PROCEEDINGS OF THE 11TH MEETING OF INTERNATIONAL COLLABORATION ON ADVANCED NEUTRON SOURCES

KEK, TSUKUBA, OCTOBER 22-26, 1990

VOL. 1

Cover Art
T. Sayama

KEK Report 90-25
March 1991
AMRD

Proceedings of the Eleventh Meeting of the

International Collaboration on Advanced Neutron Sources ICANS-XI

KEK, Tsukuba, Japan, October 22-26, 1990

Volume I

Plenary Session
Accelerator Workshop
Target Station Workshop

Editors
M. Misawa
M. Furusaka
H. Ikeda
N. Watanabe

© National Laboratory for High Energy Physics, 1991

KEK Reports are available from:

Technical Information & Library
National Laboratory for High Energy Physics
1-1 Oho, Tsukuba-shi
Ibaraki-ken, 305
JAPAN

Phone:	0298-64-1171	
Telex:	3652-534	(Domestic)
	(0)3652-534	(International)
Fax:	0298-64-4604	
Cable:	KEKOHO	

Local Organizing Committee

N. Watanabe (KEK, Chairman)
H. Asano (Univ. of Tsukuba)
Y. Endoh (Tohoku Univ.)
H. Ikeda (KEK)
K. Kaji (Kyoto Univ.)
M. Kihara (KEK)
N. Shikazono (JAERI)
Y. Yamada (Univ. of Tokyo)

Scientific Secretaries

M. Arai (KEK)
M. Furusaka (KEK)
S. Ikeda (KEK)
Y. Irie (KEK)
T. Kanaya (Kyoto Univ.)
M. Kohgi (Tohoku Univ.)
Y. Masuda (KEK)
M. Misawa (KEK)
N. Niimura (Tohoku Univ.)
I. Yamane (KEK)

Preface

The Eleventh Meeting of International Collaboration on Advanced Neutron Sources (ICANS-XI) was held on October 22-26, 1990 at National Laboratory for High Energy Physics (KEK) in Tsukuba. This meeting was hosted by KEK and sponsored by the Ministry of Education, Science and Culture (Monbusho).

The meeting covered facility status, R&D in accelerator and target station for intense spallation neutron source, and development in instrumentation for neutron scattering research. A particular emphasis was put on a topic "Total Performance".

About 130 scientists participated: about 40 from abroad and 90 from domestic. The meeting consisted of 5 status reports, 9 invited talks, about 88 workshop contributions, about 20 poster presentations, 12 summary reports of workshop sessions and 1 conference summary. Most of those are compiled in this proceedings except for some reports. A paper which we received after the deadline is compliled in the appendix. The proceedings of ICANS-XI is published as a KEK report. Questions and answers for each talk are included in the proceedings as far as we could handle. Since the total number of pages of the proceedings is so large (almost 1200 pages) we divided those into 2 volumes. We are very much thankful for all authors who have prepared manuscript quickly for the timely publication of this proceedings.

We wish to take this opportunity to thank all ICANS contacts and international advisers for their excellent cooperation in arranging the program of this meeting, and all cochairpersons for chairing their session successfully. We acknowledge with thanks the help of Local Organizing Committee, Local Program Committee, the KEK Administration Department, and the conference secretaries. Finally we would like to thank Prof. H. Sugawara, director general of KEK, for providing us an opportunity for holding this Meeting at KEK, and Prof. T. Nishikawa, former director general of KEK, for his continuous warm support for ICANS.

Conference chairman

Noboru Watanabe

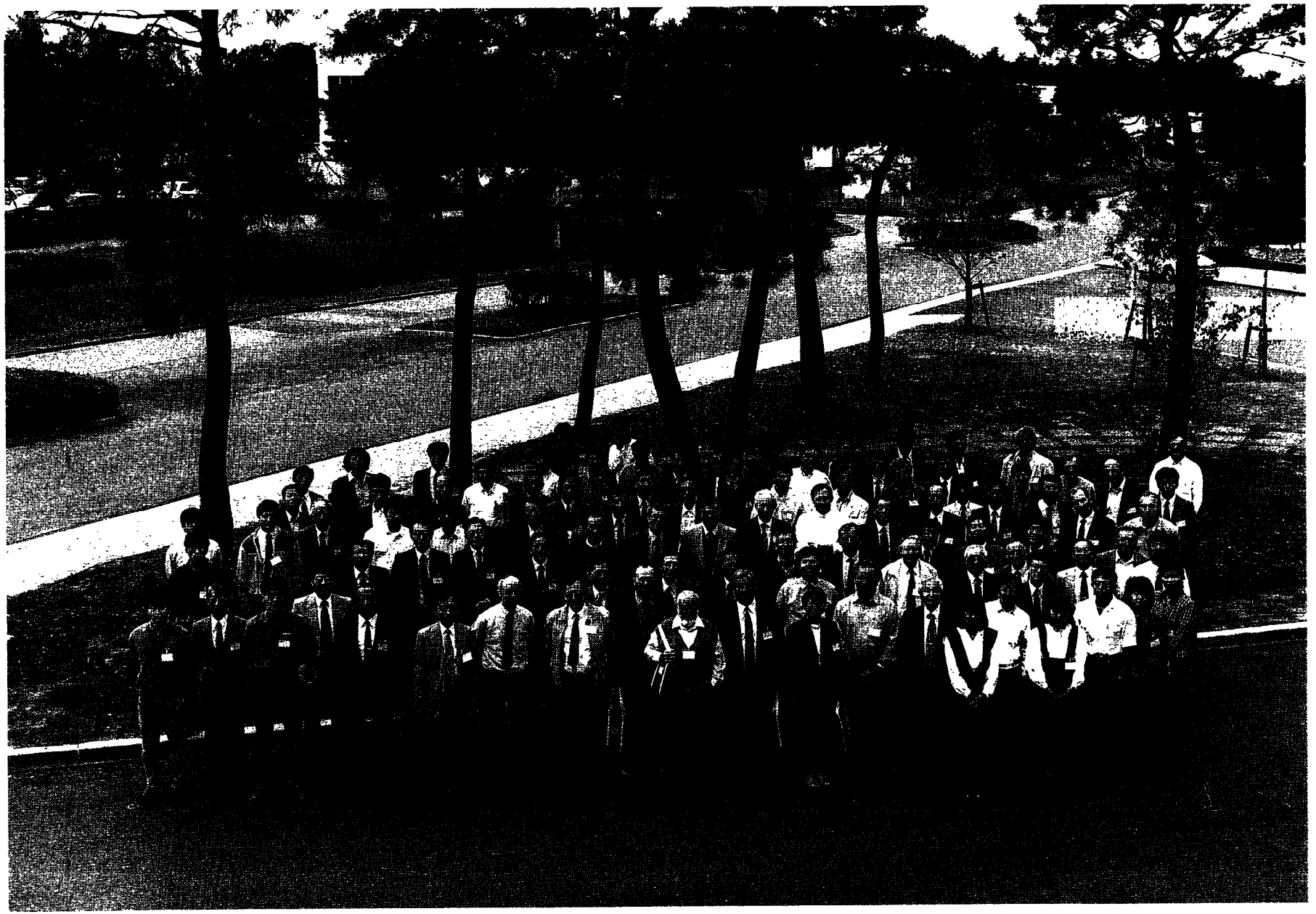

Contents

Volume 1

Preface i
Contents v

Plenary Session

Introduction to ICANS-XI 3
N.Watanabe

Status Reports

ISIS status report 5
J.L.Finney

Intense pulsed neutron source status report 14
B.S.Brown, D.E.Bohringer, F.R.Brumwell, J.M.Carpenter, R.K.Crawford, A.V.Rauchas, A.W.Schulke, and T.G. Worlton

LANSCE '90: the Manuel Lujan Jr. neutron scattering center 32
R.Pynn

SINQ -status report Oct. 1990- 41
G.S.Bauer

Status of KENS-I' and KENS-II 61
N.Watanabe

Invited Talks

Status of the Advanced Neutron Source 75
J.Hayter

Neutron facilities of Moscow meson and kaon factories 87
Yu. Ya. Stavissky

Pulsed neutron sources at KAON 100
I.M.Thorson, P.A.Egelstaff and M.K.Craddock

Pulsed neutron sources at DUBNA : their past, present and future status 109
E.P.Shabalin

Enriched vs Non-enriched vs Non-fissile targets for pulsed spallation neutron sources 119
J.M.Carpenter

General aspects of the ISIS upgrade 134
T.A.Broome, I.Gardner and G.H.Rees

Progress of the accelerator R&D for the Japanese Hadron Project 140
M.Kihara

Photons and neutrons 156
G.Shirane

Some thoughts on the future of neutron scattering 162
P.A.Egelstaff

Conference Summary

ICANS-XI Conference summary 171
G.S.Bauer

Accelerator Workshop

New Accelerator Projects (including designs) for Neutron Production

Design of the compressor/stretcher ring of the Japanese Hadron Project 179
C.Ohmori, A.Noda, Y.Kamiya, M.Kihara, and I.Yamane

Accelerator aspects of the ISIS upgrade 190
I.S.K.Gardner and G.H.Rees

INR linear accelerator and the compressor ring project for the neutron spallation source 194
S.K.Esin, A.P.Fedotov, M.I.Grachev, Q.A.Gusev, L.V.Kravchuk, V.M.Lovashev, B.P.Murin, P.N.Ostroumov, Yu. P.Severgin, and Yu. Ya. Stavissky

On the way to high-power linear proton accelerator for the long half-life radionuclides transmutation 199
G.I.Batskikh, O.S. Lupandin, B.P.Murin, and A.P.Fedotov

The intense proton accelerator program at JAERI 210
Y.Kaneko

Topics on High Intensity Accelerator Technology

High-power "Regotron"-type microwave generator for intensive technological accelerators 218
G.I.Batskikh, B.P.Murin, A.P.Durkin, O.Yu.Shlygin, and I.V.Shumakov

Treatment of H^0 and H^- beams spilled at the stripper foil at full energy charge-exchange injection scheme 224
I.Yamane

Perfect matching for the two-step H^0 injection into a ring with a DBFO lattice and minimization of the overall emittance growth 235
I.Yamane

System for generating double-pulsed magnetic fields in a kicker magnet 242
T.Kawakubo, S.Tazawa, Y.Arakida, and S.Murasugi

Intense negative ion source 247
Y.Mori

Present status of the test RF system for the KEK PS booster 251
S.Ninomiya, S.Takano, Y.Yoshii, M.Toda, and T.Katori

Summary of this session 259
G.Rees and M.Kihara

(posters)

Experimental RF proton accelerator with superconducting solenoid beam focusing 262
B.I.Bondarev, N.A.Griasnov, V.E.Keilin, A.N.Kourmanov, B.F.Lapta, A.N.Likharev, E.A.Mirochnik, A.V.Mishchenko, B.P.Murin, V.M.Pirozhenko, O.V.Plink, V.N.Saverin, I.B.Seleznev, and M.I.Surin

Particle tracking in the BSF beamline 270
T.Adachi

The accelerator complex of the Moscow Kaon factory 279
A.G.Chursin, G.A.Dubinsky, S.K.Esin, N.I.Golubeva, A.I.Iliev, V.A.Matveev, V.V.Paramonov, A.S.Pashenkov, Yu.V.Senichev, E.N.Shaposhnikova, S.P.Volin, V.A.Glukhikh, N.D.Malitskiy, Yu.P.Severgin, I.A.Shukeilo, G.I.Batskikh, Yu.S.Ivanov, R.A.Meshcherov, B.P.Murin, and Yu.F.Semunkin

Target Station Workshop

Neutronics

Spallation physics - an overview 291
G.J.Russell

Calculation code system for fission and spallation products 300
T.Nishida, H.Takada, Y.Nakahara, I.Kanno, T.Tsutsui, and Y.Kaneko

The neutronic performance of solid-target alternatives for SINQ 319
F.Atchison

Split-target neutronics 335
G.J.Russell

Neutron emission from an extended lead target under the action of light ions in the GeV region 340
R.G.Vassil'kov and V.I.Yurevich

Measurement of neutron activation cross sections by p-Be semi-monoenergetic neutrons 354
T.Nakamura, H.Sugita, Y.Kondo, Y.Uwamino, and M.Imamura

Benchmark experiment for material penetration of several tens MeV neutrons 362
K.Shin, Y.Uwamino, T.Nakamura, S. Numata, and T.Kato

Shutter system for the SINQ neutron guides 369
I.Anderson, J.Ehrat, D.Suhi, and W.Wagner

Cold Neutron Sources & Moderators

Summary report on the LANL meeting on cold neutron source 376
G.J.Russell and C.D.West

Recent experience with IPNS moderators 379
J.M.Carpenter and T.L.Scott

Optimization studies on coupled liquid hydrogen moderator 388
Y.Kiyanagi, N.Watanabe, M.Furusaka, H.Iwasa and I.Fujikawa

Reflector optimization for coupled liquid hydrogen moderator 401
Y.Kiyanagi, N.Watanabe, M.Furisaka and H.Iwasa

Some neutronic studies on flux-trap type moderator 408
Y.Kiyanagi and N.Watanabe

Theoretical thermal-hydraulic investigations of the operational and safety features of the cold D_2-moderator for SINQ 416
K.Skala, H.Spitzer, and G.S.Bauer

Technical concept of the liquid D_2-cold moderator for SINQ 430
H.Spitzer, A.Hochli, G.S.Bauer, and W.Wagner

Thermodynamic considerations on self-regurating characteristics of a cold neutron source with a closed thermosiphon 444
T.Kawai, F.Ogino, and M.Utsuro

New Concepts in Target-Reflector-Moderator Systems

Pulsed and quasistationary neutron sources based on proton beams of Moscow meson facility 454
M.I.Grachev, M.V.Kazarnovsky, V.V.Khmelshikov, N.A.Khryastov, N.V.Kolmychkov, V.M.Lobashev, V.A.Matveev, M.N.Ospanov, V.N.Sazanov, S.F.Sidorkin, Yu.Ya.Stavissky, V.I.Trushkin, and M.T.Vorontsov

Simultaneous pulsed/integral neutron facility optimization 463
I.M.Thorson

A design concept of target-moderator-reflector assemblies for KENS-II 471
N.Watanabe

The status of the ISIS targets 478
M.Holding and T.A.Broome

The LANSCE repair project 488
G.J.Russell

Thermofluid dynamics of liquid metal target for SINQ 492
Y.Takeda and W.Fischer

Thermal-hydraulics investigation for the liquid Lead-Bismuth target of the SINQ spallation source 508
B.Sigg, T.Dury, M.Hadina, and B.Smith

Design considerations for the SINQ target window 524
M.Dubs and J.Ulrich

Preliminary thermal and stress analysis of the SINQ window 536
G.Heidenreich

A solid target for SINQ based on a Pb-shot Pebble-bed 551
F.Atchison and G.Heidenreich

A high intensity beam handling system at the KEK-PS new experimental hall 569
K.H.Tanaka, M.Minakawa, Y.Yamanoi, M.Ieiri, Y.Kato, H.Ishii, Y.Suzuki, T.Suzuki, M.Takasaki, and K.Kato

Summary of this session 577
G.S.Bauer

(posters)

Measurements of the neutron yield from tungsten target irradiated by 70 GeV protons 579
A.G.Akopyan, N.V.Kolmychkov, and A.V.Kuzin

Evaluation of bulk shield for the JHP facilities 586
Y.Uwamino and T.Shibata

Multiplicating neutron targets based on the proton beam of Moscow Meson Facility 601
V.G.Miroshnichenko, S.F.Sidorkin, and Yu.Ya.Stavissky

Performance of novel moderator for pulsed neutron diffraction 607
R.E.Mayer, J.R.Granada, J.Dawidowski, and V.H.Gillette

Neutron production in thick lead target by 1-3.7 Gev protons and deuterons 612
V.A.Nikolaev, V.I.Yurevich, R.M.Yakovlev, and R.G.Vassil'kov

Superintensive pulse slow neutron source SIN based on kaon factory 628
N.V.Kolmichkov, V.D.Laptev, V.A.Matveev, L.N.Latisheva, S.V.Serezhnikov, S.F.Sidorkin, N.M.Sobolevsky, Yu.Ya.Stavissky, V.I.Trushkin, V.V.Khmelschikov, and N.A.Khryyastov

Appendix of Volume 1

Target Station Workshop

Neutronic Tuning - Some Thoughts A1
G.J.Russell

Volume 2

Contents of Volume 2 ix

Instrument Workshop

Total Performance

Why total performance 637
N.Watanabe

Performance of chopper spectrometers 644
M.Arai, A.D.Taylor, S.M.Bennington, Z.A.Bowden, R.Osborn, M.Kohgi, K.Ohoyama, and T.Nakane

Improving the resolution of chopper spectrometer at pulsed neutron sources 655
J.M.Carpenter and D.F.R.Mildner

Small-angle neutron scattering at pulsed sources compared to reactor sources 673
R.P.Hjelm,Jr, P.A.Seeger, and P.Thiyagarajan

Total performance of small-angle machines at pulsed source 677
M.Furusaka, N.Watanabe, K.Suzuya, I.Fujikawa, and S.Satoh

Total performance of LAM-80ET 684
K.Inoue, T.Kanaya, K.Kiyanagi, S.Ikeda, K.Shibata, H.Iwasa, T.Kamiyama, and Y.Izumi

Summary of this session 702
P.A.Egelstaff

Recent Progress on Instruments

•Inelastic Scattering Instruments

First results from the UK-Japanese spectrometer MARI 705
A.D.Taylor, M.Arai, S.M.Bennington, Z.A.Bowden, R.Osborn, K.Andersen, W.G.Stirling, T.Nakane, K.Yamada, and D.Welz

IPNS chopper spectrometer improvements 711
J.M.Carpenter and C.-K.Loong

Optimization of a multi-disk chopper spectrometer for cold neutron scattering experiments 717
R.E.Lechner

Crosscorrelation method using a pulsed white polarized neutron beam 733
M.Kohgi, H.Fujimoto, K.Ohoyama, K.Yamada and M.Motoya

Recent progress on MAX 739
Y.Todate, H.Ikeda, K.Tajima, and S.Tomiyoshi

Progress with the PRISMA spectrometer 743
U.Steigenberger, M.Hagen, C.Petrillo and F.Sacchetti

Advances in crystal analyser spectroscopy at ISIS 752
C.J.Carlile, U.Steigenberger, J.Tomkinson, M.A.Adams, M.Prager, and R.Mukhopadhyay

Neutron scattering on ROTAX 774
H.Tietze, W.Schmidt, R.Geick, U.Steigenberger, and H.Samulowitz

Recent progress on eVS 790
J.Mayers, A.C.Evans and A.D.Taylor

•Elastic Scattering Instruments

Recent progress in TOP spectrometer 792
S.Itoh, T.Watanabe and Y.Endoh

Collimation and background reduction design for the time of flight neutron reflectometer SPEAR at LANSCE 799
W.A.Hamilton, G.S.Smith, and R.Pynn

First results from SANDALS - the small angle neutron diffractometer for amorphous and liquid samples at ISIS 809
A.K.Soper

Status of the new GLAD instrument at IPNS 820
R.K.Crawford, J.M.Carpenter, R.Dejus, J.R.Haumann, R.Kleb, D.G.Montague, D.L.Price, and S.Susman

Use of a semi-opaque beamstop for monitoring sample transmissions at GLAD 830
D.G.Montague, J.M.Carpenter, R.K.Crawford, R.Dejus, D.L.Price, and S.Susman

EXPERIMENTS using single neutron pulses 840
C.D.Bowman, P.A.Egelstaff, and H.G.Priesmeyer

Single crystal diffraction at ISIS 849
C.C.Wilson and D.A.Keen

Future ISIS single crystal instruments 861
C C.Wilson and W.I.F.David

Analysis of a drum chopper for use on a new small angle diffractometer at IPNS 873
R.K.Crawford, J.E.Epperson, P.Thiyagarajan, and J.M.Carpenter

New Components

•Polarizers and Thin Film Multilayer Devices

Optical neutron polarizers 890
J.B.Hayter

A double reflection multilayer monochlomator for cold neutron polarizing and small angle scattering experiments 899
T.Ebisawa, S.Tasaki, T.Akiyoshi, and N.Achiwa

Polarising filter tests at ISIS 906
R.Heap, P.W.Mitchell, J.Mayers and A.D.Taylor

Investigation and growth of multilayers 910
P.Boni, I.S.Anderson, R.Hauert, P.Ruterana, K.Solt, B.Farnoux, G.J.Herdman, J.Penfold, and O.Scharpf

Optimization of the transmission of a double-trumpet neutron beam compressor 919
R.E.Lechner and F.Mezei

Summary of this session 930
W.G.Williams

•Detectors

Area detector for small angle neutron scattering at KUR 932
Y.Maeda, M.Sugiyama and S.Uehara

Scintillation detector system in neutron-nucleus experiments 937
H.M.Shimizu, T.Adachi, and Y.Masuda

Neutron detectors at IPNS 943
R.K.Crawford, J.R.Haumann, and G.E.Ostrowski

An update on ISIS detectors 957
P.L.Davidson, M.W.Johnson and N.J.Rhodes

Several experiences of using Li-glass scintillators 971
N.Niimura, H.Hirai, K.Aizawa, K.Yamada, and F.Okamura

Summary of this session 975
R.K.Crawford and N.Niimura

•Sample Environments /Peripheral Equipments

Neutron diffraction study in pulsed high magnetic field 979
M.Motokawa, H.Nojiri, M.Uchi, S.Watamura, H.Kawai, and Y.Endoh

High pressure diffraction at ISIS 987
S.Hull, W.I.F.David, R.M.Ibberson and C.C.Wilson

Feasibility studies for high pressure neutron powder diffraction experiments 995
R.B.Von Dreele

Lanthanum nuclear polarization for T-violation experiment 1002
Y.Masuda, T.Adachi, S.Ishimoto, A.Masaike, K.Morimoto, and H.M.Shimizu

Neutron scattering at ultra-low temperatures 1010
K.Kakurai

Recent Progress on Data Taking and Analysis

A summary of the workshop on neutron scattering data analysis held at the Rutherford Appleton Laboratory in March 1990 1015
M.W.Johnson

Recent improvements of the parameterization of Bragg peak profile functions 1036
J.M.Carpenter, W.C.Dimm and F.J.Rotella

Correcting beam monitor & diffraction data for chopped delayed neutron backgrounds 1044
J.M.Carpenter, D.F.R.Mildner, J.W.Richardson, Jr., and W.C.Dimm

Machine control and online data analysis using PV-WAVE 1054
G.S.Smith, W.A.Hamilton, R.O.Nelson and G.P.Cort

Future strategy for computing at ISIS 1061
W.C.A.Pulford

(posters)

Measurements of two-dimensional antimagnetic spin wave by using chopper spectrometer installed in pulsed neutron source 1078
K.Yamada, M.Arai, A.D.Taylor, S.Hosoya, A.Sano, K.Nakajima, K.Ohyama, M.Kohgi, T.Nakane, T.Perring and Y.Endoh

Crystal analyzer type spectrometer LAM-D at KENS spallation thermal neutron source 1082
K.Inoue, K.Kanaya, Y.Kiyanagi, K.Shibata, K.Kaji, S.Ikeda, H.Iwasa, and Y.Izumi

Thermal neutron small-angle scattering spectrometer (WIT) 1095
N.Niimura, K.Aizawa, M.Hirai, U.Sangawa, and K.Yamada

Diffuse scattering studies on SXD 1099
C.C.Wilson, S.Hull and D.A.Keen

High precision structural refinement from time-of-flight single crystal data 1106
C.C.Wilson

Powder diffraction at ISIS 1114
W.I.F.David, S.Hull, R.M.Ibberson and C.C.Wilson

Helium-3 neutron polarisers 1122
W.G.Williams

A new polarized target for structure studies on biomolecules at GKSS 1135
M.Hirai, W.Knop, H-J,Schink, H.B.Stuhrmann, R.Wagner, J.Zhao, O.Scharpf, R.R.Crichton, M.Krumpole, K.Nierhaus, T.O.Niinikoski, and A.Rijllart

Engineering strain measurements using the NPD at LANSCE 1144
M.A.M.Bourke, J.A.Goldstone, and K.J.Lovell

List of participants 1153

Plenary Session

Status Reports

Invited Talks

Conference Summary

Introduction to ICANS-XI

Noboru Watanabe
Conference Chairman of ICANS-XI

Ladies and Gentleman,
I would like to express our hearty welcome to all the participants at the 11th Meeting of ICANS, in particular to the foreign colleagues who came over to this meeting.

I remember the 4th Meeting of ICANS which was held just ten years ago here in KEK. It was the time just after the KENS facility began to deliver the neutron beam to users. In following ten years, large scale spallation sources were constructed in many ICANS laboratories and are now exploiting new fields of condensed matter and fundamental physics researches. I am convinced that the ICANS meetings have made a great contribution to the successes in those facilities and eventually to the world's neutron society.
In the past ICANS meetings, a first topics was historically "target station" and the second topic has alternated between "Instrumentation" and "Accelerator". In recent years, however, we had no Accelerator Workshop. We think it is always important for neutron scientists to call forth great interests of accelerator scientists for intense spallation neutron sources and their utilization. We therefore proposed that in addition to Target and Instrument, Accelerator be the three main topics covered at ICANS-XI. We hope that ICANS-XI could provide a good opportunity for this.

As you will see in the program we have so many contributions, for which the organizing committee is thankful. Since in most ICANS laboratories neutron experiments are in progress, it would be natural to have a large number of contributions in Instrumentation Workshops. The organizing committee put great emphasis on "Total Performance" as the main theme in this ICANS meeting, because the performance of an instrument should be characterized by the total system including accelerator, neutron source, instrument itself, sample environment, data acquisition and analysis, etc. We strongly hope that in all workshop sessions, the presentations and discussion will be done on this base.

We arranged two parties, and a picnic as social program. Friday afternoon Option KEK Tour is arranged.

Finally on behalf of the organizing committee I do hope that you will enjoy the meeting, excited by exchange of information and hot discussions. We also hope that you will have a good time throughout the stay in Tsukuba.

Thank you.

ICANS-XI International Collaboration on Advanced Neutron Sources
KEK, Tsukuba, October 22-26, 1990

ISIS STATUS REPORT

J L Finney
ISIS Science Division, Rutherford Appleton Laboratory, Chilton, Didcot, Oxon, OX11 0QX, UK

ABSTRACT

Two years back, I reported at ICANS X [1] that ISIS was running regularly at 100 μA, 750 MeV, with 9 scheduled neutron instruments and one muon beam line. Overall efficiency, measured as a percentage of time beam on target, was about 72%, and our stated priority was to improve reliability at 100 μA current. Over the past two years, major improvements have been made to several component parts of the system, and reliability so far in 1990 is just below 80%. Regular running periods at 100 μA have been achieved, with 100 μA average current achieved over a period of over a week. On 3 November 1989 a record integrated current over 24 hours of 2571 μA hrs was obtained. Trip rates have been significantly reduced. Three more neutron instruments are now scheduled, bringing the total to 12 neutron and 1 muon instruments. Around 350 neutron experiments were run in the 7 cycles of 1989, and about the same number are expected to be run in the 6 cycles of 1990.

Detailed reports on ISIS in the two years to March 1990 are given in ISIS 89 [2] and ISIS 90 [3]. Annual integrated currents have continued to rise, with 1989 seeing 283,000 μA hrs in 28 weeks scheduled running for users. So far in 1990, nearly 240,000 μA hrs have been achieved.

1. REVIEW OF OPERATION

As reliability has improved, integrated currents produced for user runs have risen, as shown in Figure 1. The first 4 cycles of 1990 have already produced 217,000 μA hrs: even though only 6 cycles will be run in 1990 for financial reasons (7 were run in 1989), continued running at this efficiency will lead to the 1990 figure exceeding that of 1989. Figure 2 shows the integrated beam current delivered per completed cycle to date: since ICANS X in 1988, ISIS has produced over twice as much beam as in its previous history. Figure 3 presents ISIS average beam current per cycle, and illustrates both the fall in efficiency after a long shutdown and the overall improved performance with time. The record cycle 6 in 1989 (Figure 4) included both the record day (day 16) which delivered both 2571 μA hrs (average 107 μA) and champagne to the crews. It was also in this cycle that a 100 μA average was maintained over a 9 day period (days 12-20 inclusive). 110 μA currents were achieved routinely in the second half of 1989, while the equivalent of 130 μA has been achieved at base rate during machine physics.

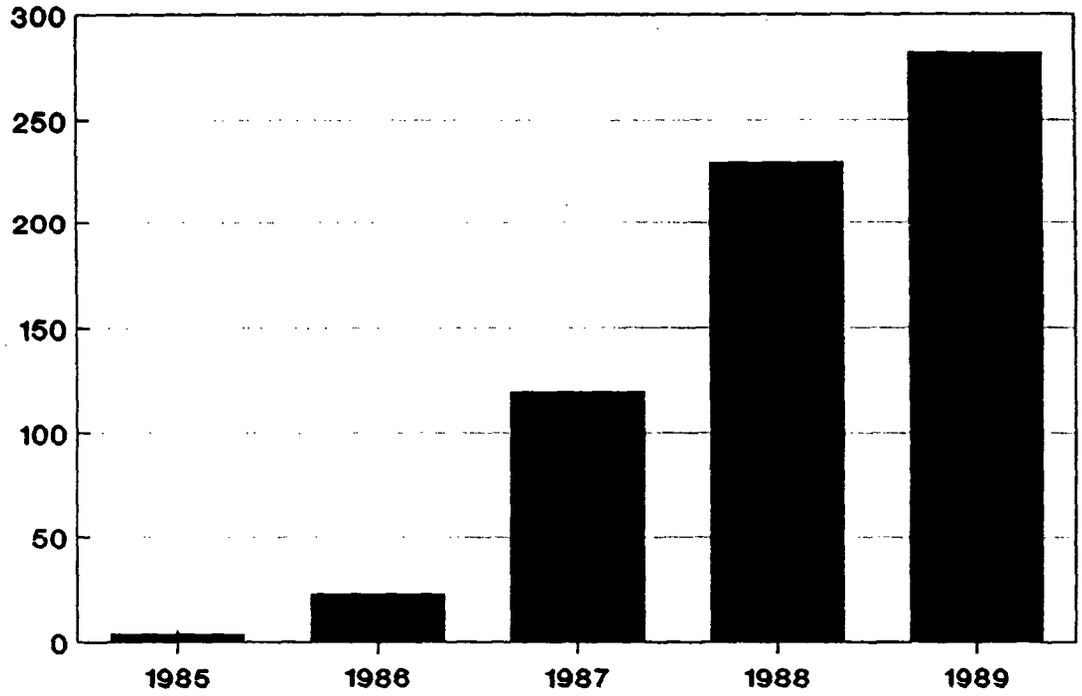

Figure 1. Integrated beam current produced by ISIS in each complete year from start-up in 1985 to 1989.

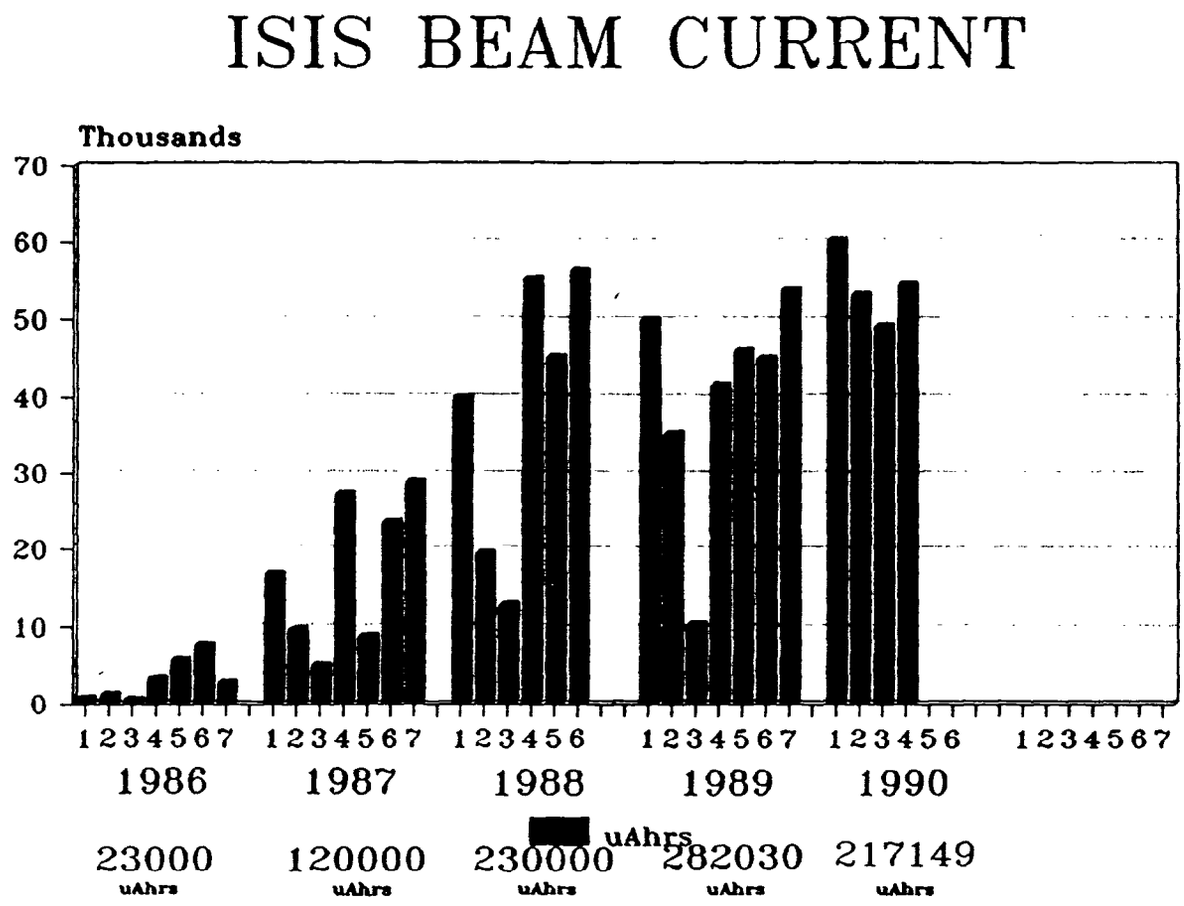

Figure 2. Integrated beam current produced by ISIS per cycle from 1986 to date.

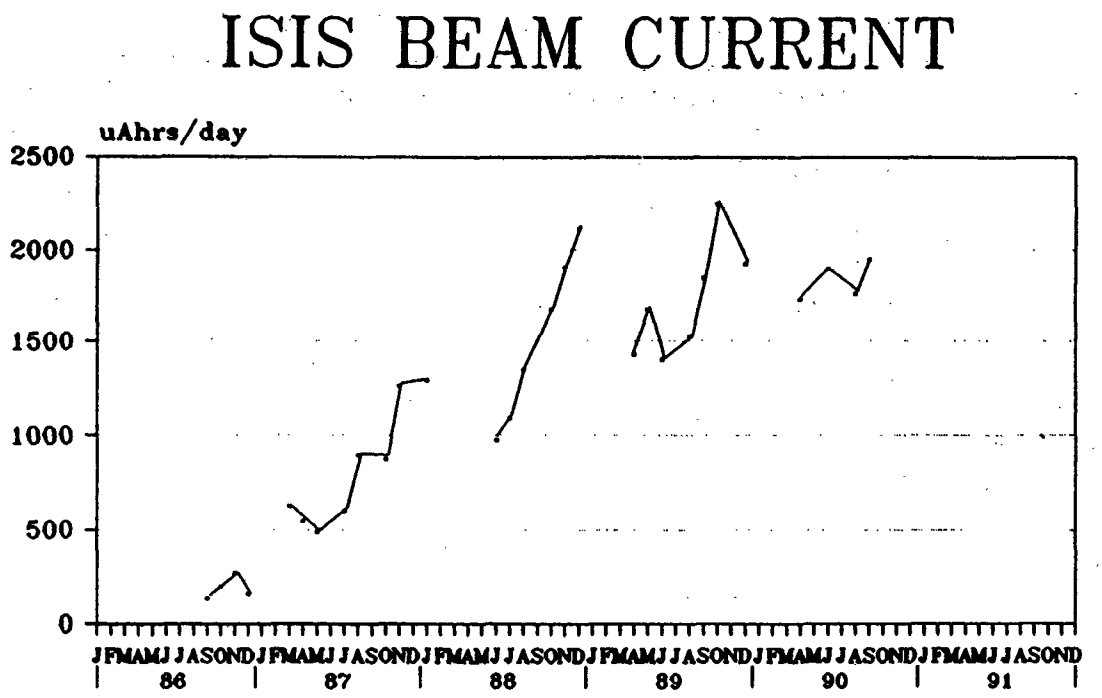

Figure 3. Average beam current per day for each cycle since 1986

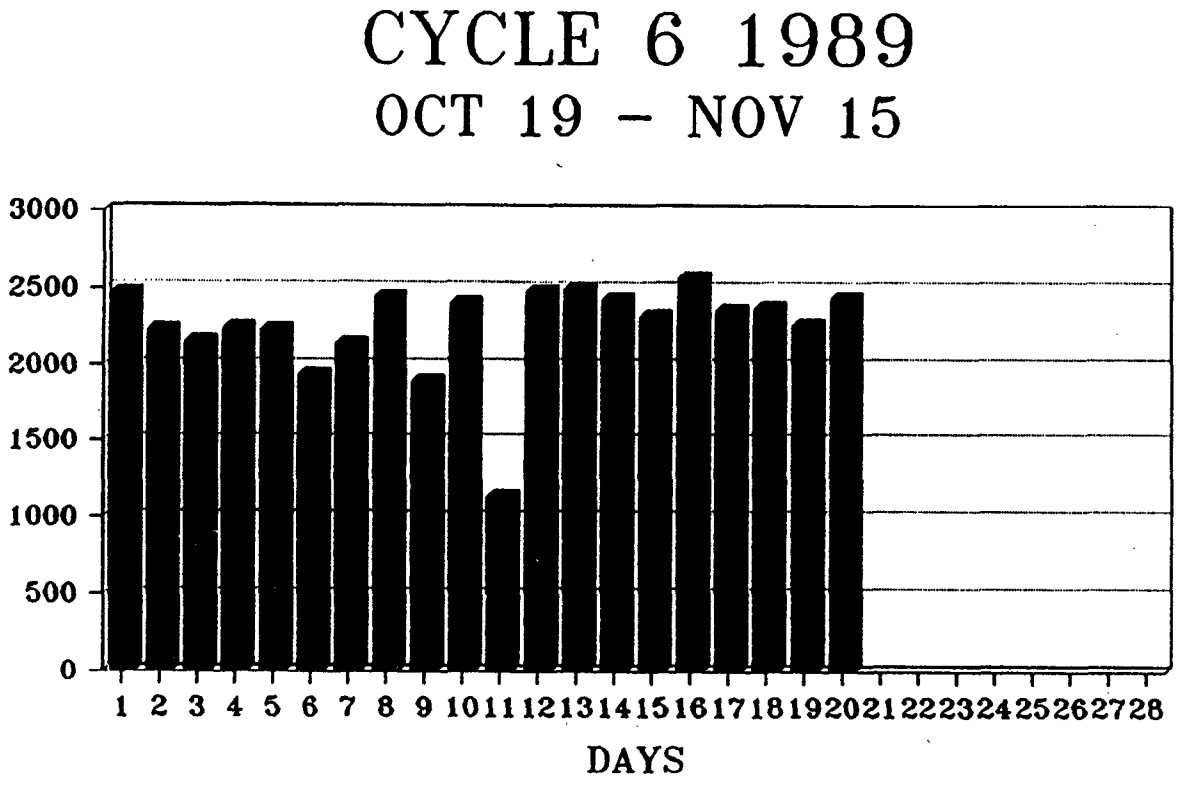

Figure 4. Beam production for each day in cycle 6, 1988. Over 100 μA was averaged for a continuous period between days 12 to 20 inclusive, with an all-time daily record of 107 μA on 3 November 1989.

Whereas in previous years, machine faults tended to come from a variety of sources and lead to short off periods, 1989 saw a shift to fewer but larger problems, with consequently longer off periods for repairs. The major failures in 1989 included the failure of a main dipole, overheating of power cables, sparking in a linac drift tube, and failure of the injection dipole power supply. Several of these problems stemmed from a major electrical storm. Some of these problems were tackled during the long shutdown between December 1989 and March 1990. A spare dipole was tested, the cable overheating problems were resolved by rerouting them, and the electrical insulation of the injection dipole magnets was improved. On the preinjector accelerating column, a modification to the electrodes was also introduced during the long shutdown to give better shielding of the insulators at the high voltage end of the structure. This has resulted in a significant reduction in the frequency of column breakdowns, and hence in the number of thermal quenches suffered by the neutron target. From an average of 68 per day in the last cycle of 1989, the trip frequency in late 1990 has fallen to 25 per day or less.

In addition to other major work, a new extraction kicker box is due to be installed in early 1991. In early 1989, it was observed that kickers 1 and 2 had been damaged by sparking, and that a large part of the copper conductor on kicker 3 had melted - although it still worked! The new kicker will allow the energy on extraction to be increased to the design 800 MeV.

At 100 μA (1.25×10^{13} protons per pulse), typical beam transfer efficiencies during routine running are :

Injection	98-99%	(98-99%)
Trapping in synchrotron	88%	(86%)
Acceleration	100%	(99%)
Extraction	100%	(99%)

The figures in brackets are those reported to ICANS-X, and demonstrate further improvement.

On the target station, new methane filters have been installed which last around 20,000 μA hrs. Uranium target number 3 failed in October 1988, after receiving 175,000 μA hrs of protons and experiencing 11,000 trips. The product of integrated current and number of trips was at 1.8×10^6 close to that for target 2: it is believed the failure mechanisms of the two targets were similar, namely swelling of the depleted uranium after repeated thermal shock. The tantalum backup target was then used for several cycles, and was found as expected to produce about 50% of the neutron yield of the uranium target. Interestingly, there was for the great majority of instruments no significant improvement in signal to noise ratio. There are thus no operational or scientific benefits apparent to offset the reduction in neutron flux. The fourth uranium target failed prematurely in August 1989: although no post mortem was carried out, a possible reason for the premature failure may have been the larger grain size of the zircalloy cladding compared to previous targets.

The asymetrically-poisoned ambient moderator, which gave rise to decay constants of 30 μs and 20 μs from opposite faces, was replaced in 1989 by a symetrically-poisoned one with 20 μs decay times from both faces. This modification was particularly beneficial in reducing the peak widths on the crystallographic instruments SXD and POLARIS. Substantial progress has also been made on the design of a system to allow the methane in the 100K moderator to be replaced as a liquid, thus removing the radiation damage products. This system, which will be essential for running at higher proton currents, will be installed in early 1991.

2. BEAM TIME DEMAND AND ALLOCATION

Seven cycles (equivalent to 28 weeks) were run for science in 1989, while financial considerations limited 1990 running to 6 cycles (24 weeks). Overall oversubscription of the instruments remained steady at around 2.5, despite the bringing on stream of new instruments. Some instruments were oversubscribed by factors of 4 to 5 or more. In 1990, 791 proposals requested 3576 instrument days, of which 403 (57%) were allocated the 1286 instrument days available. User demand from outside the UK continued to increase, and 34% of the available beam during 1990 was allocated to non-UK scientists. Figure 5 shows the distribution by country for Round 2, 1990.

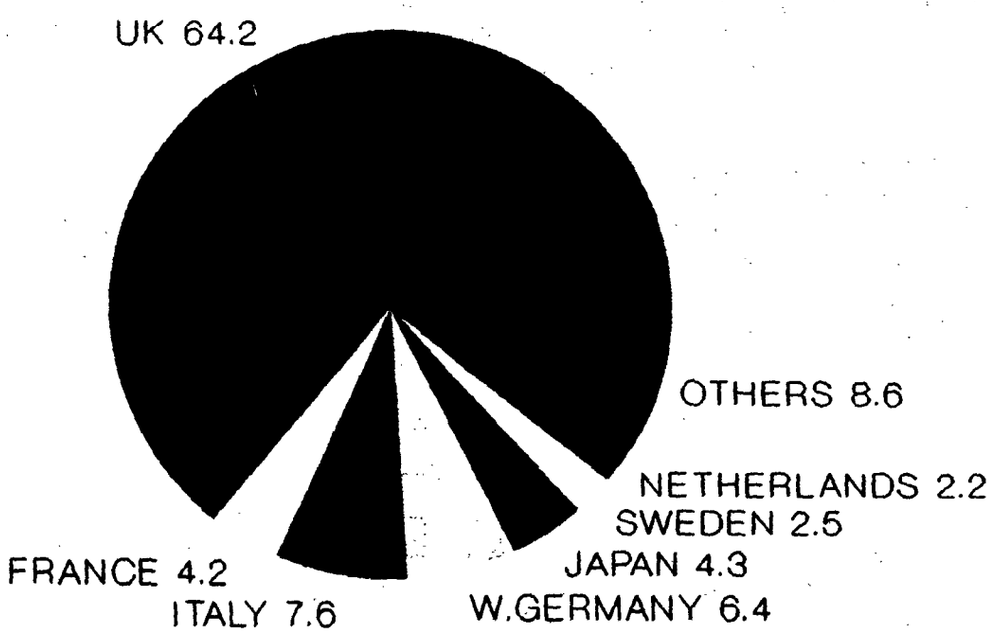

Figure 5. Allocation of ISIS beam for Round 2, 1990

3. NEW INTERNATIONAL AGREEMENTS

The agreements reported at ICANS-X as under negotiation have all been signed; as a result, agreements for the use of ISIS beams are now in operation with France, India, Italy, Japan, The Netherlands, Sweden and the University of Würzburg, Germany. In addition, a proposal to the Large Scale Facilities committee of the European Commission was approved, and consequently the present muon line will be split into three, considerably increasing the capacity of a very overloaded station. Furthermore, an important agreement was signed with the German BMFT which will provide funds to upgrade the accelerator towards its design current, and further improve reliability. Although primarily aimed at increasing neutrino production for the neutrino experiment KARMEN, this enhancement will benefit all users of the Facility. Finally, an agreement was signed with the Japanese Institute of Physical and Chemical Research (RIKEN) at the end of September 1990 for the construction of a further muon beam line and instruments on the opposite side of the muon target from the existing one. The characteristics of this line will be different from the present stopped muon line, and hence further extend the capabilities of muon science at ISIS.

4. INSTRUMENTS

Since ICANS-X, four further instruments have joined the scheduled user programme, making a total of 12 neutron instruments and 1 muon station. PRISMA - the ISIS spectrometer built by CNR Frascati, Italy - has demonstrated its suitability to perform overview measurements of dispersion curves in single crystals over an extensive range in energy and wavevector transfer. SXD - the single crystal diffractometer - joined the scheduled user programme in early 1990 and has already demonstrated the power of the time sorted Laue method, particularly in studies of disorder in crystals and magnetic satellites. SANDALS - the new generation instrument for liquids and amorphous materials designed to minimise troublesome inelasticity corrections - has just emerged from its commissioning phase. In addition to making new high quality measurements on water and silica, new science has emerged in studies of hydration of polar molecules (dimethylsulphoxide, ethylene glycol) and the tetramethylammonium ion, which appears to hydrate as a non-polar molecule.

Finally, MARI - the result of a strong collaboration with KEK, Japan - which saw its first neutrons in September 1989, has emerged from its commissioning phase and has already produced impressive results on e.g. crystal fields in ceramic superconductors, final state interactions in liquid ^4He, random network glasses such as vitreous silica, and antiferromagnetic spin waves in low dimensional systems. The instrument is clearly extremely successful, and is already in very strong demand. This is a fitting tribute to a very strong collaboration.

Papers are presented elsewhere at this meeting giving further detail on these new instruments.

Development work continues on eVS, ROTAX, and on progressing polarised neutrons at ISIS. The detectors on eVS were reconfigured to allow momentum distributions in single crystals to be measured in two mutually perpendicular directions simultaneously, and measurements on $KHCO_3$ have already produced the first unambiguous experimental evidence for the exploration of both potential wells by a single hydrogen-bonded proton.

The ROTAX principle was demonstrated on the test beam, and preparations are in hand for a test of a polarised chopped beam using the $SmCo_5$ filter developed earlier at ISIS. In addition, several instruments have been the subjects of major upgrades.

The table gives details of current ISIS instruments.

5. A CONCLUDING NOTE

ISIS produced its first neutrons at 19:16 on 16 December 1985. The occasion was marked by a 5th Anniversary celebration in and around the ISIS control room exactly five years later.

1990 was also notable for the retirement of Alan Carne, who was head of the Target Station and Muon Unit and contributed to the development and running of ISIS over many years, and also of David Gray, who was Head of Facility, and was central to the whole ISIS project from its inception. Both will be sorely missed, as will Bill Mitchell, who stood down at the end of September 1990 as SERC Chairman. Not only did the early discussions on ISIS take place in Bill's garden in 1975, but he remained a strong and sympathetic supporter of ISIS during his time in the hot seat.

INSTRUMENTS AT ISIS

Instruments commissioned since ICANS-X are underlined

Neutron Elastic

HRPD	High resolution powder diffractometer	Ab-initio structure determination, large unit cell structure refinement, phase transitions, mixed phases, line broadening, high-pressure studies.	$\Delta d/d \sim 5 \times 10^{-4}$ (backscattering), $\Delta d/d \sim 2 \times 10^{-3}$ (90° bank), guide: $\lambda^* = 0.98$ Å, minimum wavelength = 0.5 Å.
POLARIS	Medium resolution powder diffractometer	Magnetic structures, phase transitions, kinetic studies, small samples, high pressure work.	$\Delta d/d \sim 5 \times 10^{-3}$ (backscattering), $\Delta d/d \sim 8 \times 10^{-3}$ (90°), $\Delta d/d \sim 2.5 \times 10^{-2}$, (forward scattering).
SXD	Single crystal diffractometer	Reciprocal space surveying, study of structural phase changes and magnetic order, single crystal structure determination.	$0.2 < Q < 30$ Å^{-1}, $0.02 < \sin\theta/\lambda < 2.5$ Å^{-1}, 1.2-300 K accessible, position-sensitive detectors, Max. cell edge ~40 Å.
LAD	Liquids and amorphous diffractometer	Structures of liquids and amorphous solids, medium resolution powder diffraction.	$0.2 < Q < 100$ Å^{-1}, $\Delta Q/Q = 0.004$ (backscattering).
SANDALS	Small angle diffractometer for amorphous and liquid samples	Static structure factors of fluids, amorphous materials and biological systems.	Minimises inelastic corrections, $0.05 < Q < 50$Å^{-1}, $\Delta Q/Q \sim 0.01$-0.1.
CRISP	Pulsed source neutron reflectometer for surface studies	Surface structure, interfaces and surface magnetism.	Resolution 2-10% $\Delta\theta$, Q range 0.003-1.3 Å^{-1}, $0.5 < \lambda < 6.5$ Å, inclined beam for liquid surfaces.
LOQ	Low-Q diffractometer	Macromolecular, biological and other large scale structures.	$0.005 < Q < 0.2$ Å^{-1}, $\Delta Q/Q \sim 0.05$.

Neutron Inelastic

HET	High-energy transfer spectrometer	Magnetic and vibrational excitations, single particle motion in quantum systems.	Chopper incident energy 20-2000 meV, ϵ range 10-1500 meV, 1% energy transfer resolution.
MARI	Multi-angle rotor instrument	Dynamic structure factors of liquids and magnetic systems, excitations in crystalline, amorphous and disordered systems, molecular spectroscopy, momentum density.	Chopper incident energy 20-2000 meV, ϵ range 10-1000 meV, 1% energy transfer resolution, ϕ = 3-135°.
PRISMA	High-symmetry coherent inelastic spectrometer	Phonon and magnon collective excitations in single crystals.	16 independent crystal analysers and detector arms
eVS	Electron-volt spectrometer	Momentum density studies in low mass systems.	Resonance analysers in the range 1-20 eV, ϕ=30-130°
IRIS	High-resolution quasielastic and inelastic spectrometer	Rotational and translational diffusive motion in atomic and molecular systems, quantum tunnelling, crystalline electric field transitions and low lying inelastic modes.	Graphite analyser (002) reflection, 15 μeV resolution at E_a = 1.83 meV, Q = 0.25-1.85 $Å^{-1}$ (004) reflection, 50 μeV resolution at E_a = 7.2 meV, Q = 0.5-3.7 $Å^{-1}$.
TFXA	Time-focused crystal analyser	Inelastic scattering from magnetic and vibrational systems, molecular spectroscopy of hydrogenous systems.	ϵ range 2-2000 meV; ~ 1.5% energy transfer resolution, elastic line width 0.2 meV.

Muon beam

Muon Facility	μSR spectrometer and specialised equipment	Transverse, longitudinal or zero field pulsed μSR studies of magnetic materials, metals, semiconductors; muonium spectroscopy and muon catalysed fusion.	Incident momentum 20-26.5 MeV/c. Stopping range 30-90 mg/cm^2 Beam size 11 mm (v) x 20 mm (h) Intensity 5 . 10^4 μ^+/s Frequency response 100 kHz to 10 MHz

REFERENCES

1. D A Gray and J L Finney, Advanced Neutron Sources 1988, Ed D K Hyer, IOP Conf Series No 96, p11, 1989

2. ISIS 89, RAL-89-050

3. ISIS 90, RAL-90-050

Q(I.M.Thorson): I did not understand what you meant by "a three way split" in the muon beam. Could you please explain it?

A(J.L.Finney): The ISIS muon beam line accepts two sharp pulses 400ns apart every 20ms. The existence of these two pulses degrades the resolution of many μSR experiments. Currently, the new UPPSET device improves things by suppressing one of the two pulses. The EEC approved proposal will improve this situation considerably. One of the two pulses will continue to pass directly to what will be the central instrument of three. The other pulse will be split into two, with the two halves being kicked out to two experimental stations placed on either side of the central instrument. Muon capacity will thereby be increased by a factor of between 2 and 3.

Q(P.A.Egelstaff): Can you express your annual output in a convenient standard unit i.e. a 24 hour day at 100μA (2400μA hrs); in these units was your 1989 output 110 standard days?

A(J.L.Finney): Yes, of course. But the number will depend on your standard unit. Defining 2400μA hrs as 1 Egelstaff unit, ISIS in 1989 produced 118 Egelstaff's (!). We might prefer a rounder figure of 2000μA hrs, in which case 1989 produced 141 standard days.

Q(H.Tietze): Will a second target on ISIS have fully thermalized cold moderators?

A(A.D.Taylor): Probably yes.

Q(B.S.Brown): Can you say a few words about the plan and timetable for the upgrade to 200μA and 90%?

A(I.S.N.Gardner): The programme is designed to take 3years. Start of programme is 1990. The first step will be to increase the energy to 800MeV in 1991.

ICANS-XI International Collaboration on Advanced Neutron Sources
KEK, Tsukuba, October 22-26, 1990

Intense Pulsed Neutron Source Status Report

B. S. Brown, D. E. Bohringer, F. R. Brumwell, J. M. Carpenter,
R. K. Crawford, A. V. Rauchas, A. W. Schulke, and T. G. Worlton
Argonne National Laboratory
Argonne, Illinois 60439
USA

Abstract: The status and future plans of IPNS will be reviewed. At the celebration of our 10th anniversary in 7 months, IPNS will have performed over 2000 experiments and has over 230 scientists visiting IPNS annually. Plans for a new spallation source concept using a fixed field alternating gradient synchrotron will be presented.

Introduction

Seven months after the ICANS-XI meeting, IPNS will celebrate its 10th anniversary, a significant milestone and a tribute to the hard work and dedication of the scientists, users, and technical support at IPNS. The 10-year anniversary of the first delivery of the proton beam to the IPNS target will be the cause for the Fifth IPNS User Meeting, a grand celebration, and a special IPNS Progress Report.

Another milestone was recently passed with the delivery of 3×10^9 pulses to the IPNS target in July, 1990. It seems like only yesterday that we had our 2-billionth-pulse party, but then milestones such as these come quickly when operating with 95% reliability.

Our motto for the past 2 years could well have been "IPNS Keeps Chugging Along." The past 2 years have seen some large budget fluctuations (+21% and then -25%, 6 months later); some surprising personnel changes; a never-ending series of audits on safety, environment, security, etc.; and a huge effort for the scheduled visit to Argonne of the Tiger Team, a 5 week audit on Department of Energy (DOE) regulations and policies. Despite these, IPNS continues to operate successfully and in a productive manner scientifically:

- 323 experiments were performed in Fiscal Year 1989 (FY89), which began October 1988, 25% more than the previous year (FY88).
- 220 scientists visited IPNS for one or more experiments during FY89, a 10% increase over FY88.
- A second neutron reflectometer, POSY II, to be used primarily for polymer research, was commissioned in December 1988.
- The Glass, Liquid, and Amorphous Material Diffractometer (GLAD) was commissioned in April 1990.
- A proposal to DOE for manpower and instrument support for a second Small Angle Diffractometer was funded.

- A multitude of workshops were held, ranging from Momentum Distributions to the Determination of Residual Stress in Engineering Materials.

- By far the largest group of visiting faculty and high school and college students came to IPNS this past summer.

And on and on ...

A most exciting prospect for the future is the conceptual design for an advanced Pulsed Neutron Research Facility (PNRF). The goal is to build a pulsed neutron source that is as powerful as any now operating in the world which will also act as a test bed for a Fixed Field Alternating Gradient accelerator that could increase the proton current by a factor of 30, up to 3 mA. Given the very likely scenario that none of the existing DOE neutron sources will be operating in 10 years, we feel that it is very important to have a plan for the future for pulsed neutron sources as well as the very exciting prospect for the advanced steady-state reactor, the U. S. Advanced Neutron Source (ANS).

Scientific results and highlights can be found in the recently printed IPNS Progress Report, 1988-1990.

Operating status of the accelerator system

The three-billionth proton beam pulse was delivered to the IPNS target on July 16, 1990. This was less than 3 years after the last major milestone, the two-billionth pulse on target, and shows what 95% reliability can do.

The average beam current on target is continuing to increase, showing another 5% increase over the average since the previous ICANS report. Most of the increase occurred in the last six months as some nagging problems affecting accelerator system components were solved.

The reliability, already high by accelerator standards, increased to a phenomenal 95.3%. Coupled with the record-setting average beam current, this period was the most productive for the accelerator system in IPNS history. As shown in the table below, even though 161 fewer hours were scheduled between July 1988 and April 1990 than during the August 1986-June 1988 period, the accelerator was available an additional 60 hours for neutron experiments.

Table 1 Accelerator operating summary.

	11/81-7/83	10/83-2/85	3/85-7/86	8/86-6/88	7/88-4/90
Average beam current (μA)	8.65	11.90	12.89	13.47	14.12
Operating efficiency (%)	89.6	89.3	93.9	91.9	95.3
Scheduled operating time (h)	7191	5567	5263	6237	6076
Available operating time (h)	6443	4973	4942	5732	5792
Total pulses on target (x 10^8)	6.27	4.91	6.02	6.21	6.03
Total μA hours	55,732	59,179	63,702	77,210	78,865
Total protons on target (x 10^{21})	1.08	1.22	1.54	1.73	1.77
SDI linac operation (h)	0	0	1000	3125	768

Figure 1 is a plot of weekly average proton current on the neutron target since turn-on in 1981; each point represents, on average, about 148 hours of

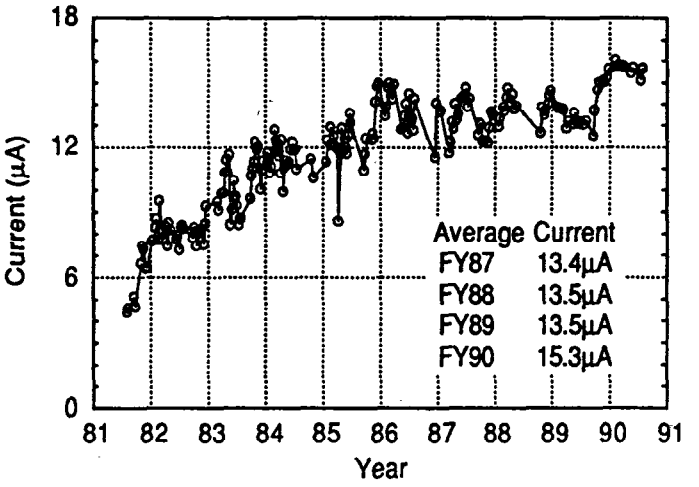

Fig. 1 Average target current of IPNS.

operation. It is clearly evident from the plot that during 1989, the average proton current had decreased after reaching a near record-setting monthly average of 14.5 μA in December 1988. In the beginning of 1989, an intermittent instability appeared in various accelerator system components. The instability was evident in numerous power supplies from the linear accelerator to the proton transport line and from the synchrotron to the neutron target. It was most prevalent in the ring-magnet power supply, which could not maintain the stability of the injection field. The worst problem was that the instability was intermittent; it would appear for several hours, disappear for another several hours, reappear again, and then disappear for several days. During the periods of instability, it would be necessary for the accelerator operators to reduce the operating current so that the imposed beam loss limit would not be exceeded. This prevented the accelerator from running at the peak level and limited the "gentle" tuning required to increase the performance. All accelerator operations personnel began investigating for possible sources of this instability. Since some intermittent problems were being experienced by the neutron chopper systems, significant investigation was centered on the variable-frequency master clock system which tracks the frequency variations of the power line and controls the phase relationship between the chopper systems and the synchrotron. This system was described in detail in the IPNS Progress Report 1983-1985.

The problem was located during June 1989 and was found to be an instability of the incoming power line. Voltage variations of a few percent and lasting only several 60-Hz cycles were affecting many of the accelerator power supplies. These power supplies are generally well-regulated, but the regulators do not have the bandwidth to respond to such short duration voltage transients. The power company was notified, and with their assistance, we were able to confirm that the noise source was not located within the laboratory, but was coming in through the power grid supplying Argonne. The power company began its own investigation in an attempt to isolate the source. Although never confirmed, the source appears to have been an industrial arc furnace facility which had converted from manual control to computer control early in the year. This would explain the appearance of the fast voltage transients on the power line. In October, the power company rearranged power grid feeders and removed the offending facility from the feeder supplying power to Argonne.

The improved accelerator stability was a major factor in the average current improvement which began in October 1989. Other contributing factors, although

much more difficult to evaluate, were the replacement of the ion source, which appeared to improve the source emittance, and the repair of a vacuum leak in an injection diagnostic in the synchrotron. Beam size measurements in the synchrotron indicated that the beam was occupying less of the injection aperture, and therefore, more beam could be injected successfully.

The real bright spot of the IPNS accelerator operations continues to be the operating reliability, that is, availability to deliver protons as scheduled. Figure 2 is a plot of this availability; each point represents the availability for a one-week period. From July 1988 to April 1990, the lowest weekly availability has been above 88%; the average for the entire period is 95.3%. This excellent performance has to be attributed to the performance of the technical personnel responsible for the accelerator system. A great deal of effort is expended in isolating potential problem areas and correcting them. Many years of accelerator operations experience provides a firm basis for extensive preventative maintenance.

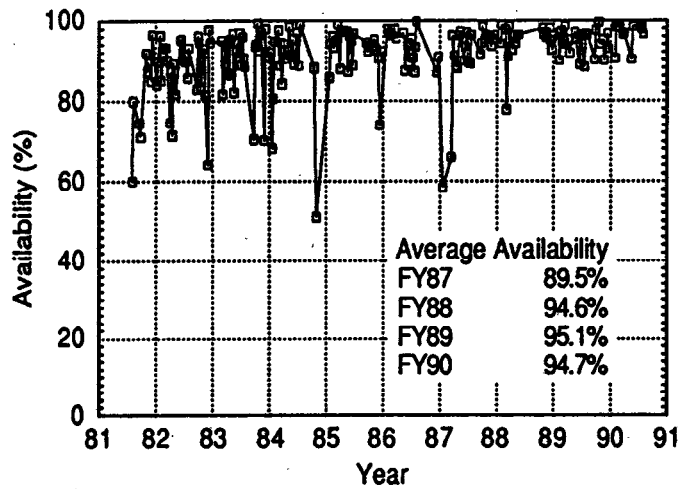

Fig. 2 Realibility of IPNS.

Achieving this high level of availability with a complex system such as an accelerator also requires some luck. There have been a few instances where equipment failures have "waited" until after the scheduled shutdown time. An example of one was a cooling hose that failed two hours after shutdown; had it occurred during operation, this would have cost six hours of downtime.

The only potentially significant problem occurred in December 1988, when a linac quadrupole magnet power supply failed to shut down when the substation feeding the linac vacuum and cooling water systems tripped off on a ground fault. It took 14 hours to repair the damage to insulation, solder joints, and current shunts. Neutron experiments lost only eight hours of beam time, since a six hour machine research period had been scheduled and was used for the repairs.

At a user facility such as IPNS, operating time is at a premium, and limited time and resources are available for major accelerator improvements. Most of the effort is used for minor upgrades. Accelerator research has been minimal and has concentrated on areas which could, with little effort, improve the accelerator performance. One area receiving attention has been the 50-MeV beam transport line from the linac to the synchrotron. Studies are underway to better characterize the beam transport system with the purpose of improving the beam matching into the synchrotron.

Another area receiving considerable attention has been the synchrotron loss monitoring system. Since the IPNS accelerator system operates loss-limited, eliminating the loss of a single proton in the synchrotron will enable an additional nine protons to be delivered to the neutron target. Studies are ongoing to improve the sensitivity and linearity of the loss monitoring system, so that the accelerator can be tuned "more precisely", thereby "squeezing" every available proton out of the synchrotron.

IPNS activity on behalf of SDI

One of the facets of the nation's Strategic Defense Initiative (SDI) program is the use of high-energy particle beams to discriminate between real and dummy warheads and to disable the real devices if necessary. Charged particle beams traveling long distances would be missteered and defocussed by the Earth's magnetic field and, of course, the electric forces between particles in the beam would tend to diffuse the beam, thus reducing its energy density. Beams of neutral particles would not suffer these deficiencies. Neutral particles cannot be accelerated, but negatively charged beams can and then, partially at least, neutralized after acceleration. It is imperative that the neutralization process does not add to the angular divergence of the beam.

While the SDI goal to put an operating 50-MeV H^- linac into space has been delayed, limited research and development is still underway. The only operating 50-MeV H^- linac in the U.S. today is the one feeding H^- ions to the IPNS RCS. Due to Department of Energy budgetary constraints, IPNS runs only one-half of the time; therefore, the IPNS linac can easily serve other users many weeks during the year.

As described in the IPNS Progress Report 1986-1988, design and construction of the larger ANL-SDI beam line started in late 1986, and the first test beam was sent down this new line on April 22, 1987. The beam optics design was supplied by members of the Argonne Engineering Physics Division, while IPNS personnel supplied much of the hardware design, installation planning, and about 90% of the installation labor and initial testing effort. Since that time, IPNS personnel have participated in the installation of a new type of electromagnetic beam expansion telescope designed at the Los Alamos National Laboratory (LANL). It includes trim multipole magnets to reduce higher order magnetic aberrations, and thus, it further decreases beam divergence. Another LANL addition to the beam line was the Wire and Fluorescent Fiber Optical Grid (WAFFOG) assembly which measures the performance of the beam expansion telescope. IPNS personnel were involved heavily in the installation and in the operations support for these tests.

However, as is evident from the Accelerator Operation Summary, the amount of SDI operation has decreased significantly. During the period July 1988-April 1990, 768 hours of SDI operation have occurred, only 25% of the time used during the August 1986-June 1988 period. Operation of the SDI facilities at IPNS will almost certainly terminate within the next year.

Instruments

Figure 3 shows the instruments now operating at IPNS, the specifications of which are given in Table 2. Although the use of epithermal neutrons (energies greater than ~100 meV) has been an important aspect of the science performed at IPNS, we are also aware that spallation sources can cover the whole useful neutron spectrum, which is why cold moderators are so important.

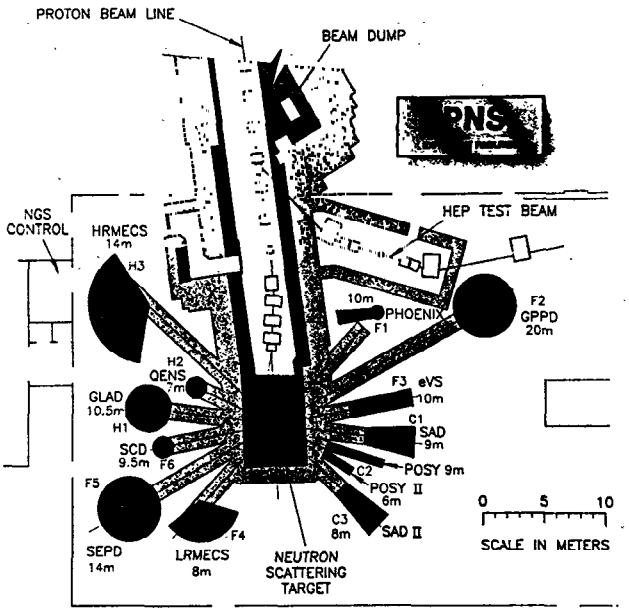

Fig. 3 IPNS neutron scattering instrument layout.

The instruments for elastic or total scattering consist of two powder diffractometers (SEPD - Special Environment Powder Diffractometer, GPPD - General Purpose Powder Diffractometer), which have excelled at high resolution and special environment work, coupled with the on-line capability of the Rietveld method and also have proved useful for amorphous systems. As one might expect, these instruments are now used increasingly with furnaces, cryostats, and pressure cells. Over the past few years, there has been considerable work on the powder diffractometers on structural and defect studies of the high-T_c superconductors and the determination of residual strains in composite materials. The Single Crystal Diffractometer (SCD) is based on the Laue technique with a two-dimensional (30 cm x 30 cm) position-sensitive scintillation detector based on the Anger method, designed and built at Argonne, and has investigated crystal structures and a variety of problems involving superstructures, diffuse scattering, and recently, texture determination and magnetic structures. The Glass, Liquid, and Amorphous Material Diffractometer (GLAD) was commissioned recently. This instrument features high intensity with low-to-moderate resolution and emphasis on low-angle detector banks to simplify inelasticity corrections. The Small Angle Diffractometer (SAD) also includes a two-dimensional position-sensitive detector and is used to investigate metallurgical, polymer, and biological systems. The broad scientific interest in the SAD and large oversubscription have resulted in the decision to build a second small angle diffractometer, SAD II, which is being designed to optimize capabilities for chemical and polymer studies.

The two chopper spectrometers (LRMECS - Low Resolution Medium Energy Chopper Spectrometer, HRMECS - High Resolution Medium Energy Chopper Spectrometer) have proved exceptionally versatile in a variety of problems involving measurements of S(Q,E). Experiments on amorphous materials, electronic transitions, and momentum distributions have all made use of the abundant epithermal spectrum. A low-temperature spectrometer, PHOENIX, is operating by a Participating Research Team (PRT) consisting of scientists from Argonne, the Pennsylvania State University, Harvard University, and the University of Illinois - Urbana for momentum density, n(**p**), measurements in quantum liquids and solids.

Table 2

IPNS NEUTRON SCATTERING INSTRUMENTS

Instrument (Instrument Scientist(s))	Beam Line	Range: Wave-vector* ($Å^{-1}$)	Range: Energy (eV)	Resolution: Wave-vector ($Å^{-1}$)	Resolution: Energy (eV)
Special Environment Powder Diffractometer (SEPD) (J. Jorgensen/K. Volin)	F5	0.5-50	**	0.35%	**
General Purpose Powder Diffractometer (GPPD) (J. Richardson/R. Hitterman)	F2	0.5-100	**	0.25%	**
Single Crystal Diffractometer (SCD) (A. Schultz/R.Goyette)	F6	2-20	**	2%	**
Glass, Liquid, and Amorphous Material Diffractometer (GLAD) (D. Price)	H1	0.05-45	**	~ 2%	**
Small Angle Diffractometer (SAD) (J. Epperson/P. Thiyagarajan)	C1	0.006-0.35	**	0.004	**
Quasielastic Neutron Spectrometer (QENS) (F. Trouw)	H2	0.42-2.59	0-0.1	~ 0.2	0.02 E_o
Low Resolution Medium Energy Chopper Spectrometer (LRMECS) (C. Loong)	F4	0.1-30	0-0.6	0.02 k_o	0.05 E_o
High Resolution Medium Energy Chopper Spectrometer (HRMECS) (C. Loong)	H3	0.3-9	0-0.4	0.01 k_o	0.02 E_o
PHOENIX (P. Sokol/Y. Wang)	F1	0.3-30	0.1-0.8	0.01 k_o	0.02 E_o
Electron-Volt Spectrometer (eVS) (P. Sokol)	F3	0.1-50	0-4	0.7%	0.08 E_o
Polarized Neutron Reflectometer (POSY) (G. Felcher/R.Goyette)	C2	0.0-0.07	**	0.0003	**
Neutron Reflectometer (POSY II) (W. Dozier)	C2	0.0-0.25	**	0.001	**

* Wave-vector, $k = 4\pi\sin\theta/\lambda$.
** No energy analysis.

Table 3

ANCILLARY EQUIPMENT AVAILABLE AT IPNS

Device	Instrument(s)	Can Be Used With	Temperature Range	Computer Control
Low Temperature				
Displex refrigerator	SEPD, GPPD, SCD, GLAD, SAD, QENS, LRMECS, HRMECS, POSY		10-300 K	yes
Helium cryostat	SEPD, GPPD, GLAD, SAD, QENS, LRMECS, HRMECS		2.5-300 K	
HeliTran	SCD		4.2-300 K	yes
^{3}He refrigerator	PHOENIX		0.3-4.2 K	
Dilution refrigerator	PHOENIX		0.03-4.2 K	
High Temperature				
"Miller" furnace	SEPD, GPPD	Controlled atmosphere	RT-1400°C	Furnace
"Howe" furnace	SEPD, GPPD, GLAD, QENS, LRMECS, HRMECS, POSY		RT-1000°C	yes
"Coffee Can" furnace	SEPD, GPPD, HRMECS		RT-400°C	yes
"Routbort" furnace	SAD	Controlled atmosphere	RT-1750°C	Furnace
"1000°C" furnace	SAD	Controlled atmosphere	RT-1000°C	Furnace
High Pressure				
0-20 kbar piston cell	SEPD, GPPD		RT	
0-7 kbar gas cell	SEPD, GPPD	Displex	10-300 K	Displex
0-5 kbar gas cell	SCD	Displex	10-300 K	Displex
0-5 kbar gas cell	GLAD		RT	
0-1.5 kbar cell	SAD	Furnace	RT-80°C	Furnace
Magnetic Field				
0-10 kG magnet	SAD		RT	
0-5 kG magnet	SAD	Displex/Furnace	10-1025 K	Displex/Furnace
0-14 kG magnet	POSY		RT	
0-8 kG magnet	POSY	Displex	10-300 K	Displex
Sample Changers				
10 position	SEPD, GPPD, GLAD		RT	yes
5 position	GLAD	Displex	10-300 K	Displex/Changer
7 position	SAD		RT	yes
Sample Positioners				
Single-axis orienter	SEPD, GPPD, GLAD, QENS, HRMECS, LRMECS	Displex	10-300 K	Displex
"x-y-z-ϕ" translator	GPPD		RT	yes

The Quasielastic Neutron Scattering Spectrometer (QENS) performs studies on molecular spectroscopy and diffusion. It takes advantage of good energy resolution (~70 μeV), coupled with the ability to measure energy changes as a function of momentum transfer.

The Polarized Neutron Reflectometer (POSY) has become a state-of-the-art instrument for obtaining magnetic information in thin films or near the surface of bulk materials. The very interesting basic information is coupled with some very promising applied interest, for example, magnetic hysteresis in materials for recording heads. A second reflectometer (POSY II) was commissioned in 1988 and was funded in part ($150,000) by IBM. This unpolarized version of POSY is primarily for studies of interfaces and interdiffusion in polymers, taking advantage of the large scattering contrast of hydrogen and deuterium. The Electron-Volt Spectrometer (eVS), designed to measure energy transfer to many eV, is used for momentum density measurement of hydrogen in various media and due to a recent reconfiguration, now functions as a high intensity, low-resolution diffractometer.

At the present time, five of the instruments at IPNS - Phoenix, GLAD, QENS, eVS, and POSY - are operated in a PRT mode. Members of a PRT supply financial support to build and operate the instrument in return for beam time (75%) that is distributed among the members. The remaining beam time is given to users that are not members of the PRT, based on proposals reviewed by the Program Advisory Committee.

Over two thirds of the experiments performed at IPNS involve some kind of special sample environment, e.g., low temperature, high temperature, controlled atmosphere (at high temperature), or high pressure. Table 3 shows the various ancillary equipment available at IPNS for use in the experimental program.

Booster target and cryogenic moderators

IPNS now operates three moderators, all cold; two of flowing liquid methane (90K) and one of static liquid hydrogen (20K). Deterioration of one of the liquid methane systems had been observed, which was due to the accumulation of radiolytically produced hydrogen. A palladium based separator has been installed which removes the hydrogen. Future plans include returning cold solid methane to the now-liquid-hydrogen system.

We were in the process of installing the Booster target at the time of the last ICANS meeting, in October 1988. In fact, one of the authors (JMC) left the meeting early for testing prior to final installation. The target has performed excellently since then, resulting in an increase in neutron beam line flux by a factor of 2.5, and is described in the IPNS Progress Report 1988-1990 and in another paper in these proceedings.

Remote examination of target growth

Previous experience has shown that enriched uranium disc materials can exhibit uranium crystal grain growth due to irradiation ("irradiation growth"). Neutron diffraction experiments at IPNS showed that the method used to fabricate the original IPNS depleted uranium discs (slicing discs from a water-cooled cylindrical mold) produced crystals with relatively small grains. Because of the small grain size and the lower neutron flux levels, irradiation growth of the discs over the predicted life of the depleted uranium target assembly was considered negligible. The process used to form the enriched uranium discs required slow cooling of the slab, which resulted in a larger grain size and an undesirable preferred crystal orientation. Due to the larger

grain, perferred crystal orientation, and higher neutron flux levels, irradiation growth of the discs became the major factor in limiting the useful lifetime of the enriched uranium target assembly. As a result, direct measurement of disk irradiation growth within the housing over the operating life of the target assembly has become highly desirable.

A test method was developed that uses ultrasonic waves to measure target growth, the distance between two metal surfaces, i.e., the top of a uranium target disc cladding and the inner wall of the housing. A sound wave is injected into the side of the vessel that contains the target. Part of the wave penetrates the vessel wall and the water that flows around each of the uranium clad target disks. The wave reflects off the disk surface and returns to the surface of the vessel. The time delay from injection to return indicates the position and, therefore, the growth of the disks. Periodic measurements of the growth permit comparison between target swelling and model predictions. The axial-length change can also be monitored using a tang that reflects the ultrasonic beam at right angles to the initial beam path so it reflects from the target spring housing. The details of the measurement and results will be published in Journal of Testing and Evaluation (D. Bohringer, et al.).

To carry out a measurement, the transducer is lowered approximately 10 ft. through a 1-in. tube (an access port), placing it in contact with the outer wall of the housing. Movement of the target back and forth under the access port tube permits monitoring of different sections of the target. A borescope inserted into the access port tube is used to align etched markings on top of the target with the tube. The etched markings identify the location of each disc and the deflection tang. The ultrasonic transducer is suspended and lowered through the tube by a signal cable attached to the back of the transducer. A weighted collar installed over the transducer provides stability and the appropriate contact pressure when the transducer is resting on the target housing. A conventional glycerol couplant is used to couple the ultrasonic wave pulse to be transmitted through the buffer, housing wall, and water. The pulse then strikes the outer surface of the disc-cladding at normal incidence and returns to the transmitting probe by the initial path.

Numerous echoes are evident in the typical oscilloscope tracing. The first echo in the train is from the housing-outer-wall buffer interface, and the second is from the housing-inner-wall/water interface. Multiple echoes from the housing-inner-wall/water interface follow. After several reverberations in the housing wall, the interface between the disc-cladding-outer-wall and the water is seen between housing wall reverberations. Establishment of the time, t, between the first echo from the housing-inner-wall/water interface and the first echo from the top of the disc, allows separation to be established from $d = v \cdot t/2$, where v is the velocity of sound in water. Calibration and a check on this measurement is carried out with a standard of the target assembly.

The gaps between target discs and housing were dimensionally inspected before the discs were finally installed. The gap between the tang and the spring housing wall was also measured during final assembly. Measurements of disc-to-housing and axial gaps obtained with the micrometer and those obtained by ultrasonic testing after final assembly are within the expected cumulative errors of micrometer measurement.

The most recent ultrasonic examination of the target pucks was carried out on July 5, 1990. Absolute estimates of gaps were on the order of 90-115 mils (1 mil = .001 in. = .0254 mm) except for puck 2 which showed an anomalous

result of 128 mils for the gap. In all cases except puck 2, the results are consistent with the initial gap measurements made on these pucks in October 1988 and the changes measured since. Total gap reductions (1988-1990) of 3-7 mils with an uncertainty of ±4 mils were observed. Average behavior is shown in Fig. 4. A clear ultrasonic signal was obtained from the reflector designed to measure axial growth. In this case the total reduction in gap (1988-1990) is about 30 mils (out of about 750 mils) with an uncertainty in change for this test of about ±9 mils.

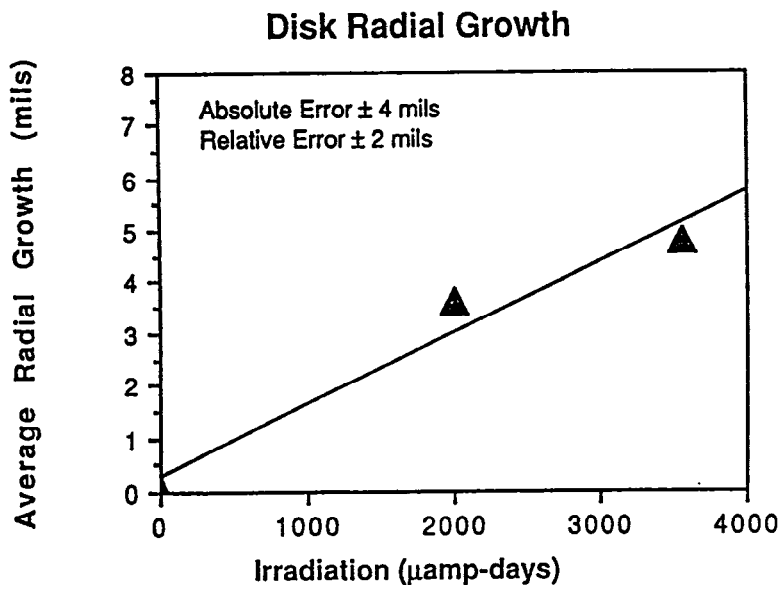

Fig. 4 Average radial growth of enriched uranium disks from October, 1988, to July, 1990.

The measurements are significant for two reasons:

1. A relatively sophisticated ultrasonic technique has been applied to a very important problem under severe test conditions. The test was performed through shielding from a distance of 3 m, on a very radioactive target (>100,000 R/hr. at the vessel surface), under corrosive conditions and requiring accurate and reproducible positioning.

2. In order to receive permission from the DOE to operate on the enriched target, very conservative estimates of growth were made, resulting in a predicted lifetime of approximately 3 years. The measurements confirm more realistic estimates of a growth rate that is less than half of the conservative estimate. The confirmation of the lower growth rate should result in installation of a new target, costing ~$1M, being delayed--for an annual savings of $300K.

Data acquisition

Introduction

Since the 1988 ICANS-X Meeting, we have continued to make improvements to the data acquisition system (DAS). Improvements to the existing system include replacement of the VAX-11/780 computer by a cluster of faster computers, conversion of additional front end computers from PDP-11's to VAXstations, installation of a 125 GB juke box library for 8 mm helical scan tape cartridges, improvement of our high-level graphics routines for the GKS

graphics system, and installation of TCP/IP networking software to give increased access for our outside users.

The PDP-11 computers used for control of the data acquisition process and the VAX-11/780 used for data analysis were based on the Unibus which is no longer produced by DEC. Communication with the microprocessors controlling the actual data acquisition was originally through a Unibus controller. As these systems were replaced by Qbus PDP-11's and VAXstations, we used a Qbus to Unibus converter so we could continue to use the same communications controllers. The communications board which we had been using has now gone out of production and there have been changes in the VMS software which have caused problems with the Unibus to Qbus conversion. Because of this we have converted our software to work with another controller board which goes directly on the Qbus.

We are gradually replacing the PDP-11 computers with VAXstations. We currently have VAXstations as front end computers on the Glass, Liquid, and Amorphous Material Diffractometer (GLAD), the Neutron Reflectometer (POSY II), and the Small Angle Diffractometer (SAD). We are in the process of installing VAXstations on the High-Resolution Medium-Energy Chopper Spectrometer (HRMECS), the other neutron reflectometer (POSY), the Single-Crystal Diffractometer (SCD), and the General Purpose Powder Diffractometer (GPPD). Replacement of the remaining PDP computers with VAXstations is expected to continue, but there may need to be additional changes in our communications with the DAS microprocessors since it appears that future DEC VAXstations will not include the Qbus, but will be busless systems. VAXstations are also being used to increase the data analysis capacity at IPNS.

Data analysis computers

The VAX-11/780 computer originally purchased for analysis of IPNS data has been replaced with a cluster of two microVAX 3500 computers and one VAXserver 3400 computer. In addition, we currently are using the GLAD2 VAXstation 3520 computer for data analysis in the IPNS computer cluster, and the GPPD VAXstation II/GPX computer is being used for analysis of powder diffraction data. A microVAX 3100 will soon replace the GPPD VAXstation for data analysis and the GPPD VAXstation will be put into service for instrument control.

The replacement of the VAX-11/780 has resulted in an increase by a factor of eight in the processing speed available for data analysis. It has also given us improved reliability since the two microVAX computers are connected in a dual-host arrangement with the system disk and one user disk on a Digital Small Systems Interconnect (DSSI) so that either system can access files on these disks when the other microVAX is shut down. Currently access to one of the disks will be lost when it is necessary to shut off power to the microVAX housing that disk in order to replace interface boards, etc. This problem will soon be solved when the disks are moved to a separate cabinet. We will also add an additional DSSI disk and reorganize files to keep critical files on the DSSI disks. We still lose access to disks directly connected to one computer when that system is shut down and expect to convert additional disk space to dual-host access as the budget allows.

Use of VAXstations

All of the initial eight IPNS instrument computer systems were based on DEC PDP-11 computers. These computers are difficult to program because of memory size limitations and give us the burden of supporting an additional operating system. Several IPNS instruments also need greater on-line computing capabilities and disk storage capacity than is available on the PDP-11 systems.

Finally, the PDP-11 systems are starting to show their age (the oldest have been in continuous operation for more than 9 years) and their failure rate is increasing. For these reasons, we have begun purchasing VAXstations to replace the PDP-11 computers. We currently have four DEC VAXstation-II GPX workstations, each with at least 300 Mbytes of disk storage, one VAXstation 3200, and one VAXstation 3520. Another VAXstation 3200 is on order. The VAXstations procured as instrument computers initially were used very successfully for data analysis. Now they are being used as instrument computers and additional microVAX and VAXserver computers have been bought for data analysis. The addition of the VAXstations has not only improved the instrument computer situation, but has also increased the total computing capacity available for data analysis since the VAXstation instrument computers place significant computing capacity at each instrument. It is expected that in the future more data analysis will be done directly at the instrument as the data are being collected, rather than on one of the central computers in the system. Our central VAX systems will continue to be used by the VAXstations for data storage and archiving as well as program development and network services.

Graphics improvements

A package of high-level graphics routines (GPLOT) for use with the GKS graphics package has been developed at IPNS. This was originally developed to provide greater access to graphics capabilities at IPNS since we did not have the budget for the expensive commercial graphics package (DISSPLA) used on the VAX-11/780 to be put on all the workstations. There also was a need for a lower cost graphics package for use by IPNS users who did not have and could not afford DISSPLA. Most of our graphics routines have now been converted to utilize GKS graphics, which is available on all of our computers. The use of GKS has allowed us to develop device-independent graphics software that can be run on the VAXstation as well as our other graphics devices. The VAXstations produce high resolution color graphics very quickly, which allows users to interact effectively with data collection and data analysis. This will also enable more interactive modes of data analysis.

One of the limitations which prevented us from using GKS for all of graphics was the lack of a 3-dimensional plotting capability. This has now been added to our GPLOT package, so we expect to continue conversion to the use of GKS, which will result in a large cost saving to both IPNS and our users.

Other improvements to GPLOT include an improved user interface with data-driven menu routines for plot device selection at run time. This will greatly simplify the installation and customization of GPLOT, and will allow individual users to create their own device menus. We have also added a plot routine which allows the user to interactively add text and vectors to the plot and to label data points. This routine also provides a continuous display of the cursor position in data coordinates on the VAXstation.

Improvements have also been made in graphics hardware. Postscript laser printers are now available in several locations, and we have added additional graphics terminals and a color ink-jet plotter.

Networking and clustering

A number of improvements have been made in the Argonne lab-wide Ethernet and more improvements are in progress. All VAX computers at the lab are now on the Ethernet and many IBM-compatible and Macintosh personal computers are now connected via Ethernet. ANL has added a Cisco router which handles both DECnet

and TCP-IP network traffic, and has purchased a site-wide license for Multinet software to provide TCP-IP capability on ANL VAX computers. We have installed Multinet software on our two microVAX 3500 computers and will add it to other computers as the need arises.

As our computer needs grew it was necessary to add a number of disk drives for users and to add additional processing power. The most cost-effective way to do this was to add MicroVAX and VAXstation computers. To simplify access and connection speed among our computer systems and many disks, it was necessary to join them together in a cluster. This has made it simpler to manage the computer systems and more efficient to store files centrally without the necessity of keeping multiple copies of files. Some of the new instruments which are now on-line have strained our computing and data storage capacity, and demand also increased with the Booster target, so a considerable expansion of the cluster has been necessary. The expansion of the cluster is expected to continue.

IPNS has now added a number of IBM-compatible personal computers and Macintosh personal computers. The IBM-compatible PC's have been networked with the VAX computers using DEC PCSA (Personal Computer Systems Architecture)/Lanworks for DOS networking software. This has improved printer sharing and will be used to improve file sharing for PC's and security of files. One of our Macintosh computers has been connected to the Ethernet and we expect to add Lanworks for Macintosh in the near future.

Future improvements to the Lab-wide network include additional connections to outside networks and the installation of a high speed (100 Mb/s) FDDI (Fiber Distributed Data Interface) fiber optic network. ANL has already installed FDDI cable between some buildings and has plans for expansion of FDDI capability. We expect to improve networked graphics through the use of X-Window terminals and will begin experimenting with this technology shortly.

Data backup, archiving, and retrieval

The large amount of data and other files on disk has required several improvements to our system for backup and archiving of data. The problem of disk back-up to tape has been solved by the use of high capacity helical scan cartridge tapes. The first drives of this type used standard VHS video tapes for backup and each cartridge could hold 2.5 GBytes compared to 0.14 GBytes on a high density 9-Track tape. This allowed us to back up two or three large disks on one tape cartridge instead of using several tapes to back up each disk. This gave us a considerable saving in operator time for changing tapes, cost of media, and storage space required.

The next generation of helical scan drives used 8 mm video tape cartridges which hold 2.2 GBytes each. These cartridges are several times more compact than the VHS cartridges and the cost of drives is lower than for the VHS units. These have been widely accepted in the industry and are starting to be used for data interchange. As we have converted to the use of VAXstations we have also put large disk drives on the front-end computers. Backup of these large disks to TK50 cartridge drives which hold 0.1 GByte proved to be unfeasible, and 8mm drives have been added to all VAXstations as well as computers used for data analysis.

Because of the cheaper and more compact storage, we are able to do weekly full backups of cluster disks and keep monthly full backup tapes permanently, instead of re-using the tapes after one year.

Another problem is the archiving of data to tape in order to keep sufficient space available on the disks. We have been using file expiration to select files for automatic removal from the disks and have used 9-Track tape to save these files. The problem with this method is that operator intervention is required to mount tapes whenever files need to be restored to disk.

We have recently purchased a juke box library system which holds 54 8mm data cartridges which can be mounted in one of two tape drives through remote commands. We have converted most of our archived files to 8 mm cartridges and have developed software for backup, archiving, and file restoration using the jukebox. This will eliminate the need for operator intervention for mounting tapes.

Current needs and future plans

IPNS has a need to continue upgrading and improving its computer systems and software. Developments in technology are very rapid in some areas and IPNS has formed a committee of users to recommend improvements to computing at IPNS. Two areas identified by this committee as primary concerns are improved interactive graphics capabilities using personal computers or workstations, and improved document production capabilities using a true What You See Is What You Get (WYSIWYG) software/hardware package. We are examining various commercial software packages in these areas for use on a Macintosh or IBM-compatible personal computer. We also plan to investigate the use of X-Windows terminals for achieving these capabilities on a shared system.

User program

Figure 5 shows that the number of requested and available days dropped off somewhat in 1985 and has been steady since that time. This is due to the decrease in operating funds which has resulted in fewer weeks of operation. This has been partially compensated by the installation of the Booster target and increase in average proton current, meaning fewer days are required per experiment.

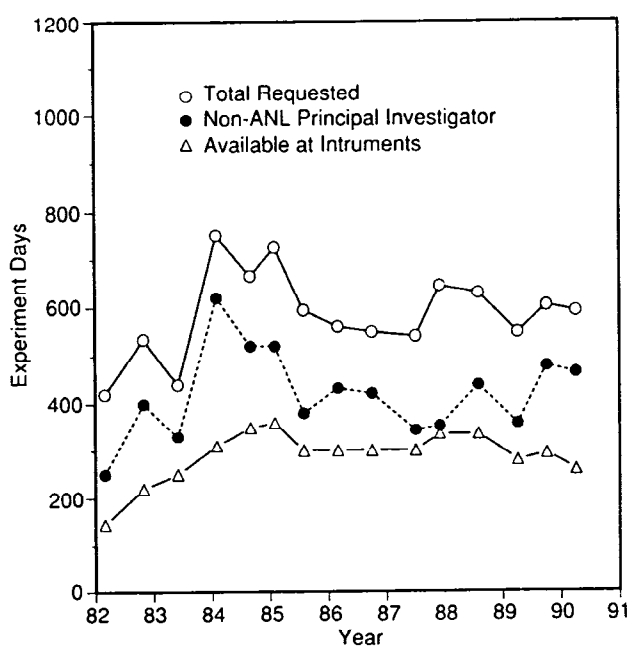

Fig. 5 IPNS statistics since 1982.

With the availability of significant fluxes of long wavelength neutrons, the Small Angle Diffractometer (SAD) has become a highly versatile and attractive instrument for research in many areas, viz., biology, metallurgy, and polymer science. This has resulted in making the SAD one of the most oversubscribed instruments for the past 4 run cycles. To alleviate this oversubscription on the SAD, a proposal to build a second SAD was developed and recently funded by the DOE; construction is underway, and the goal is to complete the instrument in collaboration with S.-H. Chen of the Massachusetts Institute of Technology by mid-1991.

The breakdown of statistics on visitors and their experiments is shown for the first 8 (fiscal) years of operation. Due to funding restrictions, the total weeks of IPNS operation decreased after fiscal year 1984 (FY84). However, since operation before FY85 included the now-defunct Radiation Effects Facility, the number of weeks for neutron scattering has been nearly constant. In addition, with the installation of the Booster target and increases in proton current and the number of instruments, the number of experiments continues to grow.

Table 4 IPNS user program statistics for FY82-FY89*.

	FY82	FY83	FY84	FY85	FY86	FY87	FY88	FY89
Experiments performed	94	110	210	180	212	223	257	323
Visitors to IPNS for at least one experiment:								
Argonne	37	41	49	44	52	55	57	60
Other government laboratories	8	9	8	7	11	15	18	16
Universities	27	33	45	51	79	78	89	94
Industry	5	5	9	7	13	24	20	24
Foreign	12	18	39	35	27	24	17	26
	89	106	150	143	182	196	201	220
User Instruments	4	5	6	6	6	6	6	7
PRT Instruments	1	1	1	2	3	3	4	4
PRT Instruments	1	1	1	2	3	3	4	4

*Fiscal Year (e.g., FY89 = October 1, 1988 to September 30, 1989, inclusive).

Recent conferences and workshops

We continue our strong commitment to sponsor conferences and workshops in connection with our efforts to spread the news about neutrons in general, and the capabilities of IPNS in particular. Financial and technical assistance from both the University of Chicago and Argonne's Division of Educational Programs is greatly acknowledged.

October 24-26, 1988
Workshop on Momentum Distributions

November 14-15, 1988
Fourth IPNS User Meeting

November 16-18, 1988
Short Course in Powder Diffraction and Rietveld Analysis

June 14-15, 1989
Neutron Scattering in Molecular Sieve Research

April 16-17, 1990
Workshop on Glass and Liquid Diffraction

May 22-23, 1990
Application of Neutron Diffraction to the Determination of Residual Stress in Engineering Materials

August 23-25, 1990
Workshop on Neutron Reflection Data Analysis

Pulsed Neutron Research Facility (PNRF)

The need for more intense neutron sources has been the subject of numerous meetings and reports. The most thorough workshop took place at Shelter Island, New York, in October 1984. The major findings of the workshop were:

1. The case for a new higher flux neutron source is extremely strong, and such a facility will lead to qualitatively new advances in condensed matter science.

2. To a large extent, the future needs of the scientific community could be met with either a 5 x 10^{15}n-cm^{-2}-s^{-1} steady state source or a 10^{17}n-cm^{-2}-s^{-1} peak flux spallation source.

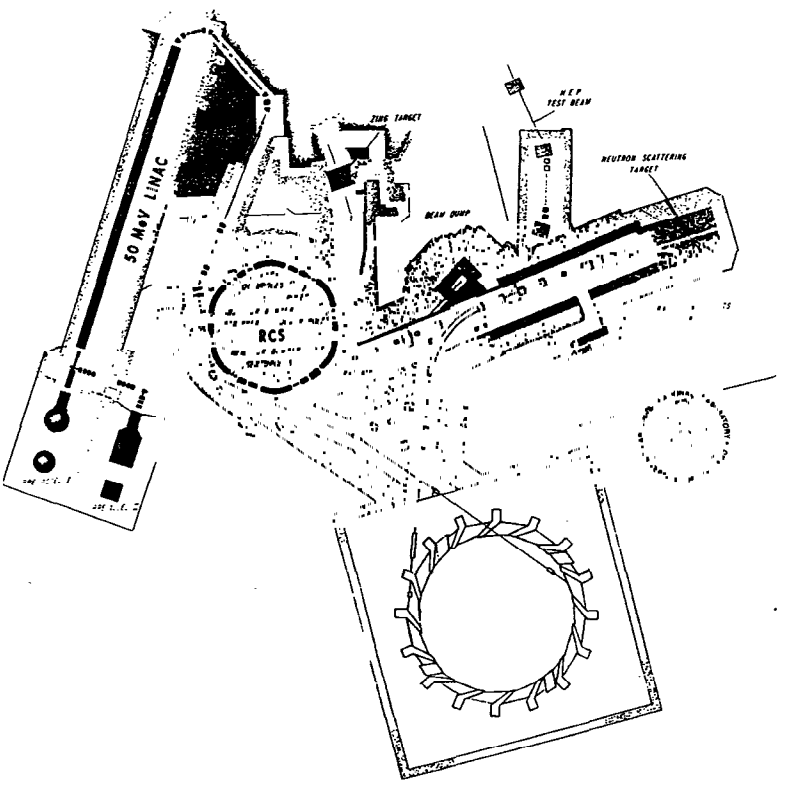

Fig. 6 Pulsed Neutron Research Facility.

Accelerator-based pulsed neutron sources have been performing neutron scattering research for just over ten years. During this decade, beam intensities have increased by a factor of 100, and there are now more than 50 spectrometers operating worldwide. The pulsed neutron sources have proved to be highly effective and are complementary to reactor-based sources in that there are important scientific areas for which each type of source has unique capabilities. We have proposed to the DOE that the capabilities of pulsed neutron sources be further pursued by means of a Fixed-Field Alternating-Gradient synchrotron concept. The program in this proposal will do the conceptual research and development for the accelerator and target systems that will produce 100-200 μA at 500-1000 MeV. Much of the present IPNS system will be incorporated in the design as shown in Figure 6. The accelerator, named Pulsed Neutron Research Facility (PNRF), will be a source comparable to the most powerful pulsed sources now operating in the world and also will act as a test bed for the basic Fixed Field Alternating-Gradient synchrotron concept for more powerful sources in the future. A preliminary conceptual design was developed in 1984 for a 100 μA, 500 MeV machine. Details of this proposal appear in the Proceeding of the Enrico Fermi Summer School on Industrial and Technological Applications of Neutrons; Lerici, Italy, June 19-29, 1990.

Acknowledgements

This work is supported by the U. S. Department of Energy. This manuscript has been authored by a contractor of the U. S. Government under contract No. W-31-109-ENG-38. Accordingly, the U. S. Government retains a nonexclusive, royalty-free license to publish or reproduce the published form of this contribution, or allow others to do so, for U. S. Government purposes.

Q(A.D.Taylor): Is your quoted thermal flux of 10^{14} n^{th} cm^{-2} mA^{-1} consistent with estimates that a 5mA SNQ would be equivalent to ILL?

A(G.S.Bauer): Yes, it is. SNQ had twice the proton energy (effectively, because of the 120MeV threshold) compared to SINQ and five times the current, which reach to somewhere around 10^{15} $cm^{-2}sec^{-1}$. Of course, the fine structure would have mach SNQ superior to the ILL-reactor by an order of magnitude or more with proper instrumentation.

Q(N.Watanabe): What are the major reasons for large difference in estimated target life compared to that of ISIS?

A(B.S.Brown): The ISIS target lifetime is determined by cladding fatigue and our by growth. The reason for the difference is in the details of target design, beam intensities, U-235 vs U-238, etc.

Q(?): Why are ISIS and IPNS target lifetime so much different?

A(J.M.Carpenter): The differences depend on details of stress distribution in the cladding. The disk designs differ substantially, so the comparison is difficult to make. Furthermore, the failure mode is in fatigue; fatigue life is a very strong inverse function of stress.

Q(Y.Endoh): I would like to ask your comment on the anisotropic growth of booster target because you showed only one direction data.

A(B.S.Brown): After 2 years of operation, the average radial disk growth was .127mm and the axial growth for the stack of 11 disks was .762mm.

Q(N.Watanabe): How can you measure the radial growing of U-235 target disk?

A(B.S.Brown): The growth is measure by an ultrasonic technique that measures the time for a signal to reflect off the outer surface of the disk.

Q(A.D.Taylor): Would you retain a ^{235}U booster target with the 100μA accelerator concept?

A(B.S.Brown): The present 80% enrichment would be very difficult at 100μA. Options include lower enrichment, 2 target stations with a booster target for low frequency operation, or a return to ^{238}U.

ICANS-XI International Collaboration on Advanced Neutron Sources
KEK, Tsukuba, October 22-26, 1990

LANSCE '90: The Manuel Lujan Jr. Neutron Scattering Center

Roger Pynn,
Los Alamos National Laboratory,
Los Alamos, NM 87545, U.S.A.

ABSTRACT

This paper describes progress that has been made at the Manuel Lujan Jr. Neutron Scattering Center (LANSCE) during the past two years. Presently, LANSCE provides a higher peak neutron flux than any other pulsed spallation neutron source. There are seven spectrometers for neutron scattering experiments that are operated for a national user program sponsored by the U.S. Department of Energy. Two more spectrometers are under construction. Plans have been made to raise the number of beam holes available for instrumentation and to improve the efficiency of the target/moderator system.

When I spoke at the last ICANS meeting in 1988 [1], LANSCE was struggling with low beam availability and a proton beam current that was less than a third of its design value. Construction of a large experimental hall had been completed and desert dust was hanging over the construction site of our new office and support building. A user program had been started and 399 days of beam time were requested for the 1988 run cycles. Occupancy of the ER-1 experimental hall during beam delivery had been achieved but relied heavily on fail-safe instrumentation to detect proton beam spills and prevent large radiation doses close to the spectrometers. The neutron powder diffractometer (NPD) and the reflectometer (SPEAR) were being commissioned: a chopper spectrometer (PHAROS) and a back-scattering machine were but concepts in the minds of their designers. We were contemplating a neutron guide for the back-scattering spectrometer but had not even decided whether it should be straight or curved.

The scene has changed in the past two years. Construction of the office/support building was completed early in 1989, on time and within the budget prescribed by the Department of Energy. Two months after we moved into our new building, the LANSCE facility was dedicated to Manuel Lujan Jr., a long-time New Mexico congressman and supporter of scientific research who is currently serving as Secretary of the Interior.

Thanks to the support and commitment of Los Alamos Laboratory management, we have been able to improve substantially the performance of the Proton Storage Ring (PSR). In recent months the proton current extracted from ring has usually been between 75 μA and 85 μA whenever beam has been delivered to the LANSCE target, averaging 75 μA with a beam availability of 74% during the most recent run cycle. During the same cycle, the

LAMPF linear accelerator was available for 84% of the time, so less than half of our lost time was due to breakdown of the PSR and beam transport systems. A beam current of 95 μA at a 20 Hz repetition rate was achieved for a shift or so last week, demonstrating that there is no fundamental technical obstacle to reaching our ultimate goal of 100 μA. For the moment however, the beam losses at 100 μA are larger than we are willing to tolerate because the activation caused by these losses is inconsistent with the Laboratory policy of reducing radiation doses received by employees In his talk later in this meeting Bob Macek will tell you what magic he worked to achieve the present PSR performance and what modifications he expects to make to achieve 100 μA on a regular basis. We are still committed to this goal, even though the present performance of PSR gives LANSCE a peak neutron intensity that is 50% higher than that of our closest rival.

The social environment in which research facilities are operated is changing rapidly in all of the industrialised nations. It is becoming increasingly clear that society will not tolerate facilities that it perceives to be unsafe or to cause environmental insult. Of course, this gives spallation sources an inherent political advantage over competing reactors, in addition to the technical advantages that are becoming increasingly apparent. Nevertheless, most of the existing spallation sources were not designed to achieve the level of safety that is now demanded. For that reason, we at LANSCE have expended a great deal of time and money over the past two years improving radiation and other safety systems. Over 800 tons of steel shielding was installed in a layer 750 mm thick on the floor of the proton transport tunnel to shield the experimental room (ER-1) that is under the tunnel from the effects of beam spill. The attenuation factor of about 100 provided by this steel substantially reduces our dependence on instrumentation for safe occupancy of the experimental hall. During our studies of radiation safety, we discovered a weakness in the shielding of the proton transport system where it passes under a road between LAMPF and the PSR. In order to deliver beam under acceptable conditions during 1990 we had to divert this road, fence off part of a parking lot and install fail-safe instrumentation to interrupt the proton beam in the event of a major spill. Such reliance on instrumentation is uncomfortable and we will install additional shielding in our road during the 1990-91 shutdown. By next year, we will have spent between $4 million and $5 million on additional shielding and instrumentation for radiation protection in a three year period.

Neutron spectrometers at most spallation sources have been designed so that access to neutron beams is prevented during beam delivery, a safety feature which is absent from all research reactors that I have ever visited. The system installed at LANSCE interlocks the door to a spectrometer cave with the shutter that prevents neutrons reaching the spectrometer. Even though this system has worked well, we have concluded that its lack of redundancy is a drawback. Accordingly we will incorporate radiation monitoring devices in our spectrometer interlock systems during the 1990-91 shutdown.

The previous paragraphs describe only two of the many safety related actions that we have taken or planned during the past year or so. There have been many others, ranging from an almost complete refurbishment of our chemistry laboratory to collaboration with the video club at our local high school to tape a comprehensive safety briefing for users of the facility. Even though I expect safety to be of continuing concern, I doubt that we will need to spend as much money on this activity as reactor centers. Nor do I anticipate that it will be necessary to interrupt research at spallation sources for safety related reasons.

Early this year we completed four new penetrations of our bulk shield. This task had to be accomplished with precision because there was very little space between the new holes and existing penetrations of our crypt. Once the holes had been bored through magnetite concrete and iron, liners were installed and welded to the crypt. The latter task proved to be highly non-trivial and it is a testament to the perseverance of Harold Robinson and his

crew that the welding was completed before the run cycles began in May. If any of you ever have to install additional beam lines at your facilities I encourage you to contact Harold: he learned many lessons the hard way. The new beam lines will eventually allow us to install four "new" spectrometers in our large experimental hall. In fact, at least two of these spectrometers (a Single Crystal Diffractometer and a Filter Difference Spectrometer) already exist and will be upgraded only in minor ways when they are moved. Unfortunately we cannot yet provide neutrons for our new beam holes. To do so requires new moderators to be installed as part of an upgrade in which we expect to increase the neutron flux to all spectrometers. Whether we will be able to obtain the $1 million or so needed for this upgrade remains to be seen.

The user program at LANSCE has expanded each year since its inception in 1988, in part because of the addition of new spectrometers. In 1988, users requested 399 days of beam time on four spectrometers. This year, 145 proposals asked for a total of 592 days on six instruments. Because funding for LAMPF has been limited, less than 50 days of beam time could be offered to users on each spectrometer, resulting in an average overload factor of 2.1. This number is close to the canonical value of 2 that seems to pertain at almost all successful neutron scattering centers, regardless of the number of spectrometers or the fraction of time during which the facility operates. Of course, it would be sensible to increase the operating time for LANSCE from five months to about nine months of each year but I doubt that this can be achieved under present budget constraints in the U.S.

The two spectrometers that were being commissioned in 1988 (NPD and SPEAR) are now an integral part of our user program. Even though we expect to upgrade the performance of both instruments by installing position-sensitive detectors during the next two years, both are already producing high quality data and are popular with users.

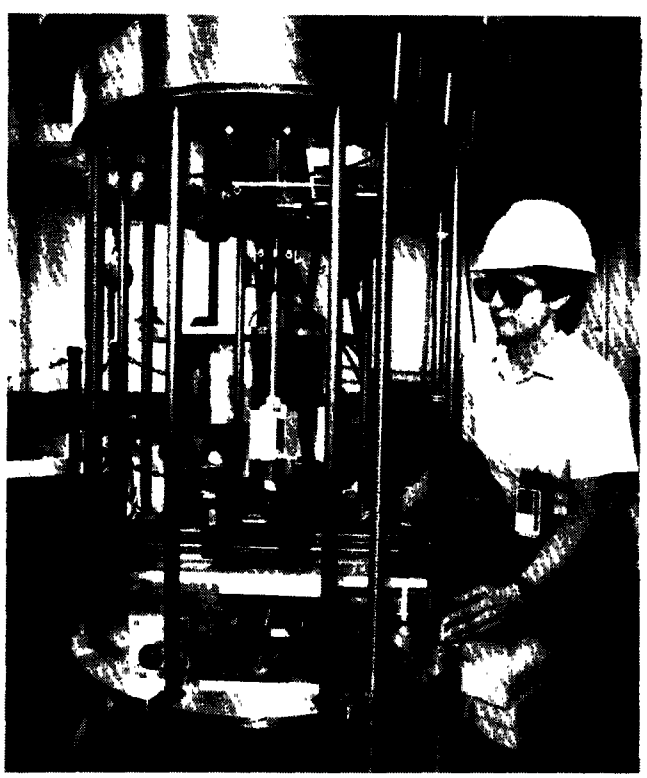

Figure 1:Joyce Goldstone with the equipment she helped design to position samples and collimate neutron beams for residual stress measurements on NPD

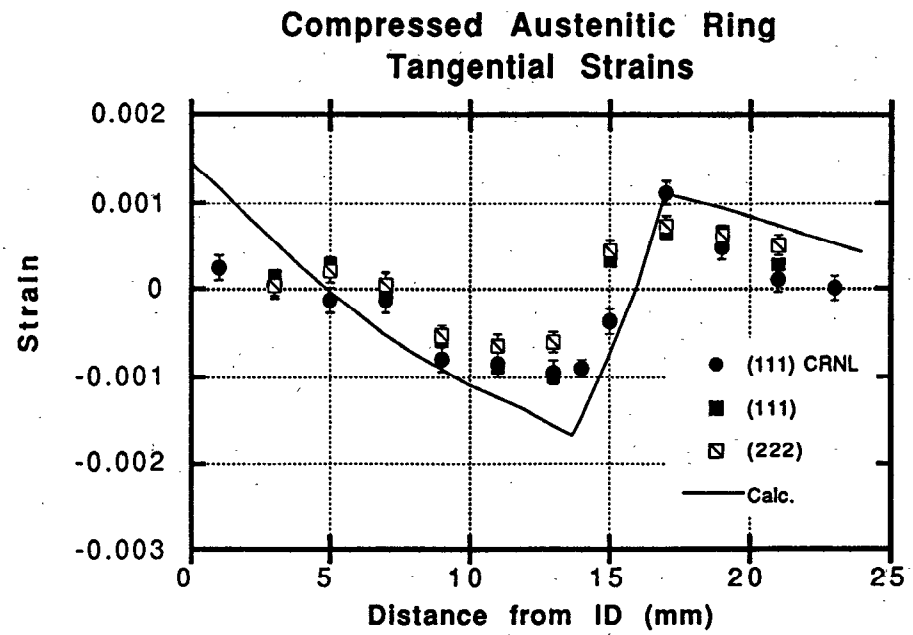

Figure 2:Tangential strain in a plastically deformed, austenitic steel ring. Measurements made at Chalk River and Los Alamos are compared with a finite-element calculation made by Elane Flower of Lawrence-Livermore Laboratory.

A system (c.f. figure 1) for positioning samples and collimating both the incident and scattered beams was installed this year on NPD to permit accurate studies of residual stress in engineering materials. To check this equipment, Joyce Goldstone and Mark Bourke, in collaboration with Tom Holden from Chalk River, remeasured the stress in a plastically deformed austenitic steel ring that had previously been examined at Chalk River [2]. Agreement between the two results was very good (c.f. figure 2). It seems that, with PSR running at 75 μA, it takes about 6 times longer to measure a single Bragg peak to a given statistical accuracy on NPD, with a resolution that is almost twice as good as that of the spectrometer used at Chalk River. Of course, the advantage of the pulsed source is that many Bragg peaks can be recorded simultaneously at two scattering angles (+90° and -90°), providing information about the anisotropy of residual stress and perhaps the density profile of stacking faults. A series of Bragg peaks would have to be recorded consecutively at a reactor to provide the same information, more than cancelling the time advantage of the reactor for measurement of a single peak. Additionally, the time-of-flight method ensures that the gauge volume within which residual stress is sampled is the same for each Bragg peak recorded. The principal disadvantage of spallation source instrumentation seems, at this stage, to be the time-consuming procedure needed for sample alignment. However, I expect this situation to improve as more experience is gained.

The LANSCE reflectometer (SPEAR) has been designed to use neutrons with wavelengths between 1 Å and 32 Å in two equal frames. This permits reflectivities to be measured for a large range of wavevector transfers perpendicular to a surface, without changing the grazing angle. Because the spectrum of incident neutrons decays rapidly at large wavelengths, the signal measured on the reflectometer only changes by a factor of a hundred or so over the 32 Å wavelength range, even though the reflectivity drops by five or six orders of magnitude. In 1990, a linear, position-sensitive detector was installed on

SPEAR. This device simplifies measurement of the scattering angle because both reflected and undeviated beams can be recorded without moving the detector. In addition, diffuse scattering can be measured, giving rise in some cases to interesting Rorschach-like patterns that we are now trying to understand. With its PSD, SPEAR is able to measure specular reflectivity at the 10^{-6} level, about an order of magnitude above the best value achievable with a well collimated and shielded single detector. It is our belief, substantiated to some extent by calculations performed by Devinder Sivia [3], that a complete reflectometry program requires both neutron and x-ray measurements. For this reason we have installed at LANSCE a conventional SCINTAG x-ray powder diffractometer that can also be used as a reflectometer. By next year, a Langmuir trough (the design of which was generously communicated to us by Jens Als Nielsen) and a single-crystal quartz cell will be available for reflection studies of liquid surfaces as well as solid-liquid interfaces.

Ancillary equipment has been added to other spectrometers. A computer controlled sample changer has replaced midnight manipulations by haggard LANSCE scientists on the Low-Q Diffractometer (LQD) and such a device will be added to NPD and SPEAR next year. A shear cell, designed by Gerry Straty of the National Institute of Standards and Technology (NIST) in Boulder, Colorado, was recently tested on the LQD. It is anticipated that both quartz and beryllium stators and rotors will be provided so that neutron and x-ray measurements can be made with the same sheared sample. As a first step towards implementing a capability for high-pressure powder diffraction, a test experiment was performed this year on the High Intensity Powder Diffractometer (HIPD) with a 49 milligram sample of $CaGeO_3$, contained in a platinum capsule and previously pressed at 65 kbar by John Parise of Stony Brook. Bob VonDreele has a poster about this work later this week.

Figure 3: The T-zero chopper used on SPEAR to eliminate the "flash" of high energy neutrons and gamma rays produced when the proton beam strikes the neutron production target. The heavy nickel-alloy rotor turns 20 times per second and is synchronised with the beam delivery system.

A great deal of progress has been made on the chopper spectrometer PHAROS, which will have an incident-energy resolution of 0.5 % as well as a Brillouin scattering capability that will eventually achieve scattering angles down to 0.65 degrees. The engineering design of the spectrometer is essentially complete and most of the 20-metre incident flight path has been installed, along with a T-zero chopper (c.f Figure 3) and much of the secondary spectrometer for Brillouin scattering. Pressure tests were successfully carried out to validate the design of the window in the tank containing the large angle detectors. The tank will allow almost uninterrupted angular coverage from -10° to +140° scattering angle with a secondary flight path of 4 metres. We are now able to phase the PHAROS monochromating chopper to an oscillator signal with an accuracy of ±20 μsec. By using the chopper to fire the PSR, each neutron pulse can be phased to the chopper with a FWHM error of ±0.25 μsec. PHAROS will rely heavily on 10-atmosphere ^{3}He, linear position-sensitive detectors that are 1 m long and 25 mm in diameter with 25 mm resolution. Since the commercially available, time-of-arrival electronics for such detectors is expensive, we have chosen to develop a charge division scheme that we believe will cost ten times less per detector. This project has proved much more difficult than we thought. The main problems have been variation of discriminator levels, temperature drift of the position calibration by as much as 10 mm, and noise in the charge division circuits. The first two problems have now been overcome but new, faster amplifiers may be needed to eliminate noise. John Sandoval, the electronics engineer in charge of the PSD's is hopeful that the detectors will be available when PHAROS is turned on next year.

The neutron guide that will provide neutrons for the back-scattering spectrometer has been ordered from Silas in France. Delivery and installation of the in-shield rotating shutter is expected in spring 1991. The guide specifications call for a 60 mm-square, 20 metre-long straight guide coated with ^{58}Ni. At the end of the guide there will be a 2-metre converging section coated with appropriate supermirror that will reduce the beam to a 30x30 mm^2 cross section at the sample. The guide will be interrupted close to the shield wall by a T-zero chopper and further out by a light, disk chopper that will define the wavelength band of neutrons transmitted. We have decided to test silicon crystals grown by the Czochralski method and annealed at high temperatures as analysers. Schneider and co-workers [4] have demonstrated that the annealing process produces domains of oxygen defects that strain the crystals and greatly enhance their reflectivity without introducing a mosaic structure. The annealed silicon crystals can be produced with a variation of d-spacing of $\Delta d/d \sim 5 \times 10^{-4}$, an ideal value for our back-scattering spectrometer. In designing the spectrometer we will make use of recent theoretical work performed at LANSCE [5] which has shown how the resolution of the primary and secondary spectrometer should be chosen to derive the greatest benefit from the asymmetry of the neutron pulses produced by a spallation source.

I am sure that Gary Russell will tell you in detail about the recent failure of our hydrogen moderator. As figure 4 shows, replacing the liquid hydrogen in this moderator by room temperature water had an enormous effect on the intensity of long wavelength neutrons used by both the LQD and by SPEAR. Nevertheless, we had no choice but to make this replacement. When the hydrogen moderator vented at the end of the first cycle this year, we found that a leak of about 0.1 mm in diameter had developed between the hydrogen transfer lines and the vacuum jacket surrounding them. Worse, there was a leak of 1.6 mm diameter into the same vacuum jacket from the crypt, which is usually maintained at a pressure of 2 torr. These leaks could have allowed small amounts of hydrogen to leak into the transfer jacket at the same time as oxygen was cryo-pumped into the same space from the crypt. Prudence dictated that we not run the hydrogen moderator under these conditions, even though the leak rates were small. Thus, for two cycles we used water and

several canisters of automobile radiator sealant instead of liquid hydrogen. Repairing the hydrogen moderator is the most important task that we will undertake during the up-coming shutdown. Unfortunately, when the present targets, moderators and reflectors were installed in 1985, the pressure of funds and deadlines did not allow sufficient thought to be given to repair operations. Accordingly we are not well equipped with remote handling tools, so the various components cannot be removed or replaced easily. The lesson to be drawn from this experience is rather obvious.

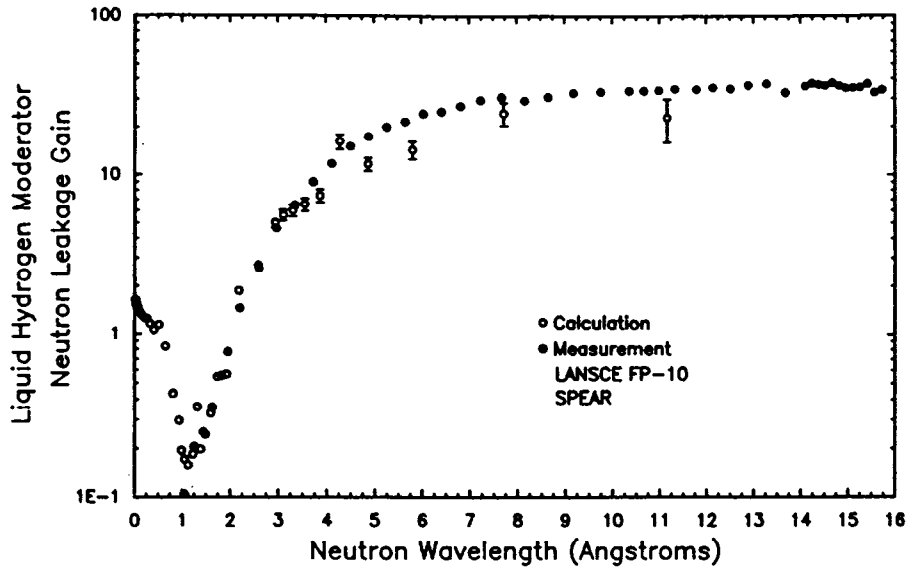

Figure 4: Comparison of the neutron spectra obtained with liquid hydrogen and water in the LANSCE "liquid hydrogen moderator". The measurements were made on SPEAR and LQD and the calculations were done by Gary Russell using the Los Alamos Monte Carlo codes.

There is a general consensus among neutron scatterers who use both spallation sources and reactors that the former provide "the big picture" while the latter are preferred for "surgical strikes". While one can debate the virtues and vices of each of these features, it is certainly true that the large dynamic range offered by most spallation source spectrometers inundates the user with more information than is easily comprehensible. The need for on-line data reduction and, above all, for display and manipulation of data in graphical form is obvious. To standardise this type of operation and to achieve a modular system capable of responding to various user needs, we have purchased a commercially available graphics and image enhancement system called PV-Wave [6]. This system uses a Pascal-like language capable of expressing sophisticated manipulations of data arrays, such as plotting, Fourier transforming, filtering and so on, in a single line of code. Commands can either be issued sequentially from a workstation or can be accumulated as a program. Windowing and menu organisation are straightforward and the system has been robust enough to convince several of our users to write their own data analysis protocols. The paper by Greg Smith and Bill Hamilton later in this conference demonstrates the way in which PV-Wave has been used on SPEAR.

I have believed for several years that neutron scatterers are lagging behind other experimental scientists in learning how to extract information from their data. For this

reason, we have been fortunate to have Devinder Sivia at LANSCE for the past two and a half years to educate us in the mysteries of the Maximum Entropy method and Bayesian logic. Several of the results he has obtained in collaboration with other LANSCE staff have been quite spectacular. His two-channel entropy method has been used successfully to separate background from sharp signals in data obtained with the constant-Q spectrometer [7]; MaxEnt is now used routinely on the Filter Difference Spectrometer (FDS) to extract information with the best possible resolution; and an application to small angle scattering data obtained with cylindrical micelles showed that the lengths of these particles was quantised [8]. Finally, application of Bayesian methods to the very difficult problem of inverting data obtained with reflectometers led Devinder to suggest a new way of performing such experiments, dubbed neutron speckle holography because of its similarity to a technique applied in astronomy [9].

LANSCE is a very different place now than it was when the last ICANS meeting was held there in 1988. At that time, LANSCE was struggling to find its place: beam current was low and unreliable, buildings were temporary and many spectrometers were not well engineered. In the two years since ICANS X, all that has changed. The main emphasis now is not on building machines but on science. I fully expect that, in the two years before the next ICANS meeting, our users will produce scientific results that justify the effort that has gone into building LANSCE.

Acknowledgements

I would like to acknowledge the LANSCE staff whose efforts have made possible the outstanding progess that has been made during the past two years. The Manuel Lujan Jr. Neutron Scattering Center is supported by the U. S. Department of Energy under contract number W-7405-ENG-36 with the University of California.

References

[1] R. Pynn, *Advanced Neutron Sources*, D.K.Hyer; ed. (Institute of Physics, Bristol, England, 1989)
[2] E. C. Flower, S. R. MacEwen and T. Holden, Proceedings of the 2nd International Conference on Advances in Numerical Methods in Engineering: Theory and Application; held in Swansea, U.K., 1987.
[3] D. S. Sivia, W. A. Hamilton, and G. S. Smith in *Neutron Scattering Data Analysis 1990*, I.O.P. Conference Series No. 107, ed: M. W. Johnson (Adam Hilger, Bristol, England)
[4] A. Magerl, J. R. Schneider, and W. Zulehner, J. Appl. Phys., 67, 533-9, (1990)
[5] D. S. Sivia, R. Silver and R. Pynn, Nucl. Instrum. and Meth., A287, 538 (1990)
[6] PV-WAVE, distributed by Precision Visuals Inc., Boulder, Colorado
[7] M. Yethiraj, R. A. Robinson, D. S. Sivia, J. W. Lynn and H. A. Mook, Phys. Rev. B (to be published)
[8] R. P. Hjelm, P. Thiyagarajan, D. S. Sivia, P. Lindner, H. Alkan, and D. Schwahn, Progess in Colloid and Surface Physics, 82 (in press)
[9] D. S. Sivia, W. A. Hamilton and G. S. Smith, Proceedings of Workshop on Methods of Analysis and Interpretation of Neutron Reflectivity Data, (to be published in Physica B, eds: G. P. Felcher and T. Russell)

Q(P.A.Egelstaff): Intensity of liq-H_2 relative to H_2O at short wavelength?

A(J.M.Carpenter): Before conclusions are drawn about relative intensities, the pulse widths must be definitively compared. Of course in principle H2O should provide shorter pulses than liq-H_2 simply because of proton density differences.

Q(N.Watanabe): I understand that time averaged proton current of 75μA was achieved at 20Hz. Do you have any program to increase the repetition rate?

A(R.Pynn): No, we believe that would be a step backwards because the performance of many instruments depends on peak neutron flux, so one does not want to increase average current by increasing repetition rate.

ICANS-XI International Collaboration on Advanced Neutron Sources
KEK, Tsukuba, October 22-26, 1990

SINQ
- Status report Oct. 1990 -

G.S. Bauer
for the SINQ project team
PAUL SCHERRER INSTITUTE
CH-5232 Villigen-PSI, Switzerland

ABSTRACT

After a lengthy period of "digging-work" which started on 8-8-88 to build the 11 m deep proton transport tunnel, most of the concrete work is now complete and the steel structure for the target and neutron guide halls has been erected. Design work on the target- and supplies system is progressing well and a basis for the safety analysis report has been established. Besides investigations towards protection against air-plane crash and earthquake this also includes research to determine the retention factor of lead-bismuth for polonium and mercury. Studies on the lead bismuth thermal hydraulics and on the D_2-cold moderator system have so far confirmed our expectations and are still in progress. Also in progress is an irradiation endurance test on the target window material at Los Alamos. In addition to intensive development work on the liquid metal target, research on a lead pebble bed target has been initiated.

I THE SOURCE CONCEPT

The final decision to add a spallation target and neutron scattering facility to the meson factory of the then Swiss Institute for Nuclear research (SIN) was made in 1987, when funding from the Swiss government was obtained.

Following this milestone, the work done in preparation of the funding request was reviewed, a formal project was established and a technical baseline was fixed.

This technical baseline took into account various boundary conditions:

- the fact that the accelerator available was a cyclotron with no macro-pulse structure on the proton beam;
- an anticipated proton current around 1.5 mA after an accelerator upgrade and a rebuild of the main meson production target;

- space limitations resulting from the fact that the proton beam line was pointing towards the steep shore of the river Aare and could only be extended by some 30 m beyond the last meson production target without violating the public requirements about distance of a building from high growing trees;
- the need of a straight-through beam line to a beam stop behind the meson production target and its associated shielding in case the spallation target was not ready for operation.

The spatial limitations can be seen from Fig. 1, which shows the PSI-West experimental complex as it is planned for future operation.

The most important feature, which is shown on Fig. 2, is the bending-down of the proton beam between the meson production target (E) and its beam dump to an inclined drift section which passes under the foundations of the Experimental Hall and the adjacent Neutron Target Hall into an 11 m deep tunnel. This tunnel will house the beam-optical devices necessary to guide the beam with very little losses and to direct it upwards again to the neutron production target.

The target concept selected for further development was close to the theoretical best, given the fact that, as a continuous source, SINQ was to ressemble very much a beamhole reactor in terms of utilization. This means that a time average thermal neutron flux as high as possible had to be achieved. The proven ways to do this are a large D_2O-moderator, high fast neutron production density and little absorption in the slowing-down regime as well as for thermal neutron.

The liquid lead bismuth target shown in Fig. 3 seemed to be almost ideal:

- the low melting point of the eutectic mixture (125 °C) allows operation at a moderate temperature level around 200 °C
- heat removal from the interaction zone by natural convection results in the highest possible material density with no cooling gaps in the reaction zone
- lead and bismuth both show good neutron yield and very little absorption
- the cylindrical geometry with a vertical axis is best for horizontal beam extraction in all directions
- the large target mass results in good high energy radiation shielding in the forward direction of the proton beam (Fig. 4) and in a low enough specific activation to make emergency removal of decay heat possible by radiation through the surface alone.

It was planned from the very beginning, to have two cold moderators at SINQ, one operating on liquid deuterium and feeding a set of neutron guides as well as a pair of beam tubes. The second cold moderator was planned to operate on liquid H_2 and to feed two pairs of beam holes. Two further pairs of beam holes were foreseen for extraction of thermal neutrons from the moderator.
For financial reasons as well as in view of the lack of experience in carrying out experiments on a non-pulsed and high power spallation source, we decided to postpone the construction of the H_2-moderator and of four of the five beamhole inserts shown on Fig. 5. In this way we expect to be able to optimize the layout on the basis of what we learn when working on the first instrument. On the other hand, four neutron guides will be available from the very beginning, with an option of a fifth one for later installation.

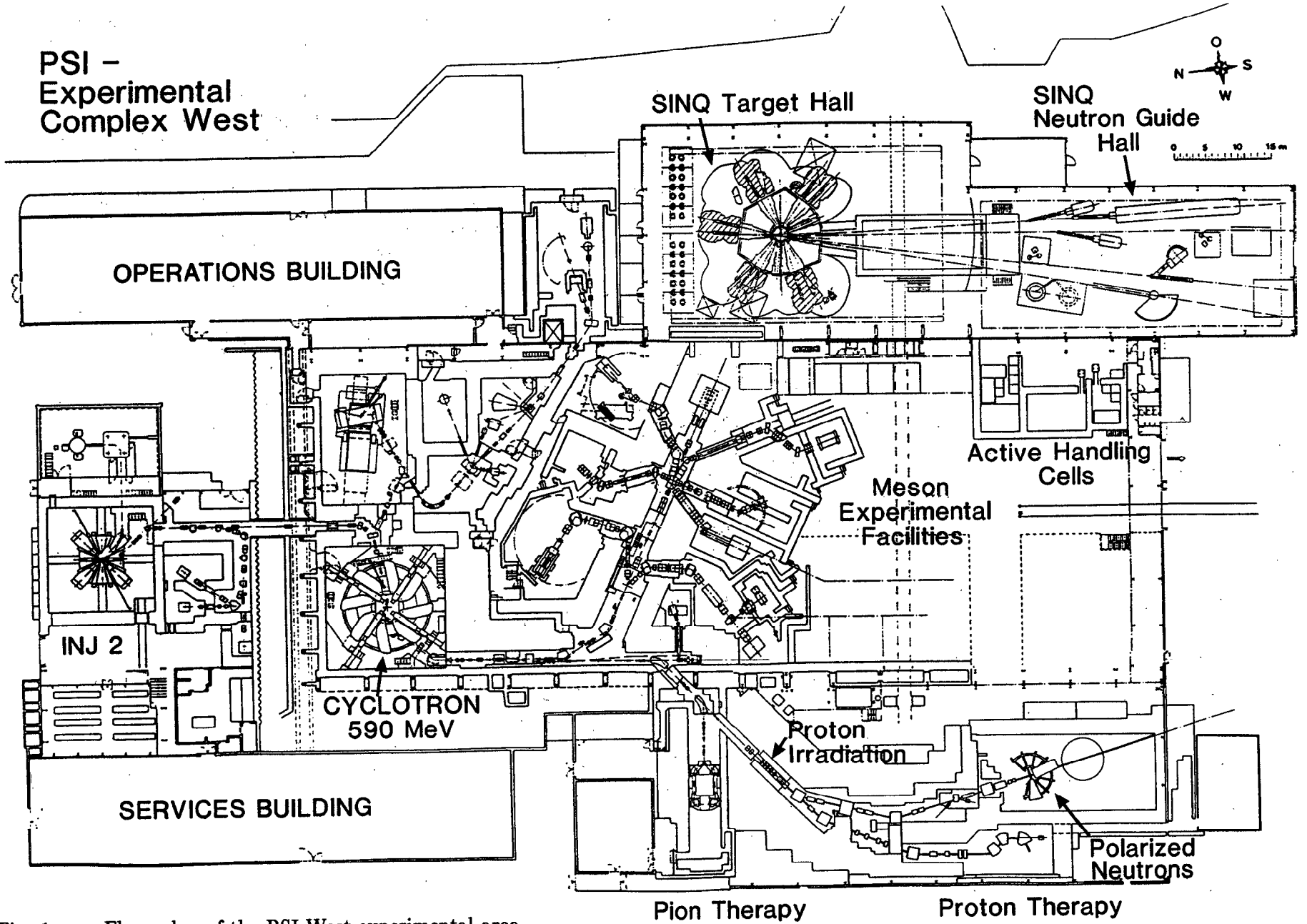

Fig. 1 Floor plan of the PSI-West experimental area as planned for operation in the mid 90's

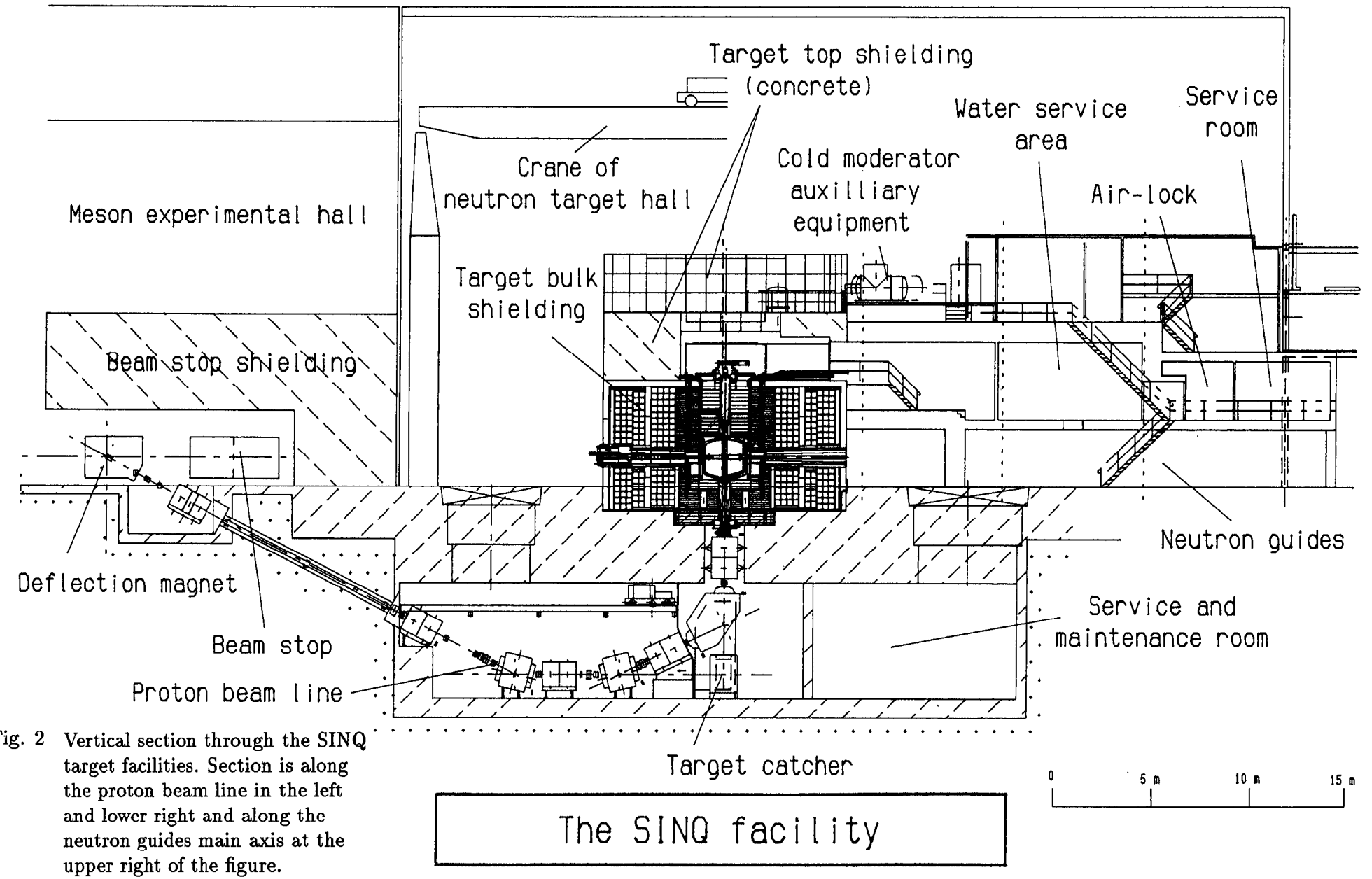

Fig. 2 Vertical section through the SINQ target facilities. Section is along the proton beam line in the left and lower right and along the neutron guides main axis at the upper right of the figure.

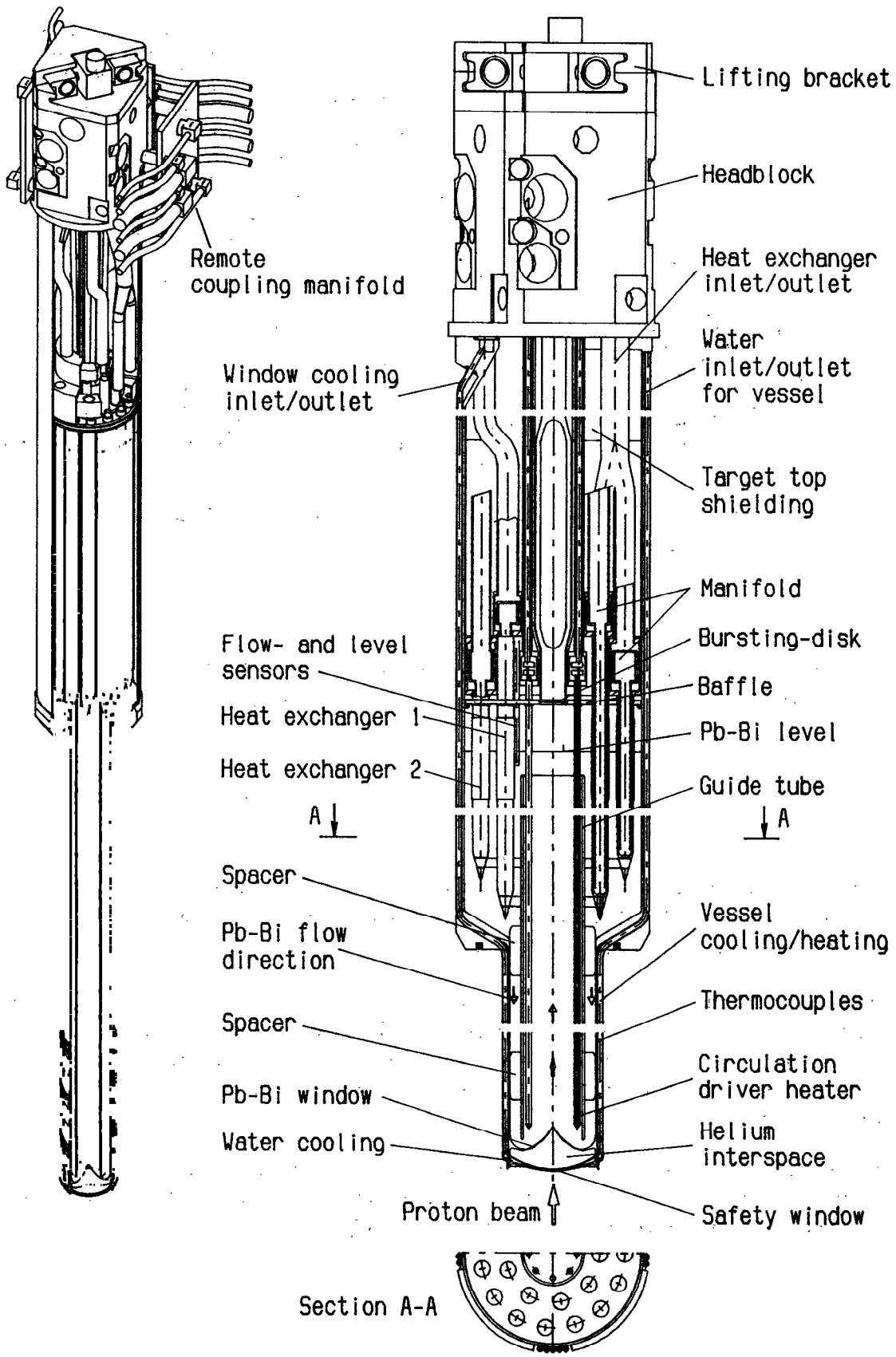

Fig. 3 Vertical section (right) and cut away view (left) of the liquid Pb-Bi target for SINQ. All connections to the target are made via four connector plates at the target head.

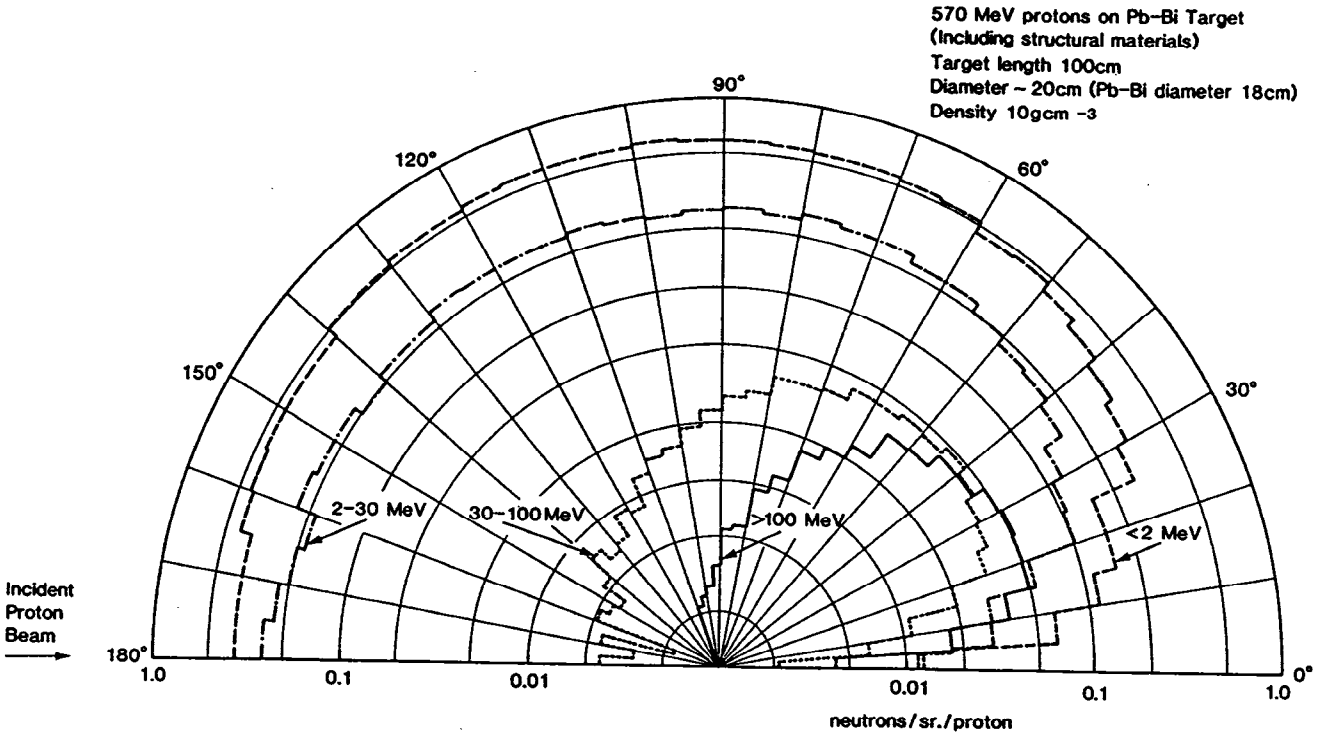

Fig. 4 Angular distribution of leakage neutrons from the liquid Pb-Bi target for SINQ. Note the self-shielding effect in forward direction for high energy neutrons.

Thus, most of the instruments scheduled for early operation on SINQ will be in the neutron guide hall. This has the additional advantage that the large access shafts to the proton channel, which are located in the neutron target hall and which will ultimately be covered with a "tanzboden" for neutron spectrometers need only be blocked after the proton beam line has been in operation for some time.

The neutron guides will have a shutter system adjacent to the main target block shielding which will be accessible by removing the heavy concrete blocks used for shielding. Following this stacked shielding there will be a cast concrete cavern extending all the way to the neutron guide hall. Above this cavern the service area will be located as shown in Fig. 6, thus forming a big service building inside the main neutron target hall.

The cold box and control system for the D_2-cold moderator will sit on top of the tunnel connecting the service building to the target block, with the D_2-ballast tank sitting on the roof of the access building for heavy equipment next to the neutron guide hall (see Fig. 1).

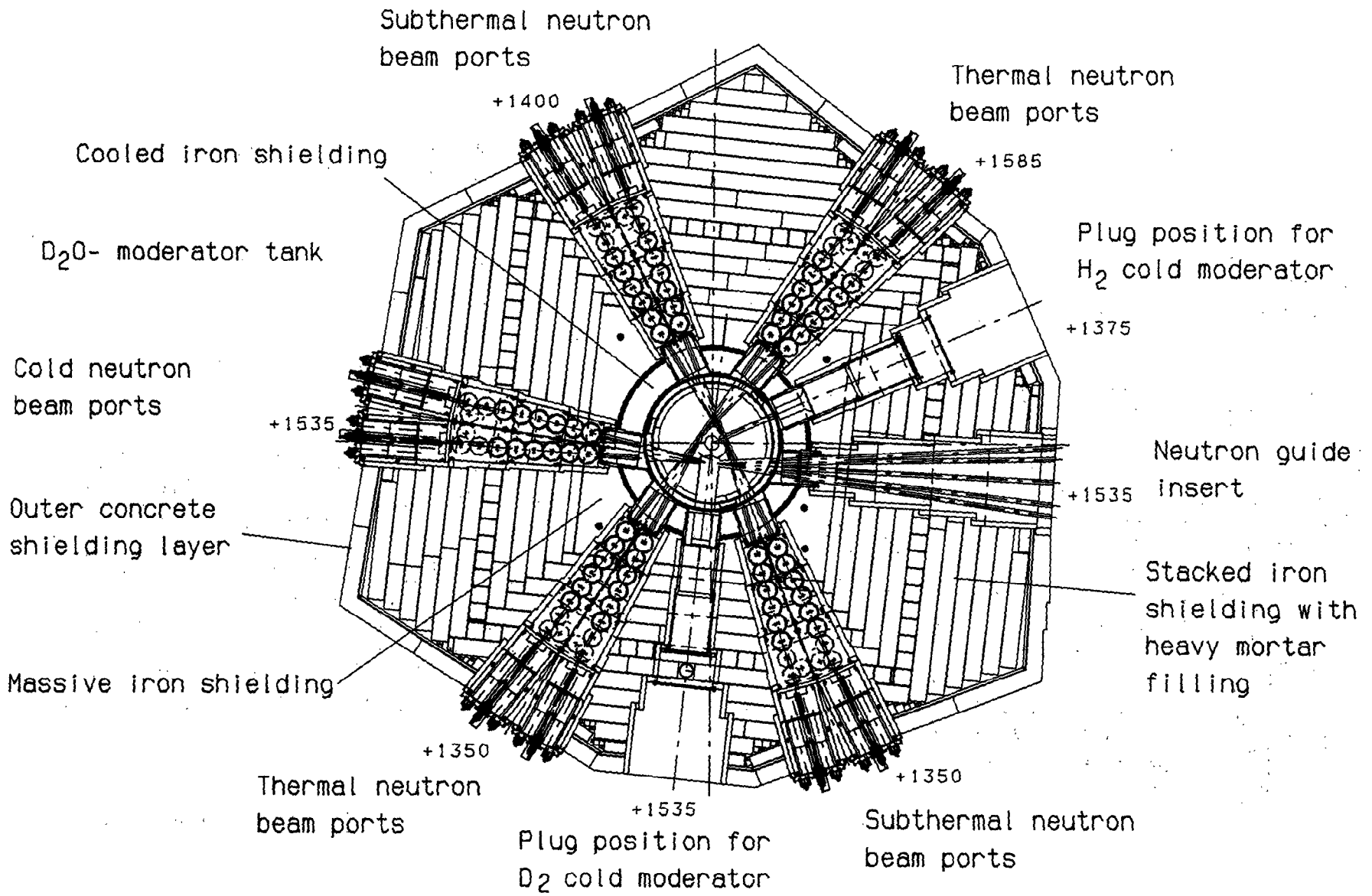

Fig. 5 Horizontal section through the SINQ target block showing the ports for beam extraction and cold moderator insertion. Beam ports viewing cold moderators are directly connected to the moderator thimbles to avoid windows and rethermalizing layers of D_2O.

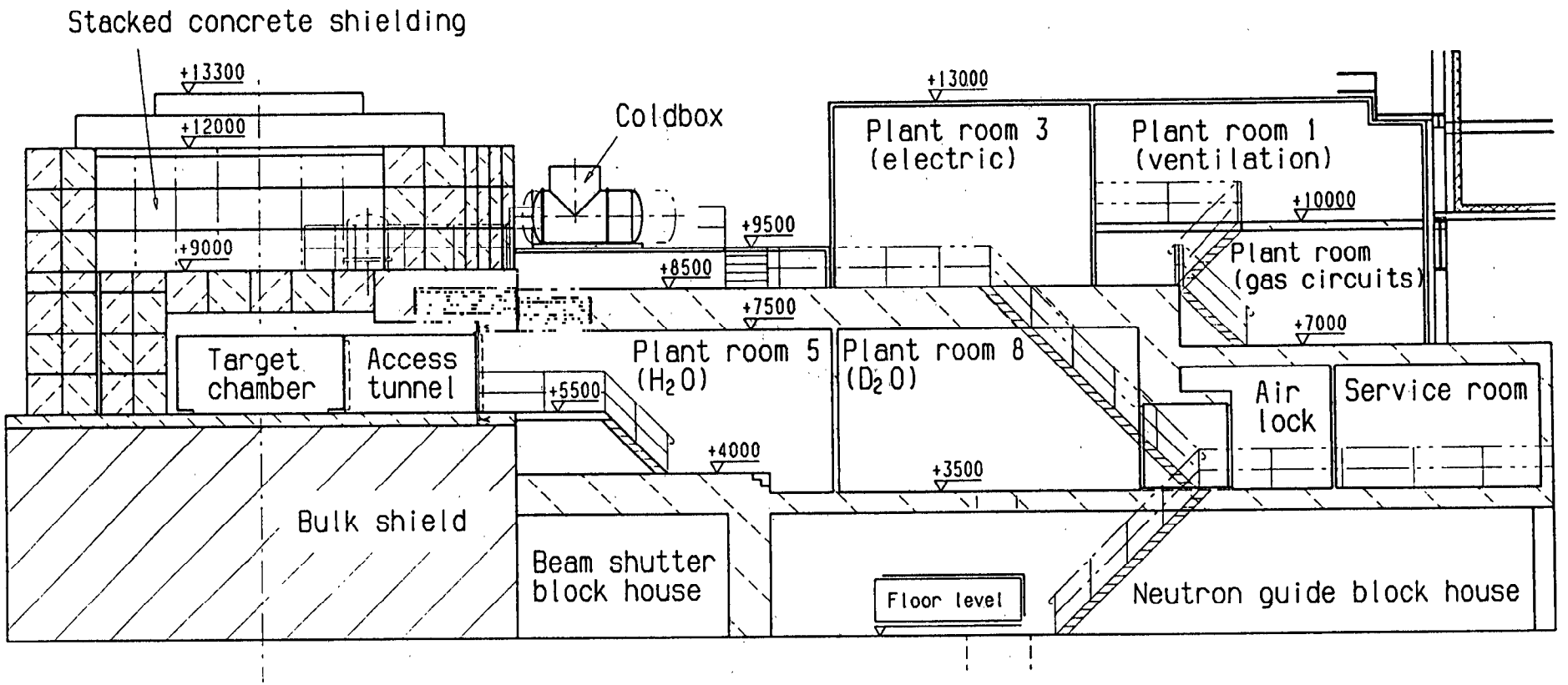

Fig. 6 Overview of the SINQ plant facilities located on top of the neutron guide block house adjacent to the target block.

II SAFETY AND LICENSING

Although not considered as a "nuclear installation" in the sense of the nuclear legislation, SINQ will require a licence from the Swiss Nuclear Safety Authorities for construction as well as for operation. This is due to the hazard potential associated with the production of polonium by neutron capture in the bismuth of the target. An estimated 9 kCi of long lived α-emitters, mainly Po, are produced during one year of target operation at 1.5 mA proton current. In an accident scenario which would destroy all protective barriers and would set free 100 % of the noble gases, 10 % of other easily volatile species including Po and Hg, 1 % of the medium volatile nuclides and 0.1 % of the less volatile spallation products it was found that 95 % of the risk potential come from the Po-isotopes. This would make emergency planning for the general public necessary. In order to avoid this, it was requested that the radioactivity in the SINQ target must remain contained in the case of

- an airplane crash with resulting kerosene fire,
- an earthquake as assumed for nuclear power stations,
- the target transport container dropping off the crane hook during target exchange.

Since the SINQ buildings will not be able to contain radioactivity over an extended period of time or withstand the crash of a (military) airplane, the safety features to meet the first two requirements will have to be built into the target shielding block and the storage holes for used targets. As a result of an analysis carried out for both kinds of events it was found that the impact of a military airplane was the more serious one. The following main measures were requested:

- the heads of the used targets in storage must be secured by 20 cm thick steel housings bolted to the concrete structure in addition to the 80 cm thick concrete covers
- the target block must have a 5 cm thick outer steel liner capable of withstanding a torque of 20 MNm and an average azimuthal stress of 70 N/mm^2 with only moderate plastic deformation
- unused beam ports must be secured by reinforced concrete or steel beams positioned in such a way that the impact force is transferred to the shielding block and not to the beam hole plug.
- the stack of iron bars inside the main target shield has to be arranged such that the impact force is distributed over the full height of the stack to avoid "spallation" of the whole shield under an impact.

These requirements will be met by the present design of the target block and target storage area.

The question, how release of radioactivity can be safely prevented in the event of a catastrophic crane failure during target transport is still under examination. Generally the risk of activity release is very small, since the radioactive nuclides will be contained by three barriers:

- the transport cask will be tightly sealed to form the outermost containment;
- the second containment is formed by the target vessel;

– thirdly, the target will be in a solid state when transported.

In order to make sure that the solid state of the target can in fact be counted as a containment of the radioactive nuclides present during transport, it is foreseen to vent and evacuate the space above the target while the target material is still liquid and thus remove practically all volatile substances from the target before transport. If necessary, the space can afterwards be filled with lead before the target is removed from its operating position. Our preliminary investigations indicate that, once the target is in a solid state and cooled down to some 50 °C for a few days, decay heat can be removed through the target surface by a contact gas. It remains to be studied, whether the shielding of the transport cask in the absence of active cooling would warm up sufficiently high to bring the target temperature back up to the melting point. At present it is our feeling, that this is rather unlikely. Detailed studies will be started soon.

Unfortunately we have some uncertainty on the radiation load in our anticipated mode of operation since we rely on the beam scattering and energy loss when the protons traverse the meson production target. It is, however, possible and even likely that a certain fraction of the beam will go past this target unscattered. This fraction may be as high as 30 % under certain operating conditions.

Partly for this reason we have not been able to quantify with a good level of confidence the life expectancy of the beam entry window at the bottom of the target. Test windows under irradiation at the LAMPF accelerator have so far stood up to 80 mAh/cm^2, which corresponds to 1200 hours of operation at 1 mA beam in our 30 % bypass situation. We hope to continue these tests.

Since the fraction of unscattered beam is very hard to monitor, we have adopted a window design in which we count on being able to detect a failure before any severe consequences develop. The idea is to have three windows at different operating conditions (pressure difference, temperature, stress situation) and to monitor the spaces between them. The first window, as can be seen in Fig. 3, is the cusp-shaped operating window cooled by the liquid lead bismuth itself and hence operating at the highest temperature. Underneath this window there will be two dome-shaped safety windows with cooling water flowing between them and with gas circulation between the operating window and the upper safety window. By suitable choice of the gas and water pressure, we can establish different load and stress situations on the three windows. If a pressure change or contamination is detected in either the gas or the water, interruption of the proton beam and closure of two safety valves in the beam line will be triggered.

These problems will be dealt with in substantial detail in the safety analysis report which we have to prepare to apply for permission from our licensing authorities for construction and operation of the source. We hope to obtain this permission by late 1991 or early 1992. It is only then that we can start building the target block and its auxiliary systems.

III SITE CONSTRUCTION AND RELATED WORK

Due to the fact that no containment functions are necessary for the neutron target and neutron guide halls, we were able to start their construction on 8-8-88. Excavations for a waste-water storage tank cavern and the 12 m deep hole of the beam transport tunnel progressed well and during the year of 1989 thousands of tons of concrete were brought to the site to form the plinth and heavy load floor (60 t/m^2) requested for the target block and target hall.

The steel structure of the neutron target and guide halls went up this summer and the halls will have walls and roofs before winter starts.

In parallel with setting up the steel structure, an 80 cm diameter inclined hole lined with concrete pipes was bored from the proton tunnel under the foundations of the existing experiment hall. It ends in a pit which had been opened in the 50 cm thick and heavily reinforced floor by cutting and lifting out a suitably large section of the concrete floor.

Although not strictly part of the SINQ project but carried out as projects of their own, it is important to note that the rebuilding of the thick meson production target and the upgrade of the cyclotron to 1.5 mA proton current are progressing well. This work was started on Jan. 3, 1990. By now, all shielding of the relevant section of the proton beam line has been dismantled. The old beam catcher and the old meson production target had to be removed with extreme precautions due to their high level of radioactivity. The new target station has been assembled and will be put in place soon. The same is true for the new beam catcher, which is ready for installation and which will be mounted as soon as the temporary concrete block house, which was set up for the construction of the inclined drift tunnel in the experimental hall, has been removed. We count on having beam again by the middle of 1991, quite a while before SINQ will be ready to accept it. This will allow the accelerator crew to do their start-up work and beam line tuning without the extra complication of the SINQ beam line section. It is planned to work up to 650 μA rather quickly after the end of the shut down period and then gradually increase the beam current by adding more rf-power to the accelerator in steps over another year or more.

IV ONGOING DEVELOPMENT AND DESIGN WORK

Although we do not anticipate to start procurement of the target station and its auxiliaries before the end of 1991, there are intense planning, design and development activities going on. In the following, only part of this work can be highlighted.

IV.1 Liquid Metal Target Development

Research and development work for the liquid metal target and its containment including the beam entry window is a major topic of research.

In this context it is important to be certain about the degree of retention of polonium and mercury in the lead-bismuth mixture. Literature data are very scarce and not convincingly consistent. For this reason we have started our own experimental investigation where we measure the amount of polonium and mercury coming off the surface of small reactor-irradiated Pb-Bi samples.

- Further experimental work in progress includes fluid dynamics investigations in a scaled-down mockup including ultrasonic velocity measurements and flow visualization by different means /1/
- theoretical thermal-hydraulics studies of the flow distribution and heat transfer problems including a suitable benchmark experiment /2/
- liquid metal corrosion tests of various materials
- measurements of the post-solidification expansion of the lead-bismuth to determine stresses in the target vessel in the event of a target solidification /3/
- flow optimization of the cooling water in the target safety window /3/
- irradiation tests of a safety window at LAMPF /3/
- detailed stress analysis for shape optimization of the target window (operating window plus safety windows) /4/

IV.2 Alternative Target Studies

Although an optimized Pb-Bi liquid metal target would be the best possible solution for SINQ from a neutronics point of view /5/, practical considerations such as the polonium problem on the one hand and materials and beam size restrictions on the other have prompted us to look into alternative solutions using solid target materials. A series of theoretical calculations on the expected neutronic performance showed that, when comparing "realistic" design of the Pb-Bi liquid metal target, to directly D_2O-cooled plate targets of Ta or W and a pebble bed target of lead shot, the unperturbed maximum thermal flux ratios at 25 cm from the centre line are /5/:

Pb-Bi : W : Ta : Pb Shot = 1 : 0.7 : 0.53 : 1.17

The reference value of 1 for the Pb-Bi is not the theoretical optimum but what one could expect to achieve under the existing boundary conditions. The relatively poor performance of Ta and W in our case is due to absorption of thermal as well as epithermal neutrons in these materials.

In view of the relatively good performance expectancy of the Pb-shot target, this alternative is now being studied in more detail /6/. One consequence of a transition to a D_2O-cooled target would be that a much more complicated D_2O-circuit with purification and recombination facilities would have to be provided at probably higher costs than for the H_2O-cooling circuit which does not intercept the beam. Also, the high local activation and after heat density of a stationary target is of some concern especially during the target exchange process. Nevertheless, a successful development of a solid target would be of substantial practical advantage. It will be actively pursued in particular for a day-one option. In this way the concept of the double safety window can be practice-tested without the risk potential of the liquid lead bismuth.

IV.3 Target Block And Moderator Tank

Detailed layout of the relatively complicated moderator tank with its double wall and its T-shaped penetrations for the beam tubes and cold moderators (Fig. 5) is in progress with stress analysis for temperature and mechanical load effects. One consequence of this analysis is that the target will now not be suspended from the moderator tank as originally planned but from the shielding block itself.

The outer part of the target shielding block will be built of existing iron rods, 30 x 30 cm^2 in cross section. Due to the relatively complicated shape of the shielding block many rods will have to be cut to size. A suitable machine has been purchased and a computer code is being developed now to minimize the number of cuts and to optimize the useage of the existing material. Tests are under way to develop a method to fill the gaps between the rods with heavy mortar. Generally the rods will be put down horizontally but as a result of the plane-crash analysis mentioned earlier there will be one "wall" of standing rods for load distribution. The rods will be contained in a 5 cm thick steel liner which will have 30 cm of boron loaded concrete to reduce the dose from the keV neutrons.

For the inner part of the shielding inside the N_2- and He-containments the possibility is under investigation of using slightly activated reprocessed scrap steel from dismantled nuclear installations.

IV.4 Cold D_2-Moderator And Neutron Guides

Design work on the cold D_2-moderator, which will be an important feature of SINQ from the first day on is well advanced /7/. The concept is based on isothermal natural circulation of a liquid-gas mixture from the moderator vessel to the heat exchanger and of liquid in the other direction through concentric tubes. The thermodynamic properties of the system are now quite well understood and calculations pertaining to accident situations such as loss of insulating vacuum have shown that no

damage will result from such situations /8/.

Four neutron guides will view the cold moderator. The guides will start at 1.5 m from the moderator surface requiring a target block insert which allows precise alignment on the one hand and minimizes parasitic radiation on the other. A system of two shutters rotating about a horizontal axis perpendicular to the guides will be installed at the outside of the target block behind heavy shielding. When open, the shutters will bridge the gaps between the inner and outer guides by neutron reflecting channels which, again, require precise alignment and a high degree of reproducibility /9/.

For the coating of the neutron guides we hope to use high performance multilayer mirrors. Development work in this direction is in progress /10/.

IV.5 Beam Port Inserts

The standard beam extraction ports in the target block will be twin ports with a separation angle of 10° between the two beam axes (Fig. 5). In view of the long distance from the target to the outside of the shielding block, an attempt was made to incorporate as many of the functions necessary for beam tube operation into the beam port inserts. These include:

- beam shutters
- filters
- exchangeable collimators

A design has been worked out which, as shown in Fig. 7, allows the port inserts to be installed for each extraction channel separately and which subdivides the whole insert into different functional units which can be handled independently. The units are: an inner shielding block, three shutter blocks, a shutter drive base and a user specific filter and collimator insert. The exploded view in Fig. 7 shows, how these parts can be mounted as separate units.

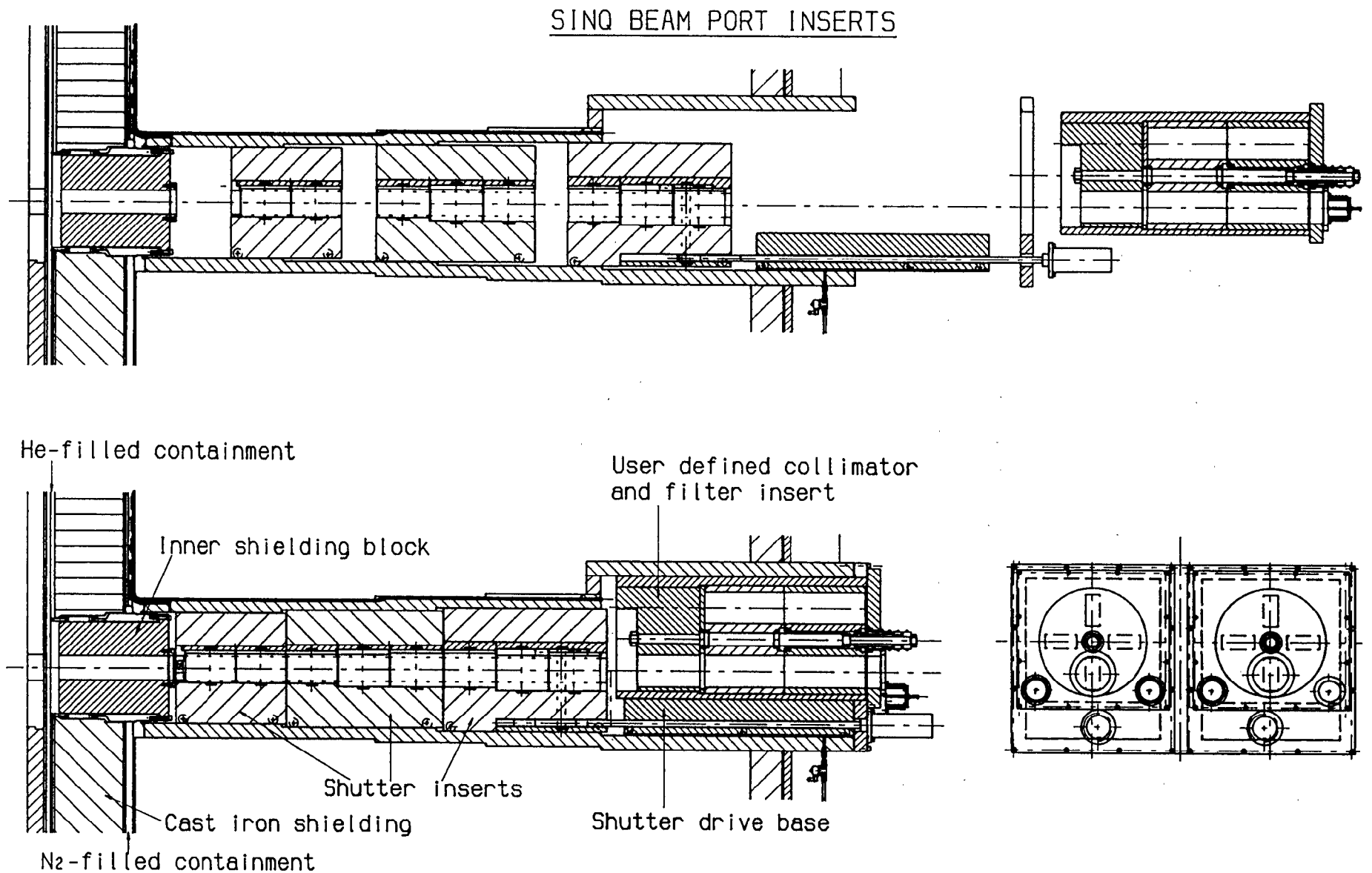

Fig. 7 Vertical section through a SINQ beam port insert. The exploded view at the top shows the units which can be removed separately. A front view of the twin channel is shown at the lower right.

V INSTRUMENT PLANNING

Based on the reference value of 1 mA beam on target and the lead-bismuth target as presently under development, we expect the neutronic performance of SINQ to be as given in Fig. 8. This shows that, in terms of time average thermal and cold neutron flux, SINQ will compare favourably with most of the medium flux reactors, such as the various DIDO-variants, that have been successfully used for neutron scattering work throughout the world during the past 3 decades.

A certain disadvantage may result from the high energy neutrons which are produced in the spallation process. Great care has been taken in the design of the bulk shield to keep them from reaching the surface of the target block. The resulting distance from the thermal flux maximum to the shield surface is 6 m. As mentioned before, part of this distance will be used to house beam shutters as well as interchangeable filter and collimator inserts.

While the shutters will be standard, filters and collimators are instrument specific and will be devised in conjunction with the respective instrument design. Controlling the high energy background contribution from the beam holes will not be an easy task. This is the main reason, why only one pair of beam holes is planned to be equipped for day one operation. The instruments selected are a high resolution powder diffractometer and a four circle diffractometer. They will use a common monochromator shielding block as shown in Fig. 9.

In this block two different concepts for variable incident energy are combined: While the HRPD will have a monochromator that can be moved to different positions to deflect neutrons of different energies to the fixed position of the instrument, the 4-circle diffractometer will be rotated around the monochromator axis as the incident energy is varied. These two concepts have been selected also in view of the need to gain experience working on a continuous spallation neutron source before further instruments are designed.

In terms of cold neutron flux, we expect SINQ to rank among the best in the world. This is due to the optimized flux position of the cold moderator and the care that was taken to minimize rethermalization of the cold neutrons by warm Al-windows or D_2O-layers /11/. It is therefore justified to put most of the emphasis in the instrumentation for day one on the cold neutron side.

The following instruments to be built on the neutron guides have been given first priority:

- Low energy transfer triple axis spectrometer
- Very high resolution time-of-flight spectrometer
- Small angle neutron scattering facility
- Polarized neutrons triple axis spectrometer
- Neutron-optical bench for ultra high precision measurements
- Diffuse-elastic neutron scattering spectrometer

The last two instruments are included on specific user's request and will be mainly under users' responsibility. Table 1 gives a summary of the main characteristics of the instruments planned for SINQ. The floor plan of the facility is shown in Fig. 10.

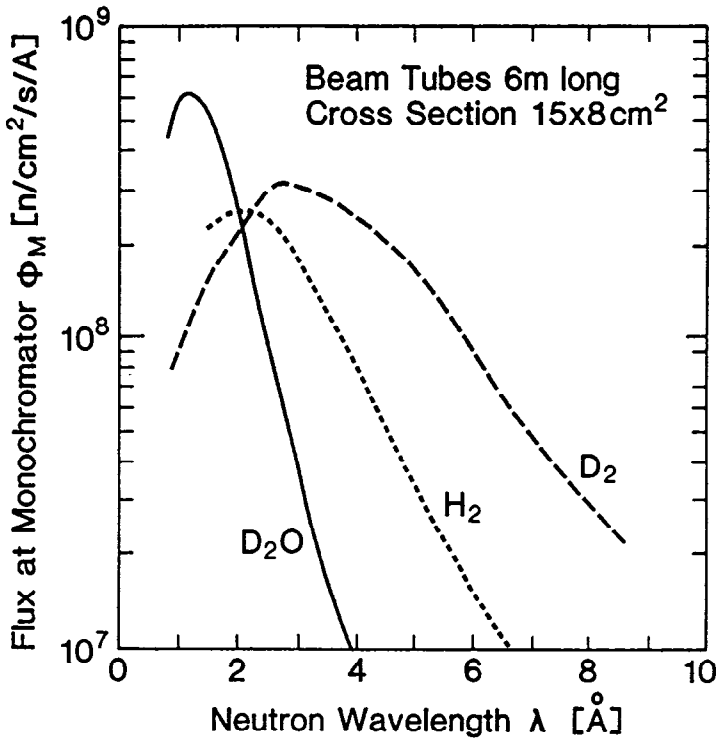

Fig. 8 Expected spectral flux distribution at 6 m from the various SINQ moderators at 1 mA proton current on target. For the D_2 moderator no effect of neutron guides has been taken into account.

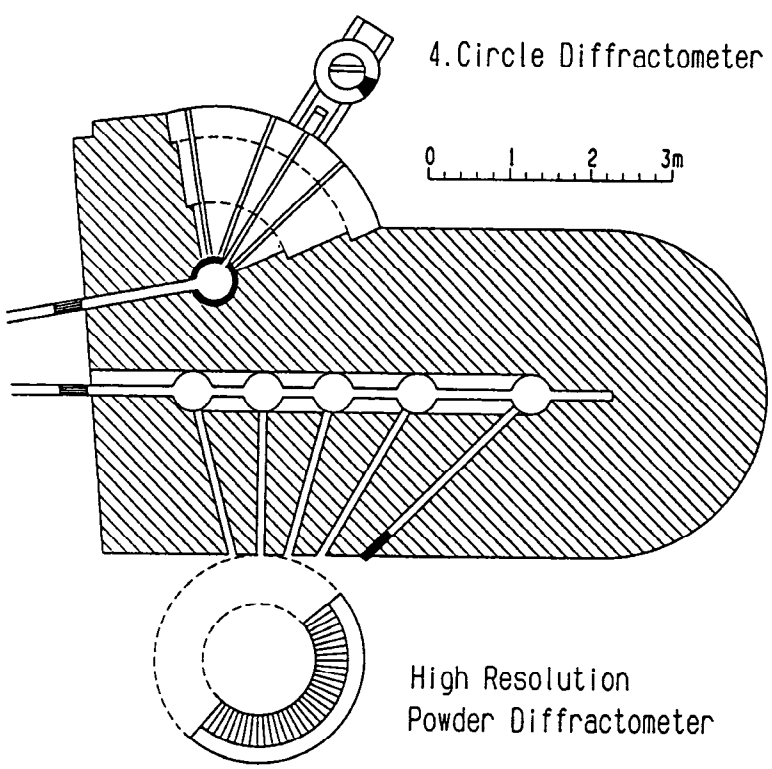

Fig. 9 Example of monochromator shielding for SINQ. Shown is the shielding block as planned for the two day one thermal neutron instruments, the HRPD and a four circle diffractometer.

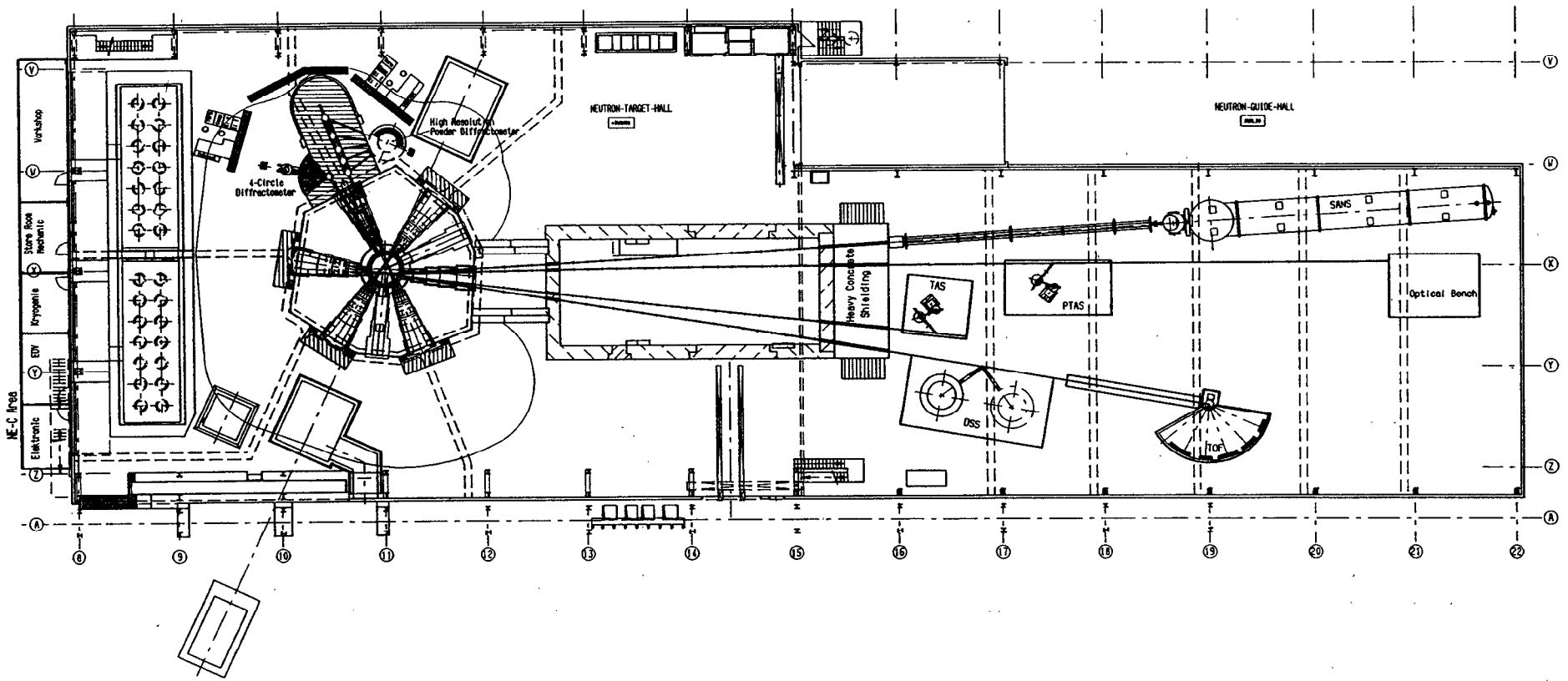

Fig. 10 Floor plan of the SINQ target and neutron guide halls showing instruments planned for early operation.

Instrument	High resolution powder diffractometer	Four circle diffractometer	High resolation triple axis	Polarized neutrons triple axis	High resoluting Time-of-flight spectrometer	Small angle scattering instrument
location	thermal neutron beam port	thermal neutron beam port	cold neutron guide	cold neutron guide	cold neutron guide	cold neutron guide
monochromator	Ge (hkl)	PG (002), Cu (220)	PG (002), Be (002)	Heusler (111) PG (002)	chopper 3-12 Å	mech. velocity selector
$2\,\theta_{mon}$	75 - 135 deg	15 - 90 deg	30 - 145 deg	30 - 145 deg	–	–
detectors	64 He-3 or linear scintillation	2 dim, He-3 210 x 185 mm^2	He-3	He-3	He-3 detector array	2 dim, 128 x 128 cells 960 x 960 mm^2
resolution/range	$\Delta d/d = 4 \cdot 10^{-4}$		$\geq 7\ \mu eV$	$\geq 7\ \mu eV$	$0.005 \div 0.5$ meV	$3 \cdot 10^{-3}\ nm^{-1} \leq Q \leq 10\ nm^{-1}$
special features/ remarks	option: position - sensitive detector; vertically focussing monochromator; GdO-mylar sollers in front of detectors	dilution cryostat; closed cycle cryostat;			counter-rotating disc choppers $100 \div 400$ Hz; detector angular range 10 - 135 °; converging super mirror	polarization (option) specimen changer cryostat; furnarce; electromagnet;

Table 1 First generation instruments planned for SINQ under PSI-responisibility

VI CONCLUSIONS AND SUMMARY

As a continuous high power spallation neutron source, SINQ will be the first of its kind. It is expected to come on line at a time when operational research reactors in Western Europe continue to decrease in number due to the fact that most of them have been build some 30 years ago. It will not only be a test facility for a new source concept but will also help to fill a gap which would otherwise be wide open. There may be a question as to what extent neutrons will be needed in the future to solve specific scientific problems, but there is no question that they will be necessary.

The rate of progress in the construction of the buildings for SINQ since it was started in August 1988 has been impressive, considering the huge amount of concrete work that was necessary. Its future progress will depend on the licensing procedure that lies ahead of us, but we are confident that construction of the "systems" part can start in early 1992. In this case we expect to produce useful neutrons in 1995. Together with the rebuild of the proton beam line and the upgrade of the cyclotron to deliver 1.5 mA this is a major undertaking for the Paul Scherrer Institute and will not only require a substantial effort from our own project team but also active support from outside, in particular from potential future users.

REFERENCES

/1/ Y. Takeda and W. Fischer
"Thermofluid dynamics of liquid metal target of SINQ"
This conference

/2/ B. Sigg, T. Dury, M. Hudina, B. Smith
"Thermal-hydraulics investigation for the liquid lead-bismuth target of the SINQ spallation source"
This conference

/3/ M. Dubs and J. Ulrich
"Design considerations of the target window"
This conference

/4/ G. Heidenreich
"Preliminary thermal and stress analysis of the SINQ window"
This conference

/5/ F. Atchison
"The neutronic performance of solid-target alternatives for SINQ"
This conference

/6/ F. Atchison and G. Heidenreich
"A solid target for SINQ based on a Pb-shot pebble-bed"
This conference

/7/ H. Spitzer, A. Höchli, G.S. Bauer, W. Wagner
"Technical concept of the liquid D_2-cold moderator for SINQ"
This conference

/8/ K. Skala, H. Spitzer, G.S. Bauer
"Theoretical thermal-hydraulic investigations of the operational and safety features of the cold D_2-moderator for SINQ"
This conference

/9/ I. Anderson, J. Ehrat, D. Suhi, W. Wagner
"Shutter system for the SINQ neutron guides"
This conference

/10/ P. Böni, I. Anderson, P. Mathieu, P. Ruterana, B. Farnoux, J. Penrose, G.J. Herdman
"Investigation and growth of multilayers"
This conference

/11/ G. Bauer
"Some Remarks on Design Criteria and Optimization Concerns for Cold Neutron Sources"
Int. Workshop on Cold Neutron Sources, March 5 - 8, 1990 Los Alamos USA

ICANS-XI International Collaboration on Advanced Neutron Sources
KEK, Tsukuba, October 22-26, 1990

Status of KENS-I' and KENS-II

N. WATANABE
National Laboratory for High Energy Physics
1-1 Oho, Tsukuba-shi, Ibaraki 305 Japan

ABSTRACT
Present status of the KENS facility (KENS-I') is reported here especially on the recent progress in instrumentation. Design concept of the KENS-II target station is briefly described with the results of recent R&D

I. KENS-I'

The present KENS Facility, KENS-I', has been successfully operated since the last ICANS meeting. The operation time of the 500 MeV Booster synchrotron in the past year was about 3500 hours, and the beam time allocated for neutron experiments was about 1500 hours. The average proton-beam intensity was 1.5×10^{12} protons per pulse (ppp) or less, which was lower than the maximum value of 2×10^{12} ppp achieved in 1988. This is due to various reasons including radiation safety problems. Since about 20% of proton-beam pulses were injected to the 12 GeV synchrotron, the average proton-beam current on the neutron target was about 4 μA. Thus, the integrated beam intensity over the past year was about 6000 μA or less which corresponds only to 3 days operation of ISIS. Nevertheless, we could perform various important experiments. We expect that the proton-beam intensity will reach 2×10^{12} ppp during routine operation. The beam transport line in the Booster Synchrotron Utilization Facility (BSF) has been improved to accept such intensity with tolerable beam loss.

The depleted uranium target has been operated trouble-free since the beginning of its operation in 1985. We experienced no serious problems with the cryogenic moderator (solid methane at 20 K) since the last ICANS meeting, because solid methane is renewed every two days before a "burp" can occur. A cold helium circulator had a problem and was repaired last year. The present cryostat which has been used for two years is still working.

During the last financial year, 76 experiments including 12 large proposals by groups responsible for the instruments were carried out. Scientists who visited the KENS facility spent about 4000 man-days. There are currently 16 instruments in the KENS facility as shown in Fig. 1. There was appreciable progress in the instrumentation since the last ICANS meeting. The construction of a new small/medium angle scattering instrument, WINK, started in 1989 and will be completed in 1991. The instrument was designed to realize a wider coverage in momentum transfer from 0.01 to 20 A^{-1} with much higher data rate, hopefully more than 10 times as high as that of the existing small angle instrument, SAN. Figure 2 shows the layout of WINK which will be equipped with more than 250 conventional He^{-3} proportional counters at a wider range of scattering angles from forward to backward. WINK was installed at the C4 beam line, sharing the beam with two existing instruments, LAM-40 (convential-resolution low-energy spectrometer) and HRP (high-resolution powder diffractometer) on the same neutron beam line as shown in Fig. 1. We were faced with various difficulties in sharing the same neutron beam by three different instruments, but now those are almost solved. Due to the relatively shorter flight path lengths for incident and scattered neutrons (9 m and 2.5 m, respectively), and to a lower repetition rate of the Booster synchrotron (20 Hz), the useful bandwidth of the incoming neutrons is quite wide, from 0.5 to 16 A, which enables the wider Q coverage mentioned above. In the last cycle, a preliminary measurement was performed on WINK with only one detector at each of 5 different angles. Figure 3 shows the result obtained with a measuring time of 2 hours. The result proved that the coverage in Q and the data rate are quite satisfactory as expected. After the full installation of detectors, measuring time of a few minutes would be adequate for a typical sample. The momentum resolution of WINK however is relaxed a bit at the lower Q range than that of SAN, because WINK employs natural beam collimation between source and sample, and the scattered neutron flight path length is limited to 2.5 m due to limited space. Details on this instrument and its performance will be presented by Furusaka[1)] at the Instrumentation Workshop "Total Performance".

There was remarkable progress on the high-resolution low-energy spectrometer, LAM-80. The LAM-type spectrometers[2)] are the inverted geometry instruments, developed by a famous Japanese neutron "Artist" Prof. Inoue, which have large analyzer mirrors composed of a large number of small analyzer crystals. LAM-80 has been improved twice. Firstly, all analyzer crystals of pyrolytic graphite were replaced by mica. This provided much better energy-resolution but with lower data rate (about one third). Then, the height of mirror was increased to realize a larger solid angle between sample and analyzer, and the number of mirrors was also increased from four to eight. As a consequence of these improvements, higher resolution with higher data rate were realized. The spectrometer is now called LAM-80ET. In order to confirm the performance of this machine, we

performed a measurement on reorientational tunneling. As a standard sample, N-oxy-γ-picoline was measured at 5 K. Figure 4[3] shows the result which demonstrates the superiority of LAM-80ET. In the present experiment, the 004 reflection of mica crystal was used to define the final energy (E_f) of the scattering process (E_f~0.82 meV). The energy-resolution is about 5 μeV with a very wide energy window of more than 1 meV. Signal-to-background ratio is excellent. Note that the measuring time was only 8 hours with a proton-beam current of only 3 μA. We are convinced that LAM-80ET is one of the best spectrometer in the world in this energy range; it is well competitive with IRIS at ISIS operated at 100 μA and IN5 in ILL Grenoble.

The total scattering spectrometer for S(Q) measurements of liquids and glasses, HIT, has been one of the most productive instrument since the beginning of the KENS facility, but now it is the oldest instrument. It has been strongly requested to update this instrument. The construction of a new instrument, which is called HIT-II, was thus decided. HIT-II was designed to have much better momentum-resolution at smaller scattering angles with higher data rate, as in GLAD at IPNS and SANDALS at ISIS. The scattered flight path length, L_2, is shorter than in the latter two due to limited space in the experimental hall, consequently resulting in relaxed resolution. HIT-II will have a ring detector bank at forward angles between 10° and 20° in 2θ, which is composed of 72 normal He-3 proportional counters, and arrays with 80 counters at higher scattering angles. L_2 of the forward ring detector bank is about 1.2 m. The momentum resolution ($\Delta Q/Q$) of this detector is about 2.5%. HIT-II will be completed by the summer of 1992.

The high resolution powder diffractometer, HRP, is also one of the most productive and busiest instrument at KENS, although it is a prototype instrument equipped with only 12 normal He-3 proportional counters. The construction of a full-scale instrument is now indispensable. We decided to construct a new instrument, HRP-II, which is designed to realize much higher data rate with better resolution. The instrument will have large counter banks, at backward, 90° and lower angles, all being composed of 1D-PSD's as GLAD at IPNS. The data rate of the backward counter bank is expected to be about 5 times higher than that of the present instrument, with better resolution of about 0.2% in $\Delta d/d$ which shall be compared to 0.3% in the present instrument. The 90° counter bank will be composed of three arrays of 1D-PSD's at three different azimuthal angles in order to cover a wider range of azimuthal angle. This counter bank will be useful not only for industrial applications such as texture measurements and strain measurements, but also for diffraction under high pressure, etc. The maximum d-spacing covered by the backward counter is 5A with a total flight path length of 20 m and repetition rate of 20 Hz. The forward counter

bank at $2\theta=17°\sim40°$ can extend the d-spacing up to 30 A. HRP-II will be completed by the summer of 1993.

A reflectometer is one of the most useful instrument at pulsed spallation neutron facilities. As an option of TOP, the polarized cold neutron instrument at KENS, the development of a reflectometer using polarized cold neutrons is in progress. By using the second frame of the KENS period of 50 ms, a wavelength scan up tp 18 A becomes possible. Preliminary, but very promising, data are being obtained.

One highlight of the scattering experiments recently achieved was neutron diffraction under high magnetic field. Scattering under extreme conditions is one of the most promising fields of research using pulsed neutrons. However, we have never performed such an experiment. The maximum magnetic field so far used in neutron diffraction was below 10 T. As a first step of high field experiments, a Kobe University group developed a pulsed field instrument which can produce a high magnetic field up to 20 T every 2 sec with a pulse duration of about 1 ms. Neutron diffraction from a single crystal of metamagnetic $PrCo_2Si_2$ was measured under various high magnetic fields on the MRP diffractometer at KENS. The pulsed magnetic field was phased to the neutron pulse. When the neutrons of a specific velocity satisfying the Bragg condition arrive at the sample, the magnet is pulsed. $PrCo_2Si_2$ shows a complicated phase transition, a so-called successive magnetic phase transition, as shown in the magnetization curve (Fig. 5)[4]. The result proved that the proposed spin configurations (Fig. 6)[4] are correct. Details on this topic will be presented by Motokawa[5] at the Instrumentation Workshop "Sample Environments".

II. KENS-II

KENS-II is a next generation pulsed-spallation-neutron-source in Japan for condensed matter research and partly for fundamental physics. KENS-II was first proposed as a part of the GEMINI (Le Générator á Méson Intense et Neutron Intense) project and then combined with a Hadron project proposed by a nuclear physics group. The joint program is called the Japanese Hadron Project (JHP) which is aimed at exploring various research fields using various kinds of unstable secondary beams based on high intensity protons from a new accelerator complex. Neutron scattering is positioned as an important part of four major fields as shown in Fig. 7[6]. After significant discussions and compromise between four research fields, we decided, as a first phase, to construct a 1GeV H^- linac and a compressor/stretcher ring (and a heavy-ion linac for exotic nuclear beams). The layout of JHP is shown in Fig. 8. The proposed site for JHP is located at the forest adjacent to the southern boundary of the present KEK site.

JHP was authorized by the Science Council of Japan almost three years ago, but is still under examination by Monbusho (The Ministry of Education, Science and Culture, Japan), and by University of Tokyo, because JHP is dependent on the conversion of the Institute of Nuclear Study, University of Tokyo, to a new national laboratory as KEK. We are expecting to have an answer at latest by next spring. The main parameters of the 1GeV linac and the compressor /stretcher ring are summarized in Table I[6]. There is remarkable progress in the R&D of the 1GeV linac, on which Kihara[7] will give an invited talk. The compressor/stretcher ring delivers two bunches of proton beams-a 200 ns pulsed beam for the neutron scattering facility and 20 ns pulsed one for the meson science facility. Figure 9 shows the structure of circulating beam and a scheme of proton beam delivery.

We are aiming to realize the world's best pulsed-spallation-neutron-source with a proposed accelerator for JHP, which is comparable to those in the existing large scale facilities. The design goal of the proposed source is as follows:

(1) the world's brightest pulsed-cold-neutron-beams;
(2) bright and narrow pulsed thermal/epithermal neutron beams, at least comparable to those at existing intense pulsed-neutron-sources;
(3) wider range of neutron spectra;
(4) as many neutron beam lines as possible.

There are increasing demands for the use of neutron beams in various fields, but the total number of available neutron-beam-lines in an existing spallation neutron facility is much smaller than that in a high flux reactor. Another important problem which must be solved for extending the neutron beam technique to various research fields including industrial applications is that neutron beams from an intense source are very expensive. In order to solve this problem to some extent, we decided to adopt a vertical proton-beam-injection scheme rather than a horizontal one as used at present KENS, IPNS and ISIS. The total number of neutron-beam-lines is mainly limited by available opening angle around the target station. The removal of the proton-beam-line in the experimental hall with it's massive shielding will provide additional neutron-beam-lines as illustrated in Fig. 10. This scheme will bring about a considerable cost saving since proton-beam-line shielding in the experimental hall is very expensive. The amount saved can well compensate the additional cost for a large 90°-bending magnet in the primary proton-beam-line and extra overhead shielding of the target station.

In a vertical injection scheme, there is another important merit, in that we can take full advantage of the so-called "flux-trap type moderator"[8]. We carefully compared by computer simulation the slow-neutron beam intensity from a flux-trap moderator with that from a traditional wing-geometry type moderator and proved that the former can provide 1.3-1.4 times higher intensity of slow neutrons than the latter. This is a very important

conclusion. Details on this topic will be presented by Kiyanagi[9] at the Target Station Workshop "Cold Neutron Sources and Moderators".

Now let us consider what kind of cold neutron source would be the most promising. It has long been believed that pulsed spallation neutron sources are not as advantageous as reactors for cold neutron experiments, especially for small-angle-scattering. This is mainly due to the fact that the time-averaged cold-neutron-beam-intensity from pulsed-spallation-neutron-sources are not adequate. The situation is gradually changing; for example, KENS has shown the usefulness of pulsed cold neutrons in various experiments even with its lower intensity, and LANSCE has proved that LQD (SANS instrument) can compete with D11 at ILL Grenoble within a certain range of Q. WINK at KENS is in the same situation. The lower time-averaged cold-neutron-beam intensity is natural because the duty cycle of a pulsed-cold-neutron-source is only $\sim 5\times10^{-3}$, and the peak flux is to the utmost comparable to a high flux reactor. The problem which we want to point out is the lower conversion efficiency (from fast to cold neutrons) in the existing large scale pulsed-spallation-neutron facilities. This is also very natural because in those facilities decoupled liquid-hydrogen-moderators are used, which can provide narrow pulses of cold neutrons but lower time-averated flux. We studied what characteristics are important for a pulsed-cold-neutron-source in various scattering experiments. We concluded that the figure of merit (FOM) of a pulsed cold neutron source for small angle scattering is, to a first approximation, proportional to the time-integrated intensity per pulse and independent of the repetition rate and the pulse width in a realistic range, while for high resolution spectroscopy it is proportional to the pulse height and again independent of the repetition rate and the pulse width[10].

Based on this result, we looked for various candidates and finally found that a coupled liquid-hydrogen-moderator with an appropriate hydrogenous premoderator at room temperature is the most promising among various realistic moderators[11]. Our preliminary experiment was very encourging[12]. Thus, we continued further optimization experiments on this type of moderator and proved that a very large gain factor relative to a traditional decoupled liquid-hydrogen-moderator can be obtained with rather modest pulse-width broadening. Measured spacial (vertical) distribution of cold neutrons on the emission surface of the proposed moderator in a wing geometry is compared with two typical decoupled cold moderators in Fig. 11. The result demonstrates the superiority of the proposed moderator-two times higher flux than solid methane at 20 K, the best decoupled cold moderator. Details on this topic will be presented by Kiyanagi[13][14] at the Target Station Workshop "Cold Neutron Sources and Moderators".

The design concept of KENS-II is based on the flux-trap type moderator with a vertical proton-beam injection scheme and the coupled cold moderator

mentioned above. In addition to these two, we proposed a new concept for the target station which has two separate target-moderator-reflector assemblies, as illustrated in Fig. 12, with a new scheme of proton-beam delivery. For every 5 pulses (100 ms), a pair of double pulses from the compressor/stretcher ring is delivered to Target-1 (dedicated to the cold neutron source), with the other 4 pulses of single pulse being fed to Target-2 (dedicated to the decoupled moderators for narrow pulses of thermal and epithermal neutrons)[10]. Both can be optimized independently. The new system with the proposed proton-beam delivery scheme can bring about several times better overall performance than a traditional single assembly of all decoupled moderators in wing geometry with a horizontal proton-beam injection scheme. Details on this idea will be presented by Watanabe[15] at the Target Station Workshop "New Concept in Target-Reflector Moderator Systems".

REFERENCE

1 M. Furusaka, K. Suzuya, N. Watanabe, J. Suzuki and I. Fujikawa : Total performance of KENS small angle machines, Proc. ICANS-XI (Tsukuba, Oct. 22-26, 1990) P-675.

2 K. Inoue, Y. Ishikawa, N. Watanabe, K. Kaji, Y. Kiyanagi, H. Iwasa and M. Kohgi : Nucl. Instrum. Methods, A238 (1985) 401.

3 K. Inoue, T. Kanaya, Y. Kiyanagi, S. Ikeda, K. Shibata, H. Iwasa, T. Kamiyama and Y. Izumi : Total performance of LAM-80ET, Proc. ICANS-XI (Tsukuba, Oct. 22-26, 1990) P-682.

4 T. Shigeoka, H. Fujii, K. Yonenobu, K. Sugiyama and M. Date : J. Phys. Soc. Jpn. 58 (1989) 394.

5 M. Motokawa, H. Nojiri, M. Uchi, S. Watamura, H. Kawai and Y. Endoh : Neutron diffraction study in pulsed high magnetic field, Proc. ICANS-XI (Tsukuba, Oct. 22-26, 1990) P-977.

6 Pamphlet "Japanese Hadron Project -the first stage-", Institute for Nuclear Study, Univ. of Tokyo (1989)

7 M. Kihara : Progress of accelerator R&D for the Japanese Hadron Project, Proc. ICANS-XI (Tsukuba, Oct. 22-26, 1990) P-140.

8 G. J. Russell, H. Robinson, G. L. Legate, R. Woods, E. R. Whitaker, A. Bridge and K. J. Hughes : Proc. ICANS-IX (Villigen, Sept. 22-26, 1986) P-177.

9 Y. Kiyanagi and N. Watanabe : Some Neutronic Studies on Flux-Trap Type Moderator, Proc. ICANS-XI (Tsukuba, Oct. 22-26, 1990) P-408.

10 N. Watanabe, M. Furusaka and Y. Kiyanagi : A design concept for KENS-II cold neutron source, Proc. Int. Workshop on Cold Neutron Sources (Los Alamos, Mar. 5-8, 1990), in press.

11 N. Watanabe : Advanced Neutron Sources 1988 (Proc. ICANS-X), Institute of Physics Conference series Number 97, Institute of Physics, Bristol and New York, P-763.

12 N. Watanabe, Y. Kiyanagi, K. Inoue, M. Furusaka, S. Ikeda, M. Arai and H. Iwasa : Advanced Neutron Sources 1988 (Proc. ICANS-X), Institute of

Physics Conference Number 97, Institute of Physics, Bristol and New York, P-787.
13 Y. Kiyanagi, N. Watanabe, M. Furusaka, H. Iwasa and I. Fujikawa : Optimization studies on coupled liquid hydrogen moderator, Proc. ICANS-XI (Tsukuba, Oct. 22-26, 1990) P-388.
14 Y. Kiyanagi, N. Watanabe, M. Furusaka and H. Iwasa : Reflector optimization for coupled liquid hydrogen moderator, Proc. ICANS-XI (Tsukuba, Oct. 22-26, 1990) P-401.
15 N. Watanabe : A design concept of target-reflector-moderator assemblies for KENS-II, Proc. ICANS-XI (Tsukuba, Oct. 22-26, 1990) P-471.

Table I Principal parameters of proton Accelerator for JHP

	Linac	Compewssor/stretcher
Energy	1Gev	1GeV
Average current	400μA	200μA
Repetition rate	50Hz	50Hz
Peak current	20mA	
Pulse width	400μs	200ns (for neutron exp.)
Size	500m long	54m in diam.

Q(G.J.Russell): Have you considered putting moderators upstream of the first target?
A(N.Watanabe): No, we have not.
Q(A.D.Taylor): On a green field site, with a solid target, would you still use vertical injection?
A(G.S.Bauer): Yes, I would. There is the advantage of a 2π region to be used for neutron beams. The cylindrical geometry is just very convenient and also the possibility of vertical target movement for exchange is a big advantage. Of course, design of the beam line needs thorough consideration.

Fig. 1. KENS NEUTRON SCATTERING FACILITY

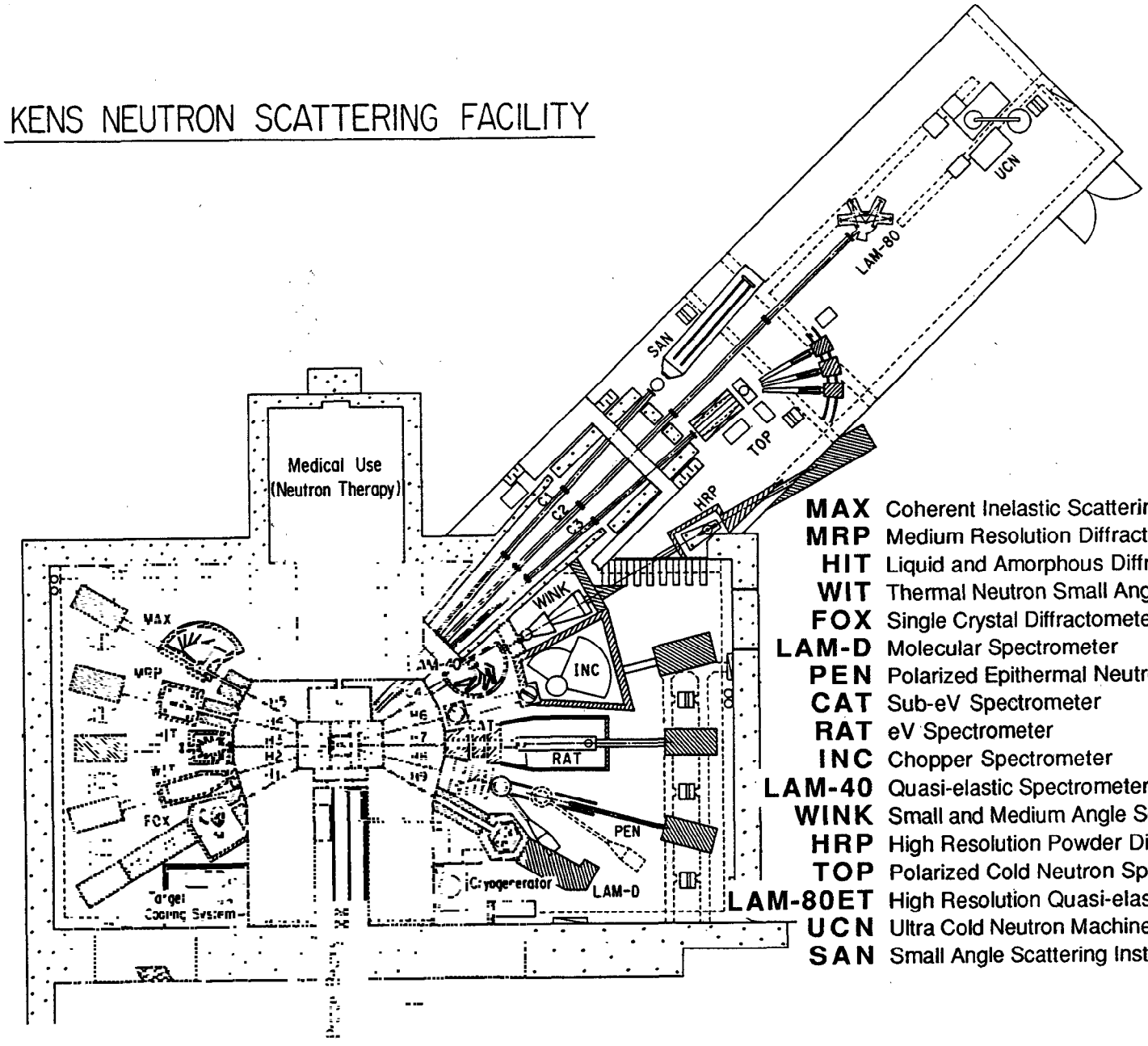

MAX Coherent Inelastic Scattering Spectrometer
MRP Medium Resolution Diffractometer under Extreme Conditions
HIT Liquid and Amorphous Diffractometer
WIT Thermal Neutron Small Angle Scattering Instrument
FOX Single Crystal Diffractometer
LAM-D Molecular Spectrometer
PEN Polarized Epithermal Neutron Spectrometer
CAT Sub-eV Spectrometer
RAT eV Spectrometer
INC Chopper Spectrometer
LAM-40 Quasi-elastic Spectrometer
WINK Small and Medium Angle Scattering Instrument
HRP High Resolution Powder Diffractometer
TOP Polarized Cold Neutron Spectrometer
LAM-80ET High Resolution Quasi-elastic Spectrometer
UCN Ultra Cold Neutron Machine
SAN Small Angle Scattering Instrument

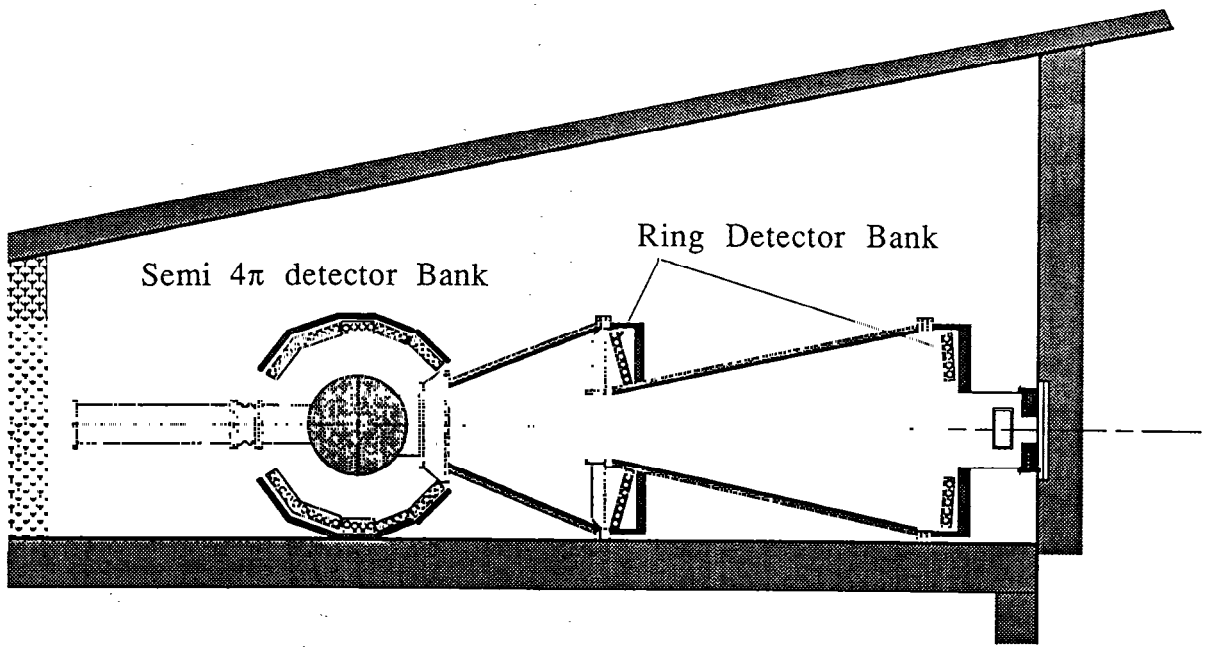

Fig. 2 Layout of WINK

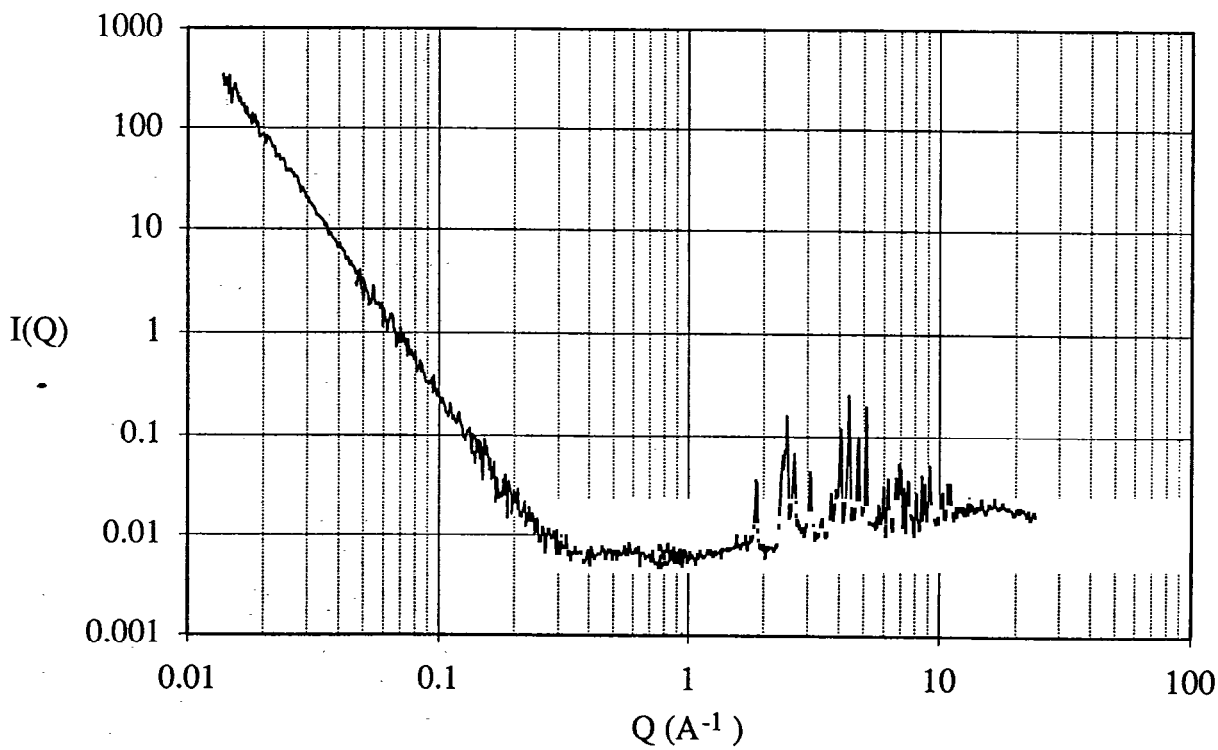

Fig. 3 Preliminary result of small angle scattering from SiC sample measured on WINK.

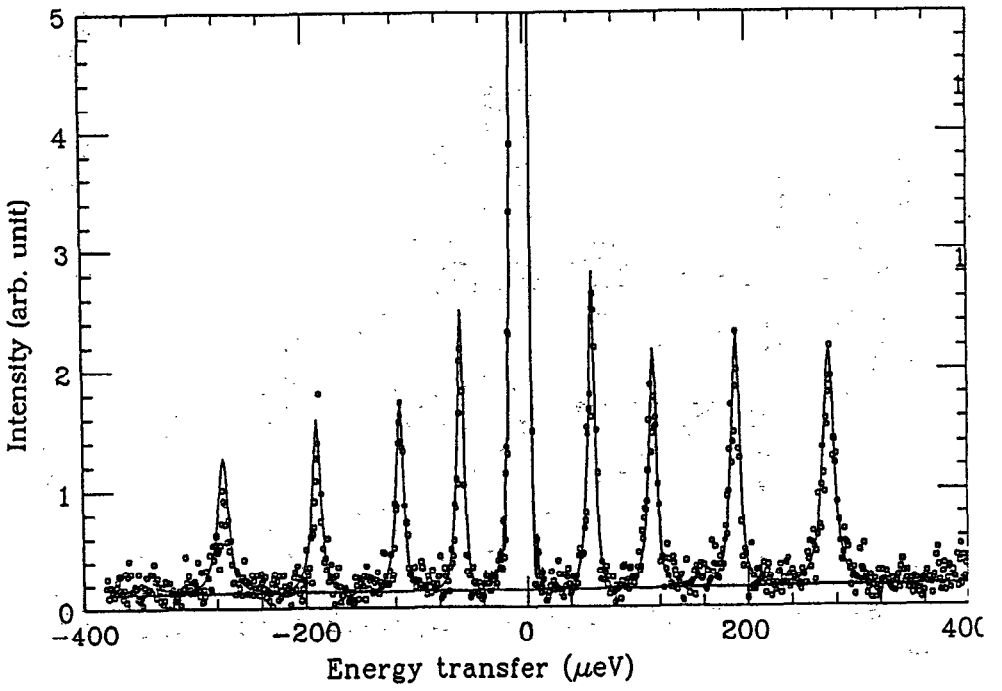

Fig. 4 Tunneling spectrum of N-Oxy γ picoline measured at 5K on LAM-80ET

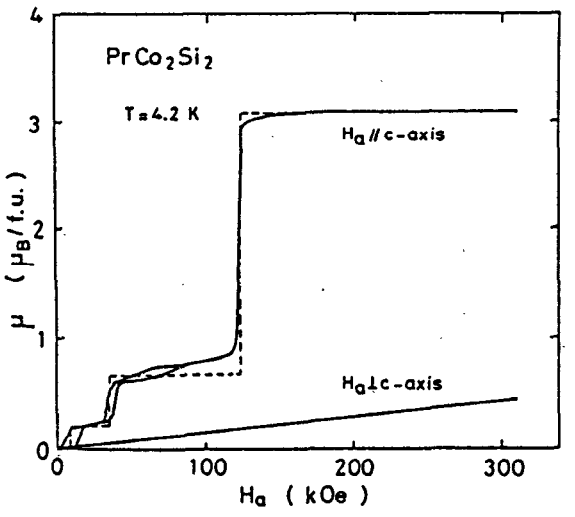

Fig. 5 High Field Magnetization curves along the a- and c-axes at 4.2K for $PrCo_2Si_2$ [after ref.4]

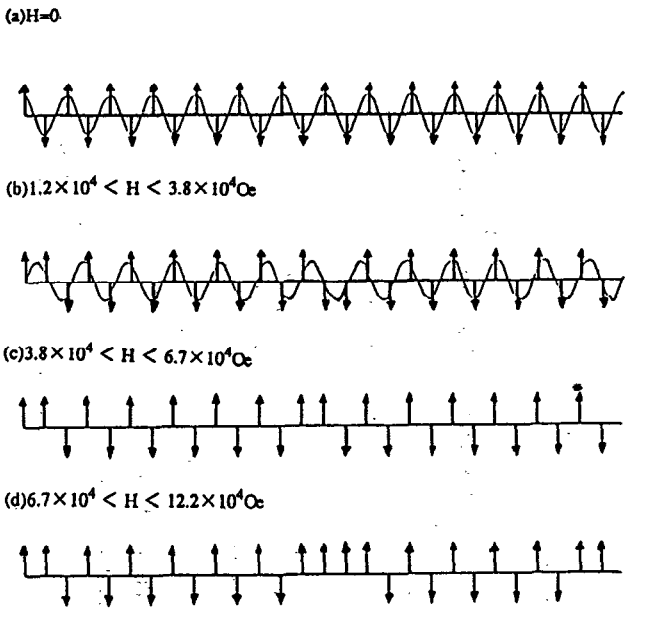

Fig. 6 A proposed spin configurations under various magnetic fields [after ref.4]

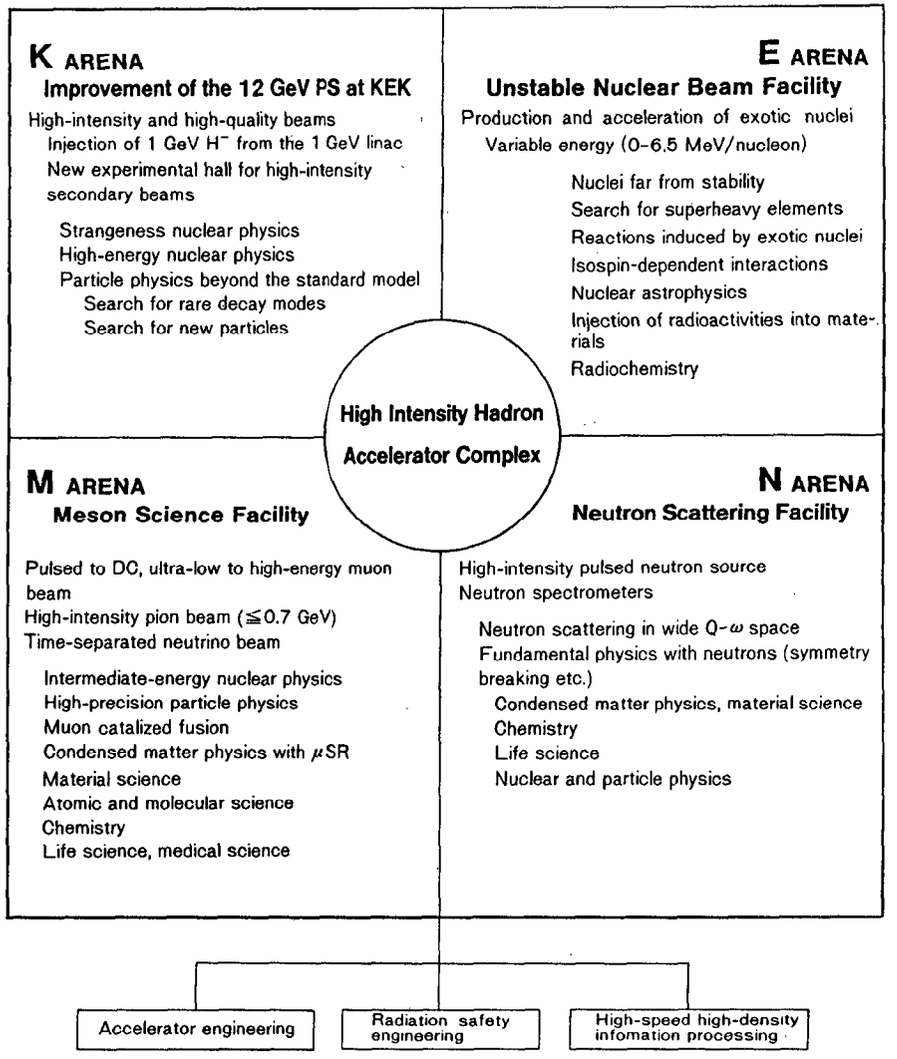

Fig. 7 Research area of JHP

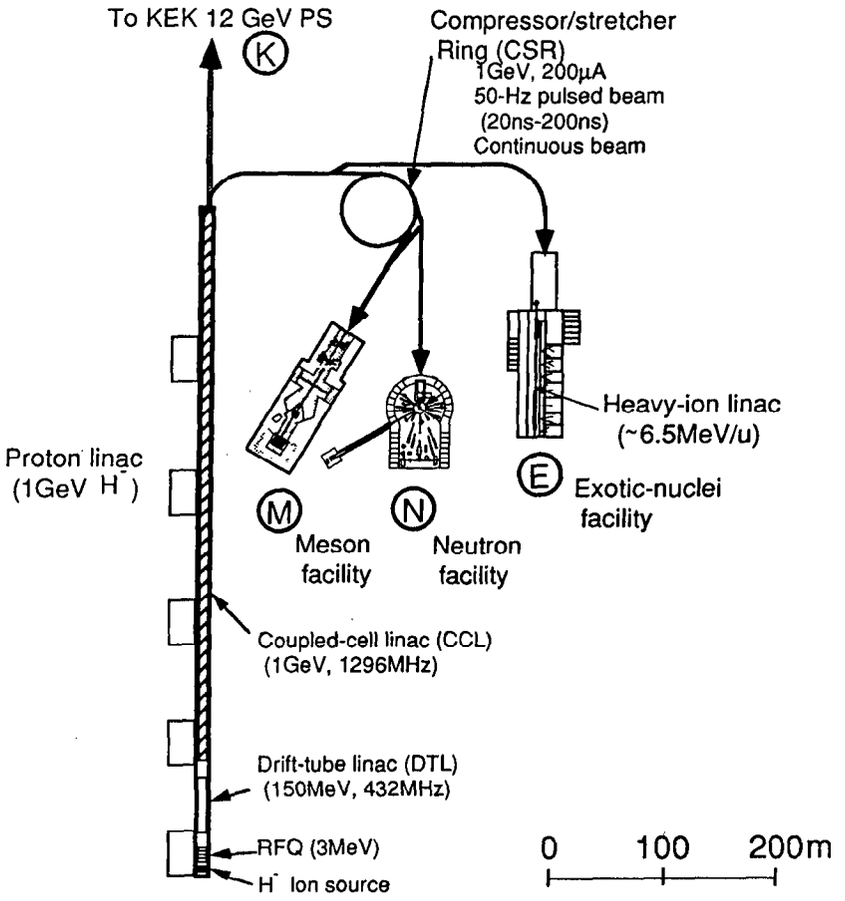

Fig. 8 Layout of JHP

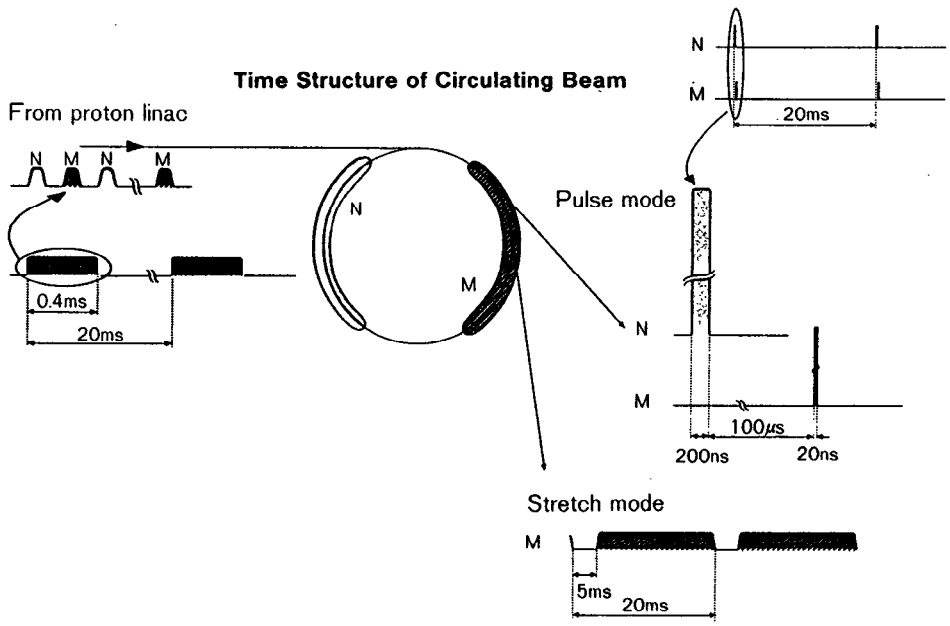

Fig. 9 Time structure of a circulating beam and a scheme of proton beam delivery

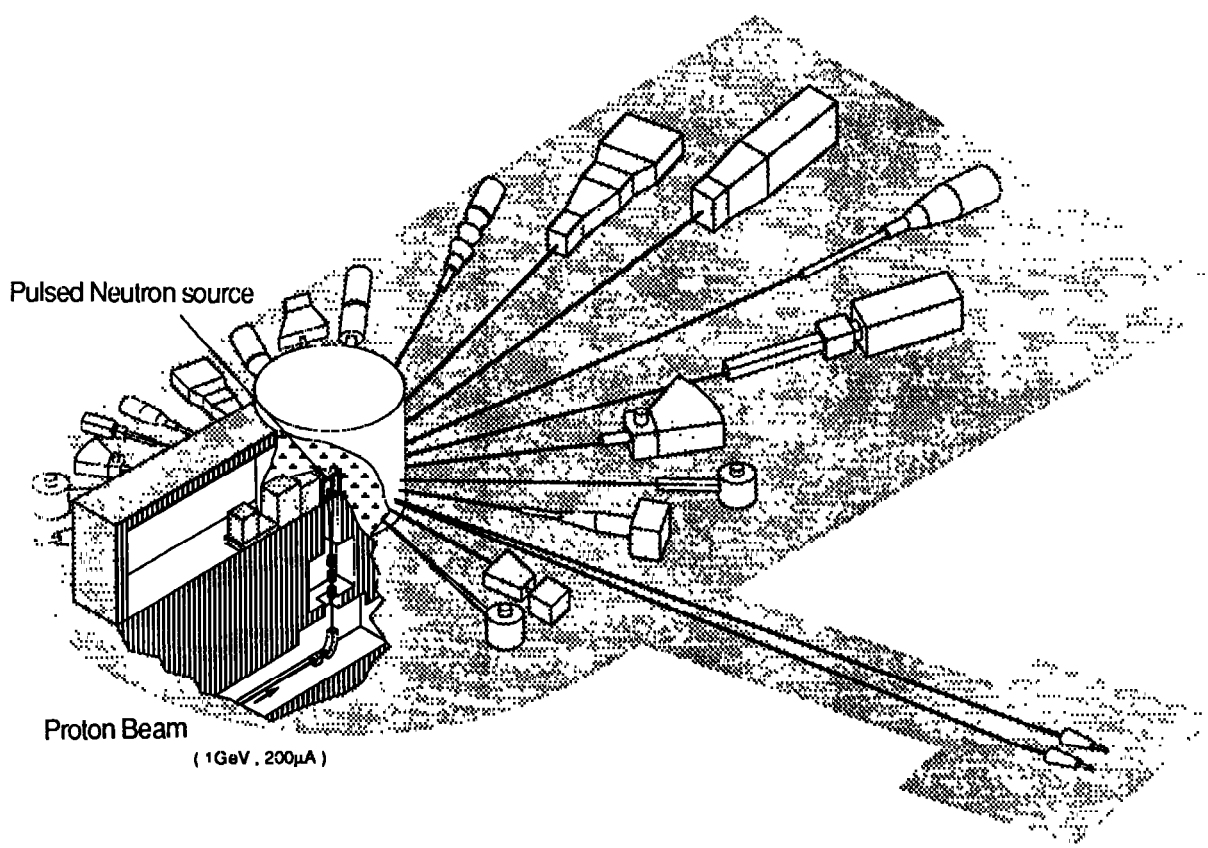

Fig. 10 Illustration of KENS-II (vertical proton-beam injection and layout of neutron instruments)

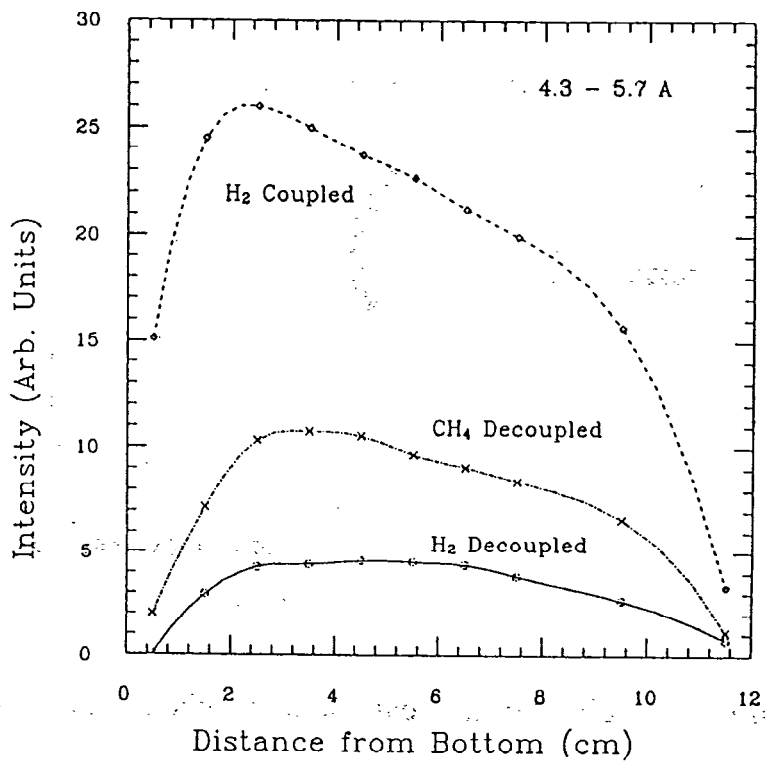

Fig. 11 Measured spatial distribution of cold neutron beam intensity along the vertical direction of the viewed surface of the coupled liquid hydrogen moderator.

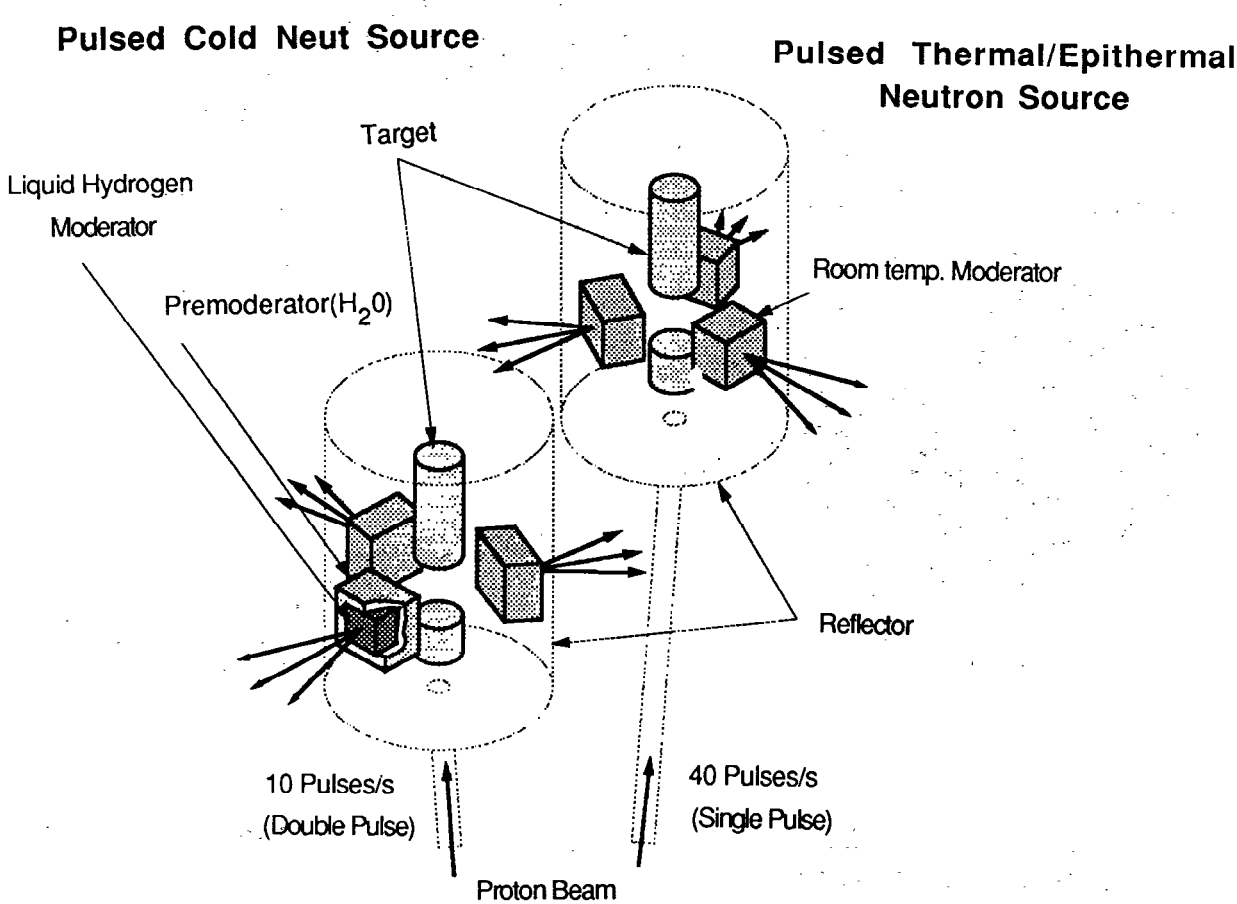

Fig. 12 Illustration of two target-reflector-moderator assemblies proposed for KENS-II

ICANS-XI International Collaboration on Advanced Neutron Sources
KEK, Tsukuba, October 22-26, 1990

STATUS OF THE ADVANCED NEUTRON SOURCE

John B. Hayter
Oak Ridge National Laboratory
FEDC/MS-8218
P.O. Box 2009
Oak Ridge, TN 37831-8218, U.S.A.

ABSTRACT
Research reactors in the United States are becoming more and more outdated, at a time when neutron scattering is being recognized as an increasingly important technique in areas vital to the U.S. scientific and technological future. The last U.S. research reactor was constructed over 25 years ago, whereas new facilities have been built or are under construction in Japan, Russia and, especially, Western Europe, which now has a commanding lead in this important field. Concern over this situation in the early 1980's by a number of organizations, including the National Academy of Sciences, led to a recommendation that design work start urgently on an advanced U.S. neutron research facility. This recommendation is realized in the Advanced Neutron Source Project. The centerpiece of the Advanced Neutron Source will be a new research reactor of unprecedented flux ($>7.5\times10^{19}$ $m^{-2}.s^{-1}$), equipped with a wide variety of state-of-the-art spectrometers and diffractometers on hot, thermal, and cold neutron beams. Very cold and ultracold neutron beams will also be provided for specialized experiments. This paper will discuss the current status of the design and the plans for scattering instrumentation.

I. INTRODUCTION

Neutron scattering was pioneered by C. G. Shull and E. O. Wollan at the X-10 (natural uranium) graphite reactor at Oak Ridge National Laboratory about half a century ago. The flux available, although low ($1\cdot10^{16}$ $m^{-2}\cdot s^{-1}$), was sufficient to show the importance of neutron scattering as a fundamental technique in materials science. Many reactors of increasingly higher flux were designed and built in the 1950's and 1960's, culminating with the high flux reactors at Brookhaven National Laboratory (HFBR) and at Oak Ridge National Laboratory (HFIR) in the United States, and at the Institut Laue-Langevin in France; all of these reactors offer fluxes of order $1.5\cdot10^{19}$ $m^{-2}\cdot s^{-1}$. However, while new research reactors have either come on-line (or are about to come on-line) since that time in Western Europe, Japan, and Russia, it is now about 25 years since the last research reactor was constructed in the United States. By the late 1970's, it was clear that the lead in the field of neutron scattering had passed decisively to Western

Europe. In 1983, the National Research Council reviewed the needs of neutron scattering *per se* [1] and the neutron scattering facilities existing in the United States [2].

The major facilities review concluded that a new, steady-state high-flux neutron facility was a high priority requirement for the United States, and recommended that design begin immediately. Among the factors contributing to this recommendation was the age of existing reactors, the evident European leadership in a field in which the U.S. had been predominant, and the important (and often unique) future applications of neutron scattering in many important areas of condensed matter physics, polymer and colloid science, metals, alloys and ceramics, chemistry, biology and medicine, and the earth sciences. The detailed needs of the community, as defined in several major workshops [3-5], helped to define the Advanced Neutron Source project. The fundamental project objective is to design and construct the world's highest flux research reactor for neutron scattering, together with state-of- the-art instrumentation. The reactor will also provide isotope production and materials irradiation facilities which are as good as, or better than, any presently operational source.

II. THE NEUTRON SOURCE

The *sine qua non* of the new facility is a reactor which can provide a flux at least five times higher than any existing neutron beam reactor, while meeting extremely stringent safety requirements. To this end, it was decided to base the design as much as possible on existing technology (although advantage will be taken of any gains from new research and development), and to carry out probabilistic risk assessment simultaneously with design; the latter is a first for such a project, and reflects the fact that safety considerations are of primordial concern. A major achievement of the project has been the completion of the preconceptual nuclear and thermal hydraulic design of the reactor, showing that the objectives can be met with a safe design. The key feature has been to choose a coaxial, split-core in which the two halves are axially displaced and separately cooled (see Figs. 1 and 2). The reactor volume of 67.4 L contains 18 kg of ^{235}U (93% enriched) in the form of involute plates of U_3Si_2 in an Al matrix. The unperturbed peak thermal flux generated in the reflector is of order $9 \cdot 10^{19}$ $m^{-2} \cdot s^{-1}$ at a power of 350 MW. The reactor core is cooled by a heavy water primary coolant loop, with coolant *upflow*. The choice of upflow provides a very desirable added safety feature, since it ensures an immediate transition to natural convection cooling (without any time delay for flow reversal) in the unlikely event of rupture of the primary circuit at a point which forestalls compensation by the independent backup circuit. (It should be noted that the normally low probability of major pipe rupture is being further reduced by designing for leak-before-break, with continuous leak monitoring.) The maximum coolant outlet temperature is 98°C, so that boiling will not occur on loss of pressure.

The reactor is controlled by four hafnium control rods in the central core channel. Each rod is provided with an independent scram mechanism, and any three of the four are able to shut down the reactor. A second, independent, shutdown mechanism is provided by eight shutdown rods placed outside the core. Each rod is again provided with an independent scram mechanism, and any seven of the rods are sufficient for total shutdown. Thus, the reactor may be shut down, even if there is total failure of one complete set of independent scram mechanisms, and partial failure of the other.

There are six major types of experimental facilities in the reactor assembly (Fig. 2). Materials irradiation (for example, for fusion research) takes place in capsules placed inside the upper fuel element, while transuranium elements are produced in targets just

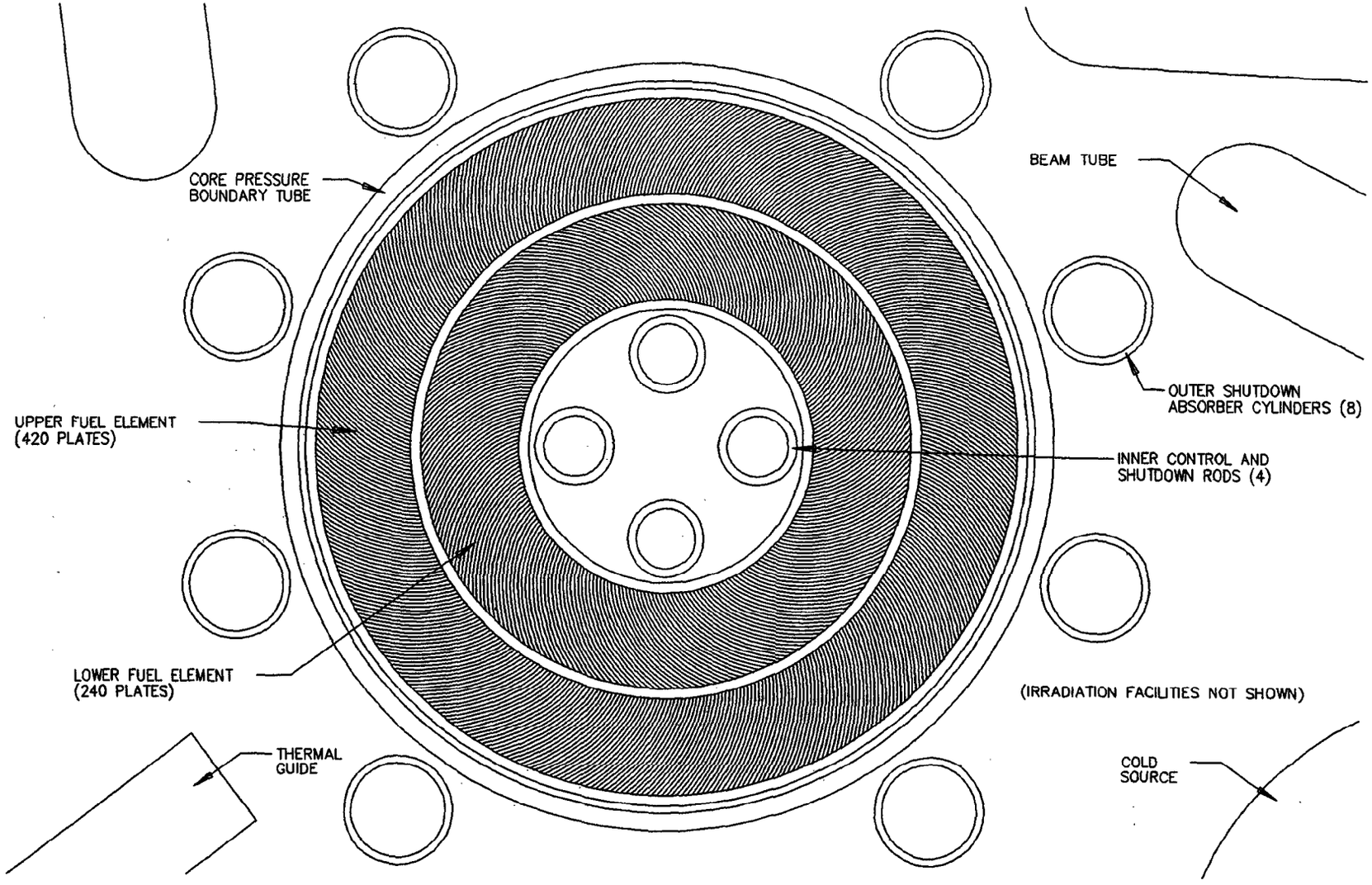

Figure 1. Plan view of the ANS reactor core.

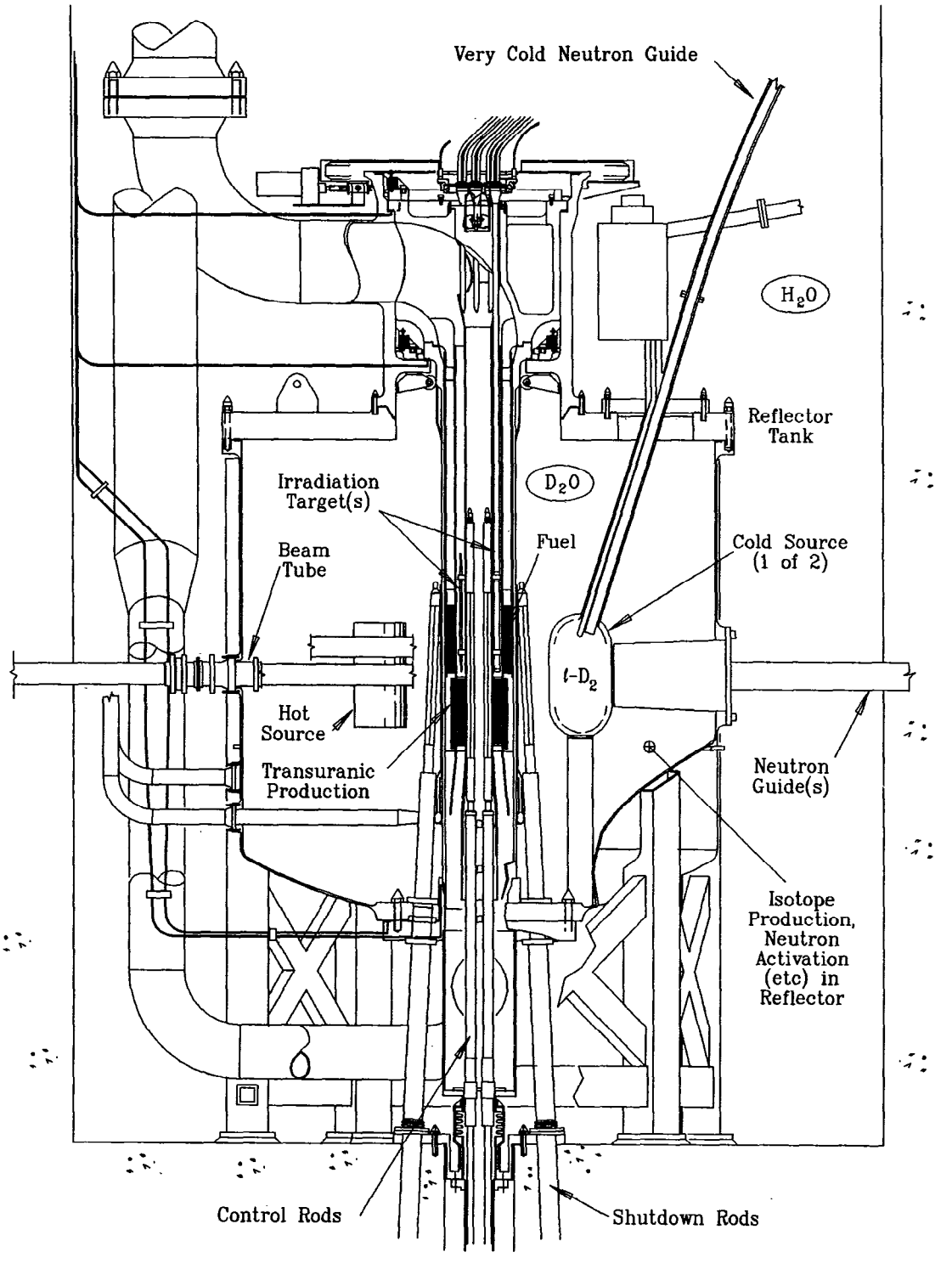

Figure 2. The ANS reactor assembly.

outside the lower fuel element. One of the achievements of the core design is that these facilities, which provide appropriate fast and epithermal neutron spectra, have minimal effect (<2%) on the fluxes of the neutron beams to the experiments. The large volume of high thermal flux available in the reflector tank is well suited to isotope production and analytical chemistry operations. To accomodate these activities, various experiment holes and "rabbit" tubes penetrate the top of the reflector tank. Four vertical and two slant holes will provide a range of thermal fluxes for isotope production; these holes will be complemented by four hydraulic rabbit tubes, and at least four pneumatic rabbit tubes for materials analysis.

Neutron beams are extracted from the reflector by beam tubes which penetrate either into the peak thermal flux region (about 400 mm from the core centerline), or terminate at the graphite hot source at the reflector tank wall. The hot source is one of two types of spectral convertor which are placed in the reflector to tailor beam energies for specific applications; conversion to sub-thermal energies is accomplished by two liquid-D_2 cold sources. Cold neutrons are transported by horizontal neutron guides into a neutron guide hall adjacent to the containment building, or by slant guides to the second-floor beam room.

III. NEUTRON SCATTERING FACILITIES

There will be three user halls provided for experimental work at the ANS (Fig. 3). The Ground Floor Beam Room will provide "conventional" access to thermal and hot neutrons from the reactor *via* horizontal beam tubes terminating at the outside of the biological shielding. Inclined beams and certain other services, such as rabbit tubes, will terminate on a higher level in the Second Floor Experiment Room. Very cold and ultracold neutron research will take place on this level, as well as such activities as neutron depth profiling and some of the fundamental and nuclear physics work. The third main experimental area is the Neutron Guide Hall, which will provide the primary instrumentation for cool and cold neutron research. The layouts presented below are tentative, as they are designed to accommodate *today's* needs and priorities [3,4].

Ground Floor Beam Room. - The ground floor beam room layout is shown in Fig. 4. This layout currently assumes that, apart from a single through tube for nuclear physics, all beams will lie in the same plane; as neutronics calculations evolve, it may become necessary to stagger the beam heights alternatively above and below this reference plane, to minimize flux perturbations due to the beam tubes themselves.

Thermal beam scattering instruments for diffraction include 4-circle diffractometers on a thermal tube (T1) or guide (T2). A polarized beam is earmarked for single crystal diffraction (T3), but, in general, it is expected that polarized neutrons (and polarization analysis) will be routinely available whenever warranted on any instrument on the ANS. High resolution (T4) and high intensity (T5) powder diffractometers and two diffuse scattering spectrometers (T6/7) complement the single crystal instruments. Inelastic spectrometers are time-of-flight (T8) or 3-axis (T11/12).

The hot source provides beams to a high energy transfer 3-axis spectrometer (H3), a high momentum transfer single crystal diffractometer (H1), and a general purpose high incident energy diffractometer (H2) for studies of liquids and amorphous materials.

Neutron Guide Hall. - The guide hall building (Fig. 5) is a wedge-shaped, single floor structure contiguous with the reactor containment building and office/laboratory complex. Two polar segment cranes will serve the guides and instruments. The guide shield

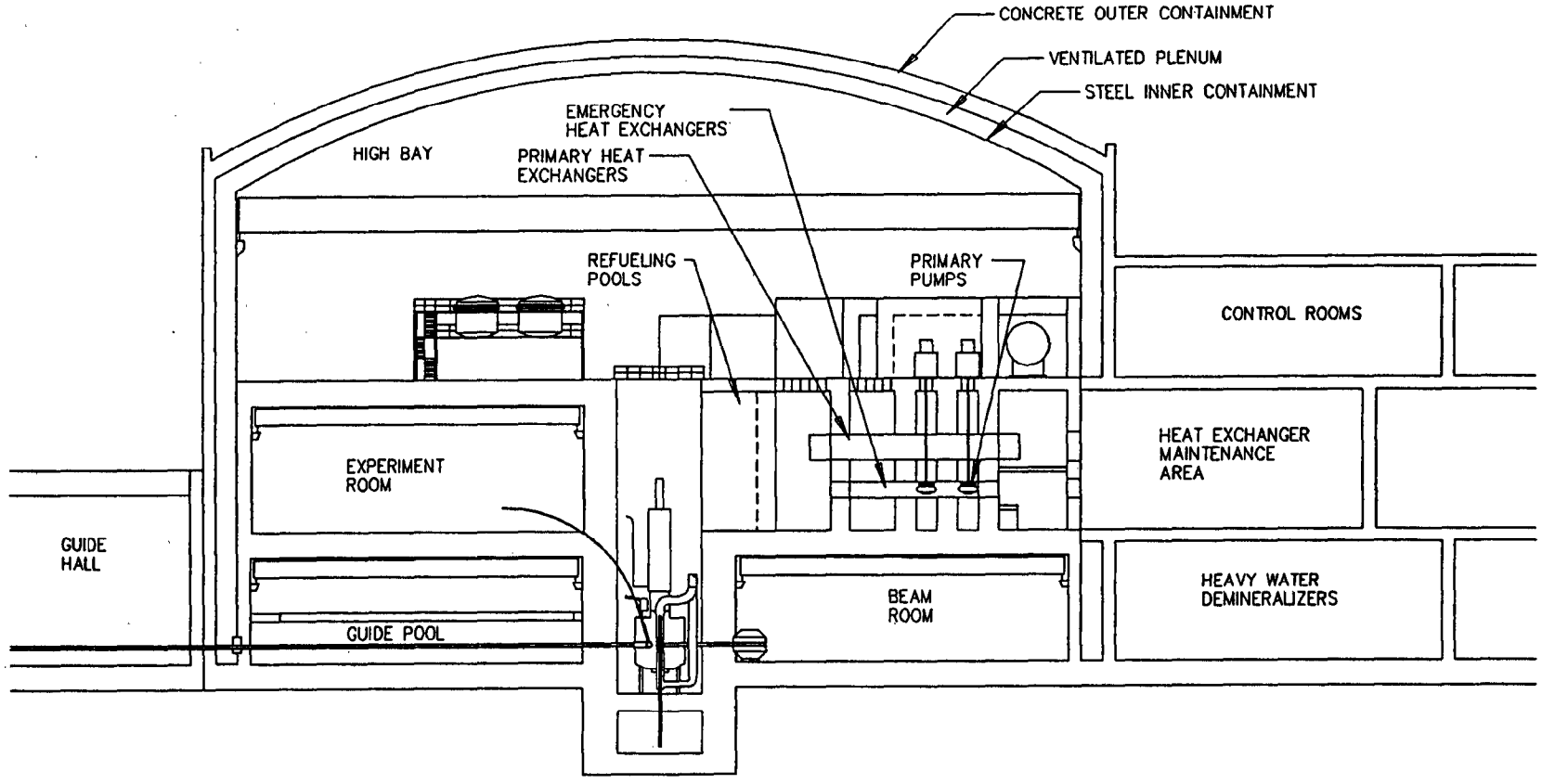

Figure 3. Vertical section through the ANS reactor building, showing experiment halls.

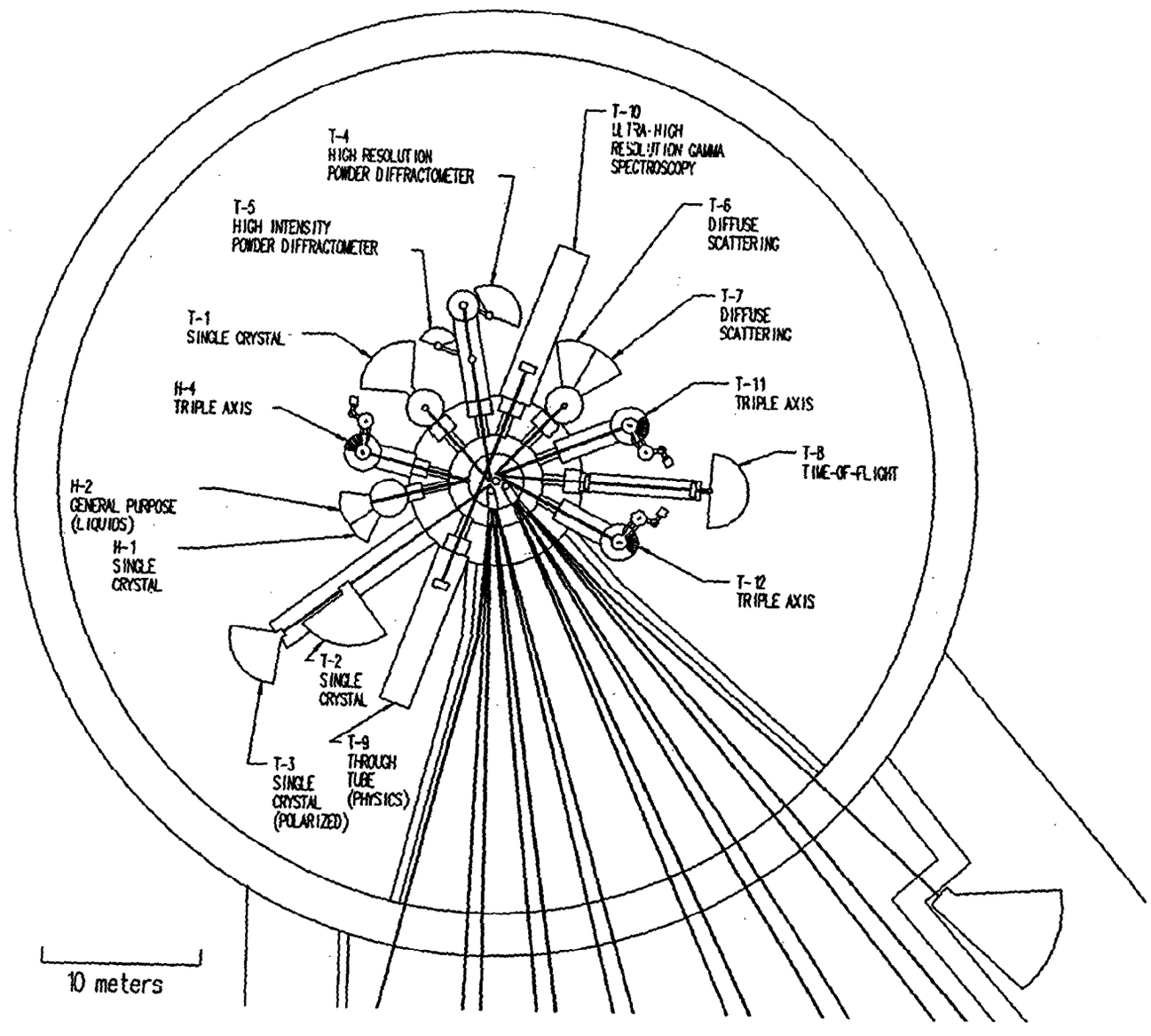

Figure 4. The Ground Floor Beam Room.

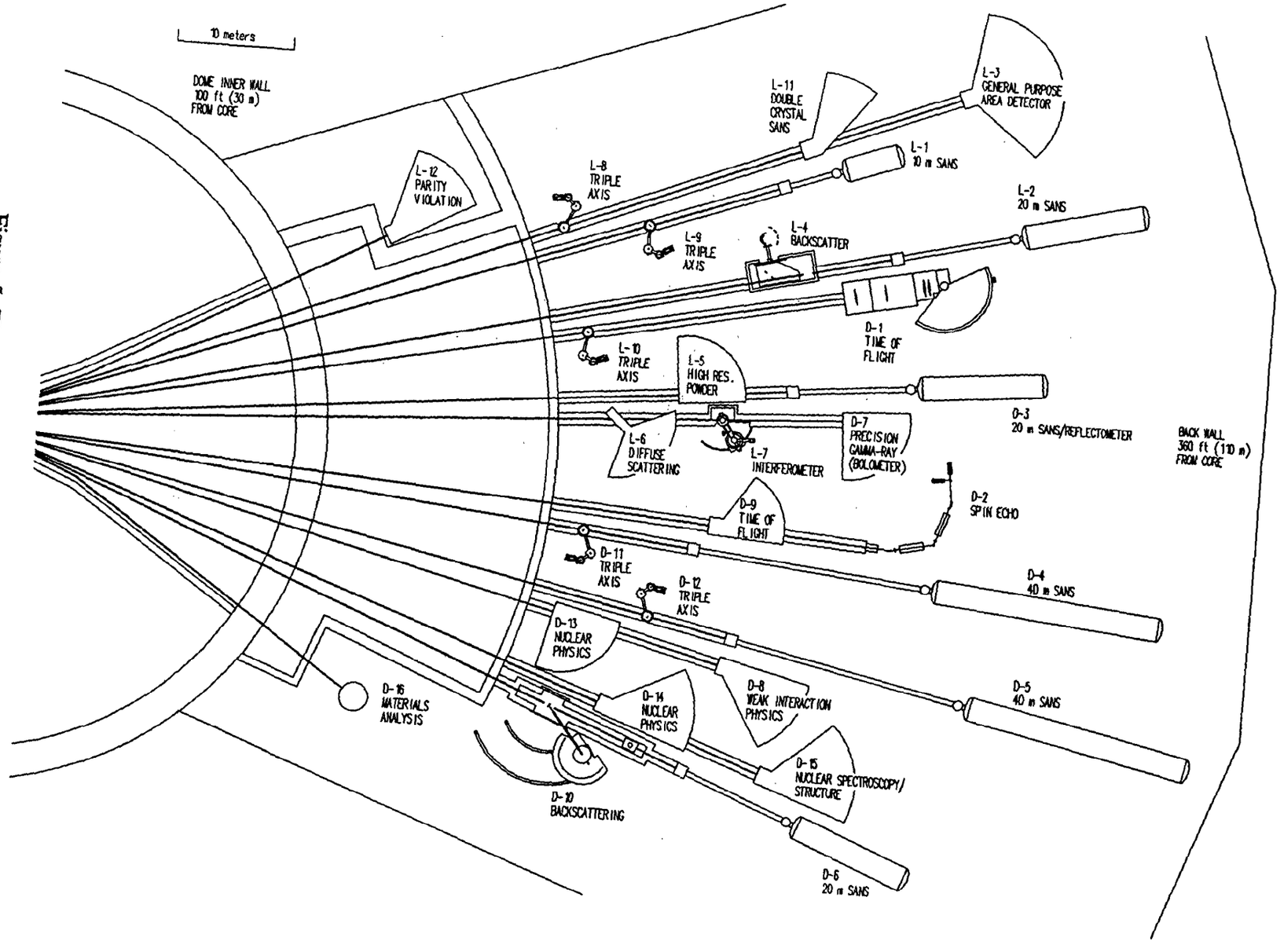

Figure 5. The Cold Neutron Guide Hall.

structure reaches out to a distance of about 50 m from the reactor axis, and the experiment area extends a further 60 m. Apart from the two extreme guides, which serve special positions for nuclear physics (L12) or materials analysis (D16), the guides will generally be straight, so that cool as well as cold energies will be available. It will be noted that about one third of the experimental stations are for nuclear or fundamental physics; only the scattering instruments will be described here.

The most prevalent elastic scattering instruments are the small-angle neutron scattering cameras (D3-6, L1, L2, L11), which offer varying degrees of resolution, and at least one of which will have reflectometer capabilities for surface studies. Diffuse scattering and high resolution powder diffraction will be available (L5, L6), together with a general purpose area detector for efficiently scanning large regions of reciprocal space, for example, to study incommensurable lattice structures. A specially isolated mounting (to screen thermal and acoustic noise) will be provided for a neutron interferometer station (L7).

Conventional, variable k_o, focussing monochromator cool and cold 3-axis spectrometers will be the workhorses for inelastic scattering studies in the guide hall (D11, D12, L8, L9, L10), together with multichopper (D1) and time focussing (D9) time-of-flight spectrometers. Higher resolution inelastic studies will use backscattering (L4, D10) or neutron spin-echo (D2) as appropriate.

Second Floor Experiment Room. - The main purpose of the second floor of the containment building is to provide experimental areas for users of the inclined beams and guides (Figs. 3 and 6). The prototypical layout shown in Fig. 6 demonstrates several key features, of which the most notable is the division of the area into two zones, one *secure*, the other *general access*. This is a particular example of the general site philosophy adopted for the ANS plant: separation of reactor operations from experimental areas, so that users may have straightforward access to their experiments and related areas (such as chemical laboratories), without requiring access to high security zones. One important role played by the second floor beam room will thus be to accommodate those experiments which have more commonly been situated in the reactor operations areas of other reactors (such as the ultracold neutron facility at ILL, Grenoble).

Current plans call for each cold source to be fitted with an inclined, curved guide (Fig. 3) for very cold neutrons (VCN). It is likely that one of these will be used directly while the other will be used as a feed for an ultracold (UCN) source (Fig. 6). A cold slant guide will provide a station for neutron depth profiling (NDP), which is a sensitive means of measuring concentration *vs* depth profiles by using reactions such as $^{10}B(n,\alpha)^{7}Li$ and detecting the resulting charged particles, whose range is a strong function of the distance they must travel in the surface being probed. NDP, which is quantitative and non-destructive, is applicable to a variety of technologies, such as microelectronics, optical signal processing, ultra- light alloys, and surface-modified materials.

A novel possibility for the ANS is to provide isotope separation on-line (ISOL). In this technique, a fission-fragment mass separator is used as the front end of an ion-implantation accelerator, providing a number of unique ions for studies of electron emission, channelling, and hyperfine interactions associated with ion-implanted radioactive atoms. Since charged beams are involved, they may be transported to ancillary equipment situated at some distance from the reactor.

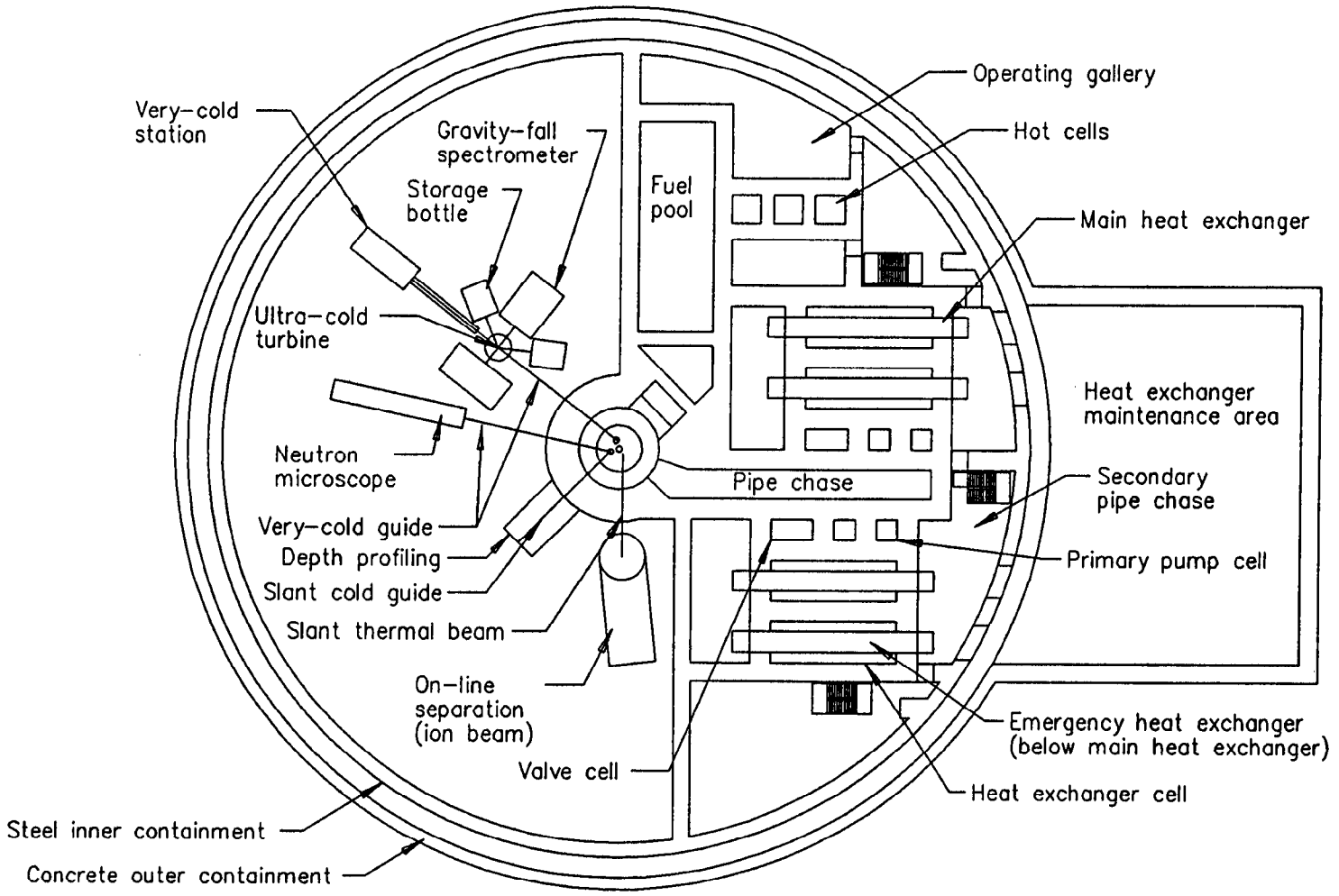

Figure 6. A possible arrangement of the Second Floor Beam Room.

IV. PROJECT SCHEDULE

The conceptual design phase of the ANS project will be finished towards the middle of 1991. Conceptual design embraces, apart from the key engineering elements, the choice of a site which meets all environmental criteria, and the considerable plant and equipment associated with the research activities planned at the ANS, for example offices, workshops and laboratories, library and conference rooms, *etc.* The next stage is preliminary engineering design, and if approved this would lead to a complete design by 1993, with construction currently planned to start in 1994. If the schedule is maintained, this will lead to reactor operation in late 1998, and will take the U.S. materials science community into the next millenium with the world's best facility of this type.

Oak Ridge National Laboratory is operated by Martin Marietta Energy Systems, Inc., for the U.S. Department of Energy, under Contract No. DE-AC05-84OR21400.

REFERENCES

1. Panel on Neutron Scattering, National Research Council: *Current Status of Neutron Scattering Research and Facilities in the United States* (National Academy Press, Washington D.C., 1984)

2. Major Materials Facilities Committee, National Research Council: *Major Facilities for Materials Research and Related Disciplines* (National Academy Press, Washington, D.C., 1984)

3. R. M. Moon, Editor: *Proceedings of the Workshop on Instrumentation for the Advanced High-Flux Reactor*, Oak Ridge National Laboratory Report CONF-8405192 (1984)

4. G. H. Lander and V. J. Emery, Editors: *Proceedings of the Workshop on Scientific Opportunities with Advanced Facilities for Neutron Scattering*, Argonne National Laboratory Report CONF-8410256 (1984); Nucl. Instr. and Meth., **B12**, 525 (1985)

5. R. M. Brugger, Editor: *Proceedings of the Workshop on an Advanced Steady-State Neutron Facility*, Nucl. Instr. and Meth., **A249** (1986)

Q(P.A.Egelstaff): Have you considered a 1/E source, for example a light water source next to the core?

A(J.B.Hayter): We have so far done very little work on the conceptual design of the hot source. A 1/E source would certainly be worth considering.

Q(A.D.Taylor): What instrument do you envisage on the hot source and how will it be complemental by spallaltion-source constitution?

A(J.B.Hayter): We currently envisage a 3-axis spectrometer, a single crystal diffractometer and a liquids diffractometer. The interest in the last instrument is to be able to extend the data to low-Q, so as to see liquid specific structure.

Q(R.Pynn): It is not clear to me that your figure of merit - total number of neutrons on total number of samples is the right one to use. Is it really to multiply flux by beam size by number of beams to get a fugure of merit?

A(J.B.Hayter): Yes, because the number of neutrons on samples is a measure of the information we can expect from scattering experiments at the ANS. The change from using only 1/3 of the guide height for each instrument at ILL to using the full height is an example of putting this concept into practice.

Q(G.S.Bauer): Is neutron scattering the main objective for construction of the ANS, in confront to the situation, when HFIR was built?

A(J.B.Hayter): Yes. The pressure to build the ANS originated with the neutron scattering community, and the highest priority optimization is for neutron scattering.

Q(G.S.Bauer): How often do you envisage you will have to change the wall separating the moderator from the core coolant and how much effort will that be?

A(J.B.Hayter): The question of whether the core pressure boundary tube will be changed each cycle, or less often, is currently under active study.

ICANS-XI International Collaboration on Advanced Neutron Sources
KEK, Tsukuba, October 22-26, 1990

To the memory of A.M.Budker

Neutron facilities of Moscow meson and kaon factories.

Yu.Ya.Stavissky, Institute for Nuclear Research
USSR Academy of Sciences.

The questions of new generation of intensive pulse neutron sources for elementary interaction physics, neutron nuclear physics, solid state and radiation physics, on the base of Moscow meson and projected kaon factories are discussed.

The neutron studies allow to obtain a unique information on fundamental questions of elementary interaction physics, on the properties and the mechanism of nuclear reactions, on the structure and the properties of the condensed matter.

The studies in neutron low energy range (cold, thermal and resonance neutrons) are of special interest.

The neutron studies development is strongly related to new neutron sources, which can allow to increase the neutron experiments luminosity.

Up till now the main volume of neutron studies were carried out on high-flux research reactors. Due to some reasons (limitation of the fuel heat release density, overloads, safety problems) the possibility for increasing neutron flux in such reactors is limited. The flux density $2\text{-}3\cdot10^{15}$ $n/s\cdot cm^2$ on the moderator surface, "radiating" into the neutron channel of a high-flux research reactor of ~ 100 MW power (for example, ILL-reactor, Grenoble, or "PIK" reactor, being constructed at LNPI, Gatchina) is close to its top limit.

Because of these circumstances, in the 60's, the suggestion was made at Canada, Chalk River, to use the spallation process with 1 GeV protons to obtain slow neutrons fluxes. The "Canadian design" is well known - a neutron source on the base of 65 mA, 1 GeV separated-orbits cyclotrons with the liquid-metal target (Pb-Bi eutectics) and the heavy-water moderator /1/.

The calculated neutron flux density value was about 10^{16} $n/s\cdot cm^2$ in this system. The calculated neutron flux density value for the system with a circular tungsten water-cooled target and the beryllium moderator (Obninsk, 1970, /2/) reached the value of about $1.5\cdot10^{17}$ $n/s\cdot cm^2$, the current of 1 Gev protons being 100 mA. However, the development of medium-energy proton accelerators for the currents about hundreds of milliampers, encounters great difficulties (energetics, exploitation, capital investments);

therefore the only neutron source SINQ /3/, based on this scheme is currently constructed in Paul Sherer Institute (PSI, Schwitzerland) with 1.5 mA current of 600 MeV protons and, accordingly, with thermal neutron flux density of $1.5\text{-}2\cdot10^{14}$ $n/cm^2\cdot s$.

The wide application of time-of-flight technique in neutron experiments opened the way for the development of intensive pulse neutron sources on the base of electron accelerators and pulse fast reactors /4/. However, the average neutron intensity from electron accelerators is relatively low. The development of pulse reactors didn't allow the sufficient increase in neutron experiments luminosity - the powerful pulse reactor "IBR-2" is close to high-flux research reactor (ILL-"PIK" /6/) by its experimental abilities.

New possibilities for neutron studies development are opened while using medium- and high-energy proton accelerators for pulse neutron sources creation. The use of charge-exchange injection in proton sinchrotrons and storage rings proposed firstly by L.Alvarez /7/ and implemented by A.M.Budker with co-workers /8/ is of principal importance in this case.

In the beginning of 60's in the Institute of Nuclear Physics, Novosibirsk and Physical-Energical Institute, Obninsk the pulse neutron source on the base of 0.5 GeV fast-cycling proton synchrotron with single-turn ejection onto the natural uranium target was worked out /9/. Currently, a number of facilities are operating on this scheme basis. These are: IPNS, Argonne laboratory; KENS, Institute of High-energy physics, Tsucuba, Japan; ISIS, Rutherford laboratory. In another scheme the proton storage ring with the single-turn ejection is used to compress linear accelerators macropulsis to short proton bursts on the neutron target /10/. This scheme is used in the following facilities: LANSCE, Los-Alamos; MMF-0,6, INR USSR Ac. of Sc. (in construction); SNQ, Julich (project); KENS-II, KEK, Tsucuba (project). High-energy protons from high-current synchrotrons of tens GeV - kaon factories being projected in a number of laboratories (Los Alamos, KEK, TRIUMF, INR Ac. of Sc. USSR), are of special interest. Some time ago R.R.Vilson suggested to use the spallation process based on high-energy protons for electro-nuclear breeding - the nuclear fuel production on the accelerators /12/. However, the energy losses, associated with the electron-photon showers in the target matter, initiated by π^0-mesons, cause 1.5-2 times decrease in nuclear fuel yield for proton energy unit, compared with 1.5 GeV protons. Therefore the high-energy protons use for electrobreeding looks rather doubtful. This circumstance is not so important for creating intensive pulse neutron sources /13/.

The neutron source facility of INR meson factory (Figs. 1, 2) /14/ involves the pulse neutron source for the beam time-of-flight experiments, time-moderation lead spectrometer, the quasi-stationary source of thermal and cold neutrons for the studies with time selection of fast neutrons background, the proton beam dump with channels, which allow one to carry out radiation studies and to produce radionuclides in proton and neutron fluxes.

The pulse neutron source includes the array of uranium rods, covered with stainless steel and cooled by water (Fig.3). For full proton current (500 μA), the heat release in the target reaches about 1 MW. During the first research stage it is planned to use metal tungsten, formed as an array of plates. The target is

adjoined by water and liquid-hydrogen moderators, "radiating" into the biological shield channels. The possibility to use the multiplicating target made of U-235 with the limited multiplication (up to about 20) for thermal and cold neutron studies is under investigation /15/. The channels of 200 mm diameter allow one to set collimators, providing the required experiment geometry. The channels come through the vertical wells on the distance of about 4.5 m from the target; wells are intended for the experimental equipment. The channels are equipped by the guillotine-type gates. The external neutron channels going through the neutron experimental hall, provide the flight path up to 500 m long.

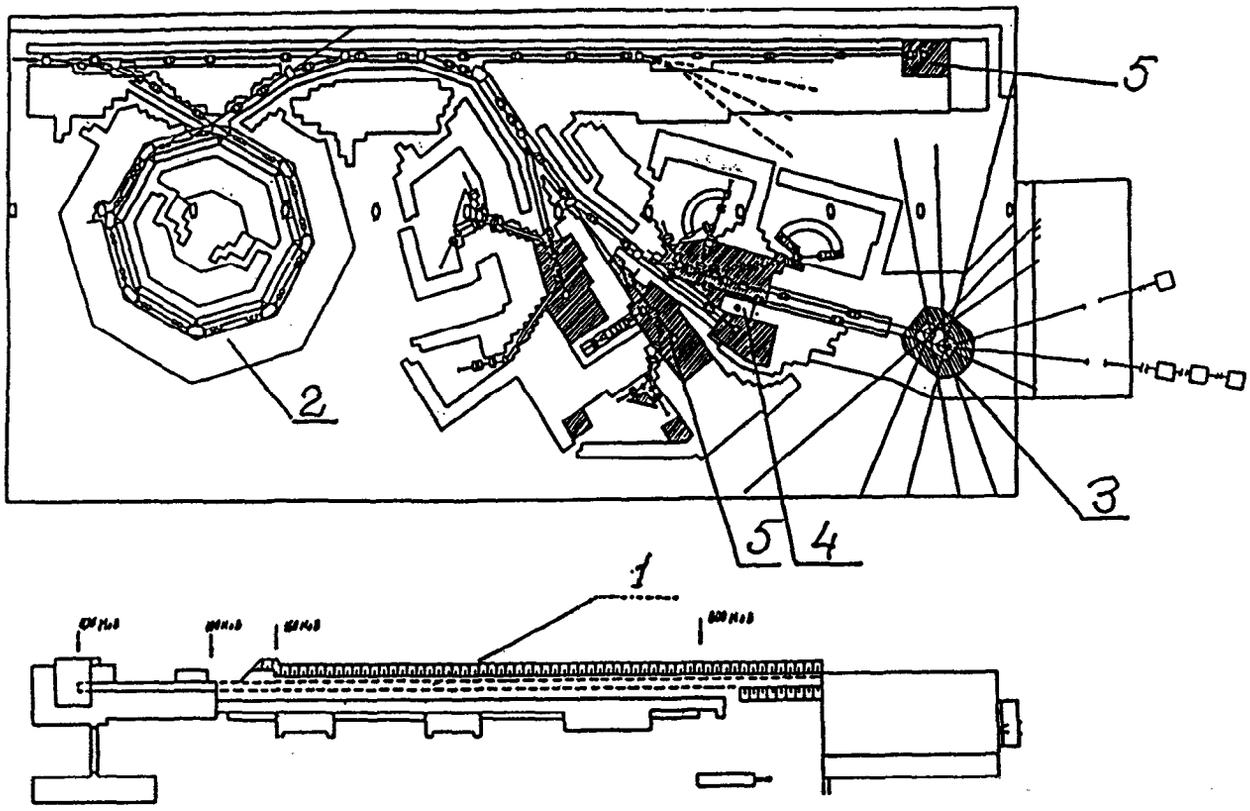

Fig. 1. Linear proton accelerator and experimental area of the Moscow meson factory. 1. Linear proton accelerator. 2. Proton storage ring. 3. Pulse and quasistationary neutron sources. 4. Time-moderation neutron lead spectrometer. 5. Proton beam dumps.

The proton current time structure in the accelerator is a sequence of 100 μs pulses following with the repetition rate 100 pps. To decrease the neutron pulse width up to 0.5-30 μs the beam interruption system after the ion source is used (with the corresponding intensity loss), or the proton storage ring with the charge-exchange injection of H^- ions and the single-turn proton ejection onto the pulse neutron source target /16/. The storage ring allows one to form proton and, correspondingly, neutron pulses about 300 ns long almost without any intensity losses, and more

short pulses with the according intensity loss.

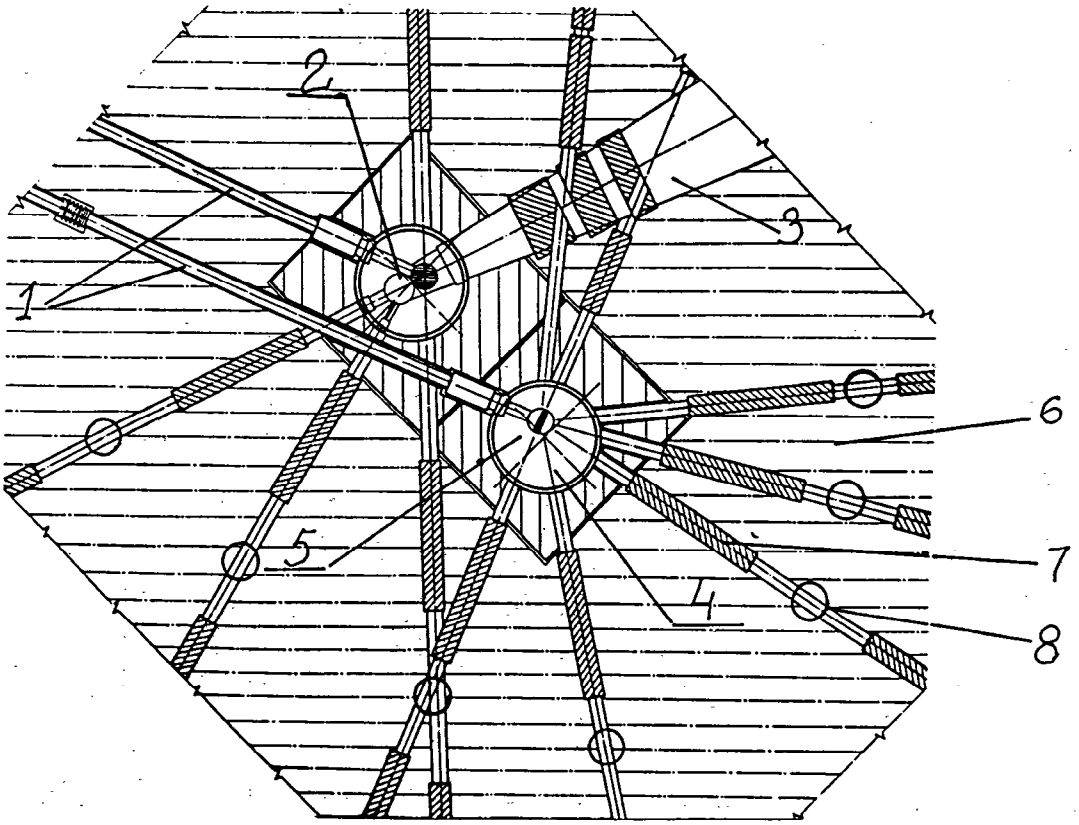

Fig. 2. Central part of the neutron facility.
1. Proton beams. 2. Heavy-water moderator with liquid-deuterium vessel. 3. Channel of n – $\tilde{n}$ experiment. 4. Vacuum vessel of the pulse neutron source. 5. Heat shield. 6. Biological shield. 7. Horizontal channels with gates. 8. Vertical wells.

The pulse neutron source allows one to develop a wide range of studies on nuclear reactions properties /11/. Particularly, the studies on the space parity violation problem in neutron reactions in the separated resonances with the help of wide-aperture neutron polarizer are planned. The high neutron source intensity will allow one to study the partial processes in the separated resonances and to obtain such phenomena detalization, which has been possible up to now only in thermal neutron experiments or in total cross-section measurement (gamma-ray spectra of neutron capture, the fission process studies, including the oriented nuclei targets and polarized neutrons, the studies on n,p- and n,α- reactions in the separated resonances of known nature etc.).

The interesting possibilities are opened by using time-moderating lead spectrometer /17/, based on grouped proton beam, which allow one to study some "low-background" processes (fission, n,p- and n,α-reactions, for example) at high intensity. For example, heavy nuclei fission cross-section measurements could

be carried out on 10^{-11} to 10^{-12} gram samples.

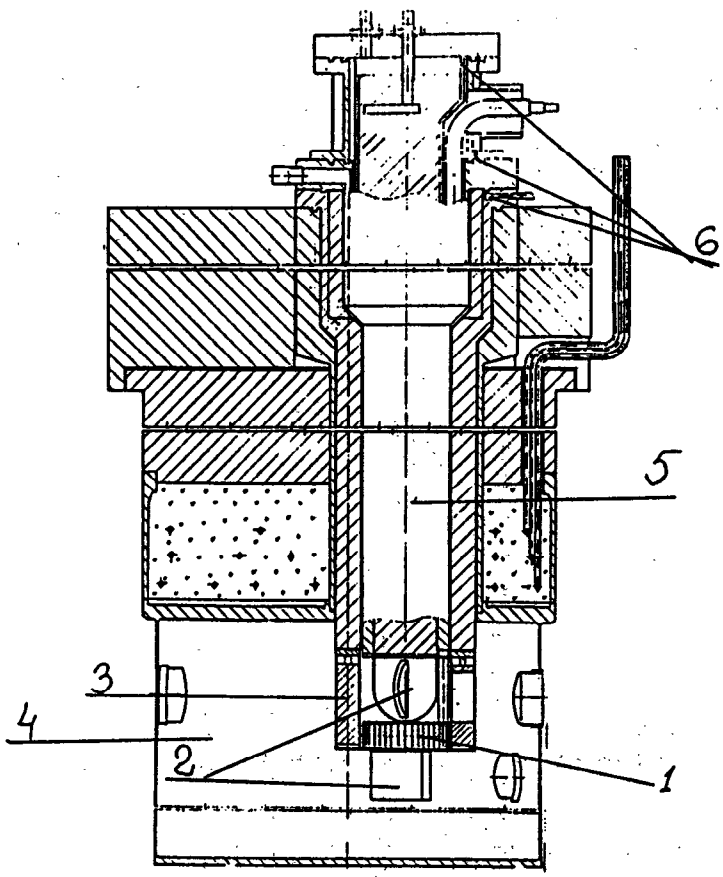

Fig. 3. Pulse neutron source.
1.Neutron target. 2. Moderators. 3. Moderator's reflector. 4. Vacuum vessel. 5. Shielding plug. 6. Vacuum seal.

The pulse neutron source will allow one to expand sufficiently a potential of experimental studies on solid state physics. The high pulse and average densities of thermal and cold neutrons allow one to perform experiments with luminosity considerably exceeding that of stationary and pulse reactors. The measurements of dispersion relationships for elastic coherent thermal neutron scattering with the help of time-of-flight spectrometer with the inverse geometry were considered as an example. The calculations showed /18/ the total luminosity to be several tens times higher, than that for three-crystal spectrometer on high-flux research reactor ILL (Grenoble).

Short neutron pulses in the electron-volt region will open unique possibilities for the high-energy phonon and electron excitation spectroscopy.

The quasi-stationary source of thermal and cold neutrons includes the water-cooled target in the form of assembly of natural-uranium or lead rods, covered with stainless steel surrounded by heavy water moderator of about 1.6 m diameter. The

liquid deuterium moderator allows one to obtain a cold neutron flux of 10^{16} n/s in the wide-apperture channel. If the liquid-deuterium moderator is removed the through channel is formed in the heavy-water. Small intensity between pulses from delayed neutrons (about 2% for uranium target and 0.2% for the tungsten one), the time selection of events, caused by epithermal neutrons, opens way for such fundamental experiments as the search for neutron - antineutron oscillations, predicted in some versions of the Grand Unification theory /19/, and with the through channel application - the experiment on direct measurement of neutron - neutron scattering length /20/, which is of fundamental interest of examination of isotopic invariancy of the nucleon-nucleon interaction.

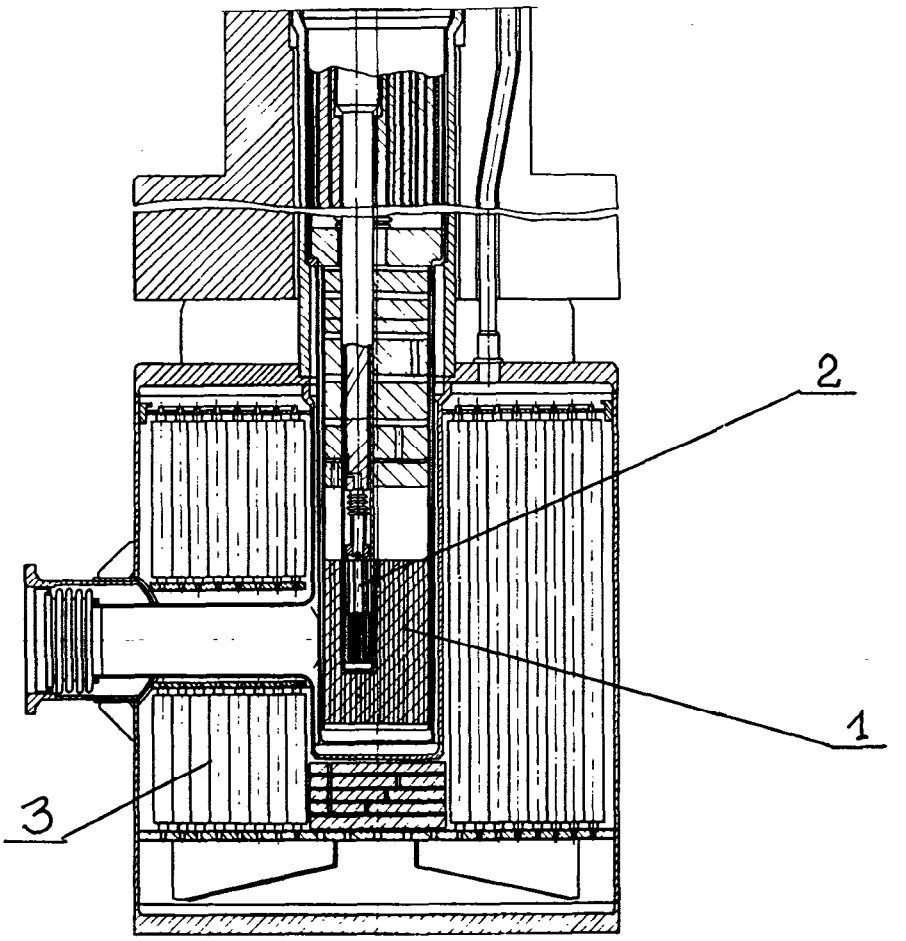

Fig. 4. Proton beam dump. 1. Tungsten plate assembly. 2. Vertical channel. 3. Iron-water heat shield.

Proton beam-dumps are positioned in proton beams, which go through the meson targets, cooled by water, and have a vertical channel, allowing samples for radiation physics studies to be inserted. The high fluxes of fast neutrons and protons, being inside the beam dump, open a unique possibility for studies of the

behavior of construction materials of atomic reactors and thermo-nuclear fusion devices. The calculations showed that the density of fast neutrons flux inside the tungsten beam-dump is about $4 \cdot 10^{14}$ $n/s \cdot cm^2$ per 1 mA current /21/. Ratio of atomic displacements number to (n,α) reactions number is approximately the same as for neutron spectrum on the 1st wall of thermonuclear fusion facilities (Figs. 5, 6, 7).

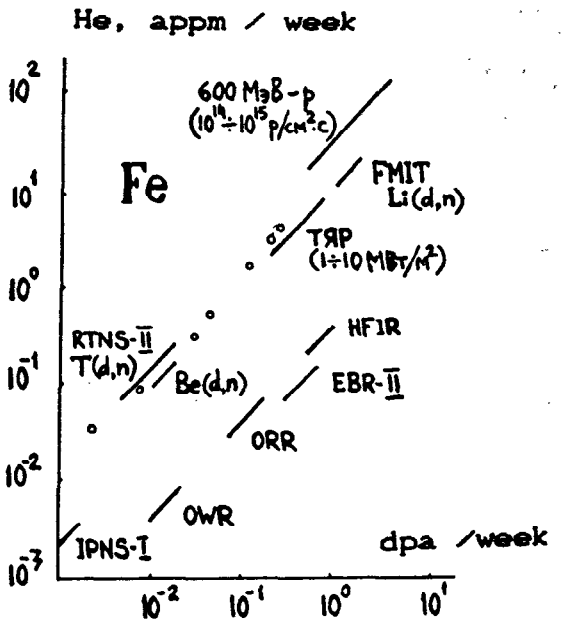

Fig. 5.

The kaon factory on the base of high-current 45 GeV - proton synchrotron with 7.5 GeV booster that is under design in INR AS USSR /22/, /23/ will use the proton linac of the Moscow meson factory as an injector. As the evaluation shows the one-turn ejection of protons from the synchrotron onto the neutron target gives the possibility to create the pulse neutron source with the average neutron intensity nearly the same as for the 15 MW reactor and with the peak thermal neutrons flux density about of 10^{18} $n/cm^2 \cdot s$. Spallation neutrons pulse duration depends on the revolution time of protons in the synchrotron and will be 1.3 μs for the beam extraction from the booster and 4.4 μs - from the main ring. Thus the pulse neutron source based on the kaon factory is of great interest for research with cold, thermal and epithermal neutrons (up to several eV, mostly for solid state physics). This neutron source, if constructed, will be used for the solid state physics research, while the neutron source with short pulses based on the Moscow meson factory (MMF-0,6) will be used mostly for research in nuclear physics.

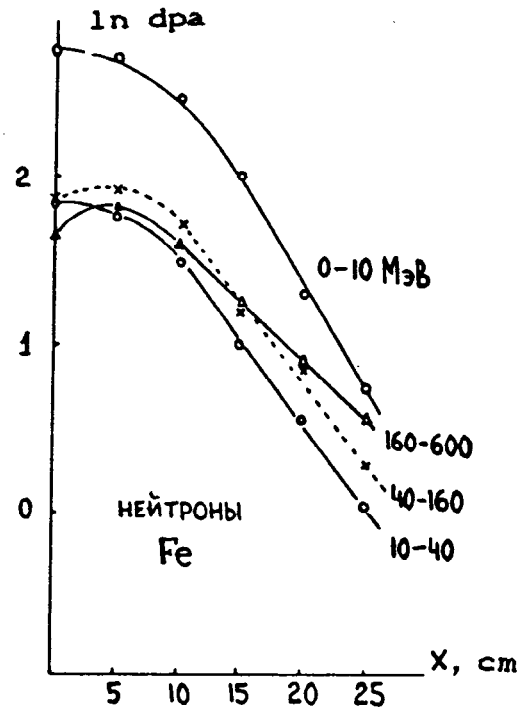

Fig. 6. Relative contribution of various energy groups neutrons to the iron damage.

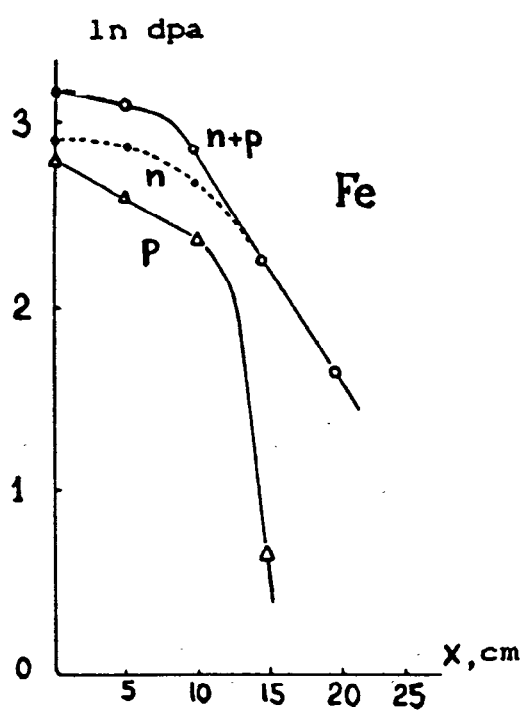

Fig. 7. Relative contribution of neutrons and protons to the iron damage.

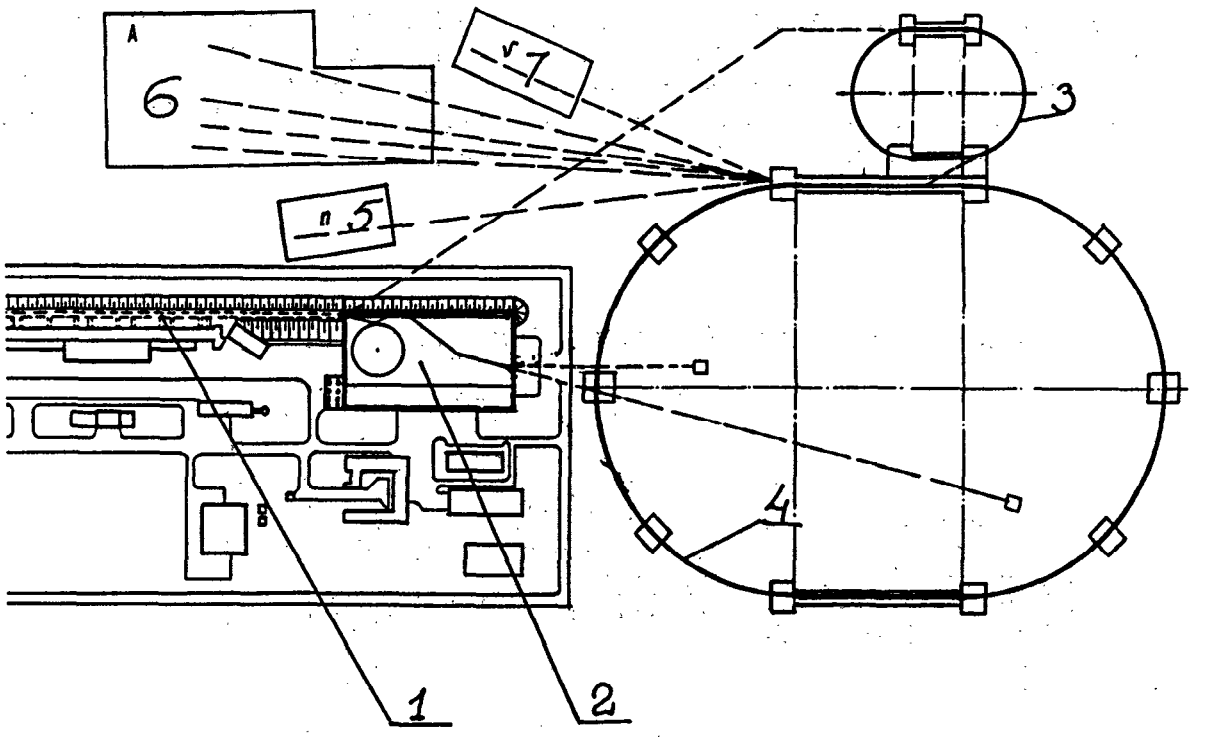

Fig.8. Scheme of the Kaon factory INR USSR Academy of Sciences.
1. Linear proton accelerator. 2. Meson factory experimental area. 3. 7.5 GeV booster. 4. 45 GeV main ring. 5. Neutron source experimental area. 6. Hadron experimental area. 7. Neutrino experimental area.

Since there were no experimental data on the neutron yield in heavy targets for proton energy greater than 7 GeV, the data on the energy balance in ionization calorimeters obtained in cosmic rays experiments /13,24/ were used for primary evaluation of spallation neutrons yield. Hadron cascade computations carried out by Monte-Carlo program SHIELD /25/ later gave similar results.

The results, obtained in the recent experiment carried out on the 70 GeV proton beam of the accelerator in IPHE (Serpuchow) /27/, are in good agreement with previous computational evaluations.

The scheme of the experimental hall of the pulse neutron source is presented in Fig. 9. The neutron source /26/ is surrounded by radiation shield consisting of iron and heavy concrete. The shield thickness in lateral direction is determined by cascade neutrons and in forward direction – by muons. The neutron target represents the compact assembly of tungsten rods cooled by water and has dimensions 40*40*16 cm^3. The target is placed inside the vertical ampoule and adjoined by liquid hydrogen and water moderators. The beam dump provided with the inner vertical and outer through horizontal channels used for experiments in inner thermal neutron fluxes (Fig. 10) is located behind the target, in the analogous ampoule. The target and beam dump are

surrounded by the reflector (made of iron-nickel alloy or beryllium). If the 45 GeV proton beam with the current 125 μA and dispersion 6.7*1.3 cm^2 (90% of protons hits the target) is directed onto the target, average heat release in the target will be 2.5 MW, average temperature in the center of tungsten rod ≈ 150 °C, maximum heating up of tungsten ≈ 60 °C per pulse at 8.3 pps.

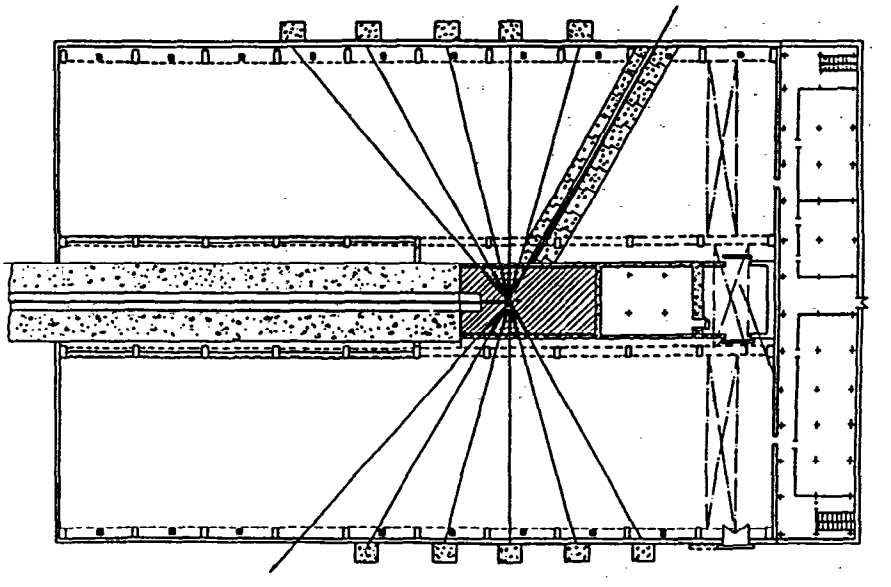

Fig. 9. Experimental area of SIN - 45.

The results of computations of hadron cascade in the target and reflector carried out by the Monte-Carlo program SHIELD for 25 GeV protons were linearly extrapolated to 45 GeV taking experimental data /27/ into account. Neutron transport calculation for energies below 10.5 MeV was carried out using the neutron data system BNAB - 64 /28/. At 8.3 pps the peak neutron flux density is about $7 \cdot 10^{17}$ $n/cm^2 \cdot s$ and time average one - $2 \cdot 10^{14}$ $n/cm^2 \cdot s$.

Operability of the neutron source depends essentially on radiation damage rate of it's main components. The comparative data on radiation damage of the first wall of neutron sources SIN-45, MMF-0.6 and thermonuclear reactor (thermal load on the first wall 1 MW/m^2) are presented in Table 1. Radiation damage computations were carried out using efficient crossections of defect production /21/.

The value of K_{dpa} 9 dpa/year corresponds to fast neutron fluence 10^{22} n/cm^2. Material properties changes are expected to be small enough at that dose.

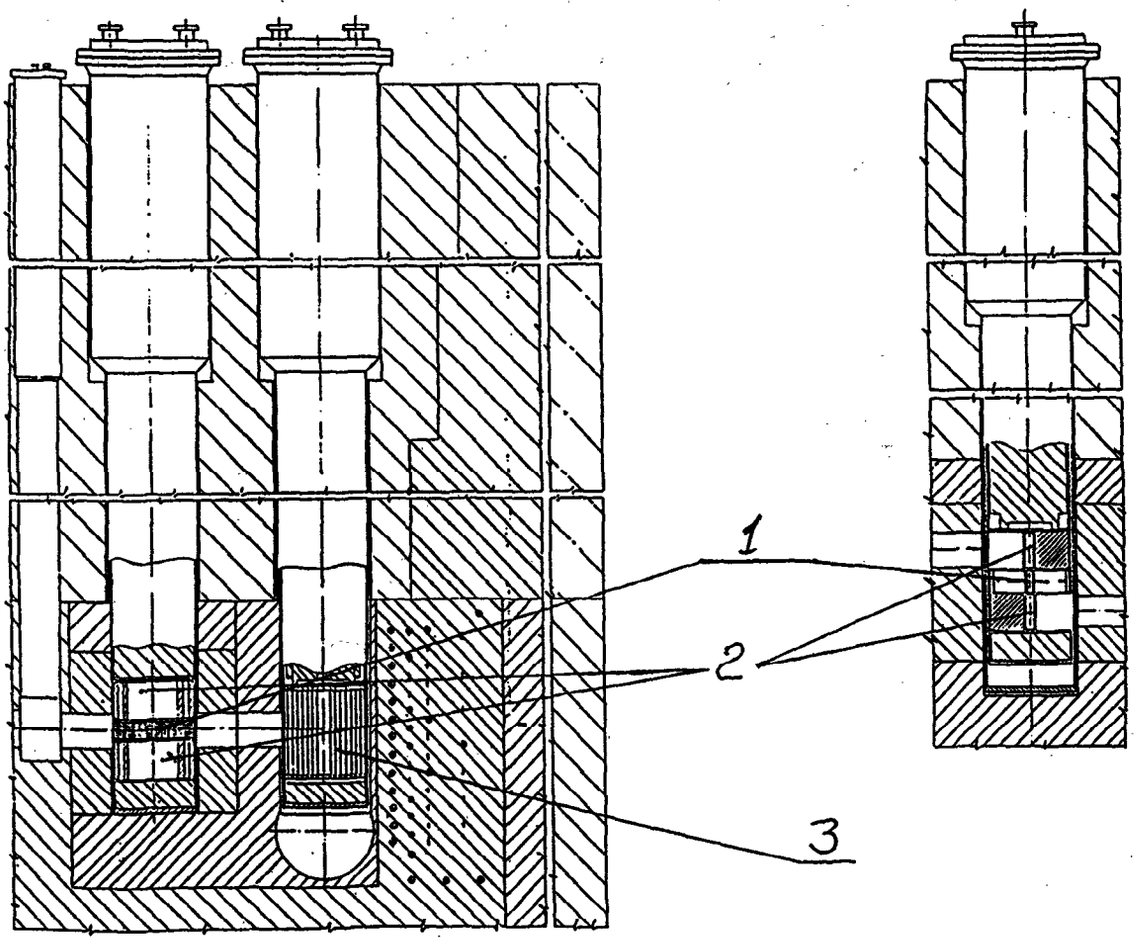

Fig. 10. Target-beam-dump device of SIN-45. 1. Tungsten target. 2. Moderators (H_2 and H_2O). 3. Beam dump.

Table 1.

system	material	damage rate dpa/year	helium prod.rate appm $\cdot 10^{-6}$/year	He/dpa $\cdot 10^{-6}$
SIN-45	Al	27	370	14
	Fe	9	430	48
	W	6	750	130
MMP-0.6	Fe	13	220	17
Fusion	Fe	14	150	11

The main parameters of pulse neutron sources MMF-0.6 and

SIN-45 in comparison with other pulse neutron sources are presented in Table 2. To compare the sources MMF-0.6 target - moderator geometry and figure-of-merit criterion $K=\bar{\Phi}_T/\theta_T^2$ were used, where $\bar{\Phi}_T$ -average thermal neutron flux density on the moderator surface, θ_T - thermal neutron pulse duration.

Table 2.

system	proton energy, GeV	θ_p, μs	f, pps	$\bar{\phi}_T$, n/cm^2·s	$\hat{\phi}_T$, n/cm^2·s	$\frac{\bar{\phi}_T}{\theta_T^2}$, r.u.	note
INI	0.5	0.01	10	$1.6\cdot10^{10}$	$3\cdot10^{13}$	0.01	project 1964
KENS	0.5	0.01	15	$4.4\cdot10^{10}$	$5\cdot10^{14}$	0.24	oper.
KENS-II	1.0	0.2	50	$2.0\cdot10^{13}$	$7\cdot10^{15}$	11	project
IPNS	0.5	0.01	30	$5.6\cdot10^{11}$	$3\cdot10^{14}$	0.3	oper.
LANSCE	0.8	0.1	12	$8.0\cdot10^{12}$	$1.1\cdot10^{16}$	4.2	oper.
IBR-2	f, 4 MW	100	5	$2.2\cdot10^{13}$	$3.5\cdot10^{16}$	1	oper.
ASPUN	1.6	0.5	60	$2.8\cdot10^{14}$	$8\cdot10^{16}$	250	project
MMP-0.6	0.6 (20)	0.3 (1)	100 (30)	$2.8\cdot10^{13}$	$5\cdot10^{15}$	15 (45)	constr.
ISIS	0.8	0.2	50	$1.4\cdot10^{13}$	$5\cdot10^{15}$	7.5	oper.
SIN-45	45 7.5	4.4 1.3	8.3 50	$2.0\cdot10^{14}$ $7.0\cdot10^{13}$	$7\cdot10^{17}$ $4.3\cdot10^{16}$	110 38	project

In conclusion I would like to express my best acknowledgements to M.A.Markov, Yu.A.Osipian, V.A.Matveev, V.M.Lobashev, M.I.Grachev S.F.Sidorkin, N.V.Kolmichkov, M.N.Ospanov, V.G.Miroschnichenko for useful discussions and collaboration.

References

1. Bartolomew G.A., Milton Y.C.D., Vogt E.W., Rep. AECL 2059, 1964.
2. Bolshov V.J. et al., At. Energy, v. 28, p.388, 1970, in Russian.
3. Bauer G., Proceedings of INES-89, Moscow, USSR, 1989.
4. Bondarenko J.J., Stavissky Yu.Ya., At. Energy, v.7, p.417, 1959, in Russian.
5. Ananiev V.D., Kozlov J.A. et al., Preprint JINR, P3-85-187,

Dubna, 1985, in Russian.
6. Konoplev K.A., Petrov Yu.V. et al., Preprint LINP, No. 376, Leningrad, 1977, in Russian.
7. Alvarez L., Rev. Sc. Instr. v. 22, 705 L, 1951.
8. Budker G.I., Dimov A.M. et al, At. Energy, v. 19, 507, 1965, in Russian.
9. Stavissky Yu.Ya. Proceedings of the seminar "Research program for meson factory", INR USSR Academy of Sciences, p. 57, Moscow, 1979, in Russian.
10. Vasiliev A.A., Mescherov R.A., Murin B.P., Stavissky Yu.Ya., US Patent 1975 3.860.828, filed aug. 30, 1972.
11. Stavissky Yu.Ya., Nuclear Energy No. 25, Bulgar Academy of Sciences, Sofia, 1987, in Russian.
12. Wilson R.R. Preprint FNAL FN-298, 1986.
13. Stavissky Yu.Ya. Preprint INR USSR Academy of Sciences, P-0215, Moscow, 1981, in Russian.
14. Bulkin Yu.M. et al. Proc. of the Conf. on Neutr. Scatt. in 90, Juelich, 1985, in Russian.
15. Miroschnichenko V.G. et al., Proceedings of INES-89, Moscow, USSR, 1989, in Russian.
16. Grachev M.I. et al., Proc. of XIII Conf. on High Energy Acc., Novosibirsk, 1987.
17. Kasarnovsky M.V. et al. Proceedings of INES-89, Moscow, USSR, 1989, in Russian.
18. Dumesh B.S., Kolmichkov N.V. et al. Preprint INR USSR Academy of Sciences, Moscow, 1982, in Russian.
19. Ilinov A.S., Kusmin V.A., Stavissky Yu.Ya. et al. Preprint INR USSR Academy of Sciences, P-0278, Moscow, 1983, in Russian.
20 Kasarnovsky M.V. et al. Proceedings of INES-89, Moscow, USSR, 1989, in Russian.
21. Boryskin S.E. et al. Preprint INR USSR Academy of Sciences, P-0431, Moscow, 1985, in Russian.
22. Laptev V.D., Matveev V.A., Stavissky Yu.Ya. Science on the Kaon Factory, Proc. of workshop, 1990, TRIUMF, Vancuver, Canada.
23. Chursin A.G., Matveev V.A., Senichev Yu.V. et al., Proc. of Advansed Hadron Facility Acc. Design Workshop, Los-Alamos, 1989.
24. Mursin V.S., Saricheva L.J. Multiproduction processes at High Energy, Atomisdat, Moscow, 1974, in Russian.
25. Sobolevsky N.M., Preprint JINR B-1-2-5458, Dubna, 1970, in Russian.
26. Boriskin S.E. et al., Preprint INR USSR Academy of Sciences P-0638, Moscow, 1989, in Russian.
27. Akopian A.G., Kolmichkov N.V., Kusin A.V., This meeting.
28. Abagian L.P., Nikolaev M.N. et al, Group constant for nuclear reactors computations, Atomizdat, Moscow, 1964, in Russian.

ICANS-XI International Collaboration on Advanced Neutron Sources
KEK, Tsukuba, October 22-26, 1990

PULSED NEUTRON SOURCES AT KAON

I.M. Thorson, P.A. Egelstaff* and M.K. Craddock
TRIUMF, 4004 Wesbrook Mall, Vancouver, B.C. V6T 2A3

ABSTRACT

The proposed KAON Factory facility at TRIUMF consists of a number of synchrotrons and storage rings which offer proton beams of energies between 0.45 and 30 GeV with varying pulse amplitudes, widths and repetition rates. Various possibilities for feeding these beams to a pulsed neutron facility and their potential for future development are examined. The incremental cost of such a pulsed neutron facility is estimated approximately.

I. INTRODUCTION

During the past ten years countries involved in major neutron scattering programs (e.g. U.S.A., U.K. and Japan) have developed pulsed neutron sources based on high intensity proton accelerators. These sources offer the neutron scattering communities in these countries, the opportunity to build programs of research in new areas of science, and to both extend and complement their existing programs on reactor sources. After several years of development the new pulsed sources are operating on a reliable, continuous basis and many neutron spectrometers are in operation at each one. Other countries are becoming interested in this field also. For example the U.S.S.R. is considering several possible pulsed neutron sources based on the Moscow Meson Factory. Canada has played an important role in the development of neutron scattering but, because of its limited resources, has limited its efforts to focused programs at its two reactor sources (NRU and MNR). The advent of the KAON Factory proposal at Vancouver offers Canada the opportunity to bring about a diversification of its neutron scattering program at a reasonable cost ($\leq$\$50 M), by building a modern pulsed neutron facility. This diversification would occur in three significant categories, geographical location, kinds of neutron scattering instruments and areas of science investigated. The object of this paper is to discuss the possible kinds of pulsed neutron sources which may be built in conjunction with the KAON Factory, and to recommend a choice which is economically and technically viable, and which is competitive in some respects with other pulsed sources and with Canada's reactor source program.

The basic KAON facility proposal has not changed substantially since the previous report to ICANS[1]. The recent Project Definition Study (PDS) funded by the Canadian federal and British Columbia provincial governments has established more detailed specifications and cost estimates for the various components of the facility. At the request of the Canadian Institute for Neutron Scattering an examination was recently undertaken at TRIUMF[2] of the incremental accelerator and target/moderator components required to achieve a compet-

*Present address University of Guelph, Guelph, Ontario

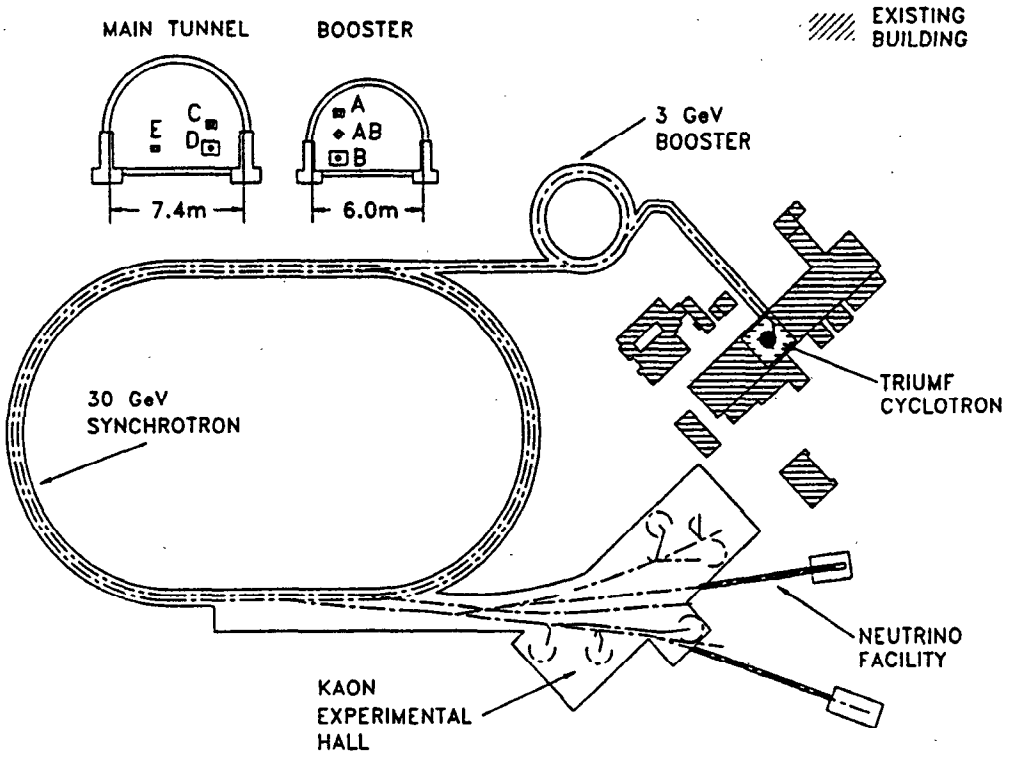

Fig. 1. The KAON facility layout following the 1989/90 project definition study.

itive pulsed neutron facility. The possibilities and requirements for simultaneous intensity optimization for both peak and integral flux beams from a single target/moderator were also addressed in reference 2 and elaborated in a later submission[3] to this meeting.

The facility layout resulting from the PDS is shown in Fig. 1. This layout takes into account the constraints of the site and others related to design contingencies and future expansion possibilities. Figure 1 shows the race-track configuration for the main rings which allows more space in the straight sections for beam conditioning and transfer elements. This layout has more possibilities for "add-ons" such as a pulsed neutron facility (PNF).

No experimental area from the intermediate energy (3 GeV) stage is currently included in the KAON plan although a 3 GeV beam could be available a year ahead of any 30 GeV staged operation. The construction schedule for the KAON project is very compressed. Only about 20 months is allowed from approval-in-principle to the beginning of the construction of the Booster tunnel and building; thus, any decisions about contingency provisions for adding a neutron facility, or any other 3 GeV facilities, without impacting other construction and installation work will need to be made early in that period.

In Section 2 we describe the components currently included in the revised KAON proposal following the PDS and enumerate the possible accelerator options and limited neutron facility possibilities within the presently planned KAON facilities and housing. Section 3 outlines the experimental hall, transfer line and target/moderator/shield assembly requirements for a dedicated add-on pulsed neutron facility. Section 4 defines the medium term developmental options that would be required to up-grade the facilities from Section 3 to a competitive world-class facility. Finally in Section 5 we discuss conclusions and some recommendations.

II. PRESENT KAON FACILITIES

A Accelerators and Beam Storage Rings

The KAON facility complex consists of two synchrotron accelerators and three proton beam storage rings as well as the present TRIUMF cyclotron used as a beam injector. The syn-

chrotrons, being pulsed accelerators, require accumulation of the cw beam from the cyclotron in a storage ring, called the A ring or Accumulator, for approximately 20 ms; this ring has a circumference of 215 m and a circulation period for the 450 MeV protons of 0.85 μs. At the end of the accumulation cycle the beam is transferred, in one turn, to the Booster synchrotron, or B ring, of the same circumference, where it is accelerated in the next cycle to 3 GeV intermediate energy; the increased proton velocity shortens the circulation time for the protons to 0.65 μs. At the end of this cycle the beam from the Booster is transferred, again in one turn, to the Collector storage (C) ring that is 5 times as long as the A and B rings. The A and B rings operate continuously with a 50 Hz repetition rate accepting beam essentially continuously from the cyclotron at a design current of 100 μA. Five successive pulses from the B ring fill the C ring; every 100 ms the content of the C ring is transferred to the D ring, the Driver synchrotron, that accelerates it on the next 10 Hz cycle to the final 30 GeV energy. At the end of that cycle the beam is transferred in one turn (3.5 μs) to either a pulsed beam line such as the neutrino experimental facility or to the Extender storage (E) ring. The circulating beam in the E ring is continuously "spilled" over the next 10 Hz cycle into the slow extraction beam lines for bombardment of the meson production targets for experiments requiring continuous beams.

The pulsed neutron possibilities at KAON are summarized in Table 1 in order of increasing additional requirements beyond the basic KAON facility. Lacking any experimental facilities for the 3 GeV beams the only "parasitic" possibility is associated with the 30 GeV neutrino facility. The plans for the facility are still in the conceptual design stage. The single-pulse intensity would be higher than that from any presently available pulsed neutron facility but at 30 GeV is far beyond the optimum energy. The energy could be reduced to the 3 GeV coming from the C-ring without substantial loss of intensity and only marginal (~3%) lengthening of the pulse length if this solved any background problems commensurate with the priority of the experiments. It would probably require a separate, but fairly modest, extraction system from the D ring to accommodate the larger beam emittance on injection to, compared to extraction from the D-ring after the acceleration cycle. The big disadvantage would, however, be the competition for beam time that reversion from parasitic to priority status of the neutron facility operations would entail.

Table 1
Pulsed Neutron Possibilities at KAON

Proton Charge per Pulse μC	Pulse Length μs	Repetition Rate Hz	Proton Energy GeV	KAON Rings Required	Target Station Location	Additional Accelerator and Transfer Line Components Required	TRI-DN-K137 Option
10	3.6	$\leq$10	3–30	A,B,C,D	KEH*	***	1,3
2	0.65–0.85	$\leq$50	0.5–3	A,B	NEH**	Beam Line BC to NEH	2,4
2	0.85	$\leq$50	0.45	A	NEH	Beam Line AB to NEH	5
10	0.4	$\leq$10	0.45–1	A	NEH	New Booster/ Compressor Ring	6
>10	$\leq$0.4	$\leq$10	~1	–	NEH	+ New KAON Injector	7

* KEH – KAON Experimental Hall, associated with neutrino facility
** NEH – Neutron Experimental Hall, additional to KAON
*** Nothing for 30 GeV; may need larger extraction line from D-ring for 3 GeV.

The options defined in the first line of Table 1 are the only ones that would not require a separate experimental hall with the advantage in cost savings and disadvantage in competition for

space in the presently envisaged KAON experimental hall that would accrue. The combined neutrino/neutron facility, however, could be moved to a dedicated experimental hall if the interest warranted the increased scope for the project. The options listed in the last four lines of Table 1 all involve beams from the KAON project at 3 GeV or less. Thus, lacking any experimental facilities associated with such beams, any neutron facilities would require an additional experimental hall as discussed below. The options in line 2 involve extraction of full beam pulses from the complete or truncated acceleration cycles in the Booster synchrotron. Extraction of beam at energies below 3 GeV would probably require larger but only modestly more expensive extraction system components, again because of the larger beam emittance at lower energies. The 2 μC single pulse is limited by the charge holding capacity of the A ring and the B ring at injection so that reduction in the 50 Hz repetition rate, which can probably be done on a pulse-to-pulse program control, would reduce time-integral intensity to both the neutron production and kaon production by complementary amounts.
The third line in Table 1 shows the most interesting possibility that would have very modest incremental accelerator requirements for a useful pulsed neutron facility. The option depends on the fact that charge holding capacity of the A-ring is limited by phase space consideration and does not depend, to first order at least, on the filling rate of the fixed-field ring. The injected current required from the cyclotron and the irreducible, absolute losses will of course be proportional to the total current to both the KAON facility and a PNF. The incremental cost associated with increasing the TRIUMF cyclotron current to 250 μA, dissipating the additional beam in beam dumps and increasing the repetition rate of the A-ring extraction system by a factor 2 is expected to be in the $5M range. In principle the repetition rate of the A ring could be increased further to say 150 or 200 Hz but the necessary intensity available from the cyclotron becomes more problematic and the frame-overlap problems greater, unless the extracted beam from the A ring is fed to further accumulation stages.
Based on a linear interpolation of the neutron yield above an effective energy threshold of 100 MeV, which fits the available data within their probable errors, the neutron yield from 450 MeV protons from the A ring on high mass targets would be one-half that at the near optimum 800 MeV of the existing ISIS and LANSCE facilities. The 0.85 μs pulse length does not degrade the thermal neutron pulse length or peak intensity significantly. The root-mean-square deviation on the thermalization time from the mean of a 0.85 μs wide square wave is 0.25 μs which broadens the 1.0 μs standard deviation for 2 MeV neutrons slowing to 1 eV in hydrogenous moderators by only 3%; at 10 eV the relative increase is about 30%. Of course, neutron conservation indicates peak intensities inversely proportional to pulse width.
The last two lines on Table 1 show options with much greater cost and potential for satisfying future pulsed neutron facility requirements. Line 4 shows the possibility of increasing the pulse charge by accumulation of say five 2 μC pulses from the A ring in a new booster-compressor ring of the same circumference, in which they would the be accelerated to 1 GeV and compressed to 0.4 μs. The design and development of such a facility appears to be feasible but would not be trivial and is estimated very roughly (and conservatively) to cost the order of $50M. Line 5 of Table 1 shows the possibility that the KAON project might at some time in the future develop an alternative injector; this would then open up other possibilities based probably on high-current linear accelerators and storage rings that might have spare capacity at modest incremental costs for feeding a pulsed neutron facility. The total cost for such an advanced facility would likely be in $100 M range, however.

B Pulsed Neutron Facilities in KAON Experimental Hall

As indicated above, the plans for the neutrino facility at KAON are still in the conceptual design stage. It consists of an optimal thickness meson production target followed in the forward direction by a long (~100 m) flight path for their decay into muons and μ-neutrinos. Because the meson (pions, kaons, etc.) mean-free-paths are longer (by 30 to 100%) than

for the incident protons approximately 70% of them suffer collisions in the primary beam targets. Previous neutrino experimental facilities have used multiple quadrupole or toroidal magnetic horn focusing systems placed immediately downbeam of the production targets to augment the "kinematic focusing" of the neutrino precursor mesons. Thus the basic target requirements for neutron and neutrino facilities are compatible but the competition for space in the immediate vicinity of the targets for moderators, target cooling and neutrino-precursor focusing devices is likely to vary from problematic to severe depending on design choices. These design requirements are overshadowed by the currently unresolved problems associated with radiation damage of the targets by pulsed, concentrated proton beams; they may well require uncontained liquid metal targets, unless the spot sizes required for neutrino-precursor production can be relaxed substantially.

The neutrino production target (but not the meson decay flight path, beam stop or neutrino detector) is currently planned to be in the KAON experimental hall, but not included in the initial installation. Thus the associated neutron facilities would compete for space outside the shielding but inside the hall with other KAON facilities.

III. INCREMENTAL REQUIREMENTS FOR A PNF AT KAON

A Transfer Beam Lines and Tunnels

The additional beam extraction components required for the options cited in Table 1 were mentioned briefly in their descriptions above. None of them requires additional components not already required for the KAON facility that are technically problematic or particularly expensive. They will be discussed further here only to the extent that they affect the possible site layout options and are constrained by accelerator/storage ring design considerations.

To minimize the cost of transfer beam lines to a pulsed neutron facility they should start at an intermediate point in the present A-B and B-C transfer lines between the rings, at the exit of a suitable dipole bending magnet. Because these transfer points in the present design are ~180 degrees apart the minimum cost transfer from both A and B rings cannot be obtained simultaneously, forcing an early selection for which option in Table 1 to optimize the layout. Although the injection and extraction points from the rings might be moved they have many soft and hard constraints. The second overall layout constraint for a pulsed neutron facility at KAON would be to leave enough space between the extraction point on the present facility and the experimental hall to install further stages of accumulation and/or acceleration of approximately the same size as the A/B-ring tunnels and tangential to the beam transfer line to the PNF hall. The layout shown in Fig. 2 satisfies these requirements for a beam from the A ring with only a modest perturbation of the reference site layout. A layout for a beam extracted at minimum cost from the B ring would require much more extensive modifications to the reference site layout but is not precluded at this stage.

Although the totals are smaller - roughly in proportion to primary beam energy above an effective 100 MeV threshold – the specific radioactivity induced in components would be the same order as those in the KAON production target areas. This provides an incentive for a layout that allows handling all such components by a common system. The layout shown in Fig. 2 does not, unfortunately, achieve that objective.

B Pulsed Neutron Facility and Hall

The only additional major components required for a pulsed neutron facility at KAON besides the beam transfer lines would be the target/moderator/shield assembly and the experimental hall to house them. Based on the PDS results the tunnels for single beam transfer lines will cost about $8K per metre and experimental halls approximately $2 K per square metre, the latter with basic services included. Thus a 75-m tunnel for a transfer beam line from the A/B ring and a 2,500 m^2 experimental hall would cost about $0.6M and $5M, respectively.

Table 2
Approximate costs of KAON PNF

	$M
Beam Transfer Line and Tunnel	1.6
Experimental Hall	5.0
Accelerator Modifications	5.0
Target/Moderators/Shielding	20.0
Total	31.6

The 100-m transfer beam line itself, as shown in Fig. 2, would cost about $1M, again based on PDS results. The largest component would be the target/moderator/shield assembly for a PNF. The capital cost of the ISIS target was £3.5M in 1979 UK£. Approximately one third of this total was for shielding which was recovered from within the laboratory and might therefore have had a considerably higher cost for new material, say double, making the effective true cost nearly £5M. At C$2=£1 the 1979 cost of reproducing the ISIS target would be approximately $10M; inflation since 1979 has probably doubled that price to $20M. The cost of an initial installation might be reduced considerably by using a simple molten lead target instead of the depleted uranium target at ISIS and fewer and less elaborate neutron beam gates and collimators, but at the price of a factor 2.3 loss of intensity beyond the factors of 2 for each of the reduced beam current and energy. The peak thermal neutron flux in a water moderator immediately following the 0.85 μs long, 2 μC pulse of 450 MeV protons on a lead target would be 6 x 10^{14} $cm^{-2}s^{-1}$, with a time integral over the 50 Hz repetition rate lower than that by a factor 100 in an "infinite" H_20 system[3]. The costs for an initial system are summarized in Table 2.

IV. FUTURE DEVELOPMENT POSSIBILITIES OF KAON

The least costly development for the improved performance of a PNF at KAON would be increasing the repetition frequency of the Accumulator ring beyond the factor 2 multiple of 50 Hz discussed above to, say, 150 or 200 Hz, and using the extra cycles to increase the repetition rate and hence the integral current to the PNF. This development would be much more interesting if it could be combined with a subsequent accumulation stage to increase the pulse size and reduce the PNF repetition rate. The limitation on how far this extrapolation of the A-ring frequency can be taken is expected to be set by gross beam spill limitations, in any of the cyclotron or the A or B rings. Because the beam from the cyclotron is extracted at 450 MeV the dominant spill mechanism, $\mathbf{v} \times \mathbf{B}$ electromagnetic stripping, is essentially eliminated leaving residual gas stripping of the H^- ions and space-charge induced emittance growth as the limitations. The present cyclotron limitation is estimated to be at approximately the 500 μA level although this must still be demonstrated within the additional constraint of restricting the longitudinal (phase) width of the micro pulses extracted from the cyclotron to the phase width capable of loss-free acceleration by the Booster synchrotron rf system operating at, basically, twice the frequency of the cyclotron system. Operation of the cyclotron at 500 μA and the A ring at 200 Hz would allow diversion of 300 μA to a PNF with a 75% duty factor, for the 1 in 4 pulses required to feed the Booster synchrotron. The only components in the A ring that would be under increased stress would be the extraction kicker magnets that would be required to operate at the increased frequency and the injection stripping foils that must operate at the higher current. The effects associated with the large number of turns collected in the A ring would, on the other hand, be relieved.
The addition of a further stage of accumulation and acceleration to an enhanced repetition rate A ring would put a KAON-based facility at the forefront of pulsed neutron facilities.

The option in line 4 of Table 1, cited above in II *A*, envisages a combined accumulator/accelerator/compressor in a single B′ ring of the same length as the A and B rings of the primary KAON facility. It would accumulate multiple – say five – 2μC pulses from the A ring; during the period when the A-ring was accumulating beam to feed to the B ring the B′ ring would accelerate its accumulated charge to 1 GeV and, possibly, compress the longitudinal 40 micro pulse beam structure using an auxillary rf system to shorten the extracted pulse length. Because the B′ ring would have the same lengths as the present A and B rings they should, if possible, share the same tunnel, avoiding the need for the second ring tunnel shown in Fig. 2.

Total beam intensities beyond the present design current of 200 μA of ISIS will require further neutron production target development to avoid the problems encountered with the present depleted uranium metal targets. Although they impose a factor of more than 2 loss in source strength, molten lead or lead-bismuth are expected to be more reliable and forgiving of transient conditions and radiation damage problems.

V. CONCLUSIONS

From the realization that there may be considerable spare capacity for accumulating 450 MeV protons in the A ring of the KAON accelerator complex the development of a pulsed neutron facility at TRIUMF must be taken as a serious possibility. A major advantage of using this starting point is the avoidance of competition with the rest of the KAON facility for beam time or intensity. It does, however, depend on adequate, increased intensity from the TRIUMF cyclotron in more restricted rf phase width than has been required for meson production. The determination of these capabilities and limitations of the TRIUMF cyclotron, required for confirmation of the KAON design in any case, should have a high

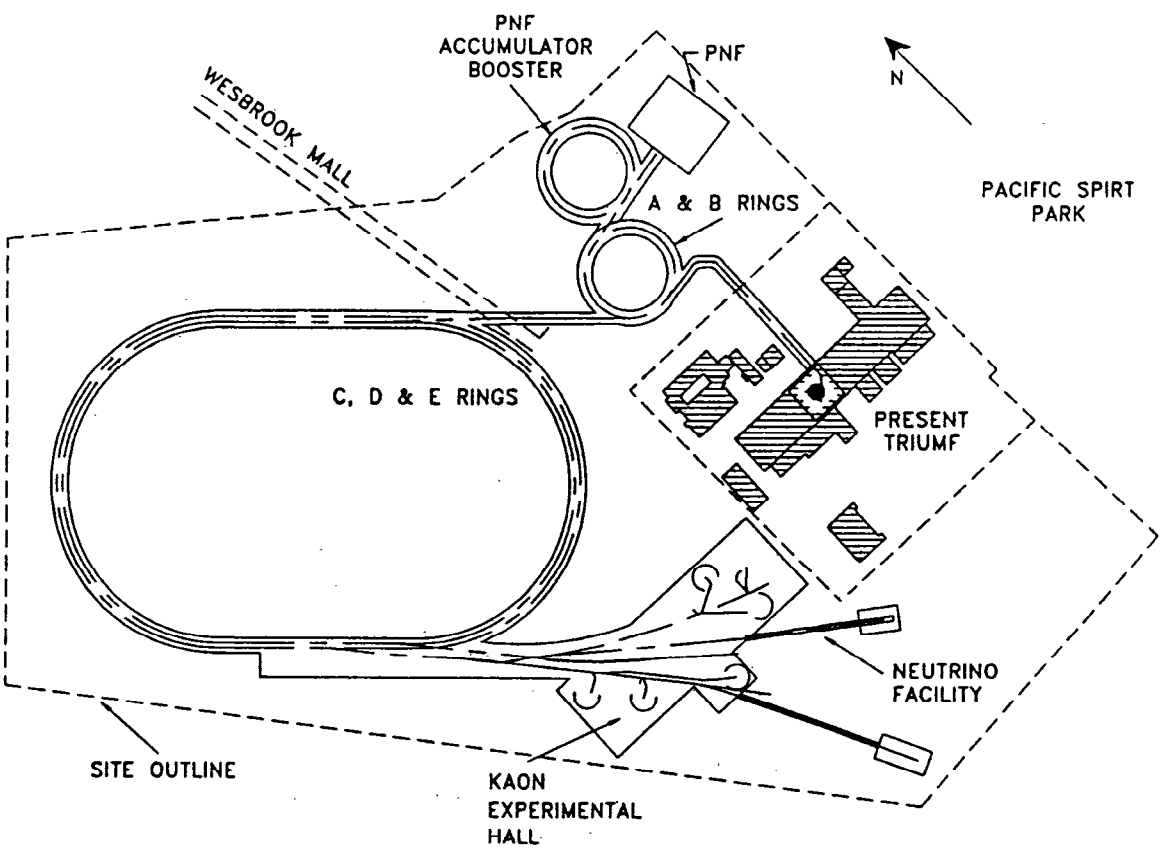

Fig. 2. The KAON layout including a possible pulsed neutron facility.

priority. If this determination is positive it would open the possibilities for the step-wise development of a competitive, world-class pulsed neutron facility that could attract national and international support and enhance Canadian neutron beam science.

The use of the full 100 μA, 3 GeV beam from the Booster synchrotron would have the advantage of increased intensity and 25% shorter pulse length compared to a facility based on direct delivery of the 0.45 GeV beam from the Accumulator. The total source strength for a 100 μA, 3 GeV proton beam on a lead target would be a factor $\sim$2 greater than that from the 200 μA, 0.8 GeV beam on the depleted uranium target at ISIS. The flux in hydrogenous moderators from such a source might, however, be discounted somewhat by the extended spatial distribution of the source depending on the target-moderator design. The disadvantage in the long term with such a facility would be the unavoidable competition for beam time and/or intensity with kaon production in the basic facility. Although the long term development of this option appears to be more limited than the preferred option discussed above, it should be preserved if possible for the initial operation of the 3 GeV facility, especially if the extraction alignments and site layout can be rearranged to allow them to feed a common target assembly from both options at reasonable beam transfer line and housing costs.

The use of the full 30 GeV, 10 μC, 10 Hz beams (although they would require separate target/moderator facilities, at least in the absence of an unencumbered neutrino facility) could have the highest single-pulse, thermal neutron intensity of any recyclable facility in the world, at least until the Moscow KAON Factory becomes operational[4].

Although the space available for a neutron experimental hall as shown in Fig. 2 appears to be adequate for an initial facility, the possible future requirements for long flight-paths and additional or specialized target halls would need to be reviewed before construction started to avoid, as far as possible, future changes of venue, with the additional cost that would incur. At a minimum, beam transfer line tunnel stubs should be installed downstream of the A-B and B-C transfer lines from the Booster tunnel to allow subsequent completion of such lines with minimum disruption to the KAON facility.

Accelerator-based pulsed neutron facilities are competitive and complementary to fission reactors and are capable of satisfying many beam users requirements, and of developing new areas of science. A PNF facility at TRIUMF that is capable of upgrading, though not initially world-leading, is a very attractive $40M initial investment in a field that has many technological spin-off possibilities.

REFERENCES

[1] I. M. Thorson, Proceedings of ICANS VII, Oxford, July 8–12, 1985, RAL Report-85-110 Vol. 1 p86, (1985).

[2] I.M. Thorson and M.K. Craddock, *Pulsed Neutron Facilities and the KAON Factory*, TRI-DN-K137 (September 1990).

[3] I. M. Thorson, *Simultaneous Pulsed/Integral Neutron Facility Optimization*, this Conference, Target Station Workshop Session.

[4] N.V. Kolmichkov, V.D. Laptev, V.A. Matveev, L.N. Latisheva, S.V. Serezhnikov, S.F. Sidorkin, N.M. Sobolevsky and Yu. Ya. Stavissky, *Superintensive Pulse Slow Neutron Source SIN Based on K-Meson Factory*, These proceedings.

Q(R.Pynn): Could you explain again the additional costs that would be involved for your various options? In particular what would 100μA, 450MeV, 10Hz & 0.4μsec pulse length cost you in addition to the currently projected cost of KAON?

A(I.M.Thorson): As will be clearer in the written text of my talk the incremental cost for a pulsed neutron facility addition to KAON would come in two parts. The first is for the target/moderator/shield assembly, experimental hall, beam transfer lines and tunnels; the approximate cost of C$30M would give us a 450MeV, 100μA, 50Hz, 0.8μs facility. A subsequent acceleration stage (to ~1GeV) and accumulation stage (to 10μC at 10Hz) is estimated at C$50M; the achievement of 0.4μs pulse length would not be a first or second priority but might be necessary for beam extraction reasons.

ICANS-XI International Collaboration on Advanced Neutron Sources
KEK, Tsukuba, October 22-26, 1990

Pulsed neutron sources at Dubna: their past, present and future status

E.P.SHABALIN

JINR,Dubna,USSR.

ABSTRACT

In 1960 the first world repetitively pulsed reactor IBR was put into operation. It was the beginning of the story how fission based pulsed neutron sources at Dubna have survived. The engineers involved have experienced many successes and failures in the course of new sources upgrading to finally come to possess the world's brightest neutron source - IBR-2. The details are being reviewed through the paper.

The fission based pulsed neutron sources did not reach their final state as yet- the conceptual views of IBR prospects are being discussed with the goal to double the thermal neutron peak flux (up to $2 \cdot 10^{16}$) and to enhance the cold neutron flux by 10 times (with the present one being as high as that of the ISIS cold moderator).

I. FEW COMMENTS ON THE PPR HISTORY AT DUBNA

Dubna is the only place where fission chain reaction based facilities are used as pulsed neutron sources. Their advantages are evident - big neutron flux and low cost of construction. But disadvantages are common famous so - more risk for pollution and too long neutron pulse duration.

The history of pulsed reactors had yet begun not in Dubna but during the Manhathen project in 1945 when special superpromptcritical experiments named "Dragon" were performed. The paper on the Dragon programme had included the part concerning the "repetitive Dragon"; the idea invented by D.Judd was to fasten a moving slug of uranium to the rotor getting so periodic pulses of fission power. The secure project was not realized and the paper was declassified only in 1960-th after the official report on the start-up of the Sovjet periodically pulsed reactor (abbrevation PPR) IBR was issued.

The IBR reactor was the first PPR in the world and it was the "bride present" to JINR from dr. Blokhintsev who arrived at Dubna from Obninsk where he and his colleagues invented (independently of Americans) the concept of a PPR. The young physicists dr. I.I.Bondarenko and Yu.Ya.Stavissky had created the exact PPR theory including the most important part concerning with power fluctuation /1/. The principle of IBR design was to divide a small fast reactor core into two parts - one of them moveable, imbedded in the fast rotating steel disk (see fig.1). The power pulse duration had appeared to be 40 μsec - more than expected 10 μsec but yet short enough for time of fligt (TOF) experiments. The time averaged power was 1 kW initially and was increased temporarily up to 6 kW for the next 3 years / 2 /.

The IBR was reconstructed in 1969; its new version, designhated as IBR-30, had 30 kW mean power. It was achieved partly by placing two uranium inserts into the disk that consequently passed the unmoving core. The reactor

could operate over the wide range of pulse repetition rates - from 100 pps to single pulses with a fission yield up to 10^{16}. The half width of fast neutron pulses was 55-60 μsec.

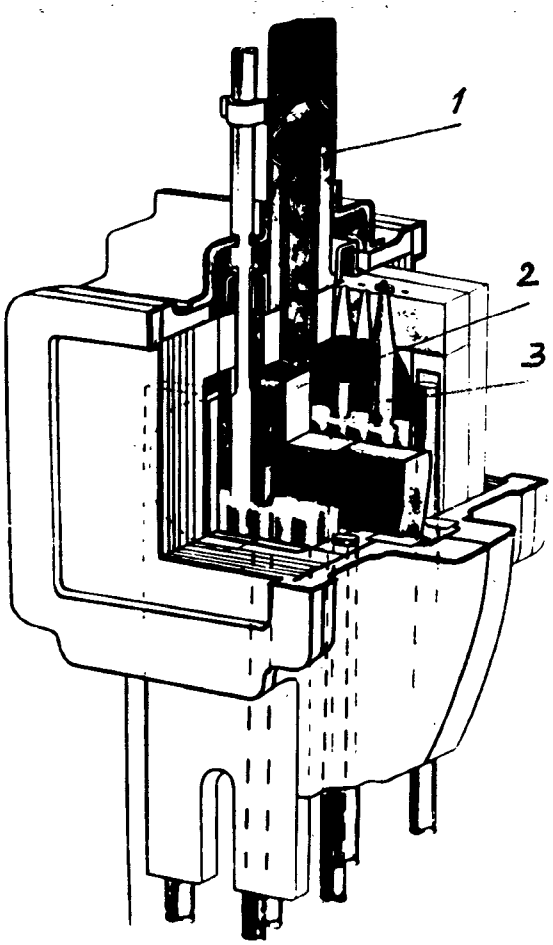

Fig.1 The IBR sketch
1-rotating steel disk
2-uranium insert
3-fuel rod of the unmoving core

To get the pulse duration in IBR shorter, it was decided in the early of 60-th to make it operating as a multiplicator of neutrons from accelarator target - "booster" mode of operation. This idea was realized earlier at Harwell but IBR was the more convenient device as the large reactivity modulation enabled a high multiplication of prompt neutrons during a pulse. The injectors (electron accelerators) for IBR and IBR-30 were the microtron (cyclic one) then LUE-40 (linear, of resonant type) that is used up to now. The pulse duration was (and is) 4 μsec at time averaged fission power from 1.2 to 13 kW depending on accelerator performances / 3 /.
The Dubna's booster scope is nuclear physics experiments by TOF method. It was the brightest neutron source in this occupation for 15-20 years until SNS appeared (the neutron luminousity of IBR booster is equal to that of 10-15 μA proton accelerator target).

It is worthy to tell about the most dramatic mode of IBR-30 operation - so called "rare pulses" one, the essence of which is in what a big reactor pulse is generated periodically but seldom - once per some seconds / 3 /. The special device was constructed to modulate reactivity with such frequency; it was the tungsten rod (reflector) swinging up and down near the core and being synchronized to the moving part of the core (uranium insert). The special emergency response facilities were established to avoid asynchronization.

The mode of rare pulses was experienced for about 2 years with energy yield in a pulse up to 100 kJ till it had finished dramatically... The mechanical part of the rod driver was not reliable enough as it became known afterwards. Once a day in the June 1972 (it was the last day before stopping for annual examination) some of the emergency systems failed, casually and simultaneously. But the maintenance stuff was ordered not to stop reactor operation. At the night the driving mechanism of swinging rod got broken, the rod started to move away the synchonized oscillation period. The reactor power started to decay according to a removal of reactivity. The emergency responce systems that might shut the reactor down were switched off and could not control situation. The power was being equal near to zero for about 15 sec Naturally, the huge amount of concealed reactivity was accumulated due to core temperature decaying. At one unpleasant moment the slowing rod found

occasionally itself in the position near to maximum reactivity simultaneously with the uranium insert so the concealed reactivity was summarized to the reactivity of the rod , and the very big power burst with about 2 MJ yield was aroused. The consequence was plutonium fuel melting. Fortunately, the fuel rod claddings successfully resisted inner pressure, and no radionuclides released outside. Otherwise the accident might be severe one with bad radioactive contamination. Since that time the rare pulses mode of operation is forbidden to maintain. Moreover, after the Chernobyl catastrophe any pulsed supercritical mode of IBR-30 operation (its fuel is metallic plutonium) is prohibited; it is used as a booster only.

In the middle of 60-th the scientific people involved in intense neutron source desighning were rather stimulated by a successful operation of IBR to be approved that PPR construction is the right way to go on. That's why so many projects of more powerful PPR's had been proposed that times - SORA in Europe, PFR in BNL(USA), KPFR in India and the others. But only one of them was realized, again in Dubna - IBR-2 (not taking into account the small PPR in Japan - JAJOI). The reason why the others designs were given up was that SNS projects won the rivals due to more broad applications and shorter pulse duration.

The principal idea and construction of IBR-2 were discussed in many papers /4 - 6/ and need not to be repeated. Let us be restricted by displaying two figures (2 and 3) and the list of IBR-2 performances (table 1).

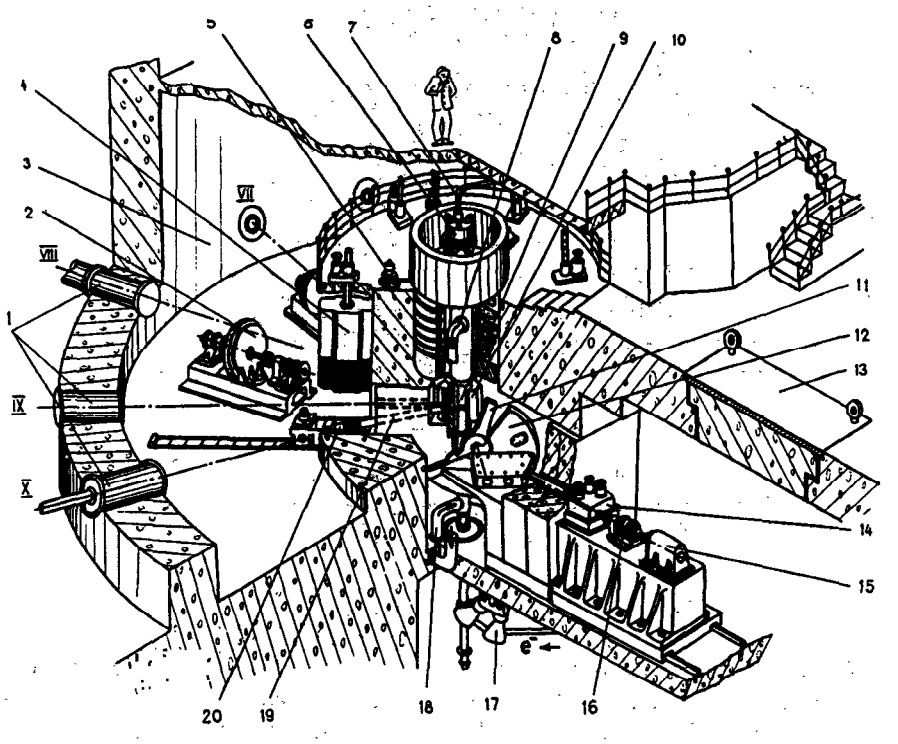

Fig.2 The general drawing of IBR-2: 1-neutron beam tubes; 2-choppers; 3-outer ring of biological shield; 4-neutron beam shutters; 5-control rod drive; 6-reactor vessel; 7-irradiation tube; 8-sodium outlet; 9-the core; 10-unmoving reflector; 11-moving reflector,MR; 12-its jacket; 13-manhole for MR withdrawing; 14,15,16-the parts of MR driver; 17-magnets for electron beam (not installed);18-sodium inlet; 19,20-safety block driving mechanism.

Table 1

The IBR-2 reactor performances.

	Today	In future
Mean power, MW	2	4
Peak power, MW	1500	10000
Pulse duration, μsec	215	70
Background power, MW	0.1	<0.15
Thermal neutron flux (n/cm ^{2}/s):		
1) time averaged	10^{13}	10^{13}
2) Peak	$0.7\ 10^{16}$	$2\ 10^{16}$

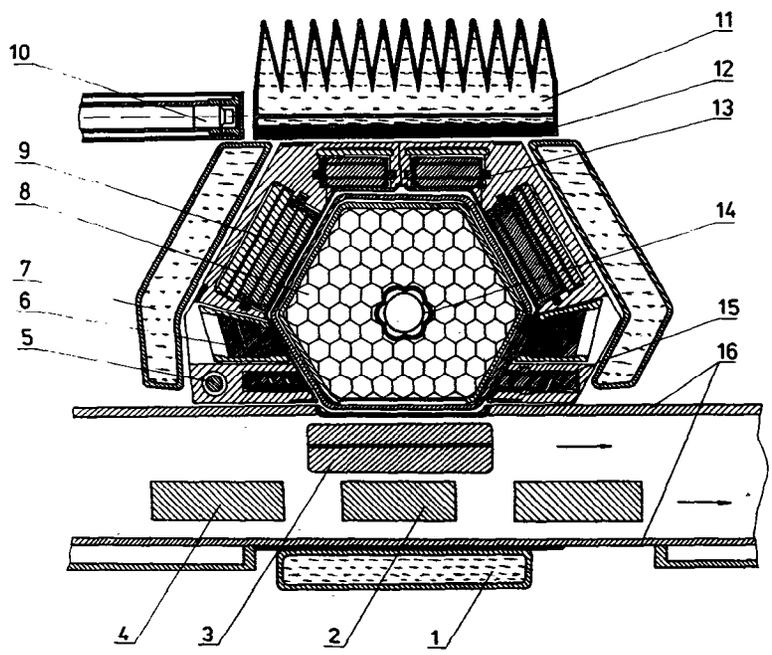

Fig.3 The IBR-2 reactor cross-section. 1,7-flat light water moderators; 2,4-auxillary moving reflector (AMR); 3-main moving rerflector (MR); 5,9,15-control blocks; 6-fast safety block; 8-fuel rods subassembly; 10-irradiation tube; 11-grooved water moderator; 12-boron filter; 13-slow safety blocks; 14 irradiation hole; 16-MR jacket.

The only thing is worthy to discuss about - the exciting scenario played by the reactor physicists to overcome difficulties with the long pulse duration. The initial value of it appeared to be more than 300 μsec - absolutely unsuitable to condensed matter reseaches. The reason for such a bad situation was so called "shadow effect" on neutron reflection, that

spoiled pulse shape at the first version of IBR-2 moving reflector MR-1 in 1978. The pulse duration is defined (it was derived by Stavissky in 1956 yet) as

$$\theta = \sqrt{2\pi\tau / \gamma}$$

where τ is the prompt neutron life time, and γ is the rate of reactivity changing at the moment of a peak power. The figure 4a shows clearly that the totally shaded auxillary reflector (AMR, used for slow reactivity modulation) is partly got open when MMR (main reflector,that is nearer to the core) is shifted in right-hand direction, and therefore some positive reactivity is released which was initially shaded by MMR. This positive reactivity decreases γ rate value in comparison with that for a single MMR. After some trials it was found that AMR of "folk type" (fig.4b) gives no shadow effects.

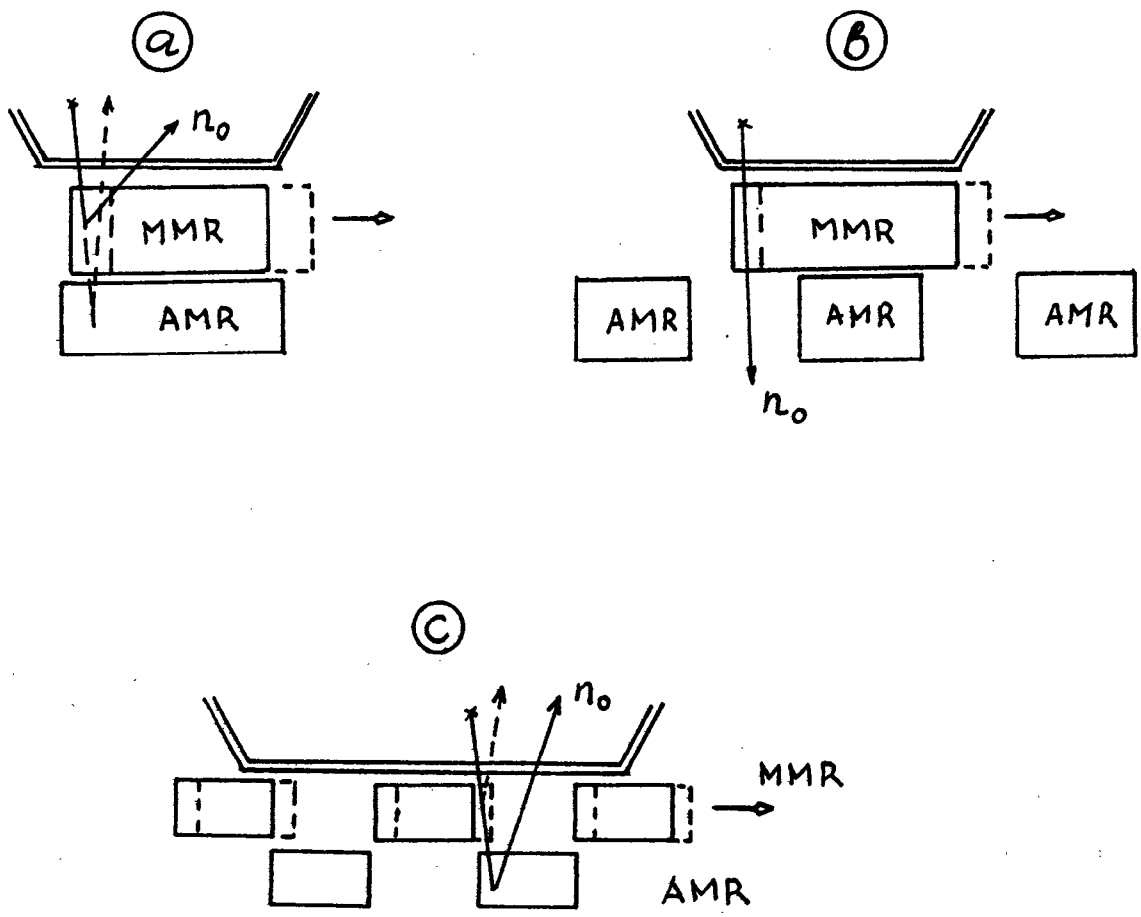

Fig.4 The diagrams of moving reflectors geometry to explain the "shadow" effect of neutron reflection. a-the first version of MR; b- MR-2; c-MR-3.

The new IBR-2 modulator MR-2 having such construction was installed in 1981 and ensured 215 μsec fast neutron pulse (fig.5).Some later (in 1983) it was proved by experimentally that the "shadow" effect could be forced to play useful role if two reflectors are shaped in special way (say, as that grid type reflectors displayed at the diagram of fig. 4c. For a such geometry of reflectors the shadow effect causes additional reactivity removing that leads to shortening a pulse duration significantly. The experiments of 1987 enabled to optimize modulator shape and material. The result is that the new project of MR-3 modulator for IBR-2 ensures 110-115 μsec pulse duration. Moreover, this modulator will be safer It is planned to be installed in 1992-1993.

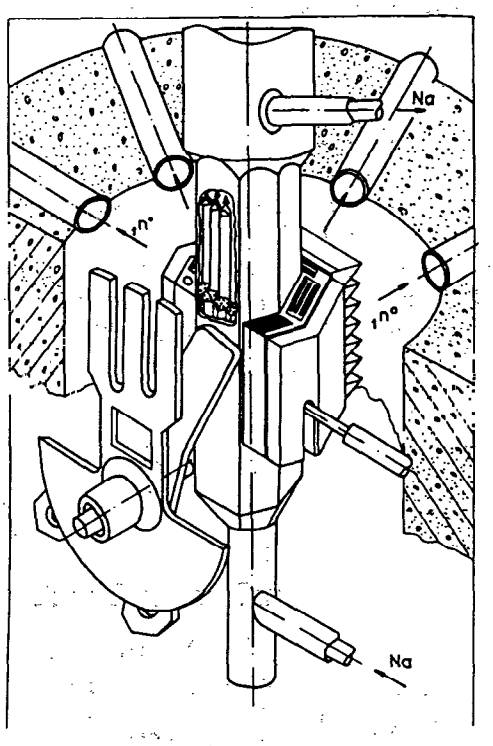

Fig.5. The IBR-2 sketch with MR-2 moving reflector rotors.

The IBR-2 started to be used for science in April 1982 mainly for condensed matter reseach by TOF method on extracted beams (but the very first experiment was concerned with searching of axion, a gypothetical particle, and not needed neutron beam).

The IBR-2 is well suit for condensed matter reseaches, especially with cold neutrons. It is resolved by 3 factors:

1. The power pulse duration is near to a cold neutrons life time in moderators.
2. The reactor core size and shape are optimized for thermal neutron intensity in outer beams.
3. The heat deposition in outer moderators per one cold neutron production is much less in comparison to that of SNS facilities or thermal reseach reactors (due to that γ-ray flux and fast neutron energy are both profoundly low).

So, yet today the cold neutron flux from the IBR-2 room temperature light water moderator equals to that of ISIS cryogenic moderator (see table 2).

Table 2. Cold neutron fluxes (λ>4Å) of IBR-2 and the others sources.

	From whole moderator surface, time averaged 10^{13} n/sec/sr	Peak density flux at λ=9Å 10^{15} n/cm^2/s/sr/eV
IBR-2 light water grooved moderator	1.2	1.3
IBR-2 solid methane	5-10	30-60
ISIS liqiud hydrogen (200 μkA)	0.8	2
ILL (Grenoble), 1 cm^2	1.5	5

As soon as the solid methane moderator would be installed at IBR-2 (see the description below) no device with the same fission density in the core could reach the cold neutron performances of IBR-2 in principle.

The IBR-2 is operated 100 days per year; the initial fuel charge ensures more than 10 years of operation with no fuel reloading.

During the IBR-2 desighning it was decided to construct a powerful electron accelerator as an injector for IBR-2 to get a short duration of neutron pulse. The induction principle was chosen to accelerate electrons as the most suitable for high current. Its essence is in that the electron beam is used as a secondary coil of a transformer with a primary one reeled on the permalloy toroidal cores. The construction of LIU-30 accelerator lasted 20 years but nothing came of it as the electron beam occured to be unstable in radial motion. All attempts to stabilize it appeared to be unsuccessful; construction was given up in the last year. We know no other electron accelerator being adequate to IBR-2 performances, i.e. so powerful as to generate more than $2\ 10^{14}$ n/sec in the target (if not proton accelerator with >2 μkA current). So, the IBR-2 operates only as a pulsed reactor contrary to the IBR-30 operating as a booster exclusively.

It is interesting to say that many uncommon effects were observed during the Dubna's pulsed facilities exploitation. Each of them worthy to tell in a proper paper / 7,8 /; here we give the headings of some of them only:

- the selfcompensating a fuel burn-up reactivity effect in IBR-2 reactor;
- the possibility of an instability of a new, "pulsed" type in PPR and transient to a chaotic behavior at a great power;
- mirror reflection of relativistic electrons of the front panel of a target.

II. THE PROSPECTS FOR PULSED NEUTRON SOURCES AT DUBNA.

We intend to install the two new devices at IBR-2 in the nearest future (1992-1993) : moving reflector MR-3 to reach 110 μsec pulse duration (yet described in the part I) and the cold moderator. The latter will be solid methane one of a grooved type at 20-25 K combined with the light water premoderator. The methane container box (fig.6) is fabricated of Al alloy and is tightly surrounded by another container to hold gaseous helium that removes heat off methane and alumium walls. Many small channels for helium flow are cut inside the front wall of methane box to enlarge the cooling surface. The heat will be transferred through low-conducting methane by the same way the Japaneses use at KENS - aluminium wires forced into the front wall, some of them twisted.

To control the methane temperature three kinds of gages will be used: gaseous thermometers,thermocouples and neutron thermometer. The latter will measure the instant cold neutron spectrum by TOF on-line method enabling to scram the reactor down just as soon as chemical energy stored at methane due to irradiation starts casually to be released.

The other pecularity of the cold moderator construction is that the back (outletting) wall of helium container is supplied with special ribs to restrain helium pressure against vacuum outside ; to avoid cold neutron absorption the ribs are placed just opposite to methane ledges at grooved side of the box. Such ribs are arranged at the vacuum container too (it is not shown in the picture).

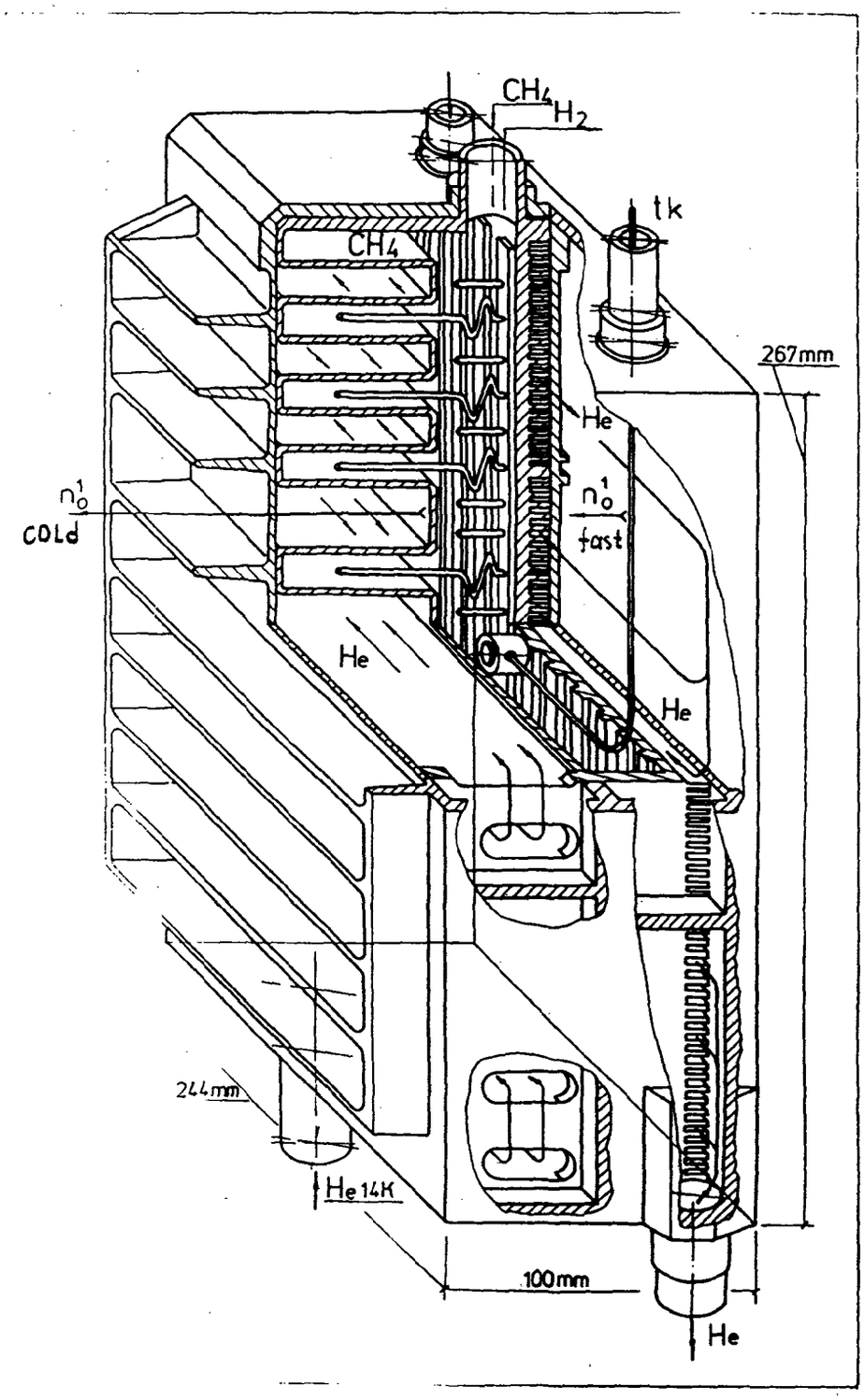

Fig.6. The solid methane moderator of IBR-2,
the cross-section drawing of the methane and helium cameras.

The power generated in methane due to neutrons slowing-down and γ-capture amounts to 110 W, in aluminium - 470 W. The maximum of heat production per unit volume will be near to that of solid methane at KENS or IPNS - about 0.1 W/g (the volume of the box is 2 ltrs). Therefore the rate of radiolysis is expected to be at appropriate grade to enable us not to replace methane by the fresh one during one run of IBR-2 operation - two weeks. If not, there is possibility to decrease heat generation in methane by adjusting the thickness of the water premoderator.

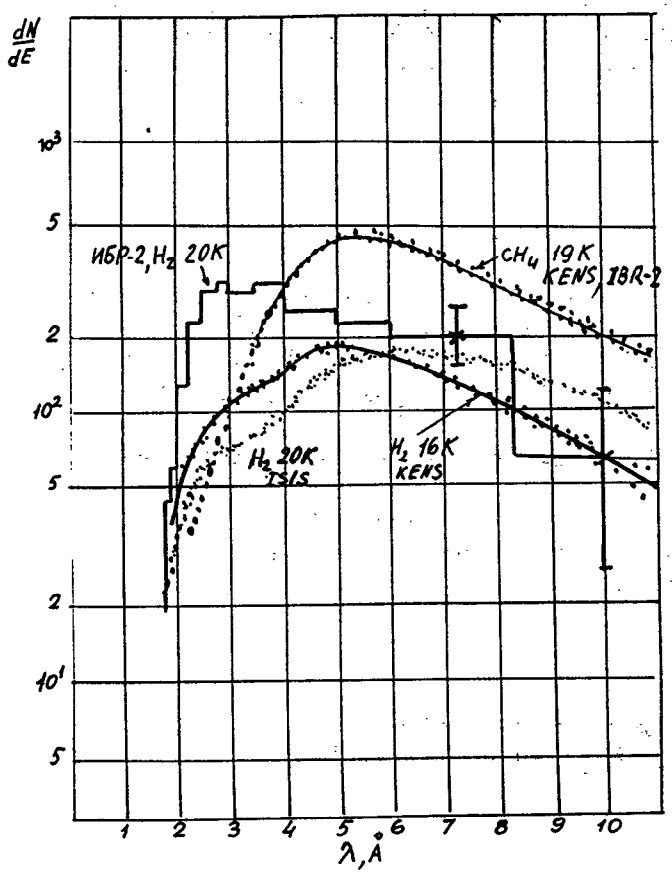

Fig.7. The relative neutron spectra for the various moderators.

It is worthy to explain that at the same heat production rate as SNS have the IBR-2 moderator supplies physicists with more cold neutrons (table 2) due to both the fast neutron mean energy kicked methane is much less than that of SNS and the moderator surface is about one order larger.

The cold moderator construction enables to optimize neutron spectrum. It is possible not to fill up the camera with methane or to fill it up partly. The goal is to get "warmer" neutrons. The most good opporturnity to get very broad neutron spectrum is to fill up the camera with liquid hydrogen instead methane(see fig.7). We were aspired by this idea after learning IPNS's experience with replacing solid methane by liquid hydrogen with no changing in the technology system. But we suffer of the strong formal limitations concerning nuclear safety to intrude liquid hydrogen at the reactor.

Besides these two up-grading of IBR-2 (MR-3 and methane moderator) we are planning more radical modifications of it. The main trend is replacing plutonium fuel by uranium one; it is desireable because of a big potencial danger of plutonium as a α-particles source. It is not easy to make such replacing not aggravating reactor performances. One possible concept of a new reactor version (let us name it as IBR-3) is to replace the reactor core of traditional type by a moving long bar placed inside the reactor vessel and cooled by sodium. This uranium slug (or few slugs) will be moved up and down so power pulses will be flashed at different parts of the slug consequently. The fissions will be diverged through all the slug enabling deminishing delayed neutrons intensities to get low background power between pulses (about 3%). Besides the duration of pulses would be reduced due to more delicate sizes of the core. No modifications are needed with nowdays cooling system, shielding, scientific instrumentation; MR-3 and the cold moderator could operate perfectly at IBR-3 too. The reactor vessel and the control blocks must be changed at some degree. Which is the most important the melting of the core is principally unprobable due to small residual power density.

The main expected performances of IBR-3 are displayed in Table 1, the second column.

And finally, a very brief comments on the future of nuclear physics by neutron experiments at JINR. After the creation of LIU-30 was finished unsuccessfully, it was decided to improve the IBR-30 booster performances to get higher time resolution. Now the desighning of a new electron injector and the new booster are under the progress. The goal is to generate short pulses <0.5 μsec at mean power of the booster 20-30 kW. The booster is proposed to be with no reactivity modulator. Thus the history revolves backwards to the first booster at Harwell but with more modern accelerator.

References

1. I.I.Bondarenko, Yu.Ya.Stavissky. Atomnaya Energia,7,417(1959).
2. B.N.Bunin et al. Proc. the 3 Int.Conf.Geneva. Report No A/28/P/324 (1964).
3. V.D.Ananiev et al.In: Fast Burst Reactors, USAEC CONF-690102,173 (1969).
4. E.P.Shabalin. Fast Pulsed and Burst Reactors. Pergamon Press,1979.
5. V.D.Ananiev et. al. Atomnaya Energia,57,227 (1984).
6. V.D.Ananiev et al. In: Neutron Scattering in the '90-th', IAEA,Vienna, IAEA-CN-46/85,p.63-73.
7. V.L.Lomidze et al. Communications of the JINR, Dubna, 3-11551 (1978)
8. E.P.Shabalin. Stochastic Dynamics of a PPR. In: Fast Reactor Safety, Proc. Conf. ANS, Salt Lake City, USA (1990)

Q(G.S.Bauer): What is the value of K_{eff} during the pulse in IBR-30 and IBR-2?
A(E.P.Shabalin): At the moment of maximum reactivity K_{eff} equals to ~0.995 for IBR-30 and ~1.001 for IBR-2.

ICANS-XI International Collaboration on Advanced Neutron Sources
KEK, Tsukuba, October 22-26, 1990

ENRICHED *vs* NON-ENRICHED *vs* NON-FISSILE TARGETS FOR PULSED SPALLATION NEUTRON SOURCES

J. M. Carpenter
Intense Pulsed Neutron Source
Argonne National Laboratory
9700 S. Cass Avenue
Argonne, IL 60439

ABSTRACT

Numerous options exist among alternatives for target material and design of the neutron producing target in pulsed spallation neutron sources. This report surveys the advantages, disadvantages and limitations of some of the alternatives, including discussions of neutron yields, delayed neutron backgrounds, source pulse widths, source-to-moderator coupling, materials performance, fabrication problems, safeguards and security and hazards questions.

I. Introduction

The purpose of "Booster" targets for pulsed neutron sources is to increase the intensity of the available neutron fluxes, above what is available from the primary neutron-producing interactions. The basic idea is to provide additional neutrons by fission in a target consisting at least in part of fissile material, which is a subcritical multiplying assembly. The pulse width demanded of the source depends on the uses to which the moderated beams are to be put, since moderation to different energies broadens the primary source pulse by an amount which is roughly proportional to the wavelength used, and by the width of the proton pulse which excites it. As will become clear below, booster targets designed to provide good resolution for measurements with eV neutrons, must operate as "fast" subcritical assemblies, that is, the fission process must be propagated by fast neutrons. If uses are confined to thermal neutrons, boosters with limited gain may be "intermediate spectrum" subcritical assemblies. For strictly cold neutron applications, low-gain "thermal" or "epithermal" subcritical assemblies may be appropriate. By way of limiting the discussion, I do not address variable reactivity boosters or reactivity pulsed reactors.

Figure 1 shows schematically the relationships among booster types classified according to the mean energy causing fission, $\langle E \rangle_F$, appropriate for different applications using conventional time-of-flight instruments (as opposed to "time-modulated" sources and instruments).

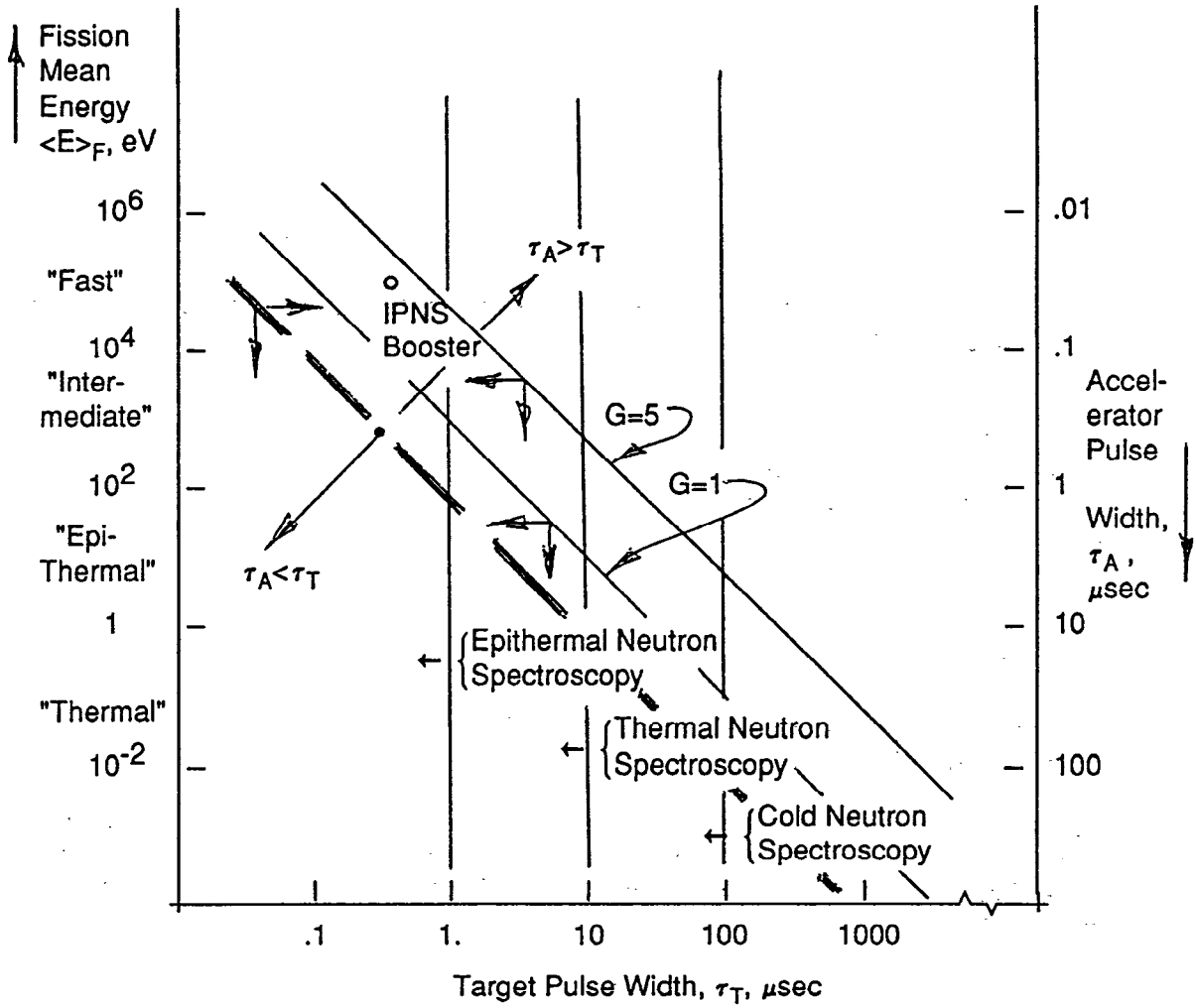

Figure 1. Relationship between the mean energy causing fission, $\langle E \rangle_F$, and the pulse width, τ_T, of subcritical booster assemblies. Two lines are shown, for no amplification, G = 1, and for a gain factor of 5. Regions shown define the pulse width requirements for efficient, conventional time-of-flight spectroscopy of epithermal, thermal and cold neutrons, assuming that appropriately designed moderators are provided; for example thermal and cold neutron spectroscopy are possible if τ_T is less than about 10 μ sec, but epithermal neutron spectroscopy is inefficient. The heavy line $\tau_T = \tau_A$ delineates the region in which the target pulse width is greater than the accelerator pulse width; the overall source pulse is dominated by whichever is greater.

Figure 2 shows the IPNS Booster Target, which was described in our earlier report[1]; the configuration is typical of "Fast" subcritical assemblies, consisting mostly of fuel with little coolant. Note the surrounding decoupling layer of ^{10}B-copper.

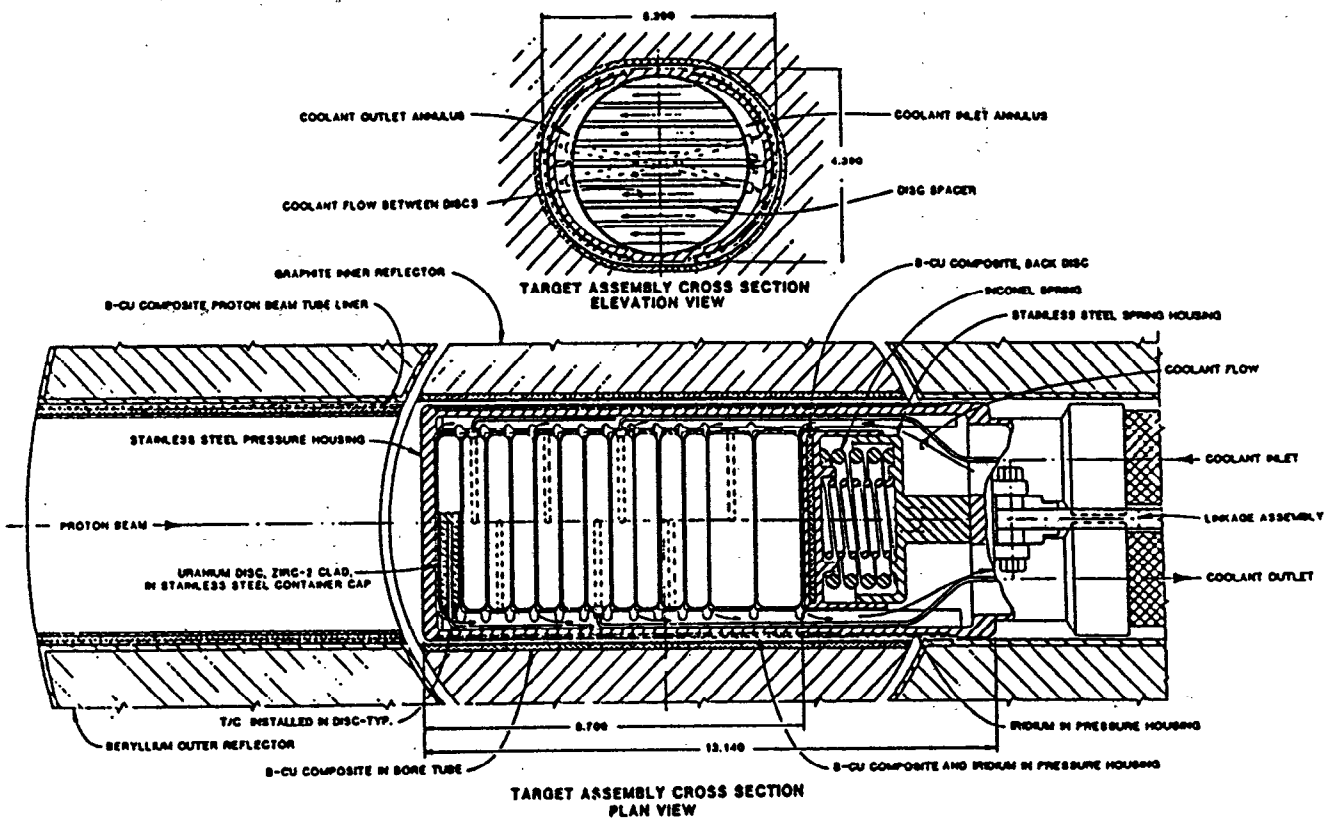

Figure 2. The IPNS Enriched Uranium Booster Target.

II. Neutron Production, The Primary Source

Figure 3 shows Fraser's well-known data on the primary spallation neutron yield (the global number of neutrons escaping the target per incident particle) from thick targets of heavy materials irradiated by protons; these are well correlated by the relationship

$$Y(E_p,A) = 0.1(E_p - .12\ \text{Gev})(A + 20)\ \text{(nonfissionable materials)} \qquad (1a)$$

$$= 5.0(E_p - .12\ \text{Gev})\ (^{238}U) \qquad (1b)$$

(E_p > .2 GeV). The yield for ^{238}U is about twice what would be calculated for nonfissionable material, because of fissions induced above the roughly 1. MeV threshold. (The distinction among the terms is traditional--"nonfissionable" having no appreciable fission cross section for neutrons of MeV energies or below; "fissionable" having appreciable fission cross section for neutrons of MeV energies, above some threshold; and "fissile" having appreciable fission cross section for neutrons extending to low energies.)

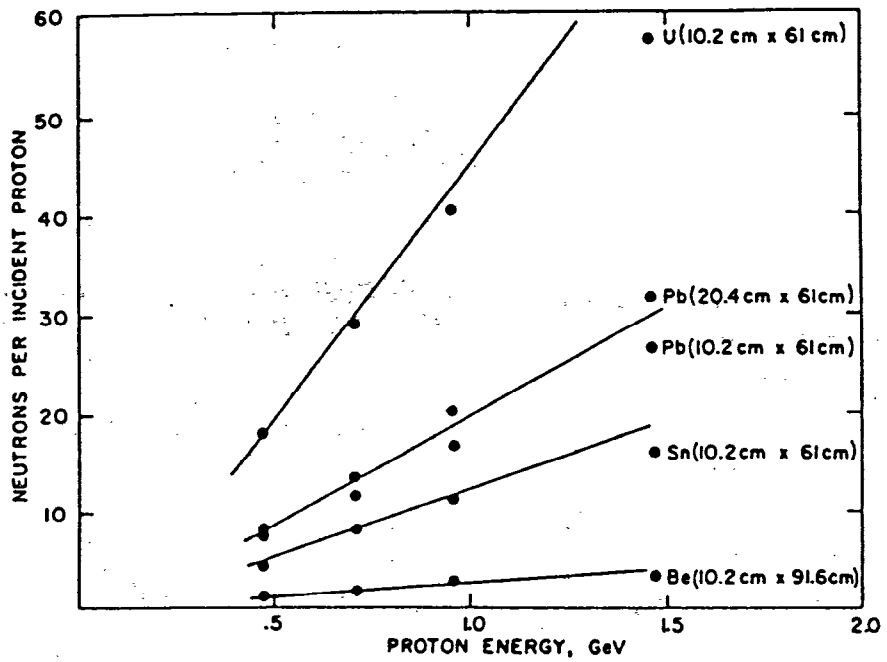

Figure 3. Measured global neutron yields vs proton energy, for various target materials. (from Fraser, et al[3])

The primary neutron producing reaction provides an externally-controlled source, either to be utilized directly or as a source which drives a multiplying, subcritical assembly, which is integral with the primary source. In the case of booster targets, it is important to recognize that the primary neutrons produced in the volume of the target are multiplied, some of which leak out and represent the source driving the moderators.

LANSCE uses a W target; other eligible non-fissionable target materials are Ta, Pb and Bi--liquid Pb is the target material in SINQ and the TRIUMF source. ^{238}U is used as fissionable, but non-fissile target material in ISIS, KENS and IPNS; Th, ^{237}Np and ^{240}Pu have similar threshold fission properties. ^{233}U, ^{235}U and ^{239}Pu are appropriate booster target materials insofar as their fission properties are concerned. Table I below summarizes the relevant attributes of some target materials.

Table I

Nuclear Properties of Some Target Materials for Pulsed Neutron Sources[a]

Material	Σ_f(~1.MeV), barns	Fission Threshold Energy, E_{th}, MeV	Delayed Neutron Fraction, β	Fission Yield, $\bar{\nu}$
		Fissionable, Non-fissile		
Th	.13	1.6	.022	2.3
^{238}U	0.52	1.35	.0157	2.6
^{237}Np	1.4	0.8	?	2.4
^{240}Pu	1.5	1.0	.0026	3.3
		Fissile		
^{233}U	1.9	---	.0027	3.0
^{235}U	1.3	---	.0065	2.7
^{239}Pu	1.95	---	.0021	3.1

a Mostly from ANL-5800[2].

Yields corresponding to Equation (1b) for fissionable materials other than ^{238}U may have been calculated or measured, but are not known to me; these depend on target size and geometry, but are not strong functions of the size of the target. Yields and the time structure of the pulses for booster targets depend very strongly on the density, enrichment of the fissile isotope, composition in terms of moderator, fuel, reflector and decoupler and on the spatial configuration of the target, and have to be computed for rather exact descriptions of the target. Beyond the question of global leakage neutron yields, there is the question of the coupling to the surroundings and moderators; this is addressed below.

While several of the materials represented in Table I have superior nuclear properties to U, practical metallurgical questions dictate the use of Uranium--which, in view of the fact that pulsed source targets are worked quite hard, is difficult enough even given the very large base of experience with that metal and its alloys. In the case of the fissile materials, the question of supply dictates the use of ^{235}U. However, in view of these superiorities, in particular the fraction of delayed neutrons, materials other than U may eventually come to the fore.

III. Booster Target Kinetics

Two aspects of the time dependence of booster target behavior are important, namely the prompt pulse width and the delayed neutron response. The number of neutrons n(t) in the system at time t, in a subcritical multiplying

assembly responding to an instantaneous externally-controlled source is described by a simple lumped-parameter theory which illustrates the main points,

$$\dot{n}(t) = n(k(1 - \beta)-1)/\ell + \lambda c + N_o\delta(t)$$

$$\dot{c}(t) = nk\beta/\ell - \lambda c \qquad (2)$$

where k is the multiplication constant ($k < 1$ in a subcritical system), β is the delayed neutron fraction, ℓ is the prompt generation time, c(t) is the number of delayed neutron precursors, λ is the average decay constant of delayed neutron precursors and N_o is the number of neutrons introduced by the external source at $t = 0$. Equations 2 assume that the external source produces no delayed neutron precursors. The solution by Laplace transform methods is straightforward,

$$n(t) = N_o\{(s_1 + \lambda)e^{s_1 t} - (s_2 + \lambda)e^{s_2 t}\}/(s_1 - s_2) \qquad (3)$$

where

$$s_{1,2} = {}^1/_2\{(\Delta k - k\beta)/\ell \pm [(\Delta k - k\beta)^2/\ell^2 + 4\Delta k\lambda/\ell]^{1/2}, \qquad (4)$$

and $\Delta k = k - 1$ (< 0). Since in a fast booster

$$\Delta k/\ell >> \lambda,$$

approximate values of s_1 and s_2 are

$$s_1 \approx (\Delta k - k\beta)/\ell \qquad (5)$$

and

$$s_2 \approx -\lambda\Delta k/(\Delta k - k\beta). \qquad (6)$$

The two terms represent the prompt response (s_1) and the delayed neutron response (s_2).

The total number of neutrons disappearing (some leak out: these are the ones we are interested in!) with the prompt pulse is proportional to

$$N_p = 1/\ell\int_0^\infty dt\,(\text{first term in eq 5})$$

$$= N_o(-1/(\Delta k - k\beta)) \qquad (7)$$

and the prompt neutron gain factor is

$$G_p = N_p/N_o = -1/(\Delta k - k\beta). \qquad (8)$$

The total number of delayed neutrons disappearing after the source pulse is, with the same proportionality as N_p

$$N_D = 1/\ell\int_0^\infty dt\,(\text{second term in eq 5})$$

$$= (k\beta/\Delta k)N_o/(\Delta k - k\beta) = \beta G_P(G_P - 1)N_o/(1 - \beta G_P) \tag{9}$$

(increasing as the <u>square</u> of the prompt gain) and the ratio of the number of delayed neutrons to prompt neutrons is

$$R_{D/P} = N_D/N_P = -k\beta/\Delta k = \beta(G_P - 1)/(1 - \beta G_P). \tag{10}$$

The delayed neutron background as a fraction of the prompt signal increases linearly with the prompt gain. (In a steady reactor, exactly critical, ($\Delta k = 0$), $R_{D/P} \to \infty$; <u>all</u> the neutrons are delayed neutrons in the present sense.) The total gain is

$$G_T = (N_P + N_D)/N_o = -1/\Delta k = G_P(1 - \beta)/(1 - \beta G_P) \tag{11}$$

and the delayed-to-total ratio is

$$R_{D/T} = -k\beta/(\Delta k - k\beta) = \beta(G_P - 1)/(1 - \beta). \tag{12}$$

The width of the prompt pulse is proportional to the prompt gain,

$$\tau_P = \ell G_P. \tag{13}$$

For representative values of the parameters, (roughly as in the IPNS Booster)

$\ell = 68.$ nanosec,
$\Delta k = -0.2$,
$\beta = .006$
$\lambda = 1.$ sec.

$$\tau_P = |1/s_1| = 340. \text{ nanosec}$$

and

$$|1/s_2| = 1.02 \text{ sec.}$$

The width of the prompt pulse, 340. nanosec, is considerably greater than the generation time ℓ; the delayed neutron pulse is so long that in, say, 30 Hz operation, the delayed neutrons appear essentially constant in time.

Roughly, for the IPNS Booster ($k = 0.80$), $G_T = 4.85$ and $\epsilon_D = R_{D/T} = .03$.

This simple analysis does not deal with the coupling of the source to different eigenfunctions (modes) of the neutron distribution, which have different multiplication constants, nor with the coupling of the target to moderators, which varies from mode to mode. On these accounts, the actual gain factor expected for beams from the IPNS booster is about 3.0 or 3.5 (determined from Monte Carlo calculations for a single moderator); figure 4 shows the calculated spectra emerging from the IPNS "H" moderator, for the depleted uranium target and for the Booster target. Measured neutron beam

intensities per unit of proton current increased on average by a factor × 2.5 over their values with the depleted uranium target. The delayed neutron fraction has been measured, with the result $\epsilon_D = 0.0283$ [4].

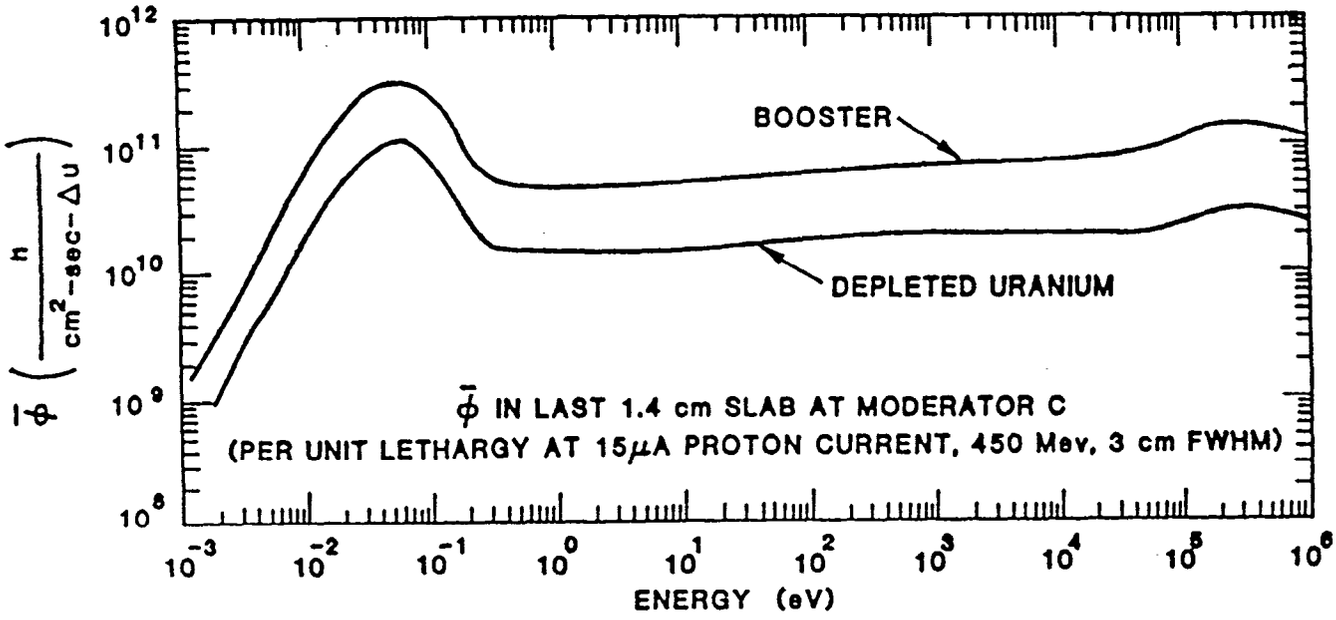

Figure 4. Time-and-spatial average scalar neutron flux in the IPNS "H" moderator, computed for the depleted and enriched uranium targets.

Reviewing the properties of the fissile isotopes in Table I, ^{233}U and ^{239}Pu are superior to ^{235}U, both in view of their higher cross sections (less fissile material would be needed to achieve a given gain) and in view of their lower delayed neutron fractions.

The discussion above deals only with delayed neutrons appearing from fission-generated precursors. In systems containing D_2O as coolant or Be as reflector, gamma rays above the relevant thresholds produce photoneutrons. These may be prompt fission gammas from the target, capture gammas from structural decoupling and poisoning materials, and activation gammas from activated components. Depending on their origins, these have different time dependence and importance in the neutron beams; some may be quick and important, as for example capture gammas produced by capture of moderator neutrons, or of reflector neutrons. As long-term delayed neutrons, these appear typically at a lower rate than delayed fission neutrons. Estimation of the photoneutron effects requires coupled gamma ray and neutron transport calculations. No source can be expected to be free of delayed neutrons; although their number may be small in sources with W or Ta targets, the measurements are easy and it is advisable to determine ϵ_D experimentally.

Delayed fission neutrons emerge from their resting parent nuclei in two-particle decays, and therefore exhibit discrete line spectra. Typical energies are in the range .1 - 1. MeV, while fission neutrons and the low-energy component of spallation neutrons have continuous evaporation spectra approximately proportional to $\sqrt{E}e^{-E/T}$, with $T \approx 1.3$ MeV. Photoneutrons have a spectrum that depends sensitively on the gamma ray energy spectrum and on the photoneutron cross section as a function of gamma ray energy.

Certain rare, light spallation product nuclei exhibit beta-delayed neutron emission, for example, $^{9}Li \rightarrow {}^{9}Be^{*}$ ($T_{1/2}$ = .17 sec), $^{9}Be^{*} \rightarrow {}^{8}Be + n$. (This is the same state that gives neutrons in $^{9}Be(\gamma,n)$.) Others, such as $^{12}Be \rightarrow {}^{12}B^{*}$ ($T_{1/2}$ = .011 sec), $^{12}B^{*} \rightarrow {}^{11}B + n$ exist which have short half lives and would appear as a time-varying delayed neutron background in repetetively-pulsed sources; as far as I know, none of these have been observed in pulsed spallation sources.

There are actually numerous species of fission-produced delayed neutron precursors, which are typically classed in groups having similar half-lives. Table II shows the relative abundances and half-lives of precursors from ^{235}U fast fission.

Table II

Relative Abundances and Half-lives of Delayed Neutron Precursors from ^{235}U Fast Fission[b]

Group	Relative Abundance a_i, %	Halflife $T_{1/2i}$, sec	Decay Constant λ_i, sec^{-1}
1	3.8	54.5	.0127
2	21.3	21.8	.0317
3	18.8	6.0	.115
4	40.7	2.23	.311
5	12.8	.496	1.40
6	2.6	.179	3.87

average decay constant = $\langle\lambda\rangle$ = .435 sec^{-1}
$T_{1/2eff} = \ln(2)/\langle\lambda\rangle$ = 1.6 sec.

b from ANL 5800[2].

Even though some of these groups have halflives of only a fraction of a second, all have halflives so long that delayed neutrons from these origins appear constant between pulses in practical pulsed sources (say, f > 20. Hz). This cannot be said of photoneutrons of certain origins, some of which may appear with short delays, both in booster targets and in non-multiplying targets.

IV. Time Response, Decoupling

It is important in pulsed sources that the prompt pulse be narrower than the width of the moderated pulse from the moderators. Inasmuch as the moderated neutron spectrum is rich in epithermal neutrons, and many instruments capitalize on this, and because the primary source must serve all of the moderators, the primary source pulse width must be narrower than the narrowest required by any instrument. In IPNS this indicates so far the use of 10. eV neutrons (in GLAD, see elsewhere in these proceedings). In dense hydrogenous moderators, the pulse width is about 2/3 μsec FWHM at 10. eV. The simple analysis above indicates that the multiplied source pulse width for the booster target will be about .34 μsec, which is comfortably less than the requirement, but not by much.

This is achieved in IPNS by decoupling the target from its surroundings, using a boron layer designed for e^{-1} attenuation of perpendicularly-incident neutrons of 100. eV. Without such decoupling, slow neutrons from the reflector and the moderators would participate in the multiplication process, significantly slowing down the response time (i. e. increasing ℓ). Such decouplers are a necessary feature of pulsed booster targets designed to preserve pulse resolution at eV energies, even though they reduce somewhat the intensity of moderated neutron beams.

V. Coupling of Source to Target and Surroundings

In highly symbolic form the Boltzmann equation describing multiplying assemblies is

$$\mathcal{H}n(\mathbf{r},\mathbf{v}) + S(\mathbf{r},\mathbf{v}) = 0 \qquad (14)$$

where

$$\mathcal{H} = \mathcal{L} + \mathcal{M}, \qquad (15)$$

and

$$\mathcal{L}n(\mathbf{r},\mathbf{v}) = -\mathbf{v}\cdot\nabla n(\mathbf{r},\mathbf{v}) - v\Sigma_{total}(\mathbf{r},\mathbf{v})v(\mathbf{r},\mathbf{v}) + \int d^3\mathbf{v}v'\Sigma_s(\mathbf{r},\mathbf{v}'\to\mathbf{v})n(\mathbf{r},\mathbf{v}') \qquad (16)$$

is the loss operator,

$$\mathcal{M}n(\mathbf{r},\mathbf{v}) = f(v)\int d^3\mathbf{v}v'\bar{\nu}(v')\Sigma_f(\mathbf{r},\mathbf{v}'\to\mathbf{v})n(\mathbf{r},\mathbf{v}') \qquad (17)$$

is the fission operator

and $S(\mathbf{r},\mathbf{v})$ is the external source density. The notation is the conventional reactor physics notation.

The task of analysis reduces to the problem of solving the eigenvalue equation

$$\mathcal{H}\Psi_n = \omega_n\Psi_n, \qquad (18)$$

with its adjoint

$$\mathcal{H}^+\Psi_n^+ = \omega_n^*\Psi_n^+, \qquad (19)$$

for which

$$\int\Psi_m^+(\mathbf{r},\mathbf{v})\Psi_n(\mathbf{r},\mathbf{v})d^3\mathbf{r}d^3\mathbf{v} = \delta_{mn}. \qquad (20)$$

Representing

$$n(\mathbf{r},\mathbf{v}) = \Sigma_n \; a_n \Psi_n(\mathbf{r},\mathbf{v}) \qquad (21)$$

and

$$S(\mathbf{r},\mathbf{v}) = \Sigma_n \; s_n \Psi_n(\mathbf{r},\mathbf{v}) \qquad (22)$$

Then

$$a_n = -(1/\omega_n)\int d^3\mathbf{r}d^3\mathbf{v}\Psi_n^{+}(\mathbf{r},\mathbf{v})\,S(\mathbf{r},\mathbf{v}), \qquad (23)$$

$$s_n = \int d^3\mathbf{r}d^3\mathbf{v}\Psi_n^{+}(\mathbf{r},\mathbf{v})\,S(\mathbf{r},\mathbf{v}) \qquad (24)$$

and

$$n(\mathbf{r},\mathbf{v}) = \Sigma_n \; (-1/\omega_n)\,s_n\Psi_n(\mathbf{r},\mathbf{v}). \qquad (25)$$

Now defining the multiplication constants k_n

$$(\mathcal{L} + \mathcal{M}/k_n)\Psi_n = (\mathcal{H} + (1-k_n)\mathcal{M}/k_n)\Psi_n \equiv 0, \qquad (26)$$

so that

$$\mathcal{L}_n \equiv \int \Psi_n^{+}\mathcal{L}\Psi_n = -\mathcal{M}_n/k_n \qquad (27)$$

where

$$\mathcal{M}_n \equiv \int \Psi_n^{+}\mathcal{M}\Psi_n \qquad (28)$$

and observing that if we order k_n's so that $k_{n+1} \leq k_n$, (for subcritical systems, allk_n's are less than 1.0), then

$$|\mathcal{L}_n| \geq |\mathcal{L}_{n+1}|. \qquad (29)$$

So

$$n(\mathbf{r},\mathbf{v}) = \Sigma_n \; k_n/(1-k_n)\,s_n/\mathcal{M}_n\Psi_n(\mathbf{r},\mathbf{v}) \qquad (30)$$

$$= \Sigma_n \; 1/(1-k_n)\,s_n/(-\mathcal{L}_n\Psi_n(\mathbf{r},\mathbf{v}). \qquad (31)$$

Integrated source and neutron densities are

$$S_T \equiv \int S(\mathbf{r},\mathbf{v})\,d^3\mathbf{r}d^3\mathbf{v} = \Sigma_n s_n \int \Psi_n(\mathbf{r}<\mathbf{v})\,d^3\mathbf{r}d^3\mathbf{v} \equiv \Sigma_n s_n f_n \qquad (31)$$

and

$$N_T \equiv \int n(\mathbf{r},\mathbf{v})\, d^3\mathbf{r} d^3\mathbf{v} = \Sigma_n k_n/(1-k_n)\, s_n f_n/\mathfrak{M}_n \tag{32}$$

$$= \Sigma_n 1/(1-k_n)\, s_n f_n/(-\mathfrak{L}_n)\,. \tag{33}$$

If the source is entirely proportional to the lowest eigenfunction,

$$S(\mathbf{r},\mathbf{v}) = S_{Fo}(\mathbf{r},\mathbf{v}) = \mathfrak{M}\Psi_o(\mathbf{r},\mathbf{v})\,, \tag{34}$$

so that

$$s_n = S_T \delta_{no}/f_o \tag{35}$$

then

$$N_T = N_{Fo} \equiv k_o S_T/(1-k_o) \text{ and } N_T \propto k_o/(1-_{ko})\,. \tag{36}$$

This is case of the "single-mode" reactor, a description that applies when k_o is very near to (but less than) 1.0 and the source distribution is similar to the fundamental eigenfunction. Otherwise and in general, since

$$f_{n+1}/(1-k_{n+1}) \leq f_n/(1-k_n)\,, \tag{37}$$

$$N_T < N_{Fo} \text{ and } N_T \not\propto k_o/(1-k_o)\,. \tag{38}$$

That is, in general, <u>the full source is not multiplied by the simple gain factor for the single-mode reactor</u>. Neither is the gain observed at a given point $(\mathbf{r},\mathbf{v})$ proportional to the simple gain factor. This is the usual situation in far-subcritical assemblies--no single eigenfunction dominates.

Criticality Monitoring

These last qualitative observations have a very significant impact on the design of procedures for measuring the fundamental multiplication constant, say during fabrication or handling (insertion and removal) of a multiplying target. Conventional reactor practice applies to situations in which the fundamental eigenfunction is dominant or nearly dominant, as in the approach to criticality. In the case of far-subcritical systems, say $k_o \approx .90$, the fundamental mode does not dominate, and many modes contribute to the total neutron density or flux at a position where it might be monitored. Procedures for monitoring k_o must surely be devised to detect incipient criticality, $k \to 1.0$, for obvious safety reasons. However, the procedures must also **succeed**, in that **false indications of approach to criticality must be ruled out**.We suffered this problem in designing the insertion procedures for the IPNS Booster target; detailed calculation of the detector response is necessary to provide predictions of the monitored neutron density, if that is the procedure followed. Other methods, such as Rossi-α measurements suffer from comparable difficulties.

VII. Power and Power Density

Producing neutrons by fission is less efficient than by spallation--about 190. MeV of sensible heat is deposited locally per fission. For ^{235}U, at best $\bar{\nu} - 1 = 1.7$ neutrons per fission remain as potential leakage neutrons (one is needed to propagate the chain reaction), so that at best, about 112. MeV of heat must be removed to provide each leakage neutron. Pure spallation, on the other hand is endothermic so that slightly less than the proton beam energy appears as heat, with about 40. MeV of heat required to be dissipated to produce a neutron from Pb. Booster targets therefore must be designed to dissipate more heat than pure spallation targets to produce the same number of neutrons; for a 15 μA proton beam current and a ^{238}U target as in IPNS, the power increases from about 6 kW to about 53 kW.

This is not as bad as it seems in terms of the total power figures, since the power density distribution in booster targets is considerably smoother than in pure spallation targets, and the local power density determines the difficulty of heat removal. Figure 5 shows the computed power density distribution in the IPNS Booster Target.

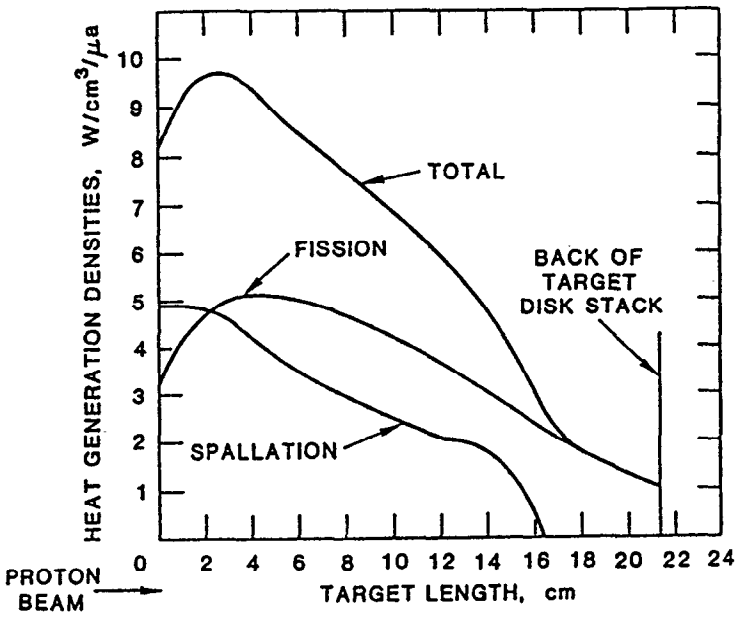

Figure 5. The power density distribution in the IPNS Booster target.

VIII. Materials and Metallurgy

Since our last report, we have had to overcome numerous difficulties in the disk fabrication process; in the end, we have succeeded.

Two general areas of uranium target design relate to questions of metallurgy: bonding and texture.

Cleanliness is next to Godliness, they say. In relation to disk fabrication, cleanliness is next to Bondedness, and we found it necessary to develop a new regimen for cleaning surfaces and handling components in order to produce reliable Zircaloy-to-uranium bonds between the cladding and the target material.

The same is true of the gas in the Hot Isostatic Pressing (HIP) apparatus. We found it necessary to send our small HIP machine to Oak Ridge for the purpose, since outgassing from the insulation in the pressure chamber of the Oak Ridge device contaminated the parts sufficiently to degrade the cladding surface.

Because it was necessary to clamp the cladding cans tightly together prior to evacuation of the welding chamber, we found it necessary to provide special vents around the periphery of the circumferential electron-beam weld, in order to release the air from the clearance space between the clad and the uranium. Even the small amount of air that remained in that space after pumping on the welding chamber without the vents, prevented good bonding, we determined.

Special attention had to be devoted to controlling the electron-beam welding parameters. Although we obviously have found a method of producing reliable welds, we must admit that we still do not understand the microscopically observed pattern of recrystallization as it relates to the zone of fusion in the weld.

The cast uranium alloy has considerably greater metallurgical texture (preferred orientation) and grains larger than the depleted uranium target material with which we have had such good experience. These observations led us to an extensive neutron diffraction investigation to characterize the material; in the process we developed newly the capability for carrying out those studies at IPNS[4]. Having obtained our best characterization, we had much to puzzle out, as to how this will affect the target. Ultimately, we adjusted the diameter of the disks, and the range of travel of the compression spring, to account for our maximal estimates of anisotropic growth of the disks. Initially, we believed that this will limit the lifetime of the target to between $3^1/_2$ and 5 years under current operating conditions. However, an ultrasonic examination program provided for in the design of the booster has shown, after two years of operation, that growth is taking place at a rate approximately 1/10th of the rate initially allowed for.

IX. Safeguards, Security and Safety

Requirements for safeguards and security (e.g. antiproliferation) and safety vary locally, and can impose significant conditions on a booster target project. Any program intended to lead to installation of a fissile booster target should be launched with ongoing simultaneous efforts to comply with these regulations, obtain the associated approvals, and provide the needed documentation. The IPNS Booster Project profited immensely from this approach.

X. Acknowledgements

We were greatly assisted in these materials assessments by Bill M^{C}Donnel of Savannah River National Laboratory, whose advice based on experience with metallic uranium reactor fuel was essential. Throughout, we enjoyed the helpful cooperation of our colleagues at Oak Ridge Y-12 Plant where the disk

processing was carried out. This work was performed under the auspices of the U.S. Department of Energy, Division of Materials Sciences, Office of Basic Energy Sciences, under Contract W-31-109-ENG-38.

XI. Conclusions

First experience with the IPNS Enriched Uranium Booster target is encouraging. The intensity gained is approximately what was expected, and the main negative effect of the increased background of delayed neutrons (also consistent with expectations) seems so far to be able to be dealt with. A considerable body of information exists concerning the performance and operational problems of moderators, which enable the design of tailored moderators for many purposes. More development should be pursued to provide better moderators, especially cold moderators appropriate for use in high-power sources.

XI. References

1. A. E. Knox, J. M. Carpenter, J. L. Bailey, R. J. Armani, R. N. Blomquist, B. S. Brown, D. R. Henley, A. G. Hins, B. A. Loomis, A. W. Schulke and H. R. Thresh, "Progress on the IPNS Enriched Uranium Booster Target" Proceedings of ICANS IX, (1986), p557.

2. Reactor Physics Constants, Argonne National Laboratory Report ANL-5800, Second Edition (1963).

3. J. S. Fraser, R. E. Green, J. W. Hilborn, J. C. D. Milton, W. A. Gibson, E. E. Gross and A. Zucker, Phys. Can. **21** (2), p. 17 (1966).

4. J. E. Epperson, J. M. Carpenter, P. Thiyagarajan and B. Heuser, Nucl. Inst. and Meth. A **289** 397-401 (1989)

5. J. W. Richardson, Jr., M. H. Mueller, F. K. Ross and D. G. Reichel, Adv. X-Ray Anal, Volume 31 (1988) p377.

Q(I.M.Thorson): Can you give us any indication of the relative importance of (γ, n) neutrons in D or Be, relative to delayed neutron problem?
Do any of the operating facilities see any significant background component that can be attributed to (γ, n) neutrons?

A(J.M.Carpenter): In reactors, photoneutrons are typically less than 10% of fission delayed neutrons; the situation in spallation sources is not known. It would be informative if measurements were made at LANSCE (W target) or ISIS (when Ta target is in place); even though the relative delayed neutron number may be quite small, it should be easily determined.

Q(N.Watanabe): You have 2.5 times more neutrons with 5 time more delayed neutrons. Is it correct? Why you have an effective gain factor 2.5 rather than $1 / (1-k_{eff}) = 5$? Is the heat distribution more flat compared to the depleted uranium target?

A(J.M.Carpenter): Yes, the average (many beams) gain is $\times 2.5$. This differs from the simple $1 / (1-k)$ because all the source neutrons do not couple into the fundamental mode. The best distribution is in fact somewhat flatter.

Q(G.J.Russell): In the context of a several target station, have you considered sub-critical dynamic booster to help in the delayed neutron problem for ^{235}U fuel? How do mechanical complexities stack-up against potential problems of substituting ^{239}Pu for ^{235}U vis-a-vis Health-Safety and Environments issues.

A(J.M.Carpenter): Yes, but only briefly (about 10 minutes in a project of 5 years' duration). The combination of mechanical complexity and potential criticality hazards makes such a proposition outside our capacity to deal with. Concerning use of ^{239}Pu, the chemical and α-activity problems, difficult in themselves, probably are outweighed by problems of metallurgy; if it is possible, Pu is metallurgically more difficult than U. This last comment is inapplicable if a "slow" booster were considered, which enables use of oxide fuel.

ICANS-XI International Collaboration on Advanced Neutron Sources
KEK, Tsukuba, October 22-26, 1990

GENERAL ASPECTS OF THE ISIS UPGRADE

T A Broome, I S K Gardner and G H Rees.
Rutherford Appleton Laboratory,U.K.

ABSTRACT
Current and proposed work on the ISIS accelerator and target station are described.

1. INTRODUCTION

The planned ISIS upgrade programme for the accelerator and target station is described. This programme aims to increase the synchrotron energy from 750 MeV to 800 MeV, and to increase the intensity from 100uA towards 200uA and also to continue the improvement in the reliability of the facility. In addition some longer term possible developments are mentioned.

As the upgrade programme for the accelerator and the target station are detailed in two other papers [1,2] for this conference only brief outlines of the work will be given here.

2. PRESENT STATUS

A comparison of the yearly operation from 1987 is shown in Table 1 with data for 1990 up to the end of September. The main effort in the last two years has been directed at improving the accelerator reliability and reducing the frequency of beam trips which are thought to shorten the lifetime of the Uranium target. The uAhrs between trips has risen by a factor of nine since 1987. The target performance is summarised in Table 2.

The fith Uranium target was installed in July this year. The investigation into the failure of Uranium target number 2 was reported at the last ICANS meeting. Since then two more Uranium targets have failed. The failure of target 3 followed a very similar pattern to targets 1 and 2 with a progressive blockage in the cooling channels at the front of the target to the point that the temperature of the Uranium plates became unacceptable and the target was changed. The behaviour of target 4 was somewhat different from the other targets in that during its operational life there were significant and abrupt, changes in the flow and pressure drop characteristics of the front cooling channels with no effect on the target plate temperatures. These changes are not understood. Finally, as with the other targets, the monitoring indicated a partial blockage and a small quantity of Uranium fission products was detected in the cooling water, indicating a cladding failure, so the target was changed.

	1987	1988	1989	1990 (So far)
Total Scheduled User Time(Days)	176	182	178	119
Total Lost Time(Days)	48	50	47	24
Total Time on Target(Days)	128	132	131	95
Percentage of time on Target	73%	72%	73%	80%
Total Integrated Current(mAhrs)	120	230	288	218
Average Current during scheduled time(uA)	28	53	67	77
Average Current with beam on(uA)	39	72	91	96
Peak Current averaged over 24 hrs(uA)	70	97	107	102
uAhrs per trip	6	18	31	53
Number of cycles for science	7	6	7	4

Table 1

Target	Gross Thermal Cycles	Integrated Current mAhr
U#1	Not measured	92.4
U#2	> 38624	53.1
U#3	10389	174.9
U#4	4147	138.8
Ta#1	18124	327.5
U#5	1657	104.1

Table 2

Some difficulties with the production of Uranium targets, which have now been resolved, resulted in extended running using the backup Tantalum target.

3 REQUIRED PERFORMANCE

It is now anticipated that the trapping efficiency in the synchrotron, at high intensity, will be about 60% and not 50% as originally envisaged. Allowing for 2% beam absorption in the thick Muon target the required and achieved performance figures for the accelerator are listed in Table 3.

	Required	Achieved
Beam on Target	2.50 E 13 ppp	1.60 E 13 ppp
Accelerated Beam	2.55 E 13 "	1.60 E 13 "
Trapped Beam	2.58 E 13 "	1.60 E 13 "
Accepted Beam (70 MeV)	4.30 E 13 "	3.30 E 13 "
Injector Beam (70 MeV)	4.39 E 13 "	4.00 E 13 "
Pre-injector Beam (650 KeV)	7.98 E 13 "	8.75 E 13 "

Table 3

With the present limit of 350 us pulse length on the linac RF system these figures indicate a current from the linac of 20 mA and a pre-injector current of 36.5 mA. Pre-injector H- currents of 50 mA have now been reached and 40 mA currents have been maintained for days with resulting 70 MeV beams of about 18 mA.

4 THE KFK/RAL IMPROVEMENT PROGRAMME

This improvement programme is outlined in Fig 1. It started this year following the completion of a KFK/RAL supplementary agreement. It is expected that all the hardware will be completed and installed by April 1993. Equipment installation will take place during each of the long shut-downs which last from January to at least April each year. The equipment required to raise the synchrotron energy to 800 MeV will be installed in the shut-down of 1991. The additional synchrotron magnets (octupoles and sextupoles) required for higher intensity operation will be installed in 1992. The Target Station modifications for 200 uA beams will be completed by 1992.

5 OTHER DEVELOPMENT AREAS

Installation of a collimator after the Muon target in the 800 MeV beam transport line has greatly reduced the radiation problems in this beam line but the levels on the beam line components at the end near the main target still make maintenance in this area difficult. A development plan to address this problem is now being investigated.

KFK/RAL ISIS UPGRADE PROGRAMME

Year ->	1990	1991	1992	1993
Planned Beam Energy				
750 MeV	XXXXXXXXXXXX			
800 MeV Trials	X			
800 MeV		XXXXXXXXX	XXXXXXXXXXXX	XXXXXXXXXXXX
Planned Linac Beam Intensity				
10 - 15 mA	XXXXXXXXXXXX	XXXXXXXXXXXX	XXX	
15 - 20 mA			XXXXXXXXX	XXXXXXXXXXXX
Planned Synchrotron Beam Intensity				
100 - 130 uA	XXXXXXXXXXXX	XXXXXXXXXXXX	XXX	
130 - 200 uA			XXXXXXXXX	XXXXXXXXXXXX
Ion Source and Pre-injector complete	XXXXXXXXXXXX	XXXXXXXXXXXX	XXX	
70 MeV transfer line power supplies complete	XXXXXXXXXXXX	XXXXXXXXXXXX	XXX	
Linac debuncher complete	XXXXXXXXXXXX	XXXXXXXXXXXX		
Octupoles, sextupoles & dipoles installed	XXXXXXXXXXXX	XXXXXXXXXXXX	XXX	
Synchrotron RF high power amplifier complete	XXXXXXXXXXXX	XXX		
Extraction kickers upgrade complete	XXXXXXXXXXXX	XXX		
800 MeV beam line power supplies complete	XXXXXXXXXXXX	XXXXXXXXXXXX	XXXXXXXXXXXX	
Target station complete for 200 uA	XXXXXXXXXXXX	XXXXXXXXXXXX	XXX	
Beam diagnostics design & installation	XXXXXXXXXXXX	XXXXXXXXXXXX	XXXXXXXXXXXX	XXX
Installed Equipment Reliability Improvement	XXXXXXXXXXXX	XXXXXXXXXXXX	XXXXXXXXXXXX	XXX

Fig 1

6 TARGET STATION DEVELOPMENT

There are several possibilities for Uranium target development which will improve the lifetime of the Uranium targets. The main thrust of this development work is to provide targets with better resistance to thermal cycling damage. This can be achieved a number of ways: by altering the details of the heat treatment of the target plates in manufacture, by changing the design of the cladding and support frame for the plates and by the use of a Uranium Molybdenum alloy as the basic target material. Details of this work are being given in another paper at this conference [2].

A new backup target is being designed and will be built using Tungsten. This will give a significantly greater neutron yield than the existing Tantalum backup target.

A major upgrade of the cryogenic plant for the methane moderator will be installed early in 1991. This will allow online replacement of the liquid methane. Radiation damage to the methane during operation produces higher hydrocarbons and hydrogen with the result that the neutron fluxes from the moderator are reduced by as much as 30% during the four week run at a mean current of 100 uA. Also many of the hydrocarbons formed are solid at the operating teperature, 100 K, with the consequent risk of blockage. It is clear that without this upgrade it will not be practical to operate at beam currents as high as 200 uA.

7 LONGER TERM DEVELOPMENTS

Some consideration is now being given to the design of a second Target Station for ISIS. Initial thoughts suggest a pulse repetition rate of about 12.5 Hz.

A facility for the production of radioactive beams in the mass range 9 to 240 with energies up to 40.6 MeV/nucleon at A=238, 123.4 MeV/nucleon at A=79 and 183.5MeV/nucleon at A=9 is also under consideration. A fraction of the ISIS 800 MeV proton beam would be used to produce these exotic nuclei by the bombardment of suitable targets. The new nuclei would be selected by an isotope seperator and then accelerated.

The future development programme will also cover the compatability of both the above facilities with the possible upgrade of ISIS to 1.6 mA beam current by changing to an 800 MeV storage ring mode of operation.

References

1 I.S.K. Gardner and G.H. Rees, Accelerator Aspects of the ISIS Upgrade, this conference.

2 T.A. Broome and M. Holding, The Status of the ISIS Targets.

Q(N.Watanabe): Do you need additional shield on the target station?

A(I.Gardner): Additional shielding will be required. It will be achieved by replacing some of the concrete on top of the target station by iron.

Q(R.Pynn): What is the projected cost of the ISIS upgrade to 200μA.

A(I.Gardner): The projected cost of the ISIS upgrade to 200μA is £3.4M plus 100 man years of effort.

ICANS-XI International Collaboration on Advanced Neutron Sources
KEK, Tsukuba, October 22-26, 1990

Progress of the accelerator R&D for the Japanese Hadron Project

Motohiro Kihara
KEK, National Laboratory for High Energy Physics
1-1 Oho, Tsukuba, Ibaraki, 305, Japan

ABSTRUCT
This paper will describe the general idea of the JHP facility, primarily from the accelerator's point of view, and up-to-date results of the research and development on accelerator components. Among others, the R&D on the proton linac has been pursued at the KEK Laboratory since 1987, efforts having been devoted mainly to the development of prototype rf power sources, the rf structure development for the coupled-cell linac and the realization of a 10-MeV linac. The R&D study on the heavy-ion linac has been made at Institute for Nuclear Study, University of Tokyo, primarily on the split-coaxial RFQ linac.

I. INTRODUCTION

The Japanese Hadron Project (JHP) aims at a new research facility for not only neutron scattering but also muon science and unstable nucleus physics. Secondary beams like neutrons, mesons, muons and unstable nuclei are produced with a proton beam of 1 GeV and 200 μA in the JHP.[1)]

To date, in Japan, research of pulsed-neutron scattering and muon science has been done at KEK since 1980, using a proton beam of the Booster Synchrotron of the 12-GeV KEK-PS. This facility provides with a beam of an average current of 6 μA at an energy of 500 MeV. There has been a strong demand for higher intensity for many years.

Physics using short-lived, exotic nucleus beams has brought about growing interests among not only nuclear physics, but also astrophysics, atomic physics and so forth. Spallation reactions from heavy elements bombarded with high-energy protons are preferable for producing a variety of unstable nuclei.

A particular feature of the JHP is that it is a combined project of various disciplines which use hadron beams. Accordingly, the time structure of secondary beams is required to cover a wide range from an ultra-short pulse of 20 ns to the continuous. Hence, we have proposed the accelerator system which is composed of a proton linear accelerator, a compressor/stretcher ring, and a heavy-ion linear accelerator. The layout of the proposed facility is shown in Fig.1.

The source of the proton beam is a linear accelerator of 500 m in length, which delivers a negative hydrogen beam with an average current of 400 μA at an energy of 1 GeV. It operates at a repetition rate of 50 Hz with a peak current of 20 mA and a macro-pulse length of 400 μs. A large fraction of the accelerated beam is transferred to the compressor/stretcher ring, and only a small fraction of the accelerated beam, e.g. 10 ~ 30 μA, is transferred to a production target of unstable nuclei.

The function of the compressor/stretcher ring is to compress a 400-μs long beam pulse delivered from the linac to much shorter one, or to make a continuous beam by stretching the accumulated beam. The rf frequency of the ring is twice as high as the revolution frequency, and two bunches are formed in the ring. The time duration of the bunch is 200 ns in the normal operation. One of these bunches is extracted to the spallation neutron source by fast extraction. The number of protons per bunch will be 1.2×10^{13}, the average current dedicated to the neutron source being 100 μA.

The residual bunch is dedicated to muon(and meson) science. The muon science arena requires an extracted beam of a time structure ranging from an ultra-short pulse to the continuous. In the normal operation, the residual bunch is extracted without any measure with a pulse length of 200 ns. If one needs an ultra-short bunch, it is further compressed with the non-adiabatic bunch rotation

technique using rf. When the continuous beam is required, the beam is moved to a specific betatron resonance and extracted over a period of 20 ms with the resonance extraction method.

The production of unstable beams applies the technique of on-line isotope separator. The proton beam of some 10 μA hits a thick target of heavy elements, and spallation products, diffused from inside, are ionized and resolved in mass with a high-resolution mass separator. Unstable nuclei so produced are accelerator to an energy of 6.5 MeV/u with a heavy-ion linear accelerator system.

II. DESCRIPTION OF THE R&D PROGRAM

The most crucial issue in the development of the accelerator system of the JHP is the proton linear accelerator. Therefore, we have been running the R&D study since 1987 in the Accelerator Department of the KEK Laboratory. In parallel to this, a development program has been pursued, at Institute for Nuclear Study, University of Tokyo, on the heavy-ion linac.

The proposed proton linear accelerator is composed of;[2)]

- a negative-hydrogen ion source (50 keV)
- a four-vane RFQ (3 MeV)
- an Alvarez section (150 MeV)
- a high-ß section (1000 MeV)

as shown in Fig.2. The design parameters of the linac are shown in Table 1. The following is a brief description of the proton linac.

A feature of the present linear accelerator is that higher rf frequencies are adopted, compared with the conventional. The RFQ and Alvarez sections will operate at 432 MHz, while many proton linacs so far have been operating in the 200-MHz domain. Taking account of the trapping efficiency across the transition region, the high-ß section will be at 1296 MHz. These choices make it possible to apply klystron amplifiers at both frequencies, which implies much more stable and reliable operation than expected with triode or tetrode amplifiers. In particular, klystrons with specifications close to the present requirement are commercially available in the 400-MHz and 1300-MHz regions. Although common in every accelerator, beam availability should be exceptionally important in the JHP linear accelerator, since the users of the experimental facilities will be a number of small-scale experiments, rather than a small number of big, long-term experiments as in high energy physics.

No working linacs in the above-mentioned frequency domains exist up to date, although test accelerators have been built; e.g. the 400-MHz region at Los Alamos. Therefore, the design must be confirmed in actual models, and experiences in operation of the technical components and their assemblies at their nominal ratings must be gained in advance of making the final design. Hence, we have set the followings as the objectives of the R&D study:

(1) Confirmation of the design, particularly of the low-energy end.
Performance of the whole system is strongly dependent on performance of the front-end. Therefore, the construction of the actual prototype of the front-end of the linac with an energy of about 10 MeV has been exhaustively pursued from the beginning.

(2) Development of the rf structure preferable for the high-ß section.
The high-ß section is the main body of the linac in size and cost.

(3) Development of prototype rf sources at both frequencies with designed ratings.
Stability and reliability in operation of the linac depend on how stable and reliable rf power sources work. Beam availability of the whole JHP facility will be certainly determined by reliability of the proton linac. Thirteen power sources are required for the RFQ and Alvarez sections, and 36 for the high-ß section. In this context, we started the R&D program from fabrication of power sources.

The negative-hydrogen ion source is of a volume-production type. Since an RFQ linac will be placed very close to the ion source, a cusp-field surface-plasma type ion source, which uses cesium vapor and could reduce breakdown voltage in the RFQ, is not preferable, although it has been working stably in the KEK-PS for many years. The volume-production type ion source is primarily free from cesium, and has been believed to be bright.

An energy of 3 MeV has been chosen for the RFQ. Higher energy of the preinjector is preferable for the following Alvarez section. Even with the high injection energy to the Alvarez section, the length of the unit cell at the entrance of the Alvarez section is 25 mm, since the rf frequency is twice as high as the conventional one. Hence, strong focusing will be required, in particular at the low-energy part, and permanent magnet quadrupoles will be used. They can produced a field gradient as high as 185 T/m for a bore radius as small as 6 mm. The RFQ and

Alvarez sections are supplied rf power by 13 klystrons, each of which will deliver a peak rf power of 1 MW.

The high-ß section is made of coupled-cell structures, as usual. The total number of accelerating cells is 3568. They are grouped into 152 tanks, and fed rf power by 36 klystrons, whose peak rf power is 3 MW.

The heavy-ion linac for accelerating unstable nucleus beams is composed of; [3)]

a split-coaxial RFQ (to an energy of 170 keV/u)
an IH-type linac (1.4 MeV/u)
an Alvarez section (6.5 MeV/u).

Fig. 3 shows the schematic of the proposed heavy-ion linac.

Unstable nuclei produced in the ISOL ion source have an energy of 1 keV/u. Since the velocity of particles is very slow, the rf frequency of the front-end of the heavy-ion linac will be as low as a few ten MHz. The conventional four-vane type RFQ will become big at these frequencies, hence a special rf structure is necessary to accelerate them. The split-coaxial RFQ(SCRFQ) with four vanes is the one which we have adopted in the present scheme. This accelerator can accept unstable particles of a charge-to-mass ratio down to 1/30. In addition to this main channel, a side channel is conceived in order to accelerate stable nuclei of larger charge-to-mass ratios.

The principal objectives of the R&D study on the heavy-ion linac are the development of the ISOL ion source system and the SCRFQ linac.

III. RESULTS OF THE R&D STUDY

III-1. Development of the front-end of the linac

(1) Volume-production type ion source

A volume source has been developed, since it is thought to be bright and free from cesium, as described before. The final goal of the ion source is a peak current of more than 20 mA with a normalized emittance of 1π mm·mrad. After fabricating a couple of models, we have achieved a current of 20 mA with a reasonable size of emittance.

A recent remarkable finding on the volume source is that introduction of cesium brings about appreciable increase in intensity. In our source, we have observed an increase of intensity; e.g. from 3.5 mA to 13mA[4)], by the introduction of a little bit of cesium. The fact that no continuous supply of cesium is necessary in the volume source is quite different from the surface-plasma type ion source, in which a fairly large amount of cesium consumption is needed in order to keep cesium coverage of the converter surface on which negative hydrogens are produced.

We have been making experiments in order to explore the mechanism of negative ion production in the volume source. It has been conceived so far that negative hydrogens are produced through dissociative attachment of electrons to highly-excited hydrogen molecules; $e^- + H_2^* \rightarrow H + H^-$. According to experiments made at KEK, the reaction of H^0 (thermal energy) + e (metal)$\rightarrow H^-$ on the surface of the anode electrode plays an important role in the production of negative hydrogens in the volume source. In this mechanism, cesium decreases the work function of the surface, and the above-mentioned reaction becomes easy to occur.

Mori and his collaborators have been measuring the reaction cross section of the above-mentioned fundamental process.[5)]

(2) RFQ linac

The RFQ linac has been recently used as the preinjector to proton and heavy-ion linacs, since it can bunch and accelerate particles with high efficiency. The conventional Cockcroft-Walton accelerators are limited in the practical maximum energy to 750keV,while it is possible to design an RFQ linac of much higher energies. The highest energy so far is 2 MeV, which was achieved in Los Alamos. We have struggled with optimization of the RFQ energy by compromising technical feasibilities of a high-energy RFQ and the front-end of the Alvarez section. An energy of 3 MeV has been adopted. The length of the RFQ becomes 2.7 m, in order to keep the maximum surface electric field less than 1.8 times the Kilpatrick limit. This RFQ is made of vacuum-melt, oxigen-free copper(0.2% of silver added). It is, in general, difficult to fabricate a four-vane RFQ long compared to the rf wavelength (4 times the rf wavelength in this case). In order to examine rf properties of the long RFQ, a cold model cavity, full in size but with no vane modulation and no

side tuners, was constructed. We have achieved an intervane distance errors of ± 10 μm, and a longitudinal and azimuthal field uniformity of ± 3.5 % with adjusting only end tuners.[6] It is expected that a more uniform distribution could be obtained if side tuners will be installed.

In general, field non-uniformities arise from geometrical imperfections. If the frequency difference between the accelerating mode and the nearest dipole or higher-order quadrupole mode is small as is the case for a longer cavity, a small amount of imperfection mixes these modes and leads to an appreciable field non-uniformity. This is a reason why mechanical accuracy is much severer for longer cavities.

According to experiences so far, tuning process was complicated even with end tuners only. Actually the field distribution was apt to be affected even with change in ambient temperature. Furthermore, when we go to a high-power model, we must anticipate thermal deformation of the cavity and situation would be much more complicated.

It is quite common in the RFQ cavity to use a measure of stabilizing fields. The most classical way is the vane coupling ring(VCR), as shown in Fig. 4(a). Although it has been known to be effective to stabilize fields in most RFQ linacs operating so far, its mechanical structure is rather complicated and cooling of vane coupling rings is very difficult. Application of the vane coupling ring specifically to high-duty RFQ seems to be unpractical. Hence, main efforts have been devoted to develop a new stabilizing mechanism which is applicable to a high-duty cavity like the present case, and a new stabilizing structure have been devised, which we call as the "π-mode stabilizing loop(PISL)",[7] as shown in Fig. 4(b).

The principle of the PISL is that the total magnetic flux normal to a surface surrounded by a conducting closed-loop is zero. As can be seen in Fig.4(b), the PISL affects mainly the field pattern of dipole modes, while leaving the quadrupole modes unchanged. As a consequence, the introduction of the PISL pushes up the frequencies of dipole modes. The larger the coupling area, the larger the frequency shift. As is easily seen, the VCR has the largest coupling area among possible PISL configurations. The PISL concept is certainly a generalization of the vane-coupling-ring concept.

As MAFIA simulations have indicated, the frequency difference of the nearest dipole mode from the accelerating mode is -14 MHz without any stabilizing mechanism, while it become +80 MHz with an introduction of the PISL. It is important that the dipole modes lie above the accelerating mode. The induced capacitance due to the PISL is several times smaller than that of the VCR. The induced current on the conductor and hence the reduction of Q-value are smaller for the PISL than the VCR, accordingly. Resultant longitudinal variations of the quadrupole field on the beam axis are 0.16 % and 0.38 % for the PISL and the VCR, respectively.

Application of the PISL structure to the cold model which we have already finished is now in progress. Confirmation of the new stabilization mechanism will be made by the end of this year. Based on these studies, a high-power model will be fabricated in FY 1991.

(3) Alvarez section[8]

Before fabricating a high-power model, a 35-cell cold model, 2.6 m long and made of aluminum alloy, was fabricated in order to confirm the design of the front-end of the Alvarez section. As seen in Fig. 5, a field flatness within 1.2 % was obtained without use of post couplers. Measurements have shown that the cavity becomes proof against perturbations when post couplers are used, and that it is the optimum to put the post couplers every other cell.

In parallel with rf property studies on the cold model, we have proceeded with development of fabrication techniques of a high-power cavity. The most crucial is the fabrication of NdFeB quadrupole magnets. NdFeB has an advantage of stronger field strength than SmCo, while weaker against radiation. Hence NdFeB will be used at the low-energy end of the linac, where a stronger field is required. From beam dynamics requirements, the deviation of the magnetic center from the axis must be less than 20 μm (r.m.s.), which predicts a deviation of the beam from the axis of 1 mm. We have already succeeded in fabricating NdFeB quadrupole magnets with the required accuracy.

The fabrication of a high-power model 1.2 m long, which corresponds to an energy from 3 MeV to 5.4 MeV, is in progress. It comprises two separate tanks, involving totally 18 cells. The tank and drift tubes are made of oxgen-free copper (OFC). This model will be finished by March 1991.

III-2. Rf structure development of the high-ß section[9)]

Among various rf structures, the annular-coupled structure (ACS) has been pursued for the high-ß section of the JHP linac, since it preserves axial symmetry, which is preferable for mechanical and electrical stabilities, and it has relatively high shunt impedance. The on-axis-coupled structure (OCS) has been used in the TRISTAN electron-positron collider of the KEK Laboratory for many years, and a lot of experience in fabrication and operation of the OCS has been accumulated there. The side-coupled structure (SCS) has been developed and used in LAMPF of LANL, and rf properties have been well understood. The structures of these coupled-cavities are shown schematically in Fig.6.

The idea of the ACS is not new, but there have been no ACS cavities so far, which have been developed up to a level sufficient for practical use. The ACS which was developed in the past was a 'two-slot' ACS. But it is inferior to other coupled-cell structures such as the SCS in many respects, and it has been ignored for many years. Problems of the two-slot ACS are that the TM_{110} mode intrudes into the accelerating passband when the slot orientation is identical in every cell, and that the accelerating mode excites a TM_{210}-like mode in the annular coupling cell, when the slot orientation alternates by 90° from cell to cell, which reduces the shunt impedance of the ACS.

In course of the R&D study, we have found, through computer simulation and model test, that these problems are all cleared up when the number of slots makes four or greater. In particular, the 'four-slot' ACS could be promising for the high-ß structure. As a matter of fact, resonant frequencies of the accelerating mode and the TM_{110} mode separate each other (Fig. 7), and the shunt impedance is fairly good; 42 MΩ/m measured at a coupling factor of 0.05. This is competitive with the side-coupled structure.

In order to check performance at high-power, we have constructed a prototype model of a reduced cell number. Figure 8 show the schematic drawing of the high-power model. It comprises a pair of ACS cavities of five accelerating cells coupled via a bridge coupler.

According to low-level measurements, the unloaded Q-value is 1.9×10^4, which is 79 % of the one calculated with SUPERFISH. Since the reduction of Q-value owing to surface finish and assembling is estimated as around 4 %, a reduction of 17 % might come from coupling slots. Figure 9 is the distribution of the accelerating-field measured on the beam axis. It was sufficiently uniform, and no tuning was necessary.

High-power test has been finished with a peak power of 300 kW, a repetition rate of 50 Hz and an rf pulse length of 300 μs. Except for the pulse length, whose designed value is 500 μs, and which is limited by the pulse-forming network of the power supply, the operating condition is the same as the designed value. Figure 10 shows a result of the first conditioning of the assembled unit. The design value was reached in 10 hours. During conditioning, no light emissions due to discharge or arcing were observed inside the cavity. A plateau at 170 kW is owing to conditioning of the rf window. Once the designed power has bee reached, no aging effects are now observed.

III-3. Rf power source development.

As mentioned earlier, we started the R&D program by designing and fabricating a prototype rf power source for 1296 MHz with the specifications similar to one unit of the coupled-cell linac, since we have thought that the power source is the most critical component of the linac, and that the development of components satisfying the specified rating is urgent. Since the required peak power is 5 MW, the capability of the klystron must exceed 5.5 MW. This power is almost the maximum which is thought technically achievable for the pulse length of 600 μs. The pulsed power supply is a line-type modulator and uses a pulse transformer of step-up ratio of 7. The power source itself has been operating, using a dummy load, with a peak power of 5 MW and a pulse length of 400 μs at a repetition rate of 30 Hz. It has been used for testing the prototype ACS cavity assembly.[10)]

The rf power source for 432 MHz has already been designed and started fabrication. It uses a klystron with a modulation anode. The high voltage power supply and the hard-tube modulator for the modulation anode have been finished and assembled in KEK. The klystron is now on order.

Table 2 shows the specifications of these power sources.

III-4. Development of the SCRFQ.

The history of research on the split-coaxial RFQ at INS is long. Arai and his collaborators have developed the SCRFQ since 1984. The particular features of the INS' SCRFQ are that it uses four vanes to generate transverse focusing and longitudinal accelerating fields, and that it applies the multi-module cavity structure, which makes it possible to fix electrodes to the cavity wall with stems firmly.

A proton model of the SCRFQ of a frequency of 50 MHz was fabricated in order to investigate rf properties of this type SCRFQ. Table 3 lists the main parameters of the proton model, and Fig.11 shows the structure of the four-vane SCRFQ. In this model, a mechanical accuracy of vane alignment better than ±0.1mm was obtained, and a good field stability was achieved. Beam acceleration test has shown that the performance on output energy, beam emittance and transmission efficiency was in good agreement with the design.[11)]

After success in the proton model, a prototype model, which works under a high-power condition similar to the final design of the JHP heavy-ion accelerator, has been fabricated, in order to examine cooling efficiency,breakdown problem and to accelerate particle beams under the working conditions. This model is completely the same as the front-end of the JHP heavy-ion linac, except for the acceptable charge-to-mass ratio. Table 4 lists the main parameters of the 25.5 MHz prototype SCRFQ, and Fig. 12 shows the schematic of the prototype SCRFQ.[12)]

The fabrication of the cavity was completed in October, 1989. As results of low-power tests, the uniformity of fields among four quadrants is satisfactory(within ±0.6%). The unloaded Q-value is 6400, which is about 84% of the calculation. In high-power tests, they have achieved an intervane voltage of 110 kV with a peak power of 70 kW. Fig.13 shows a curve of attained intervane voltage as a function of aging time. In this graph, aging time means (operation time) x (duty factor). This data was obtained with a duty factor of 0.6% ~ 3%. The multipactoring levels were overcome after aging time of 140 minutes.

High-power tests are continuing so as to increase duty factor to the designed value of 10%. Beam acceleration test will begin with N^{2+} ions by December 1990.

References

1. M. Kihara, Particle Accelerators 32 (1990) 1.
2. Y. Yamazaki and M. Kihara, submitted to 1990 Linear Accelerator Conference.
3. S. Arai, et al, Proc. 18th INS International Symposium on Physics with High-intensity Hadron Accelerators, Tokyo,March 14-16, 1990.
4. Y. Mori, et al, submitted to Nucl. Instr. Meth.
5. Y. Mori, private communication.
6. A. Ueno, et al, submitted to 1990 Linear Accelerator Conference.
7. A. Ueno, et al, submitted to Nucl. Instr. Meth.
8. F. Naito, et al, submitted to 1990 Linear Accelerator Conference.
9. T. Kageyama, et al, submitted to 1990 Linear Accelerator Conference.
10. M. Ono, et al, Particle Accelerators 32 (1990) 51.
11. S. Arai, et al, Nucl. Instr. Meth. A278 (1989) 236.
12. S. Shibuya, et al, submitted to 1990 Linear Accelerator Conference.

Table 1 Design parameters of the proton linear accelerator.

Energy	1	GeV
Total length	500	m
Average current	400	μA
Repetition rate	50	Hz
Peak current	20	mA
Beam pulse length	400	μs
Rf pulse length	600	μs
Duty factor	3	%

Table 2 Specifications of rf power sources.

A. 1296-MHz rf power source		
Modulator and pulse transformer		
Line-type		
Peak voltage	140	kV
Peak current	107	A
Pulse duration	600	μs
Klystron		
Thomson, TH2104A		
Peak output power	5.5	MW
Pulse duration	600	μs
Repetition	50	Hz
B. 432-MHz rf power source		
Modulating anode/hard-tube modulator		
Output voltage	110	kV
Peak output current	92	A
Pulse duration	600	μs
Nunber of load klystrons	2	
Klystron		
Thomson, TH2134		
Peak output power	2	MW
Pulse duration	600	μs
Repetition	50	Hz

Table 3 Main parameters of the 50-MHz proton model of the SCRFQ.

Frequency		50	MHz
Kinetic energy	2.0	59.6	keV
Normalized emittance		0.3π	mm·mrad
Vane length		2.052	cm
Cavity diameter		0.4	m
Intervane voltage		2.9	kV
Transmission			
(0mA)		85	%
(0.1mA)		76	%
(0.2mA)		62	%

Table 4 Main parameters of the 25.5 MHz prototype of the SCRFQ.

Frequency		25.5	MHz
Charge-to-mass ratio		>1/30	
Kinetic energy	1.0	45.4	keV/u
Normalized emittance		0.6π	mm.mrad
Vane length		2.135	m
Maximum intervane voltage		109.3	kV
Kilpatrick factor		2.2	
Minimum bore radius		5.21	mm
Transmission		(0mA) 92.6	%
(3mA)		61.8	%
(5mA)		47.4	%

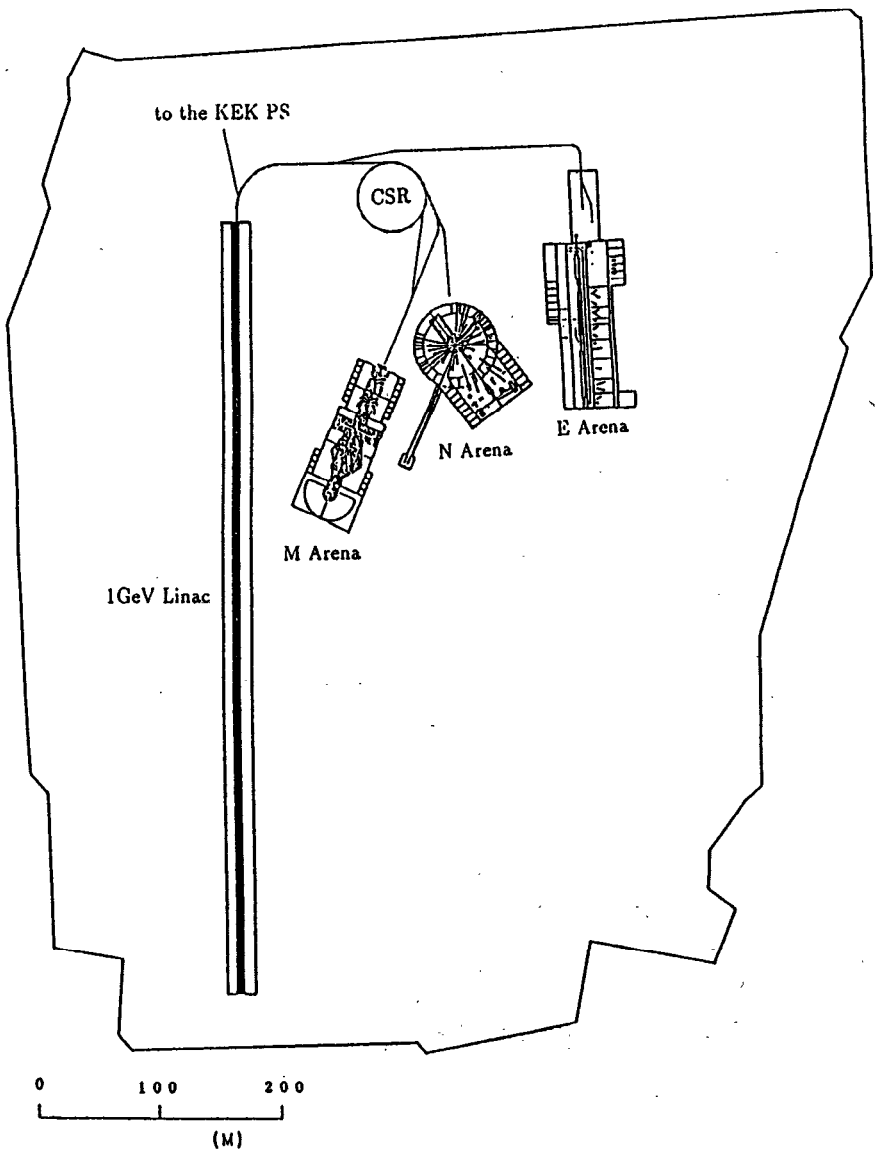

Fig. 1 Layout of the proposed facility of the JHP.

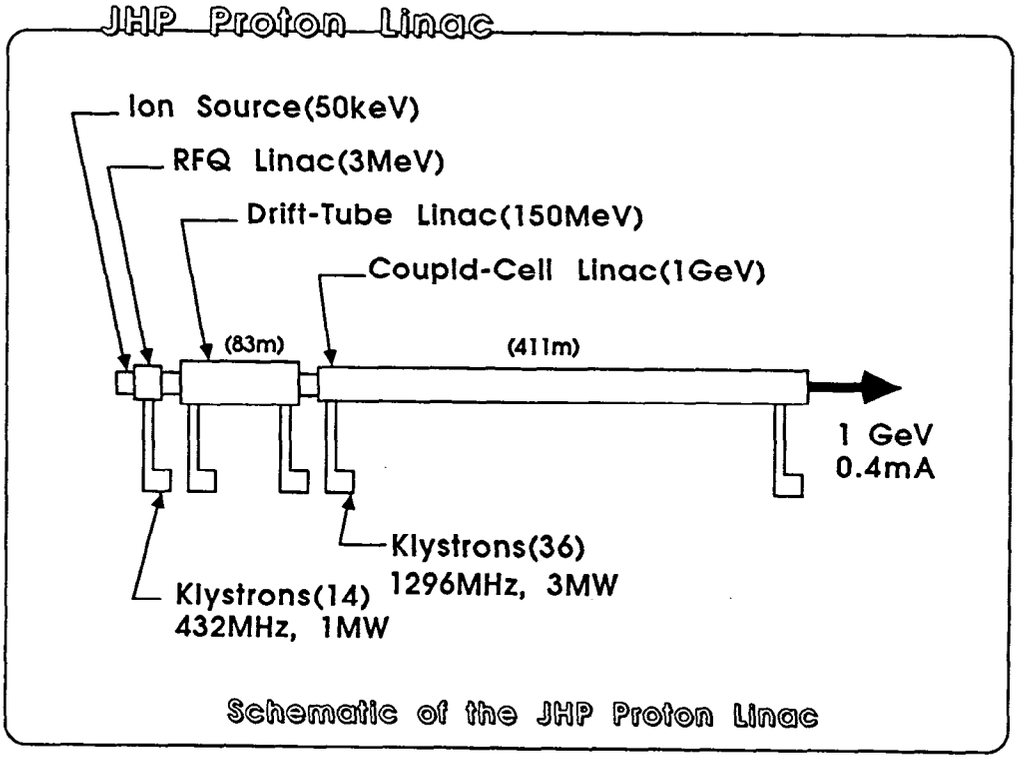

Fig. 2 Schematic of the proposed proton linear accelerator.

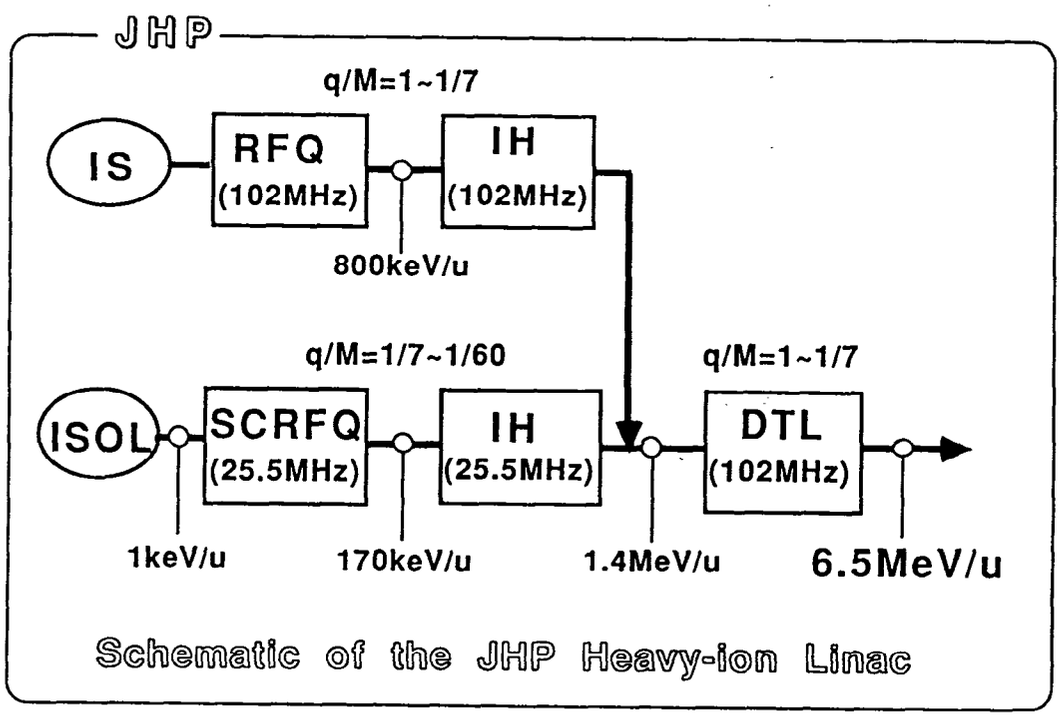

Fig. 3 Schematic of the proposed heavy-ion linear accelerator.

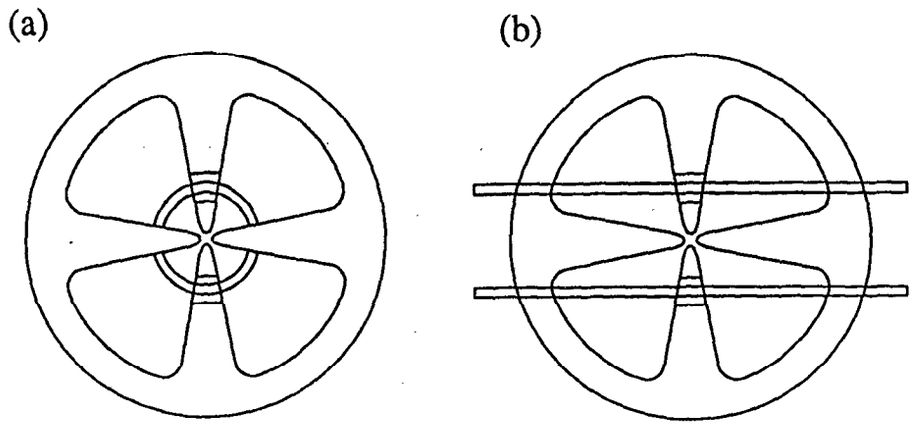

Fig. 4 Field stabilizing mechanisms.
(a) vane coupling ring and (b) π-mode stabilizing loop.

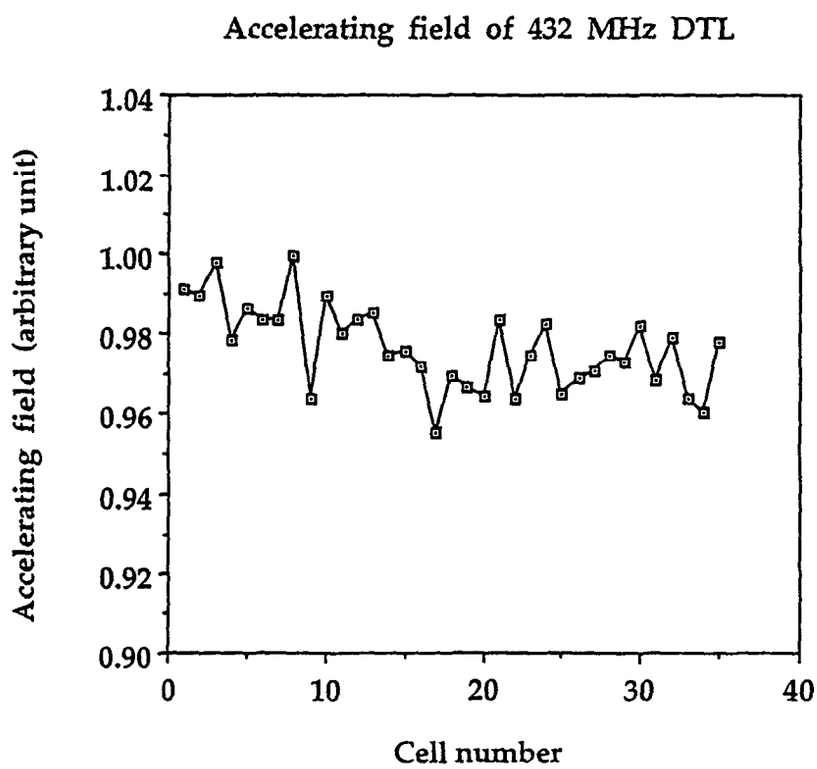

Fig. 5 Field distribution for the 432-MHz Alvarez linac cold model.

On-axis-coupled structure (OCS)

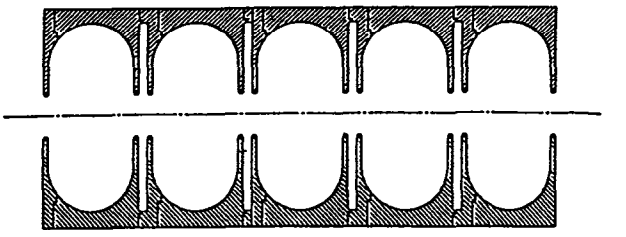

Side-coupled structure (SCS)

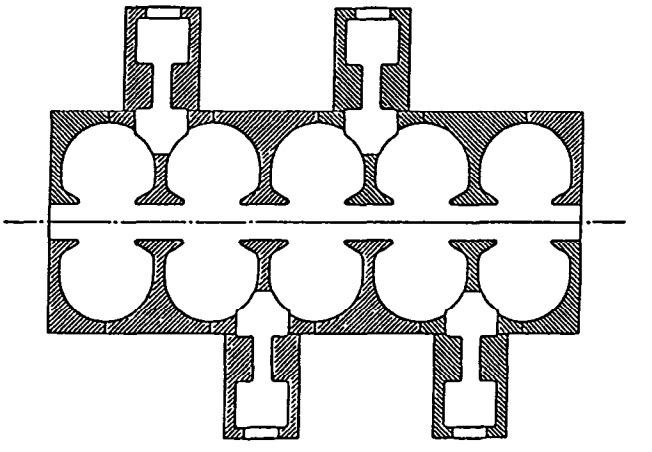

Annular-coupled structure (ACS)

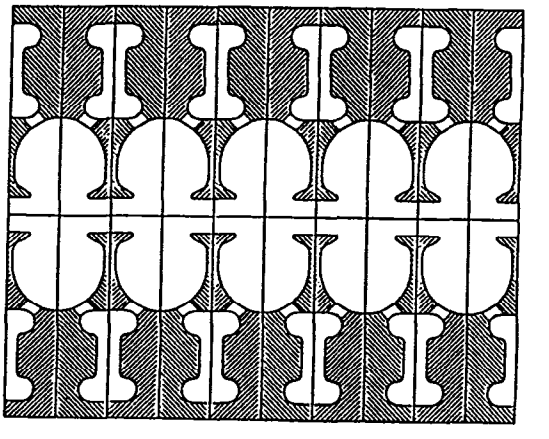

Fig. 6 Various coupled-cavity structures.

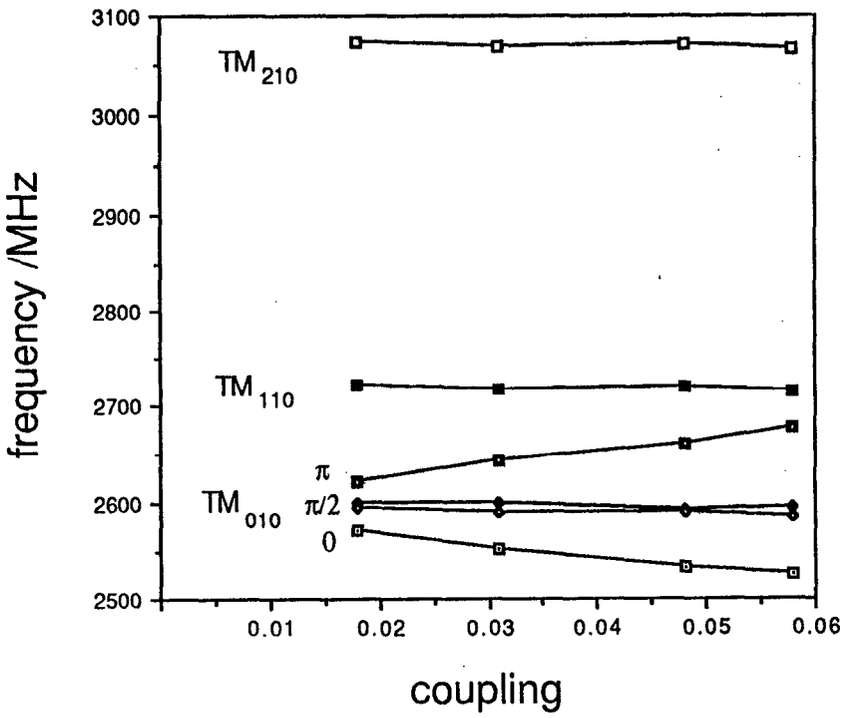

Fig. 7 Resonant frequencies of the accelerating mode and the higher-order modes for the four-slot ACS cavity.

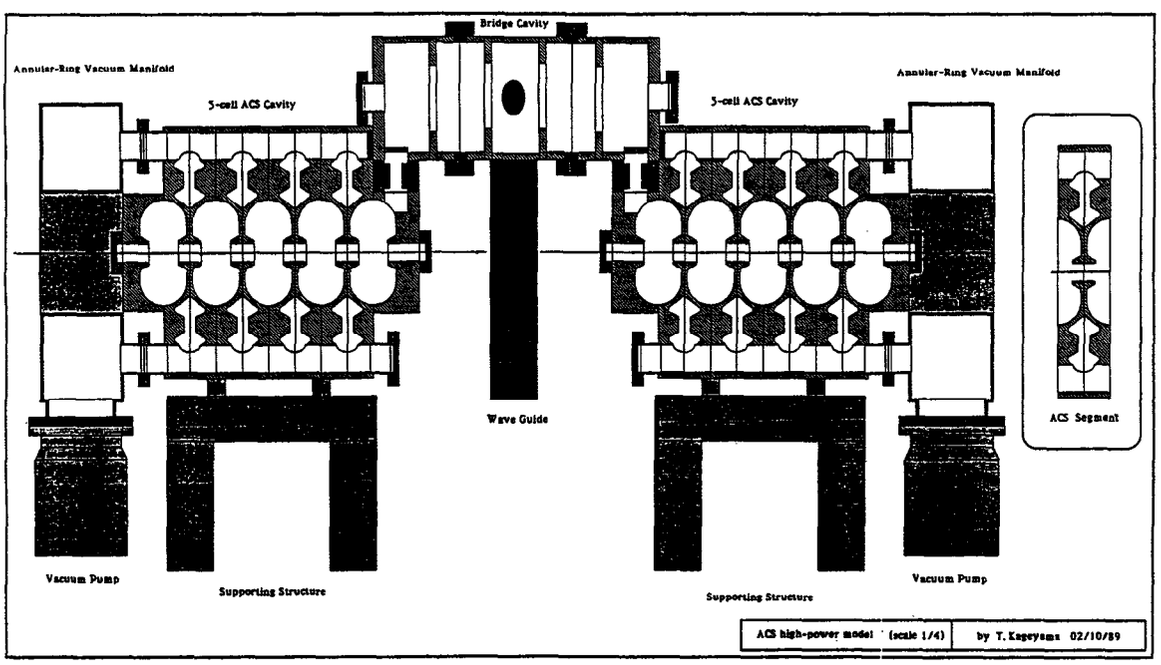

Fig. 8 Schematic drawing of the ACS high-power model.

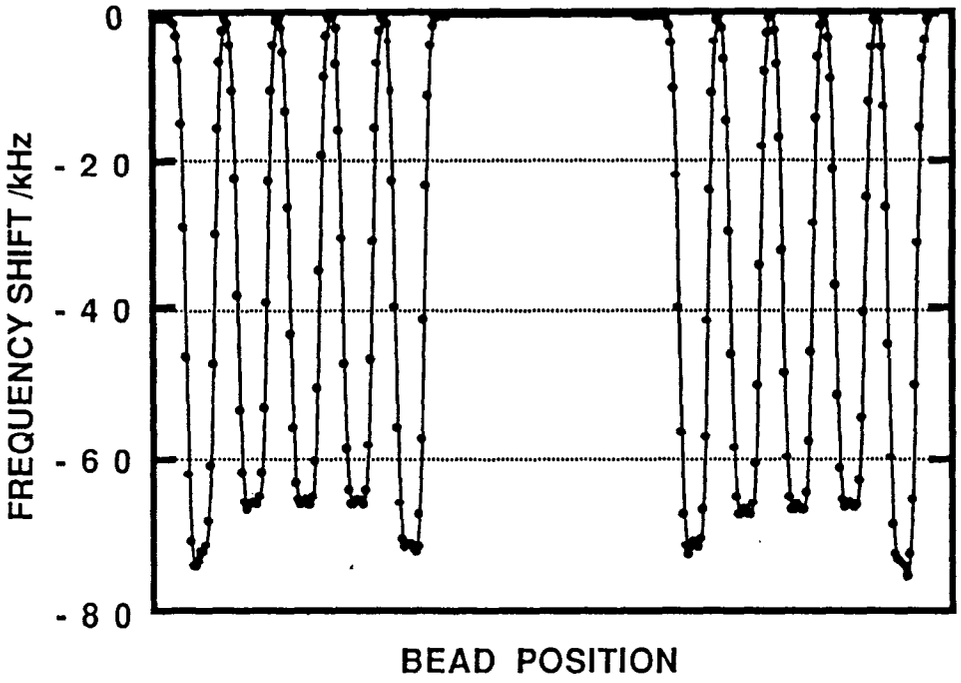

Fig. 9 Field distribution for the ACS high-power model.

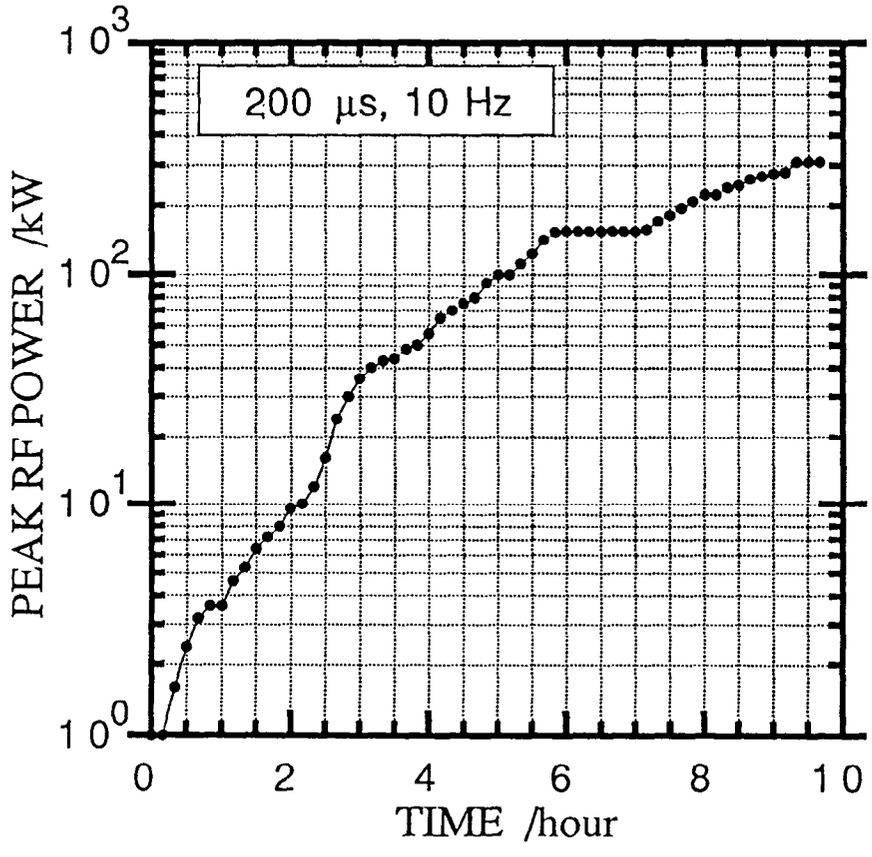

Fig. 10 First conditioning history of the assembled ACS unit.

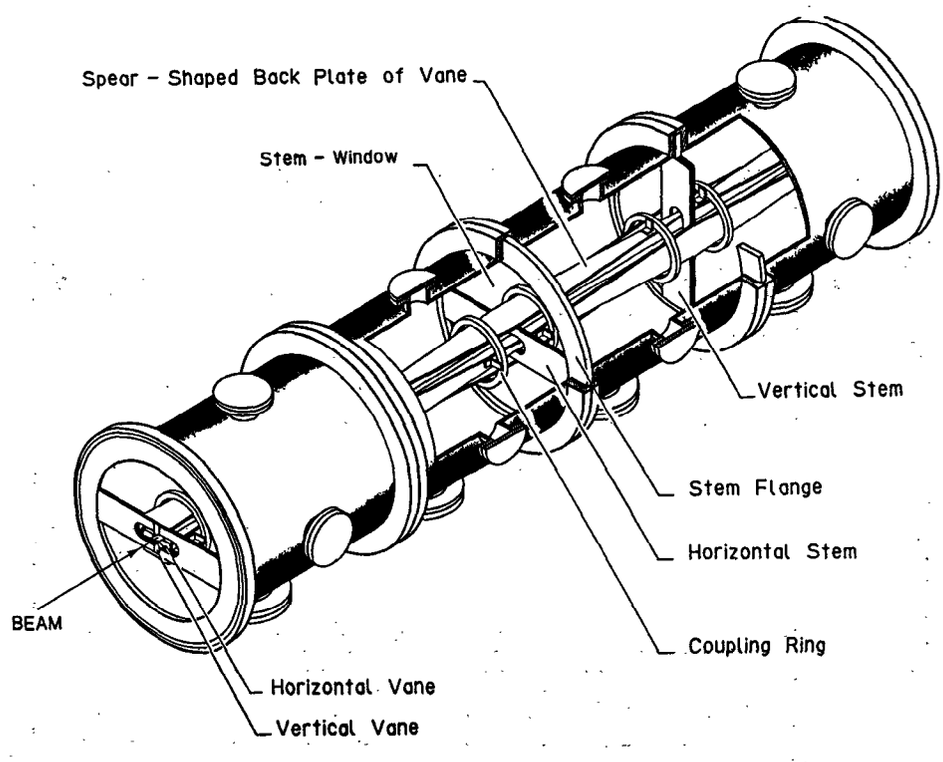

Fig. 11 Proton model of the SCRFQ.

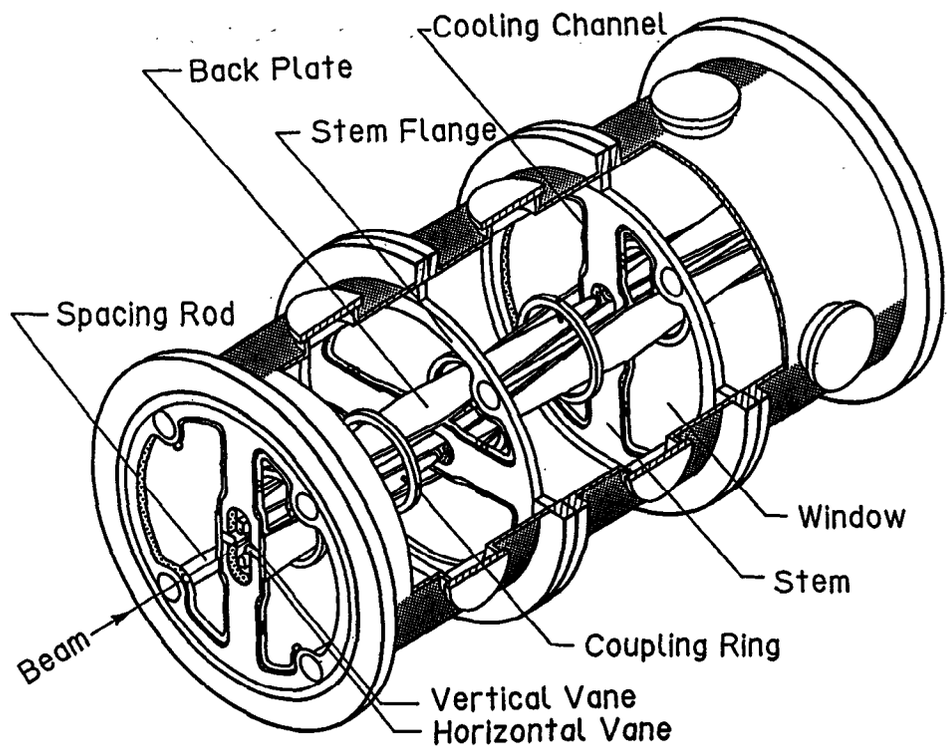

Fig. 12 25.5-MHz prototype model of the SCRFQ.

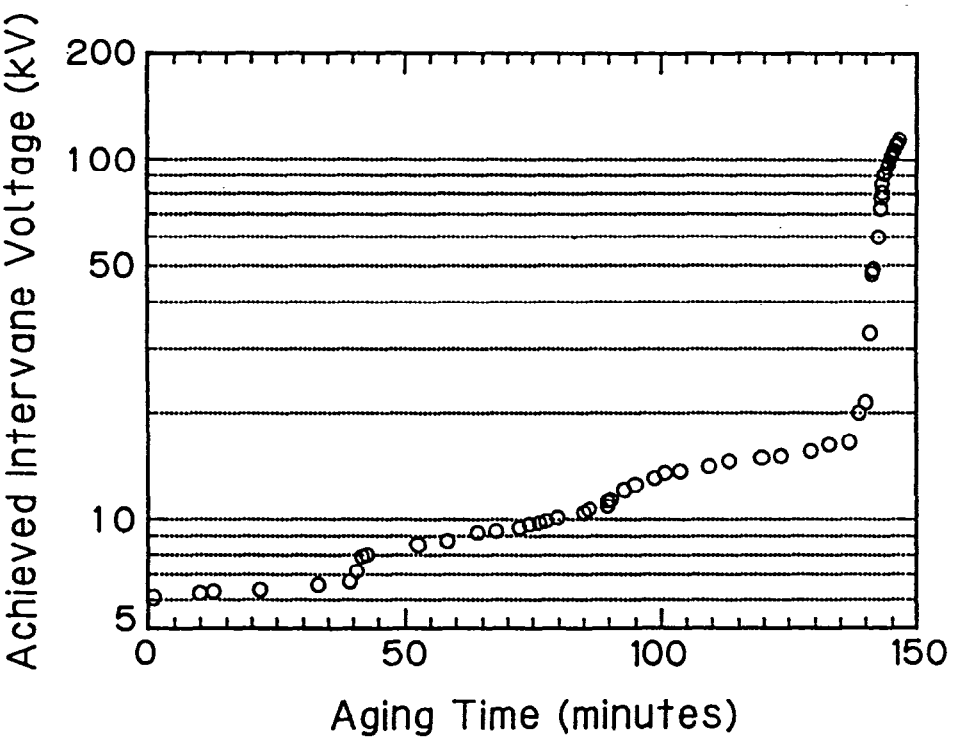

Fig. 13 Aging history of the assembled SCRFQ prototype.

Q(S.Machida): Why do you separate the DTL part of 10MeV into two tanks? I guess there is no advantage.

A(M.Kihara): We make a 10MeV section as one tank. The tank is separated into pieces for technical reasons and assembled together.

Q(A.D.Taylor): Is 400μA a physical or a fiscal limit?

A(M.Kihara): A budgetary problem exists, of course. Technically, more than 400μA is not optimistic in the present design.

Q(I.M.Thorson): What were the considerations that indicated doubling the basic operating frequency for DTL section compared to existing machines?

A(M.Kihara): The main reason is a possibility of using klystrons as power amplifiers for RFQ DTL. It gives rise to stable operation.

Q(R.J.Macek): Are you planning R&D on RF sources?

A(M.Kihara): We have finished a prototype RF source for 1296 MHz with designed specifications. A source for 432 MHz is being fabricated now and will be finished by March 1992.

ICANS-XI International Collaboration on Advanced Neutron Sources
KEK, Tsukuba, October 22-26, 1990

Photons and Neutrons

Gen Shirane
Brookhaven National Laboratory
Upton, New York 11973

A review is given of two selected topics in current activities of synchrotron x-ray studies; magnetic x-ray scattering and inelastic x-ray scattering. These are the research areas where photons and neutrons directly compete and supplement each other.

I. MAGNETIC X-RAY SCATTERING

A great deal of progress has been made in the field of magnetic x-ray scattering with synchrotron radiation. A series of high resolution studies on Ho and other rare earth magnetic structures has revealed many important features of spin arrangements, which escaped clarification by previous neutron diffraction studies. One such example is shown in Fig. 1, taken from the study of the spiral structure in Ho by Gibbs et al.(1). They discovered that the incommensurate periodicity of Ho below T_N=131K is not continuous and locks in specific rational fractions such as 2/11 and 5/27. These ratios can be naturally explained by spin-slip models. For example, the τ_m=5/27 structure is constructed by one spin slip for every 9 atomic layers; namely 4 pairs of spins followed by 1 single spin as depicted on the right side of Fig. 1.

This spin slip creates the interplanar lattice modulation caused by the magnetic-elastic interaction. This periodicity is 2/9, which is different from the magnetic period 5/27. These two peaks, one magnetic and the other charge, are clearly seen in Fig. 1 and they have different line widths. These figures are a clear demonstration of the power of the high intensity and resolution offered by synchrotron x-ray sources.

Magnetic x-ray scattering recently entered into its next stage of development when the resonance at the absorption edge(2-4) was shown to enhance the Ho magnetic cross section by a factor of 50. Fig. 2 shows the effect of the L_{III} absorption edge at 8.07KeV, on the Ho(002)+ magnetic peak. This intensity enhancement of course gives a better visibility for the magnetic peak, which is usually much weaker than the charge peak at x-ray energies outside of the resonance region. Very recently, the resonant magnetic scattering was studied(5) in antiferromagnetic UO_2; the enhancement factor here is 10^6!

One essential difference between magnetic x-ray scattering and its neutron counterpart concerns the contribution of the orbital moment. For neutrons, all magnetic scattering

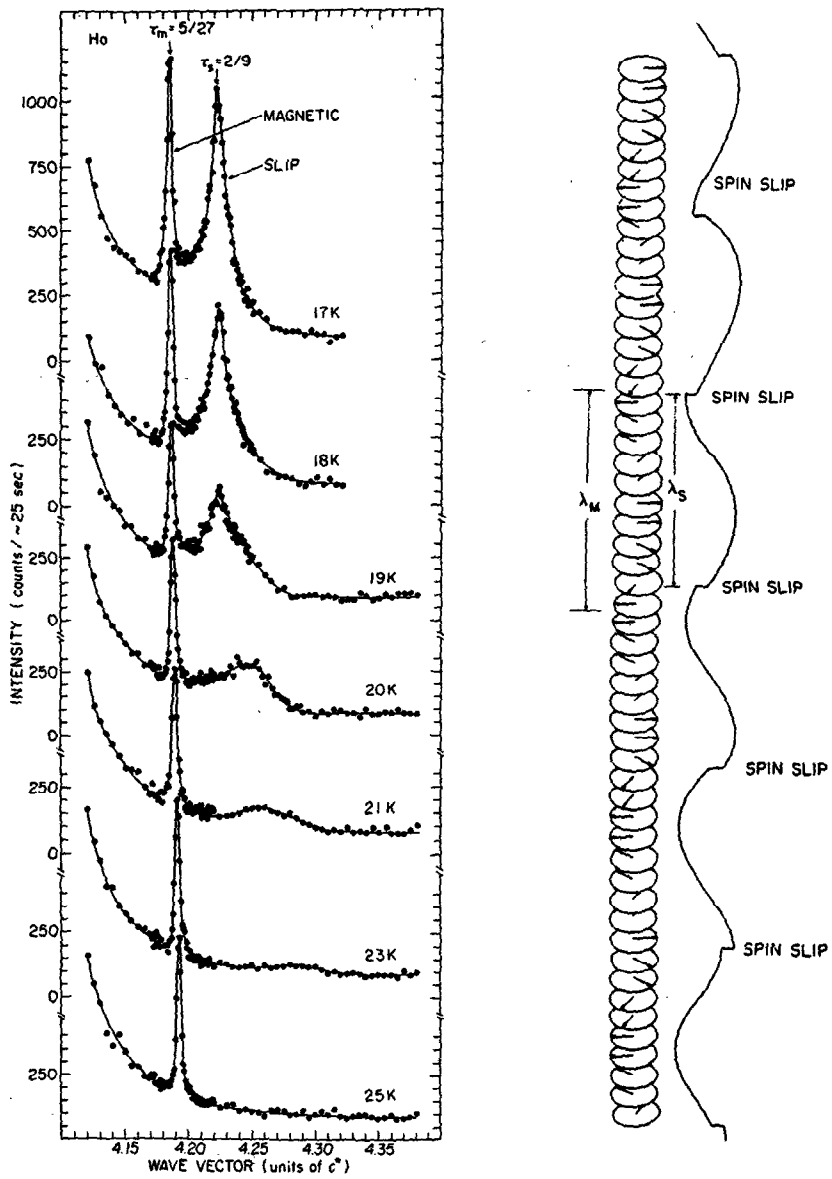

Fig. 1 Synchrotron x-ray diffraction pattern of the satellite above the (004) Bragg peak. The scattering pattern reflects both magnetic (5/27) and charge (2/9) modulations depicted on the spin slip model. After Gibbs et al. (Ref. 1)

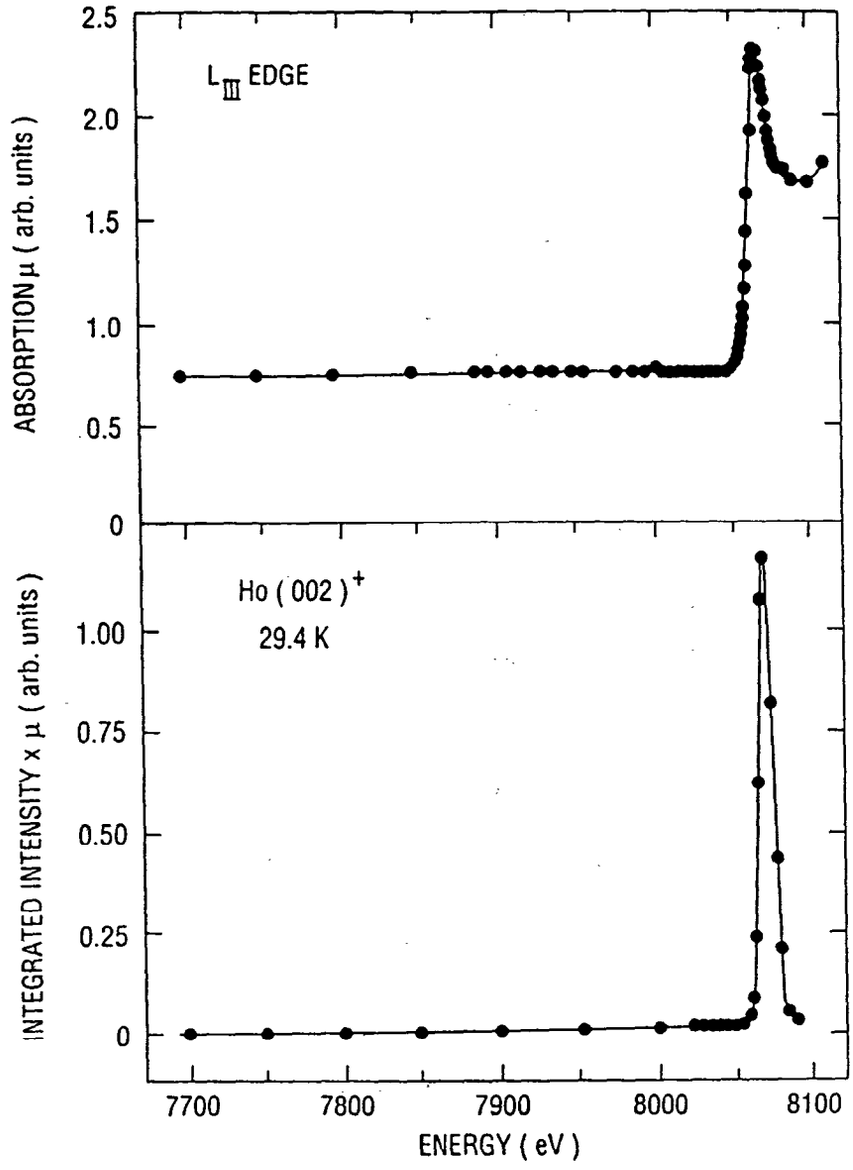

Fig. 2 Top: The absorption measured from a thin film. Bottom: The integrated magnetic intensity of the $(002)^+$ reflection of Ho near the L_{III} edge. After Gibbs et al. Ref. (4).

(spin and orbital) is governed by the magnetic interaction vector $\vec{q}$, the projection of the magnetic moment on the plane perpendicular to the scattering vector Q. Thus, the orbital moment reveals itself only by having a different form factor from that of spin. In the x-ray case, the σ and π polarizations of the scattered beam have different contributions from spin and orbital parts. Thus it is possible to separate out the two components using a polarization analyzer. This technical aspect is described in detail in a comprehensive paper by Gibbs et al[4] on Ho magnetic scattering. Thus, by combining both neutron and x-ray data, one may be able to get definitive information on both components of the magnetization.

II. INELASTIC X-RAY SCATTERING

The second area where x-ray scattering is beginning to overlap with neutron research is direct inelastic x-ray scattering. Because of its favorable energy-wavelength relation, neutron scattering has been the natural tool for the direct observation of elementary excitations in condensed matter. The most commonly used neutrons have 14 meV of energy and a 2.3Å in wavelength. The energy of x-rays with the same wavelength is 5 KeV. In order to attain a sufficient energy resolution for phonon studies, one has to use backscattering from a perfect crystal. This type of experimental arrangement became feasible recently because of the brightness of x-rays emitted by synchrotron and storage rings. A successful test experiment was already reported by Burkel et al[6,7] and is shown in Fig. 3. The monochromator I and analyzer II both consist of spherically bent silicon disks, grooved crosswise to reduce strains, and operate under extreme Bragg back reflection (777) with $\theta = 89.96$ at the monochromator and $\theta = 89.86$ at the analyzer. The beam is directed from the premonochromator III into the monochromator I and finally focused on the sample IV. The insert in Fig. 3 shows an example of phonon scans of diamond at (4,2,0,0). $\langle n \rangle$ is the Bose occupation factor. The scan clearly demonstrates the imbalance between energy gain and loss. The energy scan was carried out by varying the temperature of the analyzer crystal. A change of 1° corresponds to an energy change of 30 meV. An energy resolution of 17meV was obtained at the setup located at the hard x-ray wiggler line W2 at HASYLAB.

A similar inelastic x-ray scattering project was initiated at Brookhaven in 1980. A special crystal bender was constructed and tested by Fujii et al[8] using an ungrooved crystal. 12.9 KeV x-rays from a white beam (20 x 2.5 mm^2) were diffracted at $\theta = 89°$ by the Si (880) reflection. The best focusing position gave the smallest spot (0.2 x 0.08 mm^2) and this focused spot is more than three order of magnitude brighter than the unfocused beam. This project has recently been reactivated and a systematic effort is now underway to construct a larger beam bender for a Si crystal 125 mm in diameter. This analyzer crystal must be grooved and a procedure has been developed to dice the Si (111) surface into 0.2 x 0.2 mm blocks, 0.7 mm in height, separated by 0.05 mm wide channels[9].

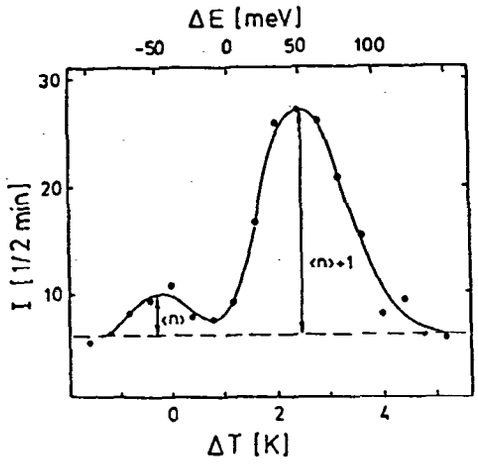

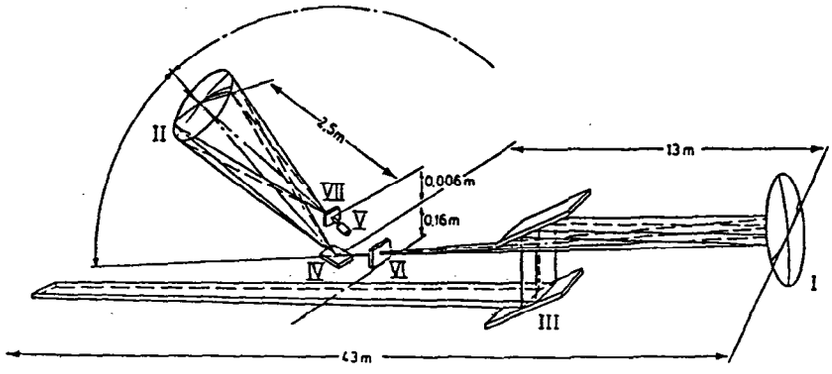

I	monochromator	III	premonochromator	V	detector
II	analyser	IV	sample	VI VII	slits

Fig. 3 Schematic setup of the instrument "INELAX" by Burkel et al (Ref 7).

It has already been demonstrated [6,7] that a direct observation of phonon excitations can be made using a back scattering x-ray arrangement and, as examples, the Be and diamond dispersion curves have been mapped out and show good agreement with neutron scattering data. The next step is the study of electronic excitations, the unique capability of the x-ray setup. With three large 7 GeV x-ray rings now under construction around the world, significant intensity gains are expected for this type of x-ray scattering in the near future.

I would like to thank Y. Fujii, P. M. Gehring, D. Gibbs, J. B. Hastings, G. H. Lander, D. E. Moncton, and D. P. Siddons for stimulating discussions. Work at Brookhaven was supported by the Division of Materials Sciences, U.S. Department of Energy under contract No. DE-AC02-76CH00016.

References

1. D. Gibbs, D. E. Moncton, K. L. D'Amico, J. Bohr, and B. H. Grier, Phys. Rev. Lett 55, 234 (1985).
2. D. Gibbs, D. R. Harshman, E. D. Isaacs, D. B. McWhan, D. Mills, and C. Vettier, Phys. Rev. Lett 61, 1241 (1988).
3. J. P. Hannon, G. T. Trammell, M. Blume, and D. Gibbs, Phys. Rev. Lett 61, 1241 (1988).
4. D. Gibbs, G. Grübel, D. R. Harshman, E. D. Isaacs, D. B. McWhan, D. Mills, and C. Vettier, Phys. Rev. B, to be published.
5. G. H. Lander and D. Gibbs, Private Communications.
6. B. Dorner, E. Burkel, Th. Illini, and J. Peisl, Z. Phys. B. Condensed Matter 69, 179 (1987).
7. E. Burkel, B. Dorner, Th. Illini and J. Peisl, Rev. Sci. Instrum. 60, 1671 (1989).
8. Y. Fujii, J. B. Hastings, S. L. Ulc and D. E. Moncton. Report at SSRL Users Group Meeting, 1981, unpublished.
9. P. M. Gehring, J. M. Tranquada, D. P. Siddons, Private Communications.

ICANS-XI International Collaboration on Advanced Neutron Sources
KEK, Tsukuba, October 22-26, 1990

SOME Thoughts on the Future of Neutron Scattering

by P.A. Egelstaff, Physics Department, University of Guelph

ABSTRACT

Attendees of ICANS meetings believe that neutron scattering has a bright future, but critics of neutron scattering argue that its practitioners are an aging group, that they use a few, very expensive neutron sources and that the interesting science may be done by other techniques. The ICANS committee asked me to comment on the future of neutron scattering in the light of this contrast.

Some comments will be made on the age distribution, on the proper distribution of sources, on the convenient availability of neutron instruments and methods, on the expansion into new areas of science, on applications to industry and on the probable impact of synchrotron sources. It is hoped that these comments will lead to an outward looking discussion on the future.

I. INTRODUCTION

Modern radiation scattering methods began in 1912 when von Laue[1] suggested that crystals would serve as natural diffraction gratings for X-rays and interpreted experimental results in this way. Subsequently the Braggs[2] improved the techniques and showed how powerful the ideas of von Laue were. From 1912 to 1942 only photons were available with sufficient intensity for good experimental work, but after Fermis' group developed the nuclear reactor a second technique became available. The first crystal spectrometer for neutrons was built by Zinn[3] in 1944 for the CP-3 reactor at A.N.L. Due to the background available from 30 years of X-ray diffraction, the development of this new technique was fairly rapid.

Enrico Fermi may be called the 'father of neutron scattering' because he (a) discovered thermal neutrons (b) built the first nuclear reactors which provided an adequate source (c) performed many of the underlying experiments upon which neutron diffraction and inelastic scattering are founded. Unlike neutron diffraction, the new subject of neutron inelastic scattering required a developmental period, but by 1957 when the first international conference took place in Stockholm it had become an established technique also. The age of the personnel then engaged in this work may be judged from the ages of the attendees at the neutron scattering conferences of this period (e.g. the I.A.E.A. meeting on inelastic scattering in 1960). A comparison with conferences held recently (e.g. the Cold Neutron Source meeting at Los Alamos 1990) shows that the average age of scientists engaged in neutron scattering has increased during the past 30 years. In fact many of those attending the ICANS-XI meeting are older than Fermi was when he made the basic experiments listed above.

It is useful to consider the trends in steady state neutron sources since the time of CP3. A plot of maximum thermal flux against year of completion is shown as figure 1. It can be seen that fluxes grew rapidly by three orders of magnitude, and that after this growth a longer time scale was required for further advances. At first the nuclear centres controlled the sources and users were centre employees. In later years the users came from many organizations (e.g. nuclear centres, Universities, Government and Industrial Laboratories, etc.), and for a number of sources the users assumed control (e.g. the I.L.L.). This trend in wider usage and user control was both natural and healthy, and is likely to be continued. However we see that in parallel with the aging of the personnel, there is an aging (and perhaps a flux limit) for the steady state sources. Pulsed neutron sources have been used since the beginning of this subject, but were not fully

competitive with the steady state sources until recently. They have shown a rapid period of development in the 80's, but may also reach a plateau during the 90's. Neutron scattering communities (e.g. Europe, U.S.A., Japan, etc.) are now considering plans for future steady state and pulsed sources at the highest levels, but the time scales and costs are both quite large.

Against this background of trends in personnel and sources it may be useful to consider the future prospects for neutron scattering. Some of the topics which our field should discuss include, the proper distribution of neutron sources, access and availability to all scientists, the introduction of new areas of science, the expansion of industrial uses, and the impact of the new synchrotron sources. An initial attempt to discuss these matters follows.

II. NEUTRON SOURCES

The high flux reactor at the Institut Laue Langevin[4] (I.L.L.) was operated from the outset as a source which was easily accessible to a wide spectrum of users. It was also one where the scientists at the many smaller sources spread throughout Europe could interact with the I.L.L. scientists and contribute to the neutron scattering facilities. In these two respects the I.L.L. differed from the major facilities in N. America, and at the latter there was some discussion on whether the new system could operate successfully? In the U.S.A. local sources were being closed in favour of 'strengthening' central sources. However experience soon showed that the I.L.L. interactive approach led to the introduction of new ideas and methods, and to the expansion of neutron scattering both in numbers of participants and in its impact on new areas of science. It is likely that the interactions between the I.L.L. and the many local sources in Europe (shown schematically in figure 2) were an important contribution to its success. The interaction worked in both directions, the local scientists developed their ideas with their own resources and with help and encouragement from the I.L.L., and then many of these ideas became part of the landscape at the I.L.L. to the benefit of the whole of Europe. The leadership of the neutron scattering field left N. America for Europe probably as a consequence of the support of and interactions with local sources in Europe compared to the run-down of local sources in N. America. The recipe for success in the 70's and 80's was probably the combination of centralization with diversity practised at the I.L.L (figure 2).

The author believes that super-sources discussed at ICANS and elsewhere are not sufficient by themselves for the success of neutron scattering. In addition two other aspects must be emphasized:-

- the interactions with local sources
- the type and quality of access and the infrastructure at the source.

We may ask the questions: will a large central source fail if there are no local sources interacting with it?, and will a large central source fail if it fails to interact with a sufficiently broad spectrum of scientists and to attract new areas of science? For the general health and development of neutron scattering three levels of neutron source are needed:-

- the teaching laboratory source
- the local source
- the high flux central source.

In the past ICANS has concentrated on the latter category, but the author believes that ICANS should widen its scope and discuss advances in the other two categories. Of great importance today is the development of ideas for local sources which will lead to cheap, safe, easily operated sources which have sufficient flux for this purpose.

By combining the views expressed in this section with those given in the Introduction, it is possible to present three observations to the neutron community:-

a) the neutron community is aging while it is still increasing in number;
b) neutron sources are aging and are decreasing in number;
c) local neutron sources are few and are decreasing, but they are essential for the success of the super-sources and of this field generally.

The neutron scattering community should discuss these observations and consider strategies to offset their adverse aspects.

III. INDUSTRIAL AND LOCAL SOURCES

New areas of science to which neutron scattering techniques may be applied successfully are difficult to predict far in advance of their appearance. However they may be encouraged to appear if, at the neutron source laboratory, there is:-

- an interaction with a broad spectrum of scientists and a 'flow-through' system for some personnel;
- a belief that neutron scattering is applicable to all areas of science and that some neutron experiments can be done by novices;
- a good level of access for all scientists (including novices) in the broadest sense.

The implementation of these points will encourage both basic and applied science: in this regard some observations on the industrial application of neutron scattering may be worthwhile. Even with the above favourable environment, each industrial use of neutron scattering is likely to require an initiation period. But once that period is over it should be possible to borrow money (from the usual lending institutions) for construction of specialized industrial application instruments, and repay the loan through industrial user charges. Such industrial programs would be evidence that neutron scattering is a growing and maturing technology. Probably neutron radiography, and strain and texture work using neutron diffraction are examples where this market oriented strategy could be applied.

It is possible that neutron scattering techniques could be included in mass production processes in appropriate cases: for example where preset orientational limits or preset strains are required. Production line samples might be sent to a central source or a portable neutron source might be used on site. In addition there are various "in the field" neutron scattering measurements for which portable sources are necessary. Many people are familiar with the bore-hole survey, airport luggage scanner, activation analysis or radiography applications. However if cheaper, simpler and more powerful portable sources were available the range of applications would increase. In this event the distinction between an 'industrial source' and a 'local source' might disappear.

In the context of this paper, a 'local source' is one large enough to do useful experiments and to serve a geographical region. They could be cheap, small accelerator based sources which can be operated with no more difficulty (or danger) than a motor-car. To achieve this target requires more inventive designs made with these requirements in mind.

The author believes that accelerator designers should work on this problem as much as they have worked on the design of super-sources, and that the discussion of local sources are properly a part of ICANS and should be included in these meetings. To keep the cost of such sources down to an acceptable level will require the production and sale of many units. Consequently if similar designs can be used for local sources, industrial sources and teaching sources that would be an advantage to both user and manufacturer.

IV. TEACHING LABORATORY SOURCES

During the whole period that X-rays have been used to study the structure of materials, there have been X-ray sources available for teaching purposes in University laboratories. As a result these techniques are taught well and widely and several generations of scientists have used them in many applications. The same is not true of neutron sources, and as a result neutron techniques do not appear in most laboratory courses. In turn this means that these techniques are neither used widely, nor properly understood by many scientists. The availability of X-ray sources compared to the lack of neutron sources is related to the energy required to produce one particle, which is very much greater for a neutron than for an X-ray photon. It is therefore unlikely that copious neutron sources can be produced sufficiently cheaply to be purchased for teaching laboratories.

At the present time radioactive sources are the most suitable for teaching laboratories, since they are inexpensive, require negligible maintenance and have a relatively constant output. The greatest flux is obtained for the spontaneous fission source (^{252}Cf), with a heavy water moderator. However it has the disadvantage that the source needs renewal in about 5 years (due to the half-life) and the heavy water container may need maintenance. The Am/Be source using a paraffin wax moderator will give about an order of magnitude fewer thermal neutrons, but has a half-life of several hundred years and requires negligible maintenance. The reaction is:-

$$\alpha + {}^{9}Be \rightarrow {}^{12}C + n(\sim 5MeV)$$

The neutron energy is greater than for fission, and hence extra fast neutron shielding is required. A 2-Curie source (4×10^6 fast neutrons/sec) is used in the laboratory neutron diffractometer (figure 3) employed for teaching purposes at the University of Guelph. Bragg reflection intensities from a graphite crystal (5 cm high and 8 cm long) are about 100/min. Table 1 shows some of the matters which may be included in a normal laboratory course using this arrangement.

Table 1

Some topics which may be studied with the laboratory spectrometer of figure 3

Basic Properties of Neutrons
Neutron Detection
Design of a neutron diffractometer
Transmission in $(CH_2)_n$ and Pb compared to X-rays
Bragg reflections from single crystals
The Spectrum of thermal neutrons
The measurement of Plancks constant
etc.

In order to improve the presentation of such topics and to include further topics, some improvement in the source is required. Possibly a cheap commercially available packaged (^{252}Cf in D_2O) source would be acceptable. Beyond this, if the local source development program (see section III) takes place, new sources at the lower end of that program may be suitable. In any event it is important for the future of neutron scattering, that the neutron community encourage the expansion of teaching laboratory work.

V. THE IMPACT OF PHOTON SOURCES

High flux photon sources are coming into general use for condensed matter science. Shirane[5] has given a good account of the properties of these sources and their use in solid state physics. It is worth listing some of the properties of these sources; in a way which compares them to neutron sources:-

- the flux is much higher than for neutron sources
- narrow, highly collimated beams are available (and may be polarized)
- electron distributions (rather than nuclear distributions) are observed
- some isotopic effects occur and are interesting (e.g. there is a quantum effect in the structure of disordered systems which can be observed by the H/D substitution method)
- some inelastic scattering effects can be seen
- some magnetic scattering effects can be seen.

When users of synchrotron radiation sources look at neutron scattering one may expect them to say that neutron scattering has, a very few expensive sources, very weak neutron beams, very large samples (beam

areas), poor statistics, poor collimation, long counting times, etc. Neutron scattering has many unique features (familiar to all neutron scattering professionals) which make experiments with all these disadvantages worthwhile, and in many ways the complimentary character of neutron and photon experiments may be exploited by able experimentalists[5]. These and similar points need to be included and explored in many teaching environments.

The growing use of synchrotron sources is likely to cause many condensed matter scientists to become familiar with radiation scattering methods and their advantages. This could offer the neutron community a fertile source of new neutron users. The scientist who shops around for the best radiation source and spectrometers for his/her scientific program, and who may use several different sources, could become the norm. The proper and advantageous ways to use all sources need to be widely disseminated in this environment. Then all kinds of users need reasonable access and convenient availability to neutron sources and spectrometers which exploit the intrinsic advantages of neutrons. In other words the neutron community needs to react in appropriate ways to a new and competitive environment.

VI. CONCLUSIONS

The object of this paper is to initiate a discussion on future directions in neutron scattering. Some of the points covered above may be regarded as 'obvious' or 'over-simplified' etc., but nevertheless need to be included in a paper of this kind. While there are many items which may be selected for further discussion from those touched on in this paper (and in other similar papers), it is important to select a few items as the most important in todays environment. In the authors view the top items are:-

(A) Local sources are in urgent need of study - while super-sources are important and worth support it may be more important to the field to study local sources

(B) Interactions with a progressively wider user base need study: new methods of developing these interactions are needed,
- with synchrotron users
- with general scientists (mainly non-experts)
- with industrial people (mainly non-experts).

These topics are not new and have been studied before - the question for today is "Can the ICANS conference do better?"

References

1. von Laue M., Münchener Sitzungsberichte p. 363 (1912), and Ann. der. Phys. 41, 989, (1913).
2. Bragg W.H. and Bragg W.L. Proc., Roy. Soc. London 88, 428 and 89, 246, (1913).
3. Zinn W.H., Phys. Rev. 71, 752, (1947).
4. Maier-Leibnitz H., p. 135 in "Fifty Years of Neutron Diffraction" ed. G.E. Bacon (Hilger, Bristol, 1986).
5. Shirane G., previous paper.

Figure Legends

1. A plot of maximum thermal flux against year of completion for steady state sources from CP3 to the present.
2. A schematic diagram showing the two-way interaction between pre-existing local sources throughout Europe and the new high flux source at the I.L.L.
3. Cross-section of the teaching laboratory neutron diffractometer at the University of Guelph.

FIG.1.

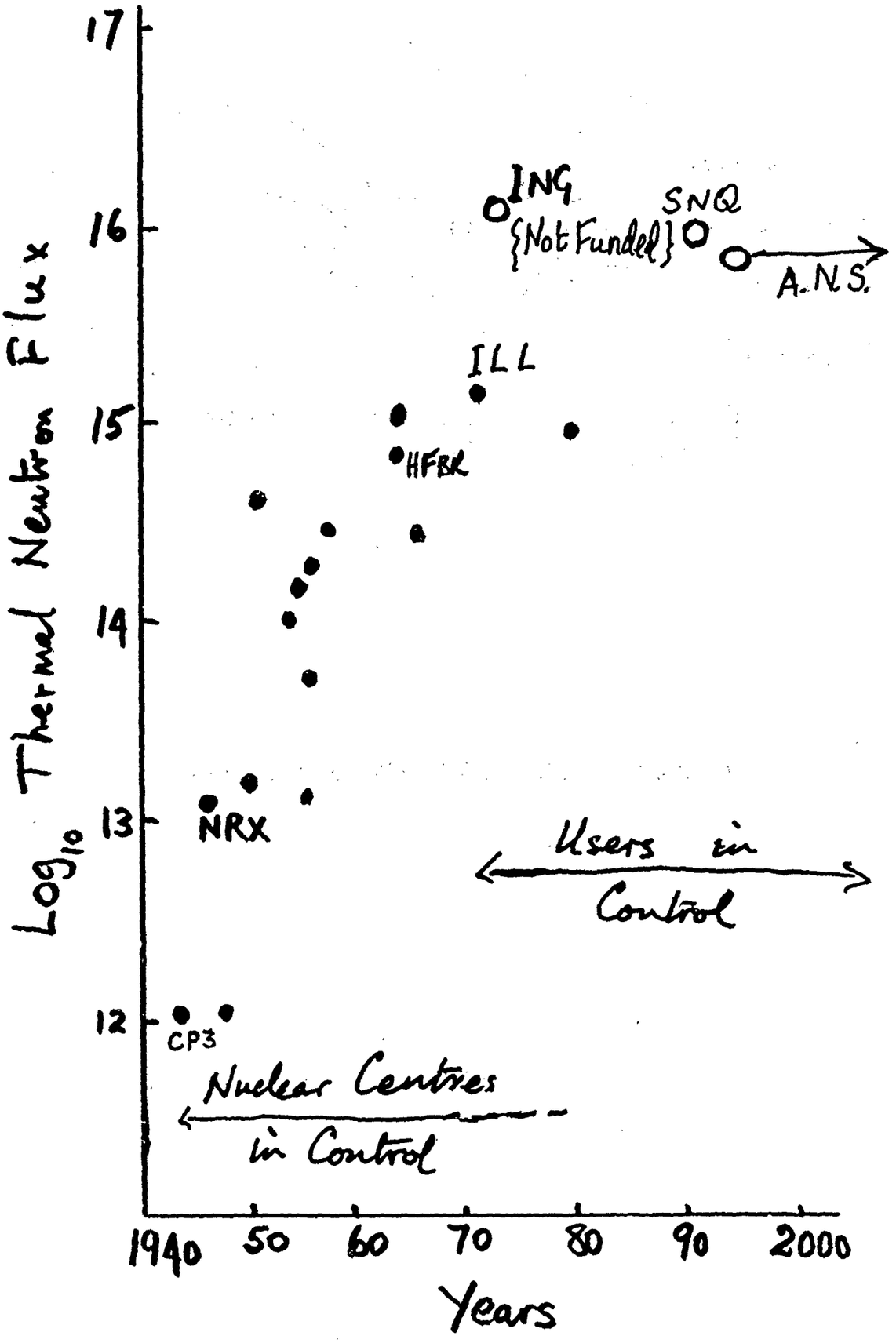
17
16
15
14
13
12
Log10 Thermal Neutron Flux
ING
{Not Funded}
SNQ
A.N.S.
ILL
HFBR
NRX
CP3
Users in Control
Nuclear Centres in Control
1940
50
60
70
80
90
2000
Years

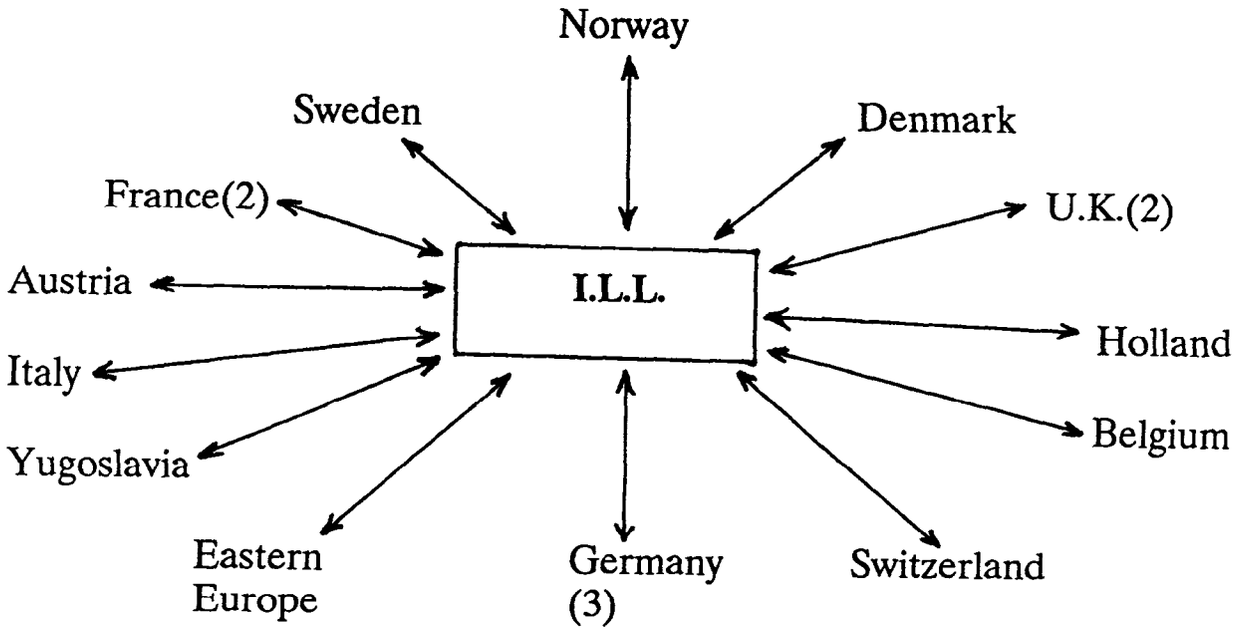

Centralization plus Diversity was a success in the 70's

FIG.2.

FIG. 3.

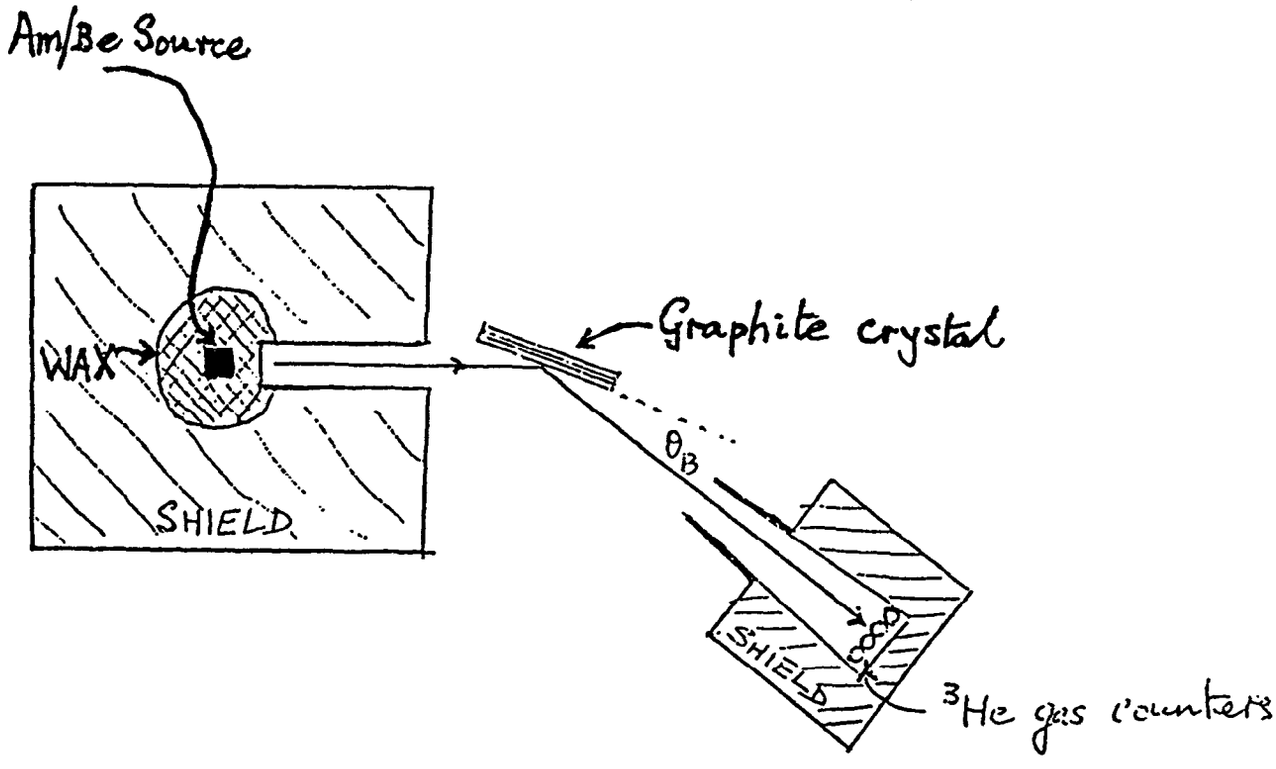
Am/Be Source
WAX
SHIELD
Graphite crystal
θ_B
SHIELD
^{3}He gas counters

C(J.L.Finney): One other positive effect of increased use of synchrotron photon sources is that it gets scientists used to working in central facility made. This in itself is encouraging wider use of the UK neutron community at least, which is growing at the rate of 10% a year.

Q(I.M.Thorson): For condensed matter science one should include muon facilities which can be associated with most pulsed-neutron facilities at modest incremental cost.

A(P.A.Egelstaff): Yes.

Q(J.B.Hayter): The average student today has more computer power at home than was available to the designers of the last U.S. reactor. Can we not exploit this as a teaching tool, e.g. by distributing programs to teachers?

A(P.A.Egelstaff): Yes, I think this is a good idea only waiting to be executed. Some people have told me that the best way to do it is to get senior high school students to do it. In this case ORNL would hire local high school students in the summer, train them in the elements of radiation scattering and let them write software for the local high schools computers.

ICANS-XI International Collaboration on Advanced Neutron Sources
KEK, Tsukuba, October 22-26, 1990

ICANS–XI

Conference Summary

G.S. Bauer
Paul Scherrer Institute
CH–5232 Villigen PSI

Generally the summary speaker of a conference is expected to report on the highlights that came up, on interesting contributions to discussions and perhaps add some of his own thoughts to this. Given the series of session summaries that were produced in this meeting, repeating the highlights over again didn't seem very appealing to me. Actually, everything I feel should be said has already been said, and so I am left with the situation, where I can scatter all that information from my own views. I want to apologize, if some of this scattering is highly inelastic. I am going to restrict any reflections to the more general questions of the meeting and to the idea behind our collaboration.

As far as the operational part of the meeting is concerned, my task is relatively simple. As it often happens on such occasions, one term starts to become dominating as the meeting goes on. On this one, this term is "total performance" and I feel that it is appropriate to make this complement to the organisers and their staff:

ICANS XI – Total Performance.

The dedication of Noburo Watanabe and his collaborators went far beyond what one could normally expect and I want to extend our sincere gratitude to them for making this such a memorable event for all of us!

Let me remind you of one event, which was not included in the summaries and which to some extent, gave me the clue for this summary. I am talking about Monday night's reception. Our hosts managed to get a few of the more prominent attendees of this meeting to give short ad hoc speeches, which I found very enlightening. In the course of his speech, Jack Carpenter noted that when the collaboration was founded and a name had to be found it was clear, that the acronym could be read

I CAN(S).

So, let me ask the question:

What **can** we – look upon today?
– be proud of?
– hope to achieve?

and, referring to the general motto of total performance:

How well did we perform in total?

It is of course not easy to answer these questions. That is, why I thought I would resort to something I learned during my travel coming here: I was waiting for the departure call for my plane at Khabarowsk in Eastern Sibiria and there was a young lady sitting next to me who did not look very happy. Having seen the trouble she had had going through customs, I thought, I knew why. But I was wrong. All of a sudden she pulled a deck of cards out of her luggage, shuffeld them thoroughly and picked three at random. Looking at them, she cheered up visibly. This aroused my curiosity and I asked her what it was all about. It turned out she was using telling cards to answer questions in her mind which there was no other way to answer. She deduced the answers from the pictures on the cards she had picked – in that case good ones –, which gave her confidence that the flight would go well (she was afraid of flying). Of course she admitted that the general moods you are in when interpreting your cards plays an important role, but she felt this was all right, actually it was what it was all about.

Now, what does this have to do with preparing a conference summary? Well, I don't have a deck of telling cards and so I had to improvise to get help in answering my questions about ICANS. I decided to collect key words starting with one of the five letters throughout the week and, at the end of each day toss them around and pick a selection. I am not going to include the full list of about twenty words for each letter here or repeat on what occasions they were used, but I would like to share with you the results of my exercise.

On **Monday** night my combination read:

International Competition on Advertising New Status Symbols

Seeing this, my scepticism about the telling card game suffered a serious blow! Had it only been the question of finding the winner of this competition, Rodger Pynn's evening speech beat them all! (By the way, fax–machines for cars **are** available).

But – should this really be the way, our group was drifting? Do we really want this? Is it the purpose of our meeting to tell each other, how good we are and how many microampere–hours we have achieved? This could not possibly be true! The result left me with an almost sleepless night, eager to repeat the exercise the following day.

On **Tuesday**, with more words in the box, the outcome was:

Instant Conversion to Adopt New Specifications

Remember, this was the "total performance" day. After some pondering over this result it dawned to me that it might have something to do with reality. It sheds some light on how idle all attempts might be to optimize a system today for tomorrow's science. Frankly, I don't believe that, for example, the success of the ILL is based on the total performance of any one of its instruments. I feel that the ILL combines several favourable factors, all of which have

their share in the overall success. In my view, the most important ones of them are:

- a large number of versatile as well as highly specialised instruments
- the highest available number of useful neutrons per year anywhere in the world
- an attractive user policy with excellent support and easy access
- a competent inhouse scientific staff as partners for frequent as well as occasional visitors
- an attractive location to spend some time at
- etc.

It is my conviction that, with such overall conditions the question becomes secondary, whether or not you have to measure 10 or 15% longer to get your desired information. The real measuring time is only a small fraction of the overall effort anyway. Now, of course, apart from "some other unnamed European neutron sources", not everyone tries to compete with ILL and, as Peter Egelstaff never fails to stress, a solid home base is necessary to be able to do the opportunities justice, that exist at large international facilities. For these sources, total performance is mainly a vehicle, and a valuable one, to stimulate extra efforts for new developments as we have seen on many national facilities such as Munich, Vienna, Tohoku and Hokkaido and, in particular, here at KENS.

So, Tuesday's result left me a little more hopeful when I repeated the game on **Wednesday** night:

Incentive Club for Announcement of New Strategies

How about that? Could Jack Carpenter's excellent iterations on the booster problem, Ian Gardener's calm and serene presentation about the new plans at ISIS and the fascinating success at KEK in new accelerator development for the Hadron factory produce such a result? Of course, there was also Gen Shirane, who made it plain to us that the times were over, when the pulsed source lobby had to prove to the world that in certain cases it could outdo a steady state reactor and when the synchrotron freaks had to demonstrate that in some cases they are able to do now what neutrons had achieved long ago. I fully agree with Gen that the best strategy for the future is to accept the virtues of the other methods and to concentrate on what one is best in oneself. The scientific questions to be answered may be limited on the long run, but at present their number and complexity are increasing rather than decreasing. This leaves enough to do for everyone without jumping on the other's domain. What we really need, as Peter Egelstaff put it, is well trained and motivated young people who know their job and who are willing to use whatever tool is best suited to solve their problems. Therefore, a strategy must be worked out to improve students' training and their knowledge about what neutrons can do and how they can be used.

On Thursday we were split in three groups so my success in adding new words to my list and do everyone justice was limited. But, remember, the girl at the airport also didn't have a chance

to add new cards to her deck. According to her conviction, what counts is the mood you are in, when picking your choice.

So, let us look at **Thursday's** results:

International Complementarity of Accessible Neutron Sources

Finally, the oracle really seemed to work my way! This is probably the point to express my satisfaction over the fact that, for the first time, we were able to welcome a number of Soviet colleagues at an ICANS meeting. Although they are not formally part of the Collaboration, their participation added significantly to the international character of the meeting. For the first time we had the opportunity to learn in considerable detail about their work and their problems.

With the pulsed reactor IBR–2 operational and with the neutron target station of the Moscow Meson Factory making good progress, the complementarity of the various sources becomes almost complete on the international scale. Although Dr. Shabalin deplored the length of IBR–2's pulses with 200 μs as being too long, I am firmly convinced that this machine, if at some day it becomes more easily accessible to a wider community, would be an ideal test bed to demonstrate concepts of instruments which, I am sure, one would have to persue if heading for a super source as it has occasionally been referred to in this meeting. Such a source would most certainly be of the SNQ–type and have pulse lengths of that order of magnitude.

Easy access to the tools we want to use is important, but it is equally important to be able to select the right tool for a given task. There is probably no such thing as an universally optimum neutron source which could be afforded by any one research centre or university. So, let us accept that some things can be done better in one place and others in others. The complementarity between pulsed and steady state high flux sources is a fact and we would be poorly advised if we tried to deny this. For this reason I am sorry we did not succeed in incorporating new reactor projects in our collaboration. At least we had John Hayter here as a guest representative from the IGORR (International Group on Research Reactors) to tell us about their exciting progress on the "Advanced Neutron Source" (ANS)–project.

Going a little beyond Thursday's result of my game, I would like to come back to Gen Shirane's talk on Wednesday and remind you that this complementarity is not restricted to neutron sources among themselves but extends to synchrotron radiation as well. From another conference I attended in Alushta in the Soviet Union two weeks ago, I would like to report to you the message given there by Gen Shiranes colleague, John Axe, that the situation is now such that X–ray and neutron scattering experiments have not only become comparable in quality, but also in cost. Synchrotron light sources and spallation neutron sources are both accelerator based machines. Almost all of the proton accelerators used for neutron sources also produce muons which, as was correctly stated during one discussion, are another tool of growing importance in condensed matter research. The same may become true for positrons.

This is, what I might have had in mind when, somewhat prematurely, I picked the last combination of words this morning for **Friday's** result:

International Commitment to Advance Nuclear Methods in Science

This, I think could be the long term perspective of a collaboration which started out as a forum for the exchange of information between laboratories of common interest in a new type of neutron source. These early projects are all operational facilities now, they make their contributions to science and the focus of the meetings has shifted towards instruments. Thoughts are being given to extensions and improvements of the sources and their uses. In that sense, let us all hope that KENS–II for which Noburo Watanabe and his collaborators have worked out such exciting schemes, will become a funded project soon!

Anyway, the scope of our interest has widened considerably and the promotion of new neutron sources can hardly remain the only long term basis of our collaboration. Yet, if we manage to direct our spirits towards this broader view, I can foresee a long and fruitful collaboration and it is my sincere wish, that this shall be the case!

I would like to end this summary by thanking the organizers of this meeting for this opportunity to express my personal views on some of the problems and prospects of ICANS.

Accelerator Workshop

New Accelerator Projects (including designs) for Neutron Production

Topics on High Intensity Accelerator Technology

ICANS-XI International Collaboration on Advanced Neutron Sources
KEK, Tsukuba, October 22-26, 1990

DESIGN OF THE COMPRESSOR/STRETCHER RING OF THE JAPANESE HADRON PROJECT

C. OHMORI, A. NODA
Institute for Nuclear Study, University of Tokyo
Tanashi-shi, Tokyo 188, Japan

and

Y. KAMIYA, M. KIHARA and I. YAMANE
National Laboratory for High Energy Physics
Tsukuba-shi, Ibaraki 305, Japan

ABSTRACT

A possibility of adopting a racetrack-type design for the compressor/stretcher ring of the Japanese Hadron Project is described. This design has two long straight sections to enable to inject the H^- beam and to produce a high β point for the slow extraction.

I. INTRODUCTION

The proposed Japanese Hadron Project consists of the 1GeV linac, the compressor/stretcher ring(CSR) and three experimental facilities. These facilities are E, M and N arenas for experiments using exotic nuclei, mesons and neutrons, respectively. The functions of the CSR are to accumulate the 1GeV proton beam with an average current of $200\mu A$ and to supply the beams to the M and N arenas with a repetition rate of 50Hz. Two bunches of the proton beam, the time duration of which is normally 200ns, are accumulated in the CSR. The N arena uses the beam of this time duration without any change in time structure. For the M arena, however, in addition to the normal operation mode just described above, two additional operation modes of different time structures are required. One mode is the ultra-short pulse mode for muon experiments, in which a bunch will be compressed to an ultra-short bunch of 20-30ns in length. In this mode, the sequence of operation is:

1. Accumulation of the beam in two RF buckets (the harmonic number h=2),
2. Fast extraction of one of the bunches to the N arena,
3. Compression of the remaining bunch by an RF system of h=1 and
4. Fast extraction of the bunch to the M arena.

Another mode is the stretcher mode for pion experiments. The beam is slow-extracted in a duration of 20ms before the next beam pulse from the Linac arrives. In this second mode, the sequence of operation is:

1. Accumulation of the beam in two RF buckets,

2. Fast extraction of one bunch to the N arena and
3. Slow extraction by a third-order resonance.

The conceptual design work on the CSR began in 1988. The design work has been almost finished and its results have been reported elsewhere[1,2]. The fundamental lattice of the CSR which was designed in this work is a FODB cell, and the whole ring consists of 16 superperiods, as shown in Fig. 1. Each cell is composed of a 2.8m bending magnet with a bending angle of 22.5 degrees, two quadrupole magnets and a 5.7m long drift space. The drift spaces are used to install the equipments for injection, fast and slow extractions, acceleration and beam collimation.

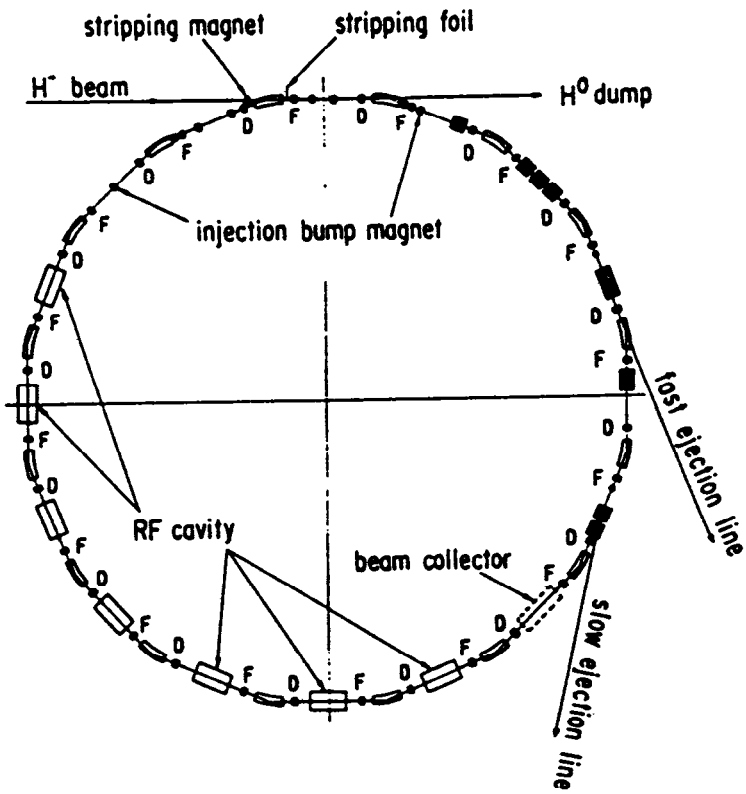

FIGURE 1. Layout of the CSR of 16 superperiod lattice.

One drift space is used to implement the H^0 injection system which is similar to that of the PSR at LANL. The H^- beam is neutralized to the H^0 beam in a stripping magnet with a magnetic field of $1.8T$. The beam is accumulated in the CSR after ionized to protons with a thin carbon foil. The H^0 injection method is simple and has a merit that it is possible to inject the beam even in a short drift space between the bending and quadrupole magnets.

Three drift spaces downstream of the injection point are used to set kickers and septums for the fast extraction. One of characteristics of this fast extraction system is to extract the beam in the vertical direction. The reason of the vertical extraction is that the horizontal beam size becomes too big to extract horizontally in the case of the ultra-short pulse, which has a large momentum spread.

Next two drift spaces include electric and magnetic septums for the slow extraction. Since the repetition rate is as high as 50Hz, the ordinary extraction method of changing the betatron tune with quadrupole magnets is not applicable to the present case. Instead, we have proposed a method to shift the horizontal tune by varying the beam energy with

RF[3]. As the CSR has a natural chromaticity of -4, it is possible to shift the horizontal tune with a momentum variation of 0.8% from 4.30 of injection tune to $4\frac{1}{3}$ of the nearest third-order resonance. The effective thickness of the electric septum seen by the extracted beam mainly determines the beam loss at the extraction point. The beam loss determined by the angular spread of the beam can be minimized by keeping the overlapping condition of outgoing separatricies of different emittances during extraction[4].

There are 17 RF cavities in eight drift spaces. One cavity operated with the frequency of 3.0MHz (h=2) is used to store two beam bunches during accumulation. Other 16 RF cavities are operated with the frequency of 1.5MHz (h=1), since it is suitable to minimize the tail of the bunch caused by non-linear RF wave form[1]. These cavities are designed to generate a voltage of 15kV per cavity. With these cavities, the high voltage of 240kV required to obtain the ultra-short pulse can be generated.

Recently, racetrack lattices which include long straight sections are proposed for special purposes in many accelerators. In the KAON factory at TRIUMF, a racetrack lattice has been proposed for reducing beam loss at the extraction septum. At the septum of the ring named Extender, the beta function is chosen to be 100m. The beam loss ratio is estimated to be about 0.2%. For a second-generation proton storage ring at LAMPF, a racetrack lattice has been also proposed for the direct H^- injection[5]. Also, Rees has pointed out merits of the lattice with long straight sections in his conceptual design of the CSR[6]. Generally speaking, however, there are some demerits when the number of superperiods decreases. For instance, the betatron resonances would be strong and may cause beam loss. Therefore, we have begun the design of a racetrack-type machine and compared it with the high-periodicity machine.

II. DESIGN CONCEPT

The general requirements imposed on the design of the racetrack-type machine are as follows.

1. Both H^- and H^0 injections are possible.
2. Two operation modes of the different time structures mentioned above are possible.
3. Both high β optics for the stretcher mode and normal β optics for the ultra-short pulse mode are possible.
4. The transition energy should not be so high compared with that of the high-periodicity lattice, since higher transition energy requires higher RF voltage for the bunch compression.
5. The fast-extraction in the horizontal direction is possible.

The design layout of the machine is shown in Fig. 2. Main parameters are listed in Table 1. The ring has a racetrack shape. The length of the long straight section is 45m. The numbers of the bending and quadrupole magnets are 24 and 54, respectively. The dispersion in the straight sections is reduced to zero by using the missing bend method. The beta and dispersion functions for the normal β and high β optics are shown in Fig. 3-a and 3-b, respectively. The beam optics near a pre-septum installed for the slow extraction are much different between two operation modes. The horizontal beta functions at the pre-septum are 25m for normal-β optics and 200m for the high β optics. The value of 200m for the high β optics was chosen from a compromise between the turn separation(5cm) of the slow-extracted beam and the horizontal acceptance($\pm$20cm) required for the quadrupole magnets nearest to the pre-septum.

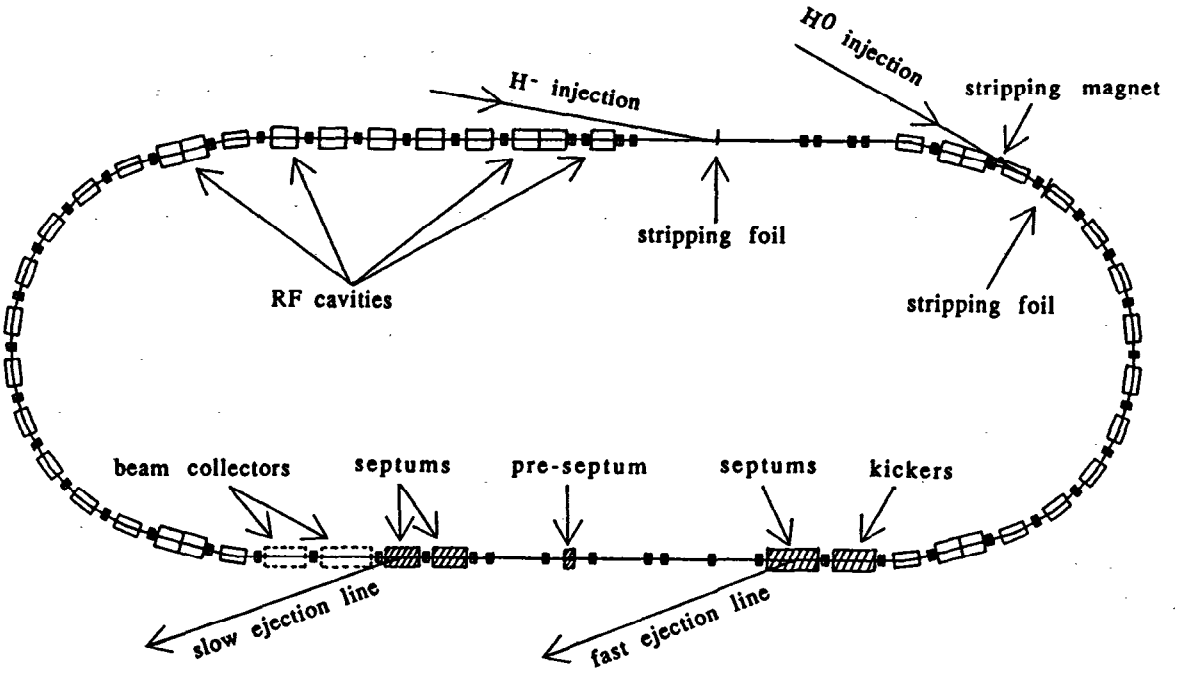

FIGURE 2. The CSR of the racetrack shape

Table 1. Parameters of the CSR of racetrack-type

Energy	$1 GeV$
γ	2.066
Particles per pulse	1.25×10^{13}
Circulation current	$5.5A$
Revolution frequency	$1.4MHz$
Harmonic number (h)	2
Circumference	$190.4m$
RF frequency	$2.8MHz$
Repetition rate	$50Hz$
Average current	$200\mu A$
Horizontal beam emittance(ϵ_x)	$30\pi mm \cdot mrad$
Vertical beam emittance(ϵ_y)	$30\pi mm \cdot mrad$
Horizontal acceptance(A_x)	$120\pi mm \cdot mrad$
Vertical acceptance(A_y)	$120\pi mm \cdot mrad$
Energy spread	$\pm0.2\%$
Max. momentum spread	$\pm1.0\%$
Momentum acceptance	$\pm1.5\%$

Beam optics parameters	High β	Low β
Horizontal tune(ν_x)	6.30(typ.)	6.28(typ.)
Vertical tune(ν_y)	6.21(typ.)	6.23(typ.)
Transition gamma (γ_T)	4.595	4.595
$\eta = (1/\gamma_T^2 - 1/\gamma^2)$	-0.187	-0.187
Horizontal chromaticity(ξ_x)	-13.1	-9.2
Vertical chromaticity(ξ_y)	-9.3	-9.5

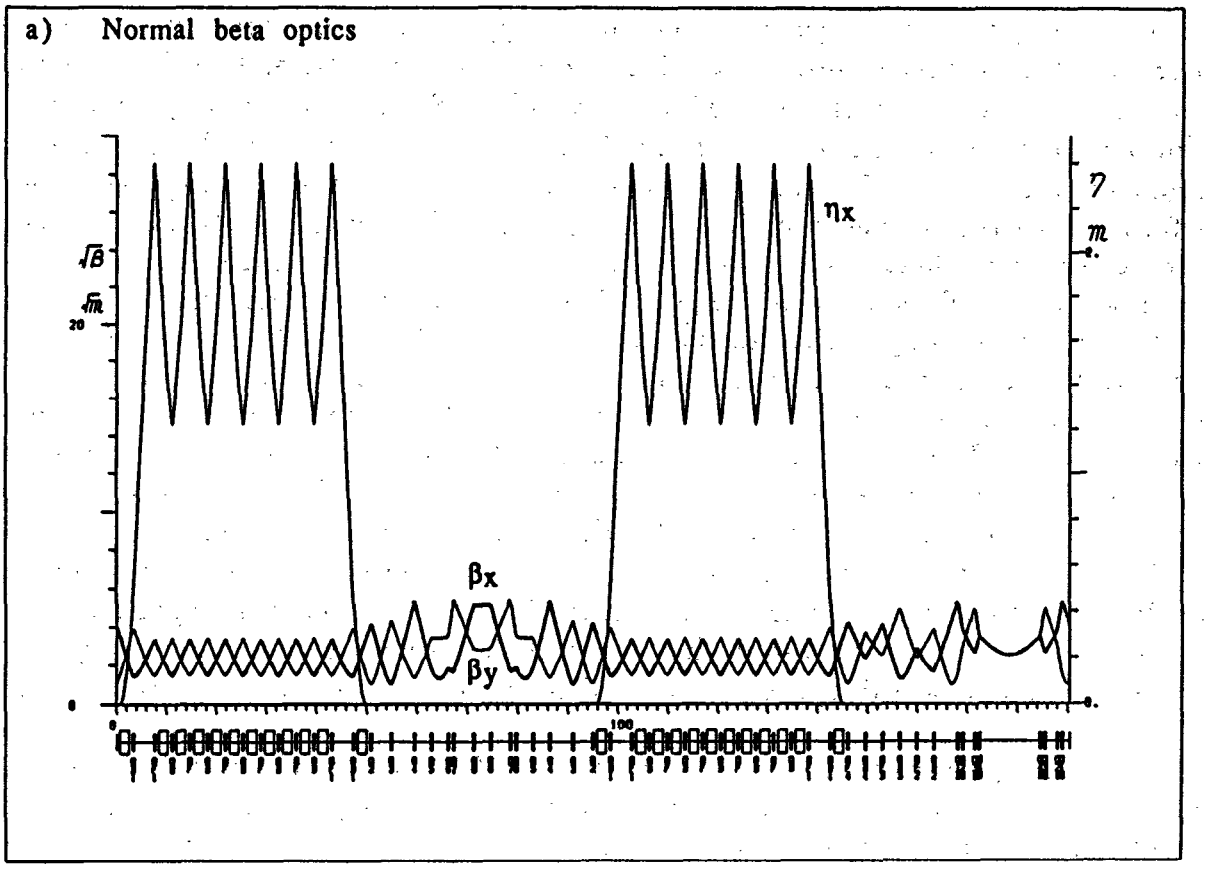

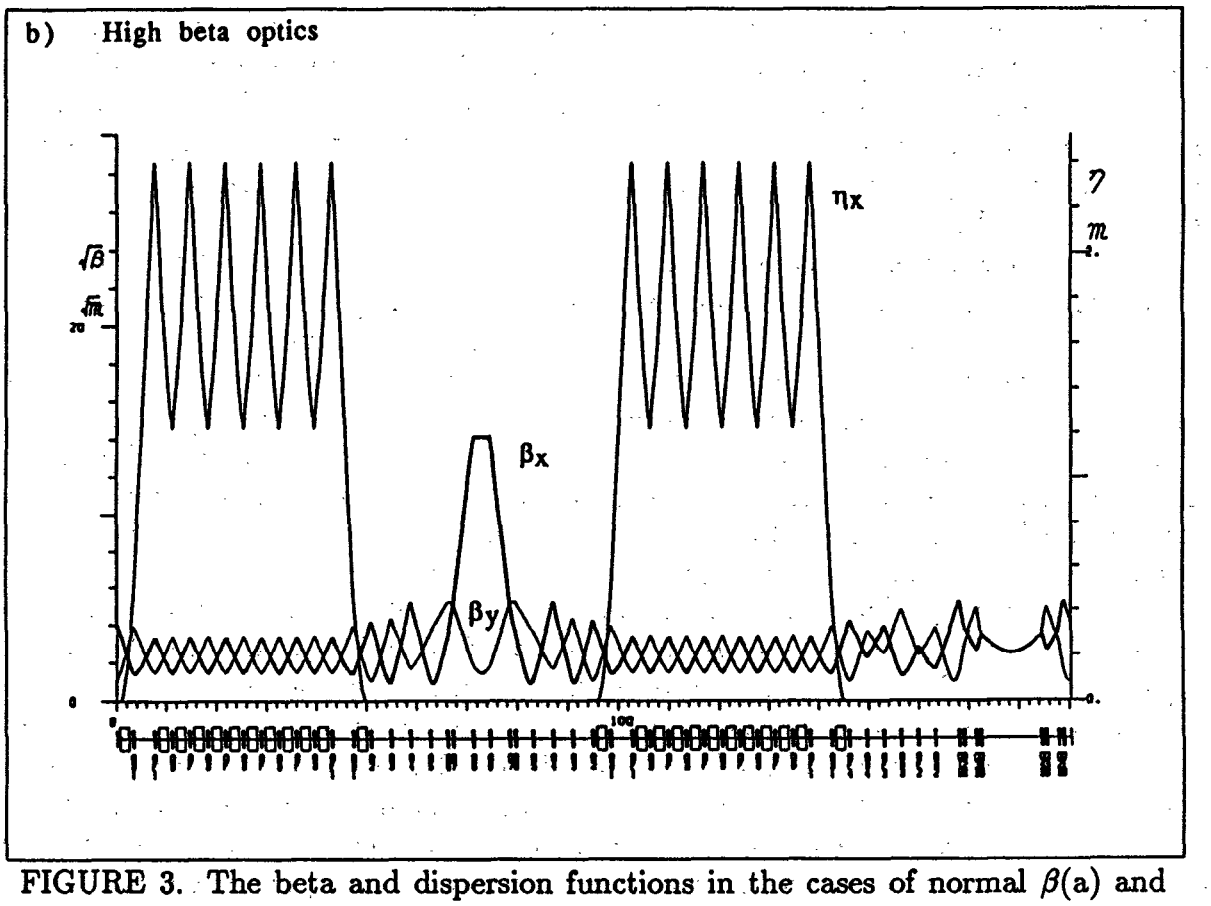

FIGURE 3. The beta and dispersion functions in the cases of normal β(a) and high β(b) optics.

When a high intensity beam is stored in a ring, the tune shift arises due to the space charge effect, and it may cause the the beam loss. The horizontal and vertical beam emittances are, therefore, chosen to be $30\pi mm \cdot mrad(100\%)$, in order to keep the tune shift below an acceptable level of 0.075. The method of phase space painting by means of bump magnets is planned in order to fill the phase space uniformly. The painting method is also useful to reduce the number of foil-hits during injection. Since it is important to decrease the beam loss from the halo of the circulating beam, both horizontal and vertical acceptances are chosen to be $120\pi mm \cdot mrad$, i.e., four times larger than the beam emittance.

One of the two long straight sections is used for injection and RF cavities. A feature of this straight section is that it has a 12m drift space to implement the H^- injection system (an injection septum, a carbon foil, bump magnets etc.). The foil is placed at the center of this drift space. The Twiss parameters, $\alpha_{x,y}$, are chosen to be zero at the foil, because it becomes easy to match the beam optics of the injected beam to that of the ring. With these parameters, the beam is injected parallel with the central orbit of the ring.

If the H^0 injection is adopted, the injection septum is not needed, since the magnetically pre-stripped H^0 beam goes straight in the magnetic field of the bending magnet. Hence, the H^0 injection can be done in a short drift space of the bending section as shown in Fig. 2. In this case, the long drift space can be used to install more RF cavities and some other instruments.

The bending magnet with the bending angle of 22.5 degrees which is designed for the high-periodicity machine is not suitable to use in this racetrack-type machine, since the phase advance per normal cell becomes much larger than 90 degrees if the dispersion is suppressed less than 2.5m. The value of 2.5m is an allowable dispersion in this lattice, as the horizontal beam size increases by 5cm when the momentum spread of the ultra-short pulse becomes $\pm 1\%$ by the compression of the bunch. Therefore, we have adopted the bending angle of 15 degrees. In this case, the phase advance per normal cell and dispersion function become 90 degrees and 2.4m, respectively. Moreover, the horizontal and vertical beta functions in the bend sections become smaller than those of high-periodicity since the distance between two neighboring quadrupole magnets becomes shorter. Therefore, the required magnet apertures also become smaller.

Another long straight section is used for both fast and slow extractions. Kicker and septum magnets for the fast-extraction are located in the drift spaces upstream of the long straight section, as shown in Fig. 2. Since this section is dispersionless, it is possible to extract the beam in the horizontal direction, even for the ultra-short pulse with the large momentum spread. The pre-electric septum for the slow extraction(see Fig. 2) is located at the center of the long straight section where the horizontal beta-function takes the maximum value. The second electric septum and two magnetic septums are located in two free spaces downstream of the pre-septum. Beam collectors in the horizontal and vertical planes would be placed in the remaining two free spaces of the long straight section.

The typical tune values are listed in table 1. The horizontal and vertical tune values of the normal β optics for the ultra-short pulse mode are 6.28 and 6.23, respectively. Since $\eta(= 1/\gamma_T^2 - 1/\gamma^2)$ is smaller by 7% than that of the high-periodicity lattice, seventeen RF cavities are required for bunch rotation. As stated before, the momentum spread is enlarged when the beam is compressed to the ultra-short pulse. Hence, almost zero chromaticity is necessary in order to avoid a large tune spread. However, the dynamic aperture generally becomes narrow, when the chromaticities are corrected with strong sextupole magnets. Therefore, we have checked the effect of the chromaticity correction on the dynamic aperture by using

a computer simulation. The result shows that a dynamic aperture is wide enough to store the beam with the emittance of $120\pi mm \cdot mrad$(see Fig. 4-a).

In the high β optics for the slow extraction, the typical horizontal tune value is chosen to 6.30, since it should be near the point of the third-order resonance. The natural horizontal chromaticity of -13.1 is corrected to -8. The value of -8 is taken so as to change the working point easily to the third-order resonance of $6\frac{1}{3}$ with a small energy variation of 0.4%. This energy variation is well inside the momentum aperture of the ring. The dynamic aperture is also larger than the physical aperture as shown in Fig. 4-b.

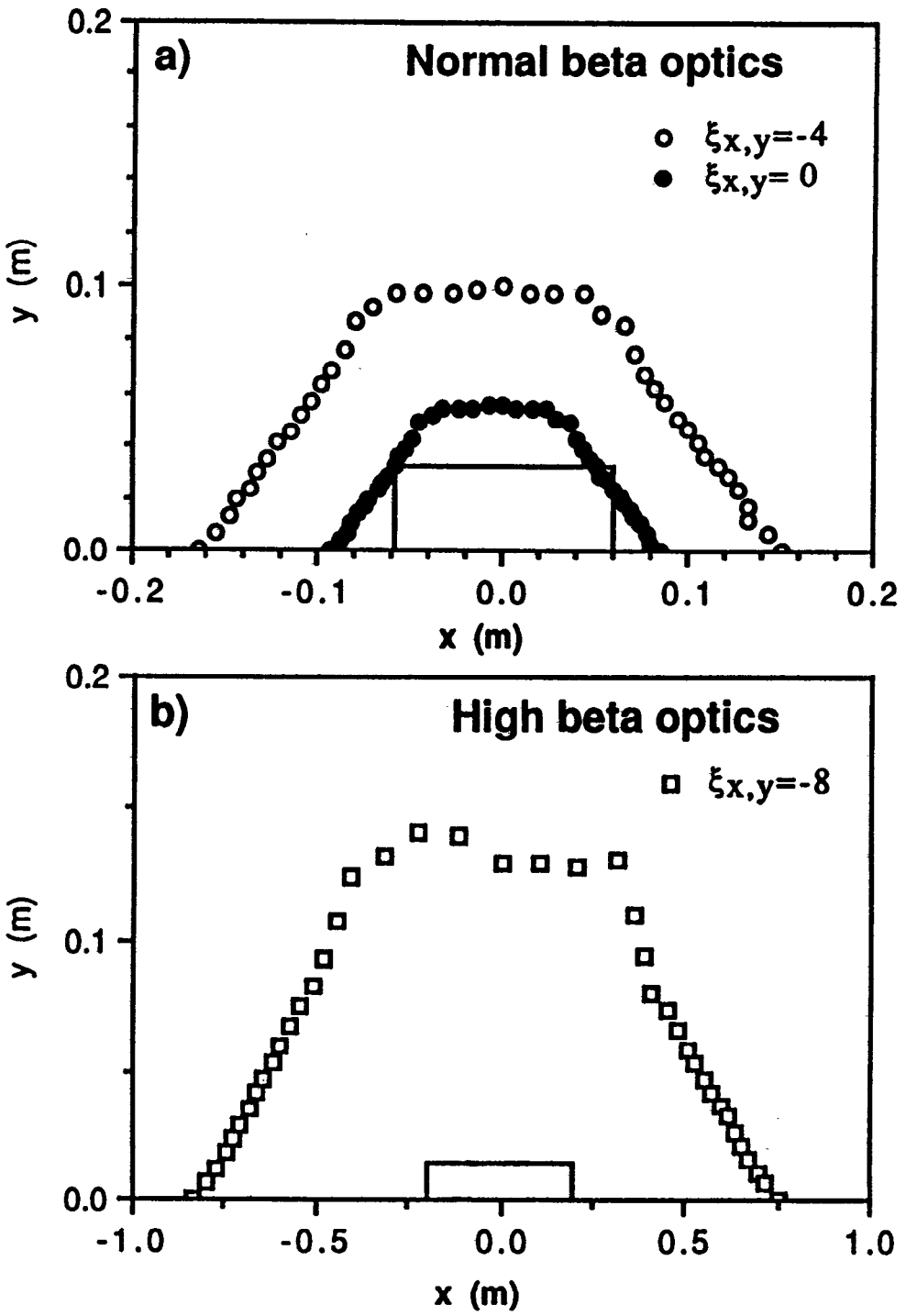

FIGURE 4. The dynamic apertures in normal β(a) and high β(b) optics. The solid line means the acceptance of $120\pi mm \cdot mrad$.

III. INJECTION

Figure 5 shows a scheme of the direct H^- injection[7]. Four bump magnets(B1-B4) are used to produce the bump orbit for phase space painting. The magnetic field of the septum magnet is chosen to be the small value of $0.4T$ in order to prevent H^- from losing an electron with Lorentz stripping during passage through the septum. This weak field requires a drift space as long as 10 to 12m.

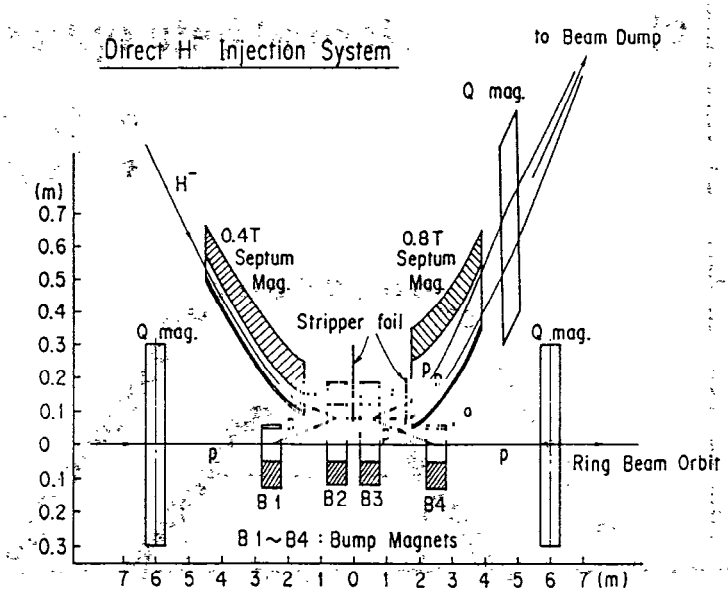

FIGURE 5. Direct H^- injection system.

The thickness of the stripping foil is chosen as thin as $200\mu g/cm^2$. The enlargement of the momentum spread caused by multiple scattering is estimated to be less than +0.1%. Since the initial momentum spread of the injected beam is 0.1 %, the resultant momentum spread becomes 0.2%. Because the ionization efficiency is 98% for this foil, the rest 2% which consists of the H^0 and H^- beams must be treated not to cause the beam loss. The H^0 and H^- beams will be ionized by another foil placed just after the bump magnet B3 and then guided to the beam dump.

IV. FAST EXTRACTION

Figure 6 shows the envelopes of the circulating and extracted beams[8]. As described before, a merit of the ring of the racetrack lattice is that it is possible to extract the beam in the horizontal direction. Five kicker magnets located in the drift space after the bend section deflect the beam into the aperture of the septum magnets in the next drift space. The design value of the total kick angle is $16.3mrad$. The total bending angle of the septums is designed to be 15.9 degrees. To decrease the beam loss at the extraction septums, the acceptances of the septums are chosen to be 120 $\pi mm \cdot mrad$, which is wide enough for the extracted beam with an emittance of 30 $\pi mm \cdot mrad$.

In the present design, the kickers will generate double-pulsed magnetic fields to fast-extract two bunches for both normal operation mode and ultra-short pulse mode[9]. The

interval of double-pulsed excitations is chosen to be about 100μs, and the rise and fall times of the kickers are designed to be 100ns in order to extract one bunch without affecting another circulating bunch[1].

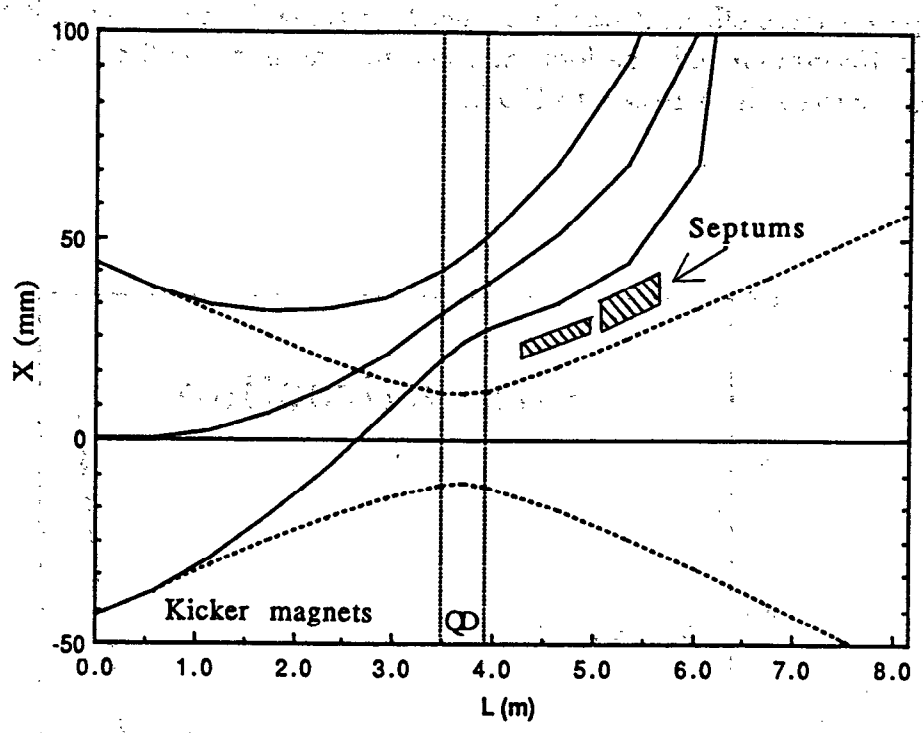

FIGURE 6. The beam envelopes of the kicked(solid lines) and non-kicked circulating(dashed lines) beams near the kickers for the fast extraction.

V. SLOW EXTRACTION

One merit to use high β optics is that it is possible to obtain a large turn separation such as 5cm of the present design. Another merit is that the angular spread of the beam at the pre-septum becomes small, so that the effective thickness of the pre-septum decreases, i.e., the beam loss can be reduced. Since the angular spread of the beam is small for the high β optics, the overlapping condition mentioned above is no longer necessary for the present design.

In the present design, the particles that enter the pre-septum with an electric field of 24kV/cm and go through its full distance are kicked by 0.7mrad. The envelopes of the kicked and circulating beams just before the extraction are shown in Fig.7. The second electric septum and the first magnetic septum are set at the position about $7m$ downstream of the pre-septum. The separation between kicked and circulating beams becomes about 3mm at the second electric septum, by which the kicked beam is further kicked by 8.0mrad and led to the magnetic septums. By the first magnetic septum the beam is kicked by 25mrad, and finally by the second septum it is deflected by 200mrad and then extracted from the ring.

By assuming that the pre-septum is 50μm thick and the angular spread of the extracted beam is 0.35mrad, the ratio of the beam loss during the extraction process is estimated to be 0.45%. This ratio is smaller than 1%, the expected value for the high-periodicity machine. Even with the small ratio of the beam loss, however, for the average current of 100μA the loss current becomes 0.45μA, which is still too much from the point of the accelerator operation and maintenance. If the acceptable loss current is to be less than 0.1μA, the beam current should be less than 22μA. However, the beam loss ratio can be further reduced. For

instance, this reduction can be made by decreasing the angular spread of the beam, since the loss ratio mainly depends on the angular spread due to the emittance of the circulating beam. Since the bean emittance is determined by the allowable amount of the tune shift due to the space charge effect, it can be reduced for a low beam current. If the emittance is taken to be $10\pi mm \cdot mrad$, the loss ratio becomes as small as 0.3% and the maximum allowable beam current is increased to 33μA.

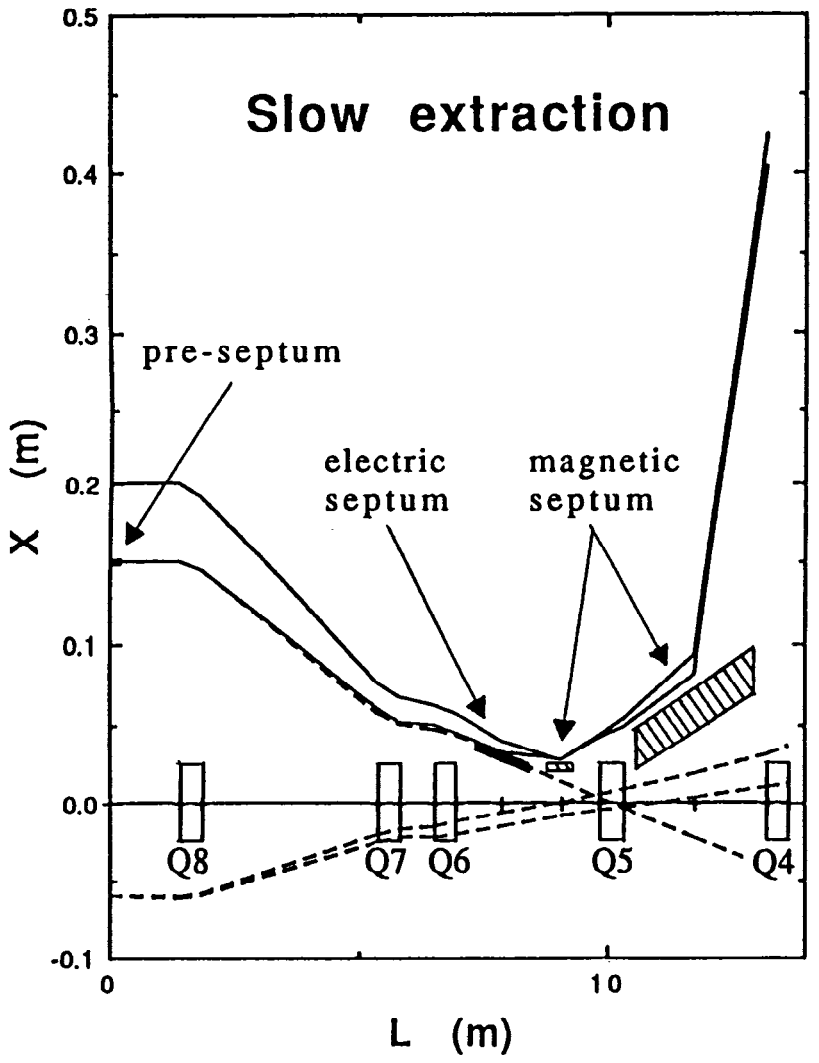

FIGURE 7. The beam envelopes of the kicked (solid lines) and non-kicked circulating(dashed lines) beams after the pre-septum for the slow extraction.

CONCLUSIONS

The design work of the racetrack-type machine has been begun. By changing the machine lattice from high-periodicity to the racetrack-type, we can obtain the following advantages. It is possible to introduce into the ring a long drift space required to implement

the direct H^- injection. The beam can be fast-extracted in the horizontal direction, since the long straight section is made dispersionless. By adopting a high β optics, the loss rate for the slow extraction can be reduced.

In the calculation of the dynamic aperture, we can find the suitable operation point to store the beam for both stretcher mode and ultra-short pulse mode. In order to optimize the machine parameters, further studies will be continued.

References

[1] Report of the design on the compressor/stretcher ring of the Japanese Hadron Project, JHP-11, KEK Internal 88-9.

[2] Y. Kamiya et al., Proceedings of 14th International Conference on High Energy Accelerators, Aug. 22-26, 1989, Tsukuba, Japan, p1499.

[3] A. Noda et al., Proceedings of European Particle Accelerator Conference, 1990, Nice, France, p1592.

[4] W. Hardt, PS/DL/LEAR NOTE 81-6(1981)

[5] G. Rees et al., Proceedings of the Advanced Hadron Facility, Accelerator Design Workshop, Los Alamos, 1988, p461.

[6] E. P. Colton, PSR Tech Note #181(1988).

[7] I. Yamane, "Treatment of H^0 and H^- beams spilled at the stripper foil at full energy charge-exchange injection scheme" in these proceedings.

[8] T. Kawakubo, private communications

[9] T. Kawakubo et al.,"System for Generating Double-Pulsed Magnetic Fields in a Kicker Magnet" in these proceedings.

ICANS-XI International Collaboration on Advanced Neutron Sources
KEK, Tsukuba, October 22-26, 1990

ACCELERATOR Aspects of the ISIS Upgrade

I S K Gardner and G H Rees
Rutherford Appleton Laboratory, UK.

ABSTRACT
A brief account is given of the future plans to attempt to increase the intensity of the ISIS proton beam.

I. INTRODUCTION

The accelerator aspects of the upgrade planned for ISIS include raising the operating energy of the 50 Hz proton synchrotron from 750 to 800 MeV and increasing the mean output current above the 100 μA level. There will be limits set to the current obtained, both by space charge effects and by the practicalities of handling the increased beam loss, but the design aim is to achieve a current approaching 200 μA. A time scale for the upgrade of three years is envisaged.

Included in the upgrade plans are a new or improved ion source, a separate power amplifier for the injection line debuncher cavity, and, for the synchrotron itself: higher power tests of the main magnet power supply, improved programming of the trim quadrupole power supplies, additional diagnostics, an increased power capability for the acceleration system, two additional steering magnets per transverse plane, six sextupole and eight octupole magnets and their associated pulsed power supplies, and a number of operational periods for machine studies. These items are to provide, respectively, increased injected beams, greater control of the input beam momentum spread, checks for magnet and magnet power supply reliability, harmonic correction for gradient errors, improved input matching, greater control for rf beam loading, improved closed orbits, chromaticity and transverse instability control, and a detailed evaluation of machine performance. Features of these plans are discussed in relation to the present ISIS synchrotron performance.

II. PRESENT PERFORMANCE OF THE ISIS SYNCHROTRON

At present the ISIS synchrotron operates routinely for neutron, neutrino and muon production at a proton energy of 750 MeV and a mean current of 100 μA. The current corresponds to two 100 ns pulses, each with 6.25 10^{12} protons, separated by a time gap of 230 ns and repeated every 20 ms. At this level, the injection efficiency for the 70 MeV beam (H^-) is 97 to 98% (with a 2% stripping loss), the acceleration efficiency is typically 88 to 92% and the extraction loss is less than 0.1%. Almost all of the acceleration loss is at low energy below 85 MeV.

The machine performance deteriorates if the beam rf feed-forward compensation is out of adjustment and also if the closed orbit deviations are not corrected adequately. Normally, it is sufficient to tune up the synchrotron at the start of a four week running period and to make only minor adjustments subsequently. Low and high energy beam losses, and the resulting activations, are localised in the long extraction straight section. There is a small high energy loss at the

extraction septum and the low energy beam, which is lost during acceleration, spirals radially inwards to the edge of the aperture, where most of it is contained in a longitudinal beam loss collector, upstream of the septum.

In experimental periods, accelerated beams have been increased from 1.25 10^{13} ppp (particles per pulse) up to 1.7 10^{13} ppp, that is, from the equivalent of 100 to 136 μA. However, it is difficult to maintain the beam at this level, and though the injection efficiency remains in the 97 to 98% range, the acceleration efficiency falls to 80% or less. Nearly all the loss is still at low energy, below 85 MeV, but there is some halo growth and a small increase in the extraction loss. To achieve the 1.7 10^{13} ppp, the low energy collectors are withdrawn from their normal positions to allow larger emittance beams, which are obtained by 'injection painting' over the ring acceptances. Most of the beam loss remains concentrated in the collector-extraction straight, though small losses do appear at other locations.

At low intensities, the betatron tunes may be varied over a wide region of the Q-diagram without affecting the performance, but at increased intensities, the operating point is important. The Q-values are ramped over injection to compensate for the combination of the changing guide field and the natural values of the chromaticities. At the field minimum, the tunes are brought to a maximum to allow maximum space charge tune depressions. Subsequently, the vertical-Q has to be lowered from 3.87 to 3.72 to limit the effect of the vertical resistive wall head-tail instability. This is a disadvantage for handling the space charge, but an advantage, when at the natural chromaticities, as it allows the lost beam of small horizontal betatron amplitude to spiral to the longitudinal collector without being lost vertically in an unprotected location.

Studies[1] have indicated that the early longitudinal loss is a sensitive function of the inter cavity phase transients, introduced as the six rf cavities are swung into phase, towards the end of injection. As the longitudinal space charge forces increase, so does the sensitivity of the beam loss with respect to these transients. Particles near the boundary may spill out of the phase stable region, so the setting of the rf beam feed-forward compensation becomes more critical.

During the first millisecond of acceleration, the beam bunches more tightly and two effects contribute to the tune spread. There is the major effect due to the transverse space charge forces and a secondary effect on the chromaticities due to the enhanced momentum spread. The latter gives a tune spread of ±0.04 for the maximum $\Delta p/p$ of $\mp 8\ 10^{-3}$ for uncorrected chromaticities, while the former is larger by more than a factor of ten for the design limit of 2.5 10^{13} ppp. At the maximum of 1.7 10^{13} ppp achieved to date, the predominant loss is longitudinal, but it is believed that the transverse tune spreads are already important.

III. INJECTION IMPROVEMENTS

Two main improvements are planned, an improved or new ion source and a separate power amplifier for the injection line debuncher cavity. In addition, more care is to be taken in setting up the linac to obtain greater repeatability of its mean output energy and longitudinal emittance. An increase of two is needed in the H^- ion source output and development will continue on the existing Penning source and also on a higher volume multi-cusp source. The debuncher cavity is powered at present from the fourth linac tank and the control for the beam loading is inadequate. A separate power amplifier is thus to be installed.

IV. SYNCHROTRON DIPOLES AND QUADRUPOLES

Synchrotron dipoles and quadrupoles are powered in series, with the units of each superperiod connected separately to one of the ten legs of a common choke which, in turn, is in parallel with a capacitor bank, to achieve overall series resonance. Separate trim quadrupoles are powered to obtain Q-adjustments. On raising the operating energy from 750 to 800 MeV, the voltages on the main magnets, the choke windings and the capacitors are all increased to near or just above their maximum voltage ratings. Thus, there will be extended running periods to confirm heating estimates and overall reliability. Also increased currents are required in the trim quadrupole magnets which will require some modified programming. Harmonic correction for gradient errors is to be investigated at low energies to see if enhanced Q-spreads may be contained.

V. INCREASED POWER FOR RF SYSTEM

Each of the six rf cavities is presently powered by one 250 kW tetrode, and the plan is to add a second 250 kW output tube in parallel. This increases the output power capability and at the same time lowers the input drive requirements, allowing both the shunt impedance of the cavities to be lowered and the accelerating voltage to be raised somewhat at mid-cycle. Copper sulphate liquid resistors may be adjusted to lower the shunt impedance, and this leads to an improved performance for the beam feed-forward compensation system. The beam loading power doubles at $2.5\ 10^{13}$ in place of $1.25\ 10^{13}$ ppp and is a maximum at the mid-point of the cycle. The planned increase in total accelerating voltage is to eliminate the tendency for small beam losses at this time.

VI. CORRECTION MAGNETS

Two additional dipole steering magnets per transverse plane are to be installed and also sets of sextupole and octupole magnets. These will be provided with programmable or pulsed power supplies. At present, there are four vertical and four horizontal steering magnets and they are used to provide fourth and third harmonic closed orbit correction. Further harmonic orbit correction will be obtained with the additional steering magnets. Six sextupoles are to be used for chromaticity correction and they are to be introduced as three sets of two to limit the possibility of resonance excitation. Eight octupoles are to be installed, similarly, as two sets of four and they are to provide Q-spreads to combat the vertical instability observed between 2 and 4 ms of acceleration. The major aim is to raise the Q_v-value at the time of high transverse space charge, 0 to 2 ms, while reducing the chromaticity; this should allow a larger space charge tune depression and enable the lost beam of small radial amplitude to spiral safely to the longitudinal collector.

VII. MACHINE PERFORMANCE AND DIAGNOSTICS

Additional diagnostics are to include high frequency pick-ups for the linac and injection line, and one or more beam envelope monitors for the ring. The former are to allow improved understanding of the linac performance and the latter, to study injection matching. The major concern in seeking a higher intensity is the control of the enhanced beam loss. It is believed that a higher intensity will only be achieved at a reduced acceleration efficiency and that the operational intensity will be determined by the practicalities of handling the beam loss. Thus, machine studies will concentrate on ensuring that the lost beam is contained in the beam loss collection system. If the loss reaches unacceptable levels, a modification of the acceleration system may be considered; in this, a subsidiary rf system would provide an initial linear rotation of the two bunches in $(\Delta p/p, \phi)$ space.

VIII. TIMESCALE

The three year timescale is set both by the funding rate and the scheduling, which must not disrupt the ISIS science programme. At this stage it is not easy to estimate the number of machine study periods that will be needed to evaluate the higher intensity performance of the synchrotron.

References

[1] I.S.K. Gardner et al, Progress at ISIS and Possible Future Developments, Proceedings of the 2nd European Particle Accelerator Conference, Nice, 1990.

ICANS-XI International Collaboration on Advanced Neutron Sources
KEK, Tsukuba, October 22-26, 1990

INR linear accelerator and the compressor ring project for the neutron spallation sources.

S. K. Esin, A. P. Fedotov*, M. I. Grachev, O. A. Gusev**,
L. V. Kravchuk, V. M. Lobashev, B .P. Murin*,
P. N. Ostroumov, Yu. P. Severgin**, Yu. Ya. Stavissky.
Institute for Nuclear Research of Academy of Science of the USSR, Moscow, *Moscow Radiotechnical Institute. **Scientific Research Institute of Electrophysical Apparatus, Leningrad,

ABSTRACT
Status of the INR linear accelerator, the proton storage ring as a compressor ring of the Moscow meson factory are discussed.

I. INTRODUCTION

The neutron scattering facility is included in the first stage of the experimental area of Moscow Meson Factory. This facility is proposed using the complex of the proton driven spallation neutron sources. At present time the proton driven spallation neutron sources are preferable to the reactors because they are ecology safe and can be optimized for the kind of the neutron scattering experiments.
The neutron sources will be described in detail at another paper /1/. Here is the description of the facility for proton driving only.
The facility for proton driving consists of a 600 MeV proton/H^- linac and a compressor ring (Fig. 1). It is possible to use the linac proton beam for driving the neutron sources with the designed peak beam current and it is possible to use the proton beam with increased peak beam current from the compressor ring after multiturn charge-exchange injection of H^- beam from the linac.

II. PROTON/H^- LINAC

Proton/H^- linac has been designed under the guidance of the Moscow Radiotechnical Institute /2, 3/.
The main linac parameters are :

the energy	600	MeV
summary peak beam current of the protons and H^-	50	mA
the pulse duration (1-st stage)	10^{-4}	s
number of particles per pulse	$3\cdot10^{13}$	ppp
the repetition rate	100	s^{-1}.

The linac consists of the injector system, the initial part of the

Alvarez type up to the energy 100 Mev (5 cavities with drift tubes) operating at frequency 198.2 MHz, and the main part with the maximum energy of 600 MeV (27 disc and washer cavities) at the frequency of 991.0 MHz. The energy variation is foreseen to be stepwise below 160 MeV and then continuously up to 600 MeV, with intermediate beam extraction at 160 MeV.
Injector system has two ion sources:

(i) a conventional duoplasmptron with a directly heated cathode and continuous flow of hydrogen as a proton source,

(ii) the Dudnikov type H^- source /4/.

The accelerating tubes of the injector system has two gaps : 5 cm with 300 KV focusing voltage and 35 cm with a voltage of 450 KV.
The tuning and initial operation of the linac is being done with a proton injector.
Presently, the 750 KeV proton injector has been installed and checked at the repetition rate 50 s^{-1}. However, the pulse rate is kept 1 s^{-1} during the linac tuning procedure to decrease the irradiation of the equipment. In 1989, the proton beam of 110 mA pulse current was injected into the first accelerating cavity and accelerated to the energy 20.5 MeV. At the output of the first cavity, the pulse current of 29 mA without prebuncher and 46 mA with prebuncher was obtained. These parameters are reasonable close to the designed values. The tuning of the whole initial part of the accelerator with beam has been obtained for the first time. The output pulse current of 23 mA (without prebuncher) has been already reached, while the pulse parameters close to the design of the initial part are expected to be achieved by the end of this year. Encouraging is the fact that the pick-up monitors placed downstream of the 2nd and 5th cavities have shown no difference in the pulse current, that indicates that the losses in the whole initial part of the linac are small.
The equipment of the main part of the accelerator (from 100 MeV to600 MeV) is installed and partly tested. By the end of this year, the proton beam at energy 160 MeV is expected to be obtained and extracted to a small experimental room adjacent to this area. The acceleration to the maximum energy 600 MeV is planned for 1991.

III. COMPRESSOR RING

Proton storage ring /5/ (Fig.2) will be used as a compressor ring. It is being under construction.
Proton storage ring was designed for transformation of the time structure of the linac beam by the Leningrad Scientific Research Institute for Electrophysical Apparatus.
The essential characteristics of the compressor ring are as follows:

orbit circumference (circulation period)	106.7 m (450 ns)	
number of storage turns	240	
maximum intensity per pulse	$3\cdot10^{13}$	
stored beam emittance	3π	cm.mrad
max. incoherent tune shift (smooth approx.)	-0.09	
peak current	11	A
momentum compaction factor	0.371	
kicker-magnet strength	0.02	T·m
kicker-magnet rise time	100	ns

Time compression of the linac macropulse is achieved by multi-turn charge-exchange injection and single-turn extraction as soon as filling process is terminated. One has to provide an azimuthal void to exclude beam loss during the rise time of kicker magnet field. Beam structure needed will be carved by the chopper, installed in an initial part of the linac.

It is reasonable to use the isochronous magnetic ring. We intend to tune it so that transition energy of the ring will be equal to linac output energy. Circulation time does not depend on particle momenta. The storage ring lattice with the required circumference may be of isochronous design at rather low cost, and short storage time (100 μs) tolerates small deviations from the exact isochronism without considerable bunch lengthening during storage. RF bunching system is absent in an isochronous storage ring. The ring of this type (IKOR) was studied at paper /6/ and at the CERN PS experiments on long-term bunch confirmed near the transition point were carried out /7/. Authors confirmed the possibility of isochronous ring realization. In a linear approximation the revolution period depends on the particle momentum as

$$\Delta T/T_0 = \eta(\Delta p/p_0) \ , \qquad \eta = \alpha - \gamma_0^{-2} \qquad (1)$$

where γ_0 is the relative energy, α is the momentum compaction factor.

Thus, the isochronous storage is possible in the ring with

$$\alpha = \gamma_0^{-2} \qquad (2)$$

The proton storage ring lattice of Moscow meson facility consisting of two achromatic periods has a variable momentum compaction factor of $0.32 < \alpha < 0.42$; $\alpha = 0.3736$ corresponds to Eq.(2).

Fig. 3 shows dynamic functions on half of its circumference. More detailed view of the lattice, the descriptions of its components operation and arrangement of the rest of the equipment may be found elsewhere /5, 8, 9/. Quadruples K3 (Fig. 3) regulate the value of the dispersion function ψ and the factor α.

The recent investigations carried out /9, 10/ shows more strong, that the linac pulse may be compressed hundredfold using an isochronous storage ring without a R.F. bunching system. There is no need to maintain strictly isochronism conditions. For example at $|\eta| \leq 0.02$ the bunch lightening during the storage period of 100 μs will not exceed 2.5 m, that seems quite tolerable, unless the goal is to obtain short bunches of several meters long. Equipment for all systems for the proton storage ring is under manufacture now. We hope it will be completed at 1992 and it will start to operate in whole at 1993.

References

1. M. T. Vorontsov et al., in Proc of This Conf.
2. B. P. Murin, Proc. of the 3d Allunion Meeting on Particle Accelerators, V.1, Moscow, Nauka, (1973), p. 234.
3. V. G. Andreev et al., Proc. of the 19th Int. Conf. on High Energy Accelerators, V.1, Serpukhov, (1972), p. 273.
4. V. G. Dudnikov, Proc. of the 4th Allunion Meeting on Particle Accelerators, V.1, Moscow, Nauka, (1975), p. 323.
5. M. I. Grachev et al., Proc. of the Int. Conf. on High Energy Accelerators, Novosibirsk, (1987), p. 264.

6. K. N. Reich, Proc. of the Workshop on High Intensity Accelerators and Compressor Rings, Karlsruhe, (1981), p. 33.
7. R. Cappi et al., IEEE TRANS. on NS, 1981, V.28, N.3, p. 2389.
8. V. P. Belov et al., Proc. of the 1987 IEEE Particle Accelerator Conference, V.2 of 3, p. 873.
9. V. A. Moiseev et al., IEEE TRANS. on NS, 1989, NS-36, V.2, p. 1406.
10. V. A. Moiseev et al., It will be published in proc. EPAC-2 conference, NICE, 12-16 June, 1990.

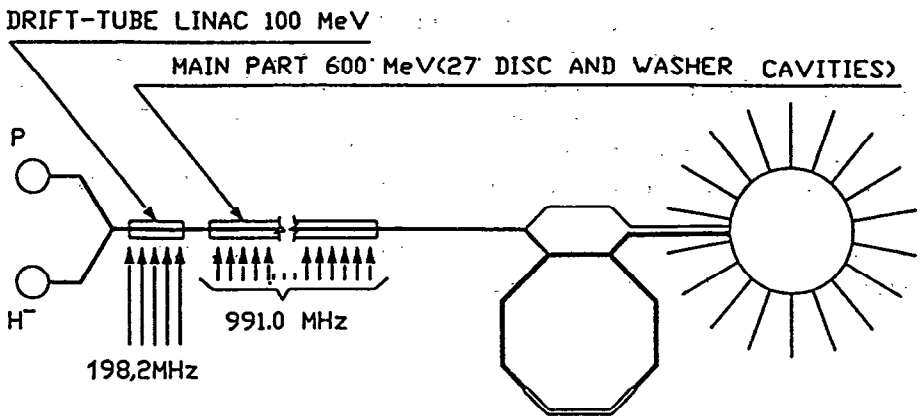

Fig. 1 The scheme of the protone driver.

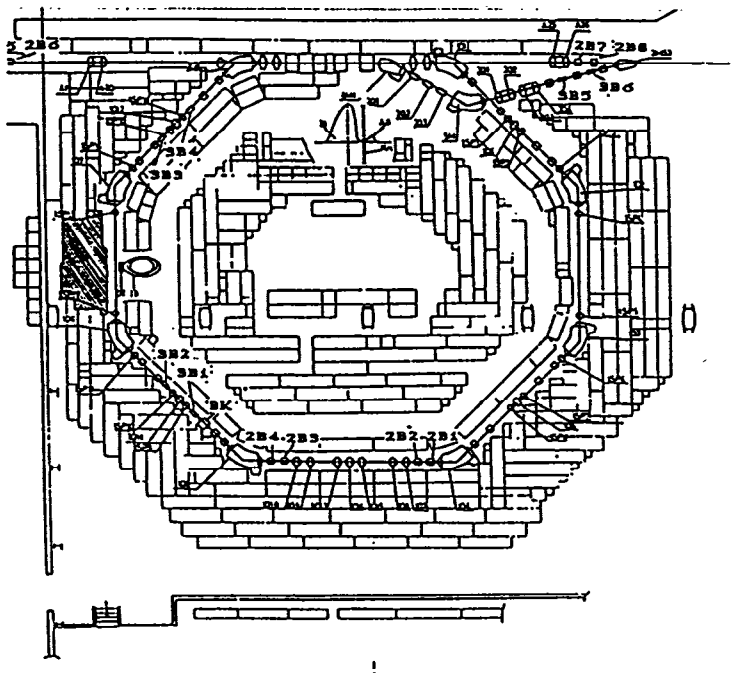

FIGURE 2 The proton storage ring. 1D1 - 1D8 - the mine dipole magnets: B = 1.45 T, aperture 20x12 cm HOR x VERT, bending angle = 45°; 1Q1 - 1Q15 - the quadrupoles: Ø = 20 cm, length = 0.4 m, G = 4.5 T/m; 1SP - the sextupoles: Ø = 20 cm; 2B1 - 2B8 - the bump magnets for injection; 3K - the kicker magnet for the one turn extraction ; DT - slow extraction target;

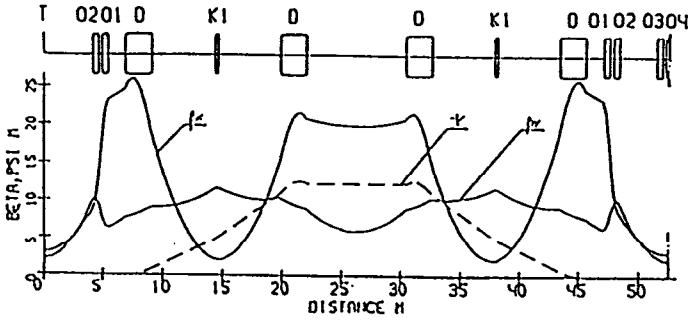

Fig. 3 The characteristic function of one half ring period for a isochronous regime.

ICANS-XI International Collaboration on Advanced Neutron Sources
KEK, Tsukuba, October 22-26, 1990

On the Way to High-Power Linear Proton Accelerator for the Long Half-Life Radionuclides Transmutation

G.I.Batskikh, O.S.Lupandin, B.P.Murin, A.P.Fedotov
Moscow Radiotechnical Institute USSR Academy of Sciences,
Moscow, USSR

ABSTRACT

The concept of continuous mode high-power linear proton accelerator with 1.5 GeV energy, 0.3 A current for the long half-life nuclides transmutation into the short ones (waste of atomic power plants (APP)) is proposed. The accelerator design main principles, scheme and parameters are presented. The accent is made on the accelerator efficiency, reliability and radiation purity.

One of the methods of APP waste treatment is based on the transmutation of the long half-life nuclides into the short ones by power proton accelerators with 1.5 GeV energy, 0.3 A current, the mean beam power of 450 MW, generating neutron fluxes for burner-reactor [1,2].

The first steps on the way to such accelerators are the linear accelerator in Los-Alamos and the Moscow Meson Facility linear accelerator at the Institute of Nuclear Research of the USSR Academy of Sciences (MMF). The accelerator and its main systems design development was carried out in MRTI [3]. The experience in the creation of the above mentioned installations and other ones designed in USSR [4-9] leads to the accelerator scheme for burner-reactor (BRLA) presented in Fig.1.

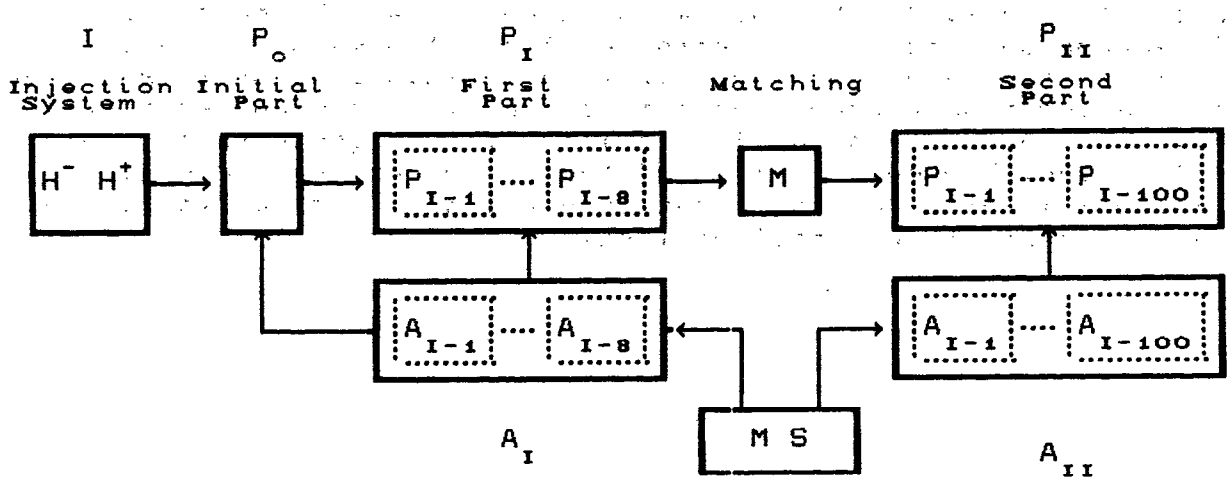

Fig.1. Burner-reactor accelerator installation diagram

The accelerator involves the injector (I), the initial (P_o), the first (P_I) and the second (P_{II}) parts, the matching system between the first and the second accelerator parts (M), amplification channel with the automatic regulation systems (A_I, A_{II}) and the power master system (MS). The following concepts were taken into account in the scheme choice.

1. Simultaneous acceleration of H^+ and H^- beams. In the case the frequency increase factor in the first and the second accelerator parts has to be odd [8]. It was chosen to be equal to 3. With larger values the bunch phase width in the first accelerator part will surpass the second accelerator part separatrix phase width due to space charge effect and accelerating channel parameters errors, and result in the beam losses at the transfer between the first and the second accelerator parts.

2. Transfer energy between the first and the second accelerator parts was chosen to be equal to 100 MeV. It's the optimal energy value as to the shunt impedances of the accelerating structures in the first and the second accelerator parts.

3. The specific acceleration was chosen to be 1 MeV/m. With larger values of specific acceleration the accelerator efficiency decreases while with smaller values the accelerator construction cost and the accelerating channel errors influence increases.

At the present design stage two pairs of operating frequencies for the first and the second accelerator parts are considered : 200 and 600 MHz; 330 and 990 MHz. The accelerating channel has the sufficiently large acceptance and the accelerating resonators are of acceptable size at the frequencies of 200 and 600 MHz. The frequencies of 330 and 990 MHz lead to the acceptance and resonator size decrease. One should note that 990 MHz is the operating frequency of the MMF accelerator second part. So we have considerable experience of the accelerating structure development at this frequency. The ratio of the operating frequencies in the first and the second accelerator parts is equal to 3. It means that the acceleration in the second accelerator part is realizes within one of three consecutive accelerating separatrix. Therefore it is possible to use the scheme presented in Fig.2. [2].

The bunches from three parallel accelerators of the first part are sequentially injecting into each separatrix of the second accelerator part. At the safe mean intensity at the output of BRLA this scheme decreases by a factor of three the mean intensity in parallel accelerators of the first and initial parts and the accelerating beam bunches amplitude in the second accelerator part. In general it will simplify the high-intensity beams acceleration. The complication of the installation as a whole will be insignificant since the first accelerator part provides only seven per cent of the total beam energy.

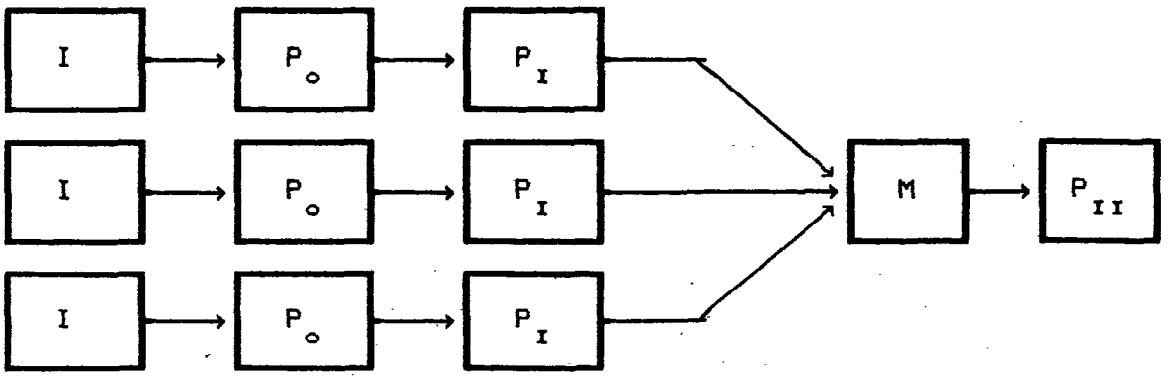

Fig.2.

I - injector system

P_o - initial accelerator part

P_I - first accelerator part

P_{II} - second accelerator part

M - matching system

Consider the accelerator parts.

Injector system (I).

Two parallel H^+ and H^- beams injectors are usedwith 100-200 keV energy.

Initial accelerator part. (P_o).

The convenient low-energy accelerators use the radio-frequency quadrupole (RFQ) [10] limiting the beam current to 0.3 A. In MRTI a structure was proposed providing for beam current increase. The proposed structure is the accelerating resonator with opposed vibrators and superconducting solenoid focusing [11,12]. The " SIU " experimental accelerator scheme is presented in Fig.3.
The superconducting solenoid with focusing 7 T magnetic field contains a resonator with opposed vibrators. RF power is applied to the resonator output by a coaxial feeder. The beam current value of 0.4 A was achieved in the SIU accelerator with 130 keV injection energy, 1,5 MeV output energy, 200 MHz operating frequency. In principle this scheme allows to accelerate the beam current up to 10 A.

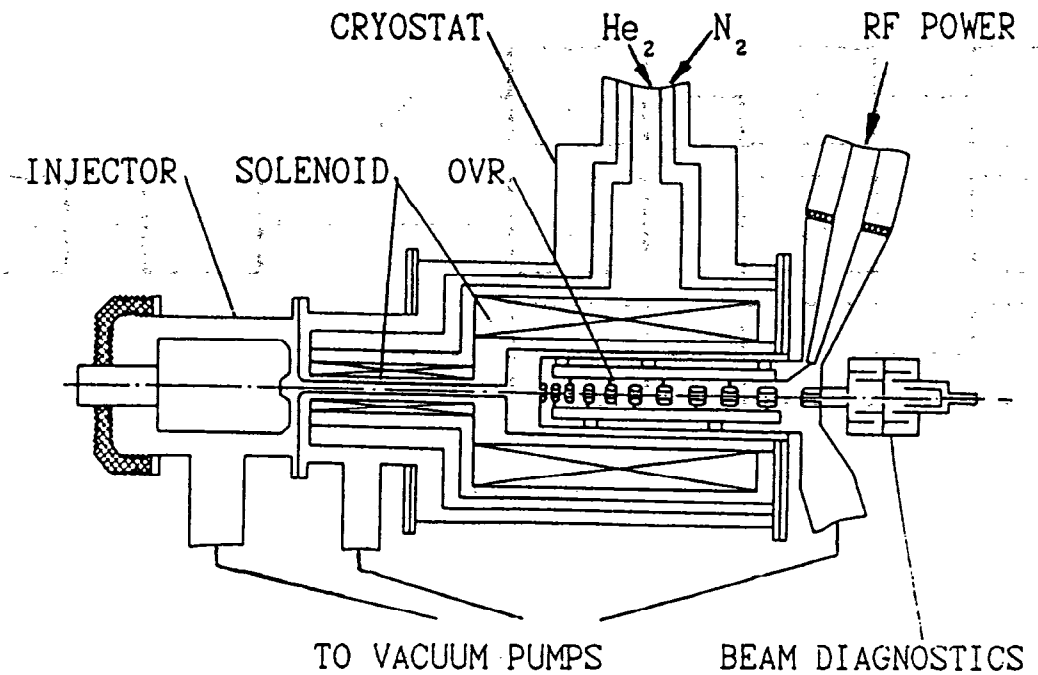

Fig.3. Outline of the SIU-1 experimental RF proton accelerator.

The first accelerator part (P_I)

The resonators with drift tubes are used in the first accelerator part. Initial energy is equal to 2-3 MeV. The field distribution stability along the resonator is realized by resonance rods [13]. This field stability method was successfully used in the MMF accelerator.

The second, main, accelerator part (P_{II})

Consider three structures for the second accelerator part : side-coupled resonator developed in Los-Alamos [14], ring-coupled resonator [15] and resonator with washers and diaphragms developed in MRTI (Fig.4.).

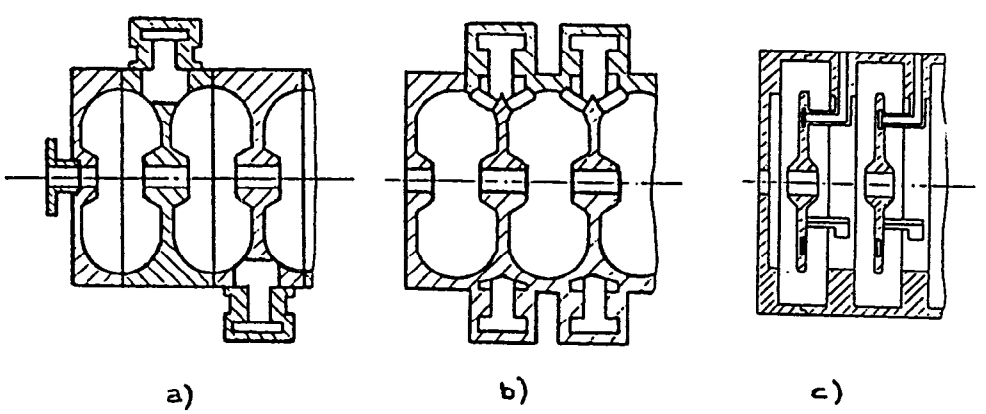

Fig.4.

a) Side-coupled structure
b) Ring-coupled structure
c) Structure with washers and diaphragms

The side-coupled resonators were successfully used for proton and electron accelerators in USA. We proposed the ring-coupled resonator for the MMF accelerator. The above mentioned resonator is equivalent to side-coupled resonator, but it has higher coupling factor. The resonator with washers and diaphragms has significant differences as compared with the above mentioned ones : the high coupling factor (40-50 per cent against 4-7 per cent for the side-coupled and ring-coupled resonators and the high vacuum conductivity. The system drawback consists in the adjacent values of the operating and parasite modes. The fault was removed by means of the T-shaped cuts in diaphragms [17]. The resonator with washers and diaphragms is used in the MMF accelerator and is proposed for BRLA. At present 32 resonators are mounted, tuned and ready to operate. The structure investigations showed its high quality . The focusing system should be based on the quadrupole lenses with permanent magnets [18,19] Such system that increases the reliability, simplifies exploitation and decreases the cost. In the first and the second accelerator parts one should use the FODO focusing structure that is less sensitive to magnetic parameters errors as compared with the FDO structure.

RF system

The new type of RF generator "regotron" is developed in MRTI [20-22]. Regotron is a high-power RF generator based on relativistic electron beam with the distributed RF power takeoffand high efficiency. The scheme of regotron is presented in Fig.5.

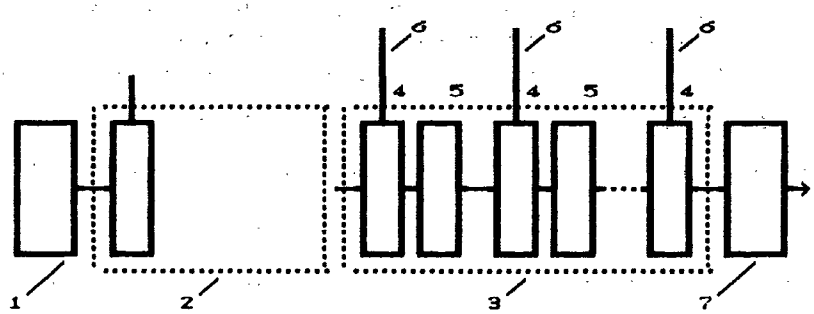

Fig.5. Regotron installation diagram.

1 - high-voltage injector (I) 2 - buncher (B)
3 - distributed power takeoff system (PS)
4 - active cavities of the power takeoff system
5 - bunching cavities of the power takeoff system 6 - output cavities 7 - beam collector

The device contains four parts :
- the high-energy accelerator generating electron beam with power W_o
- the buncher for the electron beam bunching in accordance with RF signal (B)
- the distributed system of the beam RF power takeoff. The system contains a chain of n resonator pairs (one in a pair is an active load and other is passive)

- collector (C) where the beam residual power W_r is dumped

The regotron efficiency is given by the equation :

$$\eta = 1 - \frac{W_r}{W_o}$$

High efficiency of the device is due to the autophasing mechanism in the power takeoff system [21] preventing from the electron bunches blowup. The distributed power takeoff system with n pairs of resonators allows one to remove the limitation typical for the generators with a single output takeoff resonator with 1 MW limit power [23].

The theoretical estimates and numerical simulation show that regotron is capable of generating 5...10 MW output power in continuous mode with 70-80 per cent efficiency even with low relativistic beam (500 keV energy W_o). The energy recuperation in the collector or its use is considered for the efficiency increase. At present the device development is on the stage of operating model construction.

Use of such high-power RF generators instead of klystron in continuous mode allows to simplify the accelerator RF power supply. The variant with a group of n resonators group is excited by a single regotron with the n energy outputs is possible.

Consider the BRLA design problems.

Efficiency problems

The total accelerator efficiency is basically defined by that of RF resonator energy transformation into the beam kinetic energy (resonator efficiency η_r) and electric power transformation into the RF generator energy (generator efficiency η_g). The total efficiency is equal to the product of the two components $\eta=\eta_r\eta_g$. The power consumption of the focusing, control, measurement, vacuum and subsidiary systems is negligible.

The resonator efficiency estimate has a form of

$$\eta_r = 1/\left[1+(E_y/I_n ZT^2 \cos^2\Phi_s)\right]$$

where I_n is the beam current, E_y is the voltage corresponding to the proton energy gain per unit length (its value is equal to the energy gain per 1 m of accelerator), ZT^2 is the effective shunt resistance of resonators per unit length. Accelerated particles current dependence of the resonator efficiency $\eta(I)$ is presented in Fig.6 for three values of the energy gain per unit length. If ZT^2 = 40 MeV/m, φ_s = 30 and I_n = 0.3 A then the resonator efficiency amounts to 0.9.

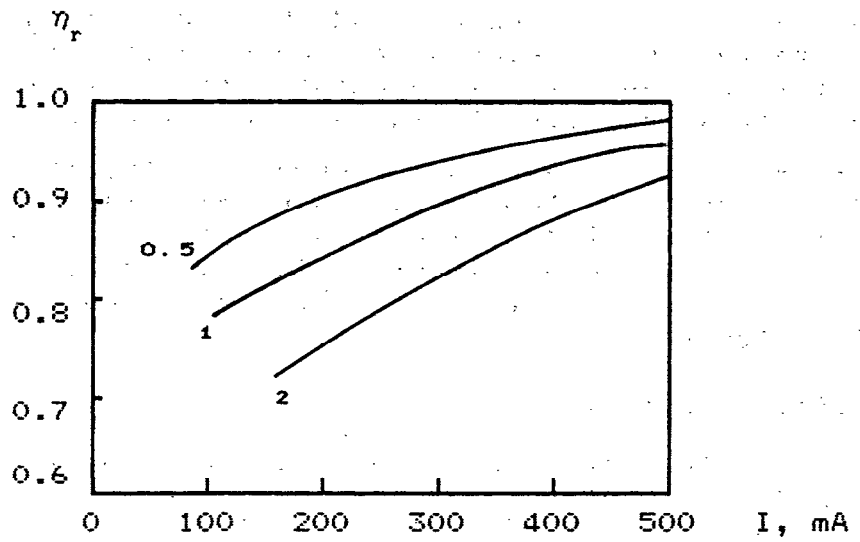

Fig.6. Accelerated particles current dependence of the resonator efficiency for three values of the energy gain per unit length (MeV)

The accelerator efficiency problem should be solved by the construction of regotron with at least 0.8 efficiency. Then $\eta_r \eta_g \approx 0.7$ and the total accelerator efficiency estimate is 0.6. It's quite feasible.

Reliability problem.

The reliability problem is essentially a problem of the installed power utilization factor (K_u) realization. The K_u factor represents the ratio of the accelerator actual operation time with the beam nominal parameters to the year hour sum. According to the nuclear power engineering specifications we present data for linear accelerators in Brookhaven and Los-Alamos to illustrate the reliability of their operation and the contribution of the separate systems.

The linear accelerator in Los-Alamos [14]

K_u=0.85

Injector	- 30 %
RF system	- 25 %
Magnet and their power supply	- 13 %
Vacuum system	- 8 %
Other system	- 34 %

The linear accelerator in Brookhaven National Laboratory

K_u=0.95

Injector	- 29 %
RF system	- 49 %
Vacuum system	- 9 %
Other system	- 18 %

It's obvious that injector and RF systems give maximum contribution to the accelerator operation unreliability.

For devices reliability improvement (first of all RF system and injector) it's necessary to increase K_u factor. For the K_u factor increase should be use the reservation schemes (as in the MMF accelerator for RF system), permanent magnets in quadrupole lenses, development of the failure prediction analysis system through the beam losses measurement. It's necessary to use the recommendation of the paper [23] for the development of RF power system on the regotron base.

Radiation purity problems.

A linear accelerator is considered to be radiation pure if the induced γ-activity doesn't exceed the occupational radiation dose of 28 mGy/hour at the distance of 1 m from the axis of accelerator after 1 hour upon its shut down. The corresponding permissible beam loss in the energy range W = 0.1 - 1 Gev amounts to [24]

$$W\ q \approx 0.05\ \text{GeV nA/m} \qquad (1)$$

The problem is essentially that of limiting the beam loss at the level given by the eq.(1). Under the condition the accelerator maintenance does not require manipulators and can be performed manually. Since the time of direct accelerator engineering service (preventive maintenance, malfunction correction) is limited, the manual service is permissible even with the dose power of 0.5 mGy/hour. The corresponding level of beam losses amounts to

$$W\ q \approx 1\ \text{GeV nA/m} \qquad (2)$$

Under the condition (2) and with specific acceleration of 1 Mev/m in the second part of accelerator (i.e. 0.1 - 1.5 GeV) the total permissible beam current losses amount to 3 μA. With the beam current of 300 mA it leads to the permissible relative losses of about 10^{-5}, whilst the condition (1) leads to the relative losses of the order of 10^{-6}.

Several methods were proposed and developed in MRTI to solve the radiation purity problem. Some of them were applied, in particular, in MMF accelerator. Among the methods are the following: beam phase volume filtering, suppression of coherent longitudinal and transverse beam oscillations, contactless beam parameters measurement, beam distortion diagnostics through the beam loss measurement, and residual gas pressure limitation in the H^- beam channel.

The phase volume filtration method essence consists in shaping such accelerator input phase volume, that would be less then further accelerator part acceptance and relative particle losses wouldn't exceed $10^{-5}...10^{-6}$ (for BRLA). Transverse phase volume filtering theory principles with space charge and longitudinal-transverse particles oscillations coupling are presented in [8,26,27].

Beam perturbations diagnostic method by beam losses analysis with the help of ionized radiation detectors (see [28-30]) is designed to determine beam perturbations source and location. Beam perturbations diagnostic problems are formulated as follows. One

assumes that the phase volume filtration is fulfilled at the beginning of accelerator, tolerances are within the calculated limits, longitudinal and transverse coherent particles oscillations depress system effectively operates. Then beam will be accelerate with possibly small losses. If a single characteristic perturbation will be realized (longitudinal motion perturbation, transverse motion perturbation, H^- ion discharge by residual gas), then a certain loss distribution will result. The reverse problem of one or several (few) perturbations search by measured beam losses distribution is just perturbation diagnostic problem. This problem can be solved. Loss distributions for characteristic beam perturbations are presented in [29-30]. The problem of beam loss distribution function reestablishment by measured neutron field distribution is solved there. Accelerating-focusing channel parameters variation and beam parameters measurement system information are also used by this method.

Current status of radiation purity problems solving as follows. In LAMPF accelerator measured losses at 70...800 MeV, accelerator 1 mA are equal to 10^{-9}. It means that condition (2) is satisfied at 1 mA mean beam current and manual accelerator maintenance problem is solved. Use of the new considered methods permits to hope that this problem will be solved for BRLA.

In conclusion it's possible to make the following inferences.

1. The analysis of linear proton accelerator science and technology development and current status along with the modern problems shows that the design and construction of continuous mode 1.5 GeV - 0.3 A linear proton accelerator is feasible and does not encounter with unsolvable science and technology problems.

2. One of the main BRLA design problems is that of generators with 5 - 10 MW mean power, 200 (300) and 600 (900) MHz operating frequencies, efficiency of order 70...80 % and 10 thousand hours of service life.

3. Further accelerating structures investigations are necessary both for low energies and for high energies.

4. On the way to BRLA implementation it's necessary to solve three important problems to say nothing of the individual linear accelerator systems perfection. The three problems are the efficiency, the reliability and the radiation purity. The basic processes for these problems solution will be simulated at MMF accelerator.

5. Current status of linear proton accelerator science and technology development, experience of the Soviet proton linear accelerator laboratories, including the very powerful MMF linear accelerator, permit to consider the construction of the proton linear accelerator for high level radioactive wastes of atomic power plants transmutation within next 15 years.

6. Since target complex problems are difficult as well, it's necessary to solve accelerator and target complex problems simultaneously. It's worth while to solve a part of target complex problems at MMF linear accelerator.

References

1. Nuclear technologies in a sustainable energy system. Editors J.S.Bauer and A.McDonald, Springer-Vearlag, Berlin-Hidelberg-New York, 19832. B.Murin,A.Fedotov, "Main Aspects of Proton Linear

Accelerators for Nuclear Fuel Breeding". Proc. 6-th All-Union Conf. on Part. Accelerators, v.1, p.241, Dubna, 1978
3. G.I.Batskikh et al. Linac for Meson Factory. In : " Acceleration Facility for Medium Energy Physics : the Meson Factory ", RTI, USSR Academy of Sciences, 1974, p.9-23
4. K.D.Sinelnikov et al. Proc. UkSSR Academy of Sciences session of peaceful atomic energy use. Kiev, UkSSR Academy of Sciences, 1958.
5. V.A.Batalin et al., 25 MeV Proton Linear Accelerator I-2, Pribory i Tekhnika Eksperimenta, No.5, p.9, 1967
6. I.M.Kapchinsky et al. On injector project for 70 GeV CW Proton Synchrotron. Atomnaya Energiya, Proc. International Accelerator Conference (Dubna), Moscow, Atomizdat, 1964
7. B.K.Shembel et al. High current CW Proton Linear Accelerator. Atomnaya Energiya, v.31, No.1, p.45, 1971
8. B.P.Murin, B.I.Bondarev, V.V.Kushin, A.P.Fedotov. Ion Linear Accelerators, v.1, Problems and Theory, Moscow, Atomizdat, 1978
9. B.Murin, V.Kulman, L.Lomize, B.Polyakov, A.Fedotov. Ion Linear Accelerators, v.2, Basic Systems, Moscow, Atomizdat, 1978
10. I.Kapchinsky, B.Teplyakov, Pribory i Tekhnika Eksperimenta, No.2, p.19, 1970 (in Russian)
11. B.I.Bondarev et al. " Focusing with Superconducting Solenoid for Current Increase in Ion Linac " Proc. of the 6-th All-Union Conf. on the Charge Particles Accelerator, v.1, 260 (1979)
12. B.I.Bondarev, N.A.Griasnov, V.A.Keilin, A.N.Kurmanov, B.F.Lapta, A.N.Likharev, E.A.Mirochnik, A.V.Mishchenko, B.P.Murin, V.M.Pirozhenko, O.V.Plink, V.N.Saverin, I.B.Seleznev, M.I.Surin. Experimental RF Proton Accelerator with Superconducting Solenoid Beam Focusing. this conference
13. V.A.Bomko et al. Field Distribution Stabilization Method in Drift Tube Accelerating Structure. Proc. 3-rd All-Union Conf. on Particle Accelerators, Moscow, Nauka, v.1, p.271, 1973
14. E.A.Knapp, B.S.Knapp, P.M.Potter. Accelerating Standing Wave Structure for High Energy Linear Accelerator, Pribori dlya Nauchnih Issledovaniy, v.39, No.7, p.31-43, 1968
15. V.G.Kulman, E.A.Mirochnik, V.M.Pirozhenko. Accelerating Ring-coupled Structure. Pribory i Tekhnika Eksperimenta, No.4, p.56-61, 1970
16. V.G.Andreev Geometry Definition of the Structure with Alternate-sign Accelerating Field on $\pi/2$-wave. Zh. Techn. Fiz., v.41, No.4, p.788, 1971
17. V.G.Andreev, V.M.Belugin, S.K.Esin, L.V.Kravchuk, V.V.Paramonov. Parasitic Mode Removal out of Operating Mode Neighborhood in DAW Accelerating Structure. IEEE Trans. on NS, v.NS-30, N.4, 1983, p.3575
18. B.P.Murin, V.I.Rogachev, A.P.Fedotov. On Possibility of Permanent Magnet Quadrupole Use for High Energy Accelerators. Pribory i Tekhnika Experimenta, No.2, p.22, 1976
19. I.M.Kapchinsky, N.V.Lazarev. On Possibility of Permanent Magnet Use in Ion Linear Accelerator Strong Focusing Channels, Preprint ITEP, Moscow, No.78, p.9,1975
20. F.A.Vodopyanov, B.P.Murin, "The Method of RF Oscillations Generation with the Use of Relativistic Electron Beam".Proc. RTI, No.22, p. 20, 1975
21. B.P.Murin, A.P.Durkin, O.Yu.Shlygin. Electron beam bunching in a microwave quasicontinuous-mode generator. In : " Relativistic microwave generators. Theory and technology ", RTI, USSR Academy

of Sciences, 1988, p.76-84
22. B.P.Murin, L.G.Lomize, A.E.Sominski. Deceleration of electron bunches in stretched cavity system. Ibid., p.96-100
23. B.P.Murin. High Power RF supply systems for Particle Accelerators. Preprint 833, RTI, USSR Academy of Sciences, 1983
24. B.Murin, A.Fedotov, "Radiation Purity and Efficiency Problem in Modern Linear Proton and H^- Ion Accelerators with High Mean Currents", Atomnaya Energiya, v.38, No.3, p.146, 1975
25 N.M.Fewell, V.Lo Destro. Operation of the Brookhaven 200 MeV Linac, Proc. of the 1979 Linear Accelerator Conf., USA, Brookhaven Nat. Lab., 1979
26. V.S.Kabanov, S.A.Lukshin, A.P.Fedotov. Transverse Particle Motion Dependence upon Longitudinal Motion and Beam Phase Volume Filtering in Proton Linear Accelerators. Pr. i Tek. Eksp., No.4, p.37-39, 1984
27. V.S.Kabanov, S.A.Lukshin, A.P.Fedotov. Transverse Beam Phase Volume Filtering with Space Charge and Longitudinal-Transverse Particles Oscillations Coupling in Proton Linear Accelerators. Pr. i Tek. Eksp., No.3, p.26, 1980
28. A.P.Fedotov et al. Beam Perturbation Diagnostics in Ion Linear Accelerators by Second Particles Distribution. Pr. i Tek. Eksp., No.3, p.26, 1980
29. V.V.Pyankov, A.P.Fedotov, V.B.Khvostov. Beam Losses Distribution Analysis in Linear Accelerator - Meson Generators. In : " Heavy-ion Accelerators, RTI, USSR Academy of Sciences, p.151, 1980
30. A.P.Fedotov. Beam Losses Measurements in Proton Linear Accelerators and Beam Perturbation Diagnostic Problems. Pr. i Tek. Eksp., No.5, p.7, 1981

ICANS-XI International Collaboration on Advanced Neutron Sources
KEK, Tsukuba, October 22-26, 1990

THE INTENSE PROTON ACCELERATOR PROGRAM AT JAERI

Yoshihiko Kaneko
Department of Reactor Engineering
Japan Atomic Energy Research Institute
Tokai-mura, Ibaraki-ken 319-11, Japan
0292-82-5517

I. INTRODUCTION

Much efforts are required to get the social understanding that nuclear energy is clean from the view point of preservation of natural environment. The social understanding is one of the premises for that the nuclear power generation is continually accepted for future like it was in the past. It is indicated in Fig.1 that share of the nuclear power in the whole primary energy supply has to be much enlarged if we want to lower the emission of CO_2 to an acceptable level while keeping the economical growth rate to the level being attained at the present.(1)

The efforts should be directed to the following two targets. One is the development of more safe nuclear reactor compared with the existing ones, for which the occurrence probability of the large scale accidents followed by the considerable level discharge of radio-active substances such as the case of the Chernobyl reactor can be thought to be effectively zero. The other is the establishment of the radio-active waste management technology.

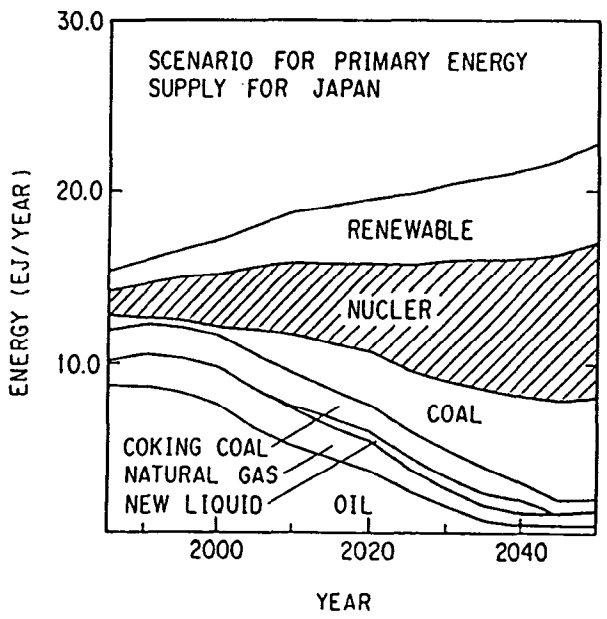

Fig.1 Primary Energy Supply under Constraint for CO_2 Emission.

In the spent fuel of the nuclear power reactor, are included the trans-uranium nuclides (TRU) such as Np, Am and Cm. Therefore, they must be kept away from the human living area for very long time, because some TRU have long lives exceeding 10^4 years. The situation is explained in Fig.2, where the decay of toxicity of nuclear wastes with time is predicted. The geological deposit is widely accepted in most advanced countries. But, it is not an easy task. If the TRU nuclides are transmuted to stable or short life ones, the technological burdens placed on the geological deposit can be substantially mitigated.

The Japanese Atomic Energy Commission concluded in Autumn 1988 to strengthen the research and development on partitioning and incineration of nuclear wastes. The Science and Technology Agency formulated the OMEGA project. The fuel cycle committee of OECD/NEA has decided to initiate an international collaboration frame work for the subject.

Incineration of nuclear wastes by use of accelerators is defined as one of the important tasks in the OMEGA program. Japan Atomic Energy Research Institute (JAERI) has been engaged for several years in the basic studies on incineration technology with use of the intense proton linear accelerator. The intense proton accelerator program intends to provide a large scale proton linear accelerator named as "The Engineering Test Accelerator". The principal purpose of the accelerator is to develop the incineration technology of the nuclear wastes. In the facility, will be made the mersurements of nuclear data, integral reactor physics

Missing Pages

211 — 226

efficiency of 98%, a stripper carbon foil with a thickness of 300 or 250 $\mu g/cm^2$ is necessary for the H^- or H^0 injected beam, respectively. The effects of this foil to the beam is as follows in the case of direct H^- injection (the estimation method is described in ref. [3]):

- Energy loss per passage (ΔE) is ~600eV.
- Emittance growth per passage ($\Delta\varepsilon$) is ~0.005 $\pi\mu$mr when the emittance of an injected beam is 1.4 $\pi\mu$mr and the beta-function at the foil is 15 m.

Though these are not so large, and even negligible when the average foil passage number is several tens, beam losses due to scattering by foil atoms and nuclei are far more severe:

- The beam loss rate per passage due to nuclear scattering (L_n) is ~5.6×10^{-6}.
- The beam loss rate per passage due to large-angle Coulomb scattering (L_c) is ~4.0×10^{-6}, provided that particles scattered by an angle larger than 2.8 mr are lost.
- The beam loss rate per passage due to large energy transfer (L_s) is ~1.3×10^{-5}, provided that particles which lose an energy larger than 1 MeV become lost from the rf bucket.

Thus, the total beam loss rate (L) is

$$L = L_n + L_c + L_s = 2.2 \times 10^{-5}. \qquad (1)$$

This means that when the accumulated particles pass the foil an average of 50 times, the fraction of the lost beam particles reaches 1.1×10^{-3} and the lost current exceeds 0.2 μA. In the JHP case, in order to accumulate 2.5×10^{13} protons the H^- beam should be injected during 600 turns of the ring cycle; accumulated particles pass the foil location 300 times on the average. Therefore, the foil-hitting probability should be suppressed to 10 % or lower. As far as the foil-hitting probability is concerned, the lower the better.

In order to reduce the foil-hitting probability, the foil is placed outside of the ring acceptance and the proton beam captured in the ring is moved away from the foil as soon as possible by varying the injection bump orbit. Moreover, the shape of stripper foil is designed as the postage stamp or the corner foil shown in Fig. 2, and the injected beam is positioned just inside of the foil edge. Fig. 3 schematically shows the situation regarding the foil and beams both upsream and downstream of the foil in the case of direct H^- injection. There are three beams downstream of the foil: a proton, H^- and H^0. Because the H^- beam is injected just inside of the foil edge, it is very possible for a part of beam periphery to wander out of and miss the foil. This part thus remains as a H^- beam. The amount of this part is expected to widely vary from negligible to several % of the injected beam, depending upon the partcle distribution of the beam and the beam positioning in the foil. Although several % of the beam is far more than the amount of the part lost by scattering, this part can be controlled and transported to a beam dump with a suitable beam guiding system. The H^0 beam downstream of the foil is produced from the main part of the injected beam, and amounts about 2 % of the beam or ~4 μA. This part is also controllable and is produced as a result of selecting a

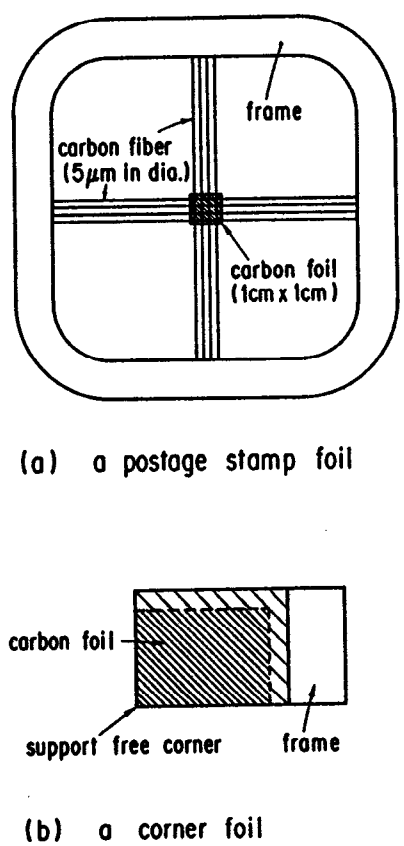

Fig. 2 A postage-stamp foil and a corner foil.

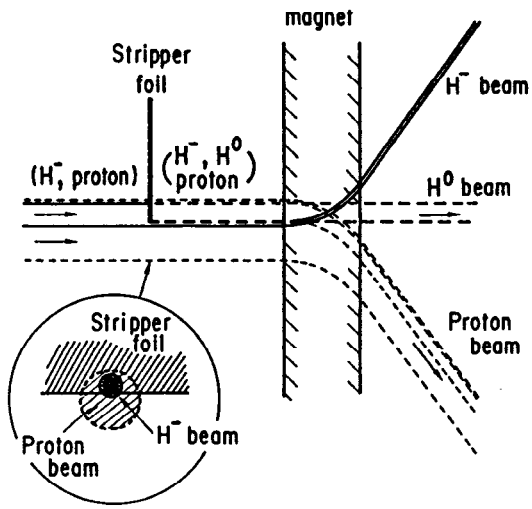

Fig. 3 Beams upstream and downstream of the stripper foil during H^- injection.

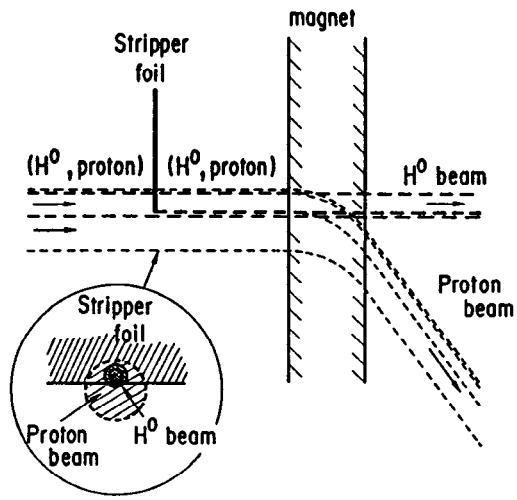

Fig. 4 Beams upstream and downstream of the stripper foil during H^0 injection.

thinner foil with a 98 % charge-exchange efficiency in order to reduce any uncontrollable beam loss due to scattering. This H^0 beam is considered to be as stable as an injected H^- beam and is desirable to be transported to an experimental room for experimental usage.

The case of H^0 injection is illustrated in Fig. 4. For the same reason as in H^- injection, the H^0 beam is injected just inside of the foil edge; a part of the beam periphery misses the foil. About 2 % of the beam which passes the foil also remains as an H^0 beam without being charge-exchanged to a proton beam. In this case, however, both of these parts are of the same kind and comprise an H^0 beam. This H^0 beam has a current of several μA and is considered to be useful in physics experiments.

In both of the cases mentioned above, one or two beams with probably several μA intensity are spilled downstream of the foil. This beam current is higher than the empirical limit (0.3 μA) of the beam loss by more than one order of magnitude. Thus, if several % of these spilled beams is lost, significant activation occurs around the injection straight section. We can not be too careful in the treatment of these spilled beams.

IV. DIRECT H^- INJECTION SYSTEM FOR A SUFFICIENTLY LONG STRAIGHT SECTION

Though examples of sufficiently long straight sections used to insert a direct H^- injection system are found in papers of G. H. Rees [6] and E. P. Colton [9], neither of these papers describe in detail the treatment of spilled H^0 and H^- beams. Although we can consider a complicated and sophisticated system for the direct H^- injection system, we restrict ourselves to a rather simple system and do not deal with any unnecessarily complicated systems.

Roughly grouping, there are four components necessary for a direct H^- injection system:
- a set of dipole magnets to form an injection bump orbit,
- a stripper foil,
- an inflection magnet system to guide the injected H^- beam near to the injection magnet, and
- an extraction magnet system for spilled H^0 and H^- beams.

In order to suppress any emittance growth and particle loss at the stripper foil as little as possible, the beta-function of the ring optics should be small at the foil in both horizontal and vertical planes. Requiring, furthermore, easiness to match the injected beam to the ring optics, we consider a special insertion that has a waist with a sufficiently small beta-function (= 3 m) in both planes at the center. At each end of this insertion, a set of quadrupole magnets is placed to match the insertion optics to the adjacent ring optics. Therefore, the four components mentioned above should be accommodated between these adjacent quadrupole magnets. Hereafter, this insertion is called "injection insertion".

When the waist with a β_0 beta-function is formed at the stripper foil, the β beta-function at a point with a distance of L from the foil is given by

$$\beta = \beta_0 + L^2 / \beta_0. \qquad (2)$$

When we take a moderate value of 15 m for the beta-function at the end of the injection insertion, then

$$L = 6\,\mathrm{m} \qquad (\text{ where } \beta = 15\,\mathrm{m}\,). \qquad (3)$$

This means that a typical length of such an insertion may be about 12 m.

Figs. 5 and 6 show examples of a conceptual design which arranges four components in the above mentioned insertion. Fig 5 shows an example which conducts both the H^0 and H^- beams together to a beam dump. On the other hand, Fig. 6 shows an example which separately conducts the H^- beam to a beam dump and the H^0 beam to an experimental room.

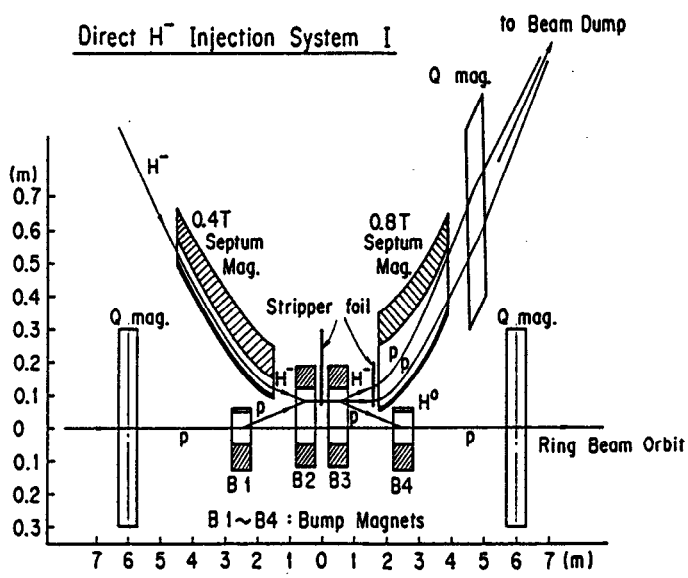

Fig. 5 Direct H^- injection system I.

The second bump magnet is called "injection magnet" in this paper. The maximun displacement of the bump orbit is usually taken so that the stripper foil at which the orbit passes comes out of the ring acceptance. Here, it is taken as 80 mm so as to meet further requirements as well; the spilled H^0 beam should sufficiently clear the fourth bump magnet and should not require a long distance for the proton beam to separate from the H^0 beam by enough space to insert the septum coil of the bump magnet between them. In such a situation, two outer bump magnets, the inflection magnet and the extraction maget should be of the septum type. The magnetic field of the inflection magnet should be taken to be lower than 0.4 T in order to avoid considerable amount of magnetic field dissociation of the injected H^- beam. It takes more than 3 m to inflect a 1-GeV H^- beam by 30 cm. Spilled H^0 and H^- beams are extracted with a septum magnet after being converted to proton beams by a stripper foil. In order to extract these beams 30 cm from the bump orbit, a septum magnet of about 2 m is necessary when a 0.8 T magnetic field is available for the septum magnet. When both spilled H^0 and H^- beams are extracted together, as shown in Fig. 5, the first quadrupole magnet downstream of the septum requires a very large horizontal aperture, since these two beams are considerably separated from each other.

When a spilled H^0 beam is used for experiments, it may be desirable that the control of one beam does not affect the other beam, as shown in Fig. 6. In both cases illustrated in Figs.5 and 6 it may be considerably useful to monitor the current and profile of each beam at a location where these beams clearly separate from each other.

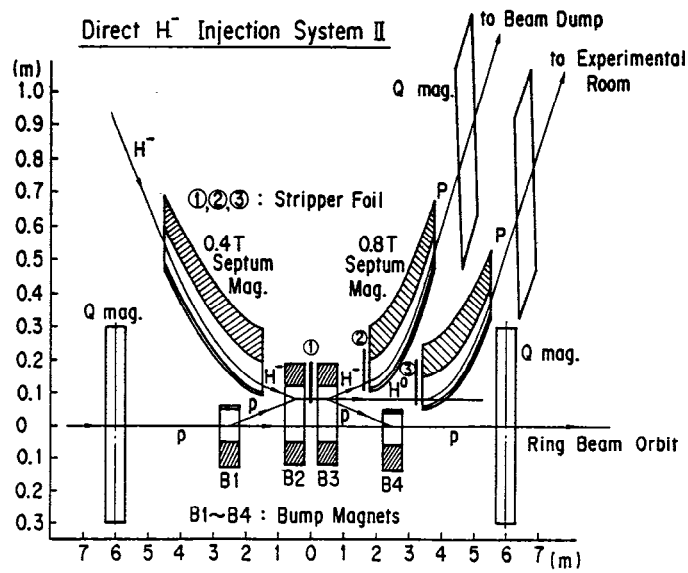

Fig. 6 Direct H^- injection system II.

V. H^0 INJECTION SYSTEM FOR A SHORT STRAIGHT SECTION

The typical length of a straight section may be 5 or 6 m for an 800-MeV or 1-GeV synchrotron with a usual higher symmetric FODO lattice. It is impossible to insert the injection insertion described in the last section in such a short straight section. Even if the ring lattice is used as it is without any insertion and, moreovere, the bump orbit is formed with an aid of the lattice focusing force, the straight section is not sufficiently long to accommodate all of the stripper foil, the injection magnet, the inflection septum magnet for the injected H^- beam and the extraction septum magnet for the spilled H^0 and H^- beams. It is therefore very difficult to accommodate a direct H^- injection system in a straight section of this type ring. When one is accepted as the superperiodicity, a special H^- injection system may be considered [10]. In such a system, treatment of the spilled H^0 and H^- beams is also one of the major subjects.

On the other hand, a two-step H^0 injection system is capable of being accommodated in a short straight section, since it does not have any inflection magnet for the injected H^- beam or any extraction magnet for the spilled H^- beam. Fig. 7 shows an example of a two-step H^0 injection system. The H^0 beam, which is formed in the stripper magnet, passes the gap of a synchrotron bend magnet without interaction and injects to the stripper foil. The stripper foil is placed outside of the ring acceptance. The proton beam formed at the foil is captured on an orbit oscillating around the bump orbit. As the bump orbit is varied, the captured proton beam wanders away from the foil and a continuously formed proton beam is painted over the phase space of the ring beam. One spilled beam is an H^0 beam which consists of two parts (as described in section III). Because the current of this H^0 beam amounts to several μA, it should be transported and used in an experimental room

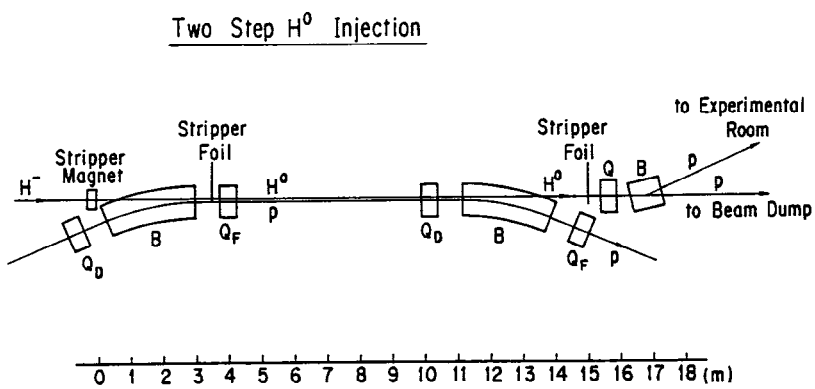

Fig. 7 Example of a two-step H^0 injection system.

after passing any current and profile monitors to obtain useful imformation concerning the injection tuning. It should be noticed that this type injection system is also applicable to the arc part of a racetrack-type ring where there is no straight section, except for very short spaces between the bend and quadrupole magnets.

A two-step H^0 injection system has been constructed and operated for several years at PSR. In the system at PSR, the stripper foil is placed at a location different from that shown in Fig. 7 and shortly downstream of the Q_F guadrupole magnet. This difference is very important to the matching of the H^0 beam to the ring optics [11]. The PSR injection system also has no magnet to switch the spilled H^0 beam to the experimental room. Experience at PSR have indicated that two-step H^0 injection has two problems [4]. One is an angular divergence accompanying the charge-exchange process in the stripper magnet, and the other is a mismatch of H^0 beam to the ring optics at the stripper foil.

Because the magnetic field dissociation is a stochastic phenomenon, the place where each H^- ion is changed to an H^0 atom is distributed along the beam path in the stripper magnet. Thus the distribution of the path length, over which each particle flies as an H^- ion, results in an angular divergence or an emittance growth of the formed H^0 beam. When the beta-function of the H^- beam at the stripper magnet is β^- and the r.m.s. angular divergence is $\Delta\phi$, r.m.s. emittances ε^- and ε_0 of the H^- and H^0 beam have the relation:

$$\varepsilon_0 = K\,\varepsilon^-, \text{ and} \tag{4}$$

$$K = \mathrm{SQRT}\{\,1 + \beta^-(\Delta\phi)^2/\varepsilon^-\,\}, \tag{5}$$

where both the phase-space particle distribution of the H^0 and H^- beams and the distribution of the angular divergence are assumed to be Gaussian. This angular divergence becomes smaller when the field gradient at the place where the stripping mainly occurs becomes steeper. The stripper magnet of PSR is an iron-core magnet which has a special pole shape in order to generate a very high field gradient [12]. Since the main gap is required to generate a field higher than 1.8 T, it is as narrow as 11 mm. Furthermore, a vacuum envelope is also inserted in the gap. As a result, the aperture for the beam is only 10 mm. In the bending plane, however, the aperture is as wide as 53 mm. The JHP compressor/stretcher ring proposal also assumes a similar stripper magnet. In such a stripper magnet, $\Delta\phi$ is ~0.37 mr for an 800-MeV beam; it is estimated to be ~0.26 mr for a 1-GeV beam. K thus has a value of about 3 for usual operation of PSR; a similar value is expected for the JHP proposal.

The other problem is that the H^0 beam formed by the above-mentioned stripper magnet can not be sufficiently matched to the ring optics at the foil. Since this problem is discussed in detail in another paper [11], only some important points are described here. In the H^0 injection system of PSR, the stripper foil is located shortly downstream of a Q_F quadrupole magnet and the bending plane of the stripper magnet is horizontal. With this arrangement, the H^0 beam may be matched in the vertical plane, but hardly in the horizontal plane. Because the gap of the stripper magnet is narrow, it is also difficult to perfectly match in the vertical plane. On the other hand, the stripper foil is placed between a bending magnet and the following Q_F quadrupole magnet and the bending plane of the stripper magnet is set to be vertical in the case of JHP proposal as shown in Fig. 7. In this case, the H^0 beam can be matched both in horizontal and vertical planes. A small mismatch, however, can not be actually avoided, since matching at the foil contradicts any suppression of emittance growth in the stripper magnet. The degree of this mismatch is defined by a mismatch factor [4],

$$C = (\beta_0\gamma - 2\alpha_0\alpha + \beta\gamma_0)/2, \tag{6}$$

where (β_0, α_0, γ_0) and (β, α, γ) are Twiss parameters of the H^0 beam and the ring optics at the foil. When matching is perfect, C reduces to 1. We then have

$$\varepsilon = C\,\varepsilon_0, \tag{7}$$

where ε is the emittance of the just-formed proton beam, and the tail of the proton distribution becomes longer than the Gaussian distribution [13]. The mismatch factor for the PSR is about 3.5 in the horizontal plane; for the JHP proposal, the mismatch factors are 1.2 and 1.6 in the horizontal and vertical plane, respectively.

VI. DISCUSSION

For full energy injection, a direct H^- injection scheme or a two-step H^0 injection scheme may be applicable. Direct H^- injection does not introduce any emittance growth like that which occurs in the stripper magnet, and is able to match the H^- beam to the ring optics at the stripper foil. However it requires a ring with a especially long straight section since a direct H^- injection system is considerably long (as is described in section IV). On the other hand, although two-step H^0 injection has noticeably atractive features (simplicity of the injection system and wide applicability to various types of rings), it introduces a beam angular divergence in the stripper magnet and an optical mismatch at the stripper foil. These eventually result in an emittance growth with a factor (K x C), where K and C are defined in equations (5) and (6), respectively. So it is desirable to minimize (KxC) factors in both horizontal and vertical planes. Minimization of these factors is described in another paper [11]. This emittance growth is basically caused by the angular divergence. Although the mismatch of the H^0 beam to the ring optics can be completely removed when the angular divergence becomes small, a small emittance growth in the stripper magnet cannot be removed. Therefore, when we can tolerate a small emittance growth, the two-step H^0 injection is very useful. Otherwise, we should adopt the direct H^- injection scheme and a ring with a sufficiently long straight section.

It may be worthwhile to examine the feasibility of a split-type superconducting solenoid as a new type of stripper magnet. An 8 T split coil magnet with a sufficiently wide gap is now commercially available. It may be possible to design a superconducting stripper magnet having a field gradient in the coil region that is a few times higher than that produced by an ordinary iron core stripper magnet. In the proposal for JHP, H^- to H^0 conversion mainly takes place around a point with 1.3 T, and the r.m.s. angular divergence is estimated to be 0.26 mr when the field gradient is 1.29 T/cm. Due to the proposed optics the emittance growth K in the stripper magnet is estimated to be 2.8 and the mismatch factor C in the vertical plane 1.6. If the field gradient is made higher and the angular divergence smaller by a factor 3, K will be reduce to 1.4 and C to 1, giving a perfect match. The mismatch in the horizontal plane may be easily removed by moving the waist slightly upstream of the stripper magnet, since the small mismatch in the proposal for JHP is to be produced by placing the waist at the gap of the stripper magnet. Furthermore, if a stripper magnet has a very high maximum field, a very steep field gradient and a beam aperture slightly larger than the currently available stripper magnet, the applicability of the two-step H^0 injection scheme is extended to such a low injection energy as the scheme is not applicable at the moment.

As described in section III, the stripper foil has many bad effects on the beam. Uncontrollable beam loss due to scattering is not negligible, especially in the full-energy injection scheme. To avoid this difficulty, it has been proposed to use a high-power laser beam instead of a foil [7]. This is a new type of two-step H^0 injection scheme. The first step involves magnetic field dissociation using a stripper magnet; the second step nvolves photoionization using a high-power laser beam. The reason why the first step does not use a laser beam is that the cross section of the photodetachment reaction (

$H^- + h\nu \rightarrow H^0 + e$) is very small. This photodetachment reaction has been fully investigated both theoretically and experimentally [14], and it is known that the cross section has the maximum value 4 x 10^{-17} cm^2 when the photon wavelength is 0.8 μm. Photoionization during the second step uses a two-step ionization ($H^0(1s) + h\nu \rightarrow H^0(2p)$ and $H^0(2p) + h\nu \rightarrow p + e$) instead of direct ionization ($H^0(1s) + h\nu \rightarrow p + e$), since the cross section of the last reaction is also as small as ~10^{-17} cm^2. The cross sections, $\sigma_{1s\rightarrow 2p}$ and $\sigma_{2p\rightarrow ion}$, of the former reactions are both ~10^{-15} cm^2 and these reactions become applicable for charge-exchange injection into a synchrotron when a laser beam with ~100 kw/cm^2 as the power density is available. Actually, in order to cover the usual beam size (several mm in diameter) and momentum spread ($\Delta p/p \sim 10^{-3}$) of a conventional injected beam, a charge-exchange system requires several commercially available standard lasers. A system using FEL (Free Electron Laser) is also applicable and may be advantageous in covering the momentum spread of the injected beam, since its intrinsic wavelength spread is fairly large. In any case, these systems seem to be quite complex. Because the area around the injection straight section is apt to contain a considerably high radiation field, any system installed in the area should be sufficiently tolerant to radiation and free from too much maintenance and tuning work which involves directly touching the machine.

VII. SUMMARY

Two methods are applicable to generate a high-intensity pulsed proton beam for a spallation neutron source. One is a low-energy injection and acceleration method and the other is a full-energy injection and compression method. The latter method has two options regarding its injection scheme: the direct H^- injection scheme and the two-step H^0 injection scheme.

Although full-energy injection is advantageous with respect to the space-charge limit, beam loss due to scattering by stripper foil atoms is very harmful. In order to suppress the amount of uncontrollable beam loss to a tolerable level, we should, instead, accept some fraction of the injected beam being spilled downstream of the stripper foil. This spilled beam is controllable and should be carefully treated, since it amounts to several μA and has two components.

A standard direct H^- injection system consists of four components: a stripper foil, a set of bump magnets, an inflection magnet system for the injected H^- beam and an extraction magnet system for the spilled H^- and H^0 beams. Because the entire injection system becomes considerably long, it requires an especially long straight section, as in a racetrack-type ring.

On the other hand, the two-step H^0 injection system does not require such a long straight section, since both injected and spilled H^0 beams pass through ring magnets without interaction. It thus has a very wide applicability to various types of rings.

Two-step H^0 injection, however, has two problems: an angular divergence due to the stripping process in the stripper magnet and a mismatch of the H^0 beam to the ring optics. In the case of the FODO lattice, the mismatch can be removed by placing the foil between the bend and the following quadrupole magnet and setting the bending plane of the stripper magnet to be the same as the divergent plane of the quadrupole magnet.

The emittance growth is based on the angular divergence introduced in the stripping process. If the angular divergence is sufficiently reduced, the mismatch at the foil can be eliminated; the emittance growth at the stripper magnet can also be reduced to a tolerable level.

Though the idea to use a high-power laser beam instead of a stripper foil is atractive, it will require much development for a complicated system comprising a high power laser or FEL to replace a foil, since the foil-hitting probability can be reduced to a tolerable level and the foil does not require so much maintenance service.

ACKNOWLEDGEMENT

The author wishes to express his heartfelt thanks to Prof. M. Kihara for many stimulating discussions and much encouragement.

REFERENCES

[1] G. P. Lawrence, Proc. IEEE 1987 Part. Acc. Conf., March 16-19, 1987, pp825-829.
[2] G. H. Rees, Proc. IEEE 1987 Part. Acc. Conf. March 16-19, 1987, pp 830-833
[3] I. Yamane et al., KEK Report 88-8, November 1988, A
[4] R. J. Macek, Proc. 1988 Eur. Part. Acc. Conf.,June 7-11, 1988, pp 1252-1254
[5] R. J. Macek and M. Borden, private communication.
[6] G. H. Rees, INS-J-172,May 1988 (Institute for Nuclear Study, Univ. of Tokyo)
[7] C. Ohmori and S. Hiramatsu, KEK Preprint 89-162, November 1989, A
[8] Y. Kamiya, Proc. IEEE 1989 Part. Acc. Conf., March 20-23, 1989, pp 660-662
M. R. Masullo and H. Schoenauer, " Transverse Painting with Linear Coupling "
E. Gianfelice and H. Schoenauer, CERN/PS 88-28 (HI)
[9] E. P. Colton, AHF Technical Note 88-025
[10] R. J. Macek, private communication.
[11] I. Yamane, " Perfect Matching for the Two-Step H^0 Injection into a Ring with a DBFO Lattice and Minimization of the Overall Emittance Growth ", another paper submitted to this workshop (ICANS XI)
[12] D.W. Hudgings, IEEE Trans. Nucl. Sci. Vol. NS-26, No.3, 3556 (1979)
[13] R. J. Macek, PSR Technical Note No. 153
[14] S. T. Smith and D. S. Burch, Phys. Rev. 116 (1959) 1028
L. M. Branscomb, " The Photoionization of One- and Two-Electron Atoms ", Physics of One- And Two-Electron Atoms, ed. by F. Bopp and H. Kleinpoppen, 1968 (North Holland)

ICANS-XI International Collaboration on Advanced Neutron Sources
KEK, Tsukuba, October 22-26, 1990

Perfect matching for two-step H^0 injection into a ring with a DBFO lattice and minimization of the overall emittance growth

Isao Yamane
National Laboratory For High Energy Physics
Oho 1-1, Tsukuba-shi, Ibaraki-ken, 305 Japan

ABSTRACT

A procedure is given for achieving perfect matching in two-step H^0 injection into a DBFO lattice. It is at first shown that the foil should be located between B and F and the stripper magnet should be set so that the bending plane is vertical in order to make the H^0 beam match the ring optics. Then, the Twiss parameters of the H^- beam are determined so as to be converted to those of the H^0 beam which matches the ring optics through the charge-exchange process in the stripper magnet. It is shown that, though perfect matching at the foil can be achieved, the emittance growth in the stripper magnet can not be made to completely disappear. A factor K is defined as a measure of the emittance growth in the stripper magnet. When C is the mismatch factor at the foil, (KxC) is a measure of the total emittance growth during the entire charge-exchange process. The (KxC) factor should be minimized in an actual application, resulting that a small K as well as a small C will remain.

I. INTRODUCTION

When we inject an H^- beam into a synchrotron through charge-exchange injection, a two-step H^0 injection scheme may be applicable, as well as a direct H^- injection scheme, if the energy of the H^- beam is as high as about 1 GeV. Of the two steps, the first is formation of an H^0 beam from the H^- beam by the magnetic field detachment of H^- ions in a stripper magnet. The second step is the stripping of the H^0 beam by a stripper foil. The H^0 beam is injected into the foil by passing it through the magnetic field of the synchrotron magnets without any interaction. The formed proton beam is finally captured in the synchrotron.

This method has been adopted in LANL PSR. The following two problems have been found from several years of operational experience[1]. One is beam angular divergence due to the stripping process in the stripper magnet; the other is an ion-optical mismatch of the H^0 beam with the ring optics at the stripper foil. Both of these bad effects result in emittance growth; a considerably large increase of emittance can be introduced during the entire charge-exchange process from an H^- to a proton beam. The two-step H^0 injection scheme, however, is very widely applicable to various types of rings, since a system of the scheme is very simple. This scheme may be very atractive when a highly symmetric ring is desirable for some reason, or when many straight sections must be devoted to the slow extraction system and/or the rf system to form extremely short beam bunches like the JHP compressor/stretcher ring. It is very important to understand the full potential of the two-step H^0 injection scheme. We, therefore, discuss how to perfectly match the beam with the ring optics in this

scheme and how much the beam emittance grows as a result. It is also discussed how small the emittance growth can be made.

II. THE MISMATCH FACTOR, C, AND AN H^0 BEAM MATCHED WITH THE RING OPTICS

Suppose that a beam with Twiss parameters β_0, α_0 and γ_0 is injected into a ring point where the Twiss parameters of the ring optics are α, β and γ. In this case, mismatching makes the emittance of the beam formed in the ring, ε, larger than the emittance of the injected beam, ε^0, by a so-called mismatch factor C:

$$C = (\beta_0\gamma + \gamma_0\beta - 2\alpha_0\alpha)/2, \text{ and} \quad (1)$$

$$\varepsilon = C\varepsilon^0. \quad (2)$$

If the particle distribution of the injected beam is Gaussian, the distribution tail of the formed beam becomes slightly longer than the Gaussian [2]. When matching is perfect, β_0, α_0 and consequently γ_0 are equal to β, α and γ, respectively, and C reduces to 1.

We now suppose injection of an H^0 beam into a ring with a DBFO lattice using charg-exchange by a stripper foil. The beta-functions of the ring may be like β_x (horizontal) and β_y (vertical) indicated by the thin solid lines in Fig. 1. This is an example from the case of the JHP compressor/stretcher ring [3]. The stripper foil is usually placed at the point FOIL1 or FOIL2 between the magnets. FOIL1 is the location proposed in the JHP compressor/stretcher ring [4] and FOIL2 is the location adopted at PSR. Beta-functions of the H^0 beam matching at respective foil location are $\beta_x(H^01)$ and $\beta_y(H^01)$ or $\beta_x(H^02)$ and $\beta_y(H^02)$ shown by thick solid or broken lines. As an H^0 beam drifts, even in the field of the bend or quadrupole magnet, its beta-function depicts a parabola that connects with the ring beta-function in such a manner that $\beta(H^0) = \beta(\text{ring})$ and $\beta'(H^0) = \beta'(\text{ring})$ at the foil location. Here, the emittance growth due to multiple scattering in the foil is supposed to be negligibly small, since the beam energy is sufficiently high and the average foil hitting number can be sufficiently small [4]. As

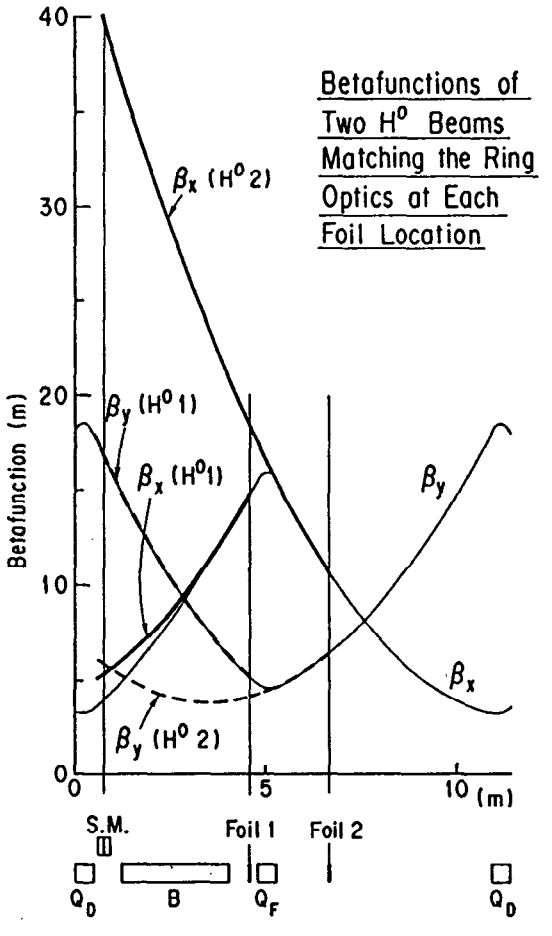

Fig. 1 Two H^0 beams matching the ring optics at the locations of FOIL1 or FOIL2. β_x and β_y are the ring beta-functions in the horizontal and vertical planes, respectively. $\beta_x(H^01)$ and $\beta_y(H^01)$ [$\beta_x(H^02)$ and $\beta_y(H^02)$] are also horizontal and vertical beta-functions of the H^0 beam matching with the ring optics at the locations of FOIL1 [FOIL2].

can be seen from this figure, beta-functions of the matched H^0 beam depend strongly upon which location the foil is placed (between B and Q_F or between Q_F and Q_D), but not so strongly upon the difference of the foil location between the two magnets for each case.The stripper magnet is placed imediately upstream of the bend magnet (shown as S.M. in the figure).

In order to generate a very high maximum field as well as a very high field gradient, the gap of the stripper magnet is considerably narrow; consequently, half of the beam aperture is as narrow as 5 mm for a currently available stripper magnet. The beam aperture in the bending plane may be taken to be sufficiently wide. Thus, when the foil is placed at the FOIL2 location, the stripper magnet should be set with the gap vertical and the bending plane horizontal. In this case, the horizontal beam size and, correspondingly, the horizontal emittance growth becomes very large in the stripper magnet. On the other hand, when the foil is placed at the FOIL1 location, it is necessary to set the stripper magnet with the gap horizontal and the bending plane vertical. This is because the vertical beam aperture is not sufficiently wide to accomodate the entire beam, including a 5σ emittance with a considerably large beta-function. For example of the JHP proposal, the 3σ emittance of the injected H^- beam is assumed to be 1.44 $\pi\mu$mr. Then, provided that the vertical beta-function is 16.69 m, a half of the 5σ beam size is 8.2 mm and can not go through the 5 mm wide half aperture.

Comparing FOIL1 and FOIL2 as the foil location, FOIL2 has a disadvatage in that the beta-function $\beta_x(H^02)$ becomes very large at the stripper magnet. It is therefore better to place the stripper foil at the location of FOIL1. In the JHP case, ring Twiss parameters at FOIL1 are as follows:

$$\beta_x = 14.84 \text{ m}, \alpha_x = -1.78 \quad \text{and} \quad \beta_y = 5.136 \text{ m}, \alpha_y = 0.867. \tag{3}$$

We have then following Twiss parameters for the H^0 beam at the stripper magnet:

$$\beta_x(H^01) = 5.348 \text{ m}, \alpha_x(H^01) = -0.709 \text{ and } \beta_y(H^01) = 16.69 \text{ m}, \alpha_y(H^01) = 2.17. \tag{4}$$

III. MATCHED H^- BEAM AND THE EMITTANCE GROWTH FACTOR, K

The stripper magnet converts an H^- beam to an H^0 beam by magnetic field detachment of H^- ions with high velocity [5] [6]. Because this detachment is a stochastic process, a distribution is introduced to path lengths that particles fly as H^- ions before being changed to H^0 atoms. The angular divergence of the beam takes place corresponding to the distribution of angles by which particles are bent by the magnetic field while they are H^- ions. The angular distribution is well fitted to a Gaussian distribution, and the r.m.s. angular divergence can be estimated from the field distribution in the stripper magnet. With the stripper magnet of PSR, the r.m.s. angular divergence is 0.37 mr for an 800 MeV H^- beam. With the same stripper magnet, the r.m.s. angular divergence is estimated to be 0.26 mr for a 1 GeV H^- beam.

When the r.m.s. emittance and Twiss parameters of the injected H^- beam are ε^-, β^- and α^- in the stripper magnet, those of the formed H^0 beam at the same location are described as

$$\varepsilon^0 = K\varepsilon^-, \tag{5}$$

$$\beta(H^0) = \beta^- / K, \text{ and} \tag{6}$$

$$\alpha(H^0) = \alpha^- / K, \tag{7}$$

where

$$K = \text{SQRT}\{ 1 + \beta^-(\Delta\phi)^2 / \varepsilon^- \}. \tag{8}$$

$\Delta\phi$ is the r.m.s. angular divergence in the stripper magnet. K is the rate of emittance growth in the stripping process, hereafter called the emittance growth factor. The beta-function of the H^- beam that is to be converted to an H^0 beam with a given beta-function $\beta(H^0)$ is derived from equations (6) and (8) as follows,

$$\beta^- = \{ (\beta(H^0)\,\Delta\phi)^2 / \varepsilon^- + \mathrm{SQRT}\{ [(\beta(H^0)\,\Delta\phi)^2 / \varepsilon^-]^2 + 4\,[\beta(H^0)]^2 \} \} / 2. \qquad (9)$$

Using these equations, vertical Twiss parameters and the emittance growth factor of the H^- beam (which is converted to the H^0 beam matched with the ring optics at the FOIL1 location) are obtained as follows:

$$\beta_y^- = 120\ \mathrm{m}, \qquad \alpha_y^- = 15.6, \text{ and} \qquad (10)$$
$$K_y = 7.2. \qquad (11)$$

Since there is no angular divergence in the horizontal plane, Twiss parameters don't change, and we have

$$\beta_x^- = 5.348\ \mathrm{m}, \qquad \alpha_x^- = -0.709, \text{ and} \qquad (12)$$
$$K_x = 1. \qquad (13)$$

Although β_y^- is considerably large, the vertical beam size is not so large, since the emittance of the H^- beam is sufficiently small. There is therefore no problem in forming such an H^- beam in the injection beam line. The emittance growth in the stripper magnet, however, is as large as 7.2.

It is thus possible to form an H^- beam which is converted to an H^0 beam matching the ring optics at the stripper foil. However, the beam emittance becomes considerably large. As the equation (8) implies, K becomes smaller as the beam size becomes smaller. However, if β_y^- is made smaller in order to reduce the emittance growth in the stripper magnet, of course, the formed H^0 beam becomes unmatched with the ring optics and some emittance growth occurs at the stripper foil corresponding to the mismatch factor.

IV. MINIMIZATION OF THE TOTAL EMITTANCE GROWTH DURING THE TWO-STEP CHARGE-EXCHANGE PROCESS

As can be seen from equations (2) and (5),

$$\varepsilon = (K\mathrm{x}C)\,\varepsilon^-. \qquad (14)$$

This means that the overall emittance growth during the two-step charge-exchange process can be expressed by the factor (KxC). It is therefore the minimum (KxC) that indicates the best condition to be realized. We should thus select the direction of stripper magnet and form an H^- beam in such a manner so as to minimize the (KxC) factor. The minimum (KxC) is easily found by calculating a map of (KxC) over the two-dimensional plane of β^- and α^- variables.

(i) When the stripper foil is placed at the location of FOIL1 and the stripper magnet at S.M. with the bending plane vertical, the minimum (KxC) in the vertical plane is obtained as

$$K_y \mathrm{x} C_y = 4.53, \qquad (K_y = 2.84, \text{ and } C_y = 1.59). \qquad (15)$$

The Twiss parameters of the H^- beam at the stripper magnet are

$$\beta_y^- = 16.74 \text{ m} \qquad \text{and} \qquad \alpha_y^- = 2.17. \tag{16}$$

In the horizontal plane, a matched H^0 beam can be formed from the H^- beam with the Twiss parameter set (12) without any emittance growth in the stripper magnet. We thus have

$$K_x x C_x = 1, \qquad (K_x = 1, \text{ and } C_x = 1). \tag{17}$$

(ii) If the increase in the (KxC) factor is shared by both planes, both of the (KxC) factors can be kept at fairly small values. In the last example, the gap direction of stripper magnet is chosen to be horizontal, since a matched H^- beam can pass the gap without any scraping. Conversely, if the gap direction is set to be vertical and the vertical beam size is diminished so that 5σ emittance can pass the gap without scraping, a remarkably small (KxC) can be obtained in the horizontal (or the stripper magnet bending) plane, although a small mismatch factor is introduced in the vertical plane. The result of searching for the minimum (KxC) factor under such a condition is

$$K_x x C_x = 2.13 \qquad (K_x = 1.80, C_x = 1.18), \text{ and} \tag{18}$$
$$K_y x C_y = 1.52, \qquad (K_y = 1.00, C_y = 1.52). \tag{19}$$

Here,

$$\beta_x^- = 5.34 \text{ m}, \qquad \alpha_x^- = -0.714, \text{ and} \tag{20}$$
$$\beta_y^- = 6.25 \text{ m}, \qquad \alpha_y^- = 0.800. \tag{21}$$

This set of (KxC) factors is considered to be the minimum atainable by the currently available stripper magnet.

V. DISCUSSION

As is shown in section III, when the H^- beam is adjusted on the condition that the stripper foil is placed at FOIL1 of Fig. 1 and the stripper magnet at S.M., with the bending plane vertical, we can make the H^0 beam formed at the stripper magnet or the proton beam formed by the stripper foil perfectly match the ring optics. However, under these conditions a considerably large emittance growth ($K_y = 7.2$) occurs in the bending plane of the stripper magnet. If the increase of KxC is shared by both the horizontal and vertical planes, emittance growth in each plane can be supressed to about 2 ($K_x x C_x = 2.13$, $K_y x C_y = 1.52$) using a currently available stripper magnet. Conversely, this indicates one of the capability limits of the present two-step H^0 injection process. Whether such an amount of emittance growth is permissible or not seems to depend upon the beam condition required for each accelerator. In the case of the JHP compressor / stretcher ring, in order to stack 2.5 x 10^{13} ppp (protons per pulse) a beam with an emittance as large as 30 $\pi\mu$mr is formed from a 1.44 $\pi\mu$mr H^- beam by beam painting. In such a situation, no serious problem can be introduced by a few times emittance growth during the charge-exchange process from an H^- to a proton beam. Beam painting will be slightly influenced by the emittance growth, because the beam size used for painting becomes about one and a half times larger. When such a small emittance growth does not matter, the

two-step H^0 injection scheme is very useful since its injection system is very simple and doesn't require such a long straight section as the direct H^- injection system.

The cause of the emittance growth is the angular divergence, $\Delta\phi$, in the stripper magnet. When an H^0 beam with a beta-function of $\beta(H^0)$ is formed from an H^- beam with an emittance ε^-, the emittance growth factor, K, is expressed as

$$K = \{ \beta(H^0)(\Delta\phi)^2/\varepsilon^- + \mathrm{SQRT}\{ [\beta(H^0)(\Delta\phi)^2/\varepsilon^-]^2 + 4 \} \}/2. \qquad (22)$$

For an r.m.s. emittance of $\varepsilon^- = 0.16\ \pi\mu\mathrm{mr}$ and $\beta(H^0) = 16.69$ m, the $\Delta\phi$ dependence of K is shown in Fig.2. This figure shows that $\Delta\phi$ should be reduced in order to suppress the emittance growth. In order to reduce $\Delta\phi$, it is necessary to increase the field gradient of the stripper magnet. A split-type superconducting solenoid may be useful for this purpose.

In paragraph (ii) of section IV, an H^0 beam mismatching with the ring optics is formed to pass through the narrow aperture of the stripper magnet in the gap direction. If the aperture is expanded to twice the size of the currently available stripper magnet, a matched H^0 beam will be formed in the gap direction from an H^- beam with the same Twiss parameters as those of the H^0 beam.

Thus, the angular divergence in the stripper magnet represents the basic shortage of the two-step H^0 injection scheme. However, if a small emittance growth due to the angular divergence is permissible, the scheme will be very useful. The usefulness of the scheme should be raised by improving the stripper magnet to generate a higher field gradient and to have a wider gap.

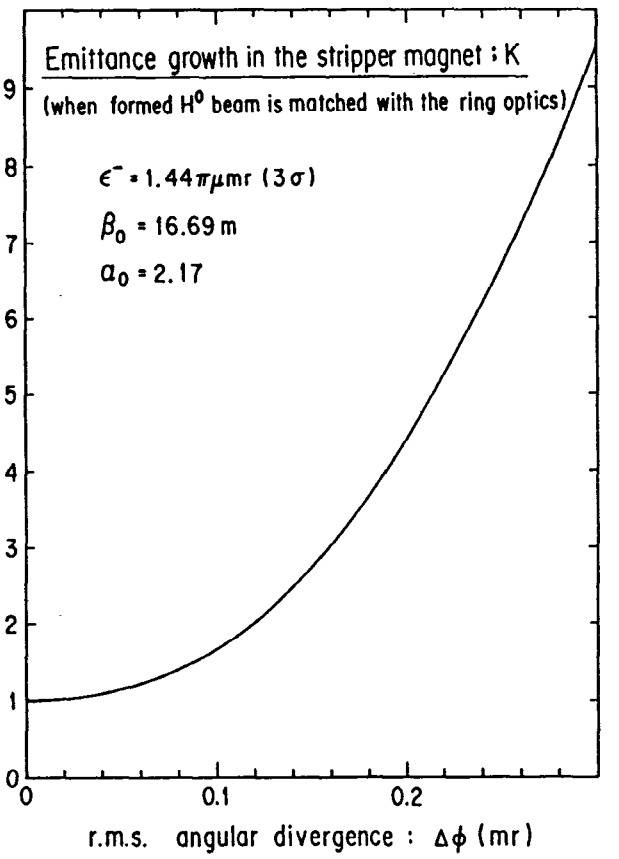

Fig. 2 Dependence of the emittance growth factor, K, upon the angular divergence in the stripper magnet. $\beta(H^0) = 16.69$ m, and ε^- (r.m.s.) = $0.16\ \pi\mu\mathrm{mr}$.

VI. CONCLUSION

Using the two-step H^0 injection scheme, an injected beam can be formed so as to perfectly match the beam optics of a synchrotron having a DBFO lattice. Then, however, a large emittance growth occurs in the same plane as that of the bending of the stripper magnet. In the case of the JHP compressor/stretcher ring, the overall emittance growth (KxC) during the charge-exchange process can be supressed to about 2 in both the horizontal and vertical planes by adjusting the emittance growth factor, K, in the stripper magnet and the mismatch factor, C, at the foil. This is one of the capability limits of the present two-step H^0 injection system. If the stripper magnet is improved to have a higher field gradient and a wider gap using such a new technique as the superconducting

solenoid, the emittance growth will be made smaller and the two-step H^0 injection scheme will be more useful.

ACKNOWLEDGEMENT

The author would like to express his hertfelt thanks to Prof. M. Kihara for many stimulating discussions and continuous encouragement.

REFERENCES

[1] R. J. Macek, Proc. 1988 Eur. Part. Acc. Conf., June 7-11, 1988. pp1252-1254
[2] R. J. Macek, PSR Technical Note No. 153, 1987
[3] "Report of the design study on the compressor/stretcher ring of the Japan Hadron Project [I]"; JHP-11, KEK Internal 88-9, September. 1988
[4] I. Yamane, KEK Report 88-8, November 1988, A
[5] G. M. Stinson et al., Nucl. Instr. Meth. 74 ('69) pp333-341
L. Sherk, Can. J. Phys. 57 ('79) pp558-563
[6] A. Jason et al., IEEE Trans. Nucl. Sci., Vol. NS-28, No 3, June 1981. pp2704-2706

Q(G.H.Rees): For 2 stage injection (H^-,H^0), have you considered introducing mismatch at the stripping foil to reduce subsequent foil transits?

A(I.Yamane): I have not yet considered. But if we can form a similar beam as the H^- beam by the two step injection, the situation does not differ so much. I think we can form a similar beam except for the emittance growth by the two step H^0 injection. Because of the emittance growth, the beam size becomes a little larger and the foil-bitting probability becomes a little larger.

Q(I.S.K.Gardner): How flexible is the H^0 injection compared with the H^- injection for the correction of small mis-alignments in the linac beam. In the H^0 case will small movements of the beam in the high gradient stripper magnet not cause match charges.

A(I.Yamane): The flexibility in the H^0 injection may be less than in the H^- injection. But the difference is not so large. The beta-function in the stripper magnet usually is considerably small. So movement of the beam in the stripper magnet is considered to be correspondingly small.

ICANS-XI International Collaboration on Advanced Neutron Sources
KEK, Tsukuba, October 22-26, 1990

System for generating double-pulsed magnetic fields in a kicker magnet

Tadamichi KAWAKUBO, Sichiro Tazawa, Yosio Arakida
and Sigeru Murasugi

National Laboratory for High Energy Physics,
1-1, Oho, Tsukuba-shi, Ibaraki-ken, 305, Japan

ABSTRACT

Two bunched beams are accelerated in the 1A ring of JHF. They are extracted for meson experiments and for neutron experiments successively. Therefore, the extraction kicker magnet should generate double-pulsed magnetic fields at intervals of about 100μsec, with a repetition rate of 50Hz. In order to test the feasibility of generating double pulses, we used two sets of thyratron housings and a kicker magnet for the KEK-PS-extraction system, which has an impedance of 25Ω. Using a thyratron cathode-loaded system, the first firing induces a second misfire by a rapid voltage drop of the second thyratron cathode. A thyratron anode-loaded system does not have the above-mentioned trouble, and has succeeded in generating the desired double pulses with half of the voltage required for the usual operation of JHF ($\sim$80kV).

1. INTRODUCTION

There are two bunched beams in the 1A ring of JHF; their timing during extraction is shown in the upper part of Fig.1. At first, one of these bunched beams is extracted for a meson measurement; then, after about 100μsec, another beam is extracted for a neutron measurement. Therefore, the extracted kicker magnet should produce 50Hz double-pulsed magnetic fields with an interval of 100μsec, as shown in the lower part of Fig.1.

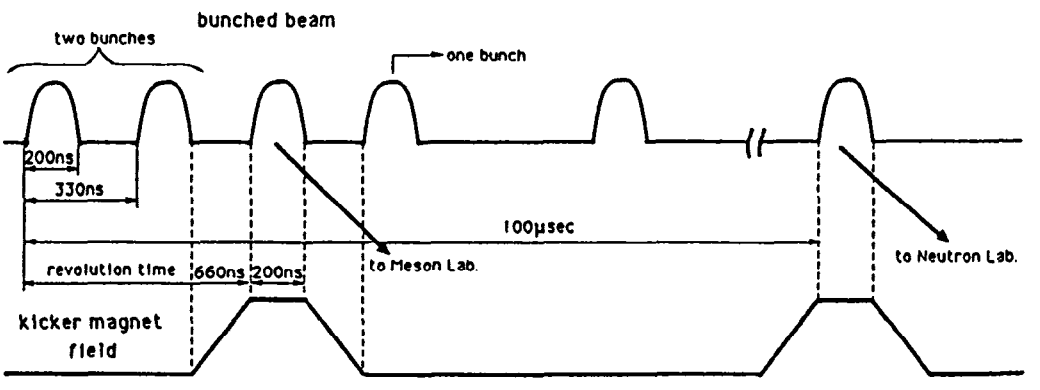

Fig.1 Timing between beam bunches and the kicker magnetic field.

In order to test the feasibility of generating double pulses, we used two sets of thyratron housings and a kicker magnet for the KEK-PS-extraction system, which has an impedance of 25Ω.

The two systems were designed to generate double pulses. One of them is a cathode-loaded system (introduced in section 2). This system works as long as the charging voltage is small. However, when the voltage is lager than a threshold value, the first firing induces a second firing without any trigger signal. The other system is a anode-loaded system. This system has no induced firing and generates double-pulse magnetic fields with an interval of about 100μsec (explained in section 3).

2. CATHODE-LOADED SYSTEM (failure case)

As shown in Fig.2, two sets of PFNs and thyratron housings are connected in parallel to a kicker magnet. At first, the thyratron 1 is triggered and the current charged in PFN1 flows to the kicker and is terminated in matching resistor. After 100μsec, thyratron 2 is triggered, and another pulse current flows to the kicker. Thus, double-pulse magnetic fields are generated in the kicker gap at intervals of 100μsec.

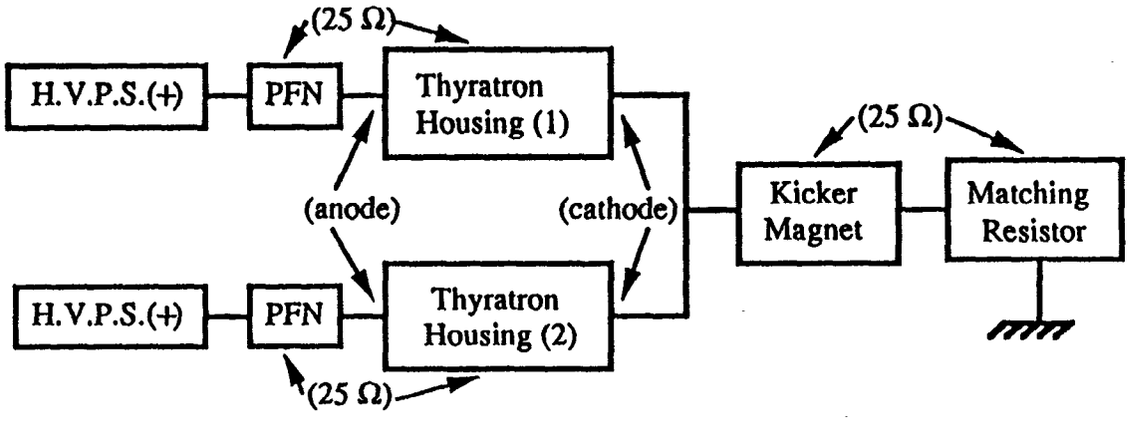

Fig.2 Block diagram of cathode-loaded system.

The thyratron in the housing is CX1171 (made by EEV company) and has a three-gap tetrode, 120kV peak forward voltage and 3kA peak anode current. Though thyratron 2 is operated without any trouble at low PFN voltage, induced firing begins to occur upon firing of thyratron 1 at a higher PFN voltage than about 12kV. This induced firing of thyratron 2 occurs even if the trigger input of the tube is shorted by a 50Ω terminator. Under this condition, the magnetic field of the kicker observed by using a long search coil is shown in Fig.3.

The time difference between the tail of the first pulse generated by thyratron 1 and the top of the second pulse generated by thyratron 2 is about 100ns. Since this time is equal to the time difference from the trigger to the start of current flow in the thyratron, the mechanism of induced firing might be as follows: the current charged in PFN 1 flows to the magnet upon firing of thyratron 1. During this stage the cathode potential of thyratron 2 increases suddenly to $V_{PFN}/2$ and the grid potential of thyratron 2 begins to gradually increase to this value. This case shows no trouble, since the potential of the grid of thyratron 2 is always lower than that of the cathode. However, just after the current passes through the thyratron 1, its cathode

We are now making a new thyratron housing for generating double pulses , which has two thyratrons (CX1171) separated from each other by a shield wall. Since the insulating voltage of the transformers is increased to 80kV, this system can generate double pulses with a PFN charging voltage of 80kV. Even if induced firing occurs, a thyratron having a screen grid like CX1171D will suppress it, because in this case the grid is effected by the anode potential.

4. ACKNOWLEDGMENT

The authors would like to acknowledge Dr.R.Sheldrake of EEV company for his interesting comments concerning the thyratron.

References

1. Private communication from Dr.R.Sheldrake, EEV.
2. EEV Technical Reprint No.130 "High power pulse generators for fast pulsed magnets; Developments and Operational experience"

Q(M.Kihara): Why do you expect an induced firing even in the second case, when you go to high voltage?

A(T.Kawakubo): I am afraid of the effect from the charge of the anode potential.

Q(I.S.K.Gardner): What is the normal operating voltage of the single thyratron cathode loaded system in use on the booster synchrotron.

A(T.Kawakubo): Our design value of PFN voltage is 80KV, but, operating one is 60KV~70KV.

ICANS-XI International Collaboration on Advanced Neutron Sources
KEK, Tsukuba, October 22-26, 1990

Intense negative ion source

Yoshiharu Mori
National Laboratory for High Energy Physics(KEK)
Oho 1-1, Tsukuba-shi,Ibaraki-ken 305, JAPAN

ABSTRACT
The volume H^- ion source has been developed at KEK. The H^- beam intensity was enhanced by introducing a very small amount of cesium vapor in the ion source. The extracted H^- beam current of 20mA was obtained in the cesium-mode operation. The measured 90% normalized beam emittance was about 1πmm.mrad for 12 mA beam. It was found that the workfunction of the cesium covered surface of the beam extracting plasma electrode had an important role to enhance the H^- beam intensity.

I. INTRODUCTION

At KEK, the pulse operated volume H^- ion source has been developed since 1988.[1] It is aiming for a pulsed H^- beam of more than 20mA with a 90% normalized emittance of less than 1 π mm.mrad. One of the difficulties in operation of the volume H^- ion source is its poor efficiency. A relatively large arc current is required to obtain an intense beam current of more than 10mA. Moreover, the total electron drain current from the ion source reaches 100 times of that of the extracted H^-beam.

Kao Leung et al have recently found that the extracted H^- beam current could be increased by injecting cesium vapor into the ion source plasma chamber.[2] We have also observed this cesium effect in our volume H^- ion source. The extracted H^- ion beam current was increased more than four times of that before injecting cesium vapor and the extracted H^- ion current reached a maximum of 20 mA. The cesium consumption rate was surprisingly small compared with the surface H^- ion source and this may hence reduce the difficulties described above in operation of the ion source with cesium vapor. We have made several experiments to examine the cesium effect on the volume H^- ion source and found that the surface condition of the beam extracting plasma electrode has a very important role in increasing the H^- beam intensity in the cesium-mode operation.

II. CHARACTERISTICS AND PERFORMANCE

A schematic diagram of the present test apparatus of the KEK volume H^- ion source is shown in Fig. 1. The ion source consists of a cylindrical plasma chamber which is surrounded by SmCo permanent magnets and a single hot filament cathode. The length and the diameter of the plasma

For our ferrite $\eta \sim 0.027$ [1/gauss], B_{rf} the average flux density in the ferrite, and $Q_0 \simeq 50$ is the value at $B_{rf} \sim 0$. The shunt impedance of the cavity at 15 kV is estimated to be 520 Ω.

If we remove the 200pF capacitance at the gap, the shunt impedance of the cavity at 15 kV will increase to ~800 Ω, which is nearly one half of what is expected. The peak power in the ferrite amounts to 140kW at 15kV.The average power and the power density in the ferrite are ~ 70 kV and 0.56 W/cm^3 respectively. The maximum permissible power density is determined by the tensile strength of the ferrite and its thickness. If we assume that the temperature at the surface of the ferrite is 30°C,the maximum temperature in the ferrite is ~50°C. The maximum tensile stress in the ferrite is ~ 1.7 kg/mm^2. The maximum tensile strength of the ferrite is ~2kg/mm^2. Therefore, the accelerating voltage of 15kV is a limit for this cavity.

The leakage inductance of anode windings on the ferrite and the gap capacitance resonated at 10 MHz. To remove this resonance from the accelerating frequency range, two 0.01μF capacitors which connect the anodes of the final tubes and the accelerating gap are installed at the accelerating gap.

BEAM CURRENT PICKUP

The gap which picks up the loading beam current is loaded with amorphous core having a large permeability. Because of the large imaginary part of the permeability, it behaves as a 100 Ω resistor for frequencies above ~ 500 kHz. The input impedance of the cathodes of the final tubes is 10 Ω. Therefore, nearly 90 % of the wall current at the pickup gap flow into the tubes.

The cathode circuit diagram including the beam current pickup is shown in Fig.8.In the diagram the drive rf current source and the wall current are connected in parallel. Our test operation was at 4kV which corresponds to a drive rf current of 3 A . This means that the final tubes will also be drive n by the wall current.

THE OTHER ELECTRONICS

We have designed power supplies for the vacuum tube grids[1]. To reduce the power dissipation at the anode,the power supplies for final tube control grids have to switch their output voltage from -400V to -200V within several 10μsec. They have a response of 50μsec. The other power supplies are working without any trouble.

All-pass networks employed in control grid circuits reduce the drive power.

ICANS-XI International Collaboration on Advanced Neutron Sources
KEK, Tsukuba, October 22-26, 1990

Intense negative ion source

Yoshiharu Mori
National Laboratory for High Energy Physics(KEK)
Oho 1-1, Tsukuba-shi,Ibaraki-ken 305, JAPAN

ABSTRACT
The volume H^- ion source has been developed at KEK. The H^- beam intensity was enhanced by introducing a very small amount of cesium vapor in the ion source. The extracted H^- beam current of 20mA was obtained in the cesium-mode operation. The measured 90% normalized beam emittance was about 1πmm.mrad for 12 mA beam. It was found that the workfunction of the cesium covered surface of the beam extracting plasma electrode had an important role to enhance the H^- beam intensity.

I. INTRODUCTION

At KEK, the pulse operated volume H^- ion source has been developed since 1988.[1] It is aiming for a pulsed H^- beam of more than 20mA with a 90% normalized emittance of less than 1 π mm.mrad. One of the difficulties in operation of the volume H^- ion source is its poor efficiency. A relatively large arc current is required to obtain an intense beam current of more than 10mA. Moreover, the total electron drain current from the ion source reaches 100 times of that of the extracted H^-beam.

Kao Leung et al have recently found that the extracted H^- beam current could be increased by injecting cesium vapor into the ion source plasma chamber.[2] We have also observed this cesium effect in our volume H^- ion source. The extracted H^- ion beam current was increased more than four times of that before injecting cesium vapor and the extracted H^- ion current reached a maximum of 20 mA. The cesium consumption rate was surprisingly small compared with the surface H^- ion source and this may hence reduce the difficulties described above in operation of the ion source with cesium vapor. We have made several experiments to examine the cesium effect on the volume H^- ion source and found that the surface condition of the beam extracting plasma electrode has a very important role in increasing the H^- beam intensity in the cesium-mode operation.

II. CHARACTERISTICS AND PERFORMANCE

A schematic diagram of the present test apparatus of the KEK volume H^- ion source is shown in Fig. 1. The ion source consists of a cylindrical plasma chamber which is surrounded by SmCo permanent magnets and a single hot filament cathode. The length and the diameter of the plasma

chamber are about 160mm and 100mm, respectively. A pair of SmCo permanent magnets, which make a dipole magnetic field, a so called virtual magnetic filter, are placed at the the outside of the plasma chamber and close to the plasma electrode. The magnetic field becomes maximum at the anode hole. Through the experiment, a single hole of 7.5mm in diameter was used as the anode aperture.

A helical coil shaped LaB_6 filament is used as a hot cathode and it is attached on the molybdenum supporting rods which are cooled by water. The operating temperature of the filament is about 1400°C and the lifetime is more than several hundred hours.

Table 1. Typical operating parameters of the KEK volume H^- ion source in cesium-mode operation.

ARC CURRENT	100-200A
ARC VOLTAGE	120-150V
FILAMENT CURRENT	70-80A
HYDROGEN FLOW RATE	15-20sccm
BEAM EXTRACTION VOLTAGE	30-40 kV

Cesium vapor is injected into the plasma chamber from the outside reservoir through a heated feedthrough. The high temperature valve, which can be closed to stop the cesium feeding immediately after the H^- ion beam current is increased, is located between the ion source and the reservoir. The reservoir temperature is normally 200-250°C.

Typical beam extraction energy is about 30-40 keV. In order to reduce the enormous amount of electrons extracted from the ion source simultaneously with H^- ions, a pair of small permanent magnets making a dipole field

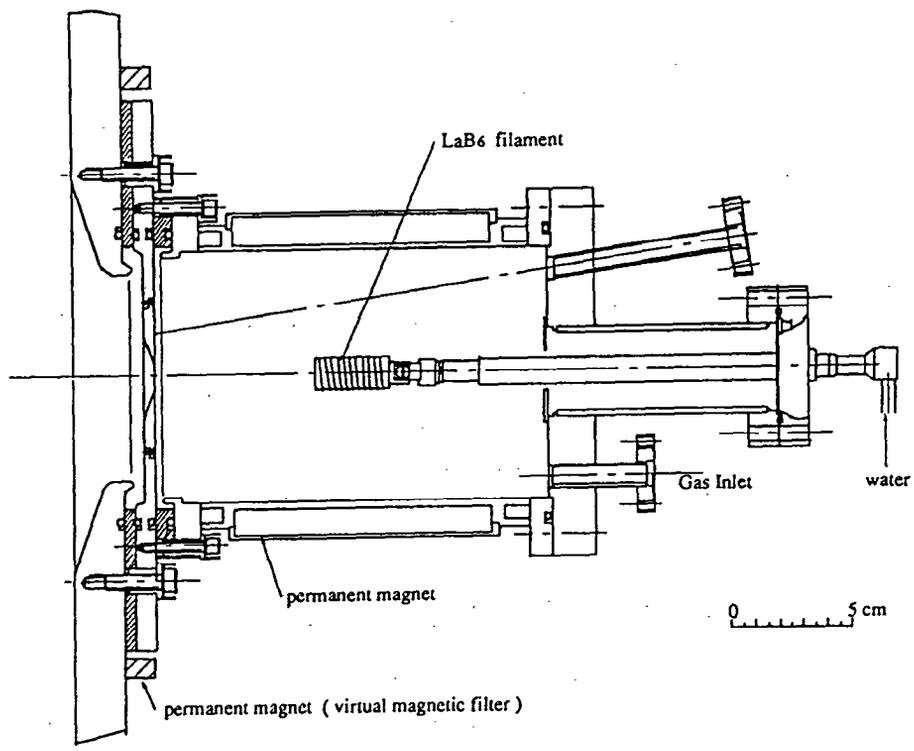

Fig.1 Schematic diagram of the KEK volume H^- ion source.

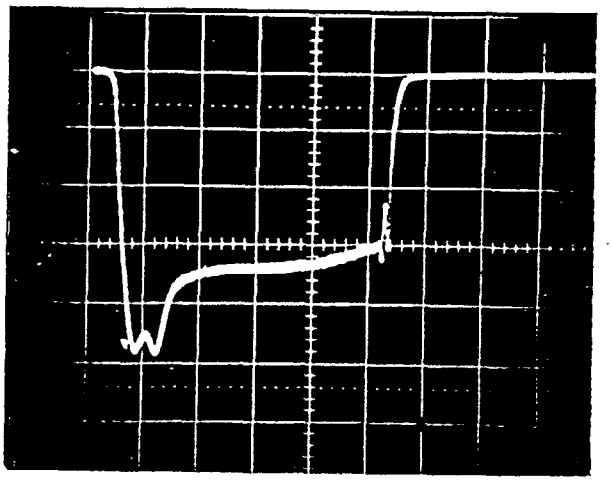

Fig.2-a H^- beam waveform before injecting cesium vapor. Vertical axis: 1 mA/div. Horizontal axis: 0.1 msec/div.

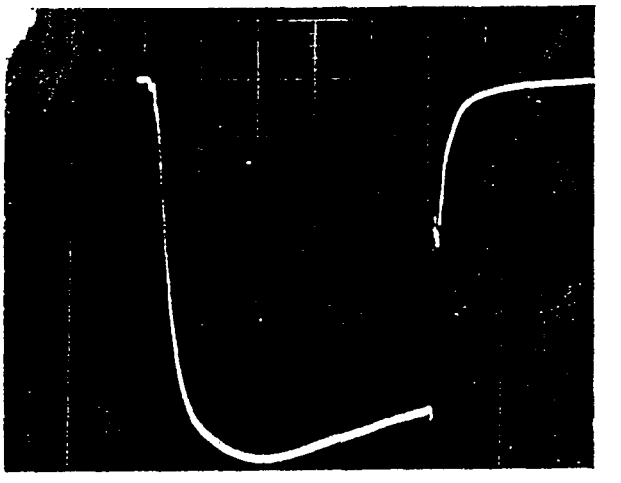

Fig.2-b H^- beam waveform after injecting cesium vapor. Vertical axis: 2 mA/div. Horizontal axis: 0.1 msec/div.

at the beam extraction point are placed. The maximum field strength of this dipole magnet is about 300 gauss. The beam can be focused by an einzel lens placed about 20 cm away from the extraction electrode and the another pair of small permanent magnets are also put at the front of the einzel lens to sweep out the electrons completely. In table 1, typical operating parameters of the cesium-mode volume H^- ion source are summarized.

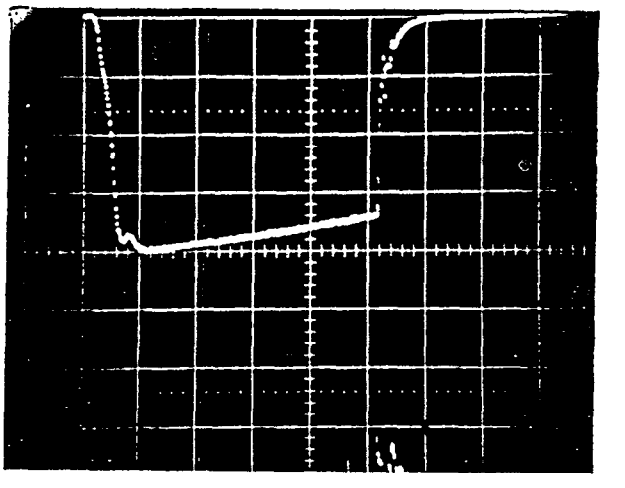

Fig.3 Optimized H^- ion beam current. Vertical axis: 5 mA/div. Horizontal

The extracted H^- beam intensity is dramatically changed by injecting cesium vapor into the plasma chamber. Figures 2-a and 2-b show the typical H^- beam waveforms before and after the cesium vapor is injected, respectively. In these figures, the total drain currents(H^- + electron) from the ion source are also shown. The H^- beam current is increased from 3mA to 12mA and on the other hand, the total drain current is decreased from 350mA to 100 mA. By optimizing the various parameters of the ion source after the cesium vapor is injected, the H^- ion beam current was increased to 20mA as shown in Fig. 3.

The cesium consumption rate was very small in operating the ion source. For example, once the beam intensity was increased after opening the valve for the cesium feed line, it kept almost constant for several ten of hours even when the valve was closed.

The beam emittance was also measured before and after the cesium injection. The magnitudes of beam emittance were little different before and

after the cesium injection when the beam intensities were not so large. However, the beam emittance substantially increased to 1 πmm.mrad when the beam intensity was increased to 12 mA. This may be explained by emittance growth due to a space charge force in a pulsed beam whose pulse width is too short for a complete space charge neutralization by positive ions generated in ionization of the residual gas.

We have measured workfunction changes of the plasma electrode before and after the cesium injection. The workfunction change was measured by detecting the photo-emission electron current which is generated by a single mode Ar ion laser beam(λ= 514.5nm). We found that the workfunction kept decreasing for long time during the operation of the ion source even after the valve of the cesium feedline was closed. This may relate to the fact that the cesium consumption rate is very small.

In order to examine which surface, the plasma electrode surface or other wall surface, is most effective in generating H^- ions when the cesium vapor is injected, we cleaned the plasma electrode surface only by Ar ion sputtering. Before the Ar ion sputter cleaning, the H^- ion current was 12 mA, however, it decreased to about 3mA just as before the cesium injection and the photo-emission electron current was also disappeared after one hour cleaning. Thus the plasma electrode surface seems to affect very much on the enhancement of the H^- ion production in the cesium-mode operation.

III. Summary

It was found that the characteristics of the ion source changed dramatically by injecting the cesium vapor into the ion source. More than four times more H^- ion beam current was extracted after the cesium injection and, nevertheless, the cesium consumption rate was very small. By the workfunction measurement with a photo-emission electron technique, it was also observed that the surface condition of the plasma electrode played an important role in the cesium-mode operation.

(REFERENCES)
(1)Y.Mori,A.Takagi,K.Ikegami,S.Fukumoto; 4th Int. Symp. on Production of Neutralization of Negative Ions and Beams,BNL ,1986, AIP conf. series,page378.
(2)K.N.Leung et al;Rev.Sci.Instr.,60(1989)531.

Q(I.Yamane): What is the energy of the H^- beam in the last figure? If the energy of the H^- beam is increased, does the emittance growth decrease?

A(Y.Mori): The beam energy is assumed to be 30KeV. The emittance growth can be reduced by increasing the beam energy.

Q(A.Noda): Have you ever studied about the effect of Cesium introduced into Volume production ion source to the break down voltage in the following accelerator? Does such voltage not go down?

A(Y.Mori): Very small amount of Cesium consumption is enough for increasing the H^- beam intensity, therefore, it might not necessary to worry about the break-down in a post-accelerator.

Q(I.S.K.Gardner): What is the current density at the output of the H^- source before and after the cesium addition.

A(Y.Mori): The H^- beam current density was ~10μA/cm^2 before Cs injection and ~60μA/cm^2 after Cs injection.

ICANS-XI International Collaboration on Advanced Neutron Sources
KEK, Tsukuba, October 22-26, 1990

PRESENT STATUS OF THE TEST RF SYSTEM FOR THE KEK PS BOOSTER

S.Ninomiya, S.Takano, Y.Yoshii, M.Toda, and T. Katori*

KEK, National Laboratory for High Energy Physics,
Oho 1-1, Tsukuba, 305 Japan

*Denki-kogyo Co. Ltd, 4052-1 Sakuradai, Nakatsu,
Aikawa-cho, Aikoo-gun, Kanagawa, 243-03 Japan

ABSTRACT

Since 1988 we have been constructing a new accelerating system for the KEK PS Booster. The system cancels the beam loading effect[1]. The system test operation result is reported. Our analysis on the beam loading effect is also described.

MECHANISM OF THE LOADING INSTABILITY OF RF SYSTEM

We have studied the of the beam loading instability mechanism of the rf system by the method described in Ref.2). The block diagram of the rf system, which is used for our analysis[3], is shown in Fig. 1. Where the radial beam feedback loop and the cavity phase lock loop are added to the diagram in Ref. 2).

The instability threshold of a rf system having a low Q cavity is shown in Fig. 2, where the horizontal scale is the transient loading angle ϕ_L, the vertical axis is the relative loading $Y = I_B/I_0$, I_B and I_0 are the beam current and drive rf current respectively. The gains of the feedback loops in the system are written in the diagram. We used the word transient loading angle, because a tuning loop in the rf system keeps the angle around $\phi_L \sim 0$. The threshold of the instability is $Y = 2 \sim 3$.

We calculated the values of the cavity transfer functions under a loaded condition.The variation of the cavity transfer function for phase modulation is shown in Fig.3.The values are evaluated at a low phase modulation frequency. For higher beam loading, the cavity transfer function reduces the value. Above a threshold, the value becomes negative. The beam loading instability mechanism is explained by this effect. That is, the loading effect changes a negative feedback loop in the rf system to a positive feedback.

The instability limit in Fig.2 is calculated by the Routh-Hurwitz criterion. Therefore, one must operate the rf system lower than the predicted value.

On the basis of the knowledge of the loading instability mechanism, we ignored the effect of the cross coupling of the loops[2], and calculated the critical damping limit of the beam phase loop. The characteristic equation of the phase loop is given by

$$(s^2 + s\cdot\Omega_p G_{pp}^{g} + \omega_s'^2)u_b = 0, \tag{1}$$

where s is the phase modulation frequency, u_b the beam phase, Ω_p the loop gain of the phase loop, $\omega_s' = \omega_s\sqrt{1 + G_{pp}^{g}C_R R}$ the synchrotron frequency shifted by the radial beam feedback, and G_{pp}^{g} the cavity transfer function of phase modulation. If we neglect higher order terms in s, it is written as

$$G_{pp}^{g} = 1 + Y\cdot\cos^2\phi_z(\sin\phi_B - \cos\phi_B\cdot\tan\phi_z), \tag{2}$$

where ϕ_z is the impedance phase angle of the cavity, and ϕ_B the synchronous phase. They are defined in Ref. 2) and 3).

The damping factor of the system of Eq.(1) has to be greater than $1/\sqrt{2}$ for damping. That is, $(\Omega_p G_{pp}^{g})/(2\omega_s') > 1/\sqrt{2}$. Therefore, we get

$$x\{ 1 + Y\cdot\cos^2\phi_z\cdot(\sin\phi_B - \cos\phi_B\cdot\tan\phi_z)\} > \sqrt{2}, \tag{3}$$

where x is the relative loop gain of the phase loop defined by

$$x = \frac{\Omega_p}{\omega_s'} \simeq \frac{\Omega_p}{\omega_s\sqrt{1 + C_R R}}. \tag{4}$$

The denominator is the synchrotron frequency shifted by the radial feedback[3]. For a normal rf system, where $\phi_L = 0$, we get for the stability,

$$Y < \frac{1}{\cos\phi_B}\left(\frac{x\tan\phi_B}{2\sqrt{2}} + \frac{x^2\tan^2\phi_B}{8} + \frac{x}{2} - 1 \right). \tag{5}$$

In the case of no acceleration $\phi_B = 0$, we get from Eq.(5),

$$Y < \frac{x}{2} - 1. \tag{6}$$

For a system which employs a feedforward compensation[3,4], where impedance phase angle of the cavity ϕ_z is adjusted to zero. Hence from Eq.(3),

$$Y > \frac{\sqrt{2}/x - 1}{\sin\phi_B} \tag{7}$$

The system is critically damped, if $x > \sqrt{2}$. The feedforward compensation is a powerful method. Note,however,that the anode dissipation of the final tube in the power amplifier increases by several factors.

The critical damping limit of the system given by Eq.(3) and is shown in Fig. 4. The critical damping limit is far less than the threshold given by the Routh-Hurwitz criterion (Fig.2).

THE TEST RF SYSTEM FOR THE KEK PS BOOSTER

Our test rf system picks up the wall current upstream of the accelerating cavity and is fed in to the accelerating cavity via the cathodes of the final vacuum tubes installed near the cavity. The current has the opposite polarity to the loading current, therefore, the loading effect at the cavity is cancelled.

The power dissipation at the anodes of the final tubes is the same value as that of feedforward compensation. The current accelerated by the system is determined by the specification of the the final tubes. In our case the final tubes are two 4CW50,000E(Eimac) connected in parallel. The parallel connection is employed, because of its higher maximum current and transconductance. A circulating beam current of 3A will be accelerated by this system.

TEST OPERATION OF CAVITY AND POWER AMPLIFIER

The test operation of the cavity voltage is limited to 4 kV, because of the discharge at the ferrite support mechanism made of FRP.The rf voltage at the accelerating gap and the phase error of the tuning system are shown in Fig. 5. The setup of the system is shown in Fig.6. The bandwidth of the aut omatic tuning system is ~ 1kHz.

24 ferrite disks with outer diameter of 620 mm are installed in the accelerating cavity, with a permeability of 250. The estimated shunt impedance of the cavity is 1.5 kΩ at an accelerating voltage of 15 kV.

The measured impedance is only 1.2 kΩ at 4kV. The impedance is calculated from the measured cathode current. The quality factor of the ferrite is far less than the expected value. The equivalent circuit of the cavity is shown in Fig.5. The Q-value of a ferrite changes with magnetic flux density in the ferrite.

$$Q = \frac{Q_o}{1 + \eta \cdot B_{rf}} .$$

For our ferrite $\eta \sim 0.027$ [1/gauss], B_{rf} the average flux density in the ferrite, and $Q_0 \simeq 50$ is the value at $B_{rf} \sim 0$. The shunt impedance of the cavity at 15 kV is estimated to be 520 Ω.

If we remove the 200pF capacitance at the gap, the shunt impedance of the cavity at 15 kV will increase to ~800 Ω, which is nearly one half of what is expected. The peak power in the ferrite amounts to 140kW at 15kV.The average power and the power density in the ferrite are ~ 70 kV and 0.56 W/cm^3 respectively. The maximum permissible power density is determined by the tensile strength of the ferrite and its thickness. If we assume that the temperature at the surface of the ferrite is 30°C,the maximum temperature in the ferrite is ~50°C. The maximum tensile stress in the ferrite is ~ 1.7 kg/mm^2. The maximum tensile strength of the ferrite is ~2kg/mm^2. Therefore, the accelerating voltage of 15kV is a limit for this cavity.

The leakage inductance of anode windings on the ferrite and the gap capacitance resonated at 10 MHz. To remove this resonance from the accelerating frequency range, two 0.01μF capacitors which connect the anodes of the final tubes and the accelerating gap are installed at the accelerating gap.

BEAM CURRENT PICKUP

The gap which picks up the loading beam current is loaded with amorphous core having a large permeability. Because of the large imaginary part of the permeability, it behaves as a 100 Ω resistor for frequencies above ~ 500 kHz. The input impedance of the cathodes of the final tubes is 10 Ω. Therefore, nearly 90 % of the wall current at the pickup gap flow into the tubes.

The cathode circuit diagram including the beam current pickup is shown in Fig.8.In the diagram the drive rf current source and the wall current are connected in parallel. Our test operation was at 4kV which corresponds to a drive rf current of 3 A . This means that the final tubes will also be drive n by the wall current.

THE OTHER ELECTRONICS

We have designed power supplies for the vacuum tube grids[1]. To reduce the power dissipation at the anode,the power supplies for final tube control grids have to switch their output voltage from -400V to -200V within several 10μsec. They have a response of 50μsec. The other power supplies are working without any trouble.

All-pass networks employed in control grid circuits reduce the drive power.

In order to get the desired frequency response, the careful adjustment of the inductances in the networks was necessary.

CONCLUSION

The improvement of the ferrite stacks will be finished within 1990. In order to increase the shunt impedance, the capacitance at the accelerating gap has to be removed. Further experiments are necessary to increase the accelerating voltage.

ACKNOWLEDGEMENTS

The authors would like to express their thanks to Profs. M. Kihara, S. Hiramatsu, and I. Yamane for their encouragement.

REFERENCES

1) S. Ninomiya et al, Particle Accelerators, Vol.32, 1990, p.1511

2) F. Pedersen, IEEE Trans. Nucl. Sci. NS-22, 1975, p.1906

3) S. Ninomiya, Beam Loading Effect on RF System in PS(in Japanese), KEK Report 89-18

4) I.S.K.Gardner, Lecture held at KEK, 1989

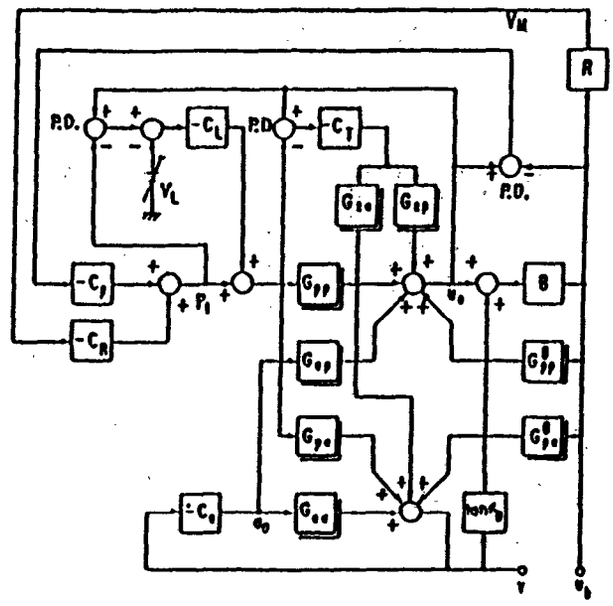

P.D.; Phase Detector

R ; ΔR monitor and circuit. $R=-\frac{N_f x_p s}{\eta \omega_{rf}}$, $V_M=Ru_b$

$C_e = \Omega_e/s$, $C_L=\Omega_L/s$, $C_p=\Omega_p/s$, $C_R=\Omega_R/s$, and $G=\Omega_T/s$

Fig. 1. The Block Diagram of The RF System Used for The Analysis.

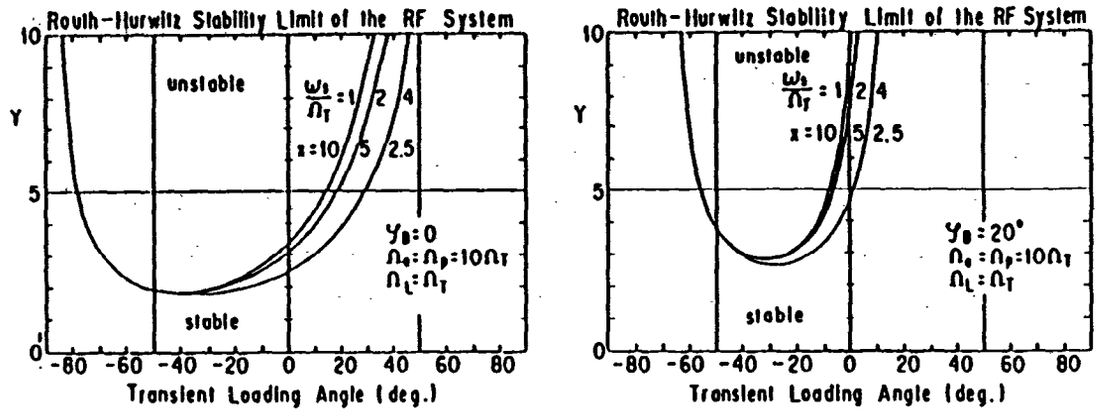

Fig. 2. The Stability Limit of The System Having a Low Q RF Cavity.

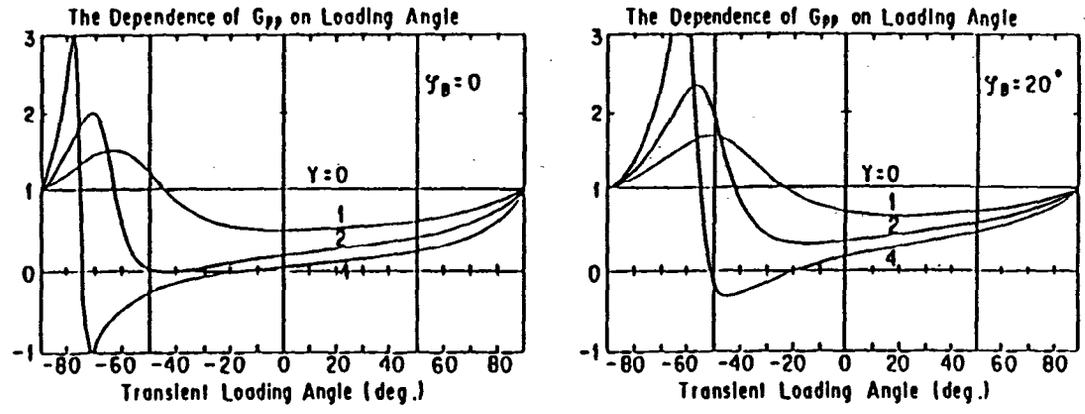

Fig. 3. The Variation of The Cavity Transfer Function for Phase Modulation.

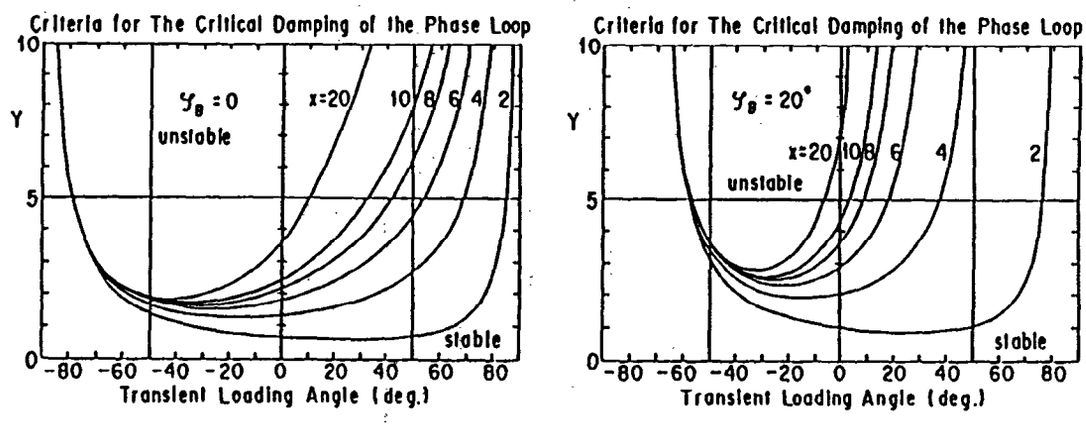

Fig. 4. The Critical Damping Limit of The Phase Loop.

Fig. 5. Upper; Phase Detector Output in Tuning Loop. (20deg/div).
Next; The Gap Voltage (4kV Amplitude).
Lower; The Bias Current. (500A/div).
Horizontal; 3 msec/div.

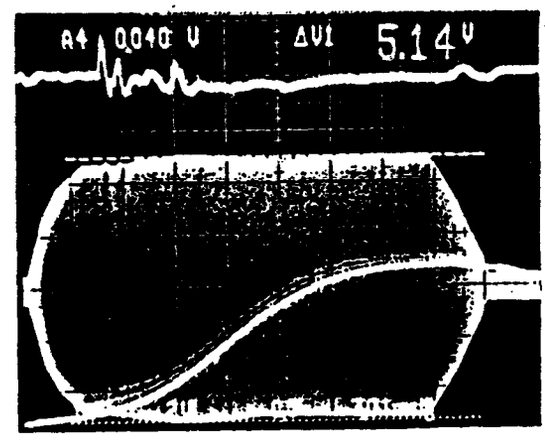

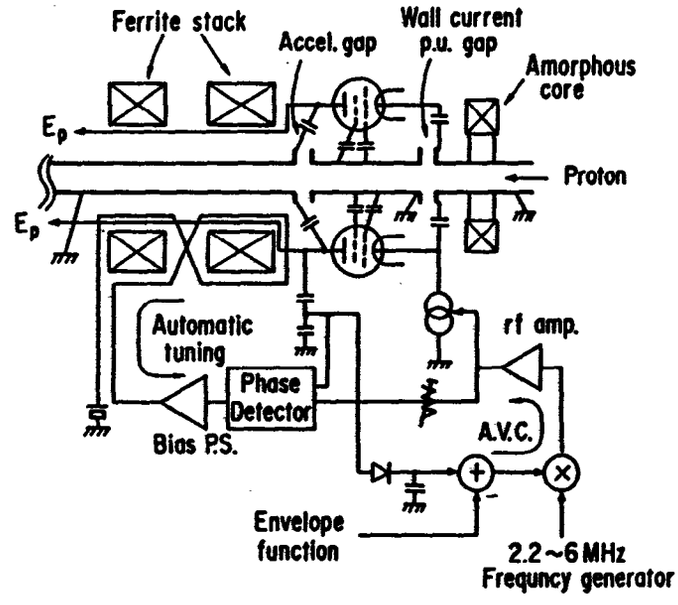

Fig. 6 Block Diagram of The Test System.

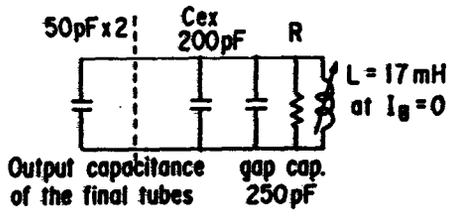

Fig. 7 Equivalent Circuit of Acceleration Gap

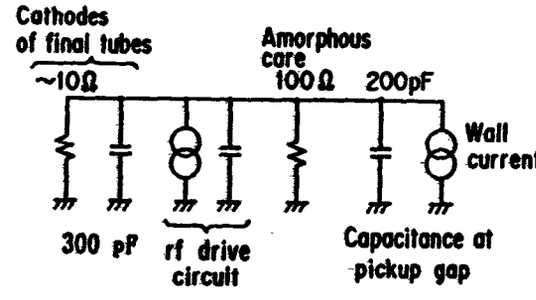

Fig. 8 Equivalent Circuit of Wall Current Pickup.

Q(Y.Mori): What happen in the ferrite situation if you can not assume a homogenity of the ferrite quality?
A(S.Ninomiya): I think that our ferrite is homogeneous.

SUMMARY of the Session on "Topics of High Intensity Accelerator Technology"

G H Rees (RAL) and M Kihara (KEK)

'TOPICS of High Intensity Accelerator Technology' were discussed at one of the parallel sessions on the afternoon of Thursday, 25 October. During the four hour session, there were eight formal talks followed by questions, and one short informal discussion on stripping foils and injection 'painting' techniques. Reports relating to the eight talks are included in the conference proceedings and the afternoon programme was as shown, but with the informal discussion included between the items A-12 and A-13:

A-8 T Suzuki; Review talk on beam instability at low energy.

A-9 R J Macek; Improvements to intensity at the Los Alamos Proton Storage Ring.

A-10 G I Batskikh°, B P Murin, A P Durkin, O J Shlygin and I V Shumakov; High power 'Regotron-type' microwave generator for intensive technological accelerator.

A-11 I Yamane; Treatment of H° and H^{-} beams spilled at the stripper foil in the full energy charge exchange injection scheme.

A-12 I Yamane; Perfect matching for the two-step H° injection into a ring with a DBFO lattice.

A-13 T Kawakubo°, S Tazawa, Y Arakida and S Murasugi; Systems for generating double pulse magnetic fields in a kicker magnet.

A-14 Y Mori; Intense negative ion source.

A-15 S Ninomiya°; S Tazawa, Y Yoshii, M Toda and T Katori; Present status of the test RF system for the KEK PS Booster.

° = speaker

These topics cover a wide range and will be discussed separately instead of in a general context. Only brief comments are given, as the details are available in the separate reports.

I. T SUZUKI; REVIEW TALK ON BEAM INSTABILITY AT LOW ENERGY

The review talk covered the relevant beam instabilities for low energy circular accelerators. Two areas were identified as being still not fully understood and these areas are the longitudual microwave instability and the basic transverse space charge limit for a ring. For the former, the intability threshold and growth rate is usually estimated from assumed values for the total ring impedance. (It is the opinion of one of the session chairmen (GHR) that an estimate for the total ring impedance is insufficient and that estimates for the individual ring impedances are required.) For the latter, the basic transverse space charge limit is found to vary widely for different rings, with typical values for the maximum tune depression in the range 0.25 to 0.6. More elaborate space charge codes are required to study the effect in more detail.

II. R J MACEK; IMPROVEMENTS TO INTENSITY AT THE LOS ALAMOS PROTON STORAGE RING

A factor of 4.6 improvement in percentage beam loss has been achieved over the last two years, following careful experimentation and development. Miscellaneous improvements have contributed a factor of 1.4, the use of 'off-set' H° injection a factor of 1.7, the use of a 'postage stamp' stripping foil a factor of 1.5 and a change in the betatron tune a factor of 1.3. The present stripping foil has a thickness of 200 $\mu gm/cm^2$ and this gives a 9% loss of unstripped beam, which presents no problem, as it is directed to a shielded external beam dump. Average extracted proton beam currents have now reached 70 μA and, at this level, the internal loss is approximately 0.5 μA. This is considered to be an upper limit for hands-on maintenance of components, and so further improvements are needed before proceeding to higher intensity. A number of suggestions have been made for possible improvements but scheduling and funding dictate the plans and rate of progress. All wished the PSR group future success.

III. G.I. BATSKIKH ET AL; HIGH POWER "REGOTRON-TYPE" MICROWAVE GENERATOR FOR INTENSIVE TECHNOLOGICAL ACCELERATOR

A new very high power microwave generator is under development for power source evaluation in relation to a 300 mA linac, needed as a "burner reactor" for the transmutation of long lived radionuclides. Under development at the Radiotechnical Institute, Moscow, is a pulsed model at 3000 MHz to provide 3.5 MW. Performance figures have also been calculated for CW power sources at frequencies of 350, 600 and 900 MHz. Planned for the linac are the use of the 600 MHz units at a 6 MW power level and a 70-80% efficiency. Initial klystron (or magnetic) bunching is utilised and there are a number of pairs of active and passive cavities for power 'take-off'.

IV & V. I YAMANE; STUDIES OF H° AND H^- INJECTION FOR JHF

The relative advantages of H° and H^- injection have been considered for the JHF project and an optimised H° system has been evaluated in detail. There are many fewer hardware components for the H° system and the straight section requirement is thus much reduced. This led to its choice for use with the original FODO storage ring lattice. However, a new racetrack lattice has now been evaluated which allows the inclusion of both an H° and an H^- injection system. This appears a wise precaution for there is some emittance growth with the H° scheme and there also appears to be more flexibility for painting with the H^- beam. A detailed comparison of 'painting' procedures for the two schemes is next required.

VI. INFORMAL DISCUSSION ON STRIPPING FOILS AND PAINTING

Descriptions were given of the stripping foils used or proposed at PSR, INR (Moscow) and RAL. The "postage-stamp" type foil used at the PSR consists of two 100 μgm/cm^2 foils supported on a backing of 4-5 μcarbon fibre wires; the technology is a spin-off from SDI research. Foil shrinkage ultimately leads to breakage. Research at INR is directed towards the development of a different type of graphite foil, formed by glow-discharge cracking. RAL has undertaken some development for a TRIUMF foil requirement. An Al_2O_3 foil of 100 μgm/cm^2 is first made which is supported on three edges. Then the foil is separated from part of the rear support and folded to make a foil with two unsupported edges. Removing stress from the foil is very important and initial studies appear promising. Finally there was a brief discussion on the possibilities for correlating the beam distributions in the different phase planes by the choice of the 'painting' procedures.

VII. T KAWAKUBO ET AL; SYSTEMS FOR GENERATING DOUBLE PULSE MAGNETIC FIELDS IN A KICKER MAGNET

The JHF has a requirement for its storage ring kicker magnet to extract separately the two circulating proton bunches. The interval between these two extractions is approximately 100 μs. The method adopted has been the feeding of the kicker from two separate thyratrons; cathode and anode loaded systems have been compared. The cathode system was found to give mis-firing but the anode loaded system has worked successfully at half the voltage levels required for the JHF. Next, a full voltage system is to be tested.

VIII. Y MORI; INTENSE NEGATIVE ION SOURCE

The JHF I GeV linac requires a low emittance, low caesium level ion source beam to feed its injector RFQ linac. The low caesium level is to prevent contamination of the surfaces of the RFQ. A volume production source has been under study using a permanent magnet cusp field and a long lifetime La B_6 filament operating at 1400°C only. The source has been found to give a few mA output H^- beam when no caesium is used and an increased beam by a factor of 4 or 5 for a low level of caesium. The physics of the source has been under study and laser diagnostics have been used for surface work function evaluation. Studies will continue in order to establish whether the H^- enhancement is a surface or a plasma effect. The source is found to have a low emittance at its exit, but next to be evaluated is how to preserve this low emittance in the subsequent beam transport.

IX. S NINOMIYA ET AL; PRESENT STATUS OF THE TEST RF SYSTEM FOR THE KEK PS BOOSTER

Detailed studies had been undertaken of the RF control loops, including the coupling effects due to the beam loading. It had been concluded that feed-forward beam compensation was required, and a direct beam feed-forward system had been developed. The system had been found to reduce the effect of a cavity parasitic resonant mode. Also studied had been the effect of a reduction in the cavity Q at the top operating frequency and estimates had been made of the resulting temperature gradients in the cavity ferrite.

ICANS-XI International Collaboration on Advanced Neutron Sources
KEK, Tsukuba, October 22-26, 1990

EXPERIMENTAL RF PROTON ACCELERATOR WITH SUPERCONDUCTING SOLENOID BEAM FOCUSING

B.I.Bondarev, N.A.Griasnov, V.E.Keilin, A.N.Kourmanov, B.F.Lapta, A.N.Likharev, E.A.Mirochnik, A.V.Mischenko, B.P.Murin, V.M.Pirozhenko, O.V.Plink, V.N.Saverin, I.B.Seleznev, M.I.Surin

Moscow Radiotechnical Institute USSR Academy of Sciences, 113519 Moscow, USSR

ABSTRACT

Theoretical and applied aspects of a beam current increase in ion linacs by using superconducting solenoid focusing are considered.Results of the SIU-1 experimental RF proton accelerator development and testing are presented.The main accelerator parameter are : the 1.5 MeV energy, the 1.75 MeV/m accelerating rate, the 200 MHz operating frequency.

I. INTRODUCTION

The main restriction of a beam current in low-energy RF ion accelerators is the Coulomb particle repulsion. Simultaneous achievement of accelerating and focusing fields high values is necessary to compensate for high-current beam Coulomb fields. This can be realized in the accelerating- focusing system with a resonator placed inside the focusing solenoid [1]. According to estimations, the beam current limit by transverse Coulomb repulsion may be increased up to several amperes and higher by using the superconducting focusing solenoid with induction of 7...8 T [1].

Development of an accelerating structure with minimum transverse dimensions is necessary to achieve a high value of a beam current. The RF accelerating channel has to provide high values of the beam current limit by longitudinal Coulomb repulsion and the capture efficiency.It is necessary to realize the required accelerating field distribution along the accelerator axis under high resonator beam loading conditions.

Use of the the strong magnetic fields for beam focusing requires solution a number of specific problems. First, one needs to solve the beam injection problem into the strong magnetic field. The resonator electrical insulation and the ion injector operation are affected by the above mentioned magnetic field.

The main results of these investigations with application to the SIU-1 linac design are briefly described below.

II. BEAM DYNAMICS ASPECTS

In the accelerating structure of this accelerator type one should use the beam adiabatic bunching with carrying out of the bunch quasi-stationary conditions during the bunching. The bunch quasi-stationary conditions allow to conserve the space-charge density distribution in the bunch and to simplify the beam matching with an accelerating-focusing system.

It can be shown that expressions for the amplitude E_m of accelerating wave and the synchronous phase φ_s, providing the bunch quasi-stationary conditions, are the following

$$\cos\varphi_s = [1+\delta^{-1}\exp(-\xi)]^{-1}; \quad E_m/E_{mo} = 1+\delta(\exp\xi-1);$$

where $\delta = (\pi/2-|\varphi_{so}|) \ll 1$, $\xi = qE_{mo}z/2W_{so}$, q is the particle charge, z is the longitudinal coordinate, W_s is the synchronous particle energy. The variables with indexes "o" and "f" correspond to the buncher beginning and the buncher end accordingly.

The buncher length L_b relates to the limiting capture efficiency k_c by the following equation

$$L_b = -\frac{2\,W_{so}}{q\,E_{mo}}\,[\,1-\pi(1-k_c)^2]\,\ln[\pi(1-k_c)^2 tg\varphi_{sf} tg(\varphi_{sf}/2)].$$

The large buncher length is necessary to achieve a high value of the capture efficiency in the adiabatic buncher with the bunch quasi-stationary conditions exact carrying out. For example, the buncher length is equal to 1.15 m for k_c= 95 %, when W_{so}= 100 keV, E_{mo}= 1 MV/m, $|\varphi_{sf}|$= 45°.

It is necessary to refuse from continuous conservation of the bunch quasi-stationary invariants along the buncher axis to shorten the buncher length. An approximate satisfiability of the bunch quasi-stationary conditions is possible for the buncher with linear change of the accelerating wave amplitude and the synchronous phase. In this adiabatic buncher it is possible to use $|\varphi_{so}| = 90°$. The buncher length and the accelerating wave amplitude rising are calculated on basis of the equality conditions of particles small phase oscillations frequencies and the separatrixes geometric length for the buncher input and the buncher output :

$$L_b = \frac{5.6\,W_{so}}{q\,E_{mo}}, \quad \frac{E_{mf}}{E_{mo}} = \frac{\beta_{sf}}{\beta_{so}\sin|\varphi_{sf}|},$$

where β_s is the normalized velocity of a synchronous particle.

In general, the RF accelerating channel contains the adiabatic buncher and the acceleration section, where the accelerating wave amplitude and the synchronous phase remain constant. Supposing that the beam current limit is defined by the adiabatic buncher end and the bunch phase length is equal to $2|\varphi_{sf}|$, we have that the beam current limit by the longitudinal Coulomb repulsion is equal to

$$I'' = 1.5\ (\beta_{sf}\ \varphi_{sf})^2 \frac{R_b}{\lambda}\left[\frac{\Omega_f}{\omega}\right]^2 I_o,$$

where R_b is the beam radius, λ is the operating wavelength, $\omega = 2\pi c/\lambda$, Ω is the cyclic frequency of the longitudinal oscillations, I_o is the characteristic beam current, c is the speed of light.

In the SIU-1 experimental proton accelerator the adiabatic bunching has been used in the accelerating field with linear rising and the bunch quasi-stationary conditions approximate carrying out. The channel characteristics are the following : the low injection energy (100 keV), the high accelerating rate (1.75 MeV/m). The main channel parameters are : E_{mo} = 1 MV/m, E_{mf}=3.7 MV/m, φ_{so}=-90°, φ_{sf}=-45°, R_b= 5 mm. For these parameters we have L_b= 0.56 m, W_{sf}= 0.7 MeV, I'' = 2.5 A when λ =1.5 m. The bunch quasi-stationary conditions disturbance is order 25 % in the SIU-1 buncher.The gap coefficient is constant along the accelerating channel axis and is equal to 2/3, the field nonuniformity parameter along a channel aperture $2\pi a/\beta_{so}\lambda$ = 2.1, that corresponds to the aperture radius a = 7.5 mm.

Numerical simulations of a beam longitudinal dynamics indicate that the beam current limit is equal to 2.75 A, the capture efficiency achieves 96 % for the beam current of 1 A.

To estimate a matching magnetic field the following relation can be used

$$B = \frac{2\ m_o}{q}\sqrt{\frac{\Omega^2}{2} + \frac{2\ c^2\ I}{\beta_s R_b^2\ I_o} + \left(\frac{c\ V_b}{R_b^2}\right)^2}\ ,$$

where m_o is the ion mass,I is the peak beam current, V_b is the beam normalized emittance.

The magnetic field value has also to provide a small value of the beam Coulomb parameter

$$h = Ic/\omega^o_{rs}\beta_s I_o V_b\ ,\ \text{where}\ \omega^o_{rs} = \left[(eB/2m_o)^2 - \Omega^2/2\right]^{1/2}.$$

The estimations and numerical simulations of a beam dynamics

indicate that magnetic fields of 5 ... 7 T are necessary to focus the beam with the current density of about 1 A/cm^2 and the phase density of several A/cm mrad for λ = 1.5 m.

During the beam injection into the magnetic field the particles longitudinal energy decreases in accordance with the relation

$$\Delta W = - \frac{(q B r)^2}{8 m_o} ,$$

where r is the distance to the solenoid axis.

For Brillouin beam the energy reduction is defined by

$$\Delta W/W = - 2I/\beta_s^3 I_o .$$

In addition to the energy reduction, the non-Brillouin beam has also an energy spread.

In practice, to reduce these effects it is necessary to use an 20-30 % injection energy increase in comparison with a calculating value.

III. ACCELERATING STRUCTURE

Combination of small transverse sizes, low sensitivity to strong beam loading, capability of uniting the large number of accelerating gaps and high value of an accelerating field can be reached in the opposed vibrator resonator (OVR) (see Fig.1).

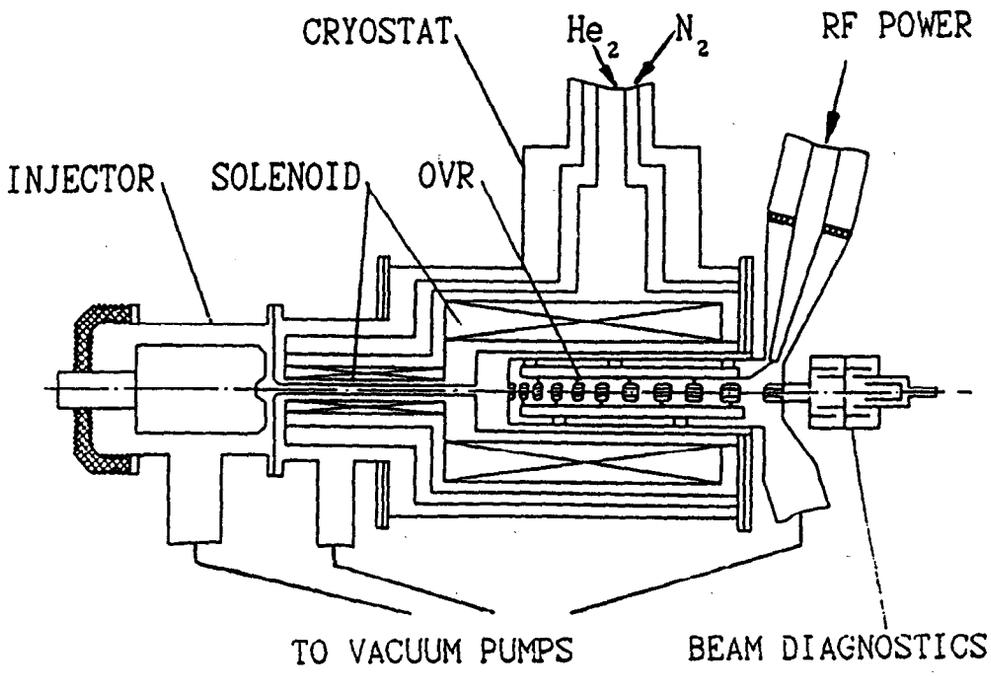

Fig.1.

The OVR can be considered as a system of the coupled lines

loaded by the lumped elements.

One can show that the structure dispersion equation is of the form

$$kl(1 + \sqrt{1 + \varkappa})/2 = \pi/2 + \alpha\cos\varphi - \beta\cos^2\varphi,$$

where k is the wave number in free space, φ is the normal wave phase advance per the l length structure section. Here α and β are the distributed and lumped coupling coefficients, $\varkappa$ is the capacitance loading coefficient.

In the lowest passband the resonance condition of the OVR, consisting of N sections, is $\varphi = \pi m/N$, $m = 0,1,\ldots,N$. Together with the large bandwidth, the small number of modes for the resonator, consisting of the great number of accelerating cells, defines good modes separation in the OVR, and, hence, low sensitivity to strong beam loading. By means of resonator sections detuning, various accelerating wave amplitude distributions are possible in the OVR, in particular, an increasing law, which is needed to realize beam adiabatic bunching and to achieve channel equal electrical insulation of the accelerating channel.

The resonant wavelength of the OVR operating mode is equal to

$$\lambda = \frac{2\,\mathfrak{L}_r}{N}\left(1 + \frac{1}{\mathfrak{L}_r}\int_0^{\mathfrak{L}_r}\sqrt{1 + \varkappa}\,dz\right)\left(1 + \frac{2}{\pi N}\sum_{i=1}^{N}(\alpha_i + \beta_i)\right),$$

where $\mathfrak{L}_r$ is the resonator length.

The OVR resonant frequency is determined by longitudinal sizes and capacitance loading of the resonator, rather than its diameter. The OVR diameter is mainly determined by electrical insulation requirement of the structure.

A high value of the accelerating wave can be achieved in the OVR. At the channel axis the accelerating wave amplitude is related to the maximum electric field at the drift tubes surfaces E_s as follows [2] :

$$E_m = \frac{E_s k_g \cos(\pi k_g/2)}{I_o\left[\pi a/h + \pi(1 - k_g)/2\right]},$$

where h is the accelerating cell length; k_g is the gap coefficient; I_o is the modified Bessel function.

The maximum accelerating gradient can be achieved with $k_g = 0.6\ldots0.7$. The accelerating wave amplitude should increase along the channel axis for $\pi a/h > 0.5$. E_m can achieve the value of about 5...10 MV/m for $E_s = 20\ldots30$ MV/m. Thus, at the SIU-1 accelerating resonator the accelerating wave amplitude of about

8 MV/m has been achieved without an external magnetic field.

The OVR has a high value of the shunt impedance in the low-energy region. The SIU-1 accelerating resonator has a shunt impedance of about 30 MOhm/m.

IV. THE PROVE OF PRINCIPLE EXPERIMENTS

The ion acceleration with superconducting solenoid focusing has been realized at the SIU-1 RF experimental proton accelerator. The accelerator scheme is presented at Fig.1.

The SIU-1 injector contains a proton source placed inside a magnetic shield, an electrostatic preaccelerator of the diode type and a beam transport channel.

The SIU-1 accelerating structure is the compact OVR placed inside the superconducting solenoid. The OVR has a length of 0.85 m and a diameter of 0.18 m.

The NbTi superconducting solenoid produces the axial magnetic field up to 7.5 T with a stored energy of about 1 MJ.

RF power supply of the accelerator is based on the RF generator which is similar that used in the first part of the Moscow Meson Factory.

The SIU-1 accelerator design, construction and investigation were carried out as follows :

1. The autonomous tests of the injector, the accelerating resonator and the focusing solenoid. All the calculating parameters were obtained.
2. The test of the accelerating resonator with focusing solenoid. The test showed the resonator electrical insulation decrease in the presence of a strong magnetic field. The achieved amplitude is 4 MV/m.
3. The injector tests with the focusing solenoid. The tests indicated the magnetic field influence on plasma in the proton source. To decrease this influence the compensating coil has been installed in the discharge chamber section. The beam current at the resonator input has been risen up to 0.6 A.
4. The beam acceleration experiments. Typical forms of voltage on measuring loop in the resonator and beam current from the Faraday-cylinder are presented at the Fig.2a. It is obvious, that the strong RF voltage decrease takes place up to the half of its value. A number of experiments were carried out using the automating amplitude tuning system to compensate this decrease. The beam current and the RF voltage pulses obtained with the operating automatic amplitude tuning system are presented at the Fig.2b. Experimental data are presented in Table I.

Table I

SIU-1 Experimental Accelerator Performances

Maximum particle energy (MeV)	1.5
Injection energy (keV)	100...130
Maximum accelerated beam current (A)	0.4
Beam pulse duration (μs)	30...70
Repetition rate (puls/s)	1

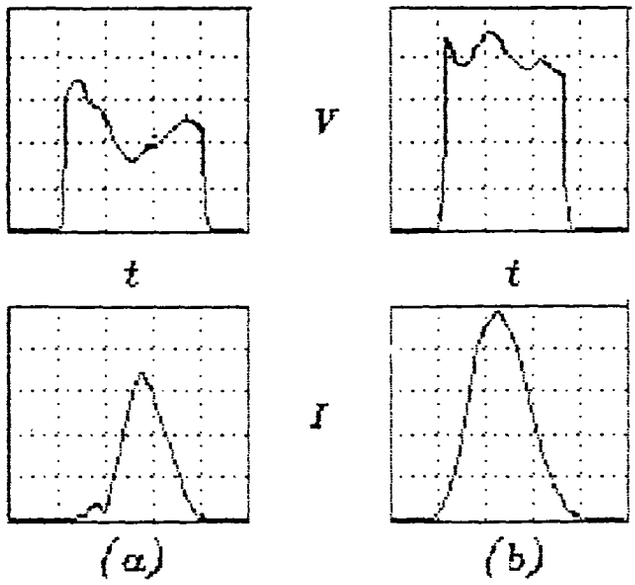

Fig.2.

V. DEVELOPMENT AND APPLICATION

The limiting calculated beam current possibilities of the SIU-1 accelerating-focusing system has not been achieved. The main reason of this is that the magnetic field distribution was not optimal because of the solenoid design. At present, the SIU-1 accelerator is under development to increase the accelerated beam current. In the SIU-2 accelerator with the injection energy rise up to 200 keV and the simultaneous accelerating wave amplitude decrease to about 1.5 MV/m it is planned to get the proton beam with the energy of about 1.5 MeV and current up to 1.5 A.

This beam current value is not a limit to this accelerator type. Physical simulations of a beam dynamic by using an electron probe indicates that a beam with the current up to 5 A can be accelerated at the frequency of about 200 MHz [3]. Further beam current increase can be achieved using the lower operating frequency. The beam dynamic calculations indicate that at the operating frequency of about 20 MHz the beam current can rise up to 15 A [3].

The accelerator with the superconducting solenoid focusing can be used as an initial part of an accelerator for the burner-reactor [4]. Beam with the average current of about 0.3 A can be accelerated in the accelerator with the injection energy of about 100 keV and the accelerating wave amplitude of about 1.5...2 MV/m.

References

1. B.Bondarev et al. " The Focusing Superconducting Solenoid Application for the Current Limit Increase in the Ion Linac ", Proc. of the 6-th All-Union Conf. on the Charged Particles Accelerators, v.1, 260 (1979).
2. O.Plink, Journ. of Techn. Phys., v.59, 196 (1989).
3. B.Bondarev et al. "High-Current RF Ion Accelerators with Longitudinal Magnetic Field Focusing ", Proc. of the 8-th International Conf. on High-Power Particle Beams (1990).
4. G.Batskikh, O.Lupandin, B.Murin, A.Fedotov " On the way to powerful accelerators for the long half-life radionuclides transmutation ", this Conference.

ICANS-XI International Collaboration on Advanced Neutron Sources
KEK, Tsukuba, October 22-26, 1990

Particle Tracking in the BSF Beamline

T.ADACHI

National Laboratory for High Energy Physics
1-1 Oho, Tsukuba-shi, Ibaraki-ken, 305, Japan

Abstract

A particle-tracking program for transverse motion was developed. It is used to calculate the particle trajectory affected by dipole and quadrupole magnetic fields. The calculation also considers multiple Coulomb scattering and energy loss in matter. The program was applied to a transport line for a 500-MeV proton beam. The result was compared with beam profiles and residual radioactivities measured along the beamline.

I. Introduction

It has become a serious problem to prevent the activation of accelerator components due to beam loss according to the increment of the beam intensity. A beam comprises core and a halo. The beam core is completely characterized in the frame of the equation of motion; it can also be defined using a few parameters. On the other hand, the beam halo cannot be defined well since it may be generated from the beam core by some stochastic processes; i.e. multiple Coulomb scattering and energy loss in matter. In a synchrotron, the stripping foil for H^- injection is the main generator of the halo. A profile monitor of secondary emission type is a candidate in a beam transport line. Such a beam halo escapes from the confining region easily and causes beam loss. In addition, the beam core may also escape from an aperture by blowing up through electro-magnetic interaction; i.e. direct space charge and instabilities. Therefore, in order to consider the behavior of a beam, both stochastic and electro-magnetic processes must necessarily be considered.

We are now developing a beam simulation program which calculates a particle trajectory affected by the dipole and quadrupole magnetic fields. The calculation also contains multiple Coulomb scattering and energy loss in matter by using a Monte Carlo method. Though we plan to include the effect of a static electric potential in the transverse plane, it has not been completed yet. This program was applied to the beam transport line which supplies a 500MeV proton beam to the beam dump, neutron, meson and medical facilities (BSF beamline). The result was compared with the beam profiles and residual radioactivities along the beamline. The beam profiles were in good agreement with the simulation. The major hot points of the beamline almost coincided with the simulation, and the

radiation level was also proportional to the calculated beam loss rate.

II. Tracking Program

§1 General

The program comprises two parts. One calculates a transfer matrix for each element as well as the twiss parameters, dispersions and momentum compaction factor if a periodic machine is selected (TRACK13). The other simulates beam trajectories taking into account of the materials and apertures (TRACK14). Those boundaries are defined by polygons using up to 20 points.

A particle is transported successively from the first element to the last element. In the periodic case, a particle is reinjected to the first element. The elements are defined by some parameters: i.e. the element name, as well as the kind of element, length, deflection angle, field gradient and aperture information . In matter, the energy loss and multiple Coulomb scattering are considered in terms of Landau and Moliere theories.[1,2] At the exit of each element, the particle position is sensed whether it stays inside or outside the aperture. When the particle is outside the aperture, it is considered to be dead.

§2 Incident Beam

The incident beam is assumed to have an elliptic boundary with a major axis of A and minor axis of B in the transverse plane, where

$$A=n\sqrt{\varepsilon_x\beta_x} \quad \text{and} \quad B=n\sqrt{\varepsilon_y\beta_y}. \tag{1}$$

Assuming that the beam profile has a Gaussian form, both the emittances, ε_x and ε_y, correspond to 2-σ beam widths. We chose 2 as the value of n, so that 99.994% of the Gaussian beam is included.

In order to assure that motions in the horizontal and vertical phase planes are independent of each other, the single-emittance model must be discarded since independent motion with single emittance in each phase plane gives a Lissajous trajectory with a rectangular envelope in the transverse plane (Fig. 1). Therefore, we adopted the following algorithm in order to obtain the particle state (x,x',y,y'). When a point (x,y) is given inside the ellipse, the allowed amplitudes are first calculated by a Monte Carlo method using the following equations:

$$\begin{aligned}
&Z_j=((-b_j-(b_j^2-4a_j(c_j+S\eta_j/2))^{1/2})/2a_j)^{1/2} \quad (j=1,2),\\
&a_1=B^2/4A^2, \qquad a_2=A^2/4B^2,\\
&b_1=-(B^2-y^2)/2, \quad b_2=-(A^2-x^2)/2,\\
&c_1=-B^2x^4/4A^2+(B^2-y^2)x^2/2,\\
&c_2=-A^2y^4/4B^2+(A^2-x^2)y^2/2
\end{aligned} \tag{2}$$

and

$$S=2a_1x^4+2a_2y^4+x^2y^2-A^2y^2-B^2x^2+A^2B^2/2,$$

where $Z_1(=X)$ and $Z_2(=Y)$ denote the allowed betatron amplitudes of the horizontal and vertical motions, whose trajectories pass through the point (x,y); S denotes the total area of the possible rectangles,

including point (x,y), and η_j denotes a uniform random number within a range of o to 1. Here, the two-dimensional probability density of the betatron amplitudes X and Y is assumed to be proportional to the rectangular area 4XY. Once a group of X and Y is selected among possible amplitudes, (x,x') or (y,y') is given as a point inside the ellipse in each phase plane determined with twiss parameters and emittance Z_j^2/β_j by using a uniform random number.

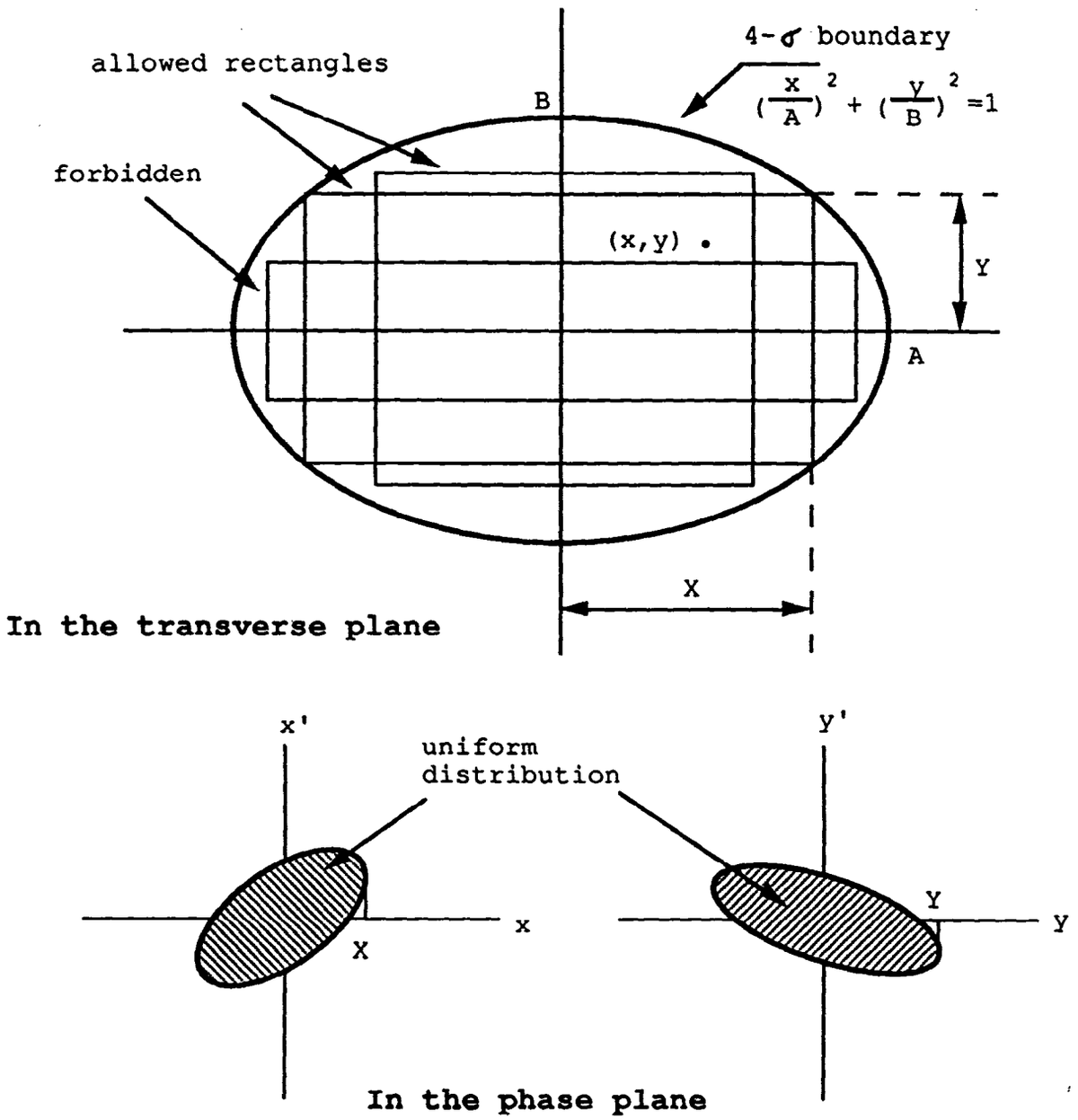

Fig. 1 Beam structure in the transverse plane and phase plane.

The momentum deviation, $\Delta p/p$, is generated so as to have an elliptic distribution given by

$$f(\delta)=2*(1-(\delta/\delta_0)^2)^{1/2}/\pi, \tag{3}$$

where δ is the momentum deviation ($=\Delta p/p$) and δ_0 is the maximum momentum deviation.

§3 Elements

The program can deal with the following elements: drift space, the sector magnet, its edge, the quadrupole magnet, and a magnet of combined type. These elements are interpreted to transfer matrices.[3] A 'Kick' element affects the beam by changing only its direction. The 'matter' option causes multiple scattering and energy loss of a particle by the Monte Carlo method. An auxiliary 'Monit' option creates histograms of horizontal and vertical beam profiles at the location where this option is found. These elements are described below.

3-1 Drift Space : DRIFT

A transfer matrix for a drift space is defined by

$$M_{ij}=\begin{vmatrix} 1 & s & 0 \\ 0 & 1 & 0 \\ 0 & 0 & 1 \end{vmatrix}, \tag{4}$$

where s denotes length of the drift space.

3-2 Sector Magnet : HSECT and VSECT

A transfer matrix for a sector magnet is defined by

$$M_{ij}=\begin{vmatrix} \cos\theta & \rho\sin\theta & \rho(1-\cos\theta) \\ -\sin\theta/\rho & \cos\theta & \sin\theta \\ 0 & 0 & 1 \end{vmatrix}, \tag{5}$$

where θ denotes the deflection angle and ρ the bending radius. In a plane perpendicular to the deflection plane, the transfer matrix is the same as that for drift space by substituting $\rho\theta$ to s.

3-3 Magnet edge : HEDGE and VEDGE

A transfer matrix for a magnet edge is defined by

$$M_{ij}=\begin{vmatrix} 1 & 0 & 0 \\ \tan\varepsilon/\rho & 1 & 0 \\ 0 & 0 & 1 \end{vmatrix}, \tag{6}$$

where ε denotes an angle between the direction of the bending radius, ρ, and the pole face. In a plane perpendicular to deflection plane, the transfer matrix is defined by

$$M_{ij}=\begin{vmatrix} 1 & 0 & 0 \\ (b/6\rho\cos\varepsilon-\tan\varepsilon)/\rho & 1 & 0 \\ 0 & 0 & 1 \end{vmatrix}, \tag{7}$$

where b denotes the range of the fringing field by a linear approximation.

3-4 Magnet of combined type : FCMB and DCMB

The transfer matrix of the combined-type magnet is defined by

$$M_{ij}=\begin{vmatrix} \cos\zeta & \sin\zeta/\sqrt{k} & (1-\cos\zeta)/\rho k \\ -\sqrt{k}\sin\zeta & \cos\zeta & \sin\zeta/\rho\sqrt{k} \\ 0 & 0 & 1 \end{vmatrix} \qquad (8)$$

in the focusing plane, where $k=(|n|+1)/\rho^2$ is for the horizontal plane, $k=|n|/\rho^2$ for vertical plane and $\zeta=s\sqrt{k}$. The transfer matrix for vertical plane is

$$M_{ij}=\begin{vmatrix} \cosh\zeta & \sinh\zeta/\sqrt{k} & (\cos\zeta-1)/\rho k \\ \sqrt{k}\sinh\zeta & \cosh\zeta & \sinh\zeta/\rho\sqrt{k} \\ 0 & 0 & 1 \end{vmatrix}, \qquad (9)$$

where $k=(|n|-1)/\rho^2$ is for the horizontal plane, $k=|n|/\rho^2$ for vertical plane and $\zeta=s\sqrt{k}$.

3-5 Quadrupole Magnet : QF and QD

The transfer matrices for quadrupole magnet are obtained from the transfer matrices for the combined-type magnet by setting $k=g/B\rho$ and $1/\rho=0$.

3-6 Kick : KICK

This element cannot be represented by a transfer matrix. When this element is found, the state vector (x,x') changes to $(x,x'+\theta)$. Here, θ denotes the kick angle.

3-7 Matter : MATTER

This element causes some deflection and displacement due to multiple Coulomb scattering as well as energy loss. The amount of energy loss is calculated in terms of Landau theory.[1] In thin matter, the energy transfer for each collision is calculated.[4] At the same time, multiple Coulomb scattering is also calculated as a succession of small-angle Rutherford scattering with a screening effect. For a thick matter, Moliere theory is adopted.[2] In order to save the CPU time, Landau distribution and a Moliere's distribution are tabulated precedently by the following formulations:

(i) Landau distribution

$$F(\lambda)=\int_{C-i\infty}^{C+i\infty}\exp(\eta\mathrm{Log}\eta+\eta\lambda)d\eta \qquad (10)$$

$$\lambda=(\Delta-\Delta_{prob})/\xi \quad ,$$

where Δ is the energy loss and $\xi=0.1536(Z/A)\rho t/\beta^2$ (MeV), using atomic number Z, mass number A, density ρ and thickness t of matter for a proton with a velocity β. The most probable energy loss, Δ_{prob}, is given by

$$\Delta_{prob}=\xi(\mathrm{Log}(2\xi m_e c^2\beta^2\gamma^2/I^2)-\beta^2+0.4228-\delta), \tag{11}$$

where $m_e c^2$ is the electron rest mass, I the mean excitation potential of matter and δ a parameter used for density correction. The value of δ for each atom was quoted from Sternheimer's works.[5]

(ii) Moliere's distribution

$$F(\theta)=\int_0^\infty \exp(\Omega(\chi)-\Omega_0)J_0(\chi\theta)\chi d\chi \tag{12}$$

$$\Omega(\chi)-\Omega_0=\chi^2\mathrm{Log}(0.29175\chi^2/\nu)/4,$$

where θ is a normalized polar angle measured with respect to the direction of an incident particle, and ν is the average collision number. The same equation gives a normalized lateral displacement upon replacing ν with 0.6492447ν. Both the actual scattering angle (θ_x, θ_y) and the displacement (x,y) are given by the following relations:

$$\theta_x=\theta\theta_c\cos\phi_1,\ \theta_y=\theta\theta_c\sin\phi_1,\ x=\theta R_c\cos\phi_2 \text{ and } y=\theta R_c\sin\phi_2, \tag{13}$$

where ϕ_1 and ϕ_2 are azimuthal angles distributed uniformly in a range between 0 and 2π. θ_c and R_c are defined by $\theta_c^2=\pi nt(2Ze^2/p\beta)^2$ and $R_c^2=t^2\theta_c^2/3$, respectively, using the particle density, n; the thickness, t; and the atomic number, Z, of the matter. The proton momentum is p and the velocity β.

3-8 Monitor option : MONIT

This element is treated as a drift space. When it is found, the horizontal and vertical profiles are created within a range between -50mm and 50mm.

III. Simulation

The program was applied to the BSF beamline. This beamline supplies a 500-MeV proton beam from a Booster synchrotron to four experimental halls: neutron, meson, medical and dump facilities. Fig. 2 shows a plan view of the beamline. Beam tracking from the entrance of the BSF beamline to the neutron facility is described below.

There are 32 quadrupole magnets, 5 dipole magnets and 19 steering magnets in this line. The calculation took into account only the quadrupole and dipole magnets. The steering magnets were treated as drift space. The beam profile monitors were considered as being a generator of the beam halo (matter option). The incident beam was generated by using twiss parameters mapped to the entrance of the beamline from the exit of the Booster. The emittances were adjusted so as to reproduce the actual beam profiles at the point of the first beam profile monitor (PR01) where dispersion was not so large. The maximum momentum deviation, δ_0, used in equation (3) was determined to be 0.4% in order to fit all of the profiles of the beamline. The beam profile monitor is a secondary-emission type and comprises 32 tungsten wires of 30μm in diameter with a 2.5mm pitch for horizontal profile measurements. The same number of wires are used for vertical profile measurements. These wires and a ceramic frame are the main scatterers of the beam. In a simulation, the wire was considered to be a square pillar.

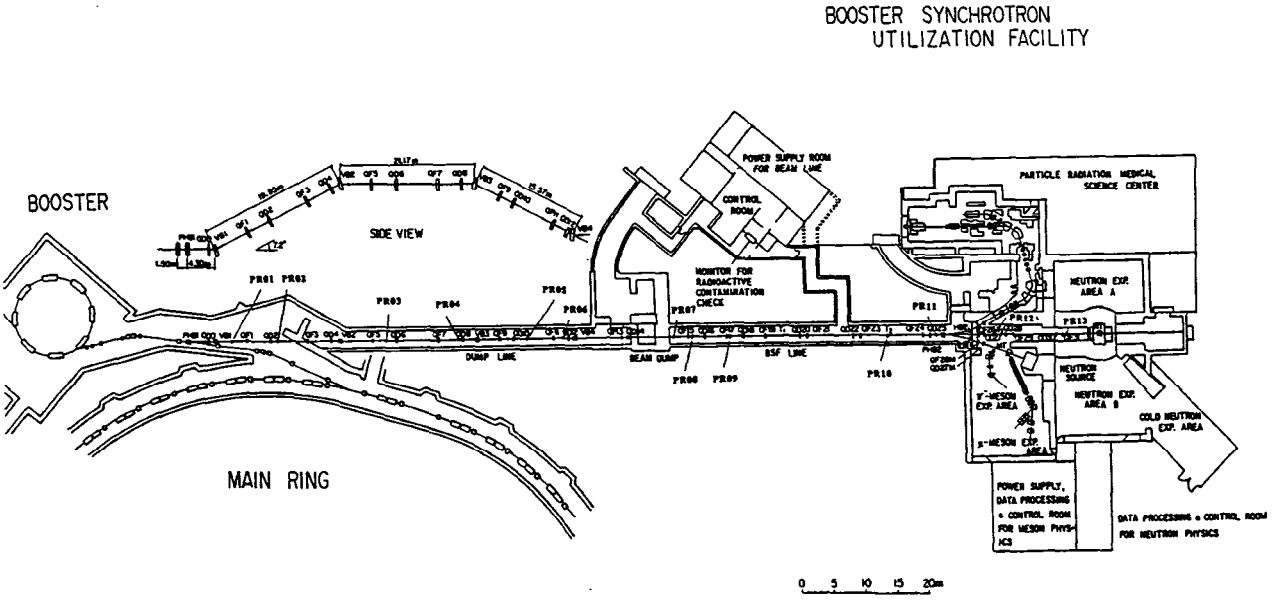

Fig. 2 Plan view of the BSF beamline.

The calculations were performed for two cases: with and without profile monitors. In the former case, the total amount of beam loss was about 1% of incident beam intensity. The latter gave a very small loss, less than 10^{-4}. This result implies that the beam halo is generated by profile monitors and is the main origin of residual radioactivity in the beamline, rather than orbit distortion. In order to test our speculation, we are planning to remove the profile monitors from the beamline during the next machine cycle.

Fig.3 compares the calculated profiles with the actual beam profiles at each monitoring point, where the line and the histogram denote the calculation and measurement, respectively. As shown, the simulation is in good agreement with the measurement, except for horizontal profile of PR13.

The beam loss count along the beamline is shown in Fig.4, together with a measurement of the radio activities (relative values). In this figure, the left edge of the knife shape histogram represents the value of relative exposure or loss count at an entrance of the element. The right edge represents the value at an exit of the element. The open and solid histograms correspond to the relative exposure and the calculated beam loss count, respectively. As shown, the major hot points almost coincide with the simulation, and the exposure level is also proportional to the calculated loss count. At the first five elements (PHB1 to ST2H), the calculation gave no beam loss. These points may occur due to orbit distortion. This will be also clarified by the next beamline study.

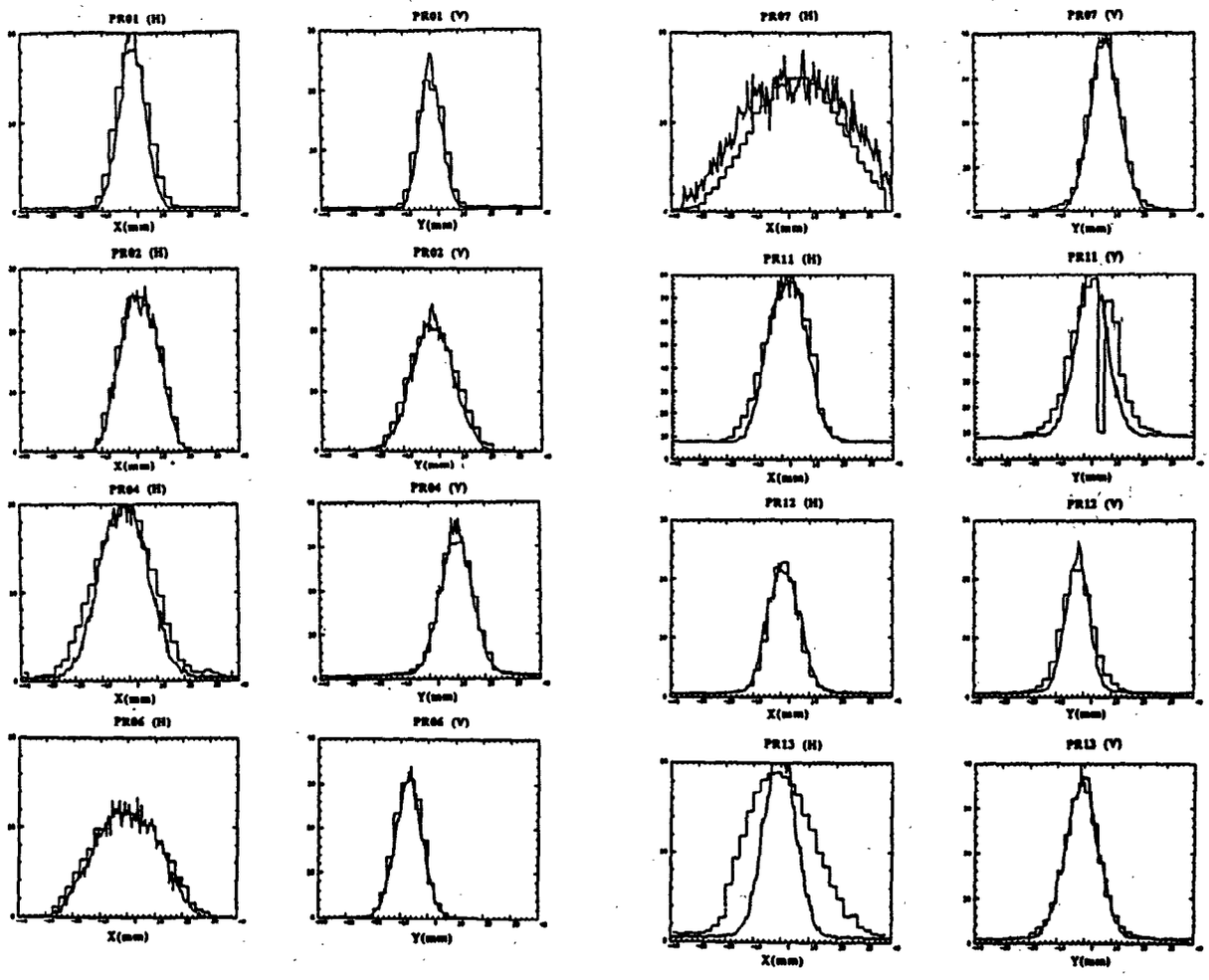

Fig. 3 Comparison between measured profiles and simulation.

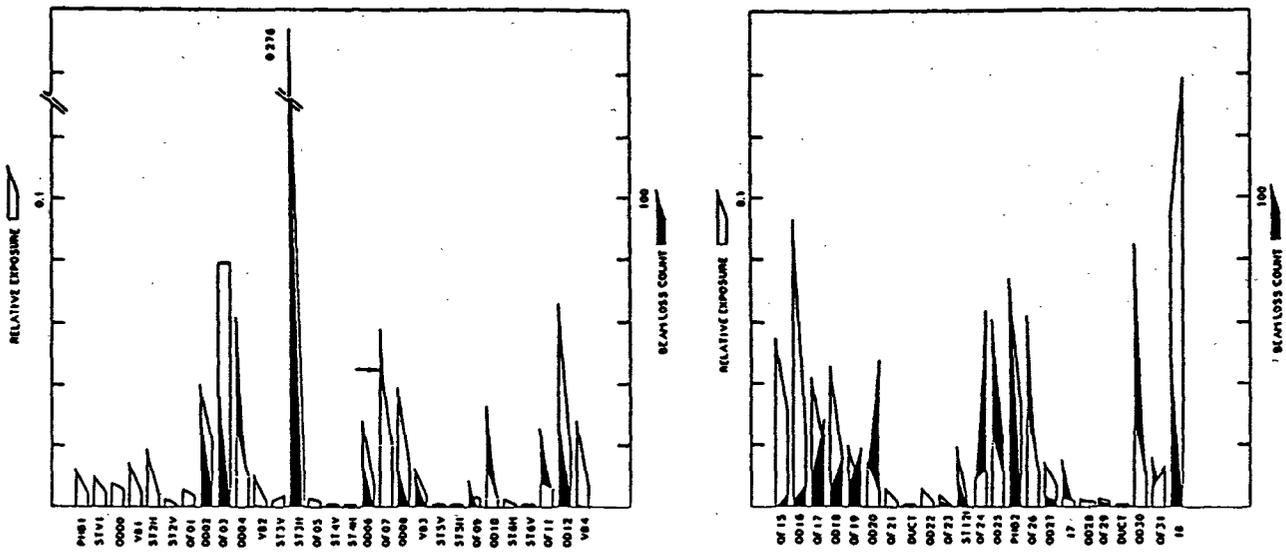

Fig. 4 Beam loss count along the beamline.

IV. Remarks

This program was applied to the BSF beamline and reproduced the actual beam profile successfully, except for the horizontal profile of PR13. The major hot points of the beamline are also consistent with measurements. This calculation implies that the tungsten wires of the beam profile monitors are the main origin of the beam halo. This idea will be tested next machine cycle by removing the profile monitors.

Acknowledgement

The author would like to thank Dr. Irie for useful discussion and continuous encouragement and Mr. Yano for useful information on the beam profiles of the BSF beamline.

References

1. L.Landau, J.Phys.USSR 8,201 (1944).
2. W.T.Scott, Revs.Mod.Phys. 35,231 (1963).
3. C.Bovet et.al, CERN/MPS-SI/Int. DL/70/4 (1970).
4. K.A.Ispirian et.al, Nucl.Instr. and Meth. 117,125 (1974).
5. R.M.Sternheimer, Phys.Rev. 145,247 (1966), 164,349 (1967) and B3,3681 (1971).

ICANS-XI International Collaboration on Advanced Neutron Sources
KEK, Tsukuba, October 22-26, 1990

THE ACCELERATOR COMPLEX OF THE MOSCOW KAON FACTORY

Chursin A.G., Dubinsky G.A., Esin S.K., Golubeva N.I., Iliev A.I.,Matveev V.A., Paramonov V.V., Pashenkov A.S., Senichev Yu.V., Shaposhnikova E.N. and Volin S.P.

Institute for Nuclear Research
of the Academy of Sciences of the USSR
Moscow

Glukhikh V.A., Malitskiy N.D., Severgin Yu.P. and Shukeilo I.A.

Scientific-Research Institute for Electro-Physical Equipment,
Leningrad

Batskikh G.I., Ivanov Yu.S., Meshcherov R.A., Murin B.P. and Semunkin Yu.F.

Moscow Radio-Technical Institute, Moscow

Introduction.

The tuning of the linear accelerator of the present Moscow Meson Factory is about to be completed. We are going to get first 600 MeV protons this year.

In accordance with the resolution on High Energy Physics of the USSR Government we have been designing the Project of Moscow Kaon Factory (MKF) since the middle of 1987. Now we collaborate with four institutes which contribute to the development of the Kaon Factory Project and we finished the Proposal of the MKF.

In the Proposal of the MKF the linear accelerator of the Meson Factory is to be used as the injector for the Booster being the first step of the MKF accelerator complex [1]. After charge exchange injection the H+ beam is accelerated in the Booster from 0.6 GeV to 7.5 GeV and in the Main Ring from 7.5 GeV to 45 GeV. At

the end of acceleration the 45 GeV beam is transferred from the Main Ring to the Extender and then extracted slowly with 100% duty cycle.

The program of physics research to be carried out at the 45 GeV high - intensity proton beam was discussed at "The 5 All Union Seminar" [2].

The Time - Energy Structure of the accelerators complex.

Figure 1 shows the time - energy structure of the accelerator complex. Every second a 100 ms long macropulse of 600 MeV H^- ions from the linac with $3.1*10^{13}$ particles is injected into the 50 Hz rapid - cycling Booster and are accelerated to 7.5 GeV. Then three out of six pulses are transferred to the Main Ring. An other three pulses of the beam are used in the experimental area of the Booster. The Main Ring is filled during the 40 ms flat bottom magnetic field. The Main Ring accelerates $9.3*10^{13}$ protons per pulse from 7.5 GeV to 45 GeV during 50 ms. The reset of the field in the Main Ring takes 30 ms, thus one cycle is 120 ms long, for a repetition rate of 8.3 Hz. The Extender is need for slow extraction with 100% duty cycle.

This accelerators complex can produce an average current of 125 mA with slows extraction with the average current from linac being 500 mA. Figure 2 shows the proposed layout of the MKF and experimental areas, together with the meson facility.

Injection from the Linac.

At injection into the Booster, the bunches follow with 198.2 MHz (the frequency of accelerating field of the last part of the linac is 991 MHz). Every bucket of the Booster is filled by three bunches from the linac. Since the rf frequency of the Booster is 33.03 MHz, three out of six bunches must be rejected which is done before injection into the linac, just after the buncher. Figure 3

shows the result of longitudinal painting with three bunches. The length of the bunch from the linac is about $\pm 1^{o}$ at 33.03 MHz and the momentum spread is ±0.6%. To improve painting it is needed to reduce the momentum spread to ±0.1% - ±0.12% with simultaneous increasing of the bunch length to $\pm 7^{o}$ - $\pm 12^{o}$ by bunch rotation. The volume of the beam in six dimensional phase space is increased by a factor 10^3 at injection. Since H^- ions are injected into the Booster by stripping them to protons as they pass through a thin foil, Liouville's theorem on phase space conservation may be circumvented and the beam is required which is injected over many tens of turns. The need to increase emittance arises from the Laslett tune shift that must not be more than 0.2. The size of the longitudinal emittance is determined by the threshold for microwave stability and a value of loading during accelerating cycle as well as by a condition of longitudinal matching between machines. To satisfy all these conditions we have chosen ±0.35% momentum spread and the ratio of bunch height to bucket height to be 0.8.

Requirements for the Lattice Design.

The MKF lattices were chosen on the basis of the following requirements:

1. For slow extraction from the Extender a dispersionless long straight section of 150 m length is needed.

2. Straight sections with zero dispersion are necessary for rf cavities for Booster and Main Ring as well as for the insertion of Siberian snakes.

3. The Main Ring and the Extender should have the same shape to be placed in a single tunnel.

4. Crossing of transition was to be avoided in both rings.

5. For increasing the threshold of microwave instability without additional longitudinal painting especially near the end of the accelerating cycle small real γ_t in Main Ring and high real γ_t in Booster are needed.

6. Suppressing of depolarizing resonances in both rings.

7. Realization of large dynamic aperture for decreasing of

losses.

All requirements are met with racetrack lattices with superperiodicity 2 and having dispersion suppressors at the ends of the arcs in all rings.

Booster Lattice

The racetrack lattice with only modulation of quadrupole strength is not convenient for Booster [3]. Because there is not enough room for collimation, diagnostic devices etc. The choice of latti ce begins with the choice of transition energy that depends on many factors. The minimum adopted value of γ_t is equal to 18. For increasing γ_t the lattice has either a high betatron tune [4] or a modulated β-function [5] or a modulated bending radius ρ or both β and ρ modulated [6]. We considered all lattices that can be divided in two types:

- the "resonant" lattices (number of superperiods of the curved section S is approximately equal to the betatron tune, $S \approx \nu_x$) and
- the "nonresonant" lattices, where S far from ν_x.

In "nonresonant" lattice for the booster there is only one family of the focusing quadrupoles and the dynamic aperture is sufficiently large. However, this lattice is unsatisfactory for lack of flexibility (an increase in γ_t requires an increase of the ring length) and there are not enough place in the arcs.

The original "resonant" lattice is the racetrack lattice with modulation of only the β-function. It consists of two arcs and two matching straight sections. The arcs together have 8 superperiods (S = 8), each superperiod includes 4*FODO cells. But this lattice is unsatisfactory because of its small dynamic aperture when chromaticity is corrected.

An alternative design investigated by us is the racetrack "missing magnet" lattice. Eight superperiods make up the two arcs. Each superperiod contains 4 regular FODO cells, but the two central halve-cells have no bending magnets ("missing magnets"). However, in this lattice it is impossible to achieve γ_t higher then 10. We therefore investigated the alternative lattice with both modulated β function and bending radius (fig.4). The arc's

construction is identical to the previous lattice. To produce zero dispersion in both straight sections the arcs are tuned to $\nu_x = 6$. In the vertical plane the phase advance of the straight sections is chosen to be $2 \cdot \pi$ for suppressing of spin-depolarization resonances and the tune of the arcs is 6.25. A high value of γ_t is obtained by the "missing magnets" and by the relatively small modulation of the β-function (2 families of QF). The numerical tracking gives a dynamic aperture of about 1300 π mm·mrad after correction of chromaticity for the on-momentum particle (fig.5). We believe that this lattice is optimal for the booster. Besides the above features there is enough place in the arcs for collimation of longitudinal losses [8] and diagnostic devices.

Extender and Synchrotron Lattice

The synchrotron lattice has been designed using a regular FODO focusing structure without superperiodicity [9]. The transition energy is determined by the horizontal tune ν_x ($\gamma_{tr} \sim \nu_x$) that equals $\nu_x = 7$. Every arc consists of 18 cells with $\pi/3$ advanced phase in the horizontal plane. The dispersion in the straight section is canceled by the "missing magnet" dispersion suppressors placed at the ends of arcs. The suppressor consists of two cells. One of them is empty and another one is the same as the arc cell. The tune for cell in both planes equals $\pi/3$ in order to have for arcs $\nu_{x,y} = 6$). The length of the straight sections is determined by the needed optics for the extender and equals 178 m. The total advanced phase is 7.25 for the horizontal plane and 8.25 for the vertical plane.

The Extender occupies the same tunnel as the Main Ring and has the same lattice in arcs. The Extender gives a continuous beam during the 120 ms cycle time via slow extraction. Dipoles have a maximum field of 1.8 T and quadrupoles of 1.1 T at the pole tip.

Slow Extraction

The Extender has two long straight sections LSS1 and LSS2. Slow extraction is performed in LSS1. LSS1 has two matching sections at its ends and extraction section EXS. Fig. 7 shows the lattice functions in LSS1 as well as the placement of the extraction elements (MPS1, MPS2 - the first and the second magnetic pre-septa, ES and MS are electrostatic and magnetic septa). The Extender is emptied by employing a third order resonance. Results of tracking studies are presented in fig.8.

The magnetic pre-septa are asymmetric quadrupoles. Both septa are identical. Each of them provides an angle of 0.5 mrad between circulated and extracted beams and has a length of 0.5 m.

The electrostatic wire septum is 5 m long with a field of ≃ 80 kV/cm. It deflects the beam by 0.85 mrad. The thickness of the wires will be 50 μm.

Magnetic septum deflects extracted beam into the derivation line. The thickness of the septum determined by the beam separation at the entrance of the magnet and is found to be 2 cm.

RF Cavities.

We consider now tunable cavities with perpendicular bias [9] as the working (first) variant. Calculations were made to chose cavities which are able to provide parameters needed with reasonable consumption of rf power and power of the bias circuit. With a maximum rf power density of less than 1 W/cm^3 in ferrites cavities for the Booster will produce an accelerating voltage 80 kV, the cavities for the Main Ring 140 kV. In comparison with the LANL-TRIUMF cavities, R/Q values and the volume of ferrite (relative) are lowered. For cooling of the ferrite rings we will use metal plates with radial slots. Development of technological processes to produce large (outer diameter 850 mm) yttrium ferrite rings is under way. An rf stand for full-scale cavity testing is under construction.

Also under consideration variant of the cavities proposal using a special varactor for capacitive tuning is . This leads to

the possibility to remove expensive ferrites and the biasing circuit.

Beam Stability.

We perform the longitudinal painting during injection into the Booster with 3 bunches spacing by 60 degrees. The maximum bunching factor B_f obtained in numerical simulation equals 0.33. The bucket height is 20% larger than the bunch. We have longitudinal emittance of 0.09 eV-s.

The space charge term of longitudinal impedance divided by mode number changes during acceleration in the Booster from -i280 to -i10. To avoid microwave instability the upper bound on the inductive wall term in the booster with γ_t=18 becomes 10 Ω.

The Main Ring operates above the transition energy with γ_t=7. Condition of longitudinal microwave stability is satisfied if inductive wall term of broad-band impedance does not exceed 8 Ω.

The parasitic modes of the rf cavities are serious sources of longitudinal instability. Passive mode damping of the parasitics helps to control them by active damping. Coupled-bunch modes around the rf frequency (n=h 1, h 2) will be damped by feedback loops connected with the rf system.

Landau damping of longitudinal modes is present only at the beginning of the accelerating cycle. Later on it is lost because the coherent frequency shift becomes larger than the half spread in incoherent frequencies.

To provide transverse stability of low frequency coupled-bunch mode the special construction of vacuum ceramic chamber and broad-band feedback system are under development. In the Main Ring the natural chromaticity must be corrected to positive value.

Conclusion

We have outlined the Proposal of the Accelerators Complex Lattice of the Moscow Kaon Factory. It allows to have simultaneous beams of the following parameters:

1. I_{av} = 250 μA, W = 7.5 GeV, f = 50 Hz, t = 1.1 ms

2. I_{av} = 125 μA, W = 45 GeV, f = 8.3 Hz, t = 3.3 ms

3. I_{av} = 125 μA, W = 45 GeV, continuously

Besides taking account of the possibilities of the linac and the 600 Mev - Accumulator - Stretcher one can consider that it will be the powerful Accelerators and Accumulators Complex for nuclear research in the field of high intensity physics and thin process.

Acknowledgement

The authors wish to thank Y.Stavis sky and V.Laptev for fruitful discusions about the parameters of MKF for experimental programm.

References.

1. Senichev Yu. et all. The proposal of the Accelerators Complex of the Moscow Kaon Factory. - Proceedings of the Advanced Hadron Facility Accelerator Design Workshop, 1989.
2. Matveev V.A., Rubakov V.A. Particle Physics at Kaon Factory. The Program of experimental research at the Moscow Meson Facility. - The 5-th All Union Seminar, 1987.
3. Servranckx R. New Lattice for C, D and E Rings. - TRI-DN-88-3.
4. Proposal for European Hadron Facility. - EHF-87-18.
5. Servranckx R.V., Wienands U., Craddock U.K. In Search for a Booster Lattice. - TRI-DN-89-K48.
6. Golubeva N.I., Iliev A.I., Senichev Yu.V. The New Lattices for the Booster of Moscow Kaon Factory. - Proceedings of the International Seminar on Intermediate Energy Physics. Moscow,1989.
7. Wienands U. Polarization in the New Racetrack Driver Ring of the TRIUMF Kaon Factory. - TRI-PP-88-14.
8. Rees G. Space for a Longitudinal Beam Loss Collector in the D Ring. - TRI-DN-89-K1.
9. The Physics and a Plan for 45 GeV Facility that Extends the High-intensity Capability in Nuclear and Particle Physics. - LA-10720-MS.

Target Station Workshop

Neutronics

Cold Neutron Sources & Moderators

New Concepts in Target-Reflector-Moderator Systems

ICANS-XI International Collaboration on Advanced Neutron Sources
KEK, Tsukuba, October 22-26, 1990

Spallation Physics - An Overview

Gary J. Russell
Los Alamos National Laboratory
Los Alamos, New Mexico

ABSTRACT

Most of you know that LANSCE uses 800-MeV protons (from LAMPF) to produce neutrons for scattering experiments. But do you know how we do it? This article explains the basics of spallation and compares it to fission, and discusses some basic target neutronics.

I. WHAT IS SPALLATION?

Spallation refers to nuclear reactions that occur when energetic particles (for example, protons, neutrons, or pions) interact with an atomic nucleus. At LANSCE, energetic (800 MeV) protons hit a tungsten target; at 100 μA, this amounts to 6.24×10^{14} protons per second striking the target. However, to illustrate the spallation process, we will describe the reactions that follow when only one 800-MeV proton, a primary particle, hits a target nucleus.

As shown in Fig. 1, spallation can be thought of as a two-stage process. In the first stage, the primary particle reacts with nucleons--neutrons and protons--inside the nucleus. The reactions that follow create an *intranuclear cascade* of high-energy (greater than 20 MeV) protons, neutrons, and pions within the nucleus. During the intranuclear cascade, some of these energetic *hadrons* escape as secondary particles. Others deposit their kinetic energy in the nucleus leaving it in an excited state. In the second stage (nuclear de-excitation), evaporation takes place when the excited nucleus relaxes by emitting low-energy (less than 20 MeV) neutrons, protons, alpha particles, etc., with the majority of the particles being neutrons. The low-energy neutrons produced during nuclear de-excitation are important in a spallation source because they can be moderated (reduced) to even lower energies for use as research probes. After evaporation, the nucleus that remains may be radioactive and may emit gamma rays.

Secondary high-energy particles produced during the intranuclear cascade move roughly in the same direction as that of the incident proton and can collide with other nuclei in the target. The reactions that follow are a series of secondary spallation reactions (see Fig. 2) that generate more secondary particles and low-energy neutrons. The so-called *hadronic cascade* is the accumulation of all reactions caused by primary and secondary particles in a target.

If the target is very heavy (for example, depleted uranium or lead), high-energy fission can compete with evaporation during nuclear de-excitation (see Fig. 3). Even more fission events can occur in fissile targets such as ^{235}U or ^{238}U.

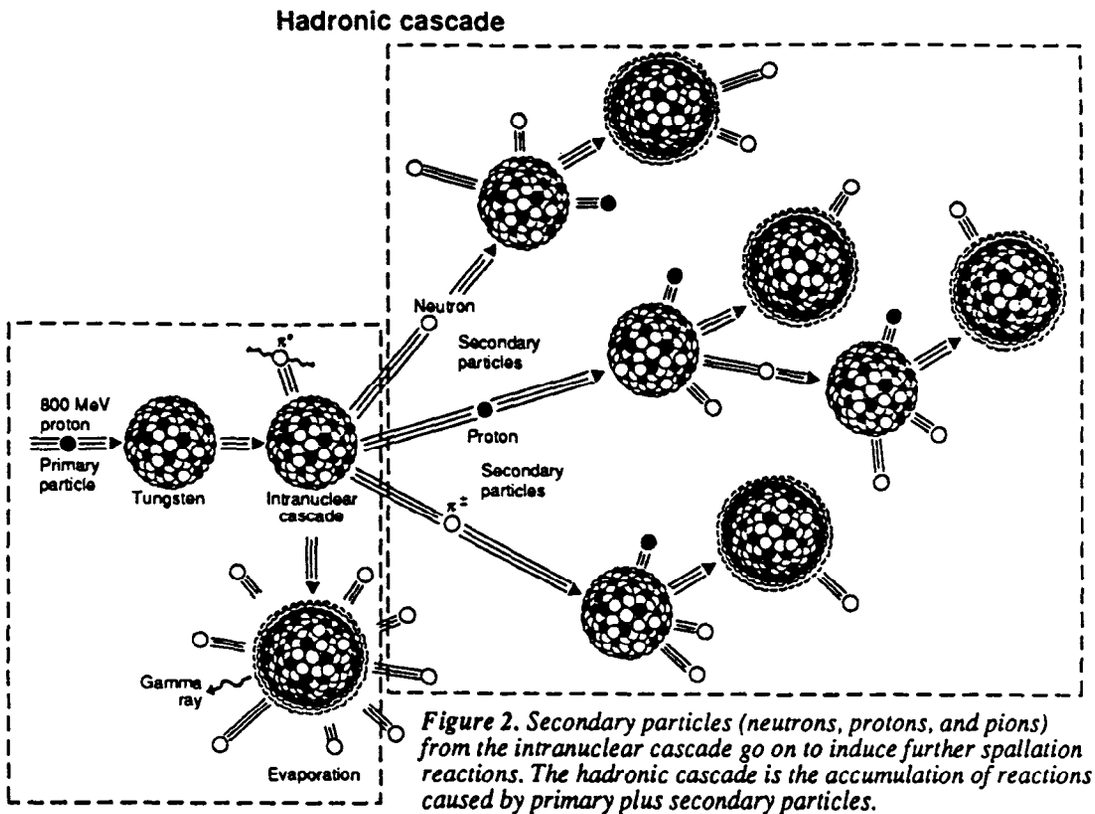

Figure 1. The primary particle (800- MeV proton) hits the tungsten nucleus, inducing spallation (the intranuclear cascade and evaporation).

Figure 2. Secondary particles (neutrons, protons, and pions) from the intranuclear cascade go on to induce further spallation reactions. The hadronic cascade is the accumulation of reactions caused by primary plus secondary particles.

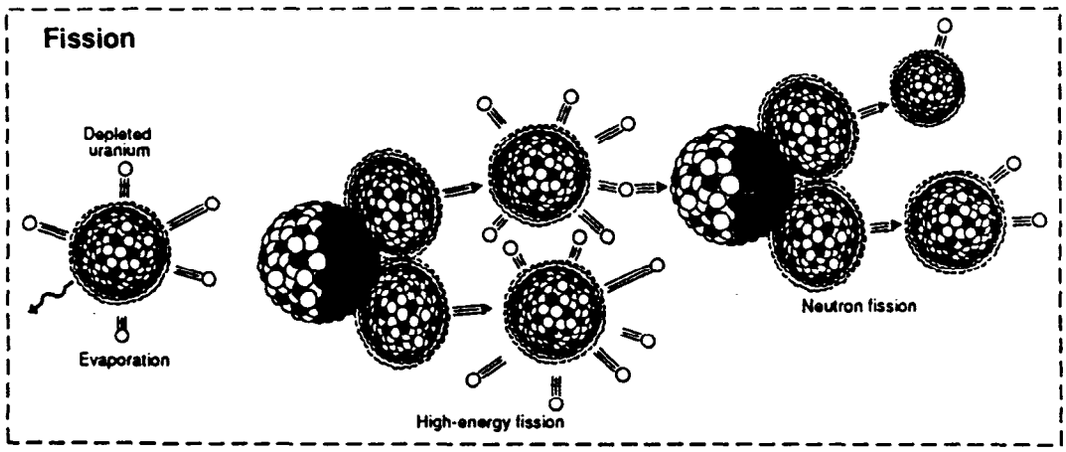

Figure 3. When a depleted uranium target is bombarded by 800-MeV protons, high-energy fission competes with evaporation during nuclear de-excitation. More neutrons are emitted from high-energy fission than from evaporation. The neutrons emitted from high-energy fission and evaporation can go on to induce more fission events.

II. HOW DOES SPALLATION DIFFER FROM FISSION?

Spallation and fission differ in several ways. One difference is in the nuclear debris remaining after the reactions. Predicted yields of spallation products from a 10-cm-diameter by 30-cm-long machineable tungsten target, bombarded on axis by 800 MeV protons, are depicted in Fig. 4. Note in Fig. 4 the more-or-less continuous distribution of spallation products down to mass number 120, the symmetric high-energy fission products in the mass range 60 to 120, and the spallation and high-energy fission products below mass 60. Spallation products below mass 60 come from the iron and nickel in machineable tungsten. Machineable tungsten used for the LANSCE targets has a density of 18.3 gm/cm^3, and is composed of 97.0 w% tungsten, 2.1 w% nickel, and 0.9 w% iron. In fission, the nucleus divides into two, producing a variety of fission products (see Fig. 3).

Another difference between spallation and fission is in the number of neutrons released. The overall number of neutrons released per fission event (about 2.5) is considerably less than that released per spallation event; about 13 neutrons for each incident proton are released from the LANSCE target (See Fig. 5). Furthermore, at least one of the 2.5 neutrons produced by fission is useless for neutron scattering--it is needed to sustain the fission reaction.

Spallation and fission also differ in other ways:

- *in the amount of energy deposited per neutron produced*

For fission, about 180 MeV of energy is deposited as heat for each neutron produced; for spallation in tungsten, the corresponding number is about 32 MeV. Although there is less heat generated with spallation, the intensity of the proton beam at a high-power spallation source can lead to cooling problems--equivalent to those of a high-power reactor source--in windows and targets, unless special care is taken.

- *in the amount of gamma-ray energy produced*

At LANSCE, about 2 MeV of gamma-ray energy is emitted for each neutron produced; about 12 MeV is released per fission event. Because spallation neutron sources do not produce as much gamma-ray energy as equivalent reactor sources, gamma-ray heating and contamination of neutron beams are less problematic.

- *in the energy distribution of the emitted neutrons*

Spallation neutrons have higher energies than fission neutrons (see Fig. 6). In a spallation source, high-energy cascade neutrons approach the energy of the incident proton (800 MeV at LANSCE). High-energy neutrons are extremely penetrating as well as being useless for neutron scattering. Well-designed shielding is needed to prevent high-energy neutrons from causing unwanted background in experiments.

III. HOW DOES SPALLATION TARGET DESIGN AFFECT NEUTRON YIELD?

The objective in designing a spallation target is to increase the leakage of low-energy neutrons and to decrease the leakage of high-energy neutrons from the target. Low-energy neutrons that leak from the target are potentially useful because suitable materials can reduce their speed (by factors of 10^1 to 10^{10}) to produce pulsed neutron beams useful for research in materials science and nuclear physics. Fortunately, low-energy neutrons from the hadronic cascade outnumber the high-energy neutrons (see Fig. 7).

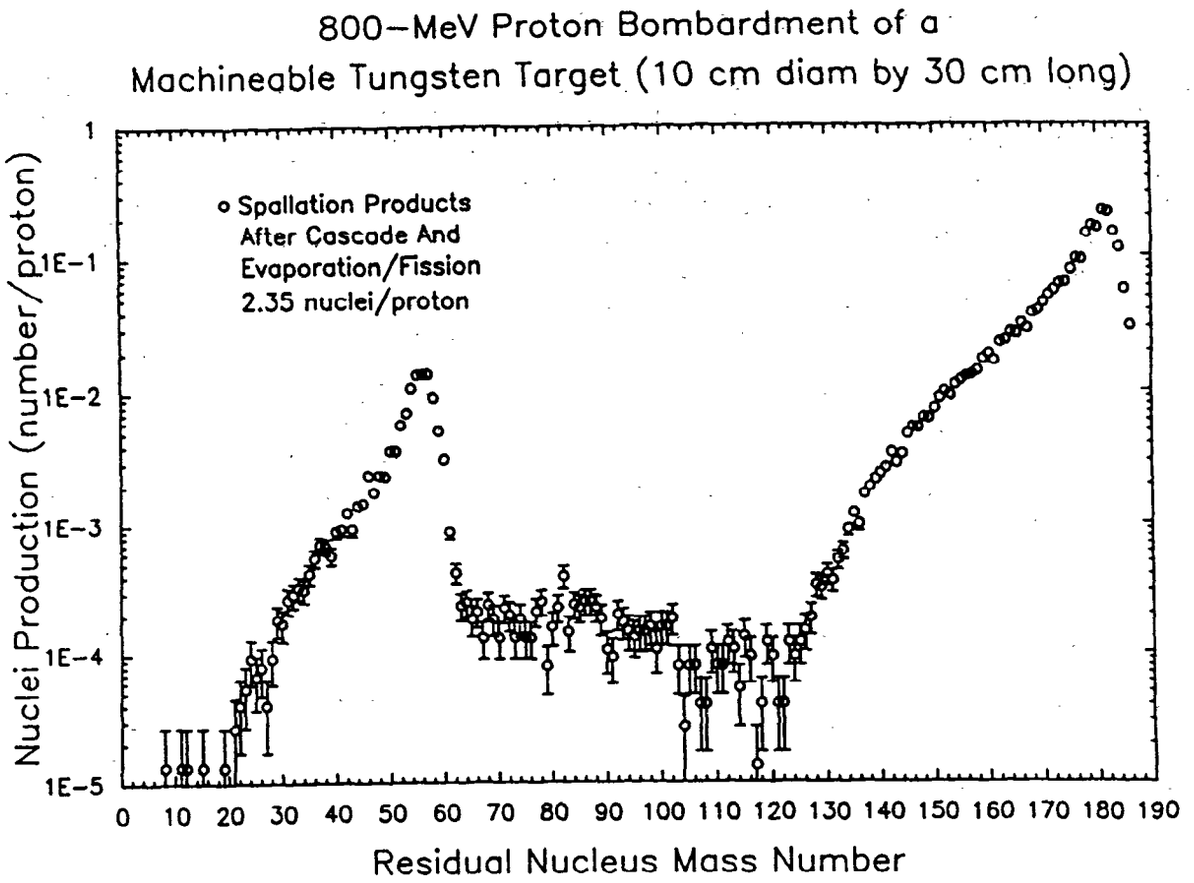

Figure 4. Calculated spallation product yields for 800-MeV protons on machineable tungsten.

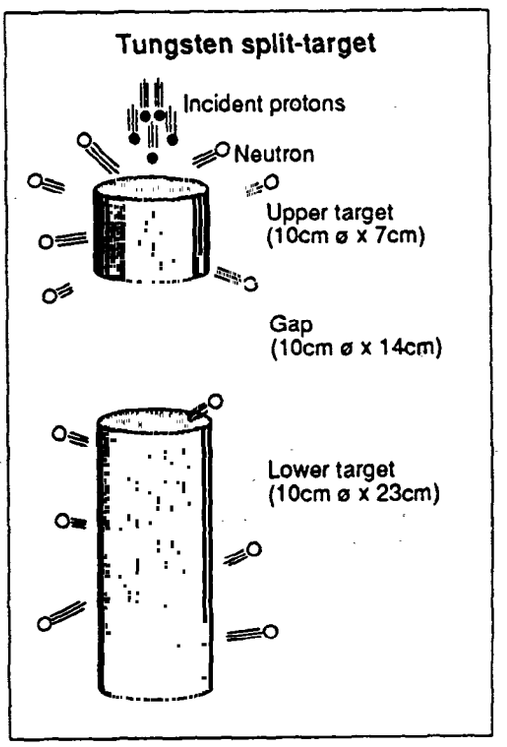

Figure 5. Illustration of the LANSCE split-target.

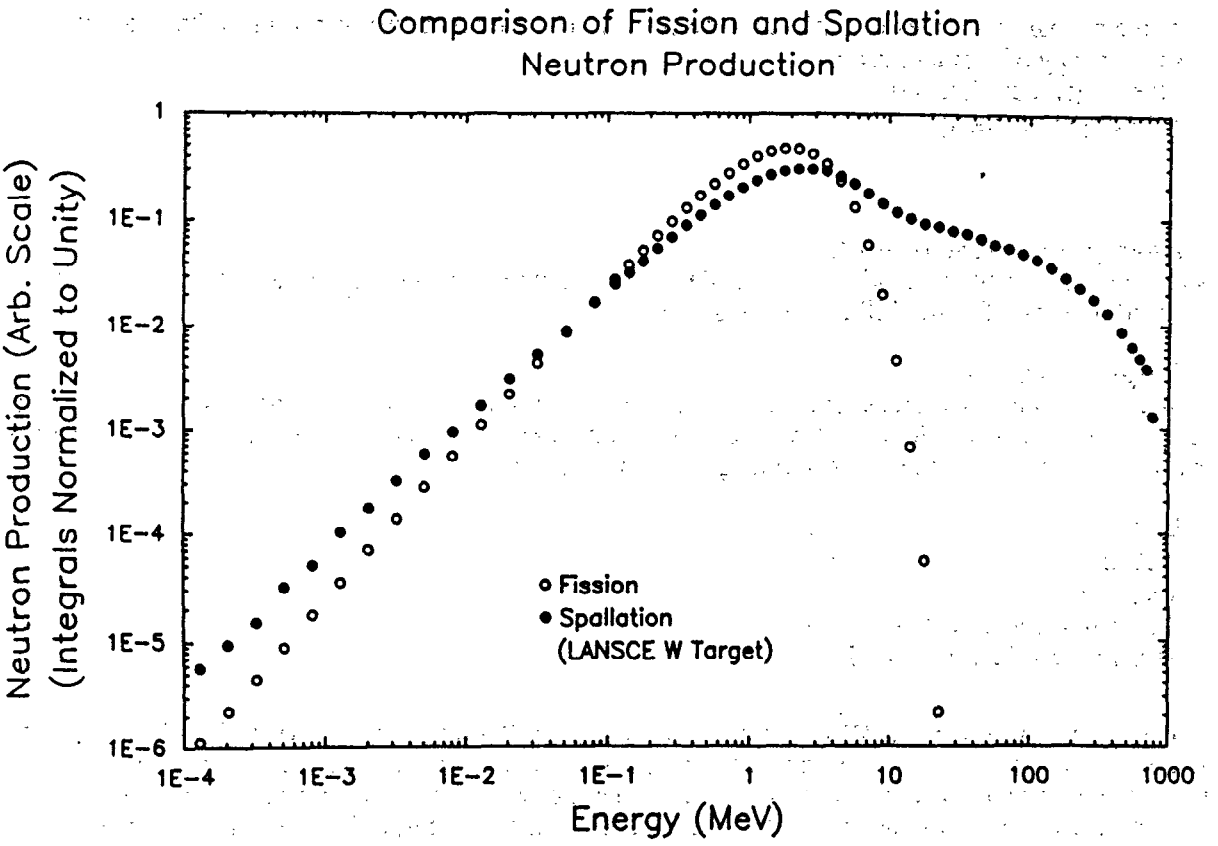

Figure 6. Neutron production from fission (o) and from spallation (•).

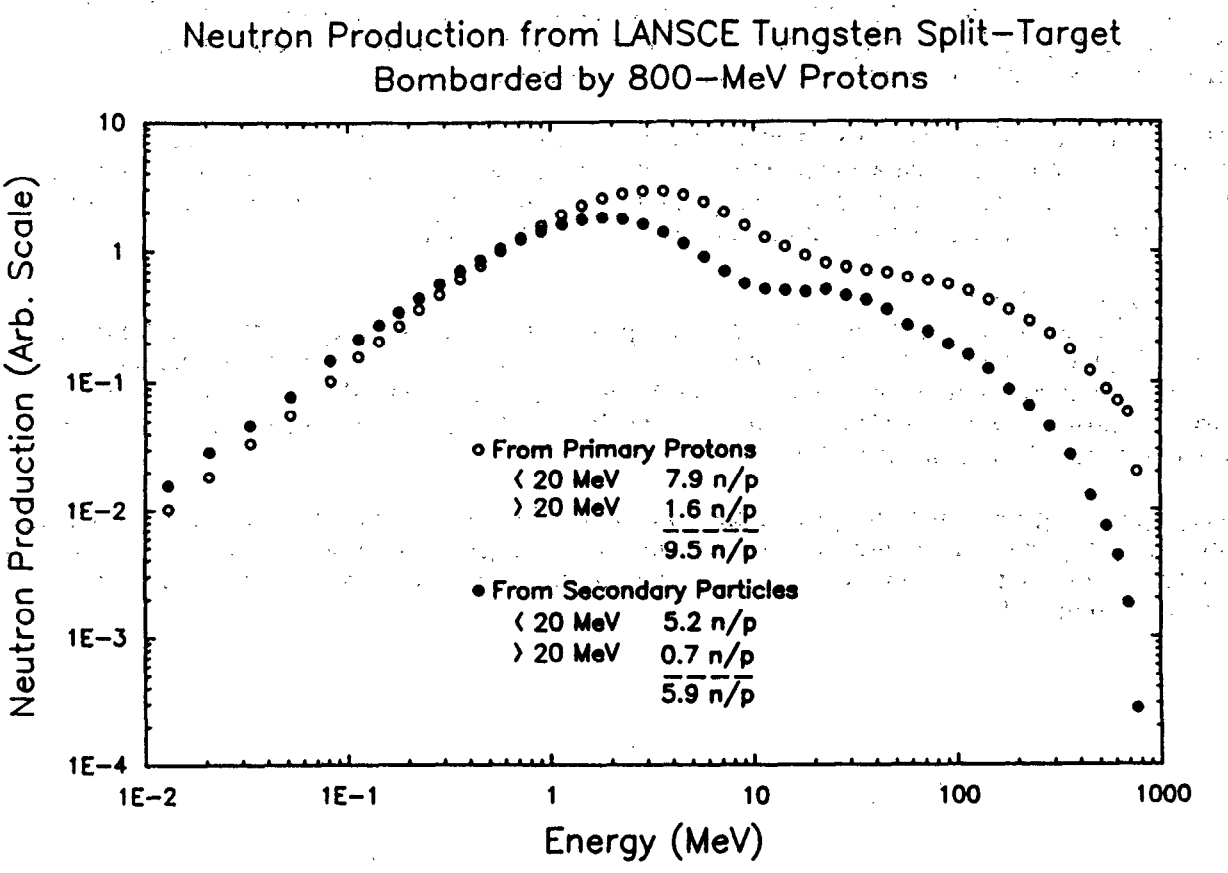

Figure 7. Neutron production from reactions caused by the primary proton (o) and the secondary particles (•) in LANSCE tungsten-target nuclei. About 85% of the total neutrons produced are low energy, and about 60% of the low-energy neutrons are produced by primary protons.

*n/p=neutrons/incident proton

Three primary variables can affect the number of low-energy neutrons produced by a target:
- the energy of incident protons,
- the target material, and
- the target geometry.

Energy of incident protons

As the energy of protons incident on a spallation target increases, the number and energy of neutrons produced increase. Figure 8 illustrates this effect.

Target material

For spallation neutron sources, practical target materials are lead, tantalum, tungsten, depleted uranium, and lead/bismuth. The calculated low-energy neutron leakages for most of these target materials having the same dimensions of the LANSCE target are as follows:

lead	*11.9*
tantalum	*12.7*
tungsten	*13.1*
depleted uranium (dilute)	*19.4*
depleted uranium (solid)	*21.4*

Compared to tungsten, a depleted uranium target designed to operate at 100 μA of 800-MeV protons must be clad to contain fission products and must be segmented more to affect target cooling. Cladding and coolant materials make the target dilute and do not produce as many neutrons as the target itself; therefore, the number of neutrons for the dilute depleted uranium target is lower than the solid depleted uranium target.

Neutrons leaking from solid split-targets of tungsten and depleted uranium are compared in Fig. 9. Neutrons emerging from a tungsten target are biased towards lower energies; these neutrons can be moderated more effectively for neutron scattering experiments.

The total neutron yield of a pulsed spallation source is not the only feature of the source that interests neutron scatterers. For accurate experiments, short pulses and low backgrounds between pulses are also important. Therefore, depending on the application, a fissile target (which produces more delayed fission neutrons between pulses than say tungsten) may not be the best choice.

Target geometry

The number of low-energy neutrons produced depends on the size of the spallation target. For example, in Fig. 10, the number of low-energy neutrons increases with target diameter and reaches an asymptotic value of about 20 neutrons/incident proton (n/p) at a diameter of about 50 cm for a 30-cm-long tungsten target bombarded with 800-MeV protons. Neutron leakage from the same target reaches a maximum value of about 15 to 16 n/p at a 20-cm diameter.

Varying the target size also changes the energy and time distribution of neutrons that leak from a target. Small targets yield more high-energy neutrons than large targets, and the change in time distribution is important in some applications (for example, nuclear physics research) in which very short neutron pulses are required.

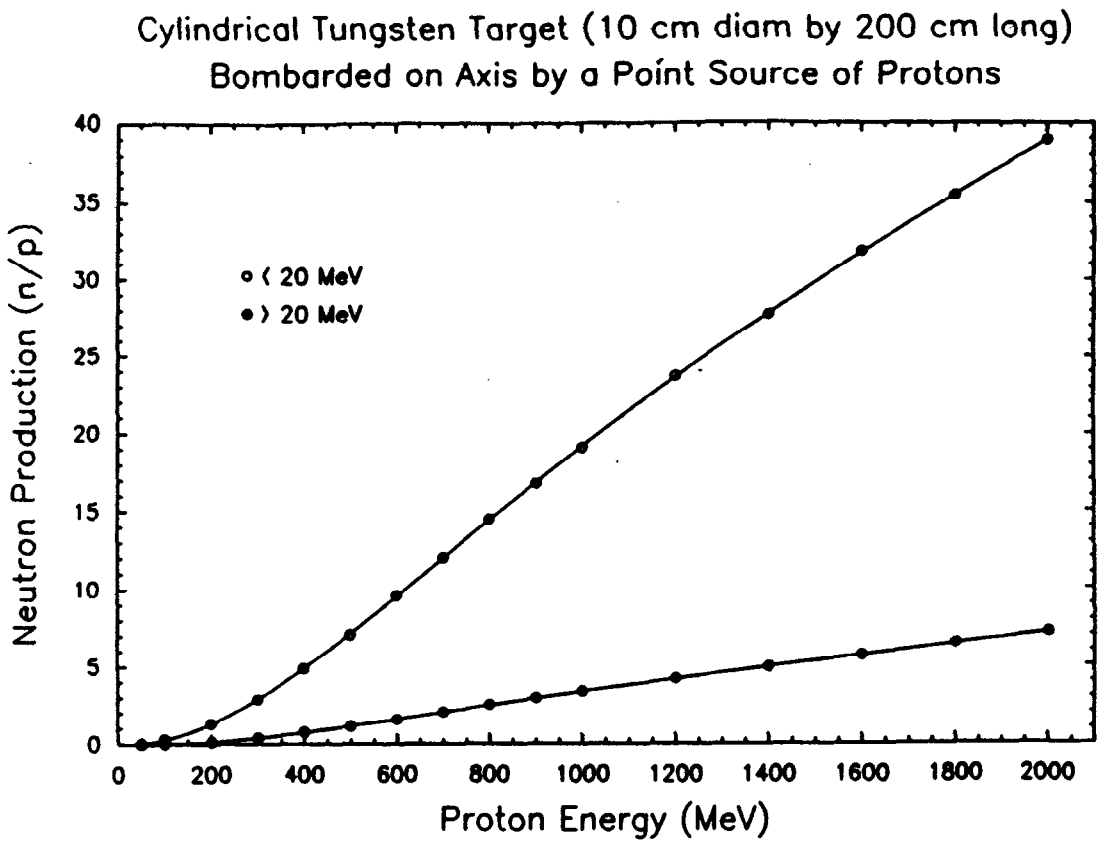

Figure 8. Production of low-energy (○) and high-energy (●) neutrons for a cylindrical tungsten target (10-cm diam by 200-cm length). The length of 200 cm was arbitrarily chosen and was long enough to range out 2000-MeV protons.

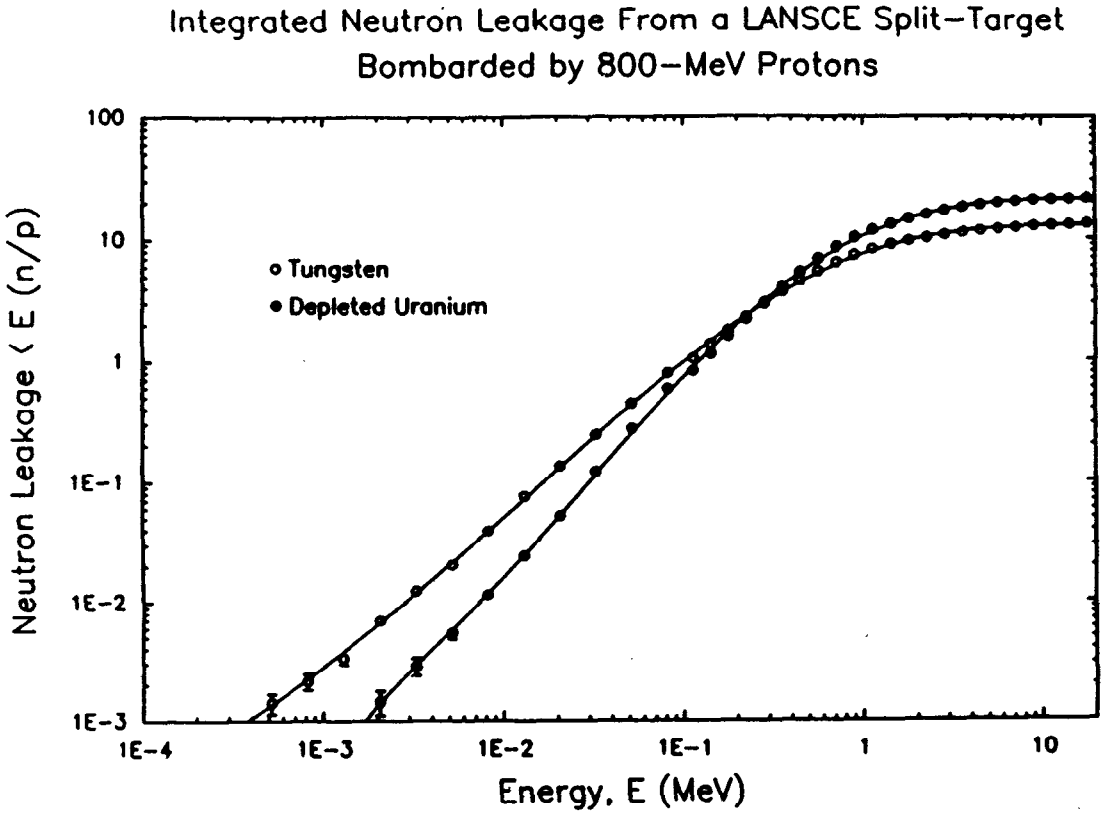

Figure 9. Low-energy neutron leakage from tungsten (○) and from depleted uranium (●) split targets, both bombarded by 800-MeV protons. More low-energy neutrons leak from the tungsten target than from the depleted uranium target.

IV. SUMMARY

Spallation is a method of producing neutrons for materials science research. Contrasted to fission, spallation differs in the following ways: a) in the nuclear debris remaining after the reactions; b) in the amount of energy deposited per neutron produced; c) in the amount of gamma-ray energy produced; and d) in the energy distribution of the emitted neutrons.

The energy of incident protons and the target material and geometry affect the number of neutrons produced. More importantly, these factors also influence the energy and spatial distribution of neutrons leaking from the target. Figure 11 illustrates the difference in spectra of neutrons produced in the target and those that leak from the target. This difference occurs because the target can be viewed as a moderator that reduces the energy of neutrons produced. For hydrogen and other moderating materials, the lower the energy of neutrons leaking from the target, the more readily these materials can moderate neutrons to energies suitable for neutron scattering experiments.

V. ACKNOWLDEGEMENTS

I appreciate the support of Roger Pynn for this work. I want to thank Tatia Vander Maat for her typing help, Gail Flower for her assistance in producing the figures, and Maria DiStravolo for proofreading the text on a very short notice. LANSCE work is supported by the US Department of Energy, Office of Basic Energy Sciences, under contract W-7405-ENG 36 with the University of California.

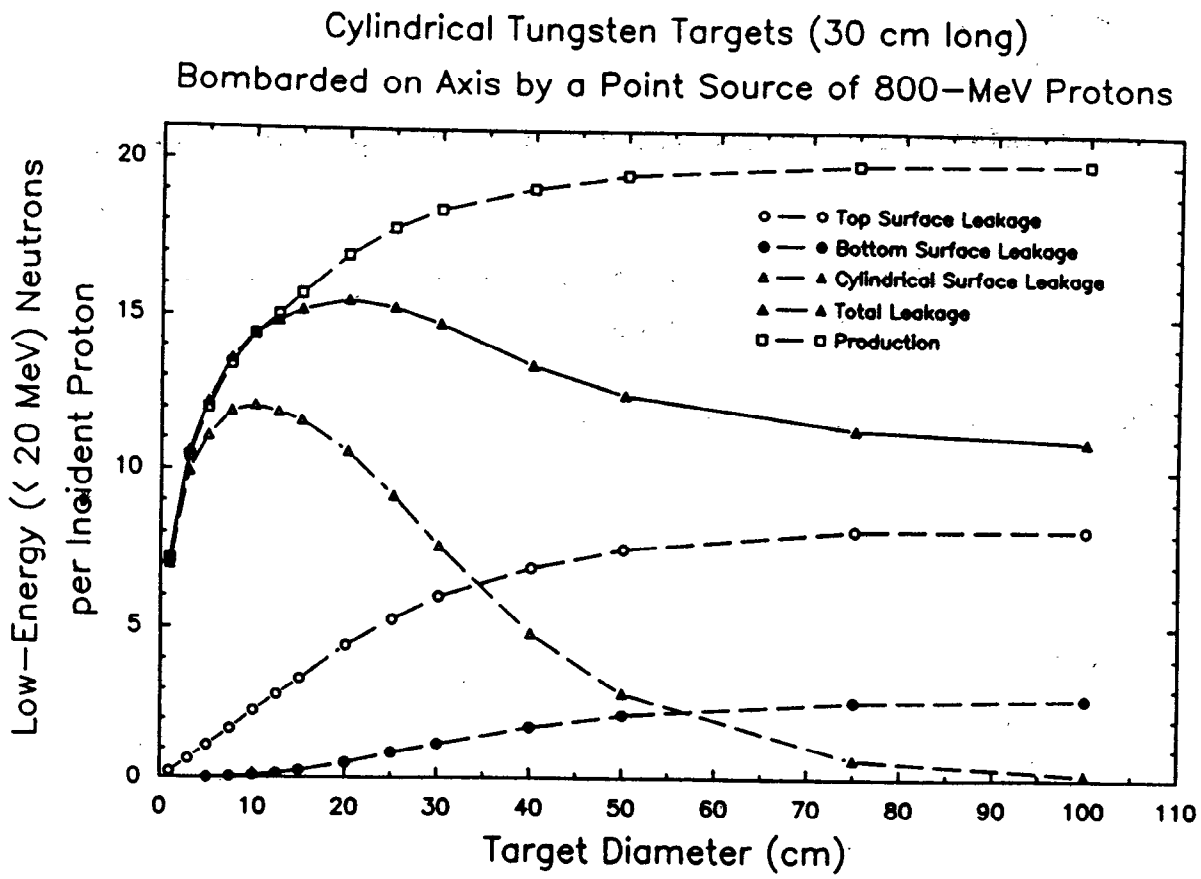

Figure 10. Low-energy (< 20 MeV) neutron production and leakage from machineable tungsten targets bombarded by 800-MeV protons.

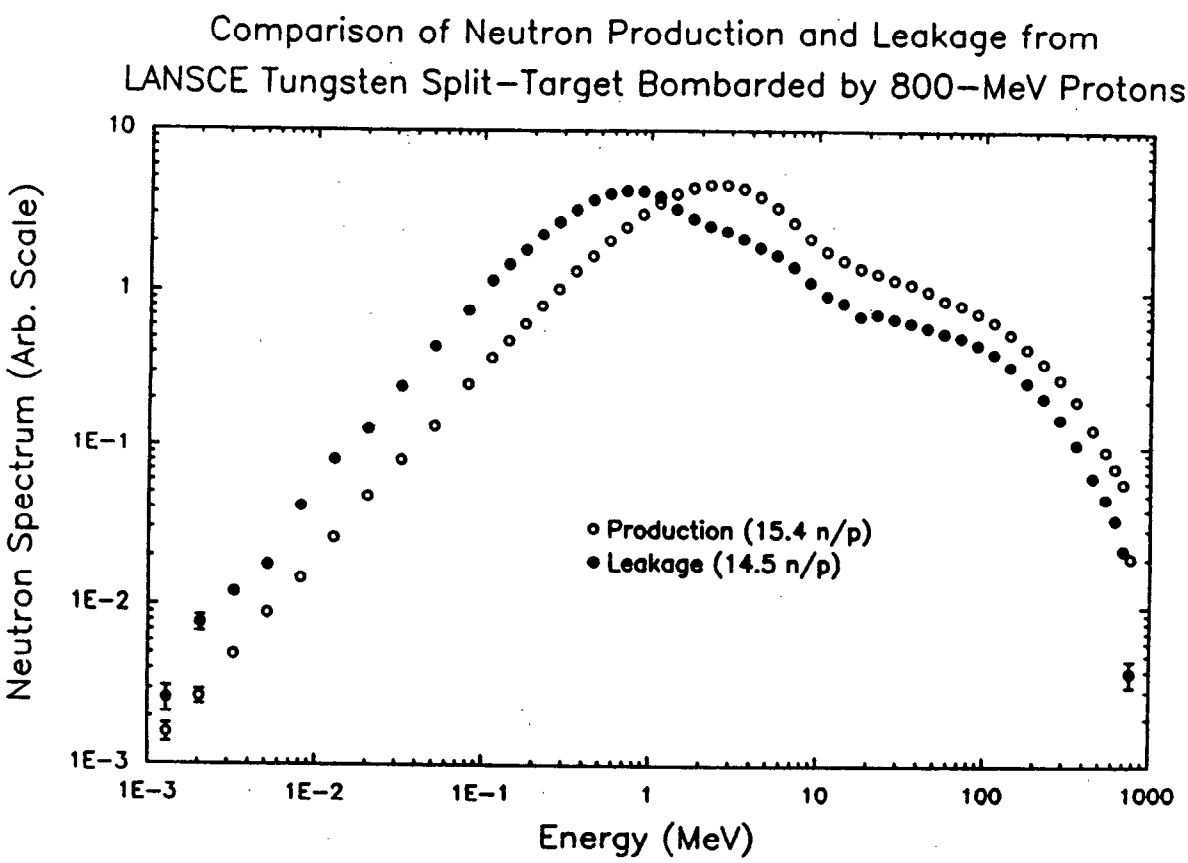

Figure 11. Spectra for neutron production (○) and neutron leakage (●) from the LANSCE target.

ICANS-XI International Collaboration on Advanced Neutron Sources
KEK, Tsukuba, October 22-26, 1990

Calculation code system for fission and spallation products

T. Nishida, H. Takada, Y. Nakahara, I. Kanno,
T. Tsutsui, Y. Kaneko

Japan Atomic Energy Research Institute, Tokai Establishment

Tokai-mura, Naka-gun, Ibaraki-ken, Japan

ABSTRACT

It is important to use computer codes with high precision for analyzing the physical process in the intense neutron source induced by the high energy proton beam. A brief description is given for the spallation and fission reactions and the particle transport codes which have been developed and upgraded at JAERI.

The simulation code for High Energy Nuclear Reaction Process in the energy range of 15 MeV to 3 GeV, NMTC/JAERI, is a JAERI version of NMTC which was developed at ORNL and revised later at LANL and BNL. In this version the high energy fission reaction can be calculated, using the statistical model, in competition with the particle evaporation reaction. The mass number A of nuclides which can be dealt in the spallation calculation has been extended from [A=1;8< A< 239] to [A=1; 6< A < 250]. A simulation code NUCLEUS for the spallation reaction of one nucleus without taking into account the internuclear cascade, was also developed to evaluate the computational model for spallation reaction and analyze effectively the data measured in thin foil experiments. For the whole energy range less than 3 GeV, two simulation code systems had been developed by connecting NMTC/JAERI with the neutron transport codes MORSE-DD and TWOTRAN-II respectively. The code SPCHAIN for calculating the time evolution process of spallation products has been developed on the base of the depletion code DCHAIN2, which had been made for the calculations of decay and built-up of fission products in a nuclear reactor. The new nuclear data have been compiled in SPCHAIN data file for about 1100 nuclides needed for TRU spallation calculation. These codes are used to calculate reaction products measured in the spallation experiment using 500 MeV protons in the booster facility of the synchrotron at KEK and to perform the conceputual design study of TRU transmutation system driven by an intense proton accelerator.

I. INTRODUCTION

It is important to use computer codes with high precision for analyzing the physical processes in an intense neutron source induced by the high energy proton beam. In this report brief descriptions are given for the spallation reaction and the particle transport codes, which have been developed or upgraded at JAERI and some results computed by using these codes are presented. Our main purposes are to perform the design study of transuranium nuclides (TRU) transmutation target-core system driven by a proton accelerator and analyze the data measured in spallation experiments. Analyses of the beam window on the spallation target and accelerator strucutral materials irradiated by high energy particle beam will be also carried out.

II. SPALLATION ANALYSIS AND TRANSMUTATION SYSTEM DESIGNING CODE SYSTEMS DEVELOPED AND UPGRADED AT JAERI

As well known, the high energy protons injecting on a target cause more complicate nuclear reactions than neutrons transporting in a reactor core. Figure 1 shows the schematic illustration of nuclear reactions and particle transport processes in a heavy metal target irradiated by the high energy proton beam. In the energy range above ~15 MeV, the intranuclear and internuclear cascades with the spallation (particle knock-on), evaporation and high energy fission reactions are induced by the proton bombardment. Through these processes many neutrons and some light particles such as proton, deuteron, triton, helium-3, α particle are emitted. Most of these spallation neutrons, which have the energy spectrum similar to one in a fast reactor, transport in the target after slowing down into the energy range lower than ~15 MeV. As nuclear reaction simulation codes, NMTC/JAERI - NMTA and NUCLEUS codes are prepared for the energy range above 15 MeV and MORSE-DD , SP-ACE and TWOTRAN-II codes for the range below 15 MeV at JAERI. ORIGEN-2 and SPCHAIN calculate the time evolution process of TRU transmutation products in the lower and upper energy ranges, respectively. The flow chart in Fig.2 shows the mutual relations among the simulation code systems prepared at JAERI. The High Energy Nuclear Reactions and Nucleon-Meson Transport Code

NMTC/JAERI is the main code in this code system. The codes included in the left side of this figure simulate the high energy nuclear reaction process above 15 MeV and ones in the other side carry out the neutron transport calculation below 15 MeV.

(1) NMTC/JAERI[1]

The code NMTC/JAERI is used for the Monte Carlo simulations of nuclear spallation induced by incident particles(proton, neutron, pion) from an external source in a heterogeneous medium. The subsequent internuclear transport processes is also calculated in the energy range of 15 MeV to 3 GeV. In the JAERI version, the fission process has been incorporated as a competing process with particle evaporation. The range of mass number A of nuclides in the target has been extended from[A=1;8< A< 239] to [A=1; 6< A < 250]. The major part of NMTC is almost the same as the old version of HETC. The detailed descriptions about NMTC/JAERI had been given by Nakahara at the former conference ICANS-IV.[2] So in this report only two graphs computed using NMTC/JAERI for the analysis of transmutation system are presented.

Figure 3 shows the dependence of the number of spallated nuclides on the incident proton energy when the ^{237}Np target(20 cm in diameter, 60 cm in length) is bombarded by protons. The number of nuclides transmutated by one proton with 1.5 GeV in energy is about 5 but it is too small to manage TRU wastes in the commercial base. It must be noted that several tens of neutrons of hard energy spectrum are emitted in the spallation reaction. The computer simulation results show that the number of spallation neutrons generated in the targets of actinides such as U, Np and Am, and heavy elements such as Pb and W increases monotonously when the proton energy increases up, as seen in Fig. 4. For the case of ^{237}Np target(20 cm in diameter, 37 cm in length) bombarded by a 1.5 GeV proton the neutron number is $\sim$40. The application of these neutrons to the transmutation system is described later.

(2) NMTA/JAERI[3]

In the improved version of NMTA, which is named to the statistical routines analyzing the Monte Carlo events in the NMTC/JAERI computation, the new subroutine HEATDP has been installed. HEATDP was developed at JAERI to calculate the energy

deposition and its spatial distribution for each component such as ionization loss energy and recoiling energy of fission and spallation products without γ -ray heating of excited residual nuclei in the high energy range. Figure 5 represents the dependece of total heat deposition in a metal target (20 cm in diameter, 60 cm in length) as a function of the injected proton enenrgy. $H_U^T$and H_U^I denote total heat deposition and ionization loss energy in a natural uranium target, respectively and H_{Pb}^T is total heat deposition in a lead target. The difference between H_U^T and H_U^I corresponds to the deposition of heat generated from the high energy fisson. The fraction of proton energy lost through the inonization decreases when the incident proton energy increases. The ionization loss becomes ~ 50 % of total heat deposition at 900 MeV. Figure 6 (a) and (b) shows the spatial distributions due to ionization loss energy and recoiling energy of SPs and FPs, respectively, for the 900 MeV proton injecting on the uranium target with 20 cm diameter and 36 cm length.

(3)NUCLEUS[4),5),6)]

The code NUCLEUS has been also developed at JAERI by modifying and combining the Monte Carlo codes NMTC/JAERI and a routine in NMTA/JAERI. The NUCLEUS can simulate the nuclear spallation reaction between a single target nucleus and a projectile without the internuclear nucleon transport process, in order to make direct evaluations of physical and computational models efficiently. The results computed by this code can also be compared directly with the data of thin foil spallation experiment, in which the internuclear multiple scattering have little effects. In NUCLEUS the counting region of reaction products was extended to avoid the count loss due to the dimension limitation in the computer program. As for a mass formula the Uno & Yamada' mass formula[7)] has been optionally adopted to upgrade the particle evaporation calculation. New several plotter routines were also provided for rapid processing of a huge amount of output data. Figure 7 compares the original calculational data with the upgraded ones for mass number distributions of reaction products with Z from 92 to 82 from a uranium nucleus spallated by a 1 GeV proton. In the central case with the extended counting region, the counting loss is recovered

and the left tail of peaks appears in the reasonable form in comparison to the left figure for the original region. By the use of Uno & Yamada's mass formula, the corrected peaks in the right figure have become wider than the central case.

On the other hand the NUCLEUS computation presents the important, basic data for researching the feasibility of TRU transmutation induced by the spallation process. In Fig. 8 the bird eye's views of yields of products are drawn in log scale for the cases of 1 GeV proton impinging on a) uranium and b) lead nuclei. The yield consists of three components, namely, the hill of spallation products, the spire of evaporated particles and the valley of high energy fission product between them. It is apparent that the yield of SP is greater than FP by two orders. Table 1 summarizes the number of produced light particle such as proton, neutron, deutron, triton, helium 3 and alpha. They are emitted from a uranium target nucleus bombarded by protons with the energy of 380 MeV to 2.9 GeV. The number of emitted particles has the maximum value around 2 GeV, where the neutrons more than 17 are emitted from one uranium nucleus. The result suggests that the incident proton energy has the optimum value around 2 GeV for neutron production. Figure 9 shows the histogram of half life distributions of products when a 2 GeV proton bombarding on ^{237}Np and ^{241}Am target nuclei. The shaded portions in the half life classifications of 7 and 9 represent tritons and deuterons & heliums respectively. The nuclides included in the classification 8 are a few. These nuclides are considered to be most harmful from the hazardous point of view. Most of SP in this case have the halflife shorter than one year.

(4) SPCHAIN, SPD

The composition and amount of residual nuclides accumulated in the target spallated by the proton beam is very improtant for the feasibility study of proton-induced TRU transmutation. Actually, however, it is almost impossible to obtain exactly the time evolution of yields of all the nuclides in the target due to enormous computing time. A code for calculating approximately the process of spallation products, SPCHAIN, has been made on the base of the depletion code DCHAIN2,[8] which was developed for the calculations of decay and build up of fission products in a

nuclear reactor. We have modified the one point depletion equation to include the transmutation, decay and build up processes of TRU and spallation products(SP) in the following,

$$
\begin{aligned}
dX_i(t)/dt = \; & \Sigma\, l_{i,j}\, \lambda_j X_j(t) + \Sigma\, k_{i,j}\, \Phi\, \sigma_{c,j} X_j(t) \\
& - (\lambda_i + \Phi\, \sigma_{c,i}) X_i(t) + \gamma_i F(t) \\
& + \Sigma\, \alpha_{i,j}\, \Phi_P \sigma_{s,j} X_j(t) - \Phi_P \sigma_{s,i} X_i(t),
\end{aligned}
$$

where the last two terms due to the spallation have newly been added to four original terms used for the reactor burnup calculation. α, σ_s and Φ_P represent the production rate of SP, the spallation cross section and high energy particle flux, respectively. The equation can be solved analytically by the Bateman method. As shown in Figure 10, some necessary data are feeded from the surrounding codes. When the halflife time of a nuclide was not obtained in the prepared data, it was calculated by using the β decay calculation program SPD[9] or guessed from the trend of data of nuclides, which are located in the neighbor of the nuclide in the Nuclear Chart. The production rate α of SP was computed by using the code NUCLEUS. The spallation cross section has been interpolated or extrapolated from the measured data[10] given for proton energy and target nucleus. The new data of decay types, decay constants, branching ratios and decay schemes have been compiled in the SPCHAIN data library for about 1100 nuclides.[11] The the preliminary result in SPCHAIN calculations is shown. Figure 11 shows the activity rate distribution of residual elements in a ^{241}Am target after one year cooling after 10 hours irradiation of 1 GeV protons with 10 mA. The high activity peaks around Z = 80 just after irradiation disappear due to the short halflives of SP and the activities buildup to Au, Os and Lu isotopes, whereas the higher actinide activity such as Np and Pu increases. So they should be transmuted through the continued spallation process. Activities due to fission products are a few.

(6) Other codes (ACCEL[12], SP-ACE)

A simulation code system ACCEL had been developed by connecting NMTC/JAERI with the neutron transport Sn code TWOTRAN-II through the neutron source file, accompanying the nuclear

data files. This system can calculate all the reaction processes occured in the target for the whole energy range less than 3 GeV as one computing job as shown in Fig. 12.

The SP-ACE code system is being developed for designing the transmutation core system driven by proton accelerator in the energy range below 15 MeV in reasonable computing time and precision. The neutron transport code RABBLE-THERMOS computes the region-wise neutron flux, using ultra fine energy group constants and the distribution of spallation neutron source, which can be obtained from Monte Carlo calculation in NMTC/JAERI. These fluxes and nuclear data are utilized to calculate the yield of products, heat generation and gamma ray intensity in each region by the burnup code COMRAD.

Ⅲ. CONCEPUTUAL DESIGN STUDY OF ACCELERATOR TRANSMUTATION SYSTEM

We have been promoting the conceptual studies on the TRU transmutation in the target-core system driven by an accelerated proton beam.[13),14),15)] For the reaction below 15MeV the Monte Carlo neutron transport code MORSE-DD [16)] was used with 52 neutron group constants edited from JENDL-2 and ENDF-B4, where spallation neutrons calculated by NMTC/JAERI code were treated as the source.

The basic conditions for the system design are (1) transmutation of 260 kg of TRU in a year, which is produced from ten commercial reactors of 1GWe and (2) good energy balance, in which it can generate enough electricity to operate the accelerator at least. Here total amount of TRU produced per year from 1 GWe PWR is about 26 kg/y, 56 % of which is ^{237}Np. Figure 13 is the target-core configuration of hybrid transmutation system driven by high power proton beam with the energy of 1.5 GeV and the current of several tens of mA. The tungsten target is installed in an TRU-fueled subcritical core surrounded by the HT-9 steel container. The system has dimensions given in the figure. A beam window is located at a depth of 0.7 m from the front face. The heat generated in the TRU fuel is removed by the forced circulation of liquid metal coolants Na/Pb-Bi. The core consists of metallic alloy fuel of TRU and provides considerably harder neutron spectrum than the other types of fuels. The fuel

pin cell geometry is shown in Fig.14 with a diameter of 4 mm cladded with HT-9 steel.

Profiles of the two-dimensional power distribution for four cases of the system cooled by Na and Pb-Bi, with and without the tungsten target, were calculated as shown in Figures 15 (a) to (d), respectively. It is apparent that the power peaking which occurs just behind the beam window is lower in the system with the tungsten target than in the one without it due to the flattening effect for cases of both coolants. The flattened power distribution allows higher beam current and increases the average number of transmuted nuclides. The system performance for these cases was summarized in Table 2. In the case of Na cooling and the tungsten target the maximum thermal power is 691 MW and the thermal power is sufficiently large to supply the electric power to the accelerator while the beam current required for the power is 22.6 mA. Without tungsten target the thermal power is 405 MW with the maximum and average power densities of 776 W/cc and 159 W/cc and its peaking factor is larger by a facter of 1.7 than the case with the tungsten target. The maximum powers of Pb-Bi cooled core are considerably lower than those of Na cooled one, while the beam current required is less than 8 mA. The maximum transmutation rate, 202 kg/year can be achieved for the core with the target cooled by Na. The changes of concentrations of some minor actinides with burn-up days in the reference system(Na cooling, with tungsten target) have been also calculated, as shown in Fig.16, using the burnup code ORIGEN2. The amounts of ^{237}Np and ^{241}Am at 1500 burning days become one half of their initial inventries, while ^{238}Pu and ^{242}Cm build up, which are not contained in the initial loading.

IV. SUMMARY

Finaly we summarize the outline of the present report as following items,

(1) Developments of NUCLEUS and SPCHAIN codes and upgrade of simulatin codes,

(2) Analysis of the spallation reaction & cascade process in the high energy range for TRU transmutation and

(3) Conceputual design study of hybrid transmutation system (

TRU alloy fuelled core type) driven by an intense proton accelerator. In the present design concept the amount of TRU produced from about 8 units of 1GWe PWR can be transmuted for the case of the core with the tungusten target cooled by Na and with the proton beam of energy 1.5 GeV and current 23 mA.

Furthermore we have the research items in the near future as

(a) Evaluation and upgrades of simulation codes based on new evaluated data and data measured in the spallation experiments which are being carried at KEK,

(b) Conceputual design study of hybrid transmutation system (TRU molten salt fuelled core type) and

(c) Analyses of irradiation tests for accelerator structural materials and the beam window in the target-core.

REFERENCES

1) Y. Nakahara, T. Tsutsui: JAERI-M 82-198 (1982) (in Japanese).
2) Y. Nakahara : ICANS-IV, Proc. (1980).
3) T. Nishida, Y. Nakahara, T. Tsutsui : JAERI-M 84-154 (1984) (in Japanese).
4) T. Nishida, Y. Nakahara, T. Tsutsui : JAERI-M 86-116 (1986) (in Japanese).
5) T. Nishida, Y. Nakahara : Kerntechnik, 50, 193 (1987).
6) T. Nishida, Y. Nakahara : Kerntechnik, 55, No.3, 147(1990).
7) M. Uno, M. Yamada : Prog. Theor. Phys., 65, No.4, 1322(1981).
8) K. Tasaka : JAERI-M 8727 (1980).
9) T. Yoshida : JAERI-M 6313 (1975).
10) W. Schimmerling et al. : Physical Review C 1, 248 (1973).
11) Table of Isotope (7th version).
12) Y. Nakahara, T. Tsutsui, Y. Taji : JAERI-memo 9502 (in Japanese, internal report).
13) H. Takano, T. Mukaiyama :" Nuclear Characteristic Analysis of TRU Burner Reactors", JAERI-M 89-072 (1989)(in Japanese).
14) T.Takizuka, I. Kanno, H. Takada, T. Ogawa, T. Nishida, Y. Kaneko : " A Study on Incineration Target System," Proc. ICENES (1989)(Karlsruhe).
15) Y. Kaneko : " THE INTENSE PROTON ACCELERATOR PROGRAM," Proc.

2nd Int. Symp. on Advanced Nuclear Energy Research - Evolution by Accelearator -, (1990)(Mito).

16) M. Nakagawa, et al., " MORSE-DD A Monte Carlo Code Using Multi Group Double Differential Form Cross Sections," JAERI-M 84-126 (1984).

Table 1 Number of light particles emitted from a uranium target nucleus bombarded by protons with the energies of 380 MeV to 2.9 GeV

Emitted particle	Energy of incident proton (MeV)			
	380	1000	2000	2900
Proton	0.994	2.924	3.697	3.276
Neutron	12.085	16.050	17.319	15.243
Deutron	0.1249	0.7063	0.9108	0.7729
Triton	0.0576	0.2719	0.3407	0.2956
Helium 3	0.0010	0.0258	0.0411	0.0361
Alpha	0.0732	0.2777	0.3079	0.2588

Table 2 Performance of the TRU transmutation system

Core system	with W target	with W target	without W target	without W target
Coolant	Na	Pb-Bi	Na	Pb-Bi
k-effective	0.92	0.86	0.94	0.95
Beam current(mA)	22.6	7.5	18.4	5.4
Thermal power(MW)	691	484	405	163
Power density(W/cc)max	889	523	776	425
ave	307	246	159	83
Burnup rate of TRU (kg / year)	202	139	114	42
Unit of 3 GWt LWR	7.6	5.3	4.3	1.8

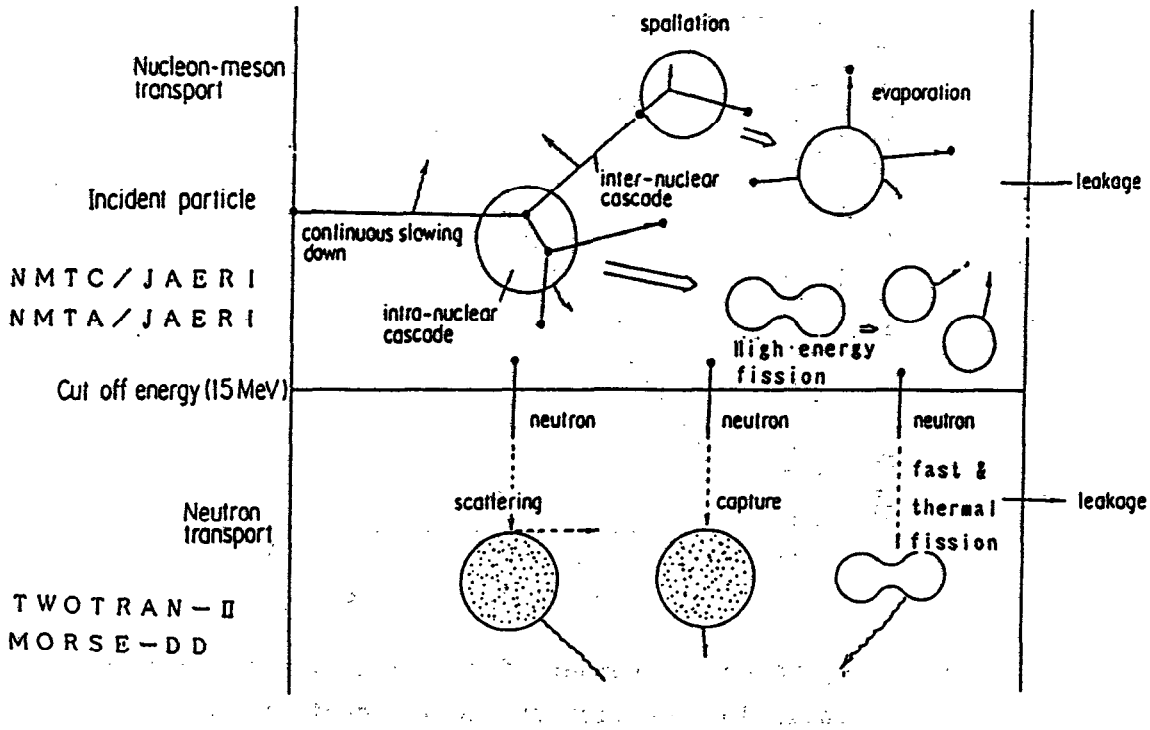

Fig. 1 Schematic illustration of nuclear reaction and nucleon transport process in a heavy metal target irradiated by the high energy proton beam.

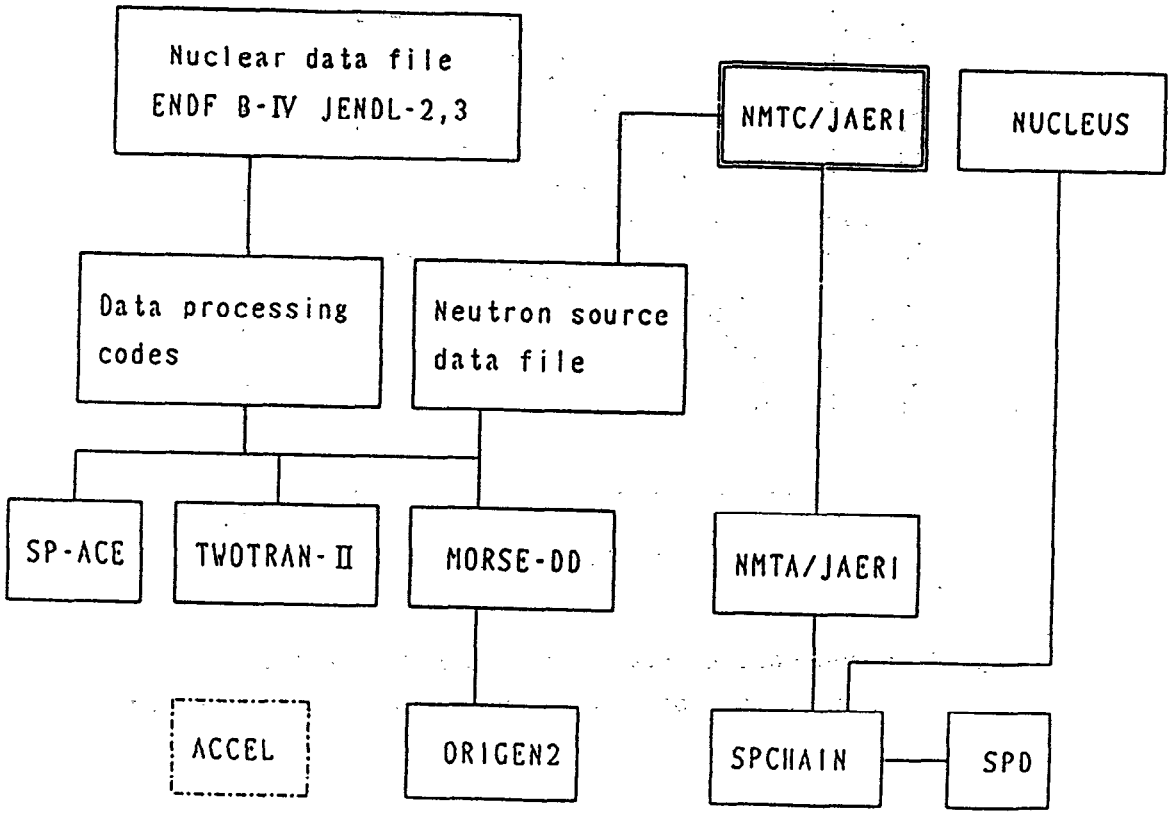

Fig. 2 JAERI code system for the spallation transmutation

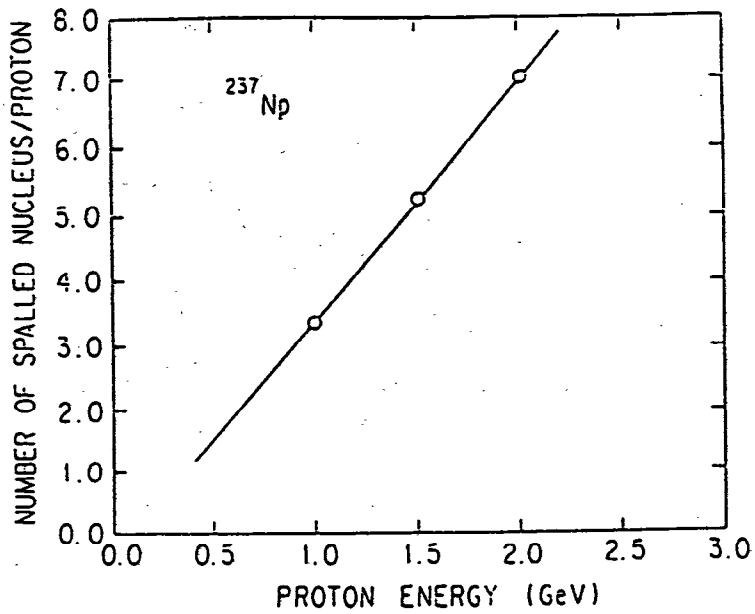

Fig. 3 Dependence of number of nuclei destructed due to spallation reaction on the incident proton energy

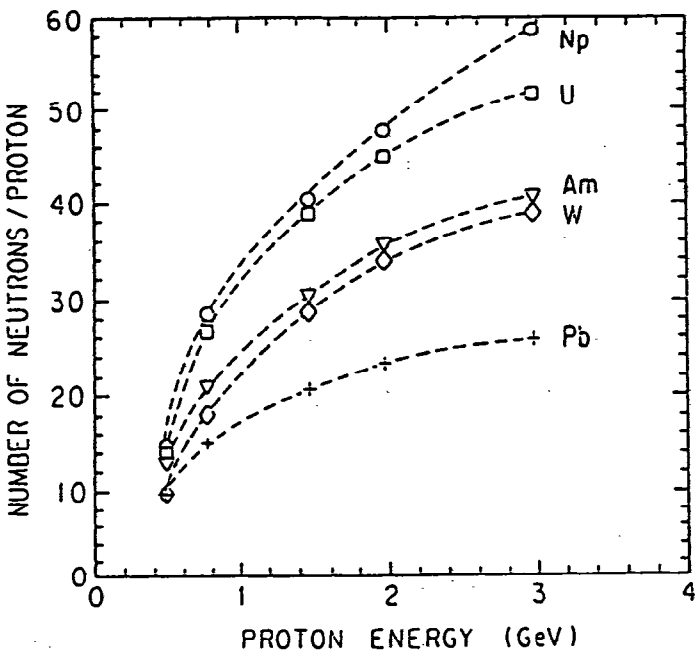

Fig. 4 Dependence of number of neutron generated in spallation reaction on the incident proton energy

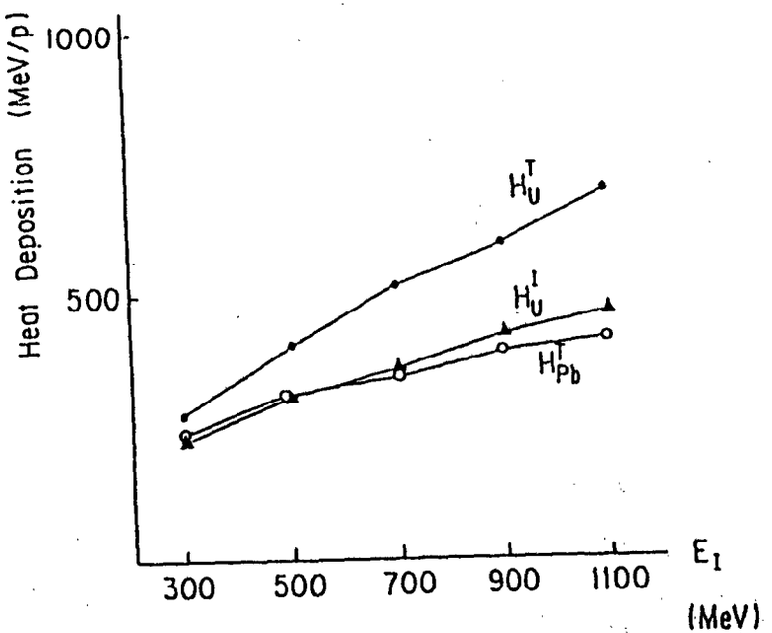

Fig. 5 Variation of total heat deposition as a function of the injected proton enenrgy

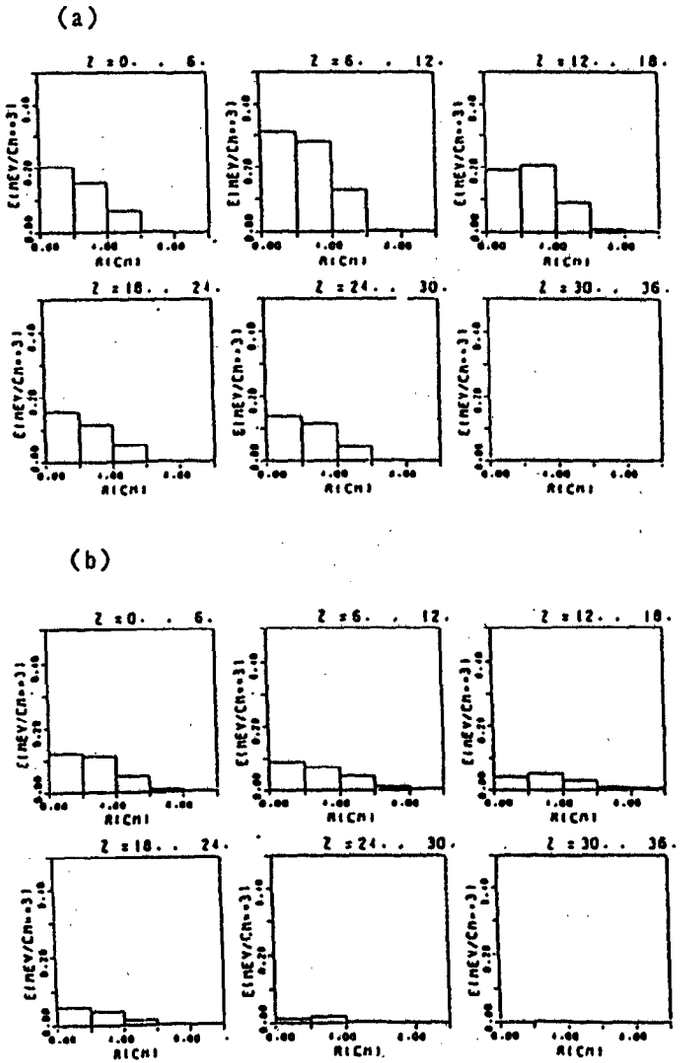

Fig. 6 Spatial distributions due to (a) ionization loss energy and (b) recoiling energy of SPs and FPs for the 900 MeV proton injecting on the uranium target

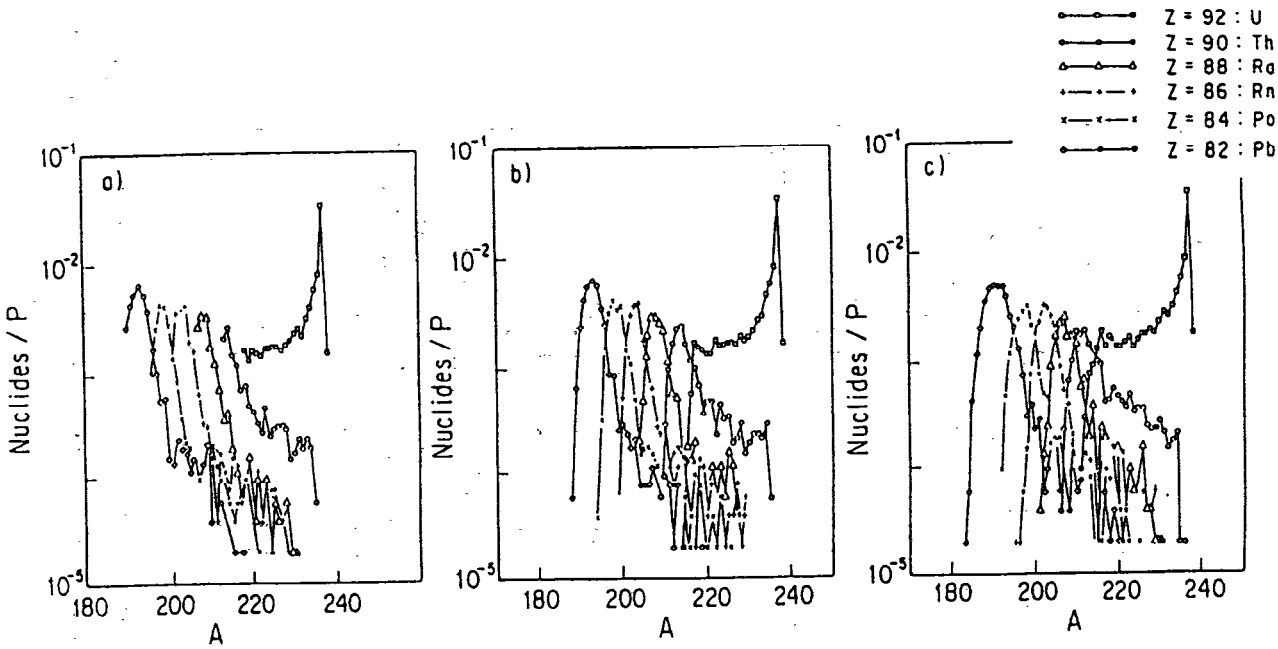

Fig. 7 Mass number distributions of products with Z from 92 to 82 from a uranium nucleus spallated by 1 GeV protons for cases of a) original version, b) extended region and c) extended region & Uno Yamada mass formula

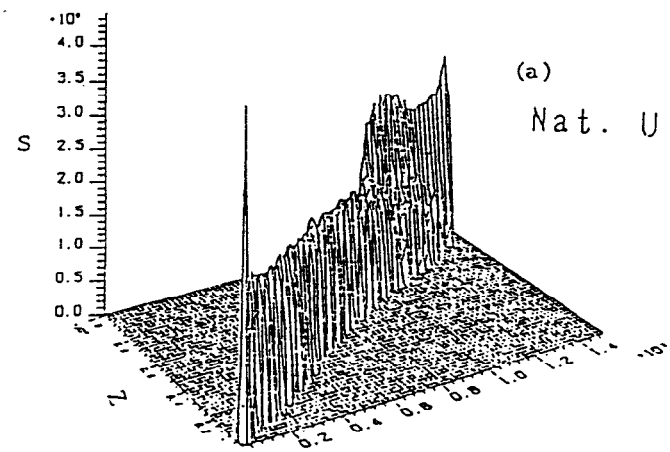

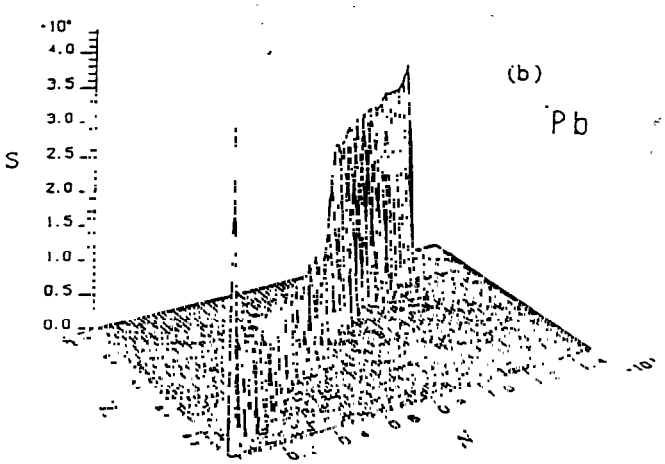

Fig. 8 Bird eye's views of yields of products for the cases of 1 GeV proton impinging on a) uranium and b) lead nuclei

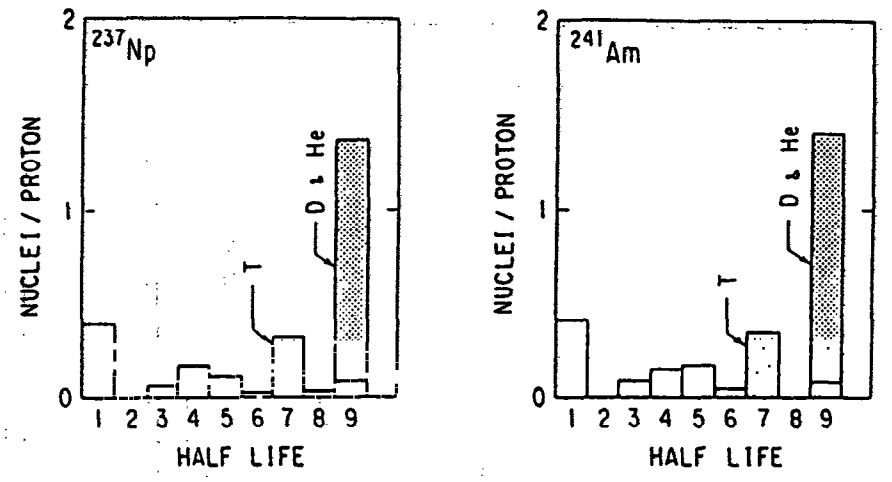

Classification by Half Life $T_{1/2}$

1 :	$0s < T_{1/2} < 10^{-3}s$	6 :	$5d < T_{1/2} < 1y$
2 :	$10^{-3}s < T_{1/2} < 1s$	7 :	$1y < T_{1/2} < 100y$
3 :	$1s < T_{1/2} < 1m$	8 :	$100y < T_{1/2} < 1 \times 10^{8}y$
4 :	$1m < T_{1/2} < 1h$	9 :	Stable Nuclides
5 :	$1h < T_{1/2} < 5d$		

Fig. 9 Histogram of half-life distributions of products when 2 GeV protons bombards on ^{237}Np and ^{241}Am target nuclei

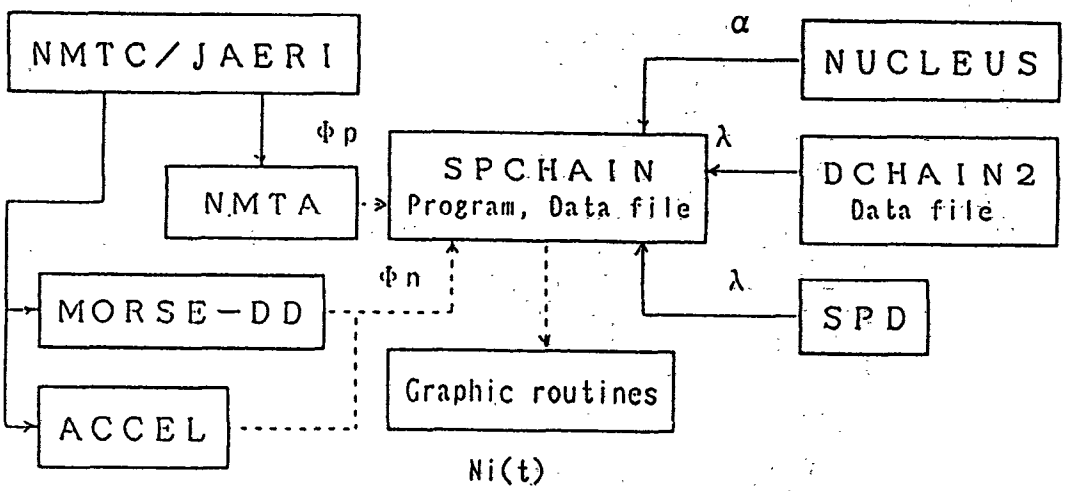

Fig. 10 Codes surrouding the SPCHAIN code

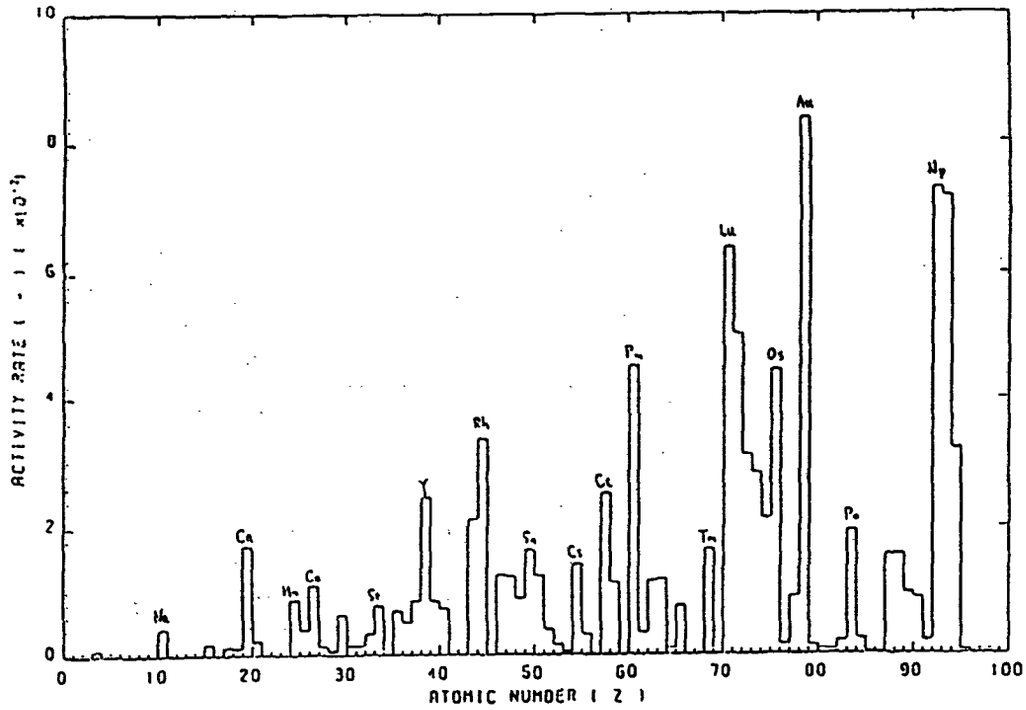

Fig. 11 Activity rate distribution of residual elements in a ^{241}Am target at the time stage of one year cooling after irradiation of ten hours of 1 GeV protons

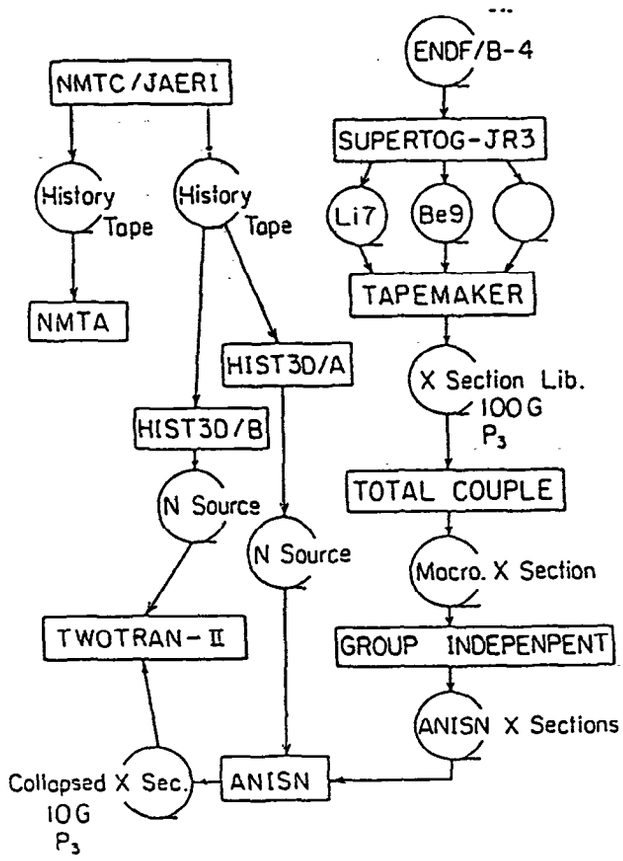

Fig. 12 ACCEL code system

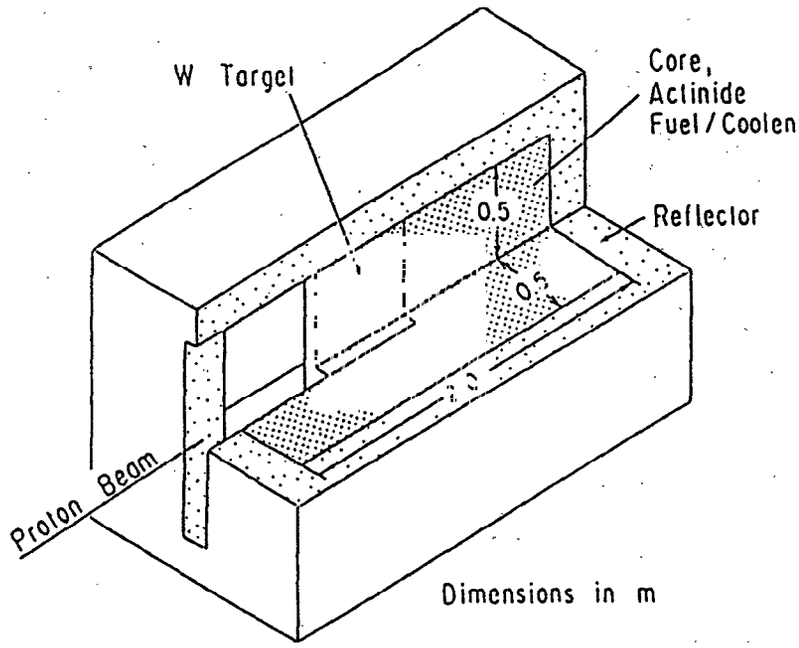

Fig. 13 Target-core configuration of hybrid transmutation system

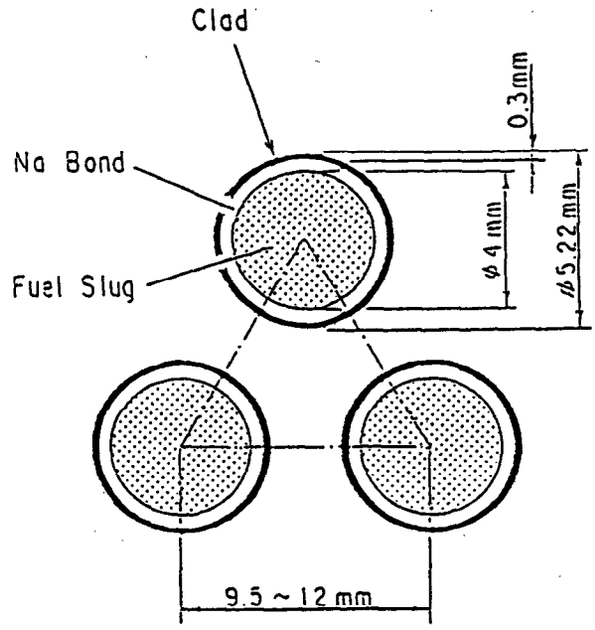

Fig. 14 TRU fuel pin geometry

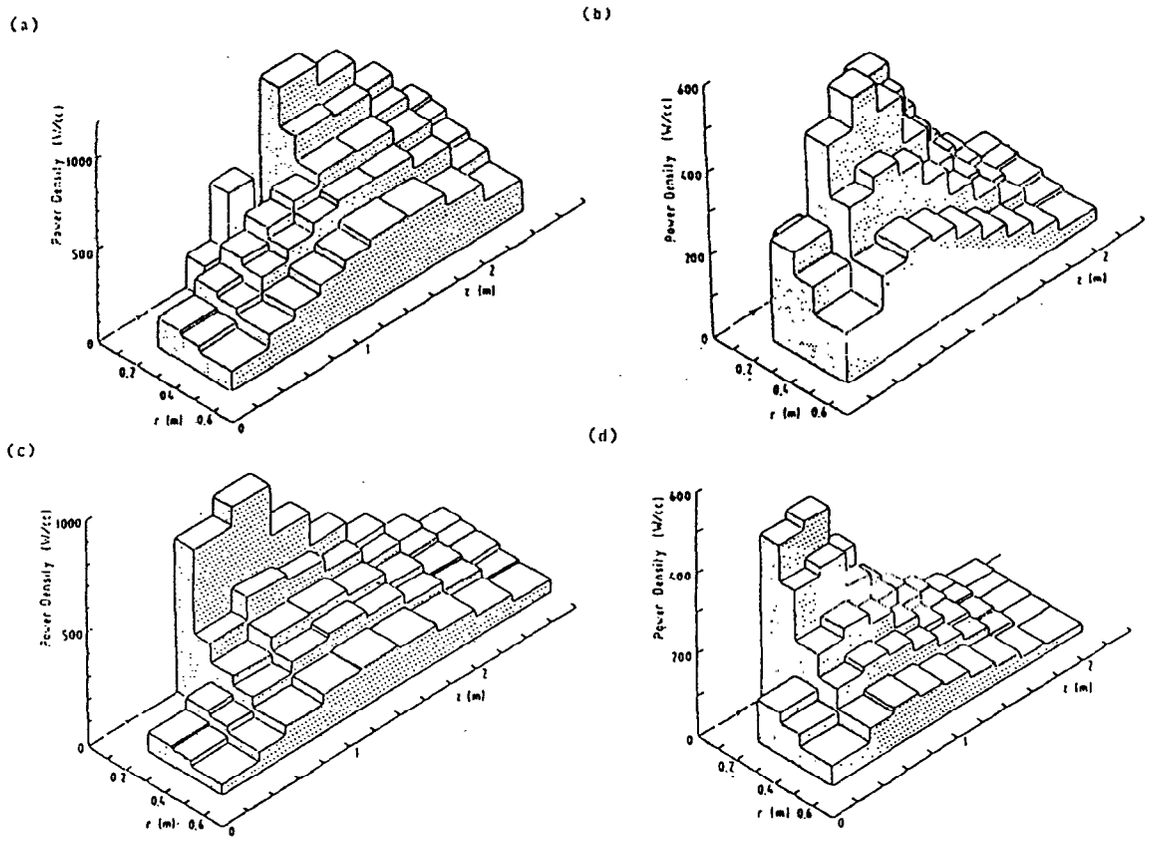

Fig. 15 Power distributions : (a) Na cooled , tungsten-loaded target, (b) Pb-Bi cooled , tungsten-loaded target, (c) Na cooled, TRU alloy target, (d) Pb-Bi cooled, TRU alloy target

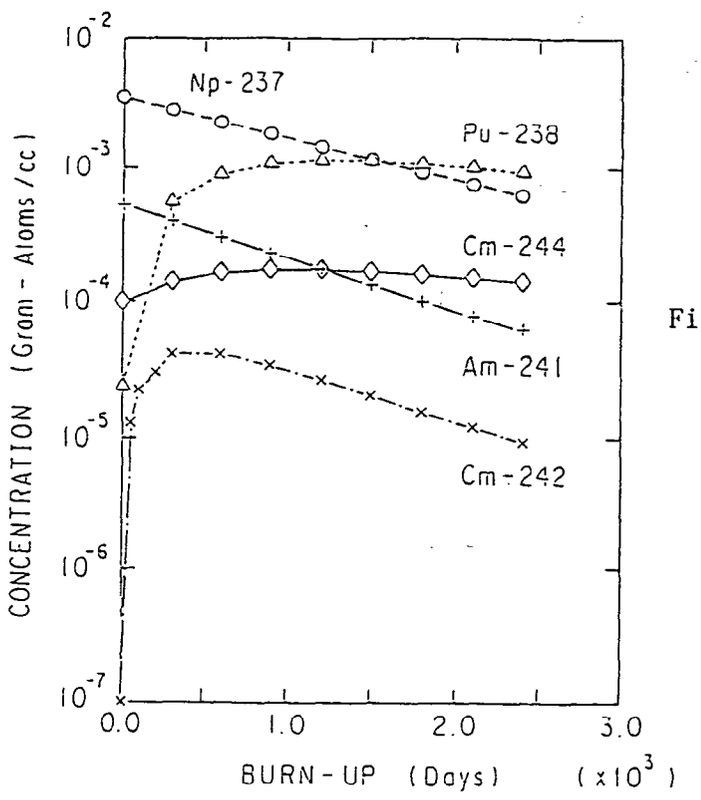

Fig. 16 Change of trans-uranium inventory with burn-up in the system

ICANS-XI International Collaboration on Advanced Neutron Sources
KEK, Tsukuba, October 22-26, 1990

The Neutronic Performance of Solid-Target Alternatives for SINQ

F. Atchison
PAUL SCHERRER INSTITUTE
CH-5232 Villigen PSI, Switzerland

ABSTRACT
The results from calculations of the neutronic performance of three possible 'solid' targets and that of the current version of the liquid Pb-Bi target are presented. Two are 'conventional' transverse cooled plate structures, one using tantalum, the other tungsten. The third is a Pb-shot based pebble-bed design. Some general results on the effect of neutron absorption on the performance of the Pebble-bed target are given.

1 Introduction

Neutronically, a liquid Pb target will always be the best possible target system for SINQ or any high-power continuous neutron source (solutions involving fissile materials discounted). The advantages are well known and are, briefly: (i) a high material density in the neutron production region, (ii) a low thermal neutron absorption cross-section, (iii) the target material can be flowed to act as its own primary coolant and has a high heat-transfer capability, (iii) radiation damage to the main bulk of the target material (at least) is not a major concern.

The realisation of such a target system has to balance neutronic requirements with practical considerations (material compatibility, safety, reliability etc.). The present design has a neutronic performance below our original hopes and still raises some doubts concerning reliability. The primary purpose of the study was to provide numbers which would allow the investment in this target system to be related to thermal neutron flux gain. The neutronic performance of the current design for the Pb-Bi target (including pertinent engineering details) and three alternative targets has been calculated. Two of the alternatives are based on transverse cooled plates of tungsten and tantalum respectively and the third is a Pebble-bed of Pb-shot [1]. The comparison of these systems is not strictly 'fair' as the alternative targets are only preliminary concepts and biased heavily to neutronic requirements, but some preliminary estimates for principal dimension (e.g. plate thicknesses to allow operation at 1.5 mA, dimensions that match those for the moderator etc.) are included.

To obtain the highest thermal neutron intensity (i) the neutron production should be concentrated in as small a volume as tolerable (which means also that the heat density will be high - about 40 MeV is deposited in the target per fast neutron produced), (ii) interactions with lighter-mass 'materials of construction' which encroach into the 'target region' should be avoided and (iii) as many of the fast neutrons as possible should be brought to thermal energies in accessible regions of the moderator.

All the neutrons will be lost eventually, at best through the outer wall of the moderator, as in this way the long random-walk involved leads to the highest concentration of neutrons in the moderator and hence neutrons available to the users. The major cause of flux reduction is neutron loss in the target region, either in the slowing-down process or as thermals by absorption: such neutrons will make only short random-walks and hence little or no contribution to the useful neutron intensity. Neutron loss in the region of the target cannot be totaly eliminated (e.g. those emitted back into the proton beam direction) but absorption loss can be kept to the minimum by the careful choice of materials.

A brief description [2] of the models of the individual systems together with calculation results, will be given in the next section. A performance comparison and some comments will be given in section 3. Section 4 will present the results of a more general examination of the effect of target neutron absorption.

Numbers in square brackets refer to entries in the section "Reference and notes": some details usefull but not strictly relevant to the main theme of the paper have been moved to this section together with references.

2 Performance of the various target systems

The calculations [3] have been made changing the target system within a fixed model of the SINQ moderator tank system as sketched in Fig. 1. The proton beam energy was 570 MeV and the beam current density distribution picked from that calculated for the present design for the SINQ proton channel [4]: the beam current density was approximately 17 $\mu A/cm^2$ at the peak (for 1 mA on target) and corresponded roughly to a radially symmetric Gaussian. The beam diverges from a focus below the beam window with an angle of approximately 30 mrad. The results are presented as (i) a two-part table with the distribution of energy in the inner parts of the system and the neutronic performance and (ii) a map of the undisturbed thermal neutron flux [5].

(a) Pb-Bi Eutectic Target: the design is fully described in (for example) [6] and the results give a reference standard for the flux comparison. The energy distribution and neutronic details are shown in Table I and the thermal-neutron flux distribution in Fig. 2.

(b) Plate Targets: the same conservative (author's claim) first estimates for the plate dimensions and coolant channel widths, to allow operation at proton currents up to 1.5 mA, have been used for both tungsten and tantalum. The systems are summarised in Fig. 3. D_2O is used as the cooling fluid and aluminium as the material of construction. The plate stack length was about 21 cm and the neutronically-sensitive region above the target and within the limits of the moderator filled with D_2O. The tantalum target was modelled with

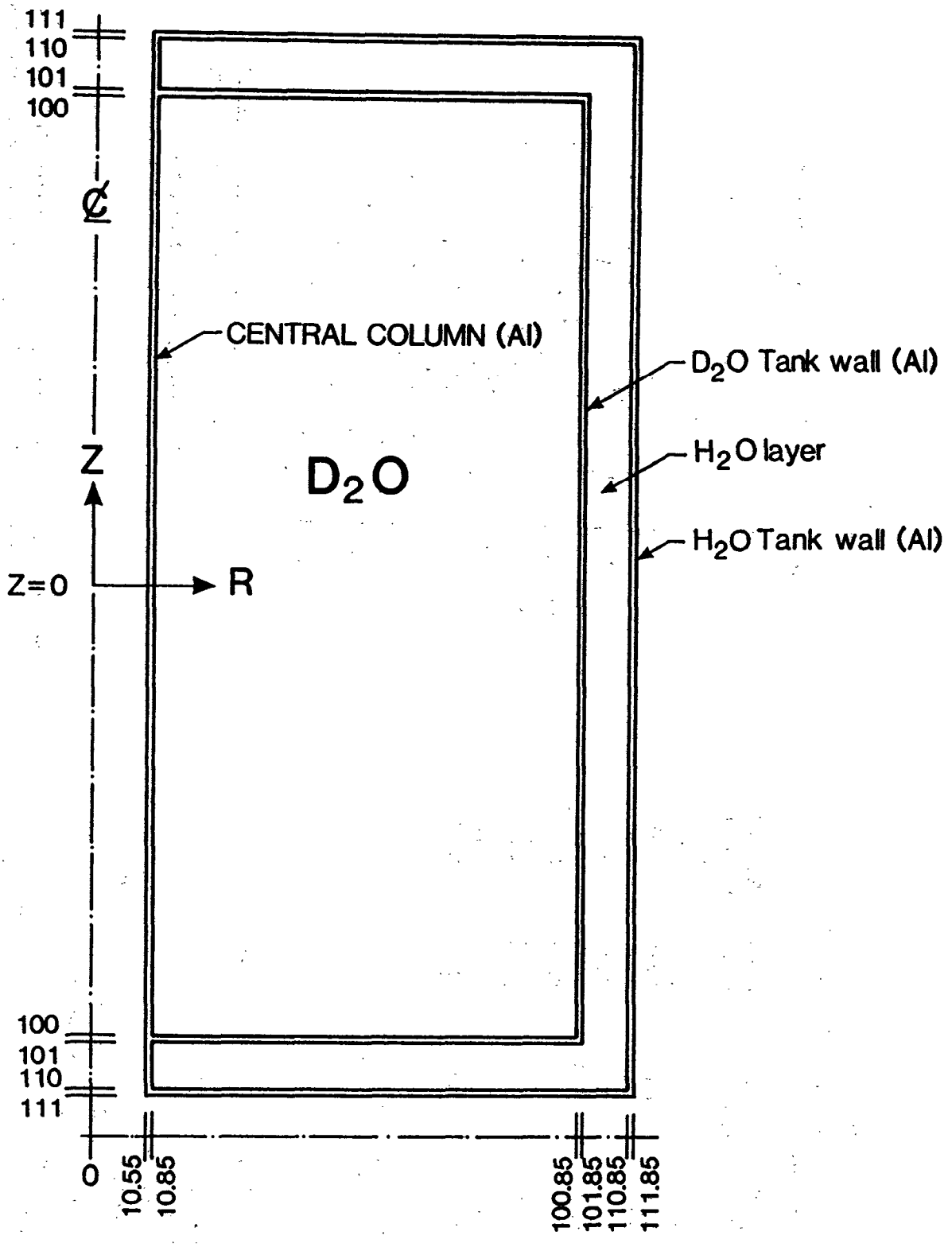

Figure 1: A sketch of the moderator tank assembly used in the calculations. The system is radially symmetric about the centre line of the central column. Dimensions are in centimetres and all walls shown are of 'pure' aluminium. Each of the target systems is mounted in the central column.

TABLE-I

(a) Energy Distribution in the Inner Regions of SINQ with the Pb-Bi Target.

Component	dE/dX(1) MeV/Proton	Gamma(2) MeV/proton	Absrptns /Proton	Energy(3) MeV/Proton
Target Material	382.06	11.25	0.235	1.59
Guide-Tube	16.07	0.64	1.053	8.01
Container Wall	2.10	0.15	1.324	10.06
Cooling Jacket	0.40	0.02	0.436	1.74
Window Complex	9.19	0.75	0.170	0.40
Central Column	0.69	0.03	0.253	2.73
D_2O	46.87	1.96	0.839	5.24
H_2O Layer	1.08	0.09	5.144	11.66
D_2O Tank Wall	0.24	0.03	0.656	7.09
H_2O Tank Wall	0.09	0.01	0.000	0.00
TOTALS	458.79	14.93	10.110	48.52

Notes:
(1) Ionization loss + Nuclear Recoil + Charged particles to rest.
(2) Prompt Nuclear Gammas + Pi zero decay.
(3) Absorption Gamma rays.

(b) Neutron Production and Loss Information

Neutrons per Interaction in Target	6.33
Interactions per Proton in Target	1.37
Neutrons per Proton in Target	8.70
Average Neutron Energy	3.42 MeV
Neutrons per Proton produced outside Target	1.30
Neutrons produced by Fast Neutrons (/proton)	0.455
Fast & Epithermal escapes	0.078
Thermal Neutron Escapes	0.213
Energy taken by H.E neutron escapes	15.93 MeV

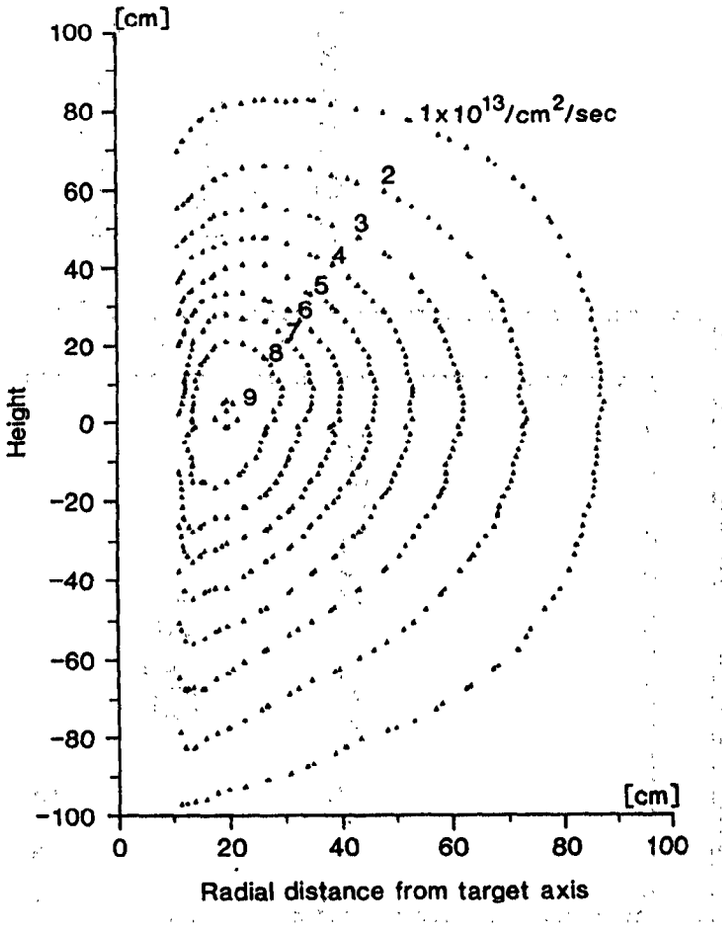

Figure 2: Contours of equal undisturbed thermal neutron flux in the heavy water for the Pb-Bi eutectic target at 1 mA proton current (see note 5 (ii)).

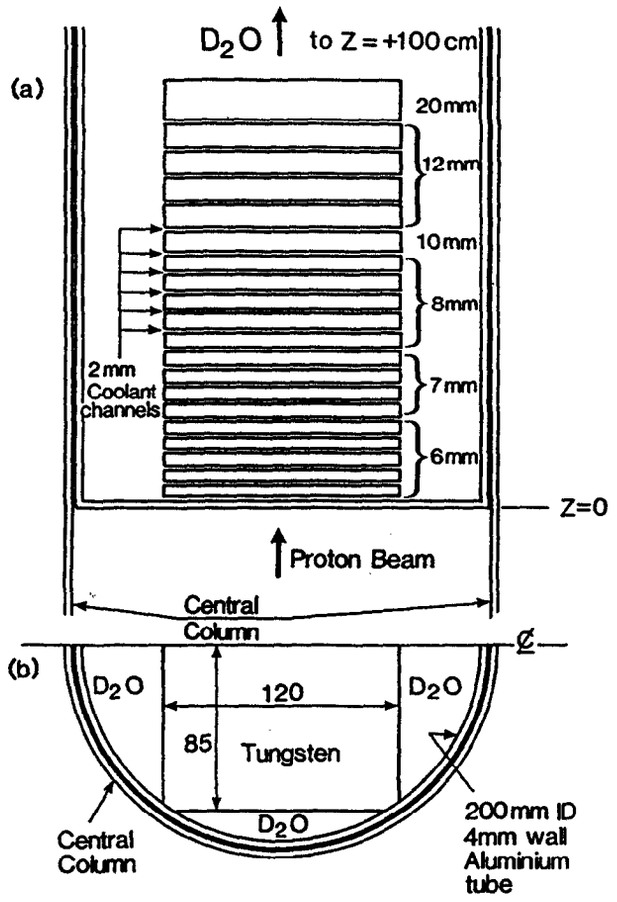

Figure 3: A sketch of the plate target systems.
(a) Vertical section: the heavy water above the plate stack extends to Z = + 100 cm.
(b) Cross-section of a tungsten plate: The 12 x 17 cm^2 plates are fitted into a 20 cm I.D. 4 mm wall aluminium tube to represent the manifold.
The tantalum plates (not shown) are 18 cm in diameter but also include an internal heavy water manifold (see reference 2 for more details).

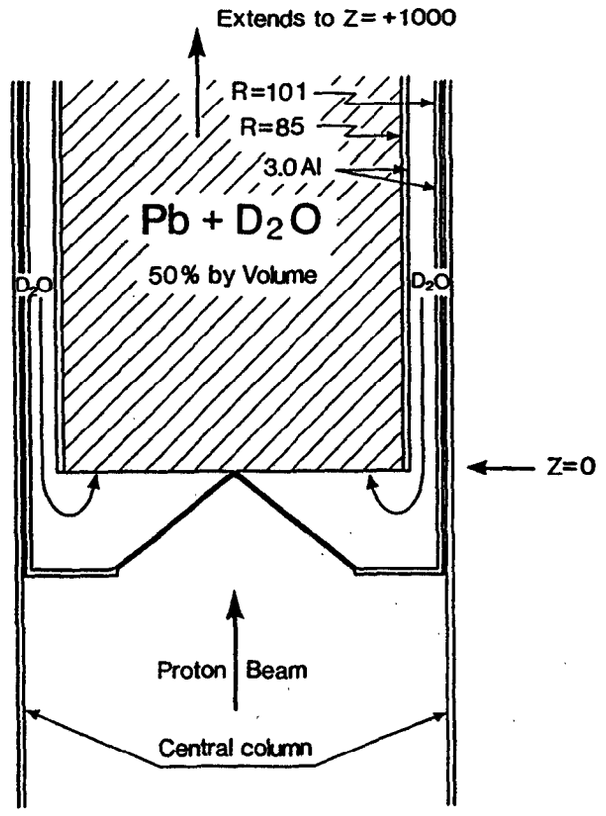

Figure 6: A sketch of a vertical section through the Pb-shot pebble bed target used in the calculation. Dimensions are in millimetres and the target extends upwards to Z = +1000 mm.

TABLE-II

(a) Energy Distribution in Inner Regions of SINQ with a Tungsten Target

Component	dE/dX(1) MeV/Proton	Gamma(2) MeV/proton	Absrptns /Proton	Energy(3) MeV/Proton
Target Material	379.037	12.018	4.961(4)	29.02
Heavy-water Gaps	14.684	1.342	0.000	0.00
Heavy Water Dump	10.294	0.359	0.004	0.03
Vessel Wall Complex	4.411	0.185	0.461	4.97
Window	2.144	0.187	0.007	0.08
Central Column	1.086	0.049	0.241	2.55
D_2O	35.144	1.754	0.525	3.28
H_2O Layer	1.324	0.078	3.234	7.21
D_2O Tank Wall	0.328	0.036	0.411	4.44
H_2O Tank Wall	0.065	0.009	0.000	0.00
TOTALS	448.517	16.017	9.844	51.58

Notes:
(1) Ionization loss + Nuclear Recoil + Charged particles to rest.
(2) Prompt Nuclear Gammas + Pi zero decay.
(3) Absorption Gamma rays.
(4) 58% of this loss during slowing-down.

(b) Neutron Production and Loss Information

Neutrons per Interaction in Target	5.64
Interactions per Proton in Target	1.50
Neutrons per Proton in Target	8.483
Average Neutron Energy	3.47 MeV
Neutrons per Proton produced outside Target	1.102
Neutrons produced by Fast Neutrons (/proton)	0.453
Fast & Epithermal escapes	0.055
Thermal Neutron Escapes	0.131
Energy taken by H.E neutron escapes	21.40 MeV

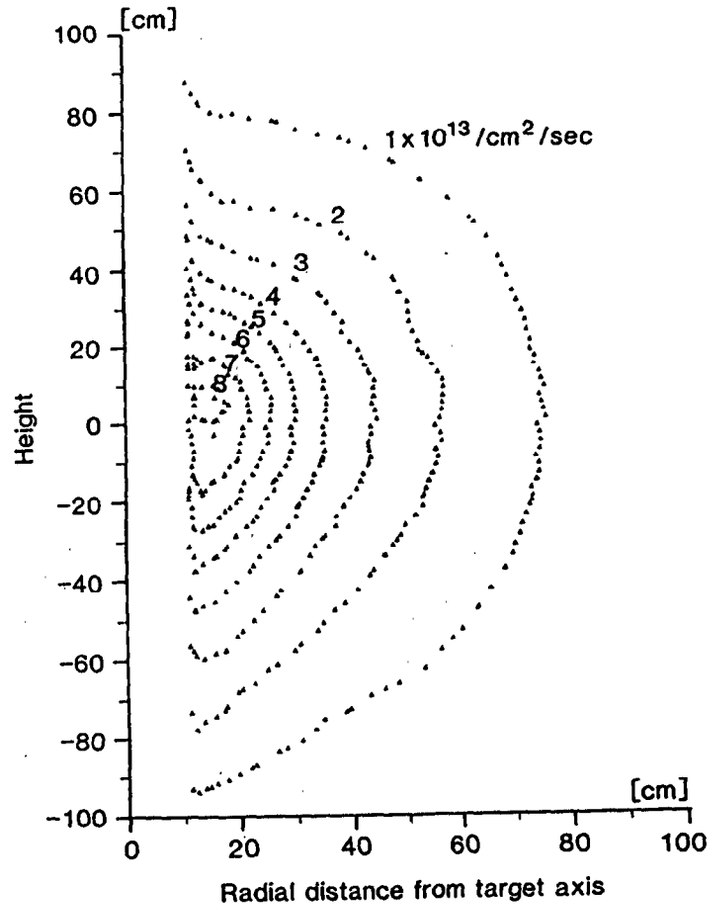

Figure 4: Contours of equal undisturbed thermal neutron flux in the heavy water for a Tungsten-plate target at 1 mA proton current (see note 5 (ii)).

a more elaborate "minimum-coolant-volume" manifold [2]. The tungsten results are shown in Table-II and Fig. 4 and those for tantalum in Table-III and Fig. 5. The quite high loss in the slowing-down process (down to 1.46 eV) should be noted.

(c) Pebble-bed Target: this target design was proposed by G. Heidenreich and is described in [1]. The geometry of the target used for the calculations is shown in Fig. 6. The values for the principal parameters assumed in the calculation were: (i) 50% volume fraction of Pb - represented by a homogeneous mixture, (ii) D_2O as cooling medium and (iii) aluminium for the beam window and target container. The energy partition, neutron production information and flux map are in Tables IV and Fig. 7.

3 Summary of Results and Comments

The neutronic information for the four systems is collected in Table-V. The relative performance is obtained from the maximum undisturbed thermal flux at a radius of 25 cm in the moderator (a typical beam-tube radial position). The importance of minimising the neutron loss in the target region is clearly evident: the lower losses in the 'Target Auxiliaries' of the Pb-shot pebble-bed target outweigh the better primary neutron production of the Pb-Bi to give a higher thermal neutron flux. Neutrons that manage to reach the outer limits of the moderator (i.e. absorbed by the H_2O or tank walls) are the ones that make the major contribution to the useful neutron flux: the '25 cm' fluxes in Table-V correlate quite well with neutron loss at the periphery of the moderator tank ($1.53 \pm .09 \cdot 10^{13}$ n°/cm^2/sec/mA for each neutron/proton lost at the periphery). Some comments specific to the individual target systems will now be given.

(a) Pb-Bi Target.

The neutronic performance of this target is about a factor of two lower than a theoretical 'best'. The principal causes are:-

20cm diameter target cf. 15cm	...20%
Interactions in guide-tube and other light nuclei	...10%
Absorption in auxiliary material within the target	...30%

0.8 X 0.9 X 0.7 = about 0.5

The first loss stems from thermo-hydraulic considerations and could be considered a consequence of being over-optimistic in defining the theoretical 'best'. The majority of the loss results indirectly from the inclusion of bismuth: it has the primary purpose of reducing the melting point and hence operating temperatures, but because of corrossion problems severely restricts the choice of materials of construction (presently a nickel-less steel). It also has considerable influence on safety system requirements (polonium). The losses also illustrate another concern in target design - the compounding of "small" loss factors to give a rather large effect overall. Work is in progress to find an alternative structural material.

(b) Plate Targets.

The high absorption cross-sections of tungsten and tantalum will always make these target materials better to avoid. Tungsten and tantalum are the highest mass materials which also have a high melting temperature and hence a good safety margin against melting when in

TABLE-III

(a) Energy Distribution in the Inner regions of SINQ with a Tantalum Target

Component	dE/dX(1) MeV/Proton	Gamma(2) MeV/proton	Absrptns /Proton	Energy(3) MeV/Proton
Target Material	387.722	11.706	6.086(4)	9.13
D2O gaps and spacers	15.447	0.462	0.266	0.40
Container Wall	0.699	0.055	0.067	0.72
Window Complex	9.227	0.608	0.174	0.26
D2O Dump above Target	2.919	0.121	0.003	0.02
Central Column	0.884	0.055	0.175	1.89
D_2O	33.254	1.731	0.434	2.71
H_2O Layer	1.082	0.089	2.756	6.15
D_2O Tank Wall	0.189	0.034	0.349	3.77
H_2O Tank Wall	0.088	0.013	0.000	0.00
TOTALS	451.511	14.874	10.310	25.05

Notes:
(1) Ionization loss + Nuclear Recoil + Charged particles to rest.
(2) Prompt Nuclear Gammas + Pi zero decay.
(3) Absorption Gamma rays.
(4) About 70% of the absorptions are during slowing down.

(b) Neutron Production and Loss Information.

Neutrons per Interaction in Target	5.80
Interactions per Proton in Target	1.51
Neutrons per Proton in Target	8.76
Average Neutron Energy	3.45 MeV
Neutrons per Proton produced outside Target	1.14
Neutrons produced by Fast Neutrons (/proton)	0.56
Fast & Epithermal escapes	0.053
Thermal Neutron Escapes	0.110
Energy taken by H.E neutron escapes	16.02 MeV

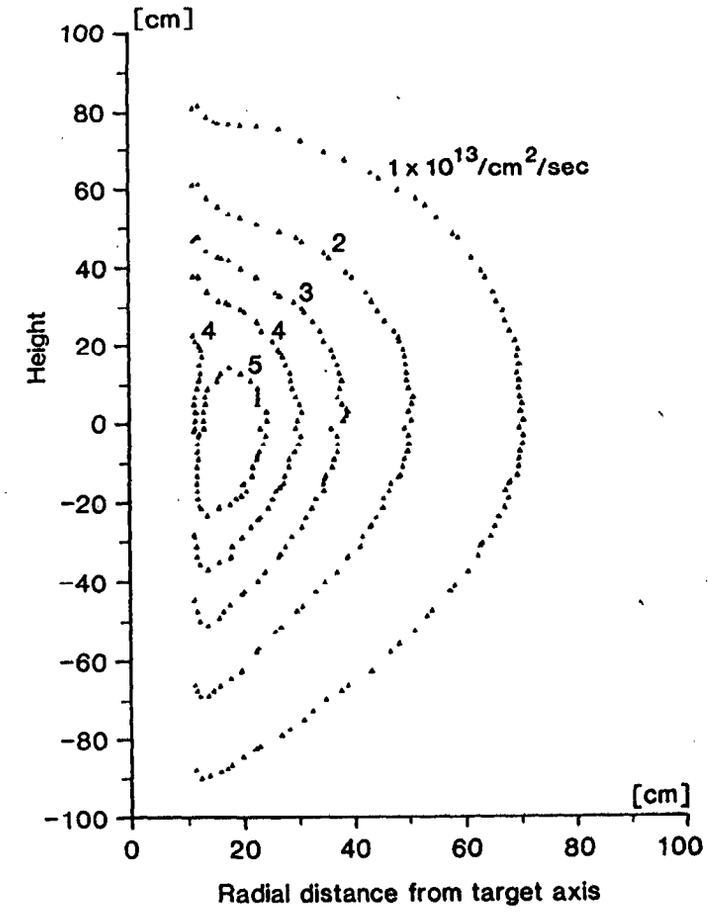

Figure 5: Contours of equal undisturbed thermal neutron flux in the heavy water for a Tantalum-plate target at 1 mA proton current (see note 5 (ii)).

TABLE-IV

(a) Energy Distribution in Inner Regions of SINQ with a Pb Pebble-bed Target

Component	dE/dX(1) MeV/Proton	Gamma(2) MeV/proton	Absrptns /Proton	Energy(3) MeV/Proton
Target Material	397.69	12.026	0.620	4.59
First Wall	2.113	0.082	0.187	2.02
Heavy-Water Downflow	4.990	0.124	0.007	0.04
Second Wall	1.523	0.076	0.255	2.75
Central Column	1.485	0.063	0.415	4.48
D_2O	49.410	2.111	0.915	5.71
H_2O Layer	1.491	0.126	5.646	12.59
D_2O Tank Wall	0.353	0.042	0.712	7.69
H_2O Tank Wall	0.078	0.012	0.000	0.00
TOTALS	459.133	14.662	8.757	39.87

Notes:

(1) Ionization loss + Nuclear Recoil + Charged particles to rest.
(2) Prompt Nuclear Gammas + Pi zero decay.
(3) Absorption Gamma rays.

(b) Neutron Production and Loss Information

Neutrons per Interaction in Target	5.682
Interactions per Proton in Target	1.298
Neutrons per Proton in Target	7.375
Average Neutron Energy	3.42 MeV
Neutrons per Proton produced outside Target	1.321
Neutrons produced by Fast Neutrons (/proton)	0.336
Fast & Epithermal escapes	0.063
Thermal Neutron Escapes	0.175
Energy taken by H.E neutron escapes	23.03 MeV

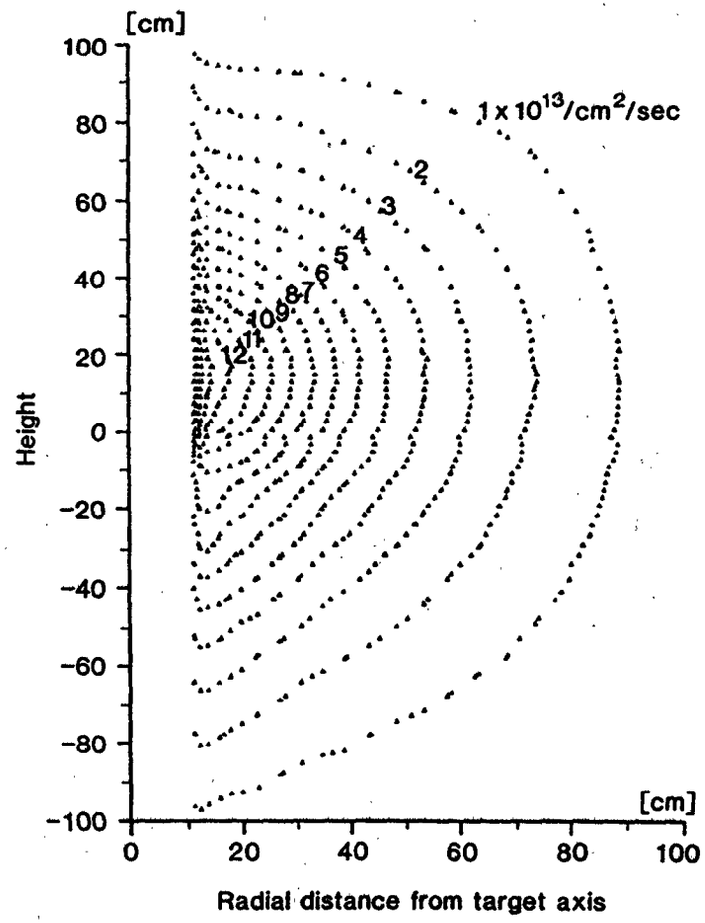

Figure 7: Contours of equal undisturbed thermal neutron flux in the heavy water for the Pb-shot pebble-bed target at 1 mA proton current (see note 5 (ii)). The Pb filling factor is 50% by volume. The low absorption in the target together with the significant quantity of moderator (D_2O) inside the target itself means that the flux maximum is close to or within the 'target'.

TABLE-V

Neutronic data for the four target systems calculated.

Target System	Pb-Bi	W	Ta	Pb Shot
Neutron Production				
(i) Target Complex	8.700	8.483	8.760	7.375
(ii) Moderator Complex	1.300	1.102	1.140	1.321
(iii) Fast Neutrons	0.455	0.453	0.560	0.336
TOTAL PRODUCTION	10.455	10.038	10.46	9.032
Neutron Loss				
(i) Fast/Epith. Escapes	0.078	0.055	0.053	0.063
(ii) Thermal Escapes	0.213	0.131	0.110	0.175
(iii) Absorption in:				
(a) Target Material	0.235	4.961	6.086	0.620
(b) Target Auxiliaries	2.983	0.472	0.510	0.449
(c) Heavy Water + CC	1.092	0.766	0.609	1.330
(d) Light Water + TWs	5.800	3.645	3.105	6.358
TOTAL LOSS	10.401	10.030	10.473	8.995
Approx. Flux Maximum	$9 \cdot 10^{13}$	$8 \cdot 10^{13}$	$5.5 \cdot 10^{13}$	$1.2 \cdot 10^{14}$
Radius of flux Max (cm)	20	15	17.5	small
Max. Flux at 25cm radius	$8.5 \cdot 10^{13}$	$6 \cdot 10^{13}$	$4.5 \cdot 10^{13}$	$1 \cdot 10^{14}$
ditto as %	100	70	53	117

operation. Tantalum is neutronically significantly worse than tungsten: its capture cross-sections are significantly higher. On the other hand, tantalum would seem to be a fairly normal metal, possibly more radiation resistant than a sintered material and has been used for (lower power) targets. With about 50% of the neutron flux of the Pb-Bi target system (or 3.8 times lower than the 'best'), it should not be considered as a contender for SINQ: that is, the plate target is only a possible alternative if it can be built using tungsten.

For tungsten, the selected plate dimensions lead to a system which gives about 70% of the flux obtained with the current Pb-Bi design (or 2.8 times lower than for a Pb-Bi target without the present loss factors): some of this might be recovered by optimisation, particularly the minimisation of coolant in the neutron production region and/or by changing to a high-mass coolant (e.g. liquid metal) to attempt reduction of the loss (about 30% of the fast neutrons produced) in the slowing-down process. Some reduction of the transverse dimensions of the plates should also bring improvement.

A major consideration could be radiation damage. The tungsten would be in the form of one of sintered agglomerates and assessment of how this would stand up to radiation damage together with the probable failure modes would need to be considered at an early stage of a design study. The major problems could be (i) swelling or other mechanical distortions constricting or interrupting the coolant flow and (ii) how to handle the activation, should failure modes involve significant fractions of the plate material entering the cooling system.

(c) Pebble-bed Target.

The calculations show this design of target to give a higher flux in the accessible regions of the moderator than the present Pb-Bi one (but 1.7 times worse than the 'best'). The actual final performance will probably be about the same, in terms of useful neutron intensity for the user, when the effect of the flux gradient is included (for a volume fraction of 50%). The shot filling density for a practical target should be about 57% (random packing), giving a slightly better performance than these calculations indicate.

This concept is being considered further to see if a practical design maintaining the neutronic performance can be realised [1].

4 The Effect of Absorption on Thermal Fluxes with a Pb-shot Target

4.1 Introduction

Calculations have been made to quantify the flux loss with the Pb-shot for small increase of the effective neutron absorption [7]. The effect of similar increases of the absorption in target 'auxiliaries' can be deduced from these results.

Two cases have been examined (i) an uniform increase of absorption cross-section throughout the whole Pb of the target (to simulate contamination) and (ii) a non-uniform distribution of absorber in the 'neutron-production' region to simulate the effect of burn-up poisoning.

This second case turns out to give a rather small effect but is of interest as it provides a natural 'background' level for assessment of the significance of absorption increase. Whilst

any increase is to be discouraged, that at the 10 or so percent level of such a "natural" background is not really significant (but the magnitude has to be known).

4.2 Burn-up Poisoning

A first look at this problem was made for the Pb-Bi target [8]. The spallation/fission products of Pb include most of the well known high thermal-neutron absorption cross-section nuclides (see Table-I in reference 8). The production rate for these is about 48 g/mA·year (0.7 nuclei/proton) and corresponds to an average effective cross-section increase of about 190 mb/mA·year but because of the high cross-sections, burn-up limits the increase to an equilibrium at about 90 mb.

We may define an effective average absorption cross-section ($\bar{\sigma}$) by:-

$$\bar{\sigma} = \frac{208}{V \times 11.3} \sum_l N_l \sigma_l$$

where N_l is the number of gramme·atoms and σ_l the capture cross-section for nuclide l, V is the volume of the interaction region. The nuclide production rates come from the Bateman equation:-

$$\dot{N}_i = -\lambda_i N_i - \sigma_i \bar{\phi(t)} N_i + \sum_j f_{ij} \lambda_j N_j + \sum_k g_{ik} \sigma_k \bar{\phi(t)} N_k$$

where N_i is the amount of nuclide i (g.atoms) and where λ_i is the decay constant for the nuclide i, σ_i the capture cross-section, f_{ij}, λ_j & N_j give the *decay* feed from N_j and g_{ik}, σ_k & N_k the *capture* feed from N_k.

The thermal flux, $\bar{\phi(t)}$, is a function of both time and position within the target making the equations non-linear. As the first step in the solution of the equation, equilibrium flux distributions [9] for fixed average absorption cross-section increases (50, 180, 360 and 540 mb) have been calculated, using a spatial distribution of absorbing nuclides based on that for energy deposition in the target. The average thermal-neutron flux in the production region of the target varies between $1.35 \cdot 10^{14}$ n°/cm^2/sec/mA with pure Pb and $1.08 \cdot 10^{14}$ n°/cm^2/sec/mA at +540 mb: this slow variation means that solutions of the Bateman equation with step-wise variation of thermal neutron flux should give adequately accurate answers. The calculated build-up of average absorption cross-sections for three fixed neutron fluxes are shown in Table-VI. Using the flux-to-peripheral-loss correlation of section 3 and the peripheral losses from the flux calculation (6.303 ± 0.032, 6.165 ± 0.033, 6.022 ± 034 and 5.914 ± 0.036 respectively for the four average absorption cross-section increases), interpolation indicates a reduction of the undisturbed thermal-neutron flux in the region of the beam-tubes of about 1.5% after 2 mA·years operation, rising to approximately 2.5% after 10 mA·years. The effect is rather small.

4.3 Uniform Increase of Absorption

The undisturbed thermal-flux in the moderator has been calculated for five cases in which the effective absorption cross-section of the Pb (170 mb) has been (arbitrarily) increased by 10, 100, 200, 300 and 400 mb [9]. The loss at 3 different heights in the moderator tank at a radius of about 25 cm as a function of cross-section increase is shown in Fig. 8. The general

Table-VI

Calculated average absorption cross-section contribution (mb) from spallation products as a function of operation time and for three different thermal fluxes.

Flux units of 10^{14}	Operation Time (mA.years) 0.027	0.27	1	2	5	10
0.0	5.1	51	187	376	943	1890
1.35	3.5	18	31	43	65	80
1.13	3.7	19	34	47	71	89

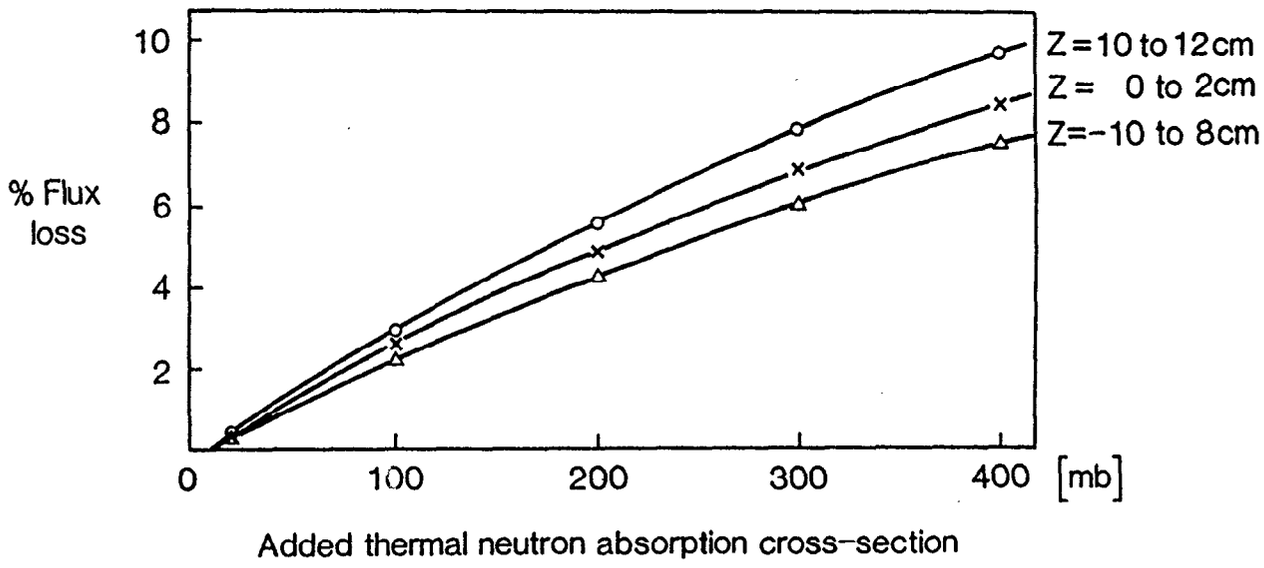

Figure 8: The percentage flux-loss at three different heights relative to the target beam-window and a radius of 25 cm as a function of added absorption cross-section.

trend is for the loss to be less as the distance from the target increases: at typical distances to the beam-tube tips (circa 25 cm) an extra 170 mb (a doubling of the absorption cross-section) gives a 4 to 5 % undisturbed flux reduction.

The results indicate that (for example) an 1% admixture of Sb (σ_{cap} = 5.4 b) would give at least a 1% loss (*there will be additional loss due to the fairly large (175 b) resonance integral which has NOT been considered*).

4.4 General Considerations

The neutron loss accounts are summarised in Fig. 9, where the loss in the various components of the system has been plotted as a function of additional absorption cross-section. The curves show the rather obvious effect that neutrons absorbed in the target (or anywhere in the inner part of the system) are lost to the number which reach the outer limits of the moderator:

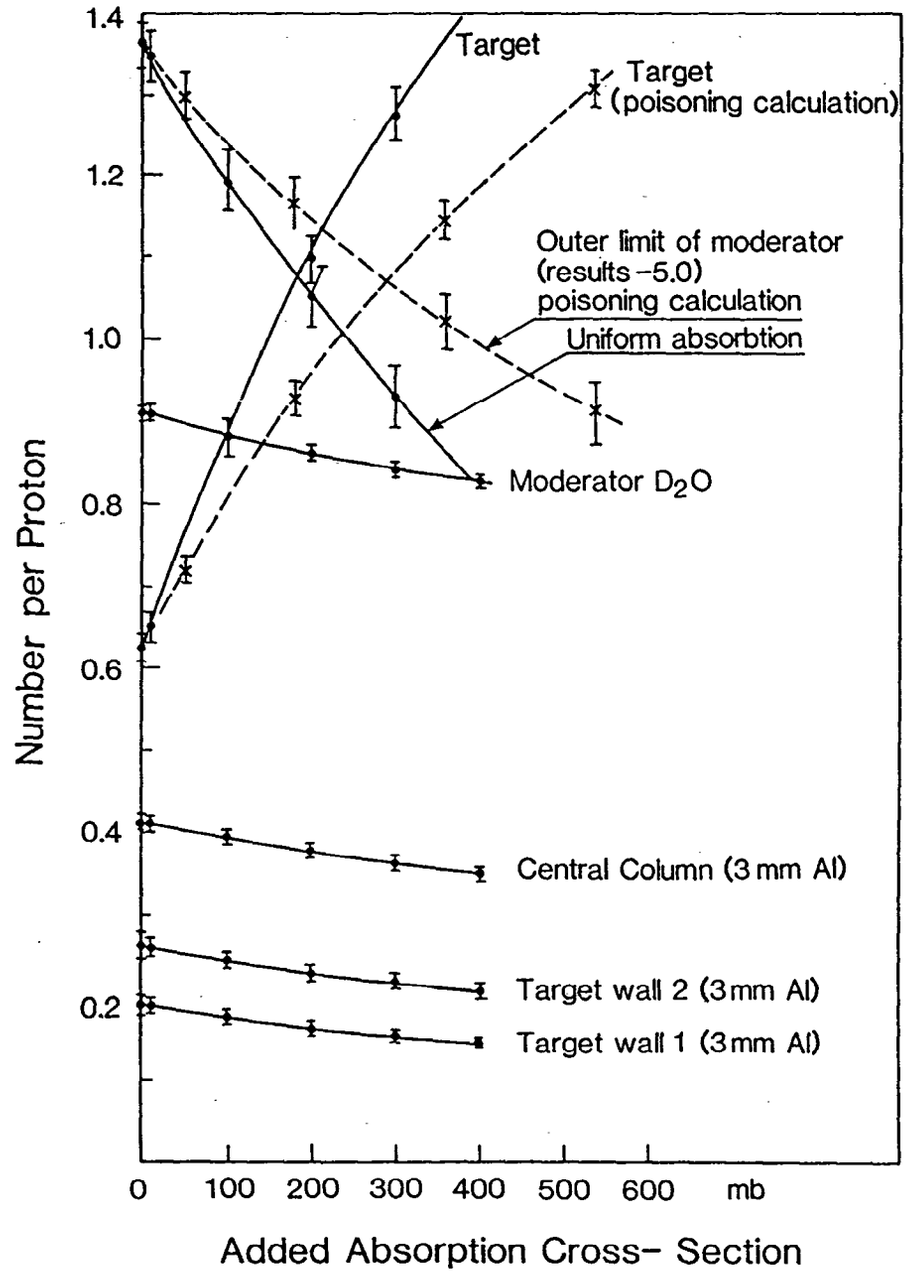

Figure 9: Thermal neutron absorption by the various components of the target-moderator system as a function of the added absorption cross-section in the target. Values shown with dots are for results with a uniform-density absorption increase and with crosses from the burn-up poisoning estimate (values for target material and periphery losses only included). Lines are drawn only as eye-guides and error bars indicate the statistical error in the estimates only.

this leads to an almost pro-rata reduction of the thermal neutron flux; the slight reduction of the loss in the other components comes from (and is a measure of) the average reduction of neutron flux in their vicinity due to these lost neutrons.

The neutron absorptions (β/proton) at the periphery of the moderator tank fit (with a correlation of 0.999_7) the relation:-

$$\beta = \frac{6.886}{1 + 0.1225 \times \sigma_{cap}}$$

where σ_{cap} is the *added* cross-section in barns and the relation simply expresses that the flux reduction is the ratio of the number of neutrons reaching the moderator tank wall with and without the extra absorption (absorption loss is proportional to flux) and system escapes (fast and thermal) are mainly geometry dependent and hence constant.

The target and periphery neutron-loss results from the burn-up poisoning calculation have been included into Fig. 9 and show (on a pro-rata average absorption increase basis) a significantly smaller effect. In some respects, one could say that the average cross-section as defined is not a correct measure of its significance. The +540 mb average corresponds to about 2.8 b in the innermost region of the target and the calculations show that for the Pb-D_2O mixture, this region is quite well decoupled from the moderator.

Two practical consequences from all this are:-

- Special treatment of the Pb in the inner (high heating, activation etc) regions which leads to a somewhat high effective absorption cross-sections can be tolerated (Note: *if such treatment also involves significant increase of the resonance integral, it would probably not be tolerable!*)
- The major importance of maintaining low absorption cross-sections for components at the outer limit of the target (particularly the container walls). Being adjacent to the moderator, these must necessarily "see" high thermal fluxes. Only 6 to 7 n°/proton are available to produce the thermal flux. With the 'pure' aluminium used in the calculations, 0.44 n°/proton are lost: a doubling of the absorption (i.e. another 0.44 lost neutrons) will mean a loss of the order of 7 %.

5 References and Comments

1. See contribution to these Proceedings : F. Atchison & G. Heidenreich, "A Solid Target for SINQ based on a Pb-shot Pebble-bed".
2. This report is a condensed version of two internal SINQ reports by the author: SINQ/816/AF38 001 and SINQ/816/AF38-003.
3. The calculations have been made with the HETC code for the high-energy transport calculations and a locally extensively modified version of the O5R code with ENDF/B-IV cross-section data for sub 15 MeV neutron transport.
   Thermal neutron transport uses the perfect-gas scattering function and fluxes have been calculated from both track-length and collision density estimators and a stopping

criterion of less than about 5% statistical fluctuation in the 'higher' flux regions. The two separate flux estimates are in reasonable agreement.

4. U. Rohrer (SINQ Internal Communication).

5. (i) The calculations use undisturbed fluxes (the beam-tube structure in the moderator tank has not been included). Neutron flux is used in this report as a measure of performance (nothing more) and on the basis that the most "useful neutrons" will be diverted to the user when a beam-tube is inserted into a region with the highest flux (calculated or measured) without the beam-tube. Thermal neutron flux is a potential function and obtains its units (/unit area/unit time) from the multiplication of the probability (per unit volume) of finding neutrons at a given position by their velocity: that is, the flux is a measure of the neutron motion maintaining the density distribution and not physical transport. Physical transport of neutrons leads to a flux gradient, so the actual intensity at the monochromator remains a somewhat open question.

   (ii) The flux maps have been prepared using double logarithmic interpolation in both the R and Z directions of the data from the path-length estimator. No data smoothing has been made: the clear separation of the contours is additional evidence that the solution has converged. The localised irregularities on the contours come from the the irregular volume mesh used and the residual statisical fluctuations and are not considered to be physically significant.

6. See contribution to these Proceedings : M. Dubs and J Ulrich, "Design Considerations of the Target Window".

7. Commercially available Pb shot would be used which will have a higher effective thermal absorption cross-section. An assay of a sample indicates an absorption increase of less than 60 mb. Using the results of this study, this would correspond to a flux loss of the order of 1 or 2% and not significant.

8. F. Atchison, Proceedings of ICANS-VIII, Rutherford Laboratory Report RAL-85-110 (1985).

9. All the results in this section have been obtained in a single run of the neutronics codes using a parallel tracking technique.

Q(N.Watanabe): What coolant are you thinking for target other than Pb-Bi?
What shape and size of block or disk are you thinking for W-target?

A(G.S.Bauer): The coolant is D_2O in all cases to minimize absorption but also moderation in the target volume. The size of the target disks in the case of W and Ta has not been optimized yet; Only the thickness of the plates has been chosen such that the surface heat flux does not lead to subcooled boiling. This leads to about 20% by volume of D_2O-content in the target.

ICANS-XI International Collaboration on Advanced Neutron Sources
KEK, Tsukuba, October 22-26, 1990

Split-Target Neutronics

Gary J. Russell
Los Alamos National Laboratory
Los Alamos, New Mexico USA

ABSTRACT

Monte Carlo simulations show that, for the LANSCE split-target of machineable tungsten, about 60% of the low-energy (<20 MeV) neutron leakage from the target comes from primary (800-MeV) proton interactions. The remaining 40% occurs from secondary high-energy reactions in the split-target. Primary protons are forward directed; secondary high-energy (>20 MeV) particles are also forward directed. Consequently, the neutronic performance of the LANSCE Target-Moderator-Reflector-Shield (TMRS) system is not adversely impacted by employing a split-target. Implementing a split-target allows us to use flux-trap moderators around the void zone between the targets to simultaneously service twelve neutron flight paths.

I. INTRODUCTION

The Los Alamos Target-Moderator-Reflector-Shield (TMRS) system[1] is a neutronically efficient target scheme for a spallation neutron source. I conceived the design in 1984, and we implemented it in 1985. One of the unique features of the device is the use of a split-target (see Fig. 1). This key concept is necessary to employ moderators in "flux-trap" geometry around the void space between the targets (see Fig. 2). This moderator arrangement allows the LANSCE TMRS to simultaneously service twelve neutron flight paths.[1] I ran a series of Monte Carlo simulations of low-energy (<20 MeV) neutron leakage from split-targets of machineable tungsten as a function of the gap-size between the targets. Machineable tungsten used in the LANSCE targets has a density of 18.3 gm/cm^3 and is composed of 97.0 wt % W, 2.1 wt % Ni, and 0.9 wt % Fe. I also studied the effects of upper-target length on low-energy neutron leakage for a gap size of 14 cm. I employed the Los Alamos Monte Carlo Code System[2] in the computations.

II. RESULTS

In all cases, the targets had a diameter of 10 cm. In the target-gap study, the upper-target length was 7 cm and the lower-target length, 23 cm. I varied the target gap from 0 to 25 cm. The computations were done for a point source of 800-MeV protons directed along the target axis. The results are shown in Fig. 3. The data in Fig. 3 are referenced to a 14 cm gap which is the size used in the as-built TMRS at LANSCE. The major reduction (≈7%) in neutron leakage occurs in opening the gap to 14 cm. Very little loss

(≈5%) results in increasing the gap to 25 cm. This minimal loss in neutron leakage allows some hope of increasing the LANSCE target gap to more than 14 cm to reduce high-energy and fast-neutron backgrounds in materials science instruments. However, one must study the effects of target-gap on actual moderator performance for realistic proton-beam profiles. These calculations are currently underway in support of the LANSCE Repair Project.[3]

The essence of the relatively minor perturbations of gap size on split-target neutronic performance depends on how low-energy neutrons are produced by spallation reactions in the split-target (see Fig. 4). In Fig. 4, about 60% of low-energy neutron leakage comes from primary (800-MeV) proton reactions.[4] These incident protons are forward directed; hence, it does not matter if the target is split or solid. Secondary high-energy particles are also forward directed. The net result is that low-energy neutron leakage from a split-target is relatively insensitive (at the <10% level) to the gap size between the targets.

I also studied the effects of upper-target length on bare-target, low-energy neutron leakage for a target gap of 14 cm. For the proton beam conditions stated above, total low-energy neutron leakage is relatively insensitive to the length of the upper target (see Fig. 5). In these studies, the length of the lower target was varied to keep the total target length (upper plus lower targets) to 30 cm.

III. ACKNOWLEDGEMENTS

I appreciate the support of Roger Pynn for this work. I want to thank Tatia Vander Maat for her typing help and Maria DiStravolo for proofreading the text on a very short notice. LANSCE work is supported by the US Department of Energy, Office of Basic Energy Sciences, under contract W-7405-ENG 36 with the University of California.

References

1. G. J. Russell, et. al., "LANSCE Target System Performance," in Advance Neutron Sources 1988: Proceedings of the Tenth Meeting of the International Collaboration on Advanced Neutron Sources (ICANS-X), Dianne Hyer, Ed. (IOP Publishing Ltd., Bristol, England), Vol 97, pp. 483-502.

2. R. E. Prael and H. Lichtenstein, "User Guide to LCS: The LAHET Code System," Los Alamos National Laboratory report LA-UR-89-3014 (September 1989).

3. G. J. Russell, "The LANSCE Repair Project," in these proceedings.

4. G. J. Russell, "Spallation Physics - An Overview," in these proceedings.

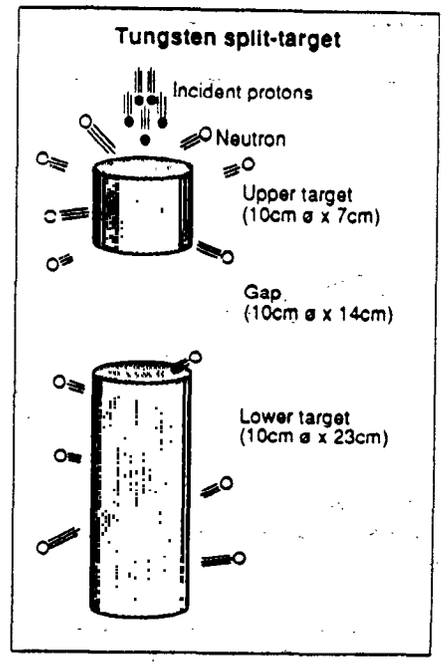

Figure 1. Illustration of the LANSCE split-target

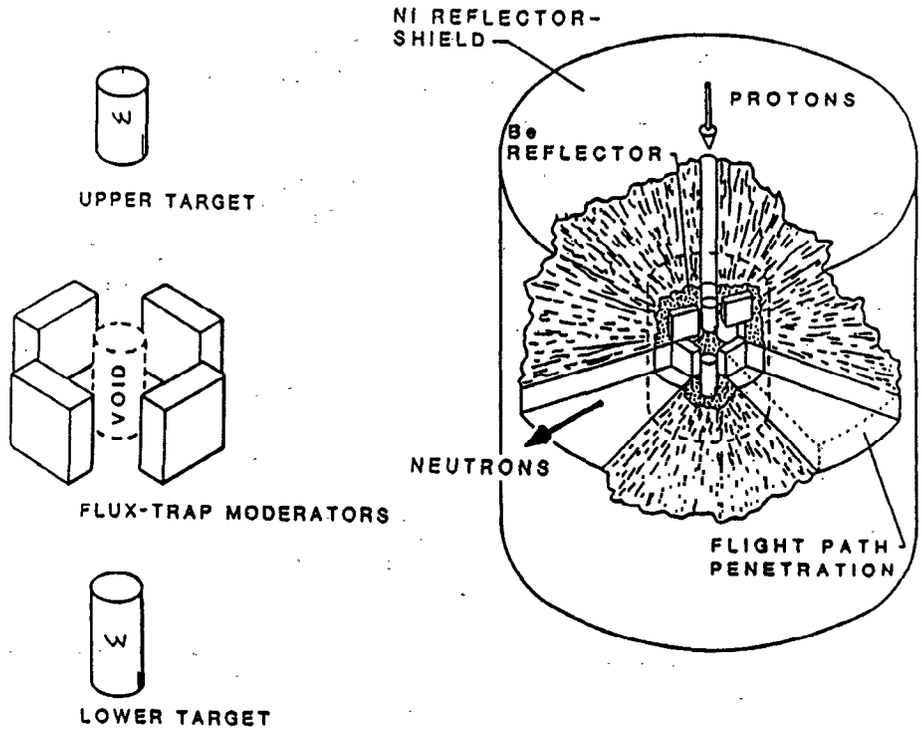

Figure 2. Illustration of the LANSCE Target-Moderator-Reflector-Shield neutron production system.

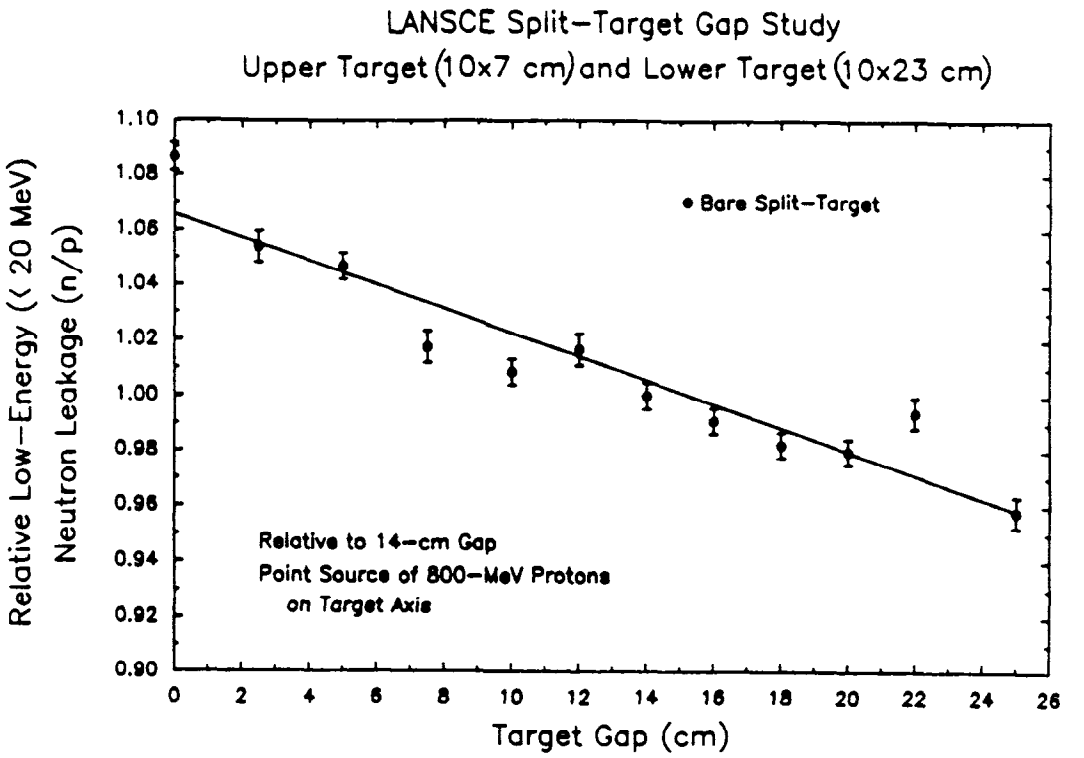

Figure 3. Neutron leakage from the LANSCE split-target. The upper-target length was fixed at 7 cm and the lower-target length was set to 23 cm.

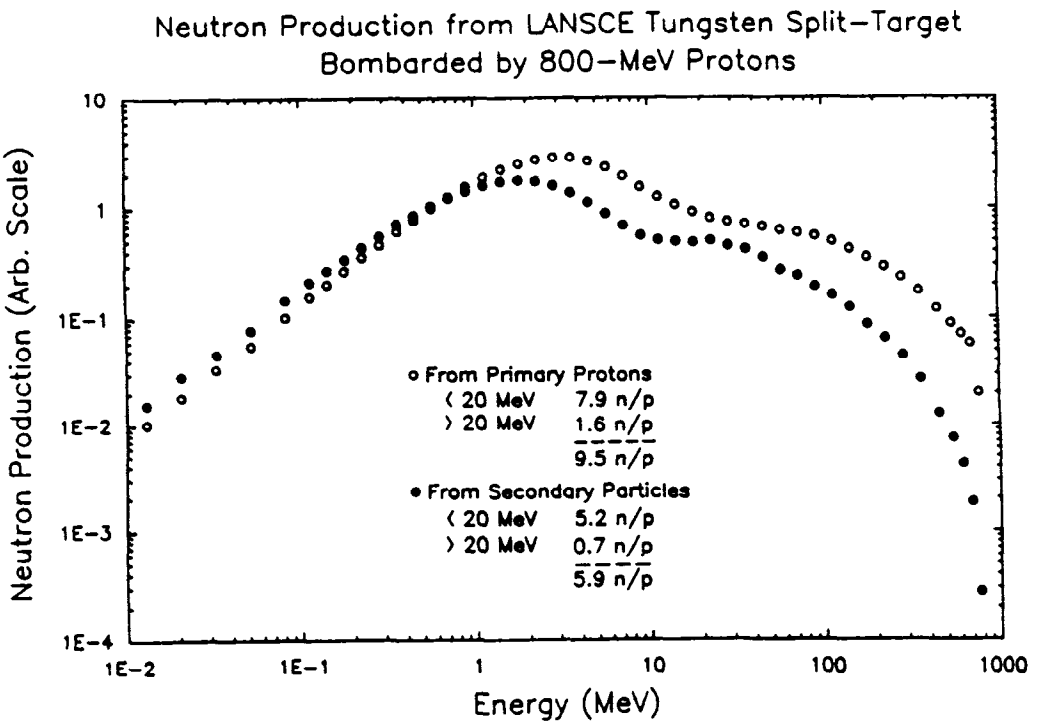

Figure 4. Neutron production from reactions caused by primary proton and secondary particles in LANSCE tungsten-target nuclei.

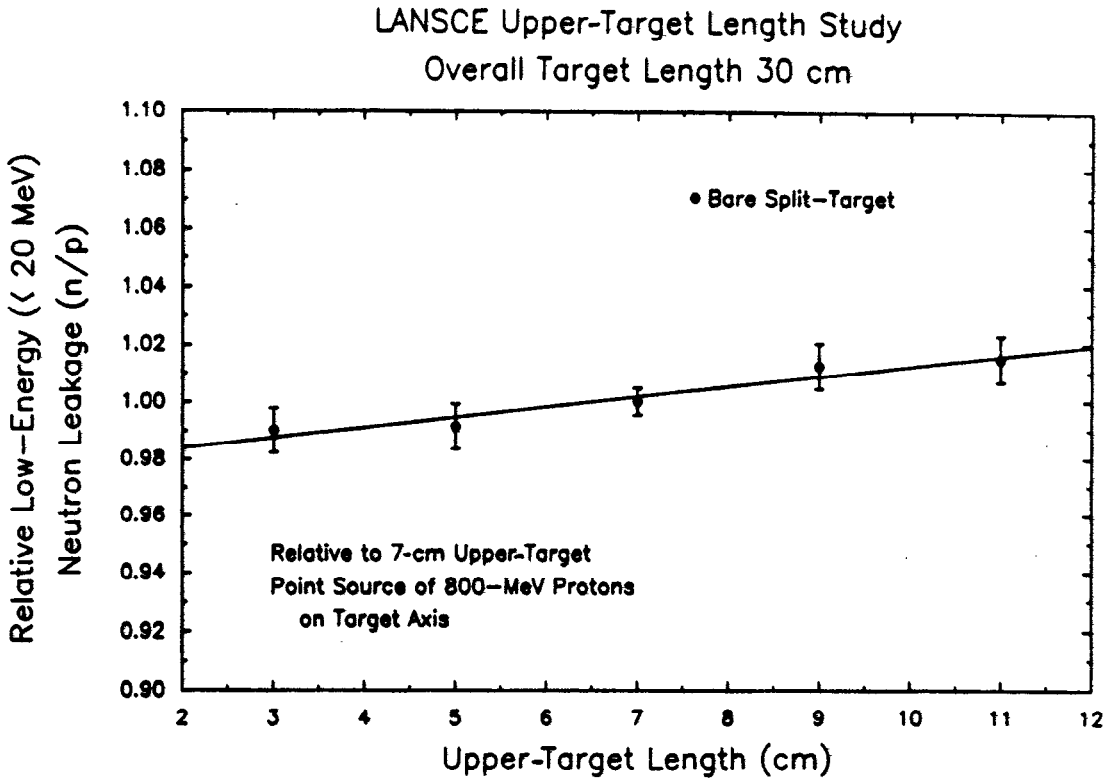

Figure 5. Neutron leakage from the LANSCE split-target. The target gap was fixed at 14.0 cm.

ICANS-XI International Collaboration on Advanced Neutron Sources
KEK, Tsukuba, October 22-26, 1990

Neutron emission from an extended lead target under the action of light ions in the GeV region

R.G.Vassil'kov
Moscow Radiotechnical Institute, Academy of Sciences of the USSR,
Warshavskoye chaussee 132, Moscow 113519, USSR
V.I.Yurevich
V.G.Khlopin Institute of Radium, Roentgen str. 1,
Leningrad 197022, USSR

ABSTRACT Experimental data are presented on yields and spectra of neutrons, emitted from a lead cylinder Ø20×60 cm, bombarded by beams of p, d, ^{3}He, ^{4}He, ^{12}C with energies 1-7,3 GeV per unit of ion charge. Measurements have been carried out by the neutron moderation technique and with solid state nuclear track detectors (SSNTD). The results obtained will be used as a scientific base for the power accelerator-based neutron sources.

1. Capability estimations and practicality considerations, with regard to large-scale accelerator-based methods of free neutron production for the nuclear fuel cycle, have prompted us to start gathering the relevant data sistematically. Experiments are carried out on some simple targets, placed at the Dubna (JINR) synchrophasotron slow ejection channel MV-2, beam line N40. Modest efforts are also being made to develop calculational codes. On the whole these activities are supported by MuCF program.

At present there are three targets on our experimental area (fig.1):

a) "naked" thick lead cylinder (as a rule Ø20x60 cm), used

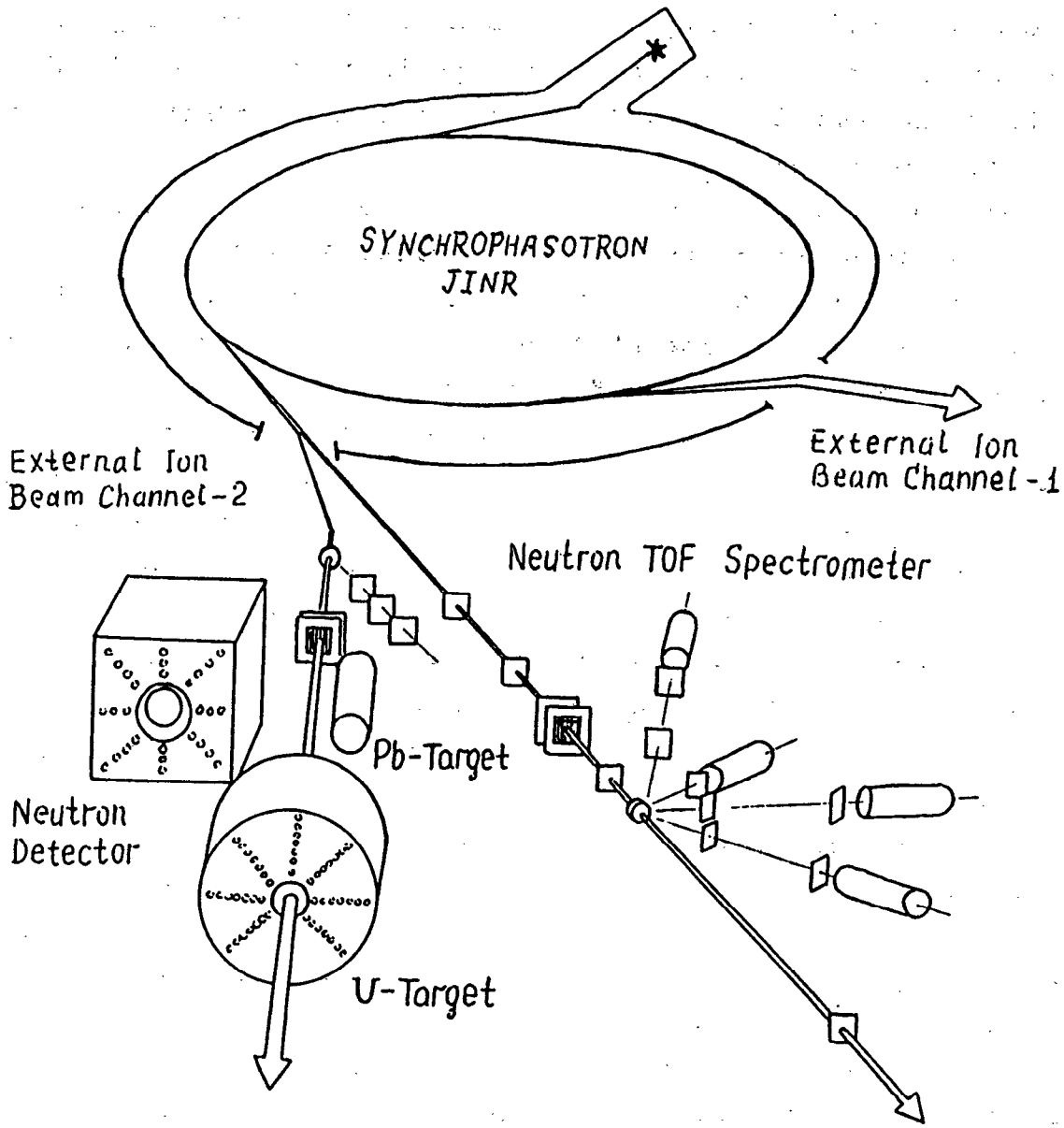

Fig. 1 A sketch of an experimental area with MRTI-IAE targets on beamline N40 of synchrophasotron JINR

for measuring neutron spectra by solid state track' nuclear detectors (SSNTD) technique; the data obtained are being combined with the results of time-of-flight spectrometer, which inhabits a neighbouring beam line and deals with thin and modest size targets of various materials.

b) The same cylinder in a hydrogenouos moderator for measuring yields of neutrons with energies ≤ 15 MeV.

c) The same lead cylinder again (later also uranium and thorium ones) will be inserted into a large uranium blanket of the depleted metal (Ø120x100 cm,full weight 21 metric ton).

The data gathered will make it possible to obtain reliable neutron characteristics for the heavy material targets bombarded by slightly relativistic hydrogen ions, i.e. in the energy region, where the energy cost of the free neutron is expected to be minimal. Moreover, the data would be useful for testing the calculational codes and improving their predictive power. Actually a calculated pattern of the total absorption of the high energy ion in, for instance, quasi infinite metal uranium block is now far from certain.

The experiments with Pb cylinders are now under way. Next january measurements will be started with a U target-blanket; work on the TOF spectrometer will also continue. However, it is feared that the synchrophasotron will be shut-down in late 1991 and subsequently dismantled.

2. The spectrum of neutrons emitted by a thick heavy target under the action of high energy ions ($\sim 10^2$-10^3 MeV) is rather complex and stretches over at least two orders more than the fission spectrum, the target size and material as well as the type of bombarding ion and its kinetic energy affect it significantly also. In order to measure a) the yield of neutrons with energies ≤15 MeV from (nonfissioning) extended target, say Pb, we have used the well developed neutron moderation technique; b) as to neutrons of higher energies the SSNTD technique was applied, with some modifications to fit our task.

The first series of the experiments was conducted on the beams of p, d, ^{3}He, ^{4}He and ^{12}C (moderation technique) with energies E_i/Z_i=1-7.3 GeV per unit of ion charge (for protons 8,1 GeV) or only p and d beams in the energy interval 1-3.65 GeV

(SSNTD technique).

a) In the neutron moderation experiments the lead cylindrical target was placed inside a CH_2 block 1.35x1.2x1.2 m^3 [1]. Counters of thermalized neutrons in 10 channels (parallel to the ion beam, i.e. target axes z). The neutron detector (counters + moderator) was calibrated by Ra-Be standard sourse ($5.22 \cdot 10^5$ n/s ±2.8%). There were neutron counters of three types: short boron (Ø 0.8x4 cm) and long (Ø 2x115 cm) filled with ^3He or BF_3.

The short counters measured reaction $(n, {}^{10}B)$ density distributions along the beam axis z; the distributions were approximated by polynoms of third power and then integrated. The long counters integrated these distributions physically. Because we did not observe any noticeable differences between the results obtained by the two methods, bulk of the data was gathered with long BF_3 neutron counters.

The primary ions bombarding the target were counted by a scintillation telescope with 1-2% errors. At beam intensities $\leq 10^5$/cycle and of slowly ejected ion pulses 350-400 ms the dead times of neutron channels did not exeed 5-6 mcs, so that missed counts amounted to ≤ 1%. An absorption of the high energy nuclear cascade in the target is rather full: the addition of 12-16 cm of lead to an initial 60 cm increases the neutron yields only by 1.5-2%.

On fig.2 E-dependences of the neutron yields Y_i/Z_i are given for various primary ions. Fig.3 shows the yields measured at a fixed energy E_i/Z_i=2.55 GeV, the yields having been set along the abscissa according to parameter $Z^2/A^{2/3}$: the grater its value is, the more is the share of ion initial kinetic energy lost before a nuclear absorption event.

A hierarchy of the bombarding ions (as to their ability to minimize the energy cost of neutron, releasing from the target) observed in fig.2, thus seems obvious, because it may qualitatively be predicted on the basis of the available data on ion-nucleus inelastic cross sections and ionization losses in extended media. A crude assumption is being done, that the yield is proportional to the mean kinetic energy of the ion left with it at the nucear absorption event. These considerations are rather primitive, because they do not take some essential issues into

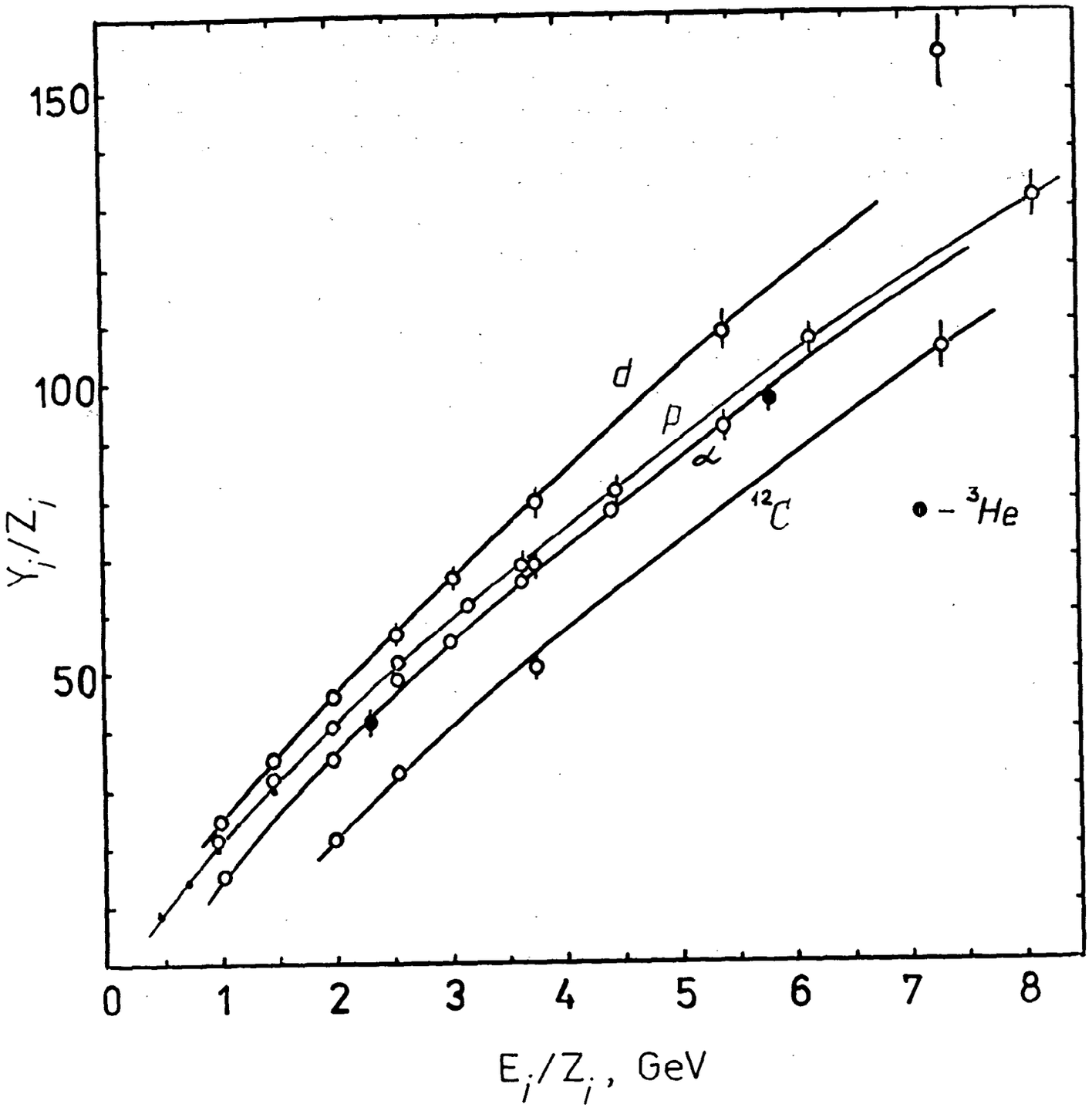

Fig. 2 Neutron yields Y_i/Z_i measured by the neutron moderation technique for lead cylinder Ø20 x 60 cm, bombarded by light ions

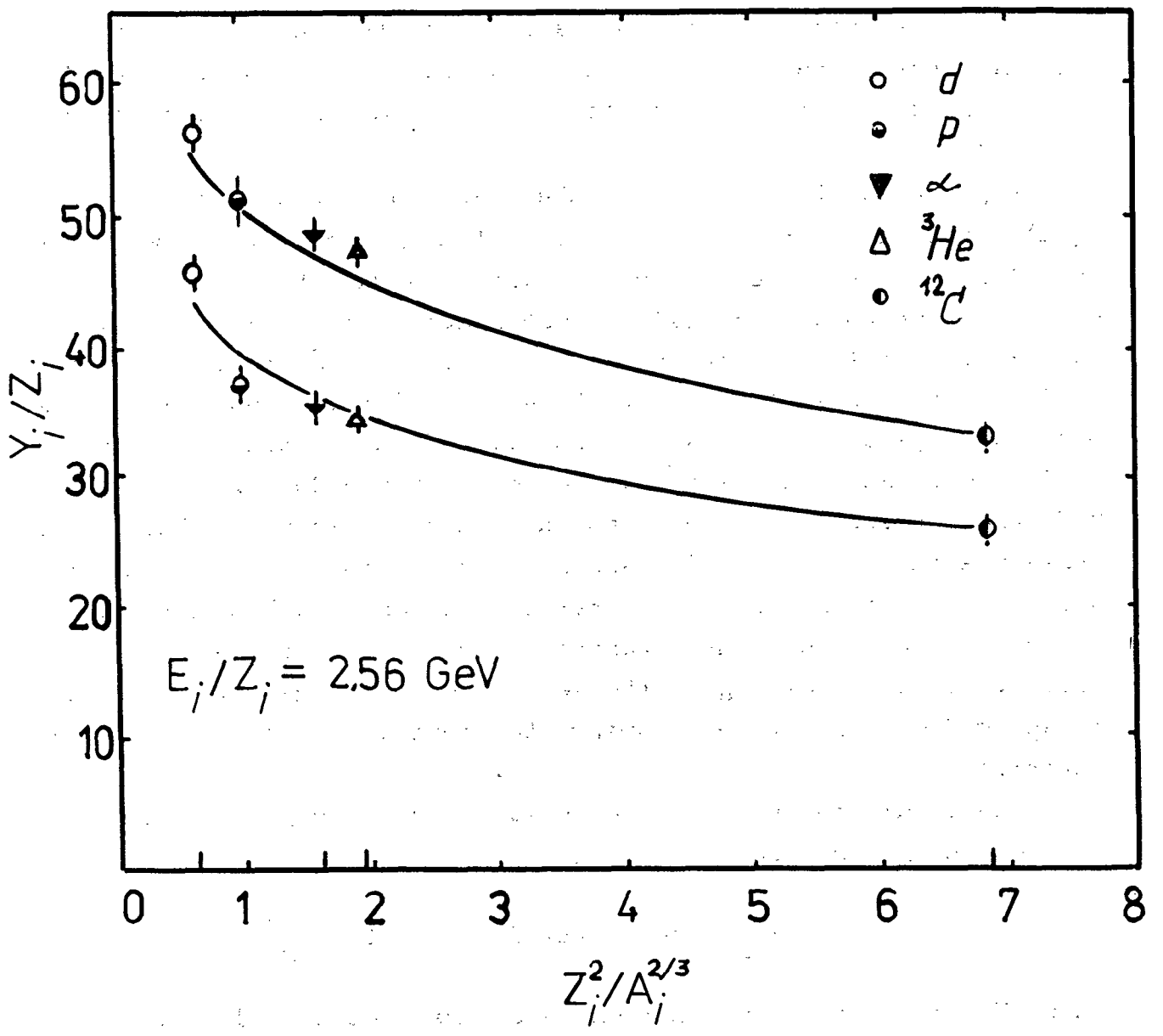

Fig. 3 Dependence of the neutron yield Y_i/Z_i on a type of bombarding ion, measured at the initial kinetic energy 2,55 GeV per unit of ion charge on the same target Ø20 x 60 cm

account, for example, the energy transfer from a hadron "component of the nuclear cascade to an electron-proton one as the ion initial kinetic energy rises, but it is not very significant for the relative qualitative pattern in a rather limited energy interval.

Fig.4 presents a curve of the neutron yield for protons, $Y_p(E_p)$, separated from the entire family on fig.2, with an addition of the previously published data obtained by the moderation technique as well: in Oak Ridge - Chalk River study /2/ for E_p=0.47-1.47 GeV, in Karlsruhe group experiments /3/ for E_p=0.59 GeV, and in ICP-MIPI work /4/ for E_p=0.4-0.66 GeV. This picture helps to realize a nonlinearity of E-dependances: it is hardly noticeable in the energy region of the order of hundreds MeV, and appears to be due to an intricate combination of at least three reasons. They are a) changing specific ionization losses and nuclear absorption cross sections; b) a steadily enhancing energy transfer from h- to e-ph-component of the nuclear cascade in the matter; c) an increasing of the mean kinetic energy of neutrons, escaping from the target owing to deficiency of the target material.

The cumulative proton data is satisfactorily parametrized by the following function

$$Y^m_p(E_p)=-8.2(\pm1.6)+29.3(\pm1.3)E_p^{0.75},$$

where E_p is in GeV. For deuterons and α-particles (only our data) we got

$$Y^m_d(E_d)=-10.5(\pm1.9)+33.6(\pm1.2)E_d^{0.75},$$

$$Y^m(E_\alpha/2)/2=-16.3(\pm1.4)+31.3(E_\alpha/2)^{0.75},$$

the upper indices in all three expressions meaning "moderation".

b) On the same fig.4 the values of neutron yields $Y^t_p(E_p)$ are displayed, which have been obtained by integrating the neutron yield distributions over the target surface and the angle θ (with respect to proton beam): dy/dS and dy/dθ. The distributions were measured by SSNTD at E_p=1-3.65 GeV. One may get from this data

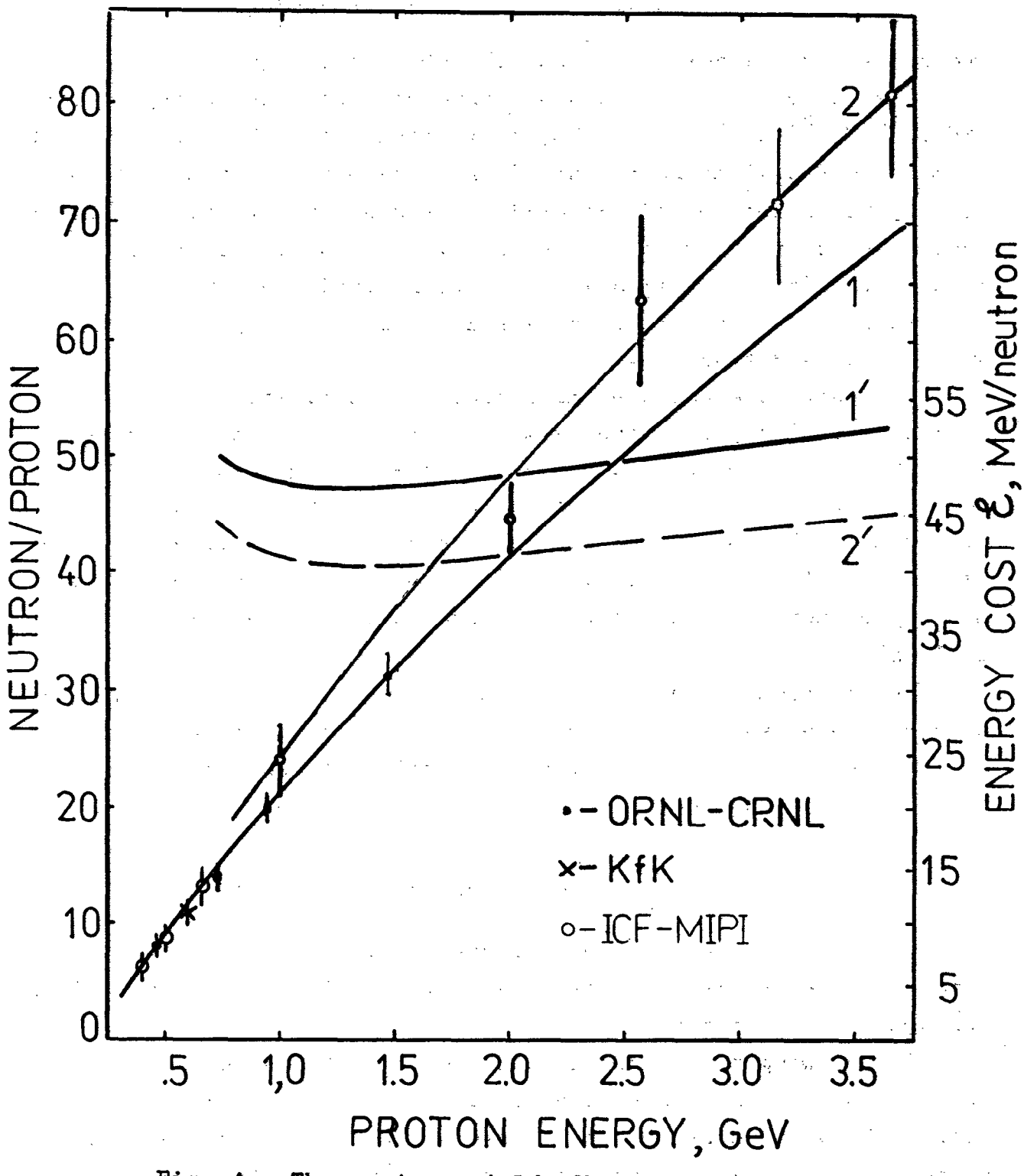

Fig. 4 The neutron yields Y_p measured by the moderation (1) and SSNTD techniques (2) on the same lead target Ø20 x 60 cm. Curves 1'and 2'refer to right ordinata.

$$Y^{m}_{p}(E_p)=-4.8(\pm1.0)+28.6(\pm2.5)E_p^{0.85},$$

where the upper index "t" means "threshold technique".

The detectors included a standard set of fissioning layers (FD): ^{235}U, ^{238}U, ^{237}Np, ^{232}Th, contacting with a 6 micron thick film of polyethylenterephtalat (PETP) (SSNTD arrangement and their setting up on the "naked" Pb cylinder and around it are shown in companion report by Nikolayev et al.). To this set we have added layers of ^{209}Bi and spallation detectors (SD) Cu and Cd, that effective neutron detection thresholds amount respectivevely to ≈ 90, ≈ 400 and ≈ 600 MeV.

In order to elucidate the detecting capabilities of the SD, a series of axillary experiments was carried out with layers of Ti,Al,Cu,Cd,,Ta,Pb on proton beam in the energy interval 0.2-4 GeV. The efficiences for an entire set of layers in SSNTD, were determined, the SD with Cu and Cd layers have the steepest energy dependence of detection efficiency in the near threshold region which provides the embracing of a broad energy interval from 0 up to ~ GeV.

The neutron yield distributions dy/dS and dy/dθ (integral spectra) were measured in various energy groups over the lead cylinder surface and angle θ. By integrating these one gets the total yield of neutrons of all energies (in 4π solid angle):

$$Y^{t}=2\pi R\cdot k\int_{0}^{60cm} dy/dS\cdot dz=2\pi\int_{-1}^{1} dy/d\Omega d(\cos\theta),$$

where R is the radius of the cylinder, coefficient k takes into account the experimental fact, that (87±4)% of all neutrons leak through the side surface.

Thus, owing to the small number of thresholds we get only the integral neutron spectrum, i.e. a set of neutron yields in some rather broad energy groups. Nevertheless, there exists a mathematical procedure for restoring the full spectrum from these experimental values (code RESTOR), which is an iterative method using some a priori information as a zero approximation in the shape of the energy spectrum. Such information may be, for example, the well known representation /5/

$$F_o(T)=\sum_{i=1}^{3} c_i(T_i/T_{oi})\cdot\exp(-T_o/T_{oi}),$$

which satisfactorily describes the spectra of neutrons from thick targets at realistic values of parameters c_i and T_{oi} /6/. The additional detectors with high thresholds sharply diminish the relative error $\delta Y(E)$ of the cascade high energy neutron yield.

The code RESTOR results in energy distributions of neutrons $F(E_n)$ and yields $y_j(E_n)$ for neutron energies,exceeding some threshold values E_{nj}(0; 0.1; 1; 6; 20; 50; 100; 250; 500 and 1000 MeV). Fig.5 illustrates the capabilities of the SSNTD technique, displaying the neutron spectra, which have been measured E_p=2.55 GeV on Pb target ø 20x20 cm at angle 90^0 by both SSNTD and TOF techniques. The SSNTD seem to be appropriate for studying neutron fields with a hard spectrum.

The spectrum of spallation neutrons generated by deutron beam is noticeably softer than in a case when primary particles are protons (fig. 6). Fig.7 compares the "hardnesses" of the neutron spectra for lead cylinder ø 20x60 cm, bombarded by protons or deuterons with energy $E_{p,d}$=2 GeV. In fig.8 the neutron spectra are given for E_p=3.65 GeV. In the immediate future we are going "to insert" the former $E_{p,d}$=2 GeV into quasi infinite uranium blanket and to compare the result obtained with the directly measured value for real assembly "beam-Pb target-U blanket" (captures, fissions, ^{237}U ect.).

Finally in fig.9 functions $\varepsilon_i=E_i/Y_i$ are presented, implying the energy cost of the free neutron, "liberated" from the lead cylinder ø 20x60 cm. If the fits for Y_i above menthioned are used, then from the condition $d\varepsilon_i/dE_i=0$ minima of the functions ε_i are obtained. ε_p^m has a minimum at $E_p\approx1.2$ GeV, functions ε_d^m and ε_α^m are achieved respectively at $E_d\approx1.4$ and $E_\alpha/2\approx2.6$ GeV. The function ε_p^t transits minimum at $E_p\approx1.2$ GeV. This fact shows apparently on a slight sensitivity of the minimum position of ε_p to a completness of the neutron spectrum, involved in a determinating the total neutron yield,or to the target diameter.

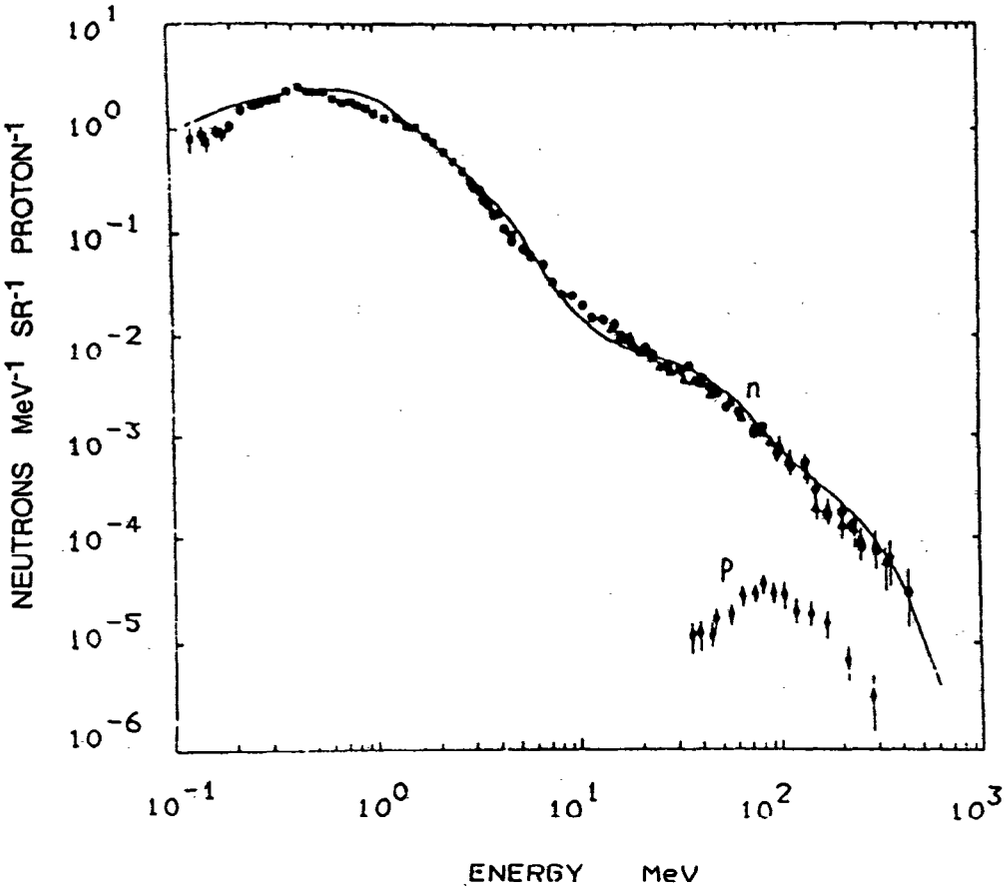

Fig. 5
Target:lead Ø20 x 20 cm, E_p = 2,55 GeV, solid line - SSNTD,points - time-of-flight

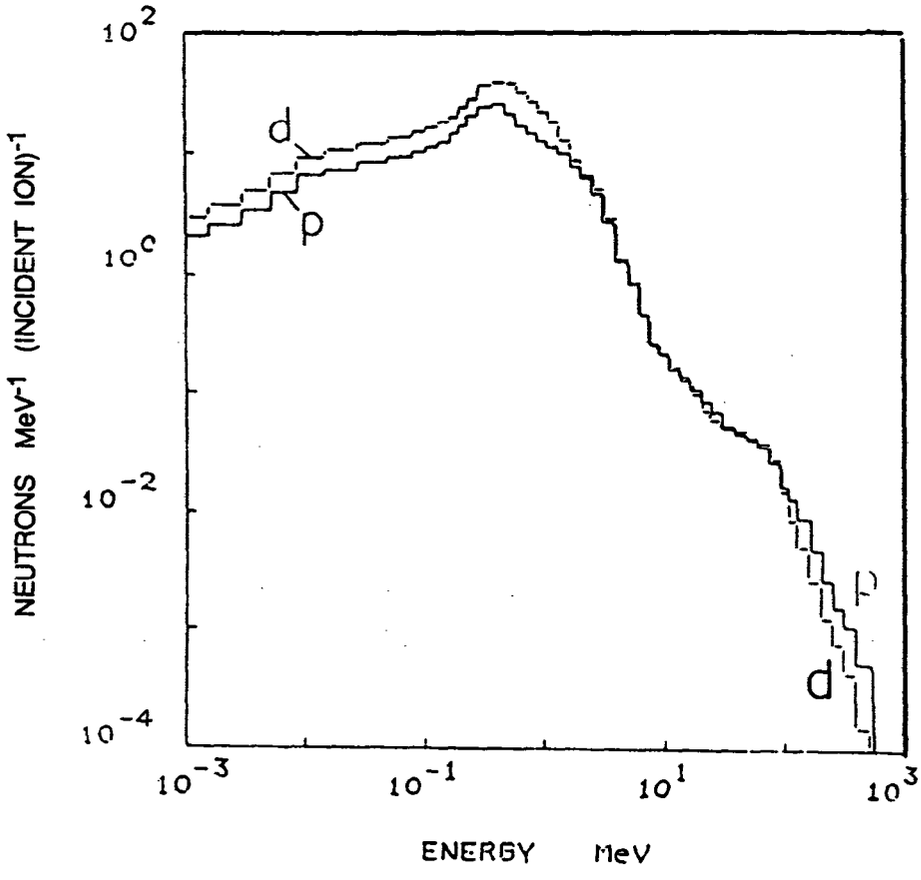

Fig. 6
Spectra of neutrons from lead cylinder Ø20 x 60 cm, measured with SSNTD, $E_{p,d}$ = = 2 GeV

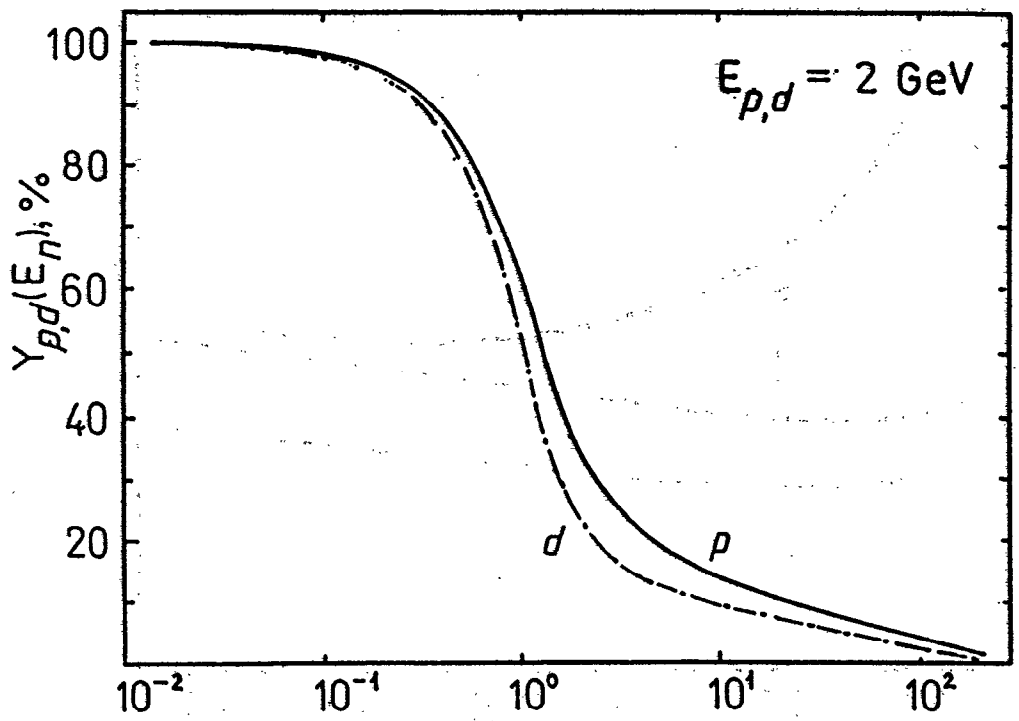

Fig. 7 "Hardness" of neutron spectra for lead target Ø20 x 60 cm, bombarded by p and d with energy 2 GeV

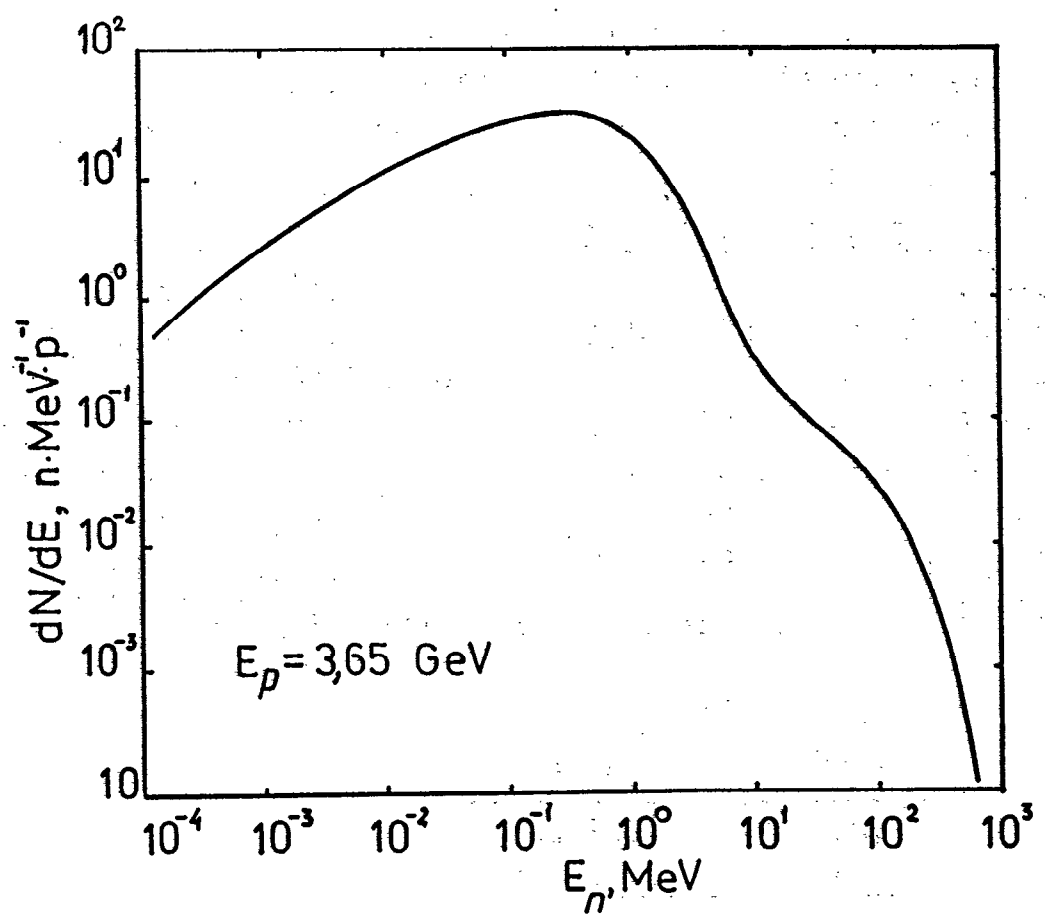

Fig. 8 Neutron spectrum for Pb cylinder ϕ20 x 60 cm, E_p = 3.65 GeV

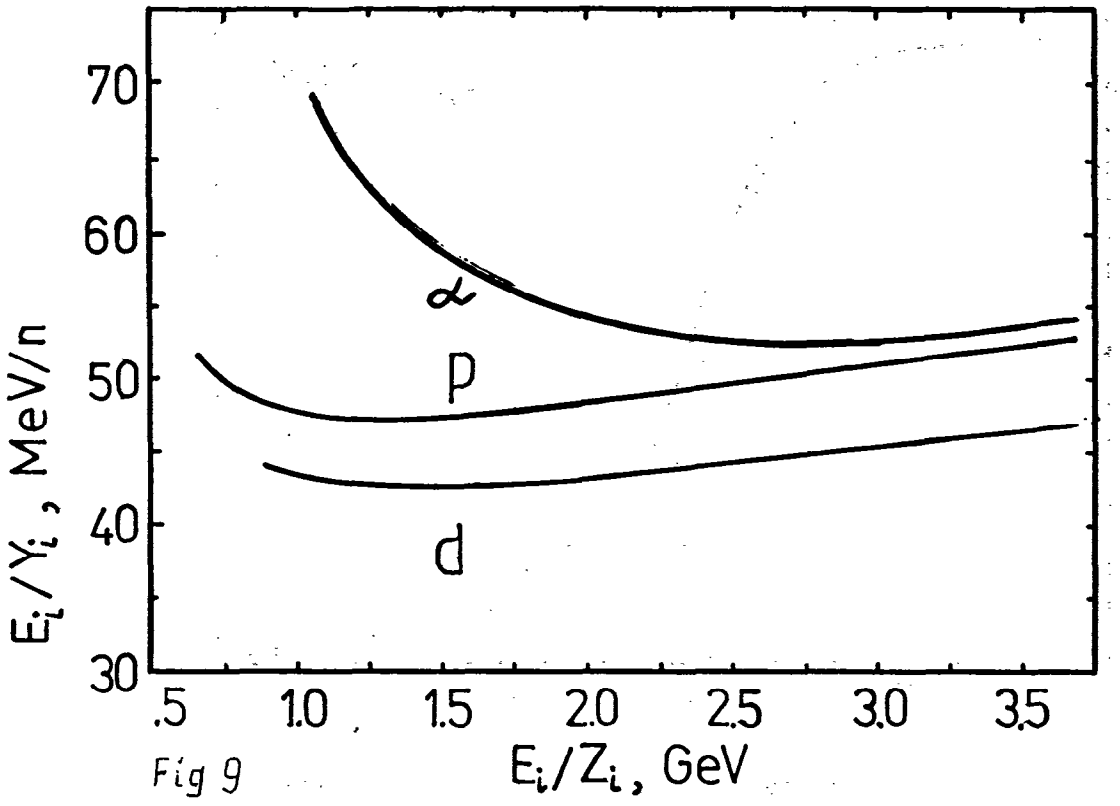

Fig 9

Neutron yields Y_i/Z_i measured
by "moderation" and "threshold" techniques,
lead target Ø 20 x 60 cm, ion energy is GeV per unit Z_i

E/Z	Y_d^m	Y_d^t	Y_α^m	Y_c^m	E_p	Y_p^m	Y_p^t
I,03	23,8±I,8	24,9±5,0	I5,4±0,8	-	0,99	2I,3±0,6	25,I±3,0
I,48	34,6±0,9	-	-	-	I,47	3I,4±0,8	-
I,98	45,8±I,2	58,5±8,2	35,2±I,4	2I,5±0,8	2,00	40,2±I,I	44,2±3,I
2,55	56,4±I,5	-	48,4±I,3	33,0±0,8	2,56	5I,3±I,5	63,5±7,6
3,03	66,6±I,7	-	55,0±I,6	-	3,I7	6I,5±I,7	7I,6±6,2
3,76	79,9±2,0	98,9±I3,8	68,8±I,9	50,3±I,3	3,65	68,I±2,5	80,7±6,9
4,42	-	-	78,7±2,0	-	4,45	8I,I±2,2	-
5,38	I08,4±2,8	-	92,6±2,3	-	6,I4	I06,8±2,8	-
7,3	I56,6±5,0	-	I36,7±4,0	I05,4±3,7	8,I	I3I,7±3,7	-

He-3

$E_{He}/2$	$Y_{He-3}/2$
2,24	42,2±I,2
5,74	98,6±2,5

REFERENCES

1. Vassil'kov R.G., Chirkin Yu.M., Chuvilo I.V. Preprint ITEP-14, Moscow, 1981.
2. Fraser I.S., Green R.E., Hilborn J.W. et al. Physics in Canada, 1965, vol. 21(2), p. 17.
3. Gompf F., Reichardt W. Progress report Kfk-3051, December 1980, p. 133.
4. Vassil'kov R.G., Goldanskii V.I., Grishkevich Ya.S. et al. Atomnaya Energia, 1968, vol. 25, p. 479.
5. Tsukada K., Nakahara Y. Atomkernenergic/Kerntechnik, 1984, vol. 44, p. 186.
6. Nakamura I., Uwamino Y. Phys. Rev. C., 1985, v. 29, p. 1317.

Q(I.M.Thorson): Was the last graph on energy cost per neutron normalized absolutely, i.e., is the cost a minimum for deuterons at ~2 GeV?

A(R.G.Vassil'kov): At Ed≈1.4 GeV, normalized absolutely in a sense of kinetic energy of d spent for neutron "liberation" (releasing) from the target (Pb ø20×60 cm).

ICANS-XI International Collaboration on Advanced Neutron Sources
KEK, Tsukuba, October 22-26, 1990

Measurement of neutron activation cross sections by p-Be semi-monoenergetic neutrons

T. Nakamura, H. Sugita, Y. Kondo, Y. Uwamino* and M. Imamura*
Cyclotron and Radioisotope Center, Tohoku University
*Institute for Nuclear Study, University of Tokyo

ABSTRACT

Neutron activation cross sections of C, Na, Mg, Al, Si, Ca, V, Cr, Mn, Cu, Zn and Au, which are mostly constituents of accelerator and building materials, in the energy range of 10 to 40 MeV, by using semi-monoenergetic neutrons from the Be(p,n) reaction. A proton beam of energies of 20, 22.5, 25, 27.5, 30, 32.5, 35, 37.5 and 40 MeV hits the 1-mm and 2-mm thick Be targets which are backed by the water coolant. The induced gamma-ray activities of the irradiated samples were measured with a pure Ge detector and of long-lived ^{26}Al were done by accelerator mass spectrometry. The activation cross section data could be obtained by unfolding technique.

I. INTRODUCTION

The radioactivities induced in accelerator and building materials, air and drain water by high energy particles, especially intense neutrons, cause severe external exposure to the workers in high energy intense accelerator facilities. To evaluate the induced radioactivities, the activation cross section data are of basic importance. The activation cross section data for protons have ever been published by several workers and for neutrons in the energy range of thermal to 20 MeV the evaluated data files exist such as ENDF/B-V and JENDL-3. While, on the other hand, there have been very few experimental data for neutrons of energy above 20 MeV and no evaluated data files.

Using a simple target system consisting of a Be disk backed by a water coolant, an intense semi-monoenergetic neutron field for activation experiment of energy up to 40 MeV was developed(1) at the SF cyclotron of the Institute for Nuclear Study, University of Tokyo. Activation experiment at this neutron field has been performed with natural samples of C, Na, Mg, Al, Si, Ca, V, Cr, Mn, Cu, Zn and Au.

II. NEUTRON FIELD FOR ACTIVATION EXPERIMENT

A proton beam of energies of 20, 22.5, 25, 27.5, 30, 32.5, 35, 37.5, 40 MeV is extracted from the SF cyclotron at the Institute for Nuclear Study, Univ. of Tokyo and hits the 1-mm thick (E_p= 20 to 37.5 MeV) and 2-mm thick (E_p= 40 MeV) Be targets which are backed by the water coolant. The water is simultaneously used to absorb the residual proton energy because of the small neutron production cross section of $^{16}O(p,n)$.
The neutron spectra at 0 deg were measured with a 51 mm diameter by 51 mm long NE-213 placed at 1.3 m from the Be target (1). An n-γ discrimination technique was utilized and the pulse height distribution by neutrons was unfolded to an energy spectrum with the revised FERDO code (2). The measured neutron spectra which subtracted the room-scattered components are shown with the unfolded errors in Fig. 1. In the figure, the monoenergetic peak neutron energy is indicated for each proton energy and the former is 4 to 5 MeV lower than the latter. The spectra also have low energy tails coming from the Be target and the water beam stopper.

III. MEASUREMENT OF INDUCED RADIOACTIVITY

The samples were irradiated by this semi-monoenergetic neutrons in the forward direction at 5 to 20 cm distant from the Be target. The proton beam current was kept to be several μA during the irradiation. The induced gamma-ray activities of the irradiated samples were measured with a pure Ge detector and the activation rates were obtained after the correction of self-absorption, parent-daughter decay and sum-coincidence effects. The measurement of long-lived ^{26}Al (half-life of 7.2×10^5 y) produced by $^{27}Al(n,2n)$ reaction was done by accelerator mass spectrometry(AMS) which has been equipped at the tandem Van-de-Graaf accelerator of the Research Center for Nuclear Science and Technology, Univ. of Tokyo (3). The $^{26}Al/^{27}Al$ isotopic ratios were obtained by AMS and were converted to the ^{26}Al activities.

IV. EVALUATION OF ACTIVATION CROSS SECTION

The measured activation rate, A_i is related to

$$A_i = N \int_0^{E_p} \sigma(E)\ \Phi_i(E)\ dE,$$

where i : ith experiment corresponding to each proton energy, E_p

N : number of target nucleus in a sample

$\sigma(E)$: activation cross section

$\Phi_i(E)$: neutron spectrum shown in Fig. 1.

Since the neutron spectrum $\Phi_i(E)$ is not purely monoenergetic but has low energy component, the $\sigma(E)$ value can be obtained by unfolding this integral equation. We finally obtained it with the SAND-II code of iterative perturbation method (4), the NEUPAC code using J-1 type unfolding method (5) and the least-square fitting (LSF) method. In the LSF, the absolute value of an initial guess of cross section was adjusted to the measured activation rates under the condition of preserving its shape as follows,

$$R = \Sigma \left\{A_i - \int_0^{E_p} k\ N\ \sigma(E)\ \Phi_i(E)\ dE\right\}^2$$

where k is determined to make R minimum. These codes required the initial guess value of $\sigma(E)$ for unfolding, and they were calculated with the ALICE code (6), in case of the lack of any experimental and calculated data. The SAND-II code does not give unfolded errors, while on the other hand, the NEUPAC code gives the errors propagated from errors of initial guess values, neutron spectrum and activation rates.

V. RESULTS AND DISCUSSIONS

Most results of activation cross sections are the first experimental data that have been obtained above 20 MeV. Some results are exemplified in Figs. 2 to 6. Figure 2 shows the $^{27}Al(n,\alpha)^{24}Na$ cross section data. Our results unfolded by three codes, SAND-II, NEUPAC and LSF, agree quite well each other, except that a small bump around 25 MeV can only be seen by the SAND-II unfolding. Our data also show good agreement with the data by ENDF/B-V and Greenwood (7) as a whole, but are 5% smaller at a peak value around 13 MeV than them. The $^{23}Na(n,2n)^{22}Na$ cross sections are shown in Fig. 3. The experimental data and the theoretically evaluated data are largely dispersed and our results are

close to the experimental data by Maslov et al. and Menlove et al. (8), and to the IRDF-85 data file.

Figure 4 shows the $^{27}Al(n,2n)^{26}Al$ cross section data. Our results given by SAND-II and NEUPAC show very good agreement each other. Our experimental results give a little lower values than Iwasakis' newest experimental data around 15 MeV (9). For comparison, the experimental data of $^{27}Al(n,2n)^{26}Al^{m}$ (half-life of 6.3 sec) cross section by Mani et al. (10) are also shown in Fig. 4. The peak value of 150 mb at 20 MeV for $^{27}Al(n,2n)^{26}Al^{m}$ is 1.6 times larger than that of 95 mb at 20-24 MeV for $^{27}Al(n,2n)^{26}Al^{g}$, but the former value in the lower energy region is much smaller than the latter value.

For $^{nat}Si(n,XnYp)^{28}Al$ cross section data shown in Fig. 5, the SAND-II results have slightly larger peak value around 12 MeV than the NEUPAC results. Our results are compared with the theoretical $^{28}Si(n,p)^{28}Al$ cross section data given by the IAEA compilation (11), and are about 10 to 25 % smaller than the latter between 10 and 15 MeV. The $^{nat}Cu(n,Xn)^{62}Cu$ cross section data are shown in Fig. 6. Our results unfolded by three codes also show good agreement within their unfolded errors. The IAEA data for $^{63}Cu(n,2n)^{62}Cu$ (11) give about 30 to 40 % higher values than our results and the GNASH calculation for $^{nat}Cu(n,Xn)^{62}Cn$ by Yamamuro (12) gives closer values to our experimental data.

The authors wish to thank to Drs. H. Nagai and K. Kobayashi and Mr. H. Yamashita for their kindful cooperation on the ^{26}Al measurement by the AMS system. This work was financially supported by a Grant-in-Aid for Cooperative Research of the Japanese Ministry of Culture and Education.

References

1 Y. Uwamino, T. Ohkubo, A. Torii and T. Nakamura, Nucl. Instr. Methods, A271, 546 (1988).

2 K. Shin, Y. Uwamino and T. Hyodo, Nucl. Technol., 53, 78 (1981).

3 H. Nagai, T. Kobayashi, M. Honda, M. Imamura, K. Kobayashi, K. Yoshida and H. Yamashita, Nucl. Instr. Methods, B29, 266 (1987).

4 W. N. McElroy, S. Berg, T. Crockett and R. G. Hawkins, AFWL-TR-67-41, Vols. I-IV, Air Force Weapons Laboratory (1967).

5 A. Sekiguchi, M. Nakazawa and N. Ueda, PNC J260 85-01, Power Reactor and Nuclear Fuel Development Corporation (1985).

6 M. Blann and J. Bisplingshoff, LLNL Report No. UCID 19614, Lawrence Livermore National Laboratory (1983).
7 L. R. Greenwood, ANL/FPP/TM-115, Argonne National Laboratory (1978).
8 Cited from D. C. Larson, Nucl. Sci. Eng., 78, 324 (1981).
9 S. Iwasaki, J. R. Dumais and K. Sugiyama, Proc. Intern. Conf. Nucl. Data for Sci. and Technol., Mito, ed. by S. Igarashi, (1988) 295.
10 G. S. Mani, G. J. McCallum and A. T. G. Ferguson, Nucl Phys., 19, 535 (1960).
11 International Atomic Energy Agency, "Handbook on Nuclear Activation Data", Technical Report Series No. 273 (1987).
12 N. Yamamuro, Private Communications (1990).

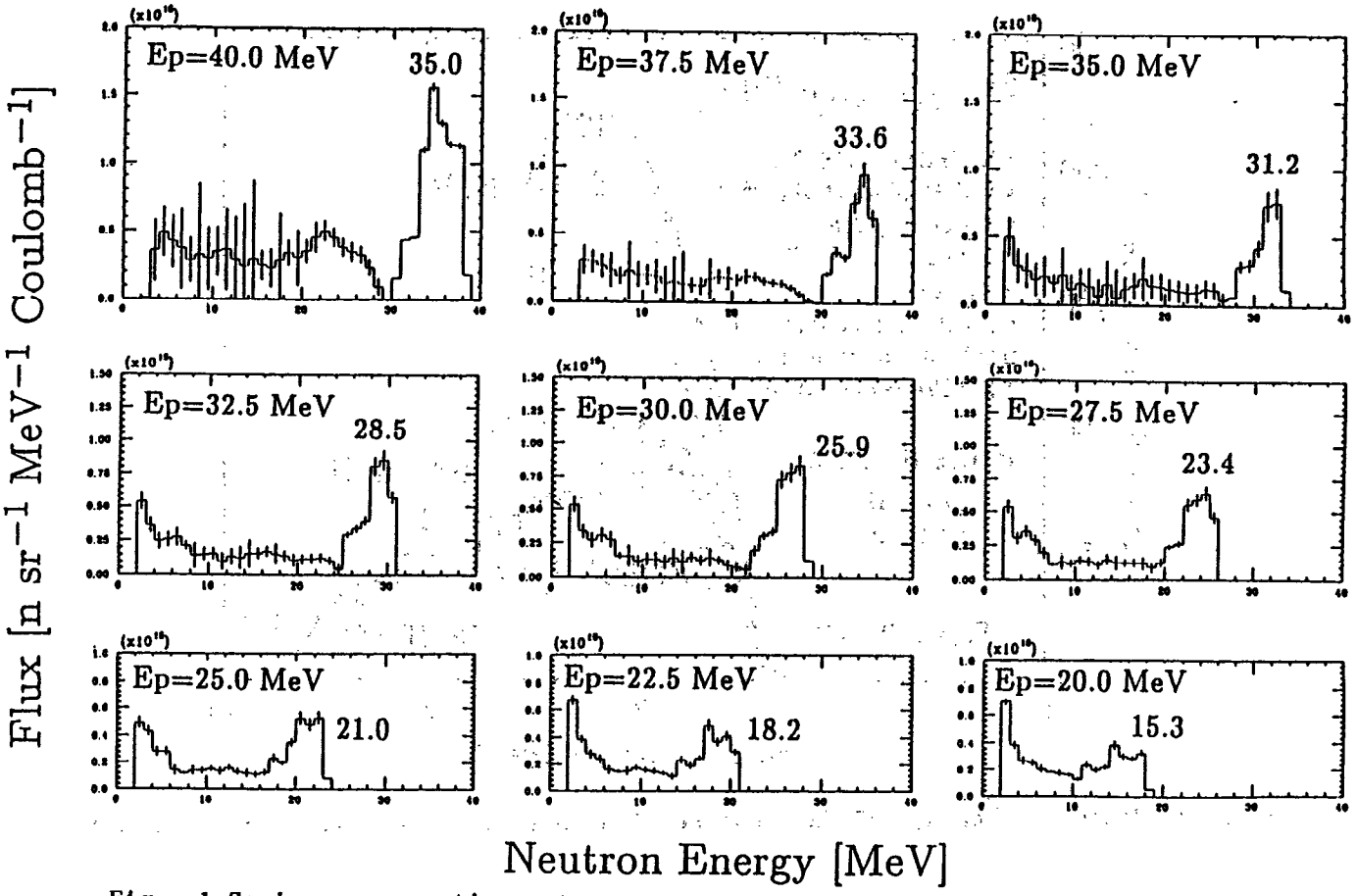

Fig. 1 Semi-monoenergetic neutron energy spectra for proton energies of 20, 22.5, 25, 27.5, 30, 32.5, 35, 37.5, 40 MeV

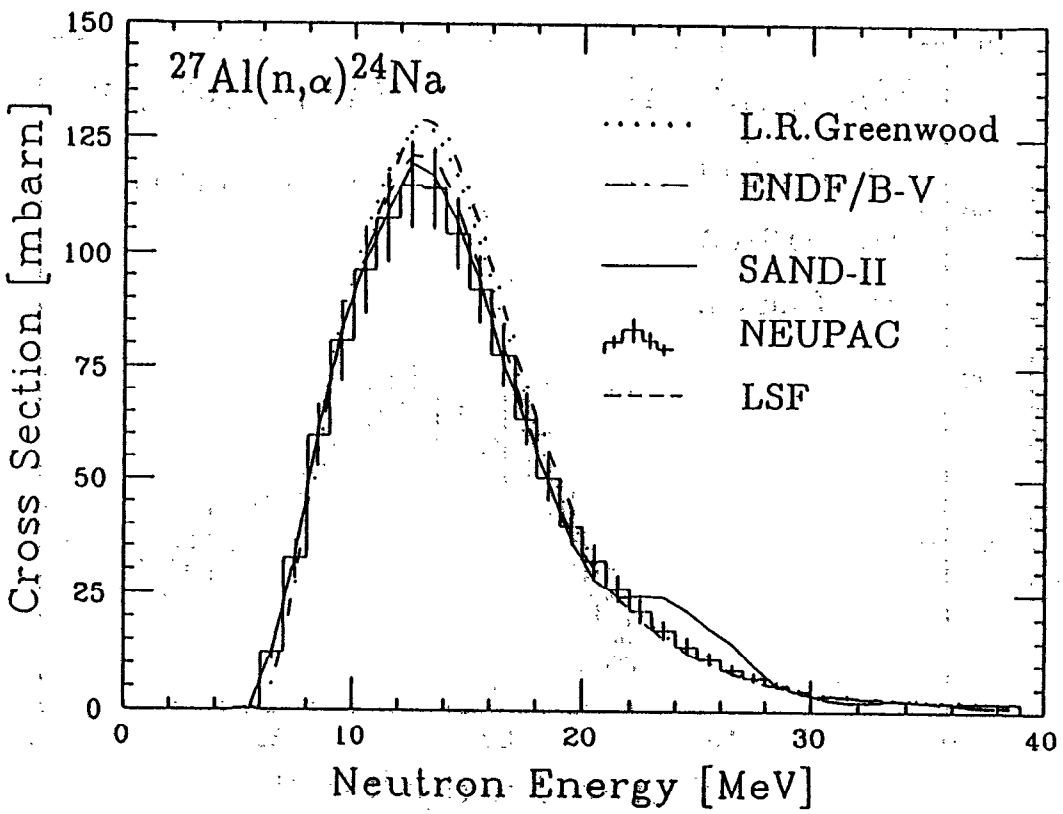

Fig. 2 Measured ^{27}Al(n,α)^{24}Na cross section data, together with the cited data

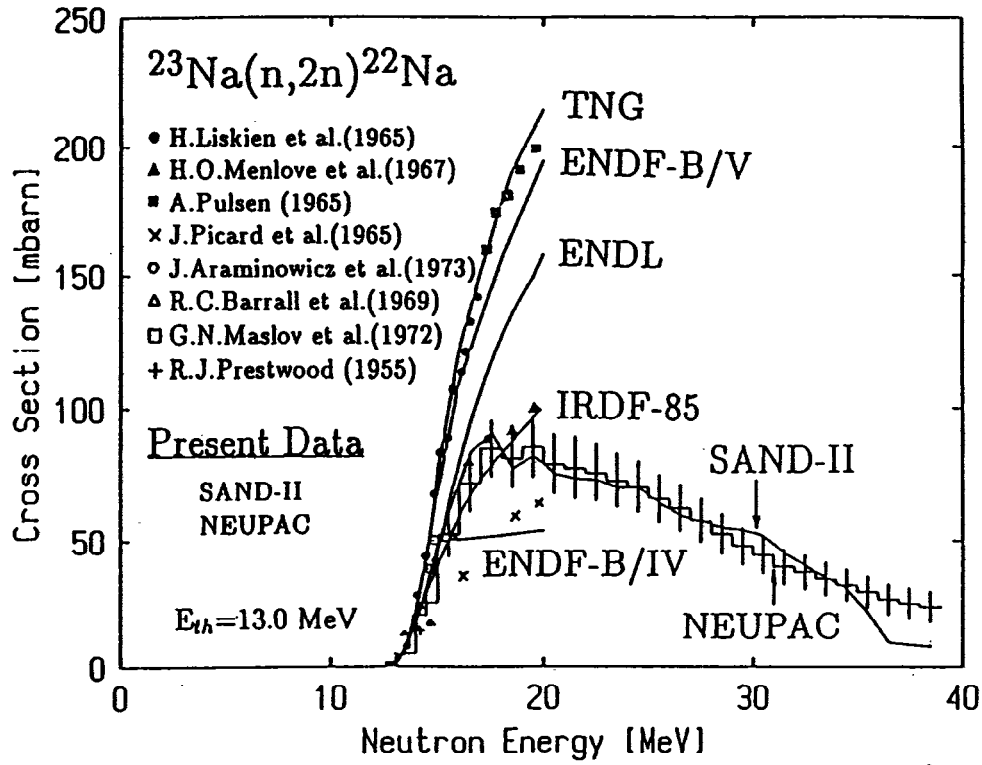

Fig. 3 Measured ^{23}Na(n,2n)^{22}Na cross section data, together with the cited data

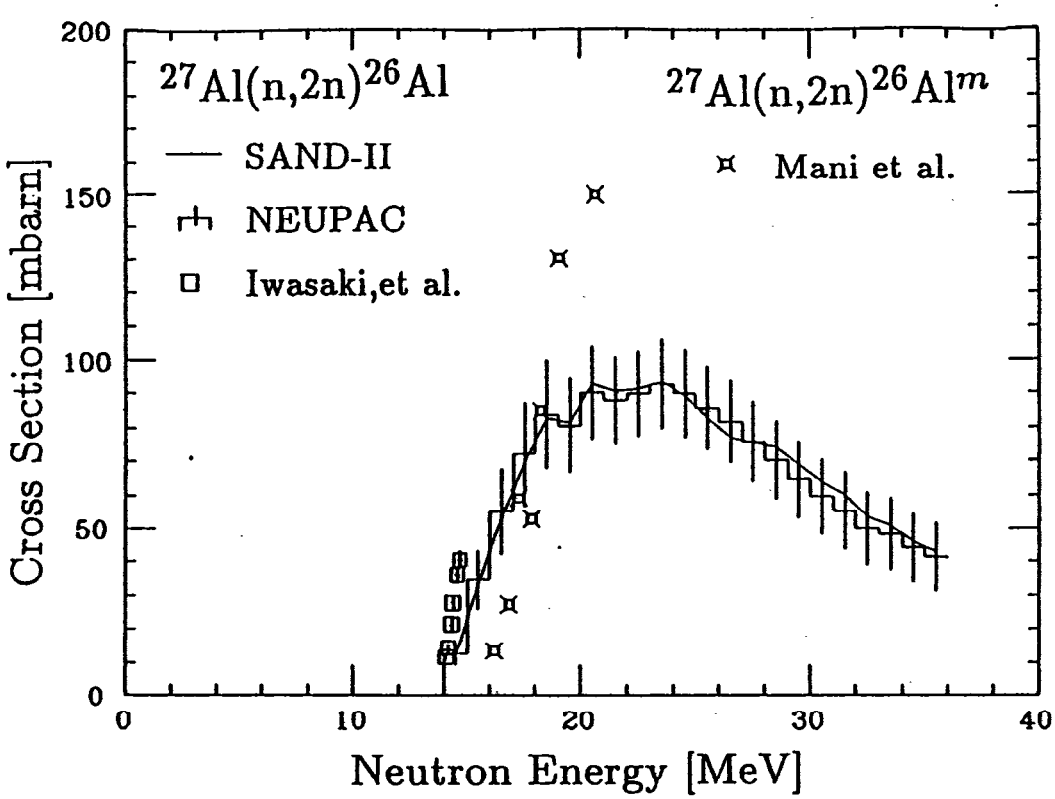

Fig. 4 Measured ^{27}Al(n,2n)^{26}Al cross section data, together with the cited data

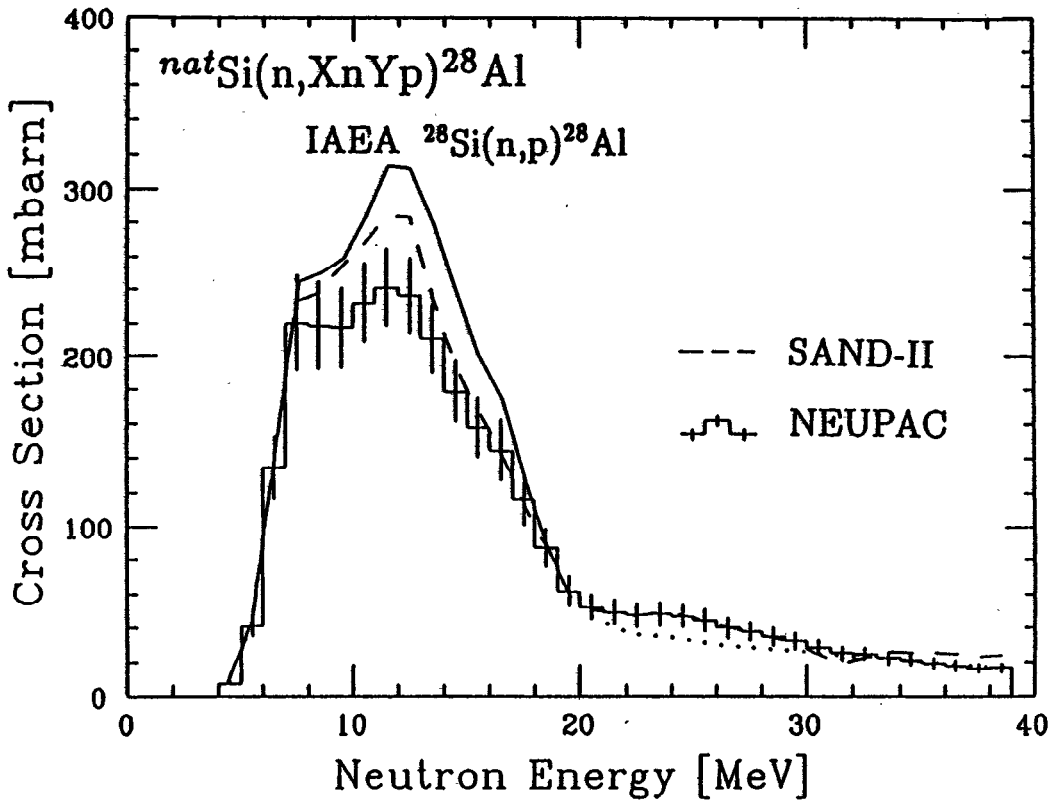

Fig. 5 Measured $^{nat}Si(n,XnYp)^{28}Al$ cross section data, together with the cited data

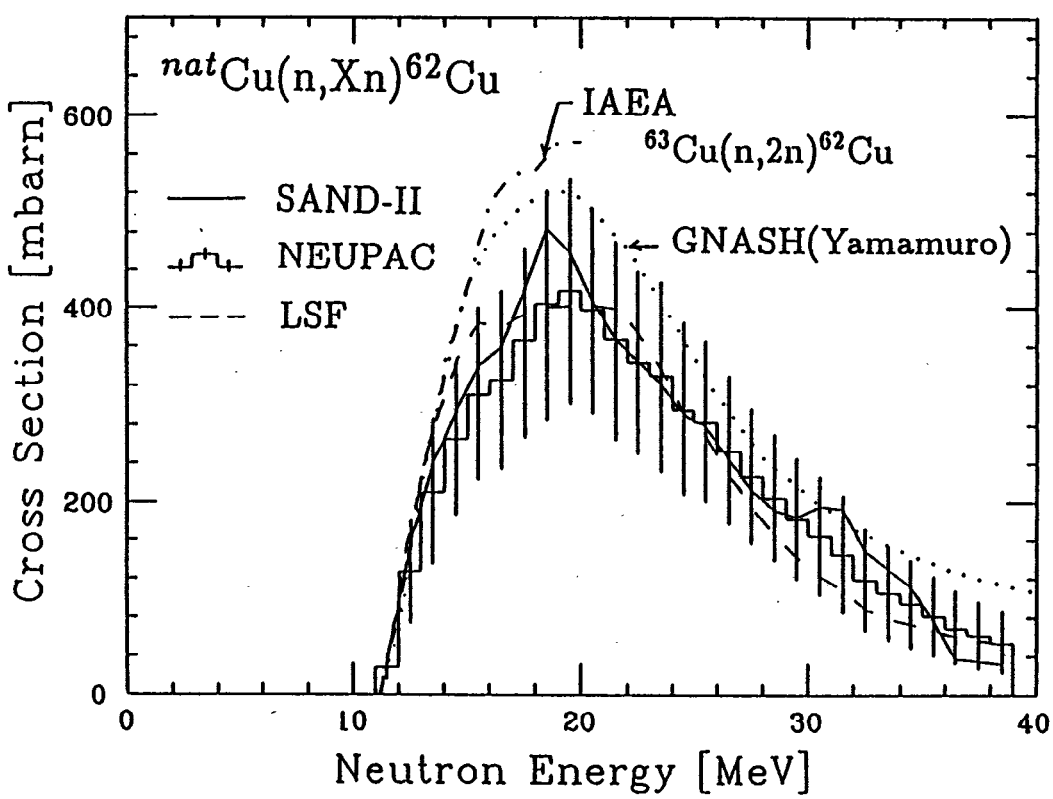

Fig. 6 Measured $^{nat}Cu(n,Xn)^{62}Cu$ cross section data, together with the cited data

ICANS-XI International Collaboration on Advanced Neutron Sources
KEK, Tsukuba, October 22-26, 1990

Benchmark Experiment for Material Penetration of Several Tens MeV Neutrons

by

Kazuo Shin[1], Yoshitomo Uwamino[2], Takashi Nakamura[3], Shigeo Numata[4], and Takashi Kato[5]

[1]Department of Nuclear Engineering, Kyoto University
[2]Institute for Nuclear Study, University of Tokyo
[3]Cyclotron and Radioisotope Center, Tohoku University
[4]Shimizu Corporation
[5]Nikken Sekkei

ABSTRACT

This paper describes (i) benchmark experiments of intermediate energy neutron transmission through iron, lead and graphite shields and (ii) estimation of thick target neutron yield by high energy ^{4}He ions.

In the neutron transmission experiments, a collimated beam of neutrons induced by 65-MeV protons in a thick Cu target was utilized in the measurements. Monte Carlo calculations by MORSE were carried out with the DLC-87 Hilo multigroup cross sections. It was found that the DLC-87 data reproduced the measured data well for the graphite shield, but gave partly higher values for the iron shield, and overpredicted the lead transmitted spectra.

Neutron yields for stopping-length target of Cu and Be were estimated for ^{4}He ion bombardment with the intranuclear cascade evaporation Monte Carlo code, HETC/KFA-1. The results were obtained for ion energies from 100 MeV/u to 800 MeV/u. The neutron spectra were fitted to simple evaporation spectra and the systematics on the nuclear temperature was studied. Total neutron yield per incident ^{4}He ion was about 5 times larger than that per proton.

I. Introduction

Treatment of neutron reactions in the energy range above 15 MeV up to 100 MeV is the most difficult part in the neutron transport calculation in high and intermediate energy range. The validity of the intranuclear cascade model, which has been very often used for the neutron transport calculation for high energy accelerators, is limited below several tens MeV energies. Multigroup cross section data DLC-87/1/ are often used in this energy range. The data were evaluated partly depending on the intranuclear cascade evaporation model. However, there are very few neutron benchmark data which enable ones to test accuracy of neutron transport calculations in this energy range./2,3/

The objective of the first half of this paper is to provide benchmark data in this energy range for neutron transmission calculation through several materials.

The remaining part of this paper treats the neutron production from

thick targets bombarded by ^{4}He ions. The work was done mostly for the design calculation of a heavy ion medical accelerator HIMAC. The accelerator is now proceeded to be built by the National Institute of Radiological Science.

Several experimental works on thick-target neutron yield have ever been published in the energy region of 100 to 800 MeV protons/4-7/, but for ^{4}He ions of energy higher than 100 MeV/u, only one experimental data exist for 710 MeV (177.5 MeV/u) ^{4}He ions./8/ We estimated the thick-target neutron yields for 100 to 800 MeV/u ^{4}He ion bombardment, using the HETC/KFA-1 intranuclear cascade evaporation Monte Carlo code./9/

II. Benchmark Experiment for Neutron Penetration through Shields

(1) Experimental Method

The experiment was made at the AVF cyclotron facility of Osaka University. A 1-cm thick (proton stopping range) Cu target was irradiated by 65-MeV protons and generated neutrons in the forward direction were pulled out to an experimental room through a 7.5-cm diameter iron-lined concrete collimator of 50-cm length. The experimental setup is depicted in Fig. 1. Experimental systems were set at locations very close to the collimator exit. Those were iron, lead and graphite shields of the size of about 40 cm by 40 cm in cross section and 10 cm to 100 cm in thickness.

Transmitted neutrons were measured just behind the shield system by a 3-inch (7.6 cm) diameter by 3-inch height NE-213 scintillator. The back-

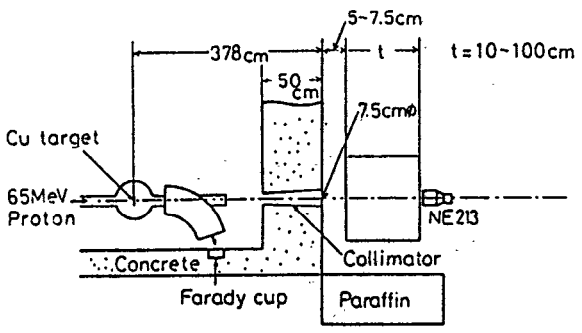

Fig.1 Experimental arrangement

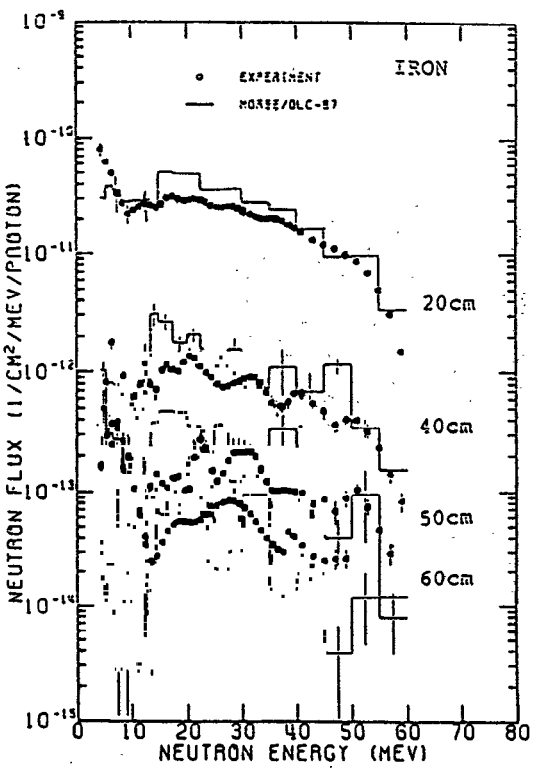

Fig.2 Transmitted neutron spectra through iron shields

background data were obtained in the same geometrical condition except that the collimator was closed by an iron plug. The source spectrum was measured without the shield.

The obtained neutron pulse-height spectra were unfolded to energy spectra by FERDO-U code./10/ Required response fucntions for the unfolding were constructed from measured response data./11/

(2) Calculation

The calculation of the transmitted neutron spectra through the shields was made by the MORSE code/12/ with multigroup cross sections DLC-87./1/ The experimental geometry after the collimator exit was simulated in the calculation. The collimator was not included in the model. Instead, source neutrons generated based on the measured spectrum were emitted from the target within a sharp cone of 3.14×10^{-4} sr.

(3) Results of the Benchmark Experiment

Neutron transmission spectra behind the iron shields are showed in Fig. 2. The measured spectra exhibit some sort of fluctuation as the shield thickness becomes larger due to poorer statistics. The overall agreement between the calculation and the experiment is well except that the systematic disagreement is seen at energies 15-30 MeV.

There are several reported measurements of the total cross sections and a few experiments for nonelastic cross sections of iron for neutrons above 15 MeV. The data in the DLC-87 are compared with those measured data.

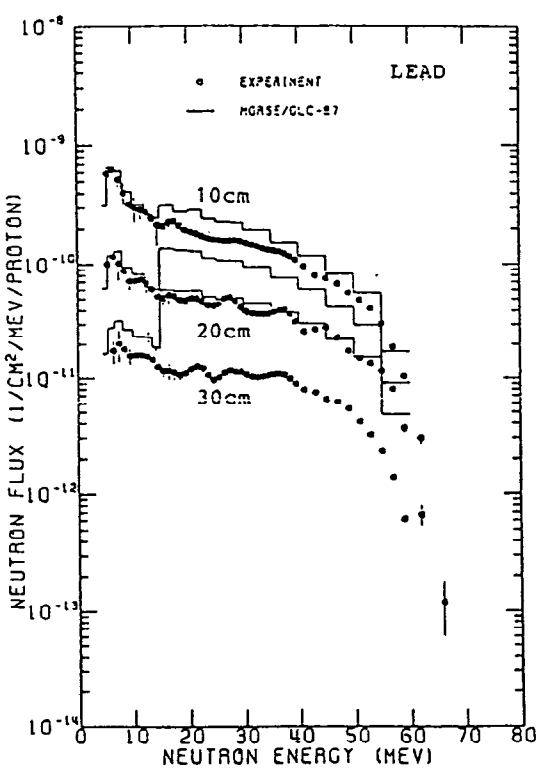

Fig.3 Transmitted neutron spectra through lead shields

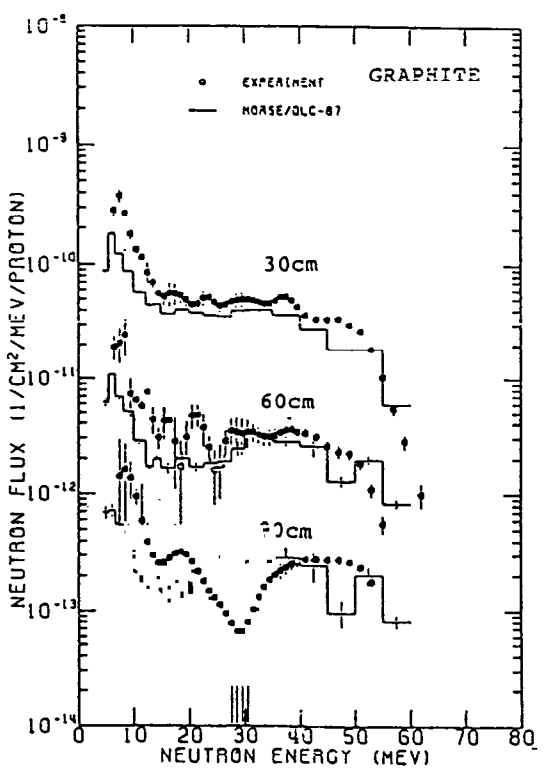

Fig.4 Transmitted neutron spectra through graphite shields

It was found that the underestimation of the iron total cross section is made at energies 15-30 MeV in the DLC-87. This is the reason for the overprediction of the transmitted neutron fluxes by the MORSE/DLC87 calculation observed in the corresponding energy range.

Figure 3 shows comparison of the lead transmitted neutron spectra between the MORSE/DLC-87 calculation and the experiment. The MORSE calculation overestimates the spectra very much in the energy range above 15 MeV, the tendency being pronounced as the lead shield becomes thicker. Because of this overestimation, the fluxes in the lower energy range below 15 MeV are also slighly overpredicted for the 30-cm thick shield, probably through the down scattering of neutrons from higher energies.

The DLC-87 lead cross section data were examined by comparing the data with some of existing measured data. The elastic scattering was ignored in evaluating the lead data above 15 MeV, and nonelastic cross sections were treated as total cross sections in the DLC-87. This is the main reason for the overprediction of transmitted fluxes. Moreover the nonelastic cross sections seemed to be somewhat underestimated above 20 MeV. This may be another reason for the overprediction of the transmitted neutron fluxes.

Neutron spectra transmitted through graphite shields are shown in Fig. 4. The overall spectra of each set of data agrees well with each other. A weak underestimation by the MORSE/DLC-87 calculation is observed at the lowest energy part below 10 MeV. The reason for this is still not clear. The big depression in the measured energy flux of the 90-cm thickness around 30 MeV is due to the subtraction of the oscillating background spectrum. A small fluctuation is also seen in the measured 60-cm spectrum.

III Estimation of Thick Target Neutron Production for ^{4}He Ions

(1) HETC Calculation and Comparison with Experiment

Neutron production by ^{4}He ions was simulated using the HETC/KFA-1 Monte Carlo code to generate systematic neutron source data for the design of the HIMAC heavy ion medical accelerator.

Before doing systematic calculations of the neutron yield, the calculational accuracy of the HETC/KFA-1 code was checked by comparing the results with the measured data by Cecil et al. They measured energy spectra and total yield of neutrons produced from a stopping length iron target (10.2cm by 15.4 cm size and 4.445 cm thickness) bombarded by 710 MeV ^{4}He ions.

Figure 5 shows the comparison between the measurement and the HETC calculation. Results of the HETC calculation were integrated over angular intervals of 0° to 30°, 30° to 70°, 70° to 110° and 110° to 180° by the SIMPEL code to decrease the statistical errors. For direct comparison, the differential neutron yield data of Cecil et al. (given at angles 0°, 6°, 15°, 30°, 45°, 60°, 90°, 120°, and 150°) were also integrated over the same angular intervals.

It is seen in the figure that the HETC calculation gives the overestimation of absolute neutron yield in the forward direction,

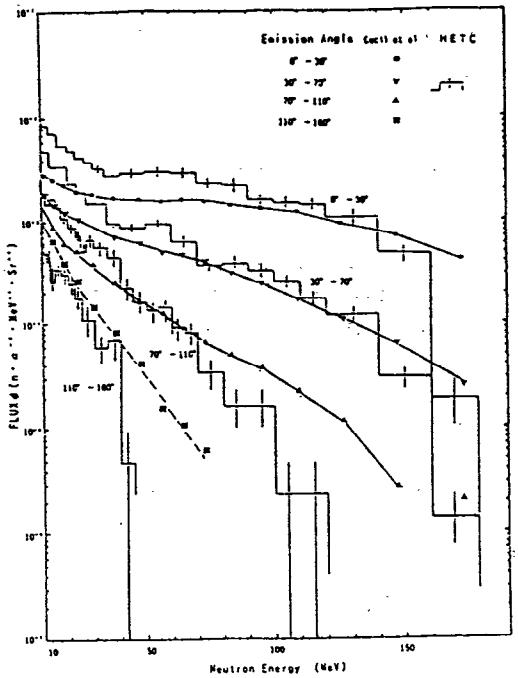

Fig.5 Neutron spectra produced from thick iron target by 710 MeV ^{4}He

Table I Targets assumed in the neutron yield calculations

Energy of α-beam E_0 (MeV)	Target Material	HxWxL (cm)	Number of History
800	Cu	20x20x40	15600
600	Cu	x30	20000
500	Cu	x20	20000
225	Cu	x10	20000
100	Cu	x 2	20000
500	Be	x80	18800
	α-beam	W, H, L	Statistical Error < 1 %

particularly in the lower energy range. This overestimation becomes less with the emission angle. The calculated spectra are softer than the measured spectra at all angles. This tendency is also shown in thick-target neutron data for protons in Refs./4-7/, but more remarkable for ^{4}He ions.

The total integrated neutron yield above 10 MeV was calculated. It was 0.65 neutron/ion. It is in a good agreement with the experimental value of 0.51 neutron/ion, being 1.27 times the measured value.

From this comparison it was revealed that the HETC code gives reasonable estimation of total neutron yield.

(2) Estimation of Neutron Yields

(i) Calculational method

The HETC calculations were performed for several ^{4}He energies and the target materials indicated in Table I. The target thickness was set to the stopping length of the incident beam. Copper was selected since it was main material in magnet, and beryllium was considered in the HIMAC design as a target for secondary radioactive beam production. The history numbers of the calculations were 20000 at maximum and the statistical errors in total yield were less than 1%.

To test the difference of neutron yields between ^{4}He and p beams, the HETC calculations were also made for copper target with the incidence of 225 and 500 MeV protons, and for the beryllium target with 500 MeV protons.

(ii) Results of Calculation

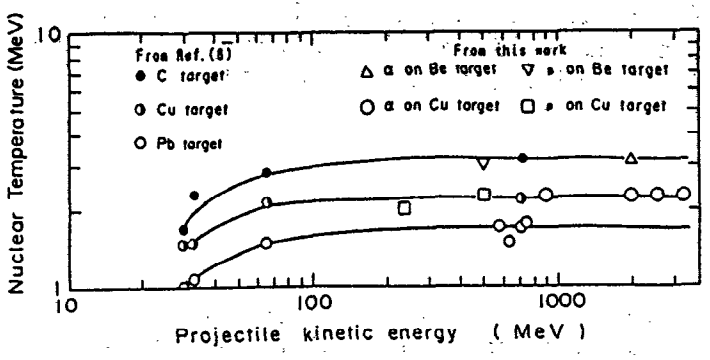

Fig.6 Nuclear temperature of the equilibrium component

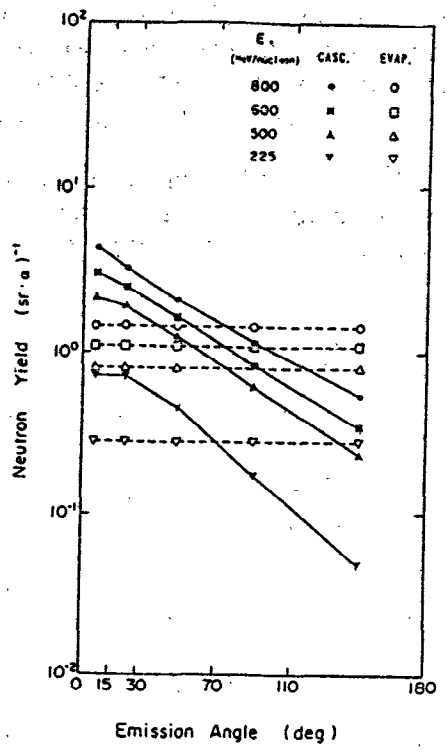

Fig.7 Angular distributions of calculated neutrons

Calculated differential neutron yield data were fitted by the phenomenological hybrid expression proposed by Nakamura/13/ with the evaporation spectrum plus two maxwellian-type spectra. The first term expresses the equilibrium component and the other two are for nonequilibrium neutrons.

Figure 6 shows the nuclear temperature of the equilibrium component as a function of projectile kinetic energy. The figure indicates that the nuclear temperature increases with increasing the projectile kinetic energy and with decreasing the target mass. It approaches a saturated value at energies higher than 100 MeV.

The angular distribution of the neutron flux was obtained by integrating the spectra over the neutron energy. The obtained fluxes for the copper target are shown in Fig. 7 for each of the cascade and evaporation components as a function of the angle. The angular distributions of the cascade and total neutron yield can be roughly approximated by the exponential shape of $\phi = \exp(-\beta\theta)$. The beta values are showed in Table II.

Figure 8 shows the total neutron yield as a function of incident particle energy per nucleon. The results obtained in this work are added to those given in Ref.14. For ^{4}He projectiles, two dashed curves for C and Cu targets were given by connecting experimental data./14/ The present results are higher than the extrapolation of the curves to higher energies.

It is noteworthy that the total neutron yields of Ref.14 were estimated values by assuming the pure Maxwellian distribution to extrapolate measured

low energy neutron spectrum to further lower energies where data were not given because of the discrimination of the measurement. In the HETC calculation, there were excess number of neutrons at lower energies whose spectrum was not represented by the maxwellian distribution. Those may be due to the neutron multiplication and energy degradation in a bulky target.

For the 500 MeV/u energy, the ratio of neutron yield by ^{4}He to that by proton was 4.37 for the Cu target and 4.15 for the Be target. This was almost equal to the ratio of number of nucleons in the projectiles.

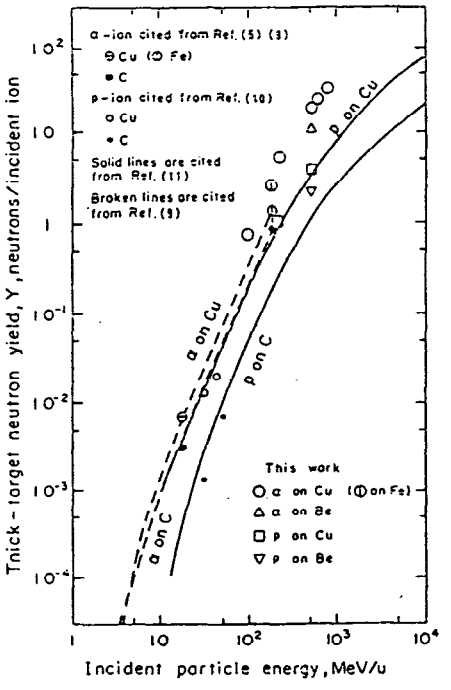

Fig.8 Neutron total yield as a function of ion energy per nucleon

Table II Beta values for exponential formula of neutron angular distributions

Projectile	Energy E_0 (MeV/nucleon)	Target	β $\phi_{casc.}(\theta)$	β $\phi_{total}(\theta)$
α	800	Cu	0.87	0.43
	600		0.92	0.45
	500		0.95	0.46
	225		1.12	0.55

References

1) R. G. Alsmiller, Jr. and J. Barish, Nucl. Sci. Eng., 80, 448 (1982).
2) K. Shin et al., Nucl. Sci. Eng., 71, 294 (1979).
3) Y. Uwamino et al., Nucl. Sci. Eng., 80, 360 (1982).
4) R. Madey and F. M. Waterman, Phys. Rev. C8, 2412 (1973).
5) S. Cierjacks et al., Proc. 4th ICANS Meeting, National Lab. for High Energy Physics, Tukuba (1980).
6) M. M. Meier et al., Nucl. Sci. Eng., 102, 310 (1989).
7) M. M. Meier et al., Nucl. Sci. Eng., 104, 339 (1990).
8) R. A. Cecil et al., Phys. Rev. C21, 2471 (1980).
9) P. Cloth et al., "The KFA-Version of the High-Energy Transport Code HETC and Generalized Evaluation Code SIMPEL" Jul-Spez-196 (1983).
10) K. Shin et al., Nucl. Sci. Eng., 71, 294 (1979).
11) K. Shin et al., prepared for publication
12) E. A. Straker et al., DNA2860T (1977).
13) T. Nakamura, Nucl. Instrum. Methods, A240, 207 (1985).
14) T. Nakamura, Genshikaku Kenkyu 29, 55 (1985) (in Japanese).

Q(I.M.Thorson): Did you do one "bad" geometry experiments when you did your "good" geometry experiment?

A(K.Shin): Since the background level in the counting room is rather high, it is not possible to measure scattered neutrons. However, it is very important thing to obtain informations in a bad geometry.

ICANS-XI International Collaboration on Advanced Neutron Sources
KEK, Tsukuba, October 22-26, 1990

Shutter System for the SINQ Neutron Guides

I. Anderson, J. Ehrat, D. Suhi, W. Wagner
PAUL SCHERRER INSTITUTE
CH-5232 Villigen-PSI, Switzerland

ABSTRACT

Viewing the liquid D_2 cold moderator of the spallation source SINQ, a neutron guide system will be provided to achieve an efficient transport of subthermal neutrons to the instruments in the remote experimental hall. Four separate neutron guides are forseen, with an option for a fifth one to be installed in future. The concept of guide shielding and performance includes a set of shutters, situated at the outside of the main target shielding, with the dual purpose of shielding the radiation from the target and inner shielding in the closed position and guiding the neutron beam in the open position. This latter function imposes strict requirements on alignment accuracy and mechanical stability while the necessity of shielding high energy neutrons from the spallation target implies the use of bulky shielding. The technical concept elaborated to fulfill these requirements is presented.

I INTRODUCTION

One of the significant features of the SINQ spallation source is a large liquid D_2 cold source which, due to an optimum position near the flux maximum in the heavy water moderator, will provide a cold neutron flux which is comparable to most medium flux reactors /1, 2/. Initially four neutron guides with large cross-section (120 x 50 mm^2) are planned which start in the main shielding at a distance of 1.5 m from the source. Additionally an option has been retained in the design of the system, in particular the in-shielding part, to install a fifth guide at a later stage. Moreover promising results in the development of high quality multilayers at PSI /3/ and elsewhere make us confident that high divergence coatings will enable us to optimize the guide system for high transmission even at relatively short wavelengths. This requirement together with the desire to retain large cross-section beams leads to rather long line of sight lengths, which may to some extent be reduced by the use of channelled guides /4/, and necessitates the installation of beam shutters which are capable of stopping the small but problematic flux of high energy neutrons leaving the target. At SINQ two such shutters (each one serving two guides) will be situated at the outside of the main shielding, Fig. 1., in a heavily shielded enclosure. Because of the restricted space available, and the possibility of installing a fifth guide and shutter at a later date, the shutters operate by rotation about a horizontal axis perpendicular to the guide axis.

In addition to functioning as a high energy neutron beam stop the shutter system must fulfill certain other requirements:

- In the open position maximal transmission of neutrons must be assured so that the shutter comprises a section of guide which must be aligned to within the nominal tolerances (0.01 mm) of the subsequent system leaving a minimum gap between successive sections and taking into account thermal distortions.
- Due to the fragility of the glass guide section and the required alignment accuracy opening and closing of the shutter must be carried out in a controlled manner to prevent shocks. In the present design the closing/opening time is of the order of 3 minutes.
- The shutter must close automatically under conditions of power or compressed air failure or when access is attempted into radiation controlled areas of the guide system. For this latter purpose end position indicators are branched into a security system.
- The shutter will remain under vacuum to reduce neutron flux losses.

All the above requirements have been integrated into the detailed technical concept elaborated in the next section.

II TECHNICAL CONCEPT

2.1 Mechanical construction

As shown in Fig. 2 the main component of the shutter is a large drum, 1880 mm in diameter and 700 mm wide, weighing 16 tons which, for ease of construction, is made up in two parts which have been stepped to prevent gaps in the shielding. The material for the drum has been selected according to the requirement of minimum Co (< 0.01 %) and Cr (< 0.8 %) content, which may be guaranteed by suppliers, and depending on cost estimates will be either Steel St 37-2 or cast iron.

Two, 2 m long guide sections separated by an angle of 2 degrees will be pre-aligned in a boral jacketed, aluminium housing which is in turn mounted on three adjustable supports within the drum. The shutter housing is essentially in the form of a flat, hollow cylinder, 2080 mm in diameter, made up of 25 mm thick steel walls to which a 50 mm thick plate is welded on one side and a similar coverplate is mounted with vacuum flange on the other side. The shielding drum turns on two precision bearings mounted in the centres of these two plates.

Taking into account the desirability of reducing to a minimum the gaps between successive sections of guide, the simplest solution for introducing the guide sections immediately preceeding and following those in the drum is to align them directly in extensions mounted on the shutter housing as shown in Fig. 2. Furthermore the ends of these connecting guide sections and those of the sections mounted in the drum will be cut in the form of an arc centred on the axis of rotation of the drum. In this way the gap between successive reflecting sections can be reduced to 2 mm. The complete shutter is mounted by means of three adjustable supports onto a positioning trolley which runs on a rail system allowing the whole system to be rolled away from the main shielding prior to removal by means of the lifting rings mounted on top of the housing. The rails are mounted on a steel ground plate which is underlayed with cement for correct alignment and the positioning accuracy of the trolley in the forward position is guaranteed by a reference pin. The total weight of the shutter system is 20 tons.

2.2 Drive system

Closing the shutter involves turning the shielding drum by 90 degrees thus bringing the guides into the vertical position. This is achieved by means of a large oil filled hydraulic cylinder operating on a rack and spur gear mounted on the side of the shutter housing.

Although compressed air is readily available at PSI, the tendency for vibration in a compressed air drive system makes it unsuitable for the precison and control required in the present application. Thus we have chosen to use a hydraulic medium transformer (compressed air/oil) which guarantees a slow and controlled rotation in both directions. The rotation speed can be adjusted by means of a throttle valve as indicated in Fig. 3.

The end positions are defined by contact of a cam on the shutter housing cover plate which comprises a shock absorber ensuring a gradual decrease of the rotation speed as the end positions are approached. In addition the accurate rotation of the drum is aided by a guide bearing mounted on the housing and running in a channel on the outer edge of the drum. This channel is so positioned to provide the necessary asymmetry in the drum which causes it to close automatically under loss of power or compressed air.

2.3 Adjustment of the guide elements.

The guides in the aluminium housing will be pre-aligned by the manufacturer before introduction into the drum. The horizontal alignment is guaranteed by the wedge shaped form of the housing itself while the vertical adjustment is achieved by means of the three adjustable supports and facilitated by the provision of reference surfaces and pins on the outside of the shutter housing. In a similar way the connecting guide sections in the extension mountings may be adjusted to match the prealigned sections in the drum. Finally the entire shutter may be aligned with respect to the rest of the guide system by means of the three large adjustable supports on the positioning trolley.

REFERENCES

/1/ G.S. Bauer
"SINQ - Status report Oct. 1990"
This conference

/2/ H. Spitzer, A. Höchli, G.S. Bauer and W. Wagner
"Technical Concept of the liquid D_2 Cold Moderator for SINQ"
This conference

/3/ P. Böni, I. S. Anderson, R. Hauert, P. Ruterana, K. Solt,
B. Farnoux, G. J. Herdman, J. Penfold and O. Schärpf
"Investigation and Growth of Multilayers"
This conference

/4/ I. Anderson and F. Atchison
"SINQ Guide Concept"
ICANS 1988

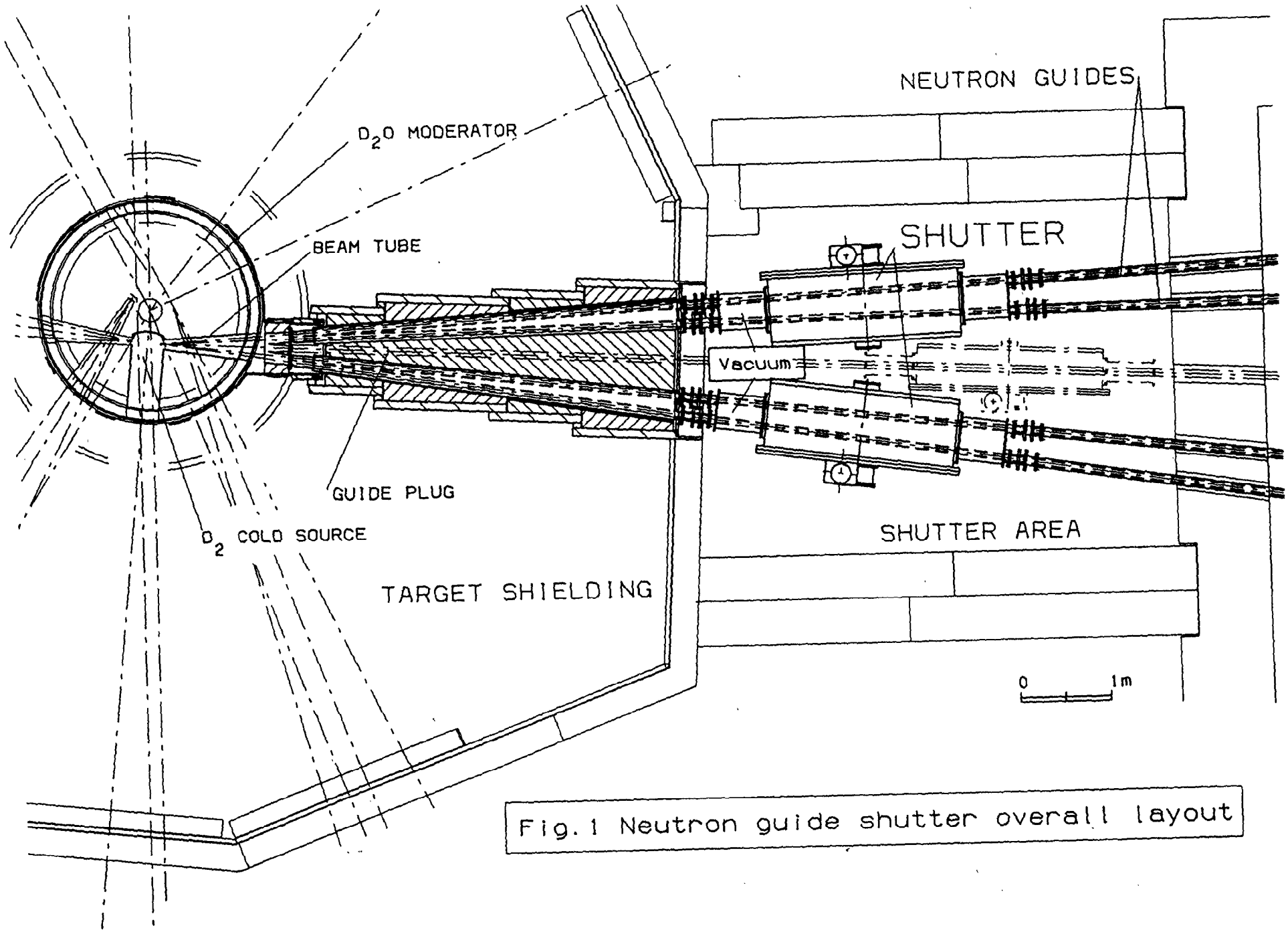

Fig. 1 Neutron guide shutter overall layout

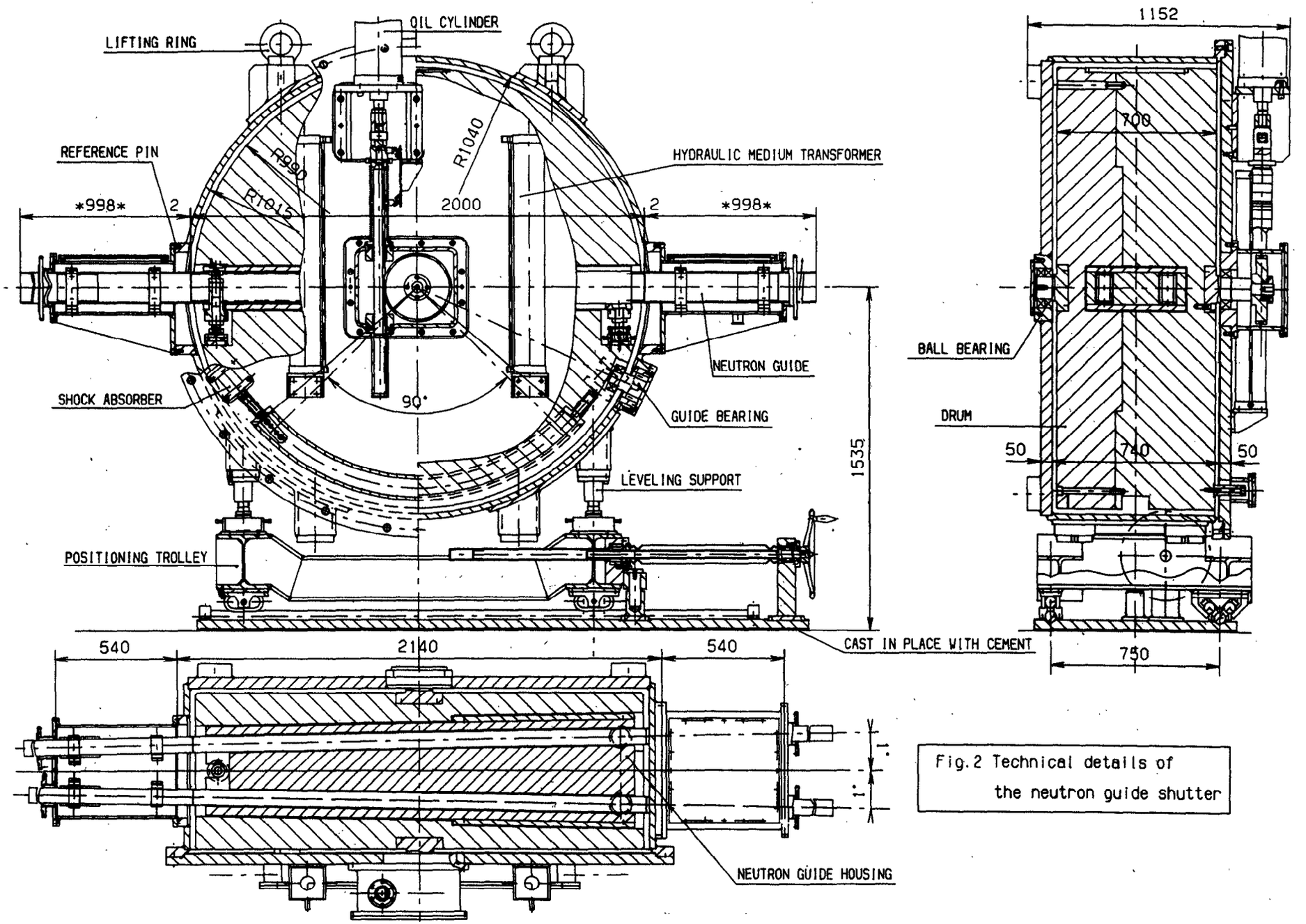

Fig.2 Technical details of the neutron guide shutter

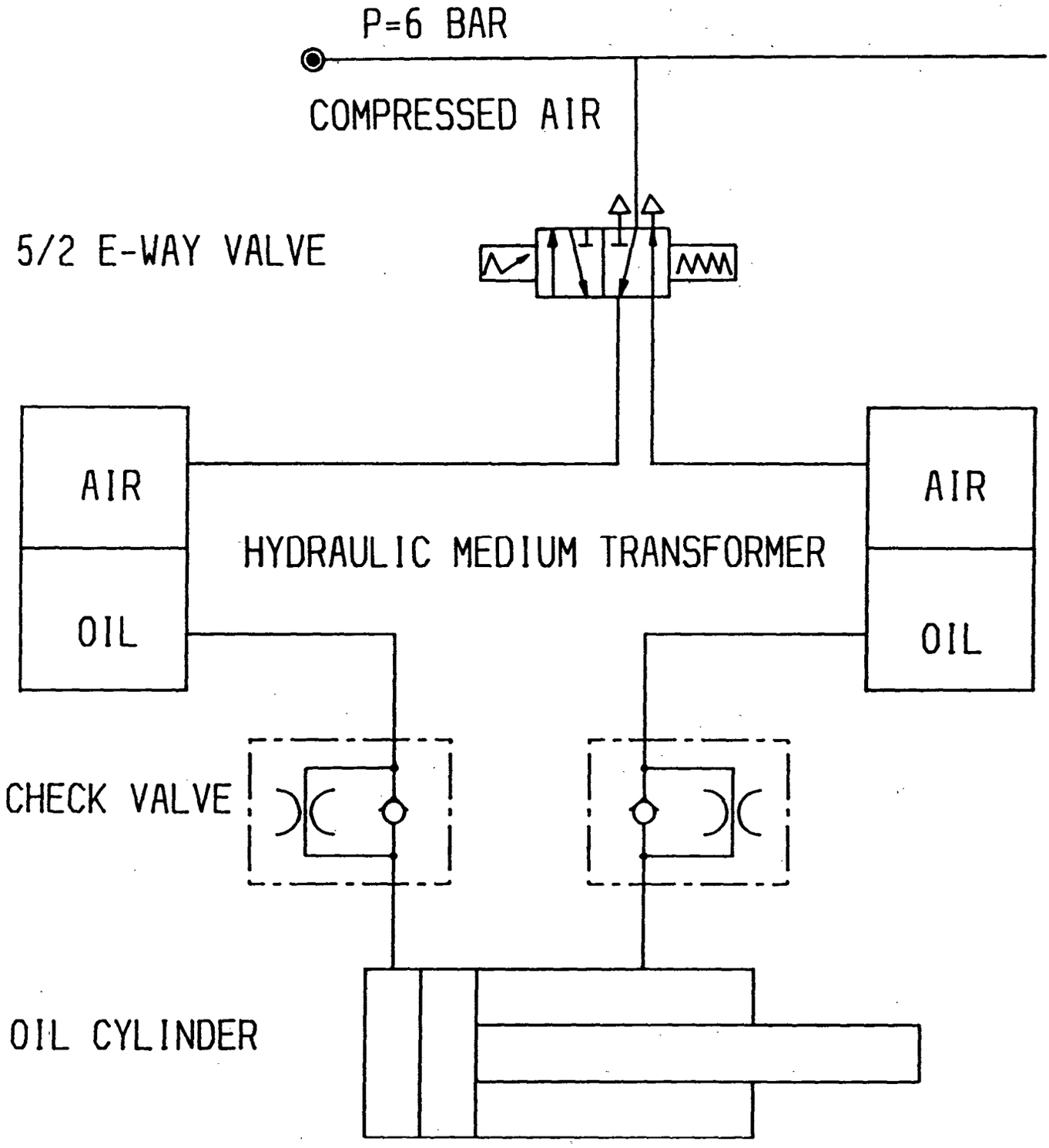

Fig. 3 Schematic of the shutter drive system

Q(I.M.Thorson): Are the shutters certainly necessary? For what? What is their cost?

A(W.Wagner): The shutters may not be absolutely necessary , but they certainly are helpful. They allow modifications at the neutron guides, e.g. at the instrumental position, with the target in operation, and fast and easy access to the neutron guide shielding bunker after the target is shut down. The estimated cost is about 800 kFr.

ICANS-XI International Collaboration on Advanced Neutron Sources
KEK, Tsukuba, October 22-26, 1990

Summary Report on the LANL Meeting on Cold Neutron Sources

Gary J. Russell
Los Alamos National Laboratory
Los Alamos, NM USA

Colin D. West
Oak Ridge National Laboratory
Oak Ridge, TN USA

The first meeting devoted to cold-neutron sources was held at the Los Alamos National Laboratory on March 5-8, 1990. Cosponsored by Los Alamos and Oak Ridge National Laboratories, the meeting was organized as an International Workshop on Cold Neutron Sources and brought together experts in the field of cold-neutron-source design for reactors and spallation sources. Eighty-four people from seven countries attended (see photograph). Because the meeting was the first of its kind in over forty years, much time was spent acquainting participants with past and planned activities at reactor and spallation facilities worldwide. As a result, the meeting had more of a conference flavor than one of a workshop.

As part of the workshop strategy, a list of questions to be addressed were sent to the participants prior to the meeting. The general topics covered at the workshop included:

- Cold source design criteria
- Neutronic predictions and performance
- Energy deposition and removal
- Engineering design, fabrication, and operation
- Material properties
- Radiation damage
- Instrumentation
- Safety
- Existing cold sources
- Future cold sources

As can be seen, a wide range of topics, from cold-moderator neutron physics to engineering and operation of cold-neutron sources were discussed.

The meeting began with review presentations on existing cold neutron sources, including design criteria, current design, and source performance. Calculational techniques for neutronic performance and available measurements on the neutronic performance of various sources were also covered on the first day. Design considerations for cold-neutron sources, including optimization, heating rates and heat removal, materials properties, radiation damage and safety, were covered on the second day. The third

day was devoted to proposals for new cold-neutron sources at both reactor and spallation facilities; this day also included a poster session and a tour of the LANSCE facility. The morning of the last day was devoted to summaries.

Here are some highlights of the items discussed at the meeting. Liquid deuterium and supercritical hydrogen appeared to be the favored choices for new cold-neutron sources at reactors. Minimizing energy deposition in the walls of reactor cold-source containers could be an improvement that could affect the engineering design of cold-neutron sources. Most attendees generally felt that neutronic gains at reactor cold sources will most likely come from more efficient coupling of the neutron source to the neutron-beam transport system rather than from improvements in cold source performance. The ability to change the moderating material viewed by a particular neutron spectrometer may be useful in some future applications. For reactors, an increase in neutron flux is always desirable if heat loads in the cold source are tolerable.

There are two types of spallation sources: steady-state and pulsed. Design problems with cold neutron sources for spallation sources are analogous to those for steady-state reactors. Heat loads are similar, but the distribution between gamma-ray and neutron heating is different. Because of inherent lower average heating rates in pulsed spallation sources, the possibility of using materials other than liquid hydrogen, such as liquid and solid methane, can be envisaged. To date, solid methane has only been used with proton currents of a few tens of microamperes, thus making it troublesome to employ as a cold moderator at proton currents in the hundreds of microampere range. Also, because target-moderator-reflector systems for pulsed spallation sources tend to be undermoderated, substantial gains in neutronic performance may result by using composite and coupled cold moderators.

A general consensus reached at the meeting was that an important design feature for both reactor and spallation cold-neutron sources is to get neutrons as cold as possible. Also, there is a real need for better data on materials properties and the effects of radiation damage at cryogenic temperatures, which could be used to improve the design of cold-neutron sources.

The meeting was deemed successful by all involved, and a follow-up meeting was proposed with the date and location to be decided later. The proceedings of the meeting will be published as a Los Alamos

National Laboratory report. A fairly extensive bibliography of work on cold-neutron sources over the past 40 years will be included.

LANSCE work is supported by the US Department of Energy, Office of Basic Energy Sciences, under contract W-7405-ENG 36 with the University of California.

Q(B.S.Brown): Is there any program to get the much needed radiation damage information on the cryogenic materials?

A(G.J.Russell): Unfortunately not. Everyone recognizes the problems, but no one has the financial resources to do anything about it at this time.

Q(Utsuro): Do you try to consider the effects of another decrease of the total cross-section of p-H_2 in meV region?

A(G.J.Russell): Yes, we have recognized this additional decrease in the total cross-section of para-hydrogen cross-section. We are presently incorporating this effect into the Los Alamos para-hydrogen scattering kernel.

ICANS-XI International Collaboration on Advanced Neutron Sources
KEK, Tsukuba, October 22-26, 1990

RECENT EXPERIENCE WITH IPNS MODERATORS

J. M. Carpenter and T. L. Scott
Argonne National Laboratory
Argonne, Illinois 60439

ABSTRACT

We describe experience with the moderators of IPNS in the two years since the installation of the Enriched Uranium Booster Target.

I. Introduction

The Enriched Uranium Booster Target was installed in IPNS in October, 1988. According to expectations, the neutron beam intensities increased by a factor of 2.5, taken as an average over the three moderators. Accompanying the higher neutron beam intensities are higher nuclear heating densities and correspondingly higher radiation damage rates in the moderators. (The delayed neutron background also increased, but this effect does not directly relate to moderator performance, and is dealt with in another paper in these proceedings.) Anticipating problems on these accounts, which would be especially severe in the cold solid methane "C" moderator, we replaced the methane there with liquid hydrogen; this required no modifications to the system. Therefore since Booster Target installation our moderators have been as shown in Table 1.

Table I.

IPNS Moderators Operating Since October, 1988

Moderator	Beams	Description
"C"	C1-3	Liquid H_2 @ 20K, stationary, grooved, decoupled
"F"	F1-6	Liquid CH_4 @ 110K, circulating, flat, poisoned, decoupled
"H"	H1-3	Liquid CH_4 @ 110K, circulating, flat, poisoned, decoupled

Below, we describe our experiences of various kinds, the means we have applied to understand new behavior we observed, and the measures we undertook to cure problems that arose.

II. Temperature Stability of the Circulating Methane Moderators

The temperature of moderators varies as accelerator beam intensity varies during operation. Transients follow beam startup of course, but occur with some frequency due to accelerator trips even though there is rapid recovery. The reason is entirely trivial, in that the temperature variation ΔT is proportional to the accelerator induced power variation ΔP,

$$\Delta T = \Delta P / (\dot{M} C_p) \tag{1}$$

where $\dot{M}$ is the mass flow rate of methane and C_p is its specific heat. Before Booster Target installation, temperatures fluctuated about ± 5K, which was tolerable for most of the experiments. After Booster installation, temperatures fluctuated more than ± 10K, which was not tolerable. We increased the flow rate of methane $\dot{M}$ and installed heaters in the inlet CH_4 stream controlled from the accelerator current. The increased flow rate stabilized the fluctuations again to about ± 5K. The heaters, which are intended to compensate for accelerator-induced power variations ΔP, have not yet been tested. Further to accommodate the temperature fluctuations and the accompanying changes in the neutron spectrum, we have incorporated monitor spectrum normalization into the data analysis routines of the white beam instruments.

III. Intensity Loss in the "F" Moderator

Over the course of each two-or three-week run, we observed that the overall intensity of the beams from the "F" moderator (<u>not the "H" moderator</u>) decreased by up to 50% or more. Simultaneously, the pressure in the ballast tanks of both the "F" and the "H" systems gradually increased. The wavelength spectrum gradually hardened during these periods. Routine gas chromatographic analyses of samples of gas from the systems showed the well-known buildup of H_2 and of heavier volatile hydrocarbons. These appear as a result of to radiolysis due to fast neutron and gamma ray damage to the methane, for example reaction (a)

$$2CH_4 \xrightarrow{n_f,\ \gamma} C_2H_6 + H_2 \ . \tag{a}$$

Table 2. shows the results of gas chromatography on a sample of gas from the circulating loop of the "F" moderator system after one week of operation, starting with a fresh charge of CH_4, with an accelerator current averaging 15. μA, and with the Booster Target.

Table 2.

Molar Concentrations in Gas
from the Circulating Side of the "F" Moderator,
After One Week of Operation at 15 μA.

Material	Concentration
H_2	22.6 %
CH_4	75.2 %
C_2H_4	$\leq$ 0.16 %
C_2H_6	1.5 %
C_3H_8	0.39 %
C_4H_{10}	$\leq$ 0.07 %

The buildup of radiolysis products is substantially faster with the booster target than with the depleted uranium target, as anticipated. The loss of intensity can be traced to the accumulation of H_2 vapor in the system; since H_2 is not highly soluble in liquid CH_4 and furthermore is a vapor at the pressure and temperature of the circulating methane, even a small amount of H2 can exclude a substantial fraction of the methane from the system. If the hydrogen vapor tends to accumulate in the moderator, then the intensity decrease and the spectrum should harden. The pulse shapes should be altered but whether broadened or narrowed depends on whether the voiding in the moderator is uniform (bubbly) or stratified; we did not observe or attempt to observe the pulse shape change. Figure 1 shows the variation of the monitor detector counting rate, integrated in the range $0.5 \leq \lambda \leq 5.0$ Angstroms, for the F2 (GPPD) beam. Figure 2 shows wavelength spectra measured with the GPPD monitor detector at different times during a running cycle. Although these results are typical, the behavior was somewhat different in different running periods. We argue on admittedly flimsy grounds that the "F" moderator container (inlet at the bottom, outlet at the top) differs from the "H" moderator container (both inlet and outlet at the top) in such a way as to explain that "H" acts like a physical phase separator collecting liquid, while "F" promotes a "bubbly" situation.

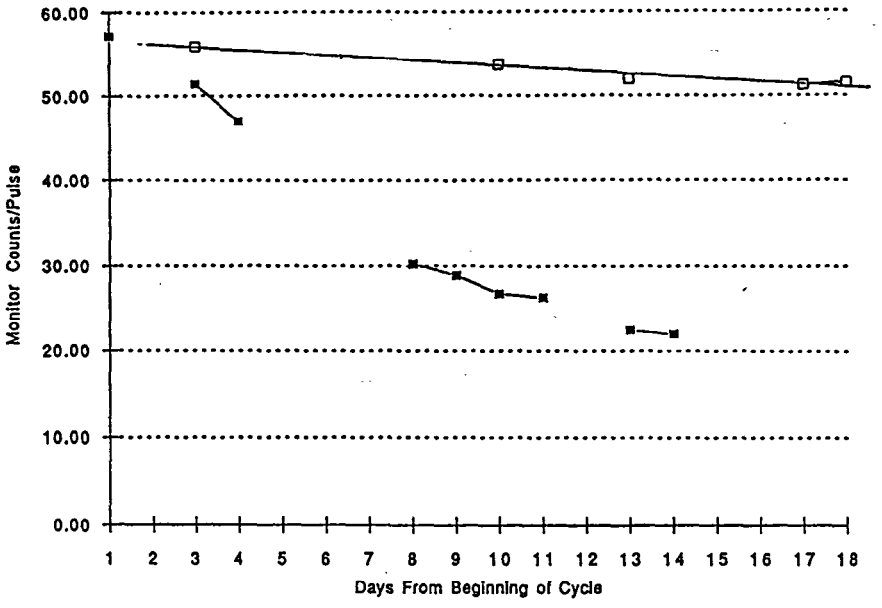

Figure 1. Variation of the intensity of the "F" moderator beam as a function of time into a running cycle. Closed symbols, March, 1990 cycle (no H_2) separator; open symbols, May, 1990 cycle (H_2 separator operating).

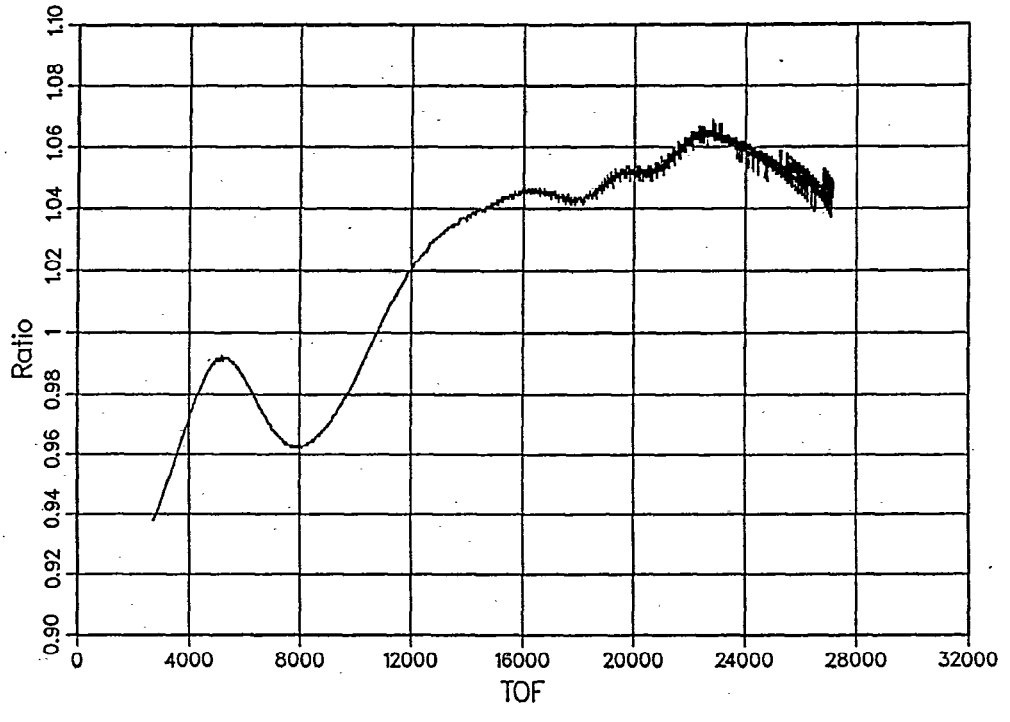

Figure 2. Variation of the spectrum during a running cycle. The figure shows the ratio of monitor counting rates, normalized according to accelerator proton current, at the beginning and at the end of a running cycle. The ratio shows the gradual increase in the temperature of the Maxwellian.

Figure 3 shows a highly schematic diagram of the circulating methane moderator systems.

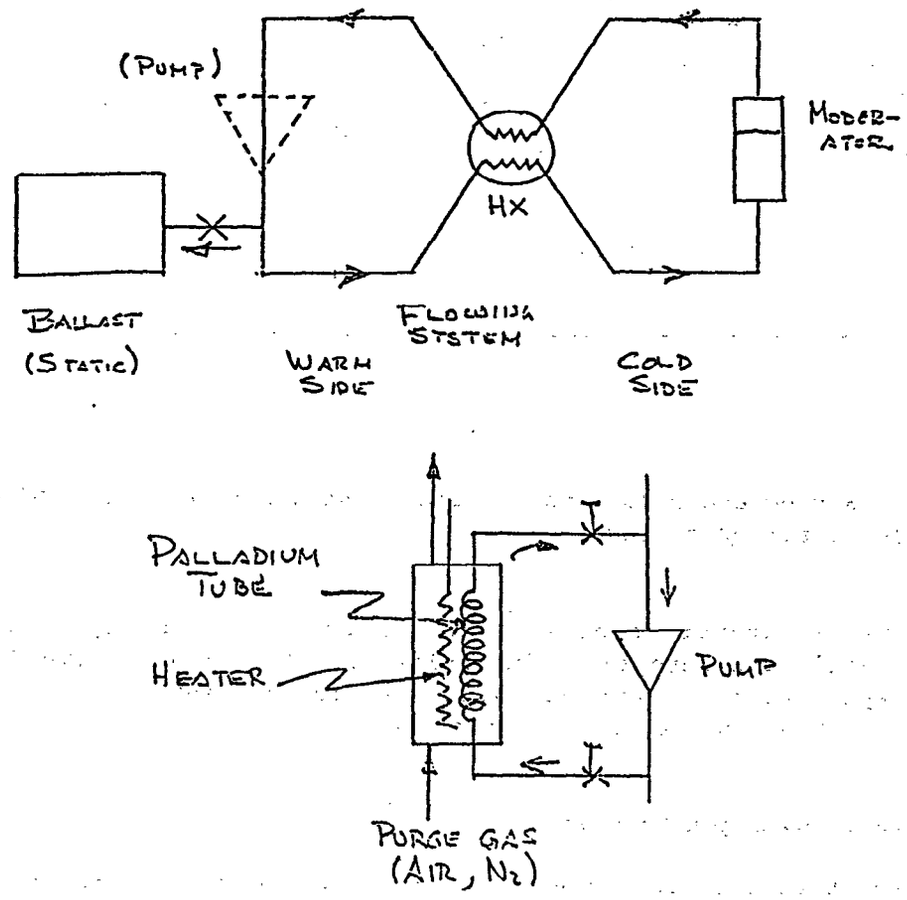

Figure 3. Schematic diagram of the circulating liquid methane moderator systems, and of the H_2 separator.

We developed a numerical model of the system, including the effects of solubility of H_2 in liquid CH_4. Calculations from this model show qualitative agreement with observations, but we have been unable to refine the unknown parameters to provide a truly acceptable match of calculation to measurement. Modeling calculations show that the ballast tank pressure is a sensitive indicator of the behavior of the system.

On the basis of the gas chromatography and numerical simulation results, we installed a commercial hydrogen separator in a bypass loop around the (room temperature) methane circulating pump. The separator, model RSD-50 by Resource Systems, Inc., E. Hanover, New Jersey, consists of a thin-walled, heated palladium tube through which the methane passes; hydrogen preferentially diffuses through the tube walls to the outside where it is removed by a nitrogen stream. The numerical model includes the effect of the separator. Figure 4 shows the calculated and measured ballast tank pressures, with calculations for two assumed H_2 production rates and for the value of the H_2 flow rate for the separator that best matches the data.

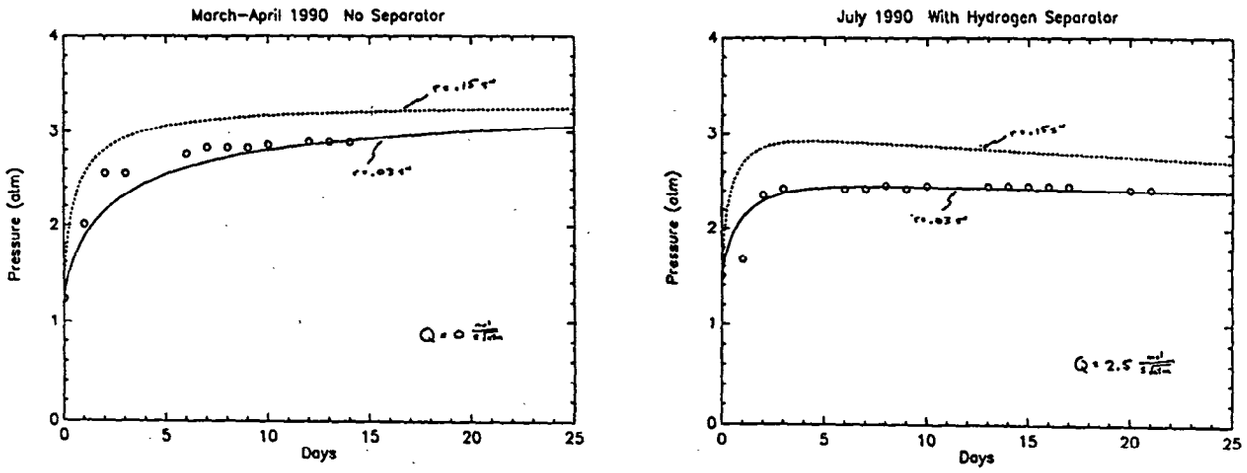

Figure 4. Measured and calculated ballast tank pressures with and without the hydrogen separator operating.

The hydrogen separator stabilizes the operation of the system. Figure 5 shows the wavelength integrated intensity as a function of time during a run with the separator operating; the intensity is constant within about 5% over the course of the two week operating cycle.

IV. The Liquid Hydrogen Moderator

With no essential modifications we now operate the "C" moderator filled with hydrogen. The liquid hydrogen moderator has behaved perfectly. However, the intensity of long-wavelength neutrons has diminished by about the same factor as was gained by installation of the Booster Target, about ×3.5 smaller than would be the case with 20 K methane. For a short time, we operated the "C" moderator filled with 20 K methane, using the Booster Target. Figure 5 shows the ratio of intensities measured with 20 K solid methane and with 20 K liquid hydrogen.

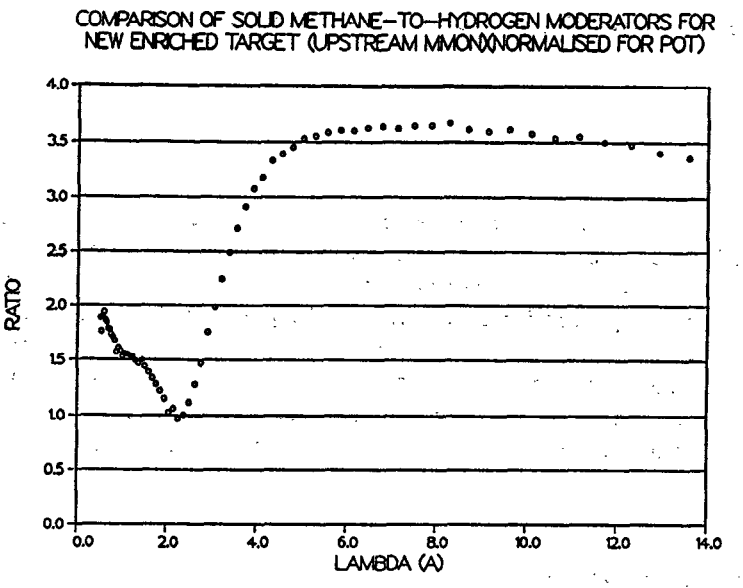

Figure 5. Ratio of intensities of neutrons, normalized to the proton beam current, from the "C" moderator filled with 20 K solid methane to the intensity when filled with 20 K liquid hydrogen, vs wavelength.

The intensity loss is due in part to the lower proton density of liquid hydrogen compared to solid methane, and in part to the inferior low temperature thermalization properties of hydrogen compared to methane. This latter is in turn due to the presence in CH_4 of closely-spaced rotational modes with approximately 1 meV (~ 12 K) spacing; the corresponding lowest energy rotational transition in H_2 is approximately 15 meV (180 K). Although we have made no careful measurements of the pulse widths, the widths of the pulses from the liquid hydrogen is greater than for solid methane at longer wavelengths, as inferred from measurements on the two reflectometers.

Our intent is to return to solid methane filling in this moderator, to recapture the lost intensity and resolution. This will require that we understand the "burping" phenomenon more thoroughly than we do at present, and control it for example by periodic annealing. Since warming the moderator leads to potentially large pressure increases due to the expansion of accumulated, trapped hydrogen, we must devise means to control the pressure increases that follow warming of the moderator, and to remove the accumulated hydrogen.

V. "Tails" on Diffractometer Bragg Peaks

Since the installation of the Booster Target, we have observed roughly 200 μsec-long "tails" on certain Bragg peaks in the powder diffractometers. The tails are about 1 % as high as the main peak and contain up to 10 % of the area, the amplitude varying with the wavelength of the neutrons. In spite of

intense efforts based on neutron beam observations, we were unable to conclusively identify the origin of these tails (but see "Post-Conference Notes, below).

VI. Conclusion

The moderators of IPNS have operated more-or-less satisfactorily since installation of the Booster Target. Problems with temperature stability and loss of intensity have been diagnosed and corrected. The 20 K solid methane moderator has been replaced with one of liquid hydrogen, which operates quite satisfactorily, but which provides fewer long wavelength neutrons and poorer pulse width resolution than the solid methane system. Work continues to obtain better understanding of the "burping" behavior of cold solid methane and to control these excursions and the consequent rises of internal pressure.

VII. Post-Conference Notes

A new problem arose immediately after the ICANS Meeting, which was not reported there but we describe briefly here. The "F" moderator methane flow stopped due to a blockage of the system between the outlet of the inlet heat exchanger and the inlet of the outlet heat exchanger, about 10 m of tubing each direction from the moderator itself. Flushing the system with tri n-butyl phosphate - heptane, heptane, methyl ethyl ketone - toluene, and toluene solvents brought out several tens of ml of involatile liquid and some insoluble chips of insoluble solid. We have not been able to identify these materials. The system was reassembled after a week's shutdown for this work, and the moderator operated successfully for one week, after which the system clogged up irreparably. We have since removed the "F" moderator and replaced it with a new, clean assembly, with inlet and outlet arrangements within the moderator container arranged to provide more effective liquid phase separation. Meanwhile we have flushed the heat exchangers and external piping with toluene. The removed materials are being subjected to chemical analysis. Results so far indicate that the solid material is insoluble in any solvent compatible with the construction materials, and is a hydrocarbon with H/C ratio of about 8:5.

The origin of the "tails" on the "F" moderator pulses has been identified; Cadmium void liner above the beam voids on both sides of the "F" moderator were accidentally omitted during assembly of the system, prior to Booster Target installation. These have been provided in the rebuilt assembly.

VII. Acknowledgements

Efforts on the IPNS moderators are pursued by the Cryogenic Moderator Problems Working Group, D. E. Bohringer, J. M. Carpenter, R. K. Crawford, W. C. Dimm, R. Kleb, A. W. Schulke, T. L. Scott and K. W. Shepard.

This work was performed under the auspices of the U. S. Department of Energy, Division of Materials Sciences, Office of Basic Energy Sciences, under contract W-31-109-ENG-38.

Q(G.S.Bauer): With the scheme of a pumped slurry of methane spheres being technically rather complicated, do you think that a pebble bed of methane spheres cooled by liquid hydrogen or even helium would limit the burping to individual pebble and thus spread it out in time without risk of the container bursting?

A(J.M.Carpenter): Yes! The consequent improvement in the effectiveness of cooling also will tend to stabilize the system.

Q(Y.Takeda): In the temperature history, are there any periodicity found, which corresponds to a limit cycle?

A(J.M.Carpenter): Yes, we observed a period of about 1 day under the conditions of IPNS depleted target operation.

Q(Y.Takeda): What are the control parameters of the nonlinear governing equation set for burping?

A(J.M.Carpenter): Principally, the coolant temperature, given that power and damage density are fixed. Otherwise, the heat transfer coefficient between CH_4 and coolant is a useful design parameter, and can be controlled somewhat by regulating coolant flow rate.

Q(R.Pynn): Have you looked at you burp equations for a range of parameters? It would surprise me if limit cycles were the solution for more than a small range of parameters.

A(J.M.Carpenter): In fact we had trouble finding parameters that produce oscillations, before the linear stability analysis. Now we have a guiding theory, which works.

ICANS-XI International Collaboration on Advanced Neutron Sources
KEK, Tsukuba, October 22-26, 1990

Optimization Studies on Coupled Liquid Hydrogen Moderator

Y. KIYANAGI, N. WATANABE*, M. FURUSAKA*, H. IWASA and I. Fujikawa
Department of Nuclear Engineering, Faculty of Engineering,
Hokkaido University, Sapporo, 060 Japan
*National Laboratory for High Energy Physics,
1-1 Oho, Tsukuba-shi, Ibaraki 305 Japan

ABSTRACT
Optimization studies on a coupled liquid-hydrogen-moderator system were performed experimentally and the results were compared with those of decoupled liquid hydrogen and solid methane moderators. A very high gain factor is obtained. Pulse characteristics were also studied and it is found that the pulse broadening by coupling is rather modest.

I. INTRODUCTION

How to realize an intense cold neutron source is one of the most important objectives for KENS-II R&D . A coupled liquid-hydrogen-moderator is the most promising candidate for this. It was revealed by our preliminary experiments[1)] that the cold neutron intensity from a coupled hydrogen moderator in a wing geometry is very much higher than that from a decoupled one and also the pulse width is not broadened so much by coupling. These results encouraged us to perform further experiments using a dedicated cryostat to this moderator system.

The cryostat used in the preliminary experiments had a large void space above the moderator chamber, resulting in a large reflector missing. We prepared a new cryostat which has a slim neck above the moderator chamber. We studied the neutronic performance of coupled liquid-hydrogen-moderators in more detail and compared the results with those of a decoupled liquid-hydrogen and solid-methane moderators.

II. EXPERIMENTAL

Figure 1 shows a coupled liquid-hydrogen-moderator system used in the present experiments. The size of the liquid-hydrogen-moderator is fixed to $12\times12\times5$ cm^3. Polyethylene plates are attached to a cryostat to compose a

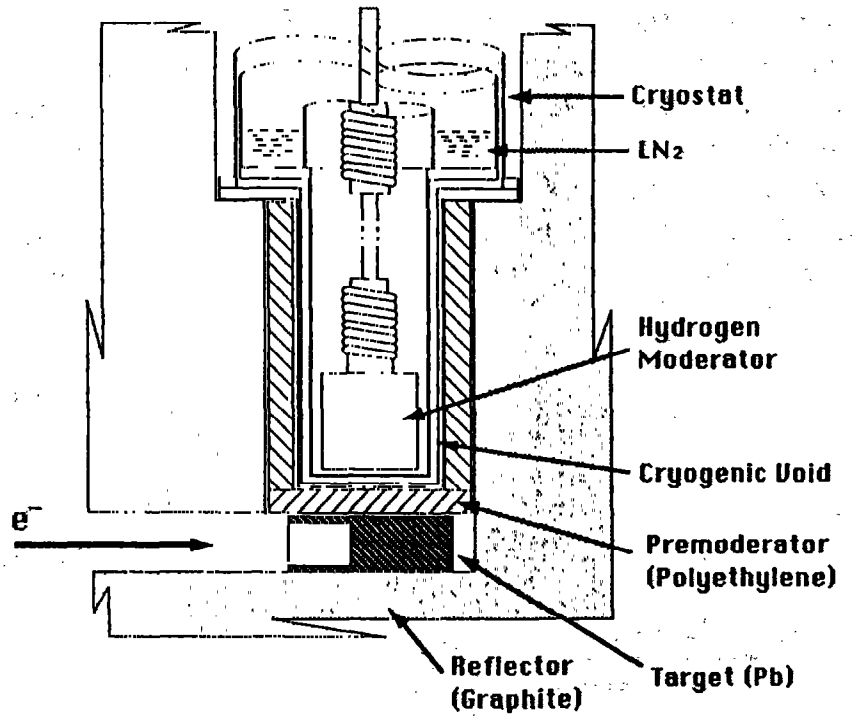

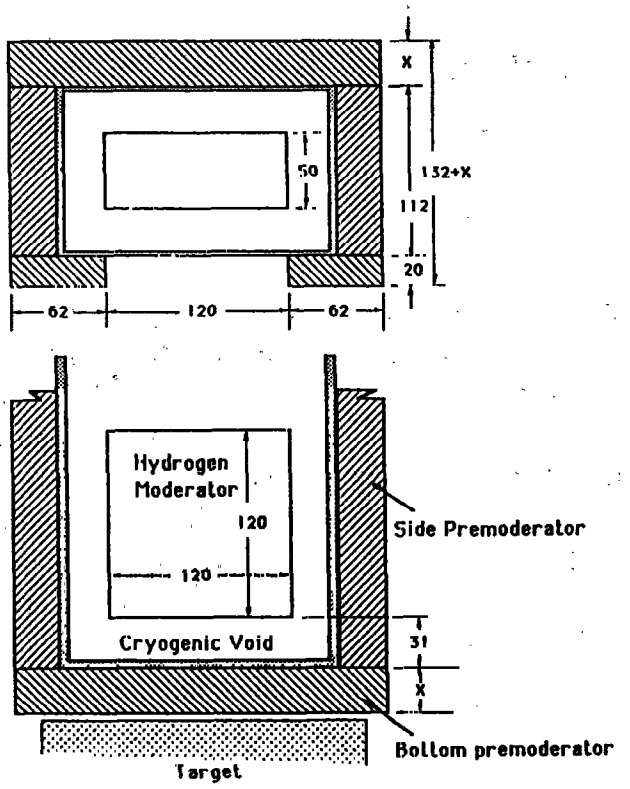

Fig. 1 Schematic representation of the target-moderator-reflector assembly for coupled liquid-hydrogen moderator with premoderator. The lower figure shows the layout of the premoderator.

premoderator. The front part of the premoderator has a window of 12×12 cm^2 for extracting the neutron beam. There is no decoupler between moderator, target and reflector; that means the system is a coupled one. Figure 2 shows the decoupled moderator system. The moderators have the same size of the coupled one and are decoupled from the reflector by 0.5 mm thick cadmium plate as shown in the figure. A neutron generating target is placed just below the premoderator or the cryostat to form a wing geometry. The target and the moderator are surrounded by a graphite reflector of about 1 m^3.

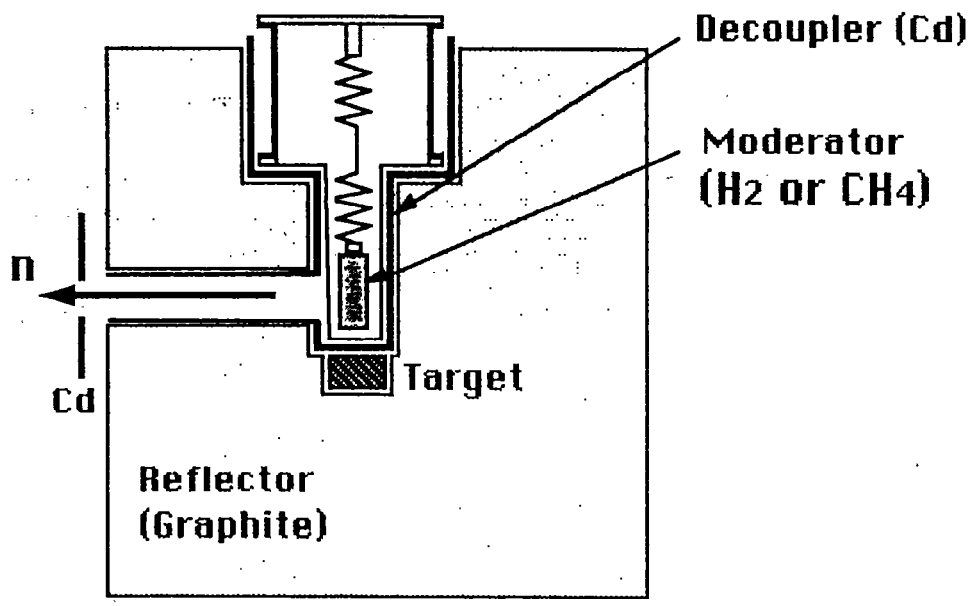

Fig. 2 Decoupled target-moderator-reflector assembly.

The electron linac at Hokkaido university was used as a fast neutron generator. Figure 3 shows the experimental arrangement for measurements of time-of-flight spectra. The flight path length between moderator and He-3 neutron detector is 5.6 m. A set of cadmium collimators is placed at both ends of an evacuated flight tube to define a viewed surface of the moderator 10×10 cm^2. The energy analyzer system used for the time distribution measurements is dipicted in the lower figure. A mica crystal is used as an energy analyzer with Bragg angle of 85°. The flight path length between moderator and analyzer crystal is 6.6 m.

III. COUPLED MODERAOTOR OPTIMIZATION

Slow neutron intensities from the coupled liquid hydrogen moderator without premoderator and the decoupled one were measured. The measured spectra are shown in Fig. 4 and the relative intensity of the coupled to the decoupled (coupling gain factor) is plotted in Fig. 5 as a function of neutron wavelength. The coupling gain factor almost saturates in

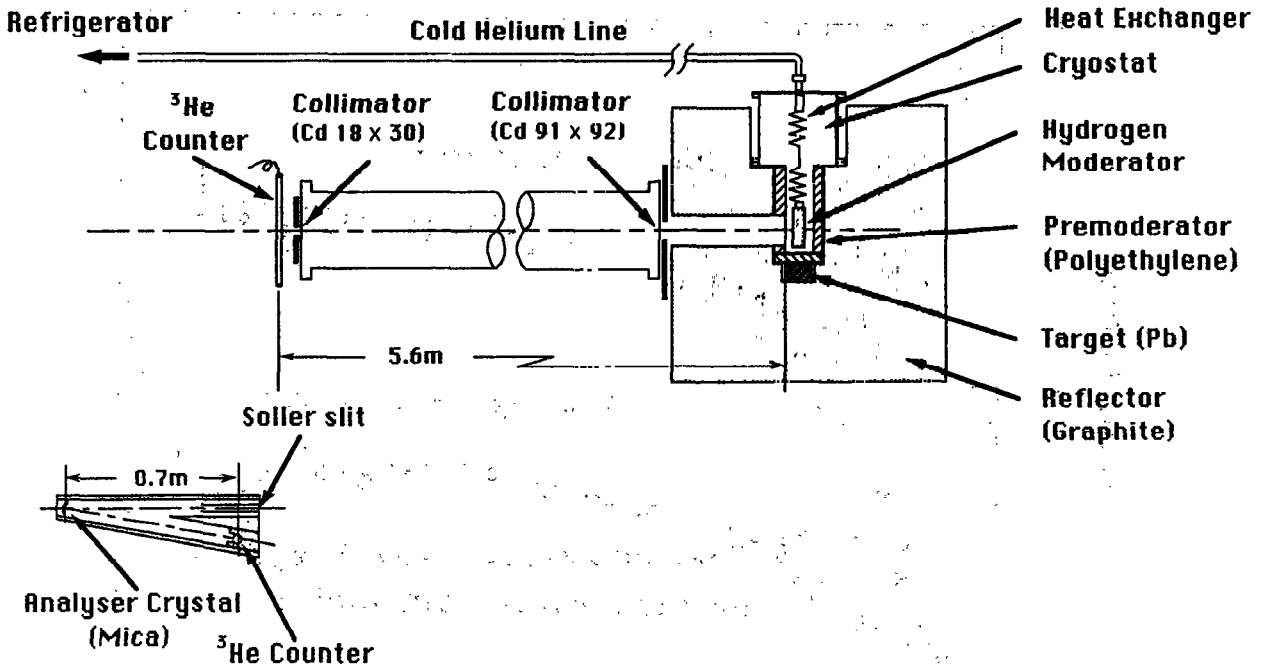

Fig. 3 Experimental arrangement for time-of-flight measurements. The lower figure shows the energy analyzer system for time distribution measurements.

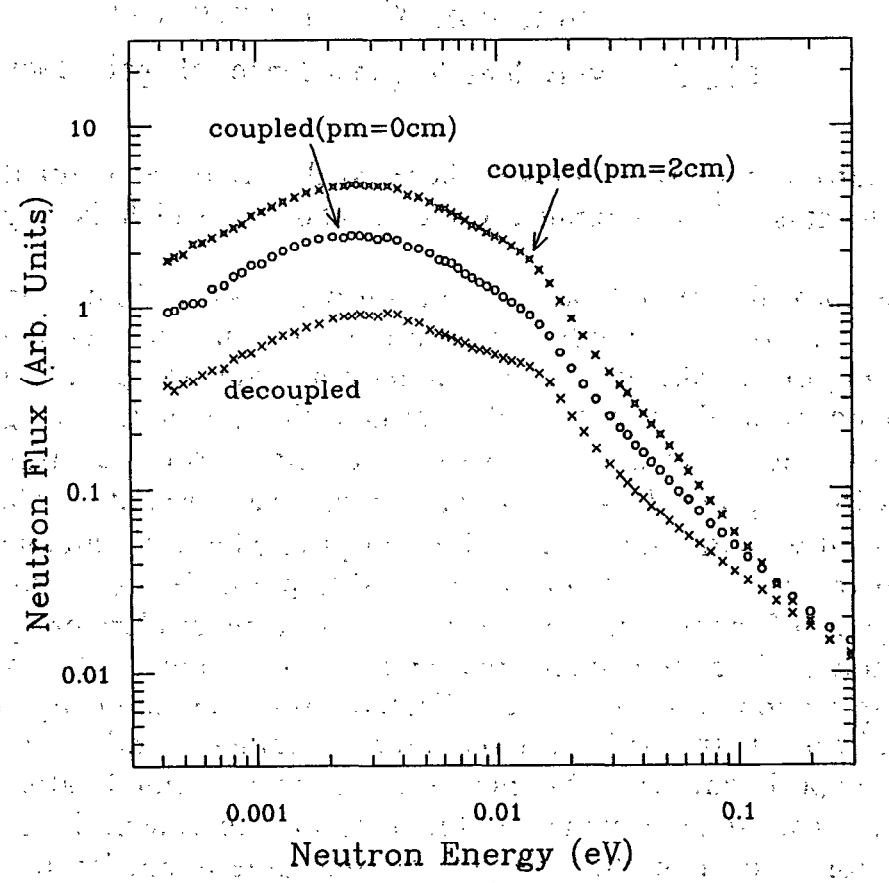

Fig. 4 Energy spectra of coupled and decoupled liquid-hydrogen-moderators. pm means premoderator thickness.

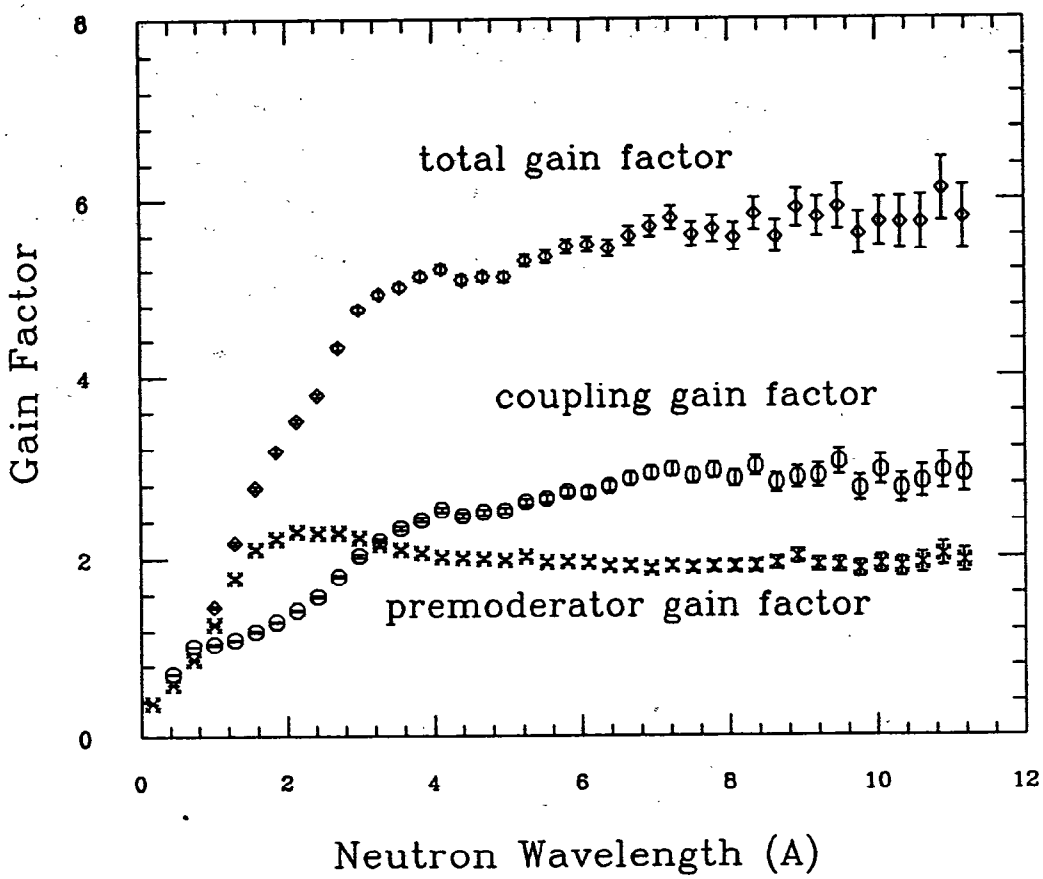

Fig. 5 Wavelength dependence of gain factors.

the cold neutron region although there still exists a gradual increase at longer wavelengths. The saturated value is about 3 which is a great.

Then we performed premoderator optimization. As a first step, we studied the effects of the premoderator thickness on the cold-neutron-beam intensity. Figure 6 shows the premoderator gain factor as a function of bottom premoderator thickness. We defined the premoderator gain factor as the ratio of the cold-neutron-beam intensity from a liquid-hydrogen-moderator with a premoderator to that from one without. The gain factor increases rapidly with increasing bottom-premoderator thickness and then saturates to a value of about 1.75. Side-premoderator brings about an additional gain of about 20 %, resulting in a premoderator gain factor of about 2 in total. The maximum appears at about 2 cm thick. We found that the bottom-premoderator is most effective for the intensity enhancement, while the effect of the side-premoderator is rather small. In the previous preliminary experiment we obtained the optimal premoderator thickness of about 3 cm. The smaller value in the present experiment is due to a better upper reflector and a higher height of the side-premoderator than in the previous.

The energy spectrum of neutrons from the coupled liquid-hydrogen-

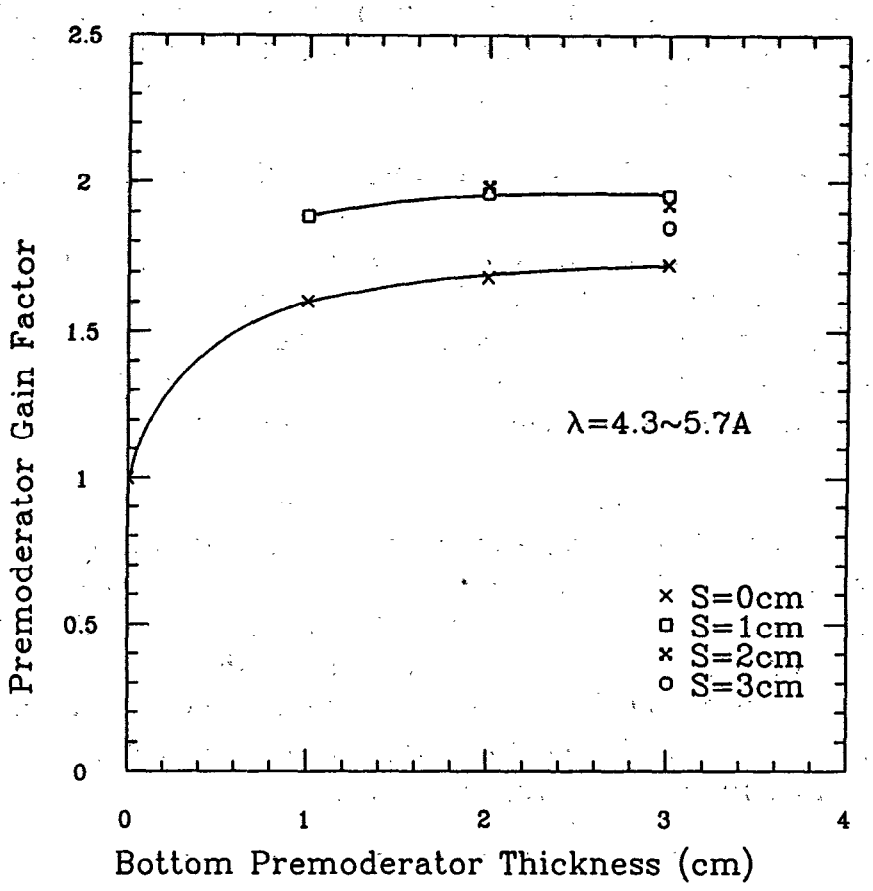

Fig 6 Premoderator gain factor at wavelength 4.3~5.7 A as a function of bottom-and side-premoderator thickness. S means side-premoderator thickness.

moderator with a 2 cm thick premoderator is also shown in Fig. 4. The energy spectra at the cold neutron region are not so different each other. The wavelength dependence of the premoderator gain factor of the liquid-hydrogen-moderator with the 2 cm thick premoderator is shown in Fig. 5. There is a broad maximum around 2.5 A and above this wavelength the gain factor approaches 2. It is also a considerable.

Grooved surface moderators were extensively studied so far and a finite gain has already been recognized. We examined a grooved-surface bottom-premoderator. The bottom-premoderator had grooves of 2 cm deep and 2 cm wide with 2 cm spacing (total thickness being 4 cm). A gain factor obtained by this was only 3 % which was unexpectedly small.

The total gain factor of the coupled liquid-hydrogen-moderator with the 2 cm thick premoderator (optimal thickness) is also shown in Fig. 5. The total gain factor is defined here as the ratio of the cold-neutron-beam intensity of this moderator to that of a decoupled 5 cm thick liquid-hydrogen-moderator. The total gain factor increases rapidly with increasing wavelength until about 3 A and approaches 6 in the longer wavelength region. Very large values of the total gain factor were attained. The values are almost as same

as previous ones in the preliminary experiments. However, the absolute intensity obtained in this experiment is about 1.5 times higher than the previous. This is due to the better reflector saving in the present system.

IV. DIRECT COMPARISON WITH DECOUPLED SOLID-METHANE MODERATOR

In the choice of cold neutron moderator system, it is important to know the beam intensity in absolute scale or in relative value to the existing best moderator for the production of pulsed cold neutrons. A decoupled solid-methane moderator of 5 cm thick as used at present KENS was adopted for this. We also performed measurements on this moderator.

Figure 7 shows the energy spectra from both moderators for direct comparison. It should be stressed that the cold-neutron-beam intensity from the proposed coupled moderator is superior to that from the reference decoupled moderator of solid methane. Figure 8 shows the ratio of the intensity of coupled liquid-hydrogen-moderator to that of the solid-methane moderator. A gain of about 2 has been attained. There is a peak at about 2.5 A which is caused by the neutron trap at this wavelength in connection with ortho-para transition of hydrogen molecule.

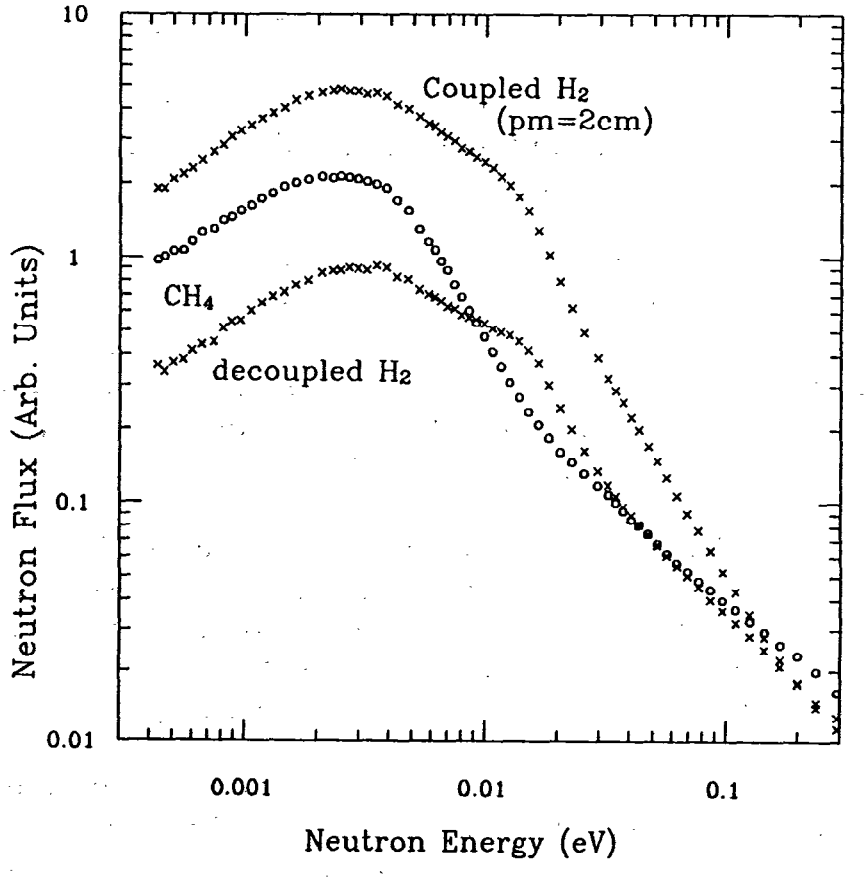

Fig. 7 Energy spectra from the coupled liquid-hydrogen-moderator with 2 cm thick premoderator and the decoupled solid methane moderator. As a reference the spectra from the decoupled liquid-hydrogen-moderator is also shown.

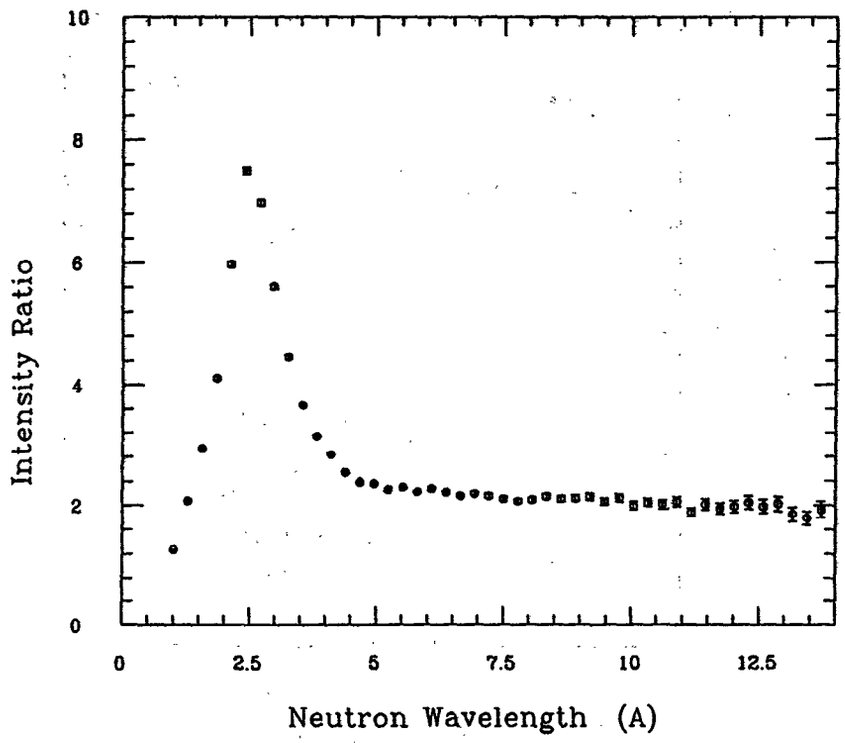

Fig. 8 Intensity ratio of the coupled liquid hydrogen moderator with 2 cm thick premoderator to the decoupled solid methane moderator.

Next, we measured spatial distributions of cold-neutron-beam intensity along the vertical direction of the viewed surface of the moderators, by scanning a cadmium slit of 1 cm-high at the entrance of the beam extraction hole (see Fig. 3). The results are shown in Fig. 9. The superiority of the proposed coupled moderator is clearly demonstrated. The peak in intensity appears close to bottom of the moderator. Such feature is enhanced more in the proposed coupled moderator. This is due to the fact that the bottom-premoderator feeds source neutrons of a more soft-spectrum to the liquid-hydrogen-moderator.

The target-moderator distance allowed for the target engineering design is one of the most important parameters, so, we measured the cold-neutron-beam intensity by changing the distance between the target and the moderator. Figure 10 shows the results. Intensities from each moderator are normalized to unity at zero distance by extrapolation. It is revealed that the intensity reduction with distance is rather modest and dose not depend on moderator.

V. PULSE CHARACTERISTICS

Time-distributions of cold neutrons from the proposed coupled liquid-hydrogen-moderator system were studied in comparison with other two decoupled moderators.

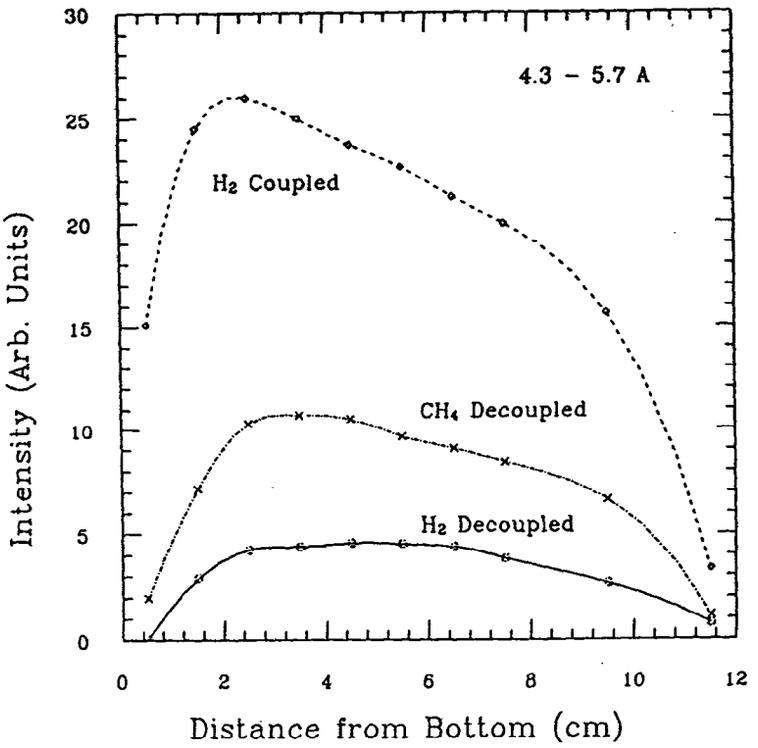

Fig 9 Spatial distributions of the cold-neutron beam intensity along the vertical direction of the viewed surface.

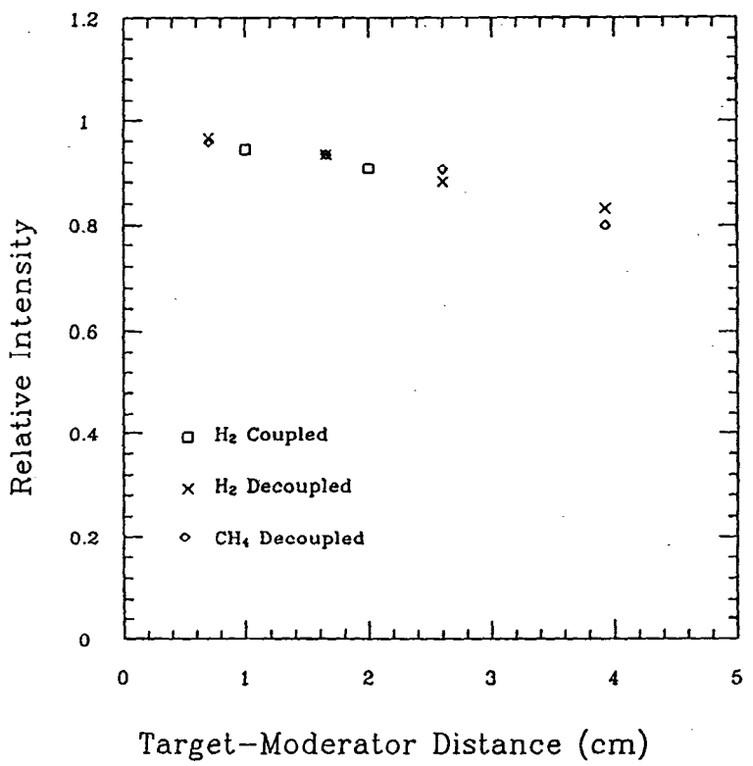

Fig 10 Cold-neutron-beam intensity as a function of moderator-target distance.

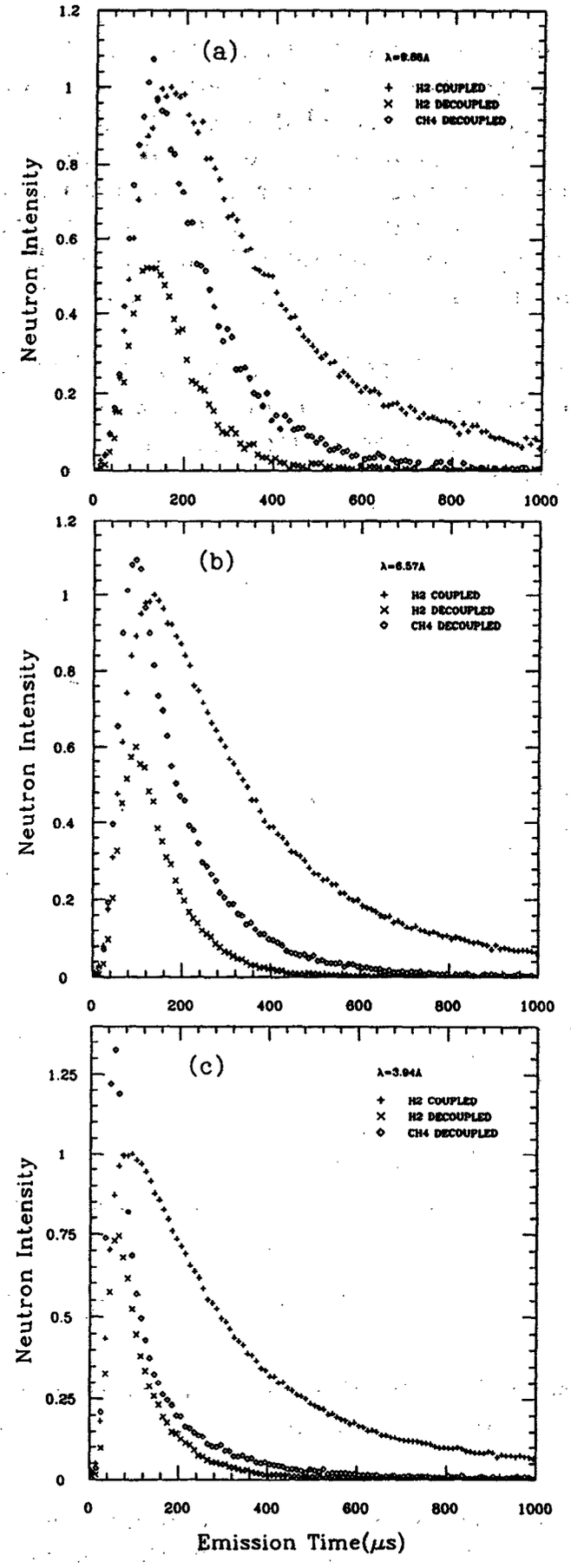

Fig 11 Time-distributions of neutrons from the coupled liquid-hydrogen-moderator with 2 cm thick premoderator and the decoupled methane and hydrogen ones at three wavelengths, (a) 9.86A, (b) 6.57 A and (c) 3.94 A.

Figure 11 compares time-distributions of cold neutrons from these moderators at three typical wavelengths. The coupled moderator gives broader pulses than the decoupled ones as expected, but the broadening is rather modest. The increase in the peak intensity is unexpectedly high compared to the decoupled hydrogen and almost comparable to the solid methane. This means that the larger gain of the coupled moderator to the decoupled liquid-hydrogen-moderator is not only due to the increase in the pulse width but also due to the increase in the peak intensity.

Pulse widths in full width at half maximum (FWHM) are plotted in Fig. 12 as a function of neutron wavelength. The pulse widths of the coupled moderator are about 2 times larger than those of the decoupled ones in the cold neutron region.

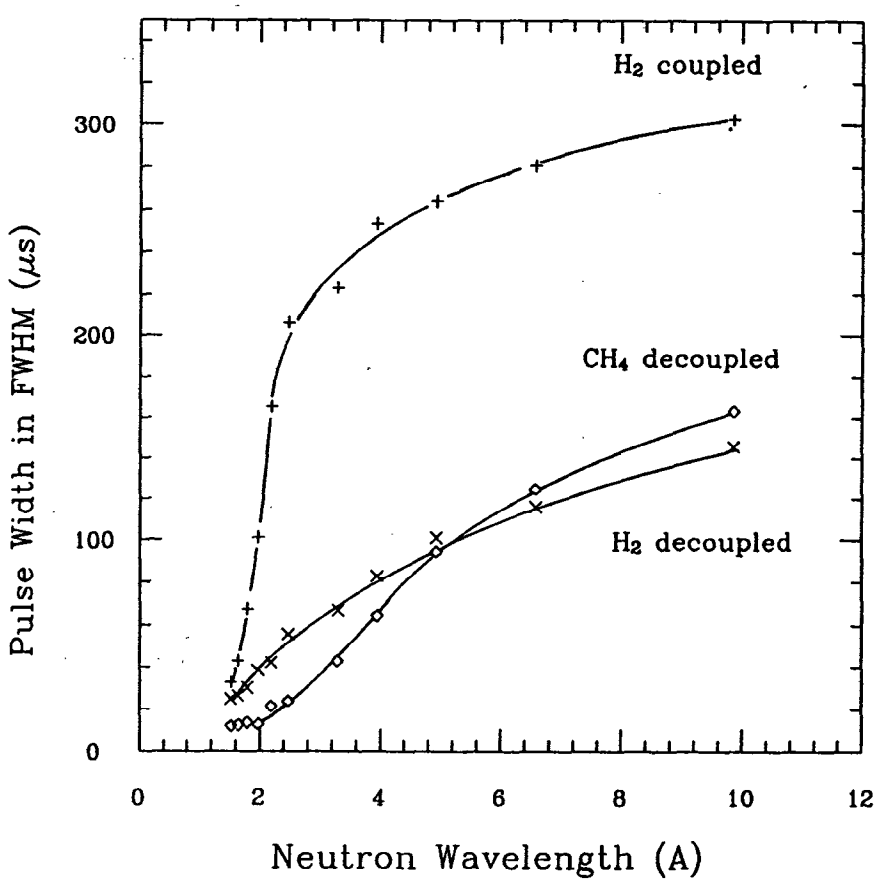

Fig 12 Pulse widths (FWHM) of neutrons from the coupled and decoupled moderators as a function of neutron wavelength.

Rising time of the neutron pulses is also plotted in Fig. 13. Here, the rising time is defined as the duration between 10 and 90 percent pulse height of the rising edge. The difference between the coupled moderator and the decoupled ones is not so large as in the pulse widths.

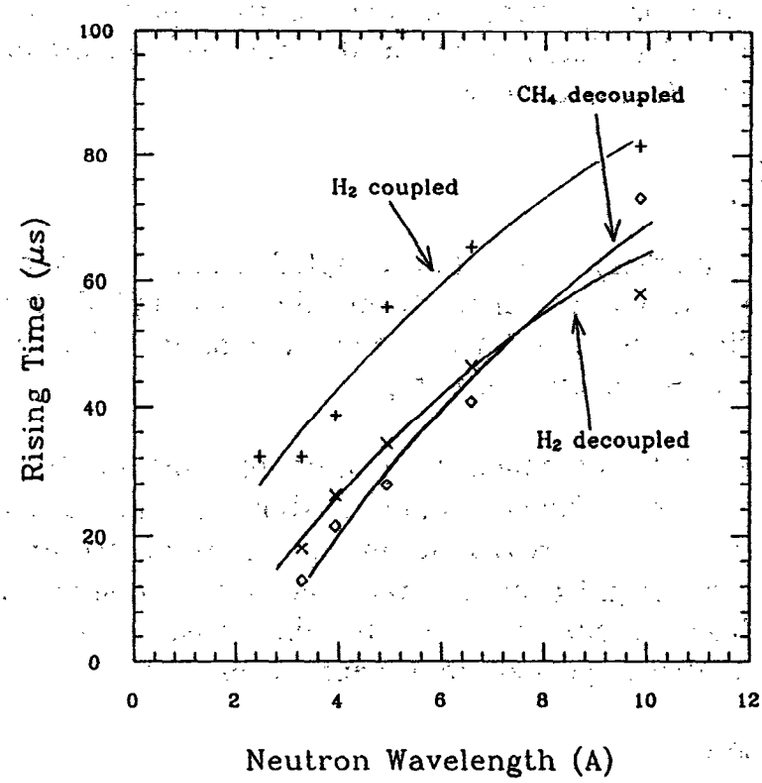

Fig. 13 Rising time of neutron pulses as a function of neutron wavelength.

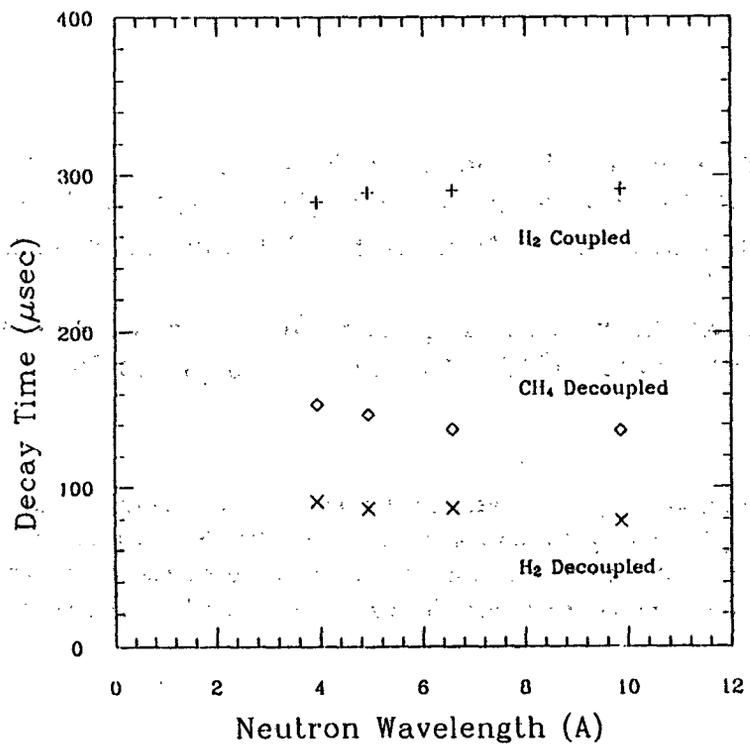

Fig. 14 Decay time of neutron pulses as a function of neutron wavelength.

Figure 14 shows the decay time of the neutron pulses as a function of neutron wavelength. The decay time of the coupled moderator is about 2~3 times as large as the decoupled one.

VI. CONCLUSIONS

The cold neutron intensity from the coupled liquid-hydrogen-moderator is about 6 times as large as that from the decoupled liquid-hydrogen-moderator and 2 times from solid-methane moderator. The increase of the intensity by coupling is considerably high.

It was so far believed by computer simulation that the pulse broadening in a coupled moderator is significant: about 5 times as broad as in a typical decoupled one[2]. It is revealed in the present experiment that the broadening is not as significant as expected by computer simulation. A coupled liquid-hydrogen-moderator will be the most intensive cold neutron moderator among realistic pulsed cold neutron moderators.

ACKNOWLEDGEMENTS

The authors are indebted to Prof. K. Inoue for his encouragement and interest shown through the course of this work.

REFERENCE

1 N. Watanabe, Y. Kiyanagi, K. Inoue, M. Furusaka, S. Ikeda, M. Arai and H. Iwasa, Advanced Neutron Sources 1988 (Proc. ICANS-X (1988)), Institute of Physics Conference Series Number 97, Institute of Physics, Bristol and New York, p-787.

2 G. J. Russell, H. Robinson, G. L. Legate, R. Woods, E. R. Whitaker, A. Bridge and K. J. Hughes : Proc. ICANS-IX (Villigen, Sept. 22-26, 1986) p-177.

Q(R.Pynn): What happens if we imagine the "premoderator" to be homogeneously embedded in the moderator? Would we gain anything by "feeding" the moderator from inside, rather than from outside?

A(Y.Kiyanagi): To feed thermal or epithermal neutrons to liquid hydrogen moderator is important for coupled hydrogen moderator. Therefore, the premoderator have to be placed outside the liquid hydrogen and may not be cooled down.

ICANS-XI International Collaboration on Advanced Neutron Sources
KEK, Tsukuba, October 22-26, 1990

Reflector Optimization for Coupled Liquid Hydrogen Moderator

Y. KIYANAGI, N. WATANABE*, M. FURUSAKA* and H. IWASA
Department of Nuclear Engineering, Faculty of Engineering,
Hokkaido University, Sapporo, 060 Japan
*National Laboratory for High Energy Physics,
1-1 Oho, Tsukuba-shi, Ibaraki 305 Japan

ABSTRACT
As a part of optimization studies on a coupled liquid hydrogen moderator system, the optimal thickness of the reflector, the effects of neutron absorbing liners and other beam hole/moderator on the cold-neutron-beam intensity were studied experimentally. It turns out that the optimal thickness is rather thick in this system and the existence of Cd liners around the beam extraction hole considerably reduces the cold neutron beam intensity, while the existence of other beam hole and moderator does not give an important intensity reduction.

I. INTRODUCTION

In a coupled liquid-hydrogen-moderator system the role of reflector is to supply thermal neutrons to liquid hydrogen, while in a decoupled system to supply fast and epithermal neutrons. So far the reflector studies have been done only for the decoupled moderator system. We therefore studied experimentally the reflector effect on the cold-neutron-beam intensity in a coupled liquid-hydrogen-moderator system in order to obtain better understanding of the reflector effects. We measured the neutron-beam intensities from the coupled liquid-hydrogen-moderator proposed in the preceding report[1)] with various reflector configurations.

II. OPTIMAL REFLECTOR THICKNESS

To find the optimal reflector thickness we performed measurements in two steps. Firstly, we examined the effect of the rear-upper-reflector. The premoderator thickness was fixed to 2 cm (optimal thickness). Figure 1 shows the neutron-beam intensity at three different energies as a function of reflector thickness of the part indicated in the inset. The reflector thickness of the lower half (below the target) was kept at 40 cm. The

intensities are saturated at a thickness of about 40 cm, independent of neutron energy. The required thickness is rather large compared to a decoupled moderator system.

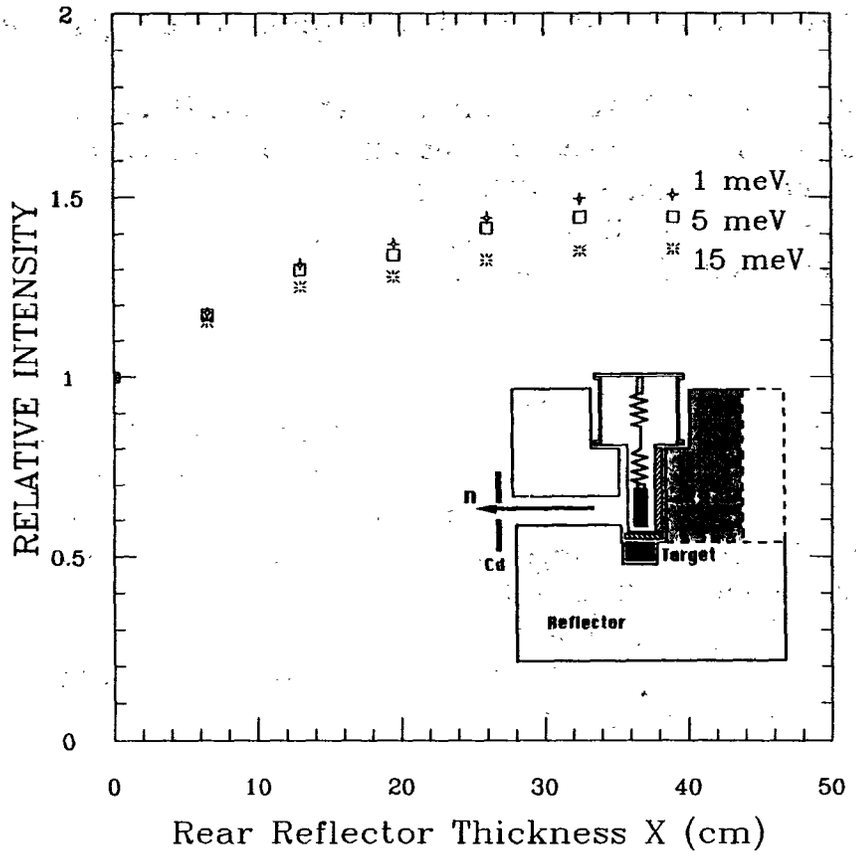

Fig. 1 Effect of the rear-upper-reflector thickness on the neutron-beam intensity. The part of reflector changed is shown in the inset.

Secondly, we examined the effect of the upper reflector. Figure 2 shows the measured neutron-beam intensities as a function of the upper reflector height (see the inset). For longer wavelength neutrons the intensity is still increasing even above 40 cm. This is probably due to the reflector missing caused by the cryogenic void. In a real system the void space produced by liquid hydrogen piping above the moderator chamber would be smaller than that of the present cryostat. However, a thicker upper reflector is important for a coupled liquid-hydrogen-moderator system.

III. EFFECT OF OPENING ANGLE OF BEAM EXTRACTION HOLE

In the KENS-II program it is strongly requested to provide as many neutron beam channels as possible[2]. For this requirement the larger opening angle of the beam extraction hole in the reflector becomes indispensable. We therefore examined the effect of the opening angle on the slow neutron

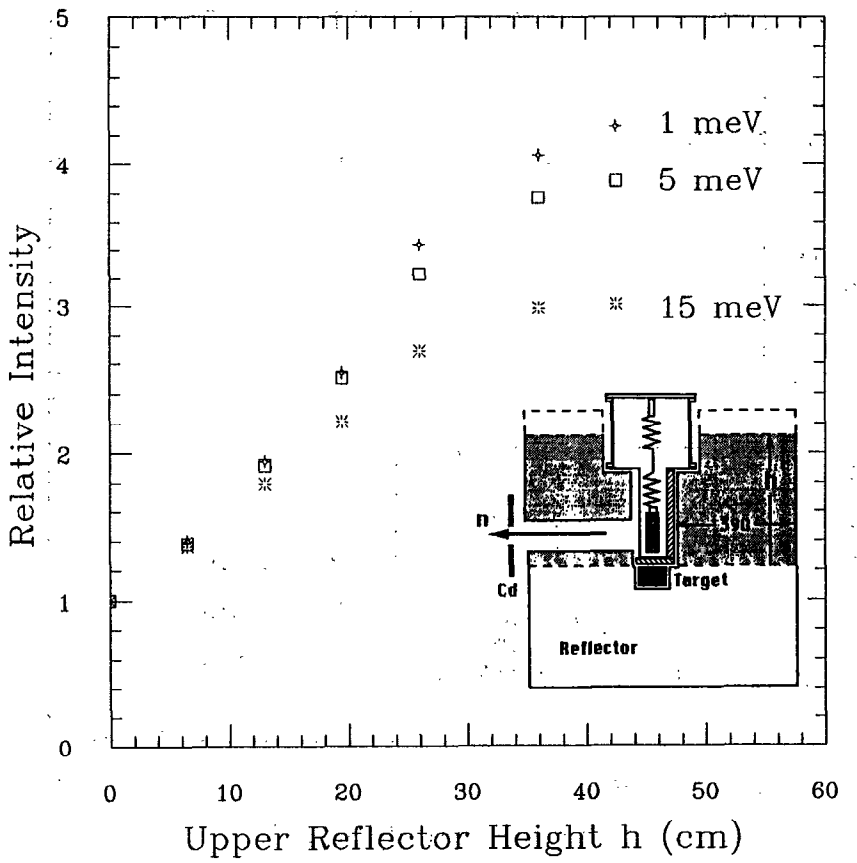

Fig. 2 Effect of upper reflector height on the neutron-beam intensity. The part of reflector changed is shown in the inset.

intensity. Figure 3 shows the intensity of slow neutrons emitted parpendicularly from the moderator surface as a function of the opening angle (see the inset). The reduction in the neutron-beam intensity is rather small (only 3-5 % even at 30°) and independent of neutron energy. In the present experiment we studied only one half of the opening angle, but the intensity reduction in the case of a symmetric opening would be less than the double in the half opening case. The intensity of slow neutrons emitted to the direction not perpendicular to the moderator surface, of course, decreases with emission angle θ as $(1+\sqrt{3}\cos\theta)/(1+\sqrt{3}/2)$ in addition to the reflector effect.

IV. EFFECTS OF Cd LINER, ANOTHER BEAM HOLE AND MODERATOR

We examined the various effects such as front-premoderator, the cadmium liner around beam extraction hole in the reflector and existence of another beam extraction hole, on the cold-neutron-beam intensity. Figure 4 shows the moderator-reflector configurations studied. The observed cold-neutron-beam intensities are summarized in Table I. We chose the configuration (a)

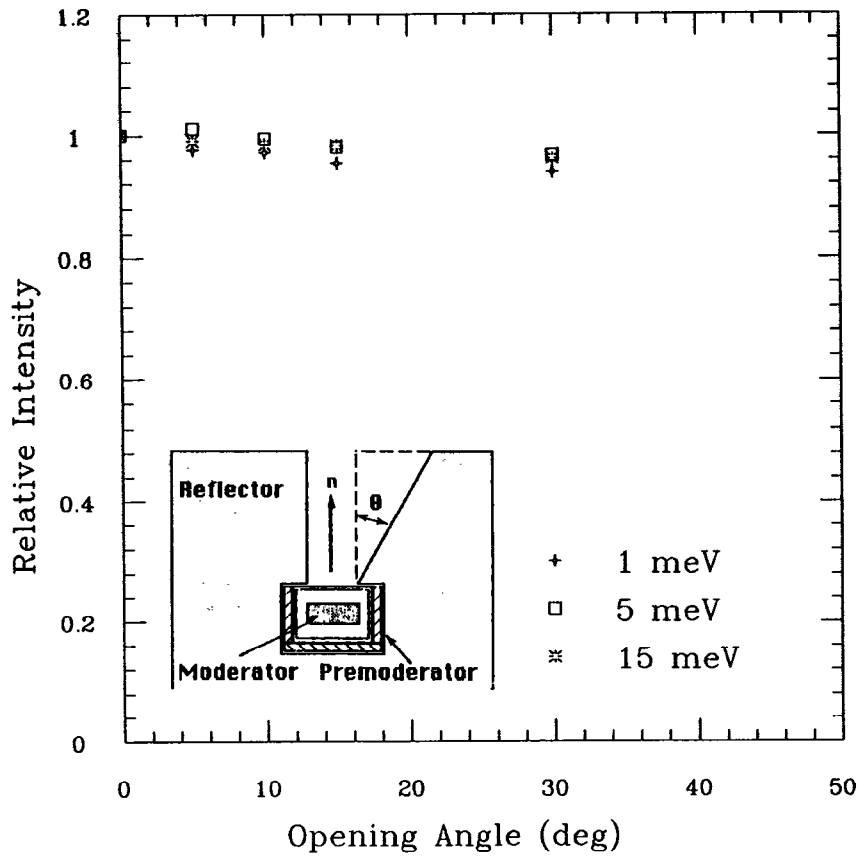

Fig. 3 Effect of the opening angle of the beam extraction hole on the neutron-beam intensity.

as a reference since it gave the highest intensity. The values in the table are the relative ones to the configuration (a).

By removing the front-premoderator (configuration (b)) we have about 12 % reduction in the beam intensity. By inserting a cadmium liner around the beam extraction hole (configuration (c)), about 40 % reduction comes out in total. The insertion of another cadmium mask in place of the front-premoderator (configuration (d)) results in the beam intensity reduction of about 50% in total.

Usually several moderators of different kinds, some are decoupled and others are coupled, will be placed around the target. Each moderator has beam extraction hole(s) on one side or both sides of the moderator. The introduction of another beam hole will bring about an additional reflector missing. We examined the case of two holes. For simplicity we made a second hole in the opposite side of the first one (configuration(e)). The size of the hole is 17×17 cm^2. This brings about 7 % loss in the beam intensity compared to the configuration(b). The insertion of a cadmium liner in the second hole (configuration (f)) gives almost no effect. The fact means that the neutrons with energies below Cd cut-off bring little effect on the cold-

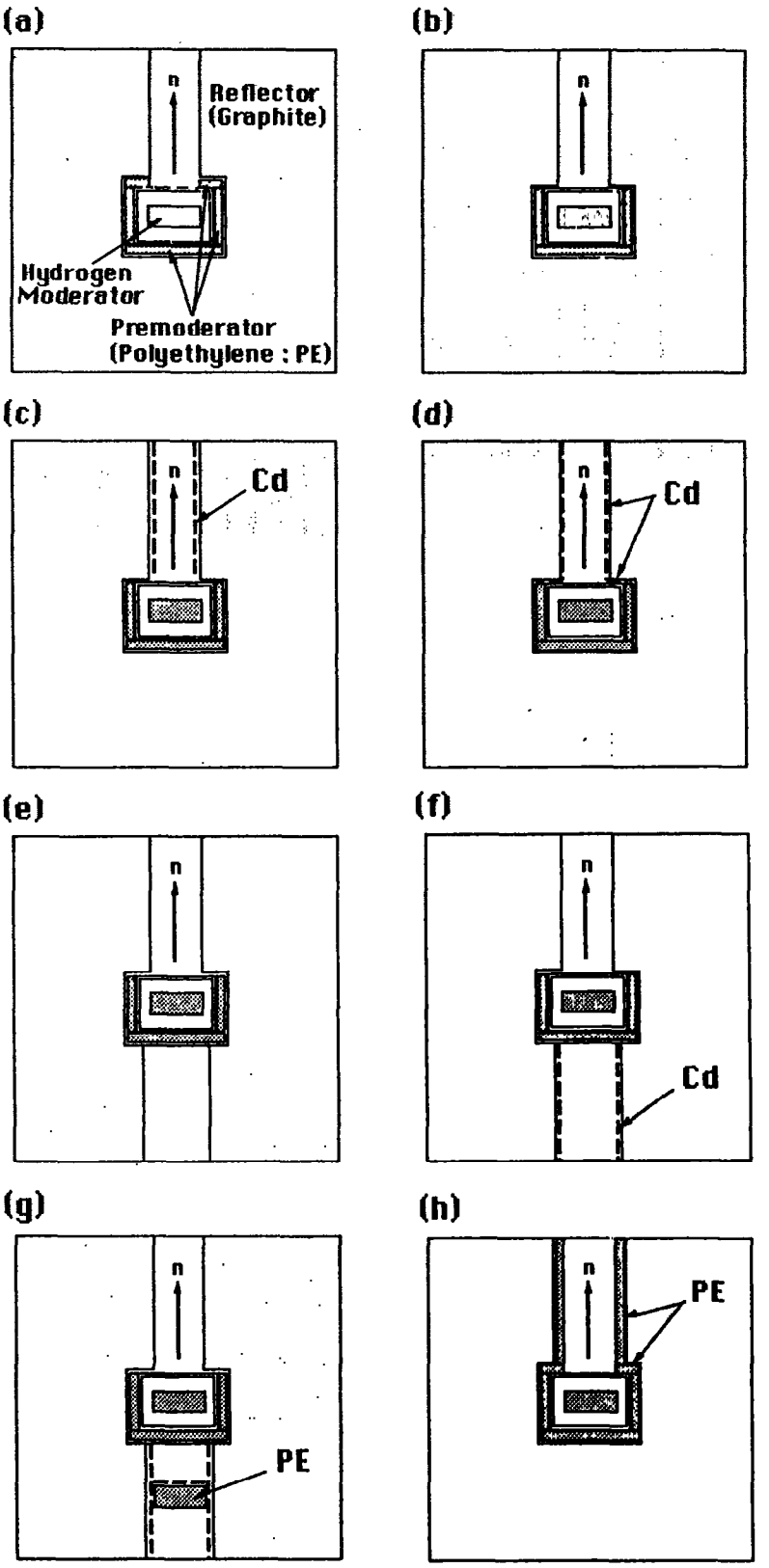

Fig. 4 Various moderator-reflector assemblies studied.

Configuration	Relative intensity to configuration (a)
(a)	1.00
(b)	0.88
(c)	0.62
(d)	0.52
(e)	0.81
(f)	0.78
(g)	0.74
(h)	1.05

Table 1 Relative intensities from the moderator-reflector assemblies shown in Fig. 4.

neutron-beam intensity. This is a great contradiction to the results obtained from the configuration (c) and (d). The reason is not understood at this moment.

In order to simulate the effect of other moderator we put a decoupled polyethylene moderator 15×15×5 cm^3 (at ambient temperature) in the second hole (configuration (g)). This does not give an appreciable reduction. The present results suggest that a coupled liquid-hydrogen-moderator with a premoderator can coexist with other decoupled moderators in the same target-moderator-reflector assembly.

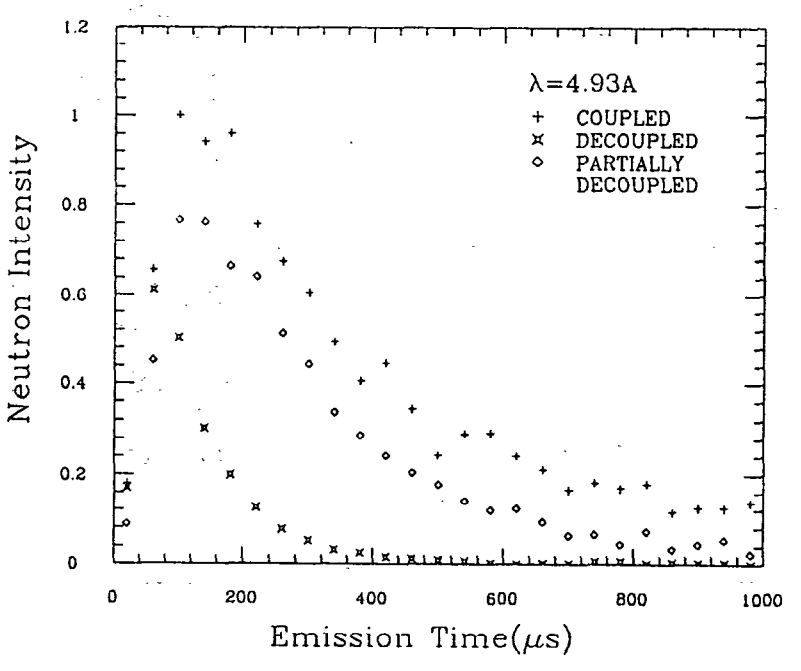

Fig 5 Time distributions of cold neutrons from the partially decoupled moderator (configuration (d)).

As an extra we examined the configuration (h) where a 1.5 cm-thick polyethylene liner was attached to the extraction hole. This configuration gives the highest beam intensity, but the obtained gain is small.

In order to understand the reason why the intensity reduction in the configuration (d) is so large, we measured time-distribution of the cold neutrons from the moderator in configuration (d). In Fig. 5 is plotted the measured time distribution of cold neutrons compared with the coupled and decoupled moderators. The pulse height and width in configuration (d) lie between both.

ACKNOWLEDGEMENTS

The authors are indebted to Prof. K. Inoue for his encouragement and interest shown through the course of this work.

REFERENCE

1 Y. Kiyanagi, N. Watanabe, M. Furusaka, H. Iwasa and I. Fujikawa : Proc. ICANS-XI (1990) p-388.
2 N. Watanabe : Proc. ICANS-XI (1990) p-471.

Q(P.A.Egelstaff): Have you tried using a heavy element with a large scattering cross-section as the reflector?
A(Y.Kiyanagi): A heavy element with a large scattering cross-section is an effective reflector for a decoupled moderator system. A moderating material is probably more suitable for a coupled liquid hydrogen moderator because slow neutrons should be fed to the liquid hydrogen moderator.

ICANS-XI International Collaboration on Advanced Neutron Sources
KEK, Tsukuba, October 22-26, 1990

Some Neutronic Studies on Flux-Trap Type Moderator

Y. KIYANAGI and N. WATANABE*
Department of Nuclear Engineering, Faculty of Engineering,
Hokkaido University, Sapporo, 060 Japan
*National Laboratory for High Energy Physics,
1-1 Oho, Tsukuba-shi, Ibaraki 305 Japan

ABSTRACT
The neutronic performance of a flux-trap type moderator was studied by computer simulation in connetion with the KENS-II target-moderator system. It was confirmed that this system can provide 1.3-1.4 times higher neutron intensity than a traditional wing-geometry moderator system.

I. INTRODUCTION

A wing-geometry in target-moderator coupling is adopted in pulsed spallation source because it can diminish the leakage of fast and high-energy neutrons into the beam holes in comparison with a slab geometry. However, the intensity of slow neutrons emitted from a wing-geometry moderator is smaller than that from a slab-geometry one. A new type of target-reflector-moderator arrangement, a so called flux-trap type moderator, was proposed by the Los Alamos group[1]. A vertical proton-beam injection sheme is one of a solution to provide more neutron beams than a horizontal one, because the proton-beam line in the experimental hall can be removed in the front[2]. In the vertical injection sheme a flux-trap type moderator arrangement is indispensable, because the tremendous stream of fast and high-energy neutrons is unavoidable in a traditional wing-geometry. We performed some optimization studies on this moderator system by computer simulation and compared the neutron intensity between flux-trap type moderator and wing geometry one in order to examine whether this can be a promising candidate for the target-moderator system in KENS-II.

II. CALCULATIONAL MODEL

The calculational model of the target-moderator system is shown in Fig. 1. The proton energy proposed for KENS-II is 1 GeV. The target is split into two parts in flux-trap type moderator system. The target, in which protons are injected, is called here a front target and the other a rear target. The

targets are made of tungsten. Total target length is 34.5 cm which is sufficient for 1 GeV protons to produce the saturated intensity of the spallation neutrons[3]. Four moderators are placed around the void space between the two targets. Light water moderators with a size of 10×10×5 cm^3 are assumed. The system is surrounded by a beryllium reflector of 30 cm thick. The beam holes in the reflector are lined with 1 cm thick B_4C decouplers. They are not shown in the figure for simplicity.

For the calculation a Monte Carlo code for low energy neutron transport, MORSE-DD[4], was used combined with a high energy transport code, NMTC/JAERI[5]. "slow neutrons" in this paper are defined here as those neutrons below 0.9 eV.

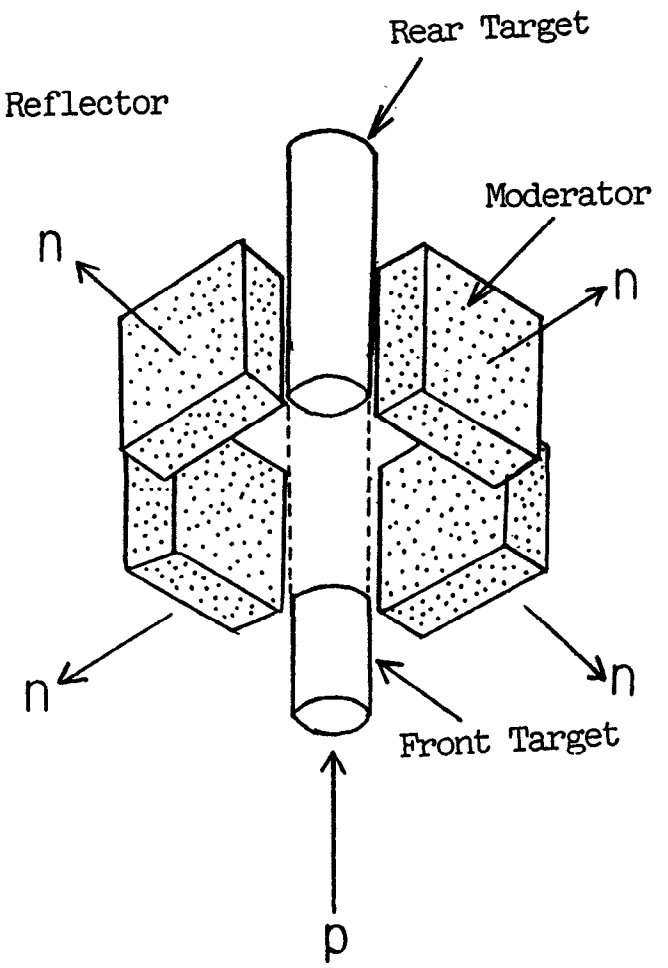

Fig. 1 Calculational model of the flux-trap type target-moderator system.

III. OPTIMIZATION STUDIES

Firstly, we examined the optimal length of the front target keeping the length of the void space between front and rear targets at 14 cm, which would just meet the moderator height of 10 cm with 1 cm thick decoupler and 1 cm allowances on top and bottom, and the target radius at 5 cm. The gap between moderator and target void was kept at 2 cm which is necessary to arrange the four moderators around the void space. Figure 2 shows the slow-neutron intensities from the moderators as a function of front-target lengths. The length dependence of the slow neutron intensity is rather modest : the optimal length is about 7-8 cm. We chose 7.5 cm for the front target length in the following calculations.

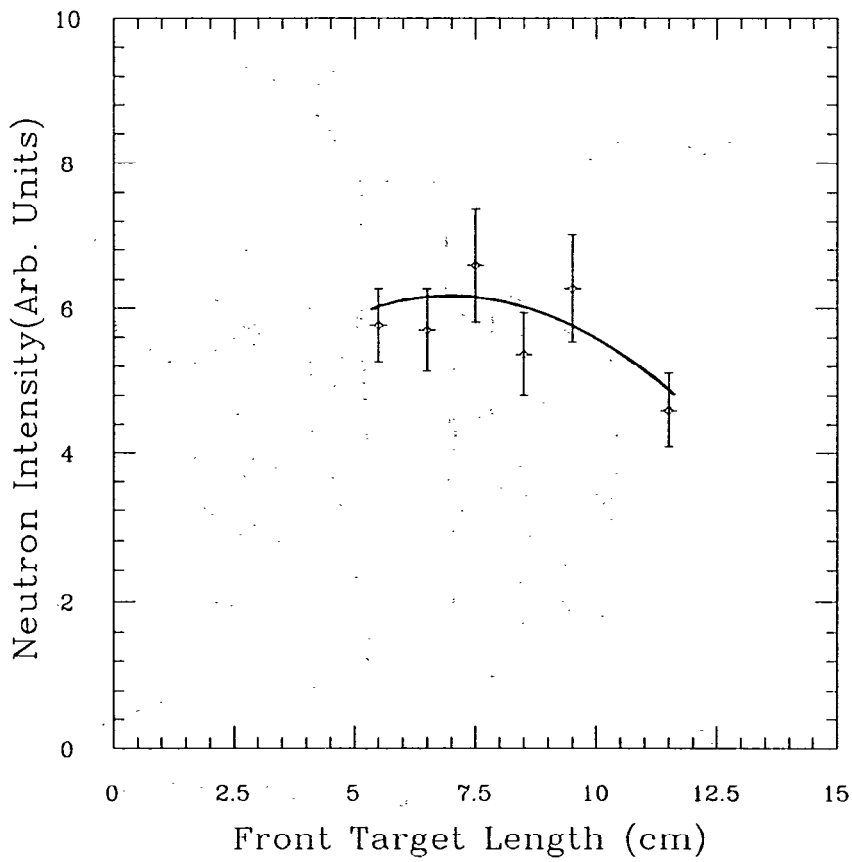

Fig. 2 Slow neutron intensity vs. front-target length.

Secondly, we examined the optimal target radius keeping the length of the target void at 14 cm, and the distance between the target center-line and the moderator at 7 cm. Figure 3 shows the slow-neutron intensities from the moderators as a function of target radius. The intensity is again unchanged up to a radius of about 8 cm. There is no gain with increasing target radius. This may be due to the tungsten target because the enlarged target simply bring about reflector missing without additional neutron production. We intend to look into a uranium target system later.

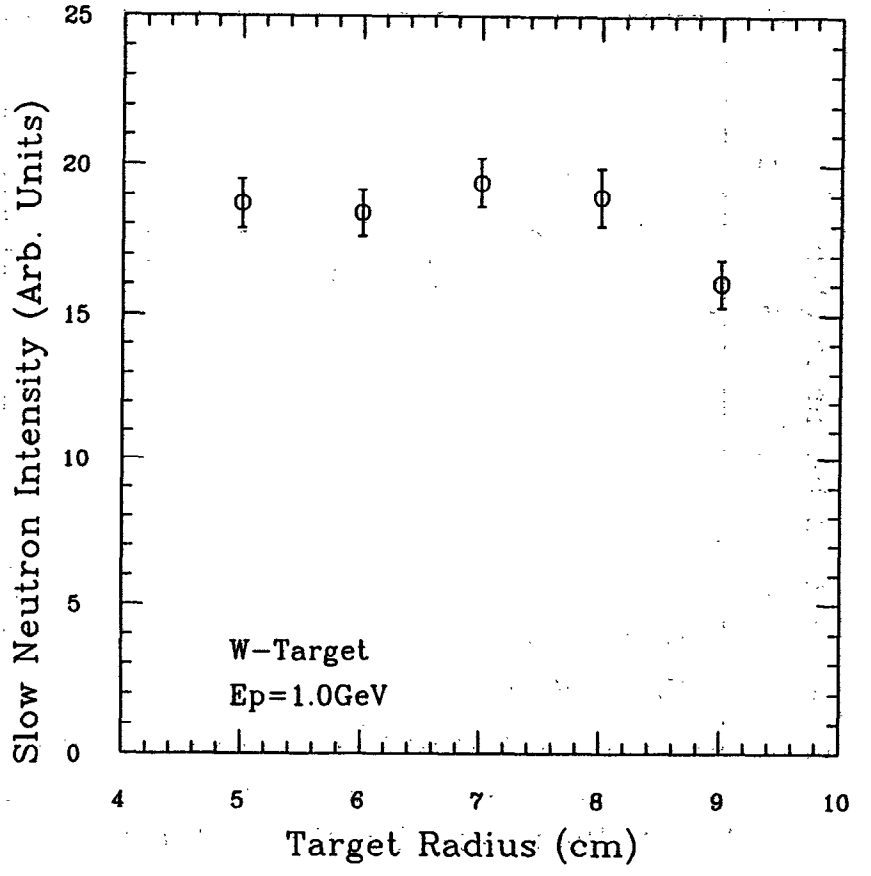

Fig. 3 Slow-neutron intensity vs. target radius.

Thirdly, we examined the optimal length of the void space between the two targets because the void length is one of the most important parameters on which the leakage of fast and high-energy neutrons to the beam holes strongly depends. The moderator was located at the center height of the target void keeping the gap between target void and moderator at 2 cm. Figure 4 shows the result. The slow-neutron intensity is almost unchanged within the statistical accuracy. This suggests the possibility to adopt a longer void space which makes it easy to suppress the hard component of neutrons leaking to the beam holes.

Next, we examined the slow-neutron intensity as a function of moderator thickness in order to obtain a better understanding of the target-moderator coupling nature of this moderator system. Other parameters were kept constant as before. Figure 5 shows slow-neutron intensity vs. moderator thickness. The maximum appears at about 7 cm. The feature is similar to the result of the slab-geometry moderator, suggesting that a flux-trap type moderator is closer to a slab-geometry moderator rather than a wing-geometry moderator in neutronic performance.

It is excepted that the rear surface of the moderator (near the target) will emit more slow neutrons than the front surface (opposite side), because the collision density of fast neutrons in the moderator will be larger in the rear

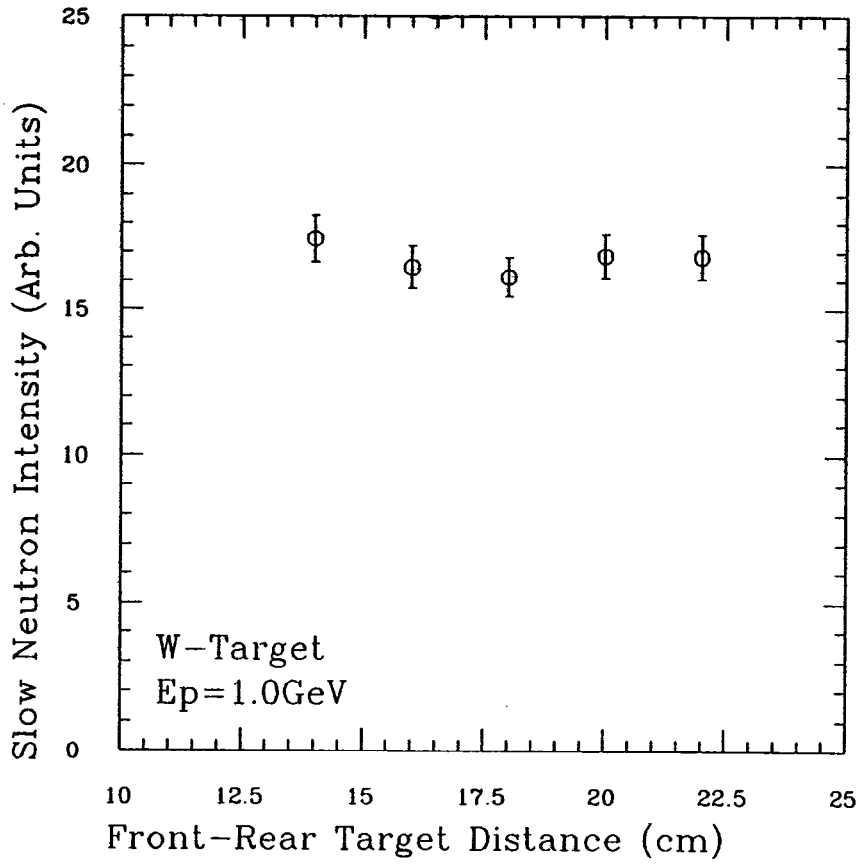

Fig 4 Slow-neutron intensity vs. void length between front and rear targets.

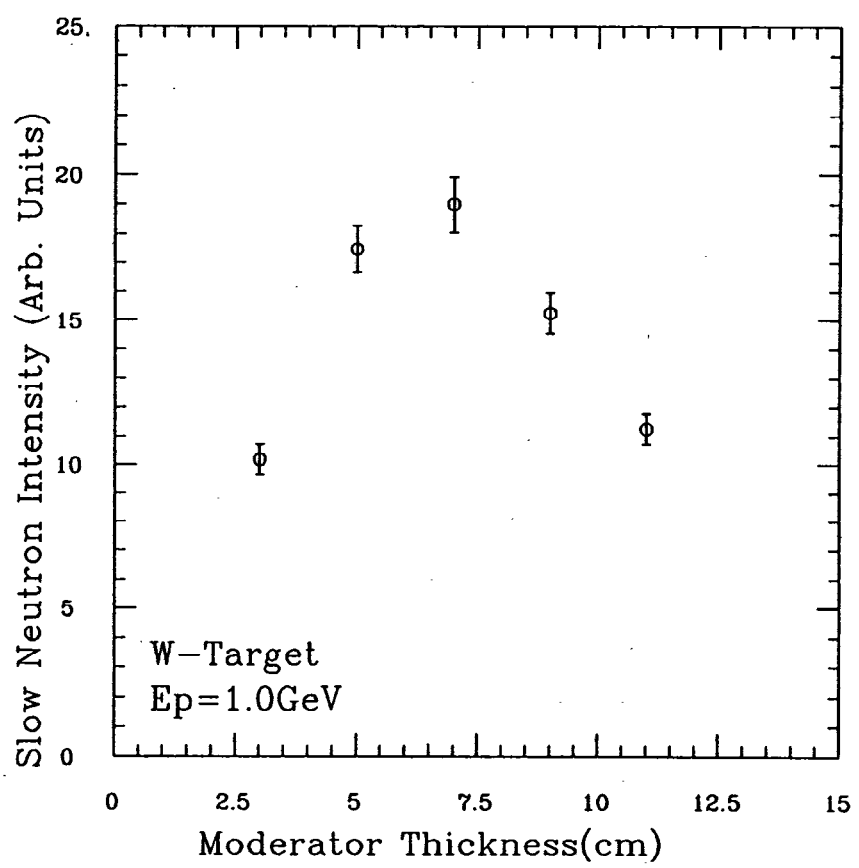

Fig 5 Slow-neutron intensity vs. moderator thickness.

side than in the front side. We can extract the neutron beam from the rear side as well because there is no target behind the moderator. In this case of course we assume that the moderator at the opposite side across the target void dose not exist. Then we calculated the neutron intensities from the rear and the front surfaces of the moderator as a function of target-moderator distance. In this case one moderator was placed around the target void for simplicity. All other parameters were fixed constant as before. Figure 6 shows the slow-neutron intensities from both surfaces of the moderator. The intensity gain from the rear compared to the front is unexpectedly small; only 10 %, suggesting that the neutron beam extraction from a rear surface of moderator is less interesting.

The slope is rather modest; approximately 10 % per 2 cm. This will make the engineering design of the target-moderator system easier: we can put the moderator around the void space with an enough spacial allowance, not sacrificing the intensity appreciably.

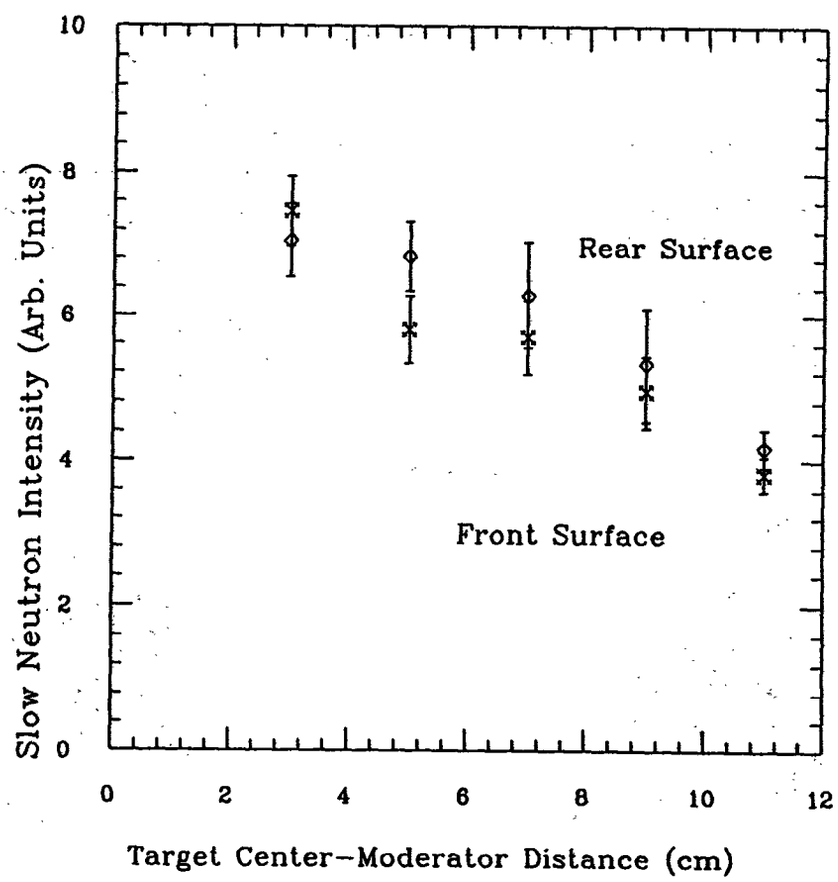

Fig. 6 Slow-neutron intensity vs. target-moderator distance.

IV. COMPARISON WITH WING-GEOMETRY MODERATOR

Finally, we compared the slow-neutron intensity from a flux-trap type

Fig. 7 Comparison of slow-neutron intensity between flux trap type moderator and wing-geometry moderator.

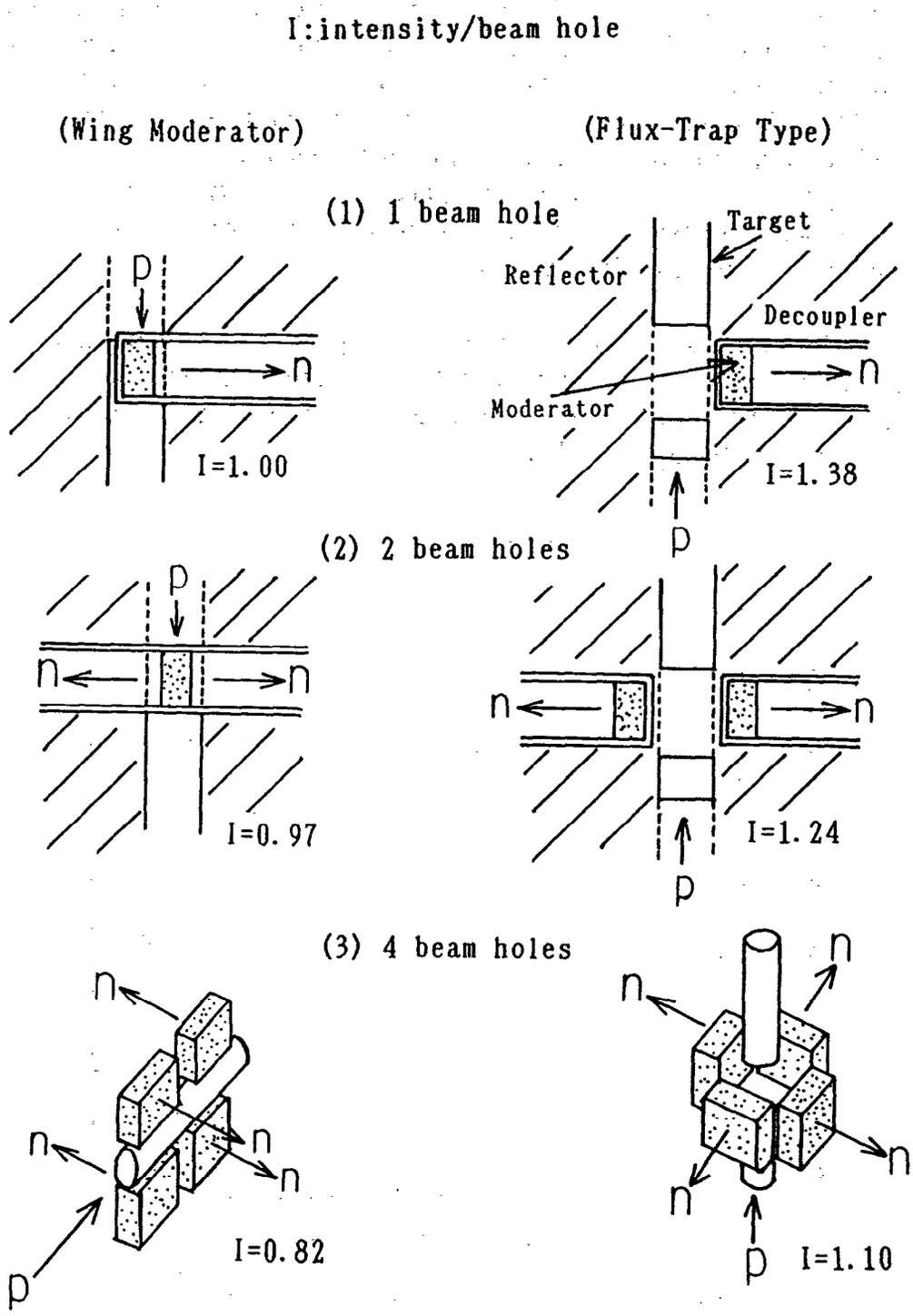

moderator system with that from a reference moderator system in a wing geometry. In all cases the gap between the cylindrical target surface and the moderator is kept at 2 cm. Figure 7 show the configurations of both systems. In the configurations of 4 beam holes, the reflector is not depicted for simplicity. The relative values of the slow-neutron intensity per moderator

surface, I, are indicated in the figure. The results show that the flux-trap type moderator can provide 1.3-1.4 times higher intensity than the wing-geometry moderator.

V. CONCLUSIONS

The present results suggest that a flux-trap type moderator is a promising candidate for the target-moderator system in KENS-II. We are now investigating similar optimization studies on a coupled liquid-hydrogen-moderator system.

REFERENCE

1 G. J. Russell, H. Robinson, G. L. Legate, R. Woods, E. R. Whitaker, A. Bridge and K. J. Hughes : Proc. ICANS-IX (Villigen, Sept. 22-26, 1986) p-177
2 N. Watanabe : Proc. ICANS-XI (Tsukuba, Oct. 22-26, 1990) p-471.
3 Y. Kiyanagi, M. Arai and N. Watanabe : Advanced Neutron Sources 1988 (Proc. ICANS-X (1988)), Institute of Physics Conference Series Number 97, Institute of Physics, Bristol and New York, p-753
4 M. Nakagawa and T. Mori: JAERI-M 84-126 (1984).
5 Y. Nakahara and T. Tsutsui:JAERI-M 82-198 (1982).

ICANS-XI International Collaboration on Advanced Neutron Sources
KEK, Tsukuba, October 22-26, 1990

Theoretical thermal-hydraulic investigations of the operational and safety features of the cold D_2-moderator for SINQ

K. Skala, H. Spitzer, G.S. Bauer
PAUL SCHERRER INSTITUTE
CH-5232 Villigen-PSI, Switzerland

ABSTRACT

In order to be able to investigate the behaviour of the gas-liquid mixture in the rather complex vessel and pipe system of the cold D_2-moderator with heat exchanger and ballast volume, a computational model of the system has been set up. The model was first benchmarked against experimental data from the cold moderator mockup for the second cold source at the ILL Grenoble. It was then used to predict operational parameters such as pressure, velocity, moisture content and others of the system under normal conditions with the anticipated distribution of heat influx. Finally, the case of total loss of insulating vacuum was investigated.

I INTRODUCTION

As compared to the cold moderators of the existing spallation neutron sources, the one planned for SINQ is different in two respects:

- SINQ being a cw-source, the cold moderator is designed to give a high time average flux of cold neutrons. This implies the use of a large D_2-filled moderator vessel.
- The high beam power of SINQ (around 1 MW) together with the large moderator volume results in a high heat input during normal operation.

Although these conditions also prevail in research reactors, other considerations such as high energy radiation shielding prevent us from simply adapting an established cold moderator design but caused us to deviate sufficiently far from existing designs to make a detailed analysis of the thermal-hydraulic behaviour necessary. Part of the work has been reported earlier /1/. This paper gives an update to include recent results from a slightly improved computational model.

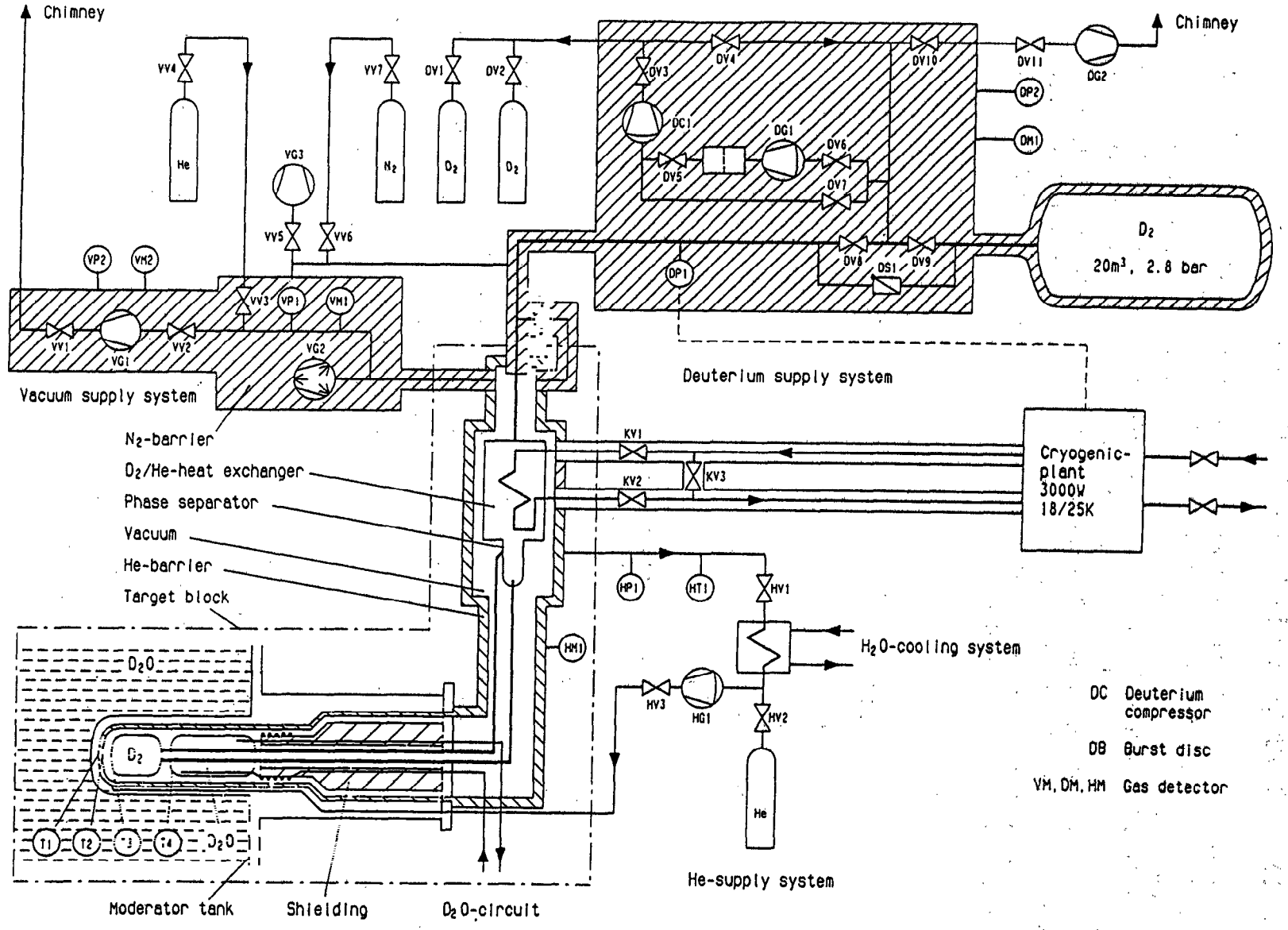

Fig. 1 Simplified diagram of the various subsystems of the D_2 cold moderator for SINQ. The cold part of the D_2 system consists of the moderator vessel, the phase separator - condenser volume and a pair of concentric pipes for circulation of the liquid and liquid-gas mixture.

II THE D_2-SYSTEM AND ITS MODEL REPRESENTATION

The technical concept of the SINQ-cold moderator system has been described elsewhere /1/, /2/. Fig. 1 shows a simplified diagram of the D_2- and auxiliary circuits. Only the D_2 part is considered in this work and is modelled as a system of three vessels representing the moderator, the phase-separator/heat exchanger and the ballast volume for the D_2-gas. These volumes are interconnected by pipes whose cross-sections have been fixed for the time being but may well be optimized as a result of ongoing calculations of the type described here. The model representation and the numbering of the pipe segments are shown in Fig. 2 and the corresponding dimensions given in Table 1. Pipe segments A and B are concentric with the forward flow (heat exchanger -to- moderator) through the inner pipe and return flow through the outer annulus.

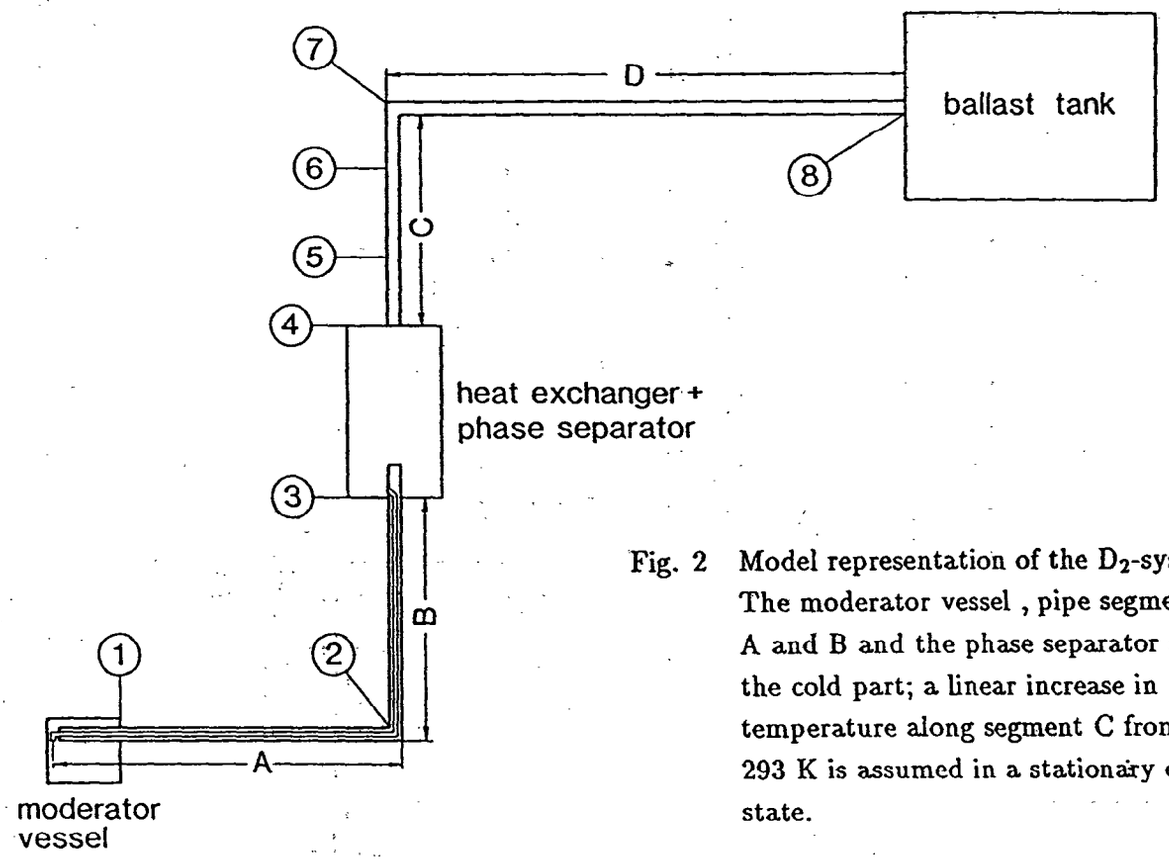

Fig. 2 Model representation of the D_2-system. The moderator vessel , pipe segments A and B and the phase separator comprise the cold part; a linear increase in temperature along segment C from 25 K to 293 K is assumed in a stationary operating state.

III THE COMPUTATIONAL MODEL

In the computational model, the three vessels are treated as "localized capacitors" where phase changes can take place and the mass content can vary. The connecting pipes are subdivided into individual elements with coupled thermodynamic properties. Coexistence of vapour and liquid and, as a new feature relative to the earlier calculations (/1/), heat input and superheated vapour is allowed in all volumes of the cold part of the system, whereas only vapour exists in the ballast volume and in pipe segments C and D.

Dynamic equilibria in mass, energy and forces are established between all neighbouring elements of the system. The corresponding coupled partial differential equations are replaced by difference equations and are applied to the finite elements. Integration is carried out numerically (with a FORTRAN programme).

The compressibility of the vapour and the variable temperatures of the superheated vapour are taken

into account where appropriate.

In order to benchmark the model and to obtain realistic values for some poorly known parameters, the data given by Hoffmann /3/ for the ILL-test experiments were reproduced in a first step with very good agreement.

Volume of the moderator vessel	22.3 litres
Volume of the phase separator/heat exchanger	30.0 litres
Volume of the D_2-ballast tank	20 m^3
Length of pipe segment A	3.9 m
Inner diameter of outer pipe in segment A	4.5 cm
Outer diameter of inner pipe in segment A	2.0 cm
Length of pipe segment B	2.7 m
Inner diameter of outer pipe in segment B	5 cm
Outer diameter of inner pipe in segment B	2 cm
Length of pipe segment C	1.8 m
Inner diameter of pipe segment C	6.7 cm
Length of pipe segment D	55 m
Inner diameter of pipe segment D	9 cm

Table 1 Dimensions of the SINQ-D_2-system

IV RESULTS FOR STANDARD OPERATING CONDITIONS

A series of calculational runs was performed to obtain a feel for the stability of the model results and also for the behaviour of the system in the event of a perturbation. It was found that the system moved towards stable operating conditions when an arbitrary, but reasonable yet non-consistent set of start parameters was given for the various system variables.

One unknown in the system, which has an effect on the set of stable parameters and which could not be derived in a theoretical manner is the liquid content of the vapour at the point of entrance from the moderator vessel to the inner pipe of segment A.

This "dryness" of the returning medium is very difficult to estimate, since it will depend on the violence of boiling in the moderator vessel, on geometry and possibly other factors. In order to get a feeling for its effect, the assumption was made, that the dryness x is a linear function of the the height h of the nominally vapour-filled volume inside the moderator vessel, i.e.:

$$x \sim \frac{h}{D}$$

with D being the diameter of the moderator vessel (Fig. 3).

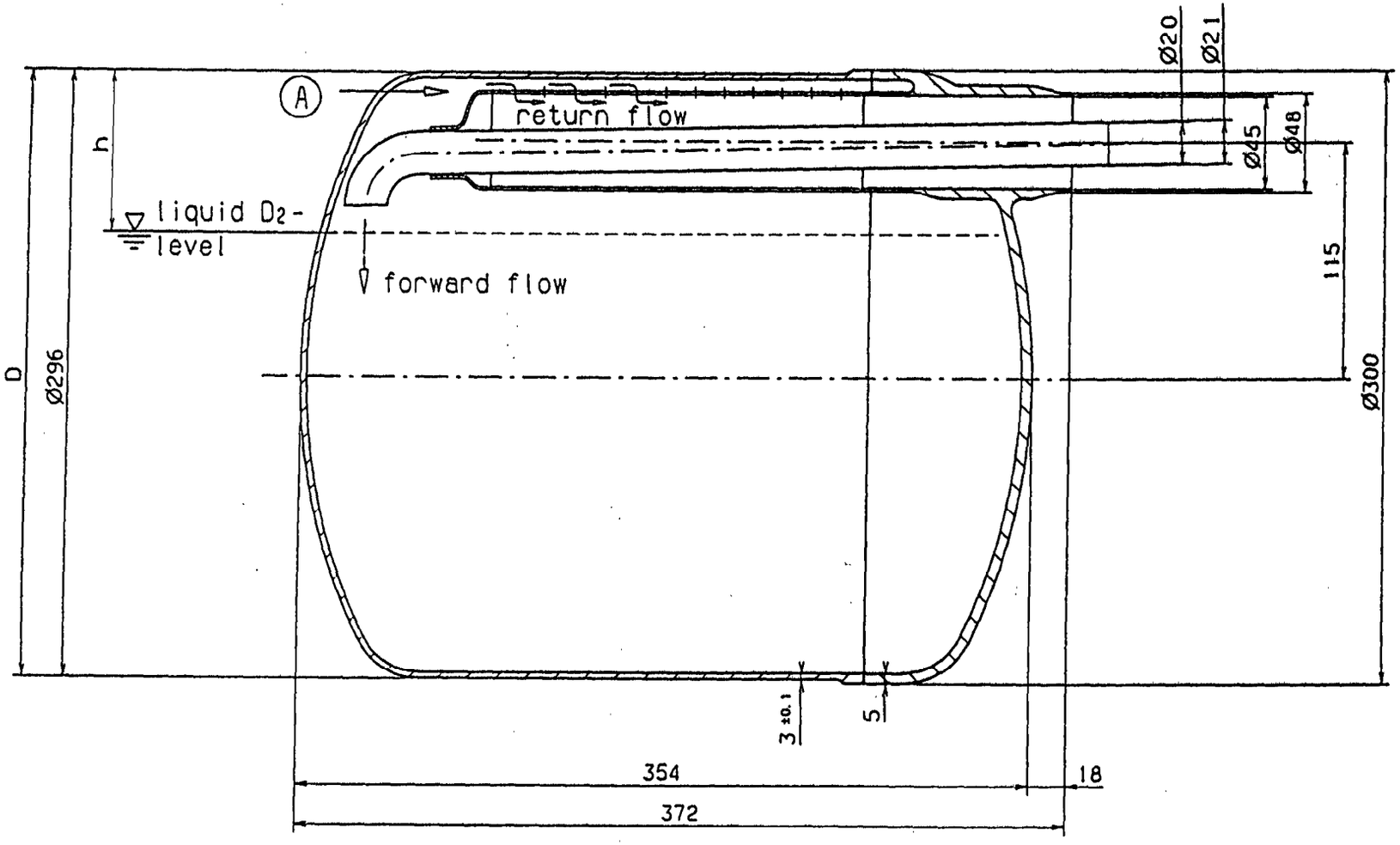

Fig. 3 Vertical section through the moderator vessel showing the definitions of h and D.

	t = 0	t = 20 sec			t = 30 sec			t = 60 sec		
		(a)	(b)	(c)	(a)	(b)	(c)	(a)	(b)	(c)
Velocity of return flow (liquid-gas-mixture) (m/s)	0.58	2.77	2.26	2.067	2.536	2.264	2.160	2.26	2.26	2.25
Velocity of forward flow (liquid D_2) (m/s)	0.40	2.10	2.08	2.038	2.098	2.078	2.058	2.08	2.08	2.08
Mass fraction of vapour in return flow (%)	15	13.4	10.6	9.1	12.3	10.6	9.8	10.7	10.7	10.5
Return mass flow (g/s)	18.0	93.47	93.89	97.5	93.3	93.9	95.9	93.6	93.9	94.25
Forward mass flow (g/s)	18.0	94.7	93.7	91.9	94.6	93.7	92.8	93.78	93.66	93.52
Total mass of D_2 in moderator vessel (kg)	3.045	3.1	3.0	2.8	3.1	3.0	2.75	3.1	3.003	2.7
Total mass of vapour in moderator vessel (g)	3.045	2.042	3.989	8.75	1.760	3.990	9.705	1.44	3.99	10.7
Relative height of liquid level (1- h/D)	0.91	0.93	0.89	0.82	0.94	0.89	0.80	0.95	0.89	0.80
Pressure in moderator vessel (bars)	1.570	1.57	1.57	1.57	1.57	1.57	1.57	1.57	1.57	1.57

Table 2 Variation of some parameters of the SINQ D_2-system as a function of time from an "arbitrary" set of starting values and under a heat input of 3 kW to the moderator vessel.

Three cases were considered (Fig. 4):

(a) x = 1 for $^h/_D$ = 0.5, i.e. dry vapour if the vessel is less than half-full

(b) x = 1 for $^h/_D$ = 1, i.e. dry vapour only if there is virtually no liquid volume in the vessel

(c) x = 0.5 for $^h/_D$ = 1, i.e. there is still a 50 % liquid fraction in the return flow even at the moment, when a stationary liquid surface cannot be detected in the vessel any more

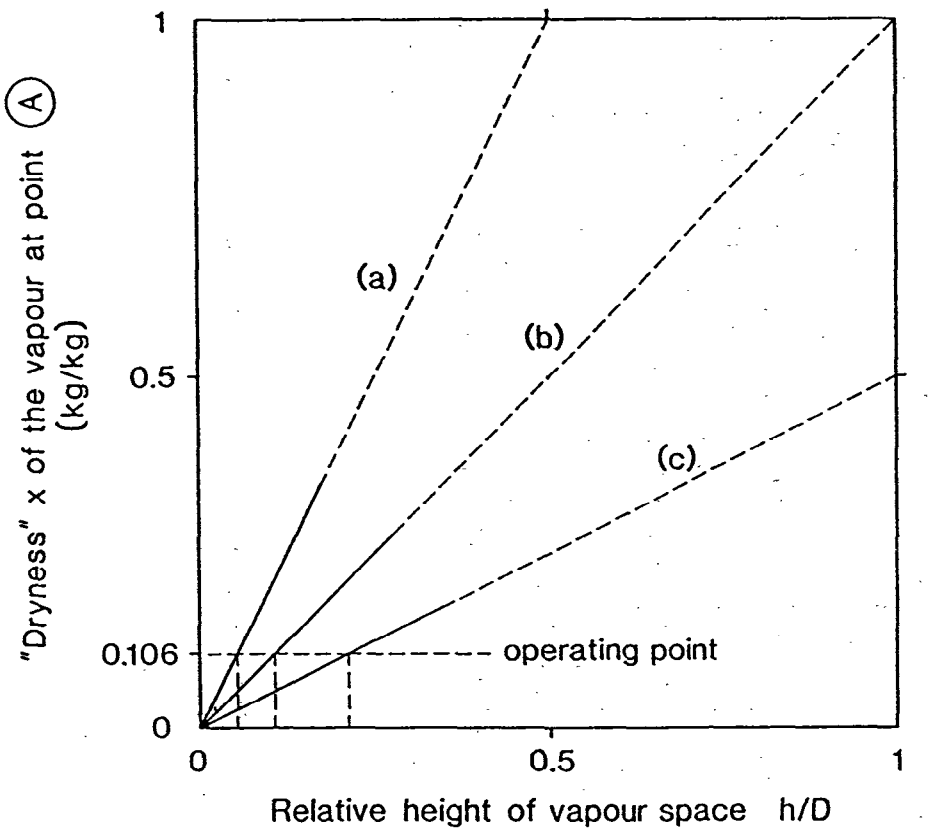

Fig. 4 Assumed relations between vapour fraction x (kg vapour per kg medium) at the level point A in Fig. 3 and relative height of the vapour space h/D in the moderator vessel. The calculated operating point to remove 3 kW of heat is at x = 10.6 %, resulting in different degrees of filling of the moderator vessel.

Of course, only the initial slope of these curves is of real importance. Table 2 gives the "arbitrary" set of starting parameters chosen at the beginning and their values 20, 30 and 60 seconds after the system was allowed to adjust to a heat input of 3 kW to the moderator vessel. While equilibrium has not yet been reached after 30 seconds in cases (a) and (c), case (b) virtually reaches its stationary situation after about 20 seconds. This is, of course, merely a consequence of the particular choice of starting parameters. After 60 seconds equilibrium has practically been reached in all cases. The fact that there exists an apparent slight difference between forward and return mass flow even after 60 seconds is a computational artifact since the calculated mass flow depends very critically on the pressure difference between the moderator and phase separator vessel. As expected, the relative filling height reached in the equilibrium situation is different for the three cases and is determined by the amount of vapour required to remove all the heat from the moderator vessel. This can be seen to be ≈ 10.6 % mass ratio in the return pipe for all cases. The filling height is important for neutronic reasons because of the effective field of view of the neutron guides.

Since the geometry is such that a loss of illumination would occur for $(1- {}^{h}/_{D}) < 0.75$, a minimum value $(1- {}^{h}/_{D}) \approx 0.8$ is desirable. This is true even in case (c) which is certainly an overly pessimistic one. An initial slope between cases (a) and (b), a situation likely to prevail in the real situation, will safely meet this condition.

The variation of $(1- {}^{h}/_{D})$ is shown for the three cases during the first 30 seconds in Fig. 5, while Fig. 6 shows the vapour content (by mass) in the return flowing liquid-gas mixture for the same time period. Although almost 90 % of the total mass leaving the moderator vessel is liquid, the vapour makes up 84 % of the volume in the pipe. The liquid does not contribute to heat transport and thus constitutes a reserve for more power to be removed from the moderator vessel. By comparing Figs. 5 and 6 it is also obvious, that, as the D_2-levels go to different equilibrium values in the three cases, the vapour fractions, after an initial "overshoot", tend towards the same mass ratio, which is achieved rather quickly in case b. The "stationary" operating point has been marked in Fig. 4 and is at 10.6 % vapour content in all cases. (Note that the "dryness" is in mass fraction, rather than volume fraction as mentioned above!)

From these results it can be concluded that safe and stable operation of the source will be possible at the anticipated power input of around 2 kW and with a large operational safety margin. Further detailed investigations of operational transients are planned for the future.

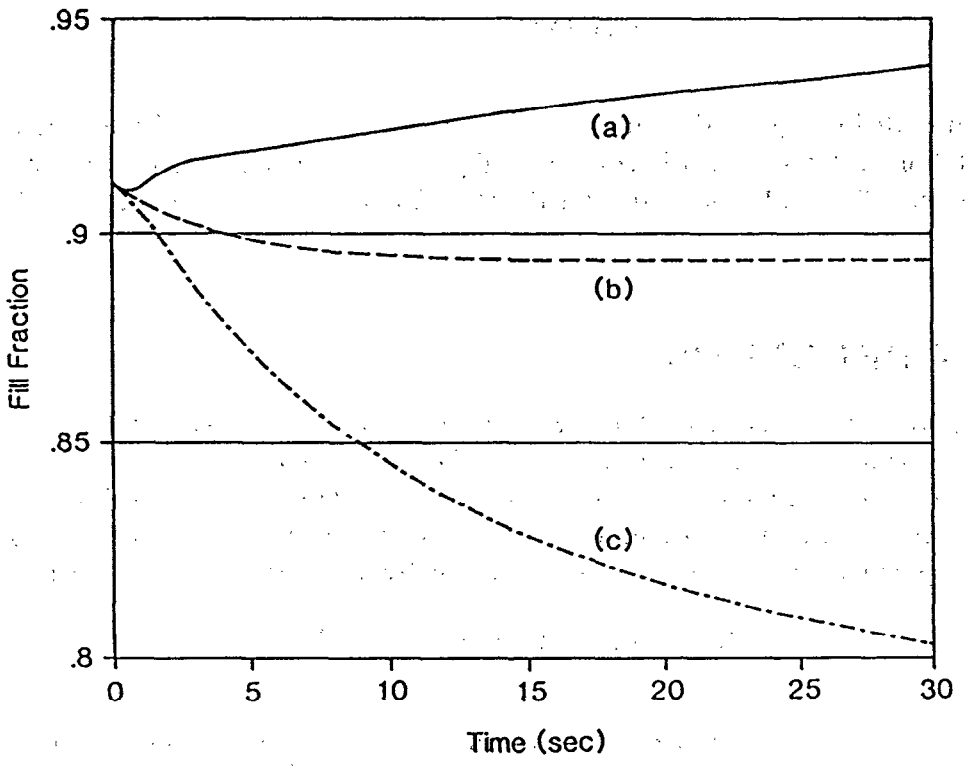

Fig. 5 Calculated filling height of the moderator vessel as a function of time for the three relations given in Fig. 4. Curve numbers (a) through (c) match in both figures. Fill fraction is (1- h/D).

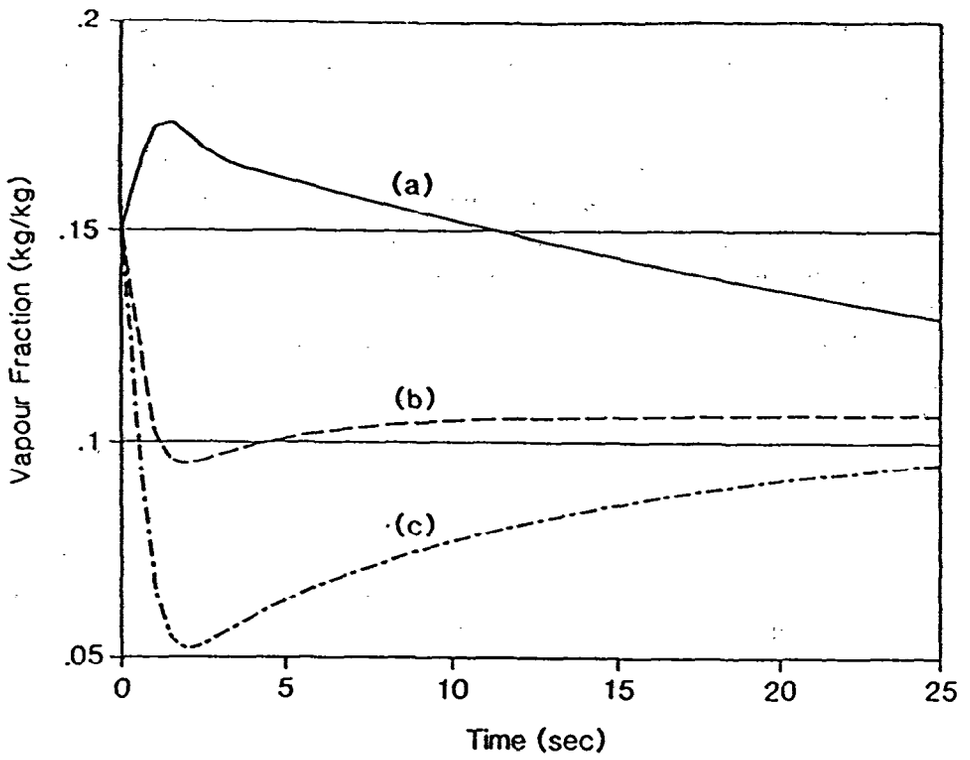

Fig. 6 Calculated change of the vapour fraction x as a function of time for the three relations between x and h/D given in Fig. 4. Curve numbers match in both figures. The equilibrium value for the three curves is x = 10.6 (kg/kg).

V SAFETY PROBLEMS

Since thermal insulation of the cold D_2-system is achieved by a vacuum environment, loss of insulating vacuum is one of the main incidents which have to be taken into account in the design. Although in general there will be a gradual increase in pressure and hence in heat transport to the cold system, it is difficult to predict exactly what sequence of events one has to consider. As a relatively flexible approximation, we assumed an exponential increase of heat transport according to the equation

$$P(t) = P_{max.} \cdot (1 - exp(-t/\tau)). \tag{1}$$

The time constant τ can be varied and the heat influx applied to any part of the system. τ is essentially determined by the thermal transport properties of the gas between the two walls. Heat conduction within the walls is much faster and has been neglected. The maximum power, P_{max} takes into account the variation in temperature and heat transfer coefficient in those regions, where superheated vapour is present, i.e. as the temperatures rise above the boiling point of the liquid.

The parameters chosen for the calculation are τ = 300 msec with a peak specific heat influx per unit area of 36 kW/m^2. Furthermore, in order to remain on the pessimistic side, it was assumed, that, at the moment of loss of vacuum, the moderator vessel was filled to the level of the outlet pipe and the connecting pipes to the phase separator were completely filled with stationary liquid (no circulation). The phase separator was assumed to be 10 % full, as given by the total amount of D_2 in the system.

The increase of heat input to the moderator vessel as a function of time is shown in Fig. 7 for the first one second. Fig. 8 gives the pressure in the moderator vessel and the phase separator for the same period of time. It can be seen that, as a consequence of the expulsion of the liquid from the pipe system, a temporary increase in pressure from the stationary value of 1.56 bars to 2.25 bars takes place, which decreases again, as more and more D_2 is expelled from the moderator vessel.

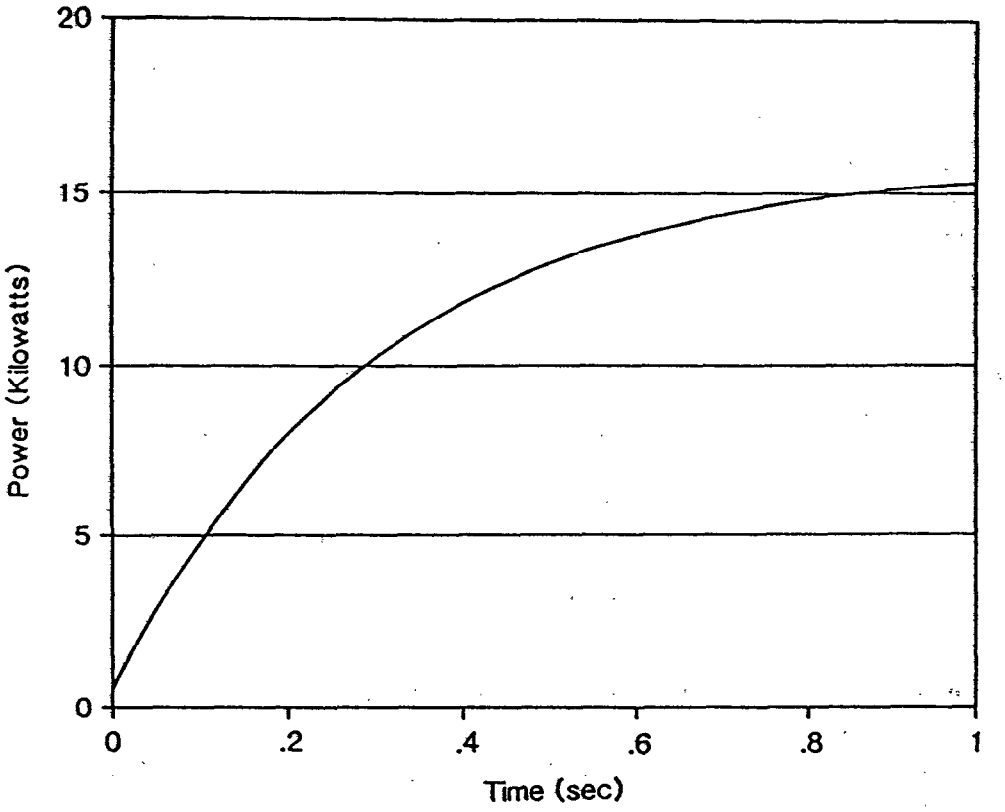

Fig. 7 Assumed variation of power input to the moderator vessel after a loss of insulating vacuum at t = 0. At t< 0 the system was in a steady state with only 0.5 kW of power input (thermal losses) and virtually no D_2- circulation.

The flow velocity of the medium at various points in the system as a function of time is shown in Fig. 9. As a consequence of the simultaneous onset of heat influx on all cold parts of the system, flow starts at t = 0 everywhere in the cold part with a delay due to the velocity of sound at the entrance to the ballast tank (curve d). The various "capacitor" volumes are also visible at that point. Furthermore, it can be observed that, at very short times, a return flow exists from segment 1 to the moderator vessel which results from the compressibility of the vapour initially present in the moderator vessel.

Taking into account that the gas pressure in the system is 2.8 bars when warm, the results found here give no cause for concern. (The system pressure of 2.8 bars will eventually be reached at long times, but 1 sec is by far, too short to notice any move in that direction).

As a consequence of the rapid expulsion of the cold medium from the moderator vessel and the phase separator, a front of cold medium is pushed through the pipe connecting the phase separator to the ballast tank. Assuming that, at stationary state, a linear temperature gradient exists over the length of pipe segment 3 between 25 K and 298 K the change in temperature at various points of the system is shown in Fig. 10. The onset of the temperature drop is linked to mass transport rather than to the velocity of sound as is the onset of mass flow. Hence the longer delay.

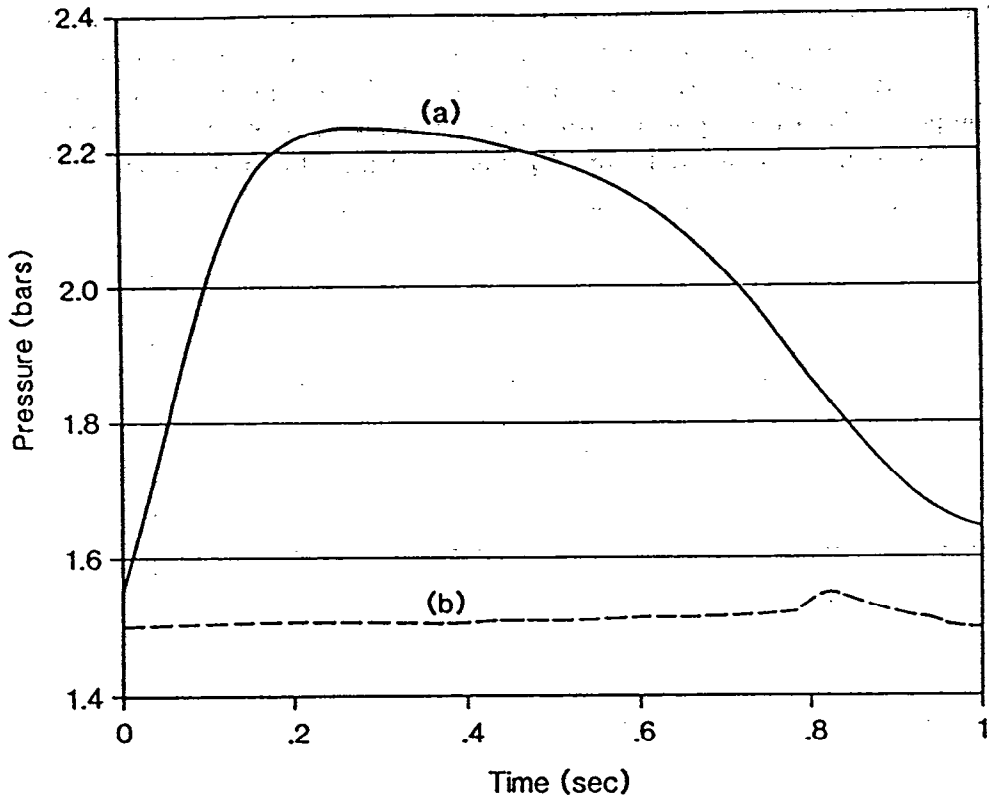

Fig. 8 Pressure in the moderator vessel (curve a) and in the phase separator (curve b) during the first one second after a loss of insulating vacuum. At longer times the pressure increases very gently as the liquid evaporates and the system warms up.

The effect of heat input to the pipe is clearly visible as a change in slope as the cold front propagates along the pipe.

It is important to note that the whole length of the transfer pipe between phase separator and ballast tank will be cooled down to 25 K in the case of a loss of insulating vacuum. (This has to be accounted for in the layout of the pipe.)

The above results are also applicable to the situation of a fairly sudden rupture of the moderator vessel with D_2-spill into the vacuum space, as long as the return flow pipe to the phase separator remains unblocked. The extra volume available in this case will even help to keep the pressure on the vacuum jacket lower. This situation remains to be considered in more detail.

For the sake of completeness, although of no real meaning, two increasingly simplified cases have also been considered:

- all heat input goes to the moderator and phase separator volumes alone, (no heating of the connecting pipes);
- as before, but in addition an effecting instantaneous increase of heat input to its maximum value (τ = 3 ms)

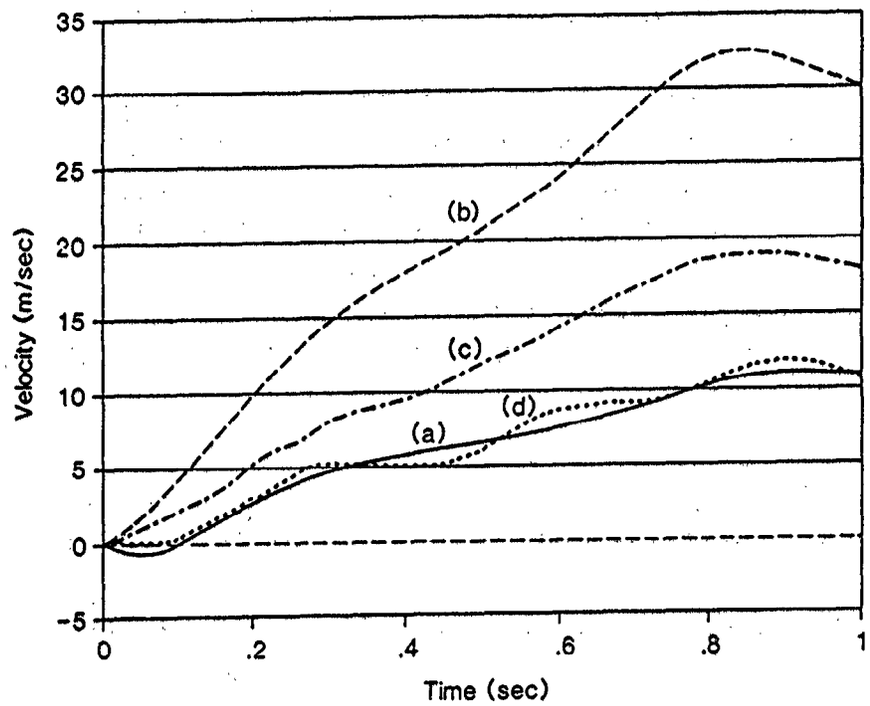

Fig. 9 Flow velocity at various points in the D_2-system after a loss of insulating vacuum at t = 0.
curve (a) : point 1 in Fig. 2 (exit of moderator vessel)
curve (b) : point 3 in Fig. 2 (entrance to phase separator)
curve (c) : point 4 in Fig. 2 (exit of phase separator)
curve (d) : point 8 in Fig. 2 (entrance of D_2-ballast tank)

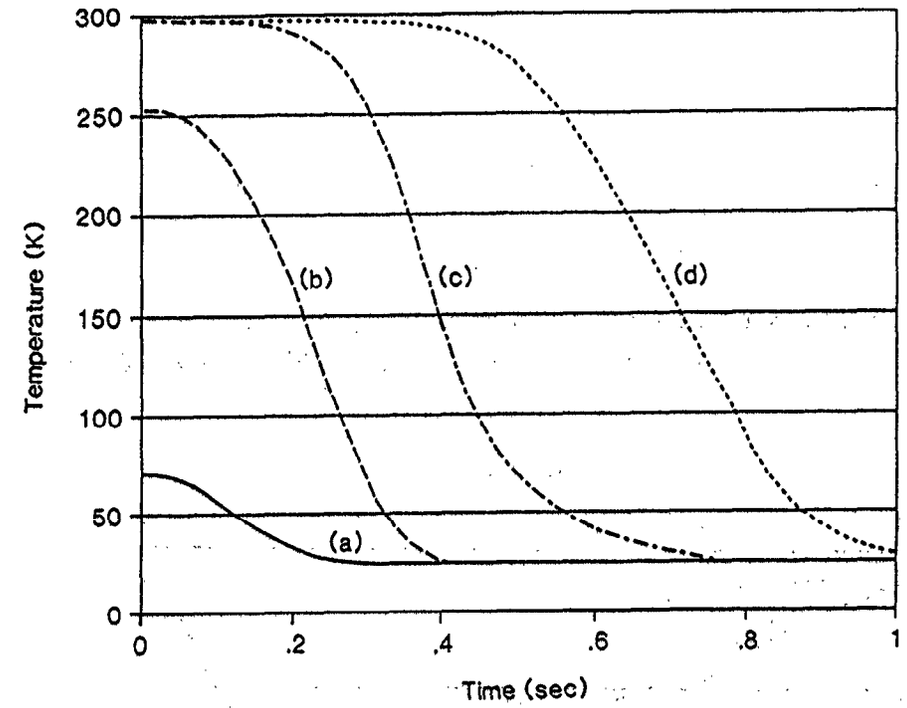

Fig. 10 Temperature evolution at various points in the D_2-system after a loss of insulating vacuum at t = 0.
(a) point 5 in Fig. 2 (at 30 cm above heat exchanger vessel)
(b) point 6 in Fig. 2 (at 150 cm above heat exchanger vessel)
(c) point 7 in Fig. 2 (at 180 cm above heat exchange vessel)
(d) point 8 in Fig. 2 (entrance to D_2-ballast tank)

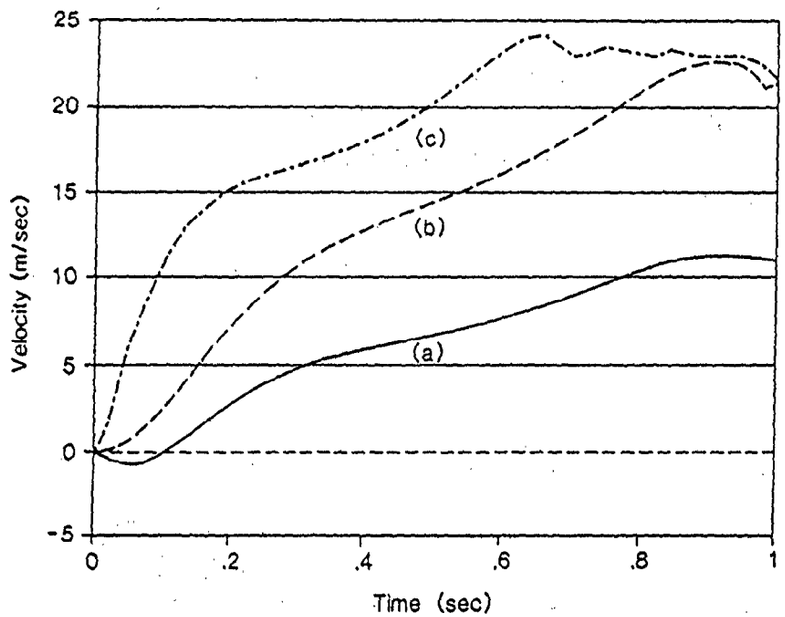

Fig. 11 Flow velocity of medium at the exit point from the moderator vessel (point 1 in Fig. 2) for three different assumptions on heat input
(a) heat input along the whole D_2-system according to Figure 7 with 3.6 W/cm^2 of surface, heat flux
(b) Heat input concentrated on moderator and phase separator volumes but matching the total heat input of curve (a).
(c) as b but time constant of power rise reduced from 300 ms to 3 ms.

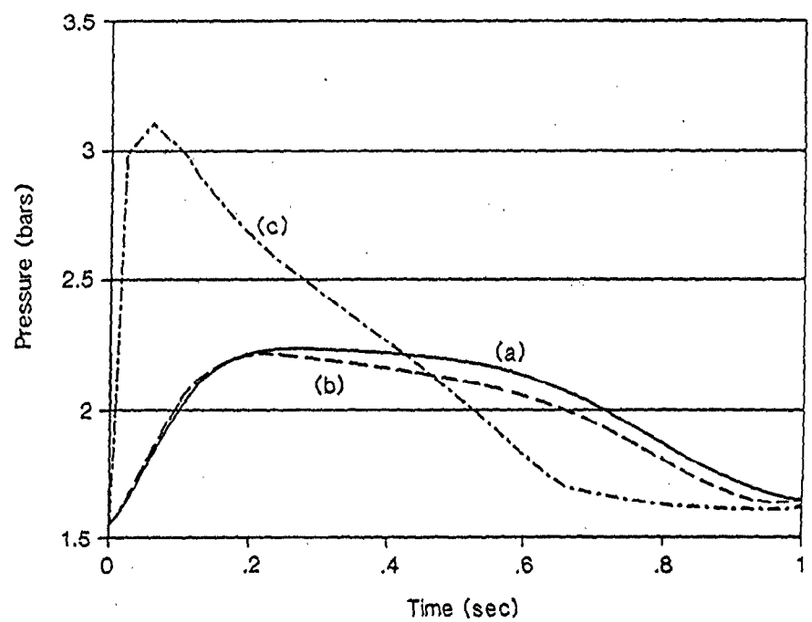

Fig. 12 Pressure rise in the moderator vessel for the three cases of Fig. 11. Curve numbers in both figures match.

The flow velocities at the entrance to pipe segment A are shown in Fig. 11 for the three cases. It can be seen that "backfiring" only occurs when heat input to the pipe is allowed. As expected, a much faster velocity results from the increased heat input, with a clearly visible faster rise in the step function case.

Nevertheless, as can be seen from Fig. 12, where the resulting pressure increase in the moderator vessel is shown, no dangerous situation with respect to the integrity of the moderator vessel will be encountered, even under the assumption of an "instantaneous" rise of the heat input (curve c). From curve a and b it can be seen that the lack of "backfiring" into the moderator vessel in case b results in a lower peak value and a faster decrease of the pressure although the total heat to the moderator vessel input is higher than in case a.

VI CONCLUSIONS

The computational model set up for the D_2-system of the SINQ cold moderator helped us to understand and predict very well the behaviour of the system under normal operating conditions as well as in the incident of a loss of insulating vacuum. It could be shown that the design pressure of the moderator vessel is not reached or exceeded in any situation, even under non-realistic assumptions. The model will be used in future to further refine our understanding of the behaviour and - if required - to study other accident scenarios.

REFERENCES

/1/ F. Atchison, G. Bauer, W. Fischer, K. Skala and H. Spitzer
"The Cold Neutron Moderator for the Continuous Spallation Neutron Source SINQ"
Proc. Int. Workshop on Cold Neutron Sources
Los Alamos, March 5 - 8, 1990

/2/ H. Spitzer, A. Höchli, G.S. Bauer, W. Wagner
"Technical Concept of the liquid D_2-cold Moderator for SINQ"
This conference

/3/ H. Hoffmann
"Natural Convection of a Cold Neutron Source with vaporizing Deuterium at Temperatures of 25 K"
NATO, Advanced Study Institute: Natural Convection, Fundamentals and Applications
July 16 - 27, 1984, Izmir Turkey

ICANS-XI International Collaboration on Advanced Neutron Sources
KEK, Tsukuba, October 22-26, 1990

Technical concept of the liquid D_2-cold moderator for SINQ

H. Spitzer, A. Höchli, G.S. Bauer and W. Wagner
PAUL SCHERRER INSTITUTE
CH-5232 Villigen-PSI, Switzerland

ABSTRACT
At the continuous, high power Spallation Source SINQ design provisions have been made in the D_2O-moderator tank for both, a D_2- and H_2-cold moderator. While the H_2-moderator will be available as a long term option, the D_2-moderator, equipped with a neutron guide system will be a day-one facility to provide the low-energy neutrons for the guide-hall instrumentation. The paper describes details of the the technical concept of the D_2-cold moderator which takes into account boundary conditions, considerations on flux optimization, operational feasiblity and safety.

I INTRODUCTION

The principle design considerations of the D_2-cold moderator for SINQ, balancing the different requirements within the boundary conditions of the SINQ general concept, were outlined at the previous ICANS meeting |1|. Meanwhile, a detailed technical design has been evaluated on the basis of the principle layout. The design is supported and refined by theoretical thermal-hydraulic investigations of the operational features, safety rquirements and failture management which are treated separately |2|. The present contribution concentrates on the technical layout of the moderator tank, the cryogenic system, shielding plug and subsystems for the D_2-handling.

II GENERAL DESIGN OF THE SINQ COLD D_2-MODERATOR

In order to minimize radiation damage of the cryogenic system, it was decided not to place any components of the cold moderator system other than the moderator vessel itself into areas of high radiation fields of fast neutrons. This means that a horizontal insertion port for the cold moderator was foreseen and the heat exchanger of the natural convection system was moved back into a well shielded region. This results in fairly long tubes between the moderator vessel (main heat source) and the heat exchanger (heat sink) and hence requires a large vertical separation of the two to overcome the frictional forces in the tube system by the buoyancy force of the liquid-gas mixture flowing back from the moderator vessel.

Experiments carried out by Hoffmann |3| in conjunction with the development of the second cold moderator at the ILL-reactor |4| showed that such a system could be operated over a large range of heat input. In our case we decided to place the vertical leg partway to the outside of the shielding

block for three reasons:

1. The need for shielding behind the horizontal leg would have blocked space valuable for neutron scattering experiments
2. Placing the heat exchanger in the shielding block automatically provides good mechanical protection
3. The length of the tube and hence the amount of liquid D_2 as well as the frictional forces could be reduced.

This design implies that the horizontal and vertical leg of the cold source cannot be installed as one unit, but have to be put in place separately with a connection made before the shielding plug behind the horizontal leg can be mounted. The vertical cut through the SINQ target station shown in Fig. 1 illustrates the geometric arrangement of horizontal and vertical leg inside the main shielding.

Cryogenic equipment (cold box) and the control system for the source will be placed next to the main shield at a level of 9.5m above ground on top of the neutron guides with a connecting channel to the service areas and to the D_2-storage tank and parts of the gas handling system, located outside the neutron target hall on the roof of the equipment access building.

A block diagram of the various sub-systems is shown in Fig. 2.

III THE COLD MODERATOR SYSTEM

The design of the cold moderator part was governed by the neutronics considerations presented earlier |1|. Its location with regard to the target centre was optimized based on flux calculations as shown in Fig. 3. In order to avoid rethermalization of cold neutrons upon extraction from the moderator, the cold moderator insertion port will be connected to the neutron extraction port resulting in a T-shaped structure inside the moderator tank, Fig. 4.

The mechanical stability of this structure under thermal loads, buoyancy forces and various differential pressure conditions is presently under investigation by computational methods.

Fig. 4 also shows the D_2 moderator vessel in the T-shaped tube structure and the D_2O reflector volume which should compensate most of the losses occuring due to reflector volumes displacement by the cold source insertion tube.

The horizontal cold moderator insert is completely independent of this T-structure. It is shown composed (Fig. 5a) and disassembled to the main sub-units (Fig. 5b) which are:

- a double-walled vacuum jacket with a helium barrier between the outer and the inner tube. The part of the vacuum jacket intruding into the D_2O-tank consists of an outer 2 mm thick $AlMg_3$-tube and an inner zircalloy tube, 3 to 4 mm thick, which is the pressure safety tube and will withstand an internal pressure of 30 bar.
- The source plug, comprising the moderator vessel, the concentric transfer tubes for liquid deuterium (inner tube) and liquid-gas mixture (outer tube) of the heat removal system and a protective support tube which changes to a massive shielding sleeve outside the D_2O tank.
- The shielding and reflector plug comprising a D_2O reflector volume to be located behind the D_2 moderator to minimize losses, its associated D_2O circulation tubes and the cylindrical central shielding plug of the insert.

The moderator vessel itself will be made of 99.5 % pure aluminium, semi-hard with one welding seam around its cylindrical surface at the far end with respect to the target. Material softening by the weld requires the wall thickness of the vessel to be increased from 3 to 5 mm in this region to obtain the desired strength to resist an internal pressure of 4.4 bar. Fig. 6 shows a vertical cut through the moderator vessel and its concentric D_2-flow tubes. Some relevant data are given in table 1.

Material	Al 99.5	
Outer diameter	296/300	mm
Length	354	mm
Wall thickness	3/5	mm
Total volume	22.3	l
Volume filled with liquid D_2	~ 20	l
Total mass of Al	4375	g
Total weight of filled vessel	~ 7.6	kg
Design internal pressure	~ 4.4	bar
Max. operating pressure	2.8	bar
Heat deposition at 1 mA proton current:		
front cover	173	W
cylindrical part	67	W
back cover	15	W
deuterium	1250	W
Total	1505	W
Max. surface heat flow	0.2	W cm^2

Table 1: *Some relevant data for the D_2-vessel of the SINQ cold moderator*

The vertical leg of the cold moderator system is shown in Fig. 7. It will be inserted from the top into the shielding, and connections to the horizontal leg will be made inside the connector box where the two inserts meet. This box will afterwards be sealed to connect the insulating vacua of the two inserts. The second flange on the connector box shown in Figs. 5 and 7 completes the protective helium barrier (see below).

The main components of the vertical insert are:

- the vacuum jacket surrounding all cold parts for thermal insulation
- the D_2/He heat exchanger (plate heat exchanger with interconnectors) to remove the total of 2.65 (Ip = 1.5 mA) kW of heat load from the D_2 (capacity 3 to 3.5 kW).
- the phase separator located beneath the heat exchanger to remove the liquid from the phase mixture coming up from the moderator vessel.
- the concentric D_2-transfer tubes ending in the phase separator in such a way that liquid D_2 is flowing downwards in the inner tube and the liquid-gas mixture comes up in the outer tube to a higher level for phase separation
- the vacuum dome above the heat exchanger where the cold He-transfer tubes and the D_2 gas tube penetrate the cold moderator insulating vacuum space.

IV THE COLD HELIUM SYSTEM

Refrigeration of the D_2 in the heat exchanger is accomplished by cold helium gas from an existing cold box whose capacity is being upgraded to $\sim$ 3 kW. With a total of 2.65 kW to be removed from the D_2-source, this offers some reserve. The helium will be supplied to the heat exchanger at 18 K and 7.5 bar and will return at 25 K, 7 bar. The cold box will operate at constant cooling power; at reduced source power heat will be provided to the system by auxilliary heaters in the helium circuit, controlled by the D_2-pressure in the system. The cold helium transfer line between the cold box and the heat exchanger will be 20 m long each way and will be in a channel inside the target shielding block. Its outer diameter will be 90 - 100 mm.

V SAFETY PROVISIONS

The safety concept of the D_2-cold moderator in the first place pursues two objects, first to ensure secure enclosure of the (tritium contaminated) deuterium, and second to prevent the formation of an inflammable mixture of hydrogen and oxygen. For these purposes, it relies on **passive** safety devices which are:

- multiple containment for D_2
- protective barrier system
- mechanical protection
- remote positioning of storage tank and gas handling devices

These passive devices are complemented by **active** devices which ensure early detection of anormal operation conditions and, in case, suitable automatic actions to prevent accidents and damage of plant components. Among these devices are:

- control of pressures and contaminations in the protective gas barriers
- pressure control and residual gas analysis in the insulating vacuum
- temperature monitoring of the moderator vessel and the surrounding vacuum jacket
- control of the purity of the deuterium before filling and during operation

The containment and barrier system is designed to avoid any possible contact between deuterium and oxygen from the air which could ultimately form an explosive gas mixture. Although the SINQ beam ports are filled with helium which also surrounds the horizontal insert of the cold moderator, it was decided to have a separate additional helium system around the cold part of the D_2 circuit for the following reasons:

- the pressure in the beam-tube gas system is below atmospheric pressure to make sure that in case of a leak the flow always is to the inside to avoid spreading possible radioactive contamination into the atmosphere. By contrast, the pressure in the protective He-barrier of the cold source should be above atmospheric pressure (1.1 bar) to avoid contamination with oxygen in case of a leak to the outer atmosphere

- the cold moderator helium barrier will be continuously monitored for oxygen contamination which suggests having as small a volume as possible
- in case of the need for access to the structural parts of the cold moderator system, the beam port helium system needs not be opened.

The helium gas in the protective barrier will be continuously circulated, carefully monitored for pressure loss and contamination by other gases and refrigerated to remove the heat it picks up from the walls in the region of high neutron flux.
Outside the main shield all system parts containing warm D_2-gas will be surrounded by a N_2-gas barrier rather than helium for the following reasons:

- N_2 is much cheaper than helium
- Helium is used for leak detection on experimental facilities and thus should be present in the smallest possible amounts in the air
- monitoring for deuterium is easier in nitrogen than in helium

The pressure in the N_2 protective barrier will also be kept at 1.1 bar to avoid oxygen-intake in case of a leak.

REFERENCES

1. F. Atchison, W. Bucher, A. Höchli, I. Horwarth and L. Nordström "The D_2 cold-neutron source for SINQ" in "Advanced Neutron Sources 1988", Institute of Physics Conference Series No. 97, D. K. Hyer, ed. Bristol and New York 1989, pp. 473 - 482

2. K. Skala, H. Spitzer, and G.S. Bauer, in these proceedings.

3. H. Hoffmann: "Natural convection of a cold neutron source with vaporizing deuterium at temperatures of 25 K", NATO, Advanced Study Institute: Natural Convention, Fundamentals und Applications, July 16-27, 1984 Izmir Turkey

4. K. Gobrecht, Proc. Int. Workshop on Cold Neutron Sources, Los Alamos NW, USA (March 1990)

Q(E.P.Shabalin): May be, I missed but you did tell nothing about vacuum layer between D_2 and He. Is there evacuated volume outside the vessel?

A(W.Wagner): The entire cold D_2-system, in the horizontal and vertical inlet, is encapsulate by cryo-vacuum.

Q(T.Kawai): Why do you use the phase separator in addition to the heat exchanger?

A(W.Wagner): Because the system is based on isothermal natural circulation, driven by bubbles of D_2-gas in the liquid D_2-back-flow line.

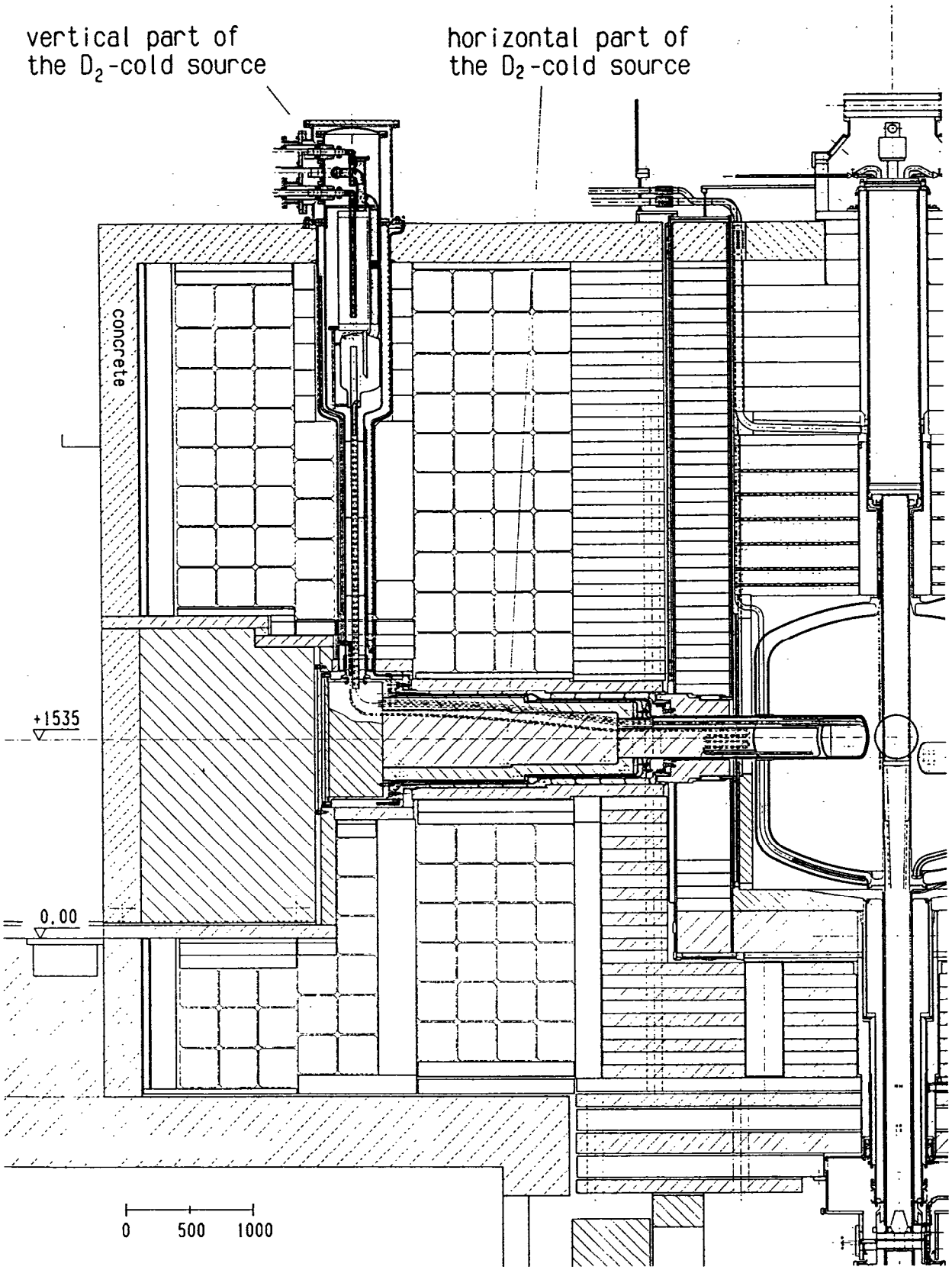

Fig. 1 Section through part of the SINQ target block along the plane of the D_2-cold moderator inserts. For detailed parts designation see Figs. 5 and 7.

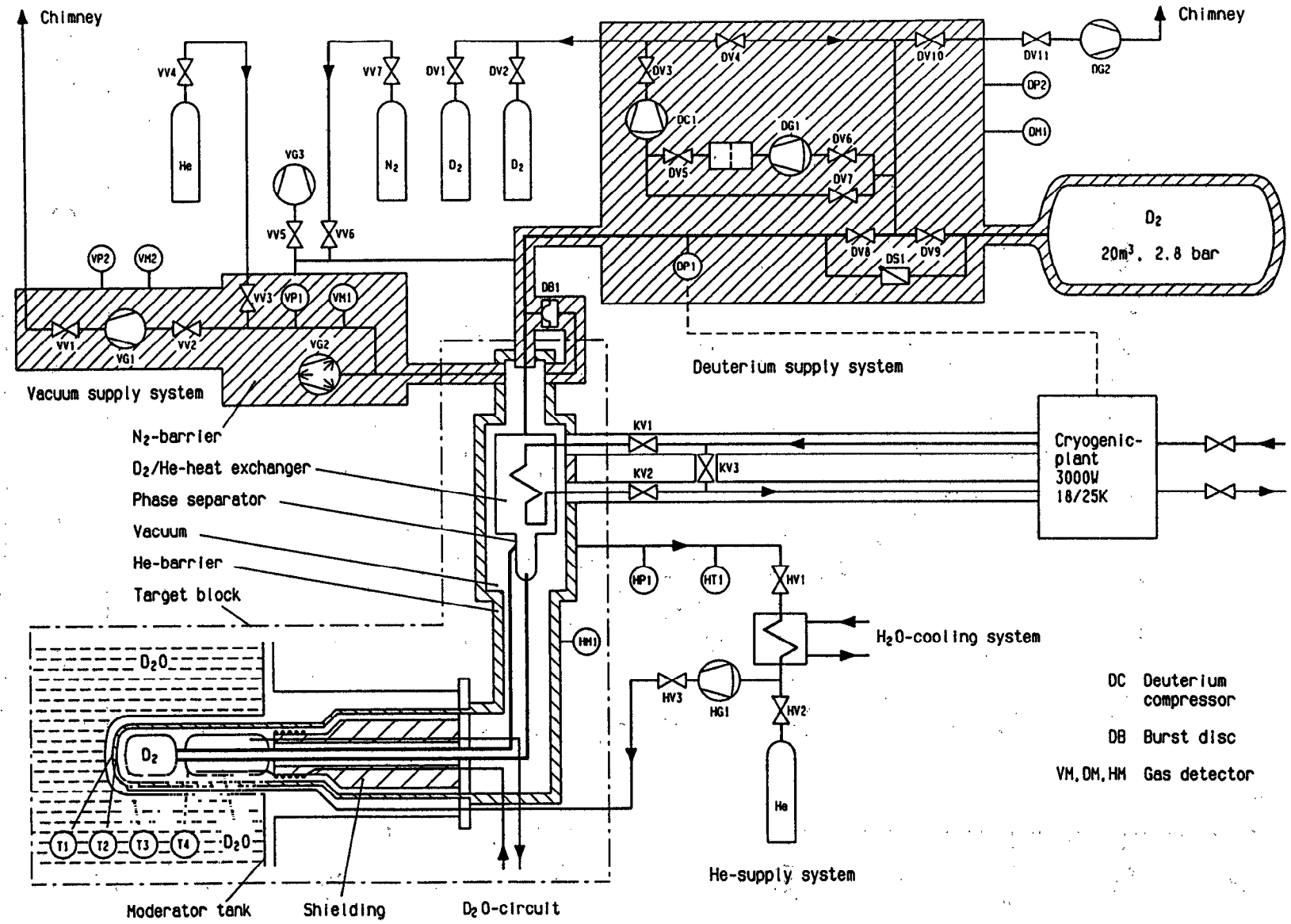

Fig. 2 Simplified diagram of the various subsystems of the D_2-cold moderator for SINQ. Helium is used for the protective barrier of the D_2-system only inside the target block. Outside the target block N_2 is used.

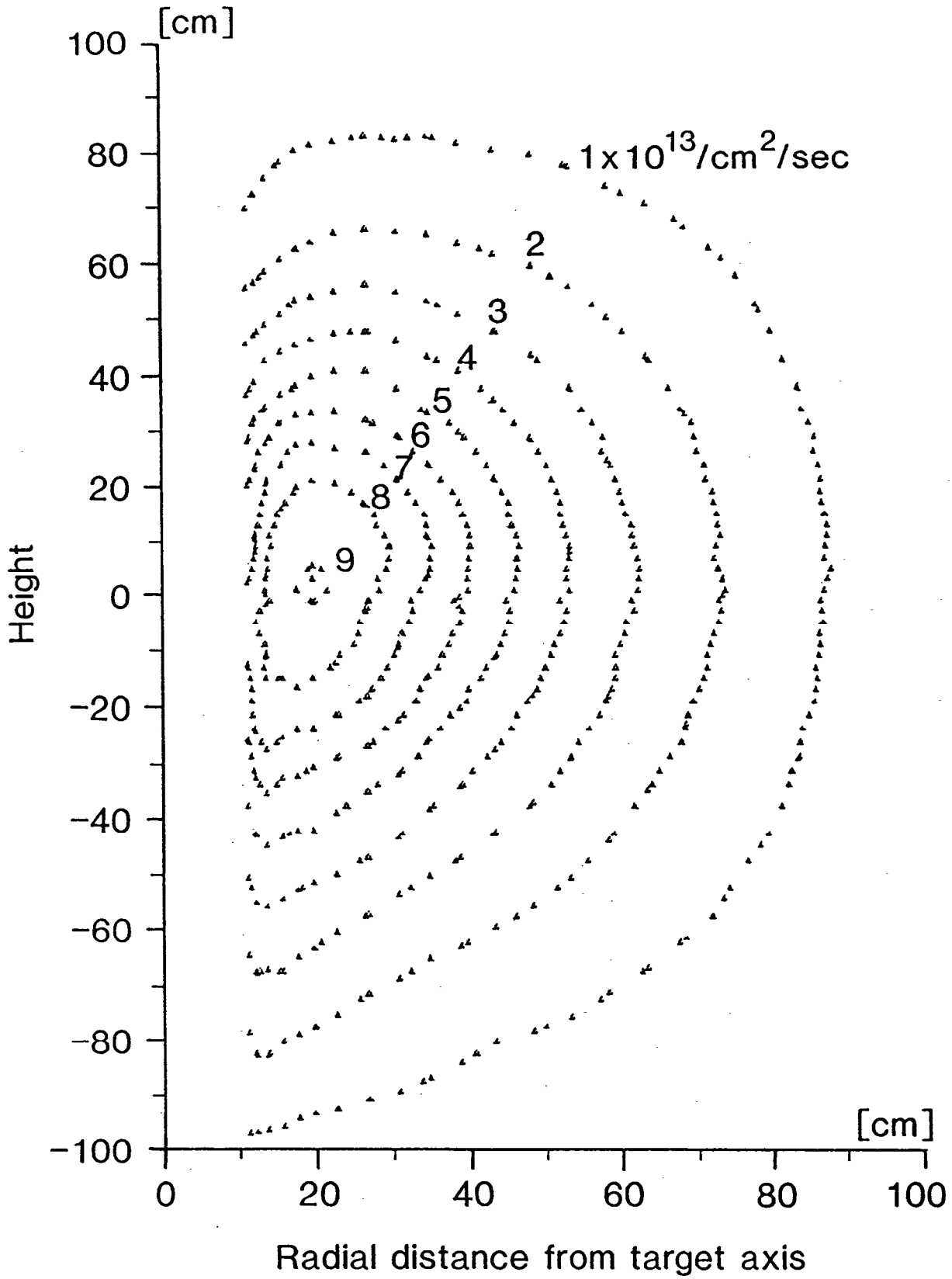

Fig. 3 Undisturbed thermal-neutron flux map in the heavy-water for 1 mA proton current on target.

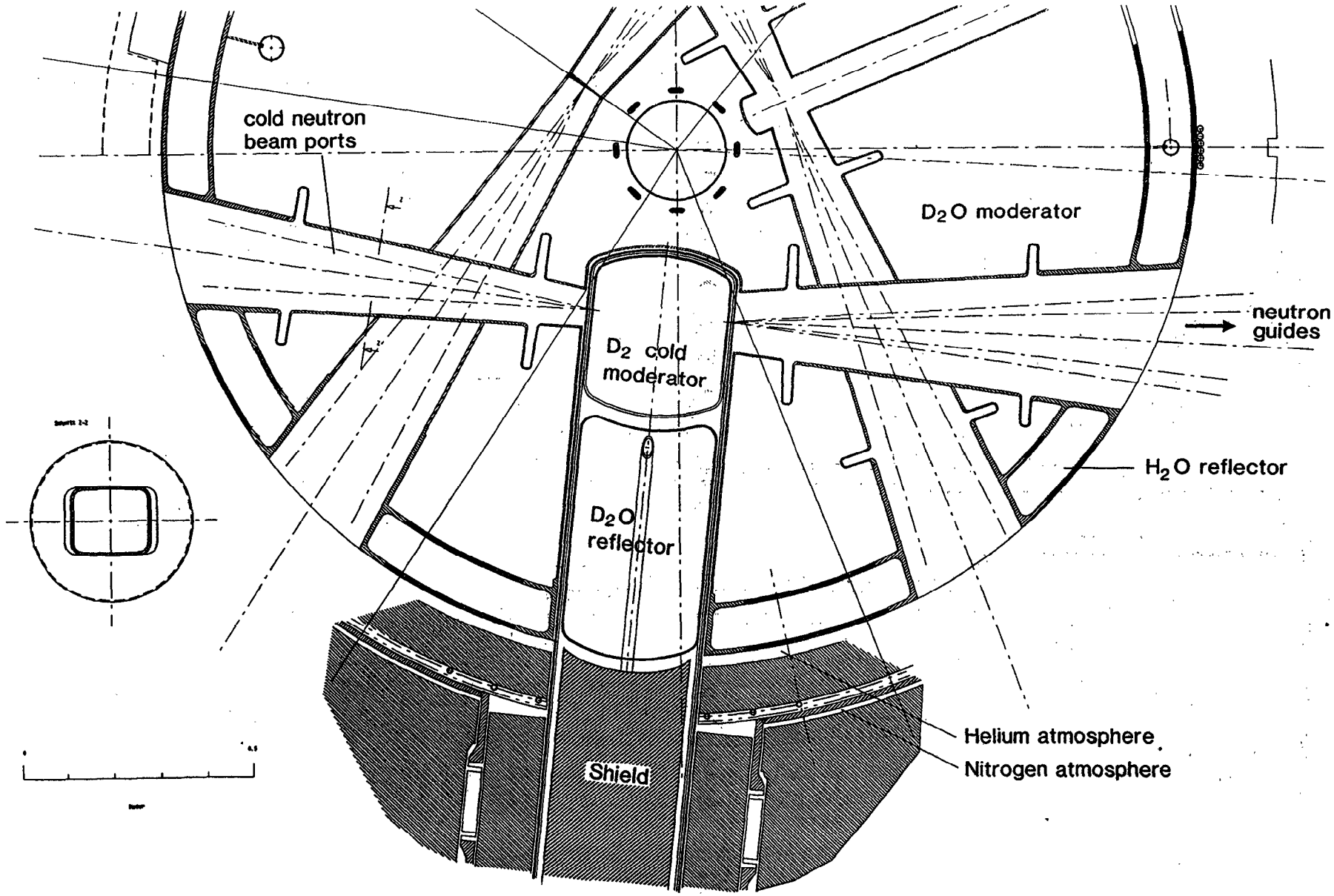

Fig.4 Layout of the SINQ-D_2O-tank with T-shaped structures for cold moderator insertion and neutron extraction, avoiding rethermalising D_2O-layers.

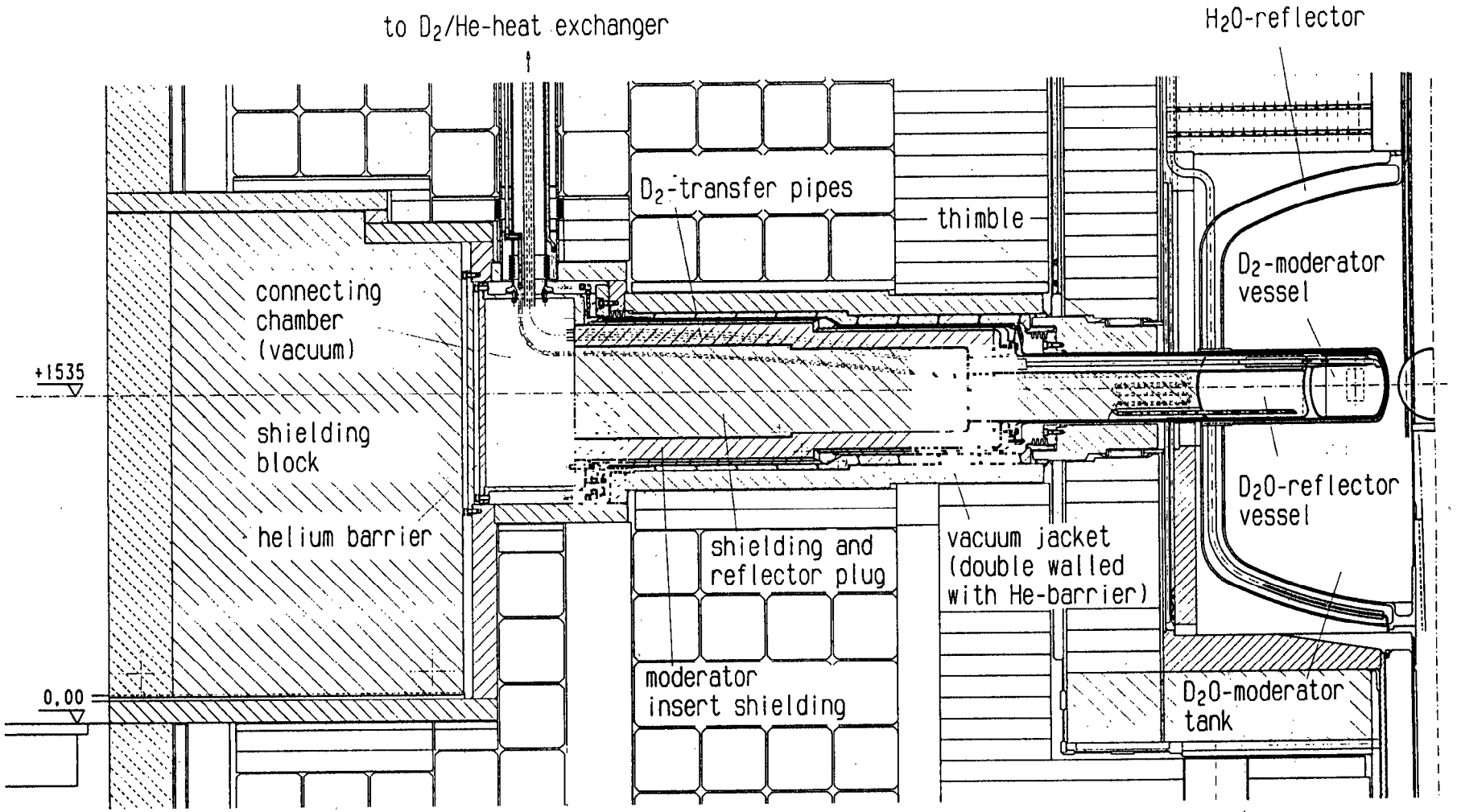

Fig. 5a Vertical section through the horizontal insert of the SINQ cold D_2-source.

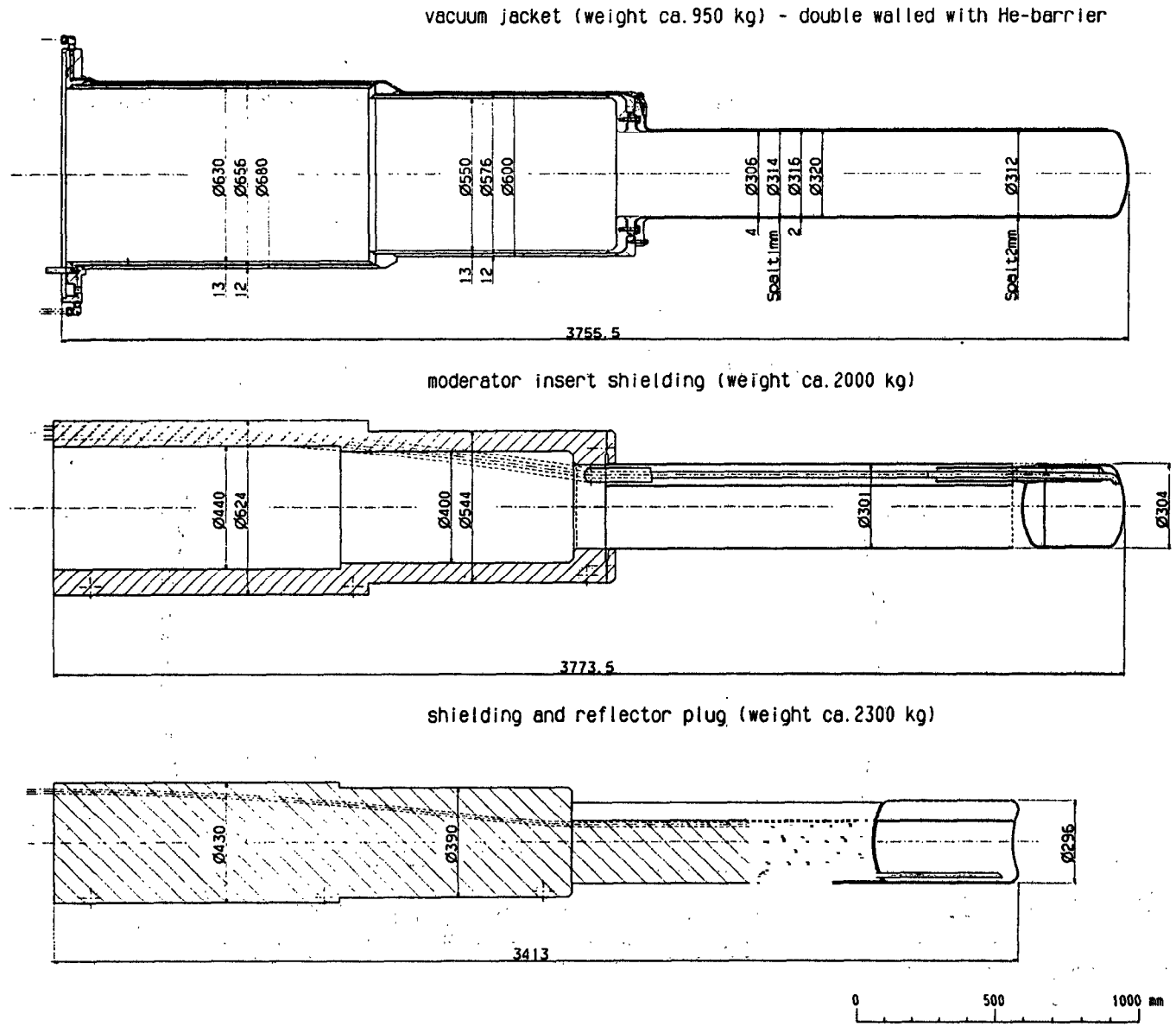

Fig. 5b Vertical section through the parts of the horizontal insert, i.e. the double walled vacuum jacket, source plug with moderator vessel and concentric transfer tube, and shielding and reflector plug.

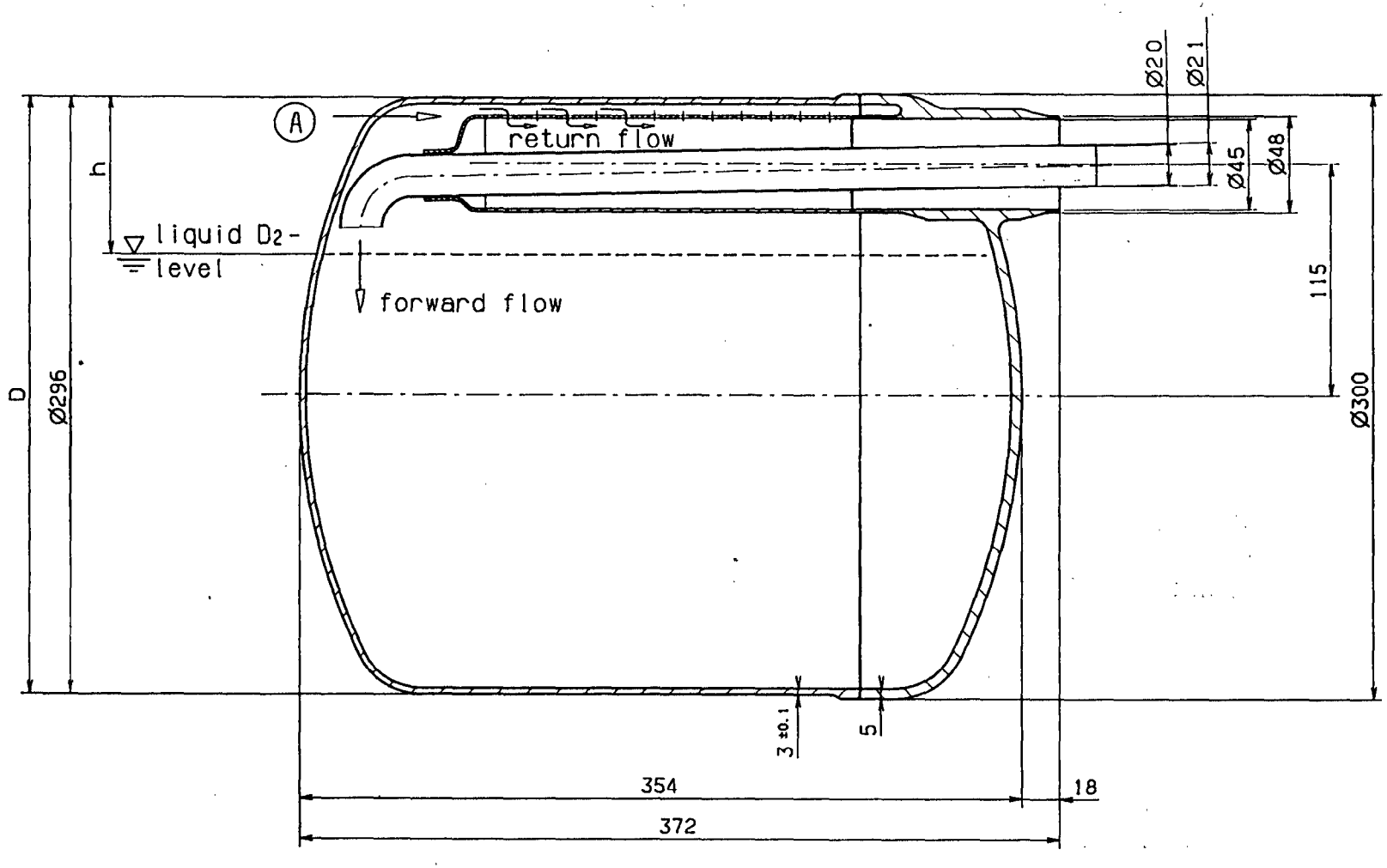

Fig. 6 The D_2-moderator vessel and its concentric flow tubes (vertical section).

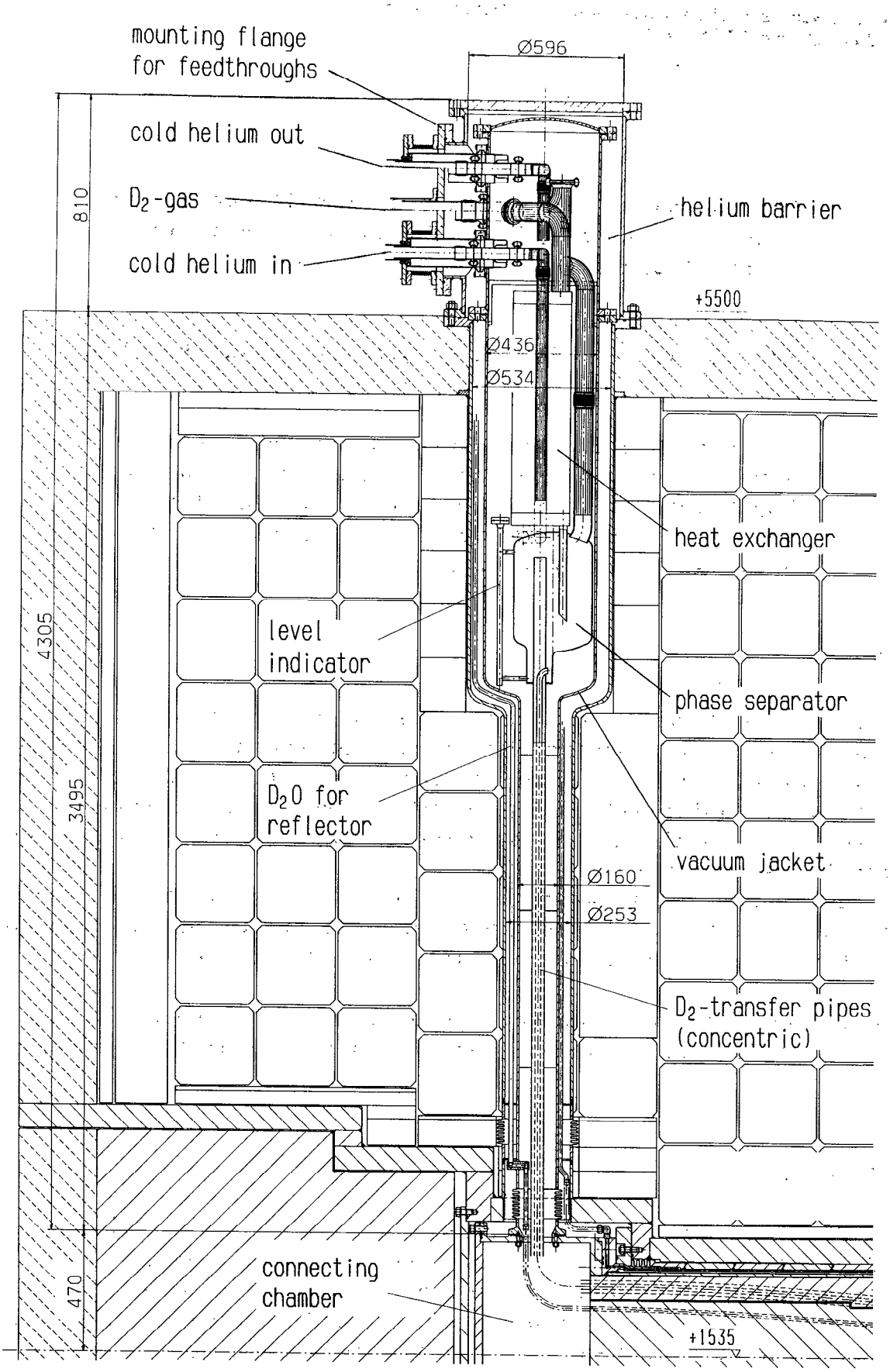

Fig. 7 Vertical section through the vertical insert of the SINQ cold D_2-source (pipe system, phase separator and heat exchanger).

ICANS-XI International Collaboration on Advanced Neutron Sources
KEK, Tsukuba, October 22-26, 1990

Thermodynamic considerations on self-regulating characteristics of a cold neutron source with a closed thermosiphon

*Takeshi Kawai, *Fumimaru Ogino and Masahiko Utsuro*

Research Reactor Institute, Kyoto University, Kumatori-cho, Sennan-gun, Osaka, 590-04, Japan.
*Department of Chemical Engineering, Faculty of Technology, Kyoto University, Yoshidahonmachi, Sakyo-ku, Kyoto 606, Japan.

ABSTRACT

The present report describes that a cold neutron source (CNS) having a closed-thermosiphon cooling loop shows a self-regulating characteristic under thermal disturbances if the effect of the moderator transfer tube is negligible. Due to this property, the liquid level in the moderator cell is kept almost constant under thermal disturbances.

The thermodynamic meaning of the self-regulating property in the idealized closed-thermosiphon and the effect of the moderator transfer tube to the self-regulation are described.

Keywords: cold neutron source; thermosiphon; self-regulation; moderator transfer tube; liquid hydrogen; liquid deuterium.

I. INTRODUCTION

The cold neutron source(CNS) is a facility to increase the cold neutron flux by cooling the moderator where the cold neutrons are extracted. Although there is a wide choice of materials as a cold moderator, liquid hydrogen and liquid deuterium have been used in many research reactors including HFR in ILL[1,2]. The principal design criteria are the safety security of personnel and the reactor, as well as the maximum increase and a stable supply of the cold neutron flux.

Recently, very cold neutrons (VCN) and ultra cold neutrons

(UCN) have been used in the field of fundamental physics. VCN are also extracted from CNS using vertical VCN guide tube, and they are further converted to UCN by using UCN turbin[3]. The superfluid helium-4 UCN source makes use of cold neutrons with the wavelength of about 9 A as the incident neutrons[4]. For this facility, CNS is also available for providing the intense cold neutrons of the wavelength of about 9 A.

From the studies on the safety and the functions of CNS described in the previous paper[5], it became evident that CNS with a closed-thermosiphon cooling loop using liquid hydrogen or liquid deuterium as a cold moderator is one of the best selections in respects of the safety and the function.

Keeping the liquid level stable in a moderator cell and preventing sudden bubbling are the important functions of CNS for supplying the stable and steady cold neutrons. Cryogenic system with a closed-thermosiphon loop is appropriate for this purpose[6]. Figure 1 shows a simplified flow diagram of a cold neutron source with a closed thermosiphon. This is a hydrogen cold system consisting of the condenser, the moderator transfer tube and the moderator cell. Gaseous hydrogen or mixture of hydrogen and deuterium is liquefied in a condenser located in a separated region from the moderator cell, and liquid moderator is transported to the moderator cell through the moderator transfer tube (a two-phase countercurrent flow tube).

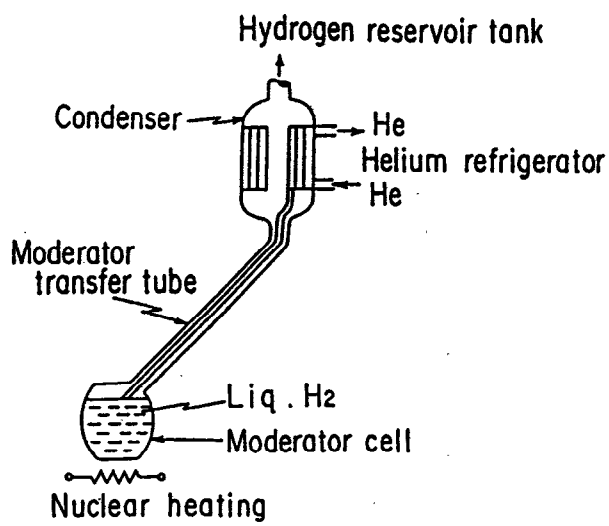

Fig. 1. Schematic diagram of the hydrogen cold system for a closed-thermosiphon.

The moderator transfer tube is required to satisfy the certain conditions for the purpose mentioned above[7].

An alternative cooling system without the transfer tube of liquid moderator is also considered and practically adopted at HFBR CNS in BNL[8]. In this system, the moderator cell itself acts as the heat exchanger with the cold helium gas, and gaseous hydrogen is transported to the cell and liquefied there. A peculiar advantage of this system is that no work is demanded for the mass transfer and thus the cooling capacity liquefying hydrogen vapor evaporated is equal to the heat absorbed in liquid hydrogen. The temperature difference between liquid and vapor is negligible and the heat-exchange efficiency is maximum. We

need not suffer from the problems relating to the moderator transfer tube such as the flooding phenomena.

However, if the heat deposition rate due to nuclear heating in the wall of the moderator cell is larger than the critical value, or the thickness of the chamber wall is great, the maximum temperature in the inner position of the wall becomes higher than the boiling point of the hydrogen. Not only the removal of nuclear heating but the storage of liquid hydrogen become, hence, impossible.

An another disadvantage of this system is that a large temperature difference between the liquid moderator and the refrigerant is required to remove a large quantity of heat generated in the liquid moderator. This brings the difficulty of keeping the liquid hydrogen from solidifying at the time when the heat load decreases suddenly, and further an excessive heat load is brought due to the additional cooling pipes.

CNS with a closed-thermosiphon cooling loop is considered to be more appropriate than that with the moderator cell acting as a heat exchanger for a high power research reactor by the reasons mentiond above.

The hydrogen system of the closed-thermosiphon loop works as a constant volume loop which consists of the reservoir tank and the hydrogen cold system. The cryogenic system consists of a helium refrigerator and the hydrogen system. The boiling point of the moderator such as hydrogen and deuterium is determined by the pressure of the closed system and these quantities are related to each other through the vapor pressure curve. Boiling point rises as a pressure of the system increases. Cooling power of the helium refrigerator increases also with a rise of the temperature of the cooling system.

When the additional thermal load is applied to the hydrogen cold system, for example owing to the reactor power fluctuations, the pressure in the system rises due to the more evaporation of a liquid moderator, and therefore the boiling point rises with it. Since the helium temperature at the outlet of the condenser rises, the liquefaction capacity of the condenser apparently increases with a refrigerating power increase of the refrigerator. Therefore, the effect of the thermal load increase is mostly compensated.

Such a cryogenic system is called here to have a self-regulation to the thermal load fluctuations[9].

We first discuss the thermodynamic meaning of the self-regulation of the idealized closed-thermosiphon.

II. SELF-REGULATING POWER OF THE IDEALIZED CLOSED THERMOSIPHON

The idealized closed-thermosiphon behaves as though the effects of the transfer tube neglected as shown in Fig. 2.

For this case, the mass balance equation for the hydrogen vapour M[gm] can be written as:

$$dM/dt=\{Q-UA(T-T_{He})\}/\Delta H \quad (1)$$

where Q[J/s] is a quantity of nuclear heating and U[W/cm²·K], A[cm²], T_{He}[K], ΔH[J/gm] are the total heat transfer coefficient of the condenser evaluated at the bulk fluid temperature T[K], the area of the cryosurface, the temperature of the helium coolant and the latent heat of evaporation of hydrogen. The first term on the right-hand side represents the quantity evaporated per unit time and the second term stands for the condensing vapour quantity. In addition, it is reasonable to assume that the state equation for an ideal gas holds for a hydrogen vapour. A much simpler analysis follows for a pressure P[atm] of the system assuming a constant T_{He} and a constant volume of the control vessel V[cm³] as:

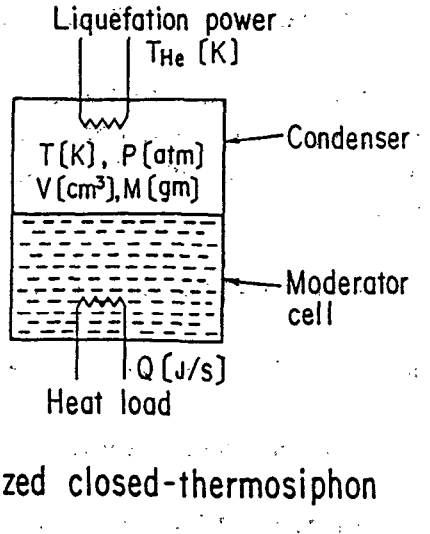

Fig. 2. Diagram of the idealized hydrogen cold system.

$$dP/P=dM/M+dT/T \quad (2)$$

Upon substitution the Clausius-Clapeyron relation

$$dP/dT= (\Delta H\ P)/(RT^2), \quad (3)$$

into Eq. (2), with a gas constant R[J/gm·K], the following results

$$dM/M=\{\Delta H/(RT^2)-1/T\}dT \quad (4)$$

where ΔH is assumed to be constant. If we represent quantities at the steady state with a subscript 0 and consider a small deviation from the steady state, then the following equation (6) can be obtained from Eq. (4) with reasonable assumptions $T\simeq T_o$ and

$$\Delta H/(RT_o^2)>>1/T_o \quad (5)$$

$$M=M_o\{1+\Delta H(T-T_o)/(RT_o^2)\}. \quad (6)$$

From Eq. (1), the mass balance at the steady state $T=T_o$ is given as

$$dM_o/dt=\{Q_o-UA(T_o-T_{He})\}/\Delta H \ . \qquad (7)$$

For the infinitesimal change of the bulk temperature, the following expression can be obtained by subtracting the respective terms in Eq.(7) from the corresponding terms of Eq.(1);

$$d(M-M_o)/dt=\{(Q-Q_o)-UA(T-T_o)\}/\Delta H. \qquad (8)$$

From Eq. (6), it also follows that

$$T-T_o=(M-M_o)RT_o^2/(M_o\Delta H). \qquad (9)$$

From substituting Eq. (9) into Eq. (8), with $m=M-M_o$ and $q=Q-Q_o$, it follows for the dynamic expression of the idealized closed-thermosiphon that

$$\Delta H \ dm/dt+\eta \ m=q \ , \qquad (10)$$

where

$$\eta=UART_o^2/(M_o\Delta H)$$

represents the liquefaction power of the condenser.

Equation (10) can be used as a starting point for the discussion about the self-regulating characteristic as a cold neutron source.

If we suppose that the stepwise heat load $q_1(=Q_1-Q_o)$ is applied at $t=0$, a change of the vapour quantity is given using (10) with $\tau=\Delta H/\eta$ as

$$m=(q_1\tau/\Delta H)(1-\exp(-t/\tau)). \qquad (11)$$

We can easily find the behavior of m for $t\to\infty$ from Eq. (11), i.e., an another equilibrium state resulting in $m=q_1/\eta$. The greater the value of $(1/\tau)$ which relates to the liquefaction power of the condenser, the more rapidly the new equilibrium state is established. Therefore, τ means the relaxation time and we call here $1/\tau$ the self-regulating power of the idealized closed-thermosiphon.

If we introduce a sinusoidal heat load $q=q^*\sin \omega t$, we obtain the solution of Eq. (10) as

$$m=(q^*\tau/\Delta H)\{\sin \omega t-\omega\tau\cos \omega t+\omega\tau\exp(-t/\tau)\}/\{1+(\tau\omega)^2\}. \qquad (12)$$

The neglect of the third term leads to the solution after the transient state,

$$m=\{(q^*\tau/\Delta H)/(1+(\omega\tau)^2)^{1/2}\}\sin\{\omega\tau-\tan^{-1}(\omega\tau)\}. \quad (13)$$

It can be seen from Eq. (13) that the phase lag of the output relative to the input approaches to $\pi/2$ for $\omega \to \infty$. When $1/\tau$ is large, that is, the liquefaction power of the condenser η is large, Eq. (13) is approximated by

$$m \simeq (q^*\tau/\Delta H)\sin \omega t. \quad (14)$$

This indicates that the cryosystem follows the change of the heat load without a significant phase lag if the cryosystem fulfills the condition required by Eq. (10). Furthermore, if $\eta >> q^*$, i.e., the liquefaction power of the condenser is sufficiently larger than the heat load, the change of the liquid quantity due to a heat load change is small. This means that the liquid level in the moderator cell is almost stable against the disturbances of the heat load applied to the cryosystem.

It is concluded that the cryosystem has a self-regulating characteristic as a cold neutron source if the moderator transfer tube fulfills certain conditions necessary for holding Eq. (10) in which the effect of the moderator transfer tube is neglected and further the liquefaction power is sufficiently larger than the heat load applied to the system.

III. EFFECTS OF A MASS TRANSFER IN THE MODERATOR TRANSFER TUBE WITH A CONSTANT FLOW RESISTANCE

When the effects of the mass transfer in the moderator transfer tube is negligible, the time lag due to the mass transfer is also negligible and the cooling loop behaves as if there were not the moderator transfer tube. The smaller the diameter or the longer the length of the moderator transfer tube is, the more steeply the flow resistance becomes large due to the pressure drop increase. The flow resistance brings about the time lag to the liquefaction power increase of the condenser owing to the pressure rise of the cooling system and the behaviour of the cooling system deviates from the ideal one described by the equation (10).

We assume that the cooling system became a steady state. In this case, the steady flow of the hydrogen vapor from the moderator cell to the condenser through the moderator transfer tube is established under the heat load of Q[W]. If we express the values at the moderator cell and the condenser by the subscripts 1 and 2 respectively, and the flow resistance by $r[cm^{-1}\cdot s^{-1}]$, the flow rate $W_f[g_m/s]$ of the hydrogen vapor can be expressed in the form

$$W_f=(P_1-P_2)/r \quad (15)$$

where P[dyne/cm^2] is the pressure of the system. The mass of the hydrogen vapor is given by equations

$$dM_1/dt=(Q/\Delta H)-W_f \tag{16}$$

$$dM_2/dt=W_f-UA(T_2-T_{He})/\Delta H \tag{17}$$

where U[W/cm^2·K] is an overall heat transfer coefficient, A[cm2] being a heat transfer area, and T_{He} the refrigerant temperature. The 2nd term in the right hand side of the equation (17) is writtten by

$$UA(T_2-T_{He})/\Delta H=(UART_{2o}^2/(M_{2o}\Delta H^2))M_2+\{UA(T_{2o}-T_{He})/\Delta H-UART_{2o}^2/\Delta H^2\}$$

$$=\eta M_2+\alpha_c \tag{18}$$

where the subscript 0 represents the value in a stationary state and the constant value α_c is the 2nd term of the right hand side. It follows by substituting the equation (18) into the equation (17) that

$$dM_2/dt=W_f-\eta M_2-\alpha_c \tag{19}$$

The following equation refering to the quantities $m=M-M_o$, $q=Q-Q_o$ and $w_f=W_f-W_{fo}$ is obtained by rearranging terms from equations (15), (16), (19)

$$dm_1/dt=(q/\Delta H)-(K_1m_1-K_2m_2)/r \tag{20}$$

$$dm_2/dt=(K_1m_1-K_2m_2)/r-\eta m_2 \tag{21}$$

where K is the conversion factor from the pressure to the hydrogen mass, being now assumed to be constant. If we eliminate m_2 from the eq. (20) and m_1 from the eq. (21), expressions refering to respective quantities at the moderator cell and the condenser are obtained,

$$d^2m_1/dt^2+2h(dm_1/dt)+k^2m_1=(1/\Delta H)(dq/dt)+(L_1/\Delta H)q \tag{22}$$

$$d^2m_2/dt^2+2h(dm_2/dt)+k^2m_2=(L_2/\Delta H)q \tag{23}$$

where,

$$2h=(K_1+K_2)/r+\eta,\ k^2=K_1\eta/r,\ L_1=K_2/r+\eta,\ L_2=K_1/r \tag{24}$$

For simplicity, we assume that the heat load changes sinusoidally in the following way

$$q=q^{o}\sin\omega t \tag{25}$$

In this case, it is easy to obtain the particular solutions m_1', m_2' for equations (22), (23), then solutions are

$$m_1'=(q_1/\sqrt{(k^2-\omega^2)^2+4h^2\omega^2})\ \sin\{\omega t+\tan^{-1}(\omega/L_1)-\tan^{-1}(2h\omega/(k^2-\omega^2))\} \tag{26}$$

$$m_2'=(q_2/\sqrt{(k^2-\omega^2)^2+4h^2\omega^2})\ \sin\{\omega t-\tan^{-1}(2h\omega/(k^2-\omega^2))\} \tag{27}$$

where

$$q_1=(q^0/\Delta H)\sqrt{L_1{}^2+\omega^2}\ ,\quad q_2=(q^0/\Delta H)L_2 \tag{28}$$

On the other hand, the general solution of the equation (22) can be expressed in three different forms according to the conditions imposed to the constant factors as follows:

(i)when $h^2-k^2<0$, the general solution m_1'' is obtained by setting $h^2-k^2=-\zeta^2$

$$m_1''=\exp(-ht)\{C_1\cos\zeta t+C_2\sin\zeta t\} \tag{29}$$

where C1, C2 are arbitrary constants determined from initial conditions. This solution exhibits the damped oscillation.
(ii)when $h^2-k^2>0$, the solution is written in the form using $\gamma^2=h^2-k^2$

$$m_1''=C_1\ \exp\{(\gamma-h)t\}+C_2\ \exp\{-(\gamma+h)t\} \tag{30}$$

This solution tends to zero when $t\to\infty$.
(iii)when $h^2-k^2=0$, the solution is

$$m_1''=\exp(-ht)\{C_1+C_2t\} \tag{31}$$

The general solution m_2'' for the equation (23) is written like m_1''.

The response of the hydrogen mass at the moderator cell and the condenser to the sinusoidal heat load applied to the system can be expressed by the particular solutions (26), (27) exclusive of the transient period. The following becomes clear from these solutions:
(i)When the variational frequency ω of the heat load is equal to k, the quantities of the hydrogen vapor at the moderator cell and the condenser approach their maximum value, that is, the resonance phenomenon appears. In this case, the phase lag at the condenser is $\pi/2$ and larger by $\tan^{-1}\{(\sqrt{K_1\eta/r})/(K_2/r+\eta)\}$ in magnitude than that at the moderator cell. (ii)At lower value of the flow resistance in the moderator transfer tube and $\omega<k$, then

the maximum quantity of hydrogen vapor becomes small and the phase lag at the condenser is approximately $\tan^{-1}\{(K_1+K_2)\omega/(K_1\eta)\}$ and nearly equal to that at the moderator cell. Thus, the system shows characteritics like the case in which the effects of the moderator transfer tube is negligible. (iii)The vapor quantities and phases are generally different between the moderator cell and the condenser. Therefore, the self-regulating characteristic disappears when the effect of the mass transfer through the moderator transfer tube is not negligible.

IV. CONCLUSION

We discussed about the thermodynamic meaning of the self-regulating power of the closed-thermosiphon type CNS when the effect of the mass transfer through the moderator transfer tube is negligible.

It is concluded that the cryosystem with a closed thermosiphon has a self-regulating characteristic as a cold neutron source if the effect of the moderator transfer tube is negligible and the liquefaction power of the condenser is sufficiently larger than the heat load applied to the cryosystem.

The self-regulating characteristics disappear when the flow resistance through the moderator transfer tube is large, because a resonance phenomenon and a large phase difference between the hydrogen vapor quantities of the moderator cell and of the condenser occur in this case.

V. ACKNOWLEDGEMENT

The authors wish to acknowledge to Prof. S. Okamoto for fruitful discussions.

References

1. P. Ageron, Proc. Conf. "Neutron Scattering in the Nineties", Julich 14-18 Jan.,1985, IAEA CN 46/016, p135.
2. C. Doose et al., Cryogenics 11(1971)107.
3. P. Ageron and W. Mampe, Proc. Workshop on The Investigation of Fundamental Interactions with Cold Neutrons, ed. G. L. Green (1985), NBS Spec. Pub. 711(1986)p.16.
4. R. Golub et al., Phys. Lett. A62(1977)337.
5. T. Kawai et al., Nucl. Instrum. Methods A276(1989)408.
6. T. Kawai et al., Nucl. Instrum. Methods A285(1989)520.
7. T. Kawai et al., Int. Workshop on Cold Neutron Source, Los Alamos, March 5-8, 1990, to be published.
8. A. Kevey, BNL Rep. 21017(1976).
9. T. Kawai et al., Cryogenic Eng. 15(1980)339, in Japanese.

Q(G.S.Bauer): Can you give an estimate for the minimum cross section of the transfer lines per unit length and unit heat input required to allow stable operation?

A(T.Kawai): It's very difficult to answer to this question correctly and practically. We can only suggest from the following points of view, that is, flooding constraints, pressure drops and flow patterns in the transfer pipe. However, this is calculated result, not experimental one, and further bubbling phenomena is not included.

ICANS-XI International Collaboration on Advanced Neutron Sources
KEK, Tsukuba, October 22-26, 1990

PULSED AND QUASISTATIONARY NEUTRON SOURCES BASED ON PROTON BEAMS OF MOSCOW MESON FACTORY

M.I.Grachev, M.V.Kazarnovsky, V.V.Khmelshikov, N.A.Khryastov, N.V.Kolmychkov, V.M.Lobashev, V.A.Matveev, M.N.Ospanov, V.N.Sazanov, S.F.Sidorkin, Yu.Ya.Stavissky, V.I.Trushkin, M.T.Vorontsov
Institute for Nuclear Research, USSR 60-th October Anniversary Prospect 7A, 117312 Moscow

The authors describe an assembly of neutron sources for physical research based on proton beams of the Moscow meson factory. The expected neutron intensity in the 4π solid angle in the regime of the resonance selector is $3*10^{16}$ n/s (25 ns, 400 Hz) while the peak density of the thermal neutron flux on the illuminating surface of the moderator is $\simeq 5*10^{15}$ $n*cm^{-2}*s^{-1}$ and the pulse duration is $\simeq$ 50 μs.

The Meson fasility of the Institute for Nuclear Research of the Soviet Academy of Sciences, which is under construction in Troitsk, is the high current accelerator of protons and H^- ions for energies of 0.6 GeV at the current of 0.5-1.0 mA. Intensive beams of protons, also including polarised protons, beams of π, μ - mesons and neutrinos resulted from the proton interactions with the matter of meson targets and beam stops give the possibility to develop the research in various fields of physics, from fundamental problems of matter structure /1/ to the study of radiation damage of materials /2,3/.

Intermediate energy protons allow intensive neutron fluxes to be obtained. Really, a proton with the energy of 0.6 GeV interacting with heavy nuclei [tungsten, lead] results in the release of 10-12 neutrons, more than 90% of which is "evaporated" neutrons with the energies of 2-3 MeV. In the case of ^{238}U target the number of secondary neutrons is about 20. Approximately the half of these neutrons are fission ones.

With proton beams available now average neutron fluxes are lower than those in experimental reactors. However, the possibility to change in the wide range the time structure of the proton beam and, correspondingly, the time structure of the neutron flux leads to unique experimental possibilities /4/.

The shaping of the short pulses of intermediate energy protons is based on the use of the stripping injection of H^- ions into the storage rings. The stripping injection proposed by Alvarez /5/ and carried out by Budker with co-workers /6/ gives the possibility to store in circular magnet assemblies the high circular currents of protons. One-turn extraction of protons from the storage ring of Moscow meson factory (Fig. 1) onto the external target gives the possibility to obtain the neutron pulses with the duration of 5-300 ns and the neutron intensity of up to $6*10^{16}$ n/s in the 4π solid angle.

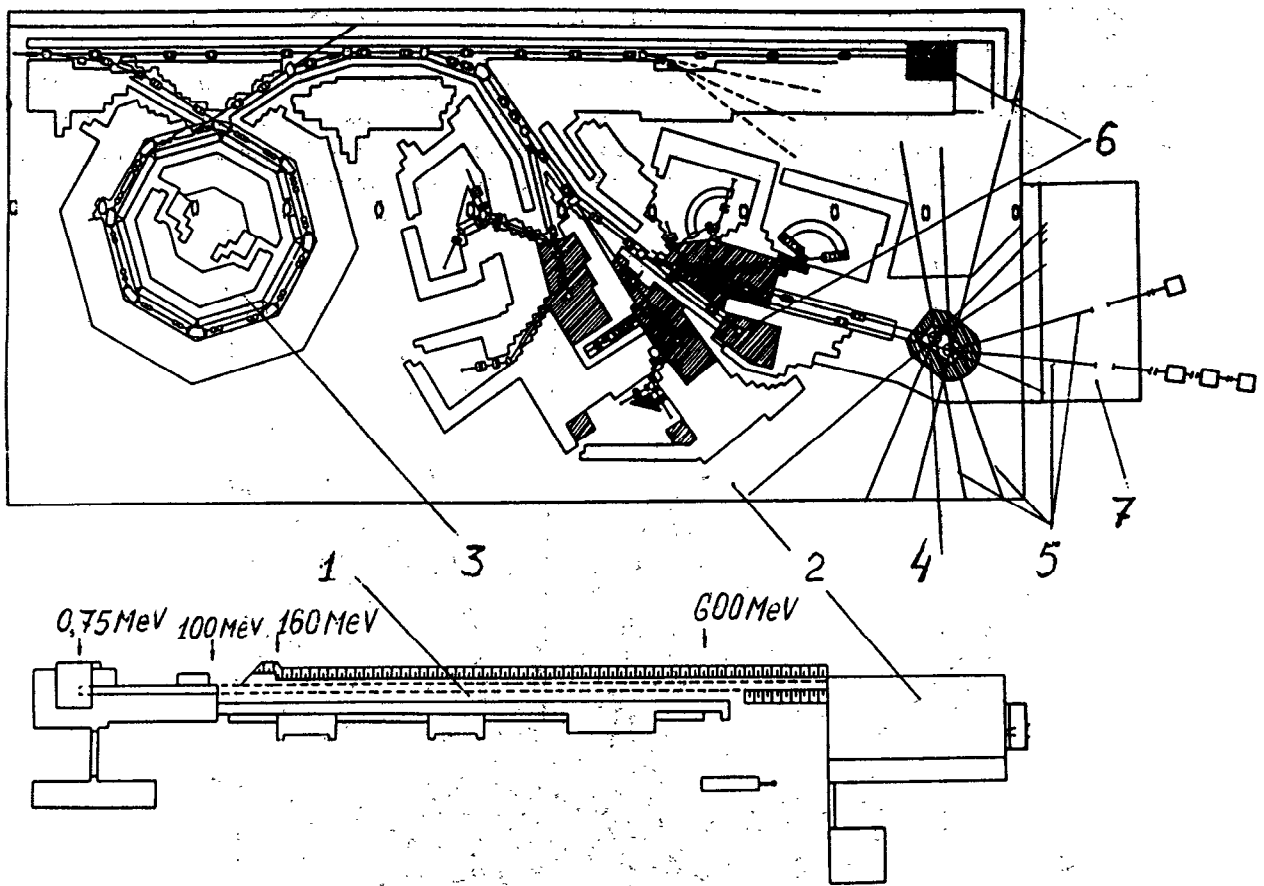

Fig.1. Moscow meson factory; 1-linear proton accelerator: 2-experimental hall; 3-proton storage ring; 4-assembly of neutron sources; 5-neutron guides; 6-beam stops; 7-neutron laboratory.

On the basis of the bunched proton beam the pulsed neutron fluxes of thermal and cold neutrons for researches on condensed matter physics as well as the fluxes of resonance neutrons may be obtained. Spectrometers of resonance neutrons based on the pulsed neutron source of Moscow meson factory will give a possibility to carry out research on the neutron nuclear physics, to study in details the partial processes of the neutron interactions with nuclei in isolated resonances and in the field of the overlapping levels.

The pulsed character of the primary neutron flux, when the neutron release between pulses is small [this release for ^{238}U ~ 1%, for lead ~0.1%, and for targets of a medium atomic weights, for example molibdenum targets, ~10^{-5}% /4/], gives the possibility to obtain in good moderators (D_2O, Be, C), if the time selection of events is used, the quasistationary fluxes of thermal and cold neutrons with the small additions of over-thermal and fast neutrons (time thermal "column"). Time selection of the background allows such experiments as the study of neutron-neutron scattering and the search of neutron-antineutron oscillations to be implemented /7/.

The assembly of neutron sources is constructed on the basis of two proton beams, which can be used simultaneously. The first one is the proton beam from the accelerator with the average current of up to 1 mA. The time structure of the beam is the sequence of macropulses with the duration ~100 μs. The repetition rate is up

to 100 Hz. This beam hits onto the neutron target of the quasistationary source of thermal and cold neutrons (Figs. 2, 3, 5). The second beam bunched in the storage ring with the stripper injection and the one-turn extraction and having the form of the pulse sequence with the duration of 5 - 300 ns and the repetition rate of up to 400 Hz at the average current of up to 500 μA hits at the neutron source (Figs. 2, 3, 6). In the assembly of neutron

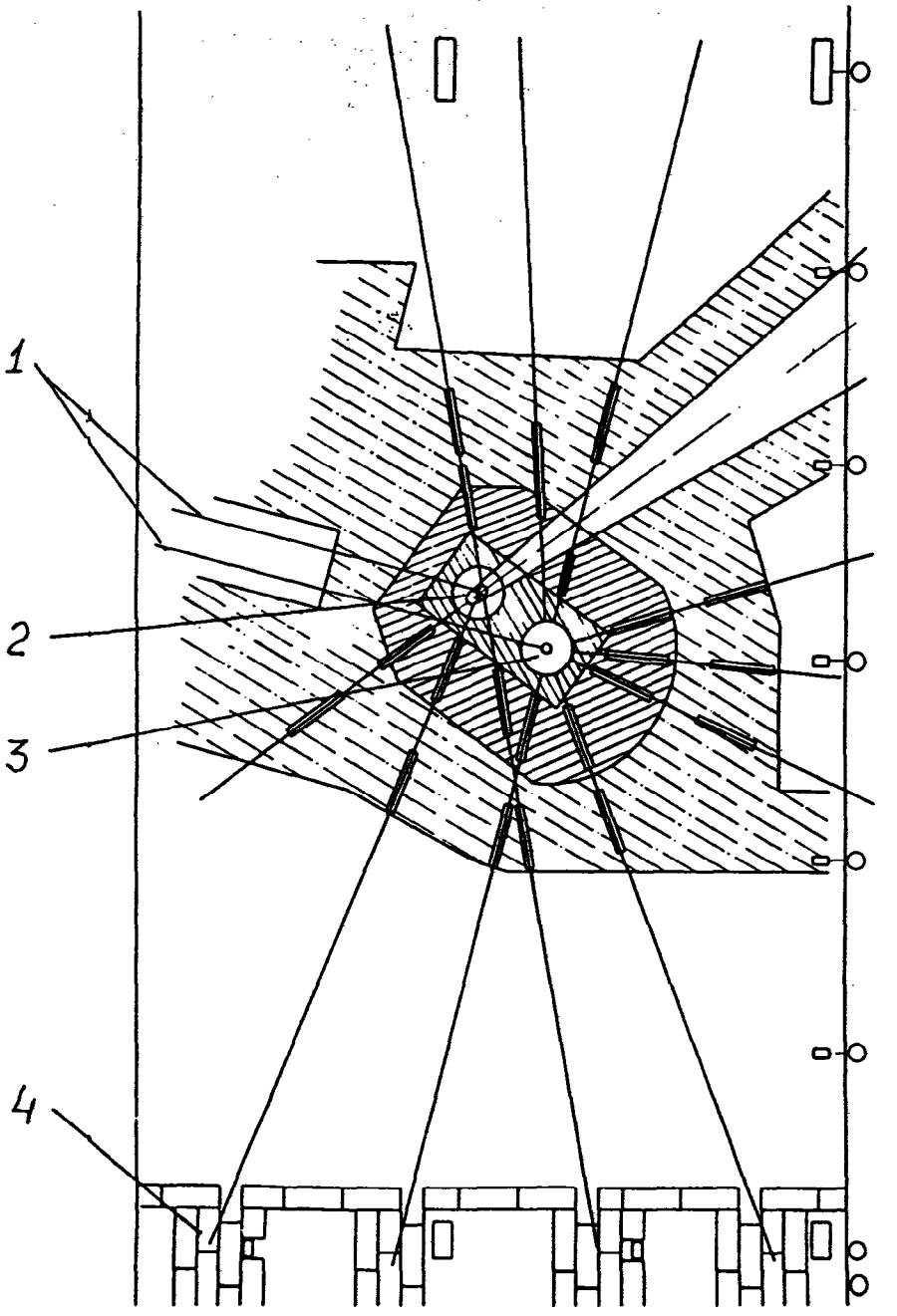

Fig.2. Assembly of neutron sources: 1-proton beams; 2-quasistationary source of thermal and cold neutron; 3-pulsed neutron source; 4-neutron beam stop.

sources there are also the proton beam stops with vertical canals to carry out experiments on radiation physics /2, 3, 9/ and to obtain neutron deficient radionuclides. The beam dumps operation is defined mainly by the programme of experiments on meson beams.

The principal construction scheme of the neutron sources and

beam stops consists of the three main parts: 1) tank with the vacuum bend, 2) ampoule with water-cooled target, 3) remote-controlled vacuum seal. By means of the vacuum bend the ampoule with the target [beam stop] is placed into the proton beam. The "first wall" dividing the vacuum set and coolant is the ampule wall made of the aluminium alloy. Vacuum seal is in the field of low neutron fluxes and made of the rubber. Such arrangement allows rapid change of target devices to be carried out. Remote-controlled vacuum seal consisting of two coaxial bellows the space between which is filled by the gas under pressure, allows the disassembly of the whole source to be carried out. If such need arises the placing of the beam pichups, scrapers, additional windows is also possible. The main dimensions of the target ampoules and beam stops is unified. So, the construction scheme is rather flexible, interchangeable and allows the further development.

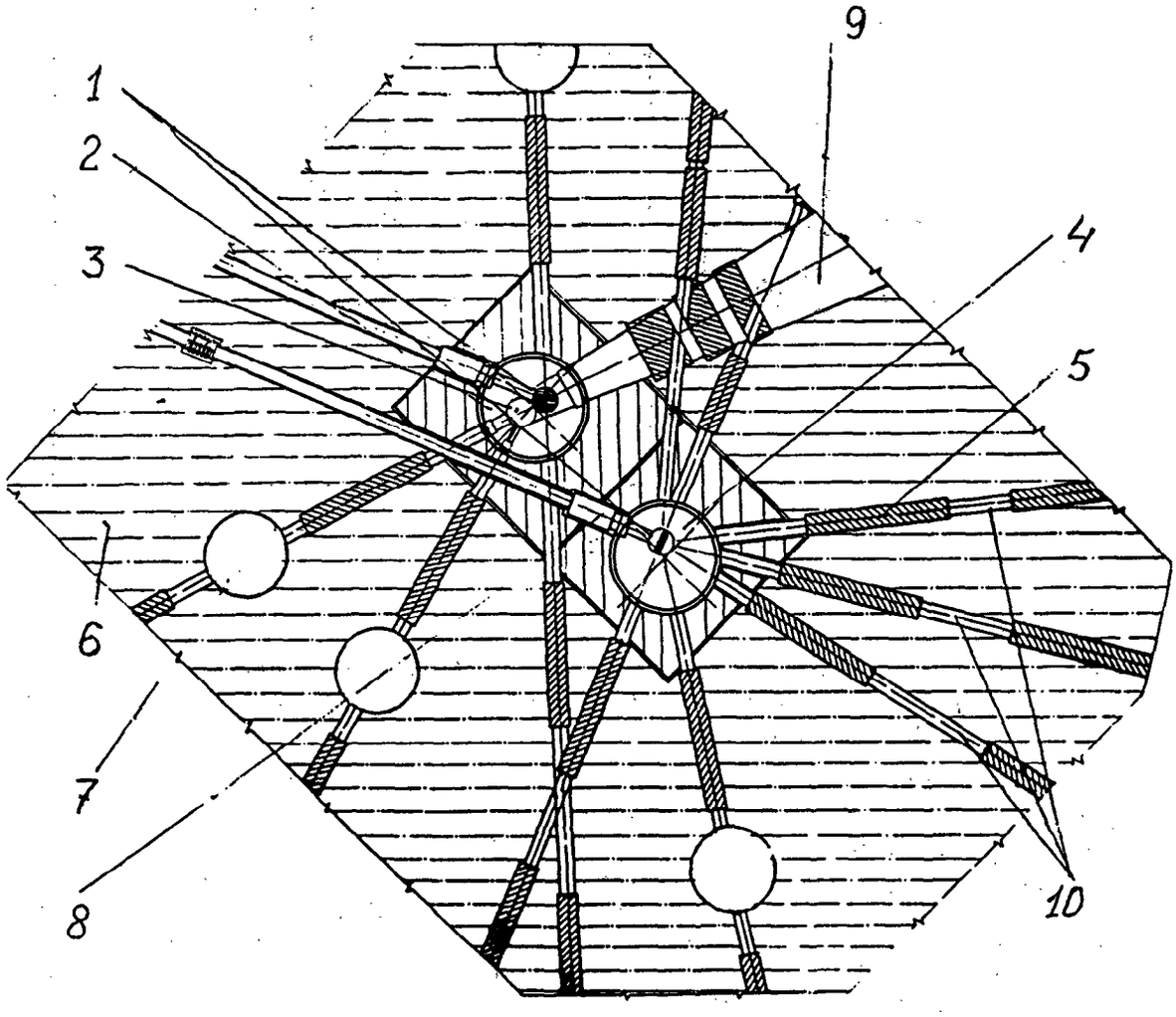

Fig.3. Assembly of neutron sources, central part: 1-neutron targets; 2-heavy water tank; 3-liquid deiterium moderator; 4-vacuum tank; 5-shut-off gate; 6-heavy concrete; 7-vertical wells of the diameter 1 m; 8-remote-controlled vacuum seal; 9-wide apperture canal; 10-canals of resonance neutrons.

Both sources are in the cylindrical boxes of the radiation protection made of steel and concrete and are looked out through the set of the canals with the shutter of the "guillotine" type.

For the placing of additional experimental equipment neutron canals have the vertical wells of 1 m diameter with the protecting valves /10/ on the distance of 3.5 - 4.0 m from the source.

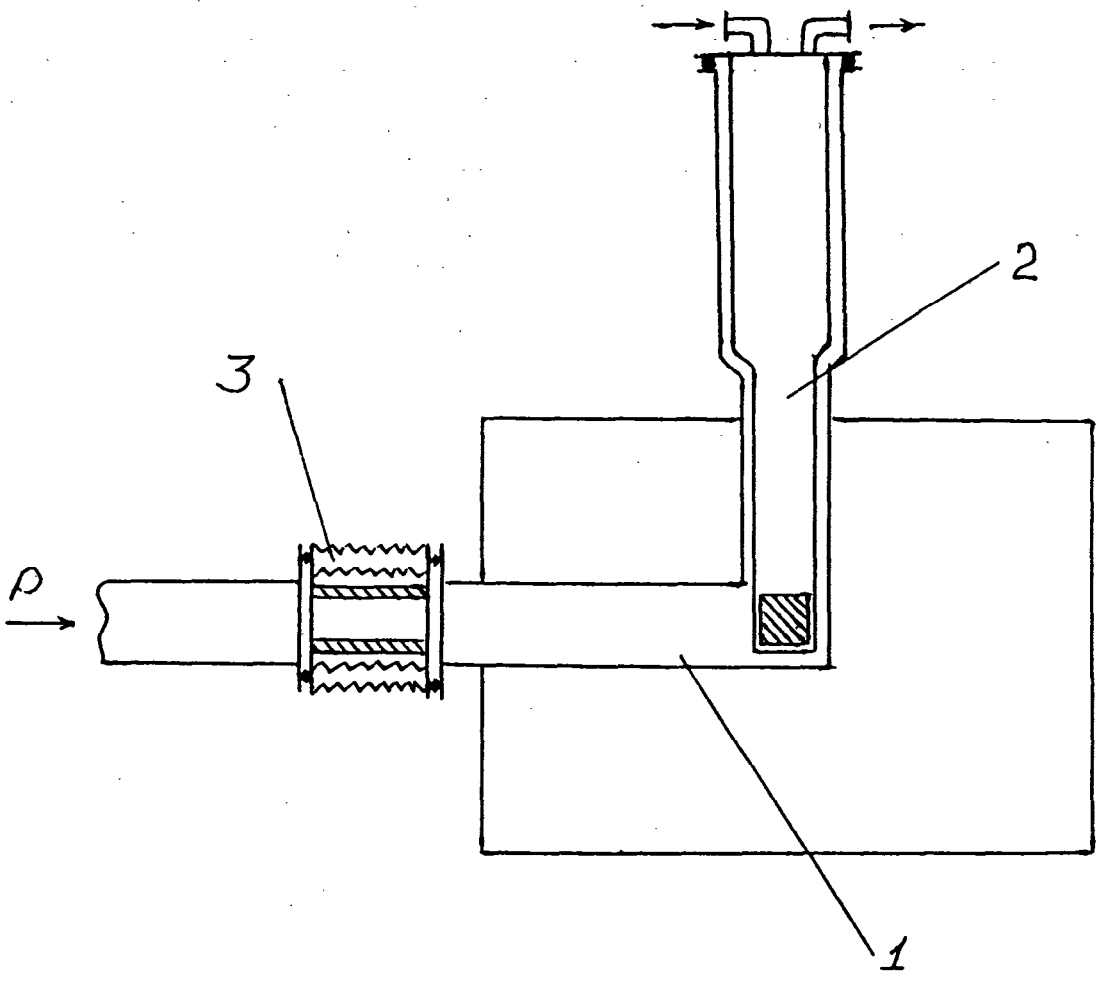

Fig.4. Design of neutron sources and proton beam dump: 1-tank with vacuum system; 2-ampoule of neutron source or beam dump; 3-remote-controlled vacuuum seal.

The quasistationary source of thermal and cold neutrons (Fig.5) consists of the water-cooled neutron target in the form of the closed package of rods made of natural uranium in stainless steel cans, heavy water moderator in the aluminium tank of 1.5 m diameter, liquid deuterium moderator of the valume ~20 l. On the first stage of the operation tungsten plates are supposed to be used. The liquid deuterium moderator radiates into the wide apperture canal for the experiments on the detection of neutron-antineutron oscillations as well as into the canals for the research with cold neutrons. With the removal of the liquid moderator the through tangential canal forms. This canal can be used for the experiment on the direct measuring of the length of neutron-neutron scattering and other researches in intensive fields of thermal neutrons /11/.

At the proton current of 0.5 mA the calculated value of the thermal neutron flux on the bottom of the experimental canal is about $3*10^{13}$ n/cm^2*s, the cold neutron flux [E < 5 meV] on the radiating surface of the cold moderator is of the order of 10^{13}

$n/cm^2 \cdot s$, with the effective neutron temperature being equal to 40° K. The radiating surface of the cold moderator is about 1000 cm^2. When ^{238}U is used and proton current ~0.5 mA the heat generation in the neutron target is of the order of 1 MW, in the heavy water 40 kW, in the cold moderator ~ 0.5 kW.

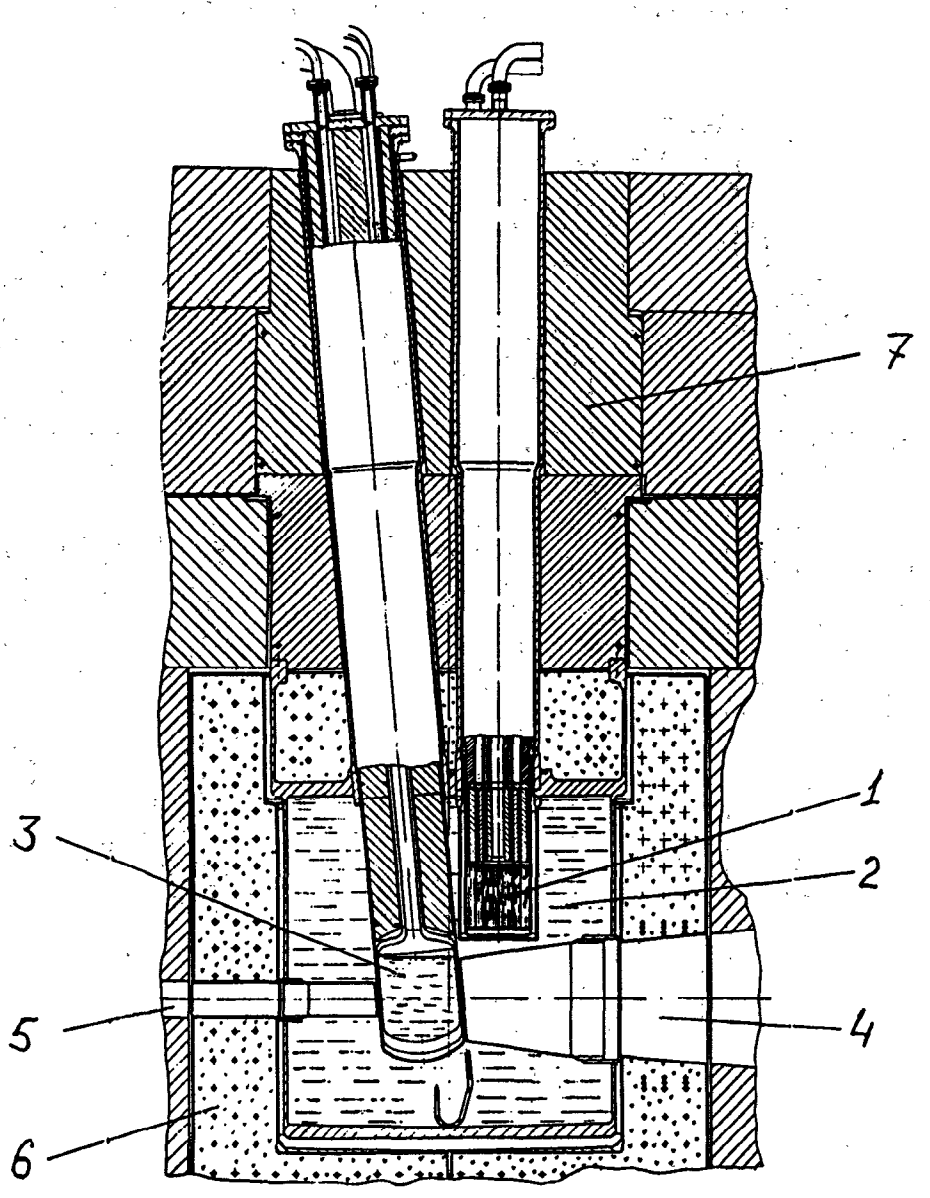

Fig.5. Quasistationary source of thermal and cold neutrons: 1-neutron target; 2-liquid deuterium moderator; 3-heavy water moderator; 4-canals for n-ν experiment; 5-extension of wide apperture canal; 6-thermal shield; 7-removable steel plugs.

The heat released in the heavy water is removed in external heat exchanger. The liquid deuterium moderator is cooled by means of the deuterium vapour condensation in the heat exchanger blown on by the helium at temperature 15•K from the refrigerator.

The pulsed neutron source consists of the target assembled from the uranium rods [tungsten plates] and cooled by water and the set of moderators (Fig. 6). The moderators are adjoined to the upper and lower surfaces of the target. To decrease the background of scattered neutrons and prevent a pulse delay in the case of the

operation with resonance neutrons both the target and moderators are placed in to the vacuum tank. Thin [~ 2 cm] light water moderator is looked out through the neutron canals for resonance neutrons with the flight distances of up to 500 m. The canals get out of the hall of the experimental complex (Fig.1). Neutron canals have intermediate pavilions. Above the target there are replaceable moderators for the work with thermal and cold neutrons. The use of

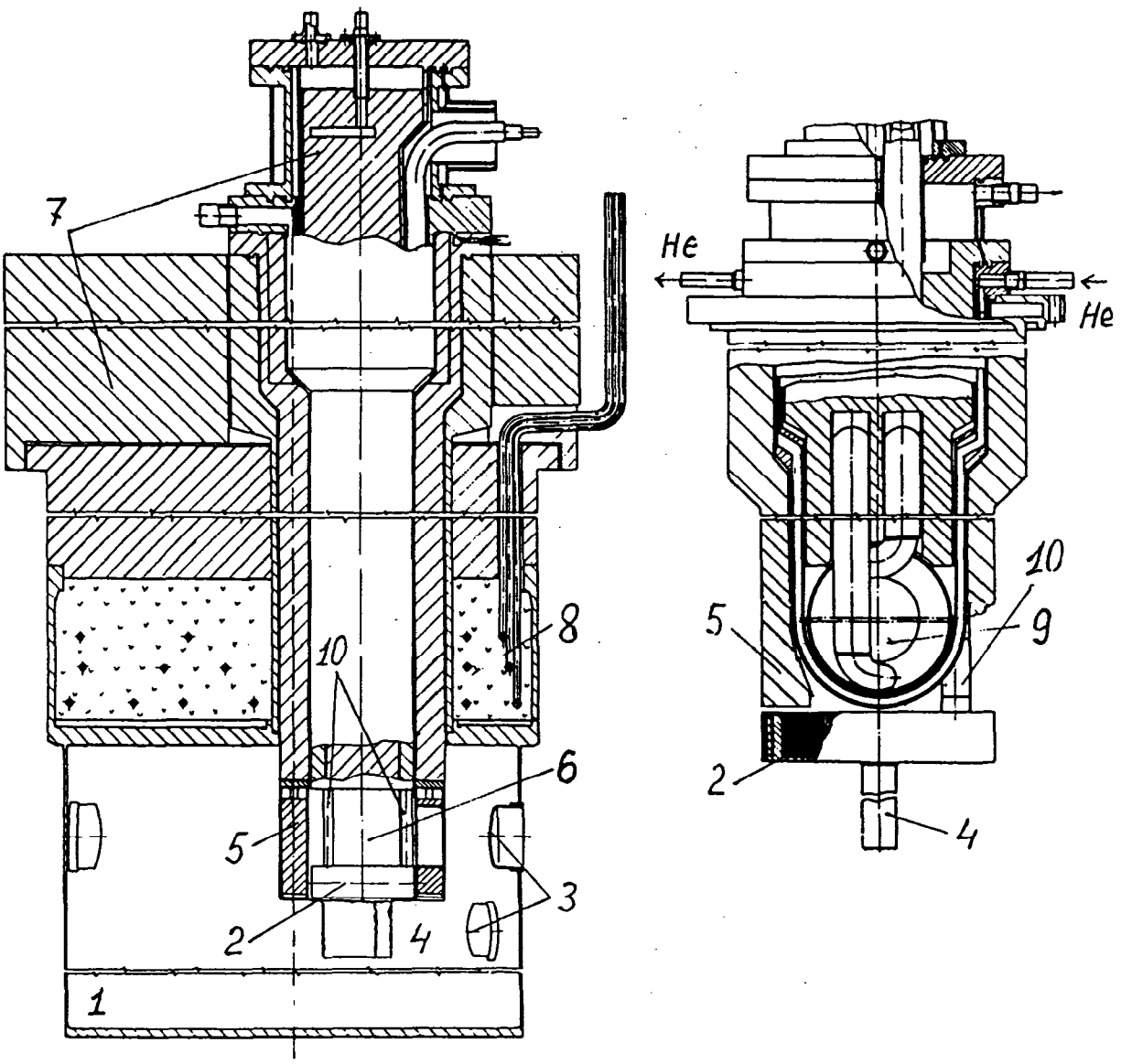

Fig.6. Pulsed neutron source: 1-vacuum tank; 2-assembly of rods made of uranium - 238 (or tungsten); 3-thin aluminum windows; 4-lower water moderator with thickness 3 cm; 5-reflector of upper moderator 6-place for the upper water or liquid-hydrogen moderator; 7-upper part of the thermal shield; 8-removable upper steel plug; 9-liquid- hydrogen moderator; 10-coolant's communications.

either the light water moderator of the thickness ~ 4 cm or the liquid deuterium moderator is supposed. These moderators have the Be reflector of the thickness 15 cm. Corresponding neutron canals look out to the experimental hall.

The peak density of thermal neutron flux averaged over the

radiating surface of the water moderator [surface area ~400 cm^2] will be about $2*10^{15}$ n/cm^2*s when pulse duration ~50 μs.

In the presence of the reflector peak fluxes of thermal neutrons will reach the value of $5*10^{15}$ n/cm^2*s on the radiating surface area ~100 cm^2.

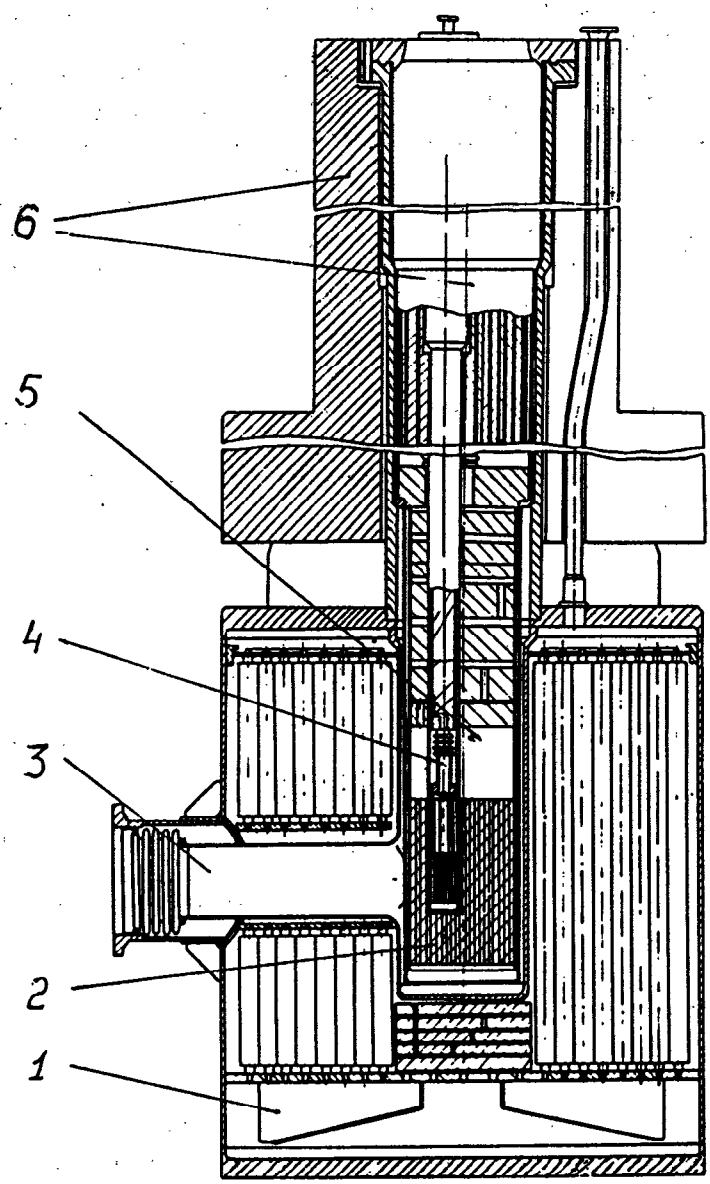

Fig.7. Proton beam dump: 1-thermal shield; 2-tungsten plates; 3-ion guide; 4-canal for sample irradiation; 5-ampoule of proton beam dump; 6-removable steel plugs.

The peak density of cold neutron flux on the surface of the cold moderator is ~10^{15} n/cm^2*s while the duration ~120 μs.

On the first stage of the neutron source operation tungsten targets will be used. In this case the average intensity and density of thermal and cold neutron flux will be approximately two times as less as compared to those in the case of the targets based on ^{238}U.

The works on further development of the assembly and improvement in performance are carried out now. In particular, the possi-

bility to use multiplicating target with the limited multiplication [up to 20] is under consideration. This will allow the pulsed neutron source intensity to be increased by 5 - 6 times in the frequency range of 10 - 30 Hz, which is most convenient to carry out most experiments with thermal neutrons.

The provided possibility to change targets and moderators will allow the optimum conditions for every group of experiments to be chosen. So, in the biological shield there are stores for the replaceable target devices and other experimental equipment.

Proton beam stops are behind the meson targets in the assembled shield made of concrete and cast iron. The target core is the assembly of water cooled tungsten plates. The core is surrounded by the iron-water thermal protection. The vertical canal of the diameter 60 cm with autonomous water cooling allows irradiated samples to be carried into the target core (Fig.7).

Average proton energy in the canal is about 450 MeV. Average flux of fast neutrons in the canal will be $2*10^{14}$ n/cm^2*s at the current 0.5 mA.

References

1. Lobashev V.M., Tavkhelidze A.N., Vestnik Academii Nauk SSSR, 21 [1983] 115.
2. Koptelov E.A., Korolev V.V., Stavissky Yu.Ya., Inst. Nucl. Res. Preprint, P - 02288, Moscow, 1983.
3. Boriskin S.E. et al., Inst. Nucl. Res. Preprint, P-0431, Moscow, 1985.
4. Stavissky Yu.Ya., Phys.-Energ. Inst.Preprint 389, Obninsk, 1973.
5. Alvarez L.W., Rev. Sci. Instrum., 22 (1951) 705L.
6. Budker G.I., Dimov G.I. et al., Atomnaja Energija [Atomic Energy] 19 [1965] 507.
7. Iljinov A.S. et al., Inst. Nucl. Res. Preprint, p-0278, Moscow, 1983.
8. Vasilev A.A., et al., USSR, USA Patent 3.860.828, 1975.
9. Stavissky Yu.Ya., All-Union Seminar on Programme of Exp. Res. on Moscow Meson Facility, Moscow, 1979, p. 37 - 39.
10. Bulkin Yu.M. et al., Proc. Conf. on Neutron Scattering in the 'nineties' Julich, 1985.
11. Kazarnovsky M.V. et al., Proceedings of INES-89, Moscow, USSR, p. 219, 1989.

Q(P.A.Egelstaff): When the liq. D_2 moderator is in front of the target, many of the neutrons from the H_2O coolant will scatter directly from the D_2O down the beam tube. But if the liq. D_2 is placed in the position indicated by Dr. Bauer many neutrons from the H_2O coolant will pass through the D_2O from behind. Does this difference change the cold neutron flux seen in these two cases?

A(S.F.Sidorkin): In the case proposed by us the cold neutron flux is not less than in the other one; neutron losses due to a big hole was taken into account at optimization study.

ICANS-XI International Collaboration on Advanced Neutron Sources
KEK, Tsukuba, October 22-26, 1990

SIMULTANEOUS PULSED/INTEGRAL NEUTRON FACILITY OPTIMIZATION

I.M. Thorson
TRIUMF, 4004 Wesbrook Mall, Vancouver, B.C. V6T 2A3

ABSTRACT

The possibilities and compromises necessary in the design of a neutron facility that would serve both pulsed and time integral users simultaneously are examined.

1. INTRODUCTION

Traditionally thermal neutron beam users have divided into two, occasionally armed camps. The maximum intensity available for monochromation by Bragg reflection of the broad thermal neutron spectrum has always been found at fission reactors. Such instruments are limited to the strictly thermal neutron energy region by two factors: the decreasing reflectivity of the monochromating (and energy analysing) crystals and the lack of epithermal neutrons in the incident neutron beams. The pulsed neutron instruments using choppers to monochromate and time-of-flight for neutron energy analysis get by with much smaller integral neutron beams by phasing the choppers to the neutron source pulses. Because the source flash is brighter by factors up to 100 for thermal neutrons and more than 1000 for epithermal neutrons they are the source of choice for such instruments. The beam power available from the present accelerators that operate in a pulsed mode is approximately 100 kW. The flux available to integral beam users from a target assembly optimized for such use would be a factor ~50 less than that available from the ILL fission reactor. As the intensity gap available between accelerator sources and fission reactor sources closes the question of optimization of target assemblies for both integral and pulsed beam users becomes important.

If a neutron facility requires N different target-moderator assemblies to satisfy the various users the overall availability of their facility for *all* users is N^{-1}. Thus the total overall availability to any user is maximized as long as the compromises necessary in a common facility design cost less than a factor at least 2 in beam availability.

The question to be addressed then is what are the approximate intensity reduction factors to the various types of instruments that common facilities would impose.

The second section uses simple one-dimensional neutron diffusion theory to estimate the epithermal and thermal fluxes available in infinite moderator assemblies of various materials. The epithermal and thermal neutron spectral components are illustrated and their spatial and temporal variations defined. In section three some of the constraints that would be necessary in the design of a "universal" target-moderator assembly are discussed. Section

four draws general conclusions and makes some recommendations on the directions for future developments.

2. NEUTRON FLUX ESTIMATION

A. Steady State or Time Integral

The diffusion theory approximation for the epithermal neutron flux in an infinite medium surrounding a void of radius R containing a source of S fast neutrons of energy E_o is given by[1]

$$\phi_{\text{epi}}(r) = \frac{S}{4\pi r}\frac{\lambda_s ln(E_o/E_{th})}{\xi}\frac{e^{-\frac{r-R}{L_s}}}{L_s(L_s+R)} \tag{1}$$

where r is distance from the source at the center of the void, λ_s is the transport mean-free-path, $\lambda_s = (\Sigma_s(1-\overline{\mu}))^{-1}$, Σ_s is the macroscopic scattering cross section and $\overline{\mu}$ is the mean cosine of the scattering angle in the infinite medium material, ξ is the mean logarithmic energy loss per (elastic) scattering collision, E_{th} is the thermal neutron energy, ~0.026 eV at room temperature, and L_s is the slowing down length

$$L_s^2 = \frac{1}{3}\int_{E_{th}}^{E_o}\frac{\lambda_s^2}{\xi(1-\overline{\mu})}\frac{dE}{E}. \tag{2}$$

Figure 1 shows the expected spatial distribution of the epithermal neutron flux for infinite media of various materials surrounding a 10 cm radius void containing a fast neutron source. The diffusion model implicitly estimates the integral over energy for a single epithermal group during the thermalization process from the intitial energy – approximately 2 MeV – to thermal, ~0.026 eV at 300° K. No neutron loss mechanism is considered except transfer to a thermal energy group at the end of the thermalization process. The neutron thermalization and diffusion parmeters shown in Table I are based on a fission reaction source spectrum; the somewhat border spectra from spallation reactions would change them only marginally. Within the epithermal group the time-averaged spectrum is expected to have an approximate E^{-1} energy dependence.

For the neutrons reaching thermal energies with the distribution given by (1) above the thermal neutron flux distribution is

$$\phi_{th}(r) = \frac{S}{4\pi r}\frac{\lambda_a}{(L_s^2-L^2)}\left(\frac{L_s}{L_s+R}e^{-\frac{r-R}{L_s}} - \frac{L}{L+R}e^{-\frac{r-R}{L}}\right) \tag{3}$$

where L is the thermal neutron diffusion length

$$L = (\frac{\lambda_a\lambda_t}{3})^{1/2} \tag{4}$$

λ_a is the thermal neutron capture mean-free-path and λ_t is the thermal neutron transport mean-free-path similar to that defined for epithermal neutrons, above. The expressions approximate both the steady state spatial distributions for continuous sources and the time-integrals for time dependent sources. It does not, however, approximate the thermal neutron spatial flux distribution immediately following thermalization, as will be discussed below.

Figure 2 shows the expected time-averaged thermal neutron flux distribution for the thermalized source distributions shown in Fig. 1 for the various infinite media. The estimate

Table I
Neutron Thermalization and Diffusion Parameters

	H_2O	D_2O (H/D=0.002)	Be (ρ=1.7 g cm^{-3})	C (ρ = 1.8 g cm^{-3})	Fe	Ni	Pb
$\lambda_{a,cm}$	45	11,300	960	3260	4.6	2.5	178
$\lambda_{t,cm}$	0.49	2.60	1.60	2.5	1.1	0.63	2.7
$L_{,cm}$	2.7	99	22.6	52	1.3	0.72	12.6
$\lambda_{s,cm}$	0.67	2.82	1.43	2.33	1.4	0.76	2.9
$L_{s,cm}$	5.5	11.0	9.3	18.7	18.5	10.4	74
ξ	0.925	0.509	0.209	0.158	0.0354	0.0337	0.0096
$\lambda_s/\xi\lambda_a$	16×10^{-3}	0.49×10^{-3}	7.1×10^{-3}	4.5×10^{-3}	8.6	9.4	1.7

λ_a – capture mean-free-path for thermal neutrons, based on 2200 m s^{-1} cross sections and Westcott convention flux.

λ_t – transport mean-free-path for thermal neutrons, $= (\Sigma_s(1-\overline{\mu}))^{-1}$, where Σ_s is macroscopic scattering cross section and $\overline{\mu}$ is the average cosine of the scattering angle.

L – thermal neutron diffusion length, $= (\frac{\lambda_t\lambda_a}{3})^{1/2}$.

λ_s – scattering mean-free-path for epithermal neutrons.

L_s – neutron slowing down length, from E_0 to E_{th}, $L_s^2 = \frac{1}{3}\int_{E_{th}}^{E_0} \frac{\lambda_s^2}{\xi(1-\overline{\mu}_s)}\frac{dE}{E}, E_0 \approx 2$ MeV

ξ – mean logarithmic energy loss per scattering collision, $\xi \approx 2/(A+\frac{2}{3})$, A is atomic weight.

uses the experimental neutron diffusion parameters from Table I for the common moderators based on measurements with fission-neutron spectra[2]. They are expected to be a reasonable approximation to the distribution around a lightly absorbing target and container (lead in zirconium, for example). The estimated thermal neutron flux in the vicinity of the target edge is the same, within a factor 2, for all of the better moderator materials. The ratio of the epithermal/thermal flux is given by

$$\frac{\phi_{\rm epi}(r)}{\phi_{th}(r)} = \frac{\lambda_s ln(E_o/E_{th})}{\xi\lambda_a} \times \frac{L_s^2 - L^2}{L_s^2 - L_s L(L_s+R)/(L+R)e^{-\frac{L_s-L}{L_s L}(r-R)}} \cdot \tag{5}$$

For $L > L_s$ this ratio decreases with increasing distance from the source, as is shown in Fig. 3. For $L_s > L$ this ratio becomes constant as the second term in the denominator vanishes, as for H_2O. The factor $\lambda_s/\xi\lambda_a$ is the ratio between the E^{-1} epithermal neutron spectrum and the thermal, Maxwellian neutron spectrum in an infinite medium with a uniformly distributed source of fast neutrons. Such spectra are shown in Fig. 4, transformed to constant reciprocal velocity, τ, interval after extracting a factor τ from the denominator. The curves as shown are proportional to the intensity seen by a time-of-flight or a perfect Bragg-reflection spectrometer for a fixed fractional velocity or reflection-angle resolution. The thermal neutron spectra for three different Maxwellian temperature are shown. The slowing-down spectra normalizations are those for uniform infinite media sources. The neutron energy, E_n, as the function of neutron reciprocal velocity, τ,

$$E_n = 5213\ \tau^{-2} \tag{6}$$

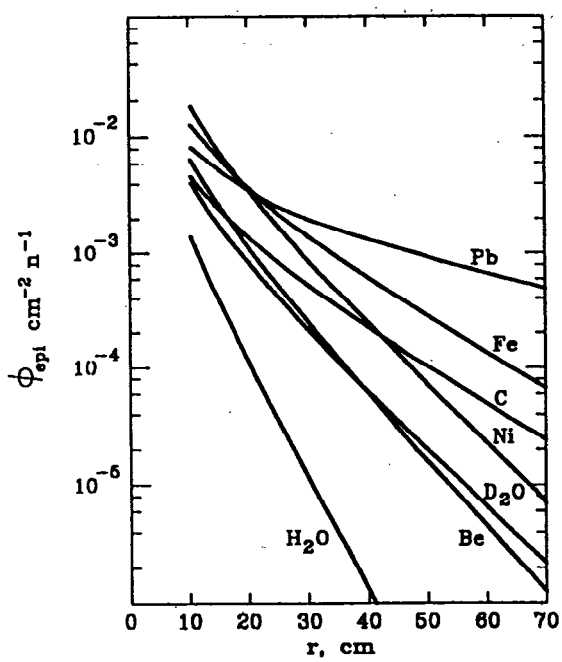

Fig. 1. The one-dimensional diffusion theory estimate of the epithermal neutron flux distribution in infinite media of various materials outside a 10 cm radius void are shown normalized to unit neutron source strength using the thermalization and diffusion parameters from Table I.

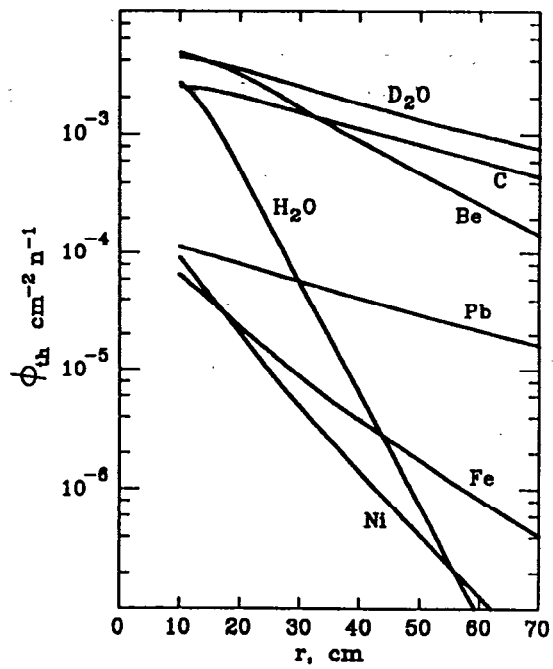

Fig. 2. The thermal neutron flux distributions are shown for the epithermal source distributions and geometry of Fig. 1.

E_n in eV, τ in μs m^{-1}, is also shown on Fig. 4. The normalization of the results in Fig. 3 is the same as for Fig. 4, i.e. the dotted lines in Fig. 4. representing the levels of the epithermal spectra in various materials track as functions of positions according to the results in Fig. 3. The dotted curve in Fig. 3 indicates the level of the (constant with temperature) maxima in the Maxwellian (thermal neutron) spectra, which can then be renormalized by the spatial distributions shown in Fig. 2.

B. Pulsed Neutron Sources

Table II shows the mean lifetimes for thermal and epithermal neutrons in the same infinite media for which the spatial distributions were estimated above. The thermal neutron lifetime is simply the quotient of the mean-free-path to capture divided by the mean neutron velocity, $v_t = 2.5 \times 10^3$ m s^{-1} for a room-temperature Maxwellian. The thermal neutron lifetimes can of course be shortened in an infinite medium only by adding absorber to the system, with a proportionate decrease in the time-integral thermal neutron flux. For moderators of finite size the relaxation rate is increased by leakage according to[3]

$$\phi_{th}(t) = \phi_o e^{-\lambda t} \tag{7}$$

where

$$\lambda \approx \alpha + DB^2 \tag{8}$$

and $\alpha = v_t \lambda_a^{-1}$ is due to neutron absorption as in the infinite system,
$B^2 = (\pi/r)^2$ for sphere of radius r,
$= (\pi/h)^2 + (2.405/r)^2$ for a cylinder of radius r and height h,
$= (\pi/a)^2 + (\pi/b)^2 + (\pi/c)^2$ for a parallelepiped of sides a, b and c.
$D = v\lambda_t/3$ is the diffusion constant for neutrons leaking out of the system,

(B is the geometrical buckling in the vernacular of fission reactor physics.)

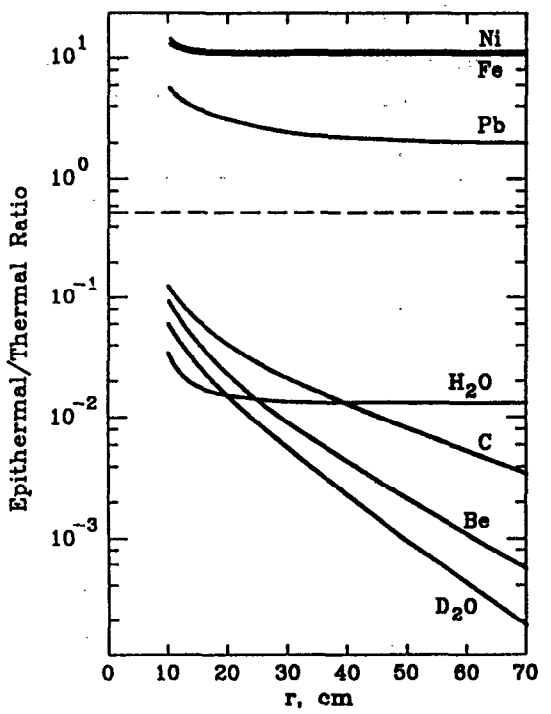

Fig. 3. The ratio of epithermal/thermal neutron fluxes are shown for the same systems and approximations as Figs. 1 and 2. (See text for normalization details).

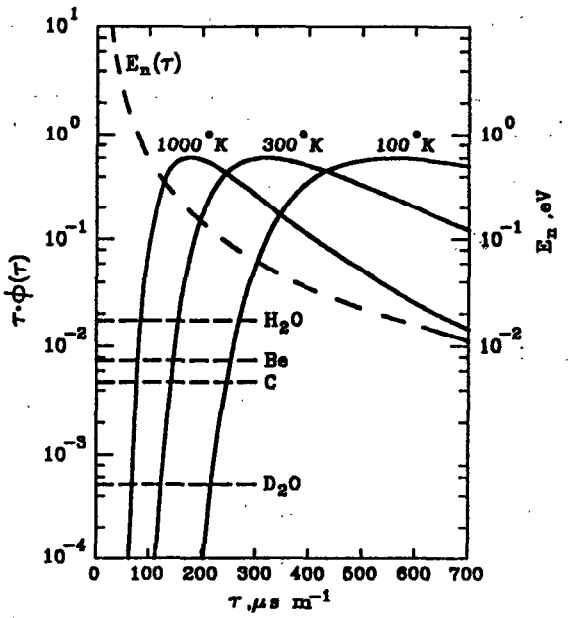

Fig. 4. The thermal and epithermal neutron spectra for infinite media with uniformly distributed sources of fast neutrons are shown for the common moderators. The spectra are shown as the functions $\tau\cdot\phi(\tau)$ where τ is the neutron reciprocal velocity (in μs m^{-1}) and $\phi(\tau)$ is the distribution per unit reciprocal velocity interval.

This expression for $\phi_{th}(t)$ is an approximation, the conditions for which are seldom, if ever, well satisfied and may not be valid for all systems of interest. In particular, heterogeneous systems of different materials may 'store' neutrons in regions with longer neutron slowing-down delays or thermal neutron lifetimes and feed them back to regions that would otherwise be more quickly populated or depleted. Thus, simple, single time-constant exponential thermalization and decay may not always be an adequate approximation for all neutron histories of interest.

Ikeda and Carpenter (ref 4) have shown experimentally that for typical compact hydrogenous moderator systems, the neutron leakage pulse at a particular neutron energy in the thermal region reqires two terms:

$$\chi(a,\beta,R,t) = \frac{a}{2}\left\{(1-R)(at)^2e^{-at} + 2\frac{Ra^2\beta}{(a-\beta)^3} \times \left[e^{-\beta t} - e^{-at}(1+(a-\beta)t+\frac{1}{2}(a-\beta)^2t^2)\right]\right\} \quad (9)$$

where a = $v\xi\Sigma_s$, defines the transferrate from the epithermal to the thermal group
β = time constant for thermal neutron loss from system, and
R = fractional yield in the thermal neutron term.

The first term represents the thermalization component that decays fairly quickly even at thermal neutron energies; the second term comes from the equilibrium thermal neutron component that has a nominal time constant of the order of $\beta = \lambda$ from Eq. (8). The thermal component weighting R value depends on the Maxwellian amplitude at the energy of interest as well as thermalization characteristics of the system. In practice it is an empirically derived parameter extrapolated from systems of a similar configuration and moderator characteristics.

Table II
Thermal and Epithermal Neutron Lifetimes

Material	γ	$\bar{t}_{th}$	$\bar{t}_s$ (to 1 eV)	$\Delta\bar{t}_s$ (to 1 eV)
		μs	μs	μs
H_2O	0.99	180	1.7	2.0
D_2O	0.56	45×10^3	4.8	4.7
(H/D=0.002)				
Be	0.148	3.8×10^3	7.9	4.7
(ρ = 1.7 g cm^{-3})				
C	0.111	13×10^3	20.2	10.8
(ρ = 1.8 g cm^{-3})				
Fe	0.0239	18	58	14.8
Ni	0.0227	10	34	8.5
Pb	0.0064	710	440	59

$\bar{t}_{th}$ – average thermal neutron lifetime.
$\bar{t}_s$ – average thermalization time.
$\Delta\bar{t}_s$ – full-width, half-maximum of thermalization distribution.
γ – thermalization parameter, $\approx 4/(3A)$ in $\bar{t}_s = (1+2/\gamma)(\gamma\lambda_s/\xi v)$ and $\Delta t_s = 2.35(1+2/\gamma)^{\frac{1}{2}}(\gamma\lambda_s/\xi v)$ where v is final neutron velocity of interest.

The epithermal neutron lifetimes, $\bar{t}_s$, are also listed in Table II for the various materials. Because of the relatively narrow fractional range of the initial energies of most of the source neutrons and the close correlation between time and energy loss, the parameter that defines the pulse length and amplitude for homogeneous systems is the straggle width of thermalization time, also shown in Table II as $\Delta\bar{t}_s$, the full-width at half-maximum, taken from reference 3 for the light moderators and estimated from the expression listed in the footnotes of Table II for the others. Except in circumstances where significant cross-feeding of neutrons takes place between regions of different thermalization times the pulse length and amplitude is controlled by the time-straggle width and the thermalization time only introduces a phase shift in the pulse cycle.
The peak fluxes, both epithermal and thermal, that contribute beam over the short periods – a few μs – sampled by time-of-flight monochrometers are then enhanced, relative to those shown for the steady state in Fig. 1 by a peak enhancement factor (F_{PE}) given by

$$F_{PE} = \frac{\tau_P/\tau_L}{1-e^{-\tau_P/\tau_L}} \tag{10}$$

where τ_P is the pulse repetition period and τ_L is the mean neutron lifetime as a thermal ($\tau_L = \bar{t}_{th}$) or epithermal ($\tau_L = \Delta\bar{t}_s$) neutron as listed in Table II for infinite systems. The mean neutron lifetimes in finite assemblies can, of course, be significantly shorter than those shown in Table II but the time-integral fluxes will be reduced by the same factor leaving the initial peak fluxes constant.
There is however another factor that must be considered in estimating the thermal neutron pulse intensity available from large moderator assemblies, namely the evolution of the thermal neutron spatial

Table III

Epithermal and Thermal Pulse Enhancement Factors for Pulse Repetition Period of 20 ms

Material	F^*_{PE} (epithermal)[1] (to 0.026 eV)	F^*_{PE} (thermal)[2] (short time)	F_{PE} (thermal)[3] (long time)
H_2O	1600	1500	110
D_2O	690	560	1.2
Be	690	620	5.3
C	300	270	2.0
Fe	220	220	1100
Ni	380	380	2000
Pb	55	55	28

1) $\tau_L = \overline{\Delta t_s}/(0.026)^{1/2}$
2) $\tau_L = ((\overline{\Delta t_s}/0.026)^2 + (\frac{\lambda_t}{3v})^2)^{\frac{1}{2}}$
3) $\tau_L = \bar{t}_{th}$

distribution with time. At thermalization the spatial distributions of the neutrons are essentially those shown in Fig. 1 for epithermal neutrons in various materials. These distributions evolve with time to give the time-integral distributions shown in Fig. 2. The pulse enhancement factor thus depends on position within the moderator, especially for materials where $L>L_s$. The asymptotic limits for the effective lifetimes are the reciprocals of the neutron capture rate at long time ($\bar{t}_{th}$ in Table II) and the reciprocals of the neutron diffusion rates ($\tau_L = \lambda_t(3v_t)^{-1}$) at short distances and short times. At short times the diffusion rates are comparable to the thermalization rates and the effective pulse enhancement factors are similar to those for the epithermal components, as shown in the last column of Table III. Thus the dominant contribution to the peak pulse intensity at all energies near the source in large moderator assemblies comes from the epithermal or recently thermalized component. Because the epithermal fluxes decrease rapidly with radial distance from the source as shown in Fig. 1, all beam tubes for such pulsed beams must penetrate to positions near the target. At these short distances, however, the three best moderators, H_2O, D_2O and Be, all give similar peak pulse intensities for both epithermal and thermal energies. The time integral intensities are also comparable for neutron source positions near the target; the Be or D_2O moderators would, however, allow geometries much less congested than for H_2O. Large all-nickel and iron moderators would also yield very good peak epithermal fluxes but would give very poor integral thermal neutron fluxes.

The time-integral thermal neutron flux is always maximum in a large D_2O moderator assembly, as reiterated by the results in Fig. 2. Its dependence on distance from target is weak enough that thermal neutron beam tubes can be terminated at least 30 cm from the target centre without suffering intensity penalties more than a factor 2. This allows off-setting of the beam tubes to tangential geometry and ahead of target entry point of the proton beam to minimize fast neutron contamination that usually dominates the background problem for most experimental instruments. To maximize the thermal neutron flux, however, the moderator, target and structural components must have minimum neutron capture cross-section.

No substantial intensity penalties are expected for either integral and pulsed neutron beam of all energies if the additional constraint of short neutron lifetimes applied to the present PNF designs is removed.

3. DESIGN CONSTRAINTS FOR OPTIMUM PULSED/INTEGRAL NEUTRON FACILITIES

The constraint of minimum absorption or leakage in small moderator assemblies to achieve optimum integral thermal neutron beams requires that all time-of-flight monochromotors include a second phased beam chopper in the vicinity of the target moderator assembly. This will be quite an acceptable price where (and when) the accelerators have power levels large enough to compete with the fission reactors. A 10^{15} cm^{-2} s^{-1} thermal neutron flux requires approximately 6 MW of beam power at approximately 1 GeV proton energy. The beam power from the KAON accelerators approaches this level but at an energy that is probably too high for optimum neutron source production.
The second over-riding constraint for a high power facility will be heat dissipation in the target. Given the intensity incentive implied by Fig. 1 for compact sources only pumped liquid metal targets are likely to be capable of the several MW per liter heat dissipation required. Fortunately both lead and bismuth, the most probable materials, are not heavy thermal neutron absorbers.

4. CONCLUSION

It appears that no fundamental neutronic constraints preclude simultaneous optimization of the integral and pulsed neutron beams available from an accelerator based neutron facility. The simple single phased chopper monochromation systems presently employed at such facilities must, however, be augmented by second phased chopper as were originally used on fission reactors more than 30 years ago[5].

REFERENCES

[1] P.R. Wallace and J. LeCaine, *Elementary Approximations in the Theory of Neutron Diffusion*, Chalk River Nuclear Laboratory report AECL No. 336, 1943.

[2] ANL-5800 *Argonne National Laboratory Reactor Physics Constants*, Second Edition, 1963.

[3] J.M. Carpenter, *Pulsed Spallation Neutron Sources for Slow Neutron Scattering*, Nucl. Instrum. and Meth. 145 (1977) pp 91-113.

[4] S. Ikeda and J.M. Carpenter, Nucl. Instrum. and Meth. A239 (1985) p 536.

[5] P.A. Egelstaff *et al.*, *A Four-Rotor Thermal Neutron Analyzer, Inelastic Scattering of Neutrons in Solids and Liquids*, IAEA, Vienna (1961) p 165.

ICANS-XI International Collaboration on Advanced Neutron Sources
KEK, Tsukuba, October 22-26, 1990

A Design Concept of Target-Moderator-Reflector Assemblies for KENS-II
-A High-Efficiency Pulsed Spallation Neutron Source-

N. WATANABE
National Laboratory for High Energy Physics,
1-1 Oho, Tsukuba-shi, Ibaraki 305 Japan

ABSTRACT
A design concept of KENS-II target-moderator-reflector assemblies is described. - one of the assenblies is dedicated to the cold neutron source, and the other, to the thermal and epithermal neutron source. A flux-trap type moderator-configuration was adopted with a vertical proton-beam injection scheme. All moderators for the cold neutron source are coupled liquid hydrogen moderators with premoderators. A new scheme of proton beam delivery is proposed. The new system can provide several times higher total performance than a reference system based on a traditional single assembly with all decoupled moderators in a wing geometry and with a horizontal proton-beam injection scheme.

I. INTRODUCTION

The traditional target-moderator-reflector assembly (TMRA) concept, based on a single assembly with all decoupled moderators in a wing geometry and a horizontal proton-beam injection scheme, has been widely adopted at existing pulsed spallation neutron sources. This concept has proved to be very useful by the successful operation of the existing facilities. The neutron scattering community has always requested more intense neutron sources, and consequently, proton accelerators with higher beam currents. The approach to an intense spallation neutron source with an intense accelerator would be orthodox, but very expensive and sometimes not realistic. When we consider a new source, generally speaking, it must be superior to the existing large scale ones, even though the proton beam power is comparable to those in existing large scale facilities. Thus, a new concept for a high-efficiency TMRA becomes indispensable. This is our situation for the fundamental design of KENS-II in the JHP project. To realize this, we proposed and developed a high efficiency cold neutron source with a coupled liquid hydrogen moderator with premoderator[1~2),4~5)] based on a

consideration of figures of merit (FOM's) of a pulsed cold neutron source for various scattering experiments[3]. We considered two typical experiments using pulsed cold neutrons: one is the small angle neutron scattering (SANS)-type, in which experiments on TOP, CRISP, spin echo machines, etc. are included, and the other is the LAM-type, high resolution spectroscopy using the time structure of the neutron pulse. We confirmed that the proposed moderator can provide much higher FOM's than a the traditional decoupled one. We have also performed detailed studies on the so-called "flux-trap type moderator", which is successfully used at LANSCE in Los Alamos. We confirmed that this moderator can provide 1.35-1.4 times higher slow neutron intensity than a traditional moderator in a wing geometry[6]. A new concept for the KENS-II TMRA described here is based on the ideas mentioned above.

II. Design Concept and Assumtions

In the TMRA concept, we assume the followings.

(1)All moderators are in a flux-trap type moderator geometry. This geometry can provide 1.35-1.4 times higher slow-neutron-beam-intensity than a traditional wing geometry not only for decoupled moderators, but also for coupled ones.

(2)For high-efficiency cold-neutron-moderators, we adopt a coupled liquid hydrogen moderator with hydrogenous premoderator at room temperature. This provides about 6 times higher performance (FOM's relative to a decoupled liquid hydrogen moderator) for SANS-type experiments and 2-3 times (depending on the neutron wavelength) higher FOM's for LAM-type experiments[3].

(3)One TMRA is not adequate for the required angular coverage of the neutron-beam (almost 360°) even with a 4-moderator configuration, because the maximum angular coverage for one viewed moderator surface is 50°, which corresponds to about 4 beams (due to the existence of other moderators). Consequently, two assemblies become necessary.

(4)We propose a 2 TMRA concept: TMRA-1 dedicated to the cold neutron source with 3 coupled moderators, and TMRA-2, to the thermal/epithermal neutron source with 3 decoupled moderators as shown in Fig. 1. Coexistence of coupled and decoupled moderators in one TMRA is not desirable from an intensity point of view[5]. This concept makes it possible to provide neutron beams over an angular range of 300° or more.

(5)We propose a new proton-beam delivery scheme as shown in Fig. 2 (scheme (1)). Since FOM's for both type of experiments are, to a first approximation, independent of the repetition rate of the neutron pulse within a realistic range[3], we allocate 10 double pulses every sec. to the TMRA-1. This will provide 2 times higher FOM's than the original proton-beam delivery scheme of 50 single pulses (another 50 single pulses are

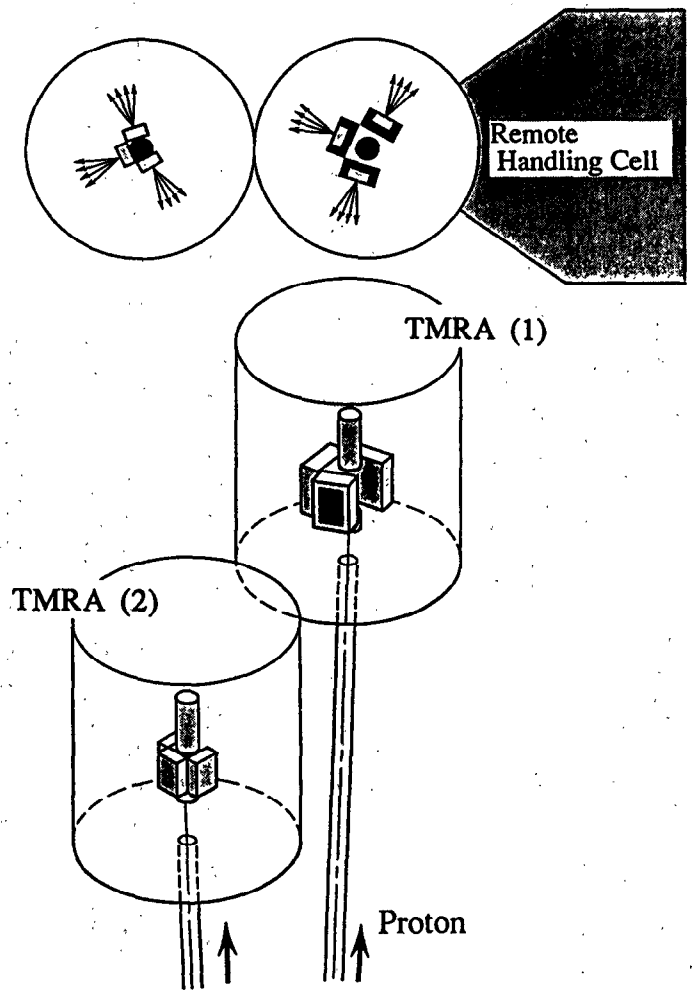

Fig. 1. Proposed TMRA's for KENS-II

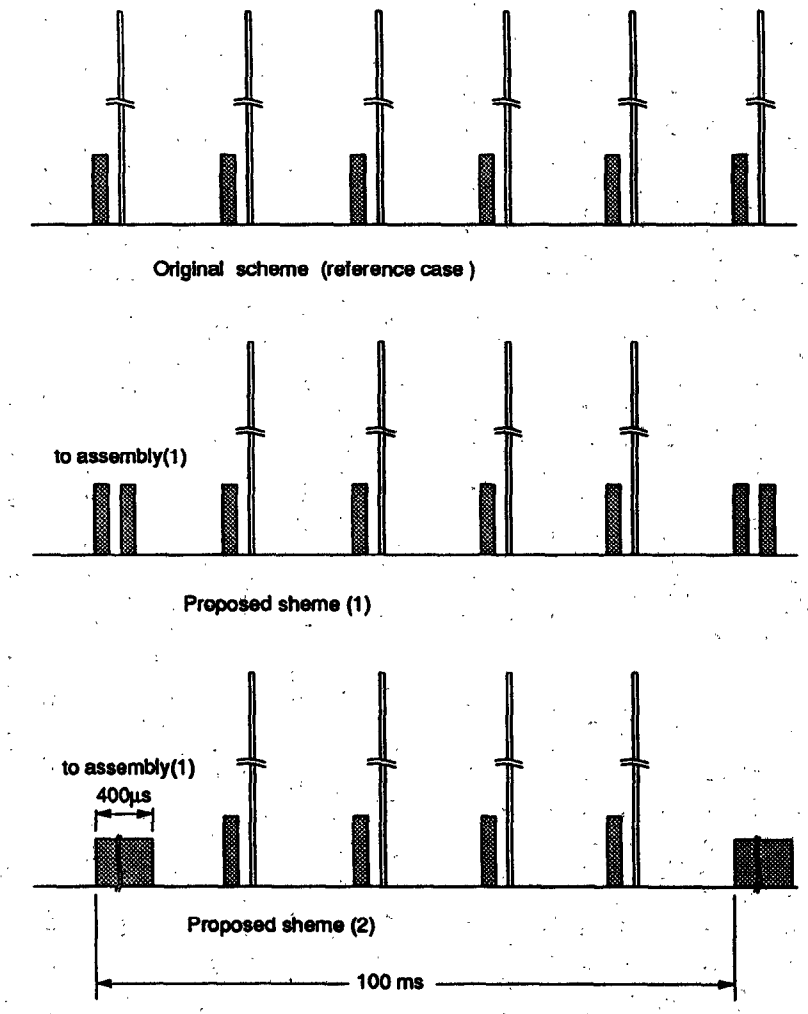

Fig. 2. Proposed proton-beam delivery schemes.
Gray pulses are to the neutron facility and white ones to the meson facility. In the reference case all gray pulses are fed to one TMRA, while in the schemes (1) and (2) first pulse(s) are fed to TMRA (1) and another ones to TMRA (2).

delivered to the meson facility) with no significant losses. The remaining 40 single pulses are fed to TMRA-2. In the JHP project, it was decided to share the total proton-beam from the compressor/stretcher ring equally by the neutron and the meson facilities. Since the meson facility has a schedule to utilize the stretched beam for about 20% of the total beam, and the simultaneous use of pulsed and stretched beams is not possible, a macroscopic beam-time sharing becomes necessary. The additional beam for the neutron facility by double-pulse delivery to the TMRA-1 just meets the 20% reduction of neutron beam-time by the stretched beam use.

(6) As an alternative to proton-beam delivery (scheme (2)), we propose to use long macro-pulses of H^- beam directly obtained from the linac, instead of double pulses from the compressor/stretcher ring. The time-averaged intensity of the H^- beam is 400 μA, 2 times higher than the short pulse beam from the ring, but the pulse duration is 400 μs. The use of this beam in the TMRA-1 gives 2 times higher FOM's for SANS-type experiments with unchanged FOM's for LAM-type experiments.

(7) The number of neutron beams available with the KENS-II concept is about 24, which should be compared to a reference case of 18 when a tradition wing geometry and a horizontal proton-beam injection scheme is used, for example, as in ISIS. The larger number in the KENS-II concept is due to the vertical proton-beam injection scheme, in which the proton beam line with its massive shielding can be removed from the experimental hall and additional neutron beams can be extracted into the space saved.

(8) It would be reasonable to allocate more neutron-beam lines for cold neutron experiments than in the existing facilities, because of the recent growth in the relative importance of cold neutrons even in spallation sources. We therefore assumed that 50% of the total neutron-beam lines are allocated for cold neutron experiments in both the reference and KENS-II cases. We also assumed that, among the cold neutron experiments, 2/3 are of the SANS-type and the remaining 1/3, the LAM-type.

For convenience, we summarize in Table I the main parameters of the neutron source in the proposed KENS-II concept compared to the reference case.

III. Total Performance and Gain Factor of Pulsed Neutron Sources

In a pulsed spallation neutron source, the total performance of the source relative to a reference case can be expressed as a sum of relative FOM's for each neutron beam,

$$\text{Total Performance} \equiv \sum_i (\text{FOM})^i/(\text{FOM})^i_{ref} .$$

For simplicity, we define

$$(\text{FOM})^i_{ref} \equiv 1,$$

Table I Main parameters of the neutron sources in the reference case and KENS-II concept

	Reference case	Kens-II Concept	
Proton-beam injection scheme	Horizontal	Vertical	
Target-moderator coupling geometry	wing	flux-trap	
Number of TMRA	1	2	
		TMRA-1 (for n_c)	TMRA-2 (for n_{th}/n_{epi})
Number of proton pulses (pulse/sec)	50 single pulses	10 double pulses	40 single pulses
Macroscopic beam time, D (relative value)	1	0.8	
Number of Moderators	4 decoupled	3 coupled	3 decoupled
Gain factor of "Flux-Trap" relative to "Wing", G_f	1	1.35	1.35
Number of neutron beams			
for SANS-type exp, N_{SANS}	6		8
for LAM-type exp, N_{LAM}	3	4	
for n_{th}/n_{epi}, $N_{th/epi}$	9		12
Relative moderator FOM			
for SANS-type exp, FOM_{SANS}	1	6	
for LAM-type exp, FOM_{LAM}	1	2.5	
for n_{th}/n_{epi}, $FOM_{th/epi}$	1		1

n denotes neutrons and the subscripts c, th and epi refer to cold, thermal and epithermal, respectively.

Table II Gain factor of proposed neutron sources relative to the reference case

KENS-II concept with proton-beam delivery scheme(1)	KENS-II concept with proton-beam delivery scheme(2)
7.6	13.5

thus, the total performance of the reference system becomes equal to the number of neutron-beam lines, that is

$$\sum_{i=1}^{18} (FOM)^{i}_{ref} = 18.$$

Let us calculate the total performance of the proposed concept for KENS-II, which can be expressed as,

$$\text{Total performance} = D\,G_f\,\{2\,(FOM_{SANS}\,N_{SANS} + FOM_{LAM}\,N_{LAM}) + (40/50)\,FOM_{th/epi}\,N_{th/epi}\}$$

where the notations are defined in Table I, and the factor 2 in the above equation comes from the "double pulse" discussed in (4) in the preceding section. Using the values listed in the table, we have

$$\text{Total Performance} = 0.8\times(1.35\sim1.4)\{2(6\times8+3\times4)+0.8\times12\}=130\sim145.$$

The relative value of the total performance to the reference case (gain factor) is thus

$$\text{Gain Factor} = (130\sim145)/18 = 7.3\sim8 = 7.6$$

If we adopt the alternative proton beam delivery scheme mentioned in (6) in the preceding section, FOM_{SANS} must be 12 instead of 6 in the above equation.
Then, we have

$$\text{Gain Factor} = 13.5.$$

Table II summarizes the result.

IV. DISCUSSIONS

We obtained a very large gain with a new concept of TMRA for KENS-II with new proton-beam delivery schemes. The large gain comes from cold neutron utilization (TMRA-1), and the overall efficiency of TMRA-2 is almost unchanged compared to the reference case. However, the gain factor 7.6~13.5 is great. In other words, <u>the neutron source in the proposed concept is equivalent to a neutron source with a proton accelerator of one order of magnitude higher beam current than is present now,</u> though more emphasis is placed on cold neutron experiments, which can well compete with those performed using a high flux reactor.

In addition to the advantage in the neutronic performance mentioned above, there are other merits to the proposed system:

(1)The heat load for Target-1 in the TMRA-1 with proton-beam deliverry scheme (1) is 2/5 of the reference case (or a maximum of 4/5 in the case of proton beam delivery scheme (2)). This makes the engineering design

of the system more easy; for example, the use of a depleted uranium target becomes less difficult.

(2)Power density and total power deposited in a liquid hydrogen moderator is almost one order of magnitude smaller than in the reference case, due to the factor mentioned in (1), and another factor saved by premoderatoion.

(3)Fast and higher energy neutrons leaking from the neutron beam holes can be minimized with a flux-trap type moderator geometry without sacrificing beam intensity by increasing the height of the void space between 2 target blocks.

(4)Smaller proton beam power, and consequently a smaller accelerator, is acceptable for a given total performance. This brings about lower costs for the construction and the operation of accelerator.

(5)Relatively thinner radiation shielding for target station and neutron beam lines is required.

(6)The radiation impact on the public is reduced.

(7)A smaller area for the site is acceptable.

REFERENCE

1 N. Watanabe : Advanced Neutron Sources 1988 (Proc. ICANS-X), Institute of Physics Conference Series Number 97, Institute of Physics, Bristol and New York (1988) p-763.

2 N. Watanabe, Y. Kiyanagi, K. Inoue, M. Furusaka, S. Ikeda, M. Arai and H. Iwasa: ibid p-787.

3 N. Watanabe, M. Furusaka and Y. Kiyanagi : A design Concept for KENS-II Cold Neutron source, Proc. Int. Workshop on Cold Neutron Sources (Los Alamos, Mar. 5-8, 1990), in press.

4 Y. Kiyanagi, N. Watanabe, M. Furusaka, H. Iwasa and I. Fujikawa Proc. ICANS-XI (Tsukuba, Oct. 22-26, 1990) p-388.

5 Y. Kiyanagi, N. Watanabe, M. Furusaka and H. Iwasa : ibid, p-401.

6 Y. Kiyanagi and N. Watanabe : ibid, p-408.

Q(J.M.Carpenter): If your four flux-trap moderators were arranged two each on two levels, with greater separation of target halves, the moderators could be viewed from both sides and provide 24 beams.

A(N.Watanabe): Greater separation of target halves does not decrease the slow neutron intensity from four flux-trap moderators on one level, but more moderators at different levels bring about lower intensity due to the shadow effect.

ICANS-XI International Collaboration on Advanced Neutron Sources
KEK, Tsukuba, October 22-26, 1990

The status of the ISIS targets

M. Holding and T.A. Broome
Rutherford Appleton Laboratory

ABSTRACT
Operational aspects of the ISIS neutron production targets are discussed and an outline given of future developments.

1. OPERATIONS

Table 1 gives an overall performance summary for the six targets which have been used to date.

At ICANS-X the failure of targets 1 and 2 were reported [1]. Since then two more Uranium targets have failed and some experience has been gained running with the backup Tantalum target.

The construction of the target and its cooling circuits have been described in detail at previous ICANS meetings so only a brief resume is given here. A schematic diagram of the construction of the target is shown in figure 1. The condition of the target is determined by monitoring the centreline temperatures of the target plates and the flow and pressure drop characteristics of the three heavy water cooling channels. The effective width of the cooling gaps between the target plates is monitored using a quantity called the 'gap constant' which is the ratio

$$\frac{\text{flow}}{(\text{pressure drop})^{0.55}}$$

This is constant over a wide range of flows and pressure drops and reduces as the cooling gaps become narrower. Measurements of the radiation levels around the cooling plant and measurement of the spectrum of gamma rays emitted from the target coolant are also used as diagnostics.

1.1 Uranium Target Running

In operation several radiation damage mechanisms lead to swelling of the Uranium so that the width of the cooling gaps between the target plates is reduced. This leads to a reduction in the gap constant and, finally, inadequate cooling of the Uranium.

The failure of target 2 followed this scenario and was described in detail at ICANS-X. This target was dismantled and the plates examined and the swelling of the Uranium was attributed to thermal cycling growth resulting from gross

thermal cycles on the target which occurred when the accelerator system tripped.

In the failure of targets 3 and 4 the changes in flow and pressure drop of the coolant followed a broadly similar pattern to that measured in the failure of targets 1 and 2. A partial blockage was detected in the cooling channel feeding the front five plates of the target with a consequent rise in Uranium temperature. The decision to change the targets was taken when the presence of fission products in the cooling water was confirmed indicating a breach in the integrity of the Zircaloy cladding of the Uranium.

During the design of the target studies of the radiation damage mechanisms lead to an estimate of about 10000 gross thermal cycles to failure. As can be seen in Table 1 the number of gross thermal cycles on target 3 was consistent with this estimated lifetime but target 4 failed after a disappointingly low number.

In operation the gap constant of target 4 changed abruptly on two occasions a long time before its failure. This behaviour has not been observed on any other target and no convincing explanation has been found. It has not been possible to dismantle either target 3 or 4 to establish detailed reason for their failures.

It is assumed that thermal cycling growth is still the dominant limitation on the lifetime of the targets. Considerable efforts have been made to reduce the frequency of accelerator trips and significant progress has been made. Figure 2 the day by day history for targets 4 and 5 and Table 2 shows the mean number of trips per day since 1987. The reliability of the accelerator systems has now improved to the point where, from the point of view of thermal cycling growth, a target lifetime of about 400 days could be expected so the fate of target 5, now in operation, is of crucial interest.

1.2 Tantalum Target Running

Some difficulties have been encountered in the manufacture, and thus availability, of Uranium targets. This has resulted in two periods, one of two months and one of seven months, where the backup Tantalum target has had to be used. This target is identical in construction to the Uranium targets with 9 cm. diameter disks of Tantalum instead of Uranium. The neutron fluxes from the moderators are 50% of that achieved with Uranium. The time independent backgrounds are lower but this was found to be of no significant advantage to the neutron scattering experiments.

There have been no operational problems with this target. Since Tantalum is not subject to the thermal cycling growth problems of Uranium there is no need for a gradual increase in current when restoring the proton beam after a trip. This results in two gross thermal cycles for each accelerator trip and is the reason for the apparently large number of gross thermal cycles for the Tantalum target in Table 1. However, a new backup is to be provided probably using Tungsten as the target material and will have a more efficient geometry. This is discussed in section 3.

1.4 Target Changes and Disposal

A great deal of work has gone into developing the remote handling of targets since ICANS-X. There have been detailed improvements to the tools including the use of air driven torque wrenches, positional readout have been added to

the remotely operated crane and the position and mounting arrangements for the cameras have been refined. As a result target changes are now essentially a routine operation without the sense of adventure evident in the early remote handling work.

The used Uranium targets have been transferred to the Harwell Laboratory for storage. This is an interim measure awaiting the procurement of a transport flask which will enable these, and all future targets, to be transferred to the Sellafield plant of British Nuclear Fuels Plc. for disposal. The contract for the flask has been placed and it is expected to be available, with full certification for use on public roads, by the middle of 1992.

2. URANIUM TARGET DEVELOPMENT

The aim of the development program is to achieve longer lifetimes for the targets. This will involve detailed changes to the design of the target plates, changes in the manufacturing procedures and possibly the use of a Uranium Molybdenum alloy for the target material. A brief description of the techniques used to produce the Uranium plates is given below together with the plans for improvements.

2.1 Uranium target module manufacturing processes

A schematic diagram of a target plate is shown in figure 3.

Depleted Uranium is melted with additions of iron and aluminium to produce the required "Springfield adjusted" Uranium alloy. This material is cast into billets which are topped, tailed and skimmed to remove most of the casting surface defects. The machined billets are then hot isostatically pressed (HIPped) to close any internal porosity, thus densifying the material. This process involves heating the material to a high temperature (typically 850C) in a pressure vessel which contains an inert gas and simultaneously increasing the gas pressure to a high level (typically 2040 bar). Any sealed void defect or casting porosity that is within the material is closed as the material yields under heating and pressure. Discs of the required thickness are sliced from the HIPped billet, heat treated to refine the structure, and surface prepared. These discs are fitted into Zircaloy-2 cups and covers which are hermetically sealed under vacuum by electron beam welding. The HIPping process is used again, but this time the high temperature and pressure are held for a set time to enable a diffusion bond to form between the Uranium disc and the Zircaloy-2 cladding. This bond is necessary in order to form a continuous thermal path from the Uranium to the water cooling. Ultrasonic inspection methods are used to check the bond and satisfactory discs are shrink-fitted into stainless steel frames to form the target plates. The target plates are then machined to reduce the cladding to the finished thickness, stacked with the window and rear closure plate, and electron beam welded together to form the target module ready for final machining.

The development programme will be staged in four parts.

2.2 Stage 1

The initial work will involve the optimisation of the HIPping cycle to produce the best diffusion bond between the Uranium and the Zircaloy-2 cladding. It will cover the possibility of eliminating the evacuation slots

in the Zircaloy cups to prevent the problems encountered on modules 5 & 6, where Uranium extruded into these slots and was found to be exposed on subsequent machining. Also the production of a more even penetration of the diffusion bond that is compatible with the automatic NDT scanning equipment, and finally to investigate the possibility of quenching the HIPped discs to further refine the grain size of the Uranium to reduce the effects of the irradiation induced growth.

2.3 Stage 2

At present the clad discs are shrink fitted into stainless steel frames and leaks have occurred through the interface to the thermocouple holes. These have to date been successfully cured on assembly by the use of custom made screw clamps and silver seals. However, internal leaks have developed subsequently during the operation of the targets and are probably due to the relaxation of the silver seals around the thermocouples caused by the normal operational temperature cycles of the targets.

This problem can be completely eradicated by replacing the stainless steel frame with an integral cup and frame manufactured from Zircaloy-2. This would utilise a square plate with a circular cavity to contain the Uranium. A solution using this method will need the development of two other items in parallel, namely longer thermowells, and a method of joining stainless steel to Zircaloy-2.

The current thermowells are manufactured in one piece and have a 1.7mm diameter hole 50mm long drilled down the centre. Experience has shown that this is the limit beyond which eccentricity occurs due to drill deflection. A programme of work is proposed which utilises electron beam welding to fabricate tubular segments to make up the longer length of thermowell required to penetrate into the centre of the larger square frames.

The final assembly stage to complete the pressure containment vessel of the target assembly involves EB welding the beam entry window to the main pressure vessel. The beam entry window forms an integral part of the target module and is EB welded to the front of the stack of 23 target plates. There will be a need to join the proposed square Zircaloy-2 frames to the stainless steel beam entry window. This is not possible by any process which involves the fusion of the two alloys because there is a tendency for brittle intermetallics to form which limit the strength of the joint. Also due to the thermal expansion mismatch between the two alloys cracks are often formed upon solidification of the weld pool.

HIP assisted diffusion bonding using a range of different thin intermediate layers to bridge the incompatibility of stainless steel and Zircaloy-2 offers a potential solution to the joining of the two alloys. This process enables bonding to take place in the solid state where it is possible to control the reaction products and therefore minimise the formation of the unwanted brittle intermetallic phases. A study will need to be carried out to optimise the nature and position of the interlayers and the HIP conditions necessary to produce metallurgically sound bonds.

2.4 Stage 3

Springfield adjusted depleted Uranium has been used so far for target production and this has well documented problems when subjected to irradiation. Some of these problems are reduced by adding molybdenum at the

rate of between 2 to 5 wt.-% to depleted Uranium to form an alloy. These alloys are less dense than the present material but will have greater resistance to radiation induced growth and swelling. Thus the neutron yield may be reduced slightly but the usable lifetime of the target will be increased. It would be beneficial to introduce this material into the front plates of the module which suffer the major damage and cause target failure whilst retaining the present material in the rear plates. That way the reduction in yield would be less noticeable but the benefits of longer lifetime would be gained.

Material casting and alloying techniques will need to be evolved and diffusion bonding trials will need to be carried out to test that the material is compatible with the existing manufacturing procedures.

2.5 Stage 4

The present 9cm diameter discs could be replaced by 9cm square blocks of similar thickness within the proposed square Zircaloy-2 frames. This would increase the volume of Uranium material in the target by about 20% and improve the coupling to the moderators. Engineering and diffusion bonding implications would need to be studied as part of a development programme.

3. NON URANIUM TARGET DEVELOPMENTS

The design of a new backup target is well advanced. The aim is to achieve the best possible neutron production from a non-Uranium target which is compatible with the remote handling facilities, disposal arrangements and the existing target cooling systems and which will require no changes to the Target Moderator Reflector Assembly,

These constraints are mainly met by retaining the pressure vessel design used for Uranium targets. Two materials have been considered namely Tantalum and the Tungsten/Iron alloy used for the LANSCE target. The Tungsten alloy has been chosen for the target as the neutron yield is about 15% higher than from Tantalum. The mechanical properties of tungsten under irradiation and thermal cycling are not well known and if the detailed design results in relatively thin block of Tungsten then this decision will be reviewed.

The gains from the geometry of the target will be achieved by using square blocks rather than the cylindrical geometry of the Uranium and existing Tantalum target. (Note that this gain could be achievable with Uranium and is the subject of Stage 4 of the development programme above.) The improvement in neutron fluxes from the moderators over the existing backup target will be about 30% thus giving fluxes about 60-65% of the Uranium target fluxes.

Commercially, the Tungsten alloy is sintered from powder and supplied in the form of hot pressed block. This has been found to have variable density, as low as 17 gm/cc compared to the expected density of 18.85 gm/cc. Also it is extremely difficult to produce holes in the block which limits the penetration depth of thermocouples to a few millimetres. A development program is underway to form the material using the Hot Isostatic Pressing technology which has the prospect of achieving uniform density and deep holes for thermocouples.

4. REFERENCE

[1] The ISIS Target A. Carne, T.A. Broome, J.R.Hogston and M. Holding
Proceedings ICANS X Los Alamos 1988
IOP Conference Series 97 (79)

Table 1. ISIS TARGET PERFORMANCE SUMMARY

Target	Gross Thermal Cycles	Integrated Current mAhr	Neutron Production mg
U#1	Not Measured	92.4	75
U#2	40000	53.1	52
U#3	10389	174.9	163
U#4	4147	138.8	130
Ta#1	18124	327.5	153
U#5	1541	106.0	97

Table 2. MONTHLY MEAN NUMBER OF TRIPS PER DAY AND MONTHLY TOTALS OF BEAM CURRENT ON TARGET

Month	Year	Trips/day	mAh	Target
September	1987	94	12.2	Uranium #2
October		367	11.0	
November		496	19.4	
December		640	10.4	
January	1988	75	27.1	Uranium #3
February		59	13.8	
June		56	19.6	
July		83	13.3	
August		76	37.1	
September		61	20.6	
October		61	43.2	
November		57	30.5	Tantalum #1
December		45	29.9	
March	1989	45	10.1	Uranium #4
April		36	40.4	
May		33	35.3	
June		32	10.7	
July		35	10.2	
August		40	32.3	
September		56	38.5	Tantalum #1
October		45	40.3	
November		49	31.4	
December		69	40.0	
April	1990	41	43.3	
May		33	34.9	
June		27	38.7	
July		24	10.6	Uranium #5
August		25	40.6	
September		26	54.8	

The calculation of trips/day only included those days when ISIS was running.

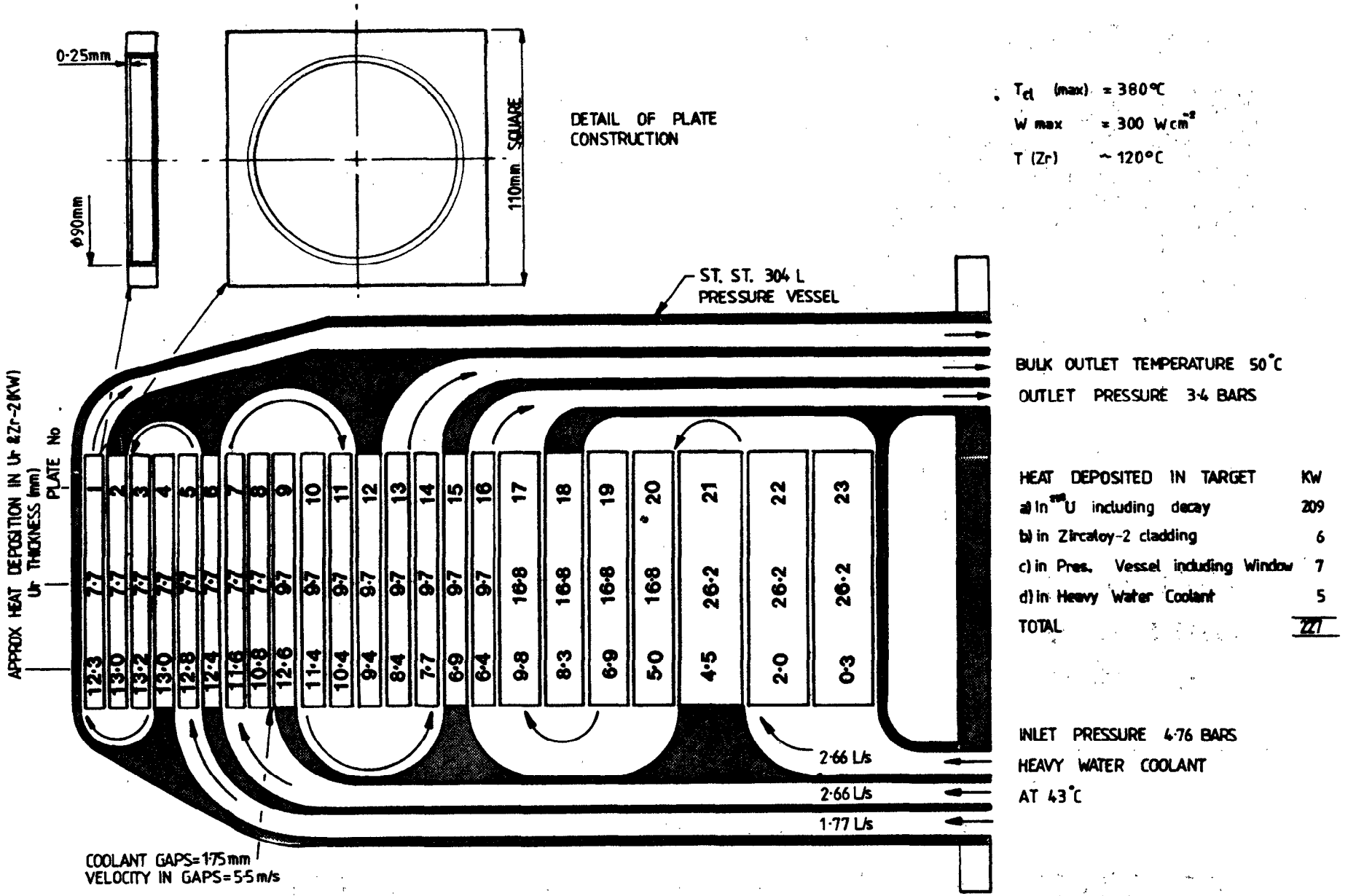

FIGURE 1 SCHEMATIC DIAGRAM OF ISIS URANIUM TARGET

Uranium targets 4 and 5

Accelerator trips per day

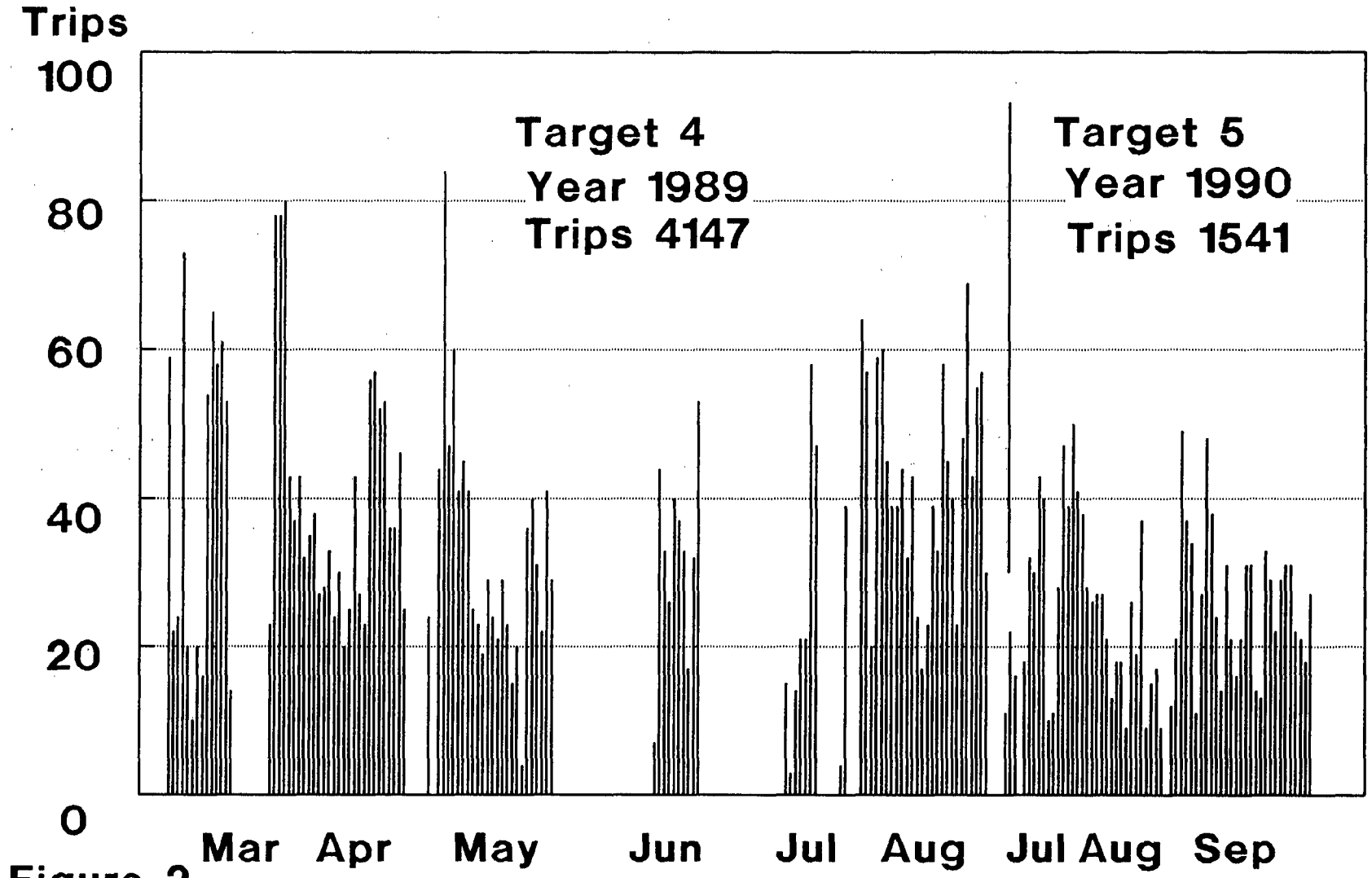

Figure 2

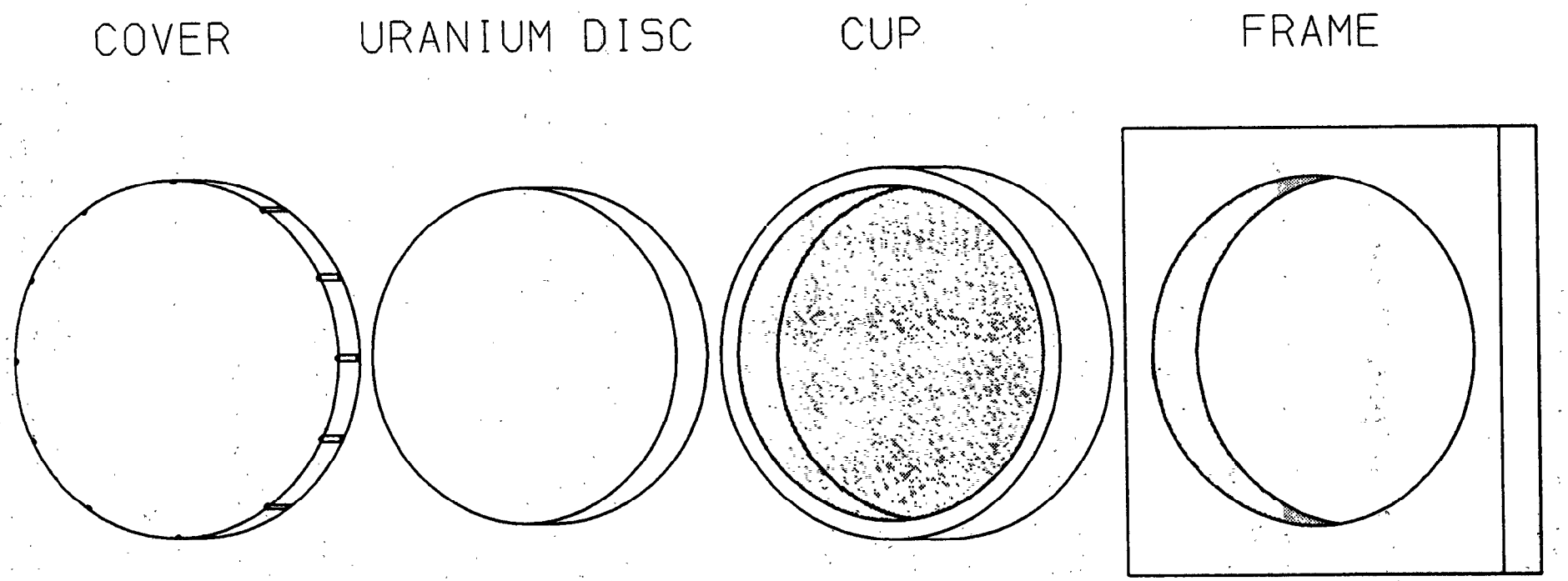

FIGURE 3 SCHEMATIC DIAGRAM OF A URANIUM TARGET PLATE

ICANS-XI International Collaboration on Advanced Neutron Sources
KEK, Tsukuba, October 22-26, 1990

The LANSCE Repair Project

Gary J. Russell, Harold Robinson, and Torben O. Brun
Los Alamos National Laboratory
Los Alamos, New Mexico USA

ABSTRACT

The LANSCE liquid-hydrogen moderator safely vented on July 2, 1990. Subsequent investigations showed two leaks in the hydrogen loop. We substituted water for liquid hydrogen and continued to run LANSCE through October 1990. This substitution was an interim solution for providing neutrons to the two instruments using the hydrogen moderator as a neutron source. For a long-term solution we will remove the liquid-hydrogen loop and replace the canister and associated piping for the liquid-hydrogen moderator. During this **LANSCE Repair Project**, we will also replace the LANSCE target. The goal of the project is to have the new target and hydrogen-moderator loop installed by the beginning of the 1991 run cycle for the Clinton P. Anderson Meson Physics Facility (LAMPF).

I. BACKGROUND

On July 2, 1990, the LANSCE liquid-hydrogen moderator[1] vented in a safe and controllable manner.[2] The LANSCE liquid-hydrogen moderator is depicted in Fig. 1. A vacuum gauge sensing the pressure in the hydrogen transfer-line jacket exceeded a preset trip point, signaling a valve to vent the hydrogen loop to the hydrogen vent stack. The overpressure resulted from one of the (three) helium compressors shutting down, which let the hydrogen system warm up, causing a "burp" (off-gassing from a cryopumped surface) and raising the pressure in the transfer line. The venting of the hydrogen loop is a normal shutdown procedure for such an occurrence.

Subsequent pressure tests with warm gas revealed two leaks:

1) *location*: in the hydrogen piping between the liquid-hydrogen and the transfer-line jacket
   leak diameter: 0.004 inches
   cause: failure in a transfer-line bellows

2) *location*: between the transfer-line jacket and the LANSCE crypt vacuum
   leak diameter: 0.065 inches
   cause: failure undetermined.

Since the LANSCE run cycle did not finish until the end of October 1990, an interim solution for providing neutrons to the instruments using the liquid-hydrogen moderator was to add a "stop leak" additive to the hydrogen loop and backfill the moderator canister

and piping with water. Figure 2 shows the calculated cold-source gain (neutron intensity from a liquid-hydrogen moderator to that of a water moderator). In Fig. 2, we also show the gain as measured by Hamilton and Smith[3], which demonstrates a penalty (intensity reduction) for the water moderator at long wavelengths. Because of this penalty, we decided to replace the hydrogen-moderator canister and associated piping with new components before the beginning of the LAMPF 1991 run cycle. This moderator replacement together with the replacement of the LANSCE target is referred to as the LANSCE Repair Project.

II. The LANSCE Repair Project

The objectives of the LANSCE Repair Project are to design, fabricate, test, and install the following by the beginning of the LAMPF 1991 run cycle:

- a new canister, associated piping, and transfer lines for the liquid-hydrogen moderator;
- new upper- and lower-tungsten targets, target canisters, and target-canister shrouds;
- new upper-crypt shielding;
- improved target (thermocouple) diagnostics; and
- better proton-beam diagnostics.

In addition, we will see if we can enhance moderator performance and increase the signal-to-noise ratio for all four LANSCE flux-trap moderators.[4]

III. ACKNOWLEDGEMENTS

We appreciate the support of Roger Pynn for this work. We thank Tatia Vander Maat for her typing help and Maria DiStravolo for proofreading the text on a very short notice. LANSCE work is supported by the US Department of Energy, Office of Basic Energy Sciences, under contract W-7405-ENG 36 with the University of California.

References

1. H. Robinson, et al., "The Los Alamos Liquid Hydrogen Neutron-Moderator System," in Cryogenic Properties, Processes and Applications 1986, A. J. Kidnay and M. J. Hiza, Eds.(American INstitute of Chemical Engineers, New York, New York, 1986), Vol 82, pp. 172-176.

2. J. H. Fretwell, et.al., "Review of the LANSCE Liquid-Hydrogen Moderator Problem," private communication.

3. W. A. Hamilton and G. S. Smith, private communication.

4. G. J. Russell, "Split-Target Neutronics," in these proceedings.

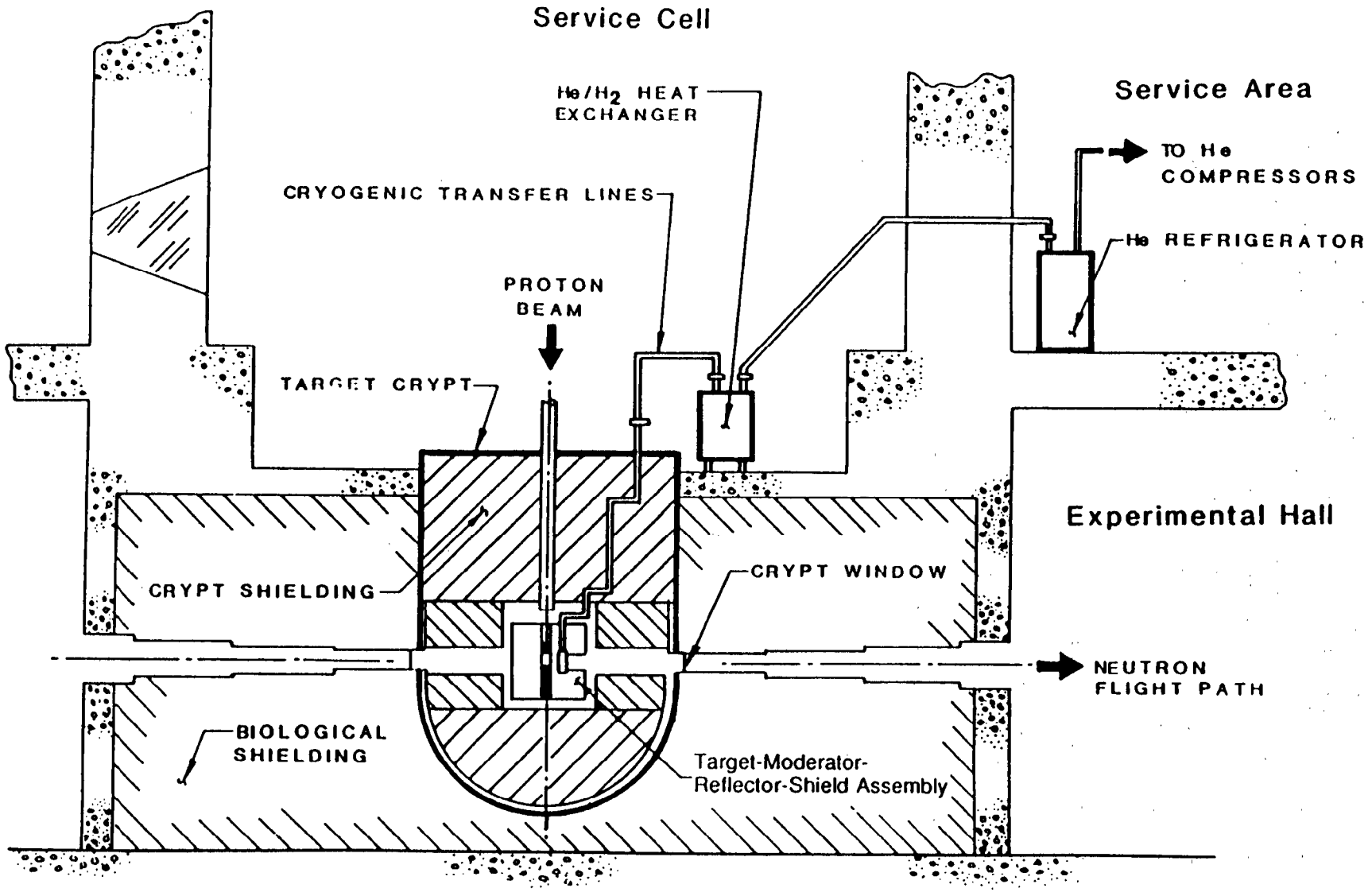

Figure 1. Section through the LANSCE target area, showing the location of the loop for the liquid-hydrogen moderator.

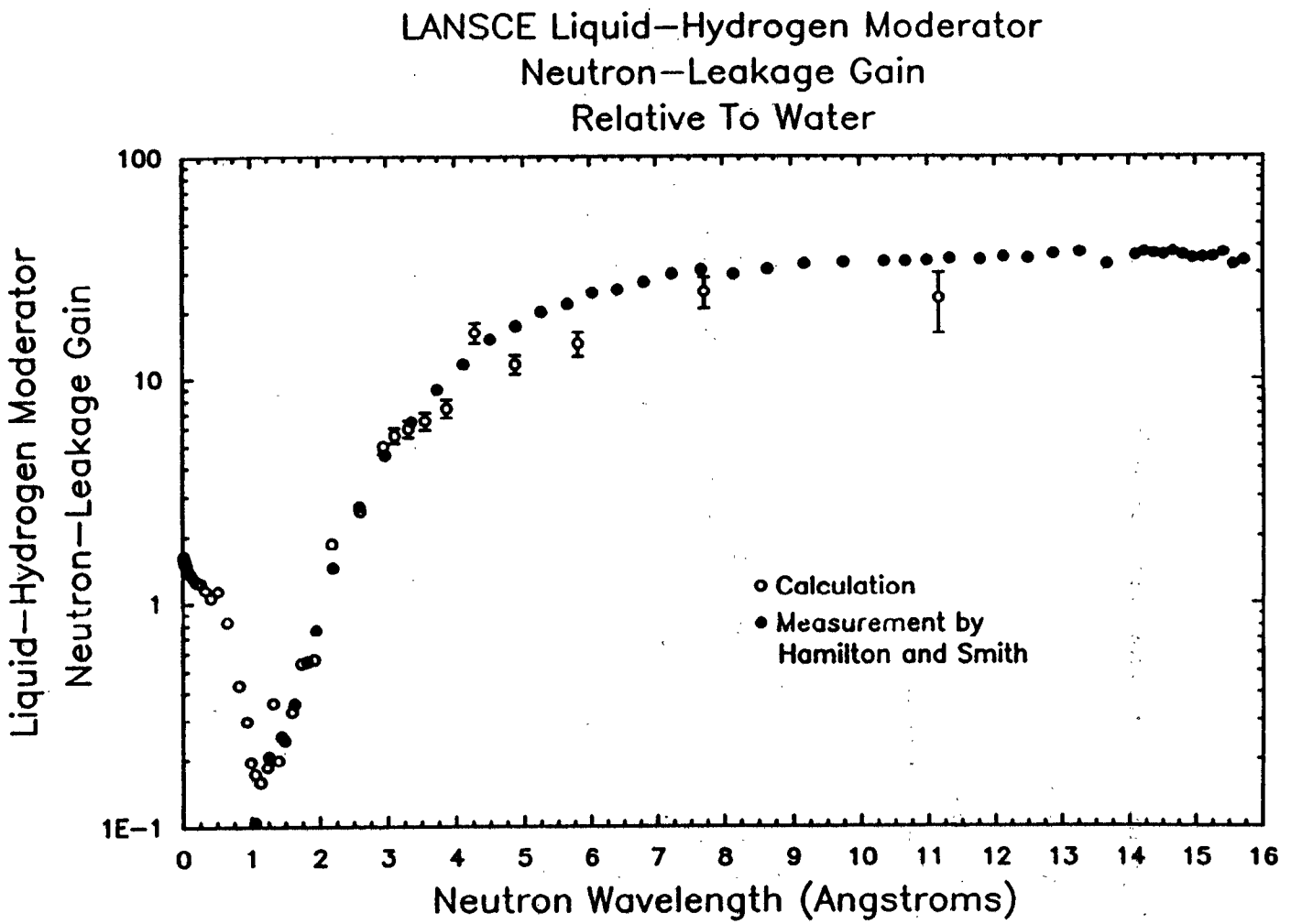

Figure 2. Comparison of calculated and measured neutron-leakage gain for the LANSCE liquid-hydrogen moderator.

ICANS-XI International Collaboration on Advanced Neutron Sources
KEK, Tsukuba, October 22-26, 1990

Thermofluid dynamics of liquid metal target of SINQ

Y.Takeda and W.E.Fischer

Paul Scherrer Institute
5232 Villigen - PSI, Switzerland

ABSTRACT
An experimental investigation on the thermofluid dynamics of the liquid LBE target for SINQ is in progress. The test section is a 1/2 scaled down mockup of the target with a maximum heat input of 200kW (heater pins are at the bottom inside a guide tube). Preliminary results up to 60kW show that generation of circulating flow is very efficient and fast. Relationships between the maximum temperature difference versus the input power and between the estimated velocity and input power both show the power law relationships as predicted by one-dimensional loop analysis. Experiments on flow patterns around the beam enterance window by flow visualization and ultrasonic technique (UVP) are also presented.

I. Introduction
The target of SINQ is a liquid Lead-Bismuth-Eutectic (LBE) contained in a double coaxial tube which forms a coaxial type loop. The proton beam enters the target from the bottom upwards and deposits its energy in the lower portion inside the inner tube (GT : guide tube), while heat exchangers are located at the upper part of the container. The natural circulation of LBE is utilized as primary cooling mechanism of this target. Details of this concept are given in [1].

A one-dimensional analysis reported earlier [1] concluded that this loop configuration exhibits simple overall behavior, high velocity level of LBE flow and maximum temperature below the specified temperature limit. The analysis also yielded useful power law relationships of the target performance with respect to the input power.

Over the past years an effort has been made to experimentaly investigate the thermofluid dynamics of the coaxial loop configuration using liquid LBE. Two test facilities were fabricated : a small scale experiment and a scaled-down target mockup. Some results are described in this report.

With regard to the cooling of the beam entrance window, an experimental investigation on the flow along the window using water was initiated. Some preliminary results are presented.

II. Summary of a one-dimensional analysis
A one-dimensional analysis of this loop configuration was reported in detail in [1,2] and it is briefly summarized here.

The analytical model is a loop which consists of two long vertical legs of the same diameter as the guide tube and of the height of the target. One leg corresponds to the inner flow channel of the guide tube and the other to the outer annular channel. Uniform internal heating is provided at the bottom of one leg and a heat exchanger at the top of the other. The heat exchanger is simulated by a volumetric heat sink. By assuming a constant flow area over the loop and by neglecting the effects arising from turns at the both ends, the problem becomes one dimensional. The governing equations are the coupled system of the momentum and energy equation. By neglecting the thermal

conduction in the liquid, a closed solution can be obtained for temperature distribution, as schematically shown in Fig.1.

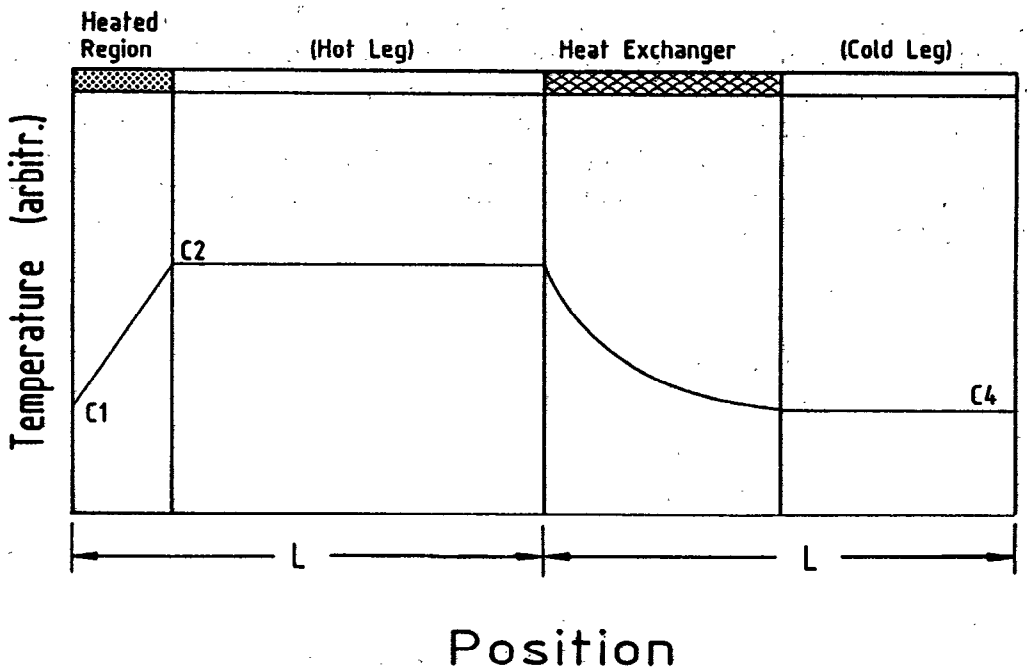

Fig.1 Typical vertical temperature distribution of the one-dimensional natural circulation loop. Left half corresponds to the hot leg and right half to the cold leg. See [1,2]

Extreme examples can be examined by this solution for the temperature distribution, giving several useful relationships on the target performance. (D, the volumetric heat deposition rate, h, height of the heated region, L, target height, Q, uniform volumetric heat deposition rate, T, temperature, v, velocity.)
The steady state velocity is related to the input power as,

(1) $v \rightarrow Q^{1/3}$

Therefore, the steady state velocity is proportional to the cubic root of beam power.
The maximum temperature is,

(2) $T_{max} \rightarrow Qh/DL$

It is linearly proportional to the input power but inversely to D and L.
The maximum temperature difference in the system is expressed as,

(3) $dT_{max} \rightarrow Q^{2/3}$

III. Liquid metal experiments

1. Experimental Facility

Fig.2 shows an illustration of the experimental facility prepared for the liquid metal experiments. It mainly consists of test sections for the Small Scale Experiment (SSE), the scaled-down Mockup (MUP) experiment and a common water loop for both the SSE and MUP. The SSE has two identical test sections ; one is for thermofluid dynamic testing and the other for corrosion testing. The water loop used for cooling maintains an outlet (supplying) temperature of 130°C and a maximum inlet (returning) temperature of 200°C (16 bars). The maximum cooling capacity is designed to be 200 kW. Each test section has its own LBE reservoir tank and LBE is always stored and frozen in this tank, not in the test section.

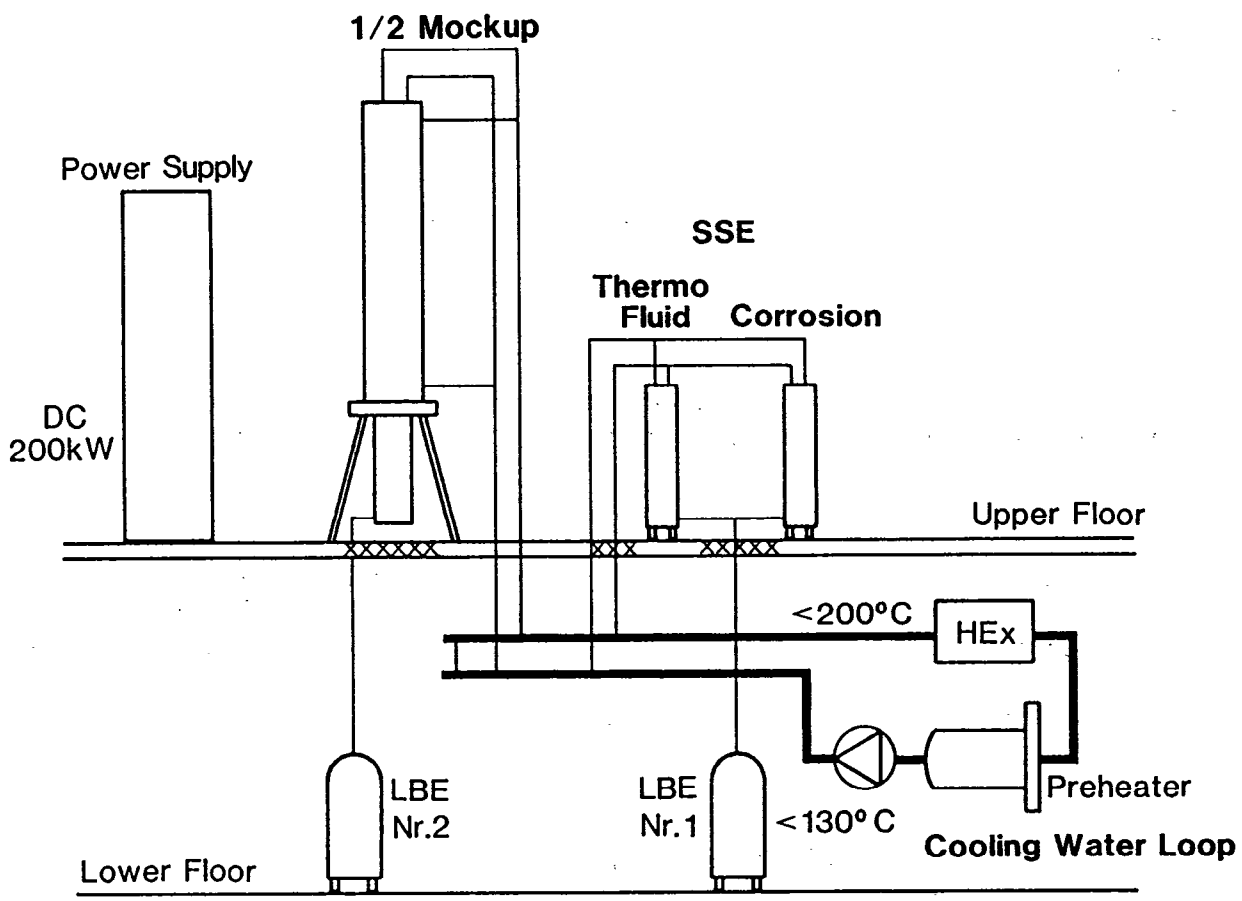

Fig.2 Schematic of the experimental facility for thermofluid dynamics of liquid LBE.

Test sections

The dimensions of the test sections are listed in Table 1 together with those of the actual SINQ target. The SSE was prepared for gaining experience in handling liquid metal and as such, configuration and instrumentation were assembled in a one-dimensional sense. The MUP is a scaled-down (1/2 scale) mockup for two-dimensional temperature distribution measurements. Whereas heating SSE is provided from the outside of the container wall, the MUP has 12 heater pins inside GT. The guide tube materials are quartz glass for the SSE and a stainless steel for the MUP.

Table 1 Dimensions of scaled Test Sections

	SSE	Mockup	SINQ
Diameter (Lower)	133.3	96	180
(Upper)		134.5	370
Height	885	1701	3340
GT diameter	100	64	123
LBE inventory (Ltr)	11	12	160
Max power (kW)	20	200	650
Heating	Outside container	Heaters inside GT	Proton beam

MUP

The MUP facility is a scaled-down mockup, as shown in Fig.3. The scaling factor is 1/2. At present, the heat exchangers are annular shell type for both the inner (within GT) and outer coolers. The lower part of the test section is insulated to approximate an adiabatic condition for heat transfer. Heat is supplied at the bottom inside GT with 12 specially fabricated heater pins affixed to a bottom flange (Photo 1). The maximum heat input with all pins is designed to be 200kW.

For measuring temperature distributions, 196 thermocouples are installed in the test section. The data acquisition system is a simple extension of the existing system which is described in an earlier report [3]. The system is monitored with the separate system which measures temperatures with 28 TCs, mass flowrate of cooling water etc.

Operation

After LBE was transported into the test section from the reservoir tank, it was left for several hours without heating in order to provide a stagnant state as an initial condition. Trial operation without such a well defined initial state resulted sometimes in the generation of a reversed flow.

Sudden heating was possible only for small heat input. This restriction is dictated by the initial sharp temperature rise inside the heater pins. Thus, the transient measurement of the temperature distribution was available only up to 25kW. For larger power, the input power was gradually increased in small steps. This was also the case for the terminating transient. An abrupt power cut can destroy the heater structure.

Data collection was made throughout the operation of the experiment with a sampling time of 5 seconds, so that a two-dimensional temperature history could be reviewed.

2. Experimental Results and discussion

SSE

1D vertical temperature distribution

The average vertical temperature distribution under steady state conditions in the SSE is plotted in Fig.4. The general behavior is in good agreement with the one-dimensional prediction. There is a sharp temperature increase in the heated region, a flat distribution above this region, a large temperature decrease in the cooled region, and again a flat distribution below. A slight discrepancy is observed in the adiabatic region. This is due to the heat conduction in the liquid as obtained by the numerical calculations including this effect [2]. In the top region, the distribution is considerably distorted because of the existence of the GT supporter.

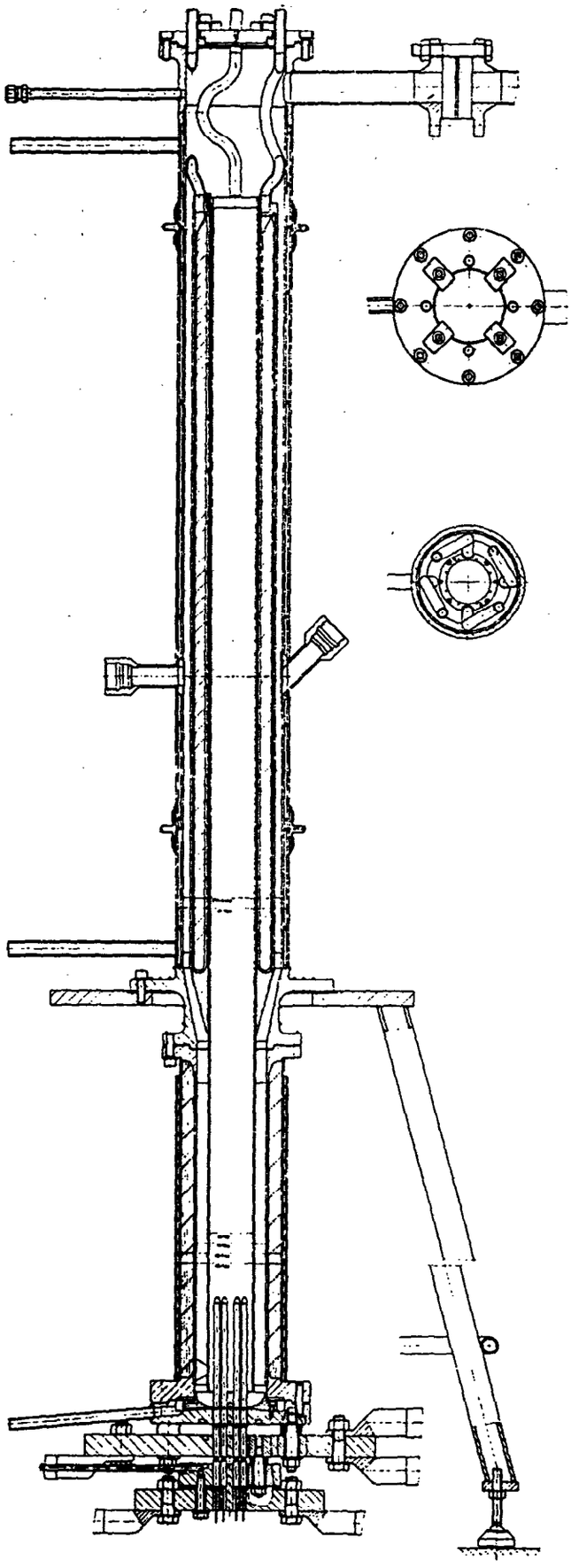

Fig.3 Detailed schematic of the mockup experiment (MUP).

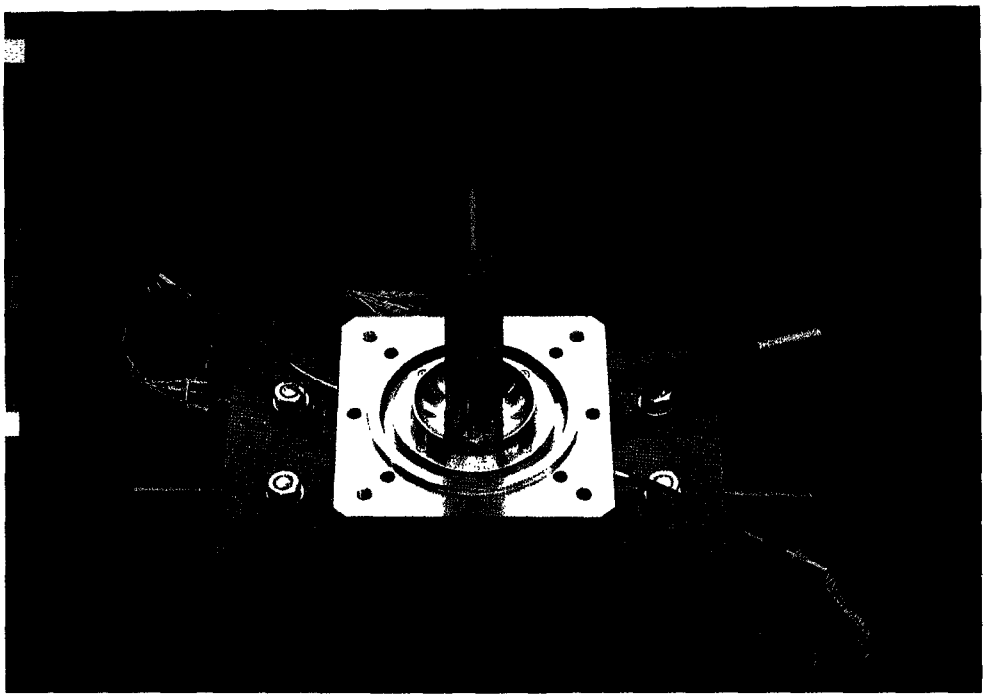

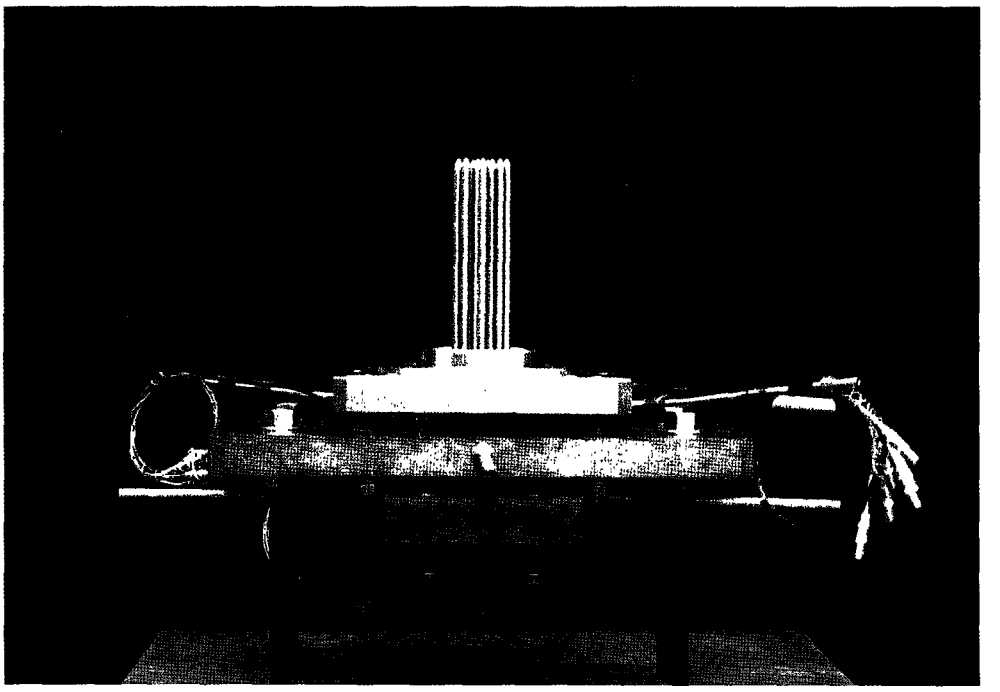

Photo 1 Heting arrangement of mockup experiment (MUP). A 12 heater pins assembly affixed to the bottom flange. Maximum heat output is 200 kW.

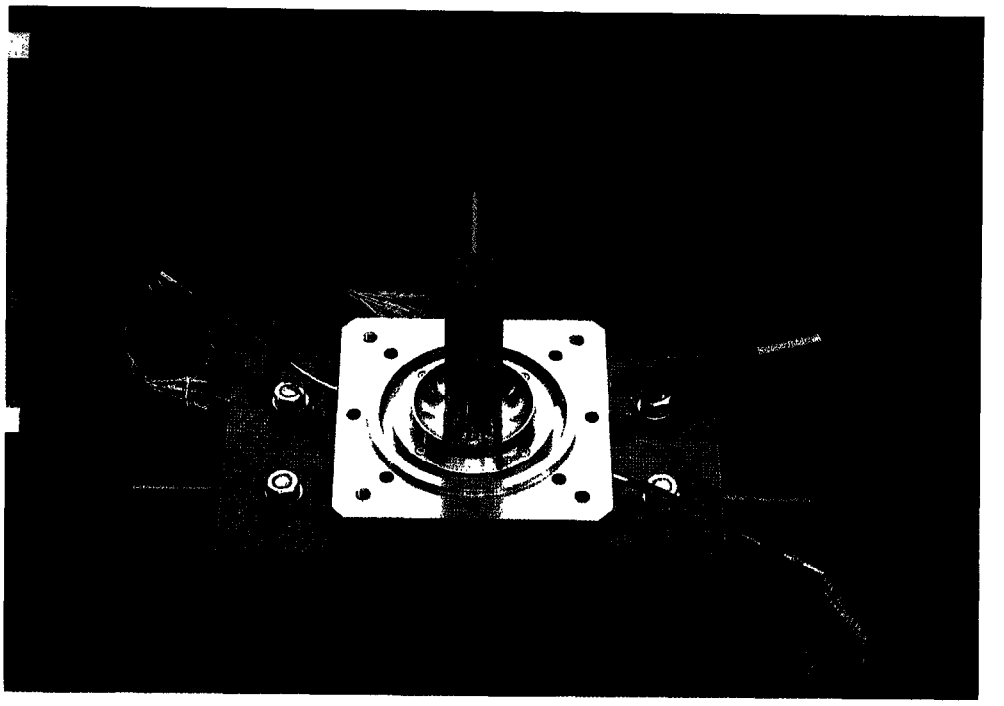

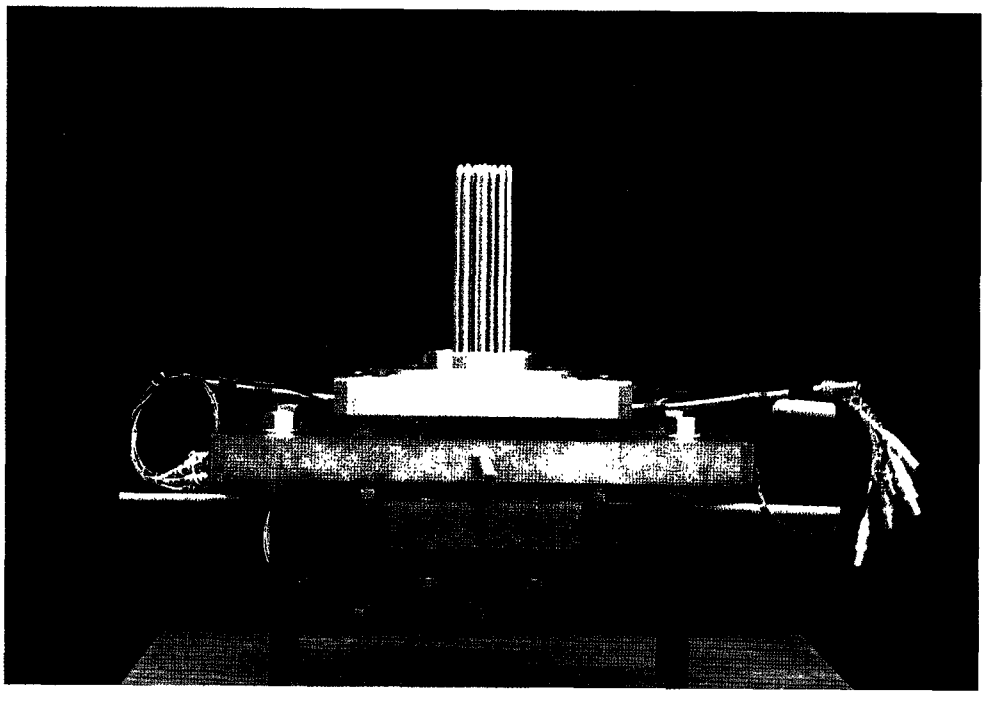

Photo 1 Heting arrangement of mockup experiment (MUP). A 12 heater pins assembly affixed to the bottom flange. Maximum heat output is 200 kW.

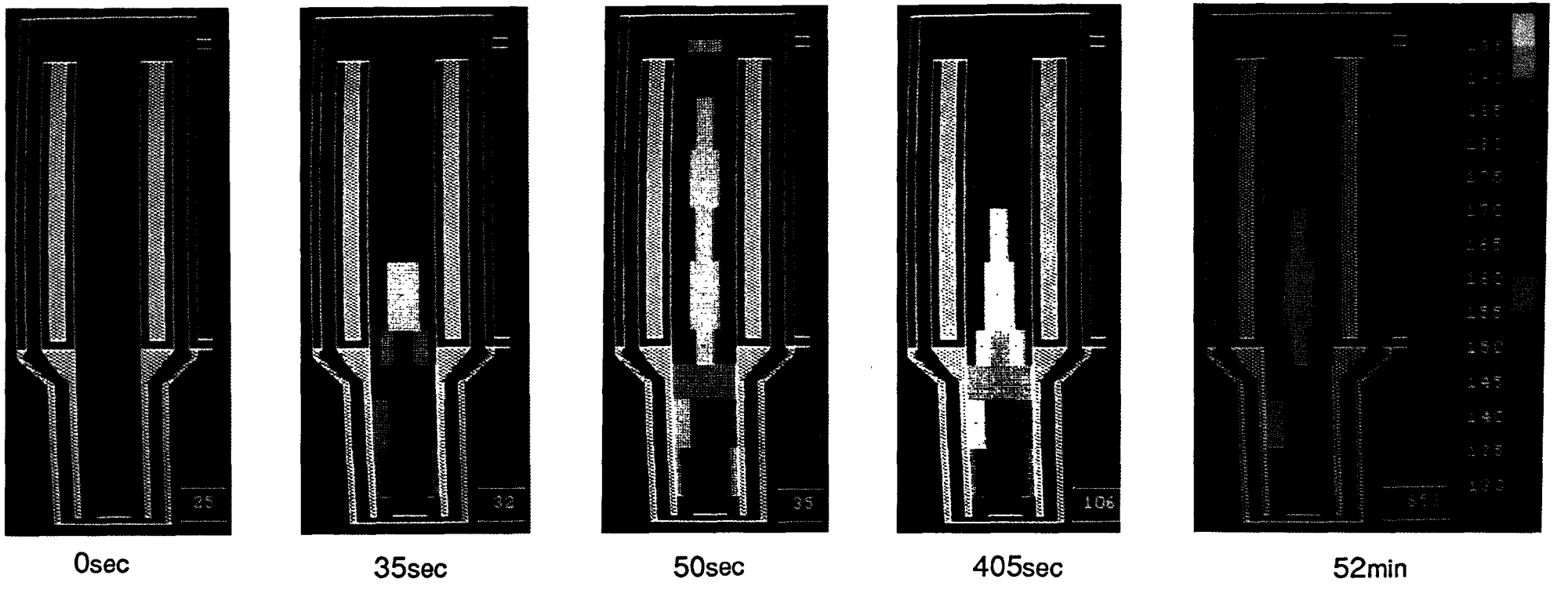

Fig.5 Time variation of two-dimensional temperature distribution after sudden start of heat input in the MUP (25 kW).

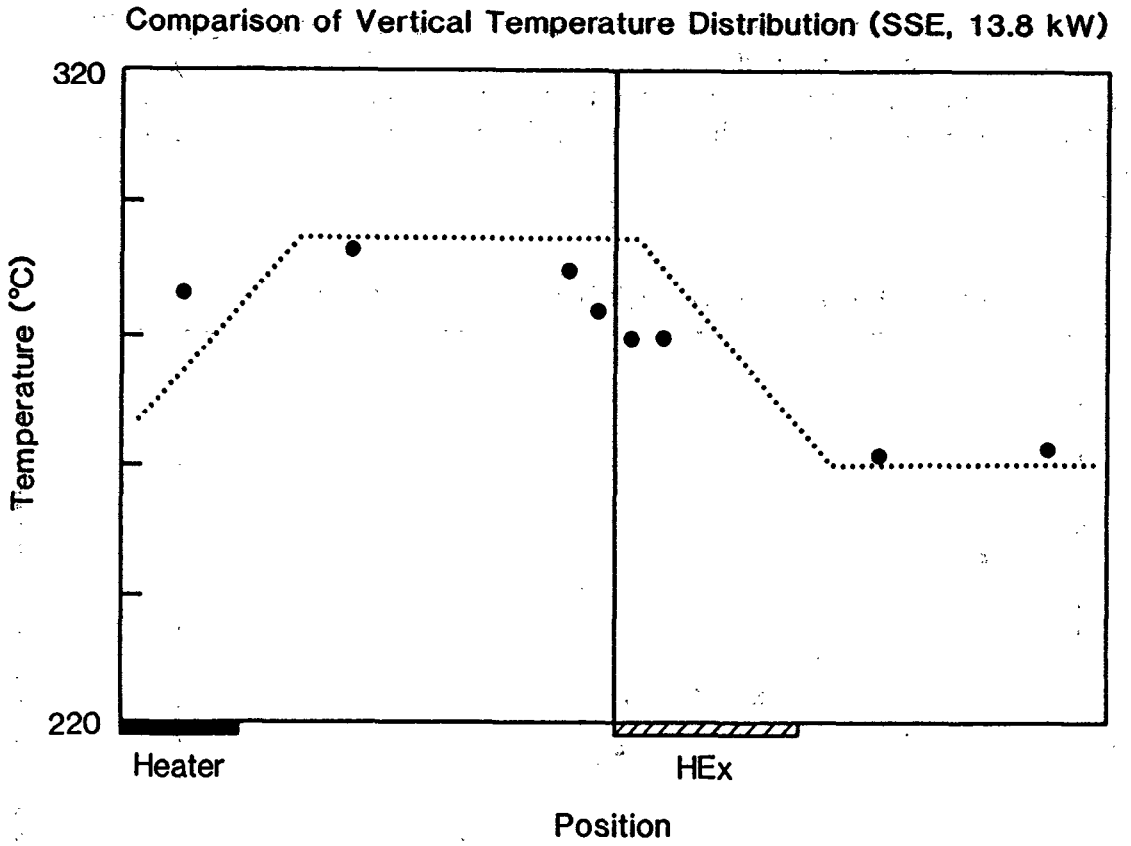

Fig.4 Measured and calculated vertical temperature distributions in SSE (13.8 kW). For numerical calculations, see [2].

MUP

2D temperature distribution

The variation of the 2D temperature distribution after a sudden power input (25 kW) is shown in Fig.5. After the beginning of heating, only a few minutes are needed until the temperature distribution becomes almost similar to that of the steady state. During this initial transient period, the hot region inside GT quickly spreads, which indicates a generation of uprising flow inside the GT, leading to a start of the natural circulation in the system. In the steady state distribution, the existence of an uprising flow inside the GT and the turning at the upper space are clearly seen.

1D temperature distributions

Vertical : Fig.6 is a vertical temperature distribution averaged over radius, angle and time. The overall behavior of this distribution is in fairly good agreement with the analytical prediction as can also be seen in SSE. However, several discrepancies have been found. There is a large temperature decrease inside the GT toward the top. This is considered to be mainly due to the cooling by the internal heat exchanger.

A large temperature increase can be seen in the annular channel at the bottom region near the heated region. A slight temperature increase was also seen in SSE, which is an effect of heat conduction in the liquid. However, this effect is much larger in the MUP, mainly due to the heat transfer through the GT wall from the inside to outside because of the larger thermal conductivity of the GT material. The heat transfer through the GT wall may correspond to the heat deposition outside the GT due to widening of the beam. It is known from a 1D analysis that this does not effect the bulk velocity of LBE but that it elevates the maximum temperature of the system [2]. These

results suggest that further investigation on the effect of a thermal conductivity of GT materials and/or a structure of GT should be made.

Temperature fluctuations observed at the position just above heater pins and at the top of the LBE layer are due to three-dimensional effects arising from the existence of heaters and cooler-supporters.

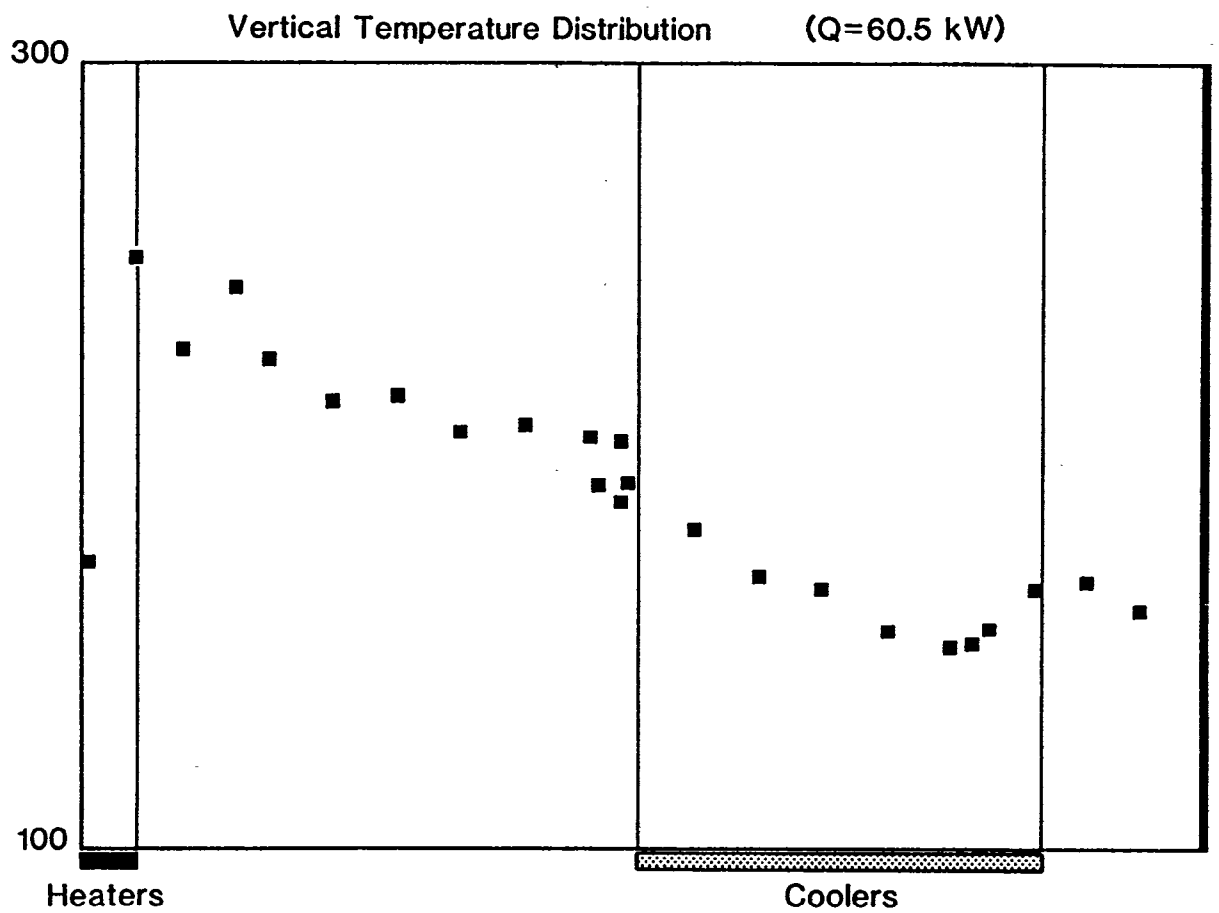

Fig.6 Vertical temperature distibution in the MUP at 60.5 kW. Averaged over radius, angle and time.

Horizontal : Fig.7 shows horizontal temperature distributions at various heights of the test section averaged over angle and time. There is a clear temperature difference between the inside and outside of the GT at all positions, which is the driving force of the natural circulation. In the lower region below the heat exchanger (eb 2 and 3), the temperature decreases monotonically outward, while in the upper region it shows a small dip at the wall of the inner heat exchanger. The former clearly indicates heat transfer through the GT and the latter is due to cooling by the internal heat exchanger. The temperature difference between the inside and outside the GT becomes smaller and the temperature distribution is flatter for the higher positions.

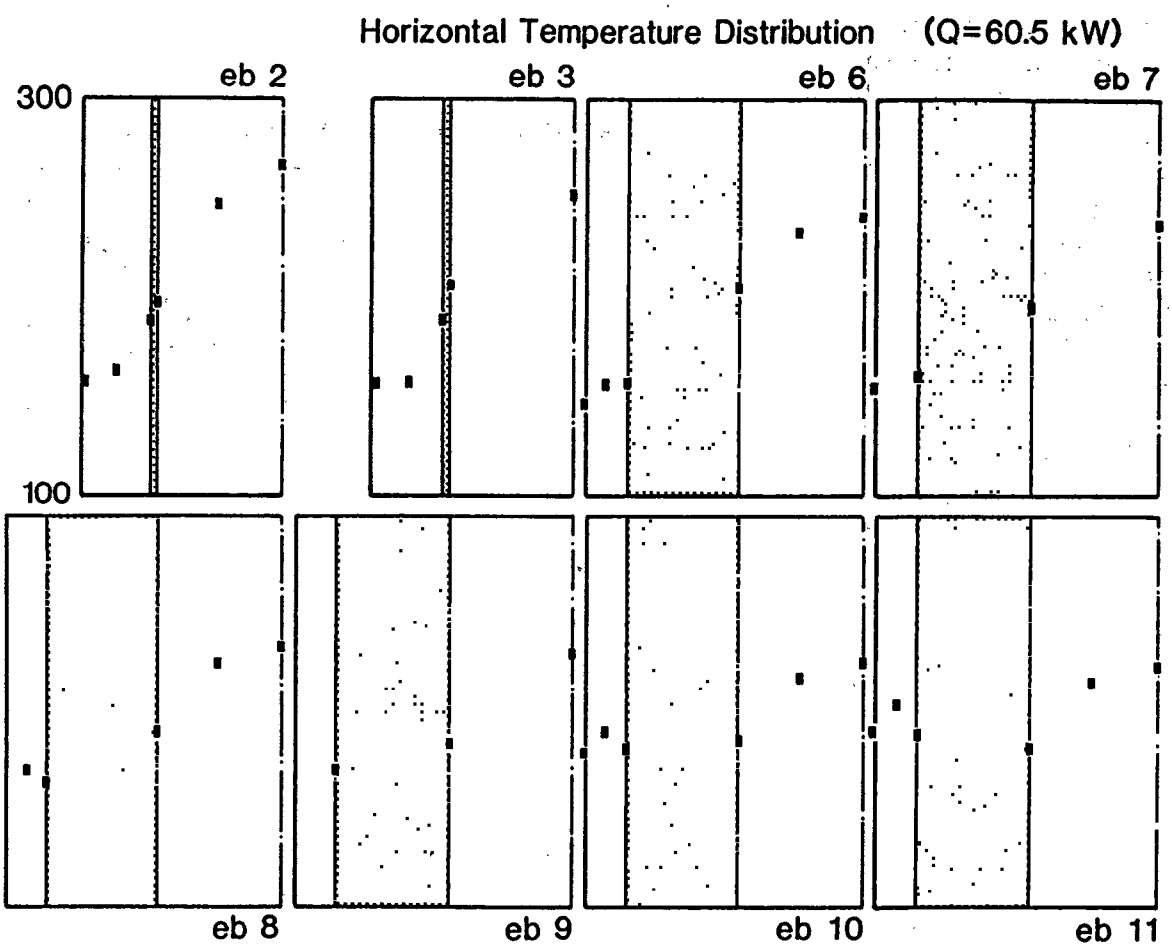

Fig.7 Horizontal temperature distributions. Same conditions as Fig.6.
Heights are eb2=18.0cm, eb3=33.5cm, eb5=53.2cm, eb6=60.2cm, eb7=80.2cm, eb8=100.2cm, eb9=120.2cm, eb10=140.2cm and eb11=160.2cm from the bottom.

Thermofluid performances of target

The maximum temperature difference in the system was estimated from temperatures at 30 cm above the heated region and at a point exiting the cooling region at the outer annular channel. This temperature difference is plotted with respect to the input power in Fig.8. It shows clearly a power law relationship as predicted by 1D analysis. The power coefficient is 0.58, which agrees well with the prediction of (Eq.3).

The bulk velocity of the circulating LBE have been estimated from an energy balance of liquid temperature flowing through the heated region, and plotted versus the input power in Fig.9. This also shows a very good power law relationship with a power coefficient of 0.33, while the predicted value is 1/3 (Eq.1).

In conclusion, the power law relationships derived from the one-dimensional analysis have been confirmed by experiments in LBE. They are useful for predicting the thermofluid performance of the target. Based on this knowledge, the temperature difference in the system at full power operation is extrapolated to be 244°C. Using another scaling law approach (Eq.2), this gives a maximum temperature of roughly 250°C. Both are below the specified operating temperature of 350 - 400°C.

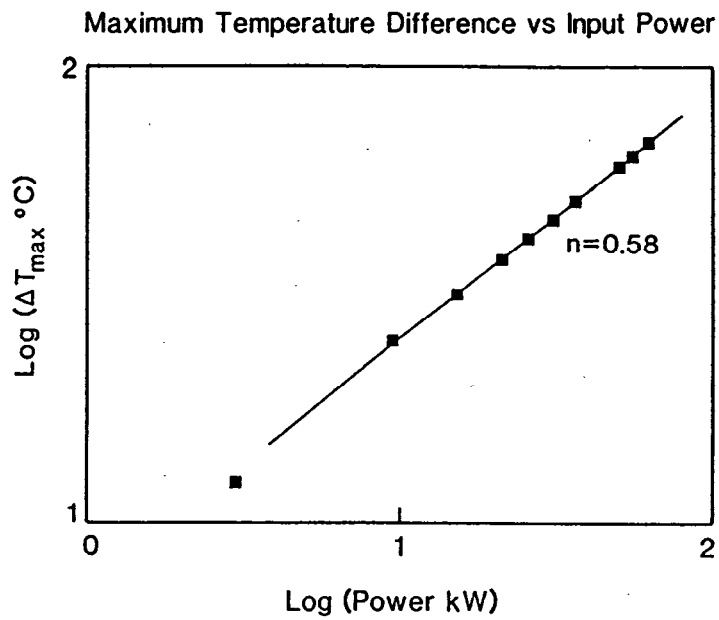

Fig.8 Target performance : Maximum temperature difference in the system versus input power.

IV. Window experiments

An investigation of the flow patterns of target liquid along the beam entrance window is in progress using water. So far, several window geometries have been tested by flow visualization technique ,and several qualitative facts have been obtained. The generation of a stagnant fluid layer in the peripheral pocket can be avoided by making the radius of the peripheral bend equal to the gap distance. The position of GT edge above the window is very important. The flatter central part generates a large stagnant layer in the central region above the window wall. With this knowledge, a cusp-shaped window was taken as a final design. A representative result of the flow visualization is shown in Photo 2. As can be seen in the photo, a stagnant layer does not appear and flow is totally smooth on the window wall. This leads us

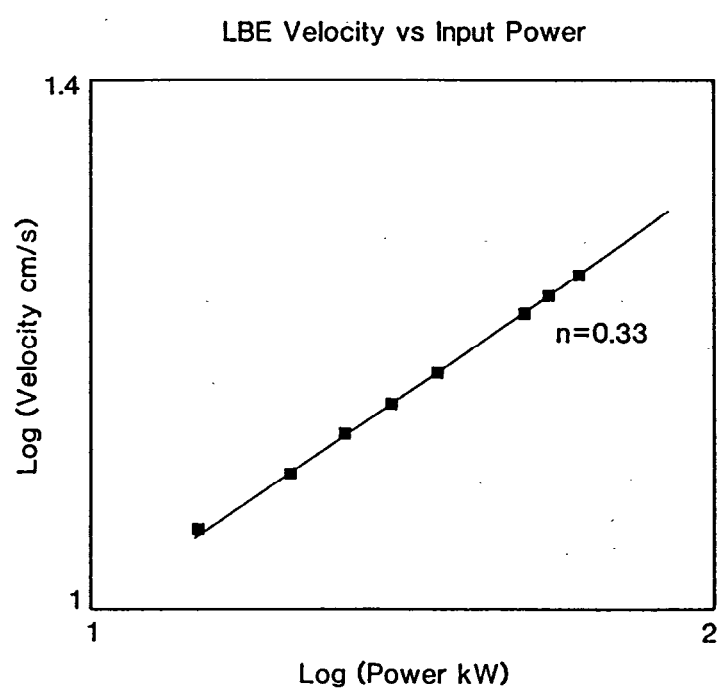

Fig.9 Target performance : Bulk velocity of LBE versus input power.

to expect that the window is sufficiently cooled by LBE. On the other hand, the development of a boundary layer on the inside wall of the GT becomes significant.

Further investigations are in progress using LBE. One method is flow visualization by neutron radiography and another by an ultrasonic velocity profile monitor. Fig.10 shows preliminary results from quantitative measurement of the vector flow field around the window using the water. The same technique will be applied to the liquid metal experiments.

Reference

1 . Y.Takeda, A Natural circulation loop as a target, ICANS-IX, 196, p259
2. Y.Takeda & W.E.Fischer, Thermofluid behavior of the SINQ target, ASME Int. Symposium on Natural Circulation, 13-18 Dec. 1987, Boston
3. Y.Takeda, Development work for the liquid lead bismuth target of SINQ, ICANS-VIII, 1985, p220

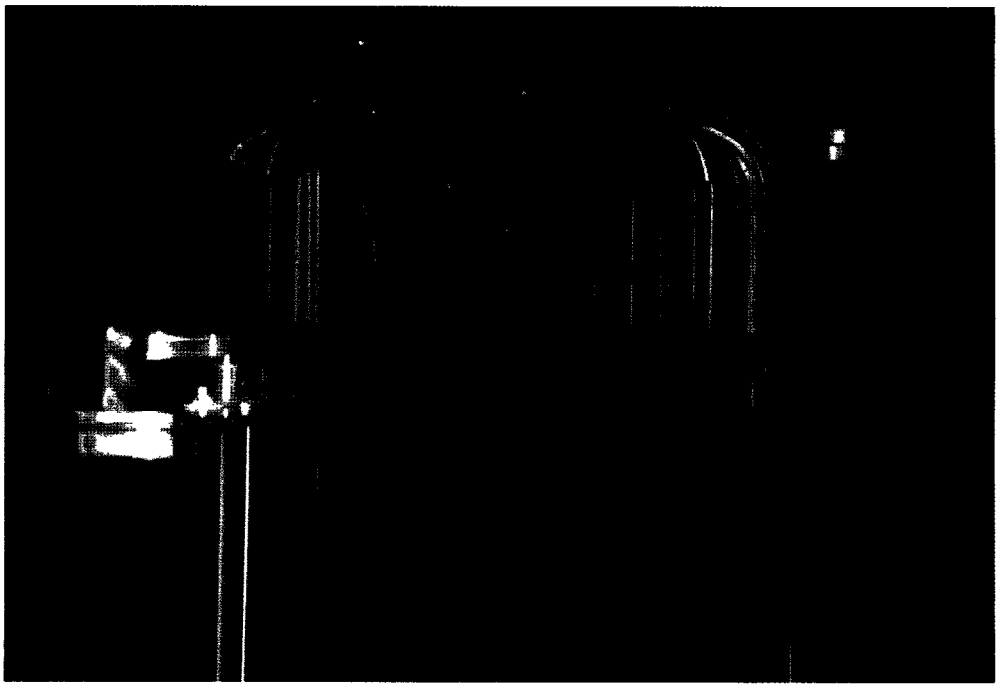

Photo 2 An example of flow visualisation of flow along the target window.

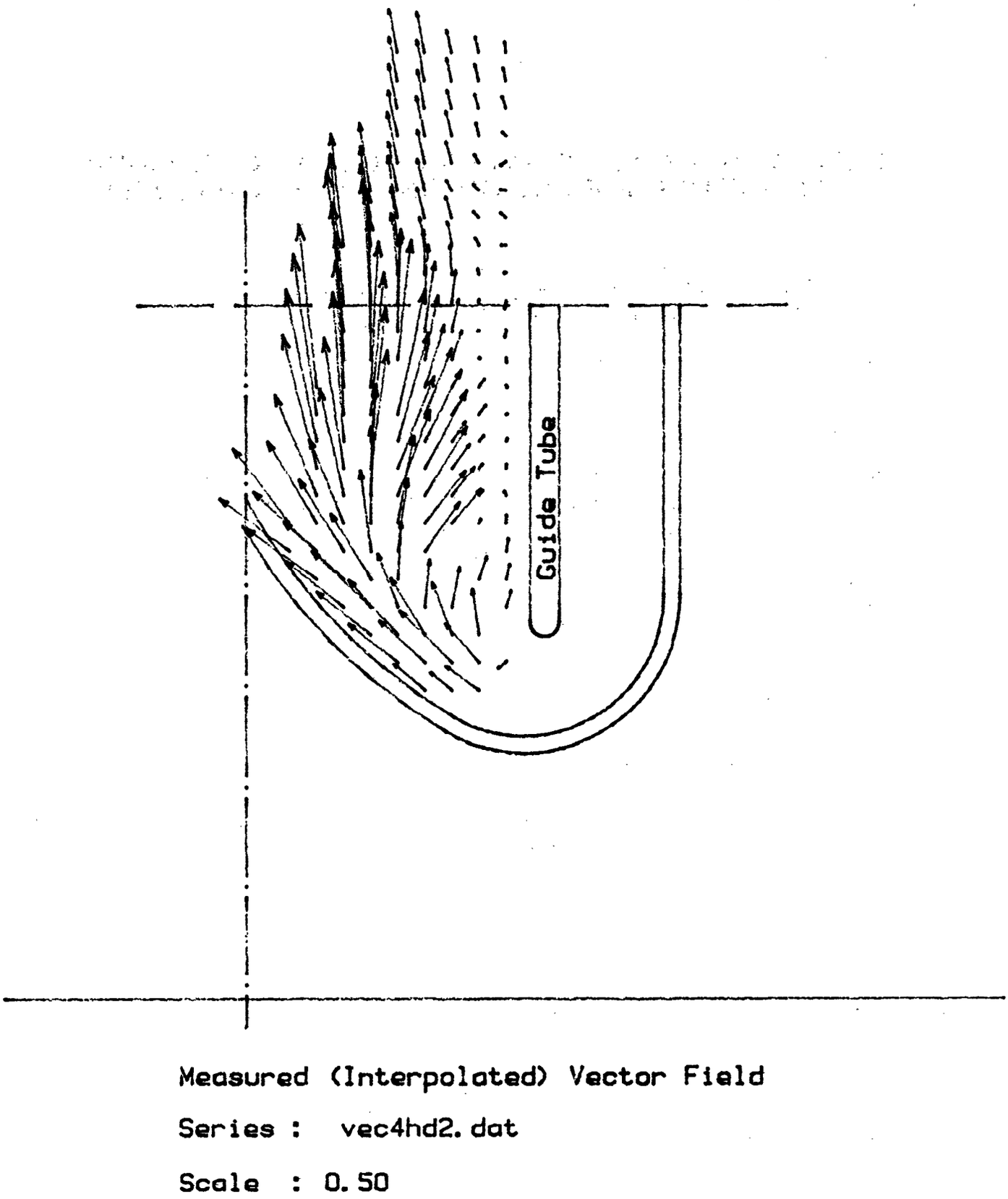

Fig.10 Measured velocity field around the target window.
(Water model, gap=1d, G=300l/h)

ICANS-XI International Collaboration on Advanced Neutron Sources
KEK, Tsukuba, October 22-26, 1990

THERMAL-HYDRAULICS INVESTIGATIONS FOR THE LIQUID LEAD-BISMUTH TARGET OF THE SINQ SPALLATION SOURCE

B. Sigg, Swiss Federal Institute of Technology, Nuclear Engineering Laboratory
T. Dury, M. Hudina, B. Smith, Thermal-hydraulics Laboratory

Paul Scherrer Institute, 5232 Villigen, Switzerland

Abstract

The paper contains a discussion of the thermal-hydraulic problems of the target which require detailed analysis by means of a two- or three-dimensional space- and in part also time-dependent fluid dynamics code. There follows a short description of the general-purpose code ASTEC, which is being used for these investigations, and examples of the target modelling, including results. The final part of the paper is devoted to a short discussion of experiments against which this application of the code has to be validated.

1 Introduction

In an earlier phase of the project, thermal-hydraulics analysis of the SINQ Liquid Lead-Bismuth Target was mainly based on experimental investigations and simplifying engineering calculation methods [1,2,3]. Later, it was found that detailed computations of the fluid dynamic phenomena had to be undertaken, in order to adequately predict temperature distributions and resulting thermal stresses occurring in the target structures, under all kinds of operational conditions. This applies mainly to the target windows, because recently detected uncertainties with respect to the proton beam profile require accurate predictions of thermal stresses to be made for cases of extreme thermal load.

2 Target description

The reference target of the SINQ Spallation source consists of a vertical liquid lead-bismuth-eutectic (LBE) column contained in a chromium-steel vessel (see Fig.1). The proton beam enters the target through a triple-walled window from below and deposits its energy mainly within the lower 0.3 m of the target. For a nominal beam current of 1.5 mA, a thermal power of 650 kW has to be removed. This is done by natural circulation of the LBE, which rises through a central guide tube to the top of the liquid column and then descends via a heat exchanger, situated in the annulus of the target container. The heat exchanger consists of a cluster of 24 water-cooled pins, distributed uniformly in the annulus. Water enters a pin by flowing down inside an inner tube and exits via the pin annulus. The closure arrangement at the bottom of the target consists of a lower, double-walled safety window, cooled internally by water, and an upper, cusp-shaped window, cooled by the LBE itself (see Fig.2). Further details on window design are given in [4]. Natural circulation within the target is not generated solely by the proton beam itself. During beam shut-down, electrical heater rods, with a total power of 40 kW and which are installed inside the guide tube above the beam-heated region,

cause sufficient pre-circulation of the target liquid to allow the proton beam to be started up within about 20 seconds.

Fig.1 also shows auxiliary heating/cooling ducts for melting/freezing of the LBE. For the transfer of the target to a near-by repository, the LBE will be solidified to reduce transportation risks. Further technical data can be found in Table 1.

3 Thermal-hydraulics problems of the target arising during normal operation, transients and malfunctions

The thermal-hydraulics problems of the target are mainly related to the task of ensuring integrity of the windows under all operating conditions, which means demonstrating that thermal stresses and temperatures remain within safe limits. The main source of concern lies in the variability of the proton beam profile. This is caused by the requirements of the users of Target E, a meson target which lies upstream in the beam channel, and by imperfect reliability of the beam control system. For the window region of the SINQ target the proton beam current density can be considered a combination of the following two, roughly Gaussian, distributions:

$$j(r) \approx \frac{J_1}{\pi\sigma_1^2}\, e^{-\frac{r^2}{\sigma_1^2}} + \frac{J_2}{\pi\sigma_2^2}\, e^{-\frac{r^2}{\sigma_2^2}} \tag{1}$$

where: J_1, J_2 = total currents of components, with $J_1 + J_2 = 1.5$ mA
$\sigma_1^2 = 1.8$ cm^2
$\sigma_2^2 = 19$ cm^2
r = Radius from beam axis.

The first term in (1) is due to protons by-passing Target E and the second to protons scattered in Target E.

If it was possible to guarantee window integrity during continuous operation with the full beam being unscattered by Target E, this would, of course, considerably simplify the target safety issue. For the design calculations, the preliminary assumption has been made that the peaked part of the beam contributes one third of the total beam, i.e. $J_1 = 0.5$ mA.

There are, of course, other parts of the target container where thermal-stress problems could arise, e.g. in the structures around the window, the lower portion of the guide tube, and the entry section of the pin coolers, where hot LBE with an undulating free surface flows by and causes thermal stressing in the walls. Additional stress problems are brought about by normal operational transients and exceptional situations due to special malfunctions. Details on window design and stress analysis calculations can be found in [4] and [5].

Table 2 presents a summary of cases which have to be analysed by means of thermal-hydraulic and stress calculations. These computations have to be repeated, if necessary, in the course of an optimisation of the target geometry (Window shape, materials of the guide tube, its distance from the window and shape at the bottom edge, geometry of pin coolers, etc.).

Adequate solutions to the resulting thermal-hydraulic calculational problems can only be obtained by means of advanced fluid dynamics codes which have the ability to solve the two- and three-dimensional, steady-state and time-dependent thermal-hydraulic differential equations in complex geometry. Beside geometrical complexity, there are a number of thermal-hydraulic phenomena which warrant the use of such a code:

1) On the window surface an internally-heated boundary layer develops. Together with the power density and geometry of the window, the velocity distribution within this layer, its thickness and its turbulent structure will determine the window temperature distribution. These properties deviate from those of

an ordinary plane boundary layer because of buoyancy forces, surface curvature and flow geometry (converging flow).

2) Behind the lower edge of the guide tube and, under special conditions, also on the surface of the window, flow detachment can occur.

3) During transients, other buoyancy-induced flow distributions may form above the window which can give rise to different window cooling behaviour. This is of particular importance for start-up transients with inadequate pre-circulation.

4) For the investigation of safety-relevant incidents, it is preferable to be able to make best-estimate calculations instead of having recourse to worst-case analyses.

The ASTEC code [6,7] was chosen to perform the necessary calculations because of its flexibility and its proven ability in solving natural convection problems [8]. Additionally, our special contacts with the code developers will guarantee good support in the event of code-running difficulties.

4 Short description of ASTEC

ASTEC solves, in general, a porous-medium form of the thermal-hydraulic, time-dependent partial differential equations in a finite volume approximation [6,7]. Fluids may be compressible or incompressible, and there is an option for the solution of additional mass transport equations. For incompressible fluids, ASTEC treats the thermal-hydraulics equations in the Boussinesq approximation. In regions of turbulent open flow (no porous medium), ASTEC solves, if required, the $k - \varepsilon$ turbulence model transport equations in order to determine space-dependent turbulent viscosities and diffusivities.

The finite-volume approach combines the flexibility of the finite-element method with the numerical stability of finite difference schemes. It allows one to subdivide the three-dimensional solution domain into hexahedra (8-node elements) of arbitrary shape. Finite volumes are formed around the corner points (nodes) according to a special geometrical procedure (see Fig.3). For the purpose of the numerical approximation, all variables are discretised at the nodes, except pressures, which are stored at the element centres.

The time-dependent discretised equations are solved by means of the time-implicit SIMPLE algorithm [9], adapted to the finite-volume arrangement of grid points. A hybrid skew-upwind scheme is optionally used for the advection terms to reduce false diffusion. Steady-state solutions are obtained by calculating a "false" transient, using very large time steps.

The code has a number of features which allow complicated problems to be solved:

- Several disconnected fluid regions with different material properties are possible.
- Heat transfer between fluids and solids may be modelled by prescribed heat transfer coefficients, if the code is not to perform an explicit boundary layer calculation.
- Additional modelling can be implemented using Fortran subroutines supplied by the user.
- The programming is adapted to vector-processing machines, an advanced version also to transputers.
- Packages for interactive pre- and post-processing (mesh generation, data analysis) are available.

ASTEC has been validated against some benchmark cases and the natural-convection experiment SONACO, which was performed at PSI [6,8,10].

5 Some results of ASTEC calculations for the SINQ-target

An ASTEC model of the target is shown in Figs. 4+5. It consists of a 22.5^0 sector of the cylindrical target, the smallest sector which allows explicit modelling of the pin coolers. Each face of the wedge model is a plane of symmetry. The central downflow-tube of the pin coolers is simulated by an annulus for simplicity, and heat transfer across the inner tube (water-to-water heat exchange) is modelled by means of heat transfer coefficients. For locations within the LBE itself, the meshing near surfaces is made sufficiently fine for the code to resolve the thermal boundary layer. The model shown in the figures has 9420 nodes and 7906 elements, and the cpu time needed to complete calculation of a stationary case is about 2-3 hours on the Cray-2 of ETH Lausanne.

In a first series of calculations, effects of window shape and guide tube insulation were investigated. Figs. 6-9 compare results of velocity and temperature distributions for a domed and a cusp-shaped window. Obviously, the latter must receive much better cooling near the target axis, since window temperatures near the centre are found to be much lower than for the domed window. In both cases no flow detachment occurs on the window surface itself, but a zone of recirculating flow forms inside the bottom end of the guide tube. Maximum velocities rise from about 0.6 m/s in the case of the domed window to about 0.7 m/s for the cusped one.

The one-third fraction of the beam reaching the SINQ target unscattered is responsible for the high window temperatures in the centre. When the full beam is diffuse, maximum temperatures for the domed window are reduced by about 400^0C.

Temperature distributions along the axis of the target show a rapid drop from the window into the fluid and a subsequent increase due to volumetric heating (see Figs. 10+11). The large temperature difference between the window surface and the relatively cool fluid layer above illustrates the importance of proper fluid flow and heat transport modelling in the boundary layer.

Using an insulating instead of a thermally conducting guide tube leads to somewhat lower temperatures in the window region ($\approx 20^0$C less) and to a slightly higher LBE circulation rate. Figs. 12+13 compare the axial temperature distributions on the outside surface of the guide tube for cases with thermally-conducting and insulated wall, respectively. The effect does not seem to be important enough to justify the resulting material and shielding complications caused by employing an insulating guide tube, although it must be said that heat exchange between the riser and the annulus leads to mixed-convection flow effects, i.e. slightly higher turbulent heat exchange and friction. Since buoyancy forces near the guide tube oppose the overall circulation forces, however, no problems with discontinuity of heat transfer coefficients and friction factors occur as in the case of buoyancy-aided flow [11].

In Figs. 14+15 temperature distributions around the pin circumference and in a cross-section of the annulus near the bottom of the cooling pins are shown. The variations around pins are not excessive and should not give rise to thermal-stress problems. The transverse temperature distribution at the bottom of the bundle shows that a current of relatively warm liquid issues from the subchannels between the inner pin coolers, whereas overcooled liquid exits near the outer wall. The arrangement of the pins could be somewhat better optimised, although the overall efficiency of the cooling arrangement seems to be acceptable. In the calculation there were 8 pins in the innner ring and 16 in the outer. A 9/15 arrangement could enable the pins to be more uniformly spaced in the annulus, though this geometry would increase the number of meshes needed for the ASTEC model. In addition, it is questionable whether such an arrangement could noticeably improve the cooling efficiency beyond that of an optimised 8/16 configuration.

Further ASTEC calculations are in preparation. These use a finer mesh near the centre of the window, to reduce discretisation errors in the temperature field computation. Transient calculations to investigate time-dependent window temperature distributions for the analysis of transient stresses are also in progress. They

will be carried out on a restricted window-region model, with prescribed velocity distribution at the inlet to avoid excessive computer time.

6 Benchmark experiments

Although ASTEC has been validated against a number of experiments [6,8,10], additional testing of the code on experiments closely related to the SINQ target geometry is considered necessary.

The first benchmark is to be the half-scale mock-up test of the target described in [12]. Its results will serve to test ASTEC with respect to integral performance, i.e. circulation rate, transient behaviour, and heat transfer to coolers.

A second experiment, called TACOS (Target Cooling Simulation), is intended to compare ASTEC calculations with measured temperature and velocity distributions in the window region. The experiment simulates flow conditions above the window and heat transfer from the window surface to the LBE stream but does not include volumetric heating. Sodium has been chosen as the simulant fluid, because of the possibility of performing the experiment in a new on-site sodium loop. The design of the TACOS test section is shown in Fig.16. It will allow the exchange of the heated part of the window as well as the lower end of the guide-tube, and variation of the distance between the bottom of the guide tube and the window. Temperature measurements will be made by means of themocouples above and below the window membrane, on the tips of a movable rake, and at various positions along the walls. Movable permanent-magnet velocity probes will enable measurements of velocity profiles to be made across the annulus and riser. There are two inlet chambers to the test section, allowing asymmetric flow distributions across the window to be generated.

The auxiliary heaters below the inlet chambers are needed for the production of temperature fluctuations. These are intended to be used in correlation analyses for determining the circumferential flow distribution in the annulus.

The setting-up of this special TACOS experiment for the testing of ASTEC is necessary because of the complicated fluid dynamic phenomena occurring in the window region, and by the strong influence which the window shape exerts on the temperatures, as exemplified by the results of ASTEC for the domed and cusped windows.

7 Conclusions

The complicated geometry of the SINQ target and the high heat load to which the target windows are exposed warrant the use of the advanced, thermal-hydraulics code ASTEC.

First results show the importance of optimising the window geometry, but more refined calculations are still needed to give better details of window temperature distributions near the central axis.

Additional benchmarking of the code, as described in the paper, is recommended in order to test its integral performance and particularly its ability to adequately predict temperatures in the window region of the target.

References

[1] Ch. Tschalär: Proc. ICANS-V, Jülich 1981.

[2] Y. Takeda: Proc. ICANS-VII, Chalk River 1984, AECL 8488.

[3] Y. Takeda: Proc. ICANS-IX, Villigen 1986.

[4] M. Dubs, J. Ulrich: These proceedings.

[5] G. Heidenreich: These proceedings.

[6] R.D. Lonsdale, R. Webster: The application of finite volume methods for modelling three-dimensional incompressible flow on an unstructured mesh.
Proceedings of 6th International Conference on Numerical Methods in Laminar and Turbulent Flow, Swansea, July 1989.

[7] R.D. Lonsdale: ASTEC, Release 1.7B: Users Manual, 14th Nov. 1989, AEA Technology, Dounreay.

[8] G. Robinson, R.D. Lonsdale, T.V. Dury: Comparisons between experimental results and numerical simulations for the SONACO sodium natural convection experiments. Proc. of the 4th Int. Conf. on Liquid Metal Engineering and Technology, 17-21 Oct. 1988, Avignon, Vol.2, p.411.

[9] S.V. Patankar: Numerical Heat Transfer and Fluid Flow. Hemisphere Publ. Corp. 1980.

[10] R.D. Lonsdale: An Algorithm for Solving Thermal-Hydraulic Equations in Complex Geometries: The ASTEC Code.
Int. Top. Meetg. on Adv. in Reactor Physics, Math. and Computation, April 27-30, 1987, Paris.

[11] M.A. Cotton, J.D. Jackson: Comparison between Theory and Experiment for Turbulent Flow of Air in a Vertical Tube with Interaction between Free and Forced Convection. ASME Winter Annual Meeting 1987, Symposium on Combined Free and Forced Convection.

[12] Y. Takeda, W.E. Fischer: These proceedings.

Table 1: Characteristics of SINQ-target

Geometry (see also Fig.1)

Height of LBE column: 3343 mm
Outer diameter in moderator region: 180 mm
Outer diameter in pin cooler region: 370 mm

Thermal-hydraulics:

Target fluid:
Thermal power with nominal beam (1.5 mA) P = 650 kW
LBE circulation rate $M \approx 37$ kg/s

Pin coolers:
Water inlet temperature $T_{in} = 128\ ^0C$
Water outlet temperature $\overline{T_{out}} = 147\ ^0C$
Total flowrate $\dot{M} = 8.0$ kg/s
Total number of pins: 24

Table 2: Normal and safety-related operational conditions of target to be investigated

1) Stand-by operation:
   - Pre-circulation by auxiliary heaters
2) Start-up transients:
   - Normal beam power ramp
   - Too-steep ramp
   - Narrow-beam ramp
   - Beam start-up with insufficient pre-circulation
   - Restart of cooling after overheating incident
3) Full-power operation
   - Design case
   - Too-large fraction of beam by-passing Target E
   - Failure of secondary cooling
   - Impeded circulation due to guide tube defects or loose parts
   - Rupture of water-cooled safety window causing water spray on lower surface of LBE window
4) Shut-down transients
   - Normal case
   - After beam control malfunction or operator error (beam profile, start-up ramp)
   - After insufficient cooling
   - After failure of safety window.

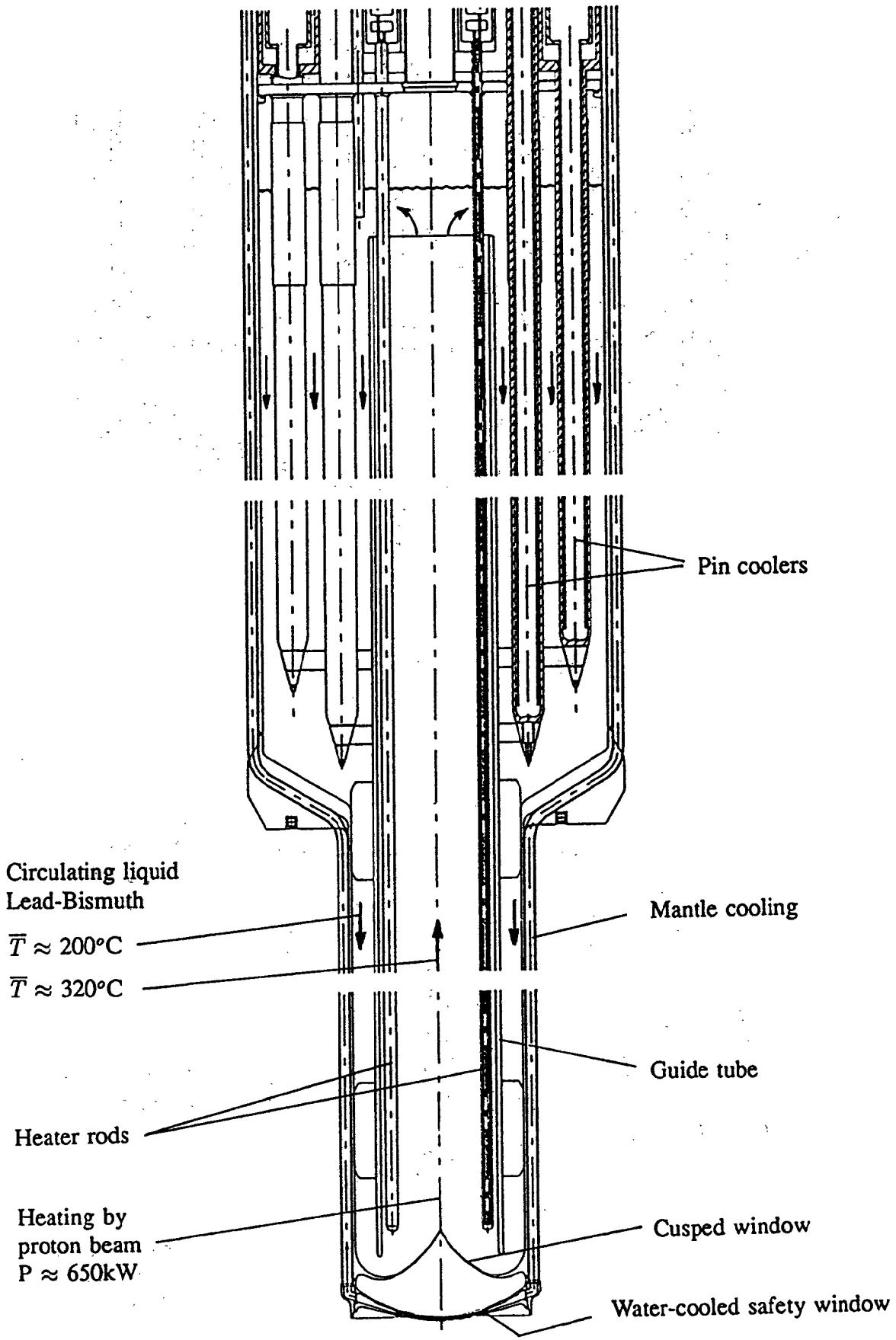

Fig.1 Sketch of SINQ target

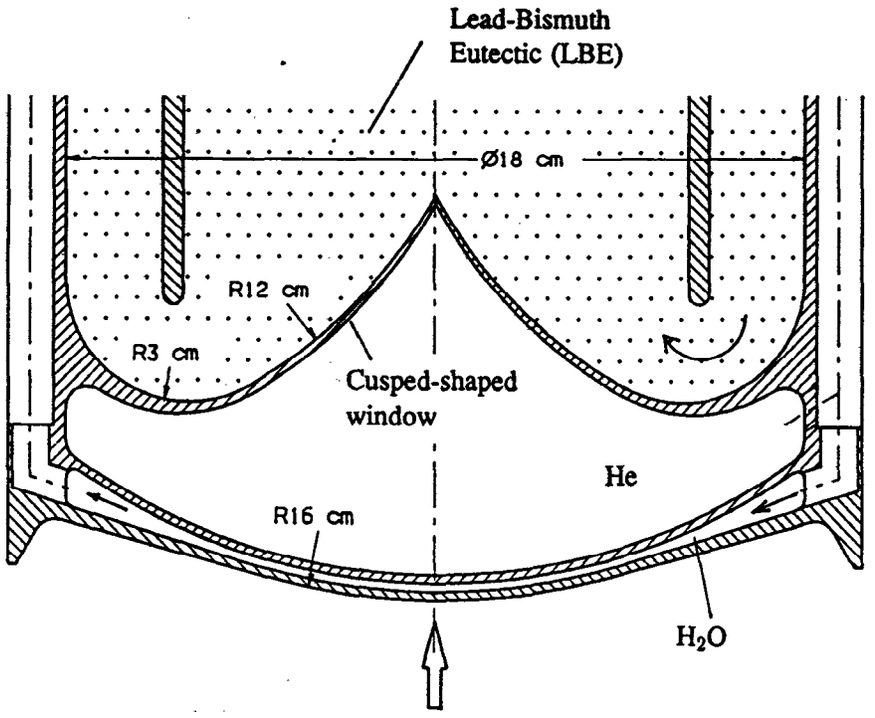

Fig.2 Cusp-shaped window design

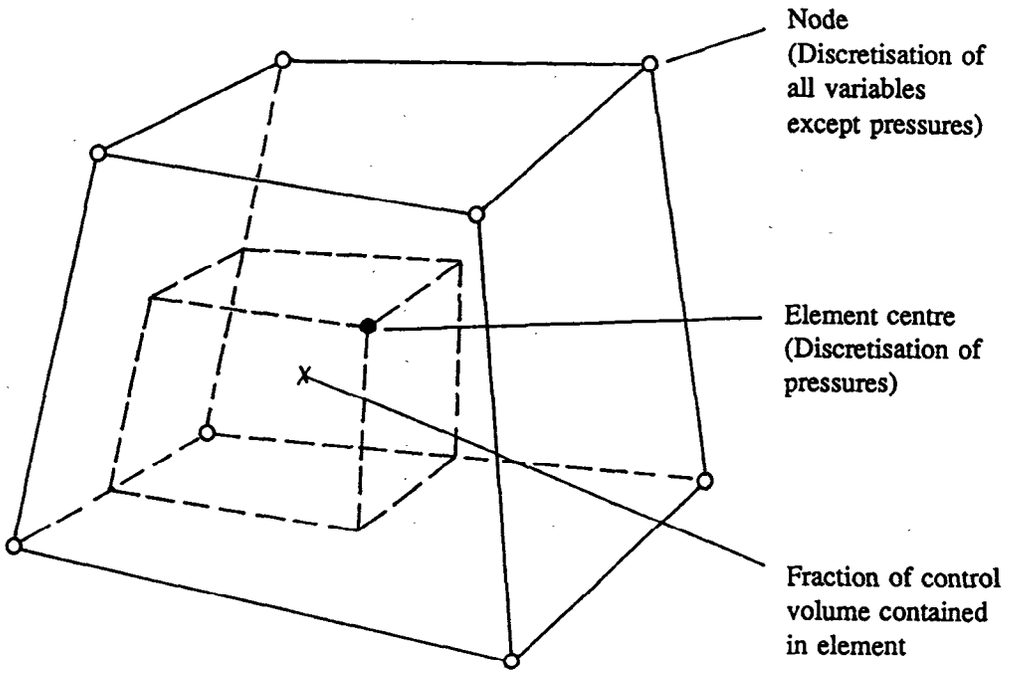

Fig.3 An 8-node element used for 3d meshes

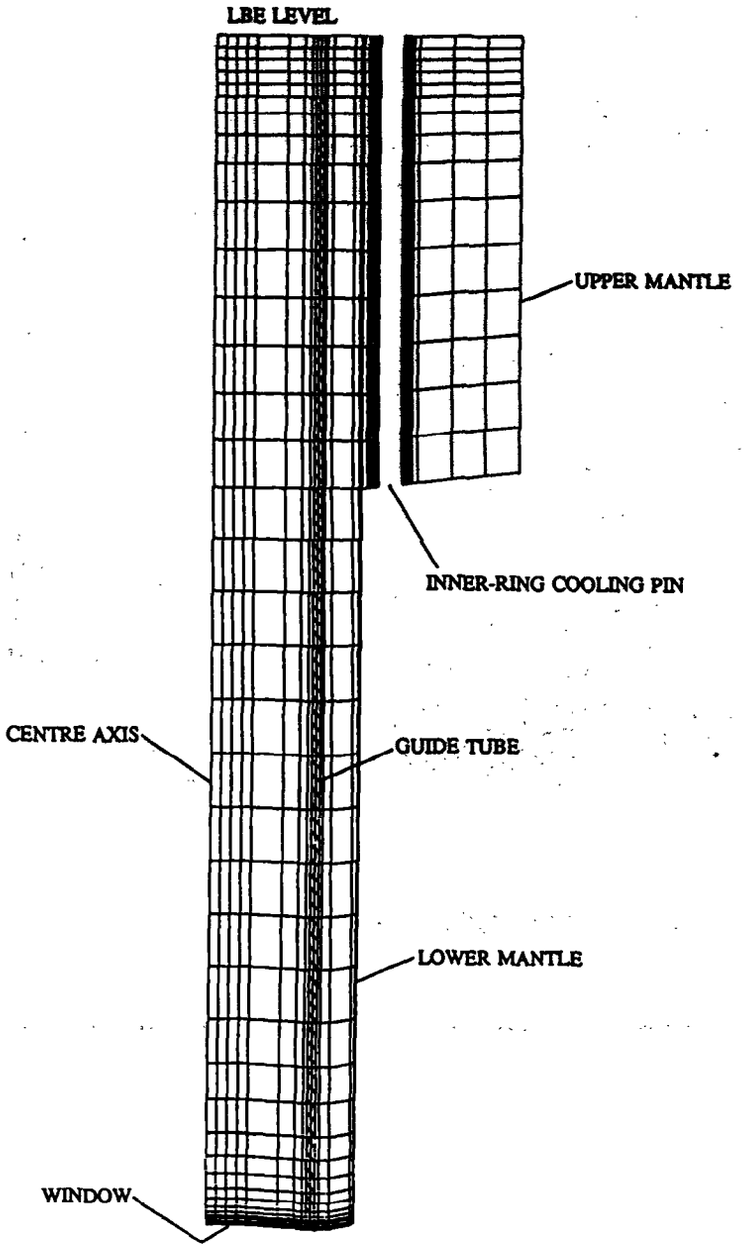

Fig.4

ASTEC target model - side view (domed window)

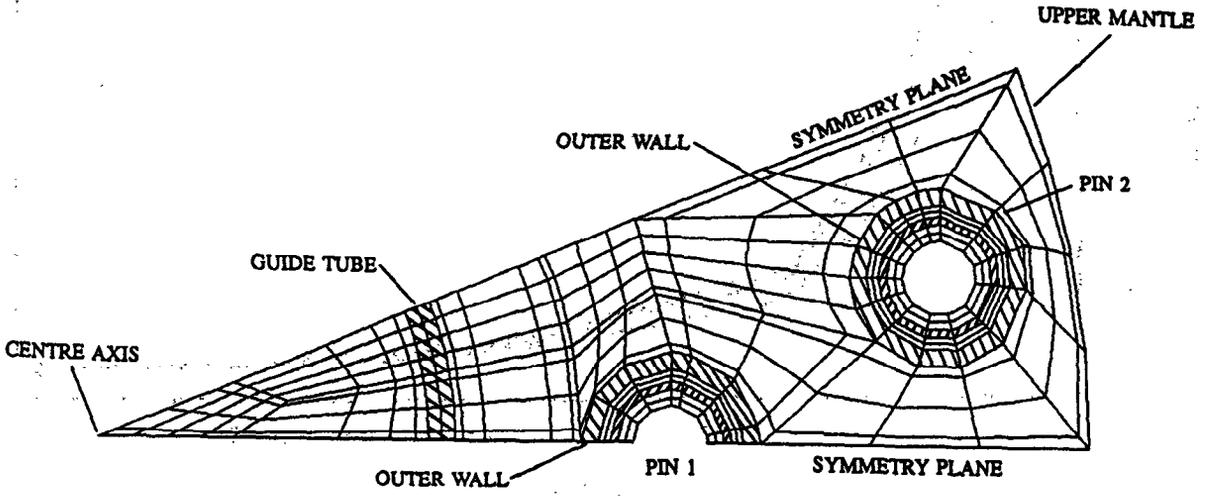

Fig.5 ASTEC mesh - Plan view of top plane

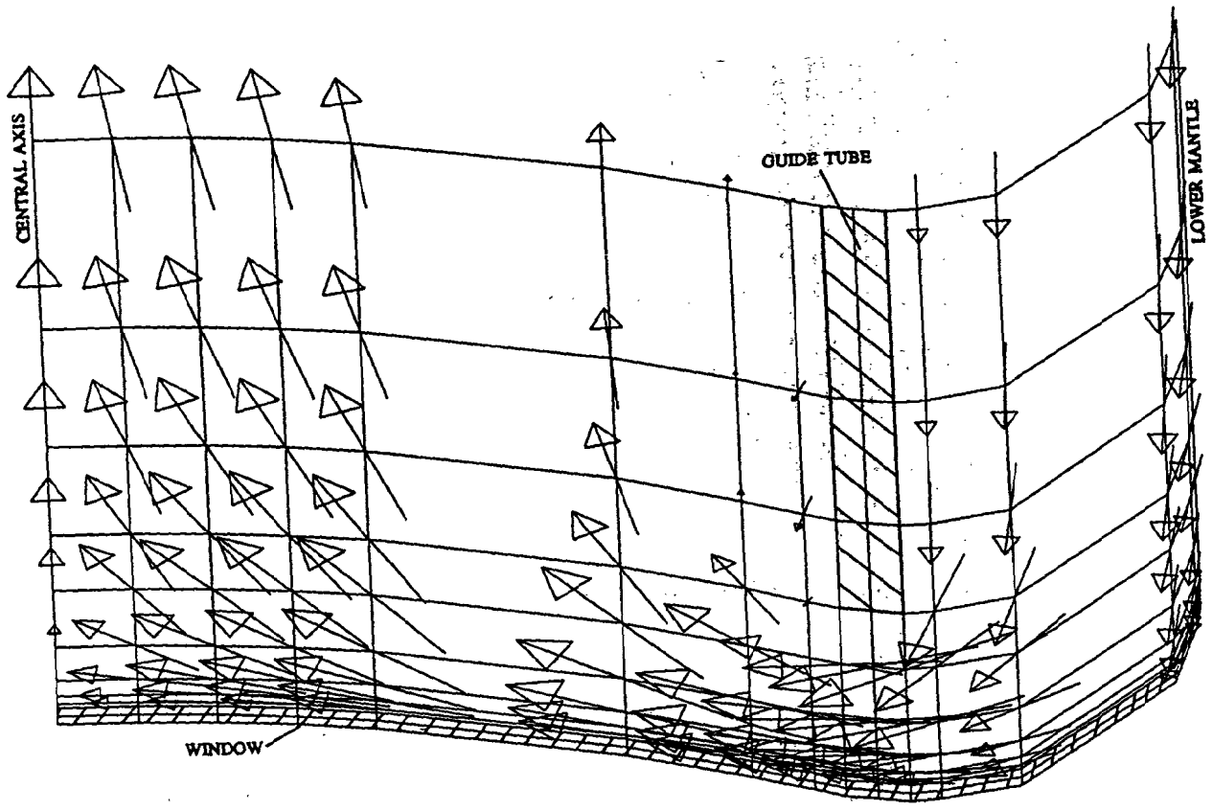

Fig.6 Domed window - velocity distribution above window

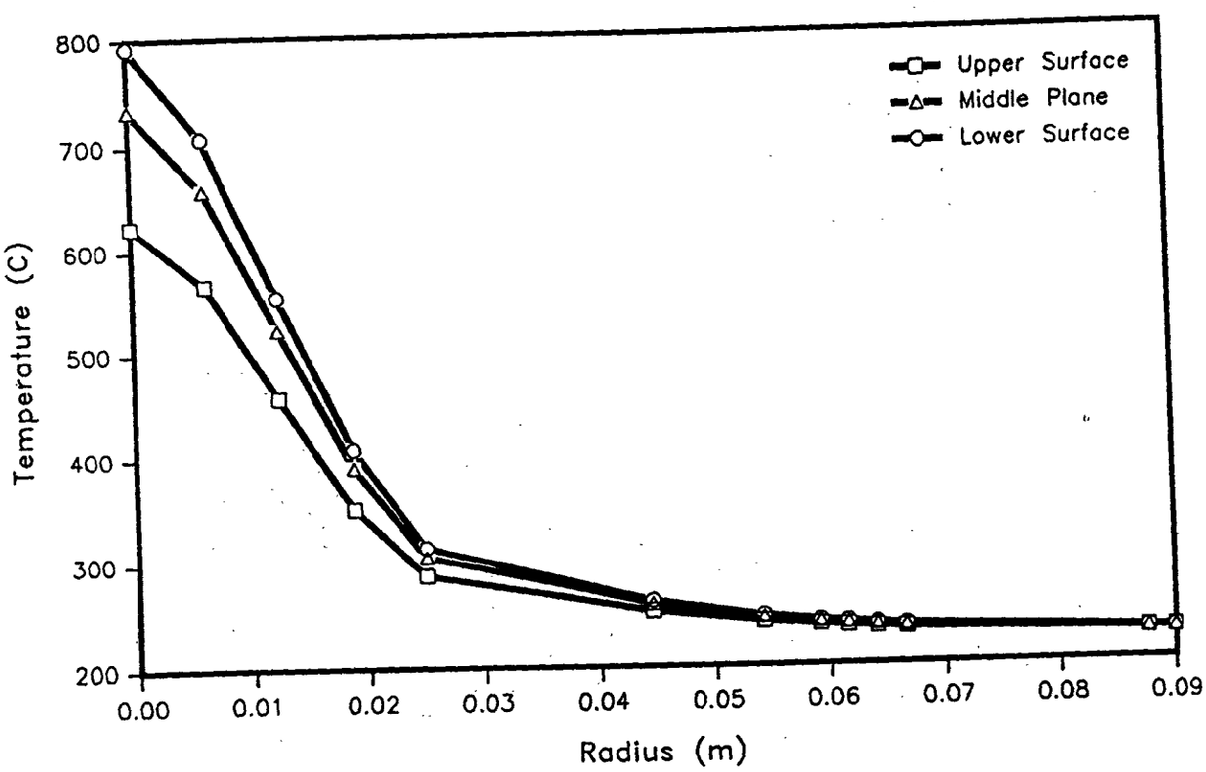

Fig.7 Domed window - Temperature distribution in window

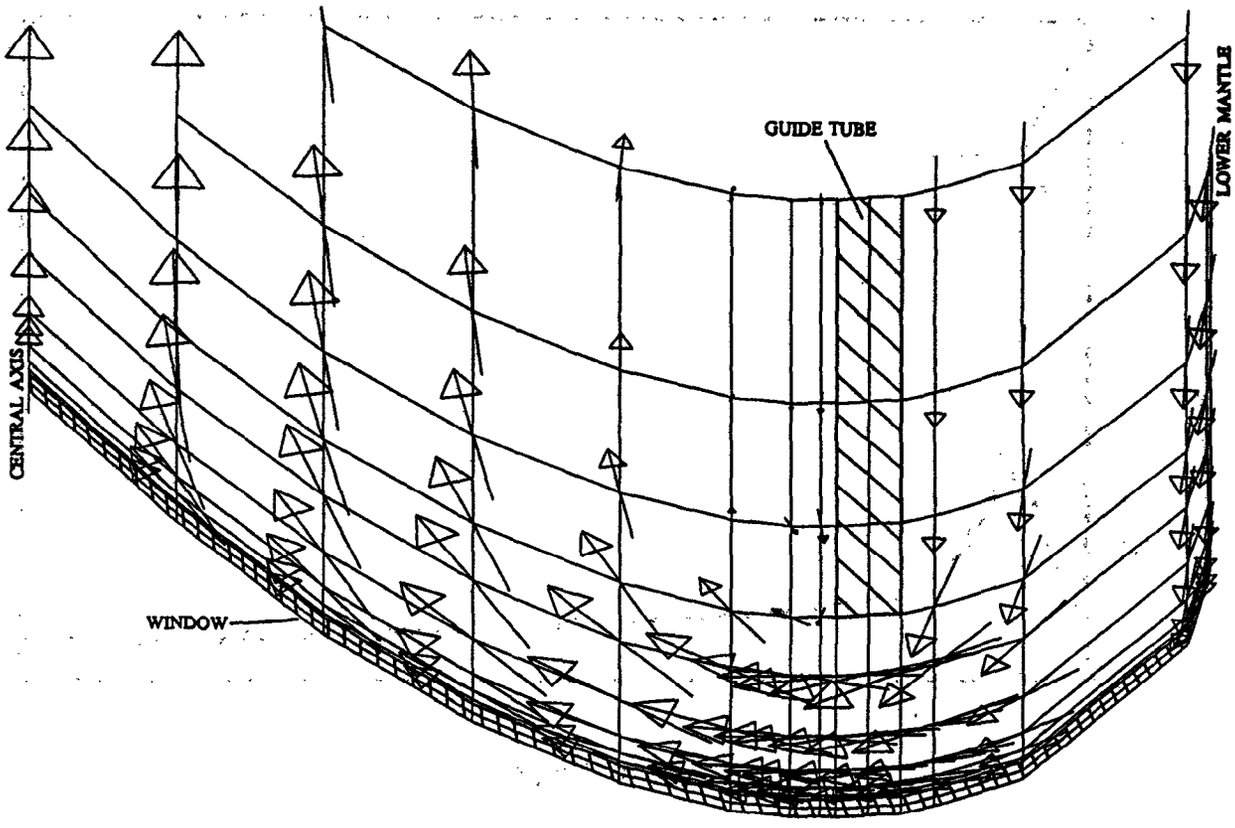

Fig.8 Cusped window - Velocity distribution above window

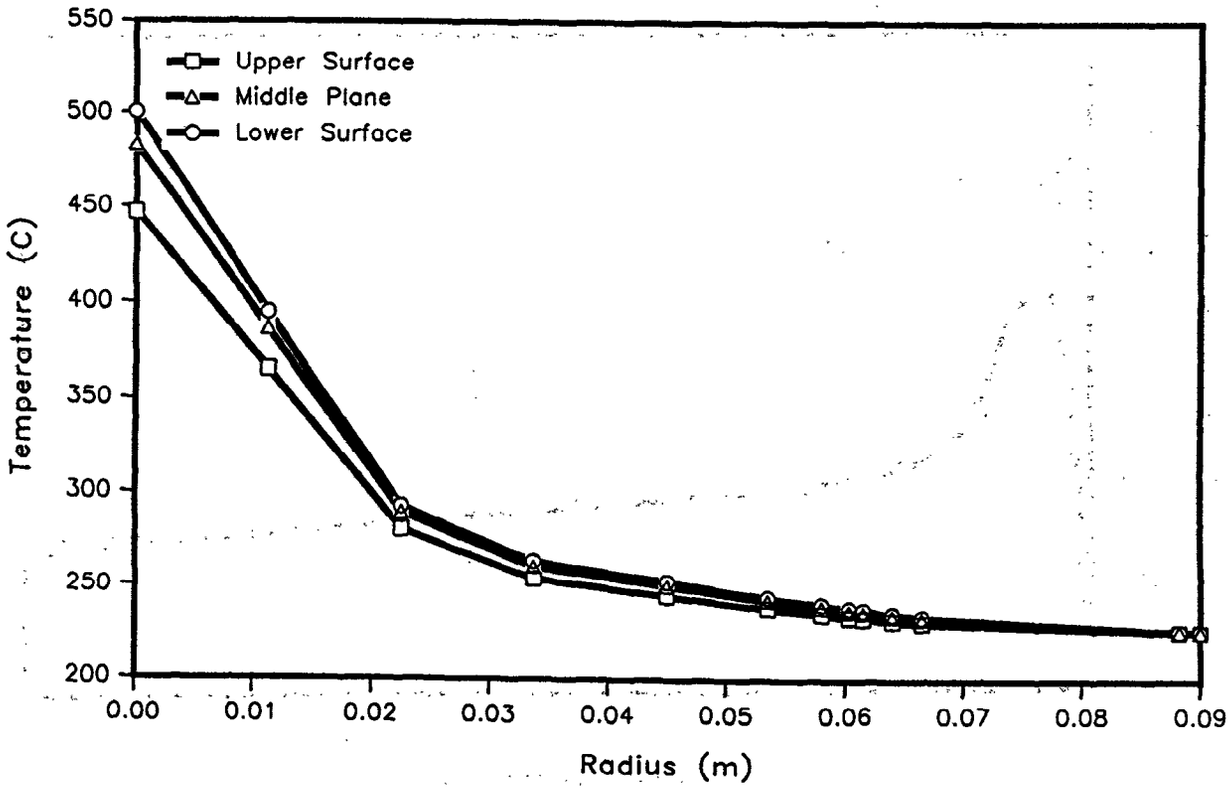

Fig.9 Cusped window - Temperature distribution in window

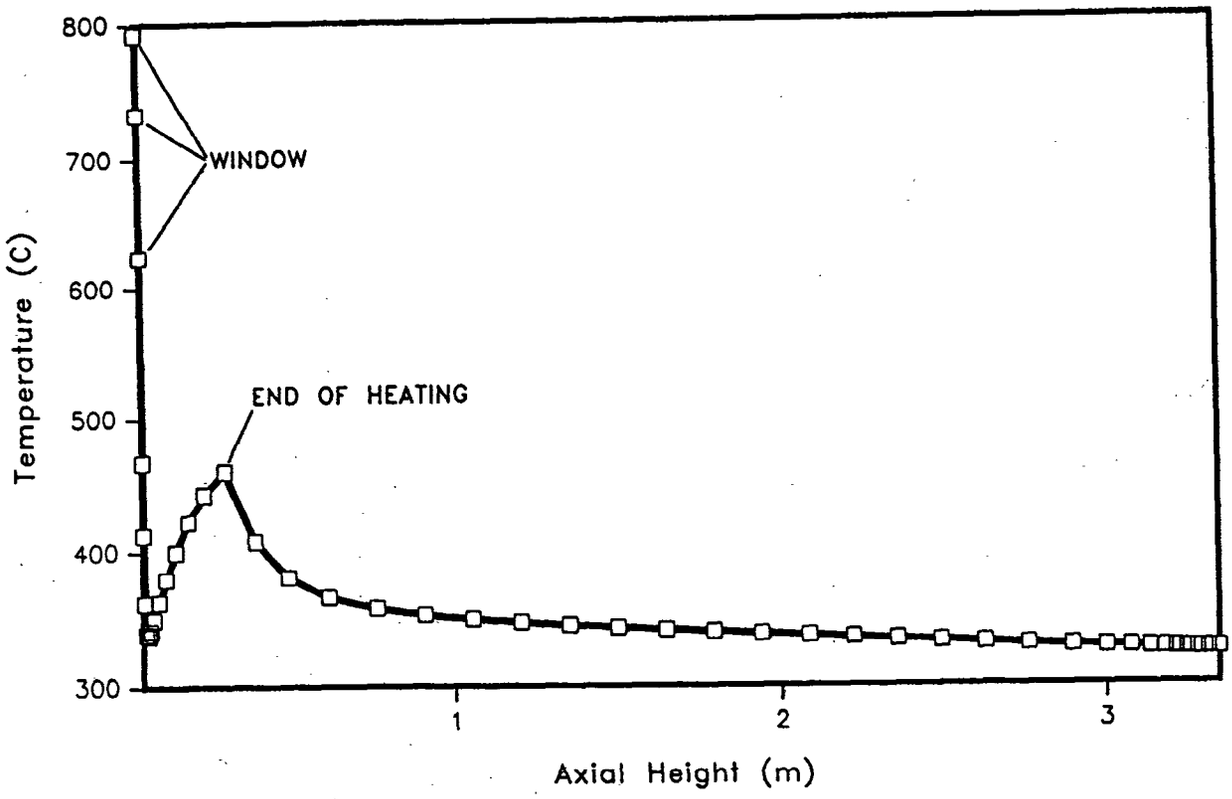

Fig.10 Domed window - Temperature distribution along target axis

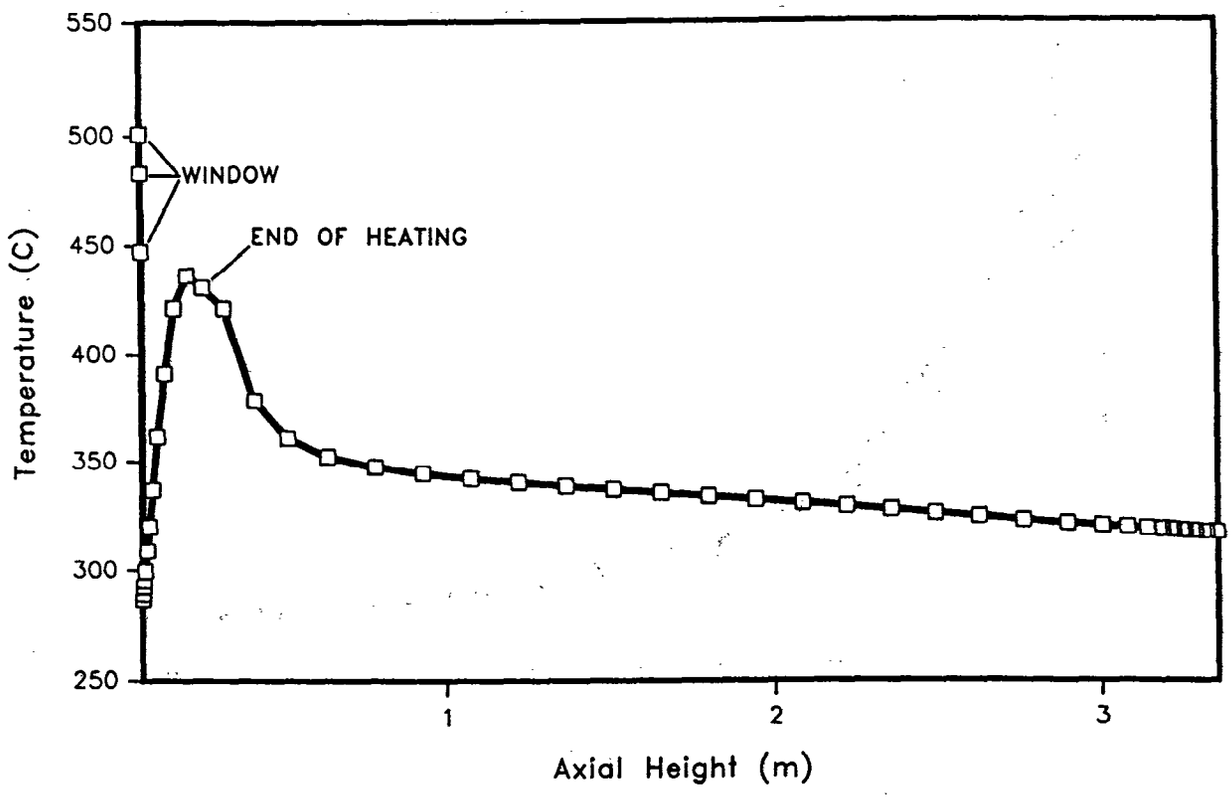

Fig.11 Cusped window - Temperature distribution along target axis

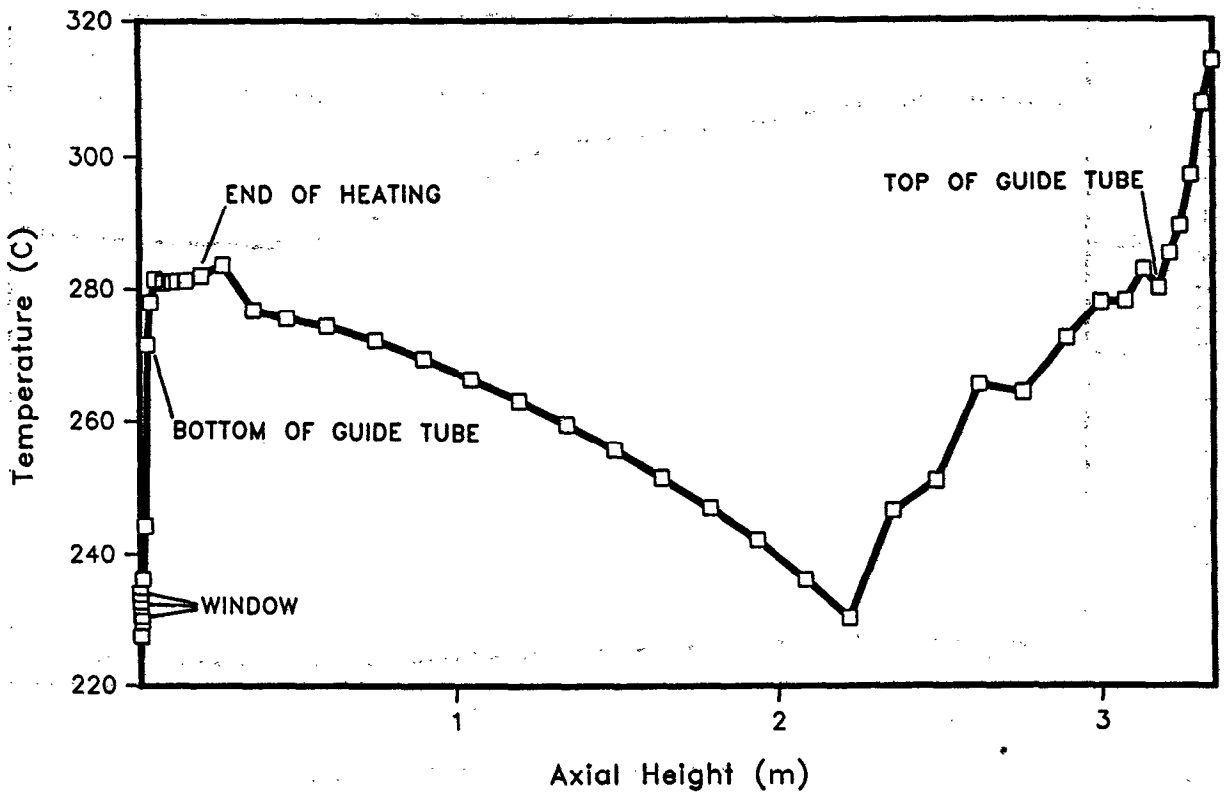

Fig.12 Axial temperature distribution on outer surface of thermally-conducting guide tube

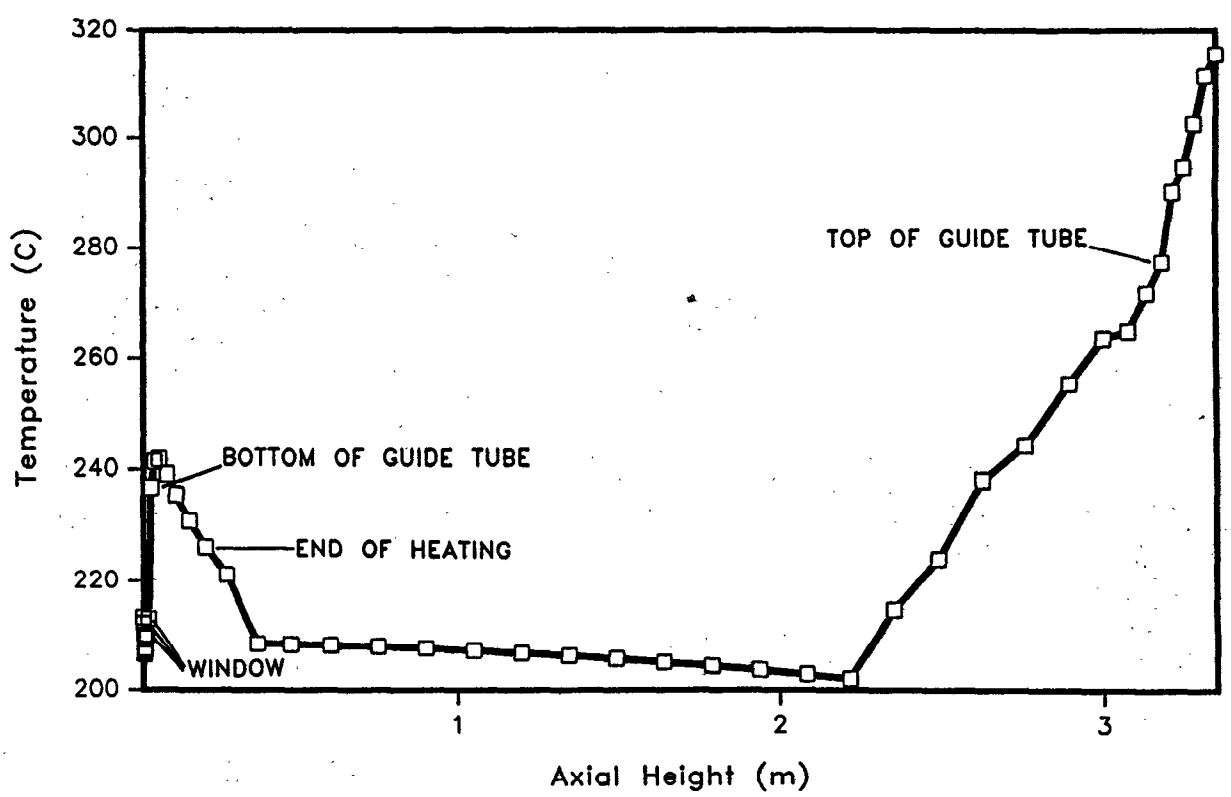

Fig.13 Axial temperature distribution on outer surface of insulated guide tube

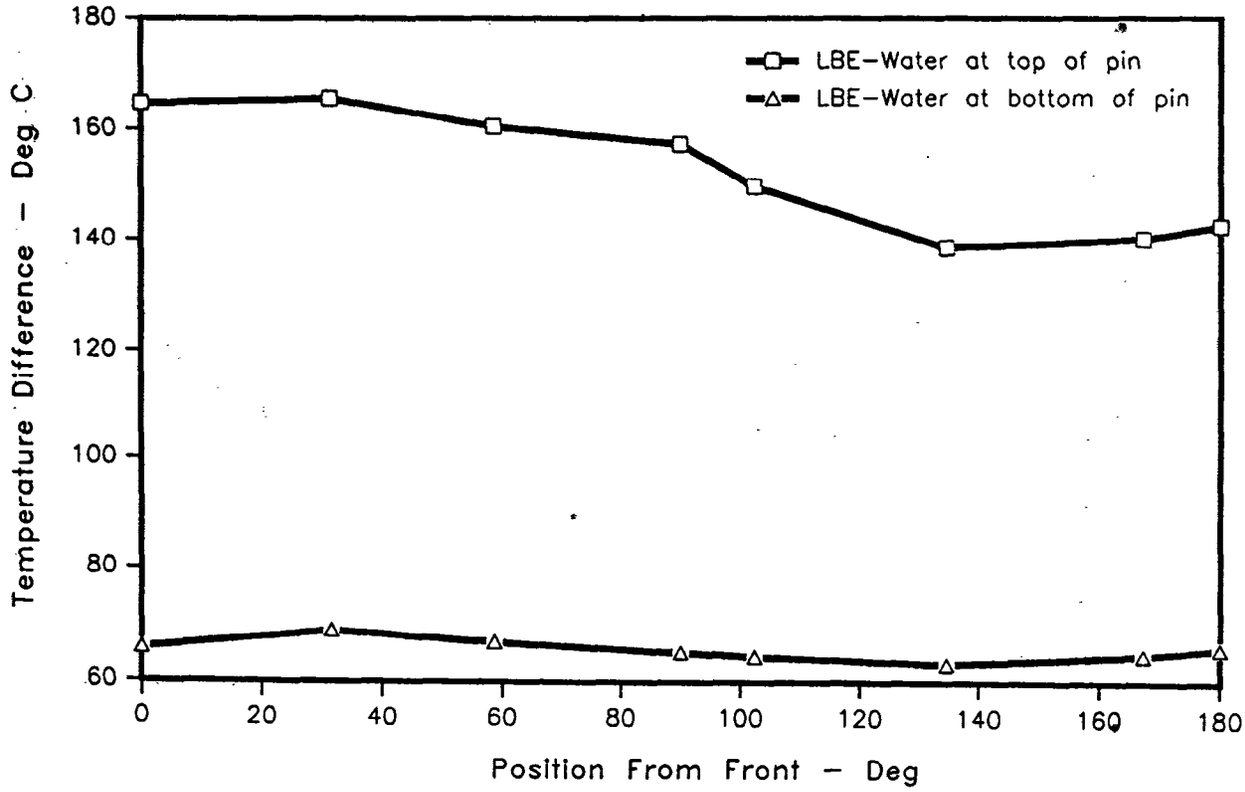

Fig.14 Temperature differences between LBE and Cooling water around circumference of Pin 1 in Fig.15

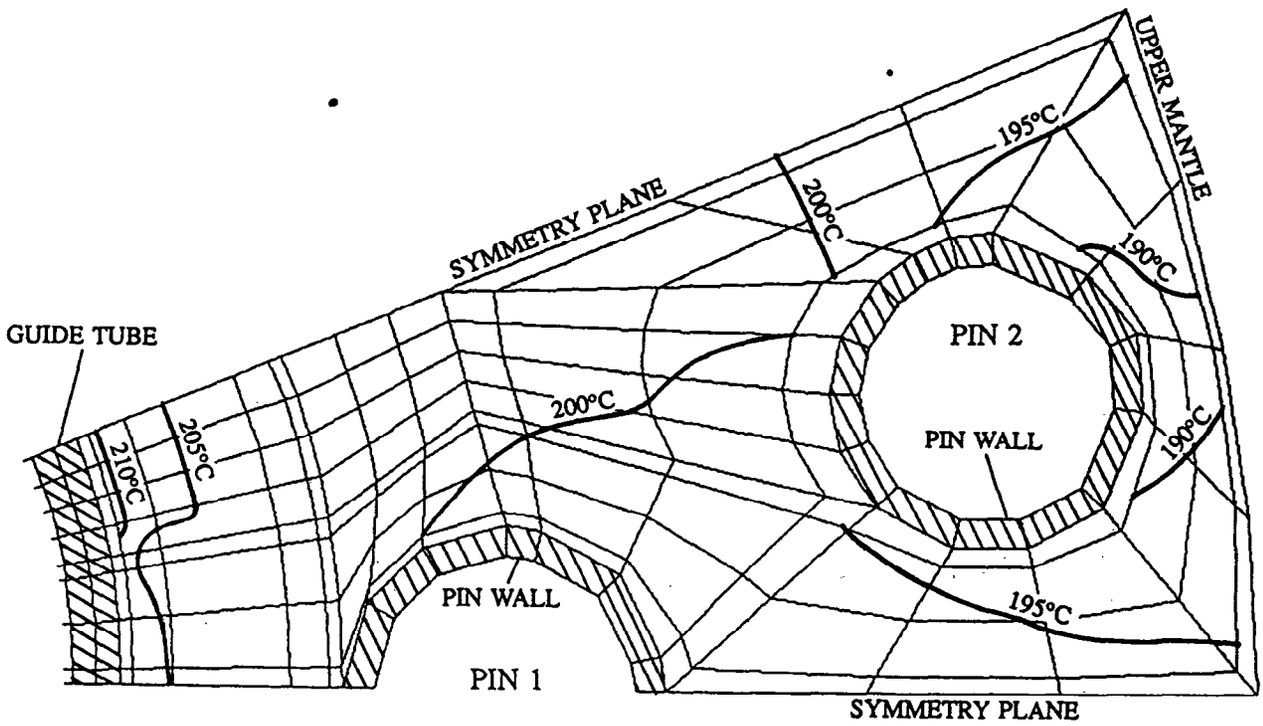

Fig.15 LBE isotherms in target annulus near bottom of cooling pins

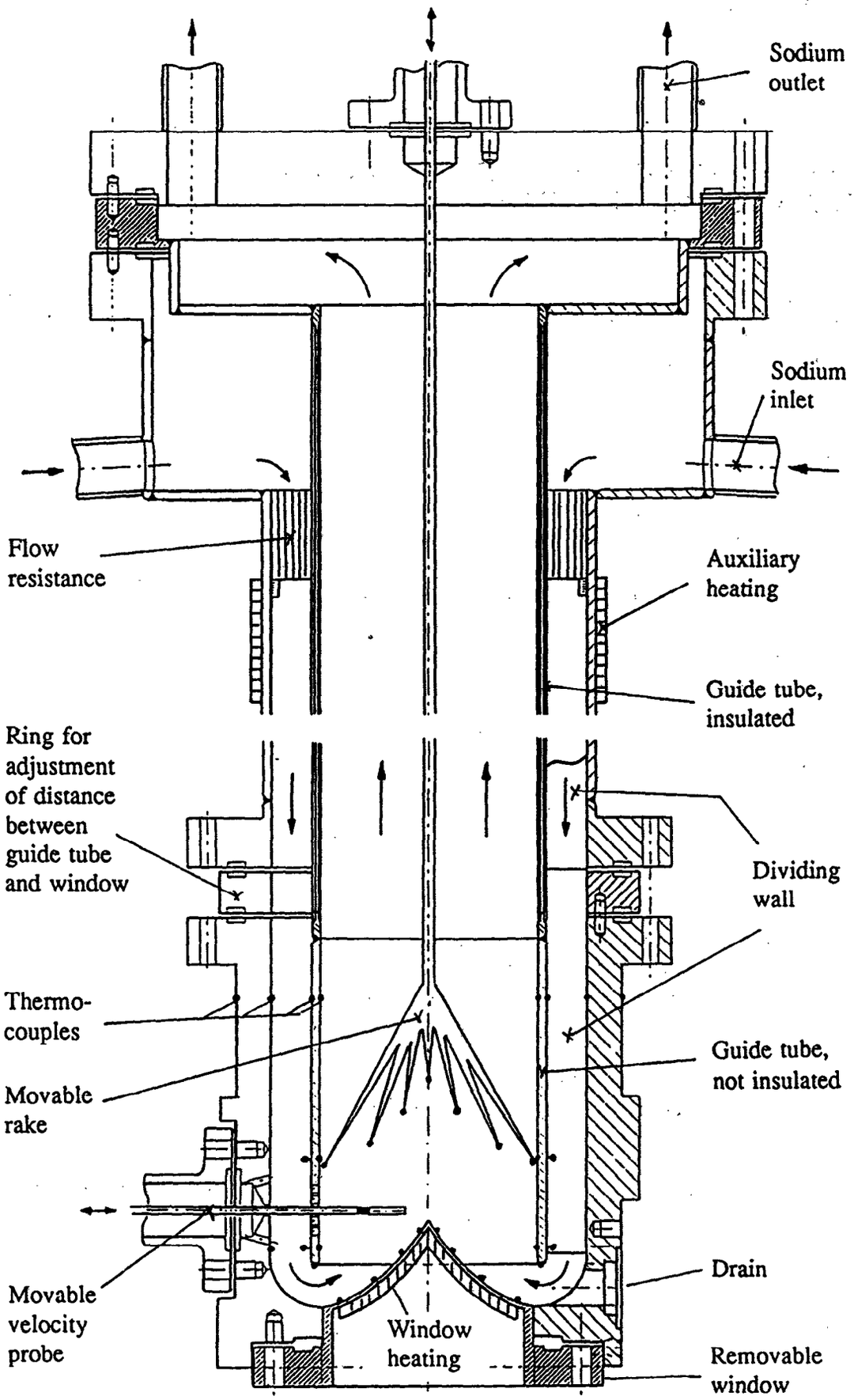

Fig.16 Sketch of TACOS test-section

ICANS-XI International Collaboration on Advanced Neutron Sources
KEK, Tsukuba, October 22-26, 1990

DESIGN CONSIDERATIONS FOR THE SINQ TARGET WINDOW

M. Dubs and J. Ulrich
PAUL SCHERRER INSTITUTE
CH-5232 Villigen-PSI, Switzerland

ABSTRACT

Since the proton-beam enters the SINQ liquid lead-bismuth target from below, a special window design is needed to attain safe operation for at least one year. The present design consist of a double-walled water cooled entrance-window and a third wall cooled by lead-bismuth. The intermediate volume contains circulating helium in order to detect any leaks in the 2nd or 3rd wall at an early stage. Several investigations have been made in the fields of radiation-damage, thermohydraulics and stress analysis.

I INTRODUCTION

This report presents an overview of the factors being taken into account in the design for the beam-window of the SINQ target.

SINQ will use the part of the proton beam left-over after passing through Target-E, the second of two meson targets here at PSI. The non-interacting part of the proton beam will be collected beyond Target-E, deflected downwards to pass under the experimental area to the centre of the source and finally pitched upwards to strike the SINQ-target from below. The spot on the target has normally a peak density of about 25 $\mu A/cm^2$ at the SINQ design current of 1500 μA.

The target consists of liquid Pb-Bi eutectic in a closed chrome-steel bottle (Fig. 1). Cooling is achieved by natural convection in the Pb-Bi transporting the heat from the neutron-production region at the bottom of the target to a heat-exchanger at the top.

The beam-window not only has to allow the protons to pass from the beam-line vacuum to the Pb-Bi but also completes the containment and supports the pressure of the liquid.

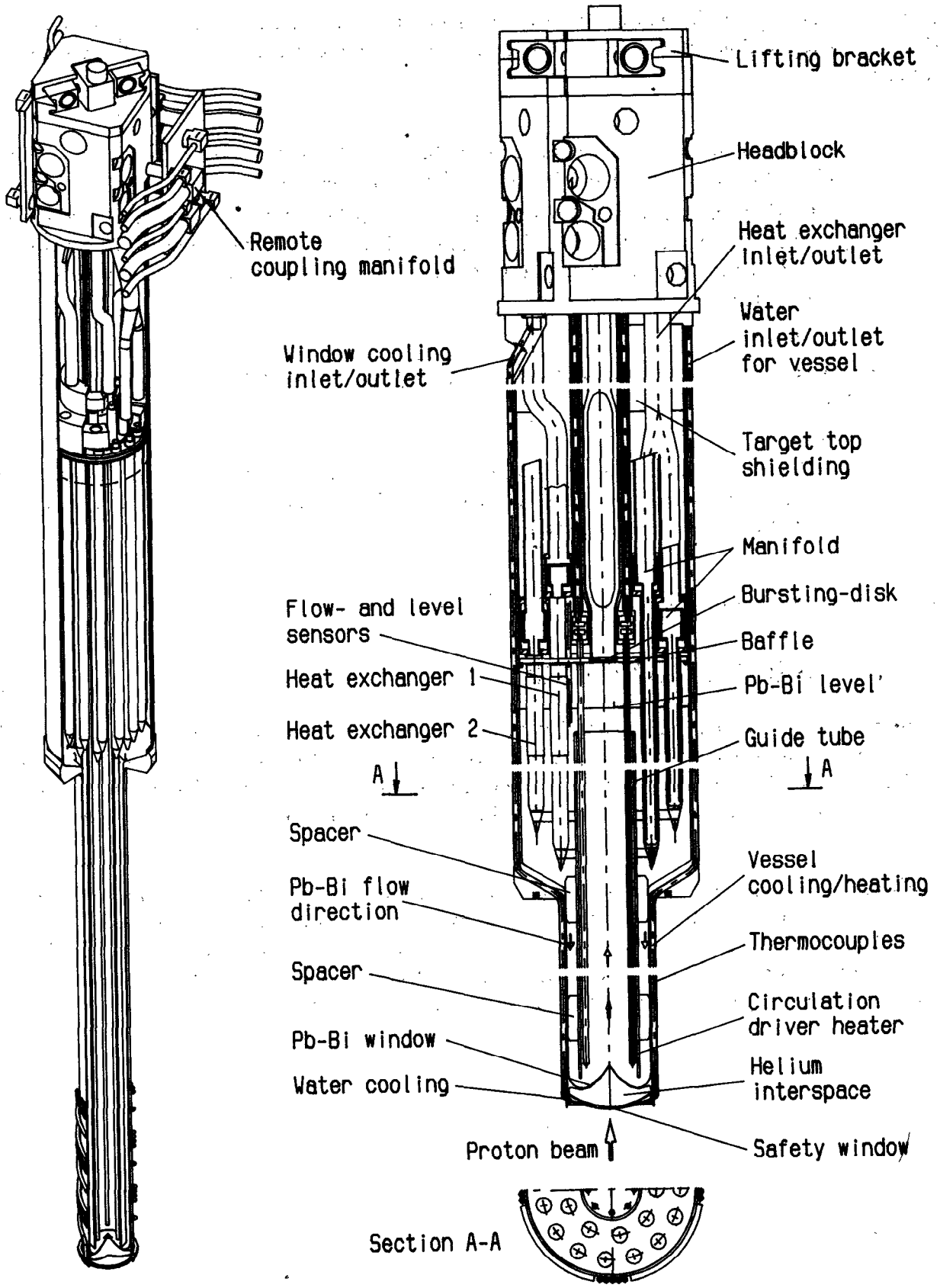

Fig. 1 Layout of the SINQ target.

The target window material will be subjected to high loading and has, as design goal, a guaranteed safe operational life-time of at least 1 mA · year. The following considerations have to be taken into account:

- The main loading comes from the stress induced by the heating caused by the proton beam. This will depend directly on the current density in the beam spot.
- Parts of the proton beam that miss Target-E will be better focused producing a higher peak to average current density. The window should be able to operate normally with up to 30 % of the beam by-passing Target-E and withstand a beam that totally misses it for a short time.
- Pressure loadings.
- Material property and geometry changes ("swelling") from radiation damage and temperature.
- Corrosion.
- Cyclic stresses from beam interruptions (at present these average at about 4 per hour and it is not unlikely that this rate will increase at least temporarily when the accelerator is operated at higher current levels).

The design study requires a combination of experiment, calculation and testing.

II TECHNICAL CONCEPT

The present window design has envolved from of an earlier water-cooled two-element concept. The high current density from the beam by-passing Target-E meant that the windows could only be cooled by using unacceptably high water pressures leading to straightforward mechanical problems and also to concern over safety: only a single mechanical barrier preventing leakage of water into the hot liquid Pb-Bi.

The overall window assembly is now in two parts (Fig. 2) and gives three material barriers between the proton-beam vacuum and the Pb-Bi: the first (safety window) consists of a water-cooled "sandwich" of two elements and the second, a single element in contact with and cooled by the Pb-Bi. The interspace contains a flowing helium atmosphere (for detection of leaks in the window assembly) at a pressure somewhat higher than that of the Pb-Bi on the inner window.

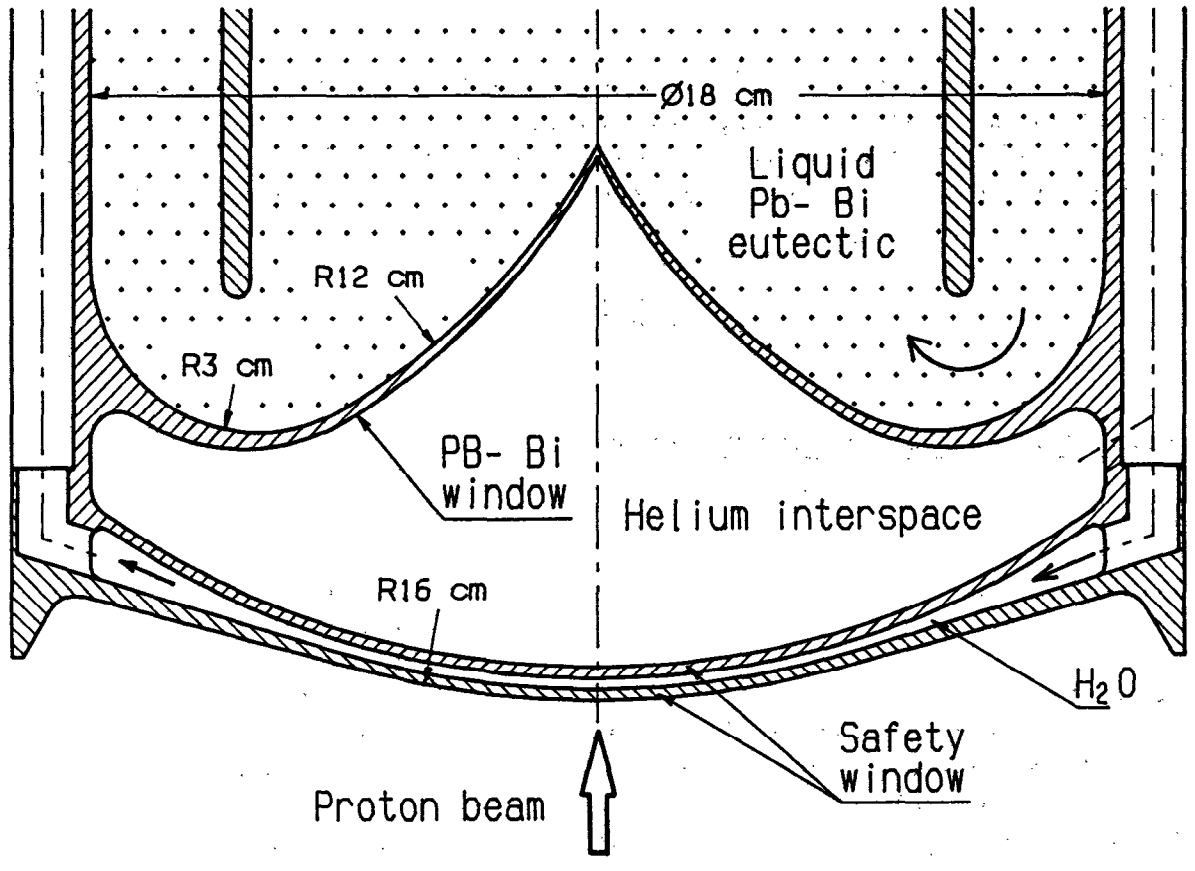

Fig. 2 SINQ-target window assembly.

Technical data and parameters for the window are given in Table 1.

The shape of the Pb-Bi window is determined by thermohydraulic considerations to give:

- good heat-transfer in the central (beam-heated) region of the window
- low pressure loss in diverting the flow of the Pb-Bi upwards into the guide-tube.

The selection of the window element thicknesses and thickness-profile depends on:

- the maximum stress (because of the three-dimensional loading, this is based on the von Mises stress) compared with the yield stress under the various operating conditions, bearing in mind all temperature gradients.
- Pressure differentials.

The safety window is cooled by a transverse flow which enters through a series of holes at the rim.

A uniform flow distribution across the full diameter of the window is achieved by suitably shaped guides (see section III.2).

The present material choice for the window complex is type X 20 CrMoV 12 1 chrome steel (similar to type HT9): this has good mechanical properties at high temperatures and is compatible with hot liquid Pb-Bi under radiation conditions. In the event that future studies show problems with this steel, an alternative is Inconel for the safety window and possibly a ceramic material for the Pb-Bi window.

Table 1

Technical data for the SINQ target window

Proton Beam Energy	570 MeV
Design Current	1500 μA
Diameter	18 cm
Thickness at Centre	0.1 - 0.2 cm
Power Deposition in Steel per cm of Window Material	30 kW
Maximum Power Density (30 % of beam by-passing Target-E)	ca. 1900 W/cm^3
Static Pressure on Pb-Bi Window	
(including 0 to 0.9 bar pressure above Pb-Bi surface)	3.3 - 4.2 bar
Helium Pressure in Interspace	4.5 bar
Water Pressure for Safety Window	10 bar

III EXPERIMENTAL TESTS

As part of the overall design study, a series of experimental tests looking at various aspects of the window, have been undertaken. These are described in the following sub-sections.

III.1 RADIATION DAMAGE

The life limit for the window will most likely be determined by radiation damage. Two experiments have been mounted at the LAMPF (Los-Alamos) radiation effects facility.

In the first, the mechanical properties of various sample materials (iron, tantalum, Fe-2.25Cr-1Mo and Fe-12Cr-1Mo) irradiated in contact with Pb-Bi were measured [1]. The materials were irradiated with 800 MeV protons to a fluence of about 5.4 x 10^{24}/m^2 which corresponds to about 1.6 dpa in steel. The HT9 (Fe-12Cr-1Mo) gave the best results (Fig. 3)

The second test is a long-term irradiation of a prototype water-cooled window (Fig. 4). Two windows have been constructed from 10.5 % Chrome-steel (X 20 CrMoV 12 1 was not obtainable within the time schedule for the experiment) and mounted at the LAMPF proton-beamline. Technical data for these windows is given in Table-II. So far the windows have been irradiated for two beam-periods (about 2000 mA hours beam current) and have received damage corresponding to about 7 dpa. The higher current densities to be handled by the SINQ-target due to the 30 % beam by-passing Target-E are estimated to correspond to a yearly damage accumulation of 40 dpa. It is hoped that the experiment can be run for some more beam-periods.

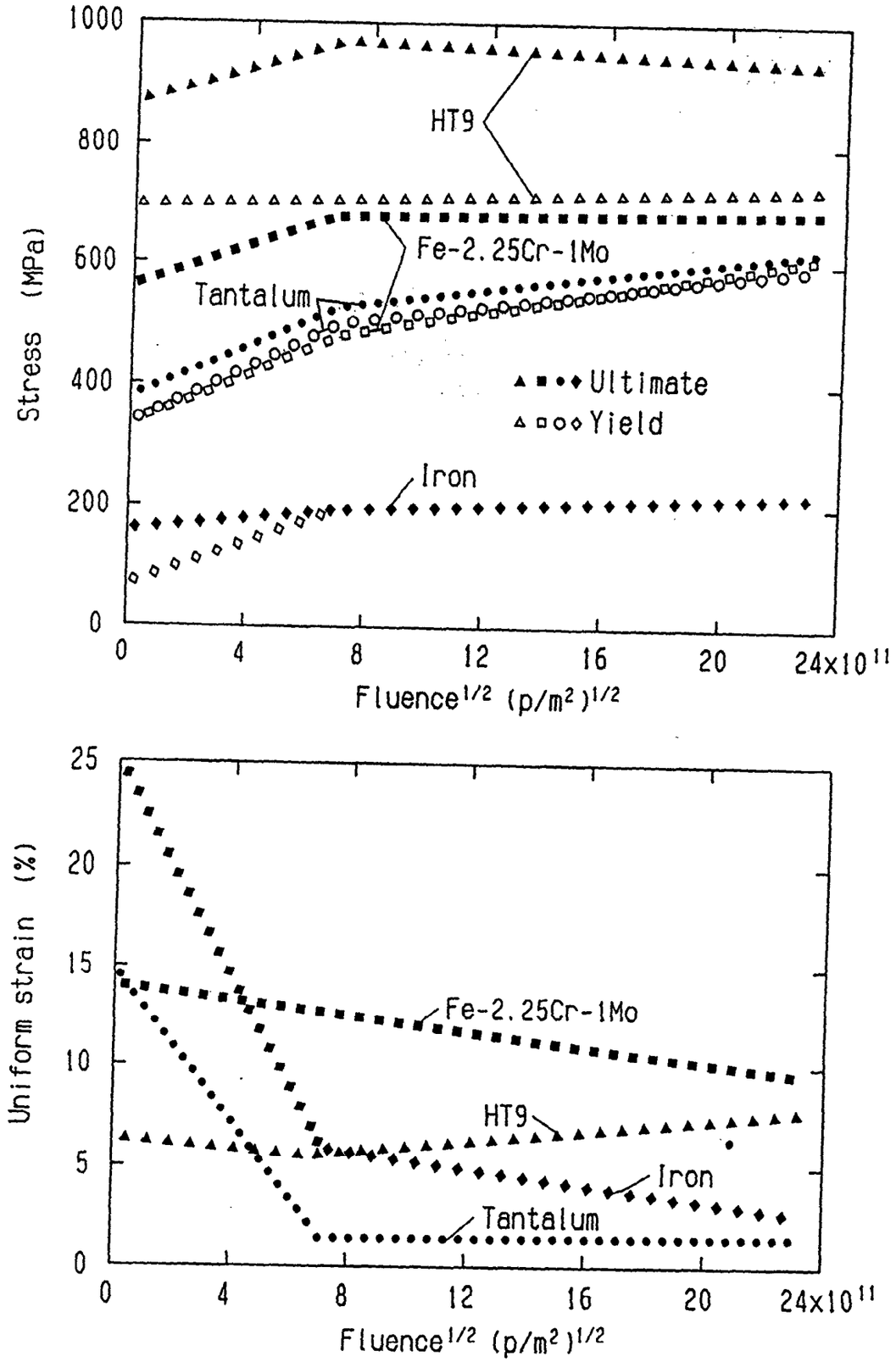

Fig. 3 Effect of irradiation with 800 MeV protons at a temperature of 400 °C for different materials.
Top: yield stress and ultimate tensile strength, bottom: uniform strain. Both are plotted as a function of the square-root of proton fluence.

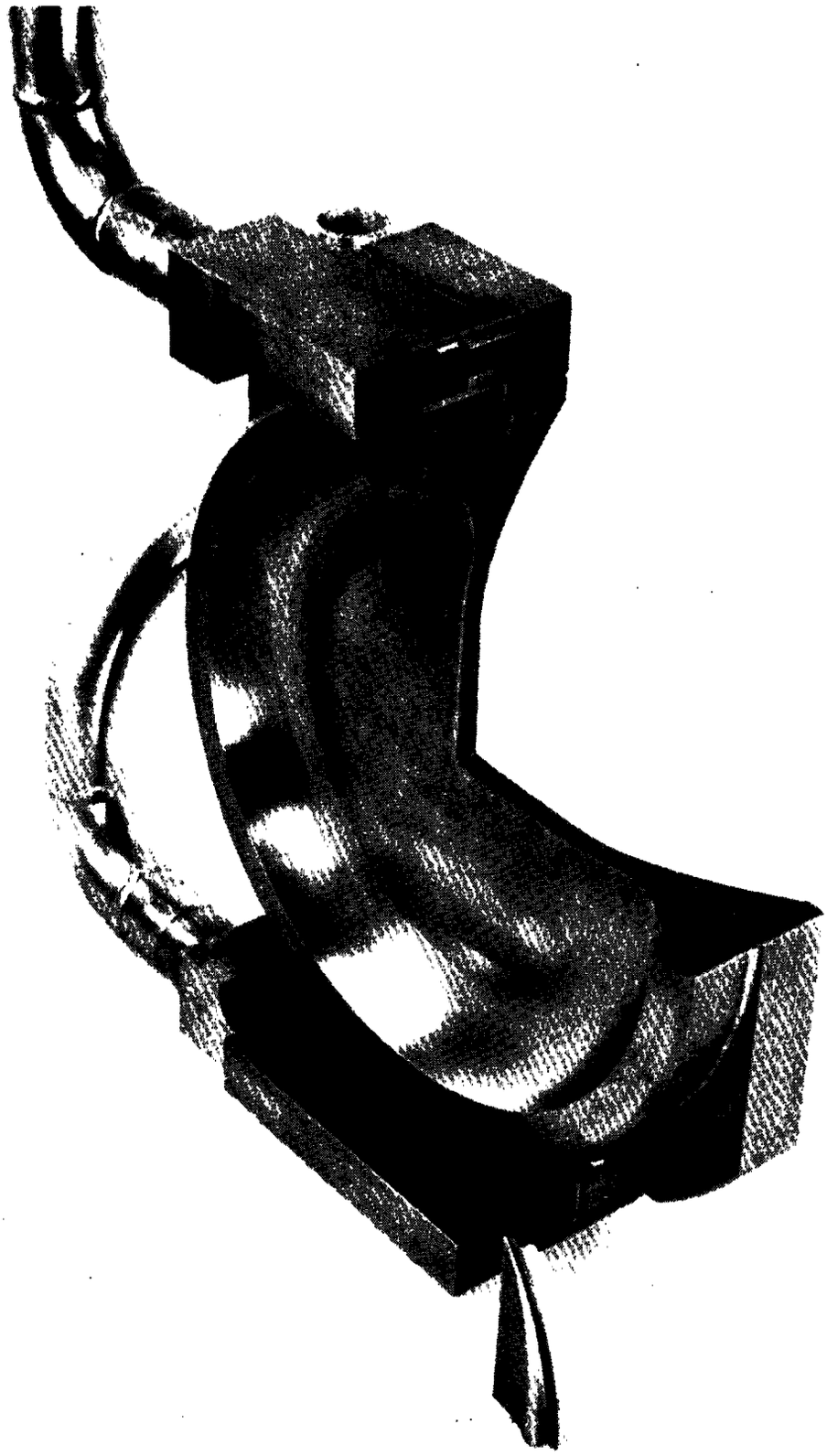

Fig. 4 Photograph of a cut-away model of the lifetime-test window mounted at LAMPF radiation effects facility. The small item standing beside the window is part of the wedge-shaped flow guide.

The fabrication of these windows has brought much valuable experience in machining and welding techniques: in particular, the importance of correct heat treatment before and after electron-beam welding (Fig. 5).

Table 2

Technical data for the Los-Alamos test windows

Proton Beam Energy	750 MeV
Average Current	700 μA
Window Diameter	18 cm
Window Material Thickness	2 x 0.2 cm
Water Channel Width	0.2 cm
Maximum Proton Beam Current Density	40 $\mu A/cm^2$
Maximum Power Density	650 W/cm^3
Water Temperature at Entrance	40 °C
Maximum Measured Window Temperature	182 °C

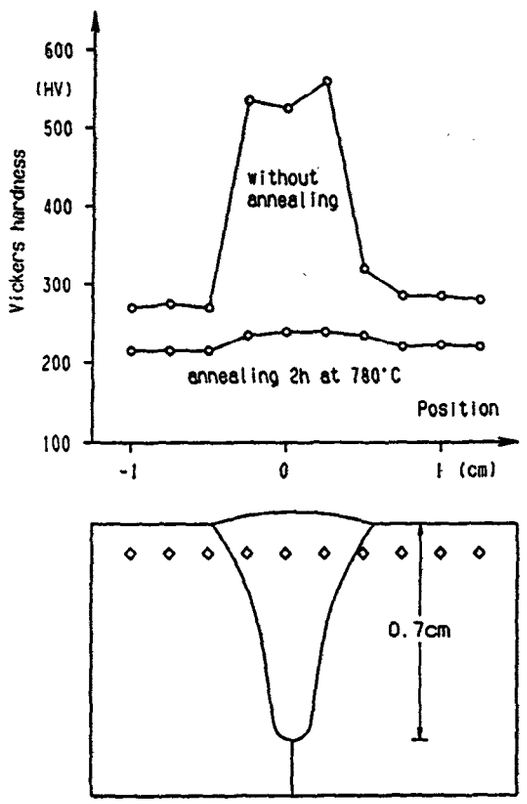

Fig. 5 Results from a test of the Vickers-hardness of a sample weld for the LAMPF irradiation-test window (Electron-beam welding at 350 °C of 10.5 % chrome-steel).
Upper: Hardness-profile of weld before and after annealing.
Lower: Profile of welding seam showing the measurement positions.

III.2 WATER FLOW IN THE SAFETY WINDOW

The window is to be constructed from a pair of dome-shaped caps and the water flow is to be across the gap from an entrance to an exit manifold. The major part of the window heating is in a small region at the centre: the water flow must be adjusted to obtain proper cooling over the whole surface with particular emphasis on the central region.

A plexiglass model of the window has been built and the flow patterns examined by injecting air bubbles. A good flow distribution was obtained by mounting wedge shaped guide-pieces at the edges of the window (Fig. 6).

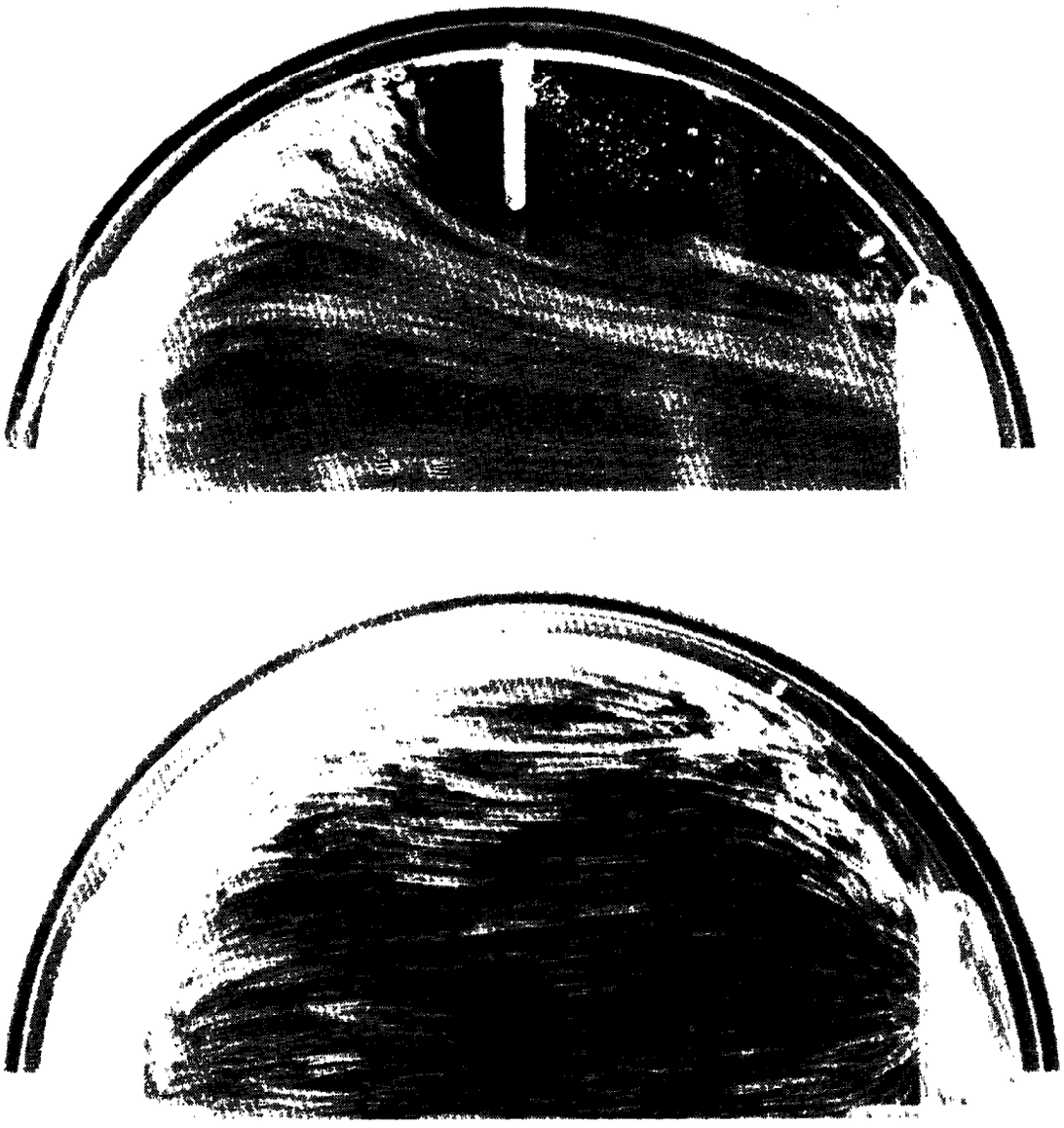

Fig. 6 Photograph of the flow in the Plexi-glass model window. The upper picture shows the effect of a simple baffle and the lower, of the wedge shaped flow-guide (see Figure 4).

III.3 EXPERIMENTS WITH Pb-Bi

A set of experiments have been made or are in progress to investigate various aspects of Pb-Bi relevant to the window design.

The temperature distribution (and hence stresses) in the inner window will depend on the flow of Pb-Bi in the neighbourhood of the window. This is complicated and has been studied by Y. Takeda [2], using a water-model. Flow conditions for various velocities and guide-tube positions have been examined.

Pb-Bi is known to corrode several materials (aluminium, nickel containing steel etc.). Samples of possible compatible steels have been mounted in an electrically heated, water cooled Pb-Bi test circuit. So far, this experiment has only run for six months and no probes have been extracted yet.

A second similar Pb-Bi test circuit is being built. There are two main aims:

- direct measurement of the heat transfer coefficient by Pb-Bi from steel
- measurements of the characteristics of a naturally circulating liquid-metal circuit [2].

A Pb-Bi eutectic mixture has the undesirable property of a delayed swelling after freezing.

A simple test to measure the size of the effect has been made: a 6.55 cm O.D. cylinder constructed from 0.175 cm thick chrome-steel was filled with molten Pb-Bi and then allowed to solidify. The diameter increased by a maximum of 0.35 % over a period of about 6 months: no measurable change of diameter occurred at later times. The consequence of this is that the Pb-Bi should be kept molten as long as the target is to be operated.

IV CALCULATIONS

The basic information required for both thermohydraulic and stress analysis is the heating rate. The major part comes from the proton beam and there is a small contribution from backscattered particles from the target. The current distribution at the beam-window for both the "normal" and the "by-pass" components of the beam comes from beam-transport calculations.

As experiments using surface-muons are to be mounted at Target-E (these require a high proton flux at the surface of Target-E), the rather high value of 30 % of the proton beam by-passing Target-E has been taken as a reference value for calculations (Fig. 7).

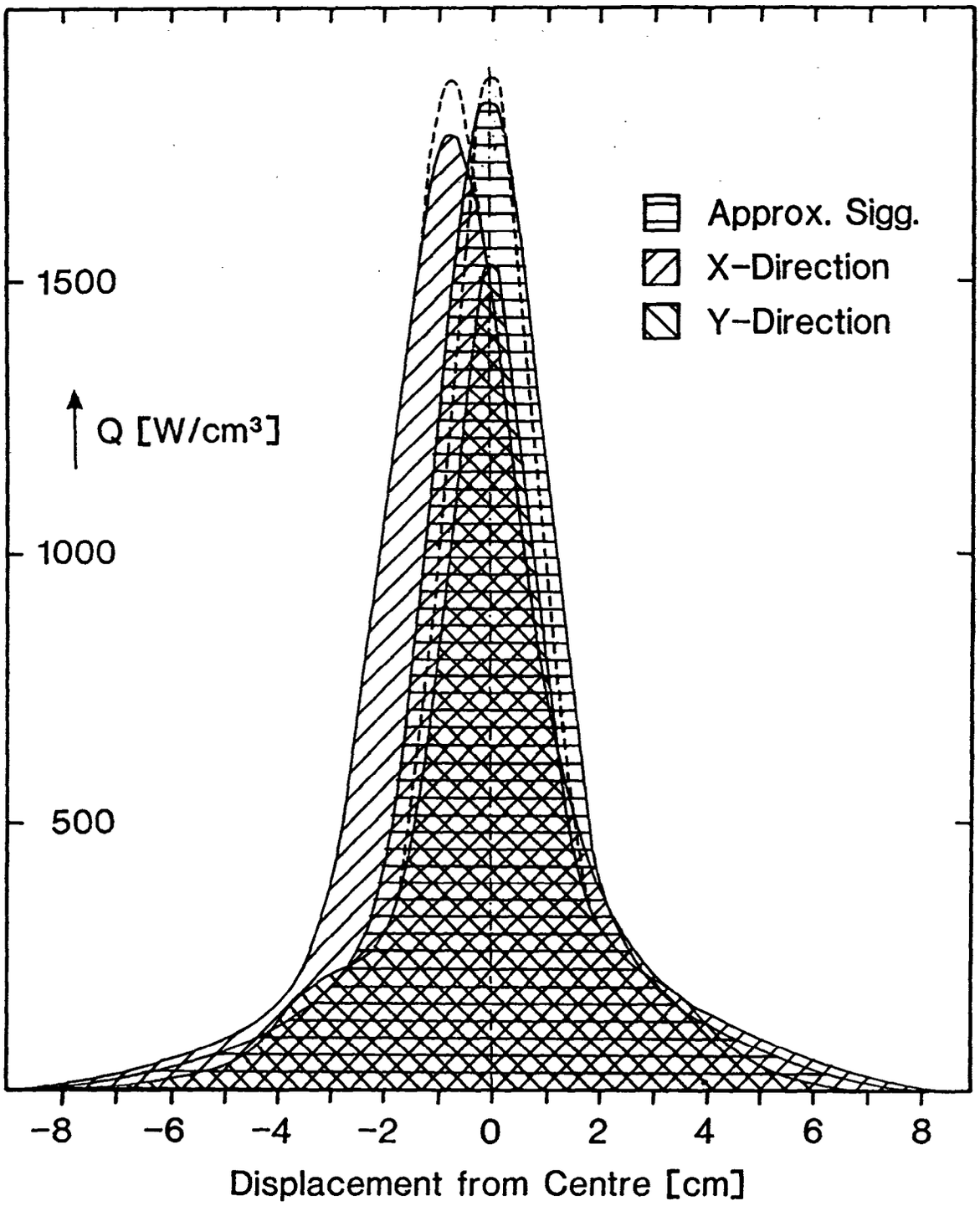

Fig. 7 Calculated profiles of power density in steel of SINQ-target window, for condition where 30 % beam by-passes Target-E, in the X- (bending plane) and Y-planes. Solid lines show the profiles on the target axes and dashed lines, through the peak of the beam. Also shown is the symmetric approximation as used by Sigg et al. [3] and Heidenreich [4].

The latest thermohydraulic calculations are presented in the report of B. Sigg et al. [3] and results of a thermal and mechanical analysis of the current window design given in the report of G. Heidenreich [4].

Both sets of calculations mainly discuss the steady state condition and also assume a radially symmetric beam exactly on the centre of the beam window. The next calculations will look at transient conditions: these will come from beam interruptions and also from the current-ramp at beam switch-on (Fig. 8).

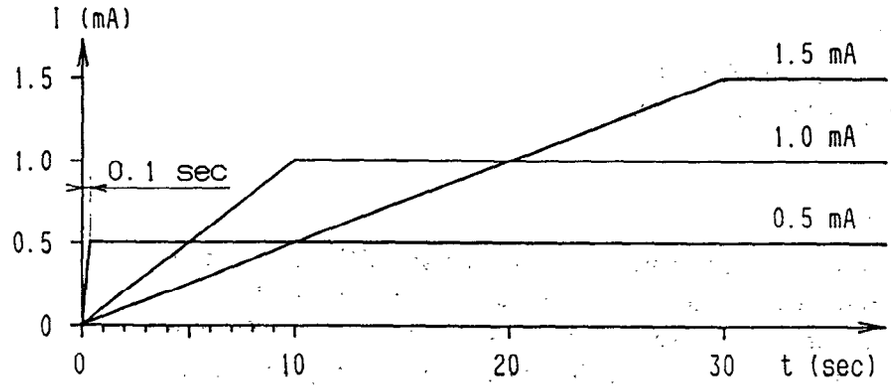

Fig. 8 Proposed accelerator start-up current ramps to different proton-beam current levels.

Future studies will need to include the effect of asymmetric loading. These will require the use of very elaborate modelling calculations and can only be justified when the design of the window is more firmly established.

REFERENCES

[1] Brown, R.D., Wechsler, M.S., and Tschalär, C., 1988, 13th Int. Symp. on "Effects of Radiation on Matter", June 23/25, Seattle.

[2] Y. Takeda, W.E. Fischer, "Thermofluid Dynamics of the Liquid Metal Target of SINQ", ICANS-XI, Japan 1990.

[3] B. Sigg et al., "Thermal-hydraulics Investigation for the Liquid Lead-Bismuth Target of the SINQ Spallation Source", ICANS-Xi, Japan 1990.

[4] G. Heidenreich, "Preliminary Thermal and Stress Analysis of the SINQ Window", ICANS-XI, Japan 1990.

ICANS-XI International Collaboration on Advanced Neutron Sources
KEK, Tsukuba, October 22-26, 1990

Preliminary Thermal and Stress Analysis of the SINQ Window

G. Heidenreich
PAUL SCHERRER INSTITUTE
CH-5232 Villigen-PSI, Switzerland

ABSTRACT

Preliminary results of a finite element analysis for the SINQ proton beam window are presented. Temperatures and stresses are calculated in an axisymmetric model. As a result of these calculations, the H_2O-cooled window (safety window) could be redesigned in such a way that plastic deformation resulting from excessive stress in some areas is avoided.

I. Introduction

A thermal and structural analysis of the proposed design for the proton-beam window for the SINQ Pb-Bi target has been performed using the commercial engineering analysis system ANSYS [1]. A full description of the window design is given elsewhere [2]. In brief, the overall assembly consists of two parts (see Fig 1): an inner window cooled on one side by the flow of the target Pb-Bi and an outer safety window made from two plates with water flowing between. The interspace has a He-flow (which plays no role in the cooling) and the whole assembly is to allow passage of the proton beam from vacuum to the target whilst also supporting the Pb-Bi. The main objects of the present study are the estimation of primary operational limits and safety margins for the window.

The temperatures and stresses depend upon the current density of the proton beam. In normal operation, all the beam passes through the up-stream meson target (Target E) and gives a peak current density of $25\mu A/cm^2$ at the design current of $1500\mu A$. Under certain operating conditions a part of the beam will bypass Target E and result in long-term peak current densities of up to $105\mu A/cm^2$. In the worst case, the full beam misses Target E giving a peak current density of up to $265\mu A/cm^2$: such an extreme fault condition is expected to be rare and to last for only a short time.

In the following analysis a safety factor ≥ 3.5, based upon the yield strength, has been calculated for the PbBi-cooled window and for peak current densities of up to $105\mu A/cm^2$. The H_2O-cooled window (safety window) can, with slight design changes, have a safety factor of ≥ 2.

At the extreme fault condition, where a peak current density of $265\mu A/cm^2$ is expected, the stresses in the PbBi-cooled window exceed the yield strength within a radius $\leq 12mm$ and plastic deformation occurs: this is due to the high peak temperature (about 830^oC).

A brief description of the model details will be given in section 2. In section 3 temperatures and stresses are calculated for a peak current density of $105\mu A/cm^2$. In section 4 the second H_2O-cooled window design changes to avoid excessive stresses are discussed. The window stresses under the extreme fault condition (peak current density of up to $265\mu A/cm^2$) will be discussed in section 5.

II. Model Details

The analysis has been performed with an axisymmetric model: the outlines of the finite element model, which corresponds to the proposed window design, is shown in Fig 1. The material properties of the selected steel X 20CrMoV1 21 (DIN 1.4922) are given below:

Elastic modulus	206 kN/mm^2
Poisson ratio	0.3
Thermal conductivity	0.024 $W/mm/^oC$
Thermal expansion	1.12 $10^{-5}/^oC$

Yield strength vs. temperature:

20	200	300	400	460	480	500	550	^oC
490	432	392	353	316	293	265	216	N/mm^2

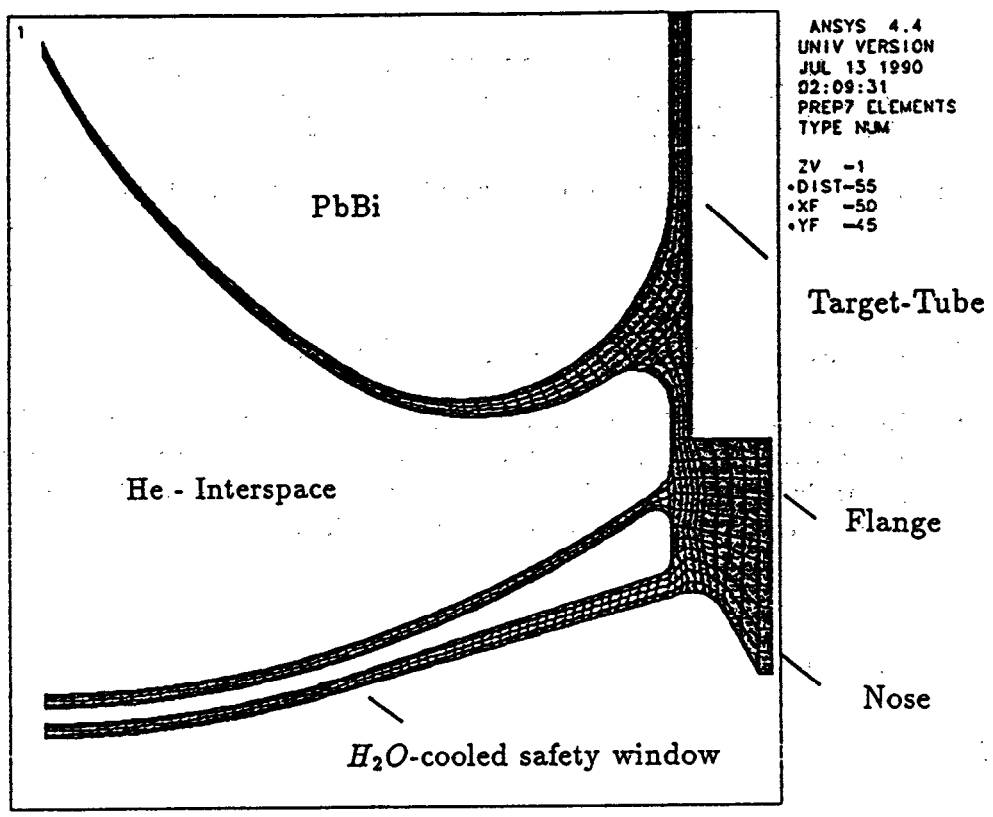

Figure 1: Outlines of the axisymmetric finite element model used in the present analysis.

II.1 Power Deposition

The power density distribution is approximated by a two-component gaussian and calculated as a function of radius r with the following equation:

$$q[W/mm^3] = I_o\ E_o[\frac{\epsilon}{\pi\sigma_1^2}exp(-\frac{r^2}{\sigma_1^2}) + \frac{1-\epsilon}{\pi\sigma_2^2}exp(-\frac{r^2}{\sigma_2^2})] + q_o$$

where

I_o = 1500 μA is the maximum total current,
E_o = 1.69 $W/\mu A/mm$, the energy deposition by ionisation-loss,
σ_1 = 13.4 mm, the S.D. of the fraction by-passing Target E,
σ_2 = 43.6 mm, the S.D. of the 'normal' beam and
q_o = 0.016 W/mm^3.

The above equation takes account of a part, ϵ, of the beam bypassing Target E, which produces a smaller beam spot with a standard deviation of σ_1. The uniform background contribution q_o comes from neutrons, gammas etc. backscattered from the target [3].

II.2 Heat Transfer on the PbBi-cooled Window

The heat transfer coefficients for the PbBi-cooled surface were derived from a thermal-hydraulic calculation [4] and are given in tabular form as a function of radius.

r(mm)	0	1	2	3	4	5	7.5	≥ 10
h(mW/$mm^2/°C$)	0	4.7	6.7	7.5	8.0	8.4	9.1	9.3

A constant bulk temperature (T_{PbBi} = 226°C) for the PbBi in the region of the window has been assumed.

II.3 Heat Transfer on the H_2O-cooled Window

The film heat transfer coefficient on the H_2O-cooled surfaces are derived from a modified Dittus-Boelter equation [5] which takes into account the thermal entrance length of the heated region.
For subcooled boiling, the Shah-correlation [6] has been used. Two regimes of subcooled boiling are defined: the low subcooling regime where the following equation holds:-

$$\Psi = \Psi_o$$

and the high subcooling regime

$$\Psi = \Psi_o + \frac{\Delta T_{sub}}{\Delta T_{sat}}$$

Ψ is defined as:

$$\Psi = \frac{q}{\Delta T_{sat} h_l}$$

and Ψ_o is the value of Ψ at zero subcooling and given by:

$$\Psi_o = 230 Bo^{0.5} \qquad Bo \geq 0.3\ 10^{-4}$$
$$\Psi_o = 1 + 46 Bo^{0.5} \qquad Bo \leq 0.3\ 10^{-4}$$

The transition point between the two regimes has been calculated by the Saha-Zuber correlation [7]:

When $Pe \leq 70000$

$(\Delta T_{sub})tr = 0.0022 q d_h / \lambda_{fl}$

when $Pe \geq 70000$

$(\Delta T_{sub})tr = 154.q d_h / (Pe \lambda_{fl})$

The cooling of the safety window can be supplied either by the main cooling circuit for the target ($T_{bulk} = 128^oC$) or by a separate circuit ($T_{bulk} = 40^oC$). The predicted heat transfer coefficients, for both bulk temperatures and for different fluid velocities and pressures, are tabulated below. A thermal entrance length of $X_l = 3cm$ has been used to calculate the film heat transfer coefficient: the value of X_l corresponds approximately to the full-width half-maximum of the beam bypassing Target E. A constant bulk temperature is assumed in the flow direction. The critical heat flux has been estimated from the empirical formula given by S.Mirshak [8]:

$$q_{chf} = 151(1 + 0.1197v)(1 + 0.00914\Delta T_{sub})(1 + 0.186p) \quad (W/cm^2)$$

$$5 \leq \Delta T_{sub}(_oC) \leq 75 \quad 1.5 \leq v(m/sec) \leq 14 \quad 1.7 \leq p(bar) \leq 6.2$$

Heat transfer for the H_2O-cooled window ($d_l = 2mm$)

case	T_{bulk}	T_{sat}	p_{H2O}	v_{fluid}	X_l	h_l	q_{chf}
	°C	°C	bar	m/sec	cm	$W/cm^2/°C$	W/cm^2
a)	40	180	10	2	3	1.4	1220
b)	"	"	"	4	"	2.6	1450
c)	"	"	"	6	"	3.7	1690
d)	128	"	"	2	"	2.0	790
e)	"	"	"	4	"	3.5	940
f)	"	"	"	6	"	4.8	1100
g)	40	160	6.2	2	"	1.4	840
h)	"	"	"	4	"	2.6	1000
i)	"	"	"	6	"	3.7	1170
j)	128	"	"	2	"	2.0	520
k)	"	"	"	4	"	3.5	620
l)	"	"	"	6	"	4.8	720

The wall temperatures T_w for the two windows as a function of the heat flux q are shown in Figs 2 & 3. As can be seen in these figures, case b) or c) should be chosen to avoid subcooled boiling at a current density of $105\mu A/cm^2$: this corresponds to a heat flux of $355W/cm^2$ for the $2mm$ thick window. In the stress analysis, only case b) has been used to calculate the temperature distribution within the H_2O-cooled window.

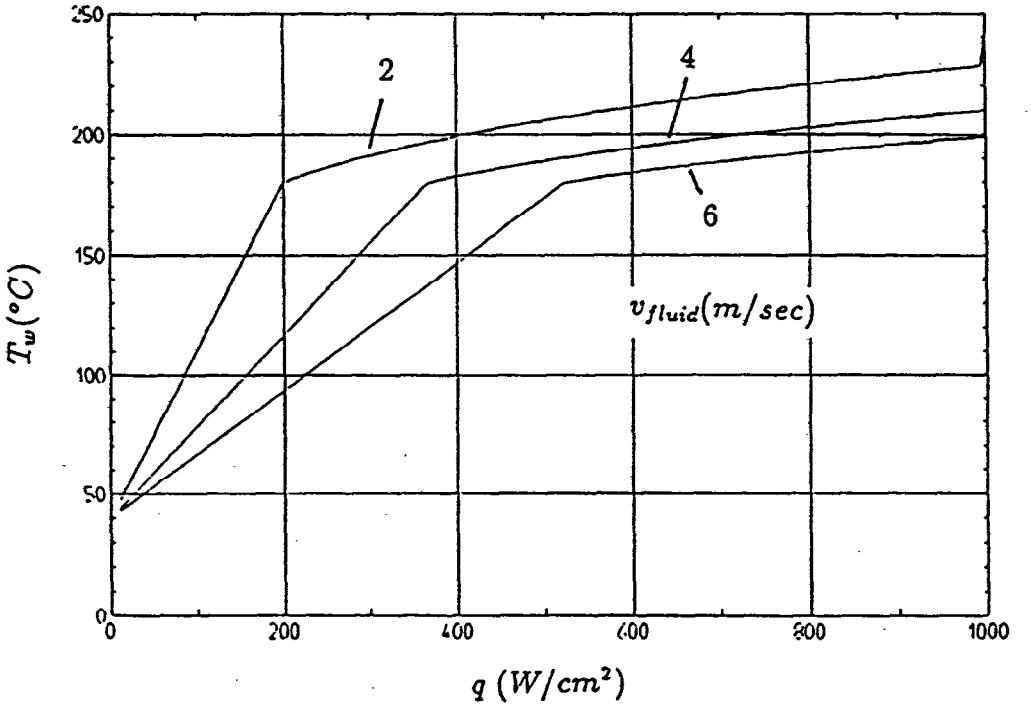

Figure 2: Wall temperature $T_w(°C)$ vs heat flux $q(W/cm^2)$: $T_{bulk} = 40°C, p_{H2O} = 10bar$

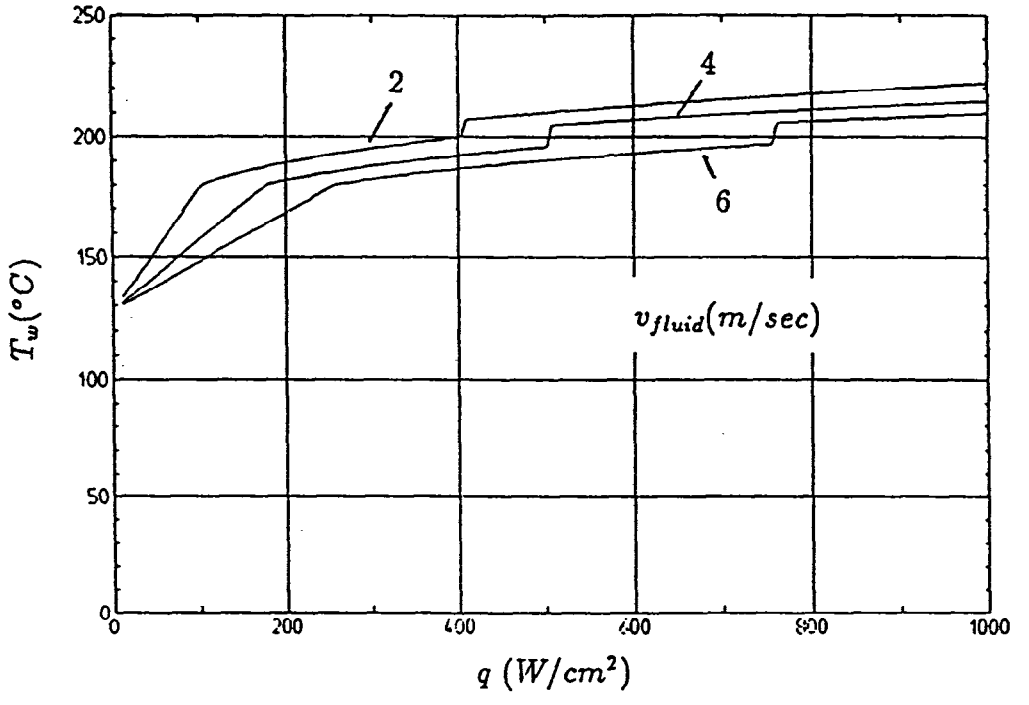

Figure 3: Wall temperature $T_w(°C)$ vs heat flux $q(W/cm^2)$: $T_{bulk} = 128°C, p_{H2O} = 10bar$

III. Thermal and Stress Analysis for a Peak Current Density of $105\mu A/cm^2$

In the following analysis it is assumed, that 33% of the beam bypasses Target E and gives a peak current density of $105\mu A/cm^2$.

III.1 Temperatures and Heat Flow

The above load and boundary conditions have been used to calculate the temperature distribution within the structure. Figs 4 & 5 show the surface temperature of the H_2O-cooled safety window and the PbBi-cooled window respectively as a function of distance along the surface to the center. The calculated heat flow from the structure to the fluids inside ($r \leq 80mm$) and outside the beam region ($r \geq 80mm$) are as follows:

Heat flow to H_2O :

1st Window element ($r \leq 80mm$)	5840 W
2nd Window element ($r \leq 80mm$)	5560 W
Both Window elements ($80 \leq r \leq 90mm$)	3310 W

Heat flow to PbBi:

Window element ($r \leq 80mm$)	6720 W
Window element ($80 \leq r \leq 90mm$)	1530 W
Target-Tube	191 W/cm

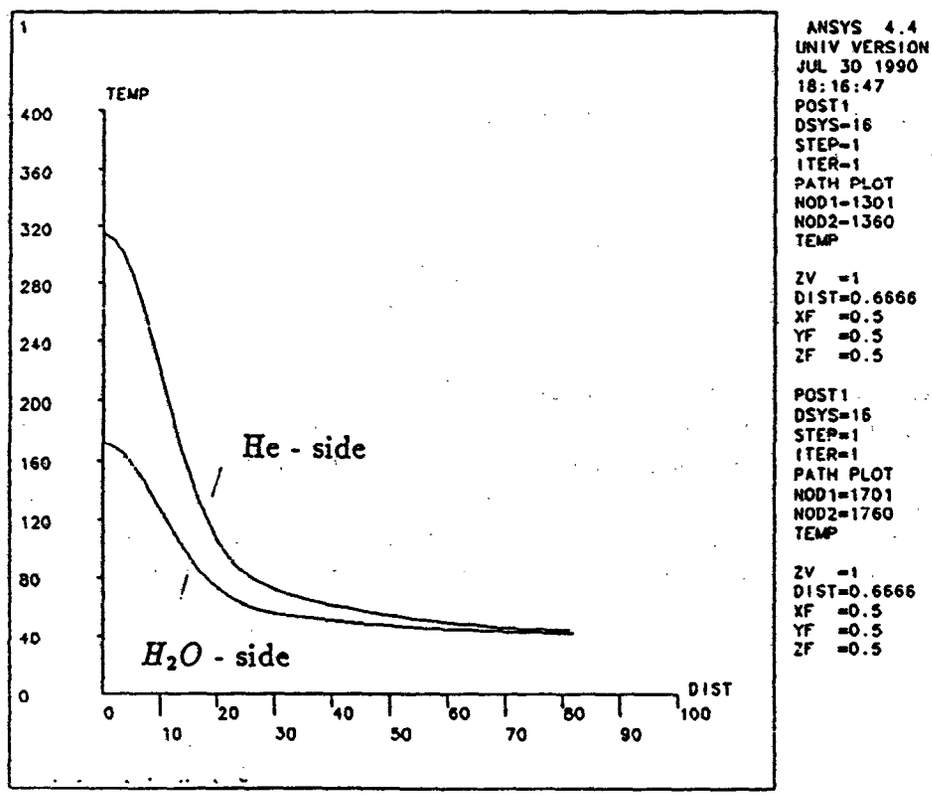

Figure 4: Temperature distribution (^oC) of the H_2O-cooled window plotted as a function of the distance (mm) to its center.

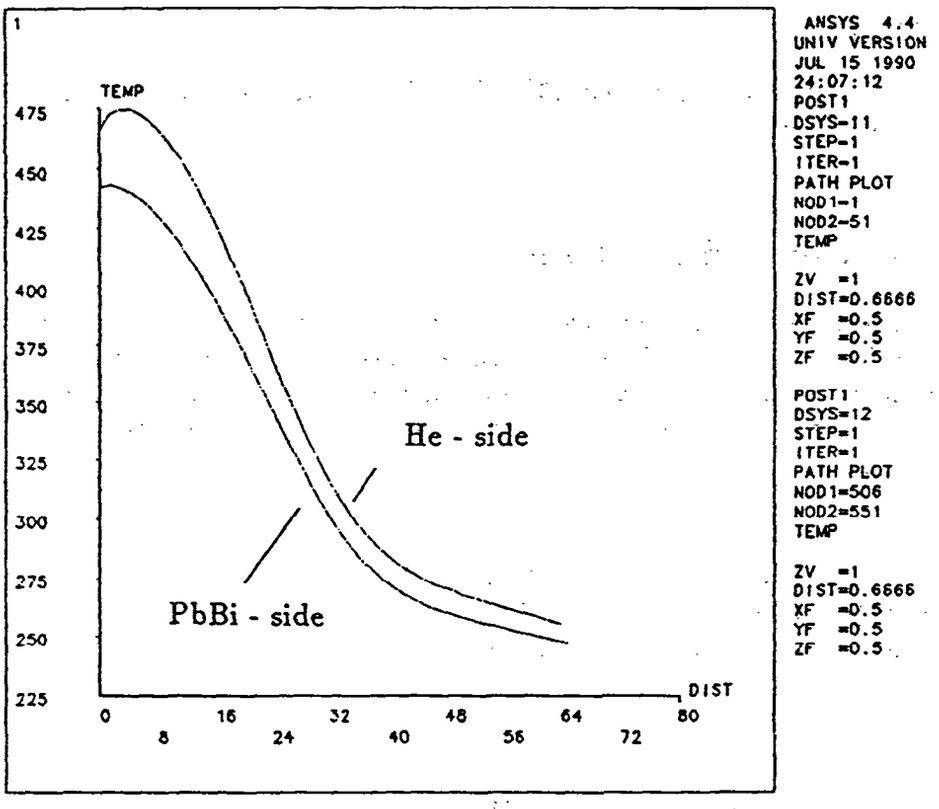

Figure 5: Temperature distribution (^oC) of the PbBi-cooled window plotted as a function of the distance (mm) to its center.

III.2 Stresses

A linear structural analysis based upon the calculated temperature distribution has been performed for the following static pressures:

$$\begin{aligned} P_{H2O} &= 10 \text{ bar} \\ P_{He} &= 0\&10 \text{ bar} \\ P_{PbBi} &= 5 \text{ bar} \end{aligned}$$

In the Figs 6 & 7, the calculated component stresses S_y for the two windows are plotted as a function of the distance along the surface to their centers. Here, S_y represents the in-plane component stress in the radial direction. As can be seen in the figures, the main contribution comes from bending stress induced by the thermal load. From the calculated stress distribution the von Mises stress has been used to evaluate a safety factor, based upon the temperature dependent yield strength. The stress maxima and corresponding safety factors are summarized below for the different load cases:

Von Mises Stress (N/mm^2) and safety factor ()
($p_PbBi = 5bar$, $pH_2O = 10bar$)

Load case	thermal	no	yes	yes
	$p_{He}(bar)$	0	0	10
$1^{st}H_2O$-cooled window	$r < 50mm$	-	150 (3)	-
	$r > 50mm$	-	160 (3)	-
$2^{nd}H_2O$-cooled window	$r < 50mm$	40	471 (.81)	432 (.88)
	$r > 50mm$	145	360 (1.3)	340 (1.4)
PbBi-cooled window	$r < 50mm$	40	100 (3.5)	100 (3.5)
	$r > 50mm$	100	190 (2.0)	170 (2.5)

The safety factor in the center part of the PbBi-cooled window reaches a value ≥ 3.5, while the second H_2O-cooled window shows a safety factor < 1 at its center, where plastic deformation may occur.

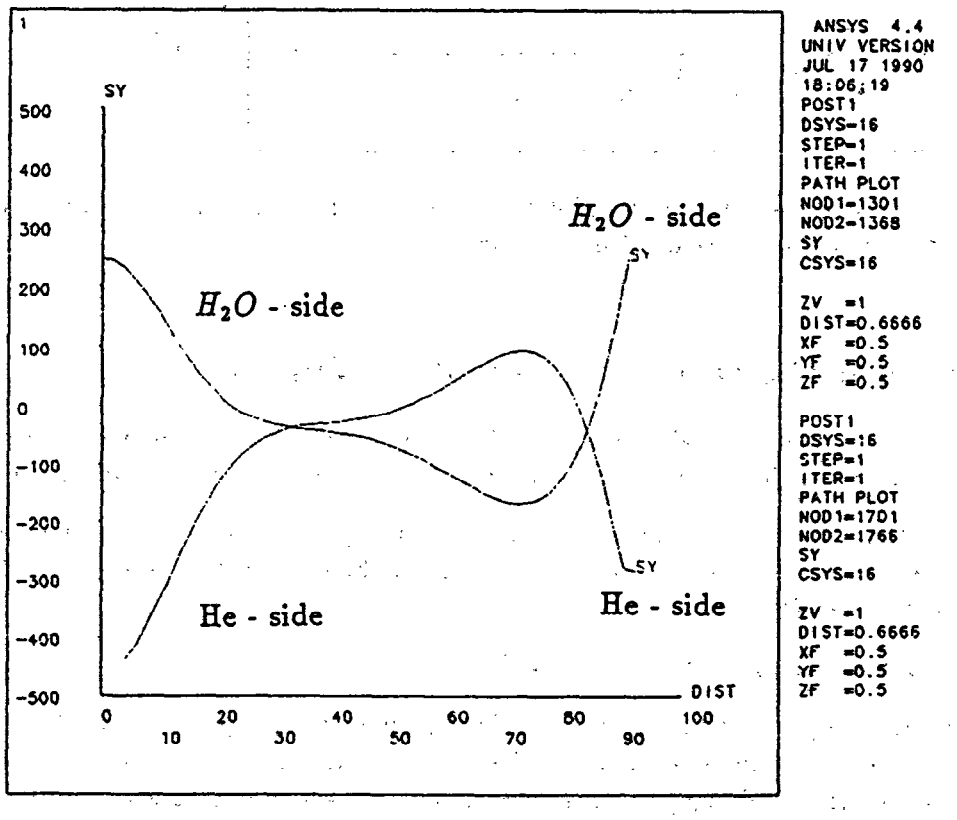

Figure 6: Component stresses $S_y(N/mm^2)$ plotted along the surface of the $2^{nd}H_2O$-cooled window as a function of the distance (mm) to its center ($p_{He} = 0bar$).

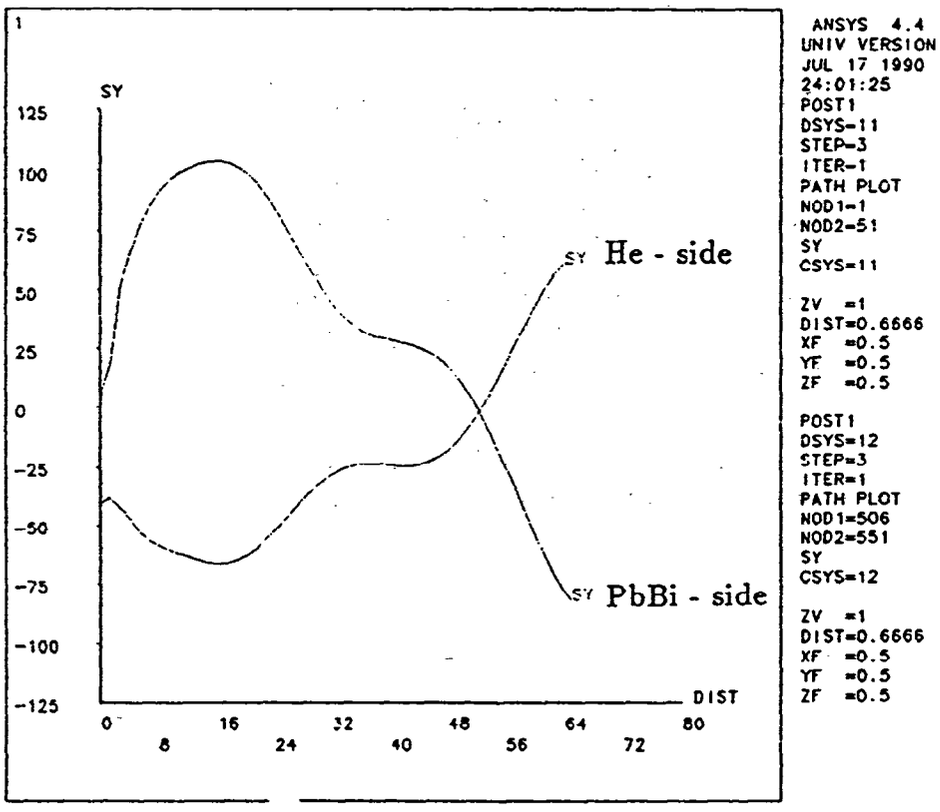

Figure 7: Component stresses $S_y(N/mm^2)$ plotted along the surface of the PbBi-cooled window as a function of the distance (mm) its center $(p_{He} = 0bar)$.

IV. Redesign of the second H_2O-cooled Window

From the present studies the essential influence of the temperature drop at the window center as well as at the flange to the stress level can be seen. Therefore, the following steps have been taken:

- The thickness of the window has been decreased from 2 to 1mm at its center and increased from 2 to 4mm at its edge. This is done by changing the radius of the spherical surface of the He-side from the original 154mm to 141.7mm.

- The nose of the support flange has been removed.

A thermal and stress analysis has been performed for this new geometry. The von Mises peak stress in the window now occurs at the edge and is $264N/mm^2$: at the center, the stress is reduced from $471N/mm^2$ (with the original design) to $220N/mm^2$. The corresponding safety factors, based upon the temperature dependent yield strength, are ≥ 2 throughout the window. The component stresses S_y plotted along the window surfaces are shown in Fig 8 and may be compared with those for the original design in Fig 6.

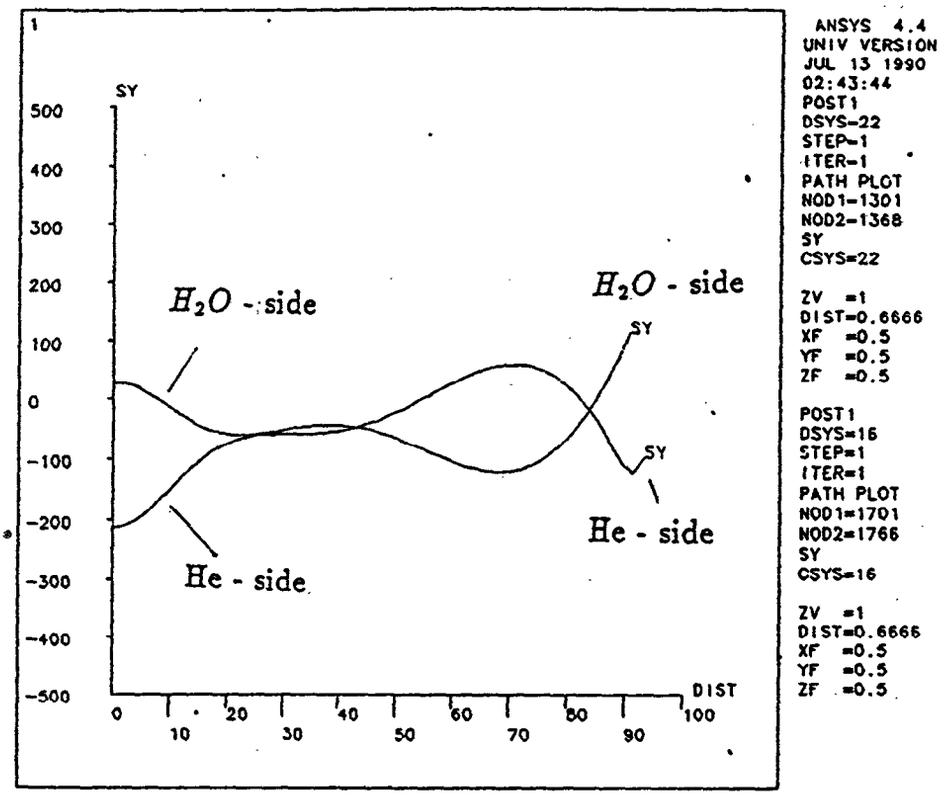

Figure 8: Component stresses $S_y(N/mm^2)$ plotted along the surface of the redesigned $2^{nd} H_2O$-cooled window as a function of the (mm) to its center $(p_{He} = 0bar)$.

V. Thermal and Stress Analysis for a Peak Current Density of $265\mu A/cm^2$

In the following simulation, the extreme fault condition is assumed, where the full beam bypasses Target E ($\epsilon = 100\%$). The same boundary conditions have been used as in the previous calculations.

V.1 Temperatures

In Fig 9, the temperature response of the PbBi-cooled window at its center has been plotted as function of time. At $t = 0$ the beam has been changed from normal operation (a peak current density of $25\mu A/cm^2$) to $265\mu A/cm^2$. The steady-state temperature distribution for each window is shown in the Figs 10 & 12. The surface temperature of the H_2O-cooled window exceeds the saturation temperature of the liquid within a radius $r \leq 12\ mm$ for the first and $r \leq 7\ mm$ for the second window and the high subcooling regime starts. The heat flux from the first window reaches a value of $\sim 900\ W/cm^2$ but is less than the predicted critical heat flux.

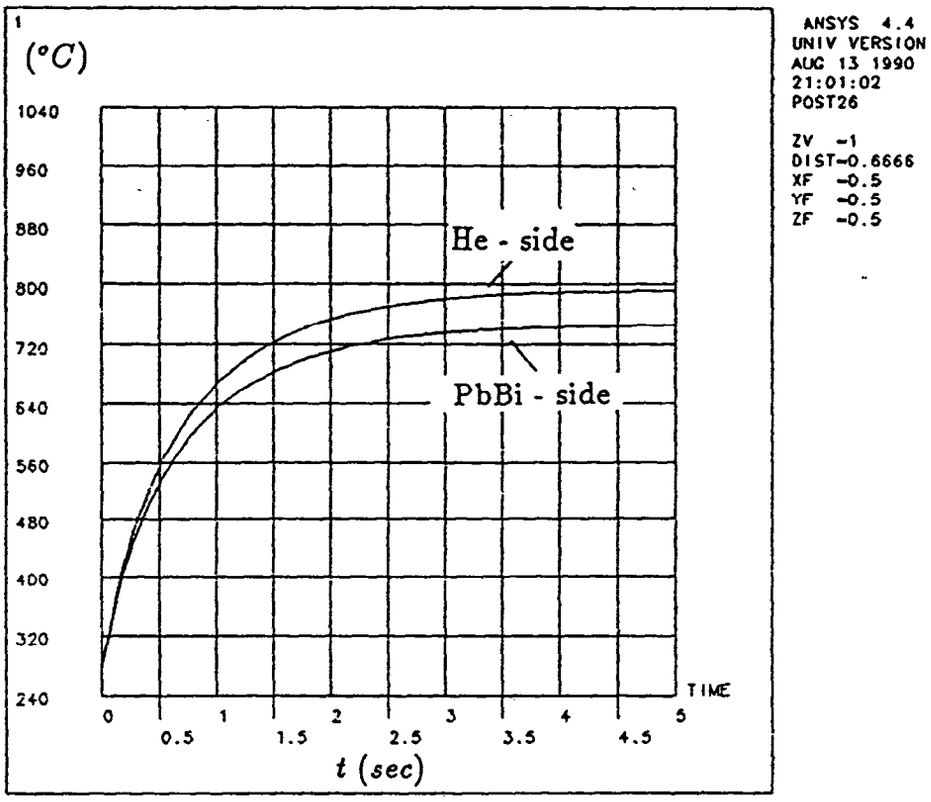

Figure 9: Temperature response ($°C$) of the PbBi-cooled window at its center plotted as a function of time t (sec). At $t = 0$ the beam size has been changed from a normal operation at a peak current density of $25\mu A/cm^2$ to a peak density of $265\mu A/cm^2$.

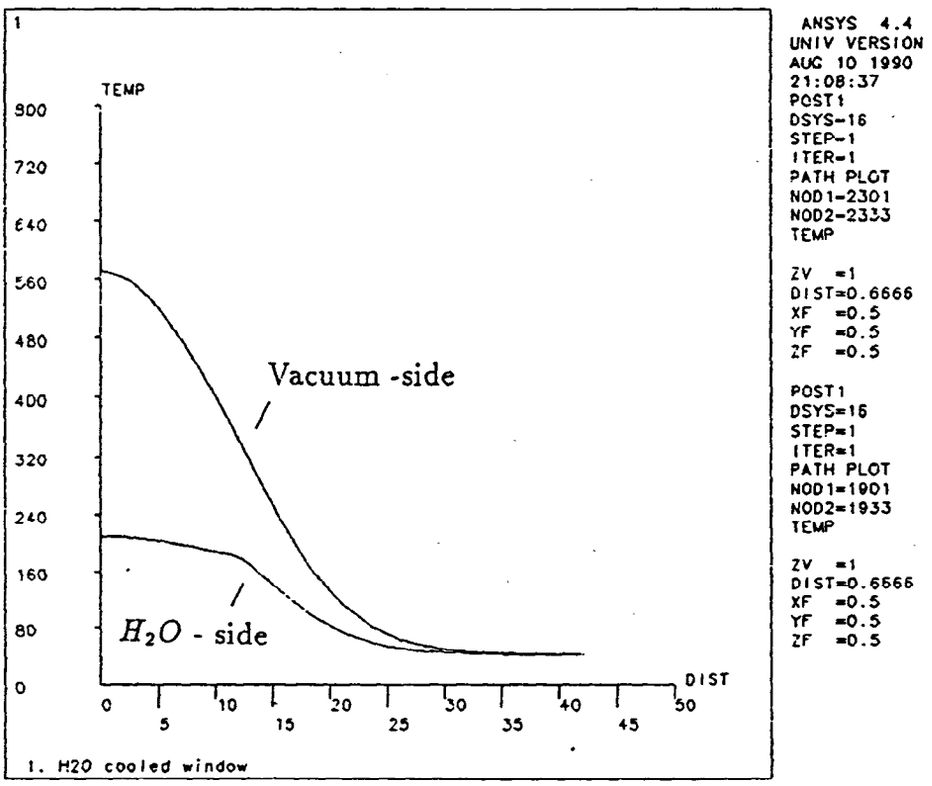

Figure 10: Temperature distribution ($°C$) of the first H_2O-cooled window plotted as a function of the distance (mm) to its center ($265\mu A/cm^2$).

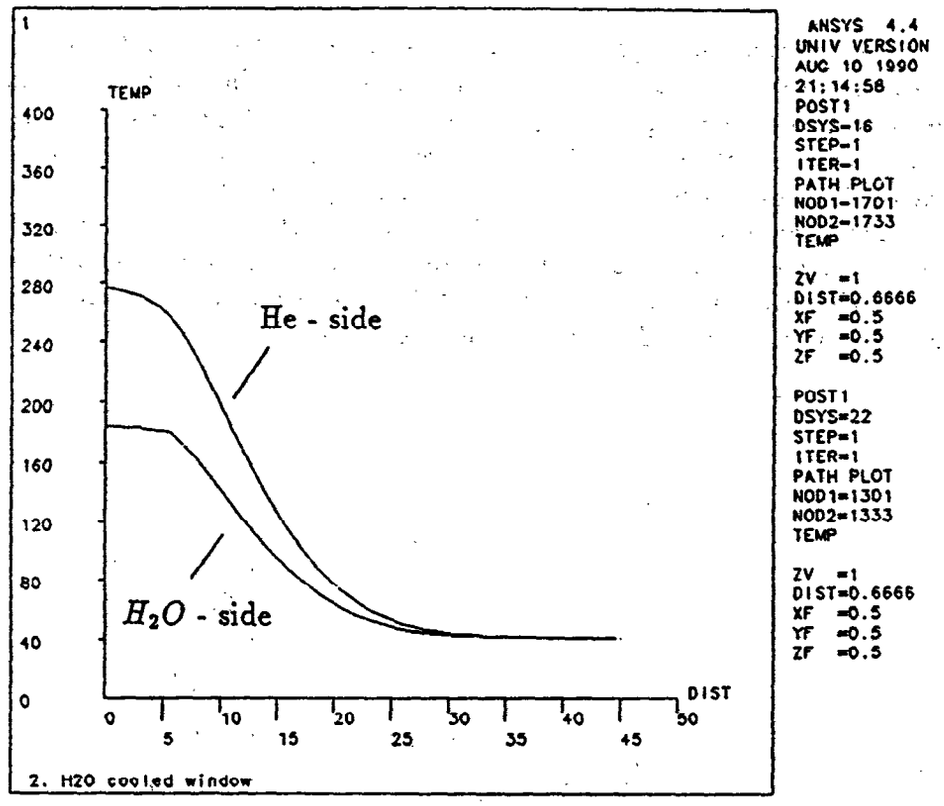

Figure 11: Temperature distribution ($°C$) of the second H_2O-cooled window plotted as a function of the distance (mm) to its center ($265\mu A/cm^2$).

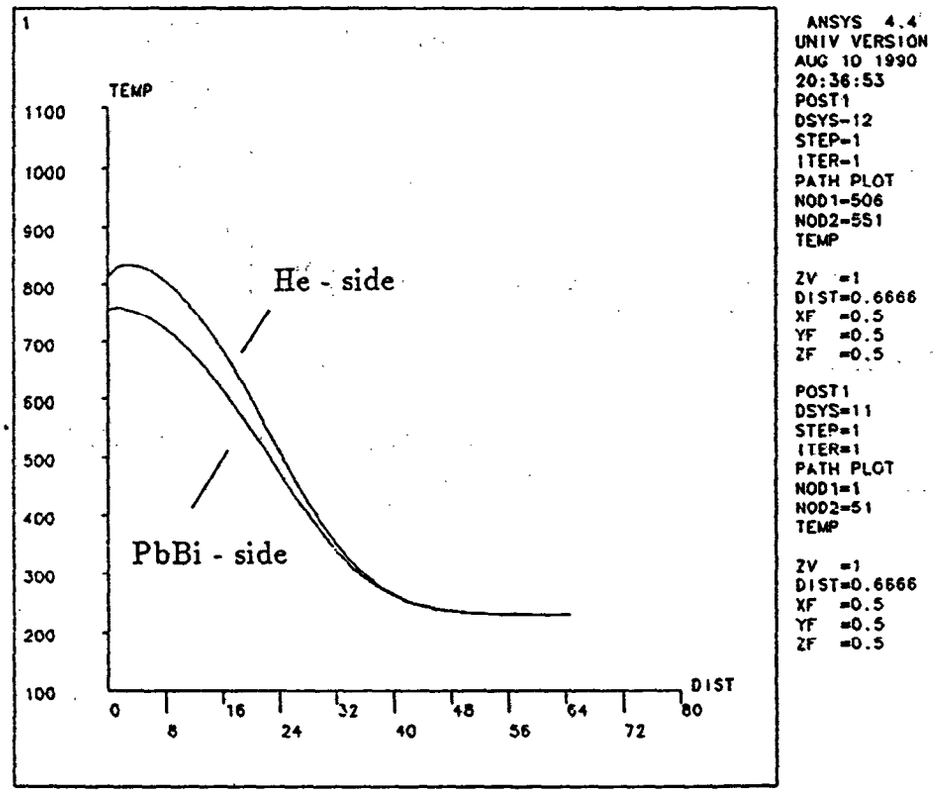

Figure 12: Temperature distribution ($°C$) of the PbBi-cooled window plotted as a function of the distance (mm) to its center ($265\mu A/cm^2$).

V.2 Stresses

In Fig 13, the von Mises stress has been plotted along the surfaces of the first H_2O-cooled window as function of the distance to its center. The stress level is less than the allowable yield strength at the corresponding temperature and at any position of the window. In Fig 14, the component stresses S_y are plotted along the surfaces of the second H_2O-cooled window. At the center, the von Mises stress exceeds slightly the yield strength within a local region. The component stresses S_y along the surfaces of the PbBi-cooled window are shown in Fig 15. Within a path length $\leq 20\ mm$, corresponding to a radius $\leq 12\ mm$, plastic deformation occurs and stress relaxation is expected, due to the drop of the yield strength at the high peak temperatures of up to $830°C$. The elastic limit is reached at $\sim 550°C$ which is about $0.5sec$ after the current-density increase (see Fig 9).

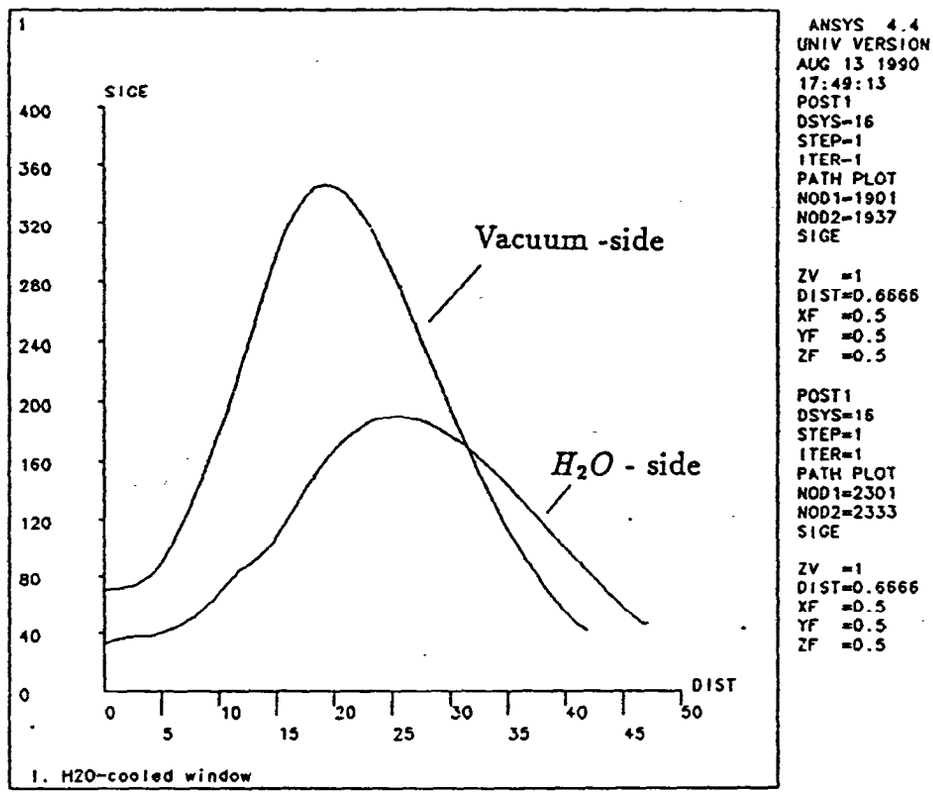

Figure 13: Von Mises stress (N/mm^2) plotted along the surfaces of the the first H_2O-cooled window as a function of the distance (mm) to its center ($265\mu A/cm^2$).

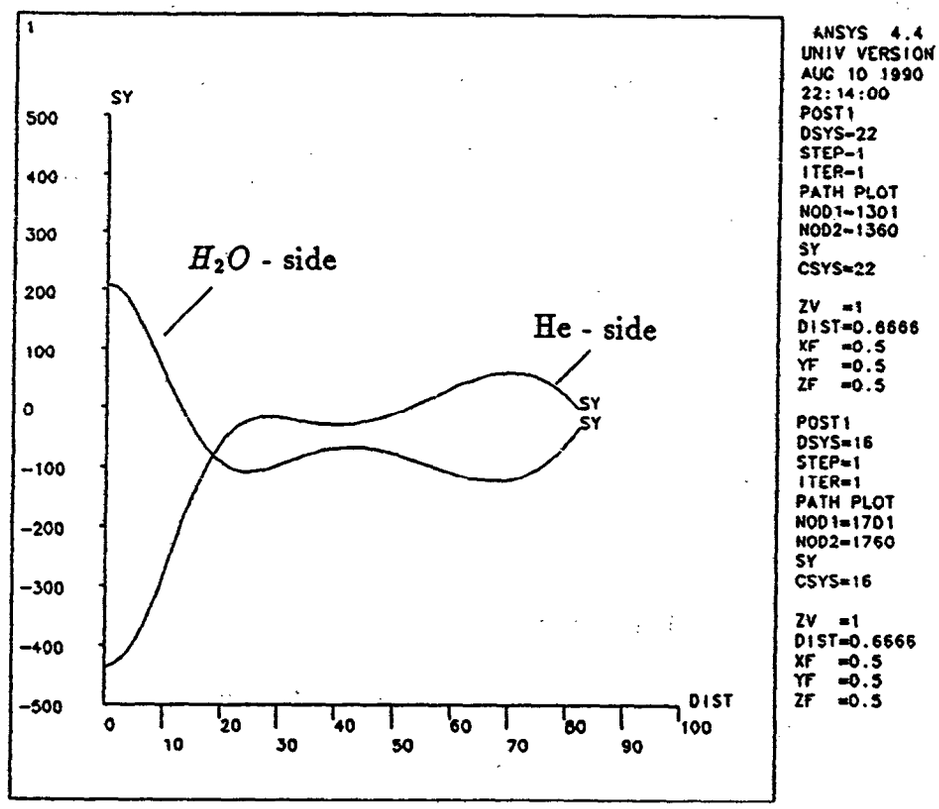

Figure 14: Component stresses $S_y(N/mm^2)$ plotted along the surfaces of the second H_2O-cooled window as a function of the distance (mm) to its center $(265\mu A/cm^2)$.

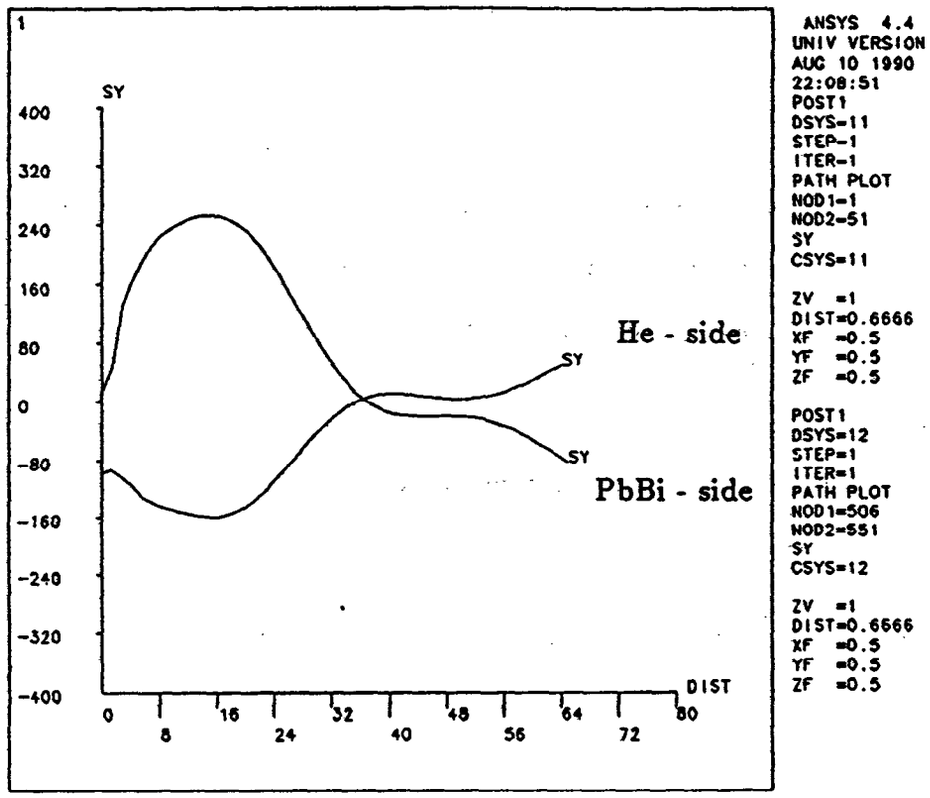

Figure 15: Calculated component stresses $(S_y(N/mm^2)$ plotted along the surfaces of the PbBi-cooled window as a function of the distance (mm) to its center $(265\mu A/cm^2)$. Note: in this case, the temperature is higher then $550°C$ and outside the range of yield-strength data.

VI. Conclusions

The present study predicts adequate safety margins for peak current densities of up to $105\mu A/cm^2$ and hence, safe long-term operation may be expected for both windows. For higher current densities, up to $265\mu A/cm^2$, the stresses stay well within the elastic range of the selected steel throughout the H_2O-cooled window. However, the present linear analysis shows that the stresses in the PbBi-cooled window exceed the elastic limit. Further investigations are required to allow prediction of the lifetime and failure mode of this window: these need to include non-linear analysis and load cycling as well as the change of the material properties due to irradiation effects.

VII. Nomenclature

$\Delta T_{sub} =$	$T_{sat} - T_{bulk}$	subcooling
$\Delta T_{sat} =$	$T_w - T_{sat}$	
T_{sat}	saturation temperature of fluid	
T_{bulk}	bulk temperature of fluid	
T_w	wall temperature	
q	heat flux, power density	
q_{chf}	critical heat flux	
h_l	single phase heat transfer coefficient	
Bo	boiling number	
Pe	Peclet number	
X_l	thermal entrance length	
d_l	channel width of fluid	
d_h	hydraulic diameter	
λ_{fl}	thermal conductivity of fluid	

References

[1] ANSYS, Swanson Analysis Systems Inc.,Houston, PA 15342 USA

[2] M. Dubs and J. Ulrich, Design considerations of the target window, ICANS-XI, Japan 1990

[3] F. Atchison, SINQ-project internal report SINQ/816/AF38-002, 1990

[4] B.Sigg et al.,Thermal-hydraulics Investigation for the Liquid Lead-Bismuth Target of the SINQ Spallation Source,ICANS-XI, Japan 1990

[5] VDI-Wärmeatlas 1984, p. Gb3,Gd4

[6] M. Shah, Generalized Prediction of Heat Transfer during Subcooled Boiling in Annuli,Heat Transfer Eng. vol.4 no.1, 1983

[7] P. Saha and N. Zuber, Proc. of the 5th Int. Heat Transfer conf., vol IV, 1974, p. 175

[8] S. Mirshak et al., Heat Flux at Burn-out, du Pont de Namours, Savannah River, DP-355, 1959

ICANS-XI International Collaboration on Advanced Neutron Sources
KEK, Tsukuba, October 22-26, 1990

A Solid Target for SINQ based on a Pb-Shot Pebble-bed

F. Atchison and G. Heidenreich
PAUL SCHERRER INSTITUTE
CH-5232 Villigen PSI, Switzerland

ABSTRACT
Preliminary results from scoping calculations examining the possibilities of implimenting a Pebble-bed of Pb-shot as a target for SINQ are presented. The primary design objects are set out and estimates of heating and activation given. Cooling circuit parameters are discussed and estimates for operating conditions presented. A short discussion of problems associated with a realisation is included.

1 Introduction

Neutronic calculations [1] indicate a Pb-shot pebble-bed target system is capable of producing thermal fluxes at least as high as with the current engineered design for the liquid Pb-Bi eutectic mixture target. A solid-Pb target system has a less hazardous nuclide inventory and the activation locked in a solid matrix. It is also subject to less severe material compatibility difficulties (which in the case of the Pb-Bi target bring the majority of the flux loss). This opens the way to the production of a target system with large operational safety margins while using materials with 'neutronically' acceptable characteristics.

The prime requirement for the design is to maintain the integrity of the beam-window and to hold the Pb under its melting point. The major consideration is proton beam current density. The peak current-density at the design current of 1.5 mA and for all the beam passing through the up-stream meson target (Target-E) is predicted to be 25 $\mu A/cm^2$. Any beam which by-passes Target-E will produce a smaller spot at SINQ. Such a beam condition is likely to arise from operational tolerances for the accelerator/proton-beam complex and may result in current densities up to 100 $\mu A/cm^2$ and for long periods; under extreme (and rare) fault conditions, the by-pass component could contain the whole beam and then the current density would reach 260 $\mu A/cm^2$.

A target system unable to stand such high current densities would require protection systems against them. If the maximum handleable current density is too low, it will cause, at the minimum, a loss of thermal-neutron fluence from excessive beam interruptions. A reasonable margin of error is required: it should allow any remedial action to keep the beam matched to Target-E to be taken at a realistic speed, but has to be limited because of the technical difficulties of handling the high-power densities.

We take as primary specification that the target/beam-window system will be capable of normal operation (satisfies thermal and mechanical criteria) with a peak current density of 100 $\mu A/cm^2$ and, to limit the scope of accident-scenario discussion, will 'survive' current densities of 260 $\mu A/cm^2$, for a short time period at least (it will have only marginal safety tolerances). Implicit in this specification is that the average peak current density over (say) one operational year remains close to 25 $\mu A/cm^2$, i.e. a hundred or so hours at the higher current levels accumulated over the year.

The final design of the Pebble-bed target is to fit into the present geometry of the Pb-Bi version [2]. The neutronically important region will be inside a cylinder of roughly 20 cm diameter and 100 cm long. This suggests an axial water flow as space limitations would make transverse cooling difficult to implement. On simplicity grounds, we consider a randomly packed bed and with the Pb-shot constrained into several sub-packets. At this stage we also restrict the considerations to the (most important) length of 50 cm which covers the main heating region. A sketch of the target is shown in Fig. 1.

Preliminary estimates for heating will be given in the next section and in the following two sections, cooling system parameters for the Pb-shot and the window respectively will be discussed. Section 5 will present activation estimates and a brief review of other considerations to be incorporated into a practical target design will be given in section 6.

2 Preliminary Estimates for Heating

A sketch of the target and moderator systems used for the neutronic estimates may be seen in Fig. 1 & 6 of [1]. Both activation (Section 5) and energy-density will vary somewhat with details of the design (maybe at the 10's of percent level) and will need recalculation when a detailed design for the whole system is available. Furthermore, the calculations have been made using a theoretical estimate for the proton beam distribution which corresponds to 'perfect matching' with Target-E (i.e. a peak current density of 25 $\mu A/cm^2$ at 1.5 mA). The energy balance for the inner part of the SINQ system with the Pb-shot target and for 570 MeV protons may be seen in Table IV of [1].

The pebble-bed has been represented in the calculation by a homogeneous mixture of 50% by volume Pb and D_2O. A simple hand estimate indicates that about 90% of the energy will be deposited in the Pb: an initial power density distribution for the Pb is based on the assumption that it receives all except the gamma-contribution (prompt nuclear and π^o). The resulting power-density distribution is shown as a contour plot in Fig. 2.

For a beam current of 1 mA, the calculation gives the following values:-

	Total Power (kW)	Average Power Density (W/g)	Peak Power Density W/g
D_2O (Direct)	33	-	-
Pb-Shot	385	6.7	37
Inner Al Wall	4.2	1.4	2.7
Outer Al Wall	4.4	1.2	2.4

The power-density for the window aluminium is given in terms of two factors: a conversion from proton beam current density at the window to power-density (2.5 W/g for 1 $\mu A/cm^2$

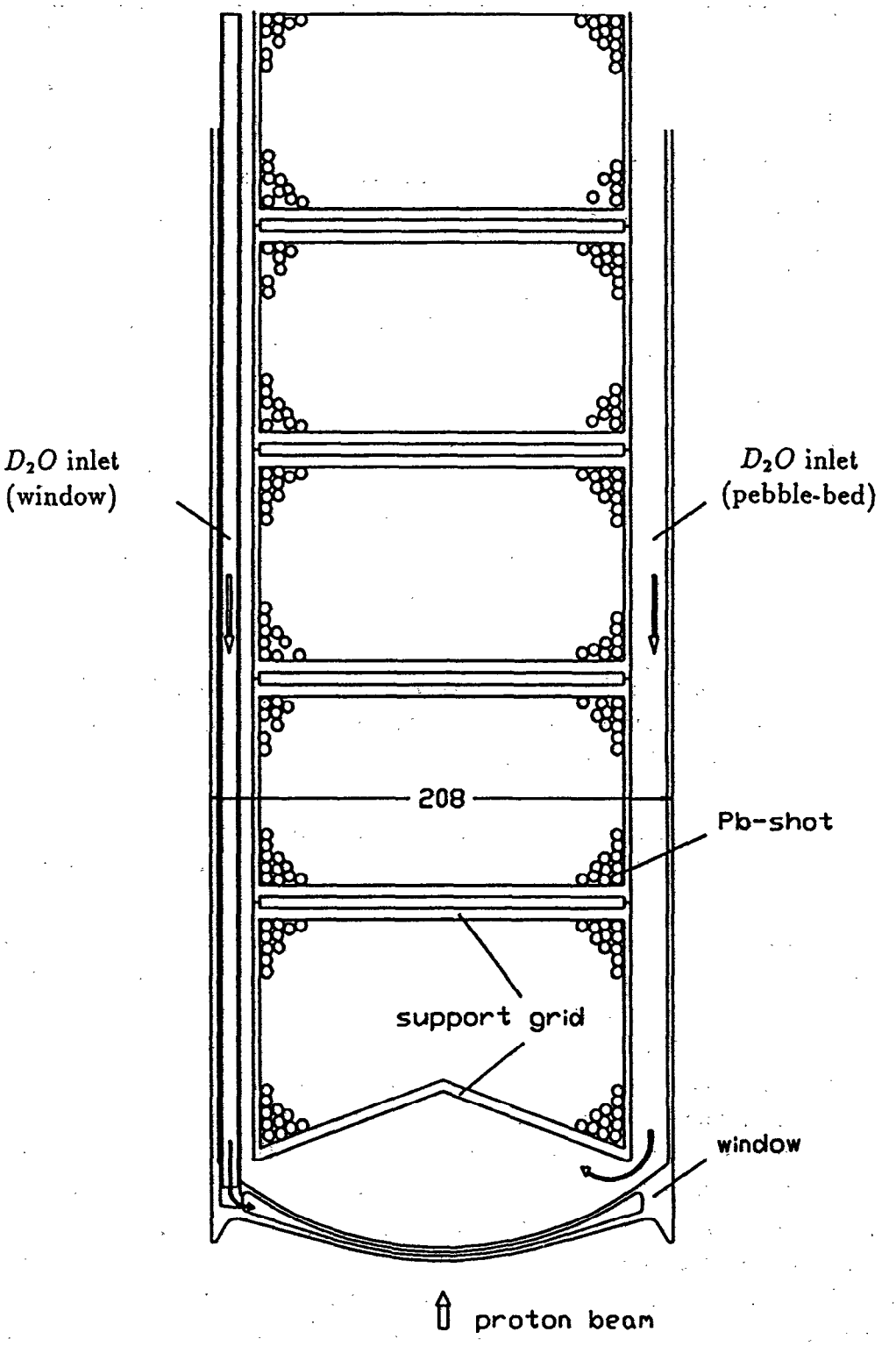

Figure 1: A sketch of the Pb Pebble-bed target. Aluminium is to be used for the material of construction and D_2O as the coolant for both the pebble-bed and the beam window.

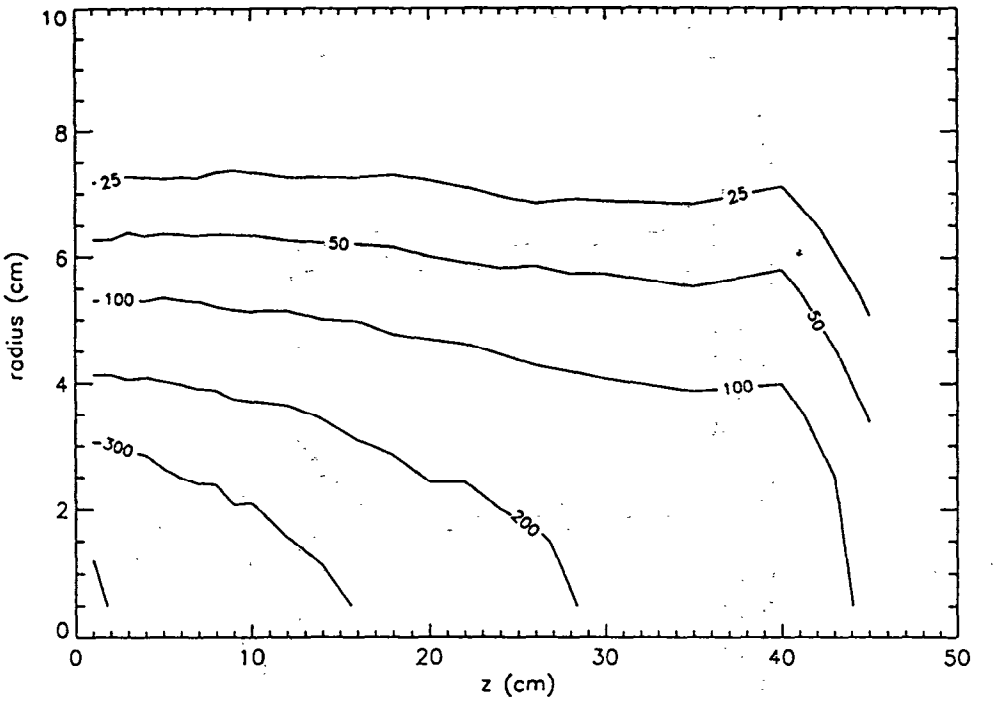

Figure 2: A contour plot of the power density distribution $q_0(r,z)$, W/cm^3, in the Pb of the pebble-bed for a total current I_0 of 1 mA, $\sigma_0 = 4.36$ cm and a void fraction $\phi_0 = 0.5$.

proton beam current density) and a background contribution of 1.4 W/g/mA from neutrons, gammas etc. backscattered from the target which is approximately uniform over the whole surface of the window.

The critical regions from the cooling point of view are the beam-window and the pebble-bed. The basic results from the neutronic calculation need some processing so that they can be applied to the varying beam-size. The power density distribution in the pebbles depends on both the proton beam density and the void fraction ϕ of the packed bed. The beam density distribution is approximated by a two component gaussian: one component represents the normal operation mode, where all the beam passes through the upstream meson target (Target E) and gives a standard deviation of $\sigma_o = 43.6mm$; the second component represents a part ϵ of the beam, which by-passes Target E and gives a standard deviation of $\sigma_\epsilon = 13.4mm$. Fig. 2 shows the power density distribution $q_o(r_o, z_o)$ for a beam current $I_o = 1mA$, the standard deviation σ_o and a void fraction $\phi_0 = 0.5$ of the packed bed. The values of $q_o(r_o, z_o)$ has been scaled by the relations below, to calculate the power density distribution $q(r,z)$ for the design current $I = 1.5mA$, the void fraction $\phi = 0.4$ of a randomly packed bed and for a part ϵ of the beam by-passing Target E.

$$q(r,z) = \frac{I}{I_o}[(1-\epsilon) + \epsilon\frac{\sigma_o^2}{\sigma_\epsilon^2}]\; q_o(r_o, z_o)$$

$$where: \quad z_o = \frac{1-\phi}{1-\phi_o} z \quad and \quad r_o = \frac{\sigma_o}{\sigma_\epsilon} r$$

3 Cooling of the Pebble-bed

The parameters of the cooling system of the bed should satisfy the following general conditions:

- The maximum centre temperature of the Pb-shot should be below the melting point of Pb (327 °C) at incident proton beam current densities up to 100 μA/cm^2 and also for at least some time at 260 μA/cm^2 (we imply by this that at the highest power density safety margins will be very small - it is considered to be an extreme fault condition).
- The surface temperature of the balls should be below T_{sat}, the saturation temperature (Note: the high pressure loss means that T_{sat} will vary along the length of the pebble bed).
- A practical beam window to withstand the high current densities specified will not be able to stand pressures above about 12 bars.

There will be a range of operating conditions and so, following some introductory general considerations on power distribution, heat-transfer and pressure-loss in the pebble-bed, the ranges of these parameters will be considered in terms of a water-velocity - shot-diameter search space.

3.1 Heat Transfer and Pressure Loss in the Packed Bed

The heat transfer coefficients, h, on the pebble surface are calculated from [3]:

$$h = Nu k_{fl} \frac{(1-\phi)}{\phi d}$$

$$Nu = (0.4 Re^{0.5} + 0.2 Re^{0.67}) Pr^{0.4}$$

$$Re = \frac{v_z d}{\nu_{fl}(1-\phi)}$$

where ν_{fl} is the kinematic viscosity and k_{fl} the thermal conductivity of the coolant.
The pressure loss dP/dz in the bed is calculated using [4]:

$$\frac{dP}{dz} = \Psi \frac{\rho_{fl} v_z^2}{2d} \frac{1-\phi}{\phi^3}$$

$$\Psi = \frac{320}{Re} + \frac{20}{Re^{0.4}} + 1.75$$

and where ρ_{fl} is the density of the fluid.
In Fig. 3 the pressure loss is presented as a function of the fluid velocity v_z measured in the empty bed and the pebble-diameter d for a void fraction $\phi = 0.4$. To avoid excessive stresses at the window, the pressure loss should not exceed ~12 bar/m, which corresponds to an entrance pressure of 12 bars and an exit pressure of 6 bars for the 50 cm long bed.

3.2 Temperature Distribution

In the present axisymmetric model the temperature distribution of the fluid $T_{fl}(r,z)$ within the packed bed is calculated by [5]:

$$\rho_{fl} c_{fl} v_z \frac{\partial T_{fl}}{\partial z} = k_r\left(\frac{1}{r}\frac{\partial T_{fl}}{\partial r} + \frac{\partial^2 T_{fl}}{\partial r^2}\right) + q_{fl}$$

where $k_r = \rho_{fl} c_{fl} v_z \frac{F}{K} d$ represents the radial convective heat transfer, F is a shape factor (F=1.15 for spheres) and K is a function of both the pebble and bed diameter (K=8.5); $q_{fl} = q(1-\phi)$ is the power density (normalized to the total volume) and c_{fl} is the specific heat of the fluid.

The surface temperature $T_s(r,z)$ and the centre temperature $T_c(r,z)$ of each spherical pebble are derived from:

$$T_s = q\frac{d}{6h} + T_{fl} \quad and \quad T_c = q\frac{d^2}{24k} + T_s$$

where k is the thermal conductivity of the solid lead.

The above formulism has been used to calculate the temperature maxima within the bed, normalized to the peak current density and as a function of the pebble-diameter and the fluid velocity. The results are presented in Fig. 4 for the D_2O temperature,Fig. 5 for the shot surface temperature and Fig. 6 for the centre temperature.

3.3 Operating Parameters

The results of the parameter survey (Figures 3 to 6) together with the constraints, allow construction of a velocity - diameter diagram describing the range where practical operating conditions exist. It will also indicate the process causing any limitation.

Taking 12 bars as the highest water pressure at the window, a pressure drop of 12 bar/m is a reasonable practical limit. This gives saturation temperatures of 190 °C at the window and 160 °C after 50 cm. As the contours indicate only the maximum values and not their position, we take 160 °C as the saturation temperature. Taking a water temperature of 40 °C at the start of the bed then the reduced temperatures at 25, 100 and 260 μA/cm^2 are:-

	25 μA/cm^2	100 μA/cm^2	260 μA/cm^2
D_2O Temperature	4.8	1.3	0.46
Shot Surface Temperature	5.2	1.2	0.5
Shot Centre Temperature	11	2.9	1.1

These values are used to construct the velocity-diameter diagram shown in Fig. 7 for 100 μA/cm^2 and Fig. 8 for 260 μA/cm^2. Any combination of values in the diagram (Fig. 7) are adequate for 25 μA/cm^2 and the range of choice to satisfy 100 μA/cm^2 is wide.

As the beam current density increases the working-space shrinks onto the '12 bar/m' line (see dashed lines in Fig. 7) indicating firstly the maximum current density handleable and secondly the optimum shot diameter: the values are about 170 μA/cm^2 and 5 mm shot diameter. The operational maximum will be at a somewhat lower current density to allow sufficient tolerance to handle the void fraction statistical variation from random packing. It

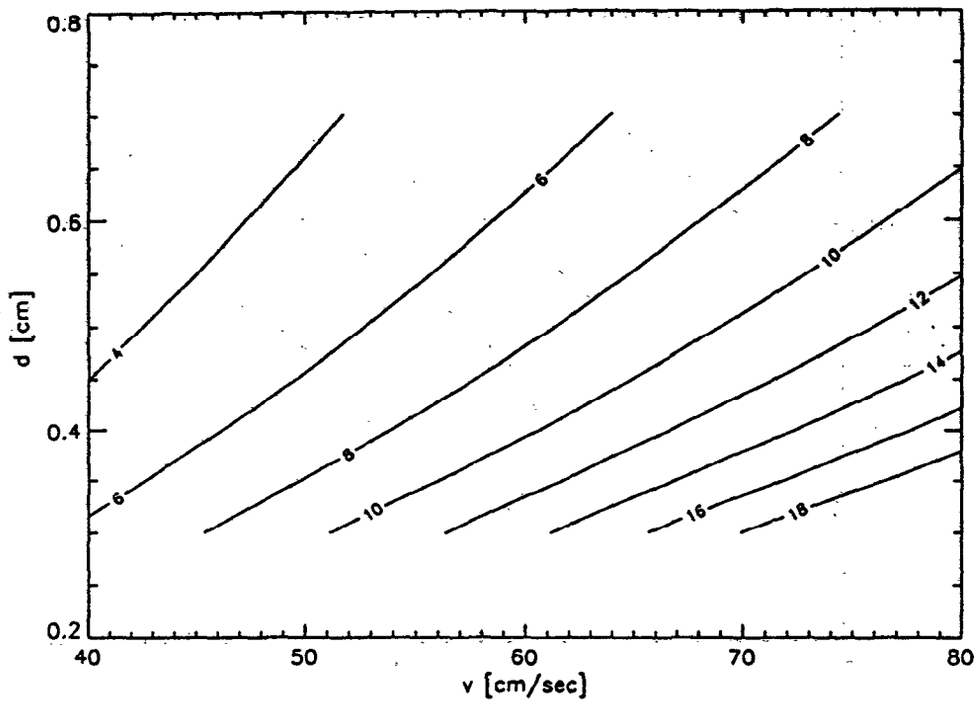

Figure 3: Contours of equal pressure loss (bar/m) as a function of water velocity and sphere diameter.

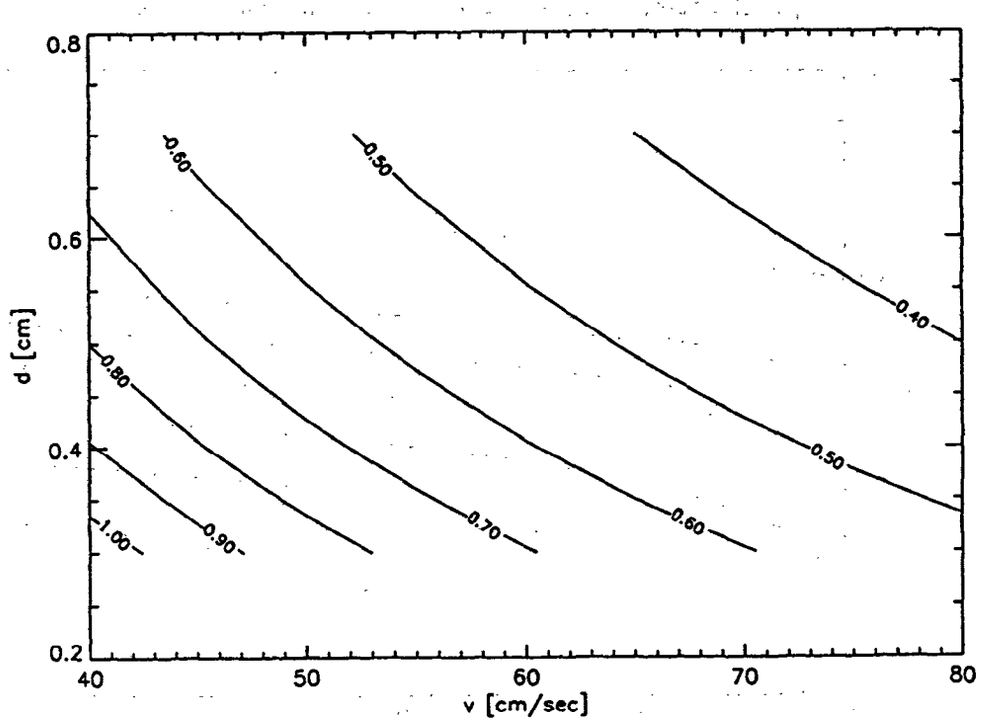

Figure 4: Contours of equal peak *reduced* D_2O temperature for a range of fluid velocities and Pb-sphere diameters. The reduced temperature is calculated from $\frac{T_{fl}-T_{fl,in}}{\eta}$, where η is the peak proton current density (μA/cm^2), T_{fl} is the actual fluid temperature and $T_{fl,in}$ is the temperature of the fluid at the start of the bed.

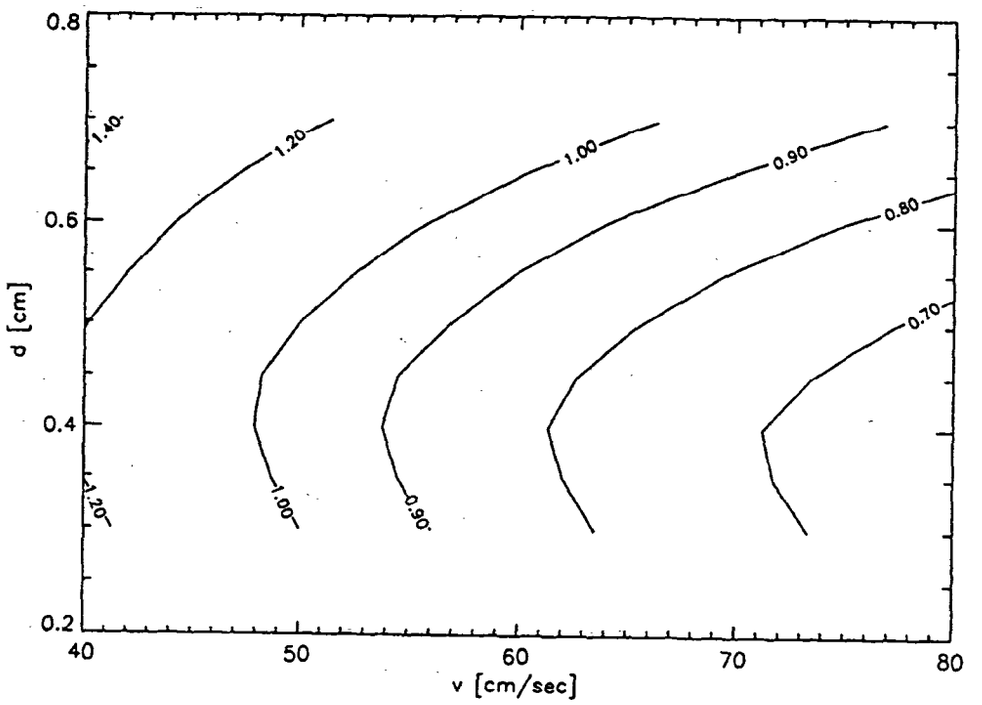

Figure 5: Contours of equal peak *reduced* Pb-sphere surface temperature for a range of fluid velocities and Pb-sphere diameters. The reduced temperature is calculated from $\frac{T_s - T_{fl,in}}{\eta}$, where η is the peak proton current density (μA/cm^2), T_s is the actual surface temperature and $T_{fl,in}$ is the temperature of the fluid at the start of the bed.

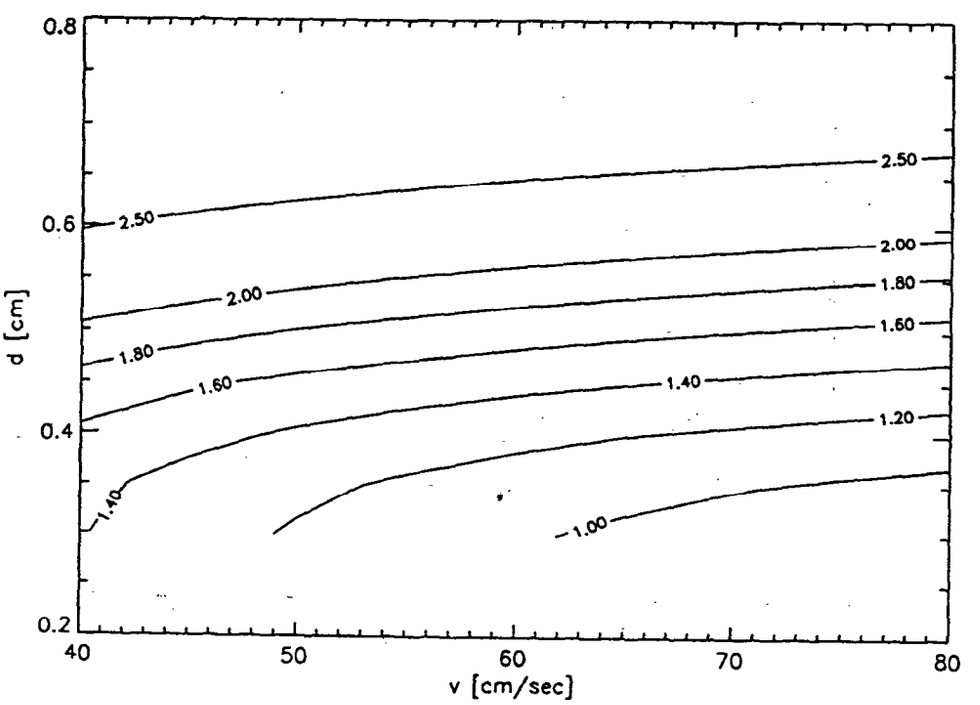

Figure 6: Contours of equal peak *reduced* Pb centre temperature for a range of fluid velocities and Pb-sphere diameters. The reduced temperature is calculated from $\frac{T_c - T_{fl,in}}{\eta}$, where η is the peak proton current density (μA/cm^2), T_c is the actual peak centre temperature and $T_{fl,in}$ is the temperature of the fluid at the start of the bed.

should also be noted that a higher maximum might be obtained if nucleate-boiling was included; this cannot be treated at this stage.

Fig. 9 shows a plot of the three pertinent temperatures (D_2O, surface and centre of the shot) along the axis of the bed for a current density of 170 $\mu A/cm^2$, a shot of diameter 5 mm and a water-velocity of 75 cm/sec. Temperatures are well below their limiting values at all positions.

Fig. 8 shows that for a current density of 260 $\mu A/cm^2$ (Note: the higher velocity range), a simple 50 cm long pebble bed would require a pressure drop of 35 bar/m. This is considered to be incompatible with a practical beam window to handle the same current density.

The main limiting factor is the temperature of the D_2O. The lateral spread of the water flow through the pebble-bed is rather low. Consequently, too small a mass of water is available to handle the high power on the axis. The distribution of water temperature through the pebble-bed is shown as a contour plot in Fig. 10. This suggests that a fruitful approach would be to introduce 'flow-diverters' between the sections of the pebble-bed. These would laterally displace the axial water flow after some suitable distance down the pebble-bed and divert cooler water to the axis for the next section of the bed. The results of Fig. 9 & 10 would suggest a displacement of 1 or 2 cm after about 10 cm as being sufficient. No detailed work has been done on this yet.

4 Beam-Entry Window

The window has to pass 1.5 mA proton current with a peak current density that can reach 260 $\mu A/cm^2$. There will be 12 bars static pressure on the inner side from the pebble-bed coolant and the proton-beam vacuum on the outer side.

The design for the outer (safety) element of the beam window for the Pb-Bi eutectic target [6] is taken as starting point. In this case, aluminium is to be the material of construction and (temperature dependent) material properties as for 6063 - T5 alloy have been used for the thermal and stress analysis made with the engineering analysis system ANSYS [7]. The window consists of two spherical caps with D_2O flowing between and is shown in Fig. 1. The aluminium thickness at the centre is 2 mm and the cooling will be supplied by an independent circuit. The power density distribution used has been described in Section 2. Heat transfer coefficients as for the earlier analysis [6] are used here: h = 2.6 $W/cm^2/°C$ for a flow velocity of 4 m/sec and a bulk temperature of 40 °C. For the present, the cooling effect of the water for the pebble-bed is neglected so that for the present both elements are identical and cooled on one surface only. The extra cooling will improve the safety-factor of the inner element but the flow characteristics for the pebble-bed coolant in this region are not yet worked out.

The maximum temperature for the window at a peak current density of 260 $\mu A/cm^2$ is 160 °C on the vacuum side. The von Mises stresses and the safety factor based on yield strength for peak current densities of 100 and 260 $\mu A/cm^2$ are given in the following table (the 50 mm radius roughly delimits the regions with and without beam heating):

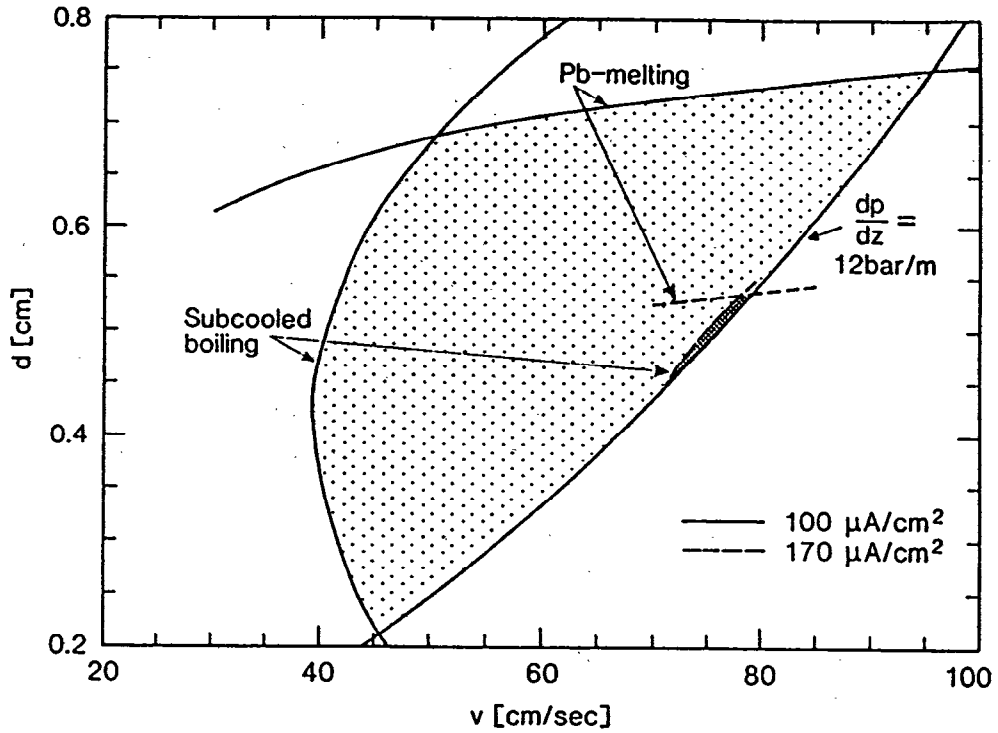

Figure 7: Operating region for velocity and shot diameter values in a simple random-packed (void fraction = 0.4) pebble-bed of length 50 cm at a beam current density of 100 μA/cm^2 and for a pressure of 12 bars on the window.
The dashed lines show the operating region for 170 μA/cm^2 (roughly the maximum) and indicates an optimum shot diameter of 0.5 cm.

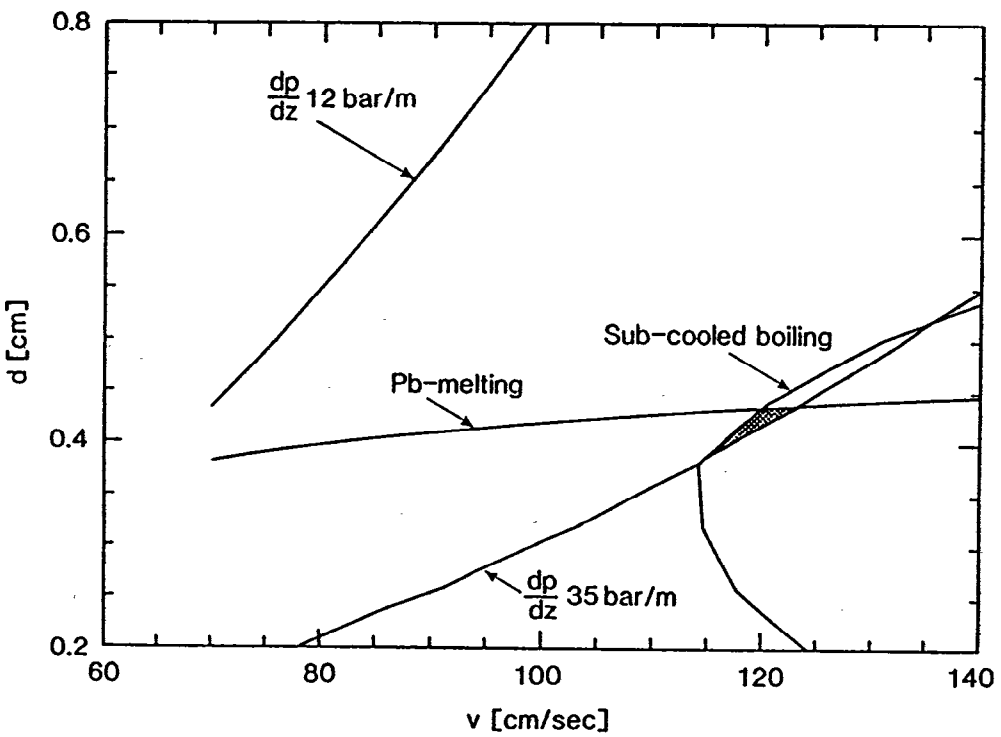

Figure 8: Operating region for velocity and shot-diameter values for 260 μA/cm^2 (Note the different velocity scale compared to Fig. 7).

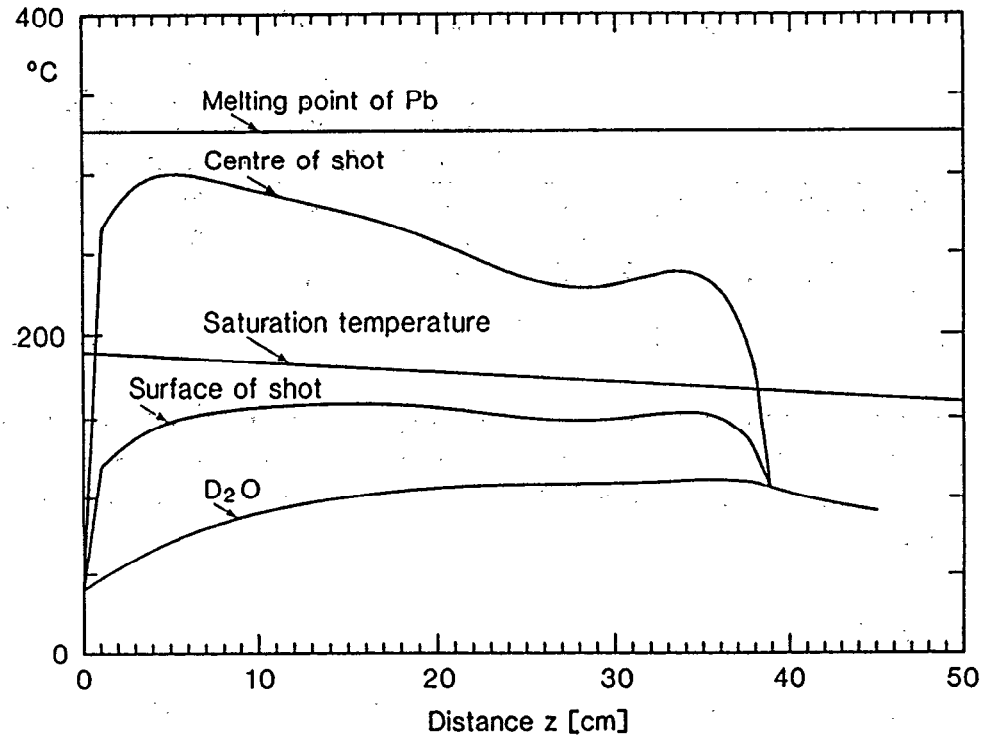

Figure 9: Axial temperature distribution at a peak current density on the beam window of 170 μA/cm^2 through a pebble-bed with 5 mm diameter Pb-shot and a D_2O velocity, v_z, of 75cm/sec. A water temperature of 40 °C at the start of the pebble-bed has been assumed.

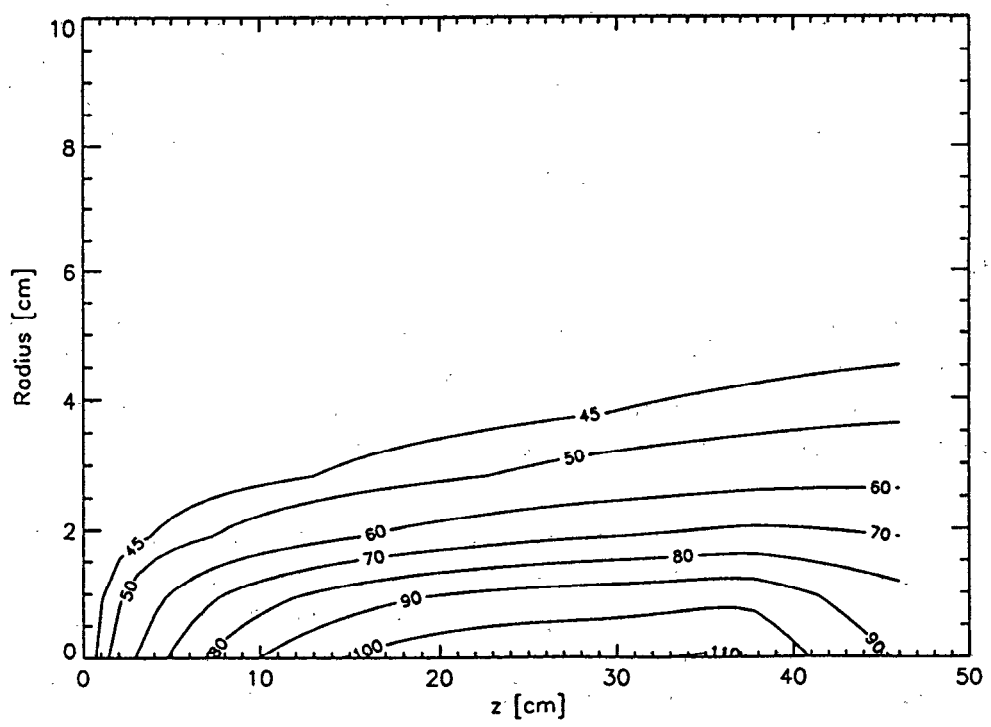

Figure 10: Contour plot of the fluid temperature in the pebble-bed as a function of depth (z) and radius. The conditions are: water velocity = 75 cm/sec, sphere diameter 5 mm, proton beam current density = 170 μA/cm^2 and inlet water temperature 40 °C.

von Mises Stress and safety factor.
(p_{window} = 10 bars, $p_{pebble-bed}$ = 12 bars)

		100 μA/cm^2		260 μA/cm^2	
		Stress N/mm^2	Safety Factor	Stress N/mm^2	Safety Factor
Outer Window	r $\leq$ 50 mm	40	3.5	70	2
	r $\geq$ 50 mm	139	1	137	1
Inner Window	r $\leq$ 50 mm	43	3.5	125	1
	r $\geq$ 50 mm	20	7	20	7

This indicates a window to pass 260 μA/cm^2 is practicable (the calculations are made with a minimally modified existing design). The main stress is caused by the static water pressure for the window coolant and the safety factor of 1 in the outer regions is indicative of the need for some design modifications.

5 Activation

A major consideration in the design is activation. A great practical advantage of the Pb-Bi target is that the main bulk of the total activation is sealed into a container and also the activation is diluted through a large mass of material. The activation of the Pb is less hazardous but the specific activation (and hence after-heat) will have a higher density and also the cooling D_2O is directly irradiated by the beam. Corrosion and the direct activation means that the external parts of the cooling circuit will have to incorporate adequate safety precautions.

The activation estimates come from the same calculation used for heating (see Section 2) and take into account nuclides produced by the high-energy particle cascade, fast and epithermal neutrons, thermal neutrons and (in the case of the Pb-shot) polonium production via α-particle induced and double production processes. No direct estimate for tritium production in the high-energy cascade is available at this time.

5.1 Lead

The build-up of secondary-product mass, activation, 'burden' [1] and decay power for 1 mA operation is shown in Table-I (a) and the decay following 1 year in operation in Table-I (b). The lower value of both activity and decay heating compared to Pb-Bi comes from the removal of the Bi: the majority of the active isotopes of Bi and Po with their relatively high decay energy are eliminated.

The activation at one year corresponds to an average value of 4.7 Ci/g and the decay power to 18 mW/g. There will be a systematic variation of the nuclide inventory within the activated region, but approximate values for the peak values may be obtained using the power density distribution. These are 27 Ci/g and 100 mW/g. Some reduction of the peak decay power will come from the energy dispersion by the (about 80%) gamma contribution.

[1] This term has been coined internally within the SINQ project to give a measure of the activation in terms of its potential hazard - the activity is multiplied by the DECO (Dose Equivalent to Critical Organ) factor to give an effective dose in rems.

Table-I

(a) The build-up of mass, activation, 'burden' and decay-power as a function of irradiation time at a current of 1 mA.

Irradiation Time	Mass g	Activation kCi	'Burden' Mrem	Decay-Power Watts
10 d	2.56	236	426	948
100 d	25.3	259	734	1030
1 y	92.2	270	962	1060
2 y	185	277	1090	1080

(b) The decay of activation, 'burden' and total decay power as a function of time following one year in operation at 1 mA. Except for short decay times, just over 80% of the decay power is radiated as gammas.

Decay Time days	Activation kCi	Burden Mrem	Decay-Power Watts
0	270	962	1080
0.1	180	930	620
10	27	490	99
100	8.3	220	21
365	2.5	95	5.8

The 'burden' for the nuclide inventory is 962 Mrem after 1 year in operation at 1 mA. This is a factor of about 74 lower than with the Pb-Bi target. The major contributors (collected by element) together with the values for Pb-Bi, are shown in Table-II.

5.2 Aluminium Container

The specific equilibrium activation (averaged over a 45 cm length of the walls) for products with half-lives greater than 10 mins (the shorter half-life products contribute about 18 Ci/g) at a beam current of 1 mA are:-

Nuclide	Half-life	Decay Mode	Equil. Activity Ci/g
^{24}Na	15.0 h	$\beta^-\gamma$	0.029
^{22}Na	2.60 y	$\beta^+\gamma$	0.046
^{21}Na	22.5 s	$\beta^+\gamma$	0.0075
^{18}F	110 m	β^+	0.037
^{3}H	12.3 y	β^-	0.13

The contribution from Tritium has been estimated using the approximation (suggested by the value from Oxygen) that production corresponds to 10% of the high-energy cross-section. The activation of the aluminium is mainly of interest as a potential contribution to activity in the coolant from corrosion.

Table-II

The major contributors to 'burden' (Mrem) with the Pb target and the Pb-Bi targets after operation at 1 mA for 1 year.

Element	Pb-Target	Pb-Bi Target
I	134	305
Sr	100	149
Ir	94	3
Hg	75	47
Y	73	116
Pb	73	39
Bi	68	13900
Tl	62	72
Po	54	56200
Xe	38	68
Os	27	20
Pt	25	27
Cd	20	42
Yb	17	17
Ce	10	21
Others	92	174
Totals	962	71200

5.3 Heavy Water

The build-up of activation and specific activation at given locations will depend on the conditions of the circuit: for an irradiation volume V in which the coolant is irradiated for a time t_{irr}, a coolant circulation time of t_{circ} and a total time in operation T ($= N \cdot t_{circ}$ and only relevant for long half-life products), the specific activation at the *end* of the irradiation volume is given by:-

$$\mathcal{I} = \sum_i \mathcal{J}_i = \sum_i \frac{\alpha_i}{V} \cdot \frac{(1 - \exp^{-\tau_i t_{irr}})(1 - \exp^{-\tau_i T})}{(1 - \exp^{-\tau_i t_{circ}})}$$

where α_i is the equilibrium activation and τ_i the decay constant for nuclide i (in the one or two cases where there is a decay chain, this expression needs an obvious modification to treat the daughters). The specific activation at some position with a time-delay from the end of the irradiation volume of t_{dec} is obtained by introducing the appropriate exponential factor into the sum over nuclides.

To give some feel for the orders of magnitude, Table-III shows values of the specific activation calculated with some 'guess' parameters (see the caption). The majority of the products are short-lived and will decay to negligible levels shortly after beam switch-off. The presence of ^{17}N will be noted in the design of the plant: being a comparatively long half-life neutron emitter it has the potential to cause activation to some degree *throughout* the cooling circuit. The tritium activity will approach 2400 Ci (but only in times given by the build-up with a 12.3 year half-life: 120 Ci at 1 year; 980 Ci at 10 years; 1900 Ci at 30 years).

Table-III

Specific activation, Ci/litre, for the D_2O coolant by nuclide and using the circuit parameters: flow velocity 0.5 m/sec, irradiation volume 8.8 lit., irradiation time (per circulation) 1.8 sec. and a circulation time of 230 sec. (i) at the end of the irradiation volume, A_{irr}, (ii) at a point beyond the end of the irradiation volume reached in 50 seconds, A_{det}, (Note: only nuclides giving significant contribution at this point are included in the table) and (iii) the equilibrium specific activation, A_{eq}.

Nuclide	Half-life	Decay Mode	A_{irr}	A_{det}	A_{eq}
^{15}O	2.03 m	β^+	7.3	5.5	520
^{14}O	70.59 s	$\beta^+\gamma$	0.42	0.26	22
^{17}N	17.0 s	$\beta^- n^o$	0.017	0.023	2.5
^{16}N	7.13 s	$\beta^-\gamma$	8.7	0.067	54.0
^{13}N	9.96 m	β^+	0.95	0.90	110
^{14}C	5730 y	β^-	$2.3 \cdot 10^{-5}$	$2.3 \cdot 10^{-5}$	83
^{11}C	20.38 m	β^+	0.33	0.32	47
^{10}C	19.3 s	$\beta^+\gamma$	0.45	0.074	7.2
^{13}B	17.33 s	$\beta^-\gamma$	0.31	0.042	4.5
^{11}Be	13.8 s	$\beta^-\gamma$	0.035	0.0028	0.41
^{10}Be	$1.6 \cdot 10^6$ y	β^-	$1.9 \cdot 10^{-8}$	$1.9 \cdot 10^{-8}$	20
^{7}Be	53.29 d	EC	0.082	0.082	13
^{3}H	12.3 y	β^-	0.039	0.039	275
Totals			202	7.3	1340

5.4 Lead Corrosion

The D_2O coolant will be contaminated by corrosion/erosion products. The principal cause for concern is the Pb-shot which will present a large surface area to the coolant and also probably collide with one another giving an erosion contribution.

Although the exact process rates have not yet been established, order-of-magnitude estimates of the activation aspects are useful at this stage to see the potential extent of the problem: cladding of the shot is planned but the degree of quality control and the consequence of failure depend critically on the hazard being inhibited.

The build-up of activation in the D_2O will be non-linear. If the production rate, in the *target*, for a nuclide with decay constant λ is $\dot{q}$ g·atom/sec, then, neglecting feeding from chains, the activity after some time t will be $\mathcal{A}$ given by:

$$\mathcal{A} = 1.628 \cdot 10^{13} \times \dot{q} \times (1.0 - \exp^{-\lambda t})$$

If the target material enters the D_2O at a rate $\dot{C}$, then the build-up of the coolant activity will be:

$$\dot{C} \cdot \mathcal{A} \cdot \frac{1}{\lambda} \cdot (1.0 - \exp^{-\lambda t}) = 1.628 \cdot 10^{13} \times \dot{q} \times \dot{C} \times \frac{1}{\lambda} \times (1.0 - \exp^{-\lambda t})^2$$

From this it may be seen that the short lived nuclides will reach an equilibrium of:

$$\frac{1}{\log_e 2} \times \dot{Q} \times t_{\frac{1}{2}} \times \mathcal{A}$$

where $\dot{Q}$ is the *fractional* rate of entry into the D_2O of the *mass of target material containing* the (equilibrium) activity $\mathcal{A}$ and the decay constant has been expressed in terms of the half-life in seconds. Expanding the exponential term, it may be seen that to first order, the long half-life nuclides will build-up according to a t^2 law.

The target activity is spread over about 1000 nuclides and requires chain-yield analysis. A first approximate numerical solution to give a feel for the orders of magnitude has been obtained using 0.1 cm/year for $\dot{Q}$ (we note that such a value is probably unacceptably high).

The activation build-up over a one-year period has been estimated by taking 10 equal time steps. The nuclide feed-rates into the D_2O are taken as constant over each time step using (i) a corrosion rate which is constant within the interval and (ii) values of the nuclide densities in the target at the middle of each period.

The build-up of the mass (Note: this is the mass of the products, NOT the mass corroded), activation and the 'burden' (see footnote above) in the D_2O for the three corrosion rates are shown in Table-IV (a) and the decay after a 1 year irradiation in Table-IV (b).

The estimated activation entering the D_2O is about 3 kCi (that is, about 1% of the activity in the target) and varies essentially linearly with total corrosion rate (i.e. $\dot{Q}$). This is of the same order of magnitude as for the (short-lived) activation of the D_2O in operation and the tritium after long-term operation.

The contributing nuclides are biased toward 'nastier' medium-to-long half-life isotopes, as may be seen from the relatively slow decrease with time and also from the 'burden' (about 6% of that for the target or a factor of six higher per Ci as compared to that for the nuclide mix in the target).

The majority of the nuclides presumably will be caught in filters or resin-beds: these will need to be shielded. The gamma intensity (summed over all nuclides in the D_2O) is about $2.3 \pm 0.3 \cdot 10^{10}$ γ/second/Ci with a mean energy of 0.58 ± 0.06 MeV where the spread in values is systematic with cooling period (rather higher at short and very long times) due to the changes in the nuclide mix.

6 Summary and Further Design Considerations

In the previous sections we have shown that the essential parts of a Pb-shot pebble-bed target system (the beam-window and the cooling of the shot) will operate with proton current densities over 100 μA/cm^2: i.e. the window has an engineering safety factor of greater than 3, the Pb-shot is well below the melting point everywhere and neutronically acceptable materials are used. The window system should also withstand the extreme 'fault-condition' current density of 260 μA/cm^2 but, at the present stage of the study, we have not completed investigations for a system in which the Pb-shot will not melt at this highest current density.

Corrosion. The Pb-shot will present a large surface area (about 6 m^2) to the D_2O and even a normal corrosion rate for the Pb-water system (0.005 cm/year) will lead to rather large quantities of Pb entering the coolant (about 4 kg/year). The extra activation lodged in the external circuit would be about 300 Ci after one year's operation. A higher corrosion rate

Table-IV

(a) The mass, activity and 'burden' for nuclides entering the D_2O by corrosion for an average corrosion rate of 0.1 cm/year and a surface area of 3 m^2.

Time y	Mass g	Activity Ci	'burden' Mrem
0.1	0.282	683	6.5
0.2	1.09	1050	14
0.3	2.39	1350	21
0.4	4.12	1630	29
0.5	6.24	1880	36
0.6	8.72	2120	42
0.7	11.5	2320	48
0.8	14.6	2490	53
0.9	17.9	2630	57
1.0	21.4	2740	61

(b) The decay of Pb corrosion product activity following one year operation at 1 mA and for a corrosion rate corresponding to 0.1 cm/year.

	Decay Time (days) ⟶						
	0.0	0.1	10.0	30.0	100.0	365.0	730.0
Curies	2740	2720	2240	1890	1260	466	225
'Burden'	61	61	55	49	35	20	17

is to be expected in the irradiated regions from radiolysis: there will be an experimental programme to measure the corrosion rates (with beam) together with the effect of water processing. It is planned to clad the Pb-shot with Sn: with appropriate circuit layout and provision of suitable shielding the problem would not seem to be too serious. The activation contribution of corrosion products would appear to make a rather insanitary water-cooling system more so, but not by a huge factor.

Afterheat. The peak decay power density immediately after beam turn-off following operation at 25 $\mu A/cm^2$ is $\leq$ 100 mW/g. This would melt the peak-rated Pb-shot in about 10 mins (starting from 40 °C) if the Pb was completely thermally isolated. The corresponding surface power density is about 100 mW/cm^2 (which would be balanced by black-body radiation at 600 k for a surface emissivity of $\geq$ 0.2). After about 10 days cool-down period (a typical time delay before a target change) the corresponding figures are 10 mW/g, 100 mins and 9 mW/cm^2. It is not yet clear how high the time-averaged current density will be over a year's operating period.

The vertical geometry implies that a complete window break will make it rather inconvenient to keep coolant in contact with the Pb. The adoption of a two-element window will alleviate this if the probability of both window-elements breaking simultaneously is significantly lower than that for one and a means of detecting the failure of either one is provided.

Radiation Damage: A major uncertainty will be the life-limit of the beam window (which most likely will come from radiation damage although thermal cycling has to be considered also). The choice of aluminium has a major advantage that we do have some practical experience. The BMA-window here at PSI (constructed from Alusuisse type AC-100 aluminium) passes 16 μA of 590 MeV protons with a beam diameter of less than 5 mm (i.e. a current density in the region of 80 $\mu A/cm^2$). To date, these windows have not failed in operation (but are regularly changed after about 40,000 $\mu A \cdot hrs$ operation). Two have been taken out, the first after about 50,000 and the second after 30,000 $\mu A \cdot hrs$ operation, for examination: neither window showed visible signs of damage.

To complete a first conceptual design study, the following points have to be worked on:-

1. Optimization of the pebble-bed: confirmation of the flow-diverter concept, choice of shot-size (the size of the Pb-shot should be increased in the lower power density regions to (i) reduce the pressure drop and (ii) reduce the surface area presented to the D_2O for corrosion).
2. A concept for the neutronically sensitive region above 50 cm. We would like to begin the shielding as early as possible but power levels are still high enough in this region to require careful cooling design.
3. Shielding: Target handling is designed to involve "hands-on" tasks in preparing the target for removal. Steel shielding will be introduced after 100 cm but has to incorporate all the service connections and will also require cooling at the bottom end.
4. A complete handling concept for the target system - uncoupling the coolant circuit - transfer vessel - provision of cooling for after-heat etc.
5. Design of the external parts of the main cooling loop, including provision of water processing and adequate shielding against accumulated activation.

References

[1] F. Atchison, "The Neutronic Performance of Solid Target Alternatives for SINQ" - Contribution to these proceedings.

[2] M. Dubs and J. Ulrich, "Design Considerations for the SINQ Target window" - Contribution to these proceedings.

[3] S. Whitaker, "Fundamantal Principles of Heat Transfer", Pergammon Press (1977)

[4] E. Achenbach, Chem. Ing. Tech. 54, 66 (1982)

[5] E.U. Schlünder, "Wärme und Stoffübertragung zwischen durchströmten Schüttungen", Chemie-Ing 38, 967 (1966)

[6] G. Heidenreich, "Preliminary thermal and stress analysis for the SINQ window" - Contribution to these proceedings.

[7] ANSYS, Swanson Analysis Systems Inc., Houston, PA 15324, USA

ICANS-XI International Collaboration on Advanced Neutron Sources
KEK, Tsukuba, October 22-26, 1990

A High Intensity Beam Handling System at the KEK-PS New Experimental Hall

K.H.Tanaka, M. Minakawa, Y. Yamanoi, M. Ieiri, Y. Kato,
H. Ishii, Y. Suzuki, T. Suzuki* and M. Takasaki
Beam Channel Group, Physics Department,
[*Radiation and Safety Control Center]
KEK, National Laboratory for High Energy Physics,
Oho 1-1, Tsukuba-shi, Ibaraki-ken, 305 Japan

K. Kato
Electromagnet Division, TOKIN Corporation,
6-7-1 Koriyama, Taihaku-ku, Sendai-shi, 982 Japan

ABSTRACT

We would like to summarize newly developed technology for handling high-intensity beams. This was practically employed in the beam-handling system of primary protons at the KEK-PS new experimental hall.

I. INTRODUCTION

Beam intensity of primary protons extracted from the KEK-PS is gradually increasing because of strong requirements of physicists and endless efforts of accelerator people. Now it can be expected that 10^{13} pps (protons per second)

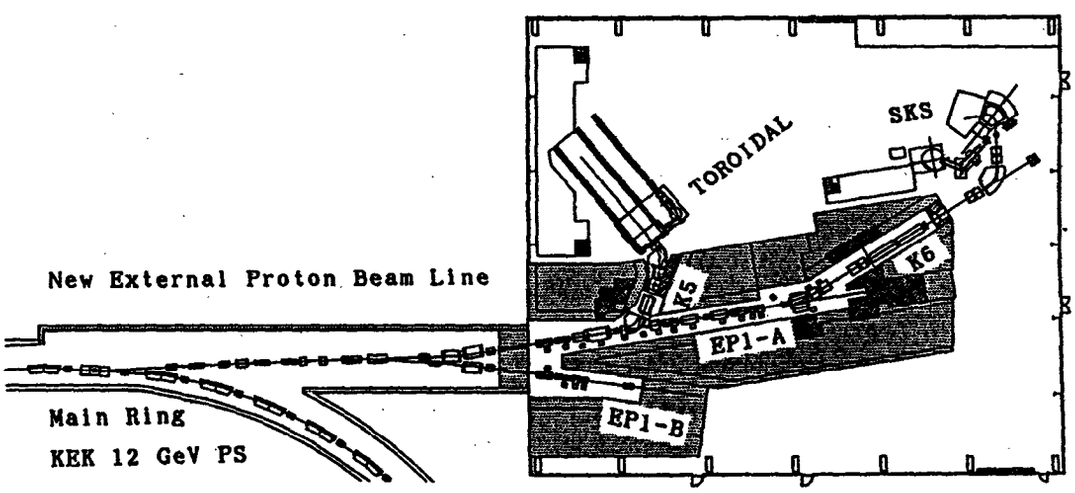

Fig. 1, Schematic illustration of the new counter experimental hall and beam lines of the KEK-PS.

will be realized in the near future by using the 1-GeV proton linac of the Japanese Hadron Facility (JHF)[1] as a new injector. This intensity is almost one order of magnitude greater than the present level of KEK-PS. The problem is that the present experimental hall was designed against 10^{12} pps and 10^{13} pps can not be extracted to the hall. We, therefore, decided to construct a new experimental hall[2] in which we can handle high-intensity beams. The construction work of the new hall started in 1987 and will be completed by the end of 1990. Tuning of the both primary and secondary beam lines will start in early 1991 at the latest. Schematic illustrations of both the new hall and the beam lines are shown in Fig. 1. The primary proton beam will be split in two directions (A and B). Two production targets will be irradiated in cascade at line A. Primary beam line B will supply protons to experiments which will require full and clean primaries.

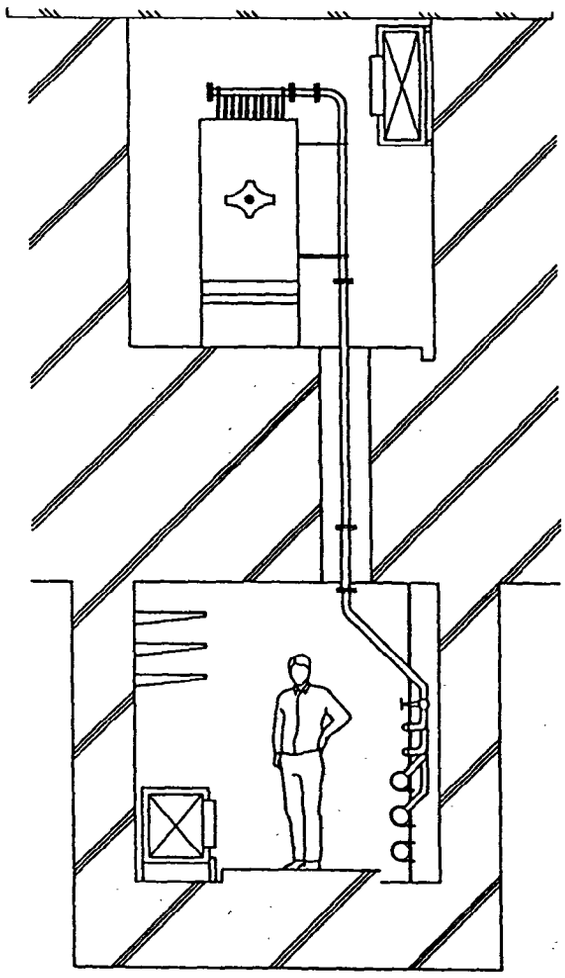

Fig. 2, Cross section of the beam line tunnel in the new experimental hall.

Beam-line components such as electromagnets of high intensity beam lines are expected to work in very high radioactive environments and will have very strong residual radioactivity even during off-beam periods. Maintenance of these components, including a routine check up, must be carried out quickly from a distant location against very high radiation in order to minimize radiation exposure to maintenance personnel. The primary beam transport system that we employed in the new hall is a two-storied structure as schematically shown in Fig. 2. The beam line components are placed in the beam tunnel. Cooling water and electric power are supplied through a service tunnel constructed parallel to the beam tunnel. The interlock signals from the beam line components can be checked in the service tunnel. Some deteriorating components, such as beam monitors, can also be replaced from the service tunnel. The pumping down of the vacuum ducts in the beam tunnel is conducted from the service tunnel. The top shielding of the beam tunnel is made of movable blocks instead that the side shielding is constructed as an immovable permanent concrete wall. If some serious trouble occurs in a beam line component, the ceiling blocks can be removed and the component is lifted out using an overhead crane. Maintenance of the component can be carried out in a hot cell prepared in the experimental hall. Therefore, most components must be easily removed from the beam tunnel. For this purpose, a quick-disconnect system of water, electric power, and interlock signals has been developed. A quick-disconnect flange for the vacuum duct has

also been developed. Details of this system are described in the next section.

It should be noticed that the most important and essential characteristic of the high-intensity beam-line equipment is its radiation hardness. In other words, those things must never break and should be maintenance free. In order to obtain the radiation hardness of the beam-handling system in the new hall, most components of the system are made of inorganic materials. The only organic material used is polyimide, which is known to be the most radiation-hard polymer[3]. The radiation lifetime of the polyimide was, however, tested by the existing proton beams from KEK-PS and no deterioration was found over 10^8Gy (10^{10}Rad). The seals employed for vacuum and water connections are metallic O-rings[4]. The insulator between the magnet coil and water manifold is made of ceramic[5]. Lubrication oil is replaced by MoS_2 or a special metal[6] which contains very fine carbon grains. The radiation-hard components, especially electromagnets, developed for making the beam line maintenance-free are described in the section III.

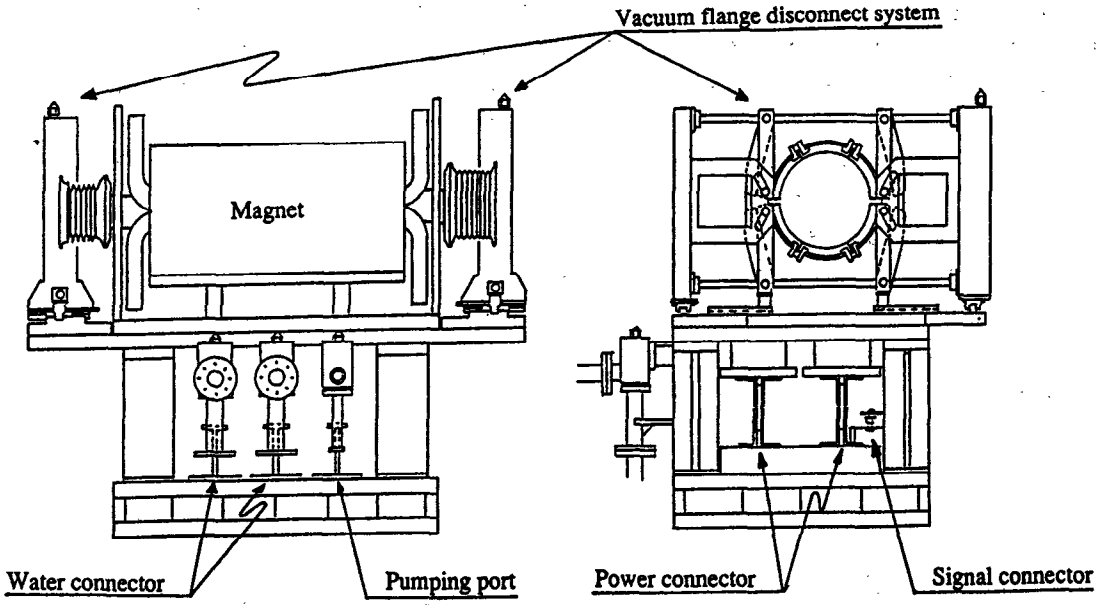

Fig.3, The magnet assembly with quick-disconnect devices.

II. Development of Quick Disconnect System

A quick-disconnect system we have presently developed is for cooling water, electric power and interlock signals for magnets, and the vacuum flange and pumping port for beam ducts. All devices are assembled on an iron base plate with the magnet as shown in Fig. 3. The base plate will be put on a floor table placed on the beam tunnel by an overhead crane. We employed a pivot fitting system between the base plate and the floor table for position reproducibility of the magnets. The floor table is well aligned and fixed on the beam tunnel. The magnet comes back from the hot cell after maintenance and is again placed on the floor table. The alignment clearance of the pivot fitting is better than 0.1mm.

The connectors of the electric power and interlock signals have a quick-disconnect structure without any external power, and are automatically joined by using the magnet weight when the magnet is brought down to the floor table. Therefore, these are set under the base plate of the magnet. The maximum

current/voltage is DC 3000A/200V. In order to resist high-level radioactivity, all the insulation parts of the connectors are made of ceramics. The connector developed for the interlock signals is 49 pin contacts. All of the insulation parts of the connectors were also replaced by ceramics.

The water joint developed is the press-joint type using a toggle-link structure, as shown in Fig. 4. The applicable pipe size is 2 inches in diameter. The gasket is attached on the magnet side of the connector, so that the gasket is also brought to the hot cell and easily replaced. The pressure of the cooling water employed in the new experimental hall is 20kg/cm^2. The water connector was tested according to the JIS 20kg flange standard. No water leakage was found up to 50kg/cm^2. The pumping port has the same structure as the water connector. The inner diameter of the port is, however, 1 inch. A helium leak test was carried out and less than 10^{-8} Torr. l/s was found. Both devices are connected by using a simple rotation motion supplied from outside the tunnel.

The beam duct in the magnet should be disconnected at both ends of the magnet when the magnet is removed from the beam tunnel[7]. A disconnect device for the vacuum flange that we developed is shown in Fig. 5. After the flange-disconnect device is released, the beam duct becomes 80mm shorter at both ends with the flange and with the disconnect device, itself, in order to clear the facing flanges. A special inorganic lubrication material was employed in the flange-disconnect device. The flange collar was made of "Devametal[7]" which contains a fine carbon powder in a brass body, ensuring very low friction at the surface of the metal. Most parts which need lubrication were also made of Devametal. MoS_2 was not used because of its long-term instability. This beam-duct disconnect device is operated also by using a simple rotation motion supplied from outside the tunnel.

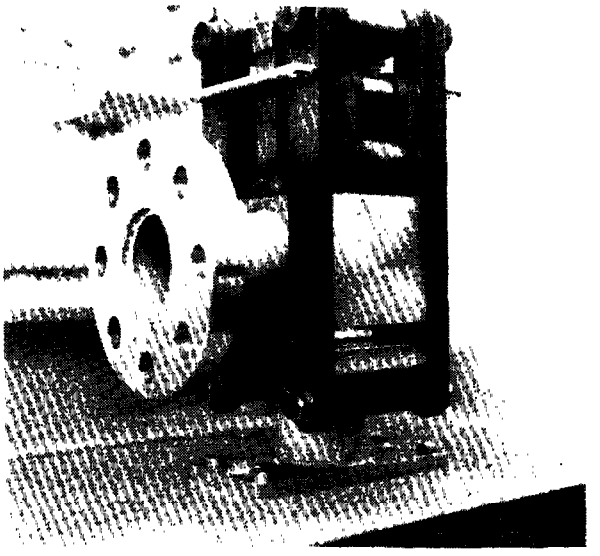

Fig.4, The press-joint type water connector using toggle-link structure.

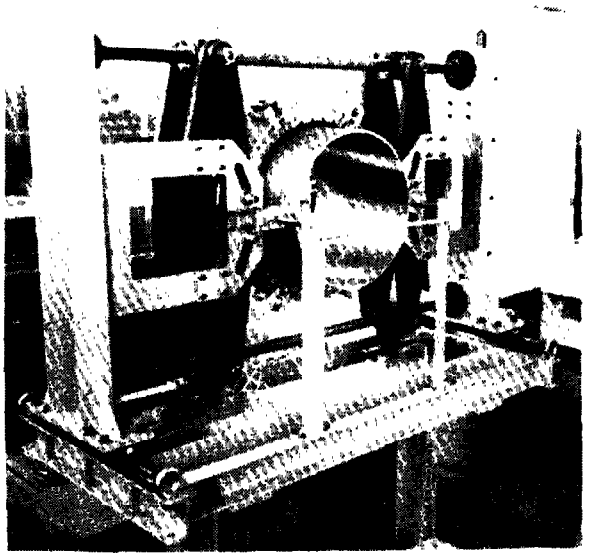

Fig. 5, Vacuum flange disconnect system.

III. DEVELOPMENT OF THE RADIATION-RESISTANT MAGNETS

It is known from our beam-handling experience at the existing experimental hall of the KEK-PS that the radiation life of the beam line magnets should be

over some 10^8Gy to realize ten years of stable operation with a beam of up to 10^{13} pps. This radiation hardness is, at least, a factor of ten more than the conventional magnets insulated by epoxy resin[8]. We therefore developed a new type of radiation-resistant magnets with use of a polyimide resin pre-impregnated (PRP) glass cloth as new insulating material of magnet coils[9]. The radiation life of PRP is expected to be several ten times longer than epoxy resin pre-impregnated and was tested at the existing external proton beam line of the KEK-PS.

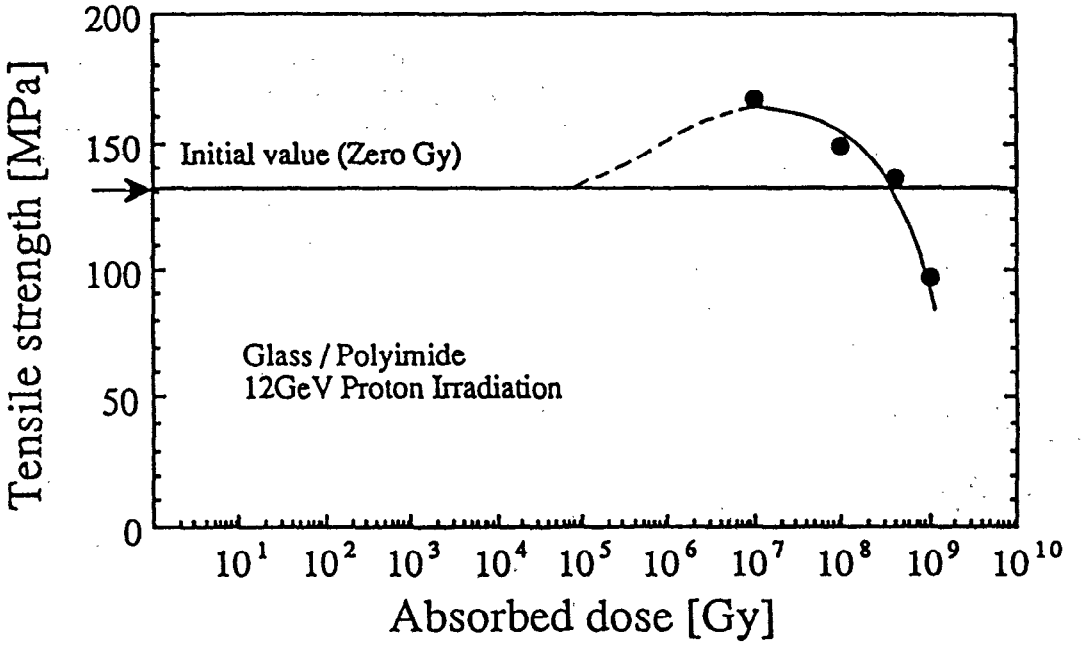

Fig. 6 Tensile strength of a cured PRP glass cloth plotted against the absorbed dose by 12GeV proton irradiation.

The polyimide we used was a BT (bismaleimide triazine) resin prepared by Mitubishi Gas Chemical Company Inc[10]. The test samples were strips 5mm wide, 50mm long and 0.25mm thick. 12-GeV protons were focused on the samples with a $1cm^2$ spot. Approximately 1.5×10^{12} protons were irradiated every 2.5 seconds, and 10^8Gy was achieved within 10 days (one experimental cycle). The tensile strength was measured at absorbed doses of 10^7, 10^8, 4×10^8 and 10^9Gy. No serious fall-off of the strength was observed up to 4×10^8Gy. However, at 10^9Gy the strength became approximately two thirds of the initial value. The results shown in Fig. 6 ensure a radiation life of the PRP insulated coil for over 10^8Gy. The breakdown voltage of the PRP insulator irradiated to 10^8Gy was also measured and was more than 4kV/mm. This fact also ensures the radiation resistivity of the PRP glass cloth for over 10^8Gy. Most magnets in the new hall were manufactured with a PRP glass cloth insulator. The glass cloth tape that we used was 0.25mm in thickness and was wrapped in a double layer on the conductor so that the insulation thickness between conductors was 1mm. No other organic material was used in the magnet, except for the PRP. Ceramic tubes were used for the electric insulation between the water manifold and the coil. Copper tubes were welded to both ends of the ceramic tube.

The magnets placed just downstream of the target station require a higher radiation hardness of up to 10^{11}Gy. In such a case the magnet must be assembled

without any organic materials. We assembled a small Q magnet (25cm in bore diameter and 40cm long) from completely inorganic materials. The magnet coil was insulated by high-alumina cement (HAC) and asbestos tape. First, a hollow conductor was wound into a final Q-magnet coil shape without any insulators. The distance between conductors was temporarily maintained by 2mm thick copper spacers. Second, the asbestos tape was wrapped by hand after the spacers were removed. An inorganic ceramic bond[11] was used to fix the asbestos tape on the conductor as needed. Figure 7 shows the coil just before being filled with cement (a mixture of 27% HAC, 55% natural Al_2O_3 and 18% water by weight).

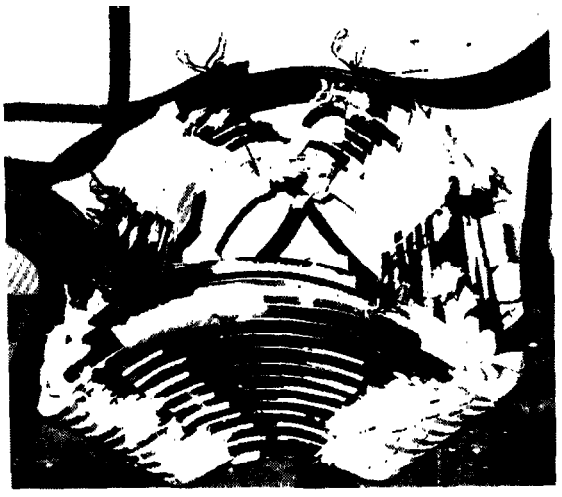

Fig. 7, Coil just before cement filling.

Fig. 8, Coil cured by the cement.

The cement was poured into a wooden box in which the coil was placed and left 48 hours for curing. The drying stage was divided into two parts. The first stage was two days in a 120 °C oven; the second was also two days, but in a vacuum tank. The electric resistance between windings of the coil was measured during each stage and 10^3M Ω was finally achieved. The coil was then hermetically sealed in a stainless-steel casing. Figure 8 shows the coil before casing. The air in the casing was pumped down for an additional two days and replaced by dry nitrogen. The pumping hole was sealed by metallic gaskets. Metalized ceramic tubes were used as power and water lead-throughs to the coil. Since the completion of the cement insulated magnet there has been no electric breakdown during the last three years.

Just after the establishment of cement-insulation coil technology[12], a trial to produce mineral insulation cables (MIC) in Japan was started. Though we can use any size of copper conductor in cement-insulation coil, the assembly technique of the cement coil is somewhat complicated and may not be suited for mass production. MIC consist of compacted MgO insulation surrounding the copper conductor, and covered with a metal sheath. The hollow conductor can be used for direct water cooling in order to achieve a higher current density. The sizes of MIC available in the world are very much limited now; there are almost three kinds of MIC with a hollow conductor[13]. The technique to form MIC into a magnet coil may be, however, relatively easy compared to the cement coil. At present the largest MIC available is 1800A class, which is sometimes insufficient to assemble higher field magnet. We, then, started a project to produce MIC in Japan. Our final goal is to prepare a larger size MIC, such as 2500A/3000A class.

At present, 750A class and 1800A class MI cables have become available in Japan. The cable length is, however, up to 30m. The quality of Japanese MI cable was tested by using bending samples and no serious failure was found. MI cable longer than 60m will be available by the end of 1991 for both 1800A class and 2500A class.

ACKNOWLEDGEMENTS

Authors would like to express their thanks to Prof. T. Nishikawa, Prof. H. Sugawara, Prof. H. Hirabayashi, Prof. M. Iwata and Prof. K. Nakai for their encouragement throughout the present study. One of authors (K.T.) is indepted to Prof. N. Watanabe who kindly gave a chance to present a talk at the ICANS meeting. A part of the present work was supported by Grant-in-Aid for Overseas Scientific Research, No. 01041095, of the Ministry of Education, Science and Culture.

REFERENCES

(1) JHP Working Group, "Japanese Hadron Project", Institute for Nuclear Study, University of Tokyo (1989).
(2) K. H. Tanaka, Present Status and Future Projects of KEK-PS, Nuclear Physics, A450, 533c (1986).
(3) R. L. Keizer and M. Mottier, Radiation-Resistant Magnets, CERN 82-05 (1982).
(4) The metallic O-ring used was "Helicoflex" prepared by Usui Kokusai Sangyo Co., Ltd., Nagasawa 131-1, Shimizu-machi, Shizuoka-ken, 411 Japan.
(5) Ceramic insulating terminals were prepared by Hitachi Haramachi Electronics Ltd., 3-10-2 Benten-cho, Hitachi-shi, Ibaraki-ken, 317 Japan.
(6) The material used was "Devametal" prepared by Daido Metal Co., Ltd., Kita-ku, Nagoya-shi, 462 Japan.
(7) M. Goujon and M. Mathieu, Raccord a vide telecommande, CERN, Note Technique SPS/SME/78-240 (1978).
(8) H. Schoenbacher and A. Stolarz-Izycka, Compilation of Radiation Damage Test Data Part II: Thermosetting and thermoplastic resins, CERN 79-08 (1989).
(9) The Coil was assembled by Electromagnet division of TOKIN Corporation, 6-7-1 Koriyama, Taihaku-ku, Sendai-shi, 982 Japan
(10) Mitubishi Gas Chemical Company Inc., 2-5-2 Marunouchi, Chiyoda-ku, Tokyo, 100 Japan.
(11) The bond used was "BOND X" of Nissan Chemical Industries Ltd., 3-7-1 Kanda-nishiki-cho, Chiyoda-ku, Tokyo, 101 Japan.
(12) K. H. Tanaka et al., Development of Radiation-Resistant Magnets for High Intensity Beam Lines, Proc. of 11th Int. Conf. on Magnet Technology [MT-11], 725 (1989).
(13) Pyrotenax Canada limited, Pyrotenax Cable for High radiation Environments, A. Harvey, Radiation-Hardened Magnets Using Mineral-Insulated Conductors, Proc. of 4th Int. Conf. on Magnet Technology [MT-4], 456 (1972).

Q(I.M.Thorson): How do you align elements in the beam line? Do you depend on pre-alignment only? Can you check alignment after installation?

A(K.H.Tanaka): It will be almost impossible to check alignment after beam irradiation on targets. We, therefore, prepared several steering magnets at every important points so that we can align beam with beamline.

ICANS-XI International Collaboration on Advanced Neutron Sources
KEK, Tsukuba, October 22-26, 1990

Summary on the session:

New Concepts in Target–Reflector–Moderator Systems

G.S. Bauer

The two sessions held under this general topic started out with an interesting presentation by S. Sidorkin on the progress and concept of the neutron target station of the Moscow Meson Factory (MMF) in Troitsk. The 100 Hz, 1 GeV linac designed for a proton current of 1 mA time average is nearing completion and acceleration has been successful up to an energy of 200 MeV. The linac will be equipped with a versatile stretcher–compressor ring which will allow a multitude of different operating modes of the neutron targets. Two targets are embedded in a common shielding block, one of them designed for short pulse operation, the other one for high average flux intensity modulated operation. The first target will be equipped with an H_2O ambient and an H_2 cold moderator whereas the second target will reside in a big D_2O tank and have a large D_2–cold moderator associated to it. The facility will also include an irradiation position in the target block upstream of the neutron targets which can be used for isotopes production and materials testing. Operation is expected to start in 1992 with full performance in 1994.

In the second contribution, Ian Thorson gave his views on the question whether one could simultaneously satisfy users who want pulsed neutrons and those for whom integral flux is what counts. He reminded us that, depending on the moderator material one uses, the spatial distribution of the slowing–down neutrons and that of the thermalized neutrons may either be quite similar, like in H_2O or differ considerably in low absorption moderators like D_2O or Be. A very extended spatial distribution of slowing down neutrons is obtained in the heavier materials such as Pb or Ni. His point is that, even at thermal energies there is always a more or less large component of slowing–down neutrons which are just entering the thermal regime and hence are more concentrated in space and time than those which are in thermal equilibrium with the moderator. His conclusion is that, if the primary fast neutron source has a sufficiently short pulse structure, one can indeed satisfy both, pulsed and integrated flux demands, if one is prepared to use additional momentum space shaping devices in the beam where necessary.

The presentation by Noburo Watanabe on the target–moderator–reflector concept for KENS–II was another proof of his total dedication to overall performance. Using the results which Dr. Kyanagi had presented in the session on cold moderators, KENS–II will have vertical injection from underneath (like SINQ) into a system of split targets (as developed for LANSCE), one of which is decoupled from its moderators whereas the other one is coupled (similar to the situation at MMF). A very clever pulse delivery management between the two targets and the muon facility will complement an optimized geometry and instrument allocation to squeeze out another order of magnitude in performance over what would be obtained from a conventional arrangement with the same proton beam power.

This set the stage for Mike Holding's discussion of the experience at RAL with the clad uranium target under the operating conditions of a medium power proton beam. To date, five uranium targets have been exhausted at ISIS with a varying number of pulses and total μA–hours. So far, no clear picture of the lifetime limiting key component has evolved, but also manufacturing

processes have not been exactly identical for the targets used so far. RAL is now on the way to go about this very systematically. One thing, which seems to be an important message to all of us who want to use materials under high load conditions is, that we will have to acquaint ourselves with the concepts of quality assurance.

In all following talks, even if not explicitly stated, quality assurance could somehow be sensed as being of prime importance. This became obvious, when Gary Russell introduced his LANSCE–repair programme by saying that the leak that had developed in their hydrogen moderator was probably due to a certain lack of care in the manufacturing. Now, as usual, Gary wants to take advantage of the fact that they have to go through all the trouble of removing the heavy binding magnet and top shield to fix also a few other problems they have encountered. One of them is the so called "target shine": If the beam channel walls outside the bulk shield can see parts of the target's surface, then one has to deal with direct high energy neutron radiation in that area. This may require a lot of bulky shielding. Gary hopes to cure this problem by opening up the gap between the two halfs of his split target, which he finds will not have a serious effect on the intensity from the flux trap moderators but could help the background radiation.

Most of the rest of the session covered by this summary was devoted to the liquid material target development at PSI. Yasushi Takeda gave an impressive account on his progress in the experimental investigation of the flow configuration in naturally circulating liquid lead–bismuth. Thanks to his work we now have a quite good idea on how the flow develops at the onset of heat input and what its distribution in the target is.

These investigations are complemented by a variety of other experiments, tests and calculations on which Martin Dubs reported. From this work we can now conclude that under standard operating conditions and in certain fault conditions which have to be considered, a liquid lead–bismuth target and its beam entrance window are feasible. The goal has not quite been reached yet, but the way to go can be seen. Nevertheless, it is felt to be prudent to develop a solid target in parallel to the liquid one, even if this is not a concept on which one would hope to build and go much further. Preliminary calculations indicate that there will be a range of operating parameters in terms of ball diameter and coolant flow velocity for a lead–shot pebble bed target, which can tolerate fault conditions resulting in a beam current density up to ten times higher than anticipated under standard operating conditions.

In any case, as we move towards higher and higher beam power, radioactivity not only on the target will become more and more of a problem. In that sense, Dr. Tonaka's presentations on his remote handling provisions in the new PS–experimental hall at KEK helped to round off the overall picture. It was impressive to see what can be done in terms of shortening necessary access times for removal of components from a radioactive environment if sufficient thought is given to the problem ahead of time. This is probably the price we all have to pay if we want to move towards higher source strength.

Barring details, the session made it very clear that quality assurance and early attention to handling and maintenance problems will be the key to a satisfactory performance of high power targets.

ICANS-XI International Collaboration on Advanced Neutron Sources
KEK, Tsukuba, October 22-26, 1990

Measurement of the Neutron Yield from Tungsten Target Irradiated with 70-GeV Protons.

A.G. Akopyan, N.V. Kolmychkov, A.V. Kuzin
Institute for Nuclear Research, Moscow, USSR

1. Introduction

In present time in a number of laboratories (LAMF, TRIUMF, KEK, Institute for Nuclear Research) the projects of the high current proton synchrotrons for the energies of tens GeV (kaon facilities) are under development. As it was shown earlier in the papers [1,2] high current proton accelerators of intermediate and high energy protons are the good base to construct high intensity neutron sources since significant growth of neutron yield from thick targets should take place when the energy of incident proton increases. Since the available suggestions on the construction of these neutron sources have been based on the theoretical estimates of the neutron yield it is interesting to detect directly on experiment the evaporated neutron yield from the targets irradiated with accelerated protons.

2. Experimental Scheme.

The yield of neutrons from tungsten target irradiated with 70-GeV protons on Serpukhov accelerator was measured in the present work. The target was assembled of tungsten plates of the sizes 160x160x300 mm.

The measurements were carried out on the 23 canal (intensity about 10^{10} p/pulse) and on the 21 canal (intensity about 10^{5} p/pulse).

In the first case the proton beam coming on the height of 1350 mm from the concrete floor was being detected by means of the copper foil placed before the target. The positions of the proton beam before and behind the target were determined by means of the photographic paper in the experiment without the target.

In the Figure 1 the experimental scheme, the final proton beam position and its sizes before the target are given.

To detect neutrons from the target the indium foils were used on the 23 canal. These foils were placed into the polyethylene balls of 127 mm diameter being in the cadmium cover on the distance of 750 mm from the geometrical target center at the angles 45°, 0° and

-22.5^0(Fig. 1). In the Figure 2 the function of the sensitivity of these ball detectors is presented.

To find neutron flux distribution on the target surface the assembly of the activation detectors made with the plastic scintillator, rhodium foils and phosphorus in the single cadmium cover and the aluminum foil was used. The basic characteristics of the detectors are given in Table 1.

Table 1.

Main characteristics of the activation detectors

Det.	Reaction	Cross Section (mbarns)	Thresh. (MeV)	Size (mm)	Density (g/cm^3)	$T_{1/2}$	Ref
Cu	$Cu(p,spa)Na^{24}$	3.90	2000	d110x0.1	8.93	15h	5
CH_2	$C^{12}(x,xn)C^{11}$	22	20	d20x9	1.06	20.4m	4
Al	$Al^{27}(n,\alpha)Na^{24}$	30	6	d40x6	2.70	15h	4
P	$P^{31}(n,p)Si^{31}$	124	2.2	d20x3	2.20	2.62h	6
Rh	$Rh^{103}(n,n')Rh^{103m}$	1000	1.0	d15x0.1	12.44	56.12m	6
In	$In^{115}(n,\gamma)In^{116m}$	160000	0	d30x0.12	7.3	5.4m	4

The verification of the aluminum and copper detectors was carried out with the single crystal scintillation gamma-spectrometer (NaJ(Tl) d150x100) on the line of $E\gamma$ =2.75 MeV.

Also the verification of the phosphorus and carbon detectors was done with the low background radiometric set (the polyester crystal of the size d45x50 mm with the photomultiplier of FEU-82 type) [7]. The rhodium detectors were verified with the semiconductor gamma-spectrometer of the DGR5 type meant for low energy Rontgen and gamma radiation. The radionuclide Rh^{103m} produced in the reaction of inelastic scattering $Rh^{103}(n,n')Rh^{103m}$ and having the half-life period $T_{1/2}$= 56.12 min was being detected on the line of $E\gamma$= 20 keV. The yield of gamma quanta of this energy is 7.865% per decay [8]. The effectiveness of the gamma quantum detection was determined with the model source Am^{241} on its line E = 25 keV. To suppress the contribution of the reaction $Rh^{103}(n,\gamma)Rh^{104m}$ ($T_{1/2}$ = 4.4 min) the foil was placed in the cadmium screen and kept there for about 1 hour after irradiation.

Calibrating measurements were carried out with Cf^{252} on the same geometry when four central plates of 10 mm thickness had been replaced by the steel plate of 40 mm thickness with the cell for the source in the center. The source was being placed both in the target center ("O") and on the side ("A") (Fig. 1).

In the measurements on the canal 21 the proton beam, which was on the height of 2250 mm from the concrete floor was being detected by two scintillation counters of 100 mm diameter with the effectiveness of the charged particle detection higher than 99.9%. The coincidence of the data of the counters was a "trigger" of the set and simultaneously gave the number of protons incoming on the target. Two additional counters in the form of the perpendicular scintillating rods of the sizes 2x2x100 mm were used for the

precise beam directing on the target center.

For the detection of neutrons from the target the neutron detector on the basis of the gas-discharge counter STS-6 enveloped by the rhodium foil was used in the 21 canal. The counter was placed into the polyethylene sphere of the diameter 254 mm. To decrease the influence of interferences and background radiation the set of detection was under operation during 2 seconds between accelerator cycles of 9.7s duration one second after the proton pulse of 0.7s duration. Since the half-life period of the basic line of Rh^{104} $T_{1/2}$= 44 s the correction caused by the relative pulse duration is equal to k= 4.50. The detector was placed at the angle 90° to the beam axis on the distance of 1.5 m from the axis.Calibrating measurements were carried out with Cf^{252} when the geometry was the same.

3. Results of Measurements.

23 canal.

The results of measurements on the 23 canal when the number of protons for the exposition was $8.54*10^{14}$ +- 5% for the time of 30 min are given in Table 2. Here the neutron fluencies from Cf^{252} per one neutron of the source are are also presented.

Table 2.

Source	Protons			Cf^{252}("O")			Cf^{252}("A")		
Position	45	0	22.5	45	0	-22.5	45	0	-22.5
Neutron Fluency $\frac{n}{cm^2*p(n)}*10^5$	1500	1600	1400	2.6	3.1	2.7	4.7	2.4	1.9

As it follows from the data of the table the angular dependence of the neutron flux around the target irradiated by protons has a little difference from the corresponding dependence for the target with the point source in the center. Taking into account the weak dependence of the neutron detector sensitivity on the neutron spectrum we obtain the following neutron yield from the target per one incident proton: Y= 514 $^{n}/_{p}$ +- 11%. In Figure 3 the distribution of the neutron flux on the target surface is presented.

21 canal.

Table 3 shows the results of measurements on the 21 canal.

Table 3 shows the results of measurements on the 21 canal.

Table 3.

Run	Presence of target	Number of protons in 21 canal, N_p $*10^5$	Detector Counts N_n	N_n/N_p 10^5	Number of protons in 8 canal 10^{14}
1	-	1.28	3885	30.4	4.19
2	W	1.07	21136	197	3.52
3	-	1.65	2376	14.4	3.08
4	W	2.19	59797	273	8.70
5*	W	1.23	278	2.3	3.19

* Measurement without Rh-foil in neutron detector

In using the neutron detector on the basis of the gas-discharge counter enveloped by the Rh-foil it is necessary to take into account the neutron and gamma background. To determine the background measurements were carried out without the target when the proton beam was going past of the set to the beam stop. In this case neutrons and gamma radiation from the protection were being detected. Measuring with the tungsten target but without Rh-foil in the detector gave the contribution of all gamma radiation. Without Rh-foil and the target we have the contribution of the gamma radiation coming from the protection only. Comparing the results of the measurements #5 with those of #1 and #3 shows that the neutron contribution is about ten times as large as that of gamma radiation. According to Table 3 there is the correlation between the value of the background and the current in the canal 8. Taking into account this correlation we can obtain the average rate of the detection $S= 1.94*10^{-3}$ per an incident proton. The background is 12% in the first measurement with the W-target and 22% in the second one.

The measurements when Cf^{252} (intensity $7.4*10^7$ $^n/s$) is in the center of the target (5% error with the credible probability 0.95) and the geometry is the same gave the following numbers of scintillations for 60 seconds : 82480 with the Rh-foil and 8278 without the foil. In account of the relative pulse duration given above, as well as the measured value S, we shall obtain the neutron yield from the W-target : $Y_{21}= 533$ $^n/p$ +- 12%.

Conclusions.

The measurements carried out on the 23 and 21 canals gave the close values of the neutron yield from tungsten target. The average value of the yield is Y= 524 $^n/p$. This value is two times less as neutron yield calculated by means of the linear dependence based on the experimental data for energies $E_p< 1$ GeV [9]. Using of the more thick target will give larger neutron yield as compared to the measured one.

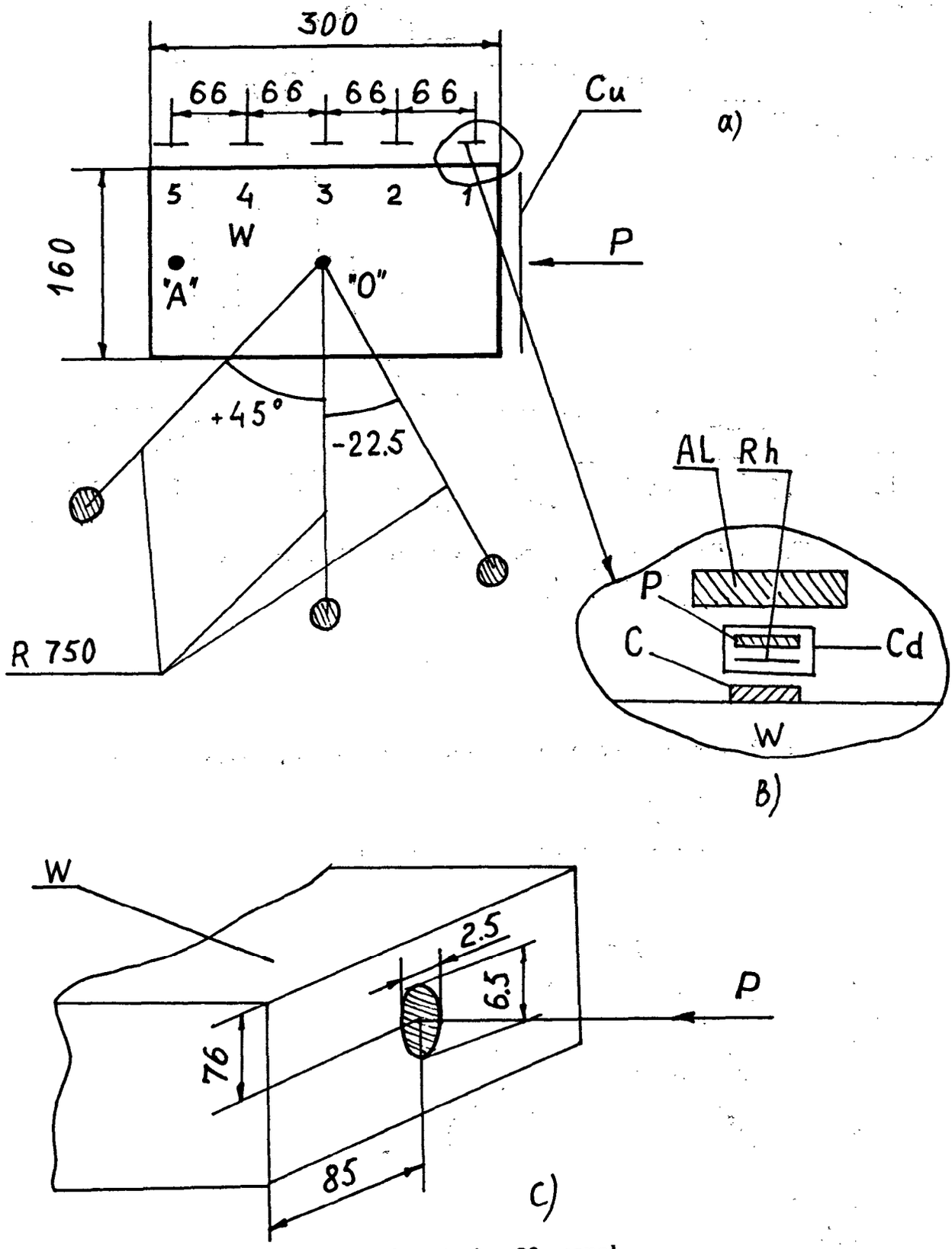

Fig. 1. Scheme of the experiment in 23 canal.
a) position of the detectors around the target
b) set of detectors
c) position of the proton beam

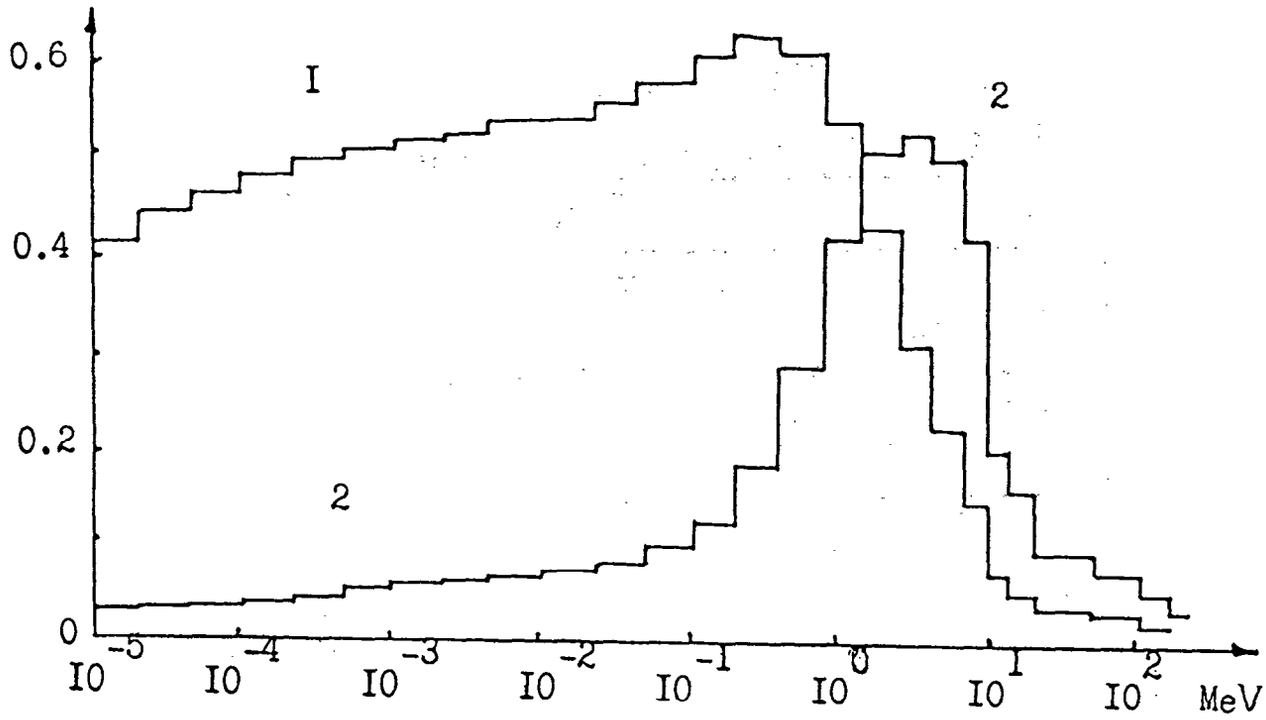

Fig. 2. Function of the sensitivity of ball detectors
1 - d127 mm
2 - d254 mm

Fig. 3. Distribution of the neutron flux on the target surface
1 - P
2 - Al
3 - C
4 - Rh (without self-absorption)

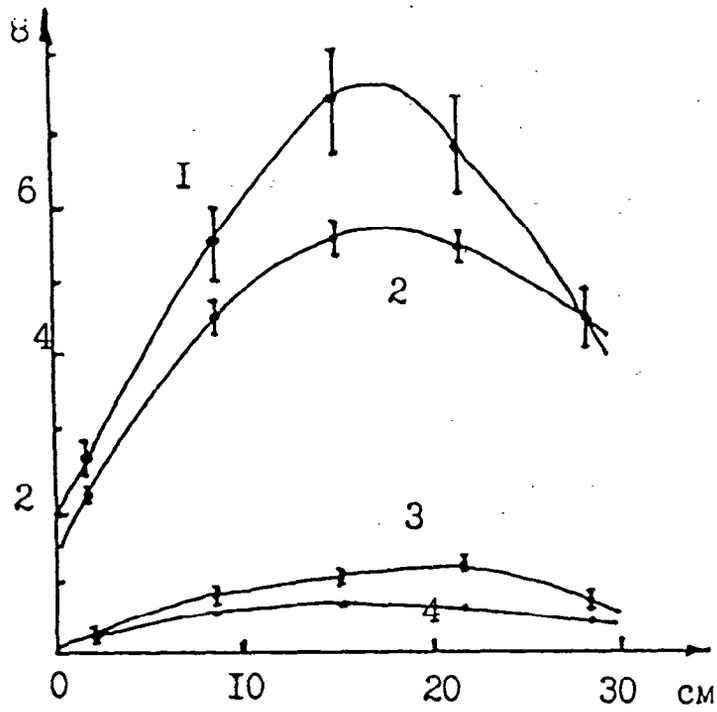

The authors would like to thank Yu.Ya. Stavissky for his interest and useful discusion. We are grateful to S.F. Sidorkin for his help in preparation of the experiment.

References.

1. Yu.Ya. Stavissky, Inst. Nucl. Res. Preprint, P-0215, M.,1981.
2. S.E. Boriskin, M.V. Kazarnovsky, N.V. Kolmychkov et al., Inst. Nucl. Res. Preprint, P-0632, M.,1989.
3. V.P. Kryuchkov, G.I. Semenova, Inst. High Energy Phys. Preprint, 87-191,Serpukhov,1987.
4. St. Chavalambus, I. Dutrannois, and K. Goebel, Preprint CERN/DT/ HP90,1966.
5. E.S. Barish, B. Blair, Y. Chu et al., Preprint CALT-68-802,1982.
6. S.S.Lomakin, V.I. Petrov, P.S. Samoilov, Radiometriya Neitronov Aktivatsionnym Metodom, Moscow, Atomizdat,1975.
7. A.I. Volynchikov, N.V. Getmanov, G.I. Krugly et al., Inst. High En. Phys. Preprint 83-86,Serpukhov,1983.
8. Schemes of Radionuclides Decay. Energy and Intensity of Radiation, vol.2, Moscow,1987.
9. J.S.Fraser,R.E.Green,J.W.Hilborn et al.Canada 21(2),1965.-

ICANS-XI International Collaboration on Advanced Neutron Sources
KEK, Tsukuba, October 22-26, 1990

Evaluation of Bulk Shield for the JHP Facilities

Yoshitomo Uwamino and Tokushi Shibata
Institute for Nuclear Study, University of Tokyo
3-2-1, Midori-cho, Tanashi, Tokyo 188 JAPAN

ABSTRACT

In the Japanese Hadron Project(JHP), a 1-GeV 200-μA proton beam will be handled, and the radiation shield of the facility will be very massive concrete and iron lump. Since the constructing cost is strongly affected by the shielding design, the design must be severely performed.

The neutron yield in thin targets and a copper beam dump was calculated by the HETC-KFA-2 Monte Carlo code. For the evaluation of the calculational accuracy, the calculational results were compared with the experimental data by Cierjacks and Raupp. The calculated result of heavy element agreed well with the experiment at a low energy region, E_n<10 MeV. The calculated angular distribution of high energy neutrons, however, have stronger forwardness than the measurement. The measured neutron yield (E_n>100 MeV) of 90 deg close to the calculated one of about 60 deg in the absolute value.

The high energy neutron transport in a 5-m-thick iron slab and in an 8-m-thick ordinary concrete slab was calculated with the HETC code and also with the discrete ordinates transport code, ANISN. In the ANISN calculation, the DLC-87/HILO and the DLC-128/LAHIMAC group cross sections were used. The ANISN calculation with the LAHIMAC cross sections gave strong underestimation compared with the HETC calculation. The difference of the shielding lengths calculated by the HETC code and by the ANISN code used with the HILO cross sections was smaller than 6% for the both iron and concrete cases.

I. INTRODUCTION

High energy neutron deep penetration is an old problem, but still a problem today for an accelerator shielding. The Moyer model is very useful for a rough shielding design of a high energy accelerator facility. This model essentially consists of two parameters, that is, the initial dose rate at the inside of an shield (H_0) and the shielding length(λ). These parameters have been measured at several accelerator facilities of GeV energy regions, but have not been constricted. For example, the CERN-LBL-Rutherford collaborative work gave the values of H_0 and λ as 2.3×10^{-13} [Sv m^2 GeV^{-1}] and 120 [g cm^{-2}]

for ordinary concrete from an experiment made at the CERN 13.7 GeV proton synchrotron. On the other hand, the KEK group gave these values as 0.88×10^{-13} and 143 for ordinary concrete. The Japanese Hadron Project (JHP) intends to handle a 1-GeV 200μA proton beam. Using the Moyer model, a necessary thickness of a shielding concrete surrounding a beam dump can be estimated. If the data of CERN-LBL-Rutherford collaboration are used, a 9.27 m thick concrete shield is expected to reduce the dose equivalent rate at the shield surface to 6μSv/h, which is a limit of Japanese law for a radiation uncontrolled area. A value of 10.16 m, however, is obtained when the KEK values are used. A 90 cm thick concrete shield reduces the dose level about one decade. If the dose rate is ten times larger than the expected level, an investment for the additional shield will be remarkable. If the situation is inverse, the lost money is not small. The affair is extremely severe for a spallation neutron source, because to reinforce the shield is very difficult and a redundant shield reduces the usable neutron intensity.

The intra-nuclear-cascade-evaporation Monte Carlo code, HETC-KFA-2, in the HERMES code system,[1] is a very powerful tool for the evaluation of the secondary neutron production by light particles and also of their penetration through a shield. The discrete-ordinates Sn transportation code, ANISN, is also very useful for an accelerator shielding design because of its short calculational time on a deep penetration problem. In this work the calculational accuracy of these codes is evaluated by comparing the calculations with each other and with experiments.

II. NEUTRON YIELD AT THIN TARGETS

Cierjacks et al.[2] measured double differential neutron production cross sections of C, Al, Fe, Nb, In, Ta, Pb, and U elements using 585 MeV protons from the SIN cyclotron. Their data are very good for a benchmark calculation of the HETC-KFA-2 Monte Carlo code. Neutron production cross sections of C, Al, Fe, In, and Pb for 585 MeV protons were calculated by the HETC code under the following condition.

Table 1 Calculational conditions for neutron yield estimation at thin targets.

Element	Density	Thickness	Atomic Densities	Number of Histories
^{6}C	2.20 g/cm^3	5.40 mm	^{12}C : 1.10×10^{23} /cm^3	8.0×10^6
^{13}Al	2.71	5.58	^{27}Al : 6.05×10^{22}	8.0×10^6
^{26}Fe	7.86	3.93	^{54}Fe : 4.92×10^{21}	5.3×10^6
			^{56}Fe : 7.99×10^{22}	
^{49}In	7.31	5.13	^{113}In : 1.65×10^{21}	4.4×10^6
			^{115}In : 3.67×10^{22}	
^{82}Pb	11.34	4.40	^{206}Pb : 8.42×10^{21}	3.5×10^6
			^{207}Pb : 7.29×10^{21}	
			^{208}Pb : 1.73×10^{22}	

The non-isotropic evaporation option was selected for the calculation of C and Al, and the high energy fission option was selected for the other elements. The in-core neutron yield analysis were performed with an angular bin structure of a 20 degree interval between 0 and 180 deg.

The calculational results of the C, Fe and Pb double differential cross sections are shown in Figs. 1, 2 and 3 in small marks connected by straight

lines, and the experimental data of Cierjacks are also shown in big marks. The Cierjacks' 90 deg data, for example, are shown in big open triangles, and the corresponding calculational results of neutron emission between 80 and 100 deg are also shown in solid triangles of which size is small. A low energy neutron yield for Pb element, $E_n<10$ MeV, shows good agreement between calculation and measurement. Since the sum of calculated neutron yield below 1 MeV is marked at 1 MeV, the calculational results are larger than the experiment at 1 MeV. For the carbon target, the difference at the low energy region is especially large for the data of 30 deg. In the 90 and 150 deg experimental data of carbon, there is a rapid decrease at about 4 MeV followed by a small bump at 7 MeV. The spectral tendency is much different for C element between the calculation and the experiment while it is in good agreement for Pb and Fe elements.

The experimental data have larger values at a high energy region, $E_n>100$ MeV, than the calculation in general, and the experimental spectrum is similar to the calculational one of more forward direction, that is, the experimental spectrum of high energy region at 90 deg is similar to the calculational one of between 60 deg and 80 deg.

Angular distributions of neutron yield are shown in Fig. 4 for C, Al, Fe, In and Pb elements. A high energy neutron emission distribution, $E_n>100$ MeV, is represented with small solid triangles connected with straight lines for the calculation, and with big open triangles for the measurements. In the same manner, squares are for the neutrons of medium energy between 100 MeV and 10 MeV, and circles are for low energy neutrons below 10 MeV. The distribution of low energy neutrons is very flat for all elements. The agreement between calculation and experiment is good for low and medium energies. The calculation gave an under estimation at 90 deg and 150 deg for high energy neutrons. The measured neutron yields at 90 deg and 150 deg are similar to the calculations at about 70 deg and 100 deg, respectively. For the lateral shielding design of a target station, the high energy neutron yield at 90 deg is the most important data. From the above consideration, the calculational neutron yield at 60 deg can be conservatively used as the source data of a shielding calculation at lateral direction.

III. NEUTRON YIELD AT THICK TARGETS

Raupp et al[3], measured neutrons produced by bombardment of 590 MeV protons on a thick uranium target. Their double differential neutron yields are very useful for a benchmark calculation of the HETC-KFA-2 code. They used a 10 cm by 10 cm by 40 cm uranium target, and measured neutron spectra at 30 deg, 90 deg and 150 deg with TOF method. A neutron yield in the whole target was estimated by them and shown in Fig. 5 with large open marks. A HETC-KFA-2 calculation was performed in a similar geometry, and the results are shown in Fig. 5 with small marks connected with lines. At a low energy region, the experiment and the calculation show good agreement for emission angles of 90 deg and 150 deg. Considering the data of Figs. 1, 2 and 3, the absolute value of the experiment at 30 deg seems to have some errors. The calculation also reproduces high energy neutron spectra which agree well with the experimental data of 90 and 150 deg when the angular biasing mentioned in the previous section is introduced.

IV. NEUTRON DEEP PENETRATION

1)HETC Calculation

A neutron deep penetration was estimated by the HETC-KFA-2 code for an 8 m thick ordinary concrete slab and for a 5 m thick iron slab. The neutron sources of these calculation were derived from a HETC-KFA-2 calculation performed with a 10 cm diam by 60 cm long copper beam dump bombarded by 1 GeV protons. The neutron yields between 0 deg and 10 deg and between 50 deg and 70 deg were selected for the source. The latter angular interval is selected as the source for a lateral shield.

Since the neutrons attenuate by several decades with these thick shields, a Monte Carlo calculation in a whole slab is nonrealistic. The calculation was divided into 1 m slabs, that is, a 1-m-thick slab calculation was performed with the source neutrons which normally hit the center of the slab, and the secondary calculation in the next 1-m-thick slab was performed with the source term of neutrons, protons and negative pions which escaped from the back surface of the previous slab. For incorporating the back scattering particles, the slabs were overlapped by 40 cm, that is, a thickness of the 1st slab was actually 140 cm and that of the succeeding slabs was 180 cm. A slab was divided into 4 regions of 25 cm thicknesses, and the neutron flux was evaluated by the track length estimator at each region. Since the lower cutoff energy of neutrons was set at 14.9 MeV, neutron spectra were obtained above 14.9 MeV. The transmission of neutrons, protons and negative pions were considered at the interface between slabs. The contribution of protons was found to be about 2% increase of the neutron flux at the next interface, and that of negative pions was much less. The effect of 40 cm overlapping gives only 0.4% increase. The calculation was performed with 100000 histories for each slab, and the cpu time was about 30 minutes on a FACOM-M780 computer.

2)ANISN Calculation

A deterministic radiation transport code, ANISN, is made on a one dimensional discrete ordinates methods. This code can perform a deep penetration calculation in much shorter time than a Monte Carlo code.

Using the same source of neutron yield in the copper beam dump bombarded by 1 GeV protons, high energy neutron penetrations through an 8 m thick ordinary concrete slab and a 5 m thick iron slab of infinite lateral size were calculated by the ANISN code with the DLC-87/HILO and DLC-128/LAHIMAC group cross sections. These neutron and gamma coupled group cross sections have neutron energy structures of from thermal to 400 MeV for HILO and from thermal to 800 MeV for LAHIMAC. The order of the Legendre expansion is P_5 and P_3 for HILO and LAHIMAC, respectively.

The ANISN shell source was placed at the left surface of the slab geometry. An S_{32} angular quadrature set was used, and the source was entered at the 33rd angle in order to simulate normal injection. Calculations were performed with sources of all the 8 directions. The source spreads up to 1 GeV, and the neutrons with energies above the upper limit of the group cross sections were treated as neutrons having the upper limit energy. For the conservation of the total energy, weights of the neutrons were increased by the ratio of the original energy and the upper limit energy. The cpu time was only several minutes for each calculation, which is less than 1/60 of the HETC calculation.

3)Results and Discussion

The calculated neutron spectra at 9 depths in the 8 m thick concrete slab are shown in Fig. 6. The source neutrons used are the yield in the copper beam dump at the angle between 50 and 70 deg. The calculated results of the HETC code are shown in small marks and the histograms represent the results of the ANISN code used with the HILO cross sections. The spectral shapes of these calculations are in good agreement. The jump at the top energy group in the ANISN spectra at shallow depths came from the energy truncation of the source spectrum mentioned in the previous section. The absolute value of the ANISN calculation, however, decreases as the depth increases.

Attenuation curves of the dose equivalent rate (H_{1cm}) in the concrete slab are shown in Fig. 7. The open and solid circles are of the HETC calculation, and the lines are of the ANISN calculation performed with the HILO cross sections. The dose rates shown in this figure are due to the neutrons of energy above 14.9 MeV. With the increase of the emission angle of the source neutrons, the absolute value of the dose rate becomes small and the slant becomes steep. At the entrance of the slab, the ANISN results are larger than that of HETC because of the weight increase in the energy truncation of the source spectrum. The difference between the HETC and the ANISN calculations is only a factor of 4 at 8 m depth, and it can be concluded that the ANISN calculation with the DLC-87/HILO group cross sections gives good results compared with the HETC code. The DLC-128/LAHIMAC cross sections, however, gave much underestimation, that is, a 1/200 value at the 8 m depth.

The dose equivalent distributions due to whole neutrons and secondary gamma rays calculated with the HILO cross sections are shown in Fig. 8. The increase coming from low energy neutrons and gamma rays is about a factor of 2.

The ANISN code can perform an adjoint calculation, in which particles are traced inversely. An adjoint transmission of the dose equivalent response function was evaluated by using this option. The results for an 8 m thick ordinary concrete are shown in Fig. 9. The adjoint flux is the same as the dose equivalent importance function, and it can be seen that the only high energy neutrons contribute to the dose rate after a thick shield.

V. CONCLUSION

Neutron emissions from thin and thick targets were calculated by the HETC-KFA-2 Monte Carlo code, and compared with experimental data. The calculation was found to give reasonable results if some angular biasing is introduced for high energy neutron emissions. Deep penetrations of the secondary neutrons produced in a copper beam dump bombarded by 1 GeV protons were calculated with the HETC code and also with the ANISN discrete ordinates transport code. The difference between these two calculations was not large.

References

1) P.Cloth, D.Filges, R.D.Neef, G.Sterzenbach, Ch.Reul, T.W.Armstrong, B.L.Colborn, B.Anders, H.Brueckmann, Jül-2203, Kernforschungsanlage, Jülich (1988).

2) S.Cierjacks, Y.Hino, F.Raupp, L.Buth, D.Filges, P.Cloth and T.W.Armstrong, Phys. Rev. C 36, 1976 (1987).

3) F.Raupp, S.Cierjacks, Y.Hino, S.D.Howe, M.T.Rainbow, M.T.Swinhoe, and L.Buth, ICANS-V, Jül-Conf-45, Jülich p333 (1981)

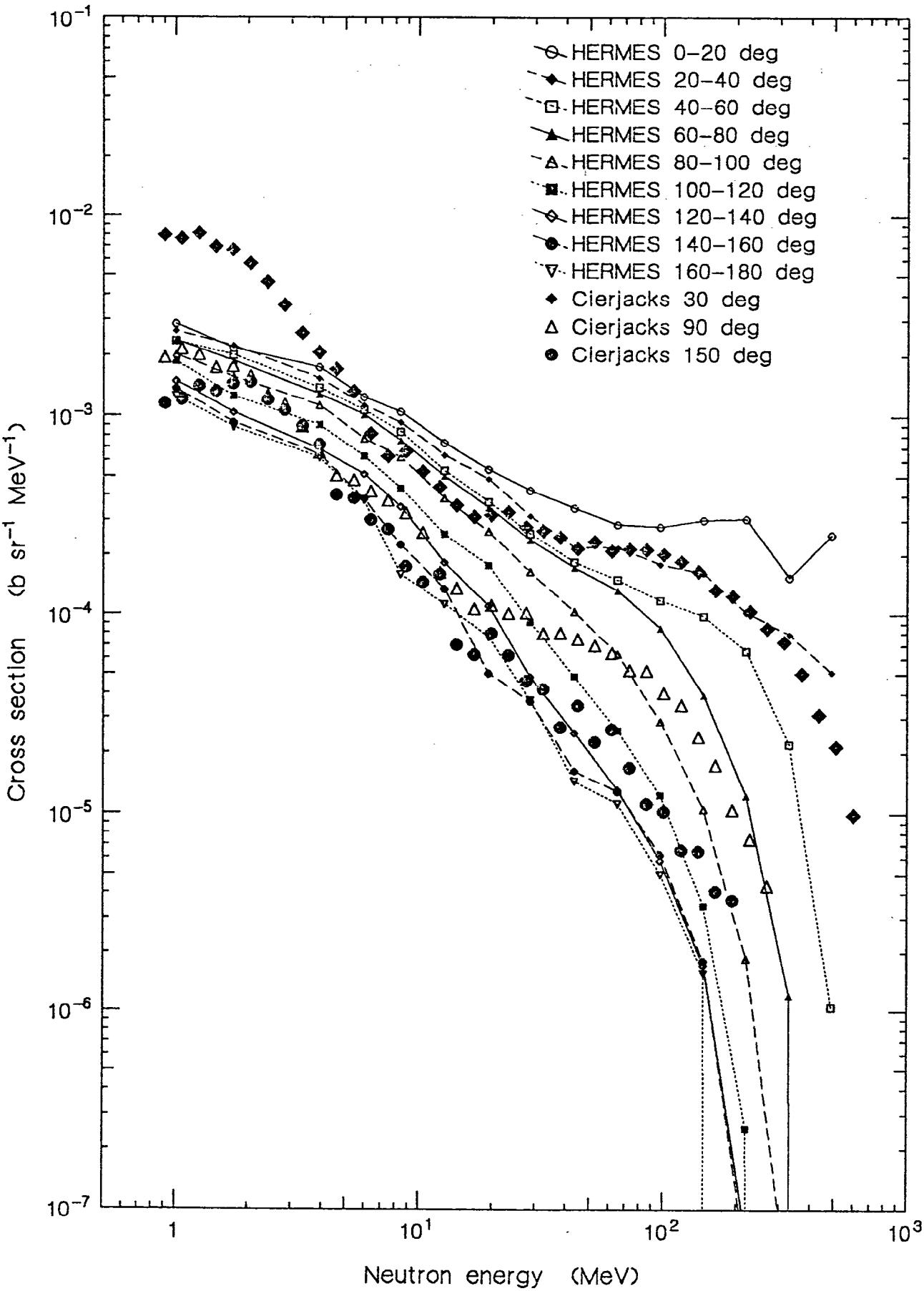

Fig. 1 Calculated and Measured double differential neutron production cross sections of carbon bombarded by 585 MeV protons.

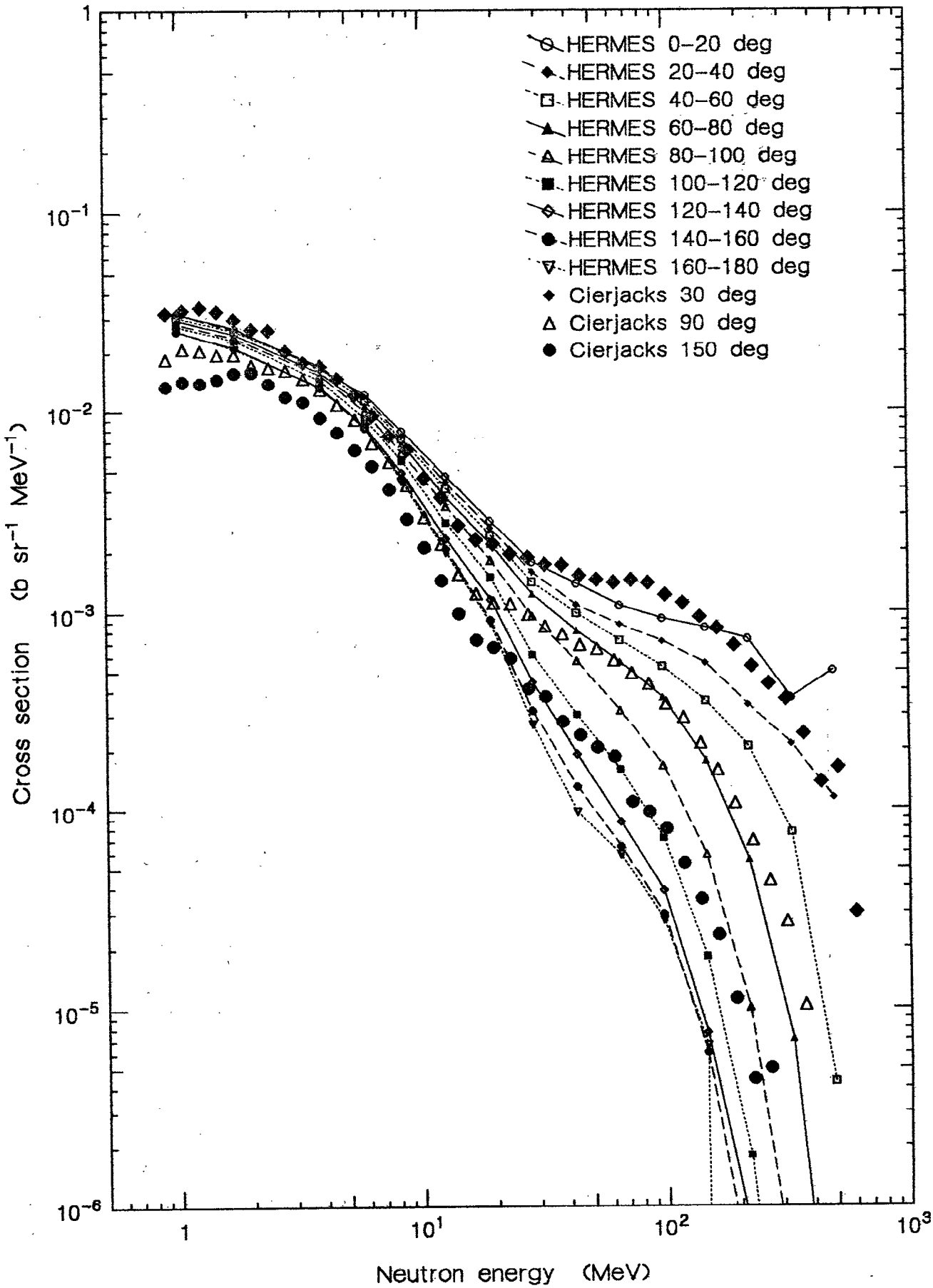

Fig. 2 Calculated and Measured double differential neutron production cross sections of iron bombarded by 585 MeV protons.

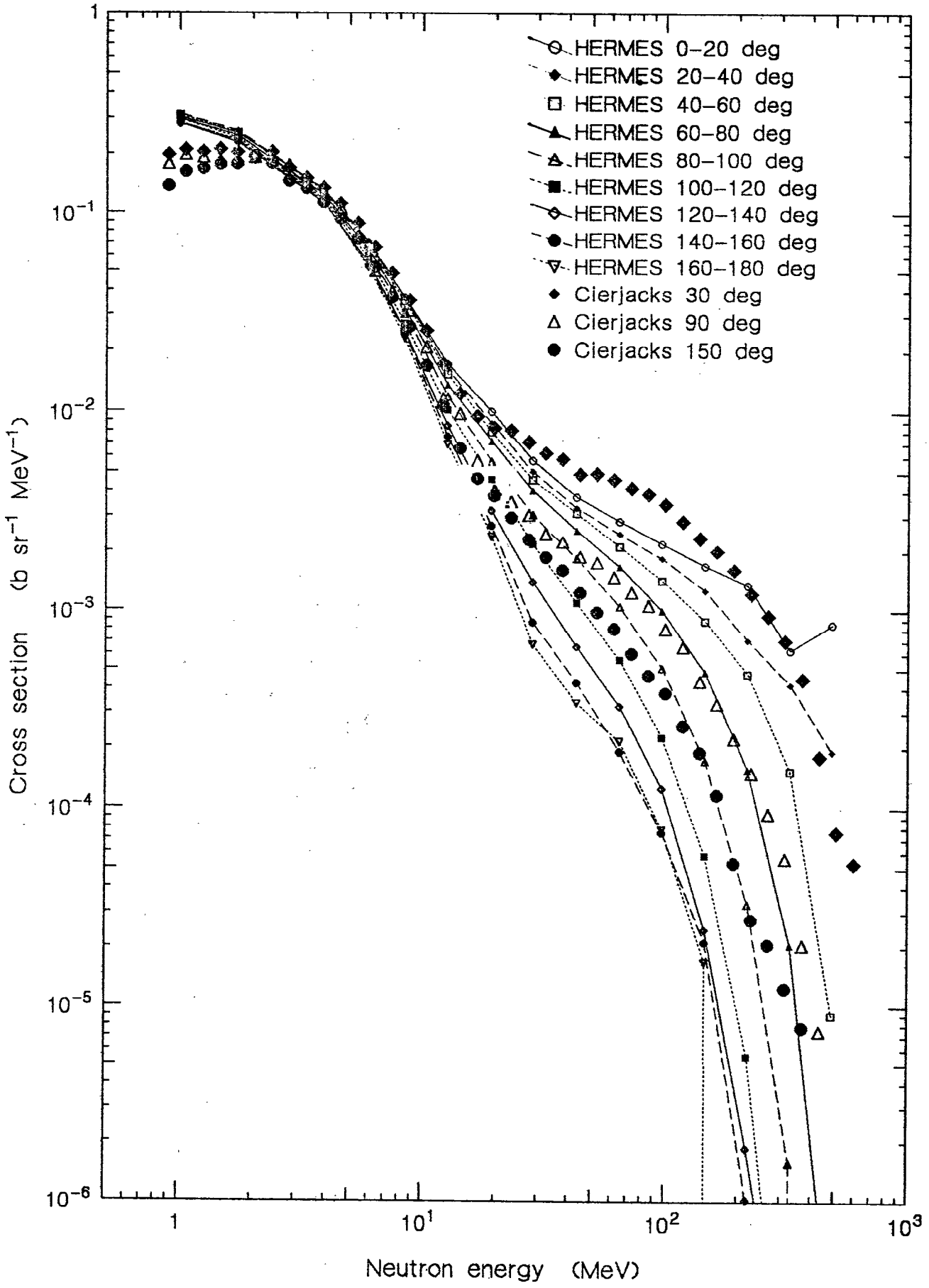

Fig. 3 Calculated and Measured double differential neutron production cross sections of lead bombarded by 585 MeV protons.

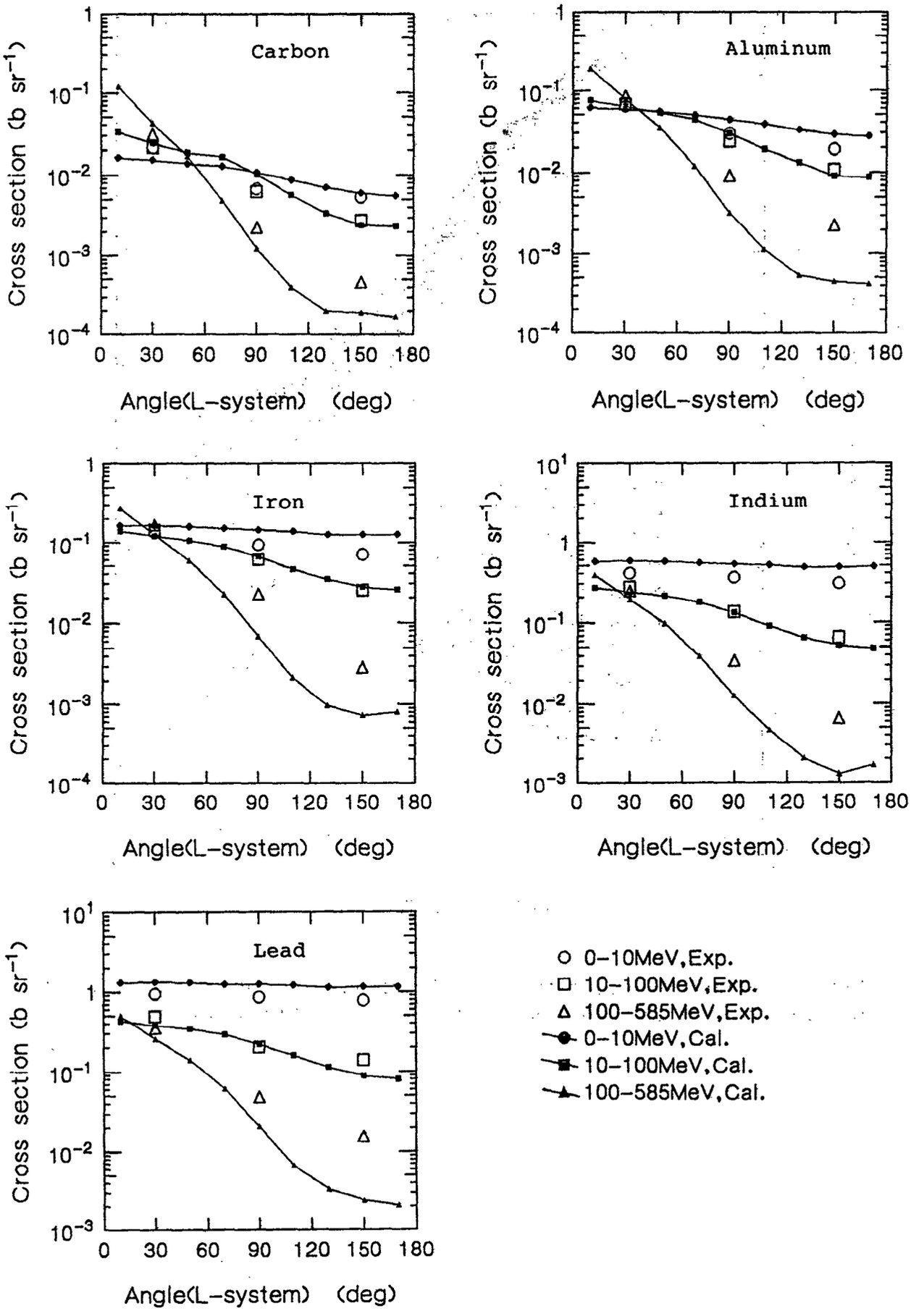

Fig. 4 Calculated and measured angular distribution of neutron yield from C, Al, Fe, In, and Pb elements bombarded by 585 MeV protons.

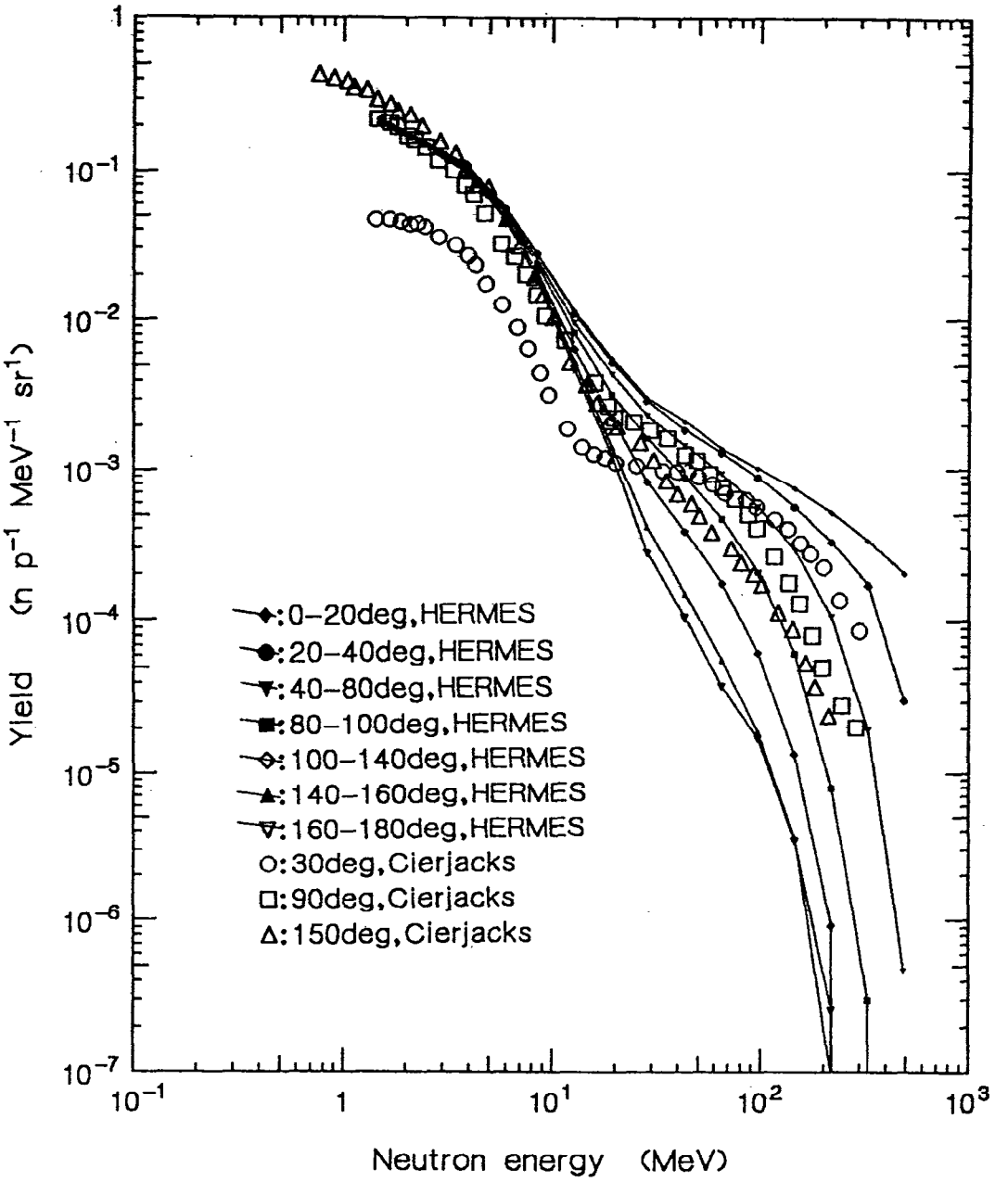

Fig. 5 Calculated and Measured double differential neutron production distribution at a thick uranium target bombarded by 585 MeV protons.

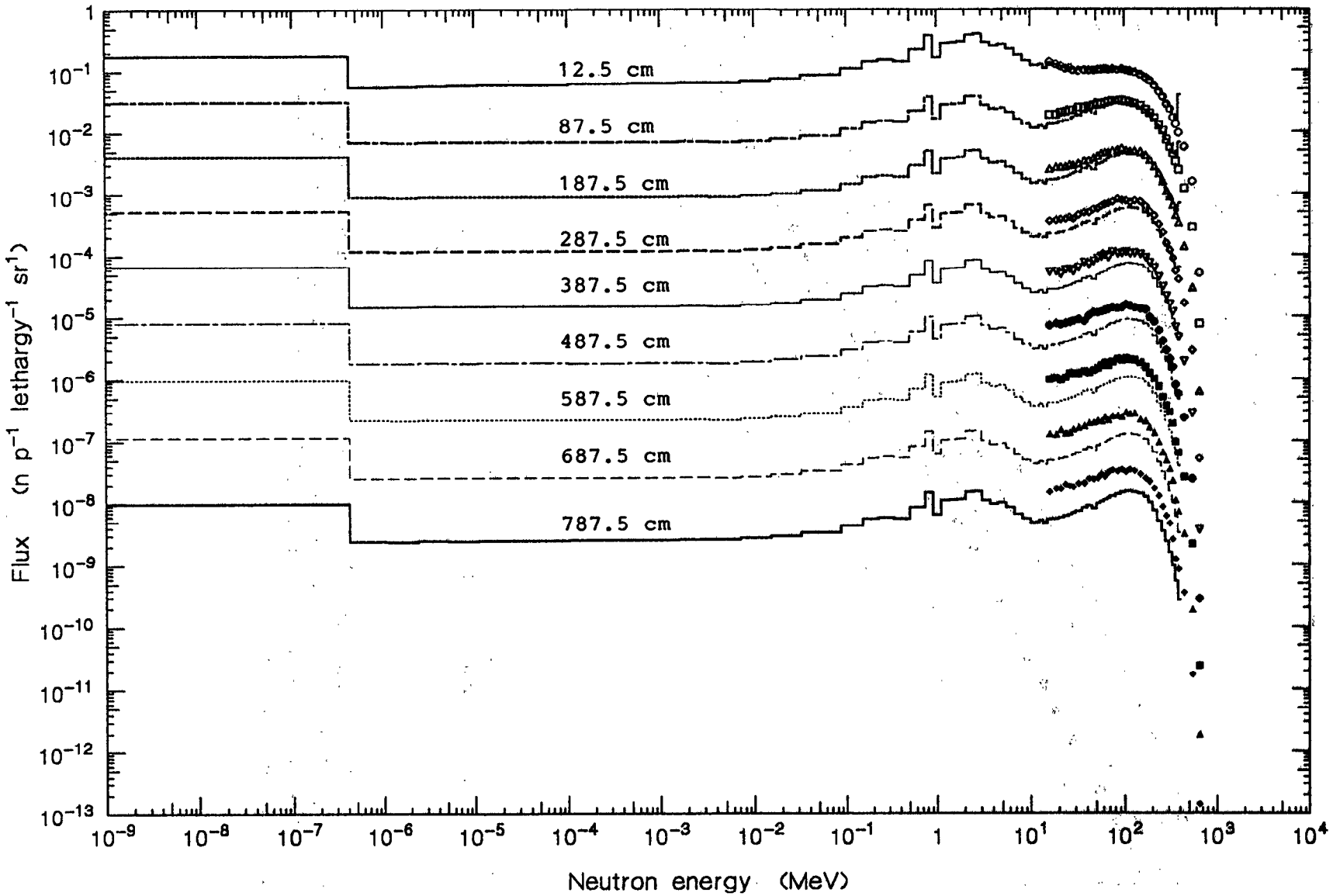

Fig. 6 Calculated neutron lethargy spectra in a 8 m thick ordinary concrete slab. The source was the neutrons produced between 50 deg and 70 deg in a copper beam dump bombarded by 1 GeV protons.

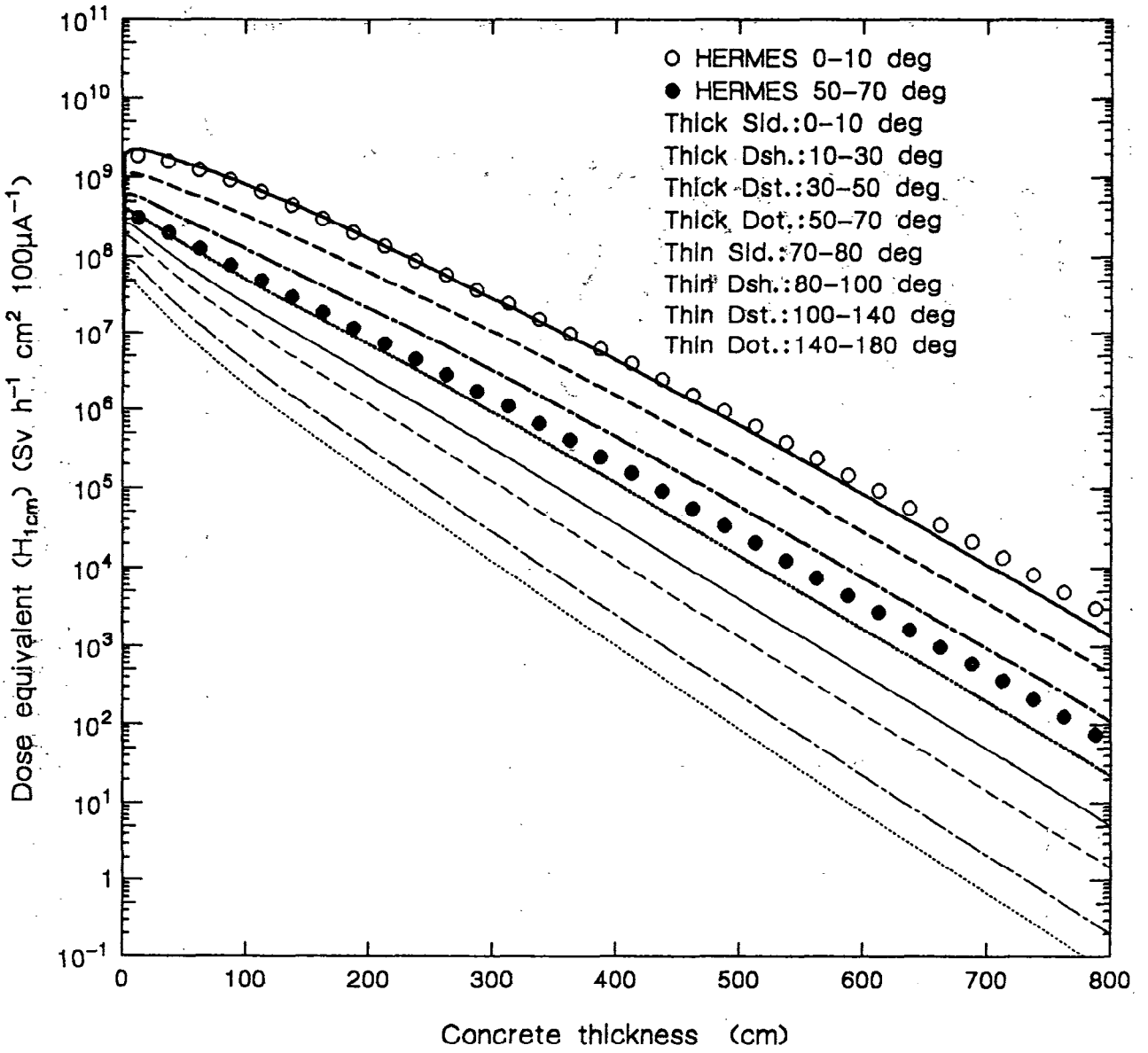

Fig. 7 Calculated dose equivalent attenuation of high energy neutrons (En>14.9 MeV) in a 8 m thick ordinary concrete slab. The source was the neutrons produced between 50 deg and 70 deg in a copper beam dump bombarded by 1 GeV protons.

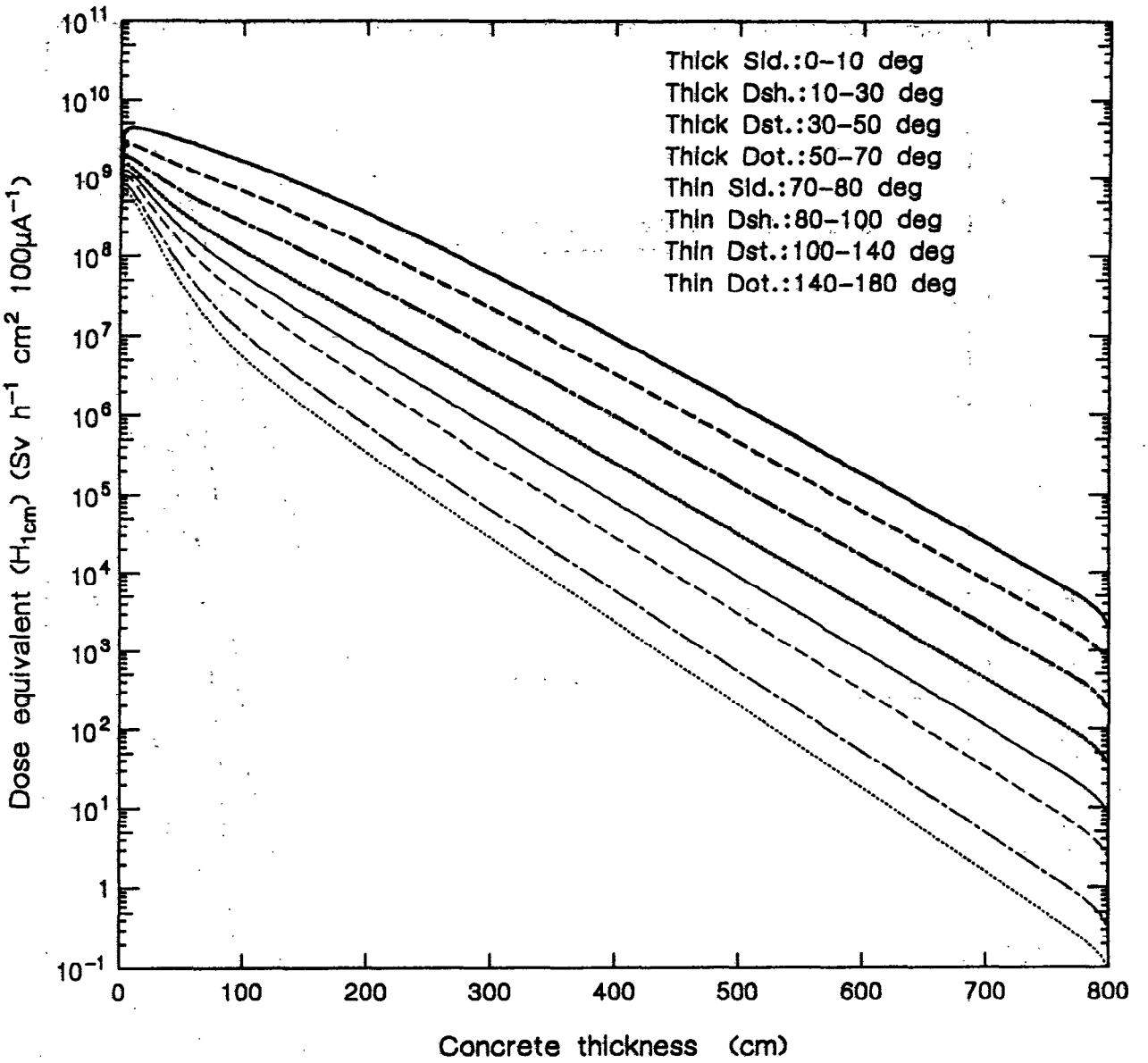

Fig. 8 Calculated dose equivalent attenuation of whole neutrons and secondary gamma rays in a 8 m thick ordinary concrete slab. The source was the neutrons produced between 50 deg and 70 deg in a copper beam dump bombarded by 1 GeV protons.

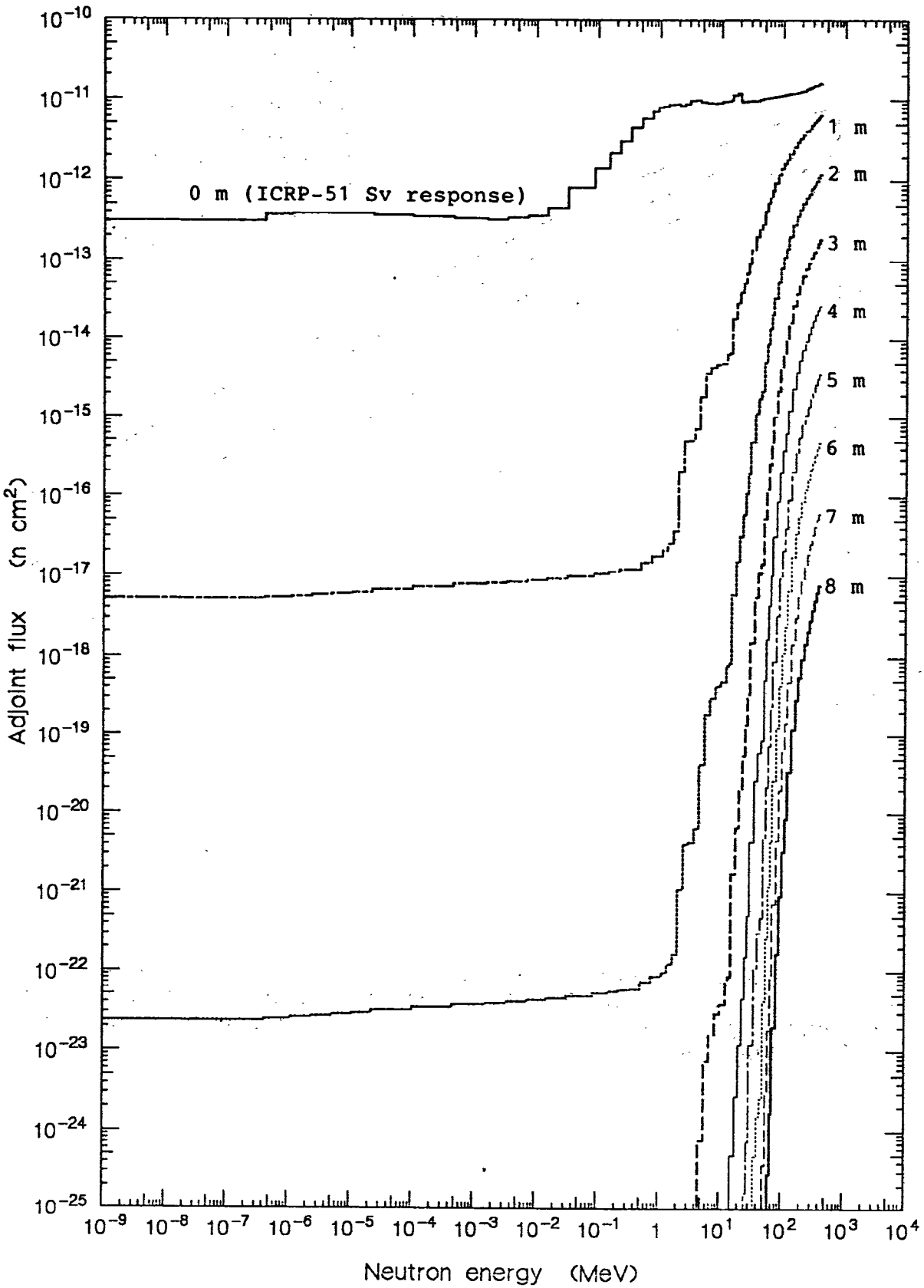

Fig. 9 Adjoint neutron flux distribution in a 8 m thick ordinary concrete slab for a source of the dose equivalent response function given in the ICRP-51.

ICANS-XI International Collaboration on Advanced Neutron Sources
KEK, Tsukuba, October 22-26, 1990

Multiplicating neutron targets based on the proton beam of Moscow Meson Facility.

V.G.Miroshnichenko, S.F.Sidorkin, Yu.Ya.Stavissky
Institute for Nuclear Research of Academy of Sciences of USSR

ABSTRACT
The main physical parameters of the pulsed neutron source with limited multiplication (⩽ 10) based on the proton beam of the Moscow meson facility are discussed. The results of calculation of an optimal multiplication coefficient are presented.

One way to increase the intensity of pulse neutron sources based on the high-current proton beams and used for time-of-flight experiments is connected with the use of multiplicating targets/3/. This gives the following possibilities:

a) to increase by several times the intensity of the pulse neutron source in the frequency range 10-30 Hz, which is the most convenient for most time-of-flight experiments;

b) to reduce the used proton beam current to 5-30% of the full accelerator intensity that allows a number of the various experiments to be carried out concurrently;

c) to provide high performance of the neutron source in the early stage of the accelerator operation when the full beam intensity will not yet be obtained.

However, multiplicating targets have greater fast neutrons pulse duration and background level between pulses comparing to non-multiplicating ones.

The optimal multiplication factor as a function of mean lifetime of prompt fission neutrons τ and energy E of neutrons used in time-of-flight experiments is shown in Fig. 1 /4/. Drawing this plot it was assumed that protons are ejected from the storage-ring-compressor with pulse duration T_s= 0.32 μs /5/. The multiplication factor K_M increases with decrease of τ and increase of the dispersion of time of slowing down of fast core neutrons to energy E and length of the diffusion in the external moderator $\tau_M(E)$, reaching its maximum value in the thermal neutrons range/4/. To determine K_M and compare pulse sources the figures of merit united into two groups were used:

$$K_{1n} = \overline{\Phi} / \theta^n, \qquad K_{2n} = \overline{\Phi S} / \theta^n,$$

where n - order of figure of merit ($1 \leqslant n \leqslant 4$),

$\overline{\Phi}$ - mean flux density of neutrons with the energy E on the radiating moderator surface,

S - area of the moderator surface that is visible from the sample side,

$\theta = \sqrt{\tau_M^2(E) + \theta_{eff}^2}$ - efficient neutron pulse duration,

θ_{eff} - efficient core neutron pulse duration /6,7/.

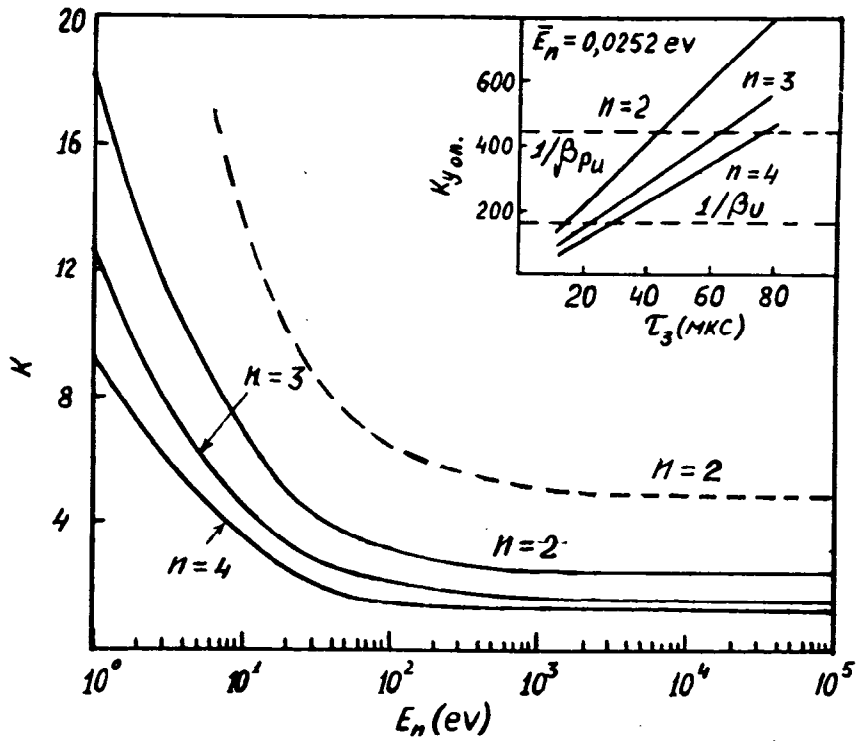

Fig. 1. Main plot: Optimal multiplication coefficient as a function of neutron energy required in an experiment for two values of prompt neutron life-time in case of using the proton beam compressor with pulse duration T_s = 0.32 μs.

Insertion: Optimal multiplication coefficient as a function of neutron moderation time spread. The dashed lines mark the lower boundary of the region where the reactivity modulator is needed for U and Pu.

On the first stage of experimental complex development it is possible to use targets with limited multiplication ($K_M \leq 15$) replacing depleted or natural uranium by highly enriched fuel and not changing the overall neutron source design /1/. This decision requires decoupling of target core and moderators to prevent increasing of pulse duration and overheating of outer core elements by thermal neutrons produced in external moderators. Design performance of the pulse neutron source with limited multiplication with core elements made of U^{233} or U^{235} alloys and ceramics operating at 25 Hz is presented in Table 1. The can of a fuel element made of stainless steel is capable to provide fuel burn-up up to 2% or 2.5 years of continuous facility operation. Proton beam

consumption constitutes 25% of a full accelerator intensity if the storage-ring-compressor is used to produce short proton pulses, and 5% - if accelerator pulses are simply "cutted" to 20 μs. It can be seen that the thermal neutrons flux density increases by a factor 6-7 as compared with the U^{238}-target.

Table 1.

Target parameters	^{235}U	^{233}U	^{238}U
Average power, MW	2.5	2.5	0.15
Background power, MW	0.0175	0.0075	0.0028
Thermal netrons pulse duration ½ θ_T, μs	35	35	35
Multiplication K_M	10	10	—
Average thermal neutrons flux density - $\overline{\Phi}_T$, n/cm^{2}s	$2.7*10^{13}$	$3.6*10^{13}$	$4.3*10^{12}$
Peak thermal neutrons flux density Φ_{peak}, n/cm^{2}s	$3.1*10^{16}$	$4.1*10^{16}$	$4.9*10^{15}$
Pulse frequency (with storage ring), Hz	25	25	25
$\overline{\Phi}_T/\theta_T^2$ *	17	17	17
I_{cold}**, n/s	$6.8*10^{15}$	$8.3*10^{15}$	$1.1*10^{15}$

*) As compared with design performance of the pulse reactor IBR-2 /8/.

**) For the quasistationary source of thermal and cold neutrons.

To evaluate optimal design parameters of the multiplicating target that provide minimum core dimensions, required multiplication factor (~ 15), and satisfactory cooling conditions (maximum fuel temperature ≤ 500°C for U-Mo-alloy and maximum temperature of the outer surface of the fuel element ≤ 120°C) the Monte-Carlo code MCU was used /11/. The target design used in computations is presented in Fig. 2. Optimal design parameters determined for the target with thermal power 2.5 MW is presented in Table 2. It should be noted that to provide fuel-coolant compatibility in a wide temperature range in case of a fuel element can destruction U_3Si - ceramics and U-Mo(9%)-alloy were considered as the fuel composition for the light-water and PbBi-eutectic coolant correspondingly.

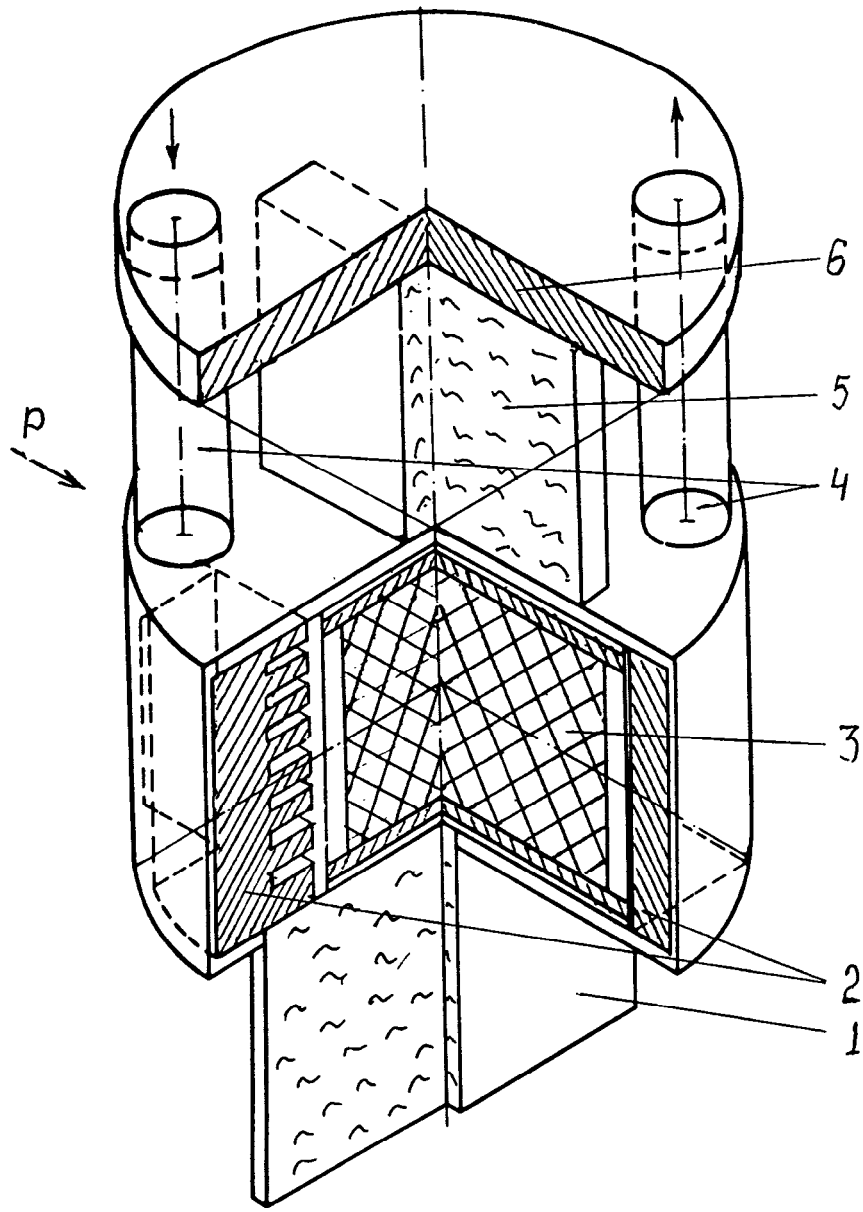

Fig. 2. Calculational scheme of the multiplicating target:
1 - lower moderator
2 - decoupler
3 - core
4 - coolant's inlet and outlet
5 - upper moderator
6 - fragment of the moderator's reflector

Table 2.

Core parameters *	^{235}U + Mo(9%)	^{233}U + Mo(9%)	Coolant
Dimensions, cm	13.2*15*22.7 (16.4*16*22.7)	7.6*15*22.7 (10*15*22.7)	H_2O (Pb-Bi)
Fuel element diameter, mm	8.5 (7.9)	6.3 (5.8)	
Maximum fuel temperature, °C	504 (505)	504 (504)	
Maximum fuel element surface temperature, °C	117 (321)	117 (314)	
Fuel content, vol.%	69.6 (68.3)	64.0 (62.3)	

*) With the tungsten reflector.

The more flat target core based on U^{233} and cooled by H_2O is the most efficient since it provides both the lowest background level and the highest neutron leakage out of the core into external moderators. Besides its dimensions are close enough to the yet designed U^{238}-target ones (6*15*22.7 cm^3) that allows neutron guides through the biological shield to be used without any changes /1/.

It should be noted that unlike the U^{238}-target the multiplicating target can not be used as the beam dump cause if the full accelerator beam is directed onto the target its thermal power will be 7 MW that exceeds the design heat release almost by a factor of three. This causes the stronger requirements to control system reliability to prevent directing of the full accelerator beam onto the multiplicating target.

Possible performance of the target with high multiplication (~ 100) was considered in detail in the paper /3/. Using this target the peak flux density of thermal neutrons on the radiating moderator surface as high as $2*10^{17}$ n/cm^2s can be obtained.

Yet another field of application of the multiplicating target is considered in detail in the paper /10/.

References.

1. Yu.M.Bulkin, M.I.Grachev, Yu.Ya.Stavissky et al., Proc. conf. on neutron scattering in the 'nineties. IAEA, Vienna, 1985, pp.369-375.
2. I.S.K.Cardner. Review of spallation neutron sources. European particle accelerator conference. Rome, June 1988.
3. Yu.M.Bulkin, N.V.Kolmychkov, S.G.Lebedev, et al., Proc. of 2-nd All-Union seminar, Moscow, 1982, pp.271-276 (in Russian).
4. S.F.Sidorkin. Inst. Nucl. Res. Preprint P - 0545, Moscow, 1987 (in Russian).
5. M.I.Grachev, V.M.Lobashev, Yu.Ya.Stavissky et al., Proc. 9th

All-Union conf. on charged particle accelerators, v.1, Dubna, 1985, p.343 (in Russian).
6. W.Kley, Nucl. Instr. Methods, v.200(1982), p.175.
7. E.P.Shabalin, "Pulsed fast reactors", Atomizdat, Moscow, 1976 (in Russian).
8. V.D.Ananiev, J.A.Kozlov, V.I.Luschikov et al., Joint Inst. Nucl. Res., Message RZ-85-187, Dubna, 1985 (in Russian).
9. S.B.Shihov, V.B.Troyansky, "Nuclear reactors theory", v.2, Energoizdat, Moscow, 1983 (in Russian).
10. S.F.Sidorkin, V.I.Derzhiev, S.I.Yakovlenko, Inst. Nucl. Res. Preprint P-0665, Moscow, 1990 (in Russian).
11. G.F.Liman, L.V.Mayorov, M.S.Yudkevich, Voprosy atomnoi nauki i tehniki, Ser. Fizika i tehnika yadernyh reactorov ,v.7, pp.27-31, 1985 (in Russian).

ICANS-XI International Collaboration on Advanced Neutron Sources
KEK, Tsukuba, October 22-26, 1990

PERFORMANCE OF NOVEL MODERATOR FOR PULSED NEUTRON DIFFRACTION

R.E.Mayer*, J.R.Granada*, J.Dawidowski**, and V.H.Gillette*

Centro Atomico Bariloche, 8400 S.C. de Bariloche (RN) - Argentina
* Also at Instituto Balseiro, Univ. Nac. de Cuyo
** Fellow of Consejo Nacional de Investigaciones Cientificas y Tecnicas. Also at CRUB, Universidad. Nacional del Comahue

ABSTRACT
Measurements of neutron pulse time-width and intensity have been carried out on grids of small moderators placed side by side and decoupled by cadmium strips. This moderator concept had been introduced at ICANS-10. The present measurements explore greater moderator thicknesses than those previously attained, yielding information on thickness optimization, while confirming the previous results on resolution which make this moderator a favourable choice in front of the conventional sandwich set-up.

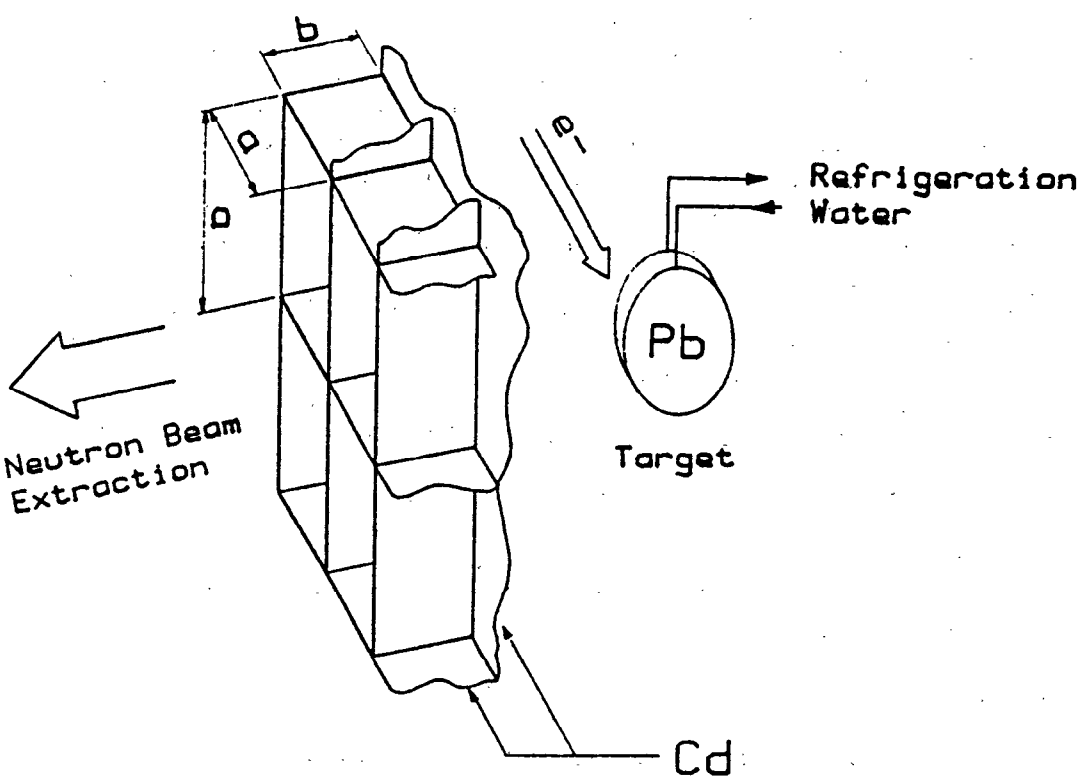

Fig. 1- Scheme of cadmium grid to be filled by moderating material, with neutron generating target shown behind.

I. INTRODUCTION

The long sought goal of finding more efficient means to slow down the fast neutrons from an accelerator's target, seems to be a subject still open for innovation. We have thus undertaken to continue exploring a concept introduced during ICANS-10 [1], and more extensively explored in a recent paper [2].

From our previous experience with thin moderators, we became convinced that their lateral dimensions are the determining parameters as far as time response is concerned. Consequently, a new system was conceived consisting of an array of small moderators placed side by side and decoupled by cadmium strips.

The sets of moderators tested consist of cadmium grids (fig. 1) filled with paraffin, which was chosen because of ease of manufacture. The aim is to selectively absorb those slow neutrons prone to have a longer residence time within the moderator and which contribute a poorer time resolution, while still retaining the possibility to increase moderator thickness in order to slow down a greater portion of the incident fast flux, without loosing time resolution; this proved to be true [1;2], and we present here a test of greater moderator thicknesses which were not available with the previous experimental set-up.

The present array differs from that studied by Day and Sinclair [3], which they later discarded, in that the depth of moderator elements is not related to their lateral size because they *are not* defined as cubes, being thus free to vary independently and reach an optimum value.

II. EXPERIMENTAL

Raw data was normalized to equal fast neutron production of the 25 MeV electron LINAC through monitor counts, and diffraction spectra from one powdered Cu sample recorded for each moderator tested, were fitted with an appropriate peak shape function [4]. The latter is the result of the analytical convolution of an exponential decay with a Gaussian; it has four parameters : peak position, its area, and the two resolution parameters ALPHA and SIGMA. ALPHA takes accout of all nonsymmetrical contributions strongly reflecting -besides minor effects- the time response of the moderator; it is the reciprocal decay constant intervening in the convolution. SIGMA is the width parameter of the convoluted Gaussian, and collects the effects of all symmetrical contributions to the time distribution, arising mostly from the geometrical characteristics of the instrument (source included). It is not greatly affected by the changes of moderators of this experiment.

For comparison purposes also a slab and a heterogeneously poisoned "sandwich" moderator were tested. The latter, according to a concept studied during 1969 [3] and of very similar dimensions as described by Windsor and Sinclair in 1976 [5].

The "sandwich" consisted of a polypropylene pre-moderator slab 20 x 20 x 1.8 cm^3, and a thin circular post-moderator 15 cm in diameter and 0.6 cm thick, decoupled from the pre-moderator by a 0.6 mm thick Cd sheet. The slab is polypropylene 20 x 20 x 2.4 cm^3. All moderator systems were wrapped in 0.8 mm thick cadmium, except on their emitting faces.

III. RESULTS

In the figures, open symbols will identify points from references [1;2], while closed symbols will be assigned to new data.

Figs. 2, 3 and 4 show how moderator related time resolution changes from grid to grid (characterized by "a") and also that this parameter is

independent of the particular moderator thickness ("b") tested.

This was a fundamental result put through by the previous work [1;2] which now appears to still hold even for thicknesses "b" much greater than that of optimal slow neutron production.

Fig. 5 is intended to show the general trend of the magnitude with which we have been dealing, while the behaviour of the other important magnitude, neutron production, is described by fig.6.

There was a (1 x 1 x 2) moderator which through extra irradiation time, was allowed to *swell* in the sense of deformation of the paraffin contained in the Cd grid, till it protruded outside of the grid boundary a few millimeters. As expected, this collapse of the boundary conditions of the experiment, produced the worsening of the time resolution and the related thermal neutron production increase visible in the figures.

This work does not intend to find "the best" moderator; its purpose, instead, is to describe the behaviour of the configuration proposed herein, and to do so in terms of parameters useful for designers. We believe it constitutes a valid alternative to other choices, especially where short flight paths are to be used, as when a premium is put on maximizing intensity in the absence of shielding limitations, or while avoiding the installation of thermal neutron guides.

REFERENCES

[1] R.E. Mayer, J.R. Granada, V.H. Gillette and J. Dawidowski, Proc. ICANS-10, Los Alamos, USA (1988), p.515.

[2] R.E. Mayer, J.R. Granada, V.H. Gillette and J. Dawidowski, Nucl. Instr. and Meth. **A288** p.467 (1990).

[3] D.H. Day and R.N. Sinclair, Nucl. Instr. and Meth. **72** p.237 (1969) .

[4] F.Kropff, J.R.Granada, R.E.Mayer, Nucl.Instr.and Meth. **198** p.515 (1982)

[5] C.G. Windsor and R.N. Sinclair, Acta Cryst. **A32** p.395(1976)..

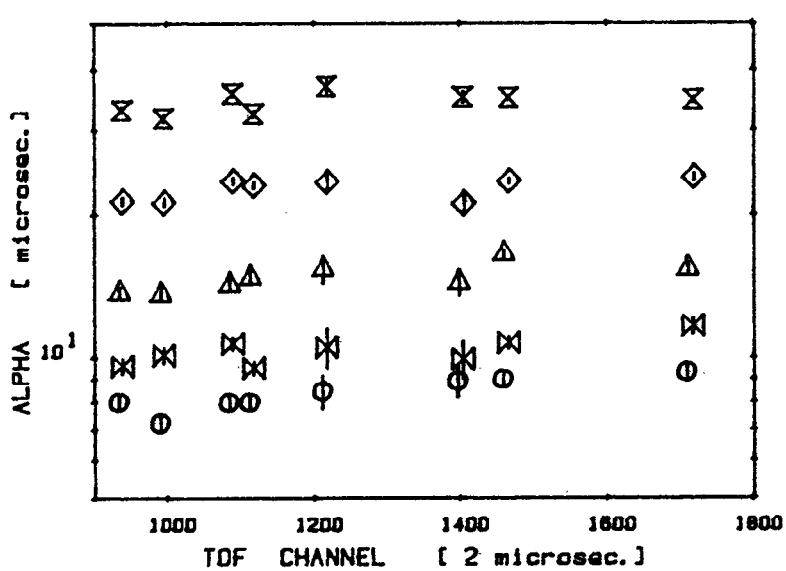

Fig. 2- ALPHA, the reciprocal exponential decay constant that intervenes in the analytical convolution with a Gaussian to yield the peak shape function [4], is most sensitive to the time response of the neutron moderator. This figure from ref. [2] displays the time response behaviour of the neutron emission for different moderator families identified by their conventional symbols (Table 1).

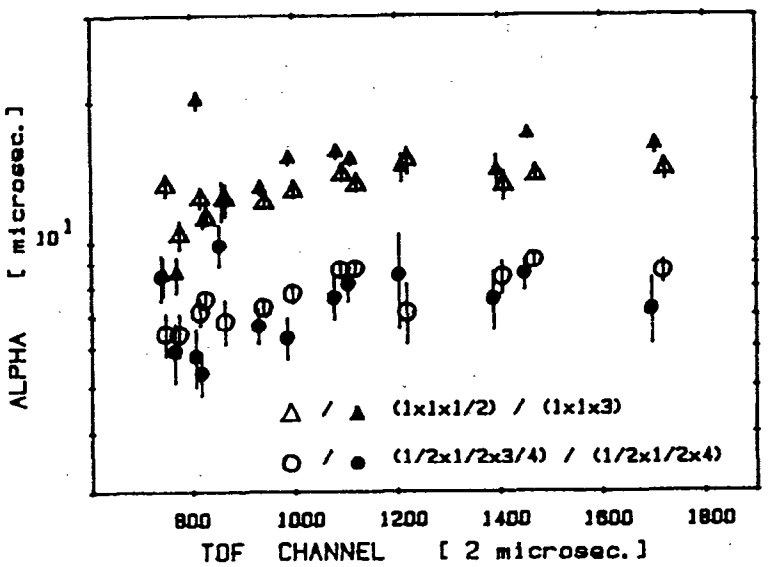

Fig. 3- Fitted ALPHA values (as explained for fig. 2) for grid spacing 1 and 1/2 in., showing the family behaviour of each grid through the insensitivity of ALPHA to very different moderator thicknesses (indicated in the plot). The (1 x 1 x 4) fit is not shown because of the low statistics of that short measurement, for which this general conclusion, anyhow, still holds.

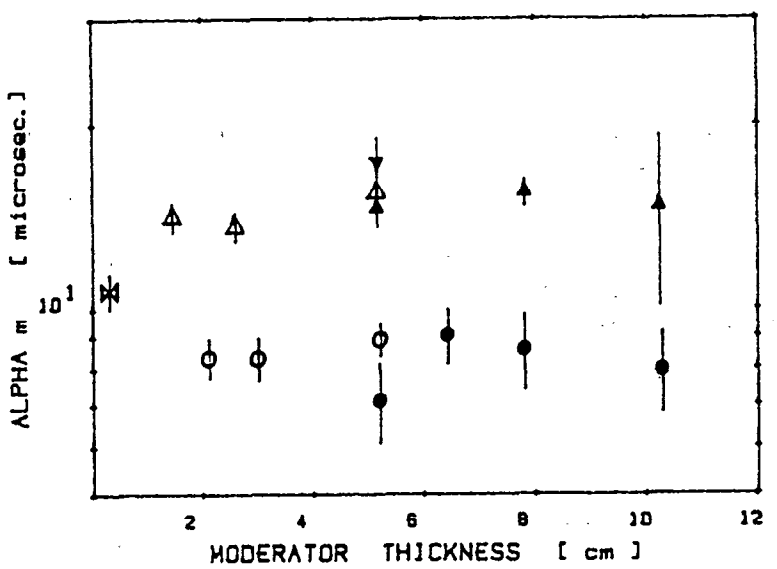

Fig. 4- ALPHAm is defined as the mean of the last four ALPHA values fitted on the lower side of the observed momentum transfer range (reflections 220; 311; 222; 400 form the Cu sample). This mean associated to the "quasi-plateau" region of each moderator, plotted against moderator thickness, better visualizes the insensitivity of neutron emission time response with the addition of moderating material. The moderator which was allowed to swell out of the Cd grid (▼) is seen to have a poorer time response, as expected. Open symbols: [1;2]; closed: new data.

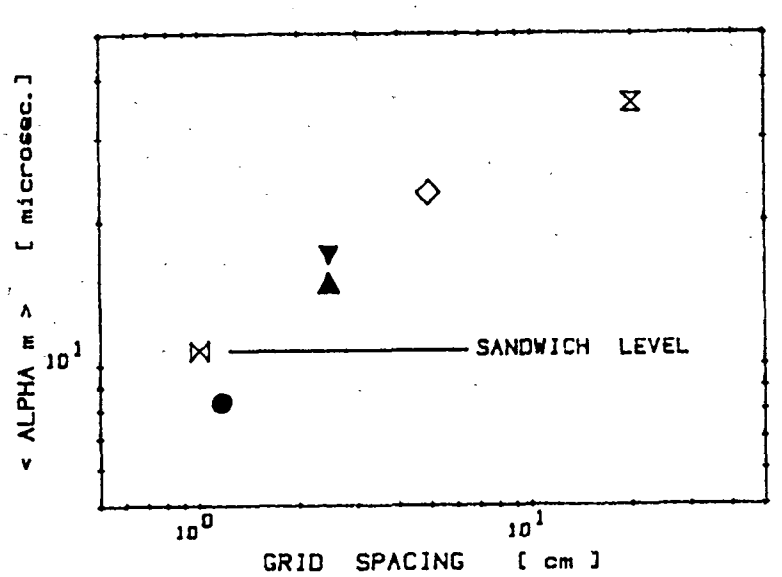

Fig. 5- <ALPHAm> is the mean of the ALPHAm values belonging to each grid family. The trend of neutron emission time response with grid spacing is clear. Slab is plotted according to its lateral dimensions as a "one-element grid". Reference sandwich moderator value is provided for comparison purposes. Open symbols: [1;2]; closed: new data.

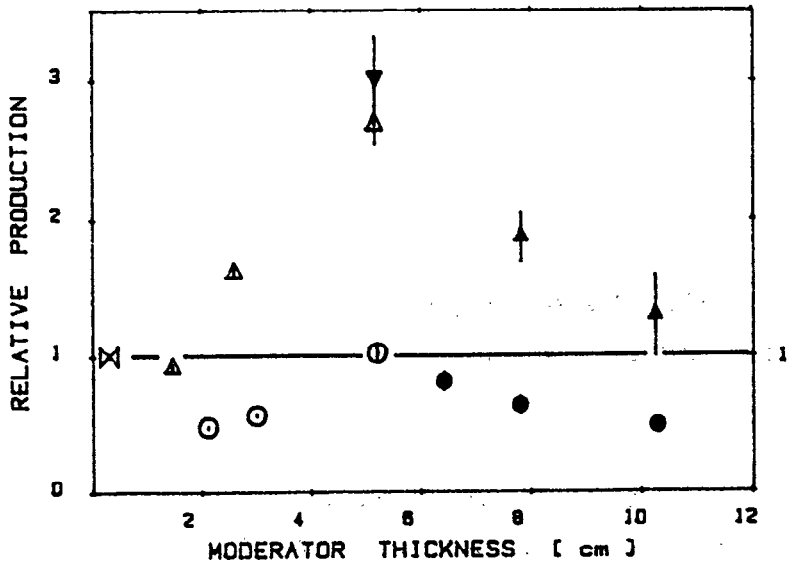

Fig. 6- Neutron production taken as the summation of eleven integrated intensities normalized by fast neutron production (monitor counts), and referred to the corresponding values of the reference moderator (sandwich). The moderator allowed to swell out of the Cd grid (▼) is exposed to less thermal neutron absorption and correspondingly exhibits a higher neutron production.

TABLE 1

Moderators identified as (a x a x b) according to Fig. 1 with their values given approximately in inches for mnemonic reasons

MODERATOR	SYMBOL	a [cm]	b [cm]
SLAB	⧗	20.0 ± 0.20	2.40 ± 0.05
(2 × 2 × 1)	◇	4.91 ± 0.01	2.54 ± 0.01
(1 × 1 × 4)	▲	2.46 ± 0.01	10.24 ± 0.06
(1 × 1 × 3)	▲	"	7.81 ± 0.19
(1 × 1 × 2)	△	"	5.15 ± 0.05
(1 × 1 × 1)	△	"	2.59 ± 0.11
(1 × 1 × 1/2)	△	"	1.45 ± 0.13
SANDWICH	⋈	-	-
(1/2 × 1/2 × 4)	●	1.17 ± 0.01	10.28 ± 0.06
(1/2 × 1/2 × 3)	●	"	7.80 ± 0.10
(1/2 × 1/2 × 5/2)	●	"	6.41 ± 0.15
(1/2 × 1/2 × 2)	○	"	5.20 ± 0.05
(1/2 × 1/2 × 5/4	○	"	3.00 ± 0.29
(1/2 × 1/2 × 3/4	○	"	2.11 ± 0.29

Cadmium separating strips thickness: (0.7 ± 0.012) mm.
Figures listed belong to moderating elements' dimensions and do not include thickness of Cd strips.

ICANS-XI International Collaboration on Advanced Neutron Sources
KEK, Tsukuba, October 22-26, 1990

Neutron Production in Thick Lead Target by 1-3.7 GeV Protons and Deuterons

V. A. Nikolaev, V. I. Yurevich, R. M. Yakovlev
V. G. Khlopin Radium Institute, Leningrad 197022, USSR

R. G. Vassil'kov
Moscow Radiotechnical Institute, Moscow 113519, USSR

The neutron field of thick lead target (20 cm diam. and 60 cm long) has been studied using the method of threshold detectors - fission and spallation detectors with SSNTD's. The investigation has been carried out at proton and deuteron beams of synchrophasotron JINR in the energy range 1-3.7 GeV. The dependence of the differential neutron distributions on a type of incident projectile and on ion energy are discussed. The data analysis has shown, that the neutron spectra for incident protons are more hard than for the deuteron beam. The relative partial neutron yields for low-energy component (<1 MeV) and high-energy component (>20 MeV) contain 38%, 10% and 45%, 7% for p and d ions respectively . The average value of the total neutron yields ratio $Y_d/Y_p = 1.20 \pm 0.15$.

1. INTRODUCTION

Rapid progress in development of high-current, medium-energy ion accelerators leaded to appearance of a new branch of neutron physics connected with desing, investigation and application of the intense neutron spallation sources. The principal idea of efficient neutron production is a conversion of ion kinetic

energy in heavy metal thick target to secondary particle radiation.

The spallation reaction of nuclei is the main mechanism for neutrons generation in passing of high-energy ions through matter. Besides neutrons, charged particles are generated to a large extent. However, as experimental studies and calculations have shown /1-4/, the relative share of neutrons quickly increases in the substance with propagation of the secondary radiation through it. Therefore even for comparatively small targets with the characteristic size above 100 g/cm^2 the neutrons yield by many times exceeds the charged particles yield. The most characteristic feature of neutron spectra of such sources is presence of the hard component in the energy range of hundreds MeV. This is more clearly illustrated in Fig.1, which shows the experimental spallation neutron spectra /2,5/ and a fission neutron spectrum for a comparison.

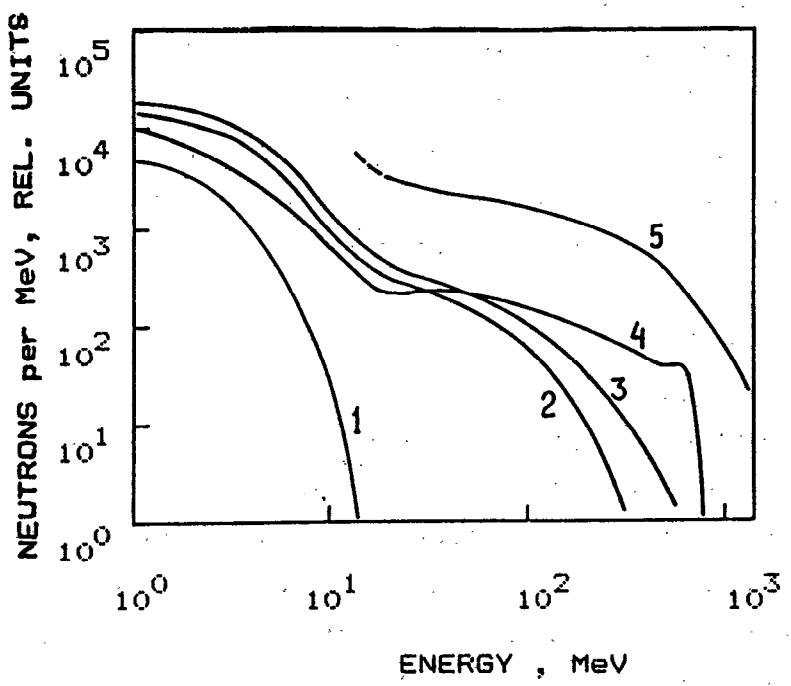

Fig.1 Energy dependence of the neutron production for fission source (1) and from medium-energy ion bombardment of various thick targets at emission angle Θ (the lines are eye-guide curves through the measured data points) : 2, 3 - 590-MeV and 1100-MeV protons on lead target 10 cm diam. x 60 cm long at Θ = 90° /2/; 4 - 800-MeV protons on tungsten target 3 cm diam. x 7.6 cm long at 30° /5/; 5 - 1-GeV/A ^{12}C ions on lead target 8x8x8 cm^3 at 30° / our results of TOF measurement /.

Meanwhile, in spite of high demand for studies of such neutron fields, there are no effective experimental methods enabling to carry out measurements under conditions of "bad" geometry. In the physics of low energy neutrons such studies are usually being done by the activation method or the method of fission threshold detectors. The latter method recently received its further development in work /6/ where the information taking from polymer solid state nuclear track detectors, SSNTD's, of fission fragments was automatized. This enabled to create an express method for determination of neutron fields' charts.

In this paper we briefly discribe the experimental method and its application to study the neutron field of thick lead target (20 cm diam. and 60 cm long) having a high neutron yield per incident ion. The considered energy region 1-3.7 GeV is the most interesting for the neutron sources design because it is characterized by a minimum of the ionization loss or a maximum of the neutron production per unit of ion kinetic energy. The precise measurements of the total yields of neutrons with energy less 15 MeV for this target were carried out by the neutron moderation technique by Vassil'kov et al. /7/. In present investigation the differential characteristics of the neutron source have been studied in detail.

2. EXPERIMENTAL METHOD

The most important requirement in construction of a hard neutron radiation detector is to broaden the existed standard set of fission threshold detectors by adding detectors with higher thresholds in the region of several hundreds or more MeV.

The detector chosen as one of such detectors was based on the bismuth's fission reaction that has been used in a number of works /8/ for registration of high energy neutrons. Study of the nuclear fragmentation of various materials, spallation reaction, under the action of high energy protons and neutrons allowed to construct a detector of new type with a very high value of the effective threshold above several hundreds MeV. For neutron measurements such a detector is used apparently for

the first time, and examining of its registering properties was paid special attention.

As to the design, a solid track detector of fission event presents a fissile layer about 1 mg/cm^2 thick, 11.3 mm in diameter (the area 1 cm^2) on an aluminum backing 19 mm in diameter and 0.2mm thick, placed close to the SSNTD. A spallation detector consists of two similar thick spallation layers (disks) embracing the track detector on both sides.

Such a design of the detector provides, firstly, a rather high efficiency of neutron registration due to making use of thick layers (the layer's thickness being greater than the maximum range of a fragment); secondly, sharp decrease of the detector's sensitivity dependence on its orientation relative to the direction of the neutrons' incidence by registration of fragments escaping both forward and backward; thirdly, shielding of SSNTD from other neighbouring material sources of background counting.

Fission and spallation products were registered by means of a SSNTD based on polyethylene terephtalate, PETP, 6 μm thick. The irradiated SSNTD are etched for 60 minutes at a temperature 60 ± 0.1 ^{o}C in a KOH solution (the density 1.252 g/cm^2 at 20° C). The efficiency of neutron registration by a thin layer threshold detector may be found by the formula

$$E = n \sigma_f \eta ,$$

where n is the number of nuclei of the fissile nuclide per cm ^{2}, σ_f – the fission cross section, η – fragment registration efficiency (η = 0.515 for isotropic escape of fragments).

Neutron fission cross sections are well known in the energy region bellow 20 MeV, and their values are part of different nuclear data libraries, for instance, ENDF/B-V. To obtain the values for higher energies of neutrons, measurements' results /5,9,10/ were used. The registration characteristics of spallation detectors were studied on a proton beam because of absence of a source of monochromatic neutrons of high energy. Besides, it was assumed that the spallation process weakly depends on the type of the incident nucleon and has

an equal possibility. In Fig.2 the measured energy dependences of efficiencies for investigated detectors are presented. From Fig.2 , it can be seen that the Cu-Cu and Cd-Cd detectors have considerably higher energy thresholds, and besides, the behavior of their efficiencies is expressed more sharply near the threshold. Note the Cd-Cd detector has a higher efficient threshold than the Cu-Cu detector.

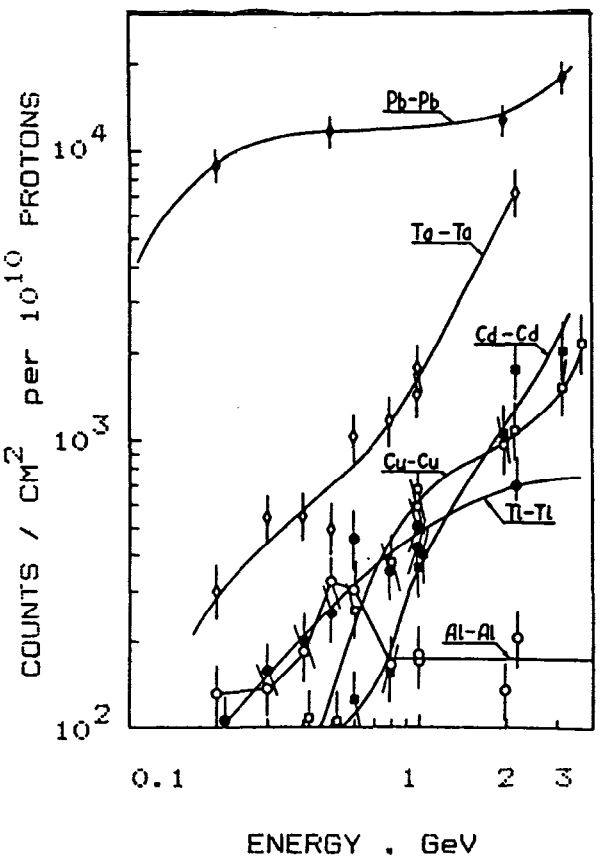

Fig.2 Energy dependence of nucleon registration efficiency for various thick layers measured on proton beam. The solid-lines are eye-guide curves through the experimental data points.

Thus, the following set of detectors were chosen, arranged in order to increase their registration treshold: U-235 in a cadmium or boron filter, Np-237, U-238, Th-232, Bi-209, Cu-Cu or Cd-Cd.

The energy dependences of efficiencies for a full set of threshold detectors, composing a neutron detector, are

presented in Fig.3. The detectors' response functions and the energy regions of maximum sensitivity for them were calculated on basis of these dependences . Analysis shows, that for all considered cases the detectors well complement one another and provide full coverage of a very broad energy range from thermal to several GeV.

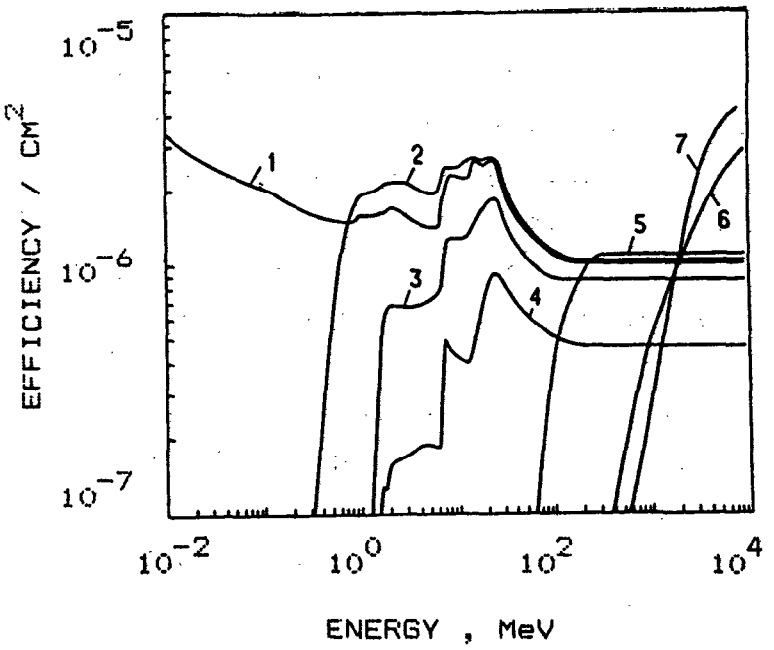

Fig.3 Energy dependence of threshold detectors' efficiencies for neutrons. The curves 1-5 are for fission detectors U-235, Np-237, U-238, Th-232 and Bi-209 respectively (1 mg/cm^2 thickness of fission layer). The curves 6,7 are for spallation detectors Cu-Cu and Cd-Cd.

For correction experimental data we studied the following distorting and background effects: 1) registration of charged hadrons; 2) angular assymmetry of fission fragments; 3) registration fragments from the backings ("the backing effect"), 4) spallation of nuclei of the fissile layer, 5) the own counting of SSNTD.

The registration characteristic and the reliability of the obtained results strongly depends on the method of processing of the irradiated SSNTD. In order to increase of the results' reliability, to decrease methodical errors, the thickness of the PETP film, was checked as well as the values characterising the process of SSNTD etching: the temperature, the concentration

of the KOH solution, the etching time.

Other sources of the errors are the uncertainties of the values of the layer's mass and the efficiency of registration of fragments, the errors of corrections for the background effects and the statistical error.

3. PROCEDURE OF DATA PROCESSING

The energy distributions of neutrons were reconstructed by iteration procedure using the results of integral measurements. The mathematical processing was realized in the computer code RESTOR. The results of data processing are the neutrons energy distribution, F(T), and the yields of neutrons, $Y(T_i)$, with kinetic energy above T_i. The value T_i is choosed from the set (0 , 0.1 , 1 , 6 , 20 , 50 , 100 , 250 , 500 , 1000 MeV).

The program allows the operator to carry out visual control of the restoration process, detecting a disagreement between the experimental results of different threshold detectors. A small number of iterations (<10) is another criterion of agreement of data-in and a good choise of the zero approximation of energy distribution, Fo(T). The zero approximation is realized in the code in two ways :

1) assignment of the table of values on the energy grid, using known results of measurements and the calculations of neutron spectra ;

2) analytic representation of the energy distribution.

The details of the measurement and data processing method take place in paper /11/.

The method was tested in the neutron field of a lead target (20 cm diam. and 20 cm long) irradiated by 2.55-GeV protons The three-component representation of neutron spectrum /12,13/ with realistic values of parameters was used for assignment of the zero approximation.

The results of measurements were compared with the ones obtained by the time-of-flight technique. The energy distributions measured by these experimental methods at angle 90° are presented in Fig.4. Good agreement of the results with each other in the

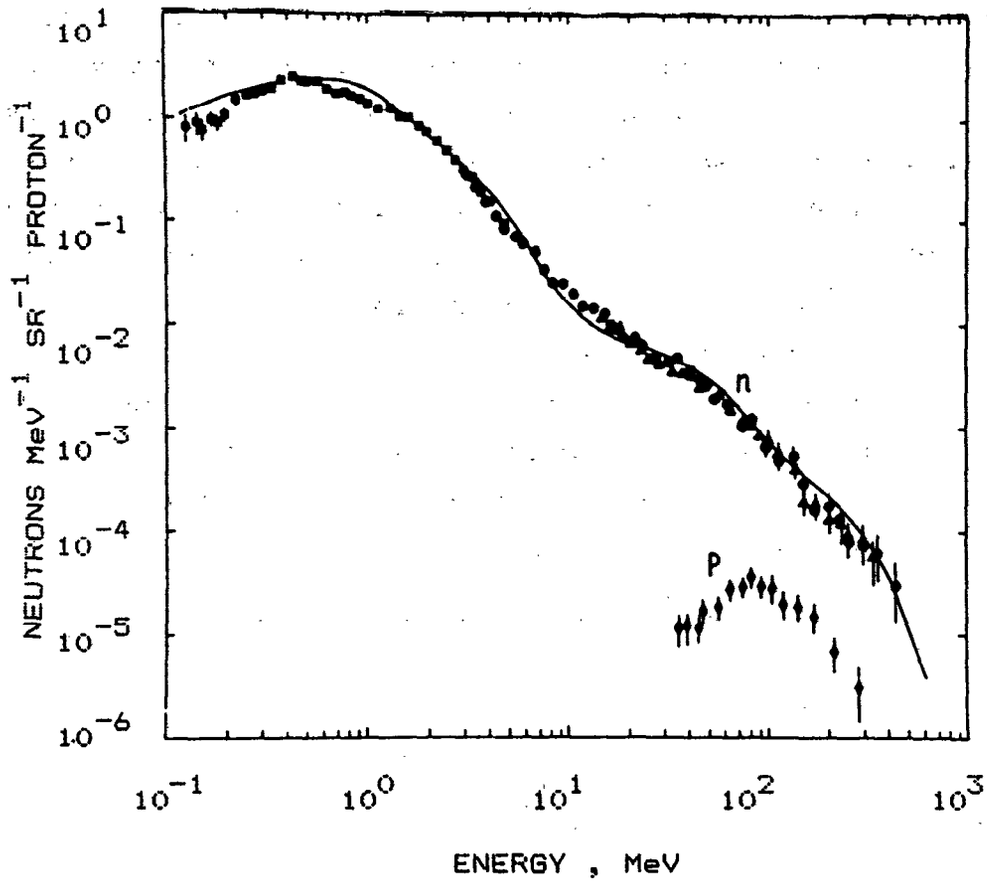

Fig.4 The spectral distribution of neutrons at emission angle 90° from bombardment of lead target 20 cm diam.x 20 cm long with 2.55-MeV protons has been measured by both the time-of-flight technique (the points) and the threshold detectors' method (the curve). The TOF spectrum of secondary protons is shown too.

whole energy range confirms applicability of the described method for studying the neutron fields of a hard energy spectrum.

As shown in Fig.4 , for thick lead target the neutron output is higher proton output more than order for all energies.

4. EXPERIMENTAL SETUP AND PROCEDURE

The neutron field of the lead target (20 cm diam. and 60 cm long) has been studied at synchrophasotron JINR using external proton and deuteron beams with energy about 1 , 1.5 , 2 , 2.5 , 3.1 , and 3.7 GeV. The beam intensity during the measurements

was typically of the order of a few 10^8–10^9 ions per second. The position and the profile of the beam at front surface of the target have been measured by multiwire proportional chamber. The beam spot at the target position as typically 20 – 30 mm (FWHM) in the vertical and horizontal directions. The ion flux has been monitored using activation reactions on aluminum $^{27}Al(p,x)^{24}Na$ and $^{27}Al(d,x)^{24}Na$. Aluminum monitoring-foil has been placed ~40 cm in front of the target. On a base of the experimental data for the first monitor reaction we have supposed the cross section about constant with a value 10.0±0.3 mb. But for the deuterons only in one experimental work /14/ a value of the cross section was determined 15.25±1.5 mb at energy 2.33 GeV. Our

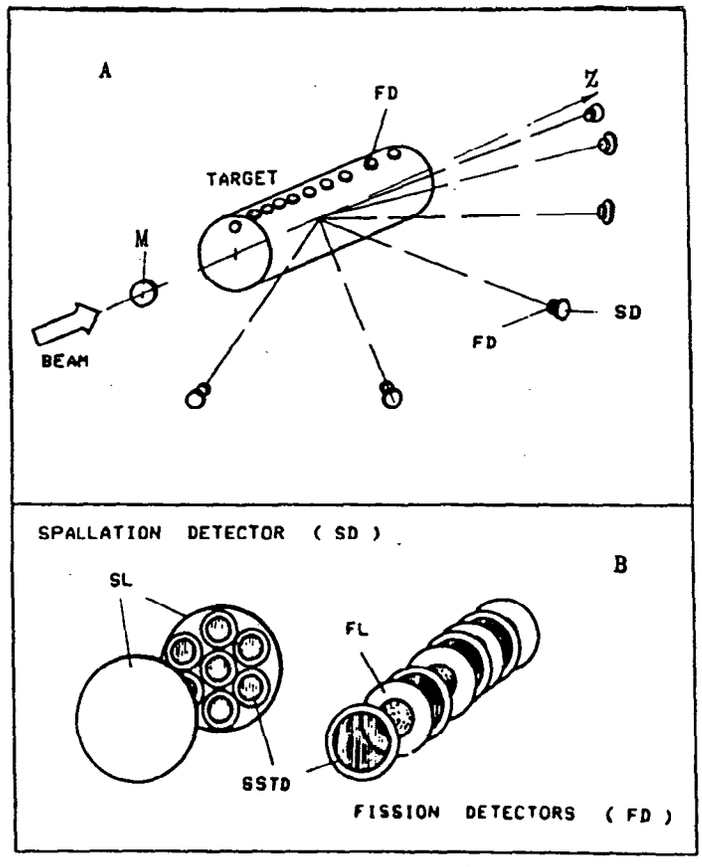

Fig.5 Schematic drawing of the target-detectors arrangement (A) and the construction of neutron detector (B) : M – aluminum monitoring foil ; FL – foil with fission layer ; SL – spallation layer.

relative measurements have shown that for the deuteron with energy 1-4 GeV a value of the cross section may be supposed about constant too. The experimental set-up and the neutron detector construction are shown in schematic Fig.5. The detectors have been placed along beam direction on the target surface and at angles of 10°, 30°, 60°, 90°, 120° and 150° at a distance 1 m from the centre of the target.

The typical neutron detector has consisted of the fission detectors and for angular measurements we have added the spallation detectors, where seven SSNTD's have been used for decrease of the methodical and statistical errors.

The measurements of the neutron background counts for different threshold detectors have been carried out with heavy concrete brick (50 cm long).

The data analysis has been performed by using our code RESTOR. The energy distributions mesured by time-of-flight technique for the lead target (20 cm diam. and 20 cm long) on 2.55-GeV proton beam have been used as a prior information to construct the zero approximation of the neutron spectrum.

The double differential neutron production distributions, $dF/dTdS$ and $dF/dTd\Omega$, have been determined for each value of beam energy. Then from these data the integral neutron spectra have been calculated for fixed values of the energy, $dY(T_i)/dS$ and $dY(T_i)/d\Omega$. Finaly, these differential distributions have been integrated for a determination of the total neutron energy spectra, $F(T)$ and $Y(T_i)$.

5. EXPERIMENTAL RESULTS

DIFFERENTIAL CHARACTERISTICS

The typical differential neutron distributions $dY(T_i)/dS$ on target surface along the direction of the incoming ions with energy 2.0 GeV is shown in Fig.6 All distributions have one maximum at Z = 12-22 cm. A value of the maximum position increases, when we pass from the total yield to the yield of the neutrons with energy T_i above 100 MeV, and besides with a rise of beam particle energy. An analysis of spatial dependent neutron production rates in the target shows that the most

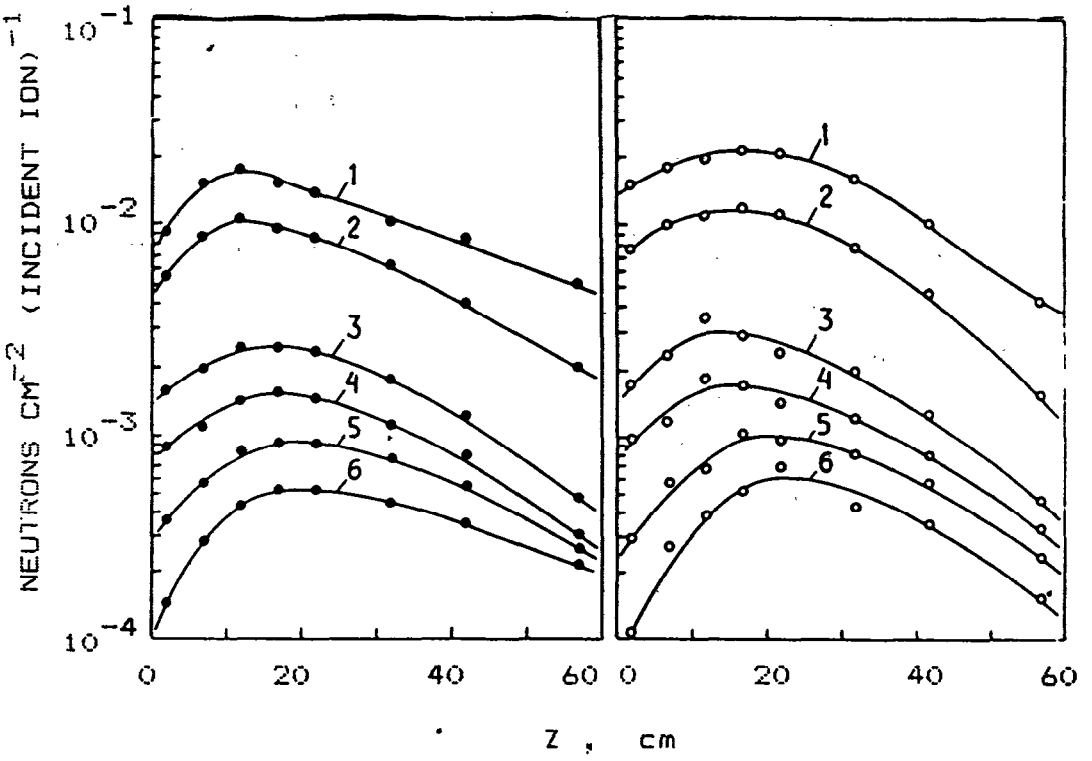

Fig.6 Side surface distributions of neutron production on the lead target by 2.0-GeV protons (●) and deuterons (O). The distributions 1-6 correspond to neutron energy above 0, 1, 6, 20, 50, 100 MeV respectively. The solid lines are eye-guide curves through the measured data points.

neutrons are emitted from the first half of the target (Z<30 cm). However the contribution of the second half of the target in the neutron yield increases to pass from 1-GeV to 3.7-GeV ions. The estimate has shown that about 87±4 % neutrons are emitted through the side surface of lead target and the contribution of the back surface in neutron emission only a few percents (this contribution increases as the beam energy rises). The angular dependences of the emission of neutrons with energy higher 1, 20 and 100 MeV, $dY(T_i)/d\Omega$, have been ploted in Fig.7 for the protons and the deuterons with energy 1 and 3.7 GeV. A comparison of a shape of angular distributions for the protons and the deuterons leads to a conclusion that only a few difference is observed between ones. The similarity of the shapes is partly place when the distributions measured at 1 GeV and 3.7 GeV are compared.

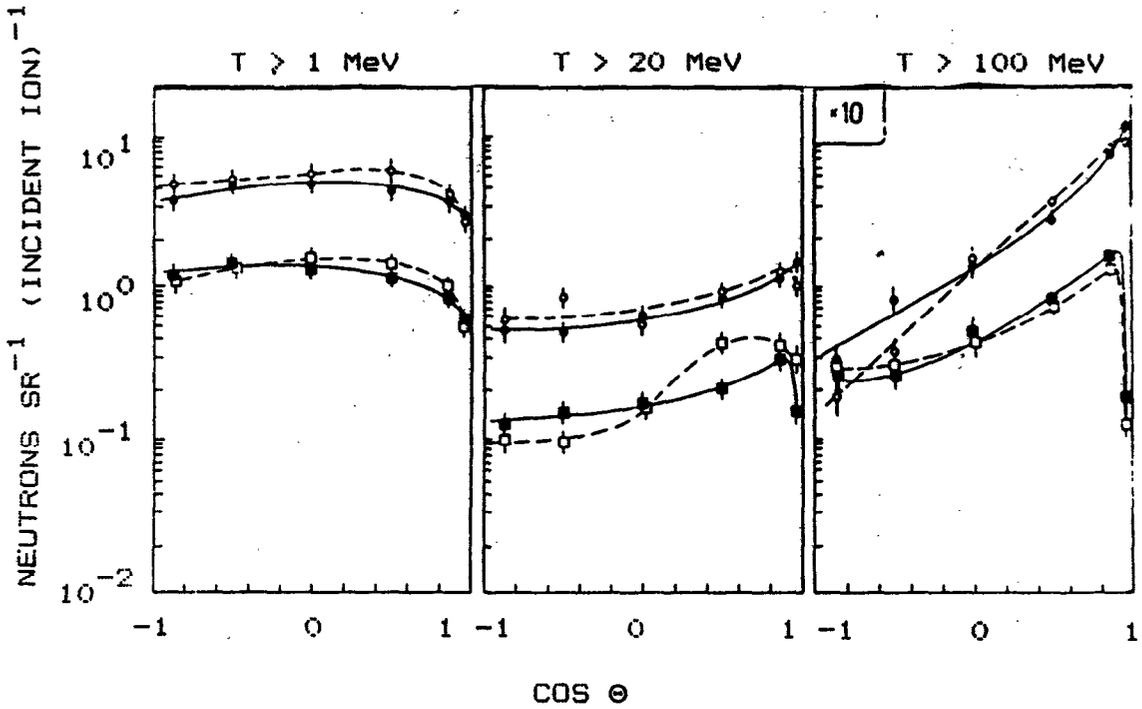

Fig.7 Angular dependence of neutron production with energy above 1 MeV , 20 MeV , and 100 MeV on the lead target by 1.0-GeV and 3.7-GeV protons (dark symbols and solid-lines) and deuterons (clear symbols and dotted-lines). The squares and circles correspond to 1-GeV and 3.7-GeV data. The lines are eye-guide curves through the measured data points.

In contrast, the shape of the distributions strongly changes moving to high-energy neutron region. The energy spectrum in the forward direction is much harder than in the backward direction and the angular distribution of the low-energy neutrons is more isotropic than for the high-energy component, which is strongly forward peaked.

INTEGRAL CHARACTERISTICS

The integral characteristics describe the production of neutrons for the whole target at all angles. As example, the absolute neutron energy spectra for incident protons and deuterons with energy 2 GeV are shown in Fig.8. This spectra have one maximum in the energy region 0.1-1 MeV and above a few MeV the intensity of both spectra monotonically and quickly falls with neutron energy. For protons the neutron spectrum is

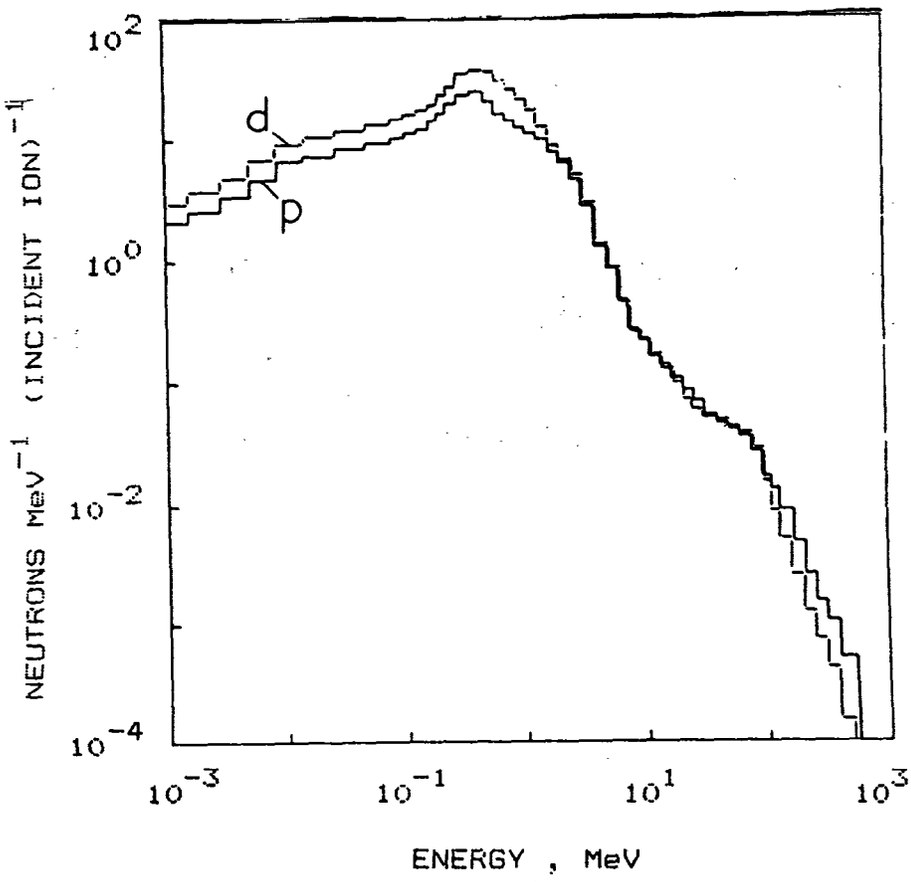

Fig.8 Comparison of the measured neutron energy spectra from the lead target bombarded by 2.0-GeV protons (solid-line histogram) and deuterons (dotted-line histogram).

more hard than one for deuteron which produce the most number of low energy neutrons but give the less high-energy neutron yield. The numerical values of secondary neutron yields at incident projectile energy about 1, 2 and 3.7 GeV are shown in Table 1.

Table 1. Experimental neutron yields for lead target (20 cm diam and 60 cm long).

energy group of neutrons	energy of incident ions /GeV/					
	protons			deuterons		
	0.994	2.00	3.65	1.032	1.98	3.76
total	25.1±3.0	44.2±3.1	80.7±6.9	24.9±5.0	58.5±8.2	98.9±14.
>1 MeV	16.3±2.1	27.5±2.0	49.9±4.5	13.9±2.8	31.3±4.7	56.6±8.5
>20 MeV	2.1±0.3	4.7±0.4	8.6±1.0	1.7±0.4	4.1±0.7	8.2±1.5

It should be noted that experimental error of data for deuteron beam is higher than one for proton beam. For deuterons this leads to a large scatter of experimental points in the energy dependence of the neutron yield. As can be seen from Table 1, p and d ions produce in the lead target (20 cm diam. 60 cm long) about 38% and 45% neutrons in energy region below 1 MeV and about 10% and 7% above 20 MeV respectively. Our estimate of the

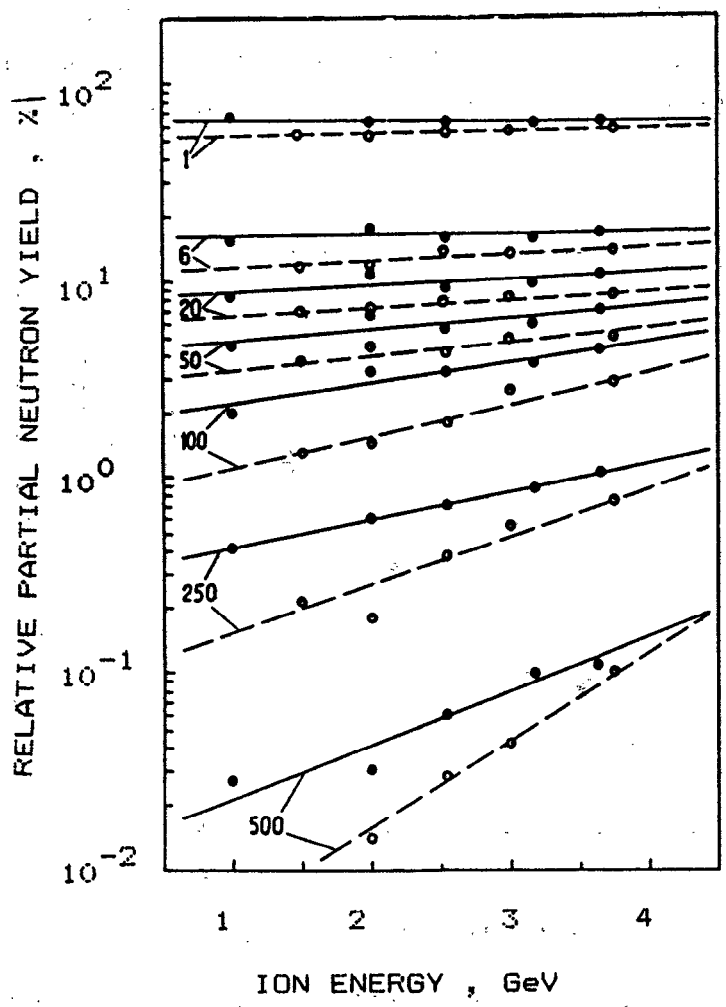

Fig.9 Relative partial neutron yields from the lead target as a function of incident ion energy for the neutron groups with energy above 1, 6, 20, 50, 100, 250 and 500 MeV. The data for the proton beam are the dark symbols and solid-lines, ones for deutron beam are the clear symbols and dotted lines. The lines are eye-guide curves through the measured data points.

average value of the total neutron yield ratio for various projectiles has given a result $Y_d/Y_p = 1.20 \pm 0.15$. The relative partial neutron yields as function of the incident ion energy have been plotted in Fig.9. As seen, their energy dependence becomes more strong for both types of the projectiles as the neutron energy is rising.

A comparison of the present experimental total neutron yields and the yields of neutrons below 15 MeV with the energy dependence of Vassil'kov et al. /7/ obtained by neutron moderation technique for proton beam and lead target (20 cm diam. and 60 cm long) is carried out in Fig.10. It shows a good

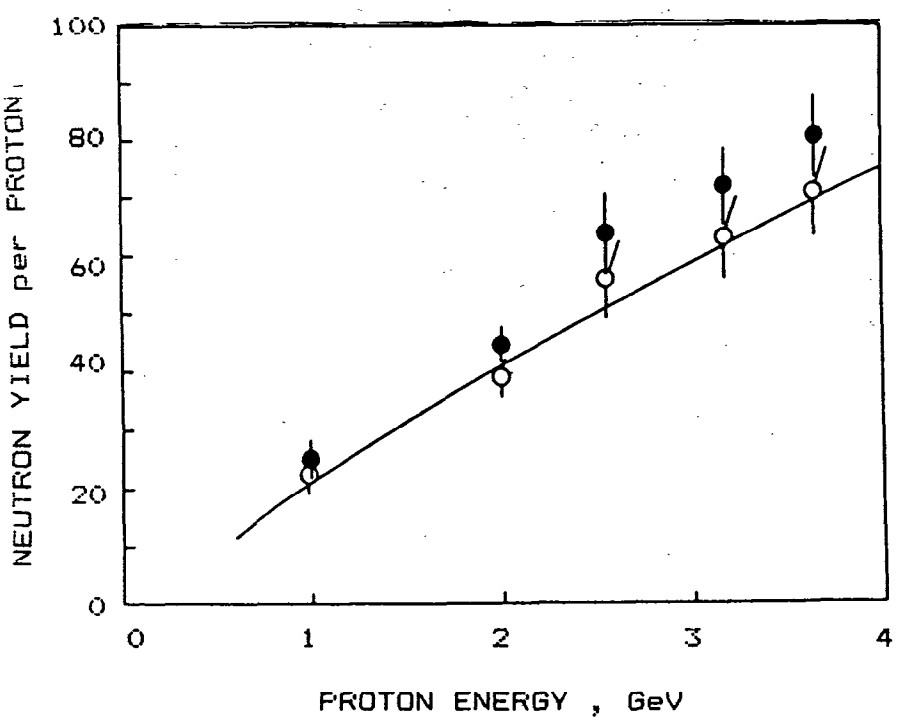

Fig.10 Comparison of the present results on total neutron yields (●) and the yields of neutrons below 15 MeV (O) with the energy dependence of Vassil'kov et al. /7/ obtained by the neutron moderation technique (solid-line) for the lead target (20 cm dium. x 60 cm long) bombarded by protons.

agreement between the present results for neutrons below 15 MeV and the dependence from paper /7/. A simple explanation of this is a neutron leakage. The neutrons with energies above about 15

MeV with high possibility go away from the moderator of experimental set-up. The data analysis is still being continued.

The authors would like to acknowledge the help in present measurements realization Y. M. Chirkin, N. S. Myzin, I. O. Tsvetkov, I. B. Vorob'ev.

REFERENCES

1. M. Nieminen, J. J. Torsti, Nucl. Instrum. Methods, v.179, 77 (1981).
2. H. M. Conrad, Nouvelle de SATURNE, n.8, 29 (1983).
3. A. R. Krylov et al., Report 16-85-347, JINR, Dubna (1985).
4. V. P. Bamblevsky et al., Report 16-86-486, JINR, Dubna (1986).
5. S. A. Wender et al., Proc. of the First Inter. Conf. on Neutron Physics, 1987, Kiev, Moscow, Atomizdt, v.4, 17 (1988).
6. I. B. Vorob'ev et al., Atomnaya Energiya, v.61, 35 (1986).
7. R. G. Vassil'kov et al., In this conference.
8. P. F. Denisov, V. N. Mehedov, Nuclear Reactions at High Energies, Moscow, Atomizdat (1972).
9. V. I. Gol'dansky et al., JETP, v.29, 778 (1955).
10. P. W. Lisowski et al., Proc. of the Inter. Conf. on Nuclear Data for Science and Technology, 1988, Mito, JAERI, 97 (1988).
11. I. B. Vorob'ev et al., Proc. of the 15th Inter. Conf. on Particle Tracks in Solids, 1990, Marburg, FRG (will be published in Nuclear Tracks in Radiation Methods).
12. T. Nakamura, Y. Uwamino, Phys. Rev. C, v.29, 1317 (1984).
13. T. Nakamura, Nucl. Instrum. Methods, v.A240, 207 (1985).
14. J. Banaigs et al., Nucl. Instrum. Methods, v.95, 307 (1971).

ICANS-XI International Collaboration on Advanced Neutron Sources
KEK, Tsukuba, October 22-26, 1990

Superintensive pulse slow neutron source SIN based on kaon factory.

N.V.Kolmichkov, V.D.Laptev, V.A.Matveev, L.N.Latisheva, S.V.Serezhnikov, S.F.Sidorkin, N.M.Sobolevsky, Yu.Ya.Stavissky
INR of Soviet Academy of Sciences

V.I. Trushkin, V.V.Khmelschikov, N.A.Khryastov
NIKIET

Possibility of intensive pulse slow neutron source creation based on 45-Gev proton synchrotron of K-meson factory, planned to construction in INR AS USSR is considered. Calculated peak thermal neutrons flux density value, averaged on "radiating" light-water moderator surface of 100 cm^2 is 6.6×10^{17} neutrons/(cm^2sec) for pulse duration of 35 microseconds.

Creation of high-current proton accelerators for 50 Gev energy gives way for the following development of new neutron sources generation based on proton beams /1/. Possibility of intensive pulse slow neutrons source creation based on K-meson factory was considered earlier in /2/. This article deals with superintensive pulse neutron source SIN features based on K-meson factory with following accelerator parameters:

Proton energy (GeV)	45
Average current,μa	125
Pulse frequency,Pps	8.3
Pulse duration,μsec	4.4

General scheme of neutron source SIN is analogous to one of pulse neutron source based on Moscow meson factory (MMF-0.6) /3/. Fig. 1 shows neutron source geometry for calculations. Target is compact packing of wolfram rods cooled by water (volume water fraction about 20%). Target and light water moderator are surrounded by iron reflector also cooled by water. Neutron source with reflector are located in the biological shield made of iron and heavy concrete. Figs. 2 and 3 show the location of neutron source and experimental channels in the shield.Shield thickness in side direction is determined by cascade neutrons, in proton beam direction - by μ-mesons.

Calculation of heat generation and neutron flux density were carried out by SHIELD and MKT programs. Detailed description of calculation technique is presented in /2/.

Hadron cascade calculation was carried out for proton energy of 25 GeV. 383 vaporized neutrons with average energy of 3.3 MeV are produced per one incident proton in the whole system - including 250

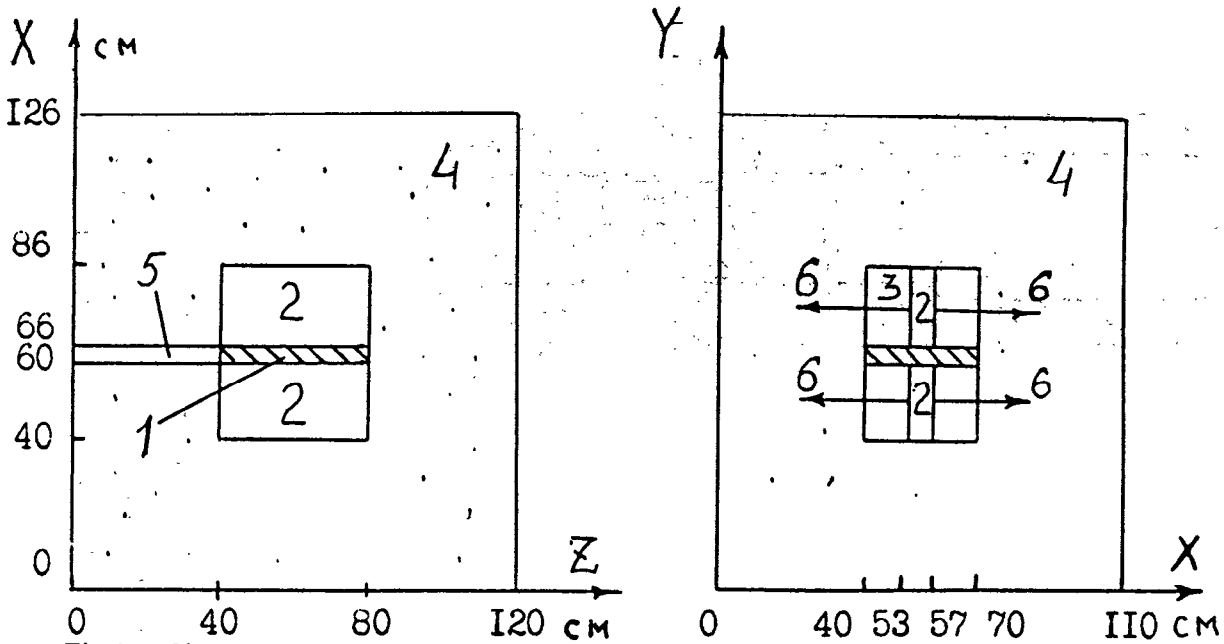

Fig.1. Neutron source SIN geometry for calculation 1 - target; 2 - water; 3 -vacuum; 4 - reflector; 5 - proton beam tube; 6 - experimental neutron channels.

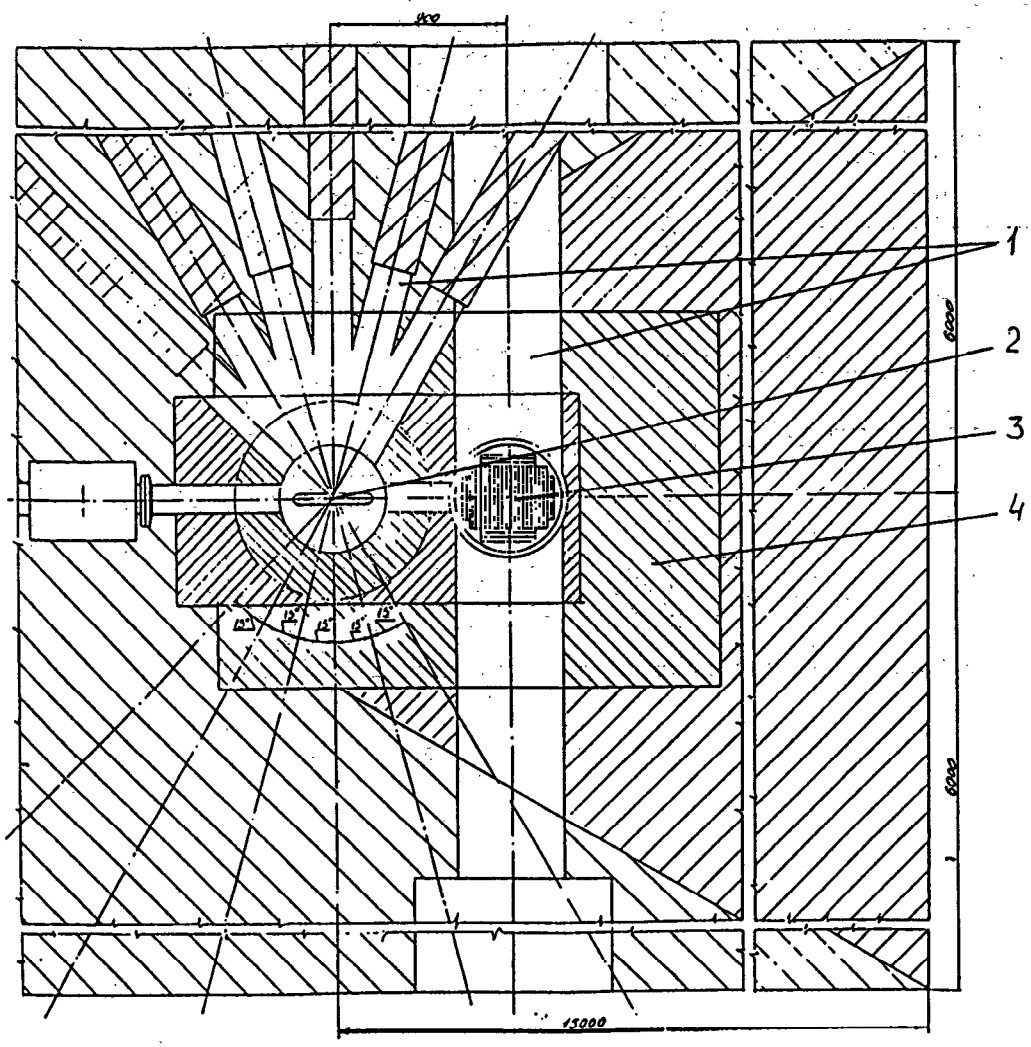

Fig.2. General view of SIN: 1 -experimental neutron channels; 2 - moderator; 3 - beam dump; 4 - shield.

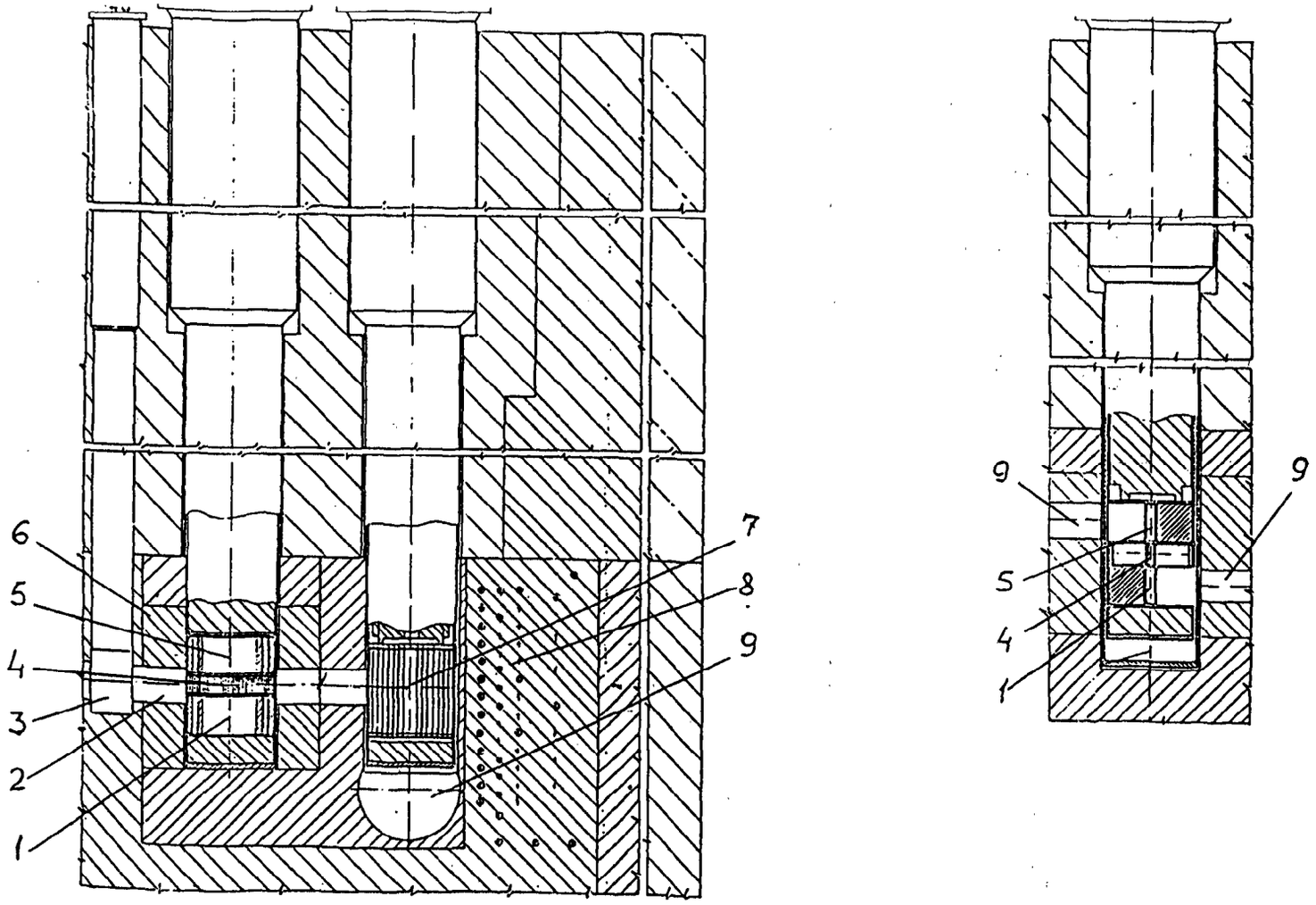

Fig.3. SIN vertical cross-section: 1 - water moderator; 2 - proton beam tube; 3 - vacuum switch; 4 - SIN target; 5 - liquid hydrogen moderator; 6 - reflector; 7 - beam stop target; 8 - heat shield; 9 - experimental neutron channels.

neutrons in wolfram target. Figs. 4 and 5 show neutron production distribution in wolfram target (20% of water in the volume) from the point proton beam.

Table 1 presents number of neutrons going from "radiative" moderator surface of 20*40 cm^2 to differential solid angles perpendicularly to the surface, calculated for one falling proton (Ep=25 GeV).

Efficient width θ of thermal neutron pulses (E < 0.215 eV) for moderator thickness of 3 cm is about 35 μsec. For moderator parameters presented above the average thermal neutron flux density $\overline{\Phi}_2$ = 5.9×10^{13} neutrons/(cm^2sec) and peak density is 2.0×10^{17} neutr/(cm^2sec) (Ep=45 GeV). For moderator of 10x10 cm^2 corresponding flux densities are: 2.0×10^{14} and 6.6×10^{17} neutr/(cm^2sec) respectively.

Table 2 shows thermophysical parameters for neutron target with dimensions 100x300x400 mm^3.

When Gaussian cross distribution of proton beam intensity has σ_x and σ_y dispersions, specified in the table, 90% of beam protons hit the target.

Time constant τ for cooling of wolfram rod is about $c\rho R^2/\lambda$, where c - specific heat, ρ - density, R - rod radius and λ - heat conductivity. This value τ = 82 msec is close to pulse period T = 80 msec and is sufficiently greater than heat-carrier transition time through half-target being 15 msec. It causes sufficiently pulse character of rod and heat-carrier temperature fields.

Table 3 shows relative data for radiation damages in first-wall materials of SIN, MMF-0.6 neutron sources and thermonuclear reactor with thermal load of first wall about 1 Mw/m^2. The radiation damages calculation were carried out by analogy with /2/.

Data for SIN are given for proton current of 125 μA and dispersions of 7.9 and 2.63 cm, for MMF-0.6 - for the current of 500 μA and 3 cm dispersion.

Fast neutron fluence of about 10^{22} neutr/(cm^2year) corresponds to K_{dpa} about 10 dpa per year. Expected material features alterations for such radiation dose are small.

Table 4 gives relative parameters for SIN, pulse fast reactor IBR-2 (Dubna), for ISIS neutron source /4/ and for neutron source based on MMF-0.6.

In conclusion we are like to acknowledge for support and for interest to the work A.N.Tavchelidze, V.M.Lobashev, V.D.Burlakov.

Table 1.

Angle, deg.	5	10	30	90
Neutron energy				
E < 0.215 eV	0.18	0.38	3.5	16.9
0.215ev<E<10,5Mev	0.36	1.2	12	60.5
E > 10.5 MeV	0.001	0.003	0.05	2.6
fraction, %	0.2	0.2	0.3	3.3
0 < E < 8	0.54	1.6	15	80

Table 2.

Proton beam	
Proton energy, GeV	45
Average current, μA	125
Pulse per sec	8.3
Dispersion σ_x, σ_y, cm	7.9, 2.6
Fraction of beam on the target,%	90
Target:	
Heat release, Mw	2.5
Size, mm	100x300x400
Rod length, mm	300
Rod diametr, mm	4
Max.aver.heat release,w/m^3	$1.3.10^9$
Max. wall temp., ^{0}C	135
Heating up per pulse, ^{0}C	60
Coolant - H_2O :	
Initial temp., ^{0}C	30
Velocity, m/sec	10
Flow rate, m^3/h	290
α, w/m^2grad	5.10^4
Heating up on half length of rod, ^{0}C	
Min	12
Max	16
Heating up - α, ^{0}C	
Min	23
Max	62

Table 3.

Facility	Material	Damage production rate K_{dpa}, dpa/year	Helium production rate K_{He}, nuc/year x10^6	K_{He}/K_{dpa}x10^6
SIN (1st wall)	Fe	9	430	48
	Al	27	370	14
	W	6	750	130
MMF-0.6 (1st wall)	Fe	13	220	17
Thermonucl. reactor	Fe	14	150	11
SIN (target)	W	15	1200	80

Table 4.

Neutron source	Pulse width therm.neutr µsec	Peac flux dens.therm neutr/cm^{2}s	Av.flux dens.therm neutr/cm^{2}s	PPS	Fig.of merit, Φ_{av}/θ^2
IBR-2	215	1.0.10^{16}	1.1.10^{13}	5	0.16
IBR-2*)	120	3.7 10^{16}	2.2.10^{13}	5	1
ISIS**	35	4.9.10^{15}	8.5.10^{12}	50	4.5
MMF-0.6	35	4.9.10^{15}	1.7.10^{13}	100	9
SIN	35	6.6.10^{17}	2.0.10^{14}	8.3	110

*) Expected data after modernisation.

**) Evaluated data for target-moderator scheme analogous to the one of MMF-0.6.

REFERENCES

1.Stavissky Yu.Ya. Gigantic Pulses of Thermal Neutrons in Targets of Superhighenergy Accelerators. INR AS USSR, Prepr. P-0215, Moscow (1981).

2.Boriskin S.E. et al. Proc. Vsesoyusnogo seminara po programme mesonnoi fabriki. IYaI AN SSSR, Moskva (1988).
3.Bulkin Yu.M.et al. Proc.of a Conf.on Neutron Scattering in the Nineties. IAEA, Vienna. pp. 369-375 (1985).
4.Gray D.A. Proc. of a Conf. on Neutron Scattering in the Nineties. IAEA, Vienna. pp. 261-266 (1985).
5.Ananyev V.D.et al. Pulse Reactor IBR-2 in Nineties. JINR. Prepr. R3-85-187 (1985).

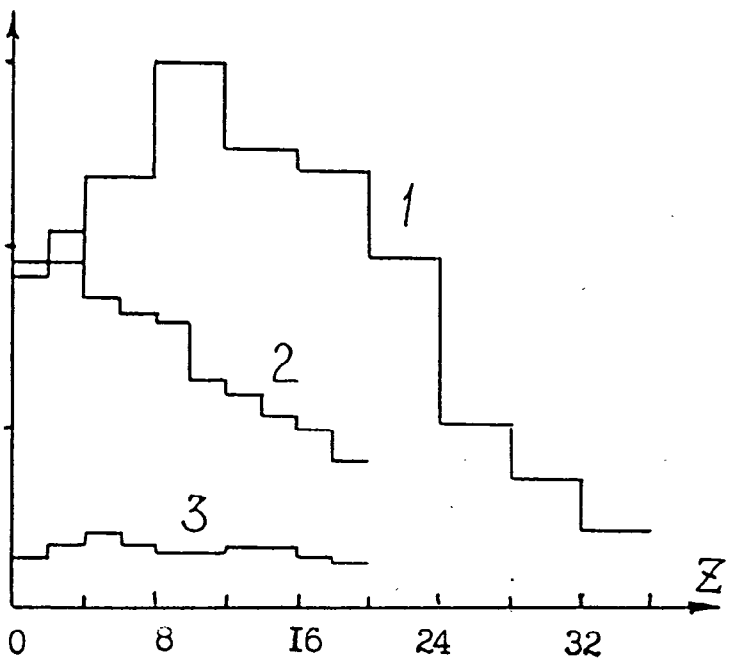

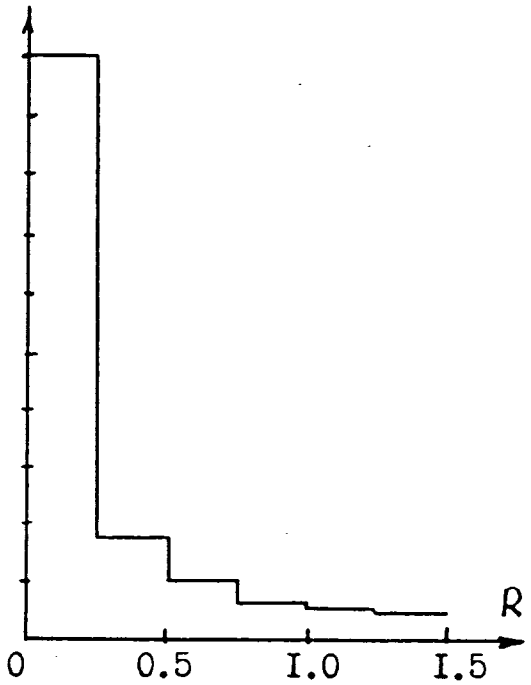

Fig.4. Z-dependence of vaporised neutron production density(1), of total heat release (2), of heat release without π^0 contrbution(3).

Fig.5. R-dependence of vaporised neutrons production density.

ICANS-XI International Collaboration on Advanced Neutron Sources
KEK, Tsukuba, October 22-26, 1990

Neutronic Tuning - Some Thoughts

Gary J. Russell
Los Alamos National Laboratory
Los Alamos, New Mexico USA

DEFINITION

"A ***useful*** neutron is one heading in the right direction with the correct energy at the right time."

"...uncontaminated and as many as possible!"

Anonymous

I. SUMMARY

The above definition of a ***useful*** neutron offers a real challenge to the designers of spallation target systems for pulsed and steady-state neutron sources. (A spallation target system is the composite of many individual components, which are listed in Table I.) The designer's job is to produce as many useful neutrons as possible. It is an extremely complicated optimization problem.

Neutronically tuning a spallation target system is the process of optimizing the production of useful neutrons. Many variables exist in neutronically tuning a spallation target system (see Table II). Enhancing the neutronic performance of a spallation neutron source by neutronically tuning the target system is much more cost effective and prudent than increasing the output of the accelerator, which feeds the spallation target system. Gains in useful neutron production of 10% are very worthwhile to attain. For LANSCE, a 10% increase in useful neutron production corresponds to 10 μA of proton current in the Proton Storage Ring (PSR), which feeds 800-MeV protons to the Los Alamos Neutron Scattering Center (LANSCE).

In ***neutronic tuning***, the designer should isolate individual components (where possible) to understand the neutronics of that component. However, the designer should take this approach only so far. Because of synergistic effects, the designer must optimize the neutronics of the *entire* target system for useful neutron production. Even with an optimized target system, other variables are also important when looking at the ***total performance*** of a spallation neutron source. Table III shows the main variables affecting total performance.

II. ACKNOWLEDGEMENTS

I appreciate the support of Roger Pynn for this work. I thank Tatia Vander Maat for her typing help and Maria DiStravolo for proofreading the text on a very short notice. LANSCE work is supported by the US Department of Energy, Office of Basic Energy Sciences, under contract W-7405-ENG 36 with the University of California.

Table I

What is a Spallation Target *System*?

- Target(s)
- Moderator(s)
- Reflector(s)
- Poisons/Decouplers/Liners
- Structural Materials
- Cooling Material(s)
- Shielding

Table II

Neutronic Tuning Variables

- Proton Beam

  - *Energy/Beam Profile*

- Target

  - *Material*

    * tantalum
    * tungsten
    * lead
    * lead/bismuth
    * depleted uranium
    * enriched uranium

  - *Geometry/Size*

    * cylinder
    * square
    * slab
    * split
    * composite

- Reflector(s)

  - *Material/Size*
    * beryllium
    * graphite
    * heavy water
    * nickel
    * lead

- Moderator

  - *Material*
    * light water
    * heavy water
    * liquid methane
    * solid methane
    * liquid H_2
    * liquid D_2

  - *Temperature*
  - *Size*
  - *Decoupled*
  - *Poisoned*
  - *Coupled*
  - *Reentrant*
  - *Grooved*
  - *Honeycombed*
  - *Composite*
  - *Field-of-View*

- Poisons/Decouplers/Liners

  - *Material/Thickness*
    * gadolinium
    * cadmium
    * ^{10}B
    * boral
    * ^{6}Li

- Target-Moderator-Reflector-Shield geometry

  - *Coupling*
    * geometric
    * neutronic

  - *Target*
    * solid
    * liquid
    * split
    * composite

  - *Moderator geometry*
    * wing
    * slab
    * flux-trap
    * backscattering
    * composite

- Time

  - *Neutron-pulse shapes*
    * pulse width
    * rise time (leading edge)
    * decay time (pulse tails)

- Synergistic effects